Characterization of Most Promising Sequestration Formations in the Rocky Mountain Region (RMCCS)

Final Report
Reporting Period: October, 2009 – September 2013

Principal Authors:
Brian McPherson, University of Utah, Salt Lake City, Utah USA
Vince Matthews, Ph.D., CPG-11610, LeadvilleGeology LLC, Leadville, CO USA

January, 2014

DE-FE0001812

Submitted by
Brian McPherson, University of Utah, Salt Lake City, Utah 84112

Other Significant Sub-Recipients and Report Contributors:
Leadville Geology, LLC, 519 W 7th St, Leadville, CO 80461
Colorado Geological Survey, 1500 Illinois St., Golden, CO 80401
Utah Geological Survey, 1594 W North Temple, Salt Lake City, UT 84116
Arizona Geological Survey, 416 W. Congress St., Suite 100 Tucson, Arizona 85701
New Mexico Bureau of Geology and Mineral Resources, 801 Leroy Place, Socorro, NM 87801
Schlumberger Carbon Services, 300 Schlumberger Dr. Sugar Land, Texas 77478
Shell Oil Company, 4582 S Ulster ST, Denver, CO, 80237
Tri-State Generation and Transmission Assoc., Inc., 1100 W 116th Ave, Westminster, CO 80234
Trapper Mining, Inc., 25910 Colorado 13, Craig, CO 81625

DISCLAIMER
This report was prepared as an account of work sponsored by an agency of the United States Government. Neither the United States Government nor any agency thereof, nor any of their employees, makes any warranty, express or implied, or assumes any legal liability or responsibility for the accuracy, completeness, or usefulness of any information, apparatus, product, or process disclosed, or represents that its use would not infringe privately owned rights. Reference herein to any specific commercial product, process, or service by trade name, trademark, manufacturer, or otherwise does not necessarily constitute or imply its endorsement, recommendation, or favoring by the United States Government or any agency thereof. The views and opinions of authors expressed herein do not necessarily reflect those of the United States Government or any agency thereof.

Abstract

The primary objective of the "Characterization of Most Promising Carbon Capture and Sequestration Formations in the Central Rocky Mountain Region" project, or RMCCS project, is to characterize the storage potential of the most promising geologic sequestration formations within the southwestern U.S. and the Central Rocky Mountain region in particular. The approach included an analysis of geologic sequestration formations under the Craig Power Station in northwestern Colorado, and application or extrapolation of those local-scale results to the broader region. A ten-step protocol for geologic carbon storage site characterization was a primary outcome of this project.

TABLE OF CONTENTS

EXECUTIVE SUMMARY 1

NARRATIVE 2

1. Regional Assessment and Data Gathering 2

2. Identification and analysis of appropriate local sites 3

UTAH 5

NEW MEXICO 14

ARIZONA 15

3. Public engagement: outreach, planning and permitting 16

PLANNING 17

PERMITTING 17

PUBLIC OUTREACH 19

4. Geologic and geophysical studies at local characterization site 22

5. Stratigraphic well drilling and coring 37

Pre-Drilling Activity 37

Pre-Drilling Risk Mitigation 39

Drilling Chronology 40

Discussion and Key Points 40

Conclusion 48

6. Core analysis and interpretation with other geological and geophysical data 49

Core Sampling and Inventory 49

Plug Acquisition 49

Core Slabbing 52

Core Analysis 54

Total Organic Carbon (TOC) 55

X-Ray Diffraction (XRD) 55

Spectral Core Gamma (SCG) 56

Fracture Analysis 56

Porosity and Permeability 56

Noble Gas Tracers 59

Capillary Pressure 59

Relative Permeability 63

7. Database assembly and static model development 69

8. Capacity assessment 77

9. Simulation and uncertainty assessment 87

10. Final risk assessment 95

11. Project Summary and Conclusions 115

Identification and Analysis of Appropriate Local Sites 116

UTAH 116

ARIZONA 118

NEW MEXICO 119

COLORADO 121

Public Engagement 123

Detailed Local-Scale Analysis: Geologic and Geophysical Data for the Sand Wash Basin 123
Detailed Local-Scale Analysis: Stratigraphic Well Drilling and Coring 124
Detailed Local-Scale Analysis: Core Analysis and Interpretation with Other Geological and Geophysical Data 125
Detailed Local-Scale Analysis: Database Assembly and Geologic Static Model Development 128
Capacity Assessment 129
Uncertainty Assessment Workflow 130
Simulation and Risk Assessment 131
Appendix A: References 134
Appendix B: Bonanza Site (Utah) Analysis 133
Appendix C: Woodside Site (Utah) Analysis 158
Appendix D: CGS Outreach Presentations 184
Appendix E: Public Engagement Documentation 218
Appendix F: Sand Wash Basin (Colorado) Data 239
Appendix G: Short Versions of Drilling Plan and Safety Plan 258
Appendix H: Drilling Chronology 267
Appendix I: RMCCS #1 Well Log 273
Appendix J: Niobrara Well Log and Associated Information 275
Appendix K: Core Analysis Results 279
Appendix L: Sample of Petrography Results 469
Appendix M: Capacity Assessment Methodology 479
Appendix N: Arizona Capacity Assessment 513
Appendix O: New Mexico (San Juan Basin) Capacity Assessment 569
Appendix P: Utah Geological Survey Capacity Assessment 614
Appendix Q: Colorado Geological Survey Capacity Assessment 666

EXECUTIVE SUMMARY

The four state geological surveys of Arizona, Colorado, New Mexico, and Utah conducted regional geologic assessments of three of the most promising sedimentary units for sequestering CO_2 in the Colorado Plateau physiographic province. The maps and interpretations are important contributions because they were a coordinated effort to use the same techniques and interpretations across state boundaries, which is rarely done. The studies included structural contour maps, net sand and porosity maps, geothermal data, and salinity data. Sequestration capacities were modeled at the University of Utah from these regional studies resulting in the conclusion that the three formations could provide between 12.9 and 136.8 billion metric tons of storage. The medium case would provide more than 150 years of sequestration potential at current rates of emission.

A stratigraphic characterization well was drilled to 9750' depth in the Sand Wash Basin, Colorado near the town of Craig. The well plan called for taking cores in the Dakota, Entrada, and Weber formations. Because the drilling exceeded budgeted costs, the Weber Formation was never reached. A number of key lessons were learned about drilling a well of this nature which are outlined in the drilling and coring section.

Lack of nearby well control, and variable stratigraphy made it difficult to forecast where the Dakota Sandstone would be encountered, so full-core sampling of that formation was not possible. The most full-core samples were taken from the Entrada Formation. However, the targeted formations encountered in the well were sampled with sidewall cores and sophisticated, wireline geophysical logs. These enabled excellent characterization of the targeted formations. The sidewall cores also allowed petrographic and X-ray diffraction analysis of the targeted formations, even though full-core samples were not obtained in all targets.

Public outreach took a variety of forms from informal meetings with stakeholders, to public meetings with print and radio media in attendance. A website provided up-to-date information to the public. Public, informational meetings were held both before and after drilling of the Sand Wash Basin well.

The Colorado Geological Survey, Schlumberger, and the University of Utah built a geocellular model of the area surrounding the drilled well in order to model the potential injection of CO_2 into this area. The data used in constructing the model included information from the stratigraphic characterization well, more than 1,000 surface measurements, 2700 geophysical well logs, 15,000 formation tops, all available core data, 78 miles of 2-D seismic lines, and published geologic studies. The seismic lines were all processed to the same standard.

The development of a new workflow based on random "pseudo wells" placed in the geocellular model allowed the derivation of the minimum number of characterization wells necessary to acceptably model the capacity of an area like the Sand Wash Basin. This analysis clearly showed that the appropriate density of characterization data/well is dependent on the character of the geologic formations, even within the same basin.

NARRATIVE

This project narrative section expresses the comprehensive results of the RMCCS project in the form of the Final 10-Step Protocol for CO_2 Storage Site Characterization. All references cited are listed in Appendix A. Remaining appendices are related to the individual steps of the protocol, discussed in this narrative, beginning with step 1, Regional Assessment and Data Gathering.

1. Regional Assessment and Data Gathering

The first step in any geologic sequestration project involves regional assessment and data gathering. For this project, the State Geologists from Arizona, New Mexico, Utah, and Colorado met and conducted a preliminary regional assessment. They agreed that the Colorado Plateau presented an excellent opportunity to conduct a broad scale, regional study of the potential for carbon capture and sequestration. The Dakota, Entrada, and Weber were formations (and their equivalents) that were widespread throughout the Plateau and generally had good permeability and porosity.

Prior to the initial meeting, each geological survey was asked to select one or more areas that might be suitable for a pilot project to characterize the three formations. Several criteria were necessary for a successful site to propose. First, a site must be found where the landowner is willing to allow for a characterization well to be drilled. Second, the site must have structural and stratigraphic characteristics that would make it suitable for long-term sequestration of CO_2. It would be preferable if the site had a preliminary estimate of CCS capacity. And third, the site should have potential for attracting industry partnership and investment.

Colorado brought a site located near Craig, Colorado to the initial meeting. The site had all three formations present and the appearance of large structural closure near the margin of the Plateau. The site was located on Colorado state lands. The Colorado State Land Board (a sibling agency of the Colorado Geological Survey) is in the Colorado Department of Natural Resources providing the opportunity for a close working relationship. The Craig Power station, a coal-fired electric generating station was located on the structure. Shell and Tri-state Generation and Transmission indicated a possible interest in joining the project. The location was situated near a coal plant with significant emissions, near several gas processing plants with emissions, and near a potential oil-shale operation that would generate new emissions. It was also considered to be an attractive site for new cement plant operations or any other industry that might need to control emissions. The site had also had a preliminary estimate of storage capacity under Phase II of the Southwest Partnership for Carbon Sequestration.

Each of the other states also brought potential sites within their boundaries. However, none of these sites ultimately were able to meet all of the necessary criteria. And, all agreed that the Colorado site was the only one that would have any chance of moving forward.

Because of the long, and excellent, relationship that the Colorado Geological Survey had experienced with Dr. Brian McPherson and the Southwest Partnership for Carbon Sequestration, Dr. McPherson and his team at the University of Utah was invited to join in the proposal to DOE. Additionally, he brought Schlumberger Carbon Services into the partnership.

Each state geological survey was to investigate those basins on the Plateau where the three formations (or their equivalents) were present at depths sufficient for injection and storage of CO_2. For Colorado that included the Sand Wash, Piceance, San Juan, and Paradox Basins; for Utah the basin selected was the Uinta; for New Mexico, the San Juan Basin; and for Arizona, the

Black Mesa Basin. Formations analyzed were Dakota, Entrada, Weber, Hermosa, Cedar Mesa, De Chelly, and Leadville.

Data that were gathered for the analyses were derived from subsurface well logs (digital where available), regional literature, and existing core descriptions. Data used in the analyses included salinity, porosity, depth, thickness, and temperature.

Well log data were analyzed, interpreted, correlated, and incorporated into various interpretive software programs available to each survey (Petra and ArcGIS). Structural contour maps on the tops of the potential formations were prepared by each survey. Isopach maps of the potential formations in the Colorado Plateau were also prepared by each survey. The data were exported in ARC for inclusion in NATCARB V. Ultimately the data were incorporated into Petrel for modeling capacity.

2. Identification and analysis of appropriate local sites

The geology of the Colorado Plateau, located in the Southwestern United States, contains several deep saline formations that are suitable for geological carbon sequestration. These formations occur below 3000' depth, are capped by seals and their salinity is generally higher than 10,000 mg/l. Three ubiquitous reservoirs within the four-state region of AZ, CO, NM and UT are the Cretaceous Dakota Formation, the Jurassic Entrada Formation and the Permian Weber Formation, mainly occurring in the northern sedimentary basins of the Colorado Plateau Region the main emphasis of this study. Additional formations studied at the regional scale in the Four Corners area on the southern end of the Colorado Basin, were the Hermosa Group, the stratigraphic equivalent of the Weber in the NM San Juan Basin, the DeChelly Formation in AZ, CO and UT, the Cedar Mesa Formation in AZ, and the Leadville Formation in NM.

The Geological Surveys of the four states in which the Colorado Plateau Region is located, AZ, CO, NM and UT, were tasked to improve the regional geologic assessment of the listed formations. That was accomplished by generating structure and thickness contour maps for each of the formations for which they were responsible. These maps were not just based on interpolating well-derived data, but also incorporated additional available information and studies. Each of the partnering geologists contributed in-depth, sedimentary-basin expertise during the compilation of the regional geology. In addition to digital contour maps, the surveys also provided regional porosity data and geothermal gradient values.

Besides the regional assessment carried out on the deep saline formations occurring across the state boundaries, each of the four states were asked to prepare a site-specific study. For Colorado this site was the Sand Wash Basin (Figure 2.1), the main location of the detailed site characterization efforts. Utah looked at several sites and found two with potential, willing outside-cooperating partners: Woodside Dome site near Green River Utah and the Bonanza site,— both in the Uinta Basin (Figure 2.1). Several potential storage sites were identified in the San Juan Basin (Figure 2.1) also, but no outside cooperating partners were available. The regional assessment for Arizona indicated the best storage site occurs near the Navajo Generating Station (Figure 2.1) but because of lack of detailed well data at that site, this site requires more in-depth study, comparable to the Craig-site, before a final determination about the suitability of the site can be made. The site specific storage capacity estimates are included in this report as well. Selection of local (specific) sites in Utah, New Mexico and Arizona are described in the following subsections. For Colorado, the local site (Craig, CO) and associated comprehensive analyses are detailed in Chapters 4 through 7 of this report, with additional complementary details about Colorado and the Craig site in all other chapters.

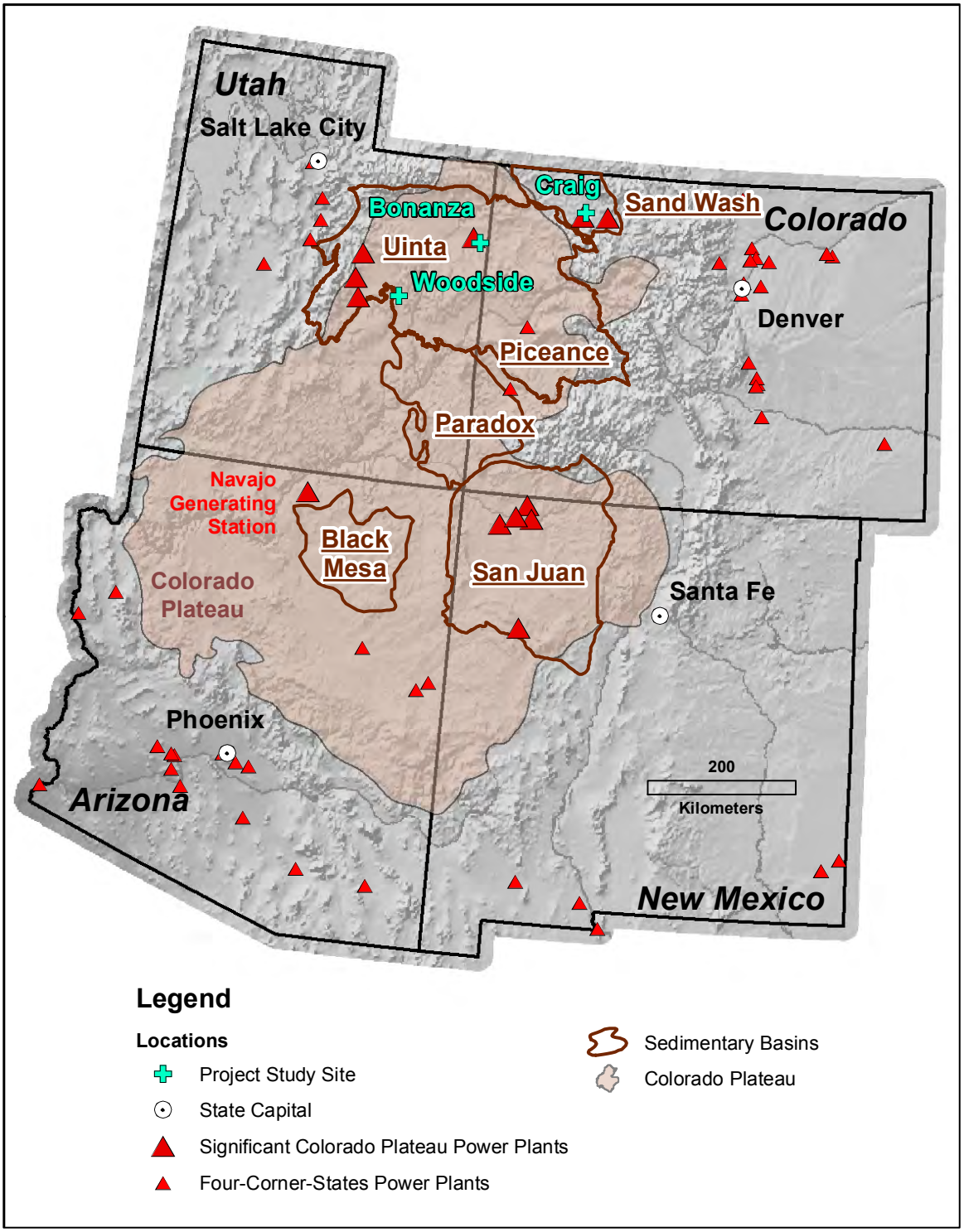


Figure 2.1: *Colorado Plateau carbon emission sources in relation and potential site-specific geological sequestration reservoir candidates.*

UTAH

Geologic, oil and gas field, and structure contour maps of the Uinta Basin were used to identify nonproducing structures, abandoned oil and gas fields, and areas with potential stratigraphic traps for the Weber, Entrada, and Dakota Sandstones. A table of potential CO_2 storage sites was compiled. Data added to the table included the area of each site which was defined using geologic maps; the depth, thickness, and porosity were defined from published reports or from a representative well log. Reservoir pressure and temperature were calculated from standard pressure and geothermal gradients for the area. Storage capacity was determined two ways: (1) using CO_2 density from a chart published by Hardage and Sava (May 2009), and (2) calculating CO_2 density from an ideal gas law equation. The storage capacity equation used was: area (ft^2) * thickness (ft) * porosity * CO_2 density (lbs/ft^3) * 0.04 (efficiency) = lbs (lbs/2204 = lbs/metric ton).

Minimum site qualifications were:

(1) must have at least one of the three primary targets (Weber, Entrada, or Dakota),
(2) potential reservoirs must be at least 2500-ft (760-m) drill depth [this was later changed to minimum 3000-ft (1000-m) drill depth],
(3) must have minimum storage capacity of 30 million metric tonnes (MMT)
(4) must contain saline water with 10,000 total dissolved solids (TDS) or more, and
(5) must be within the Colorado Plateau.

Table 2.1 shows the sites, the basic reservoir parameters, and the storage calculations. We also included land ownership, current status of land usage, and relevant infrastructure. Some of the sites did not meet the minimum qualifications and are designed with an X in the ranking column. Copies of Table 2.1 (without rankings) were given to four UGS geologists who were asked to rank the sites following instructions below Table 2.1. The rankings in column 1 of the table are based on the input from the geologists.

Table 2.1. Preliminary site evaluation for CO_2 storage capacity in the Uinta Basin. Each site must have at least one of the three primary reservoirs—Weber, Entrada, and Dakota.

Rank	***Location***	***Area***	***Depth (ft): Kd Je Pw other***	***Thickness (ft): Kd Je Pw other***	***Porosity (%)***	***Status***	***Land***	***Resource: Power plant Coal Rail***	***Pressure (psi) Calc. @ 0.45psi/ft***	***Temp (^{0}F) Calc. @ 60+1ºF/ 100 ft***	***Storage Estimate MMT- Chart***	***Storage Estimate MMT- Equation***
1	Bonanza 9S-10S 24E-25E	100 sq mi 528,000 acres. Potentially much larger 2,790,000,000 ft^2	Kd 11,000 Je 12,000 Jn 12,250 Pw 13,800	Kd 80 Je 150 Jn 600 IPw 200	Kd 15 Je 12 Jn 10 Pw 10	Gas wells Tw – Kd. Natural Buttes area. Very active gas drilling	BLM, SITLA	Within 6 mi. of Bonanza Power Plant. Remote location.	Kd 5000 Je 5400 Jn 5500 Pw 6200	Kd 170 Je 180 Jn 180 Pw 200	Kd 25.5 Je 41.0 Jn 136.7 Pw 40.5 TOTAL 243.6 MMT	Kd 30.2 Je 45.3 Jn 151.9 Pw 50.3 TOTAL 277.7 MMT
X	Cisco Dome 19S-20S 21E-22E	24 sq mi 13,440 acres 669,000,000 ft^2	Kd TS Je 2822 Jn 3500 Pw NA	Je 400 Jn 300	Je 18 Jn 12	Prod Kd - Jm Je abd Jn non-productive	BLM	75 mi. from Castle Dale. Next to undeveloped coal, rail and freeway access.	Je 1300 Jn 1600	Je 90 Jn 95	Je 37.6 Jn 18.8 TOTAL 56.4 MMT	Je 6.4 Jn 13.7 TOTAL 20.1
X	Gordon Creek 14S 7E-8E	13 sq mi. 68,640 acres 362,000,000 ft^2	Kd 4025 Je 6400 Jn 8400 Pwr 11,150	Kd 50 Je 270 Jn 350 Pwr 500	Kd 6 Je silt & sh 2-4 Jn 16 Pwr 0-4	Kf prod. SWP site	mix	High Plateau 20 mi from Castle Dale. SWP demo site.	Kd 1800 Je 2900 Jn 3800 Pwr 5000	Kd 100 Je 125 Jn 140 Pwr 170	Kd 0.9 Je 1.7 Jn 18.4 Pwr 2.8 TOTAL 23.7 MMT	Kd 0.8 Je 1.7 Jn 18.3 Pwr 3.3 TOTAL 24.1
X	Green River south Little Grand Fault 21S 17E	12 sq mi 63,360 acres 335,000,000 ft^2	Kd-Jn TS Pwr 3000 Mm 10,000	Pwr 260 Mm 400+	Pwr 6-16 Mm 2-6	Non-productive	BLM, military, SITLA	Next to I-70 and rail line 36 mi from Castle Dale; 20 mi from undeveloped coal.	Pwr 1400 Mm 4500	Pwr 90 Mm 160	Pwr 5.4 Mm 4.4 TOTAL 9.8 MMT	Pwr 3.2 Mm 4.8 TOTAL 8.0 MMT
3	Last Chance Anticline 26S 7E	24 sq mi 126,720 acres 669,000,000 ft^2	Kd-Jn TS Pwr 3050 Mm 4600	Pwr 150 Mm 900	Pwr 14 (30 ft) Mm 16	SI gas wells; Moenkopi	BLM, SITLA, part WSA	90 mi south of Castle Dale. Remote location.	Pwr 1400 Mm 2000	Pwr 90 Mm 105	Pwr 2.2 Mm 80.4 TOTAL 82.6 MMT	Pwr 1.3 Mm 80.4 TOTAL 81.7 MMT
4	Peters Point 12S-3S 15E-17E	30 sq mi. 158,400 acres 836,000,000 ft^2	Kd 13,000 Je 13,970 Jn 14,578 Pw 16,088	Kd 30 Je 80 Jn 50 IPw 320 Mm 600	Kd 10 Je 6 Jn 8 Pw 6 Mm 6	Tertiary-Jn. Very active field	BLM - BBC lease.	Remote location 40 mi from Castle Dale.	Kd 5900 Je 6300 Jn 6500 Pw 7200 Mm 7500	Kd 190 Je 200 Jn 200 Pw 220 Mm 230	Kd 2.0 Je 2.9 Jn 2.9 Pw 14.6 Mm 27.3 TOTAL 49.6 MMT	Kd 2.3 Je 3.6 Jn 3.1 Pw 14.6 Mm 27.3 TOTAL 50.9

			Mm 16,615									
X	Summit SRS 19S 11E-12E & all SRS	1300 sq mi. 6,864,000 acres 36,250,000,000 ft^2	Pwr outcrops Mm 4100	Mm 700	Mm 2-10	Non-productive	Location is SITLA. Potential is BLM with lots of WSA	20 mi from Castle Dale. Good access.	Mm 1800	Mm 100	Mm 847.0 TOTAL 847.0 MMT	Mm 716.2 TOTAL 716.2 MMT
2	Woodside Dome 19S 13E-14E	40 sq mi. 126,720 aces 1,115,000,000 ft^2	Kd NA Je - Jn TS Pwr 3000 Mm 6400	Pwr 450 Mm 700	Pwr 6-8 Mm 2-10	SI well BBC	BLM	30 mi from Castle Dale. Good access.	Pwr 1300 Mm 2900	Pwr 95 Mm 120	Pwr 26.1 Mm 27.2 TOTAL 53.3 MMT	Pwr 9.9 Mm 28.0 TOTAL 37.9 MMT

Kd = Dakota Sandstone, Je = Entrada Sandstone, Jn = Navajo Sandstone, IPw = Weber Sandstone, Pwr = White Rim Sandstone, Mm = Madison (Redwall, Leadville, Deseret), Kf = Ferron Sandstone of the Mancos Shale, Jm = Morrison Formation, Tw = Wasatch Formation, WSA = Wilderness Study Area, BLM = Bureau of Land Management, SITLA = School and Institutional Trust Lands Administration, mi = miles, Sq mi = square miles, ft^2 = square feet (calculated from sq miles), psi = pounds per square inch, F = Fahrenheit, NA = not applicable (usually absent), prod = producing, SI = shut in well, BBC = Bill Barrett Corporation, SRS = San Rafael Swell, MMT = million metric tonnes.

Storage estimate chart versus equation. Storage is calculated area * height (thickness)* porosity * density of CO_2 * efficiency (using 0.04). Density of CO_2 can be very difficult to determine. The chart was published in the AAPG Explorer but without a reference. The equation is based on ideal gas law. The big difference comes at lower pressure when near the triple point of gas, liquid, and super critical. The only significant difference in storage capacity using the two methods is at Cisco Dome.

The top two sites were the Bonanza and Woodside locations (Figures 2.1 & 2.2). Bonanza was ranked number 1 because the area is similar to the RMCCS Craig, Colorado test site. Bonanza has all three primary targets, is closest to the Craig test site, and has very similar stratigraphy. The location is next to the Bonanza coal-fired power plant. The Dakota reservoir is gas productive and may have to be eliminated from near-term consideration. There is not a well-defined trap in the Bonanza site but structural and fault traps are present updip (southeast) of the site on the Douglas Creek Arch in Colorado. A stratigraphic trap may exist for both the Dakota and Weber reservoirs within the Bonanza area, but more data is needed. The storage area is potentially much larger than what was evaluated in Table 2.1.

Woodside Dome was ranked number 2. The Dakota Sandstone crops out along the flanks of Woodside Dome and the Entrada Sandstone is too shallow for consideration. But the White Rim Sandstone (Weber equivalent) along with the deeper Redwall Limestone combined, may have sufficient storage capacity. Woodside Dome has easy access, is a well-defined anticline on the surface, and is near newly developed coal. It is close enough that a CO_2 pipeline could be constructed from the power plants in the Castle Valley area to the west.

Last Chance Anticline was ranked number 3. The potential reservoirs are the White Rim Sandstone and the Mississippian Redwall Limestone. Most of the potential storage capacity is in the Redwall which is not one of the primary target reservoirs. The location is very remote but has a well-defined structure.

Peters Point was ranked number 4. Peters Point has numerous potential reservoirs but most of the storage capacity is in the Redwall Limestone. Peters Point is a very active gas field with production from the Navajo, Dakota Sandstone, Mesaverde Group, and Wasatch Formation. The natural gas drilling and production would be a significant impediment to any near-term CO_2 storage.

Cisco Dome was eliminated from consideration due to the water quality (6800 TDS in the Entrada Sandstone determined after the initial rankings). Cisco Dome was initially ranked 1 or 2 by most of the geologists due to excellent reservoir quality, well-defined structure and easy access near undeveloped coal. The temperature and pressure data are near the phase shift from gas to super critical. As a result, Cisco Dome has more than 30 MMT or less than 30 MMT of storage capacity depending on how the CO_2 density is derived.

Gordon Creek was eliminated because (1) the storage capacity was less than 30 MMT and (2) this field had been scheduled to be extensively studied by another project. Green River South was eliminated because the storage capacity was less than 30 MMT. Summit SRS (San Rafael Swell) was eliminated because it lacked any potential in the three target reservoirs. The area has potential in the Redwall but the White Rim Sandstone was dropped from consideration because the formation crops out near the crest of the SRS.

Evaluation of the Bonanza Site

The Bonanza site in eastern Uinta Basin is in T. 8 S. to 10 S., and Range 23 E. to 25 E., Uintah County, Utah (figure 2.2). The Bonanza coal-fired power plant lies within the down dip portion of the site. Several wells have penetrated the Dakota Sandstone in the northwest portion of the site but only one well has penetrated the deeper Entrada and Weber Sandstones. The Bonanza site is a down dip extension of the Hells Hole field (Moretti Jr., and others, 1992). A detailed characterization of the Bonanza is presented in Appendix B. The parameters used to calculate the CO_2 storage capacity are shown in Table 2.2, the calculated storage volumes are shown in Table 2.3.

The preliminary calculation (Table 2.1) used 4% efficiency and resulted in 243.6 to 277.7 MMT total storage capacity. The preliminary calculation included the storage capacity of the Navajo Sandstone which was not evaluated in the final analysis. Subtracting out the storage capacity of the Navajo the preliminary total capacity for the Bonanza site was 106.9 to 125.8 MMT. The final CO_2 storage capacity for the Dakota, Entrada, and Weber reservoirs at the Bonanza Site at 4% efficiency is 232 MMT, significantly more than the preliminary calculation. Additional storage capacity exists in the Castlegate Sandstone of the Cretaceous Mesaverde Group and Jurassic-Triassic Navajo (Nugget) Sandstone. The Dakota Sandstone has the least storage capacity of the reservoirs evaluated. The thin lenticular sandstone beds in the Dakota provide good stratigraphic traps but very little storage capacity. The Entrada Sandstone has the most storage capacity. The Entrada is laterally continuous thick eolian sandstone with good porosity. The lateral continuity of the Entrada means it is less likely to have local stratigraphic traps and needs fault closure or structural closure for a trap. The Weber Sandstone has large storage capacity but with limited well data we used the gross formation thickness as the reservoir thickness. The Weber interfingers with the arkosic red beds of the Maroon Formation in the Bonanza site. As a result, the actual reservoir thickness and therefore storage capacity of the Weber may be much less than what we calculated.

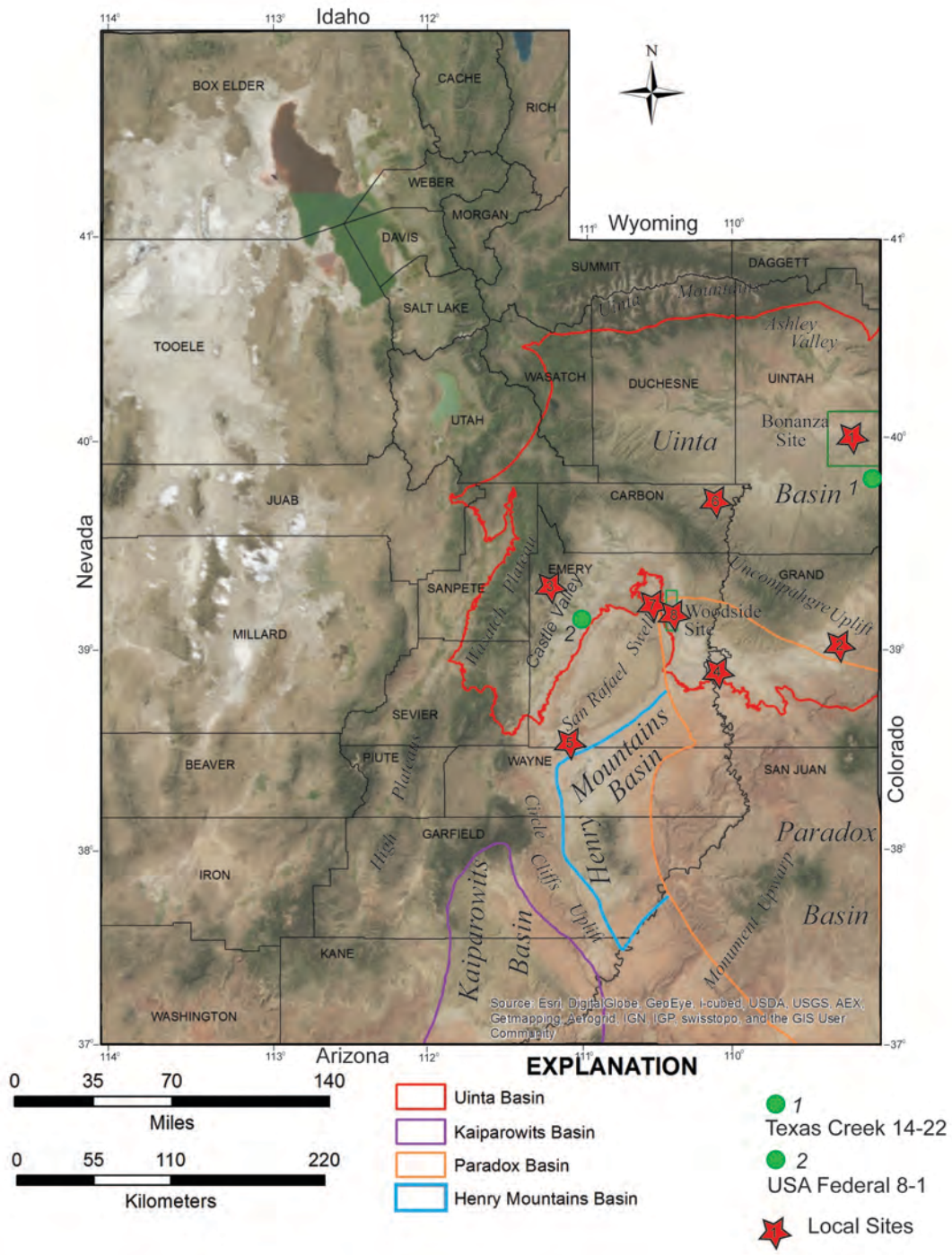


Figure 2.2. Map of Utah showing basins and uplifts of the Colorado Plateau. Local sites eva as potential storage sites (see table 1), 1 = Bonanza, 2 = Cisco Dome, 3 = Gordon Creek, 4 = River South, 5 = Last Chance, 6 = Peters Point, 7 = Summit, and 8 = Woodside. The Bonanz Woodside sites (rectangular outlines) were selected for detail characterization. Wells (green 1 has a Weber Sandstone (?) core and 2 has a White Rim core.

CO_2 storage.

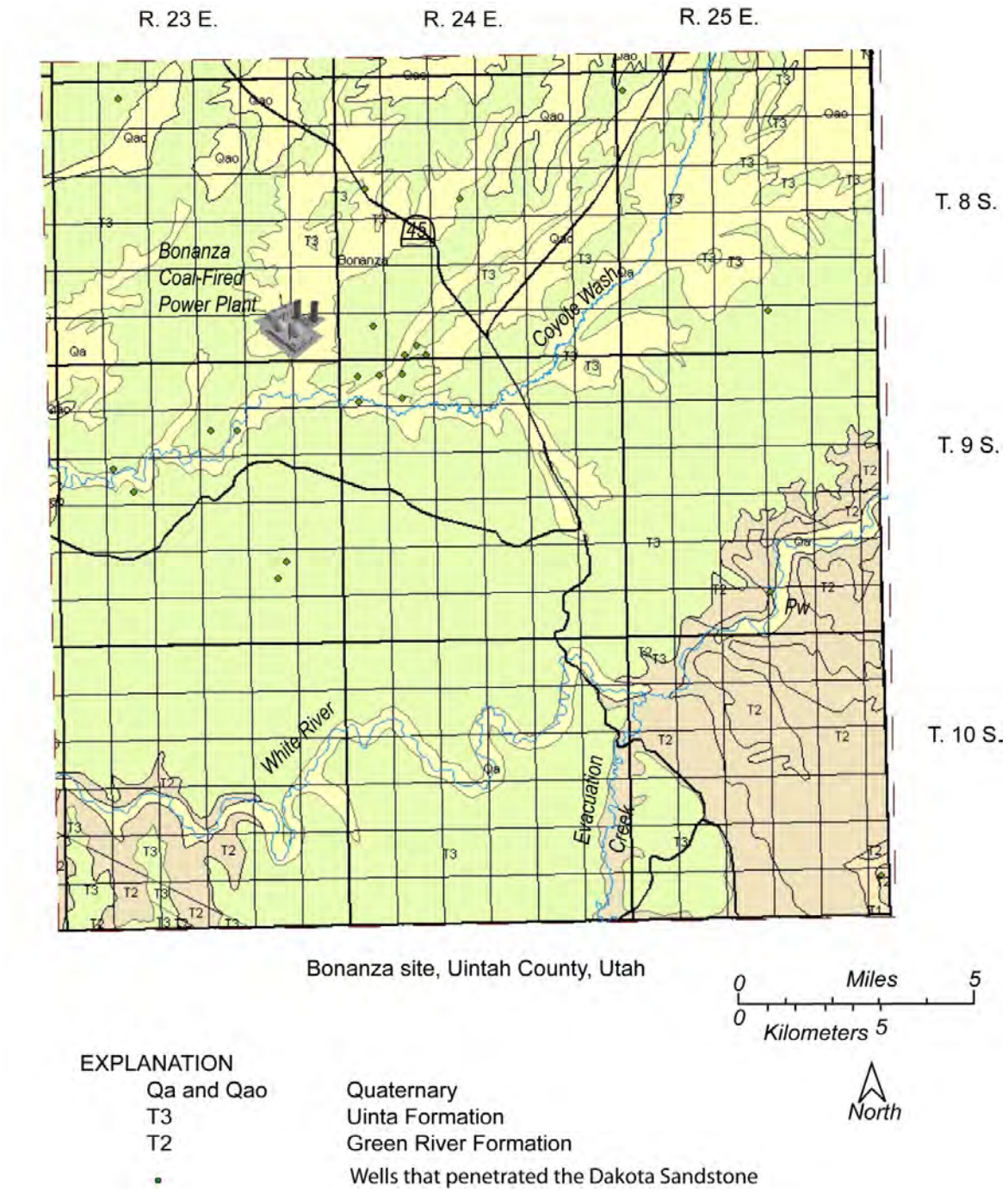


Figure 2.3. Geologic map of the Bonanza site from Hintze and others (2000). Structure contours are on the top of Dakota Sandstone from Roberts (2003); contour interval is 500 feet (150 m), mean sea level datum. Pw shows the location of the one well in the Bonanza site that penetrated the Entrada and Weber Sandstones.

Table 2.2. Parameters used to calculate the CO_2 storage capacity of the Dakota, Entrada, and Weber reservoirs at the Bonanza site. ft = feet, m = meters, km^2 = kilometers squared, F = degrees Fahrenheit, C = degrees Celsius, D = depth, psi = pounds per square inch, and kPal = kiloPascals.

	Area	Average Depth	Average Reservoir Thickness	Average Porosity	Temperature Gradient	Pressure Gradient
Dakota	328 $miles^2$ 850 km^2	12,122 ft 3695 m	20 ft 6 m	12%	55 °F + (0.015*D) 0.03 °C/m	0.45 psi/ft 10.2 kPal/m
Entrada	326 $miles^2$ 845 km^2	13,016 ft 3967 m	94 ft 29 m	16%	55 °F + (0.015*D) 0.03 °C/m	0.45 psi/ft 10.2 kPal/m
Weber	328 $miles^2$ 850 km^2	14,604 ft 4451 m	186 ft 57 m	7%	55 °F + (0.015*D) 0.03 °C/m	0.45 psi/ft 10.2 kPal/m

Table 2.3. CO_2 storage capacity of the Dakota, Entrada, and Weber reservoirs at the Bonanza site using three different efficiency factors.

CO_2 Storage Capacity in Million Metric Tonnes			
	Efficiency Factors		
	0.5%	2.0%	5.4%
Dakota	2.29	8.97	24.21
Entrada	14.22	55.78	150.59
Weber	13.07	51.25	138.38
TOTAL	***29.58***	***116.0***	***313.18***

Evaluation of the Woodside Dome Site

A detailed characterization of the Woodside Dome site is in Appendix C. Woodside Dome is a doubly-plunging anticline on the east flank of the San Rafael Swell (Figure 2.4). The Jurassic Curtis Formation is exposed on the crest of the structure. The Dakota Sandstone has been eroded off of the crest of the anticline and the Entrada Sandstone is too shallow (less than 3000 feet [1000 m]) to be considered for CO_2 storage. The Permian Black Box Dolomite, White Rim Sandstone, and Redwall Limestone contain 12.6 MMT (at 2% E) of CO_2 storage capacity in 13.5 square miles (35 km^2). Structural closure is controlled by a blind reverse fault which oil operators have indicated is visible on seismic, but the amount of displacement and extent of the fault is unknown to us. We evaluated the capacity with a very conservative fault that has minor displacement and minor length. A more extensive fault could greatly increase closure and, as a result, increase the storage capacity at Woodside.

Table 2.4 shows the parameters used to calculate the CO_2 storage capacity at Woodside. Table 2.5 gives the storage capacity for the Redwall Limestone, White Rim Sandstone, and Black Box Dolomite at Woodside using three different efficiency factors. Table 2.6 compares the preliminary parameters and storage capacity, and the final parameters and storage capacity at 4% efficiency, for the Redwall and White Rim. The area is the parameter that has the greatest effect on the difference between the preliminary and final storage calculation for the White Rim reservoir. The area and thickness were both significantly reduced in the final evaluation of the Redwall reservoir.

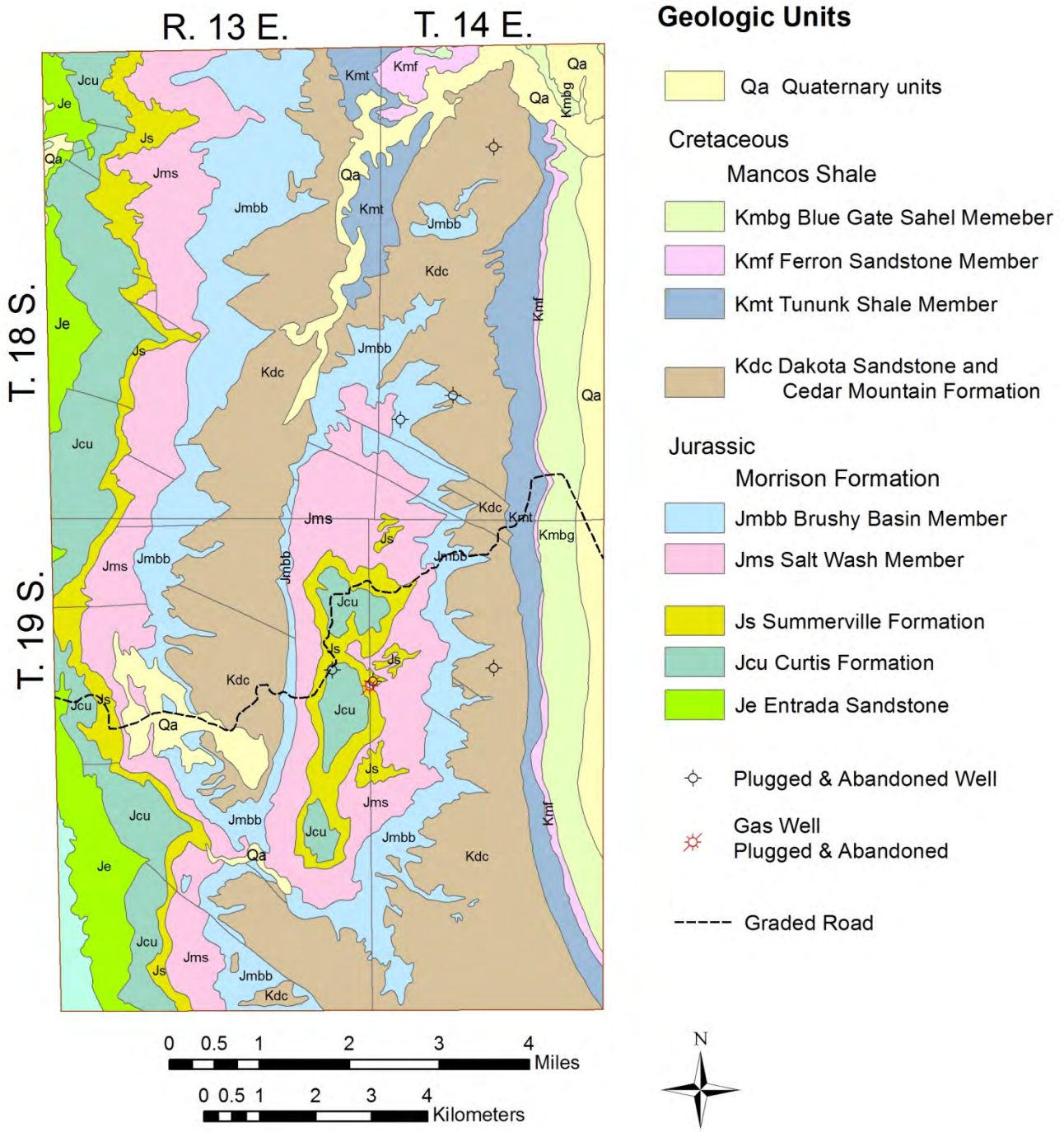


Figure 2.4. Geologic map of the Woodside Dome site from Witkind (2004). The crest of the anticline is the Jurassic Curtis Formation (Jcu), the flank is the Dakota and Cedar Mountain Formations undifferentiated (Kdc). Modified fromWitkind (2004).

The preliminary area was based on the full extent of the anticline mapped on the surface. The final area is based on subsurface cross sections and structure contour mapping of the White Rim Sandstone and Redwall Limestone. Closure at the level of the two reservoirs is controlled by a blind reverse fault. We do not have seismic data over Woodside to accurately determine the displacement and extent of the fault so we took a very conservative approach to mapping the closure. Acquisition of seismic data to map the displacement and extent of the fault could result in greater area of closure and therefore larger storage capacity.

Table 2.4. Parameters used to calculate the CO_2 storage capacity of the Redwall Limestone, White Rim Sandstone, and Black Box Dolomite at Woodside. ft = feet, m = meters, D = depth, km^2 = kilometers squared, F = degrees Fahrenheit, C = degrees Celsius, psi = pounds per square inch, and kPal = kiloPascals.

	Area	Average Depth	Reservoir Thickness	Average Porosity	Temperature	Pressure
Redwall	16.6 $miles^2$ 43 km^2	6749 ft 2058 m	345 ft 105 m	5%	55º F + (0.013*D) 0.03º C/m	0.42 psi/ft 9.5 kPal/m
White Rim	11.9 $miles^2$ 31 km^2	3445 ft 1050 m	420 ft 128 m	15%	55º F + (0.012*D) 0.04º C/m	0.42 psi/ft 9.5 kPal/m
Black Box	13.5 $miles^2$ 35 km^2	3422 ft 1043 m	75 ft 23 m	16%	55º F + (0.012*D) 0.04º C/m	0.42 psi/ft 9.5 kPal/m

Table 2.5. CO_2 storage capacity of the Redwall, White Rim, and Black Box reservoirs at the Woodside Site using three different efficiency factors.

CO_2 Storage Capacity			
	Efficiency Factors		
	0.5%	2.0%	5.4%
Redwall	0.8	3.2	8.8
White Rim	2.0	7.9	21.4
Black Box	0.4	1.5	4.1
Total	***3.2***	***12.6***	***34.3***

Table 2.6. Comparison of the preliminary parameters (from table 1) and final (in parenthesis) parameters and resulting storage capacity calculations at an efficiency factor of 5.4%. Black Box Dolomite was not evaluated in the preliminary calculations.

	Area ($miles^2$)	Thickness (feet)	Porosity (%)	Temperature (ºF)	Pressure (psi)	Capacity (MMT) 4%
Redwall	40 (16.6)	700 (345)	0.04 (0.05)	120 (141)	2900 (2835)	27.2-28 (6.5)
White Rim	40 (11.9)	450 (420)	0.07 (0.15)	95 (98)	1300 (1447)	9.9-26.1 (15.9)
Total						37.1-54.1 (22.4)

NEW MEXICO

The search for reservoirs with appropriate properties for sequestration, including

- accompanying tight seals that occur between 3,000 and 13,000 feet
- total dissolved solids of greater than 10,000 μg/l and
- apparent capacity in excess of 500K barrels of oil equivalent (BOEs)

is straightforward in New Mexico because of its long history of oil and gas production in the San Juan Basin (Figure 2.5). The tremendous size of many of the fields in this basin is sufficient to render them prospective sequestration targets. In addition, many deep saline aquifers also provide additional sequestration opportunities. Several large power plants in the area could take advantage of the many identified sequestration reservoirs.

Within the San Juan Basin, several horizons were selected as possible sequestration targets: the Dakota Group, Entrada Formation, Hermosa Group (equivalent to the Weber) and the Leadville Limestone. They are locally thick, porous and deep enough to be possible CO_2 sequestration targets. Associated seals for each of the units are in place in all areas, but ultimately, the thick sequence of shales and siltstones of the Mancos Shale is an excellent upper seal for all the units in the basin.

Within the San Juan Basin area, primary CO_2 point emissions were identified. These include the San Juan Generating Plant, Four Corners Generating Plant, Escalante Generating Plant, San Juan Gas Plant, Lybrook Gas Plant and the Giant Refinery. Of these sites, the San Juan and Four Corners Generating Plants were considered the most likely candidates for a CO_2 sequestration project because the units of interest were deep enough and thick enough to meet all of the criteria for injection.

For the primary RMCCS local site analysis, the main issues that ruled out a New Mexico site early in the selection process included:

- The lack of a partner (a source of CO_2) willing to work with the group. Both Tri-State Energy in New Mexico and PNM Resources, the operators of the two selected power plants, were contacted and declined involvement.
- The San Juan Basin is an area with complex land ownership issues. The area is a patchwork of private, state and federal lands that included both public and Indian lands. The nature of the permits and ownership issues would have made a site selection a long and uncertain affair.

These issues are not insurmountable for possible future projects, but far more upfront time will be required for site selection and permitting in the San Juan Basin than the selected Craig Well site. In most areas of the San Juan basin, agreements would probably require Federal, Tribal, State and private landholders involvement in the site selection process.

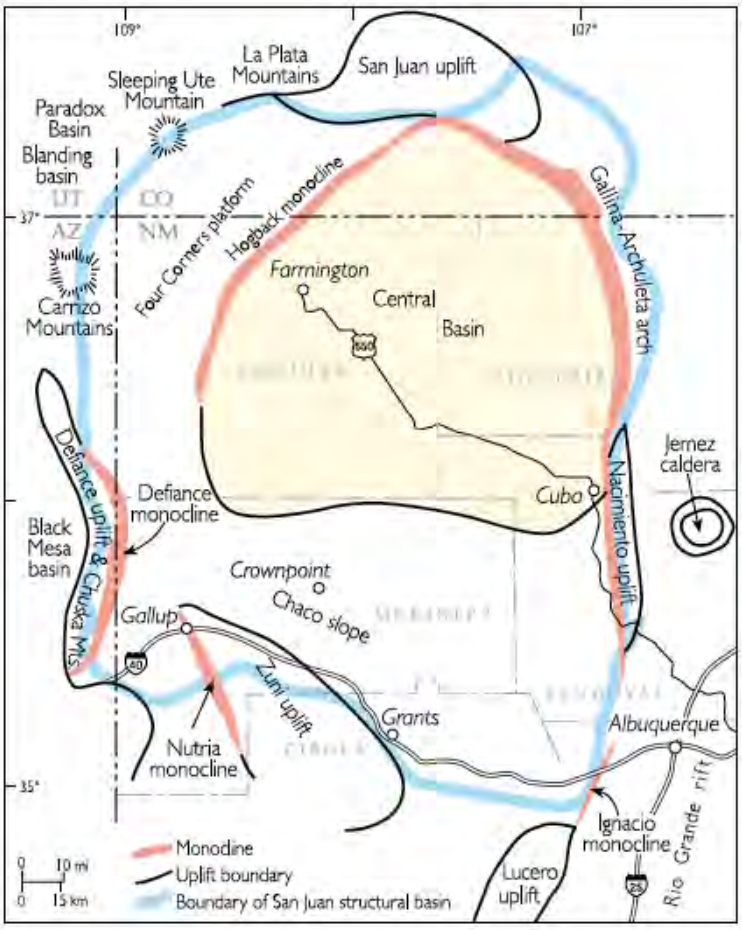


Figure 2.5: The San Juan Basin of Colorado and New Mexico which was evaluated by the Colorado Geological Survey and the New Mexico Bureau of Geology and Mineral Resources.

ARIZONA

Northeastern Arizona encompasses the southwestern part of the Colorado Plateau (Figure 2.6), an area of gently dipping to slightly tilted Paleozoic and Mesozoic strata that includes porous and permeable sandstone units. The Lower Permian Cedar Mesa Sandstone was identified for study as a potential target for CO_2 sequestration. The Cedar Mesa Sandstone is overlain by the impermeable Organ Rock Formation, which forms a seal. The salinity of groundwater in the Cedar Mesa Sandstone is unknown, and must be determined before CO_2 can be sequestered. Well logs for 755 drill holes were used to evaluate the extent, depth, and thickness of subsurface formations. The ESRI® ArcMap™ GIS software was then used to calculate the volume of the Cedar Mesa Sandstone in all areas where the top of the unit is below 3000 feet (915 meters) depth. Well logs were used to evaluate porosity, which were then used to calculate the amount of pore space at least theoretically available for CO_2 storage (the effective porosity). The Arizona Geological Survey calculates between 30 km^3 and 80 km^3 of pore space in the Cedar Mesa Sandstone. The net fraction of pore-space accessible to CO_2 injection is estimated to be approximately 0.5% to 5%. For context, application of this storage efficiency to the Cedar Mesa Sandstone indicates that 0.15 km^3 to 4.3 km^3 of pore space is accessible to injected CO_2, and that 0.114 to 3.24 billion tons of CO_2 could be sequestered in this pore space at a density of approximately 750 kg/m^3.

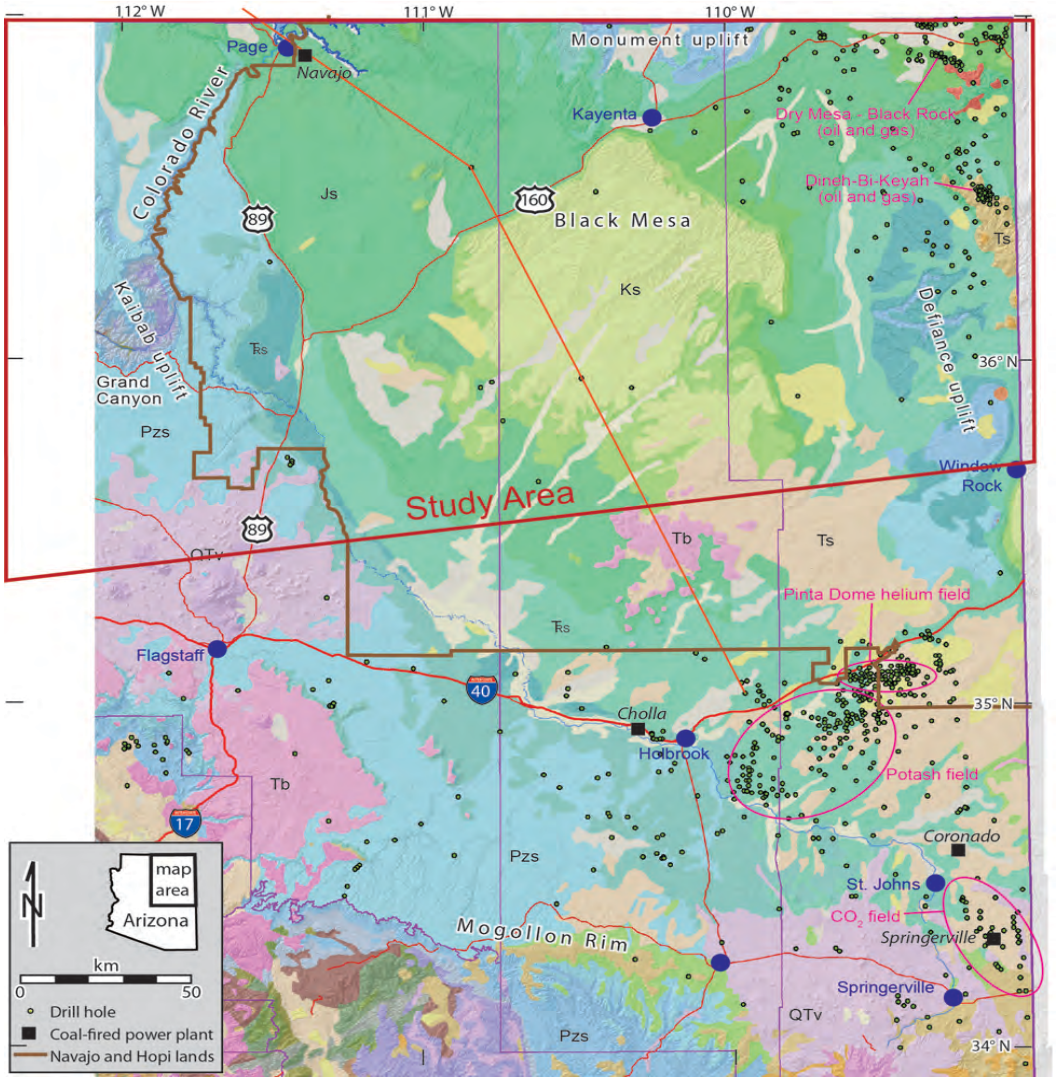


Figure 2.6: Area of northeastern Arizona where the Arizona Geological Survey studied the Cedar Mesa sandstone for its sequestration potential.

3. Public engagement: outreach, planning and permitting

The Rocky Mountain Carbon Capture and Sequestration (RMCCS) project team identified public engagement as an essential and necessary component of the projects' success. The process of public engagement involved contact and outreach to a broad spectrum of organizations and individuals at the local and regional level. Landowners, mineral rights owners, industry, state and local government/regulatory agencies, private citizens and the print/radio/television news media were all a part of the public engagement process. Each of the contacts was purposeful and necessary to inform members of the public about the project activity, promote an understanding of the technology, address fears and concerns, secure permissions and access, obtain permits, seek funding and in-kind contributions and to generate good will toward the research, development and potential future subsurface storage of carbon dioxide. Many of the public engagement efforts were required steps in the process. As a result, many of the RMCCS team members were involved in the public engagement process.

PLANNING

The Colorado Geological Survey (CGS) took the lead in the overall planning efforts for the project. There were several key stakeholders that needed to be contacted and many of these were in the project area or located in the State. Working with the RMCCS project team, CGS developed presentation materials (Appendix D) that were used to communicate information about carbon sequestration in northwest Colorado and the proposed Craig Geologic Characterization project to key stakeholders ((see Appendix E for some details about stakeholders and associated information). CGS made presentations to the Colorado State Land Board, the State of Colorado's Carbon Sequestration Task Force, the Tri-State Generation and Transmission Association Board of Directors (Tri-State), the Trapper Mine Board of Directors, to locally elected officials from the Town of Craig and to County Commissioners from Moffatt and Routt Counties. The State Land Board holds title to some of the surface rights and most of the mineral rights upon which the project was located. The geologic characterization well and the seismic surveys to be conducted for the project were all located on the Trapper Mine property. Tri-State operates the Craig generating station located adjacent to the Trapper Mine and uses all of the coal it produces. The Town of Craig is located just a few miles from the Trapper Mine, Craig Station and the RMCCS project. The Trapper Mine representatives were very helpful and accommodating in the completion of the seismic surveys and in the drilling of the characterization well. Presentations made to local elected officials also provided a forum for presenting information to members of the public about the project. Early contact with the public was an important aspect of the project that helped to develop a greater understanding of carbon storage in deep saline formations and build a foundation for good relationships. CGS also made presentations to the State Geologists of Utah, Arizona, and New Mexico to explain the DOE project and how the information to be collected would be useful. In many cases, the planning efforts were a useful preliminary step to satisfying requirements from landowners, mineral right owners and various state and local agencies, to conduct many of the activities required by the RMCCS project.

PERMITTING

It is required by state and local regulators to obtain permission from landowners, mineral right owners and various state and local agencies, to conduct many of the activities required by the RMCCS project. Specific requirements vary greatly from state to state and county to county, time of year and the nature of the work being done. It is strongly recommended that project leaders identify sub-contractors familiar with the permitting requirements in the specific area for any future projects. This pertains to gaining access to the drill site within the Trapper Mine, conducting of the surface seismic survey and the drilling of the RMCCS State No. 1 site characterization well. The objective of drilling the characterization well was to obtain valuable data from the subsurface and was classified as a "Stratigraphic Test". Since there would be no production or injection with the well, the permitting process was straight forward and relatively fast. In the project, no individual permit took longer than 60 days from the time of submission to approval. Obtaining approvals for permits to drill wells for the purpose of CO_2 injection take considerably longer. Even in projects where the ultimate purpose for a well is for injection it may be more expedient to initially permit the well as a stratigraphic test well, allowing drilling to proceed while the injection permits are being processed separately.

For the RMCCS project, permitting involved three different components. The first was obtaining permission from the Trapper Mine for access to the site that would be used for drilling the well. Selecting a well site within the boundaries of an operating surface mine added additional

considerations in the permitting process. After significant work with the mine, the drill pad was located in a previously mined, inactive area, not yet reclaimed reducing reclamation expenses and mitigating much of the environmental risk associated with well drilling. The access permit obtained from the Trapper Mine specified the liability for any financial damages due to the drilling process onto the RMCCS project, documented insurance requirements for Schlumberger as the owner of the well and all major sub-contractors to Schlumberger, and specified time limits for access to and from the well site under the agreement. The access agreement required approval by the Trapper Mine General Manager and also the mine insurance provider. For the RMCCS project there were two separate agreements, one for permission to conduct the seismic survey and the second agreement for well drilling. The process to obtain the permits took approximately six weeks from initial discussions to final approval for each agreement. A similar type of agreement will be typical when requiring access to any commercial industrial property.

The second permitting component involves obtaining permits from surface owners and mineral right owners to conduct a project surface seismic survey. A seismic survey was conducted to obtain detailed imaging of the subsurface using reflection of acoustic energy from rock layers deep below the surface. The permits included permission to access the property, a pre-negotiated damage fee and terms for compensation if additional damage occurs. For mineral right owners, the permits were to allow data to be acquired and specified who would be allowed to receive the data and what data, if any, would be given to the mineral rights owner. The permitting for the seismic survey was conducted by St. Croix Environmental, an organization specializing in seismic permitting. Maps and data used as a basis for developing the seismic permit applications are provided in Appendix F.

The third, and most extensive, permitting component was for the drilling of the RMCCS State No. 1 characterization well. Although the permit requirements to drill a stratigraphic test well are the least complex to obtain, the number of permits and number of entities that need to be contacted is large. The primary agency regulating well drilling for the RMCCS project is the Colorado Oil and Gas Conservation Commission (COGCC). The land on which the well was drilled is owned by the State of Colorado and an exploration permit is required by the State Board of Land Commissioners. Additionally, Colorado's Department of Natural Resources - Division of Parks & Wildlife, Colorado's Department of Public Health & Environment and the federal Department of Labor's Mining Safety and Health Administration also has jurisdiction over various aspects of the operation. In order to assure all applicable requirements and jurisdictions were identified and fulfilled, Northwest Corporation, based in Grand Junction, Colorado, was employed as the project permitting agent. A forty-eight point compliance plan was developed to summarize all forms, notices and other requirements detailed. The primary permitting requirement for well drilling is the Application for Permit-to-Drill (APD). Prior to submitting the APD the drill pad site had to be surveyed and a layout of the site construction prepared. Detail information on the drilling rig, drilling fluid system, drilling plan and well completion plan was required to be developed and submitted with the application.

Once the engineering plan for the well drilling was complete, the drilling rig selected and the exact site located, a series of forms were required to be completed and submitted to the Colorado Oil and Gas Conservation Commission for approval. The forms included: Form 1 – Operator Application, Form 2 – Application for Permit-to-Drill, Form 2A – Oil and Gas Location Assessment, Form 3 – Performance Bond, Form 4 – Sundry Notice and Form 15 – Earthen Pit Permit. In addition to COGCC requirements, the project was required to obtain a waiver of wildlife stipulations from the Colorado Division of Parks & Wildlife which restricts drilling during winter months in certain areas in Moffat County. A mitigation plan was agreed upon to limit impact on elk common in the area by the well drilling. A Storm Water/Erosion Control Plan was submitted and approved by the Colorado

Department of Public Health & Environment. The COGCC requested acknowledgement of drilling fluid containment, spill/release mitigation plans, and drill cuttings low moisture content requirements. Approval to drill was granted on October 27, 2011. Basic summaries of the drilling plan and an associated safety program was also provided, and a copy of these brief details is included as Appendix G. A "letter of intent" to drill was sent to each land owner and to Moffat County after the COGCC approval was received. During the drilling operations a weekly storm water inspection was performed and sundry notices of key drilling operations were required to be provided to the COGCC. Typically the Occupational Health and Safety Administration would have exercised jurisdiction over all field activities in regards to health and safety, however since the project site was located within the boundaries of the Trapper Mine, the Mining Safety and Health Administration (MSHA) exercised jurisdiction over the project. The special requirements for complying with MSHA regulations are extensive and are explained in the drilling section of this report.

Once the well was drilled and cored, and geophysical well logs were obtained, additional COGCC forms were required to be completed and submitted for plugging the well, restoring the drill pad and well abandonment. Form 6 – the Well Abandonment form was submitted and approved. In addition to the submission of COGCC Form 6, the RMCCS project was required to submit a letter from the Director of the Board of Land Commissioners, Craig Region, stating that the restoration of the site met the approval of the land board. Although the well has been abandoned in accordance with all state requirements, the well abandonment was engineered in such a way that it could be re-entered and put back into service with minimal cost.

PUBLIC OUTREACH

Upon receiving the RMCCS award from the DOE, the University of Utah began efforts to develop a web presence for the project. The first RMCCS project website for public use was developed by a University of Utah web development team and was housed on University of Utah servers. The rmccs.org website went "live" in late 2010. In May 2011 the rmccs.org web site (screenshot in Figure W1) was transferred to another University of Utah server (Apache), file system and RAID array purchased using RMCCS funds. The RMCCS website was built using standard HTML language with a flat (non-database) file system.

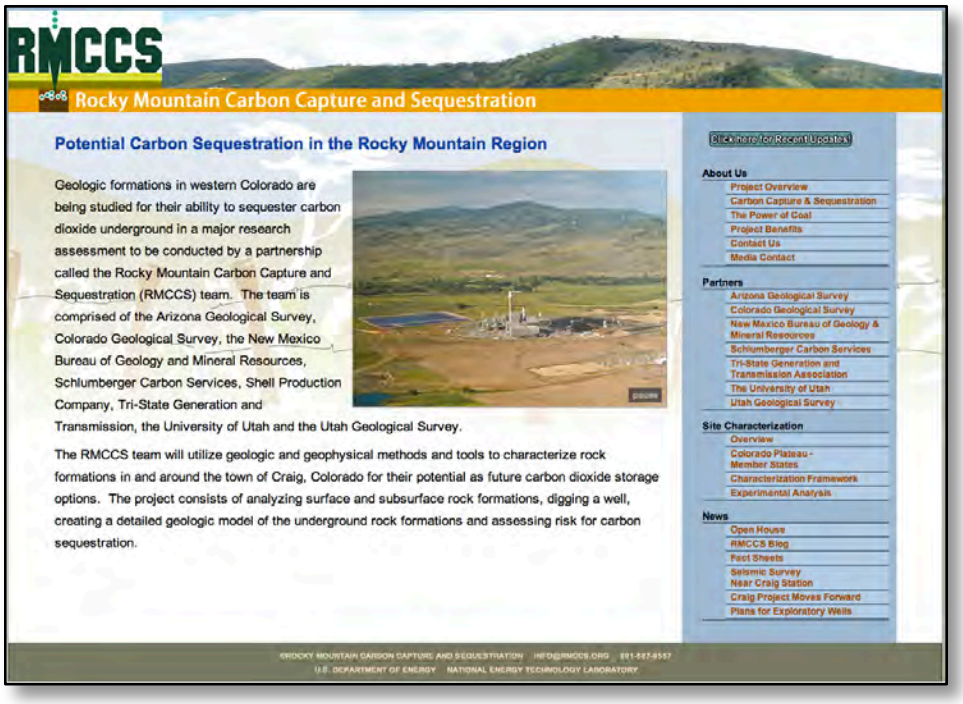


Figure 3.1. Screenshot of RMCCS.org website.

The initial RMCCS website introduced visitors to the concepts of CO_2 sequestration, the goals of the RMCCS project, and some economic background of northwest Colorado, including the benefits of coal mining and coal-fired electric power generation. As the project moved forward with surface field mapping, seismic surveys, well drilling, core analysis and modeling, the website was updated by University of Utah staff, with input from RMCCS project partners. An "Update" link provided visitors with an up-to-the-minute status report of the well drilling progress and a "News" link provided information about open house events and press releases developed through the communications plan and other significant project developments. Significant website updates and changes were stored on secure, password protected subdomains (e.g. http://testing.rmccs.org) and passed along to the NETL/DOE for approval before being moved to the public site.

The RMCCS project also maintained an internal website, called "Unite". Unite is a collaboration system used to assist multi-user groups and projects in their research efforts and goals. Unite for RMCCS (accessible from the main RMCCS website to authorized users) was intended to house all documents and data for the project, and to be a communication tool to discuss project tasks and deliverables. The RMCCS Unite site was prepared and presented to the RMCCS project team in September 2011, however, the project team never fully utilized the Unite system. Project team members eventually reverted to traditional means of communication and data-sharing, such as email and 3rd party file-sharing services.

Later in the project, the flat file/HTML system for the RMCCS website proved to be limiting for many of the project needs, especially for data-sharing and data-management (e.g. the dissemination of project core analysis results to the public). The RMCCS partners also wanted to better understand the organizations expressing the most interest in the data gathered by the RMCCS project to allow future site characterization and CCS/CCUS projects to more effectively reach stakeholders. To address these needs, the rmccs.org website was shifted to a dynamic, database-

driven system (WordPress) in the summer of 2013. The updated site can be seen at http://testing.rmccs.org/wordpress352/. The new site maintains the overall look and feel of the original site, but benefits from an authentication system, where logged in users can create/edit pages, view pages and download analytical data, depending on predetermined permission levels. The public is able to register for access to all RMCCS data. The University of Utah, the RMCCS project, its partners and/or the NETL/DOE will not sell or otherwise provide the registration information (email address and organization) to any 3rd party.

The rmccs.org site served a total of 2,446 unique visitors, with over 15,000 page hits during the life of the project. Most site visitors were from Colorado and other locations in the United States.

The RMCCS project team also developed a comprehensive communications plan that worked in partnership with the website to define and prioritize the stakeholder groups impacted by the project, finalize necessary messages, materials and communication channels, prepare public relations efforts, and determine long-term campaign strategies, issues, milestones and initiatives. The outreach strategy included an on-site open house at the Trapper Mine and a viewing of core samples at Triple-O-Slabbing in Denver. Two press releases were submitted to media outlets to promote these events.

The written communications plan for RMCCS identified the project partners, state, county and city government stakeholders and external influencers such as the media and special interest groups. A specific list of these key audiences and stakeholders are located in the communications plan in Appendix E. The plan defined the strategy and planning of communications for the project, outlined materials to be developed in the communication efforts, media relations protocol, community outreach including open houses at the project site and at the slabbing office, and programs, tools and tactics the RMCCS used for outreach efforts.

The first open house was held at the Trapper Mine in Craig, Colorado on January 24, 2012 from 4:00 pm to 7:00 pm. The open house was promoted to the Craig community through newspaper ads in the Craig Daily Press and postcards mailed to stakeholders identified in the communications plan. The newspaper advertisements and postcard can be found in Appendix E. At the open house meeting, informational boards on the project were located throughout the conference room and team members were on hand to answer questions about the project. The informational boards (Appendix E) covered a general project overview, an overview of the project partners, information on carbon capture and sequestration, seismic testing, how a well for this type of project is drilled, safety of storing carbon underground and an update on the current drilling project at Trapper Mine. A tour of the drilling rig was offered at 3:00 pm just prior to the start of the open house meeting. Members of the public interested in the tour were taken by shuttle bus to the rig site where they were provided an overview of the drilling rig and progress on the overall project of drilling the well. A total of 21 people attended the open house, including two local county commissioners and a representative from US Senator Udall's office.

The second public event was an opportunity to view the core that was taken from the well drilled at the Trapper Mine and was held at Triple-O-Slabbing on August 16th, 2012 from 1:00pm to 2:00pm. Members of the press were invited to view core samples via a broadly distributed press release (Appendix E) and through personal invitations. Several members of the project team were present for the core viewing and were available to discuss the potential for long-term carbon storage sites with the media. RMCCS received 33 media hits from this event, totaling 7,704,687 unique visitors. A detailed press report on coverage of this event can be found in Appendix E. A total of four radio stories were aired as part of the media coverage. Barbara Walz of Tri-State gave an interview to Colorado Public Radio that subsequently air on the local radio station in Denver. KOA radio also

attended the event and conducted interviews with Sarah Carlisle of Tri-State and Vince Matthews of the Colorado Geologic Survey that subsequently aired on the local radio station. Transcripts of radio interviews can be found here.

CONCLUSION

Effective communication and public outreach were critical to the success of the RMCCS project. Investing the time necessary to understand the requirements and establish good relationships with federal, state and local government agencies as well as members of the media and individual citizens made challenging issues more manageable. Access and permitting activities were required in all phases of the field activity from planning and execution through completion and abandonment. Project implementation required obtaining permits and complying with numerous terms and conditions that vary greatly from state to state depending on the specifics of the operation. For this reason it is highly recommended to engage sub-contractors that are experienced in permitting for the specific requirements of each project. Compliance with permit terms and access requirements was also an important component to successful project completion and for being a responsible community partner. Communication with the local and regional community provided education and acceptance for the viability of long term carbon storage in deep saline formations. Outreach efforts included providing internet access to general background information about CCS and the project specific data as well as locally hosted public events and television/radio/print media contacts. The outreach efforts successfully educated the public about the project, its perceived issues and promoted the use of long term carbon storage as a safe and effective strategy.

4. Geologic and geophysical studies at local characterization site

The Sand Wash Basin is a basin within the CSA in northwestern Colorado that was selected as the focus of this study. It contains the Craig Power Station and the location of the stratigraphic test well (RMCCS State #1) that was drilled as part of this study; it was the area of the most detailed mapping.

Two key objectives of the RMCCS partnership are to:

1. Characterize in detail the saline aquifers and their seals in the vicinity of a stratigraphic test well that was to be drilled as part of this project. The well was drilled in February and March, 2012, in the SW SE of Section 34, Township 6 North, Range 91 West, six miles south of Craig, Colorado and was named the RMCCS State #1.
2. Expand that characterization to the entire Colorado Plateau incorporating the data acquired from the drilling of the stratigraphic test.

To achieve these objectives, the CSA was examined at three scales (Figure 4.1):

1. At the local scale, a very detailed examination has been made of the geology within a single Laramide-age structure called the Yampa Block surrounding the site of the RMCCS State #1 stratigraphic test well.
2. At the basin level, the structural framework for a detailed three-dimensional geocellular model was created that covered the Sand Wash Basin and a portion of the adjacent Piceance Basin in northwestern Colorado.
3. At the regional level, the top and base of each of the saline aquifers were mapped within the Colorado portion of the Colorado Plateau.

To achieve the primary objective of characterizing the targeted saline aquifers and their seals, a three- dimensional geocellular model was created that covered the Sand Wash Basin study area (Figure 4.1). This will be used for simulating carbon dioxide injection into the RMCCS State #1

stratigraphic test well, which is to the south of the Craig Power Station. Characterization of the reservoir quality of the saline aquifers in the Sand Wash Basin was made by examining cores and cuttings; researching published porosity and permeability values for oil and gas fields within the basin; crossplotting porosity and permeability data from core analyses from existing wells; and mapping net sand, porosity and pore volumes from digital geophysical logs.

To achieve the secondary objective of expanding the characterization to the Colorado Plateau, maps were made depicting the structural tops and bases of the three saline aquifers and their equivalent formations, as well as the Mancos seal; these covered the CSA. Near the end of the project digital logs were obtained and were used to identify more accurately net sand, average porosity and pore volumes; maps of these parameters were constructed for the CSA.

Because the majority of this report was prepared prior to the simulation of CO_2 injection, analyses of geologic and structural controls on fluid flow are minimal.

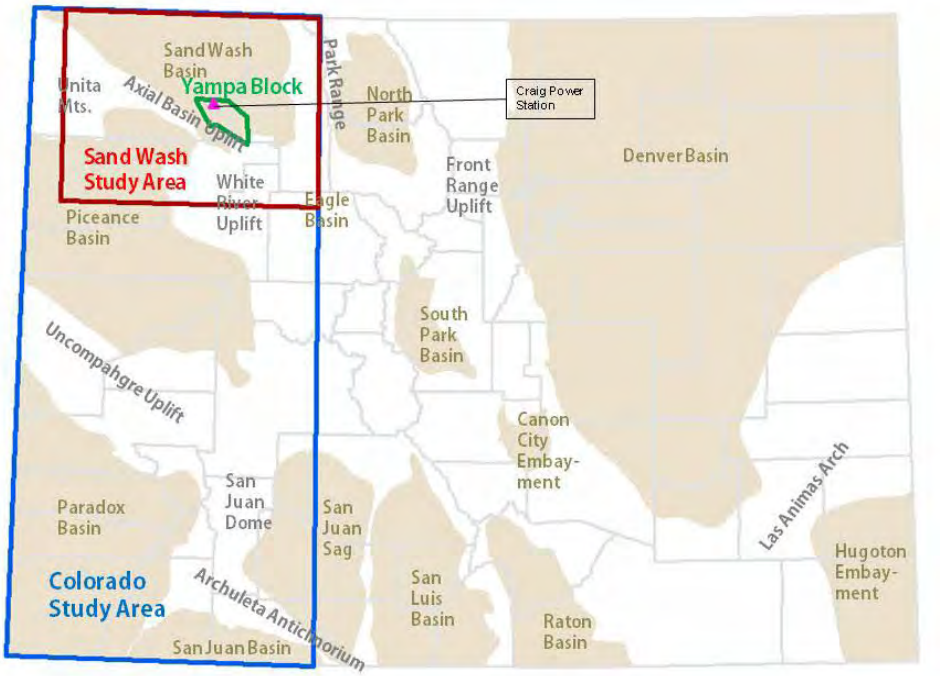


Figure 4.1. Extent of Colorado study areas including Yampa Block (green) and Sand Wash Basin (red).

Mapping of Structural Surfaces

Data

A goal of this project was to incorporate all existing publicly available data into maps depicting the structural configuration of the saline aquifers and their seals. The data utilized in this mapping included:

- Records from over 30,000 oil and gas wells. These were obtained primarily from the IHS commercial database for the Rocky Mountain region. This database was augmented by data from the Colorado Oil and Gas Conservation Commission's website. The locations of these wells are shown in Figure 4.2A.
- Raster images of geophysical logs from over 18,000 oil and gas wells in the CSA. These

were purchased from MJ Systems, a company that scans and archives raster logs. Geophysical logs record the physical properties of the rocks and fluids that surrounding the wellbore and were used to determine the depths of the saline aquifers and other formations in the subsurface. They were also used to estimate porosity and net sand in the saline aquifer. Locations of wells with raster geophysical logs are shown in Figure 4.2B.

- One thousand surface measurements of bedding strikes and dips. Nearly 1500 measurements were collected by a team of geologists from the Colorado Geological Survey covering an area of approximately 800 square miles, predominantly in the region of the Yampa Block. 470 of these measurements were deemed less reliable and were not used. Approximately one thousand strike and dip measurements were used to modify hand contours depicting the structural configuration of the Dakota Formation in the subsurface. Figure 4.3 shows the locations of the strike and dip measurements used in this project.
- Approximately 70 miles of existing two-dimensional seismic data in 11 lines. These were purchased through Seismic Exchange, Inc. to help define the structures in the southern part of the Yampa Block, which is updip from the stratigraphic test well, the direction that sequestered CO_2 is expected to migrate. The locations of these lines are shown in Figure 4.4.
- Approximately eight miles of two-dimensional seismic data in two lines were shot by Western Geco, a Schlumberger Company. These cross the stratigraphic test well location and were shot to define the subsurface structure in the immediate area of the test well. The locations of these lines are shown in Figure 4.4. For work on this portion of the project, these newly acquired lines were used qualitatively to manipulate the shape of the Dakota surface. The precise depth of the Dakota horizon was not picked from the seismic lines because existing maps of the structural configuration of the shallow Twenty-Mile Sand and the Trout Creek Sand, as well as surface strike and dip measurements, conflicted with the information in the deeper seismic horizons. More work can and should be done with these seismic lines assuming processing and calibration are robust.
- Published geologic maps that depict the rocks and structures at the surface. These include:
    - Outcrop patterns from surface geologic maps, including Tweto (1977).
    - Locations of fold axes from surface geologic maps, including Tweto (1977).
    - Elevations of surface contacts between the Dakota and the overlying Mowry Shale depicted on digital elevation models.
- Geologic publications that contain subsurface maps, cross sections, and/or rock characteristics and properties. Sources of formation tops, including published geologic maps, are listed in Appendix F.
- Data collected from the drilling of the stratigraphic test well RMCCS State #1, including:
    - Geophysical well logs that help determine rock and fluid properties of the penetrated strata.
    - Full-diameter cores and sidewall cores from which direct measurements of rock properties of the saline aquifers and their seals can be obtained.

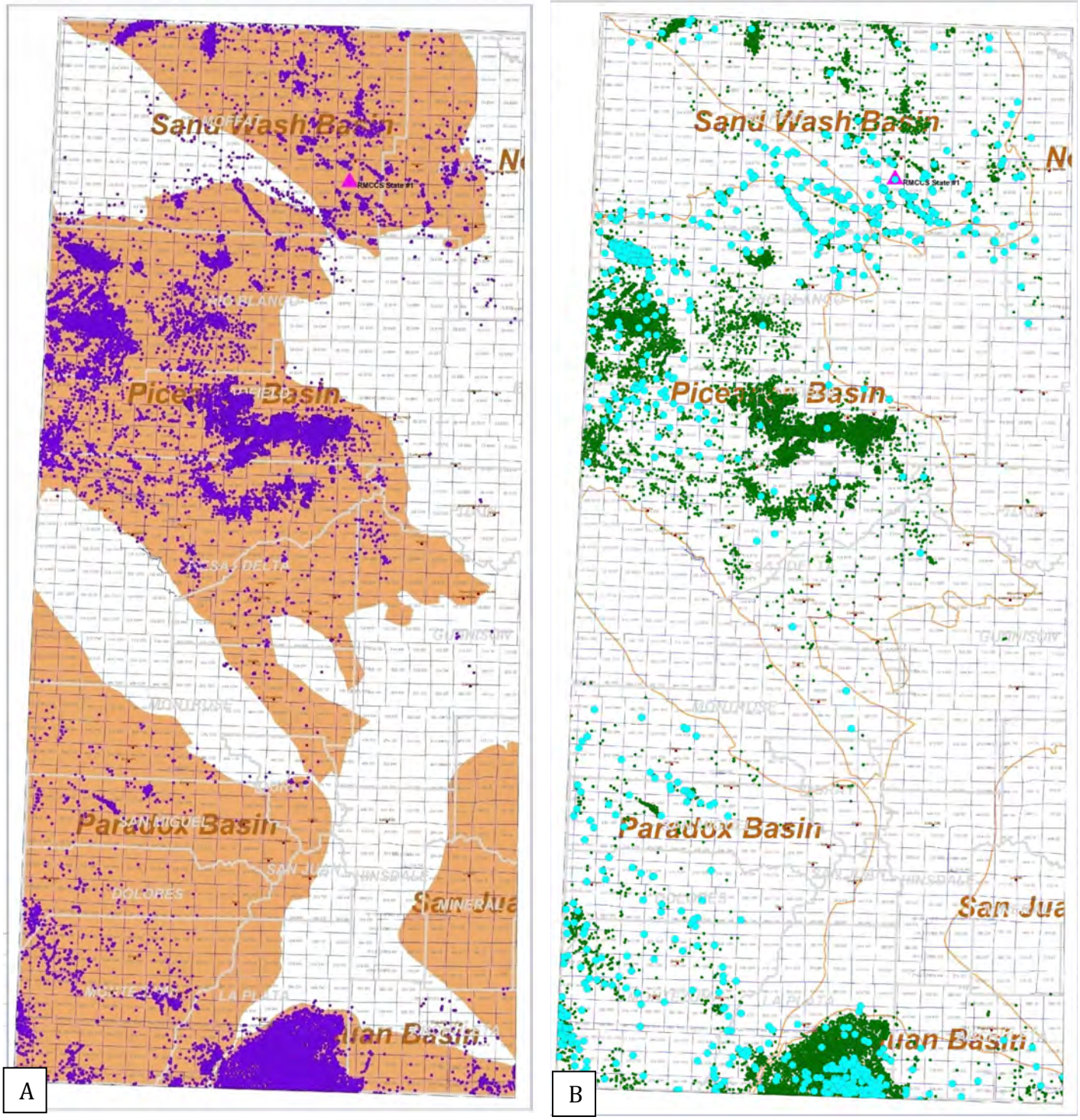


Figure 4.2: A.) Location of wells in the Colorado Study Area. B.) Location of wells in the Colorado Study Area with raster images(dark green, smaller dots) and digital logs (larger turquoise dots).

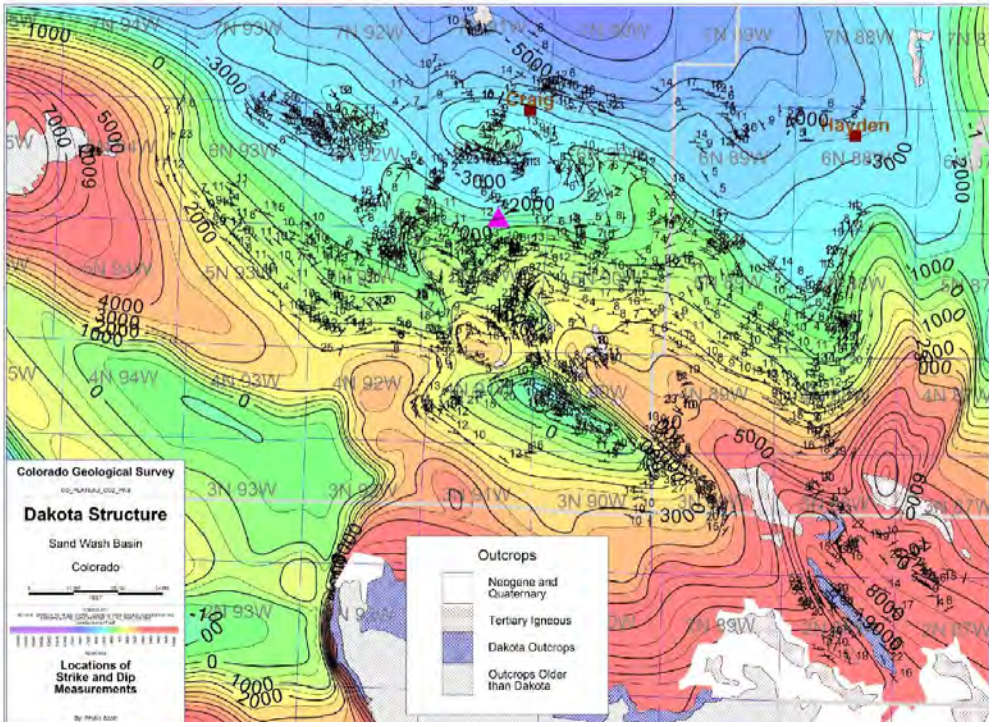


Figure 4.3: Location of surface strike and dip measurements made by the Colorado Geological Survey superposed on structure map on top of the Dakota sandstone.

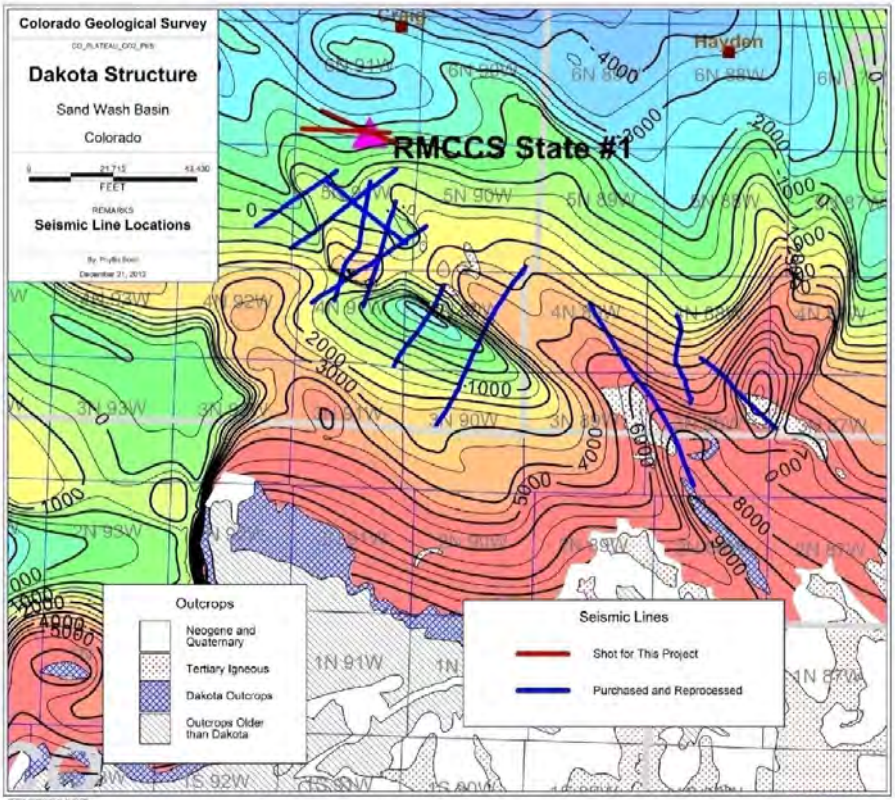


Figure 4.4: Location of seismic lines purchased or shot for the study superposed on top of Dakota structure map.

Extent of Maps of Structural Surfaces

The sequestration potential of the saline aquifers in Colorado has been examined at three scales as was shown in Figure 4.1:

1. Yampa Block: a very detailed analysis of the geology of the Laramide-age Yampa Block south of the town of Craig, Colorado. All of the data types listed above were used in this detailed study component. This block covers approximately 230 square miles and generally dips about 10 degrees to the north. It is bounded on all sides by forced folds.
2. Sand Wash Study Area: a detailed characterization of the three saline aquifers within a 40-mile radius of Craig. This study component augments the Yampa Block mapping with IHS data for oil and gas wells in the expanded area. Also utilized were additional geophysical logs, surface geologic maps and other published data. This characterization included most of the Sand Wash Basin and the adjacent Axial Basin Uplift that separates the Sand Wash and Piceance basins. The final products from this characterization were structure maps of fourteen formation top surfaces that were used for building a geocellular model.
3. Colorado Study Area: a regional scale mapping of the three saline aquifers and their equivalents. This report presents the maps created for Colorado portion of the Colorado Plateau, also referred to as the Colorado Study Area (CSA). Mapping from the Sand Wash Study Area was expanded to the CSA by incorporating more IHS well data, geophysical logs, surface geologic maps and other published data. The tops and bases of the three saline aquifers and their equivalents, as well as the top of the Mancos seal, were mapped at this scale.

Mapping Software

Three mapping software packages were used to create these maps:

1. Petra™: an IHS software package designed for geologic interpretation and mapping based on data from oil and gas wells. Petra was used to correlate formation tops and to create a detailed, hand-contoured map depicting the structural surface of the Dakota Sandstone.
2. Petrel™: a Schlumberger application for geocellular modeling and visualization. Petrel was used to generate multiple, sub-parallel formation surfaces using the Dakota structure map and other formation tops interpreted in Petra. A static geologic model was created from this framework that was ultimately used for fluid injection simulations.
3. ArcGIS™: a popular ESRI tool for GIS based mapping. ArcGIS™ has been chosen as the primary RMCCS spatial database format.

Methods

Overview

The general workflow consisted of correlating formation tops in Petra™ and creating a detailed, hand-contoured, Dakota structure map. The correlated tops and gridded Dakota structure map were transferred to Petrel™, which was used to create structure maps of other formations. Finally, the Petrel™ gridded surfaces were imported into ArcGIS™ where they were combined with surfaces created for other portions of the Colorado Plateau in the final report.

Sand Wash Basin

Petra™

Petra™ was the primary software tool used for analysis and interpretation. Well data from the IHS database and scanned geophysical log images from MJ Systems were central to this interpretation. Formation tops as reported by operators are notoriously unreliable, with inconsistencies common from company to company. Oftentimes tops do not correlate exactly, creating errors in mapped surfaces. To produce the most accurate maps, formation tops were identified and correlated anew throughout the study area. This detailed correlation process resulted in a high level of consistency throughout the area.

The tops correlated in this project were used to create a detailed structure contour map on the top of the Dakota Sandstone. The Dakota Sandstone was chosen as the key surface because it is regionally extensive and often easy to distinguish on geophysical logs. It is also the shallowest of the regionally targeted saline aquifers.

Initially only the Sand Wash Basin study area (including the Yampa Block and the Axial Basin Uplift) was examined and mapped. On the Axial Basin Uplift, the saline aquifer targets are near the surface, and in some cases have been removed by erosion. In contrast, deeper parts of the basin have thick sections of younger sediments overlying the saline aquifers, with few wells drilled deep enough to penetrate the aquifers. To overcome this problem, depths to the aquifers could be projected from the positions of shallower or deeper formations. Many more formation tops not associated with the targeted aquifers were correlated and mapped. From these the tops of the aquifers could be estimated in wells that did not actually penetrate the aquifers.

The Sand Wash study area contained 4924 wells, of which 2708 had at least one geophysical log. Of those wells with logs, 2000 had either an actual or projected Dakota formation top that was correlated for this project. Altogether, 37 formation tops ranging in age from the Cretaceous Fox Hills Sandstone to the Precambrian erosional surface were correlated for the Sand Wash study area totaling 15,000 individual tops.

The Dakota tops were hand contoured to incorporate the individual data points as well as all the other data sources. The structures were contoured as forced folds overlying the edges of fragmented and differentially uplifted basement blocks.

The Dakota structure map of the Sand Wash Basin study area, shown in Figure 4.5, was then imported into Petrel and subsequently used for generating other modeled surfaces .

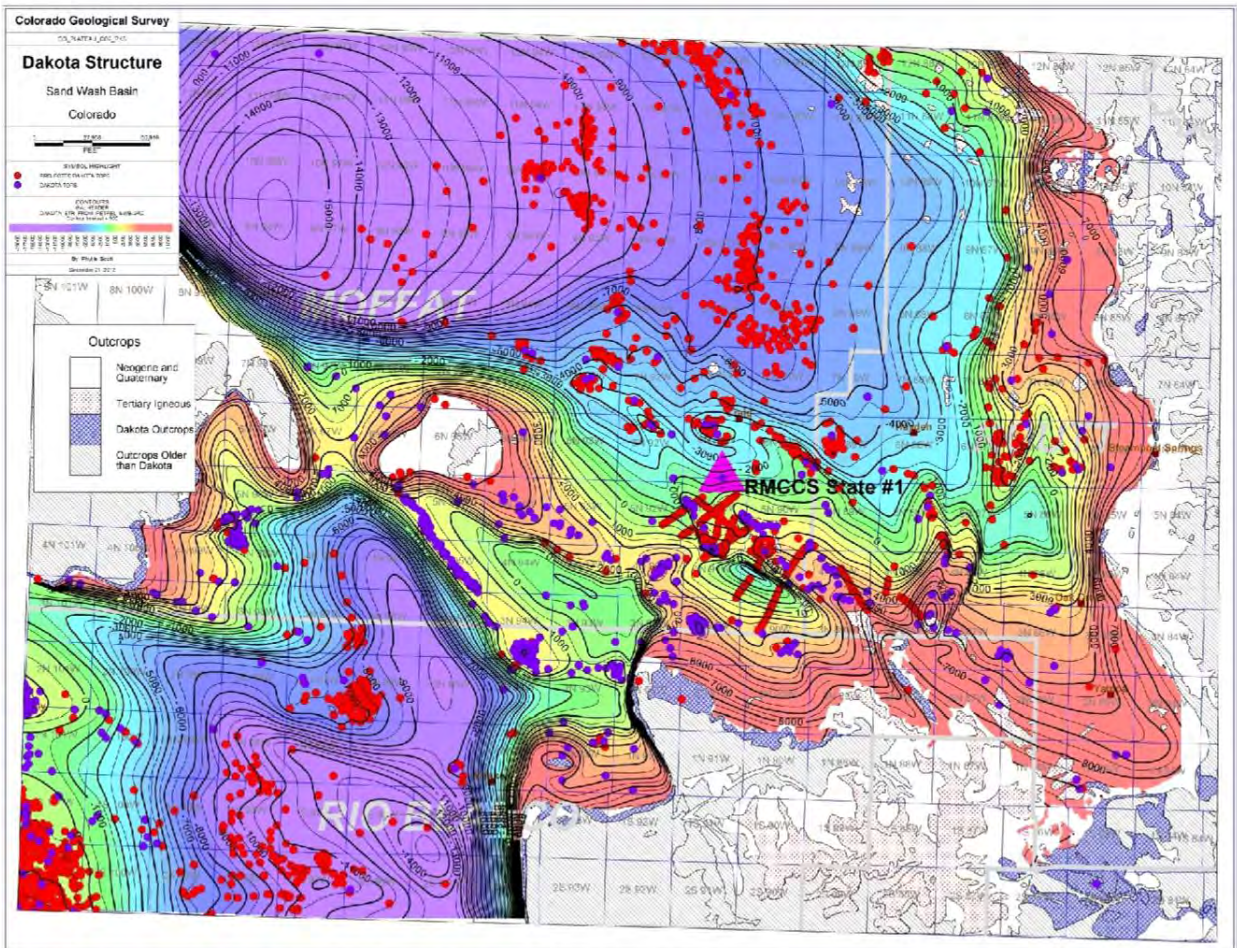


Figure 4.5. Petra™ structure map on top of the Dakota Sandstone saline aquifer, Sand Wash Basin Study Area. Locations of Dakota tops shown as purple dots; projected Dakota tops are shown as red dots.

Petrel™

Petrel™ is a software package designed by Schlumberger for generating and visualizing static geologic models from a myriad of oil and gas well data. Petrel™ was used to create a three-dimensional model within the Sand Wash Study area to be used as the structural framework for simulating the injection of CO_2 into the saline aquifers from the RMCCS State #1 well.

The Dakota surface that was generated in the Petra project was imported into Petrel along with the locations of wells within the study area and formation tops for those wells. Petrel used these data to map other surfaces by comparing formation tops for an unmapped surface with an adjacent mapped surface and creating a new, sub-parallel structure map. For example, the top of the Morrison was mapped by using the Dakota structural surface and Morrison formation tops to create a Morrison structural surface that is sub-parallel with the Dakota surface. The use of both a surface and the formation tops provides much more information for the creation of the secondary surface than tops alone. Relying only on formation tops to create surfaces in this structurally complex area usually resulted in impossible geometries with surfaces that intersected.

Fourteen surfaces were created in Petrel (Table 4.1 and Figure 4.6). From shallowest to deepest they are:

Formations Mapped in the Sand Wash Basin Geostatic Model		
Formation Top	***Average Interval Thickness***	***Description***
Mancos	888	The name of the group that comprises all of the formations deposited within the Cretaceous Seaway (including all formations down to the Dakota saline aquifer). The Mancos Group is the ultimate seal overlying the saline aquifers.
Morapos	2311	A prominent sand within the Mancos Group deposited in the Cretaceous Seaway
Niobrara	1528	A calcareous section within the Mancos Group deposited in the Cretaceous Seaway
Carlile	199	A shale within the Mancos Group deposited in the Cretaceous Seaway
Frontier	295	A coarsening-upward shale and sand unit deposited within the Cretaceous Seaway.
Mowry	102	A shale unit directly overlying the Dakota saline aquifer. It is the seal for the Dakota saline aquifer
Dakota	166	A saline aquifer comprised of fluvial and marine sands, silts and shales.
Morrison	415	Fluvial sands and shales. The Morrison top is the base of the Dakota saline aquifer. This unit is a seal for the Entrada saline aquifer, although there are some porous sandstones in the western part of the study area.
Curtis	65	A marine deposit of sand, shale and siltstone that forms the seal for the Entrada saline aquifer.
Entrada	347	A saline aquifer comprised of eolian sandstone. It includes the Navajo Sandstone in the western part of the study area.
Chinle	779	Sands and silts deposited by large river systems. The Chinle is the base of the Entrada/Navajo saline aquifer. This interval includes the Moenkopi, which underlies the Chinle. The entire interval is a seal for the Weber saline aquifer.
Phosphoria	187	Marine limestone, sandstone and shale that acts as a seal for the Weber saline aquifer.
Weber	411	A saline aquifer comprised of eolian sandstone.
Maroon		Alluvial fan redbeds and the base of the Weber saline aquifer.

Table 4.1. Summary of stratigraphic formations mapped for the Sand Wash Basin geostatic model.

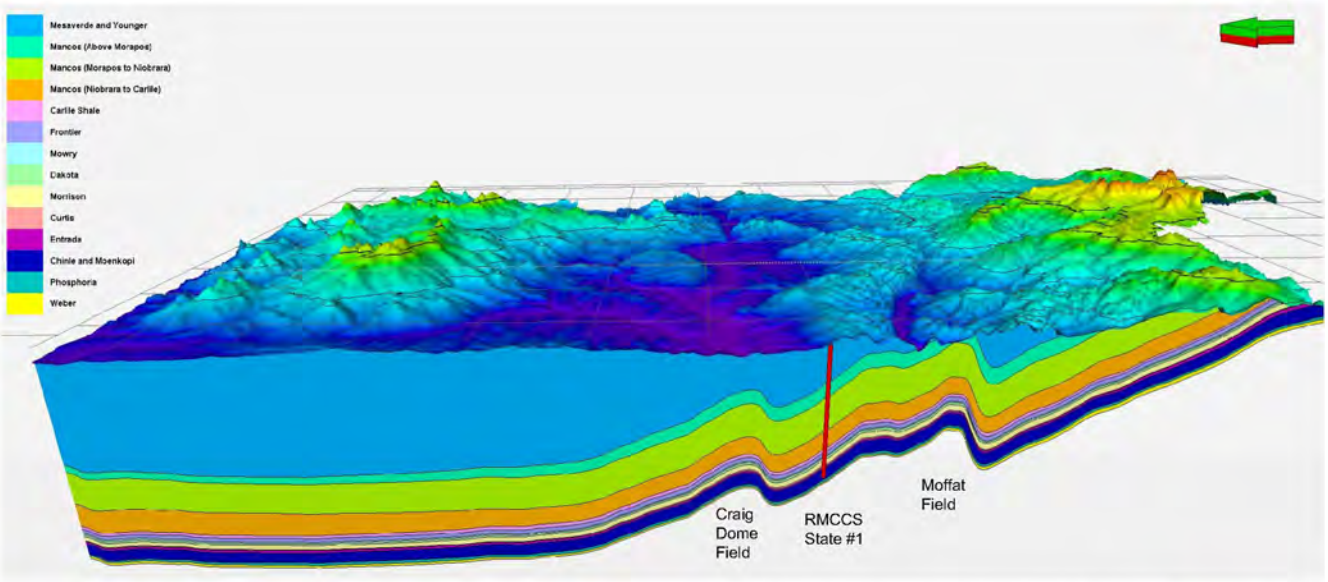


Figure 4.6. North-South cross section through Sand Wash Basin Petrel™ model. Wyoming border is at the left of the image and the White River Uplift (south) is on the right. The RMCCS State #1 stratigraphic test well is shown in red.

Geocellular Model

Surfaces for the geocellular model were generated using a minimum curvature algorithm and a grid size of 500 by 500 feet. A digital elevation model was imported into Petrel™ and used to trim each of the surfaces to prevent projections above the ground surface. Fourteen surfaces and their respective isopach maps were migrated from Petrel™ into Petra™ and ArcMap™ for visualization and database archiving. A cross section through the Petrel model is shown in Figure 4.6 which is a north-south cross section.

Discussion

Accuracy of Mapped Surfaces

Potential sources of error in the oil and gas well data and resultant maps include the following (listed in order of significance):

- In areas of sparse well control, the surfaces may be mapped incorrectly. Structural features, both faults and folds, may be completely missed if there are no well control or outcrop patterns that suggest that structures are present.
- The thickness of a formation (or the thickness between two formation tops) may appear to be highly variable. This can be due to:
    - The wellbore cutting a normal fault which has removed part of the section by extension, resulting in an anomalously thin isopach. Anomalous data points were ignored.
    - Incompetent formations such as the Mancos Shale appear to have been deformed and either thickened by compressional forces or thinned by extensional forces.

    - Steeply dipping beds make a section appear thicker than normal because a vertical wellbore does not penetrate the formation at a 90 degree angle. In areas of steep dip, anomalous sections should appear as elongate thicks or thins that parallel the strike of the section; however, computer gridding algorithms contour these anomalies as bullseyes when there are no other wells nearby for additional control. Because of this, other contoured surfaces that were made from the isopach maps would be in error. However, in areas of steep dip the contour lines are very close together, so a thicker section would result in a very small lateral shift in the contour lines.

- Tops may be miscorrelated because they are difficult to discern, especially on different types of geophysical logs that have been run over the years. Correlations were made on many formation tops above and below the saline aquifer tops in an attempt to insure accurate correlations.
- Formation tops oftentimes are gradational and difficult to pinpoint.
- The datum may have been measured incorrectly. Reported surface elevations were compared with digital elevation model data to gauge the correctness of the surveys.
- Locations may be misspotted. Data points that did not make sense were checked on the Colorado Oil and Gas Conservation Commission's website. If they could not be rectified, they were ignored.
- Wells may not be vertical. If this is the case, the measured depth of a formation top or an isopach interval may be too great. Anomalous points were ignored.
- Formation tops were picked with the geophysical logs compressed on the screen so that a longer section of the log could be viewed. Because of this, the top could be off by as much as 10 or 15 feet from where the actual pick would be if the log were enlarged.
- Because of the scale of the mapping project, the mapped surfaces are generalized and smoothed.

Potential Pathway for Injected CO_2

Detailed mapping suggests:

- There are barriers to the updip migration of sequestered CO_2 to the south, west and east of the RMCCS State #1 well.
- At this scale of mapping there are no clear barriers to the southeast that would prevent injected CO_2 from traveling from the wellbore updip to the Dakota outcrop.
- It is very possible that barriers exist either as faults that have not been identified or as permeability barriers. If an injection program is pursued, this potential pathway must be examined in greater detail.

Mapping of Reservoir Properties

Porosity and permeability, and therefore storage capacity, vary considerably over the lateral extents of the aquifers. They are affected by the environments that existed during deposition of the formations and also by subsequent factors that occurred during burial and lithification including cementation and diagenetic changes. Reservoir parameters can be measured from core analyses and from geophysical logs. These parameters were examined in this study in an attempt to depict their spatial distributions and to quantify storage capacity (Figure 4.7).

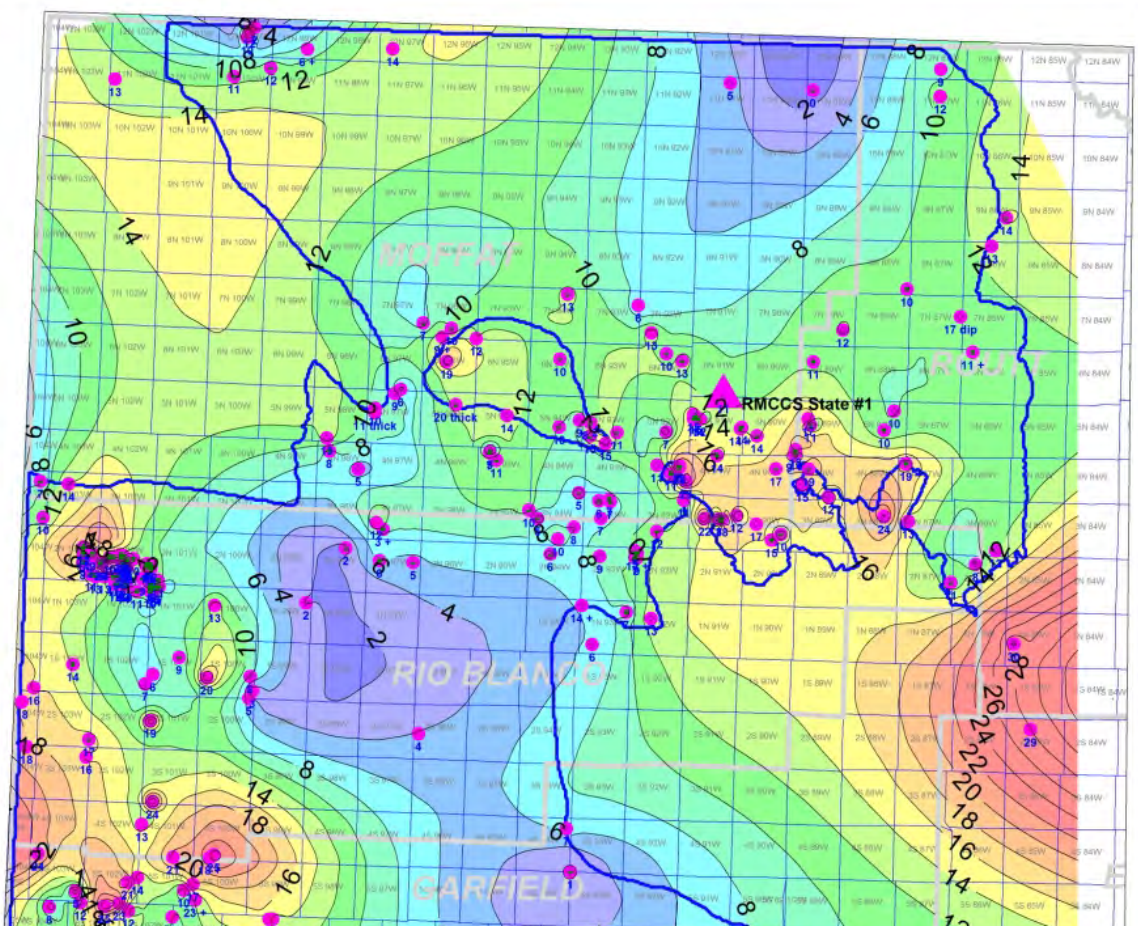


Figure 4.7: Pore thickness map (feet) for the Dakota saline aquifer in northwest Colorado. Purple dots show location of wells with data points.

Data

Data measuring reservoir properties were collected to understand the range and distribution of the properties that would affect storage capacity. These data include:

- Raster images of geophysical logs from over 18,000 oil and gas wells in the Colorado Study Area (CSA). These were purchased from MJ Systems, a company that scans and archives raster logs. Geophysical logs record the physical properties of the rocks and fluids that surround the wellbore. They were used to make an initial estimate of net sand within each saline aquifer. The locations of wells with raster geophysical logs are shown in Figure 4.2 B.

- In the final months of this study, digital logs were obtained for 818 wells in the (CSA) from IHS. These were used to map the reservoir parameters of net sand and porosity within the CSA. The locations of wells with digital geophysical logs are shown in Figure 4.2 B.
- Published average porosity and permeability values from field studies.
- Porosity and permeability measurements from older wells that had been cored and whose core analyses were available from the Colorado Oil & Gas Conservation Commission's website.
- Data collected from the drilling of the stratigraphic test well RMCCS State #1, including:
    - Geophysical well logs that help determine rock and fluid properties of the penetrated strata.
    - Full-diameter cores and sidewall cores from which direct measurements of rock properties of the saline aquifers and their seals can be obtained.

Published Porosity and Permeability Values for Oil and Gas Fields

As a part of this study, a cursory examination of published porosity and permeability measurements was made in an attempt to better estimate the storage capacity of the saline aquifers. Estimates of average porosity and permeability values were tabulated from published field studies.

Porosity and Permeability Crossplots

Additionally, core analysis data sheets were downloaded from the Colorado Oil & Gas Conservation Commission's website for wells in the Sand Wash Basin study area. Porosity and permeability measurements from six Dakota cores, three Entrada cores, and five Weber cores were manually entered into an Excel spreadsheet and crossplotted.

The data from the Dakota cores are shown in Table 4.2 and Figure 4.8; their average porosity is 13.7% and the median permeability is 19 md. One of the included cores had anomalously high permeability values. The porosity and permeability values are also dependent on the position of the core within the section; they vary greatly depending on whether the cores were cut through zones of the highest porosity or through more shaly intervals.

Dakota Cores					**Porosity %**		**Permeability (md)**	
API Number	**Location**	**Top of Dakota**	**Dist. from RMCCS State #1**	**No. of Samples**	**Average**	**Median**	**Average**	**Median**
05-081-06683	SE SW SW 20-5N-90W	4893	6 mi SE	8	11.7	12.8	84	43
05-081-06198	NE SE SW 21-5N-90W	4850	6mi SE	35	16.4	16.4	16	1
05-107-06162	NW SE 29-4N-89W	3183	14 mi SE	13	14.0	14.7	158	72
05-103-07055	NE SE 1-2N-93W	6996	20 mi SSW	51	13.7	14.7	748	240
05-107-06133	NW NE 36-4N-88W	891	22 mi SE	11	9.8	9.3	0.36	0.03
05-081-06666	NE NW 30-5N- 93W	2752	16 mi	7	8.3	7.5	9.1	0.16
All 5 Cores				125	13.7	14.4	325	19

Table 4.2: Porosity and permeability data from COGCC public records.

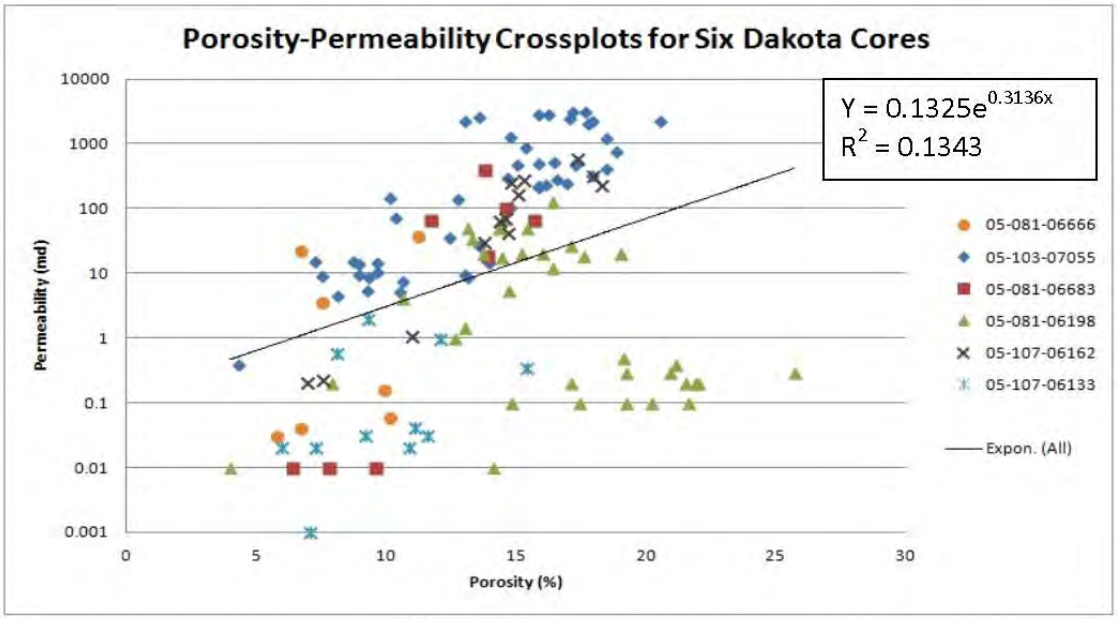


Figure 4.8: Cross-plot of permeability/porosity for 125 Dakota samples.

Table 4.3 and Figure 4.9 show the porosity and permeability data for the three Entrada cores. The table shows more detailed information for each individual core. The average porosity for the three cores is 15.0 percent and the median permeability is 23.5 md.

Entrada Cores					**Porosity %**		**Permeability (md)**	
API Number	**Location**	**Top of Entrada (MD)**	**Dist. from RMCCS State #1**	**No. of Samples**	**Average**	**Median**	**Average**	**Median**
05-081-05278	SW SE 20- 5N-	5421	5.5 mi SE	7	13.7	14.9	26	24
05-081-05284	NW SW 13- 5N-	5254	28 mi W	10	18.8	21.2	187	161
05-107-06162	NW SE 29-4N-89W	3814	13.7 mi SE	45	14.4	14.7	21	18
All 3 Cores				62	15.0	14.9	48	23.5

Table 4.3: Porosity and permeability data from COGCC public records.

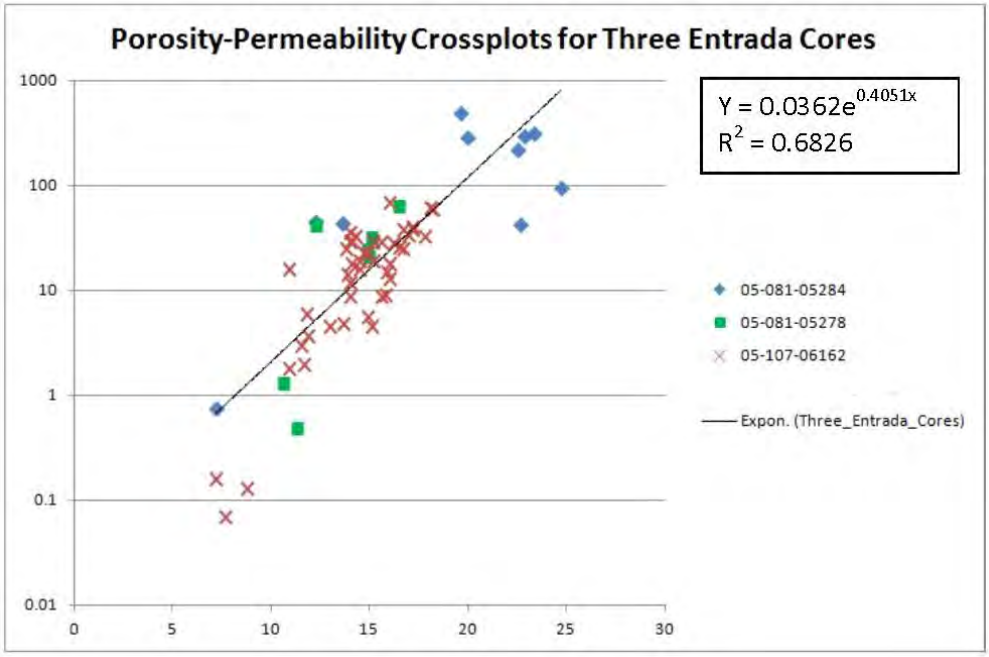


Figure 4.9: Cross-plot of permeability/porosity for 62 Entrada samples.

Table 4.4 and Figure 4.10 show the porosity and permeability data for five Weber cores. Four of these cores are from more than 60 miles to the west of the location of the RMCCS State #1 well. The one Weber core near the stratigraphic test well (05-081-06621) shows very low porosity and permeability. The Weber thins considerably from the west where the the other four cores were taken, to the east where this core was cut. However, the extremely low permeability in this core is somewhat misleading in that it was cut through a tight sandstone; a more porous zone containing about 40 feet of sand exists higher in the section.

Weber Cores					**Porosity %**		**Permeability (md)**	
API Number	**Location**	**Top of Weber (MD)**	**Dist. from RMCCS State #1**	**No. of Samples**	**Average**	**Median**	**Average**	**Median**
05-081-06621***	NW SW NW 20-5N-91W	8300	4 mi SW	17	2.9	2.2	.04	.01
05-081-06340	NW NW 12-3N-104W	9303	77 mi WSW	31	9.4	8.8	2.6	0.24
05-103-09287	NW NW SE 17-1N-100W	9968	61 mi SW	25	3.7	2.9	0.08	0.02
05-103-09262	NE SE 1-2N-93W	7661	69 mi SW	26	8.0	7.5	0.75	0.23
05-103-08021	NE SE 31-2N-101W	6160	67 mi SW	257	7.1	6.1	1.3	0.1
All 5 Cores				356	6.9	6.15	1.3	0.1

Table 4.4: Porosity and permeability data from COGCC public records.

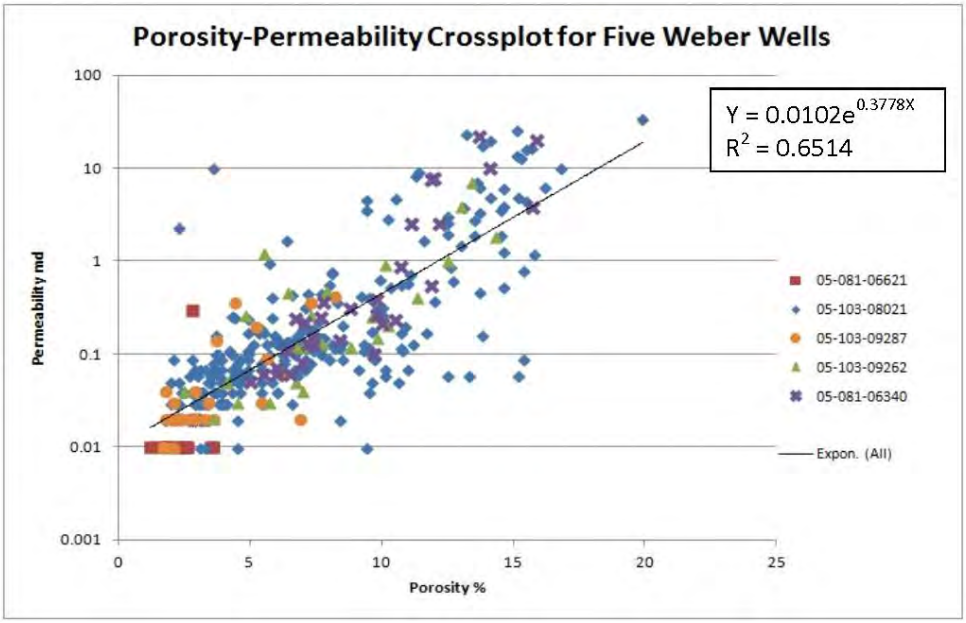


Figure 4.10: Cross-plot of permeability/porosity for 356 Weber samples.

5. Stratigraphic well drilling and coring

Pre-Drilling Activity

Drilling Plan

The drilling of any well begins a minimum of six months prior to spudding, or initiating drilling operations. The approximate well location, projected depth of the target and the overall objectives of the well are required to begin planning. In the case of the RMCCS well there were two potential locations under consideration, both approximately 5 miles south of the town of Craig, Colorado in Moffat County. The deepest target formation was the Weber Sandstone with an estimated depth of 7,500 Ft, based on the best estimated available data at the time the project management plan was submitted in January 2010. The immediate area surrounding the potential locations were sparsely drilled and so this well would generally be referred to as a "Wildcat" well due to the lack of key data. The primary objectives were to: obtain full-bore core in three injection zones of interest and their respective sealing formations, obtain a full suite of geophysical well logs, and construct a well following current Department of Energy NETL best practices.

From this basic information a well budget, generally referred to in the oil and gas industry as an Authorization for Expenditure (AFE) was generated. Drilling bit records in the general area were analyzed to estimate drilling times, quotes obtained for all key costs elements, and drilling contractors meeting the selection criteria interviewed. For the RMCCS well the initial drilling contractor selected was Nabors Drilling in Q1 2011. In the RMCCS project there were two over-riding external influences impacting the critical component surrounding securing a top tier drilling contractor. The first was a significant increase in drilling costs compared to estimates from 2010 when the project budget was developed and approved. This was primarily due to a historic boom in shale oil activity in North Dakota attracting a significant number of rigs from the Rocky Mountain region. This included Nabors Drilling which moved the rig selected to drill the RMCCS

well from Colorado to ND. The second was the reluctance of the remaining drilling contractors in the area surrounding our location to mobilize a large distance to drill one well. After a prolonged search consuming all of Q3 2011, Patterson 166 was selected to drill the RMCCS well.

The final pre-drilling component was the selection of the actual drill site. Two viable sites were identified meeting all project criteria. The first was in Township 6N, Range 91W, a state section in Moffat County within the boundaries of Trapper Mine. Project partner, Tri-State Generation and Transmission, is a majority owner of Trapper Mining Company. The second location was in Township 5N, Range 90W, also a state section.

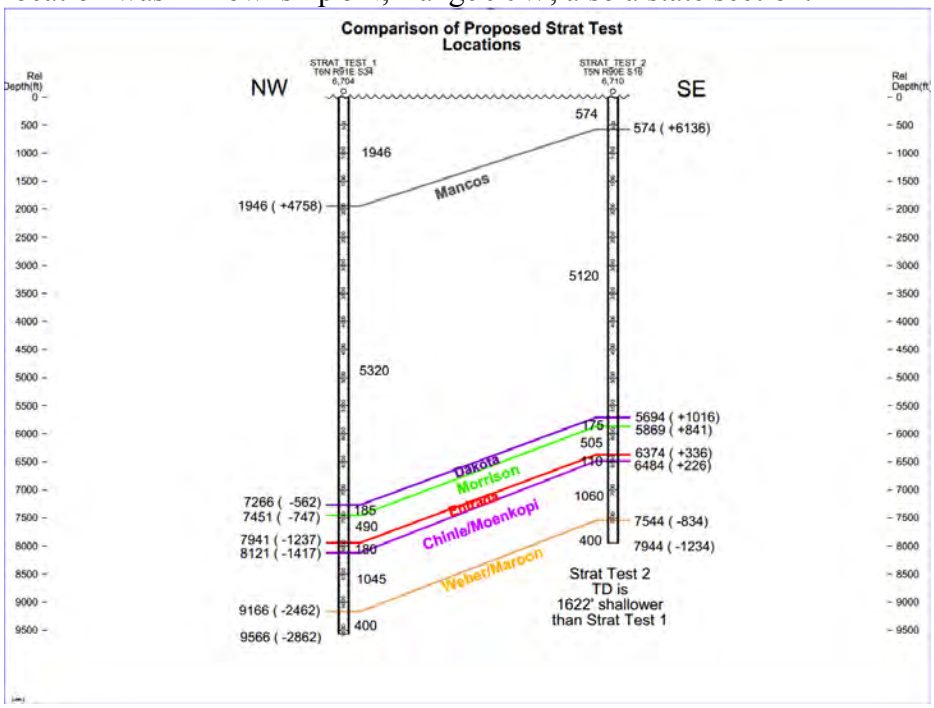


Figure 5.1: Cross-section with two potential drill sites

The second location had the advantage of a lower ground elevation that would reduce drilling cost, was not within the boundaries of an operating mine that added significant additional drilling safety regulations and rig access complexities. On the negative side, the location was long and narrow significantly increasing pad construction cost, was directly adjacent to a county road increasing public safety risk and was located on a drainage watershed that would make permitting more difficult and dramatically increase environmental risk and the cost of drilling insurance. The Trapper Mine site had the advantage of a large, flat surface area, low pad construction costs, proximity to the Craig Station power plant (for possible future sequestration demonstration) and very low environmental risk. After careful consideration by the RMCCS technical team, the Trapper site was selected. With all key pre-drilling decisions complete the well plan was developed (a very basic summary is included in Appendix G). On November 10 and 11 representatives from all project partners and sub-contractors met to review the drilling plan in detail in what is referred to as a drill the well on paper (DWOP) workshop. The workshop was held in Ft Lupton, Colorado and each step of the drilling plan was reviewed and evaluated.



Figure 5.2: Drill Well On Paper workshop, Ft. Lupton, CO.

Pre-Drilling Risk Mitigation

Prior to initiating drilling operations a number of steps were taken to reduce risks associated with field activity. The first step was creating what is commonly referred to as a "Bridging Document". This is a single document that combines the safety procedures for each of the primary organizations involved in the drilling operations. In the case of the RMCCS project this included Schlumberger, Patterson Drilling and Trapper Mining. A representative from each organization met and reviewed each organization's respective safety programs and policies. A comprehensive unified document was prepared and in cases of conflicting requirements, the more stringent was always used. Once the final document was compiled, each organization signed off on the document signifying this was the safety document that all parties involved in field operations would adhere.

The second risk mitigation step was performing a drilling risk assessment. In the risk assessment, a team of drilling experts reviewed the operation, identified the potential risks and ranked them for likelihood and severity. Each identified risk outside of safe operating conditions was treated with a mitigation plan until it fell within safe operating levels. The highest identified risk was site access within the boundaries of the mine by the numerous subcontractors involved in drilling operations. To reduce this risk to a minimum a full time on-site Safety Supervisor was added to the project during field activity. The Safety Supervisor had extensive oilfield experience, was a trained Paramedic and a certified Mining Safety and Health Administration (MSHA) instructor. From the beginning of field activity to the end the safety supervisor was on duty twenty-four hours a day, seven days a week. The safety supervisor performed MSHA training for every subcontractor entering the mine for access to the drill site, escorted traffic on and off the site, conducted twice daily safety meeting with rig crew, safety meetings with each subcontractor prior to any operation, maintained safety statistics, acted on hazard identification efforts by field crews and generally managed all aspects of safety during the entire field operation. The results were zero safety incidents, including not even minor incidents, for the entire project. There were 293 individuals trained in MSHA site training and 19,426 man-hours worked without incident. This performance is outstanding and well outside the norm in even the best of circumstances.

The third risk mitigation step was to develop a plan to assure Mining Safety and Health Administration (MSHA) compliance throughout all field operations within the boundaries of the mine. Oilfield drilling operations are generally regulated by the Occupational Safety and Health

Administration (OSHA) and drilling contractors and all drilling service providers are organized to maintain compliance to OSHA regulations. However, all activities within the boundaries of an operating mine are regulated by MSHA. MSHA compliance standards are generally much more stringent and comprehensive than OSHA. Additionally, significant violations or repeated minor violations of MSHA regulations by RMCCS project subcontractors would potentially have devastating consequences for the project host, Trapper Mining. Therefore, ever effort was made to fully comply with MSHA requirements. Numerous meetings were conducted with the MSHA field superintendent in Craig, Colorado and with Trapper Mining safety engineers to develop the compliance plan. Once the plan was completed a meeting was held in the MSHA Division office in Denver, including Schlumberger, Patterson and Trapper representatives, to review the plan in detail. The RMCCS MSHA Safety compliance plan was approved on December 1, 2011 and a short version of that plan is included in Appendix G. An additional step was to have an MSHA certified inspector visit the selected rig, November 28, 2011, on location in Wyoming while it was drilling for another operator. The inspector identified modifications to be made to the rig to bring it within compliance to MSHA regulations.

An important lesson learned was to attempt to secure permission from the operator of the well the rig was drilling for, to complete as many the modifications while on this location. Four days at a daily rate of $19,000 per day were used after rigging up on the RMCCS site making the necessary modifications. Overall, this MSHA compliance risk mitigation effort was also a motivating factor in having a dedicated safety engineer on site with MSHA certification. Overall, the MSHA compliance plan was extremely effective and there were zero MSHA citations for any project partner, service provider or subcontractor for the entire project.

Drilling Chronology

A drilling chronology of significant events is provided in Appendix H.

Discussion and Key Points

Drilling Under MSHA Oversight

Drilling a well for deep geologic storage draws heavily on people, equipment and expertise from the oil and gas industry. Safety for drilling rigs and operations in the oil and gas industry are generally regulated by the Occupational Safety and Health Administration (OSHA). Consequently, drilling rigs and procedures are constructed for compliance with OHSA rules and guidance. The RMCCS well was drilled within the boundaries of an operating coal mine and thus, under the oversight of the Mining Safety and Health Administration, or MSHA. Many coal-fired power plants are situated in close proximity to the mines supplying the coal reducing the cost of transporting the coal to the plant. Since CO_2 transportation is a major cost component for geologic storage as well, having injection wells placed within the boundaries of a mine will not be uncommon. For this reason, the lessons learned by drilling the RMCCS State No. 1 within the boundaries of the Trapper Mine will be valuable for future operations. Many of the issues surrounding site access, rig worker certification and transportation to and from the site have been discussed. However, conducting drilling operations with a drilling rig and rig crews under MSHA oversight, rather than OSHA, had considerable impact on the cost of drilling the RMCCS well. This impact was due almost exclusively to modifications necessary to the rig and drill pad living quarters to make them compliant with MSHA regulations.

To proactively assess the condition of the rig we were to use for drilling the RMCCS well, we contacted the drilling company and the operator of the well they were drilling for and obtained

permission to have an MSHA inspector visit the rig. On November 28, 2011 the unofficial inspection was conducted by an MSHA certified electrician. None of the observations were considered serious and it was estimated that it would take minimal time to bring the rig into compliance. A local MSHA certified electrician in the Craig, Colorado area was identified and secured to begin preparing he rig for MSHA certification once it arrived at the RMCCS site.

On January 3rd, the rig was released by the operator of the preceding well and by January 7 the entire rig was at the location. Rig up activity took an additional three days and under normal conditions, the rig would have been ready to begin drilling on January 10. However, it would take another five days to get the rig operational and fully compliant with Mining Safety and Health Administration (MSHA) regulations. The difficulty was in complying with Federal Metal and Nonmetallic Mine Training, Safety & Health Standards CFR 30 Section II, subpart K.12001 – K.12038 related to electrical overload protection, conductors, distribution boxes and grounding. The time and effort to bring the rig and living quarters to compliance was much greater than anticipated. It is important to note that it is not the electrician hourly wages and material cost that impacted the project budget. It is the fact the once the rig is functionally ready to commence drilling operations the rig goes on "Day Rate" or begins charging a daily sum as specified by the drilling contract. In the case of the RMCCS well, the negotiated day rate was $19,000 per day. Additionally, all daily rental fees associated with living quarters, rental tools and expendables increased the daily cost to $27,950 per day. Consequently, the 5 day cost of bringing the rig into MSHA compliance was $139,750.

- *When drilling a well for geologic storage under MSHA regulations, make every attempt to have the rig pass an inspection by MSHA prior to taking possession of the rig.*

For future drilling operations within the jurisdiction of MHSA guidelines, there are three potential actions to mitigate the cost of bringing compliance of a drilling rig generally operating under OSHA regulations up to the much more stringent MSHA standards. The first is to attempt to secure a rig that has already been made MSHA compliant. The second is to attempt to gain a waiver from the MSHA District Superintendent from MSHA oversight. In the case of the RMCCS well a partial waiver was obtained in regard to training of the rig workers, but not to drilling operations oversight. There is a potential pathway to obtaining a waiver that should be rigorously pursued. There is a "Memorandum of Understanding" between OSHA and MSHA that allows oversight by OSHA within specific areas within the boundaries of the mining operation under certain circumstances. This avenue was pursued in the RMCCS project but a waiver not granted. The third option is to attempt to gain access to the rig while it is either idle or "stacked", or obtain permission to work on the rig while drilling for another operator, bringing the rig into compliance without being subject to the rig and associated day rate.

Coring Operations

In most drilling applications there are nearby wells penetrating the same formations providing an accurate geologic cross-section allowing the well-site geologist to make an accurate estimation of the depth that equivalent formation to be encountered in the well being drilled. In these cases, if a particular formation is to be cored, the well-site geologist can determine the point at which the drilling of the desired formation is immanent and at what point to pull the drill bit out of the well-bore and re-enter with the coring assembly. The general objective for coring in the RMCCS project was to attempt to obtain full diameter core (4") from the bottom of the sealing formation and into the top of each of the three potential storage targets. Three target seal combinations are: Mowry Shale / Dakota Sandstone, Curtis Shale / Entrada Sandstone, Phosphoria / Weber Sandstone. The plan was to attempt to core through the contact interface between each seal/injection formation pair. In the case of typical coring operations there is a single formation

that core is to be obtained in each coring run. In this instance, the geologist observes drill cuttings to watch for evidence that the bit is penetrating the desired formation. To core though the interface between two formations, the geologist must have an accurate prediction of the thickness of the first formation to be able to predict at what point the core bit will approach the top of the interface. If the first interval is thinner than predicted the drill bit could unexpectedly pass all the way through the interface. If the first formation is thicker than predicted and the coring begins too soon, it is possible to fill the 90' core barrel with the first (sealing) formation, thus requiring adding a second core run to continue into the target injection formation. At depths typical to geologic storage, it takes from eight to sixteen hours to pull out of the well with a core barrel, retrieve the core, and go back into the well to either resume drilling or resume coring. Therefore, picking the core point too early or too late can have significant impact on the scientific objectives of the well, or significantly increase drilling cost.

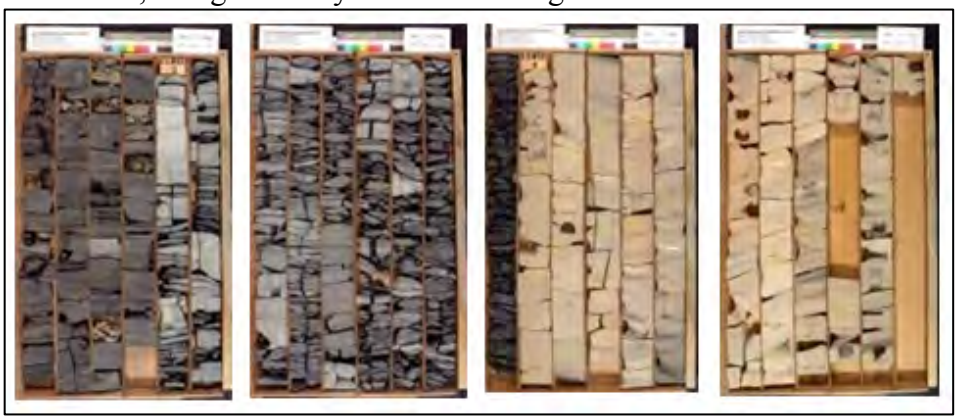


Figure 5.7 – Core obtained from the RMCCS Well.

In areas where there are few nearby well penetrations, such as the case for the RMCCS well, it is difficult to predict the relative thickness and depth at which the bit will penetrate the intervals to be cored. Matching drill cuttings to well correlations to distant wells resulted in too much uncertainty for predicting proper core points. It was decided to add a gamma ray measurement to the bottom hole drilling assembly. Having a more precise depth correlation and a measurement that could be compared to similar measurements in the correlation wells dramatically improved the confidence in the depth of the drill bit in relation to the geologic structure and the desired intervals to core. Therefore, it is highly recommended to add a gamma ray measurement, at a minimum, to the drilling assembly, if full core is to be obtained in a well without nearby wells (within one to three miles). Additional measurements, such as resistivity and porosity, can be added to further reduce uncertainty, if the budget allows.

Managing Drilling Cost

The single largest budget component for the entire RMCCS project was the cost to drill the characterization well. The primary objective in drilling the well was obtaining the site specific data necessary to complete the scientific objectives of the project. This data includes geophysical well logs and full core to permit detailed characterization of the injectivity and capacity of the Dakota, Entrada and Weber formations, and their respective sealing formations. However, the lessons learned in performing the drilling and coring operations provide additional significant benefits to further the development of best practice documentation by the NETL and providing a significant economic impact to the local economies.

The initial drilling budget was developed in the spring of 2009 for the original grant proposal. At the time, rig availability, drilling supplies, third-party contractors, trucking, tubulars and all of the costs associated with drilling, were generally plentiful. The estimated well total

depth was estimated at 7,500' and not for a specific site, but was thought to be a representative depth for the general area. Furthermore, the cost estimate was based on typical drilling practices and bit records gleaned from oil and gas development wells were from the Piceance Basin to the south, where the vast majority of drilling activity in NW Colorado was underway. The development of the drilling budget started by defining a percentage of the available funding, the available cost share and was distributed proportionally by the cost expectations of completing all of the proposal tasks. Consequently, the drilling budget started at roughly one-third of the total project budget. The original drilling budget dated July 31, 2009 was $1,005,302. The final AFE amount, prior to drilling, with an expanded Niobrara coring program and projected total depth of 10,380' was $4,119,721. The final actual drilling cost was $4,666,757 with an actual total depth of 9,745'.

There were several categories of drilling expenditures significantly higher than the initial drilling budget (AFE). The "Preparation and Termination" category exceeded the budget by $106,312. The majority of the overages within this category are directly attributable to the additional expense of bringing the rig and location within MSHA regulation requirements. Alterations of the well pad, camp facilities, and electrical work and rig costs associated with approximately four days of extended rig up were all required to pass inspections and meet the MSHA standards.

A second area of significant overage are related to the loss circulation encountered in drilling the surface section prior to setting the intermediate protection casing at 5,340'. Lost circulation occurs when the pressure exerted by the column of drilling fluid encounters open fractures, extremely permeable formations or rock layers with pore pressures much less than hydrostatic. The weight of the drilling fluid must be maintained to prevent the potential for blowout. Drilling through multiple coal layers within the surface strata made the potential of a blowout caused by drilling into trapped accumulations of methane a significant project risk. However, the rock formations in this interval were not able to support the slight overbalance in the mud weight and consequently, thousands of gallons of excess water and drilling fluid materials had to be trucked in on a continual basis until casing was cemented in place to prevent the lost circulation. The impact on the drilling costs were $93,190 in additional "Mud Chemical and Engineering Services" and $62,363 in Water.

A third category of drilling cost exceeding the budget is directly related to the drilling environment. The toughness of the rock layers is higher than expected, lowering bit efficiency and resulting in the utilization of additional bits, both for drilling and coring. The expense for "Bits, Reamers and Coreheads" exceeded the budget by $85,649. The well also exhibited a tendency to drift to the south due to formation dip. The drilling manager felt it was critical to maintain a deviation from vertical less than 10 degrees, and ideally less than 3 degrees. This was to assure the successful retrieval of core barrels and reduce the risk of sticking the logging tools. To combat the well deviation and the development of doglegs in the well trajectory, directional drilling capabilities were added to the bottom-hole assembly (BHA). Later, a gamma ray tool was also added to the BHA to help the wellsite geologist correlate the well to distant offset well control to aid in picking core points. Both of these additions to the BHA resulted in $260,616 to the drilling costs above the budget.

In addition to the drilling related cost overages described, there was $209,771 in additional "General" expenses directly attributable to cost inflation experience in the period between preparing the drilling budget (2010-2011) and the beginning of 2012. The cost inflation was a result of a rapid drain of available service capacity driven by an historic boom in activity in North Dakota with the success of drilling efforts in the Bakken Oil Shale. The final drilling expenditures

exceeded the budget by $545,771 (13%) necessitating the curtailing of the core plan and abandoning the attempt to drill to the deepest formation of interest, the Weber Sandstone. To cover the additional drilling costs $90,000 were moved from the regional characterization budget of the state geological surveys and Shell provided an additional $507,000 in cost share to allow drilling to continue and to preserve logging a full and comprehensive wireline logging suite to augment the full core in developing the site specific characterization project task.

- *Exercise caution in basing drilling cost estimates on nearby oilfield experience.*

There are several cost efficiencies built into drilling expenditures in the oil and gas industries providing an important analog for drilling wells for geologic storage. However, it is important to consider unique differences that may impact drilling costs. The majority of wells drilled for oil and gas development are in areas where a great number of wells have been drilled previously and a particular drilling technique is more fully optimized. Additionally, it is common practice to add 10% - 15% to the estimated drilling expense (AFE) to cover overages that are common, but difficult to anticipate in what category the overages may occur. Very seldom does every cost group fall within the AFE amount in normal oil and gas drilling activities, even in mature areas. Periodically there will be an extreme overage, as much as 100% or more of the AFE cost, and is absorbed within the long term asset budget not tied to an individual well budget. A relevant example is the well drilled by the Patterson 166 just prior to moving to the RMCCS well. The operator encountered unanticipated drilling hazards that increased total drilling time from the original 30 day estimate to 65 days, increasing the drilling cost by an estimated 80% and delaying the start of the RMCCS well.

- *Well construction for Geologic Storage has lower risk acceptance than drilling for oil and gas and extra drilling methods need to be used to mitigate risk to as low as reasonably possible.*

Oil and gas exploration and production is a high risk – high reward activity. Typical rate of return on expenditures is generally over 25%, even with below average commodity prices. Consequently, operators have the ability to absorb significant, unexpected costs. Commercial operations engaging in industries producing anthropogenic CO_2 often operate at lower margins or have margins regulated and have a much lower risk tolerance. Additionally, for geologic storage in a saline reservoir, there are few surrounding wells to provide nearby drilling experience inherently increasing the risk. In the case of the RMCCS well, risk tolerance is also low, due to a fixed budget and high visibility associated with a publically funded demonstration project. In such cases it is prudent to perform a thorough and complete risk assessment for the drilling operation and apply mitigation strategies to bring all identified risks within an acceptable range. It is often above and beyond what may be acceptable risk in oil and gas operations. For the RMCCS well, a risk assessment was initiated on June 24, 2011 and completed, presented and approved on July 7, 2011. A summary of the identified risks, with likelihood and severity ratings before and after mitigation, was developed. Some of the significant mitigation strategies employed in the RMCCS project included: securing a high performing rig and crew with local drilling experience, utilizing a rig with greater than 200 ton hook capacity to minimize the risk of sticking the bottom hole drilling assembly, a sub-structure to accommodate the required Blow-Out-Preventer, maintaining well deviation below 3 degrees, twenty-four hour on-site safety supervision, setting an intermediate casing string above intervals to be cored, close engagement with district and local MSHA managers and Trapper Mine managers.

- *Well construction costs can be quite volatile for intervals as short as six months. The volatility is tied to oil price, and to a lesser extent, the price for natural gas. The impact on*

well construction is compounded if the site is greater than 50 miles from centers of oilfield activity, which is often the case for geologic storage into saline aquifers.

The cost of drilling rigs and services is closely tied to rig utilization, which is in turn closely tied to the price of oil and gas. The fleet of available drilling rigs and skilled personnel is relatively stable for periods of two to three years. This is due to the cost to build new rigs and infrastructure cost required to increase service availability limits the ability to match supply with demand. Conversely, a drop in oil prices results in a reduction in drilling activity and an accompanying drop in rig costs. The variability goes beyond daily drilling rates, but extend to contract terms as well. When rig availability is high, rig owners are willing to negotiate contract terms potentially extending to offering turnkey contracts where the driller agrees to reach a specified depth for a fixed price and often absorb some or all of the cost to mobilize and demobilize to the drill site. A turnkey contract significantly reduces drilling risk for the well operator. When rig availability is tight, drillers generally adhere to general contract terms outlined by the International Association of Drilling Contractors, or IADC. The general terms of a standard IADC specify a day rate for the rig, pass all mobilization costs, possibly de-mobilization costs and place virtually all risk associated with the drilling operations on the well operator.

In the case of tight rig availability, the effect on geologic storage into saline aquifers can be compounded. Many potential sites for saline aquifer storage are in areas remote from concentrated oil and gas activity. Any distance greater than 50 miles from centers of oilfield activity place additional burdens on well construction costs. The cost of rig mobilization, fuel, casing, wellheads, etc., are directly related to distance from the service center. At the time of the drilling of the RMCCS well (2012) the typical cost to move a rig was roughly $1,000/mile. Additionally, the greater the distance a rig must move, the more reluctant a drilling contractor is to leave a particular area because the day rate only applies when the rig is on site and operational; the drillers favoring multiwall contracts and short moves.

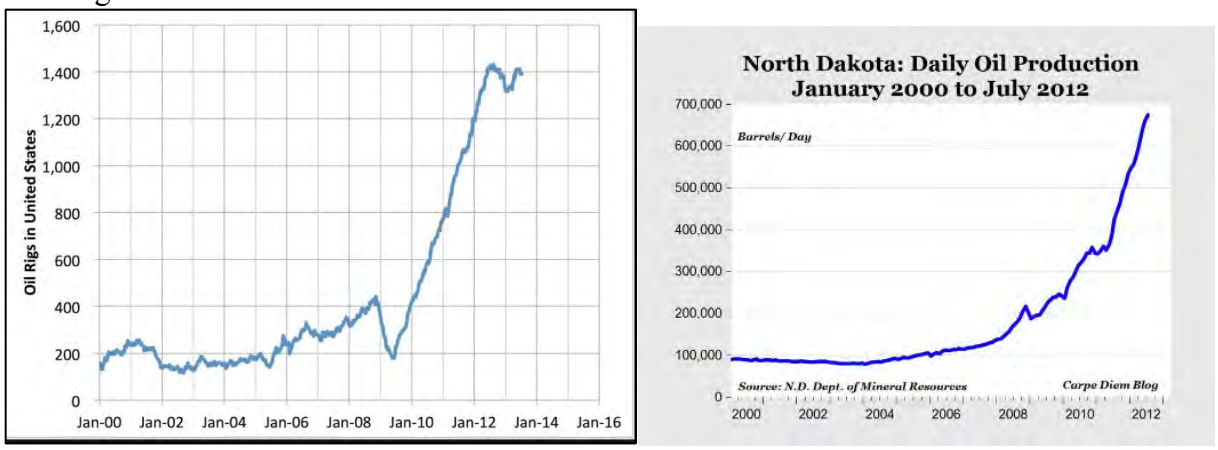


Figure 5.8 – Rig Utilization during RMCCS project primarily as a result of oil boom in North Dakota.

All of these factors related to rig utilization impacted the RMCCS project. At the time the original proposal and budget where being prepared in mid-2009, rig utilization was low as seen in figure 5.8. At this time, rig day rates were moderate, service costs low and drilling contractors willing to consider favorable contract terms. At that time, Nabors drilling was identified as the best option and the drilling budget was based on prevailing costs at that time. By the time the project schedule was ready for the well in mid-2011 the landscape had experienced dramatic change. An increase in oil prices, coupled with technical success in applying new hydraulic fracturing technology in the Williston Basin of North Dakota had initiated a boom in activity there

of historic proportions. This initiated a drain in rig capacity, skilled personnel and services in NW Colorado to North Dakota. This included Nabors moving our designated rig there. Additionally, the remaining rigs in NW Colorado were generally engaged in long-term, multi-well projects in the Piceance Basin 50 miles to the south of Craig. It took many months to find a drilling rig willing to mobilize to Craig, Colorado to drill the RMCCS well. Fortunately, by September of 2011, we were able to come to contract terms with Patterson Drilling rig 166. The impact of the volatility of drilling costs within the oil and gas industry was evident with the RMCCS project. When drilling actually began in January 2013, the drilling spread rate, or total daily costs for well drilling, had nearly doubled from $37,500 in 2009 to $71,000 in 2012.

TIME CATEGORY	HOURS
RIG UP/DOWN	248
DRILLING	437
REAMING	9
CORING	127
COND. & CIRC.	101
TRIPS	243
LUBRICATE RIG	30
C/O DRILL LINE	7
DEVIATION	10
WIRELINE LOG	76
RUN CSG & CMNT	37
NIPPLE UP BOP	44
TEST BOP	24
DIR. WORK	21
MISC.	192
TOTAL HOURS	**1,604**
(Days)	67

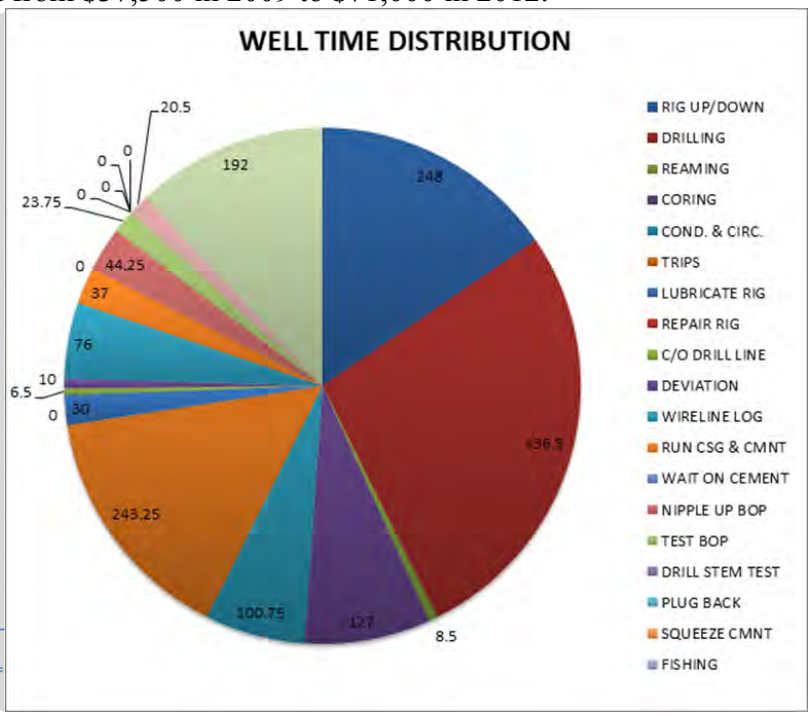


Figure 5.9 – Cost element distribution by hours.

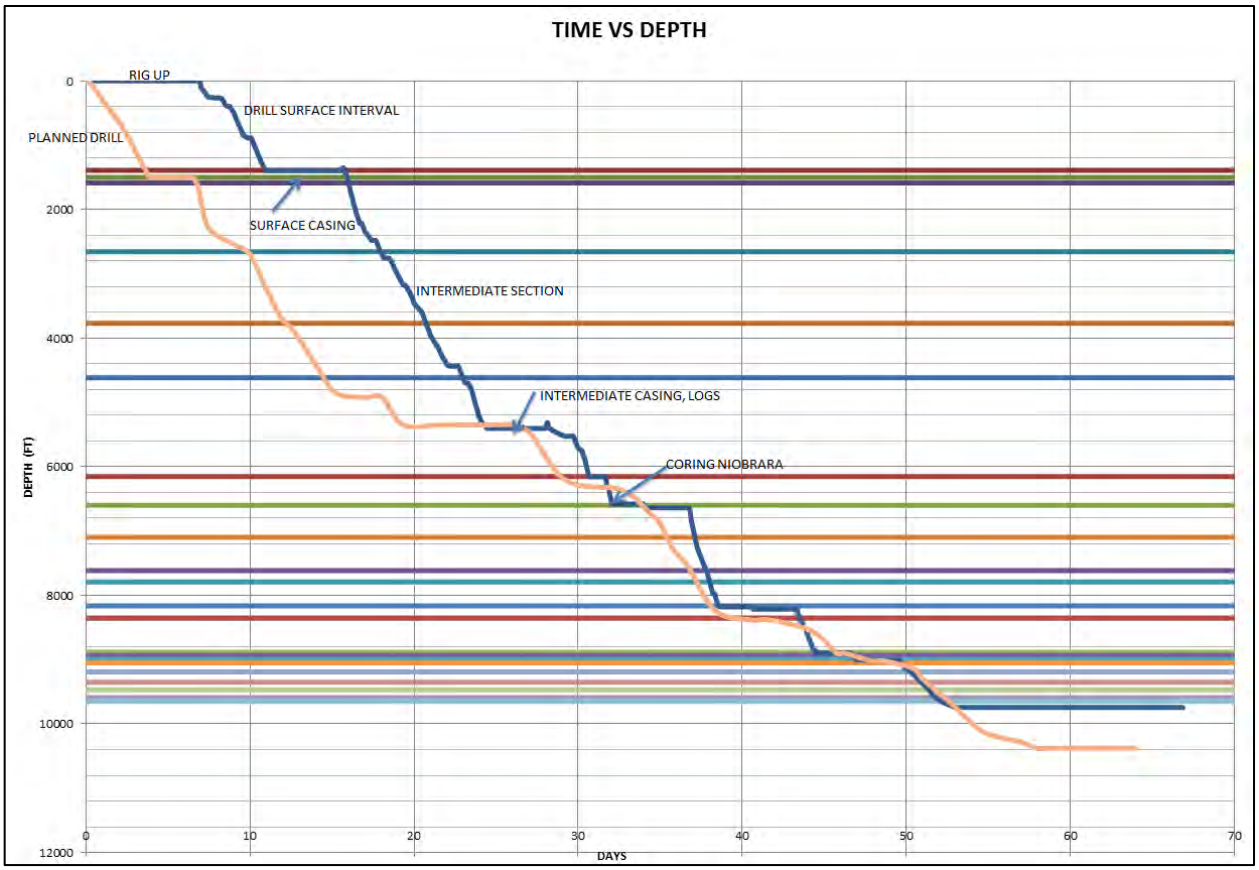


Figure 5.10 – Drilling time, projected VS actual.

- *Well construction with a fixed budget requires additional cost tracking methods beyond what is normally employed in oil and gas operations where reserve funding is readily available with approval by asset management.*

In normal oil and gas drilling operations a drilling budget, or AFE, is developed prior to initiating drilling. A contingency item of 10%-15% is included as a line item in virtually all cases. Cumulative daily costs are distributed each morning. If drilling costs are exceeding the AFE amount, the partners are contacted and if approved, additional funds are made available. In rare instances, the decision is made to stop at an intermediate point and abandon the original objective. Although projecting the final cost as drilling in progress, it is seldom rigorously done.

In the case of many scientific projects, the overall budget is fixed and cannot be exceeded. This was the case with the RMCCS well. Although there is the ability to change scope and move budget dollars between tasks, drilling expenses can escalate quickly and overwhelm a project's ability to absorb overages. Therefore, continually projecting the total costs forward to completion in drilling a well with a fixed budget is critical. Costs associated with drilling operations are in three categories: time driven, episodic and depth driven.

Time driven costs include the rig day rate, rental tools and equipment, fuel, trailers, and supervision. All combined these costs are referred to as the spread rate. The spread rate for the RMCCS well was approximately $71,000 per day. During drilling the time driven costs remaining are computed by the penetration rate time's thickness of the remaining formations, plus number of bit trips times average trip time, plus logging time, plus completion time and rig down time. Time driven costs are the dominant costs determining the episodic costs include running casing, running

geophysical well logs, well completion or plug and abandonment, rig demobilization, site restoration and reclamation.

Depth driven costs generally become components of the time driven costs and episodic costs. For example, the time it takes to come out of the hole to change drill bits and go back to bottom to resume drilling (referred to as trip time) is a function of depth. The cost to run casing is a function of depth based on the number of joints of casing required. The cost of geophysical well logs has a depth component.

For the RMCCS well the estimated cost going forward using this methodology was computed daily and provided to project partners. This allowed "what-if" scenarios to be calculated to continually adjust scope to assure there would be remaining budget to finalize all necessary work all the way through to rig demobilization and site restoration. It was using this methodology that the determination was made that there would be insufficient remaining funds to drill to the ultimate objective of 200' below the top of the Weber formation. This resulted in achieving most of the scientific objectives of the well while finishing all well related work without exceeding the available budget.

Conclusion

The drilling of the RMCCS State No. 1 well provided an abundance of critical site-specific scientific data (Appendix I includes the master well log for the well). This data is the foundation for developing a detailed geologic description of the Dakota and Entrada formations, two of the primary targets for potential future geologic storage, and their respective sealing formations. Equally important is the operational experience, lessons learned and recommended best practices gathered through the drilling operations.

6. Core analysis and interpretation with other geological and geophysical data

Core Sampling and Inventory

Due to technical and budgetary issues related to drilling, coring and core recovery, as described in previous sections, only 131 feet of RMCCS core was obtained for the project. Initial plans for the project called for 780 feet of core, from the Dakota, Entrada and Weber sandstones, and their associated seals: the Mowry, Curtis and Moenkopi shales, respectively. Sub-cores (plugs) of these three formations and their seals were to provide a comprehensive evaluation of the capacity, injectivity and seal integrity of the most promising CO_2 sequestration targets on the Colorado Plateau. The 131 feet of core obtained only included the Mowry, Curtis and Entrada Formations. However, several downhole trips with a rotary sidewall coring tool were able to obtain small plugs of the Carlile, Frontier, Dakota, Morrison, Curtis (Sand), Entrada, Chinle, Shinarump and Moenkopi Formations. Core from the Niobrara formation were also extracted and analyzed by RMCCS Partner Shell Oil (see Appendix J for these data).

Plug Acquisition

The full diameter core was transferred from the RMCCS drill site to CoreLab of Denver for acquisition of sub-core/plugs. Based on in-person consultations from Rich Esser, Tony Rice, Chris Eisinger and Dave Noe after viewing the core, sample points (n=537, including "duplicates") along the 131 feet of core were chosen. The RMCCS team elected to plug the core prior to slabbing to maximize sample size and recovery. It was also decided to plug the shale core (Mowry and Curtis) at 1.0 inches in diameter and the Entrada core and 1.5 inches in diameter in an effort to maximize recovery of coherent plugs. The three principle orientations (horizontal, vertical and 45°, relative to the axis of the core) were selected throughout the cored section to assess anisotropy of the analytical data. Where the full diameter core was deemed sufficiently coherent, multiples from a single location (i.e. immediately adjacent location) were attempted to accommodate duplicate analyses for QA/QC purposes. Table 6.1 shows the plug locations, orientations and multiples requested by the RMCCS team.

In the interest of petrophysical tests requiring larger diameter core, a 21-inch section of the RMCCS core from the Entrada Formation was spared from plugging and slabbing activities. The unadulterated, full diameter (4.0 inch) core spans from 9038 ft to 9039.75 ft. It is currently housed at the University of Utah.

Table 6.1. Requested plug attempts from RMCCS team to CoreLab. In some cases, multiples of a specific location were requested (x2, x3, x4) to accommodate duplicate analyses.

RMCCS Core plugging plan (based on observations from CoreLab visit of March 28, 2012)

1 inch diameter plugs (by at least two inches long)
1.5 inch diameter plugs (by at least three inches long)

Hor - parallel to bedding
Vert - perpendicular to bedding
45Deg - 45° to bedding

Formation	Core	Box	Depth (in feet) Hor1	Vert1	45Deg1	Hor2	Vert2	45Deg2	Hor3	Vert3	45Deg3
Mowry (~8180-8206 ft)	1	1		8180							
	1	2									
	1	3	8187	8187	8187†	8187.6	8187.6				
	1	4		8189.4		8191.7	8191.7	8191.7			
	1	5	8192	8192	8192	8194.4	8194.4	8194.4			
	1	6	8195	8195	any 1	8197	8197				
	1	7	8198	8198	8198	8199	8199				
	1	8	8201 (x2)	8201 (x2)	8201 (x2)	8203	8203				
	1	9	8204 (x2)	8204 (x2)	8205	8206	8206				
	1	10	8206	8206	8206						
Mowry (~8216-8261 ft)	2	1	8216 (x2)	8216 (x2)	8216 (x2)	8217 (x2)	8217 (x2)	8217 (x2)	8218	8218	
	2	2	8219	8219	8219	8221 (x2)	8221 (x2)	8221 (x2)			
	2	3	8223 (x2)	8223 (x2)	8223 (x2)						
	2	4	8226.8	8226.8	8226.8	8227.6	8227.6				
	2	5	8228.9	8228.9	8228.9	8230.9	8230.4				
	2	6	8233 (x2)	8233 (x2)	8233 (x2)						
	2	7	8235	8235	8235	8236	8236				
	2	8	8238	8238		8240	8240	8240			
	2	9	8241.9	8241.9	8241.9	8243 (x2)	8243 (x2)	8243			
	2	10	8244	8244	8244	8245	8245		8246	8246	8246
	2	11	8246.8	8246.8	8246.8	8249.6	8249.6				
	2	12	8250	8250	8250	8251	8251				
	2	13	8253.4	8253.4	8253.4	8254.5	8254.5	8254.5			
	2	14	8255.5	8255.5	8255.5	8258	8258	8258			
	2	15	8259.5	8259.5	8259.5	8260.6	8260.6	8260.6			
Curtis (~8896-8924 ft)	3	1	8896	8896		8897.2	8897.2	8897.2			
	3	2	8898.5	8898.5		8900.5	8900.5				
	3	3	8902.5	8902.5		8903.5	8903.5				
	3	4	8904	8904	8904	8905	8905		8906	8906	8906
	3	5	8907	8907		8908	8908				
	3	6	8909				8910				8911
	3	7	8911.8	8911.8		8913	8913.4		8914	8914	8914
	3	8	8915	8915		8916	8916	8916			
	3	9	8918	8918		8919.8	8919.8	8919.8			
	3	10									
	3	11	8924	8924							
Entrada (~9011-9046 ft)	4	1	9011 (x4)	9011 (x4)	9011 (x3)	9012 (x4)	9012 (x4)	9012 (x3)	9013.5 (x4)	9013.5 (x4)	9013.5 (x3)
	4	2	9015 (x4)	9015 (x4)	9015 (x3)	9016 (x4)	9016 (x4)	9016 (x3)	9017 (x4)	9017 (x4)	9017 (x3)
	4	3	9017.5 (x3)	9017.5 (x3)	9017.5 (x3)	9019.5 (x3)	9019.5 (x3)	9019.5 (x3)			
	4	4	9020.1 (x4)	9020.1 (x4)	9020.1 (x3)	9021.2 (x4)	9021.2 (x4)	9021.2 (x3)	9022.2 (x4)	9022.2 (x4)	9022.2 (x3)
	4	5	9023.2 (x4)	9023.2 (x4)	9023.2 (x3)	9024 (x4)	9024 (x4)	9024 (x3)	9025.2 (x4)	9025.2 (x4)	9025.2 (x3)
	4	6	9026 (x4)	9026 (x4)	9026 (x3)	9027 (x4)	9027 (x4)	9027 (x3)	9028 (x4)	9028 (x4)	9028 (x3)
	4	7	9029 (x4)	9029 (x4)	9029 (x3)	9030 (x4)	9030 (x4)	9030 (x3)	9031 (x4)	9031 (x4)	9031 (x3)
	4	8	9032 (x4)	9032 (x4)	9032 (x3)	9033 (x4)	9033 (x4)	9033 (x3)	9034 (x4)	9034 (x4)	9034 (x3)
	4	9	9035 (x4)	9035 (x4)	9035 (x3)	9036 (x4)	9036 (x4)	9036 (x3)	9037 (x4)	9037 (x4)	9037 (x3)
	4	10	9037.5 (x4)	9037.5 (x4)	9037.5 (x3)						
	4	11	9040 (x4)	9040 (x4)	9040 (x3)	9041 (x4)	9041 (x4)	9041 (x3)	9042 (x4)	9042 (x4)	9042 (x3)
	4	12	9042.8 (x4)	9042.8 (x4)	9042.8 (x3)	9043.7 (x4)	9043.7 (x4)	9043.7 (x3)			
Total Count			84	84	62	74	75	47	40	40	31
											537



Figure 6.1. "Chatter mark" left by CoreLab technicians on some RMCCS plugs.

CoreLab technicians utilized a drill press with diamond coring tools and liquid nitrogen as a drilling lubricant to attempt to cut as many of the plugs at the orientations requested (some plugs in the Entrada were drilled with a salt water solution). Due to the fractured nature of the core, in particular the shale sections, only about 60% (313 out of 537 plugs) were considered a "good" recovery by CoreLab. The remaining plug points were either not attempted by CoreLab because of the poor quality of the core section, or the plug recovery was too poor to be useable/saved. However, of the 313 recovered plugs that were labeled "good" by CoreLab, only 183 were longer than 1 inch, a length sufficient for many of the petrophysical analyses that were going to be attempted by the project. CoreLab labeled most of the plugs as an "A" on their Core Quality Index (CQI – a visual description of core grain recovery based on core quality (e.g. shattering, fracture, mud invasion, etc) and core recovery size (i.e. length)) though some of the plugs exhibited "chatter marks" (Figure 6.1), where the core barrel left grooves around the plug leaving it generally unusable for petrophysical testing.



Figure 6.2. Example photographs of plugs sampled from RMCCS core.

The RMCCS plugs were wrapped in plastic and aluminum foil, to minimize significant dehydration, and shipped to the Energy & Geoscience Institute at the University of Utah. Each plug was unwrapped, inspected, measured and photographed (Figure 6.2). From this assessment, a matrix was constructed listing all available plugs, their core depth, formation of origin, size, orientation, length, CQI, extra notations and potential for various petrophysical tests. In general, it is preferable if plugs have a 2:1 length to diameter ratio, especially for geomechanics tests. The matrix visually identifies those samples adhering to this 2:1 ratio (green icons). Likewise, certain hydraulic tests ideally should have samples of a certain length (relative permeability tests should be at least 1.5" inches in length, but more accurate results are yielded when samples are at least 2 inches in length).

Table 6.2 shows an excerpt from the sample matrix. The full matrix and all resulting data is presented in an Appendix K.

Table 6.2. RMCCS sample matrix showing physical measurements and description of each plug sampled from the full core. Based on diameter, length and CQI, each plug received a grade potential for petrophysical tests. A green icon indicates sufficient material, a red icon indicates insufficient material, and a yellow icon indicates marginally sufficient material.

Depth	Plug orientation	Plug No.	Formation	Size (inch diameter)	Max Size (inches)	Recovery Size	CQI	XRD	SEM	Petrography	Porosity	Permeability	Relative Perm	Capillary Pres
8188.17			Mowry							NMT				
8188.92			Mowry							NMT				
8191.6	Hor		Mowry	1.0										
8191.65	Vert	2V	Mowry	1.0	0.2	1	D							
8191.65	Vert	2VB	Mowry	1.0	1.1	4	B				TT	TT		
8191.85	45°	2°B	Mowry	1.0	1.3	4	B							
8192	Hor	3H	Mowry	1.0	1.0	3	B				TT	TT		
8192.1	Vert	3V	Mowry	1.0	0.9	3	A							
8192.4	45°	3°	Mowry	1.0	0.8	3	C	NMT						
8193.5			Mowry							NMT				
8194.4	Hor	3HB	Mowry	1.0	1.1	4	B							
8195.1	Hor	4H	Mowry	1.0	NR		D							
8195.1	Vert	4V	Mowry	1.0	0.3	1	D							
8195.65	45°	4°	Mowry	1.0	NR		D							
8197.3	Hor	4HB	Mowry	1.0	0.2	1	C							
8197.67			Mowry							NMT				
8198.1	Hor	5H	Mowry	1.0	NR		D	NMT						
8198.15	Vert	5V	Mowry	1.0	0.7	3	C							
8199.45	Hor	5HB	Mowry	1.0	1.6	4	B							
8199.45	Vert	5VB	Mowry	1.0	NR		D							
8200.5	Hor	7HA	Mowry	1.0	NR		C							
8200.6	Hor	7HB	Mowry	1.0	1.3	4	B							
8200.5	Vert	7VA	Mowry	1.0	0.4	2	D							
8201.1	Vert	7VB	Mowry	1.0	0.7	3	D							
8201.5	45°	7°	Mowry	1.0	0.8	3	B							
8201.5	45°	7°B	Mowry	1.0	0.4	2	D							
8203	Hor		Mowry	1.0	1.5	4	A							
8203.75	Hor		Mowry	1.0	1.5	4	A	NMT			TT	TT		
8203.83			Mowry							NMT				
8204	Hor	9H	Mowry	1.0	2.7	4	A			NMT				
8204	Hor	9HB	Mowry	1.0	1.6	4	A							
8204.3	Vert	9V	Mowry	1.0	0.9	3	B							
8204.3	Vert	9VB	Mowry	1.0	0.9	3	B							
8205	45°	9°	Mowry	1.0	NR		D							
8205	45°	10°	Mowry	1.0	1.3	4	A							
8206	Hor	10H	Mowry	1.0	1.6	4	A				TT	TT		
8206	Hor	10HB	Mowry	1.0	1.3	4	A				CL	CL		CL
8206	Vert	10V	Mowry	1.0	1.0	3	A							
8206	Vert	10VB	Mowry	1.0	1.6	4	A							
8216	Hor		Mowry	1.0										
8216	Hor	11HB	Mowry	1.0	NR		D							
8216	Vert	11V	Mowry	1.0	NR		D							

Core Slabbing

Following core plugging at CoreLab (Denver), the whole core was transferred to Triple-O Slabbing where it was slabbed to 1/3 to allow for more precise observations of petrology and sedimentary features by the team geologists. Figure 6.3 shows one box of

the seven slabbed core; all slabbed core photos are in the Appendix K. Soon after the core was slabbed, Triple-O hosted a viewing event for the RMCCS team, its partners and local media.



Figure 6.3. Sample photograph of the slabbed RMCCS core.

The slabbed core was housed at Triple-O's Denver facility for the active period of the RMCCS project. In October of 2013, the core and ownership was to be transferred to the USGS Core Research Center at the Denver Federal Center in Colorado.

In December of 2012, Dr. Daniel Soeder of the National Energy Technology Laboratory in Morgantown, West Virginia contacted the RMCCS team and inquired about the possibility of obtaining a selection of plug samples from the RMCCS well (Table 6.3). Dr. Soeder was interested in conducting "lithologic and petrophysical analyses of porosity, permeability, two-phase flow, and response to net stress on gas shales to determine how they may behave as carbon dioxide storage reservoirs after depletion". As the samples were not earmarked for analysis by the RMCCS team, they were shipped to Dr. Soeder in early 2013. All analyses performed by Dr. Soeder are presumed to be "destructive" and no expectation of sample return is expected by the RMCCS project.

Table 6.3. RMCCS plug samples sent to Dr. Soeder (NETL) for testing.

Depth (ft)	Plug orientation	Plug No.	Formation
8221	Hor	15H	Mowry
8221	Hor	15HB	Mowry
8221	Vert	15V	Mowry
8223.15	Hor	16H	Mowry
8223.15	Hor	16HB	Mowry
8223.45	Vert	16V	Mowry
8226.5	Hor	17H	Mowry

8226.6	Hor	17HB	Mowry
8241	Vert	24V	Mowry
8241	45°	24°	Mowry
8254.3	Hor	34H	Mowry
8254.3	Vert	34V	Mowry
8254.55	45°	34°	Mowry
8898.5	Hor	43HA	Curtis
8900.5	Hor	44HA	Curtis
8900.5	Vert	44V	Curtis
8903.5	Vert	46V	Curtis
8911	45°	54°	Curtis
8911.6	Hor	54H	Curtis
8911.6	Vert	54V	Curtis
8916.3	Vert	58V	Curtis
9012.1	Hor	63H	Entrada
9022.1	Hor	72H	Entrada
9022.3	Hor	72HB	Entrada
9022.5	45°	72°	Entrada
9042.55	Hor	92H	Entrada
9042.6	Hor	92HB	Entrada
9042.9	Vert	92V	Entrada
7863.00	Sidewall	99	Frontier
8515.00	Sidewall	16	Morrison

Core Analysis

The objective of the core analysis program was to obtain essential lithologic descriptions and hydraulic/geochemical/geomechanical properties of the cored rock formations. These parameters were going to be used to populate models and simulations that evaluate the potential for CO_2 storage at the RMCCS site, the region and the Colorado Plateau. The RMCCS team originally elected to perform a comprehensive suite of petrophysical tests to gather conventional petrophysical (porosity, permeability), mineralogy (XRD), chemistry (Total Organic Carbon, noble gases), physical (CT Scans, petrography, SEM), SCAL (capillary pressure, relative permeability) and geomechanics (scratch test, compressive strength, triaxial) data. The testing was going to be split between New Mexico Tech, the University of Utah and at least two commercial laboratories. However, because of budgetary constraints and analytical "overreach" (i.e. analyses that were not going to be incorporated into final RMCCS models or simulations), the planned testing was scaled back. Table 6.4 lists the petrophysical tests and number conducted by the RMCCS team on plugs sampled from the RMCCS whole core.

Table 6.4. Petrophysical tests conducted by the RMCCS project on plugs sampled from the whole core.

Analysis	New Mexico Tech	University of Utah	Service Company (TerraTek, CoreLab)
XRD	80	0	0
Petrography	41	0	0
Porosity	0	22	31
Permeability	0	22	31
Relative Permeability	0	2	4
Capillary Pressure	0	0	13
TOC	0	2	0

Total Organic Carbon (TOC)

Total Organic Carbon (TOC) analyses were performed on two samples from the Curtis Formation for the purposes of assessing CO_2 adsorption potential (CO_2 capacity) of the seal unit immediately overlying the Entrada. Table 6.5 shows the TOC results from analyses performed at the University of Utah. By comparison, the TOC contents of the Curtis Shale are significantly less than those yielded by the Niobrara Formation (TOC range from 2.35% to 4.10%).

Table 6.5. TOC results on 2 samples from the Curtis Formation, obtained at the University of Utah.

Sample ID	Formation	Sample Mass (mg)	Organic Carbon (mg)	TOC (%)
47V0 a	Curtis	88	0.128	0.15%
47V0 b	Curtis	171	0.954	0.56%
47V0 c	Curtis	128	0.583	0.46%
			Mean	**0.39%**
59H0 a	Curtis	135	0.267	0.20%
59H0 b	Curtis	128	1.106	0.86%
59H0 c	Curtis	108	0.222	0.21%
			Mean	**0.42%**

X-Ray Diffraction (XRD)

Dr. Dana Ulmer-Scholle of New Mexico Tech performed XRD analyses on 80 samples obtained directory from the core and from plugs sampled for petrophysical testing. Figure 6.4 shows XRD data for some key CO_2 sequestration-significant minerals within the Entrada Sandstone and its immediately overlying seal, the Curtis Shale. Although specific reactive transport simulations are beyond the scope of this section, the mineralogy data will be useful for determining long-term trapping mechanisms within the Entrada reservoir as well as seal efficiency of the Curtis and Mowry Shales.

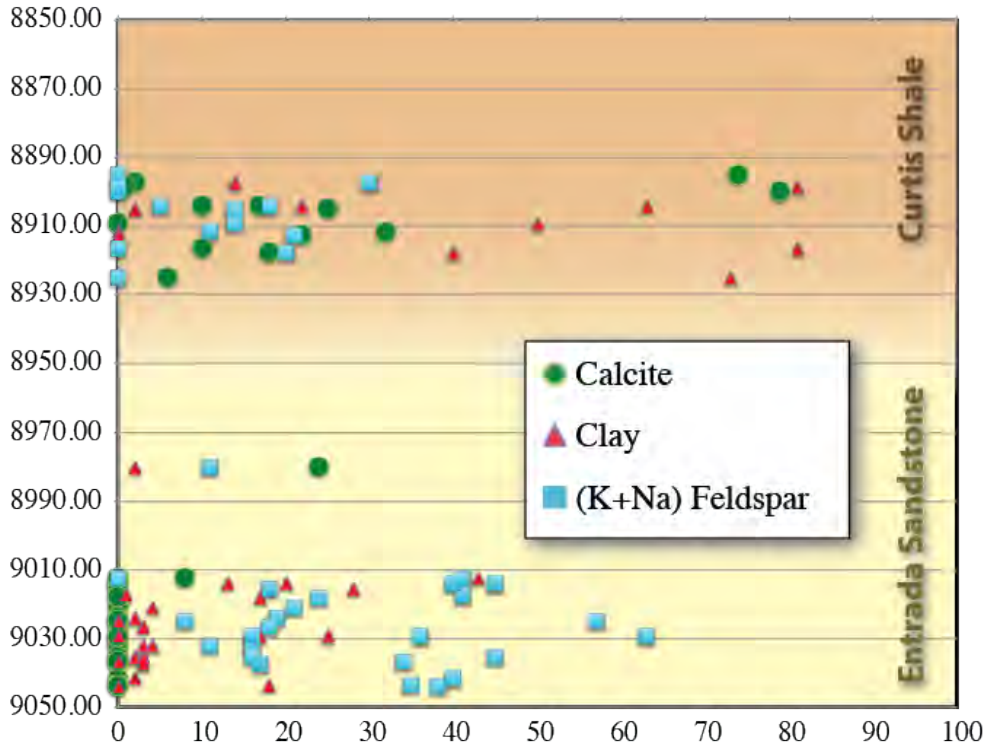


Figure 6.4. Plot of Calcite, Clay and Feldspar totals from the XRD analyses for the Entrada Sandstone and the overlying Curtis Shale. Of importance are the differences in reactive constituents between the two formations.

Spectral Core Gamma (SCG)

CoreLab performed Spectral Core Gamma (SCG) scans on the whole core when it was received from the RMCCS wellsite. The SCG System measures the natural radioactivity and is primarily used to calibrate core depths to downhole logging tools. The full SCG results from CoreLab are presented in Appendix K.

Fracture Analysis

Prior to plugging operations, the whole core was examined by CoreLab geologist Ron Cormier for lithologic/fracture descriptions. Additionally, seven core sections were scanned by X-Ray CT to determine interior structures. The full Fracture Analysis is presented in Appendix K.

Porosity and Permeability

RMCCS plugs and rotary sidewall cores were tested for (Helium) porosity and permeability using standard methods. Table 6.6 lists all of the values obtained by the University of Utah, CoreLab and TerraTek. Detailed analysis reports are included in Appendix K. All values reported in this section and in Table 6.6 were obtained using a Net Confining Stress (overburden) calculated from the depth the individual plugs were sampled. Nine unique formations were tested for porosity and permeability, but the majority of samples were from the Mowry Shale and Entrada Sandstone. The Mowry plugs yielded an average porosity of 2.25% (min=0.63%; max=5.95%) while the average permeability was 0.25 mD (min=0.07 mD; max=0.58 mD). The Entrada plugs yielded an average porosity of 8.57% (min=1.22%; max=18.60%) while the average permeability

was 15.48 mD (min=0.05 mD; max=307 mD). While anisotropy of the individual formations is difficult to assess with the limited number of oriented samples, it is worth noting that the average vertical permeability of the Entrada Sandstone is 3.83 mD, while the average horizontal permeability is 8.03 mD.

Correlating the Helium porosity values from the plugs to downhole log data is tenuous given the sparseness of the plug data. However, for the section of the Entrada core that has sufficient Helium porosity data, the values correlate well to the neutron porosity values obtained from the wireline logs (Figure 6.5).

At the net confining stress values for each sample (>3500 psi), many of the values of porosity and permeability were too low (labeled as "N.A." in Table 6.6) to be determined by the individual method or instrument. This minimum limits are generally approximately <<0.1% for porosity and <<0.001 mD for permeability.

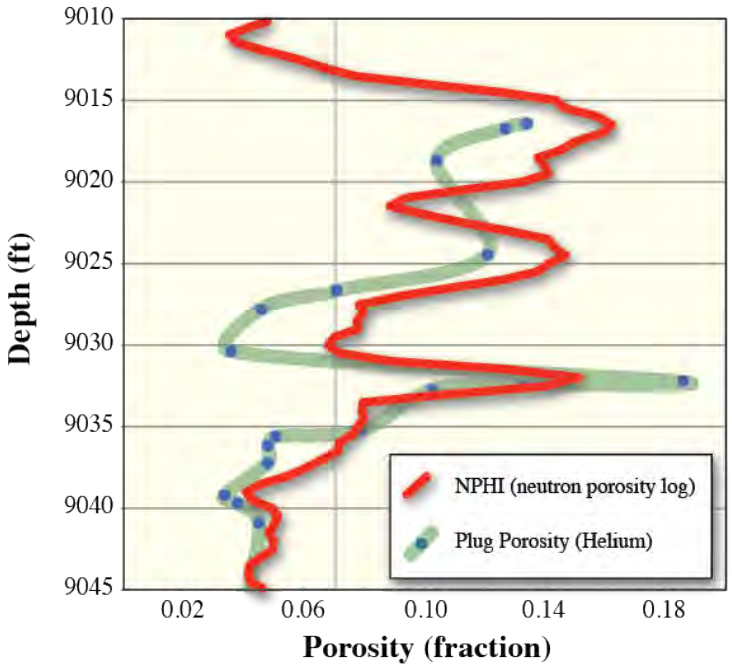


Figure 6.5. Correlation between Helium porosity values from the RMCCS plugs and the NPHI wireline log data. It must noted that there is an apparent ~3 ft offset between the two curves to maximize correlations.

Table 6.6. Porosity and Permeability results for plugs and rotary sidewall core from the RMCCS well. "N.A." indicates porosity and/or permeability values below detectable limits, at Net Confining Stress (i.e. overburden – greater than 3000 psi).

Depth	Plug (orientation) or Sidewall	Sample ID	Formation	Helium Porosity (%, confined)	Permeability (md, water/Klinkenberg)
8191.65	Vertical	2VB	Mowry	1.98	N.A.
8192	Horizontal	3H	Mowry	0.98	N.A.
8206	Horizontal	10HB	Mowry	5.40	0.09
8206	Horizontal	10H	Mowry	5.95	N.A.
8218.3	Horizontal	13H	Mowry	1.39	0.07
8228.9	Horizontal	18H	Mowry	1.55	0.00
8235	Horizontal	21HB	Mowry	1.60	0.58
8235	Horizontal	21H	Mowry	1.98	N.A.
8243.15	Horizontal	25HA	Mowry	1.29	N.A.
8258	Horizontal	36H	Mowry	0.63	N.A.
8259.5	Horizontal	37H	Mowry	1.95	N.A.
8288.00	Sidewall	42	Dakota	4.95	N.A.
8358.00	Sidewall	40	Dakota	5.66	0.01
8490.00	Sidewall	17	Morrison	N.A.	N.A.
8780.00	Sidewall	14	Morrison	N.A.	N.A.
8807.00	Sidewall	36	Morrison	5.22	N.A.
8882.00	Sidewall	35	Morrison	7.83	0.02
8896.1	Horizontal	41HA	Curtis	0.51	N.A.
8904	Horizontal	47H	Curtis	0.32	N.A.
8916.35	Horizontal	58H	Curtis	2.58	0.03
8992.00	Sidewall	34	Curtis Sand	N.A.	N.A.
9012.3	45°	63°	Entrada	11.40	1.40
9012.8	Vertical	63VB	Entrada	11.90	5.24
9012.8	Vertical	63V	Entrada	12.40	2.84
9013.3	Horizontal	64H	Entrada	13.40	2.11
9013.4	45°	64°	Entrada	12.25	5.22
9013.6	Horizontal	64HB	Entrada	12.70	4.59
9015.6	Horizontal	65HB	Entrada	10.40	0.64
9015.85	45°	65°	Entrada	12.10	3.04
9021.35	Horizontal	71HB	Entrada	12.10	13.90
9021.55	45°	71°	Entrada	11.80	3.64
9023.35	Vertical	73V	Entrada	13.10	3.41
9023.55	Horizontal	73H	Entrada	7.10	19.80
9024.65	Horizontal	74HB	Entrada	4.60	0.64
9026.7	45°	76°	Entrada	5.80	N.A.
9027.3	Horizontal	77H	Entrada	3.60	0.17
9027.45	Horizontal	77HB	Entrada	N.A.	0.18
9027.8	45°	77°	Entrada	1.22	N.A.
9029.15	Horizontal	79H	Entrada	18.60	307.00
9029.35	Horizontal	79HB	Entrada	13.30	10.66
9029.6	Horizontal	79HC	Entrada	10.30	N.A.
9032.15	Horizontal	82H	Entrada	7.87	1.41
9032.5	Horizontal	82HB	Entrada	5.05	0.16
9033.1	Horizontal	83H	Entrada	4.80	0.10
9034.1	Horizontal	84H	Entrada	4.80	0.46
9036.1	Horizontal	86H	Entrada	3.35	0.26
9036.6	Horizontal	86HB	Entrada	3.80	0.10
9037.8	Horizontal	88HB	Entrada	4.50	0.07
9042.1	Horizontal	91H	Entrada	4.20	0.05
9043.7	45°	93°	Entrada	3.48	N.A.
9380.00	Sidewall	6	Chinle	2.83	N.A.
9603.00	Sidewall	2	Shinarump	N.A.	N.A.
9675.00	Sidewall	26	Moenkopi	N.A.	N.A.

Noble Gas Tracers

The RMCCS team, with the assistance of Dr. Kip Solomon of the Geology and Geophysics Department at the University of Utah, collected eight sub-samples of core to perform noble gas tracer analyses (Table 6.7). Noble gas (i.e. ^{3}He and ^{4}He) profiles have been used successfully as analogs to evaluate gas/fluid diffusion in seal units. Though the 8 samples (from the Curtis and Entrada Formations) were sampled (directly from the core at the well site) in February of 2012, the samples are required to sit and outgas in a vacuum-tight canister for at least several months. The "head space" gas in the canister is then analyzed for the isotopic signature of the noble gases. Unfortunately, a series of breakdowns and ultimately a significant laboratory upgrade by Dr. Solomon pushed the noble gas analyses back into late 2013. As of the end of the RMCCS project, the noble gas samples have not been analyzed. However, the integrity of the vacuum vessels remains intact and Dr. Solomon is committed to the analyses of the RMCCS noble gas samples and a publication of their results at a near future date.

Table 6.7. Samples collected by Dr. Kip Solomon for Noble Gas profiles.

Sample ID (Depth(ft))	Formation	Exposure Time (s)	Total Mass (g)	Mass in Flask (g)
8901	Curtis	1020	1417.13	287.53
8907	Curtis	5880	1403.44	215.04
8913	Curtis	6720	1026.26	215.16
8919	Curtis	6720	1268.26	234.36
9020	Entrada	4560	1096.6	208.63
9026	Entrada	4980	N.A.	197.67
9032	Entrada	5340	892.6	241.19
9038	Entrada	5820	631.3	217.42

Capillary Pressure

Thirteen samples (plugs) from the RMCCS core were selected for capillary pressure measurements, two of which were duplicates to evaluate quality control between the two service companies performing the analyses (TerraTek and CoreLab). Additionally, the three plug samples sent to CoreLab were analyzed using both high-pressure mercury injection method and the centrifugal method. Table 6.8 lists the samples for which capillary pressure measurements were performed.

Table 6.8. RMCCS Plug samples for which capillary pressure values were determined.

Sample ID	Service Company	Method
21HO	TerraTek	HPMI
36HO	TerraTek	HPMI
37HO	TerraTek	HPMI
41HA	TerraTek	HPMI
48HO	TerraTek	HPMI
63DO	TerraTek	HPMI
63VO	TerraTek	HPMI
64HB	TerraTek	HPMI
79HO	TerraTek	HPMI
93DO	TerraTek	HPMI
64HO	CoreLab	HPMI & Cfg
21HB	CoreLab	HPMI & Cfg
10HB	CoreLab	HPMI & Cfg

HPMI: High Pressure Mercury Injection
Cfg: Centrifugal

Complete mercury injection and centrifuge capillary pressure results are presented in the Appendix K. Figure 6.6 and Figure 6.7 show the capillary pressure (drainage) curves for the Entrada and Mowry plugs, respectively (TerraTek analyses only). Overall, the Corelab and TerraTek data yield entry pressures for the shales (Mowry and Curtis) between 3,357 and 10,031 psi, with a mean of 7085 psi. In general, the capillary pressures curves suggest that the Mowry and Curtis Shales will act as good CO_2 seals provided the entry pressures are not exceeded. Note: Capillary pressure curves from TerraTek and CoreLab on duplicate samples (Figure 6.8 and Figure 6.9) show good agreement between the two laboratories.

The mercury injection method yields pore throat size distributions that are expected for shales and sandstones.

Figure 6.10 shows typical pore throat size histograms for the two rock types. In general, the shales yield pore throat sizes ranging from 0.002 to 0.05 μm in diameter. The sandstones yield pore throat sizes greater than 0.05 μm in diameter.

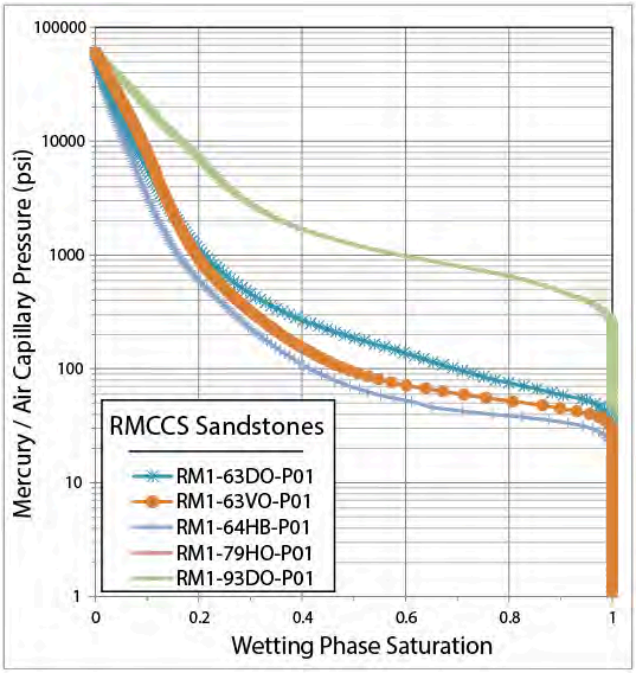


Figure 6.6. Capillary pressure curves for the Entrada Sandstone plugs sampled from the RMCCS core (TerraTek analyses).

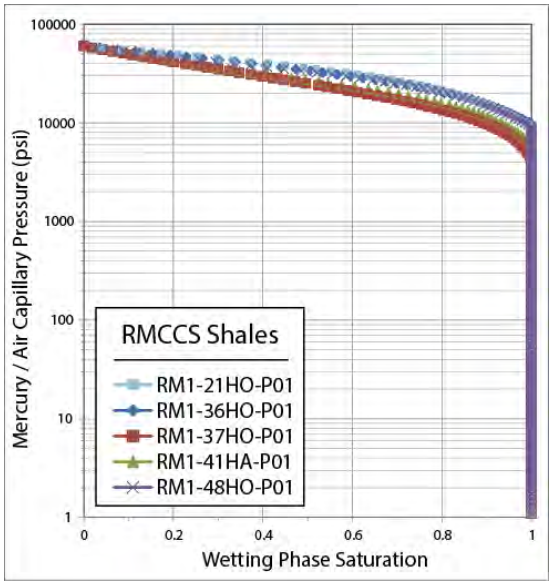


Figure 6.7. Capillary pressure curves for the Mowry Shale plugs sampled from the RMCCS core (TerraTek analyses).

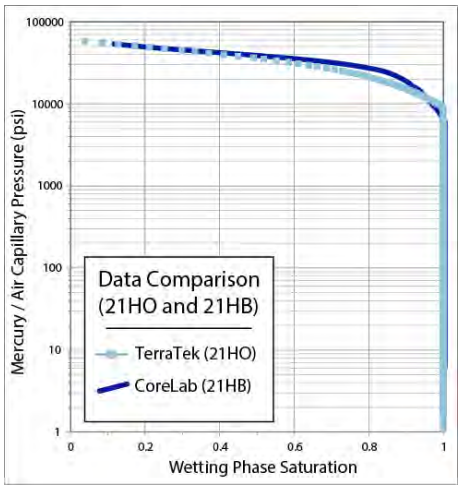


Figure 6.8. Data comparison of Capillary Pressure curves between TerraTek and CoreLab for plug 21H.

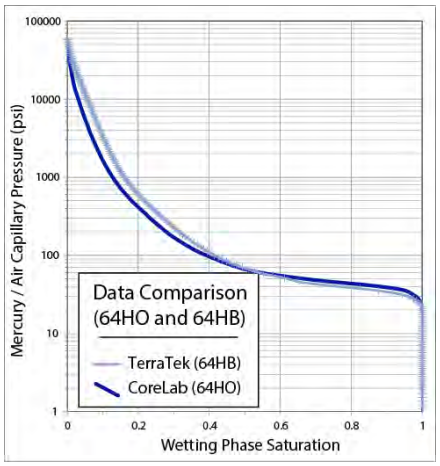


Figure 6.9. Data comparison of Capillary Pressure curves between TerraTek and CoreLab for plug 64H.

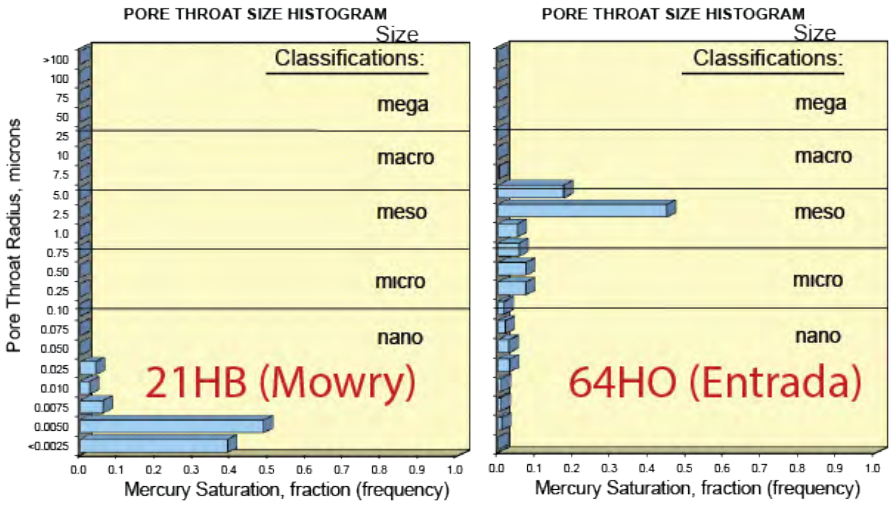


Figure 6.10. Typical pore throat size distribution for RMCCS shales (left) and sandstones (right).

Relative Permeability

TerraTek performed unsteady-state relative permeability analyses on plug samples 63°, 63V, 64HB and 79H (Figure 6.11).

The University of Utah performed *steady*-state relative permeability analyses on plug samples 73H (Figure 6.12) and 73V. Unsteady-state relative permeability tests were chosen for the TerraTek samples due to the prohibitively high cost and difficulty of obtaining steady-state results. The full analytical results are in Appendix K.

For the four Entrada samples tested by TerraTek, the relative permeability curves are not exceptionally different, despite all three orientations (45°, horizontal and vertical) being represented. Although a simulation of the relative permeability outcomes are beyond the scope of this section (see the section on model development), this is suggestive that anisotropy will not have a significant impact. The data also indicates that the irreducible water saturation is greater than 50%.

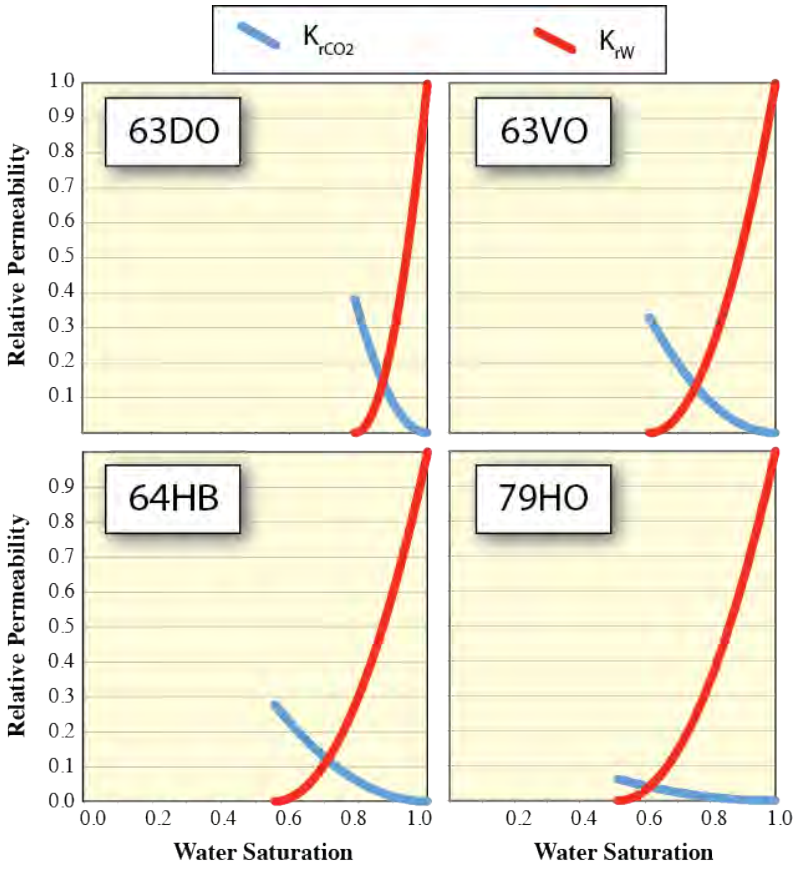


Figure 6.11. Relative Permeability (unsteady state) plots for the 4 Entrada samples analyzed by TerraTek.

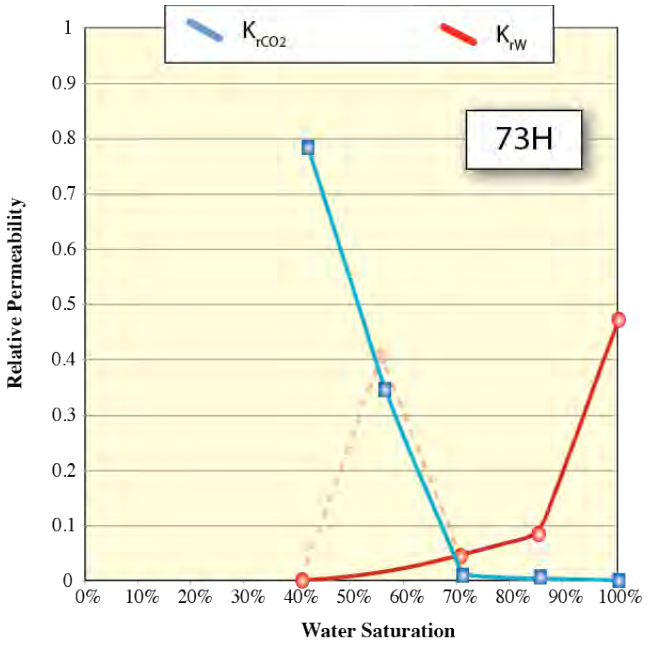


Figure 6.12. Preliminary relative permeability (steady-state) curve for plug 73H analyzed at the University of Utah.

Samples for petrographic thin-sections were obtained by Dr. Dana Ulmer-Scholle of New Mexico Tech. Detailed descriptions of the petrographic results, including lithology, depositional environment, diagenesis, porosity analysis, and photomicrographs are posted on the RMCCS website, http://rmccs.org, under the link "RMCCS Petrographic Results," and will also be submitted for publication as a Topical Report (for those seeking this report later, the senior author will be Dana Ulmer-Scholle, and the title of the report will be "Petrographic Analysis Results Associated with Characterization of the Most Promising Sequestration Formations in the Rocky Mountain Region"). A brief summary of selected results for the Dakota Sandstone is provided in Appendix L of this report. The following are examples from this and other selected formations:

Mowry Formation petrographic results

Depositional Environment:

Most of the thin sections are dominated by silty shales and shaley siltstones.

One of the reasons that the water depth is interpreted to be great (deep) is due to the lack of an overall diverse or abundant fauna within these units. For the most part, siliceous, pelagic radiolarians are a dominant microfossil in this section of the core. The shales in the section are composed of illite and mixed layered clays (I/S). X-ray diffraction was not done on these units, so the identification of these clays is based on petrographic observations. Many of the shale zones also appear to have been partially silicified, resulting in hardening (more brittle) of some of the shale zones. Others also contain carbonate (both calcite and dolomite).

Diagenesis:

An idealized diagenetic sequence was developed for the rocks of the Mowry formation. Compaction was not a single event, but rather shows a progression during burial. The following are the diagenetic events in order of their occurrence based on cross cutting relationships:

- Pyrite replacement of organics, grains and groundmass;
- Minor illite and chlorite cements (rare);
- Phosphate cements and phosphate-replaced feldspars and other grains (sedimentary bioclasts and rock fragments);
- Quartz and plagioclase overgrowths. Also minor euhedral megaquartz replacements;
- Poikilotopic calcite cements filling interparticle porosity in sandy laminae and burrow fills;
- Silicification and phosphatization of shales;
- Calcite replacing radiolarians, VRFs and feldspars;
- Plagioclase alteration to sericite;
- Compaction (due to overburden):
    - Wispy pressure solution, horizontal stylolites, flattened grains and compactional drape,
    - Fractures (partially to completely filled with calcite, minor gypsum and matrix). These fractures commonly show multiple generations of opening and filling;
- Euhedral to subhedral dolomite cements and oil migration;
- Leaching of feldspars and radiolarians;
- Anhydrite and gypsum cements;
    - Compaction (due to compressional tectonics): Horizontal, shear fractures filled with calcite cement,
    - Vertical stylolites.

Dakota Formation petrographic results

Based on one thin section, the conglomeratic nature of the sediments and the composition (quartz, quartzite, feldspars and chert/chalcedony), indicate that these deposits were formed most likely in a fluvial or alluvial channel deposit feeding from highlands to the west of the Craig well site. The distance is moderately far because of the dominance of quartz grains and the scarcity of feldspars and other grains.

Diagenesis:

The diagenetic sequence for the one thin section made from Dakota Formation was:

- Early feldspar (both K-spar and plagioclase) overgrowths
- Quartz overgrowths
- Leaching of K-spar and chert/chalcedony grains
- Kaolinite and illite cements
- Pyrite replacement (very minor)

Because of the early quartz cementation, the sands were well cemented prior to significant burial, and few compactional fabrics were found.Porosity makes up about

12% of the thin section with most of the porosity being secondary intraparticle, vuggy and intercrystalline (10%) and primary interparticle (2%).

Morrison Formation petrographic results

The plug was probably taken from the Salt Wash member of the Morrison Formation (but the Brushy Basin member is possible). The thin section is dominated by pebble-sized chert clasts and quartz sand. A probable depositional environment was a high-energy fluvial channel or braided stream environment. All of the less durable clasts were removed both mechanically and chemically.

Diagenesis:

Like the Dakota Formation, we only had one sample from the Morrison Formation to characterize its diagenesis. The observed diagenetic sequence was:

- Quartz overgrowths on monocrystalline quartz grains
- Leaching of unstable grains and minerals like dolomite and microcrystalline quartz
- Kaolinite and illitic (minor) clays are found in both primary and secondary porosity
- Fracturing
- Calcite fracture fills
- Oil migration

Porosity is made up of both primary interparticle and secondary fracture, dolomoldic, biomoldic and intraparticle. Primary porosity dominates over the secondary porosity.

Curtis Formation petrographic results

Depositional Environment:

Burrows and abundant fauna indicate well-oxygenated conditions and normal salinity. Scattered grains like ooids indicate a nearby high-energy shallow water environment. Mud clasts and coarsely crystalline dolomite clasts were ripped up from a intertidal to supratidal environment during storms. Fauna includes: brachiopods, crinoids, echinoids, pelecypods, ostracods, rare foraminifera, calcispheres, and sponges. Glauconite is very common in these sediments and is indicative of slow sediment accumulation rates in marine shelf settings.

Diagenesis**:**

A generalized paragenetic sequence for the Curtis slides is:

- Isopachous, fibrous marine calcite cements,
- Glauconite, chert/chalcedony and phosphate replacement pellets, bioclasts and grains and filling porosity within bioclasts on the sea floor,
- Syntaxial overgrowths and blocky cements on echinoid and crinoid debris,
- Pyrite replacement,
- Soft-sediment deformation,
- Dolomite cements,
- Leaching of grains and matrix,
- Gypsum/anhydrite and chalcedony replacement of matrix and grains,
- Compaction associated with fractures, horizontal stylolites and wispy pressure solution,

- Calcite filling of fractures,
- Dolomite cements and hydrocarbon migration
- Horizontal compression producing vertical stylolites

Porosity within this unit is very limited due to the lack of early quartz cementation and extensive compaction. The porosity that is in this slide is minor primary intercrystalline and intergranular and secondary microfracturing, fracturing and intraparticle porosity.

Entrada Formation petrographic results

Overall, the Entrada Formation in the core is dominated by large cross-bed sets interbedded with a few planar-laminated sections. The cross bedding are the dunes and planar units are probably the playa deposits.

Diagenesis**:**

The diagenetic sequence developed for the thin section from the Entrada Formation varied very littlewithin the thin sections. The sequence was:

- Minor quartz overgrowths on grains
- Minor pyrite replacement of organics and matrix
- Illite cements incompletely coat grains
- Quartz and feldspar (less common) overgrowths fill primary porosity and provide support to the sediments
- Kaolinite cements
- Euhedral, zoned dolomite and anhydrite cementation
- Minor titanite (sphene) cementation and replacements of dolomite
- Leaching of unstable grains like feldspars and rock fragments (volcanic and sedimentary
- Overburden compactional fabrics include fractures, wispy pressure solution seams and stylolites. Fractures are filled:
  - First with euhedral, baroque dolomites and
  - Followed by dogtooth calcite spars
- Leaching associated with fracturing. Both the dolomite and calcite fracture fills are stained by hydrocarbons
- Hydrocarbon migration and filling of late formed pores
- Overburden compaction. Unlike the other units, there are few fabrics indicating compressional shortening of the region. It may be due to the extensive silicification of the unit.

Porosity ranges from less than 1% to over 15% of the thin sections. Both primary and secondary porosity are common. Of the primary porosity types, intergranular and intercrystalline, the most important factors controlling porosity preservation was the relationship between the amount of quartz cementation and the timing of compaction. The key to porosity in this unit was to have enough quartz overgrowths to support the rock during compaction, but not enough to fill all the pore spaces. Porosity in the upper parts of the core was significantly higher than the lower sections of the core where compaction had larger impacts. Intercrystalline porosity is formed within kaolinite books. While this doesn't have a large impact on the overall porosity, the kaolinite does impact the permeability of the unit by possibly blocking pore throats. Secondary porosity types include moldic, fracture and intraparticle. While fracture

porosity enhances permeability and porosity, moldic and intraparticle can improve the porosity, but depending on the interconnectivity of the molds, the impact on the permeability may be minimal.

Chinle Formation petrographic results

The plug the thin section was made from may be from the Chinle Formation, but there is some uncertainty about it.

Diagenesis**:**

The diagenetic sequence in the one plug from the Chinle(?) Formation is:

- Minor illite cements with iron staining
- Quartz overgrowths
- Leaching of feldspar grains
- Kaolinite and dickite (similar to kaolinite compositional, but usually larger, coarser vermicular books)
- Quartz overgrowths continued
- Compaction produced microstylolites and compromised crystal boundaries
- Hydrocarbon staining.

The porosity within this sample is good, and it consists of a combination primary and secondary pores. Primary porosity is intergranular and intercrystalline, and secondary porosity is moldic after dissolution of feldspars and sedimentary rock fragments.

Moenkopi(?) Formation petrographic results

Based on previous literature, a sample from the Moenkopi Formation in the area around the Craig well site should be a terrestrial siltstone, sandstone to conglomerate, but the sample provided for thin section is none of those. It is a marine shale that was deposited on a distal platform or in a basin due to the grain size and fauna.

The slide appears to have Inoceramid fragments/prisms in it in addition to siliceous radiolarians, foraminifera and ostracods. If the prisms are from Inoceramid sp., then this slide has to be Cretaceous in age and probably from the Mowry Formation. Could there be a fault between the previous sample and this one? It is something that should be investigated geophysically.

Diagenesis**:**

The diagenetic sequence for the Moenkopi(?) sample is:

- Minor quartz replacements;
- Pyrite replaces matrix and bioclasts
- Kaolinite infills of foraminifera chambers
- Calcite fills the remaining tests of the foraminifera tests
- Compaction associated with wispy pressure solution and possible fracturing

The only visible porosity in this sample is secondary fracture porosity. It may result from plugging or it may be natural.

7. Database assembly and static model development

Schlumberger Carbon Services and the Colorado Geologic Survey (CGS) worked together to develop a static geologic model in Petrel of the Sandwash Basin and Piceance Basin in northwestern Colorado (Figure 4.1). The model was developed to properly assess the geologic structure, CO_2 storage capacity, CO_2 injectivity, and CO_2 confinement of the Sandwash Basin and Piceance Basin. In order to develop this geologic model, geologic and geophysical data was integrated and ultimately used to characterize potential repositories, traps, and sealing mechanisms that would be needed to design and implement a CO_2 storage project.

Like many geologic models, this model was developed in stages and was updated when new data became available. Phase 1 of the model was constructed prior to the drilling of the stratigraphic test well RMCCS State #1 (Craig Project Site) and was used, from a CO_2 storage perspective, as a tool to understand the geological characteristics of the Sandwash Basin and Piceance Basin. This geologic understanding was used to shortlist suitable locations to drill RMCCS State #1 which ultimately provide valuable geologic information specific to a CO_2 injection scheme. This model was also used for a well prognosis of RMCCS State # 1 to estimate likely conditions (formation tops and associated geological characteristics) to be encountered while drilling at the location. Once RMCCS State # 1 was drilled, new well data and 2D seismic survey data became available, which allowed for subsequent more detailed site specific Phase 2 modeling.

Figure 4.1 displays the Regional Model area and the two subareas (Geostatistical Model and Simulation Model) which were utilized to meet the RMCCS modeling project objectives. The below points and Table 7.1 summarize the three model areas. For structural consistency across multiple scales, the structural control for Geostatistical Model grid and Simulation Model grid was extracted from the Regional Model grid. The Regional Model was built first than scaled down into the Geostatistical Model and then to the Simulation model to meet project objectives that required a finer scale around RMCCS State # 1.

- **Regional Model -** A 3D structural framework model was generated for this model area with the main structural control surfaces being provided by CGS. This area covers an aerial extent greater than the available petrophysical data. This model area is 108 miles x 83.5 miles.
- **Geostatistical Model** – This local subarea of the Regional Model covered by the available petrophysical data is roughly 40 mile x 40 mile centered on the stratigraphic test well (RMCCS State # 1). This model was used for geostatistical analysis of petrophysical properties.
- **Simulation Model -** This subarea of the Geostatistical Model was the area used for simulation work and porosity and permeability stochastic modeling. Simulation engineers at the University of Utah (UU) specified a 20 mile x 20 mile area centered on RMCCS State # 1 to be appropriate for the project objectives.

Table 7.1: Geocellular Model Area Grid Summary

Model Area	Model Size (mile)	X-Y Cell Size (feet)	Total Cells (Dakota, Entrada, Weber) (Y, X)	Vertical Cell Thickness (Z)
Regional Model	108 x 83.5	1000 x 1000	570 x 441	Selected for each zone based on geophysical logs
Geostatistical Model	40 x 40	500 x 500	216 x 211	
Simulation Model	20 x 20	100 x 100	1056 x 1056	

During the development of the Regional Model, 15 formation surfaces were modeled. These formation surfaces were the structural framework for subsequent stochastic property modeling (porosity and permeability) of 7 formations in all three model areas (Table 7.2). Of these 7 formations, the Dakota, Entrada and Weber were the primary formations of interest because they are the Potential CO_2 injection Reservoirs.

Table 7.2: Modeled Formation Surfaces and Formations with Property Modeling Results

Modeled Formation Surface	Formation with Property Model Results			Formation Notes
	Regional Model	Geostatistical Model	Simulation Model	
Mesa Verde (Surface DEM)				Digital Elevation Model
Mancos				
Marapos				
Niobrara				
Carlisle				
Frontier				
Mowry				
Dakota	x	x	x	Potential CO_2 injection Reservoir
Morrison	x	x	x	
Curtis	x	x	x	
Entrada	x	x	x	Potential CO_2 injection Reservoir
Chinle	x	x	x	

Phosphoria	x	x	x	
Weber	x	x	x	Potential CO_2 injection Reservoir
Maroon				

Property modeling results (porosity and permeability) from all three modeled areas were utilized to provide the site specific foundation for subsequent RMCCS project objectives. The Regional Model was built first, then scaled down into the Geostatistical Model and then to the Simulation model to meet project objectives that required a finer scale around RMCCS State # 1.The subsequent RMCCS project objectives are listed below:

- Capacity assessment (Pore Volume Distribution) in the Sandwash Basin (Section 8 of this report) (Utilized Regional Model)
- Uncertainty assessment workflow (Section 9 of this report) (Utilized Geostatistical Model)
- Simulation and risk assessment (Section 10 of this report)(Utilized Simulation Model)
- To support regulatory and permitting requirements (Utilized all model areas).

Phase 1 Static Model Development (Before Drilling RMCCS State # 1)

The RMCCS Petrel static model development began with acquiring the data types listed below from various sources such as IHS and from the State Geologic surveys. Before this data was imported into Petrel, it underwent a QA\QC process to ensure its reliability and relevance to the project.

RMCCS Phase 1 Model: Database Assembly

The data types below were incorporated into the Petrel model (Figure 4.6):

- Well names, type and coordinates (X, Y, Z, TD, TVD) (4202 wells)
- Well deviation surveys
- Well formation tops (Table 3)

Table 7.3: Formation Tops Used in the Model

Modeled Formation Surface	Number of Well Tops used in Regional Model
Mancos	319
Marapos	346
Niobrara	553
Carlisle	504
Frontier	506
Mowry	488
Dakota	523
Morrison	479
Curtis	381
Entrada	387
Chinle	253
Phosphoria	198
Weber	201

- Selected Applicable Well logs – Within a 40 mile proximity to RMCCS State # 1 (Geostatistical Model area), a well log search focus was for porosity, resistivity, and gamma ray logs because they are required for petrophysical analysis which computes permeability. Based on the available data from this search, 20 wells were selected for petrophysical analysis. Additional logs selected for incorporation to the model included density, neutron, sonic, SP and caliper.
- Cultural Data
    - Oil and gas activity
    - Sandwash basin fault locations
    - Dakota, Entrada and Weber Outcrop locations
    - Digital elevation model (DEM)
    - Power plant locations (3 within the Regional Model Area)
    - Local roads and highways

RMCCS Phase 1 Model: Model Development

Phase 1 of the model was constructed prior to the drilling of RMCCS State # 1 and was used as a tool to understand the local and regional geological characteristics (porosity, permeability and pore volume) of the Sandwash Basin and Piceance Basin from a CO_2 storage perspective. This geologic understand was used to shortlist suitable locations to drill RMCCS State #1 which ultimately provide valuable geologic information specific to a CO_2 injection scheme. This model was also used for a well prognosis of RMCCS State # 1 to estimate likely conditions (formation tops and associated geological characteristics) to be encountered while drilling at the location. A summary of the Phase 1 model development steps are presented below:

1. After a rigorous QA\QC process, relevant data was uploaded into Petrel.
2. The Regional Model area was defined.
3. With the guidance of CGS, who has unique geological expertise in the area, formation surfaces were generated to fit the known local geology characteristics and surface outcrop locations.
4. The generated formation surfaces were the foundation for a structural framework geocellular model.
5. Available log data (porosity, resistivity, and gamma ray logs) were utilized for petrophysical analysis, which calculated a permeability log. Much of the available log data was of early vintage, limited and unreliable. Based on the proximity to RMCCS State # 1 and the available budget, 20 wells with appropriate log data, in a 40 mile proximity to RMCCS State # 1, were selected for advanced petrophysical analysis (Figure 4). At these wells, available data varied but several wells had density and sonic data available for porosity computation. Before drilling RMCCS State # 1, these 20 wells represented the best information as to porosity and the derived permeability in the area around RMCCS State # 1. The spatial extent of these wells defined the extent of the Geostatistical Model area and an associated finer scale geocellular model was generated.
6. The porosity and permeability data at these 20 wells were upscaled into the Geostatistical Model cells (Dakota, Entrada and Weber Formations).
7. Using these 20 selected wells, variogram analysis was conducted to understand the variation in porosity as a function of separation distance between wells. It was also used as means of determining directions/degree of anisotropy. The results of this analysis are presented below in Table 4.

Table 7.4: Log Porosity Statistical Summary

Formation	Porosity Mean	Porosity Standard. Deviation	Variogram Analysis		
			Major Range	Minor Range	Azimuth
Dakota	0.102	0.046	30,979	23,595	141
Entrada	0.085	0.036	29,177	29,144	160
Weber	0.053	0.022	31,182	29,729	160

1. Using the variogram parameters, Sequential Gaussian Simulation (SGS) was then used to populate the porosity values to each grid cell

within the Dakota, Entrada and Weber throughout the Geostatistical Model and Regional Model areas.

2. Formation Pore Volume (PV) (ft^3) was calculated individually for the Dakota, Entrada and Weber Formations via the below simple calculation:
    - Formation PV=Formation SUM(Cell Pore Volume=Cell Volume*Cell Porosity)
3. Formation Permeability Thickness (Kh) (mD-ft) was calculated individually for the Dakota, Entrada and Weber Formations as a proxy for well injectivity. While KH serves as a good proxy for injectivity on a localized basis, long term injectivity is highly dependent on lateral connectivity of pore space. Therefore, long term injectivity estimates should be verified with numerical simulation. Formation Kh, localized at the planned RMCCS State # 1 well location was calculated via the below simple calculation:
    - Formation Kh (RMCCS State # 1)= At RMCCS State # 1, Formation Vertical SUM (Cell Height*Cell Permeability)
    -

Phase 2 Static Model Development (After Drilling RMCCS State # 1)

RMCCS Phase 2 Model: Database Assembly

The data types below were appended to the already existing Petrel model:

- RMCCS State # 1 coordinates (X, Y, Z, TD, TVD)
- RMCCS State # 1 Wireline logs and associated Elemental Analysis (ELAN) data provided excellent porosity and permeability data.
- RMCCS State # 1 Core Analysis results
- RMCCS State # 1 Well Tops
- 12 recently depth converted 2D seismic surveys within the Simulation model area. These lines were converted from time to depth by Schlumberger WesternGeco. Two of these lines were newly acquired and cross directly at RMCCS State # 1.

RMCCS Phase 2 Model: Model Development

Once RMCCS State # 1 was drilled, new well data and 2D seismic survey data became available. The new data collected from RMCCS State # 1 was more specific to a CO_2 injection project than previous data that had already been incorporated into the model. RMCCS State # 1 also provided excellent porosity and permeability data, which when benchmarked to the petrophysical analysis of the 20 wells in the Geostatistical model area, showed that the initial petrophysical analysis was accurate. With this new data, Phase 2 of modeling was now able to move forward and the model was updated with this valuable data. A summary of the Phase 2 model development steps are presented below:

1. After a rigorous QA\QC process, relevant data acquired from RMCCS State # 1, was uploaded into Petrel.

2. CGS, who has unique geological expertise in the area, regenerated the formation surfaces with the new well tops from RMCCS State # 1 and from interpreted horizons interpreted from the recently depth converted 2D seismic survey lines. These generated formation surfaces were the new foundation for a structural framework geocellular model.
3. A new geocellular model was regenerated for the Regional Model area and the finer scale Geostatistical Model area.
4. The 20 wells with porosity and permeability data in the Geostatistical Model area were compared to results from RMCCS State # 1 and showed the initial petrophysical analysis was accurate.
5. From these 20 wells and RMCCS State # 1, porosity data were upscaled into the new Geostatistical Model cells (Dakota, Entrada and Weber Formations).
6. Given the addition of spatial porosity data from RMCCS State #1 to the 20 selected wells, the previous variogram analysis was reviewed. This review concluded that the addition of RMCCS State # 1 did not significantly impact the previous variogram analysis.
7. When conducting property modeling within the Geostatistical Model area there is a great deal of uncertainty between known data points because there are only 20 wells and RMCCS State # 1, with porosity and permeability data available in this large area (40 mile x 40 mile). Because these wells are spaced so far apart, correlation ranges for porosity extracted from experimental variograms were very long and not felt to be representative of actual heterogeneity. Because of this poor spatial sampling an uncertainty analysis was conducted to understand how changes in variogram parameters ultimately affect the porosity and permeability results of SGS within the geocellular model areas. The results showed this to be a useful proxy to understand the spatial geologic uncertainty and how it impacts understanding of porosity distributions.
8. A finer scale geocellular model was generated for the Simulation Model area.
9. Using the results from the above described variogram uncertainty analysis, the P50 set of variogram parameters were selected. Using these parameters, SGS was then used to populate the porosity values to each grid cell within the Dakota, Entrada and Weber Formations of the Simulation Model area, the Geostatistical Model area and the Regional Model area.
10. Pore Volume (PV) ft3 for the Dakota, Entrada and Weber Formations were recalculated.
11. Permeability-Height (KH) mD-ft, at the RMCCS State # 1 location was calculated with the newly acquired data from RMCCS State #1 for the Dakota, Entrada and Weber Formations.

12. These results were used to support subsequent RMCCS modeling objectives as described previously.

8. Capacity assessment

The Geological Surveys of the four states in which the Colorado Plateau Region is located, AZ, CO, NM and UT, were tasked to improve the regional geologic assessment of the listed formations. That was accomplished by generating structure and thickness contour maps for each of the formations for which they were responsible (Appendices N, O, P, & Q). These maps were not just based on interpolating well-derived data but also incorporated additional available information and studies. In addition, each of the partnering geologists contributed in-depth, sedimentary basin expertise during the compilation of the regional geology. Besides digital contour maps, the surveys also provided regional porosity data and geothermal gradient values.

Methodology and Workflow

Storage capacity was estimated through the volumetric method (Atlas III; U.S. DOE 2010) using the following formula: $GCO_2 = A_t h_g \Phi_{tot} \rho E_{saline}$. This formula generates the CO_2 storage-resource, mass estimates (GCO_2); based on combining data for the total area (A_t), gross formation thickness (h_g), total porosity (Φ_{tot}), CO_2 density (ρ) and the storage efficiency factor (E_{saline}). The first two input parameters account for the total bulk volume; the CO_2 density converts the reservoir volume of CO_2 to mass while the storage-efficiency factor reflects the fraction of the total pore volume that will be occupied by the injected CO_2.

The University of Utah, in cooperation with the State Geological Surveys, developed a five-step workflow method for processing the regional data. This workflow combined GIS procedures and spreadsheet calculations, to generate storage capacity estimates and convert the input data into the by NETL predefined NATCARB Atlas format (Table 8.1). The details of each step can be found in the 'Regional Significance' Topical Summary Report attached as Appendix M. The regional capacity estimates describe the numbers derived for the saline formations of interest occurring in the northern UT and CO sedimentary basins (Uinta, Piceance and Sand Wash Basins) and those occurring in the in the basins of the Four Corners area of AZ, UT, CO and NM (San Juan, Black Mesa, Paradox basins). See Appendices N, O, P and Q for capacity assessment details for Arizona, New Mexico, Utah and Colorado, respectively. The "local storage capacity estimates" refer to those derived from the small-scale geocellular model of the specific Sand Wash Basin site characterization study in northwestern Colorado.

The first step for the regional workflow consisted of extracting depth and thickness values from the contour maps by converting the data to 1–km^2 gridded data using GIS tools. After the grid attribute values were converted to point data, they were further manipulated in a spreadsheet. This spreadsheet – the EGI capacity calculation spreadsheet – contained a macro that generated CO_2 density values based on temperature and pressure data derived from the depth values. The CO_2 capacity numbers, at three different efficiency factors (0.51%, 2% and 5.4%), were derived by combining the CO_2-mass values and the available pore volume derived from thickness, grid cell area and porosity for each record. These capacity estimates were further manipulated in GIS to resolve data problems that occurred along State Boundaries and to integrate the points for each formation into a single feature class across State Boundaries. Finally the data were

aggregated into the 10km^2 predefined NATCARB polygons and all the data, including outlines of the area representing the spatial extent of the formations, were integrated into a single GIS geodatabase.

Table 8.1: Major methodology workflow steps:

Workflow step	Processing environment	Data Scale	Responsibility
1. Regional Data Preparation	GIS	Regional	AZ, CO, NM & UT Geological Surveys
2. CO_2 storage capacity calculations	Spreadsheet	1 km^2	State Surveys and University of Utah
3. Creation of GIS CO_2 storage capacity point database	GIS	1 km^2	University of Utah
4. Edge matching formation data across state boundaries	GIS & spreadsheet	1 km^2	University of Utah & State Surveys
5. Integration of the regional 1-km-spaced Rocky Mountain CO_2 capacity GIS database	GIS	1 km^2	University of Utah
6. Aggregating (upscaling) the data into 10 km^2 NATCARB predefined polygons	GIS	10 km^2	University of Utah

The storage capacity calculations for the local Sand Wash basin model were generated based on the static geocellular petrel model properties. This required a few modifications to the workflow designed to process the regional data (Laes et al., 2013b). The petrel geocellular model is a corner-point-defined grid. The height of the cells (= thickness of the formation) in such a grid is not constant. Thickness, a required NATCARB Atlas database field, was also not a parameter stored specifically in the model as a property but the volume for each cell was. The area of each cell was constant for all cells so an average thickness was derived from the cell volume. Another difference between the regional and the local capacity calculations was how the porosity was handled. The regional model was based on a single porosity value for each formation that was assigned a single value is each state. The local model assigned variable porosity values derived by sequential Gaussian simulation (sGs) based on variogram models. Porosity data from 20 deep wells in the basin were the input data for the variography. After the values were extracted from the geocellular model and the data, which were originally processed in ArcGIS using the projection parameters of the Petrel model (UTM, zone 13, NAD 83 with units in feet), the data were projected to the projection required for the NATCARB Atlas (Lambert Azimuthal Equal Area, WGS 1984 with the units in meters). The cell size was scaled up from 1000ft originally, to 1000m so the data would conform to the regional data.

Storage capacity estimate input parameters

The input parameters used to estimate the carbon storage are listed in Table 8.2. The parameters differ by formation and by state. The minimum values represent a minimum depth of 3000' below the surface. This is a conservative cut-off value, also used for the existing carbon storage capacity numbers in the southwest region of the US. Generally, under average conditions CO_2 stays in the supercritical state at around 800m (approximate 2650').

For all the formations in all four states, except Colorado, a constant geothermal gradient was used to calculate the temperature at the top of the formation. Due to buoyancy effects the CO_2 will migrate to the top of the formation where it will be trapped assuming there is a suitable seal to cap the saline formations in place. If the center of the formation had been taken to calculate the CO_2 density, the temperature would have been higher resulting in a slightly lower density and a corresponding lesser amount of CO_2 that could be stored. The geothermal gradients are listed in Table 8.3. Colorado used a geothermal gradient that is location dependent. The gradients were calculated based on data from deep wells that were interpolated across the sedimentary basins.

Table 8.2: Input parameters for the carbon storage capacity estimates for the deep saline fromations in the Colorado Plateau.

Formation	Unit	Statistic	Dakota				Entrada				Weber		Hermosa	De Chelly			Cedar Mesa	Leadville
State			CO	CO	NM	UT	CO	CO	NM	UT	CO	UT	NM	AZ	CO	UT	AZ	NM
Basin			Piceance Sandwash	San Juan	San Juan	Uinta	Piceance Sandwas	San Juan	San Juan	Uinta	Piceance Sandwas	Uinta	San Juan	Black Mesa	Paradox	Paradox	Black Mesa	San Juan
Area	km^2	total	28522	3214	19599	28834	30052	4595	16511	29989	15577	27789	9444	10053	1934	1579	17139	12247
Thickness	ft	min	60	149	89	14	6	90	167	431	0	0	965	731	2	43	0	67
		mean	185	245	236	131	332	215	299	905	434	499	1,577	1,286	99	160	195	125
		max	522	373	413	373	957	379	661	2,317	1,452	1,600	2,133	1,661	238	373	705	257
Depth	ft	min	3,000	3,002	3,010	3,003	3,000	3,002	3,345	3,000	3,000	3,001	4,693	3,000	3,003	3,000	3,000	3,639
		mean	10,635	6,375	5,858	12,031	10,950	6,362	6,993	11,925	13,000	13,201	9,233	3,820	4,528	3,971	4,349	10,145
		max	22,142	10,325	8,796	27,045	22,794	11,400	9,678	29,227	24,377	35,550	12,051	4,754	6,627	8,218	5,906	13,810
Temp	F	min	91	95	139	93	91	101	148	93	95	90	183	97	89	101	97	156
		mean	238	162	213	222	245	162	243	220	250	207	301	103	134	113	107	325
		max	523	279	290	436	541	292	313	467	556	464	374	110	190	159	119	420
Pressure	psi	min	1,299	1,300	1,303	1,351	1,299	1,300	1,449	1,350	1,299	1,711	2,032	1,299	1,300	3,180	1,299	1,576
		mean	4,605	2,760	2,537	5,414	4,741	2,755	3,028	5,366	5,629	15,039	3,998	1,654	1,960	4,210	1,883	4,393
		max	9,587	4,471	3,809	12,170	9,870	4,936	4,191	13,152	10,555	40,527	5,218	2,059	2,869	8,711	2,557	5,980
Porosity	%	min										1.12						
		mean	10	10	6.34	12	15	15	10	16	8	6.22	9.87	14.3	10	20	4.62	4
		max										22.45						
CO_2 density	kg/m^3	min	259	264	262	711	258	286	283	712	249	746	442	386	335	371	386	300
		mean	587	556	378	720	586	551	410	720	648	989	733	636	484	481	691	453
		max	935	651	444	722	937	702	454	723	940	1,040	830	748	741	925	774	482

Table 8.3: Rocky Mountain Carbon Sequestration Project geothermal gradients used to derive temperatures at top of formation depth for deep saline CO_2 storage formations

State	Basin	Formation(s)	Gradient*	Temp @ depth Formula = Surface temp (F) + gradient
AZ	Black Mesa	Cedar Mesa De Chelly	13.5°C/km	75 + (0.0074 * D**)
CO	Piceance/S andWash	Dakota Entrada Weber	Spatial dependent	55 + (gradient in the 1km^2 cell * D)
	Paradox	De Chelly		
	San Juan	Dakota		
UT	Uinta	Dakota	25°C/km	55 + (0.0138 * D)
		Entrada		
		Weber	20°C/km	55 + (0.0115 * D)
	Paradox	De Chelly	20°C/km	55 + (0.0115 * D)
NM	San Juan	Dakota Entrada Hermosa Leadville	47°C/km	61 + (0.026 * D)

* Geothermal conversion factor from °C/100m to °F/100ft: 0.549 (Klett 2005)
D** = depth in feet

Salinity and Permeability data are not required input parameters to calculate the carbon storage capacity. Only NM provided those data as mean values for each formation within the San Juan Basin (Table 8.4).

Table 8.4: Salinity and Permeability data from the NM deep saline formations

State	Formation	Salinity (TDS)	Permeability (mD)
NM*	Dakota	25000	0.83
	Entrada	35000	0.09
	Hermosa	85000	0.2
	Leadville	35000	-

*Only NM provided salinity data

Sand Wash Basin storage capacity input parameters

The carbon storage capacity estimates were generated based directly from the exported geocellular model properties. For these estimates the original cell size of 1000' was used and a geothermal gradient was extracted from the spatial dependent grid created for Colorado based on measured regional deep well temperatures.

The input parameters to calculate the storage capacity data for the Sand Wash Basin model for the geocellular model in UTM are listed in table 8.5. They represent a cut-off of the data at 3000' depth and a geothermal gradient of 31°C/km. A combination of these two parameters generates the most conservative estimate for the Sand Wash Basin.

Table 8.5. Sand Wash Basin geocellular model parameter ranges for the Dakota, Entrada and Weber at the 3000' depth constraint and a geothermal gradient of 31°C/km)

		Min	mean	Max
Dakota	Thickness (ft)	52	177	243
	Depth (ft)	3,001	13,345	22,248
	Porosity (%)	1.65	6.37	14.34
	Temperature (F)	107	286	440
	Pressure (psi)	1299	5778	9633
	CO_2 Density (kg/m^3)	340	618	641
Entrada	Thickness (ft)	1	321	804
	Depth (ft)	3050	14089	23120
	Porosity (%)	1.63	4.68	13.64
	Temperature (F)	108	299	455
	Pressure (psi)	1320	6101	10011
	CO_2 Density (kg/m^3)	346	623	642
Weber	Thickness (ft)	1	316	836
	Depth (ft)	3006	15392	24765
	Porosity (%)	1.50	2.98	7.22
	Temperature (F)	107	321	483
	Pressure (psi)	1301	6665	10723
	CO_2 Density (kg/m^3)	341	628	643

Storage capacity estimates

Rocky Mountain Region estimates

CO_2 capacity numbers grouped by formation but separated by state and sedimentary basin are listed in Table 8.6. Figure 8.2 shows the spatial distribution of the total cumulatively capacity numbers summed over all of the formations at the 1-km^2 data-distribution scale. The total, calculated CO_2-storage-capacity for all seven formations (using the average porosity for most data) varies between 13.6 and 143.7 billion metric tonnes depending on the efficiency factor (Table 8.7). For the three major, deep-saline formations the values vary between 9.8 and 104.0 billion metric tonnes. The regional storage capacity numbers for the Dakota, Entrada and Weber formations, represent an approximate 8% decrease in capacity when compared to the 2012 NATCARB Atlas IV numbers (Laes et at 2013a). This decrease is attributed to better characterization of the geologic formations.

Table 8.6: Rocky Mountain Carbon Sequestration Project deep-saline, CO_2-capacity numbers derived from the 1 km^2 scaled points:

				CO2 Storage Volume (metric Tonnes)		
State	Basin	Formation	Area (km^2)	Low Efficiency (0.51%)	Medium Efficiency (2%)	High Efficiency (5.4 %)
CO	Piceance_ Sandwash	Dakota	28,522	482,624,867	1,892,646,535	5,110,145,645
CO	San Juan		3,214	68,252,705	267,657,665	722,675,695
NM	San Juan		19,599	172,502,878	676,481,873	1,826,501,060
UT	Uinta		28,834	507,104,513	1,988,645,149	5,369,341,904
CO	Piceance_ Sandwash	Entrada	30,052	1,393,361,516	5,464,162,810	14,753,239,586
CO	San Juan		4,595	127,397,634	499,598,566	1,348,916,127
NM	San Juan		16,511	300,019,280	1,176,546,181	3,176,674,688
UT	Uinta	Entrada-Navajo	29,989	4,857,039,869	19,047,215,174	51,427,480,970
CO	Piceance_ Sandwash	Weber	15,577	549,361,376	2,154,358,336	5,816,767,507
UT	Uinta		27,789	1,361,192,180	5,338,008,549	14,412,623,083
NM	San Juan	Hermosa	9,444	1,672,530,703	6,558,943,933	17,709,148,619
AZ	Black Mesa	De Chelly	10,053	1,820,718,060	7,140,070,822	19,278,191,219
CO	Paradox		1,934	13,715,122	53,784,794	145,218,943
UT	Paradox		1,579	35,650,148	139,804,502	377,472,155
AZ	Black Mesa	Cedar Mesa	17,139	168,097,713	659,206,719	1,779,858,142
NM	San Juan	Leadville	12,247	42,728,636	167,563,275	452,420,844
			Totals:	**13,572,297,199**	**53,224,694,882**	**143,706,676,188**

Table 8.7: Rocky Mountain Carbon Sequestration Project deep-saline, CO_2-capacity numbers summarized by formation

	CO_2 Storage Volume (metric Giga Tonnes)		
Formation	Low Effciency (0.51%)	Medium Effciency (2%)	High Effciency (5.4%)
Dakota	1.23	4.83	13.03
Entrada	6.68	26.19	70.71
Weber	1.91	7.49	20.23
Partial Total:	**9.82**	**38.51**	**103.96**
Hermosa	1.67	6.56	17.71
Cedar Mesa	0.17	0.66	1.78
De Chelly	1.87	7.33	19.80
Leadville	0.04	0.17	0.45
Total:	**13.57**	**53.22**	**143.71**

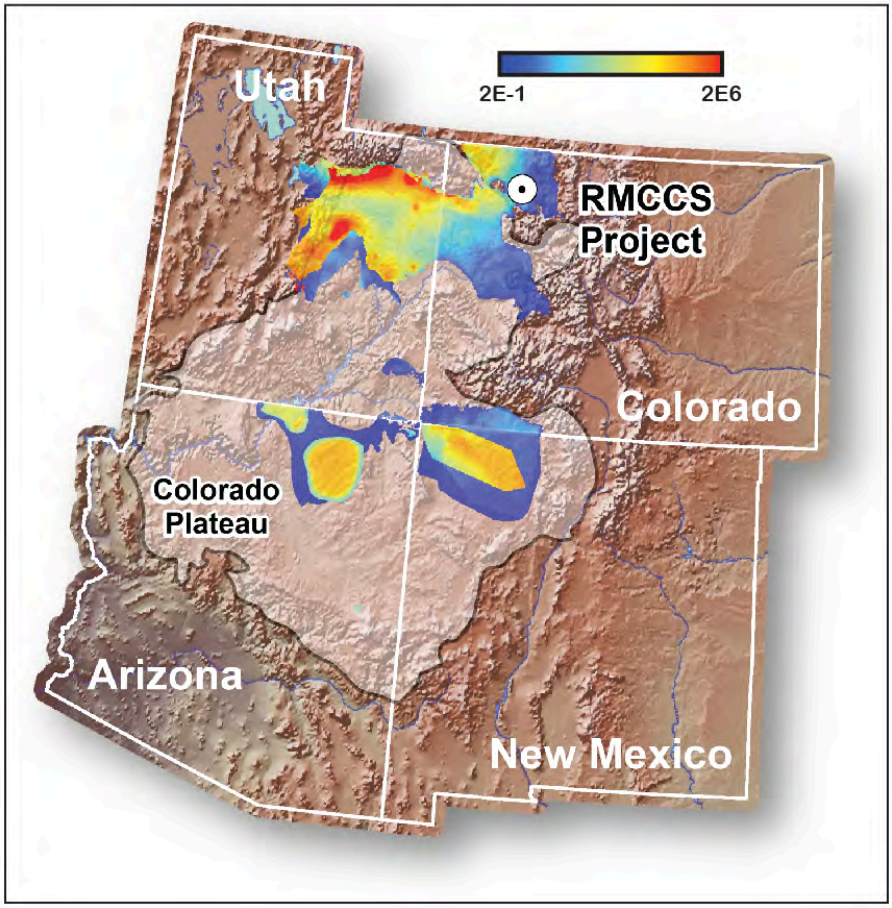


Figure 8.2: Spatial distribution of the CO_2 storage capacity summed over all 7 formations using a 1-km^2 cell size. The legend represents the medium efficiency CO_2 capacity data in metric tons.

Sand Wash Basin Estimates

The site-specific storage capacity estimates for the Dakota, Entrada and Weber Formations, the only formations assessed for the Sand Wash Basin, are listed in Table 8.8. The capacity numbers derived from the parameters as extracted from the geocellular model based on a constant geothermal gradient throughout the Sand Wash Basin area resulted in a 10% higher estimate using the lower geothermal gradient (Laes et al. 2013b). Applying the spatial determined gradient, which varied between 10°C/km and 50°C/km, provided the largest storage capacity numbers (Table 8.8). The differences in the estimates were approximately 5% and 16% when compared to the 27°C/km and to the 31°C/km gradient respectively. The spatial cumulative storage capacity distribution summed for the three formations shows that the northwestern section of the basin could accommodate more CO_2 than eastern part of the basin (Figure 8.3).

Table 8.8. Sand Wash Basin CO_2 storage capacity estimates calculated for records below 3000' deep after converting the geocellular model derived data to the required NATCARB atlas required Lambert Azimuthal Equal area projection using a spatial dependent geothermal gradient.

			CO_2 Storage Capacity Estimates (million metric Tonnes)			
Formation	# of 1 km cells	# of 250 m points	Low Efficiency (0.51%)	Medium Efficiency (2%)	High Efficiency (5.4%)	Adjusted area (km^2)
Dakota	8446	131860	102.093	400.363	1,080.980	8,241
Entrada	8420	131528	144.380	566.196	1,528.730	8,221
Weber	8462	131865	86.810	340.431	919.163	8,242
		Total Σ:	333.282	1,306.990	3,528.873	

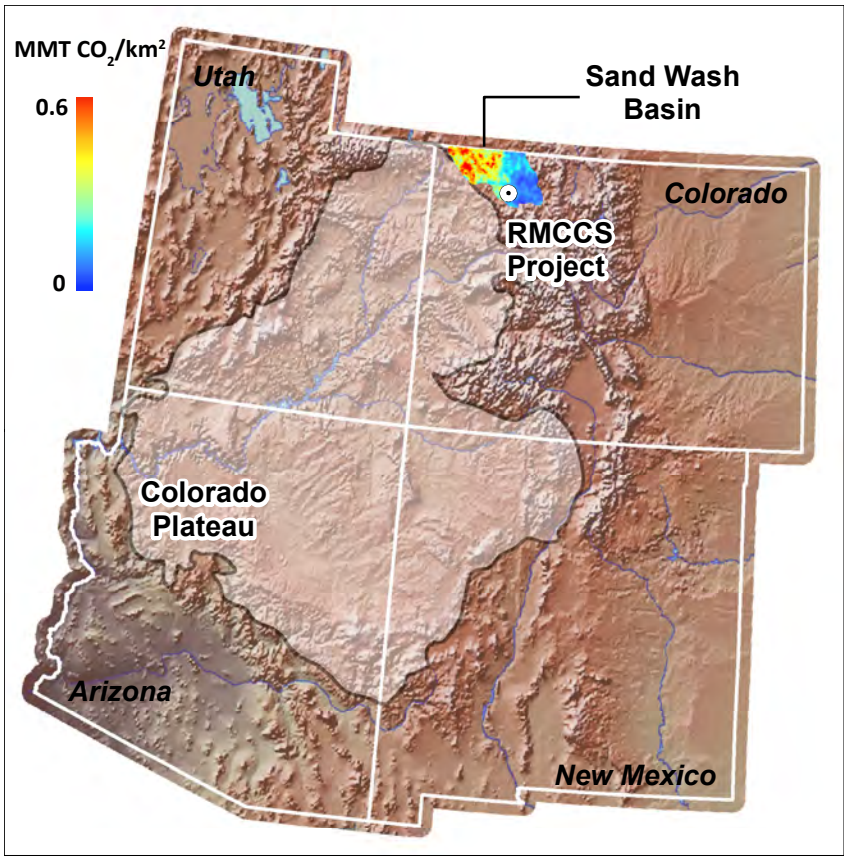


Figure 8.3: Spatial distribution of the CO_2 storage capacity summed over all 3 saline formations in the Sand Wash Basin using a 1-km^2 cell size. The legend represents the medium efficiency CO_2 capacity data in million metric tonnes (MMT). The distribution pattern for other efficiency levels is the same but the numbers will vary according to the efficiency level.

Significance

The 2010 CO_2 emission rate for the coal- and gas-fired power plants in the region is listed as about 320 million tonnes per year (EPA 2010). Based on the medium efficiency storage capacity of 38.5 GT for the three main formations characterized in this study (Table 8.9), this corresponds to 120 years of capacity. When the other formations characterized in this study are included, the storage capacity potential climbs to 166 years. These numbers are based on near constant CO_2-emission numbers and assuming all of the calculated storage volume is available for CO_2 sequestration.

This study estimated a carbon storage capacity ranging between 0.33 and 3.53 metric GT for the Sand Wash Basin. The storage capacity at the medium efficiency factor is 1.3 metric GT. The two coal-fired power plants located within Sand Wash Basin in Craig and Hayden emitted a combined total of 13.5 and 12.2 million metric tonnes of CO_2 during 2010 (U.S. EPA, 2010) and 2011 (U.S. EPA 2011). Using the highest geothermal gradient and a cut-off storage depth of 3000', the saline formations within the Sand Wash basin have the capacity of storing CO_2 for approximately 97 years at the medium storage efficiency level of 2%.

There are 3 coal-fired power plants within a distance of 60 to 80 miles to the west and northwest of the Woodside Dome site. Their combined 2010 CO_2 emissions summed to 15.9 million metric tonnes. The storage capacity estimate of 12.6 million metric tonnes at the 2% efficiency levels derived using conservative geologic constraints would provide storage for less than a year. Because the listed storage capacity numbers are conservative estimates the site would benefit from additional study to characterize the extent of the geologic structure better.

According to the UGS research, the Bonanza site is the best potential Utah commercial CO_2 storage site in the Colorado Plateau. At a combined estimated storage capacity of 116 million metric tonnes (2% efficiency), the Dakota, Entrada and Weber Formations could handle the 2010 reported CO_2 Bonanza plant emissions of 3.4 million metric tonnes for 34 years.

Conclusions

The newest capacity data reported here are markedly different when compared to the regional data reported to DOE/NETL for the NATCARB Atlas IV version (DOE 2012). The primary explanations for the contrast in results include more data, better quality data, and more-robust geological analysis of those data. The data improvement can be attributed to the cooperation with the state geological surveys providing a partnership that gave the project access to expert knowledge of the sedimentary basins. Because the data and interpretations are better, the regional capacity estimates may be considered to be more significant in the context of reliability and usefulness. The upshot is that regional capacity estimates will be better and more significant as more resources are invested in the analysis.

Some of the saline formations occur in very deep parts of the studied sedimentary basins. Because of limited well information in the deeper parts, the stratigraphic boundaries of the formations are not as well constrained there. Of the wells that do penetrate to top of the oldest and deepest formations, few penetrate the entire formation leading to a higher level of uncertainty of the thickness and thus the storage capacity numbers, of the older formations at greater depth.

Although the cooperation required between groups of geologist from the states involved resulted in improved data, it did however also create problems that would not have occurred if the same person had generated all data. Notably were geological continuity problems across administrative state boundaries. Those problems were solved in cooperation with the different groups using GIS techniques. Another continuity problem across state boundaries was related to different states using different cut-offs for bounding basal and top of formation layers leading to differences in thickness occurring at the state boundaries. There were a few data structural problems because it took a while before the group had a system worked out that was workable for all the participating geologists. Despite all the problems that needed to be solved, the quality improvement of resulting dataset is an indication that the system of using partnering experts and the data streamlining method developed by this project could serve as an example for the other carbon sequestration data compilation efforts, not just in the southwest but most likely for other regional carbon sequestration partnerships as well.

9. Simulation and uncertainty assessment

During the characterization activity, potential of a site/reservoir for CO_2 storage is generally examined by three criteria: capacity, injectivity, and seal integrity.

- Capacity defines how much CO_2 can be stored within a target formation in terms of available pore space (e.g., porosity, thickness, and areal extent) for the storage.
- Injectivity is dependent on permeability, fracture pressure; geometry and connectivity, and CO_2-water-rock interactions, which determines the relative mobility of CO_2 within the pore space.
- Caprock or seal integrity is the ability to contain CO_2 within the injection zone determined by seal extent, fault stability and maximum sustainable fluid pressure.

Due to the lack of economic interest, CCS target formations (especially saline aquifer) typically have relatively low, well penetration compared to hydrocarbon production reservoirs. Therefore, the available subsurface data sets within the potential CCS target formations are often sparse and suffer from a relatively higher level of uncertainty. In order to understand this uncertainty, we focused on the uncertainty in the storage capacity estimation and demonstrated how the local data (e.g., well data, number of wells, and location of wells) affect the storage capacity estimates and what the degree of well density (number of wells) is required to appropriately estimate the capacity within a specified degree of confidence. In other words, this study is not intended to provide specifics as to the true storage capacity of a reservoir/basin, but is intended to provide an understanding how much information is required in the characterization process to adequately estimate the storage capacity in practice. To do this, we developed a new workflow accommodating the addition of random pseudo wells to represent the virtual characterization wells.

Geocelluar Model

Within the Sand Wash Basin, the stratigraphic formation top picks, well information, and well log images available from the project site were gathered to establish the geocellular model. Porosity values were assigned to the grid cells of the Dakota, Entrada and Weber Formations. This process began by taking porosity data from 20 existing wells within the Sand Wash Basin model boundary. Variogram analysis was conducted to understand the variation in porosity as a function of separation distance between existing wells. It was also used as means of determining directions/degree of anisotropy. Using the sample variogram results, Sequential Gaussian Simulation (SGS) was used to assign porosity values to each cell within the Dakota, Entrada and Weber Formations of the Sandwash Basin.

In this study, the geocellular model (porosity) within the basin boundary shown in Figure 1 serves as a true geology. The constructed 3D model contains 6 formations starting with the Cretaceous Dakota formation to the Weber formation from top to bottom. The static model domain covers 107.7 miles by 58 miles in the x and y direction. The grid configuration is 569x306x26 cells in x, y, and z direction, respectively, with a cell dimension of 1,000 ft by 1,000 ft.

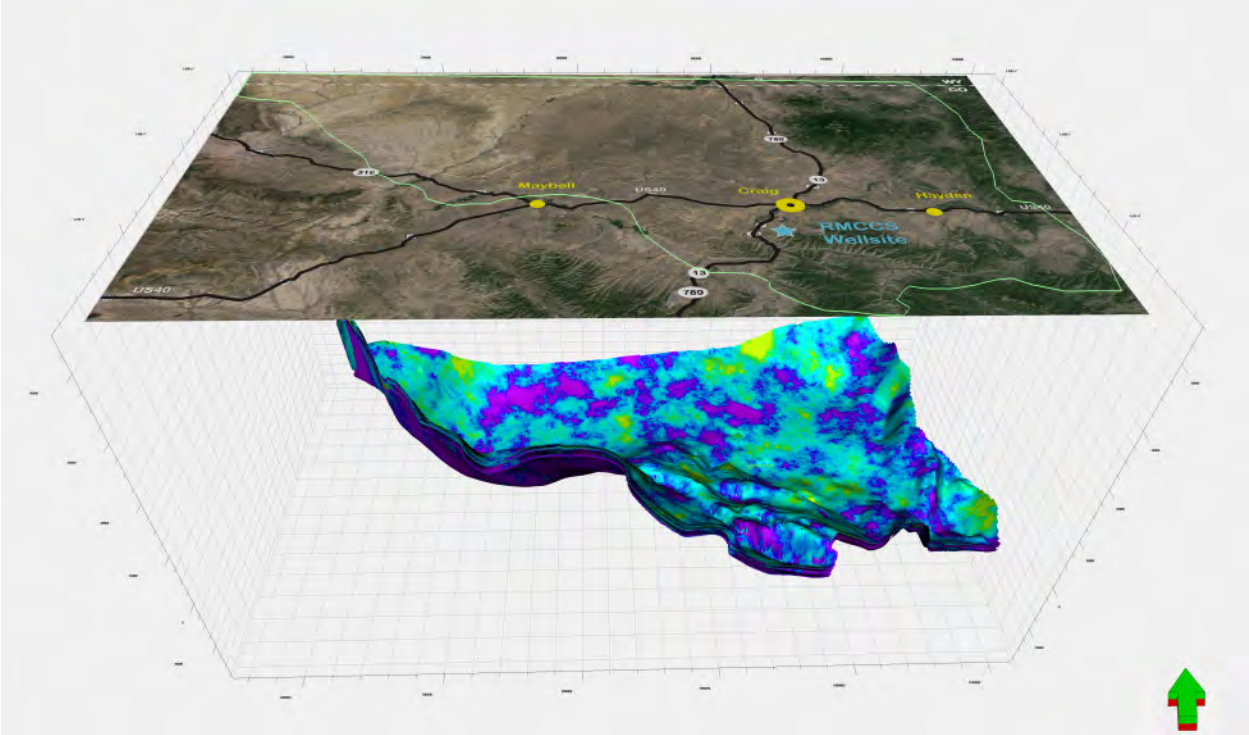


Figure 9.1. The Sand Wash Basin boundary and simulated porosity field within the boundary. Vertical exaggeration is 2x.

Methods

One newly drilled characterization well will provided good additional information on storage capacity; however, how close this new well progresses the project to understanding the true storage capacity estimate within the Sand Wash Basin is uncertain. It is also uncertain as to how many additional wells would be required to approach the true pore volume within the Basin. To understand this uncertainty a methodology was developed focusing on randomly placing "pseudo-wells" in a basin-scale model. Therefore, each randomly pseudo-well was assumed to provide new well data and additional geologic information. The recently developed geocelluar model of Sand Wash Basin was considered to be "true" or best estimate of real geology. We evaluated how the degrees of data density (well density) represented by the pseudo-wells affects the capacity estimates of target formations within the Sand Wash Basin. Note that we considered the estimated pore volume as a proxy to the capacity estimate in this work.

Figure 9.2 shows the general workflow we followed in this study. Based on the geocellular model of Sand Wash Basin, for 25 individual cases, we randomly sampled the location of pseudo-wells (or new characterization well) up to 25 within the model. As each well was placed, porosity and formation thickness information within each well was extracted from the Sand Wash Basin geocellular model which is considered to be "true" or best estimate of real geology. Starting from a first randomly sampled point, we sequentially added a new pseudo-well into the previous well(s) and calculated the estimated pore volume at each step to see how the new information affects the capacity estimates. That is, addition of pseudo-well(s) is supposed to provide additional information within the Sand Wash Basin.

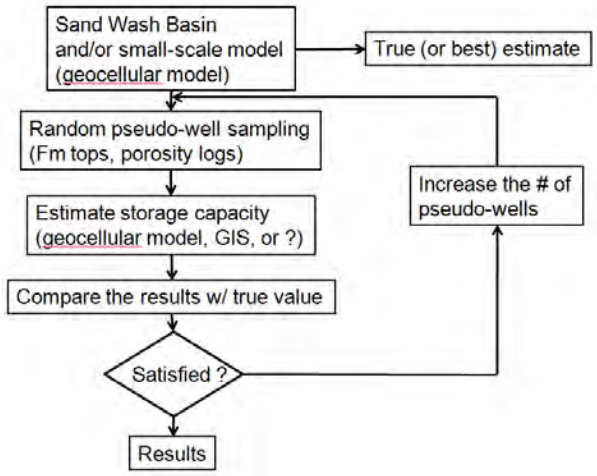


Figure 9.2. Workflow for the pore volume estimation with the incremental addition of pseudo-well.

Average porosity value and thickness of a target formation were determined from each pseudo-well and assigned uniformly to the subarea corresponding to the pseudo-well. The estimated pore volume of a subarea was simply computed by the product of average porosity value, thickness, and size of the subarea. For example, Figure 9.3 shows 25 subareas of Dakota formation corresponding to the randomly selected 25 pseudo wells for case 1. The boundary of each subarea was determined by the closest distance from each pseudo-well. Total estimated pore volume of the basin is the sum of each subarea's estimated pore volume. We repeated the same process for a total of 25 cases with a different starting pseudo-well location for statistical analysis.

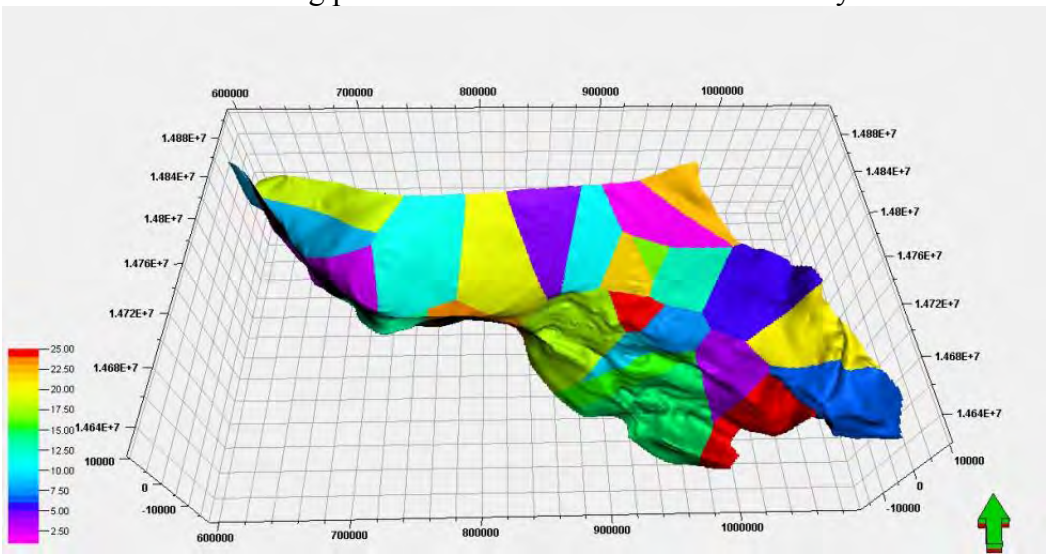


Figure 9.3. Case 1, 25 subareas applied in the Dakota formation based on the closest point from corresponding pseudo wells within the Sand Wash Basin. For this method, 24 other cases like the above were run and produced alternate data sets. Vertical exaggeration is 2x.

Results and Discussion

Figures 9.4-9.6 show the obtained relative differences of the capacity estimates from the true value of geocellular model for Dakota, Entrada, and Weber formation,

respectively for cases 1-25. The relative difference is defined by $\frac{V_{est}-V_{true}}{(V_{est}+V_{true})/2}$ where V_{est} is the estimate of total pore volume and V_{true} is the true capacity value from the geocellular model. That is, if the relative difference reaches zero, the pore volume (or storage capacity) estimate is close to the true value. Positive relative difference represents the overestimation and negative value is underestimation to the true value.

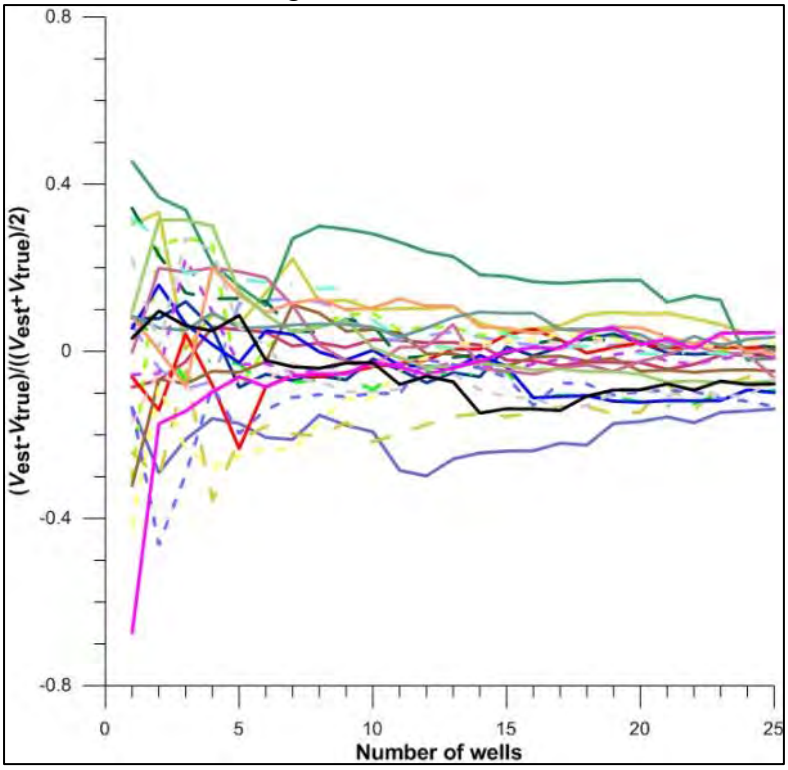


Figure 9.4. Case 1-25 combined data set, relative differences of the capacity estimates from the true value of geocellular model for Dakota formation. Each line represents 1 of the 25 cases.

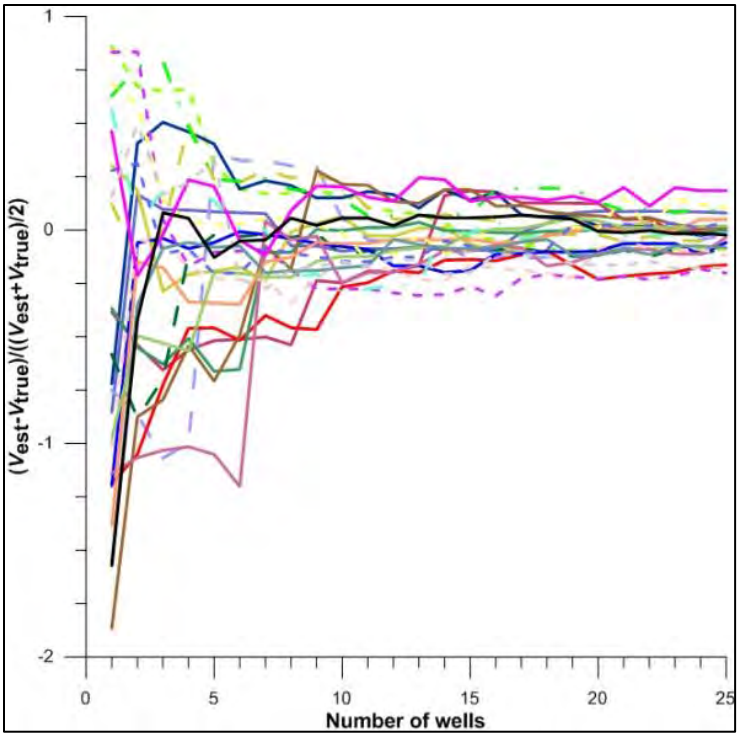


Figure 9.5. Case 1-25 combined data set, relative differences of the capacity estimates from the true value of geocellular model for Entrada formation. Each line represents 1 of the 25 cases.

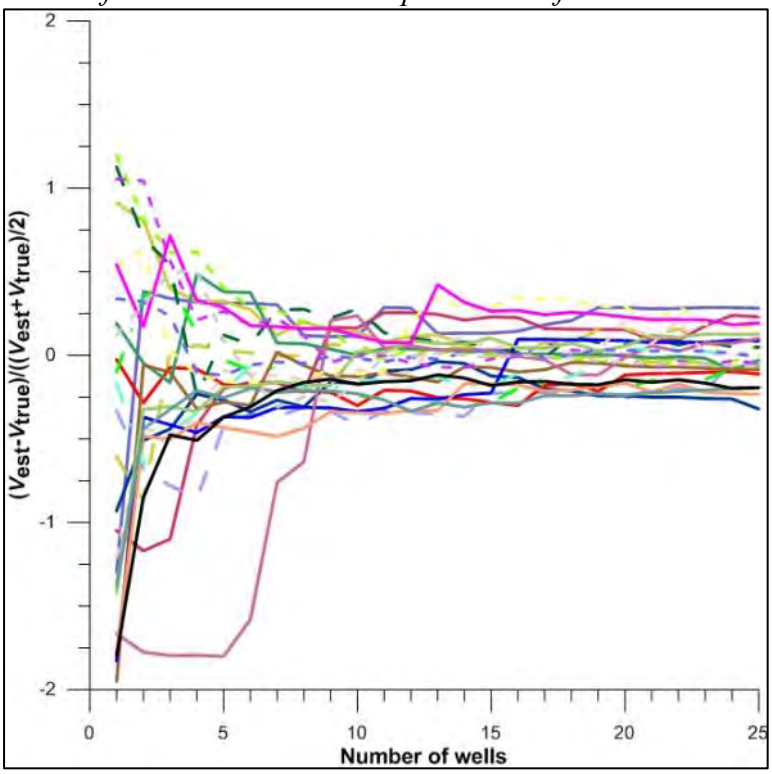


Figure 9.6. Case 1-25 combined data set, relative differences of the capacity estimates from the true value of geocellular model for Weber formation. Each line represents 1 of the 25 cases.

As expected, our results show that the difference between the estimated pore volume and true value is decreasing with the addition of new data (pseudo-wells) (Figures 9.4 – 9.6). However, pore volume estimation for the Dakota (Figure 4) shows better fit especially with less number of pseudo-wells compared to Entrada and Weber formation (Figures 9.5 and 9.6). Since the estimated pore volume of a subarea is computed with the single porosity and thickness value given by the corresponding pseudo-well, the difference will increase if there is a large spatial variation in the porosity and thickness within a subarea. In other words, our results indicate that Dakota formation has relatively less spatial variation in the porosity and thickness. Targeting ±30% relative difference as a tolerable error range, our results show that we would need at least 5 characterization wells for the Dakota and 9 wells for Entrada and Weber formations, respectively. Note that appropriate density of characterization data/well is dependent on the geologic formations even within the same basin.

With the minimum, lower quartile, median, upper quartile, and maximum, Box-Whisker plots shown in Figures 9.7 – 9.9 graphically summarize the results for cases 1-25 of the pore volume estimates (relative difference) at different number of pseudo-wells for the Dakota, Entrada, and Weber, respectively. The bottom of the box is the 25^{th} percentile and the top is 75^{th} percentile. The horizontal line within the box shows the median value and the end of whiskers are the minimum and maximum. The range/distribution of relative difference value for the small number of wells is significantly larger for the Entrada and Weber formation compared to the Dakota. Even with the single characterization well, median of relative difference out of 25 cases is close to zero. Whereas, the Entrada and Weber formation exhibited large negative median (underestimation) with a single characterization well and gradually decreased the difference as the number of wells increased.

As our relative difference measurement shows the deviation from the true value, we also analyzed which factor is more significant in terms of pore volume estimation. Note that our pore volume estimates in this work involves the uncertainties only in porosity and cell volume (geometry of geologic structures). To adequately quantify the degree of variation in the geologic structures and its effect on the capacity estimation, we calculated volume-weighted average dip angle of each target formation. Being consistent with our relative difference measurements, the volume-weighted dip angle for the Dakota is the smallest (4.95 degrees) among three target formations (Table 9.2). Entrada and Weber are characterized by higher volume-weighted dip angle of 11.32 and 9.49 degrees, respectively. That is, a formation with a large dip angle is likely to have more uncertainty and greater error in the capacity estimation with the limited characterization data. However, unlike the volume-weighted average dip angle, the degree of heterogeneity in the porosity was not consistent with our relative difference results. Table 9.2 summarizes the general statistics of the porosity from the original well logs and simulated true porosity field.

Although our results did not consider the cost analysis in this study, greater characterization efforts and cost should be accounted for the reliable capacity estimates in the Entrada and Weber due to their more complicated spatial variation in geology and/or petrophysical properties. Our findings demonstrate with confidence that spatial geologic variation strongly affects the capacity estimation and associated uncertainty.

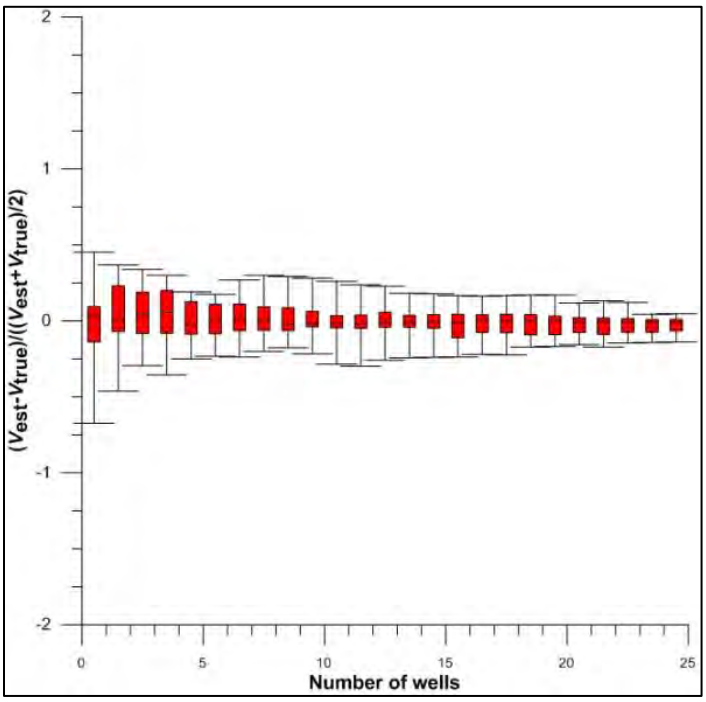


Figure 9.7. Case 1-25 combined data set, Box-Whisker plot of the relative difference of the capacity estimates for Dakota formation from the true value of geocellular model.

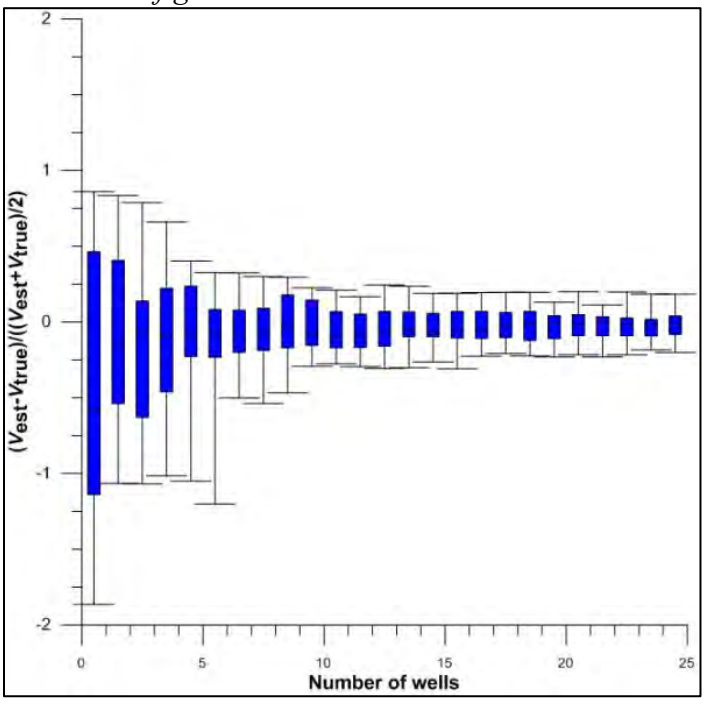


Figure 9.8. Case 1-25 combined data set, Box-Whisker plot of the relative difference of the capacity estimates for Entrada formation from the true value of geocellular model.

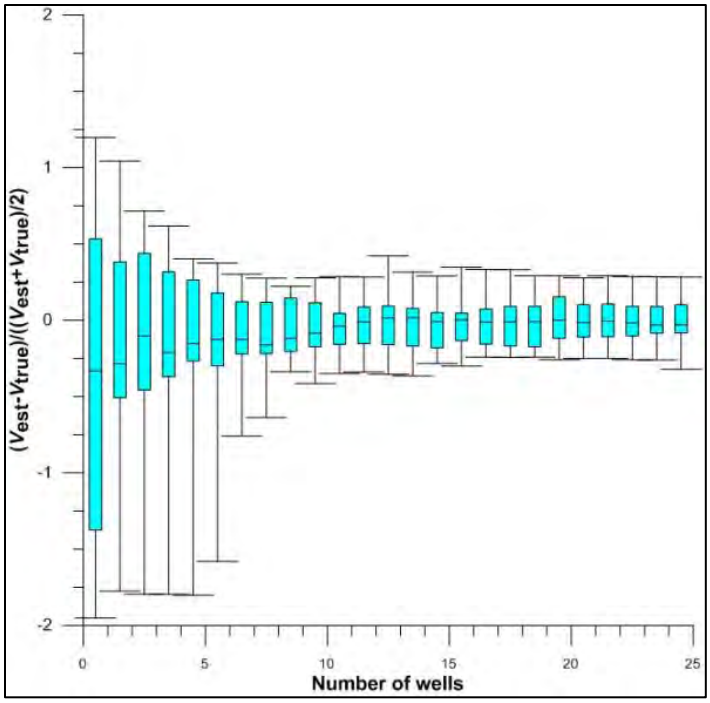


Figure 9.9. Case 1-25 combined data set, Box-Whisker plot of the relative difference of the capacity estimates for Weber formation from the true value of geocellular model.

Table 9.2. Volume-weighted average dip angle and general statistics of porosity field.

		Dakota	***Entrada***	***Weber***
Volume-weighted average dip angle		4.95	11.32	9.49
Minimum	Property	0.0165	0.0163	0.015
	Well Logs	0.015	0.015	0.015
Maximum	Property	0.1434	0.1364	0.0722
	Well Logs	0.3706	0.1558	0.1168
N	Property	89173	88549	88862
	Well Logs	2886	2366	840
Mean	Property	0.0637	0.0468	0.0297
	Well Logs	0.0667	0.0517	0.0342
Std. Dev.	Property	0.0172	0.02	0.0136
	Well Logs	0.0365	0.0247	0.021

10. Final risk assessment

Introduction

Carbon dioxide (CO_2) storage in the deep subsurface has been considered a potential option combined with CO_2 capture for the mitigation of global climate change [*IPCC*, 2007]. For reliable and successful project performance, predictive tools integrated with site characterization, Monitoring, Verification, & Assessment (MVA), and risk assessment need to be routinely applied and updated as more scientific and operational data are collected throughout the life of a project. However, due to the incomplete knowledge of subsurface environment with CO_2 injection and storage, a commercial-scale geologic CO_2 storage project requires the predictive tools that account for the uncertainties, and subsequently can help build confidence that a system will meet its design targets as well as regulatory requirement within the probabilistic framework [*Mathias et al.*, 2013; *Sato*, 2011; *Walter et al.*, 2012].

Recent EPA's Underground Injection Control (UIC) Program for geologic CO_2 sequestration wells (Class VI) is an example of federal requirement imposed on the geologic CO_2 storage in the US [*EPA*, 2010]. The Class VI rule is under the authority of the Safe Drinking Water Act's UIC program designed to protect Underground Sources of Drinking Water (USDW). This rule specifies the use of computational modeling to predict the migration of CO_2 plume and formation fluids. The definition of an Area of Review (AoR) for a Class VI well is the region surrounding the geologic sequestration project where USDW may be endangered by CO_2 injection activities. However, given the unavoidable uncertainty in the deep subsurface environment, prediction on the environmental impacts such as AoR, CO_2 leakage, or groundwater vulnerability always includes the certain uncertainties in the outcome.

In order to quantify the uncertainty, Monte Carlo-based method is traditionally used to estimate a system's output response (e.g., probability density function) from known or estimated statistical distributions of input parameters. While Monte Carlo simulation method is simple, it typically requires a large number of probability-weighted samplings of inputs and subsequently high computational cost to yield a probability distribution of an output metric. Furthermore, numerical simulation of geologic CO_2 sequestration involves computationally intensive multi-phase simulation efforts [*Deng et al.*, 2012; *Han et al.*, 2010]. Thus, new efficient and readily-applicable methodology within the probabilistic framework is necessary for better compliance with the project goals and regulatory requirement in timely manner.

Monte Carlo methods are commonly used for forecasting uncertainty associated with reservoir simulations. However, Monte Carlo methods typically require tremendous computational power (or time), and thus we elected to use a response surface methodology (RSM) instead. In comparison to traditional Monte Carlo methods, application of RSM with appropriate experimental design is relatively efficient for a variety of reservoir engineering analyses including performance prediction, upscaling, history-matching, and optimization (design) studies[*Bu and Damsleth*, 1996; *Chu*, 1990; *Willis and White*, 2000]. RSM with a statistically linear model uses only a small

number of runs at specified input points. Recently, RSM has also been introduced for assessing geologic CO_2 storage [*Ghomian et al.*, 2010; *Liu and Zhang*, 2011; *Rohmer and Bouc*, 2010; *Wood et al.*, 2008]. Using a first-order model with a two-level Plackett-Burman design of experiment , [*Liu and Zhang*, 2011] focused on a parameter sensitivity analysis of upscaled aquifer models to 7 parameters (vertical gradient of background aquifer flow, geothermal gradient, degree of heterogeneity (variance), maximum residual gas saturation, salinity of formation water, injection rate, and caprock permeability). They found that residual gas saturation, degree of heterogeneity (variance), and salinity are the most critical parameters for the fully heterogeneous model. However, the first-order Plackett-Burman design of experiment does not include the interaction among the parameters and the effect of higher order terms. [*Ghomian et al.*, 2010] used the design of experiment (DoE) and RSM to investigate the uncertainties in CO_2 flooding design parameters for EOR and CO_2 sequestration. They used a fractional factorial design for sandstone and a D-optimal design for carbonate reservoirs. [*Wood et al.*, 2008] applied the Box-Behnken design (BBD) to screen CO_2 flooding and storage in the Gulf Coast reservoirs based on dimensionless groups. *[Rohmer and Bouc, 2010]* applied a first-order polynomial approximation with Latin hypercube sampling for cap rock failure assessment due to the CO_2 storage. In addition to the RSM approach, this study proposes the integration of Monte Carlo samplings combined with the obtained RSM to achieve the uncertainty quantification within the probabilistic framework.

The project team caucused regarding the most significant risk features, events and processes, or "FEPs," for the RMCCS project site, and elected to focus risk analyses on the top two (most significant) FEPs, (1) plume size or Area of Review (AoR), and (2) injection-induced pressure buildup. Specifically, we probabilistically delineated the spatiotemporal responses (e.g. AoR and injection-induced pressure buildup) resulting from CO_2 injection into the subsurface. In the RMCCS project, we applied RSM, but combined it with Monte Carlo sampling (Kalla, 2005) to facilitate a probabilistic assessment of potential CO_2 storage in the candidate formations within the Sand Wash basin near Craig, Colorado.

Saline Aquifer Description

The Craig site is located in Moffat County, northwestern part of Colorado (Figure 10.1). The three potential storage formations (Dakota, Entrada, and Weber) are deep saline aquifer targets. The Weber and Entrada formations consist of mostly aeolian deposits and the Dakota is comprised of fluvial and marginal marine deposits. The Weber Sandstone, target formation of this study, is one of the major saline reservoirs that are present throughout the Colorado Plateau and Rocky Mountain basins, including the adjacent Piceance and Green River basins. The Weber Sandstone is estimated to have a storage potential of nearly 5 billion tons of CO_2 in Colorado, and potentially an equal amount from the same reservoirs in Utah, northeast Arizona, and northwest New Mexico [*DOE*, 2010; *NATCARB*, 2010]. Local and regional sources of CO_2 include the Craig coal-fired power plant and the Hayden coal-fired power plant approximately 35 km to the east of Craig, Colorado. The Craig and Hayden plants output at least 9.5 and 3.5 MMT of CO_2 per year, respectively [*NATCARB*, 2010].

The proposed injection site is geologically situated on northerly dipping beds that plunge into the Sand Wash Basin. Regional dips are typically between 5 and 13 degrees north into the basin. South of the proposed injection site, dips become steeper (~10 to 15 degrees or more). Superimposed on the regional north dip, asymmetrical anticlines plunge northwest into the basin. The southwestern limbs of these anticlines are typically steeply dipping forced folds and possibly faulted. Structural closure is created by the Axial Basin Uplift to the south.

Uncertainties associated with the geology of the region are limiting the accuracy of both total CO_2 capacity and CO_2 injectivity [*Bradshaw et al.*, 2007]. Sparse data from the 233 oil and gas wells within the 50 km radius (7,854 km^2) around the proposed injection site results in large areas where basic petrophysical data is lacking. Extrapolation/interpolation of down-hole geophysical data attempts to reduce the uncertainty where data is lacking, but the geophysical logs are also incomplete, or not available, especially for the deep saline aquifers.

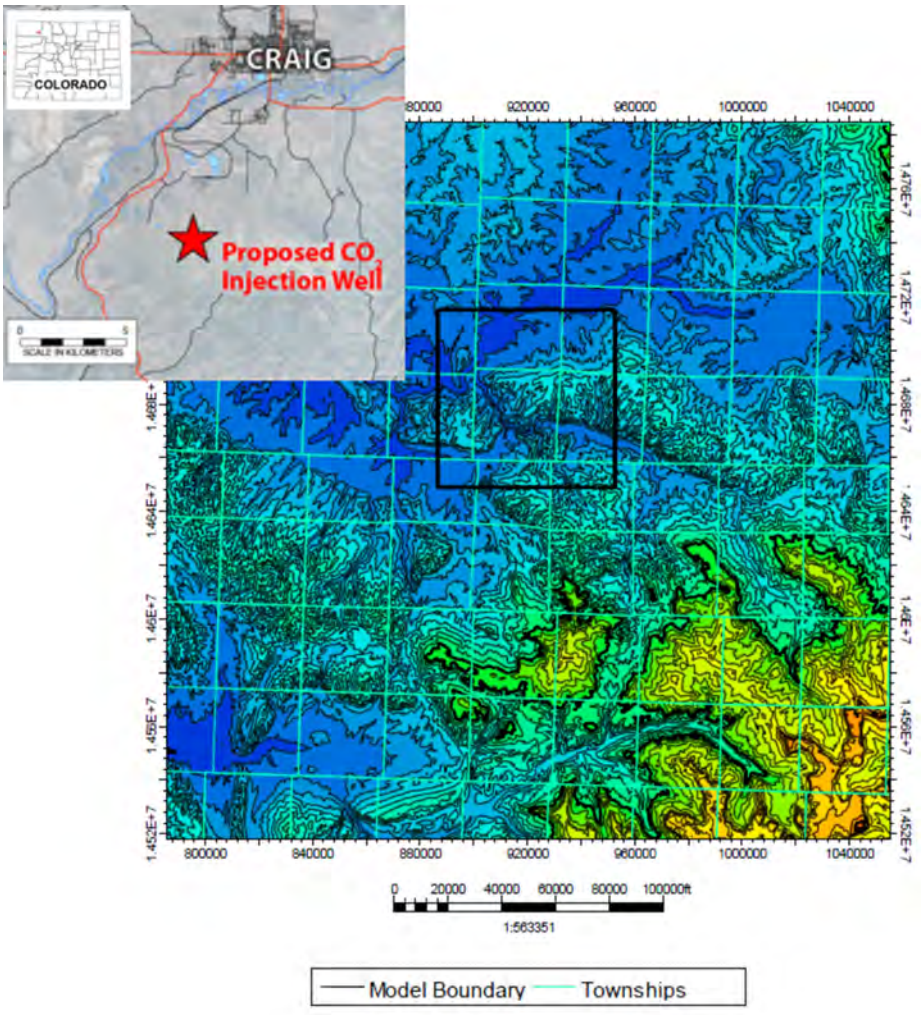


Figure 10.1. Location map of Craig site in Moffat County, Colorado.

Geologic Model

The stratigraphic-formation, top picks, well information, and well log images available from the project site were gathered to establish the numerical model grid. We built a site-specific aquifer model for the numerical simulation based on the regional geologic model developed and provided by Colorado Geological Survey and Schlumberger. The site-specific static model within the model boundary is shown in Figure 10.2. The constructed 3D model contains 6 formations starting with the Cretaceous Dakota formation to the Weber formation from top to bottom. Among them, we only considered a single well injection into the deepest target formation (Weber) interval for our study. The assumption was made that the overlying Chinle formation works as a perfect seal and thus no flow at the top of Weber. The static model domain covers 20.1 km (66,000 ft) by 20.1 km (66,000 ft) in the x and y direction. The grid configuration is 200x200x20 cells in x, y, and z direction, respectively, with a cell dimension of 100.6 m (330 ft) by 100.6 m (330 ft). Twenty cells were equally spaced vertically in the target formation.

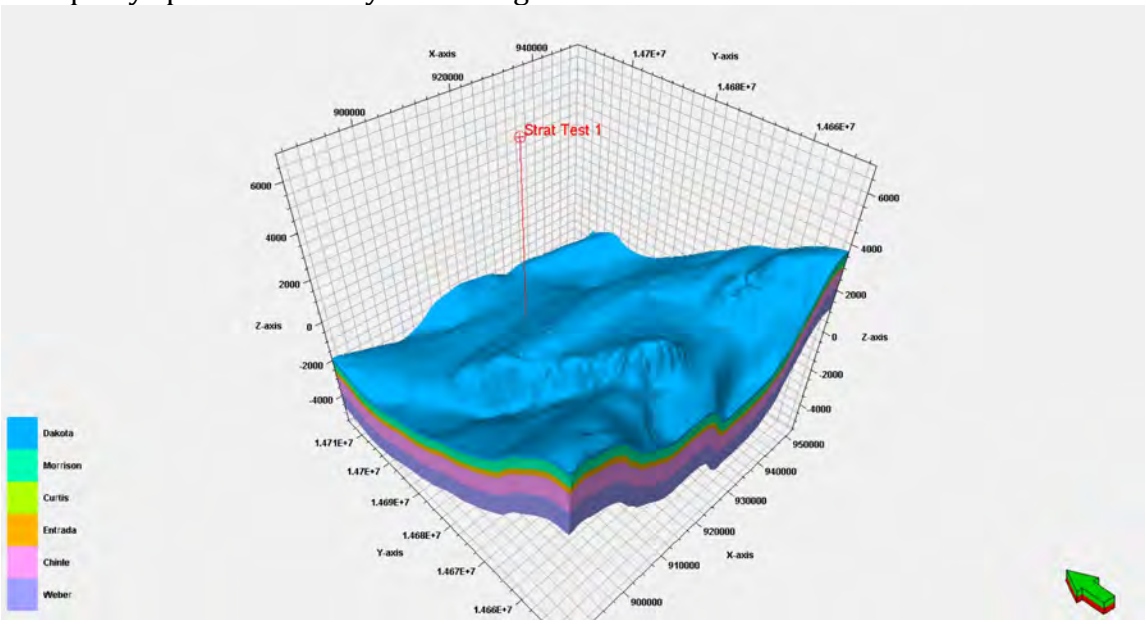


Figure 10.2. Stratigraphic distribution of geologic formations starting from Dakota formation within the Craig site model boundary. Vertical exaggeration is 5x.

Methods

Figure 10.3 summarizes the workflow we followed in this study. We first determined independent variables/factors to construct the DoE based on the BBD followed by the numerical experiments. Then, the spatiotemporal evolution of CO_2 migration and pressure build-up was delineated by constructing the response surface (or proxy model) for each different time. We utilized stepwise regression technique to eliminate insignificant factors from the regression equation. Then, several goodness-of-fit measurements examined the performance of the regression model. Lastly, Monte Carlo samplings of mutually independent, input parameters

through the obtained, response-surface models for each time-generated, temporal evolution in the CDFs of output responses from the given input distributions.

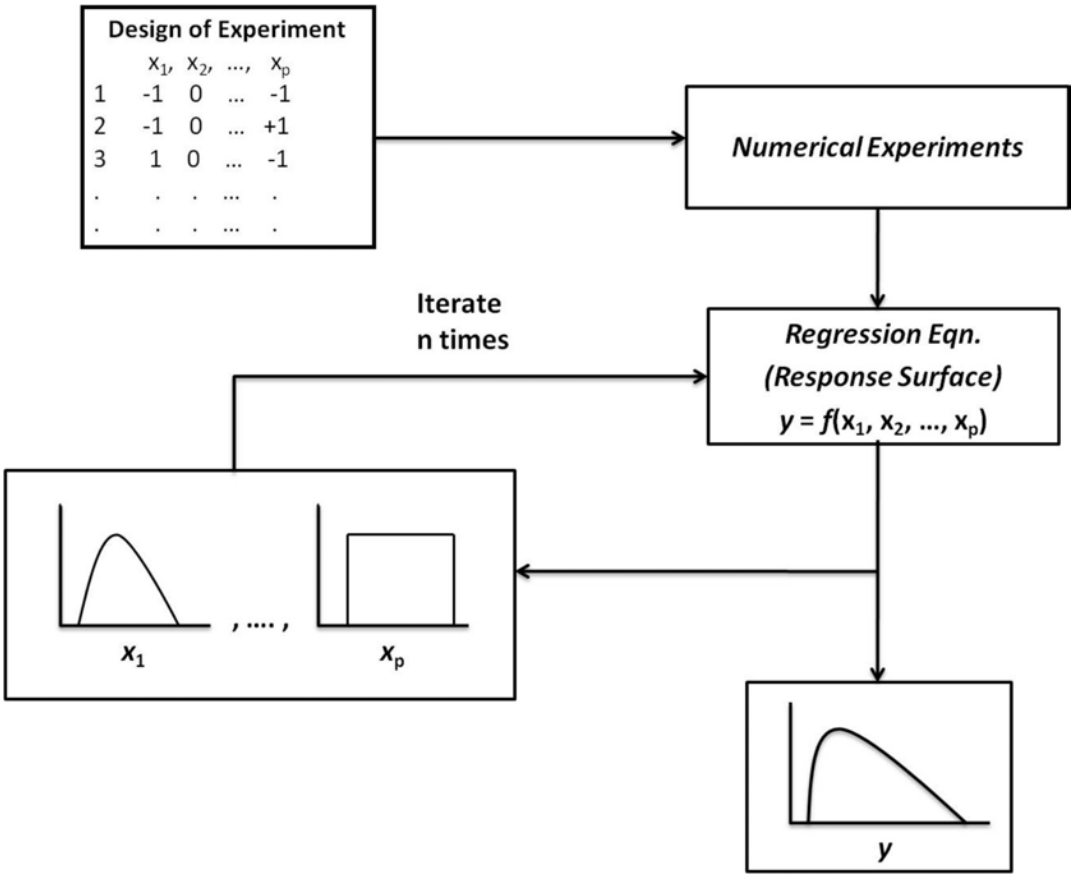


Figure 10.3. Workflow of the response surface method combined with the Monte Carlo simulations.

Design of Experiment (DoE)

RSM estimates a statistically linear model that fits to the responses from the DoE, which initially involves the identification of appropriate factors or design variables to be varied in the prediction of responses or outcome. Major goal of DoE techniques is to represent sampling space as much as possible given a limited set of laboratory or numerical experiments. Design space of factors should represent possible values and usually follows linear scaling of factor into the range of -1 (min) and 1 (max). Note that the invalid selection of the design space range in the input factors will lead to poor predictability beyond the range of -1 and 1.

In this study, BBD was used for the experimental design. The BBD is a particular subset of the factorial combinations from the 3^k factorial design, which consists of three levels (-1, 0, 1) for each factor. Each factor is placed at one of the three equally spaced values. The BBD has been widely used because of its economical design (less number of runs) compared to the full factorial designs

[*Montgomery*, 2008]. Full factorial design with 2-level (-1, 1) or 3-level (-1, 0, 1) is fully crossed design requires 2^k and 3^k runs, respectively. For example, for 5 factors BBD requires 41 runs while 3-level full factorial design requires 243 experiments. In addition, BBD contains not only the interaction terms of factors but also the higher-order quadratic effects. BBD includes the midpoint in the design and is nearly orthogonal and rotatable mathematically.

We selected 4 independent variables to be considered key factors for the BBD; thickness and permeability of Weber formation, permeability anisotropy ratio, and formation temperature. Likely variations in each factor are scaled to -1 and 1 for minimum and maximum of the range, respectively. Table 1 summarizes the three levels for each factor. Log-normal distribution is assumed for the permeability of Weber formation with mean (u=100 mD) and standard deviation (σ=1). Minimum, midpoint, and maximum of Weber formation's permeability in Table 1 correspond to u-2σ, u, and u+2σ in the log-normally distributed permeability, respectively. Uniform distribution is assumed for the remaining factors with each lower endpoint, midpoint, and upper endpoint given in Table 1. The thickness of Weber formation ranges from 61 to 244 m (200 to 800 ft) based on the initial geologic interpretation. The anisotropy ratio (k_v/k_h) is assumed to be constant but ranges from 0.1 to 1. Reservoir temperature is assumed to be isothermal and its variation among the numerical experiments is from 150 to 198 °F. Total 25 runs specified by BBD provide the corresponding output variables from the numerical experiments.

Table 10.1. Independent variables used in the design of experiment.

Independent variables (Xi)		Low (-1)	Mid (0)	High (+1)	Statistical distribution
X1	Thickness of Weber (m)	61.0	152.4	243.8	Uniform
X2	Permeability of Weber (mD)	13.5	100	738.9	Log-normal
X3	Anisotropy ratio	0.1	0.55	1	Uniform
X4	Reservoir Temperature (°C)	65.6 (150)	78.9 (174)	92.2 (198)	Uniform

Numerical Simulation

Given the design of experiment specified with the BBD, we performed numerical modeling work for the 25 cases. For initial conditions of the model, we assumed that the model is fully saturated with brine. A hydrostatic pressure ($P=\rho_w gh$) ranging from 1,872 psi to 4,948 psi was initially assigned according to the formation depth. Reservoir temperature was assumed to be isothermal and its variation among the numerical experiments is given in Table 1 as a dependent variable. The assigned pressure field and temperature values maintain the injected CO_2 in its supercritical phase within the model domain.

Both top and bottom layers of this model impose no-flow conditions, imitating the situation where the CO_2 injection formation is present under the regionally extended, low-permeability caprock and above basement rock. For the lateral boundaries representing extended aquifer beyond the simulation grid, we assign a large aquifer block to the lateral boundaries. Under these boundary conditions, the injected brine displaced by the CO_2 is allowed to flow laterally away from the injection region, such that the brine displacement does not exert a downward force on the CO_2 plume and permits buoyancy to act without interference.

In all simulations, supercritical-phase CO_2 was injected into the Weber formation during the initial 2-year period with the rate of 1 MMt/year, totaling 2,000,000 metric tons. We assumed that the injection well is fully perforated through the target formation. Total simulation time for this study is chosen to be 100 years including the injection period. Simulated results were collected and post-processed to obtain the dependent variables for the regression and assessment. Figure 10.4 shows the simulated CO_2 plume distribution of case 1 at 40^{th} year after the CO_2 injection activity ceases. Effect of hysteresis in the relative permeability was separately examined with and without the hysteresis option in the simulation. In this paper, we selected the Killough (1976) hysteresis method for the generation of scanning curves in the relative-permeability, hysteresis model.

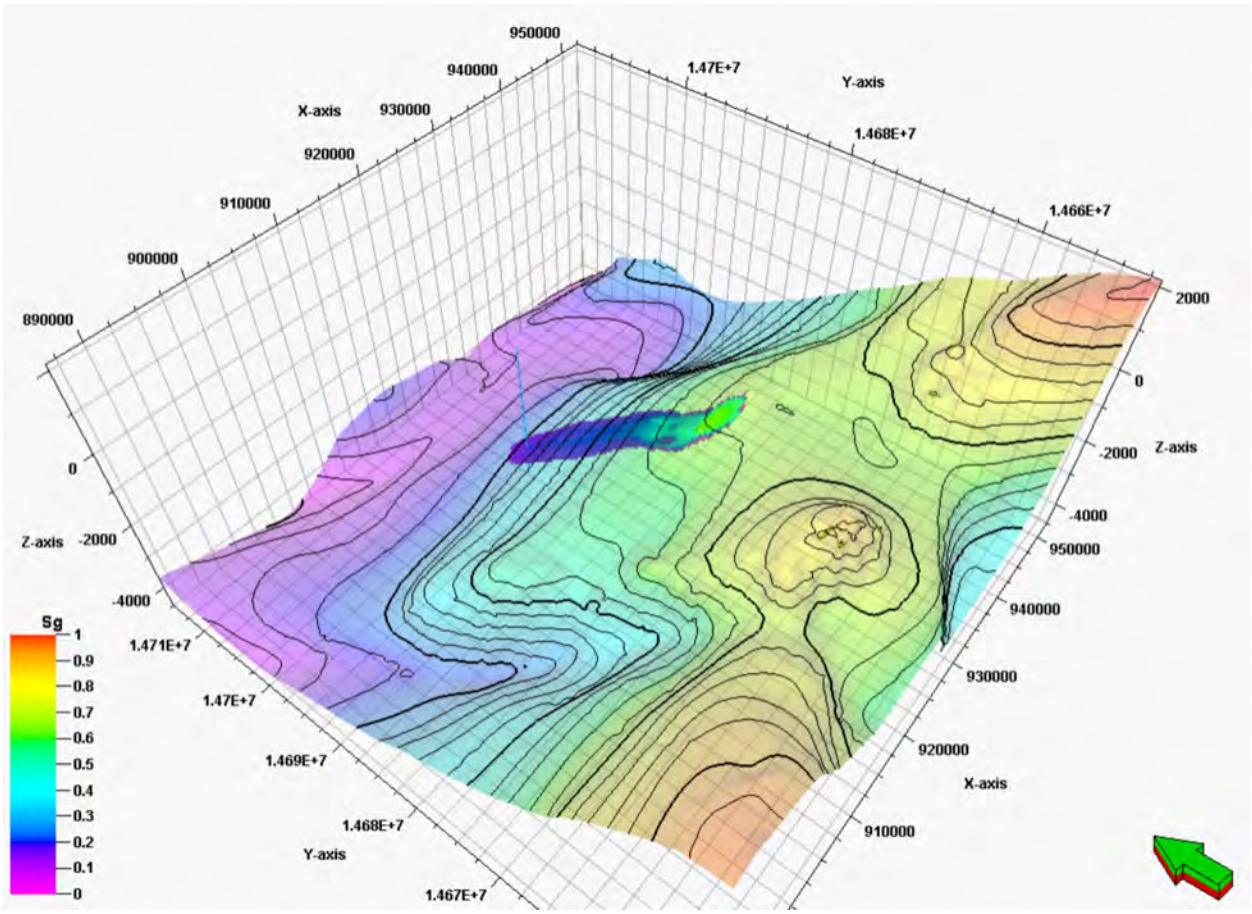


Figure 10.4. Simulated CO_2 plume distribution on top of the Weber at 40th year after the CO_2 injection activity ceases. Horizontal cell dimension is 330ft x 330ft. Vertical exaggeration is 2x.

Response Surface Model

Response surface method (RSM), or regression modeling, consists of mathematical and statistical techniques to develop a functional relationship between a response or dependent variable (y) of interest and associated independent variables or factors (x_1, x_2, …, x_k). The RSM typically involves the development of a polynomial approximation to the responses (y) obtained with a linear regression given the input/design variables (X_i) in a chosen DoE. A full second degree RSM for k independent variables is

$$y = \beta_0 + \sum_{i=1}^{k} \beta_i X_i + \sum_{\substack{i=1,j=2 \\ i<j}}^{k} \beta_{ij} X_i X_j + \sum_{i=1}^{k} \beta_{ii} X_i^2 + \varepsilon \qquad \text{Equation (1)}$$

where β_i, β_{ij}, and $_{\beta ii}$ represent regression coefficients and ε is random error assumed to have a zero mean. "k" is four in this study. Unlike the laboratory experiment, the random error due to the non-repeatability does not exist in a deterministic numerical experiment and is ignored in this study. Eqn. (1) contains linear, two-way interactions, as well as quadratic terms. We used least square method to

determine the coefficients of the polynomial equation at each time. Least squares estimator of beta is:

$$\hat{\beta} = (\mathbf{X}'\mathbf{X})^{-1}\mathbf{X}'y \qquad \text{Equation (2)}$$

Only significant variables and interaction terms (at the 95% significance level) were included in the RSM after application of stepwise regression procedure. The stepwise procedure is a multi-linear regression of the response values with iterative stepping based on their statistical significance in a regression. That is, it is repeatedly altering the model at the previous step by adding or removing a predictor variable in accordance with the entry and removal criteria, respectively until the stepping or altering is no longer possible given the stepping criteria or the maximum number of steps is reached.

We post-processed the numerical results for AoR (the areal CO_2 plume extent), x- and y-directional 1st moment of CO_2 plume, and pressure buildup as dependent variables. To quantity AoR, we evaluated the areal extent of CO_2 plume in the top layer and first spatial moments of the CO_2 plume with respect to x (M_x) and y (M_y) directions with the following equations [*Freyberg*, 1986; *Han et al.*, 2010; *Tompson and Gelhar*, 1990]:

$$M_{ij} = \int_{-\infty}^{\infty}\int_{-\infty}^{\infty} \emptyset\rho_{CO_2}(x,y)\, S_{CO_2}(x,y)x^i y^i dxdy \qquad \text{Equation (3)}$$

,

$$M_x = \frac{M_{10}}{M_{00}} \qquad \text{Equation (4)}$$

,

$$M_y = \frac{M_{01}}{M_{00}} \qquad \text{Equation (5)}$$

.

The first spatial moments represent the location of the mass center of the CO_2 plume.

The pressure build-up resulting from the CO_2 injection activity was evaluated at the injection well and three monitoring wells in the top layer. Three monitoring locations at 500 m, 1 km, and 5 km south of the injection well were chosen to investigate the effect on the proximal, middle, and distal region. Simulated pressure values were recorded at the top of each well perforation.

Goodness-of-Fit Measurements

To quantitatively examine and validate the simulated outcome/response fit to the observed values properly, we used two measures including mean absolute error (MAE) and coefficient of determination (R^2). Mean absolute error (MAE) is obtained by

$$\text{MAE} = N^{-1}\sum_{i=1}^{N}|y_i - f_i| \qquad \text{(Equation 6)}$$

where y_i and f_i are observed and simulated response, respectively at case *i*. MAE is given in the units of the variable. Coefficient of determination (R^2) is determined by

$$R^2 = 1 - \frac{\sum_{i=1}^{N}(y_i - f_i)^2}{\sum_{i=1}^{N}(y_i - \bar{y})^2} \qquad \text{(Equation 7)}$$

where $\bar{y}$ is the mean of the observed data. R^2 measures the degree of variation in the response that can be explained by the model. In addition, we also looked at mean squared error (MSE), normalized MSE (NMSE), normalized root-mean-squared error (NRMSE), mean-absolute-relative error (MARE), coefficient of correlation (R), and coefficient of efficiency (COE) to further investigate whether the response model was statistically acceptable or not. Figure 10.5 showed the cross-plot of the simulated and predicted pressure build-up response at t=3,650 days with the goodness-of-fit measure results. We first considered the results with $R^2 > 0.9$ as the acceptable model criteria. Although R^2 is not above the acceptable level, we considered the model as acceptable regardless of the goodness-of-fit measures when the maximum absolute error is less than 0.1% of its corresponding actual value.

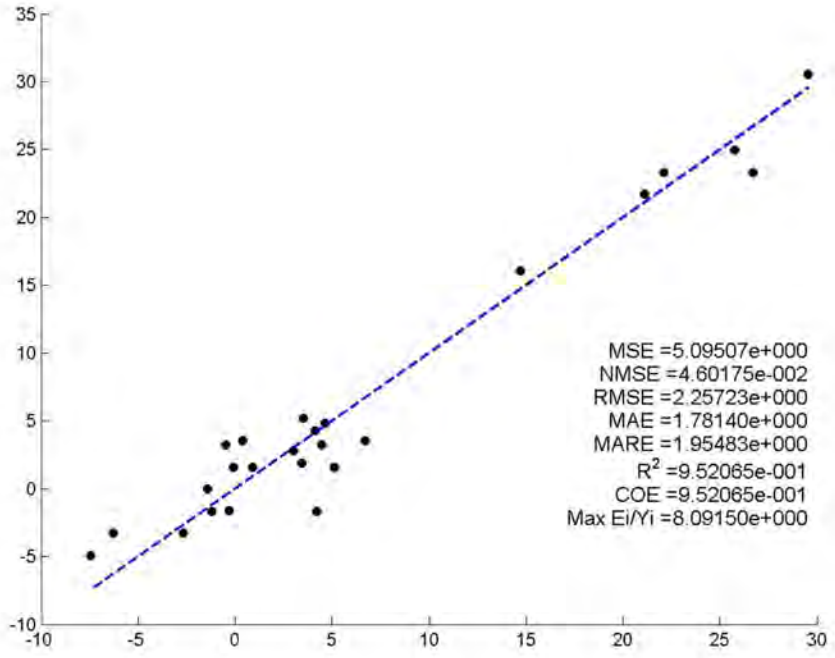


Figure 10.5. Observed vs. predicted pressure build-up (psi) of injection well at t=3,650 days.

Monte Carlo simulation through RSM

A series of random combinations drawn from the input distributions of the input factors is applied to the fitted response surface equation and creates a large number of realizations, resulting in a probabilistic distribution function of the output variable. We performed 10,000 iterations of Monte Carlo samplings associated with the identified RSM for each dependent variable and time. Note that dependent variables are statistically mutually independent. Each iteration represents a combination of input variables sampled from the given probability distributions and contributes to the construction of probability distribution in the outcome. Figure 10.6 showed the series of separate, probability-density functions

(PDFs) obtained at each specified time. Smooth change in the PDFs was made possible due to the appropriate adjustment in output interval, leading to the interpolation of probability distribution functions from one to the next time. Because of the rapid change in pressure response during the injection period, it was necessary to reduce the time steps during, and right after, the injection period. Thus, temporal evolution of the probability distribution functions was mapped for each dependent variable as a final result.

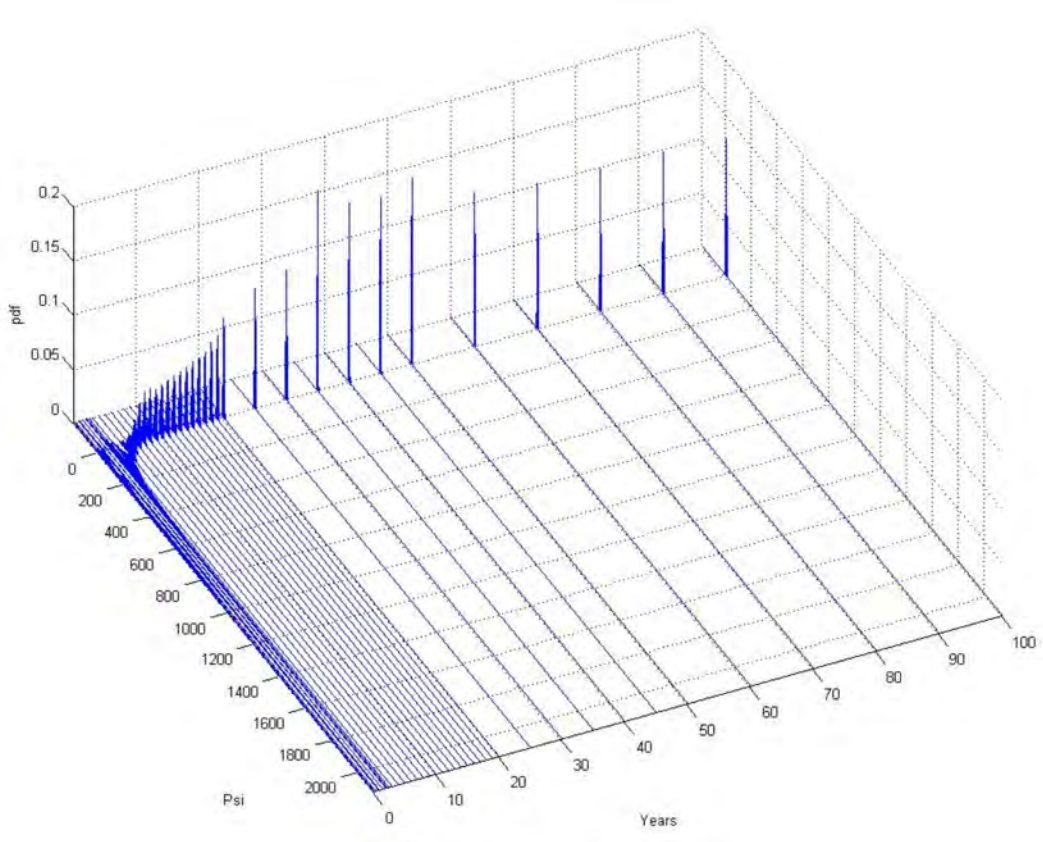


Figure 10.6. Probability density functions for the pressure build-up (psi) at the injection well.

Results

As described in the previous sections, we have constructed a RSM associated with 4-factor BBD experimental design and performed the regression modeling with the stepwise regression method on the outcomes (responses) from the specified numerical runs. After validating the regression model with various goodness-of-fit measures, we applied Monte Carlo simulation with the fitted RSM at each time. Post-processed results include the collection of the dependent variables (y = aerial extent, spatial 1st moments of CO_2 plume, pressure build-up in the injection well and three monitoring wells) for the assessment of geologic CO_2 storage.

Either PDFs or corresponding cumulative distribution functions (CDFs) can display the probability distribution in the outcome. CDFs shows the probability level associated with the dependent variable (e.g., CO_2 plume size) greater than or less than a certain level. In Figure 10.7, the 95th percentile (P95) of projected plume size falls below approximately 6x10^7 ft^2 after 20 years. Similarly, the 50th percentile (P50) or median of the projected plume size indicates the plume size is about 2x10^7 ft^2. Figure 10.7 also shows the likely range of the projected plume size between lower quartile (P25) and upper quartile (P75) gradually increases and gets stabilized as 2x10^7 ft^2 after 20 years. The likelihood, or probability, of being greater than, or less than, a certain plume which can be a design target can also be obtained from this result.

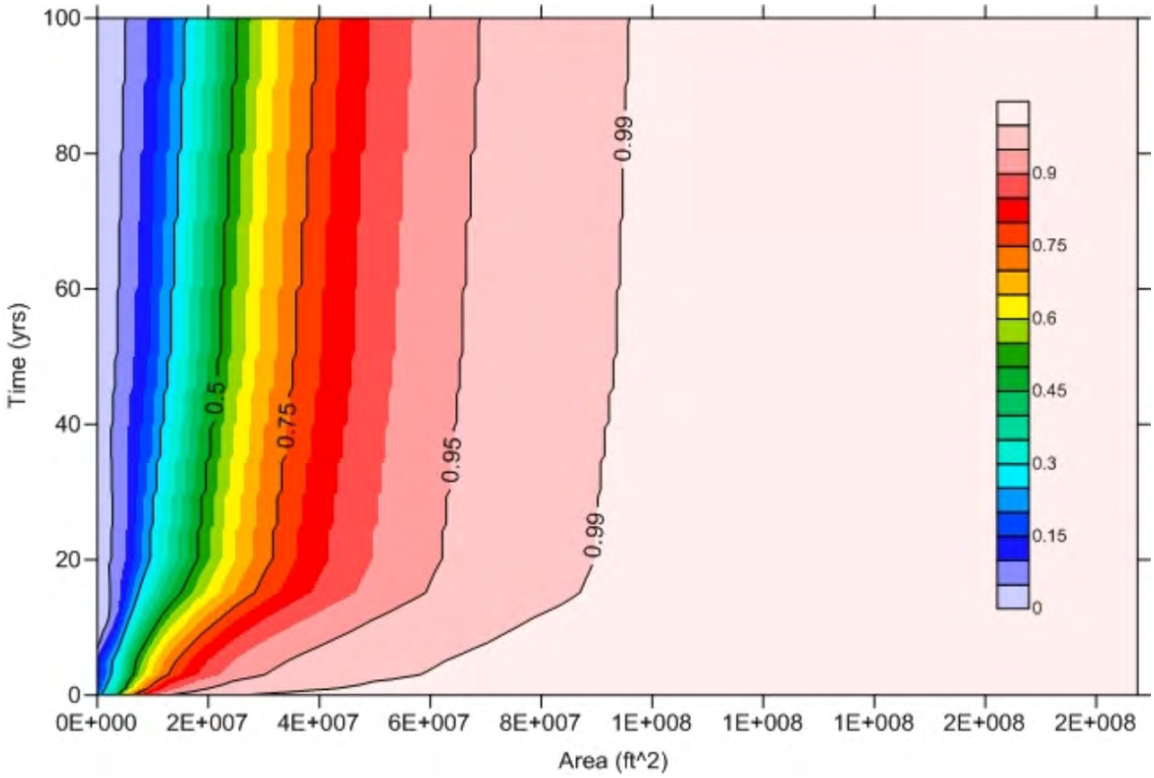


Figure 10.7. Contour map of the CDFs for the CO_2 plume extent in the top layer of the Weber formation.

Given the range/distributions of input variables, the predicted CO_2 plume size tends to increase rapidly for the initial 20 years (Figure 10.7). Our results indicate that the CO_2 plume keeps growing, but slowly, even at the end of the simulation time (year 100). This could be related to the low irreducible gas saturation used in the relative permeability function. Under the conservative perspective, this can provide the maximum CO_2 plume migration, but better prediction can be made from the relative permeability function that will be obtained from the collected core samples.

Since the results of CO_2 plume size do not provide the migration information, x- and y-directional 1st moment results were used to delineate the center of the CO_2 plume (Figures 10.8a and 10.8b). Both x- and y-directional 1st moment results

showed the CO_2 plume tending to migrate toward the east and south, respectively. P95 of x-dir 1st moment is about 875 ft east of the injection well location and 5,000 ft south for the P95 of y-dir 1st moment at the end of the simulation time. Calculated plume migration rate in the up-dip direction (y-dir) after the injection stops is approximately 25 ft/yr in the model with the hysteresis whereas it was about 70 ft/yr without the hysteresis. Our results showed the strong dependency of plume size and migration rate/distance on the hysteresis model especially in the long-term prediction. In addition, the variation/range in the outcomes was reduced notably with the hysteresis model.

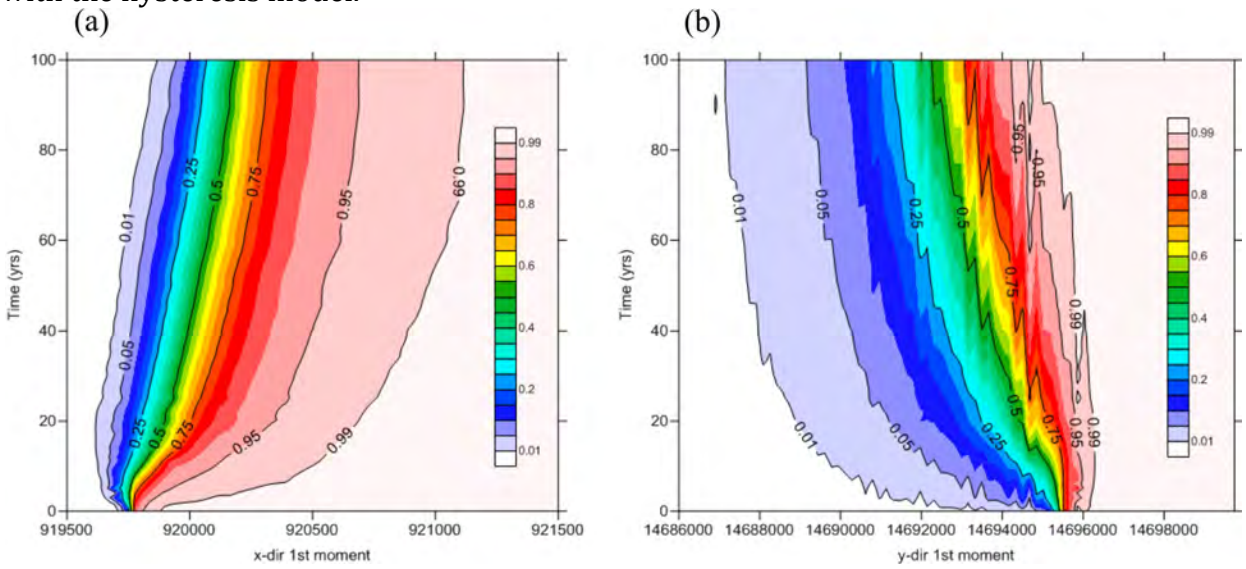


Figure 10.8. Contour map of the CDFs for the x- (a) and y-directional (b) lst spatial moment of CO_2 plume.

Figure 10.9a showed the predicted pressure build-up at the injection well. The immediate pressure response resulted from the CO_2 injection and reached the peak at about 1 year after the injection starts. After the peak, the pressure build-up decreased and quickly diminished after two years of CO_2 injection. The P95 of the outcome is within the 1,600 psi increase and P50 of the results are less than, or equal to, about 750 psi increase at the peak. It seems it takes about 5 years to return to the original pressure condition after CO_2 injection terminates. At the proximal location (500 m from the injection well), pressure is building up continuously until the injection stops (Figure 10.9b). However, the magnitude of pressure build-up is smaller than the one at the injection well (700 psi within P95 at the peak). In addition, returning to the pre-equilibrated pressure takes a little longer. At the second monitoring well located 1 km south of the injection well, we found the pressure response is very similar to the one at the proximal location. The magnitude of the pressure build-up decreased (about 500 psi within P95 at the peak) and the arrival time of the peak was slightly delayed (Figure 10.9c). Figure 10.9d shows the CDF map of pressure build-up at the distal location (5 km from the injection well). Unlike the pressure build-up at the injection well and proximal well locations, the pressure returns to the original state slowly. The pressure

build-up reached the peak at the end of injection activity (t = 2 yrs) for all the monitoring wells and diminished thereafter.

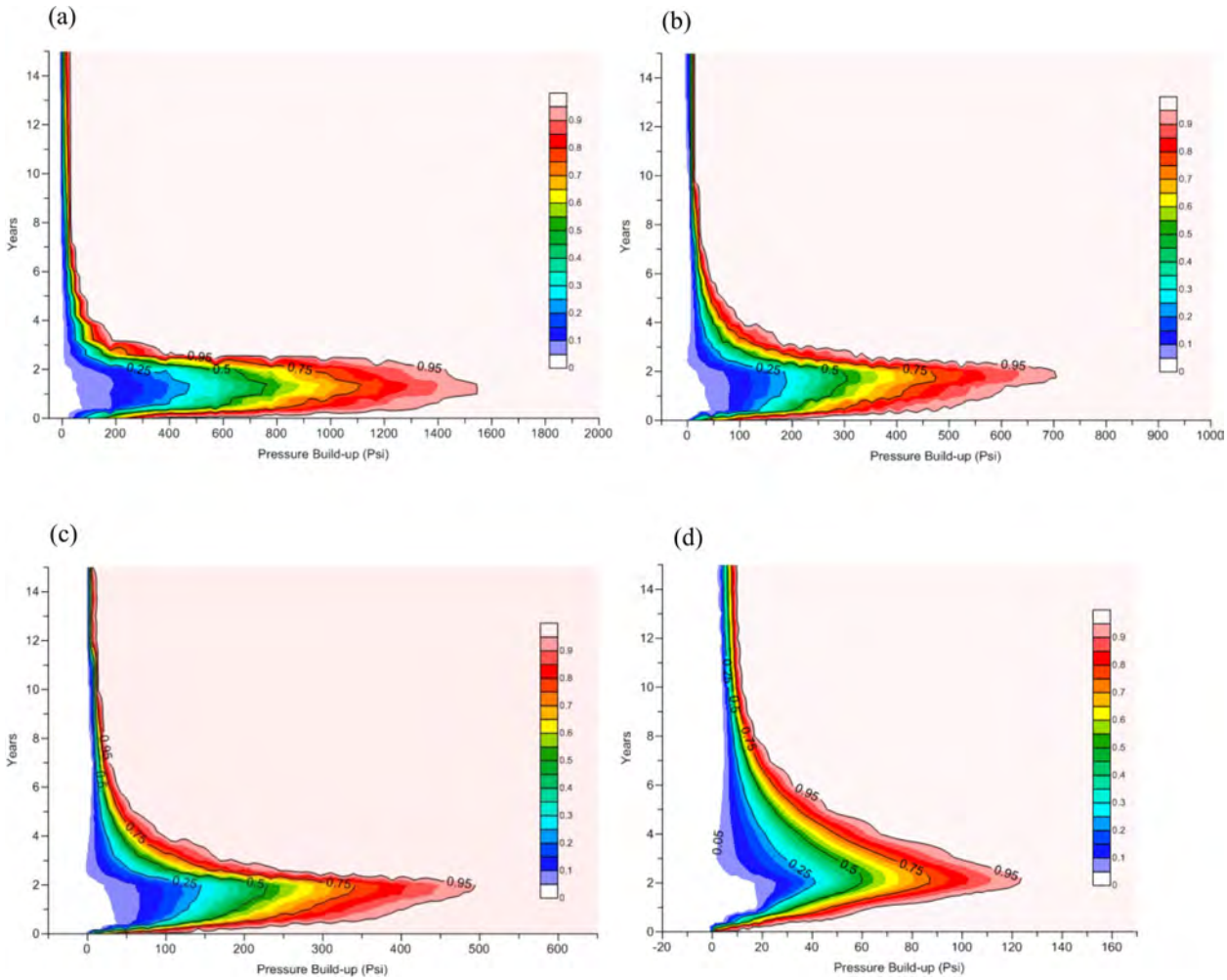


Figure 10.9. Contour map of the CDFs for the pressure build-up at the injection well (a) and three monitoring locations at 500 m (b), 1km (c), and 5 km (d) south of the injection well.

In general, pressure build-up, both in the injection and monitoring wells, exhibited extreme, positively-skewed distribution, which suggests the tendency of low pressure build-up in the mean sense given the range of input parameters. During the injection period, rapid jump in the pressure build-up was well shown both in the injection and monitoring wells. However, its magnitude is smaller in the monitoring well. Likewise, maximum pressure buildup during the injection period was significantly smaller in the monitoring well. In addition, unlike the injection well, the simulated pressure at the monitoring wells exhibited the increase in time lag in the pressure response according to the increase in the distances from the injection well and monitoring wells. Note that the pressure dissipation after injection period took about 6 years to return to the original condition.

Mitigation Strategies

As discussed in detail in the previous sections, estimated PDFs and CDFs for specific risk features, events or processes, or "FEPs," provide a quantitative measure of the likelihood of that risk FEP. Also essential for comprehensive risk management, is an appropriate mitigation strategy. However, for this, and probably all, geologic carbon storage sites, mitigation plans are predicated on the number and types of wells involved in the project. Thus, for purposes of this topical report, we propose only a generalized Mitigation Strategy that accounts for the most likely permutations of project design and setting.

Figure 10.10 exhibits a generalized geologic carbon storage site under normal conditions, including an injection well and at least two observation wells.

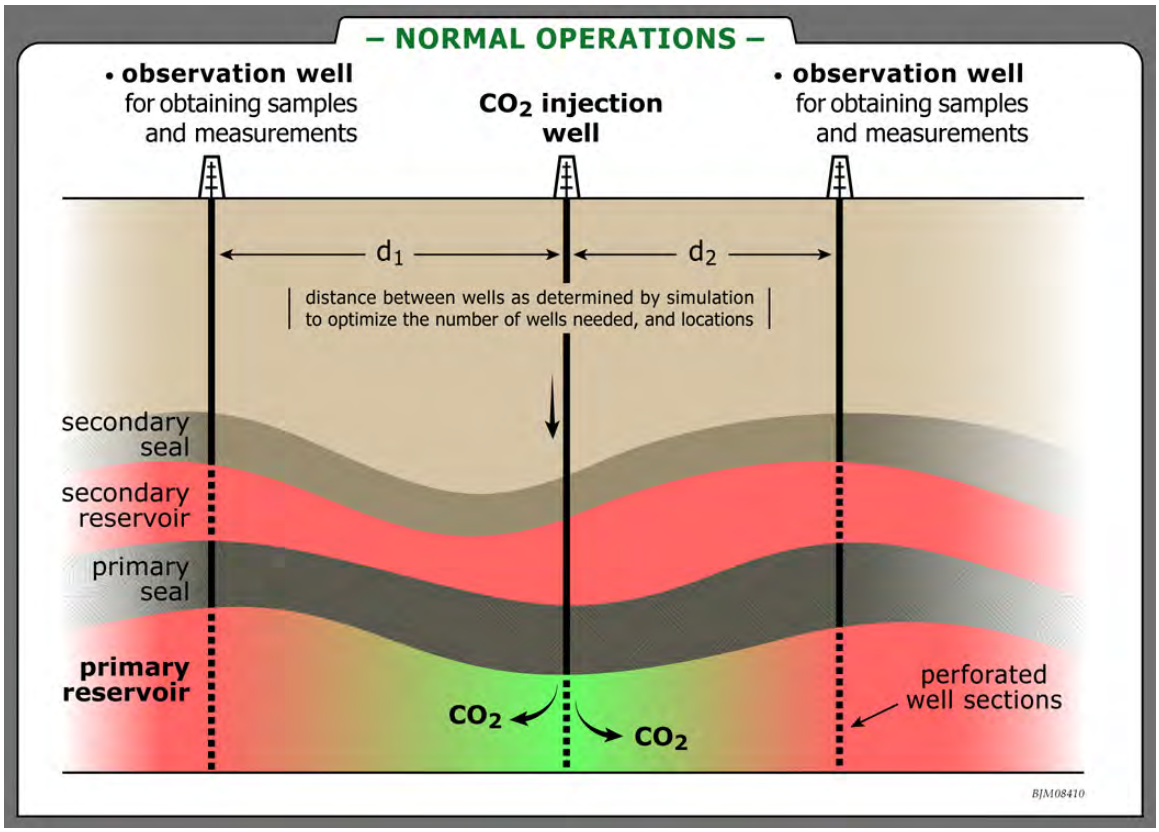


Figure 10.10. Schematic of "normal" operations of a geologic storage site. Adapted after McPherson (2009).

Figure 10.11 expresses how leakage from the primary reservoir (into a secondary reservoir above) may be managed by injection of water into the secondary reservoir, thus imposing a "fluid pressure seal" in that secondary reservoir. Such an approach assumes that observation wells can be used for injection, or that separate injection wells are ready.

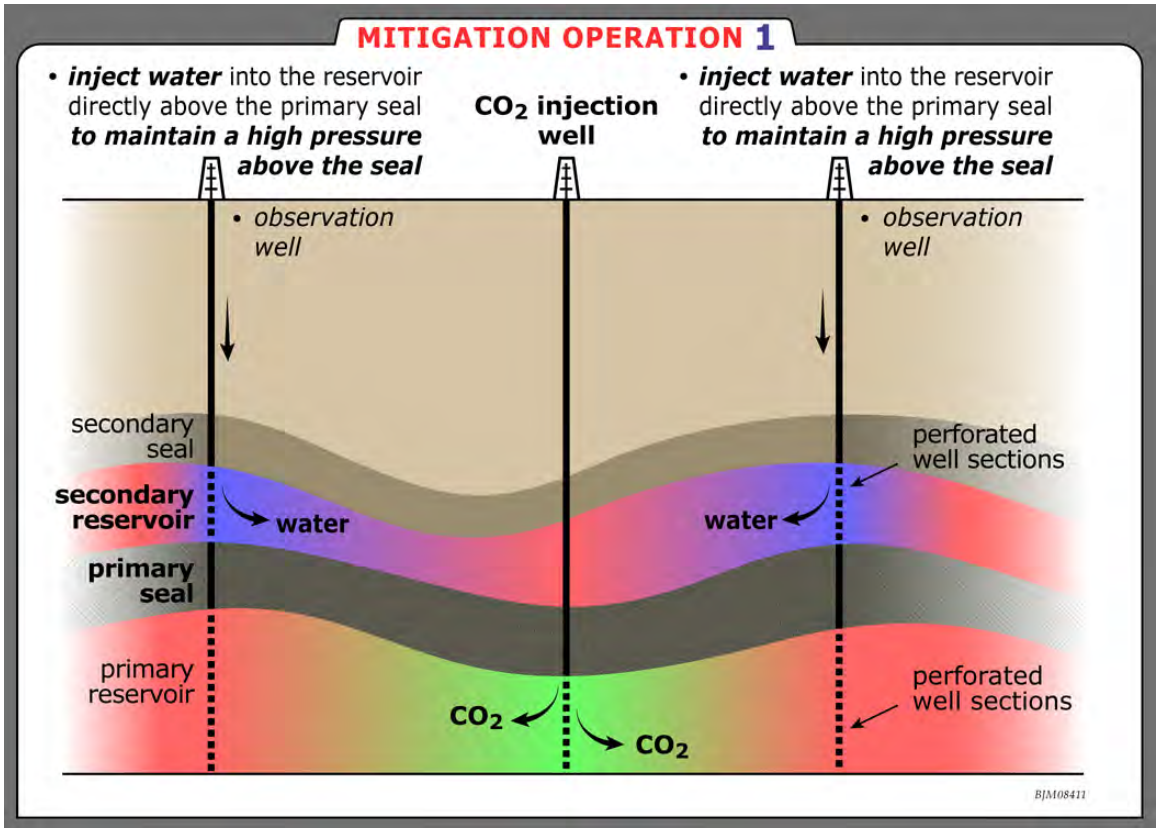


Figure 10.11. Schematic showing injection for inducing a "fluid pressure seal" in the secondary reservoir, to minimize leakage from the primary reservoir into that secondary reservoir. Adapted from McPherson (2009).

Figure 10.12 expresses a mitigation approach with respect to containing a CO_2 plume and reducing AoR. Specifically, injection of water into the primary reservoir could be used to create a pressure "wall" to contain the plume. Such an approach is predicated on sufficient injection well availability.

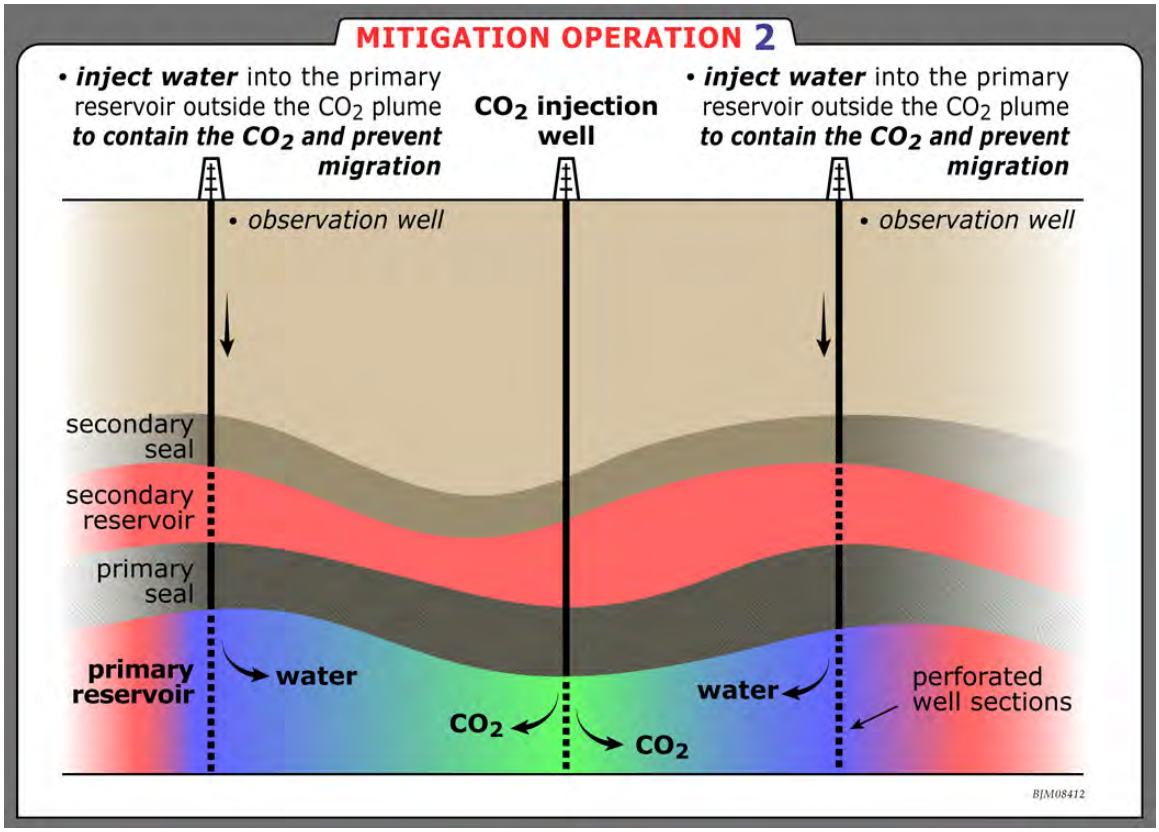


Figure 10.12. Schematic of how injection wells may be used to create a "pressure wall" that contains a CO_2 plume and limits AoR. Adapted from McPherson (2009).

Regarding effective reservoir pressure reduction, or relief, from excessive pressure buildup associated with injection, Figure 10.13 expresses the simplest of concepts: vent CO_2 to the atmosphere. Of course, hydraulic diffusivity may be such that the time for pressure to decay is too long, in which case either water/brine production from the secondary reservoir (Figure 10.14a) and/or CO_2 production from the primary reservoir (Figure 10.14b) may be necessary to facilitate faster pressure reduction. Other permutations are possible, depending on the FEP in question and the project design, specifically, the number of production/injection wells available for mitigation operations.

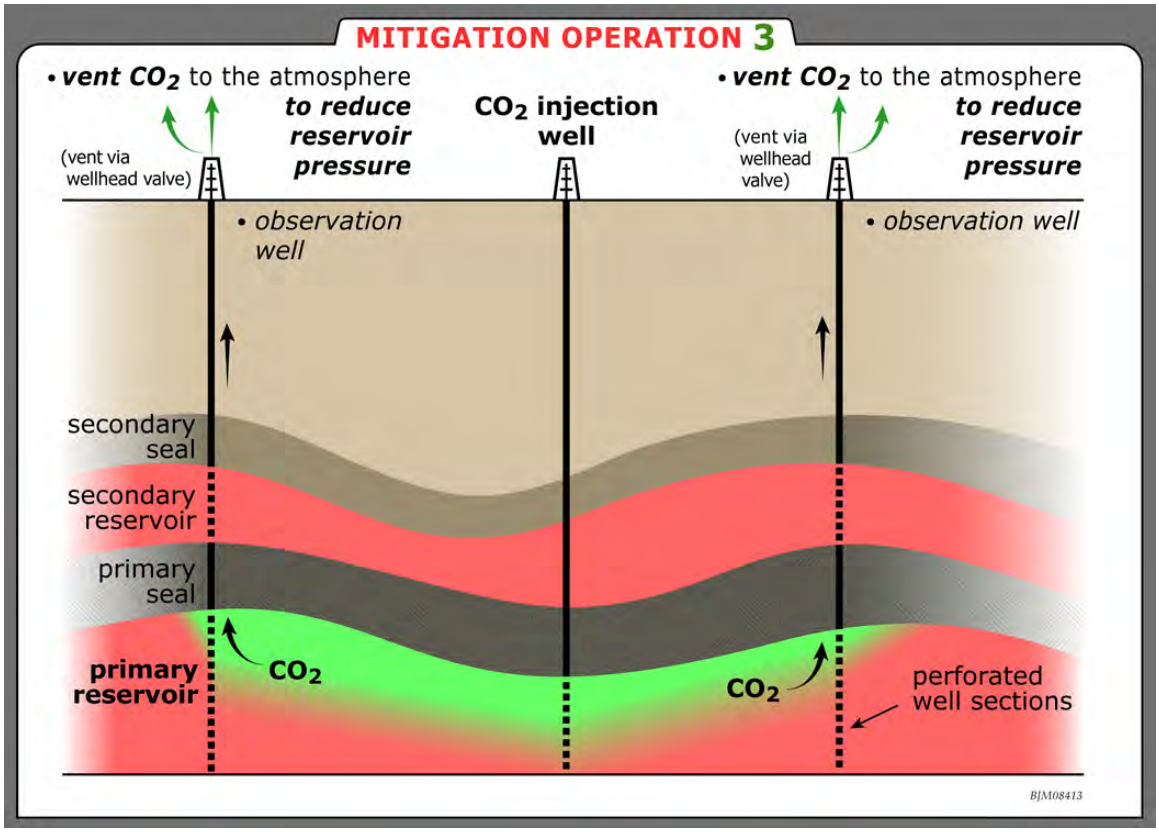
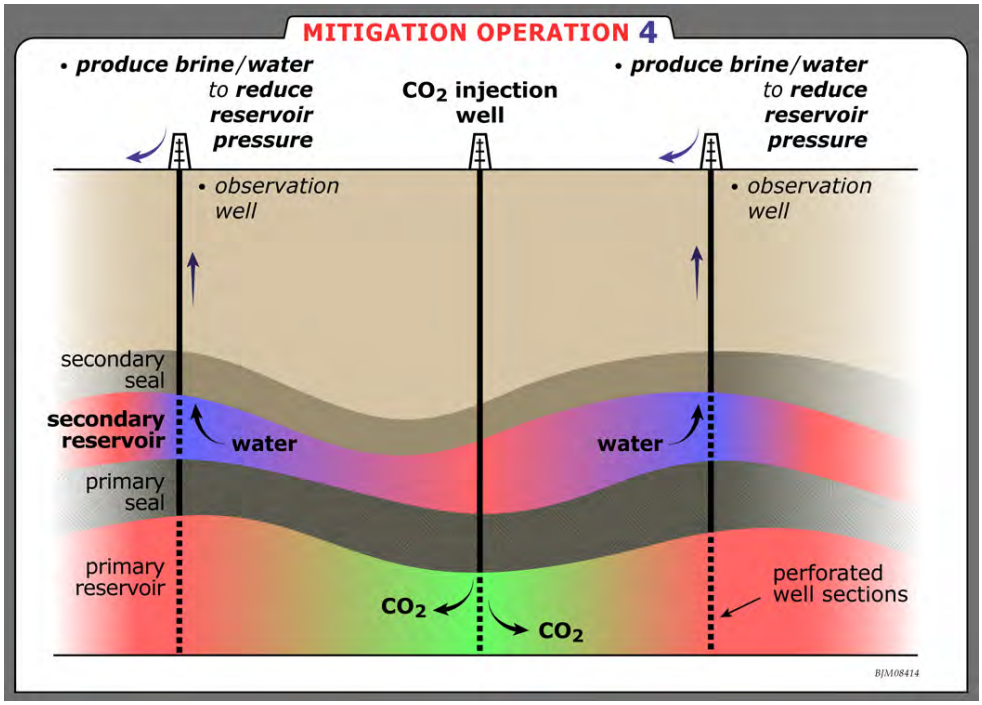


Figure 10.13. The simplest mitigation approach for excessive pressure buildup is CO_2 venting. Adapted from McPherson (2009).

(a)



(b)

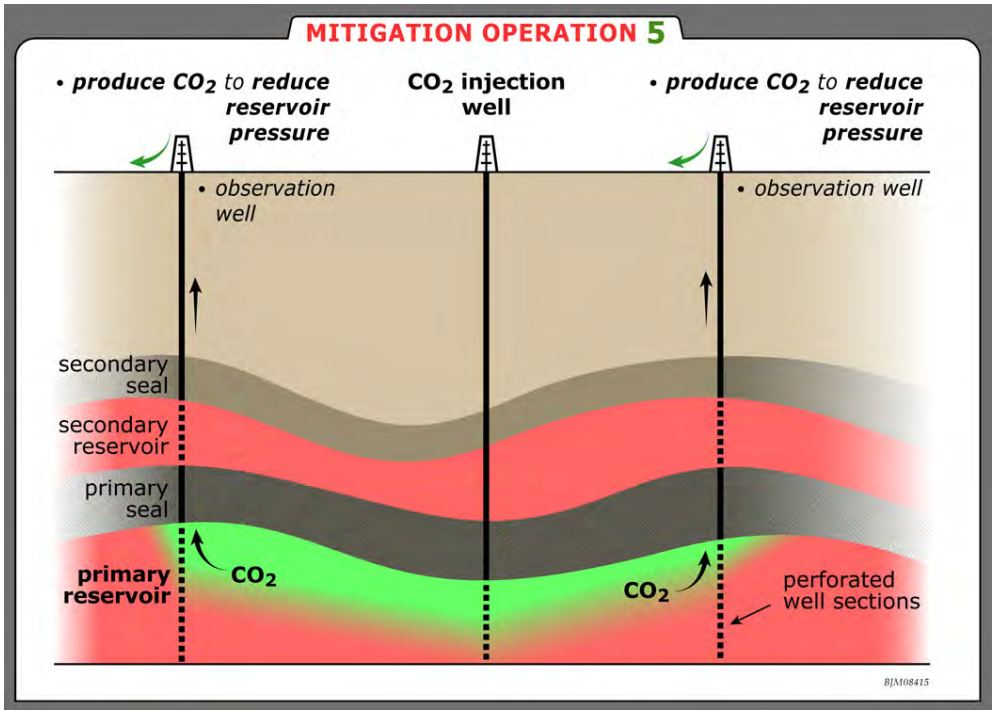


Figure 10.14 (a) Water production from the secondary or primary reservoir may be a means of pressure management; (b) CO_2 production from the primary reservoir is also a means of pressure reduction. Adapted from McPherson (2009).

Conclusions

We presented the probabilistic evaluation of growth and migration of injected CO_2 plume and pressure build-up in the proposed injection well and monitoring wells, in Craig site, Colorado. Our approach includes the development of

response surface model (RSM) associated with the Box-Behnken design (BBD), corresponding numerical modeling experiments, and Monte Carlo simulations. Our approach accounted for the probability distributions to characterize variability or uncertainty in prediction estimates for the probabilistic evaluation of geologic CO_2 storage and allows us to effectively analyze the risk or uncertainty in the site selection (pre-injection) stage and easily update the results upon the availability of additional data throughout a project (during- and post-injection stage). Furthermore, it can also be applied to the site screening and project management, monitoring plan, optimization, and risk mitigation plan given the uncertainty in the input parameters.

11. Project Summary and Conclusions

The RMCCS (Rocky Mountain Carbon Capture and Sequestration) project concept was initiated with a meeting of the State Geologists of Arizona, New Mexico, Utah, and Colorado. All agreed that the Colorado Plateau presented an excellent opportunity to conduct a broad scale, regional study of the potential for carbon capture and sequestration. The Pennsylvanian Weber, Jurassic Entrada, and Cretaceous Dakota Sandstones (and their equivalents) are formations that are widespread throughout the Plateau and generally exhibit good permeability and porosity, suggesting they are the most promising carbon sinks in the region. A number of significant point sources of CO_2 throughout the Plateau are documented (Figure 1). All sources are proximal to one or more of these promising sink formations.

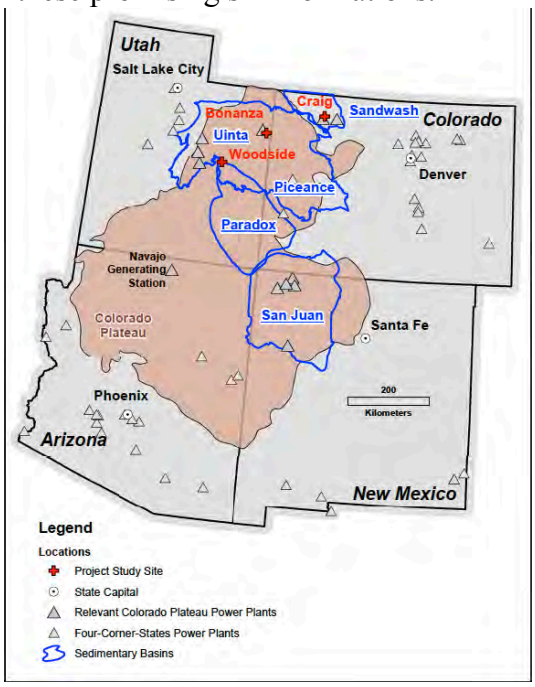


Figure 11.1: Colorado Plateau shown in tan. The site-specific studies done by the Utah and Colorado Geologic Surveys are indicated with red crosses and prominent basins evaluated are outlined in blue. Locations of coal-fired electrical generating stations in the four states are shown by triangles.

In addition to characterizing promising targets, the RMCCS partnership aims to develop protocols for characterization and storage capacity calculations to support eventual commercial development of stacked, high-potential storage formations throughout the Colorado Plateau and the Rocky Mountain Region.

Because of the state geological surveys' long relationship with Dr. Brian McPherson through the Southwest Partnership for Carbon Sequestration (SWP), he and his team at the University of Utah were asked to join the project. Tri-State Generation and Transmission, Shell Exploration and Production, and Schlumberger Carbon Services also joined the project as industry partners.

A site near Craig, Colorado was selected for a stratigraphic, characterization well based on several criteria: location near a major point source of CO_2, presence of a large

structural trap, preliminary estimates of ample storage capacity by the SWP Phase I study, presence of all three formations, affirmative landowner permission, and regional potential for storing large emissions from oil shale and gas processing facilities.

A proposal was submitted to the Department of Energy's (DOE) National Energy Technology Laboratory (NETL) in the summer of 2009.

Identification and Analysis of Appropriate Local Sites

The four state geological surveys conducted regional studies of their parts of the Colorado Plateau for overall CO_2 storage capacity in the target formations. As part of these analyses, they identified specific candidates for sequestration.

UTAH

The UGS evaluated potential CO_2 storage sites in the Uinta Basin that have one or more of the primary reservoirs—Pennsylvanian-Permian Weber, Jurassic Entrada, and Cretaceous Dakota Sandstones. First a table was constructed of potential sites based on geologic maps and published reports of the basin. These sites had to have one or more of the primary reservoirs at 2500 feet (760 m) or more depth and contain saline water with 10,000 TDS or more. Area and reservoir parameters from published maps, reports, and regional databases were added to the table and a preliminary storage capacity was calculated for each site. Included in the table were landownership, usage, and infrastructure. The table was then given to four UGS geologists who were asked to rank the sites as potential storage sites.

Some of the sites were eliminated because preliminary calculations indicated they had less than 30 million metric tonnes (MMT) of potential storage capacity. One site was eliminated because it had water quality less than 10,000 TDS. The evaluation team reached a consensus and the Bonanza site was ranked number 1 and the Woodside site was ranked number 2; both were selected for detailed characterization.

The detailed characterization of Bonanza site calculated more storage capacity than in the preliminary table. However, the Dakota reservoir is currently gas productive in the area limiting the near-term CO_2 storage potential. The Entrada and Weber reservoirs have very limited data in the Bonanza area and could change significantly if more data is gathered. Additional significant CO_2 storage capacity may exist in the Cretaceous Castlegate Sandstone and Tertiary Wasatch Formation; neither were evaluated as part of this study.

The detailed characterization of Woodside site resulted in less storage capacity than in the preliminary table. The lower storage capacity was due to significantly less area for both the Mississippian Redwall Limestone and Permian White Rim Sandstone reservoirs and much thinner net reservoir thickness for the Redwall. The study revealed that the Permian Black Box Dolomite (Kaibab Formation) can be both a seal for the White Rim and a storage reservoir. Seismic data is needed to determine if the storage area, or structural closure, is larger than we calculated. The net thickness of the Redwall reservoir (4% or more porosity) was based on one well that penetrated the entire Redwall at Woodside. Additional drilling could reveal a significantly thicker porous reservoir greatly increasing the storage CO_2 capacity.

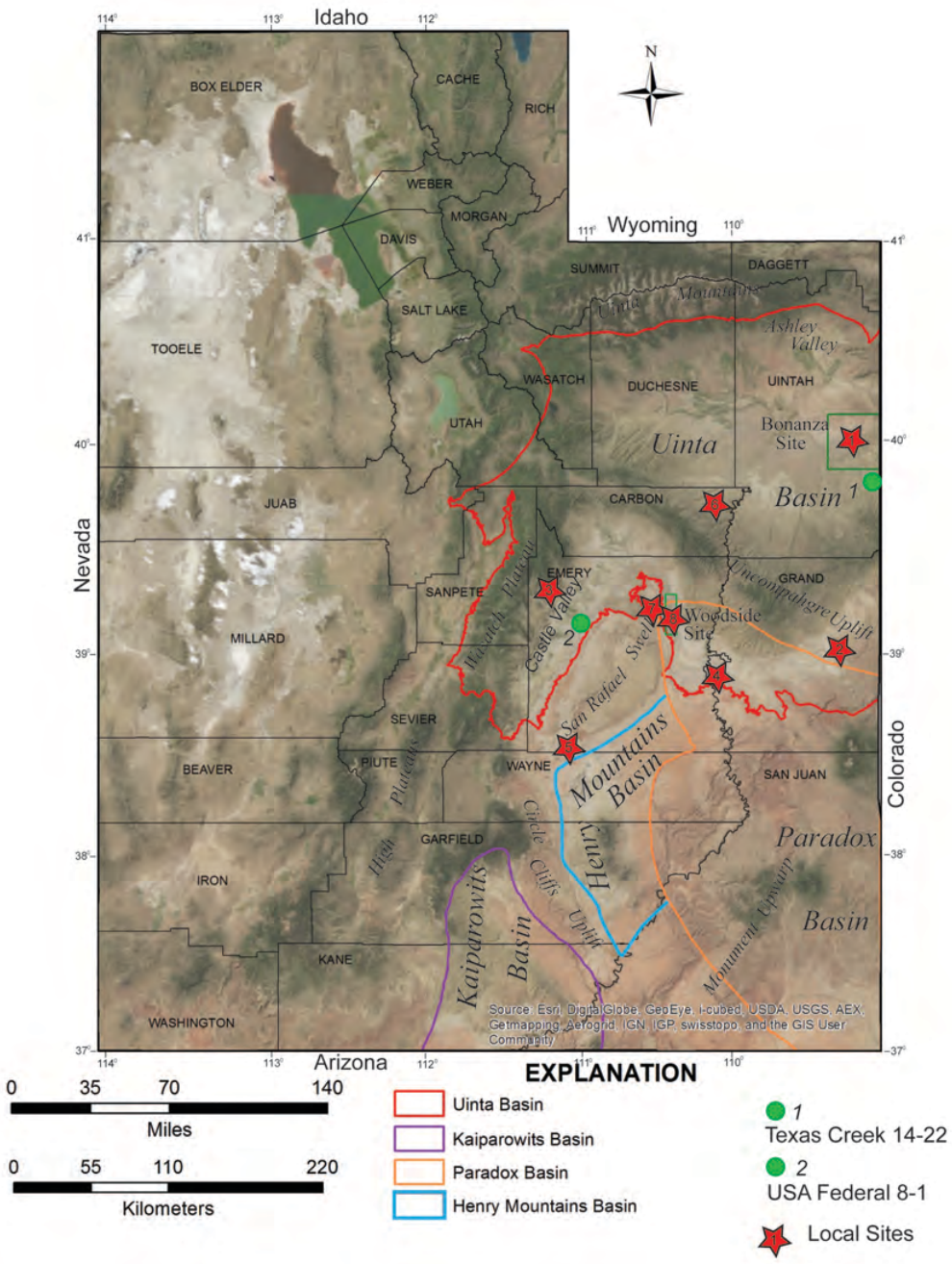


Figure 11.2 . Map of Utah showing basins and uplifts of the Colorado Plateau. Local sites evaluated as potential storage sites (see table 1), 1 = Bonanza, 2 = Cisco Dome, 3 = Gordon Creek, 4 = Green River South, 5 = Last Chance, 6 = Peters Point, 7 = Summit, and 8 = Woodside. The Bonanza and Woodside sites (rectangular outlines) were selected for detailed characterization. Well (green circle) 1 has a Weber Sandstone (?) core and Well 2 has a White Rim core.

The detailed characterization of Woodside resulted in less storage capacity than in the preliminary inventory. The lower storage capacity resulted from estimates of area for both the Mississippian Redwall Limestone and Permian White Rim Sandstone reservoirs that were far less than initial estimates, and because the estimated net reservoir thickness of the Redwall was much less than initially estimated. The study revealed that the Permian Black Box Dolomite (Kaibab Formation) can be both a seal for the White Rim and a storage reservoir. Seismic data are needed to determine if the storage area, or structural closure, is larger than what the UGS calculated. The net thickness of the Redwall reservoir (4% or more porosity) was based on one well that penetrated the entire Redwall at Woodside. Additional drilling could reveal a significantly thicker reservoir and therefore a much larger estimate of storage capacity.

ARIZONA

Northeastern Arizona encompasses the southwestern part of the Colorado Plateau, an area of gently dipping to slightly tilted Paleozoic and Mesozoic strata that includes porous and permeable sandstone units. The Lower Permian Cedar Mesa Sandstone was identified for study as a potential target for CO_2 sequestration. The Cedar Mesa Sandstone is overlain by the impermeable Organ Rock Formation, which forms a seal. The salinity of groundwater in the Cedar Mesa Sandstone is unknown, and must be determined before CO_2 can be sequestered (because CO_2 sequestration is not permitted in potable groundwater under current regulatory conditions). Well logs for 755 drill holes were used to evaluate the extent, depth, and thickness of subsurface formations. The ESRI® ArcMap™ GIS software was then used to calculate the volume of the Cedar Mesa Sandstone in all areas where the top of the unit is below 3000 feet (915 meters) depth, the minimum depth necessary for optimum CO_2 sequestration conditions. Well logs were used to evaluate porosity, which were then used to calculate the amount of pore space at least theoretically available for CO_2 storage (the effective porosity). The Arizona Geological Survey calculates between 30 km^3 and 80 km^3 of pore space in the Cedar Mesa Sandstone. The net fraction of pore-space accessible to CO_2 injection is estimated to be approximately 0.5% to 5%. For context, application of this storage efficiency to the Cedar Mesa Sandstone indicates that 0.15 km^3 to 4.3 km^3 of pore space is accessible to injected CO_2, and that 0.114 to 3.24 billion tons of CO_2 could be sequestered in this pore space at a density of approximately 750 kg/m^3.

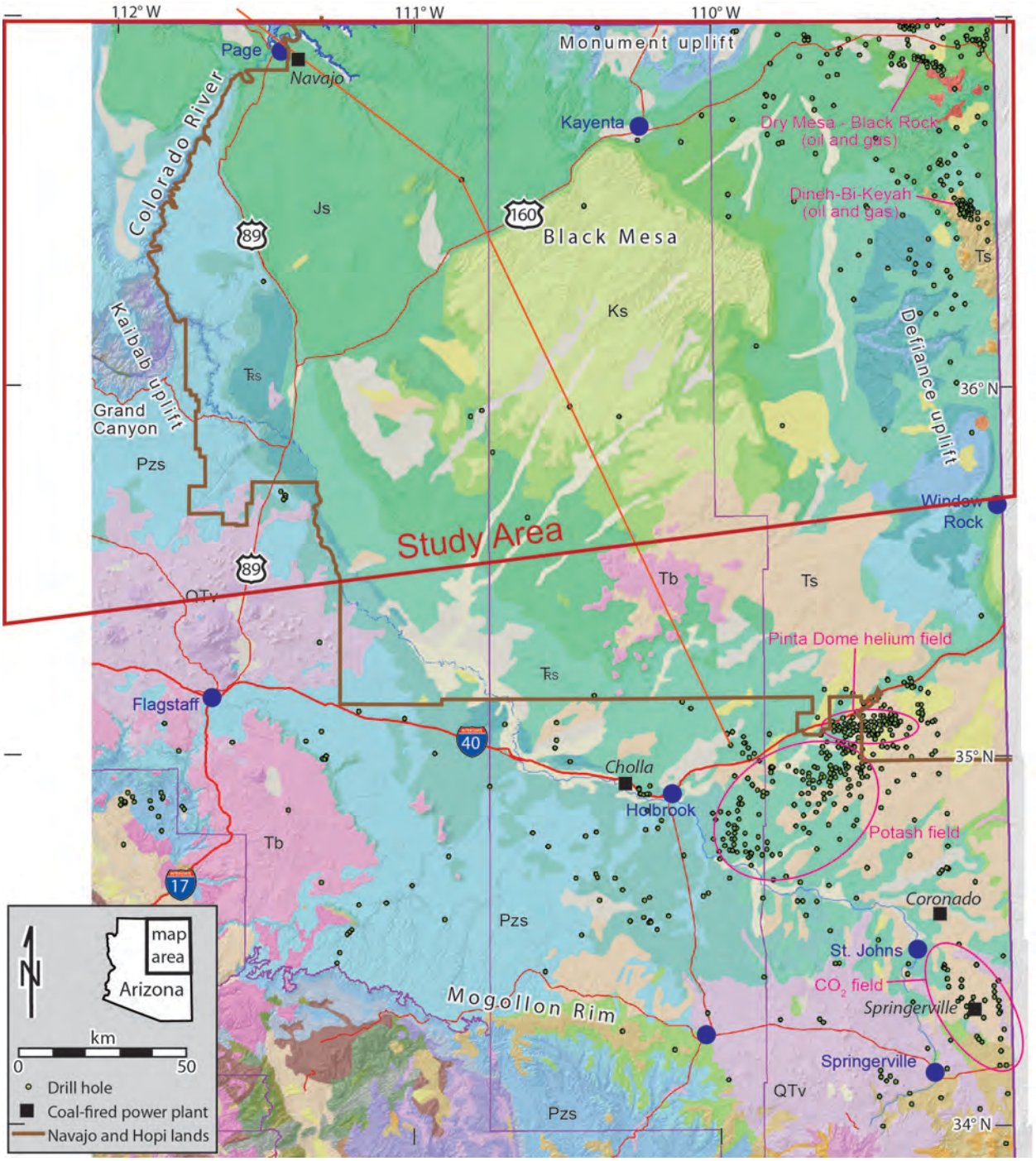


Figure 11.3: Area of northeastern Arizona where the Arizona Geological Survey studied the Cedar Mesa sandstone for its sequestration potential.

NEW MEXICO

The search for reservoirs with appropriate properties for sequestration, including

- accompanying tight seals that occur between 3,000 and 13,000 feet
- total dissolved solids of greater than 10,000 µg/l and
- apparent capacity in excess of 500K barrels of oil equivalent (BOEs)

is straightforward in New Mexico because of its long history of oil and gas production in the San Juan Basin. The tremendous sizes of many of the fields in this basin are sufficient to render them prospective sequestration targets. In addition, many deep saline aquifers also provide additional sequestration opportunities. Several large power plants in the area could take advantage of the many identified sequestration reservoirs.

Within the San Juan Basin, several horizons were selected as possible sequestration targets: the Dakota Group, Entrada Formation, Hermosa Group (equivalent to the Weber) and the Leadville Limestone. They are locally thick, porous and deep enough to be possible CO_2 sequestration targets. Associated seals for each of the units are in place in all areas, but ultimately, the thick sequence of shales and siltstones of the Mancos Shale is an excellent upper seal for all the units in the basin.

Within the San Juan Basin area, primary CO_2 point emissions were identified. These include the San Juan Generating Plant, Four Corners Generating Plant, Escalante Generating Plant, San Juan Gas Plant, Lybrook Gas Plant and the Giant Refinery. Of these sites, the San Juan and Four Corners Generating Plants were considered the most likely candidates for a CO_2 sequestration project because the units of interest were deep enough and thick enough to meet all of the criteria for injection.

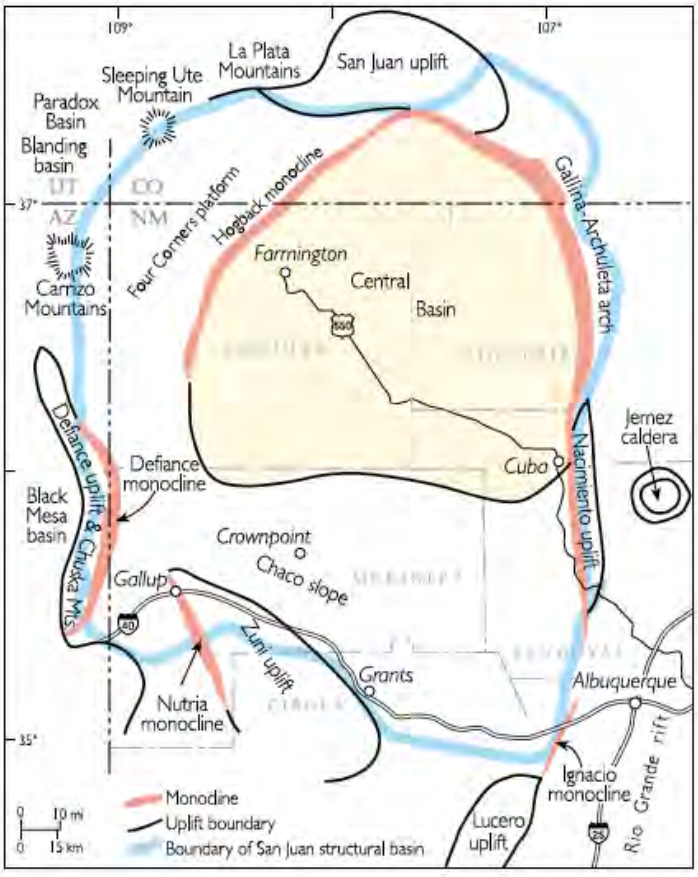


Figure 11.4: The San Juan Basin of Colorado and New Mexico which was evaluated by the Colorado Geological Survey and the New Mexico Bureau of Geology and Mineral Resources.

For the primary RMCCS local site analysis, the main issues that ruled out a New Mexico site early in the selection process included:

- The lack of a partner (a source of CO_2) willing to work with the group. Both Tri-State Energy in New Mexico and PNM Resources, the operators of the two selected power plants, were contacted and declined involvement.
- The San Juan Basin is an area with complex land ownership issues. The area is a patchwork of private, state and federal lands that included both public and Indian lands. The nature of the permits and ownership issues would have made a site selection a long and uncertain affair.

These issues are not insurmountable for possible future projects, but far more upfront time will be required for site selection and permitting in the San Juan Basin than the selected Craig Well site. In most areas of the San Juan basin, agreements would probably require Federal, Tribal, State and private landholders involvement in the site selection process.

COLORADO

The area of the Colorado portion of the Colorado Plateau is approximately 35,000 square miles. The RMCCS team focused on the broader region that includes the Sand Wash, Piceance, Paradox and San Juan Basins and the intervening Uncompahgre and Axial Basin Uplifts. The same procedure was followed as for the basin scale analysis: formation tops were correlated and the Dakota surface was mapped in detail using Petra ™. That grid was then transferred to Petrel™.

The RMCCS areal project contains a total of 30,678 wells, of which 18,796 have one or more geophysical logs. Eighty-three formations were identified and correlated and 48,700 individual tops were picked. Altogether 11,146 Dakota tops were used in the construction of the regional Dakota structure map; 2,816 were picked directly off logs and the rest were projected from shallower (or occasionally deeper).

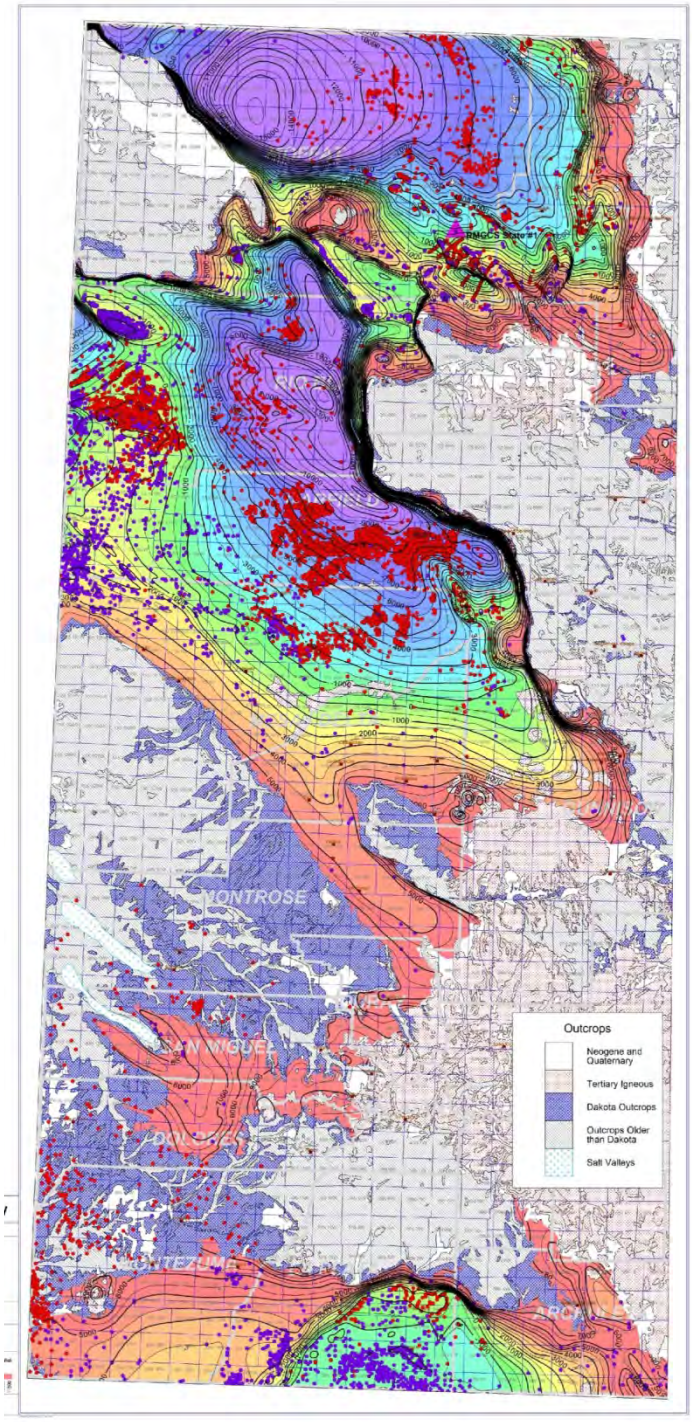


Figure 11.5: Structure map on top of the Dakota saline aquifer prepared from more than 11,000 well tops in the principal basins of the Colorado Plateau in western Colorado. Purple dots are measured Dakota tops; red dots are projected Dakota tops. Purple shaded area without contours are Dakota outcrops.

Public Engagement

The Rocky Mountain Carbon Capture and Sequestration (RMCCS) project team identified public engagement as an essential and necessary component of the projects' success. The process of public engagement involved contact and outreach to a broad spectrum of organizations and individuals at the local and regional level. Landowners, mineral rights owners, industry, state and local government/regulatory agencies, private citizens and the print/radio/television news media were all a part of the public engagement process. Each of the contacts was purposeful and necessary to inform members of the public about the project activity, promote an understanding of the technology, address fears and concerns, secure permissions and access, obtain permits, seek funding and in-kind contributions and to generate good will toward the research, development and potential future subsurface storage of carbon dioxide. Many of the public engagement efforts were required steps in the process. As a result, many of the RMCCS team members were involved in the public engagement process. Examples of various materials generated and used are in Appendices D & E.

Detailed Local-Scale Analysis: Geologic and Geophysical Data for the Sand Wash Basin

A goal of this project was to incorporate all existing publicly available data into maps depicting the structural configuration of the saline aquifers and their seals. The data utilized in this mapping included:

- 4,924 wells, of which 2708 had at least one geophysical log. Of those wells with logs, 2,000 had either an actual or projected Dakota formation top that was correlated for this project. Altogether, 37 formation tops ranging in age from the Cretaceous Fox Hills Sandstone to the Precambrian erosional surface were correlated for the Sandwash study area totaling 15,000 individual tops.
- Approximately one thousand surface measurements of bedding strikes and dips. Nearly 1500 measurements were collected by a team of geologists from the Colorado Geological Survey covering an area of approximately 800 square miles, predominantly in the region of the Yampa Block. Of these measurements, 470 were deemed unreliable and were not used. Approximately one thousand strike and dip measurements were used to hand-modify contours of the Dakota Formation's structure in the subsurface.
- Approximately 70 miles of existing two-dimensional seismic data in 11 lines. These were purchased through Seismic Exchange, Inc. to help define the structures in the southern part of the Yampa Block, which is updip from the stratigraphic test well, the direction that sequestered CO_2 is expected to migrate.
- Approximately eight miles of two-dimensional seismic data in two lines that were shot by Schlumberger Carbon Services. These cross the stratigraphic test well location and were shot to define the subsurface structure in the immediate area of the test well
- Published geologic maps that depict the rocks and structures at the surface. These include:
    - Outcrop patterns from surface geologic maps, including Tweto (1977).
    - Locations of fold axes from surface geologic maps, including Tweto (1977).

    - Elevations of surface contacts between the Dakota and the overlying Mowry Shale depicted on digital elevation models.
- Geologic publications that contain subsurface maps, cross sections, and/or rock characteristics and properties. Sources of formation tops from published geologic maps are listed in the Appendix F.
- Data from relevant well cores and cuttings. Published porosity and permeability data were collected for wells in the Sand Wash Basin. Average data from published field studies were tabulated to be used in estimates of storage capacity for sequestration. In addition, porosity-permeability crossplots were created for data from six Dakota cores, three Entrada cores and five Weber cores. Median Dakota porosity was 14.4 percent and median permeability was 19 md for the six Dakota wells. Median Entrada porosity was 14.9 percent and median permeability was 23 md for the three wells. Median Weber porosity was 6 percent and median permeability was 0.1 md for the five wells.

Detailed Local-Scale Analysis: Stratigraphic Well Drilling and Coring

Permissions to drill the RMCCS stratigraphic well, a key component of the local-scale characterization effort, were obtained from the Colorado Oil and Gas Conservation Commission, Colorado Department of Public Health and Environment, and the Colorado Division of Wildlife. Because the drill site was within an active mine-site, MSHA had authority over the operations, rather than OSHA (as is normal for most oil and gas activities). This added an additional layer of cost and training.

An attempt was made to reduce risk during drilling in several ways. Because three entities (Trapper Mining, Patterson Drilling, and Schlumberger Carbon Services) could be affected by the drilling, a single document was created that combined safety procedures and policies of the three, with the highest standard of each as the ruling policy. All parties signed off on the combined document before drilling began. A second risk-mitigation step was to add a full-time, on-site Safety Supervisor who had oil and gas experience and was also an MSHA safety instructor. As a result 293 people received MSHA site training and 19,416 man hours were safely worked without incident. The third risk-mitigation step was to develop a plan to assure compliance with all MSHA regulations which was successful and resulted in no citations to the RMCCS group.

The cost for a drill rig escalated between the time the project began and when drilling actually began, because of industry demands for new wells. Also, early estimates of the depth to the Weber were too shallow, causing the overall estimate of drilling the well to be too low. During field operations, a number of unanticipated occurrences drove up the cost of drilling and prevented reaching all three characterization targets because of a lack of funds. Modifying the rig to make it MSHA compliant, took five unexpected days. Lost circulation problems increased costs and slowed drilling. Overall penetration rates were slower than predicted, which increased costs.

Lack of nearby well control made it difficult to accurately predict coring points, thus increased costs and made it difficult to obtain coring targets. Addition of unanticipated steering and formation detection equipment also increased the costs. These increased costs, combined with a lack of contingency funding in the approved AFE under DOE guidelines, caused the project to drill to only two of the three objective formations: Entrada and Dakota. The Weber was not reached.

Detailed Local-Scale Analysis: Core Analysis and Interpretation with Other Geological and Geophysical Data

The RMCCS project extracted 131 feet of full diameter core from the well outside of Craig, Colorado. . Greater than 300 sample plugs were collected from the core for the purpose of performing a suite of petrophysical tests to evaluate CO_2 capacity, injectivity and seal efficacy The test data includes standard hydraulic (porosity and permeability) and mineralogical (XRD) analyses, as well as specialty analyses (capillary pressure and relative permeability).

Additionally, detailed petrographic analyses describe each of the 7 unique formations sampled by the coring and rotary sidewall sampling activities. Petrographic analysis of the core and core plugs was performed at the New Mexico Bureau of Geology and Mineral Resources. Thin sections of core from the Mowry, Dakota, Curtis, Entrada, Chinle, and Moenkopi(?) were examined and described.The petrographic data collected for this project were used to calibrate geophysical logs, construct more accurate geologic models and perform more accurate simulations.

Fifty nine samples from sidewall core and full core were analyzed for bulk mineralogy (Quartz, Potassium Feldspar, Plagioclase, Calcite, Dolomite, Halite, Siderite, Pyrite, and Clay) by semi-quantitative X-ray diffraction (XRD). These samples were from the Mowry, Lakota, Curtis, Entrada, Chinle, Shinarump, and Moenkopi formations. The clay fraction was then analyzed for clay mineral groups: illite, smectite, kaolinite, chlorite and illite/smectite. Each of those nine samples was run three different ways on the XRD machine.

Shell Exploration and Production had Core Laboriories perform numerous analyses on the Niobrara core including gas desorption, isotope analyses, triaxial stress tests, spectral gamma ray, fluid sensitivity, clay content, total organic carbon, and routine core analyses. For brevity, those data are not tabulated here, but will be published as a separate topical report (for those seeking this report later, the title of the report will be "Results of Core Analysis for the Niobrara Formation in the Sand Wash Basin, Colorado"). For reference, the well logs for the Niobrara are included in Appendix J.

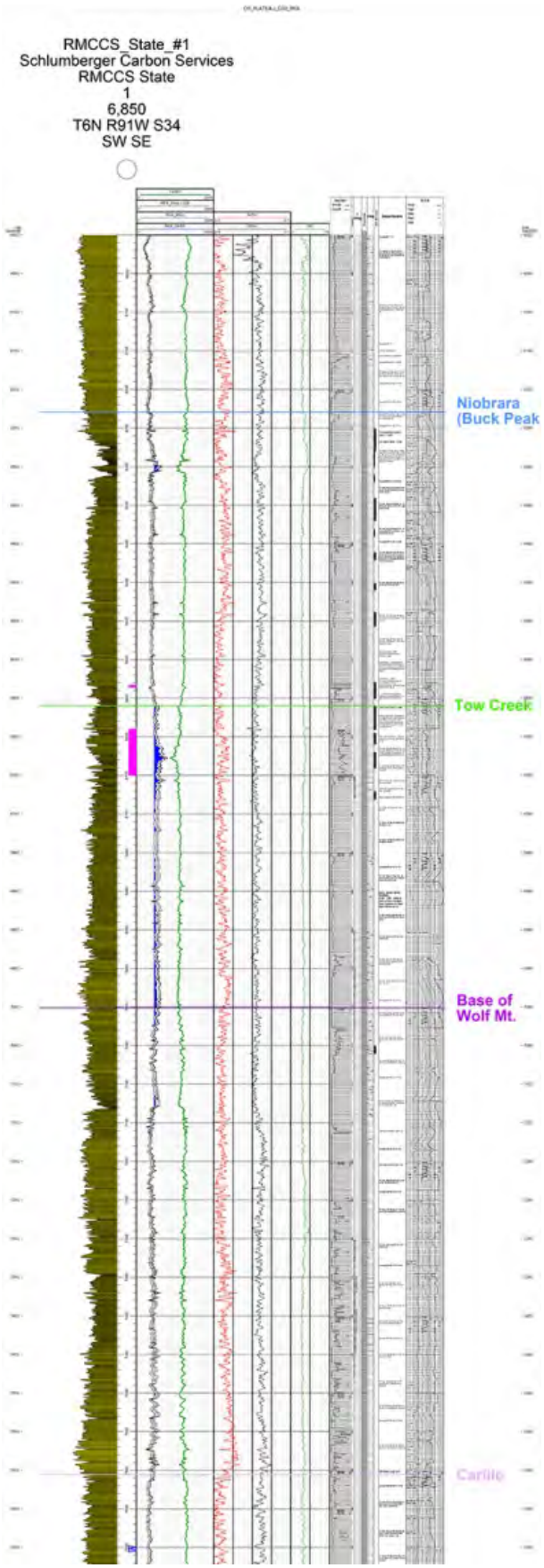


Figure 11.6A: The upper half of the geophysical logs run in the wells showing labelled tops of formations, location of cores (purple), sidewall cores (blue open triangles).

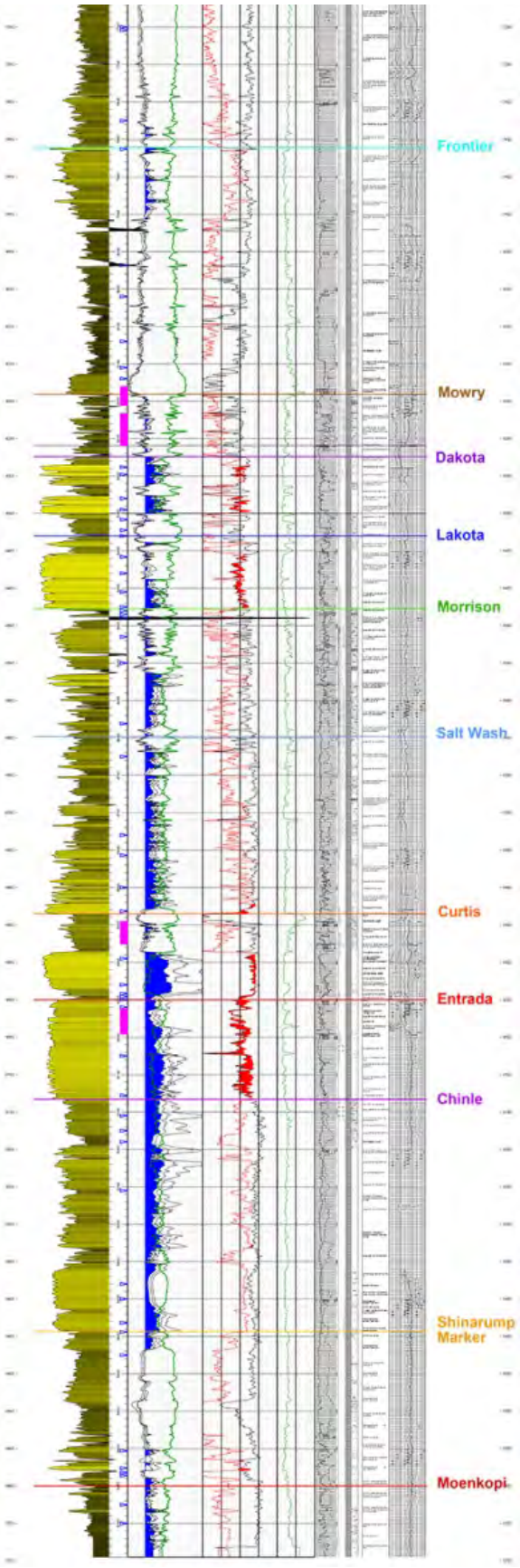


Figure 11.6B: The lower half of the geophysical logs run in the wells showing labelled tops of formations, location of cores (purple), sidewall cores (blue open triangles)

Detailed Local-Scale Analysis: Database Assembly and Geologic Static Model Development

Schlumberger Carbon Services and the Colorado Geologic Survey (CGS) worked together to develop a static geologic model in Petrel of the Sandwash Basin and Piceance Basin in northwestern Colorado (Figure 7). The model was developed to assess the geologic structure, CO_2 storage capacity, CO_2 injectivity, and CO_2 confinement of the Sandwash Basin and Piceance Basin. In order to develop this geologic model, geologic and geophysical data were integrated and ultimately used to characterize potential repositories, traps, and sealing mechanisms that would be needed to design and implement a CO_2 storage project.

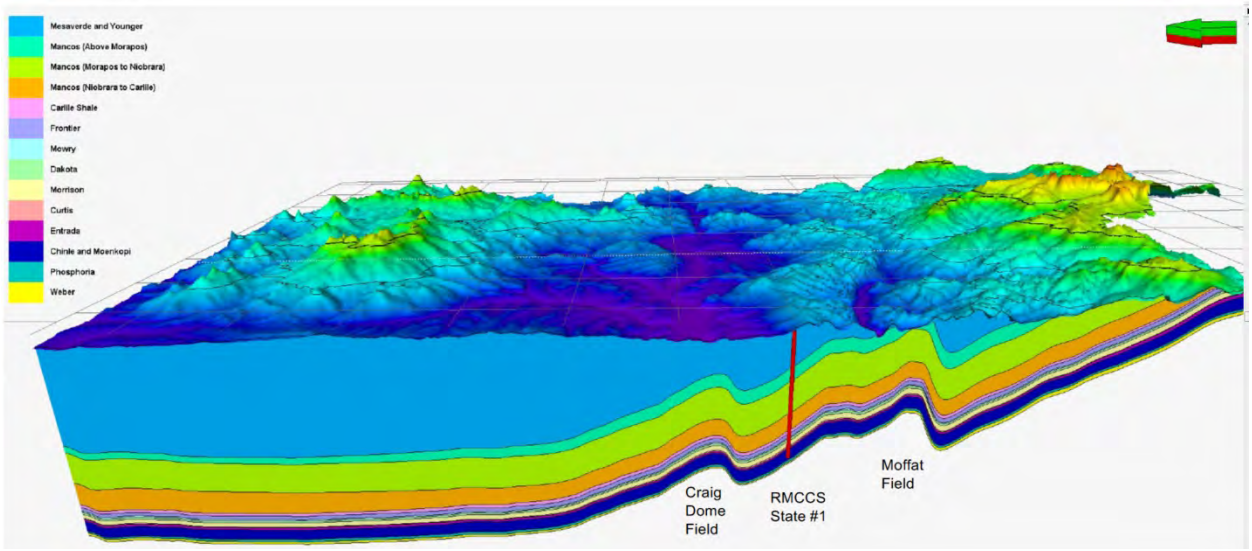


Figure 11.7. North-south cross section through Sand Wash Basin Petrel model. Wyoming border is at the left of the image and the White River Uplift is on the right. The RMCCS State #1 stratigraphic test well is shown in red.

Like many geologic models, this model was developed in stages and was updated when new data became available. Phase 1 of the model was constructed prior to the drilling of the stratigraphic test well RMCCS State # 1 (Craig Project Site) and was used as a tool to understand the geological characteristics of the Sandwash Basin and Piceance Basin. This geologic understanding was used to shortlist suitable locations to drill RMCCS State # 1 which ultimately provide valuable geologic information specific to a CO_2 injection scheme. This model was also used to evaluate the likely conditions to be encountered when drilling the RMCCS State # 1 at its proposed location. Once RMCCS State # 1 was drilled, new well data and 2D seismic survey data became available, which allowed for subsequent more detailed site specific Phase 2 modeling.

Property modeling (porosity and permeability) results were utilized to provide the site specific foundation for subsequent RMCCS project objectives listed below:

- Capacity assessment (Pore Volume Distribution) in the Sandwash Basin (Section 8 of the Narrative within this Final Report)

- Uncertainty assessment workflow (Section 9 of the Narrative within this Final Report)
- Simulation and risk assessment (Section 10 of the Narrative within this Final Report)
- To support regulatory and permitting requirements.

Capacity Assessment

The project generated carbon storage capacity estimates for deep saline formations of the Colorado Plateau with a concentration on the Dakota, Entrada and Weber Formations. Four additional formations were included for the southern part of the Colorado Plateau. The total regional estimated storage capacity for all evaluated formations ranges between 13.6 and 143.7 GT (Giga Tons) depending on the applied efficiency factor. For the three main formations the capacity ranges between 9.8 and 104 GT. At the 2% efficiency the Colorado Plateau has the capacity to store the 320 million tons per year CO_2 emissions generated by the gas and coal-fired power plants of the region for 120 years in the three main formations. The capacity increases up to 166 years when the other four formations are included.

				CO2 Storage Volume (metric Tonnes)		
State	Basin	Formation	Area (km^2)	Low Efficiency (0.51%)	Medium Efficiency (2%)	High Efficiency (5.4 %)
CO	Piceance_ Sandwash	Dakota	28,522	482,624,867	1,892,646,535	5,110,145,645
CO	San Juan		3,214	68,252,705	267,657,665	722,675,695
NM	San Juan		19,599	172,502,878	676,481,873	1,826,501,060
UT	Uinta		28,834	507,104,513	1,988,645,149	5,369,341,904
CO	Piceance_ Sandwash	Entrada	30,052	1,393,361,516	5,464,162,810	14,753,239,586
CO	San Juan		4,595	127,397,634	499,598,566	1,348,916,127
NM	San Juan		16,511	300,019,280	1,176,546,181	3,176,674,688
UT	Uinta	Entrada-Navajo	29,989	4,857,039,869	19,047,215,174	51,427,480,970
CO	Piceance_ Sandwash	Weber	15,577	549,361,376	2,154,358,336	5,816,767,507
UT	Uinta		27,789	1,361,192,180	5,338,008,549	14,412,623,083
NM	San Juan	Hermosa	9,444	1,672,530,703	6,558,943,933	17,709,148,619
AZ	Black Mesa	De Chelly	10,053	1,820,718,060	7,140,070,822	19,278,191,219
CO	Paradox		1,934	13,715,122	53,784,794	145,218,943
UT	Paradox		1,579	35,650,148	139,804,502	377,472,155
AZ	Black Mesa	Cedar Mesa	17,139	168,097,713	659,206,719	1,779,858,142
NM	San Juan	Leadville	12,247	42,728,636	167,563,275	452,420,844
			Totals:	**13,572,297,199**	**53,224,694,882**	**143,706,676,188**

Table 11.1: Summary of capacity estimates for basins in the Colorado Plateau.

The Sand Wash Basin has a combined saline storage capacity ranging between 0.3 and 3.5 GT. The emissions from the Craig and the Hayden coal-fired power plants can be stored for approximately 97 years when the storage capacity is estimated using a

2% efficiency factor. The other site-specific locations need more in depth study to assess the storage capacity with a higher degree of accuracy.

Uncertainty Assessment Workflow

We evaluated the uncertainty in the storage capacity estimation and demonstrated how the local data (e.g., well data, number of wells, and location of wells) affect the storage capacity estimates. Further, we estimated the well density (number of wells) required to appropriately estimate the capacity within a specified degree of confidence. To accomplish this, we developed a new workflow that used random, pseudo wells to represent the virtual characterization wells.

The focus of the modeling was on the three potential storage formations (Weber, Entrada, and Dakota sandstone formations) within the Sand Wash Basin. A geocellular model was constructed using the stratigraphic boundaries, well information, and well log images available from the project site. Using the sample variogram results, porosity values were assigned to each cell by the Sequential Gaussian Simulation (SGS) for each of the Dakota, Entrada and Weber Formations. The analysis assumed that the 3-D geocellular model (porosity) within the basin boundary serves as a true, or best, estimate of real geology.

A new workflow was developed that focused on randomly placing "pseudo-wells" in the Sand Wash Basin geocellular model. Each random pseudo-well was assumed to provide new well data and additional geologic information. We evaluated how the degrees of data density (well density) represented by the pseudo-wells affects the capacity estimates of target formations. The estimated pore volume in the geocellular model was considered as a proxy to the capacity estimate in this work.

As each pseudo-well was placed, porosity and formation thickness information within each well was extracted from the geocellular model. Starting from a first randomly sampled point, we sequentially added a new random pseudo-well up to a total of 25 wells. The estimated pore volume was calculated at each step to see how the new information affected the capacity estimates. Average porosity value and thickness of a target formation were determined from each pseudo-well and assigned uniformly to the subarea corresponding to the pseudo-well. The estimated pore volume of a subarea was simply computed by the product of average porosity value, thickness, and size of the subarea. The boundary of each subarea was determined by the closest distance from each pseudo-well. Total estimated pore volume of the basin is the sum of each subarea's estimated pore volume. We repeated the same process for a total of 25 cases with a different starting pseudo-well location for statistical analysis.

Relative differences of the capacity estimates from the true value of the geocellular model were computed for the Dakota, Entrada, and Weber formations, respectively for 25 cases. Our findings can be summarized as follows:

- The difference between the estimated pore volume and true value generally decreases with the addition of new data (pseudo-wells).
- Pore volume estimation for the Dakota shows a better fit, especially with less number of pseudo-wells compared to the Entrada and Weber formations.
- The Dakota formation has relatively less spatial variation in the porosity and thickness in the geocellular model.

- Targeting ±30% relative difference as a tolerable error range, we would need at least five characterization wells for the Dakota formation and nine wells each for the Entrada and Weber formations.
- The range/distribution of relative difference value for the small number of wells is significantly larger for the Entrada and Weber formation compared to the Dakota.
- The appropriate density of characterization data/well is dependent on the geologic formations even within the same basin.

As our relative difference measurement shows the deviation from the true value, we also analyzed which factor is more significant in terms of pore volume estimation. Since the estimated pore volume of a subarea is computed with the single porosity and thickness value given by the corresponding pseudo-well, the difference will increase if there is a large spatial variation in the porosity and thickness within a subarea.

We also calculated volume-weighted average dip angle of each target formation. Being consistent with our relative difference measurements, the volume-weighted dip angle for the Dakota is the smallest (4.95 degrees) among three target formations. Entrada and Weber are characterized by higher volume-weighted dip angles of 11.32 and 9.49 degrees, respectively. That is, a formation with a large dip angle is likely to have more uncertainty and greater error in the capacity estimation with the limited characterization data. However, unlike the volume-weighted average dip angle, the degree of heterogeneity in the porosity was not consistent with our relative difference results.

Simulation and Risk Assessment

A major goal of this study is to delineate probabilistically spatiotemporal responses (e.g. the areal CO_2 plume extent and injection-induced pressure buildup) resulting from subsurface CO_2 injection. Comprehensive simulations with the conventional Monte Carlo approach may be computationally expensive given the uncertainties in model parameters. Consequently, we applied a response surface method associated with the Monte Carlo technique for a probabilistic risk assessment of geologic CO_2 storage into Permo-Penn Weber formation at a potential site near Craig, Colorado. We built a site-specific aquifer model for the numerical simulation based on the regional geologic model.

Our response surface method (RSM) approach includes the Box-Behnken design (BBD) of experiment, numerical simulations, stepwise regression modeling, and Monte Carlo simulation at each time step. We identified four independent parameters (thickness of target formation, permeability, anisotropy ratio, and reservoir temperature) for the design of experiment according to their significance. A total of 25 runs specified by BBD provide the corresponding output variables from the numerical experiments.

For initial conditions of the model, a hydrostatic pressure was initially assigned according to the formation depth. Both the top and bottom layers of this model were assigned no-flow conditions. For the lateral boundaries representing extended aquifer beyond the simulation grid, we assign a large aquifer block to the lateral boundaries. In all simulations, supercritical-phase CO_2 was injected into the Weber formation during the initial 2-year period with the rate of 1 million metric tons per year, totaling 2,000,000

metric tons. Total simulation time for this study is chosen to be 100 years including the injection period.

We performed 10,000 iterations of Monte Carlo sampling associated with the identified RSM for each dependent variable and time. Each iteration represents a combination of input variables sampled from the given probability distributions and contributes to the construction of probability distribution in the outcome. The results of the modeling show the following:

- The projected plume size falls below approximately $6x10^7$ ft^2 after 20 years at 95 percentile (P95).
- The median projected plume size would be about $2x10^7$ ft^2 at 50 percentile (P50).
- The projected plume size gradually increases and tends to be stabilized as $2x10^7$ ft^2 after 20 years between the lower quartile (P25) and upper quartile (P75).
- The CO_2 plume tended to migrate toward the east (875 ft) and south (5,000 ft) from both x- and y-directional 1^{st} moment results at the P95 level at the end of the simulation time.
- Calculated plume migration rate in the up-dip direction (y-dir) after the injection stops is approximately 25 ft/yr in the model.
- P95 of pressure buildup at the injection well is within the 1,600 psi increase and P50 of the results are less than or equal to about 750 psi increase at the peak.
- At the proximal location, pressure is building up continuously until the injection stops. However, the magnitude of pressure build-up is smaller than the one at the injection well (700 psi within P95 at the peak).
- Unlike the pressure build-up at the injection and proximal well locations, pressure build-up at the distal location returns to the original state slowly at the distal monitoring location.

This study accounted for the probability distributions to characterize variability or uncertainty in prediction estimates for the probabilistic evaluation of geologic CO_2 storage. We presented the temporal evolution of cumulative distribution functions of output responses. Our approach has demonstrated that the response surface method (RSM) combined with Monte Carlo simulation can be efficiently applied for evaluation of geologic CO_2 storage within a probabilistic framework.

Appendix A: References
Appendix B: Bonanza Site (Utah) Analysis
Appendix C: Woodside Site (Utah) Analysis
Appendix D: CGS Outreach Presentations
Appendix E: Public Engagement Documentation
Appendix F: Sand Wash Basin (Colorado) Data
Appendix G: Short Versions of Drilling Plan and Safety Plan
Appendix H: Drilling Chronology
Appendix I: RMCCS #1 Well Log
Appendix J: Niobrara Well Log and Associated Information
Appendix K: Core Analysis Results
Appendix L: Sample of Petrography Results
Appendix M: Capacity Assessment Methodology
Appendix N: Arizona Capacity Assessment
Appendix O: New Mexico (San Juan Basin) Capacity Assessment
Appendix P: Utah Geological Survey Capacity Assessment
Appendix Q: Colorado Geological Survey Capacity Assessment

APPENDIX A

References

Contents

Reference List Only

APPENDIX A – REFERENCES

Akers, J.P., M.E. Cooley, and C.A. Repenning, 1958, Moenkopi and Chinle Formations of Black Mesa basin and adjacent areas, *in* Black Mesa Basin, Northeastern Arizona: New Mexico Geological Society Guidebook 9th Field Conference, p. 88-94.

Anderson, O.J., and S.G. Lucas, 1996, Stratigraphy and depositional environments of Middle and Upper Jurassic rocks, southeastern San Juan Basin, New Mexico, *in* Jemez Mountain Region: New Mexico Geological Society Guidebook 47th Field Conference, p. 205-210.

Armstrong, A.K., and E.D. Holcomb, 1989, Stratigraphy, facies and paleotectonic history of Mississippian rocks in the San Juan Basin of northwestern New Mexico and adjacent areas, *in* Southeastern Colorado Plateau: New Mexico Geological Society Guidebook, 40th Field Conference, p. 159-166.

Armstrong, A.K., and B.L. Mamet, 1977, Biostratigraphy and paleogeography of the Mississippian system in northern New Mexico and adjacent San Juan mountains of southwestern Colorado, *in* San Juan Basin III: New Mexico Geological Society Guidebook, 28th Field Conference, p. 111-127.

Bachu, S., 2003, Screening and ranking of sedimentary basins for sequestration of CO2 in geological Bachu, S., 2003, Screening and ranking of sedimentary basins for sequestration of CO2 in geological media in response to climate change: Environmental Geology, v. 44, p. 277-289.

Berman, A. E., Poleschook, D., Jr., Dimelow, T. E., 1980, Jurassic and Cretaceous Systems of Colorado, *in* Kent, H. C., and Porter, K. W., eds., Colorado Geology: Rocky Mountain Association of Geologists—1980 Symposium, p. 111-128.

Blakey, R.C., 1989, Triassic and Jurassic geology of the southern Colorado Plateau, *in* Jenny, J.P., and Reynolds, S.J., eds., Geologic evolution of Arizona: Arizona Geological Society Digest 17, p. 369-396.

Blakey, R.C., and Knepp, R., 1989, Pennsylvanian and Permian geology of Arizona, *in* Jenny, J.P., and Reynolds, S.J., eds., Geologic evolution of Arizona: Arizona Geological Society Digest 17, p. 313-348.

Bradshaw, J., et al. (2007), CO2 storage capacity estimation: Issues and development of standards, *International Journal of Greenhouse Gas Control*, *1*(1), 62-68.

Bradshaw, J., S. Bachu, D. Bonijoly, R. Burruss, S. Holloway, N. P. Christensen, and O. M. Mathiassen (2007), CO2 storage capacity estimation: Issues and development of standards, *International Journal of Greenhouse Gas Control*, *1*(1), 62-68.

Brister, B.S., and G.K. Hoffman, 2002, *in* Brister, B.S., and L.G. Price, eds., New Mexico's Energy, Present and Future: Policy, Production, Economics, and the Environment: New Mexico Bureau of Geology and Mineral Resources, Decision-Maker Field Conference 2002, p. 21-25.

Brister, B.S., and L.G. Price, eds., 2002, New Mexico's Energy, Present and Future: Policy, Production, Economics, and the Environment: New Mexico Bureau of Geology and Mineral Resources, Decision-Maker Field Conference 2002, 153 p.

Bu, T., and E. Damsleth (1996), Errors and Uncertainties in Reservoir Performance Predictions, *SPE Formation Evaluation*, *11*(3), 194-200.

Burton, G.C., Jr., 1955, Sedimentation and stratigraphy of the Dakota Group in the San Juan Basin, *in* Geology of Parts of the Paradox, Black Mesa and San Juan Basins: Four Corners Field Conference, p. 78-88.

Cain, Mary Reinarts, 1986, Depositional Environment of Upper Cretaceous Sandstones of the Lewis Shale, Sand Wash Basin, Colorado *in* Stone, D. S., ed., New Interpretations of Northwest Colorado Geology, Rocky Mountain Association of Geologists 1986 Symposium, p. 171-182.

Chapin, E. C., and Cather, S. M., 1983, Eocene Tectonics and Sedimentation in the Colorado Plateau--Rocky Mountain Area *in* Lowell, J. D., ed., Rocky Mountain Foreland Basins and Uplifts: Rocky Mountain Association of Geologists, p. 33-56.

Chidsey, Jr., T.C., and Sprinkel, D.A., 2005, Petroleum geology of Ashley Valley oil field and hydrocarbon potential of the surrounding area, Uintah County, Uutah, *in* Dehler, C.M., Pederson,

J.L., Sprinkel, D.S., and Kowallis, B.J., editors, Uinta Mountain Geology: Utah Geological Association Publication 33, p. 347-368.
Chu, C. (1990), Prediction of Steamflood Performance in Heavy Oil Reservoirs Using Correlations Developed by Factorial Design Method, paper presented at SPE California Regional Meeting, Ventura, California, 4-6 April, 1990.
Clarkson, G. and M. Reiter, 1988, An overview of geothermal studies in the San Juan Basin, New Mexico and Colorado, *in* Geology and Coal-Bed Methane Resources of the Northern San Juan Basin, Colorado and New Mexico: Rocky Mountain Association of Geologists, p. 285-291.
Craigg, S.D., 2001, Geologic framework of the San Juan structural basin of New Mexico, Colorado, Arizona, and Utah, with emphasis on Triassic Through Tertiary Rocks: United States Geological Survey, Professional Paper 1420, 70 p.
Currie, B.S., McPherson, M.L., Hokanson, W., Pierson, J.S., Homan, M.B., Pyden, T., Schellenbach, W., Purcell, R., and Nicklaus, D., 2012, Reservoir characterization of the Lower Cretaceous Cedar Mountain and Dakota Formations, northern Uinta Basin, Utah: UGS Open-File Report 597, CD-ROM.
Deischl, D.G., 1973, The characteristics, history and development of the Basin Dakota Gas Field, San Juan Basin, New Mexico, *in* Cretaceous and Tertiary Rocks of the southern Colorado Plateau, Four Corners Geological Society Memoir, p. 168-173.
Deng, H., P. H. Stauffer, Z. Dai, Z. Jiao, and R. C. Surdam (2012), Simulation of industrial-scale CO_2 storage: Miltu-scale heterogeneity and its impacts on storage capacity, injectivity and leakage *International Journal of Greenhouse Gas Control*, *10*, 397-418.
DeVoto, Richard H., 1980, Pennsylvanian Stratigraphy and History of Colorado, *in* Kent, H. C. and Porter, K. W., eds., Colorado Geology: Rocky Mountain Association of Geologists—1980 Symposium, p. 71-101.
DOE (2010), Carbon Sequestration Atlas of the United States and Canada, edited, U.S. Department of Energy, Office of Fossil Energy, National Energy Technology Laboratory.
Dubiel, Russell F., 1992, Sedimentology and Depositional History of the Upper Triassic Chinle Formation in the Uinta, Piceance, and Eagle Basins, Northwestern Colorado and Northeastern Utah: U. S. Geological Survey Bulletin 1787, 25p.
Engler, T.W., B.S. Brister, H.-Y. Chen and L.W. Teufel, 2001, A 20-year, Reasonable Foreseeable Development (RFD) Scenario Supporting the Resource Management Plan for the Farmington Field Office, Bureau of Land Management: New Mexico Bureau of Geology and Mineral Resources Open-File Report 463, 125 p.
EPA (2010), Federal Requirements Under the Underground Injection Control (UIC) Program for Carbon Dioxide Geologic Sequestration Wells, *[EPA-HQ-OW-2008-0390 FRL-9232-7] RIN 2040-AE98*.
Fassett, J.E., 1983, Stratigraphy and Oil and Gas Production of Northwest New Mexico Updated Through 1983, *in* Fassett, J. E., ed., Oil and Gas Fields of the Four Corners Area, v. III: Four Corners Geological Society, p. 849-863.
Fassett, J.E., 2006, The San Juan Basin: A complex giant gas field, New Mexico and Colorado: The Mountain Geologist, Vol. 43, No. 3, p. 225-230.
Fassett, J.E., 2010, Oil and gas resources of the San Juan Basin, New Mexico and Colorado *in* Four Corners Country: New Mexico Geological Society 61st Field Conference Guidebook, p. 181-196.
Fassett, J.E., and J.S. Hinds, 1971, Geology and fuel resources of the Fruitland Formation and Kirtland Shale of the San Juan Basin, New Mexico and Colorado: United States Geological Survey Professional Paper 676, 76 p.
Finn, T. M., and Johnson, R. C., 2005, Niobrara Total Petroleum System in the Southwestern Wyoming Province, Chapter 6 of Petroleum Systems and Geologic Assessment of Oil and Gas in the Southwestern Wyoming Province, Wyoming, Colorado, and Utah: U. S. Geological Survey Digital Data Series DDS-69-D, 27 p.

Freyberg, D. L. (1986), A natural gradient experiment on solute transport in a sand aquifer. 2. Spatial moments and the advection and dispersion of nonreactive tracers, *Water Resour. Res.*, ***22***(13), 2031-2046.

Fryberger, S. G., and Koelmel, M. H., 1986, Rangely Field: Eolian System-Boundary Trap in the Permo-Pennsylvanian Weer Sandstone of Northwest Colorado, *in* Stone, D. S., ed., New Interpretations of Northwest Colorado Geology, Rocky Mountain Association of Geologists, p. 129-149.

Geldon, A. L., 1986, Hydrostratigraphic Characterization of Paleozoic Formations in Northwestern Colorado *in* Stone, D. S., ed., New Interpretations of Northwest Colorado Geology: Rocky Mountain Association of Geologists, p. 265-281.

Ghomian, Y., K. Sepehrnoori, and G. Pope (2010), Efficient investigation of uncertainties in flood design parameters for coupled CO2 sequestration and enhanced oil recovery, paper presented at SPE International Conference on CO2 Capture, Storage, and Utilization.

Grammer, G. M., Eberli, G. P., Van Buchem, F. S. P., Stevenson, G. M., Homewood, P., 1996, Application of High-Resolution Sequence Stratigraphy to Evaluate Lateral Variabilityin Outcrop and Subsurface--Desert Creek and Ismay Intervals, Paradox Basin *in* Longman, M. W., and Sonnenfeld, M. D., Paleozoic Systems of the Rocky Mountain Region: The Rocky Mountain Section SEPM (Society for Sedimentary Geology), p.235-266.

Grant, K., and D.E. Owen, 1974, The Dakota Sandstone (Cretaceous) of the southern part of the Chama Basin, New Mexico—A preliminary report on its stratigraphy, paleontology, and sedimentology: New Mexico Geological Society 25th Field Conference Guidebook, p. 238-249.

Han, W. S., S.-Y. Lee, C. Lu, and B. J. McPherson (2010), Effects of permeability on CO_2 trapping mechanisms and buoyancy-driven CO_2 migration in saline formations, *Water Resour. Res.*, ***46***(W07510).

Hardage, B., and Sava, D., May 2009, Seismic steps aid sequestration: American Association of Petroleum Geologists Explorer, p. 38-39.

Harston, W.A., and Morris, T.H., 2013, Facies analysis of the Permian White Rim Sandstone, Black Box Dolomite, and Black Dragon Member of the Triassic Moenkopi Formation for CO_2 sequestration at Woodside field, San Rafael Swell, Utah, Part I, *in* Morris, T.H., and Ressetar, R., editors, The San Rafael Swell and Henry Mountains basin—geologic centerpiece of Utah: Utah Geological Association Publication 42, p. 145-172**.**

Hasket, G. I., 1959, Niobrara Formation of northwest Colorado, *in* Haun, J. D., and Weimer, R. J., eds., Symposium on Cretaceous Rocks of Colorado and Adjacent Areas: Rocky Mountain Association of Geologists 11th Field Conference, p. 46-49.

Hereford, R., 1977, Deposition of the Tapeats Sandstone (Cambrian) in central Arizona:Geological Society of America Bulletin, v. 88, no. 2, p. 199-211.

Hettinger, R. D., and Kirschbaum, M. A., 2003, Stratigraphy of the Upper Cretaceous Mancos Shale (Upper Part) and Mesaverde Group in the Southern Part of the Uinta and Piceance Basins, Utah and Colorado: Chapter 12 of Petroleum Systems and Geologic Assessment of Oil and Gas in the Uinta-Piceance Province, Utah and Colorado: U. S. Geological Survey Digital Data Series DDS-69-B, Plate 2.

Hintze, L.F., and Kowallis, B.J., 2009, Geologic history of Utah: Brigham Young University Geology Studies Special Publication 9, 225 p.

Hintze, L.F., Willis, G.C., Laes, D.Y.M., Sprinkel, D.A., and Brown, K.D., 2000, Digital geologic map of Utah: Utah Geological Survey Map 179DM, scale 1:500,000.

IPCC (2007), The Physical Science Basis. Contribution of Working Group I to the Fourth Assessment Report of the Intergovernmental Panel on Climate Change, 996 pp

Irwin, Dennis, Chairman of the R.M.A.G. Research Committee, 1977, Subsurface Cross-Sections of Colorado: Rocky Mountain Association of Geologists Special Publication No. 2, 24 cross sections by a number of authors.

Johnson, R. C., 2003, Depositional Framework of the Upper Cretaceous Mancos Shale and the Lower Part of the Upper Cretaceous Mesaverde Group, Western Colorado and Eastern Utah, Chapter 10

of Petroleum Systems and Geologic Assessment of Oil and Gas in the Uinta-Piceance Province, Utah and Colorado: U. S. Geological Survey Digital Data Series DDS-69-B, Plate 1.

Johnson, Samuel Y., Chan, Marjorie A., and Konopka, Edith A., 1992, Pennsylvanian and Early Permian Paleogeography of the Unita-Piceance Basin Region, Northwestern Colorado and Northeastern Utah; U. S. Geological Survey bulletin 1787-CC, 35 p.

Kalla, S. (2005). Use of Orthogonal Arrays, Quasi-Monte Carlo Sampling, and Kriging Response Models for Reservoir Simulation with Many Varying Factors(Doctoral dissertation, Faculty of the Louisiana State University and Agricultural and Mechanical College in partial fulfillment of the requirements for the degree of Master of Science in Petroleum Engineering in The Department of Petroleum Engineering by Subhash Kalla B. Tech., Regional Engineering College)

Kaiser, W. R., Scott, A. R., Hamilton, D. S., Tyler, Roger, McMurry, R. G., Zhou, N, Tremain, C. M., 1993, Geologic and Hydrologic Controls on Coalbed Methane: Sand Wash Basin, Colorado and Wyoming: Colorado Geological Survey Resource Series 30 and Bureau of Economic Geology Report of Investigations No. 220, 151 p.

Kent, Harry C., 1972 Review of Phanerozoic History, IN Mallory, W. W.; Mudge, M. R.; Swanson, V. E.; Lumb, W. E.; and Stone, D. S., eds., 1972, Geologic Atlas of the Rocky Mountain Region, Rocky Mountain Association of Geologists, 331 pp

Kirkland, D.W., R.E. Denison, and R. Evans, 1995, Middle Jurassic Todilto Formation of northern New Mexico and southwestern Colorado; marine or nonmarine?: New Mexico Bureau of Mines and Mineral Resources Bulletin 147, 39 p.

Kirschbaum, M. A., 2003, Geologic Assessment of Undiscovered Oil and Gs Resources of the Mancos/Mowry Total Petroleum System, Uinta-Piceance Province, Utah and Colorado: Chapter 6 of Petroleum Systems and Geologic Assessment of Oil and Gas in the Unita-Piceance Province, Utah and Colorado: U. S. Geological Survey Digital Data Series DDS-69-B, Plate 4.

Kluth, C. F., 1986, Plate tectonics of the ancestral Rocky Mountains, *in* Peterson, J. A., ed., Paleotectonics and sedimentation in the Rocky Mountain region, United States: American Association of Petroleum Geologists Memoir 41, p. 353-370.

Kluth, C. F., and DuChene, H. F., 2009, Late Pennsylvanian and Early Permian Structural Geology and Tectonic History of the Paradox Basin and Uncompahgre Uplift, Colorado and Utah, *in* Houston, W. S., Wray, L. L., and Moreland, P. G., eds., The Paradox Basin Revisited--New Developments in Petroleum Systems and Basin Analysis, Rocky Mountain Association of Geologists 2009 Special Publication, p.178-197.

Knight, R.L., and Cooper, J.R., 1955, Suggested changes in Devonian terminology in the FourCorners area, in Cooper, J.C., ed., Geology of parts of Paradox, Black Mesa, and San JuanBasins, Four Corners Field Conference: Four Corners Geological Society Guidebook, p. 56-58.

Koelmel, M. H., 1986, Post-Mississippian Paleotectonic, Stratigraphic, and Diagenetic History of the Weber Sandstone in the Rangely Field Area, Colorado *in* Peterson, J. A., ed., Paleotectonics and sedimentation in the Rocky Mountain region, United States: American Association of Petroleum Geologists Memoir 41, p. 371-396.

Laes Denise, Chris Eisinger, Rich Esser, Craig Morgan, Steve Rauzi, Dana Ulmer-Scholle, Vince Matthews and Brian McPherson. 2013a. Regional Capacity and Significance Summary Topical Report. U.S. Department of Energy - National Energy Technology Laboratory. 46 pages.

Laes Denise, Chris Eisinger, Craig Morgan, Dana Ulmer-Scholle, Phyllis Scott and Wade Zaluski. 2013b. Sequestration capacity and associated aspects of the most promising geologic formations sequestrations candidates summary topical report. U.S. Department of Energy - National Energy Technology Laboratory. 144 pages.

Lamb, G.M, 1978, The lower Mancos Shale in the northern San Juan Basin: Geological Society of America Bulletin, v. 89, p. 59-82.

Lausen, C., and Wilson, E.D., 1925, Gold and copper deposits near Payson, Arizona: Arizona Bureau of Mines Bulletin no. 120, 44 p.

Litynski, J., Deel, D., Rodosta, T., Guthrie, G., Goodman, A, Hakala, A., Bromhal, G., andFrailey, S., 2010, Carbon sequestration atlas of the United States and Canada (Atlas III):U.S. Department of Energy, Office of Fossil Energy, National Energy TechnologyLaboratory (NETL), 3rd ed., Appendix B, p. 136-152.

Liu, B., and Y. Zhang (2011), CO2 modeling in a deep saline aquifer: a predictive uncertainty analysis using design of experiment, *Environmental science & technology*, *45*(8), 3504-3510.

Lucas, S.G., and Anderson, O.J., 1997, The Jurassic San Rafael Group, Four Corners region: New Mexico Geological Society, 48th Field Conference Guidebook, p. 115-132.

Lucas, S.G., K.K. Kietzke, and A.P. Hunt, 1985, The Jurassic System in east central New Mexico: New Mexico Geological Society, 36th Field Conference Guidebook, p. 213-242.

Lucas, S.G., S.C.H.A.B. Semken, W.R.H.G. Berglof, B.S.C.L.S. Kues, and J.C. Aubele, 2003, First-day road log, from Gallup to Gamerco, Yah-ta-hey, Window Rock, Fort Defiance, Navajo, Todilto Park, Crystal, Narbona Pass, Sheep Springs, Tohatchi and Gallup: New Mexico Geological Society, 54th Field Conference Guidebook, p. 1-6

Mallory, W. W., 1972, Pennsylvanian Arkose and the Ancestral Rocky Mountains *in* Mallory, W. W.; Mudge, M. R.; Swanson, V. E.; Lumb, W. E.; and Stone, D. S., eds., Geologic Atlas of the Rocky Mountain Region, Rocky Mountain Association of Geologists, 331 pp.

Mallory, W. W.; Mudge, M. R.; Swanson, V. E.; Lumb, W. E.; and Stone, D. S., eds., 1972, Geologic Atlas of the Rocky Mountain Region, Rocky Mountain Association of Geologists, 331 pp.

Masoner, L. O., and Wackowski, R. K., 1995, Rangely Weber Sand Unit CO2 Project Update; SPE Reservoir Engineering, p. 203-207.

Mathias, S. A., J. G. Gluyas, G. J. González, M. de Miguel, S. L. Bryant, and D. Wilson (2013), On relative permeability data uncertainty and CO_2 injectivity estimation for brine aquifers, *International Journal of Greenhouse Gas Control*, *12*, 200-212.

McLemore, V.T., R.F. Broadhead, W.L. Chenoweth, K. Cook, J.M. Barker, G. Roybal, R.M. North, P. Copeland, J.S. Hingtgen, M.R. Bowie, and K.B. Brown, 1986a, A Preliminary Mineral-Resource Potential of San Juan County, Northwestern New Mexico: New Mexico Bureau of Mines and Mineral Resources Open-file Report 232, 258 p.

McLemore, V.T., R.F. Broadhead, G. Roybal, W.L. Chenoweth, J.M. Barker, P. Copeland, M.R. Bowie, K. Cook, J.S. Hingtgen, K. Kline, and K.B. Brown, 1986b, A Preliminary Mineral-Resouroe Potential of Western Rio Arriba County, Northwestern New Mexico: New Mexico Bureau of Mines and Mineral Resources Open-file Report 233, 157 p.

McPherson, B.J., (2009) Geologic Carbon Sequestration: Challenges of Mitigation Planning, presentation exhibited at the Eighth Annual Conference on Carbon Capture & Sequestration, Pittsburgh, Pennsylvania, May 5, 2009.

Molenaar, C.M., 1977, Stratigraphy and depositional history of Upper Cretaceous rocks of the San Juan Basin area, New Mexico and Colorado, with a note on economic resources: New Mexico Geological Society Guidebook 28th Field Conference, p. 159-166.

Molenaar,C. M., 1981, Mesozoic Stratigraphy of the Paradox Basin--An Overview, IN Wiegand, D. L., ed., Geology of the Paradox Basin: Rocky Mountain Association of Geologists, p. 119-127.

Molenaar, C. M., 1983, Principal reference section and correlation of Gallup Sandstone, northwestern New Mexico: Contributions to mid-Cretaceous paleontology and stratigraphy of New Mexico (Part 2): New Mexico Bureau of Mines and Mineral Resources Circular 185, p. 29-40.

Montgomery, D. C. (2008), *Design and Analysis of Experiments*, John Wiley & Sons, Inc., New York, NY.

Moretti Jr., G., Lipinski, P., Gustafson, F., and Slaughter, A., 1992, Dakota Sandstone deposition and trap door structure of Hells Hole field, eastern Uinta Basin, Utah and Colorado in Fouch, T.D., Nuccio, V.F., and Chidsey, Jr., T.C., editors, Hydrocarbon and mineral resources of the Uinta Basin, Utah and Colorado: Utah Geological Association Guidebook 20, p. 313-323.

Morgan, C.D., Carney, S., and Nielsen, P., 2013, Recent characterization of Gordon Creek, Farnham Dome, and Woodside fields, Carbon and Emery Counties, Utah, *in* Morris, T.H., and Ressetar,

R., editors, The San Rafael Swell and Henry Mountains basin—geologic centerpiece of Utah: Utah Geological Association Publication 42, p. 393-414.

NATCARB (2010), National Carbon Sequestration Database and Geographic Information System, edited.

National Energy Technology Laboratory, 2012, The United States 2012 Carbon Utilization and Storage Atlas, 4th Edition, U.S. Department of Energy, 130 p. http://www.netl.doe.gov/technologies/carbon_seq/refshelf/atlasIV/index.html

Nummedal, D., and C.M. Molenaar, 1995, Sequence stratigraphy of ramp-setting strand plain successions: The Gallup Sandstone, New Mexico, *in* Van Wagoner, J.C., and G.T. Bertram, eds., Sequence Stratigraphy of Foreland Basin Deposits: AAPG Memoir 64, p. 277-310.

Oriel, S. S. and Craig, L. C.,1960, Lower Mesozoic Rocks in Colorado *in* Weimer, R. J., and Haun, J. D., eds., Guide to the Geology of Colorado, Geological Society of America, Rocky Mountain Association of Geologists, and Colorado Scientific Society, p. 43-58.

O'Sullivan, R. B., C.A. Repenning, E.C. Beaumont, and H.G. Page, 1972, Stratigraphy of the Cretaceous rocks and the Tertiary Ojo Alamo Sandstone, Navajo and Hopi Indian reservations, Arizona, New Mexico and Utah: U.S. Geological Survey Professional Paper 521-E, 65 p.

Peterson, J. A., and Hite, R. J., 1969, Pennsylvanian Evaporite-Carbonate Cycles and Their Relation to Petroleum Occurrence, Southern Rocky Mountains: American Association of Petroleum Geologists Bulletin V. 93, No. 4, p. 884-908.

Quigley, M. D., 1959, Correlation of the Dakota-Cedar Mountain-Morrison sequence along the Douglas arch: Rocky Mountain Association of Geologists, Guidebook to 11th Field Conference, pp. 33-36.

Rauzi, S.L., and Spencer, J.E., 2012, An Evaluation of CO2 Sequestration Potential of Paleozoic Sandstone Units, Northeastern Arizona: Arizona Geological Survey Open File Report 12-10, 29 p., with appendix.

Reiter, M., and Clarkson, G., 1983, Relationships between heat flow, paleotemperatures, coalification, and petroleum maturation in the San Juan Basin, northwest New Mexico and southwest Colorado: Geothermics, v. 12, p. 323-339.

Repenning, C. A., Cooley, M. E., Akers, J. P., 1969, Stratigraphy of the Chinle and Moenkopi Formations, Navajo and Hopi Indian Reservations, Arizona, New Mexico, and Utah: United States Geological Survey Professional Paper 521-B, 34 p.

Richard, S.M., Reynolds, S.J., Spencer, J.E., and Pearthree, P.A., 2000, Geologic map of Arizona: Arizona Geological Survey Map 35, scale 1:1,000,000.

Roberts, L.N.R., 2003, Structure contour map of the top of the Dakota Sandstone, Uinta-Piceance Province, Utah and Colorado, *in* USGS Uinta-Piceance Assessment Team compilers, Petroleum systems and geologic assessment of oil and gas in the Uinta-Piceance Province, Utah and Colorado, USGS DDS-69B, 14 p.

Rohmer, J., and O. Bouc (2010), A response surface methodology to address uncertainties in cap rock failure assessment for CO2 geological storage in deep aquifers, *International Journal of Greenhouse Gas Control*, *4*(2), 198-208.

Sato, K. (2011), Value of information analysis for adequate monitoring of carbon dioxide storage in geological reservoirs under uncertainty, *International Journal of Greenhouse Gas Control*, *5*, 1294-1302.

Simpson, J., 2006, Characterization of produced groundwater within the San Juan Basin: New Mexico Bureau of Mines and Mineral Resources Open-file Report 499, 23 p.

Sloss, L.L., 1988, Tectonic evolution of the craton in Phanerozoic time, *in* Sloss, L.L., ed., Sedimentary Cover - North American craton: Geological Society of America DNAG v. D-2, p. 25-51.

Stern, E. J., and Constenius, K. N., 1997, Space-Time Relationships Between Magmatism and Tectonism in the Western United States Between 120 Ma and 10 Ma: a Regional Context for the Front Range of Colorado *in* Bolyard, D. W., and Sonnenberg, S. A., eds., Geologic History of the Colorado Front Range: 1997 RMS-AAPG Field Trip #7, p. 85-100.

Stevenson, G. M., 1983, Paleozoic rocks of the San Juan Basin: an exploration frontier, *in* Fassett, J. E.,

ed., Oil and Gas Fields of the Four Corners Area, v. Ill: Four Corners Geological Society, p. 780-788.
Stevenson, G. M., and D.L. Baars, 1977, Pre-Carboniferous paleotectonics of the San Juan Basin: New Mexico Geological Society, Guidebook to the 28th Field Conference, p. 99-110.
Stevenson, G. M., and Baars, D. L., 1988, Overview: Carbonate Reservoirs of the Paradox Basin *in* Goolsby, S. M., and Longman, M. W., eds., Occurrence and Petrophysical Properties of Carbonate Reservoirs in the Rocky Mountain Region: Rocky Mountain Association of Geologists, p. 149-162.
Stewart, J. H., Poole, F. G. and Wilson, R. F., 1972, Stratigraphy and origin of the Triassic Moenkopi Formation and related strata in the Colorado Plateau region: U. S. Geological Survey Professional Paper 691, 336 p.
Stone, D. S., 1986, Seismic and Borehole Evidence for Important Pre-Laramide Faulting Along the Axial Arch in Northwest Colorado, *in* Stone, D. S., ed, New Interpretations of Northwest Colorado Geology: Rocky Mountain Association of Geologists, p. 19-36.
Stone, W.J., F.P. Lyford, P.F. Frenzel, N.H. Mizell, and E. Padgett, 1983, Hydrogeology and water resources of the San Juan Basin, New Mexico: New Mexico Bureau of Mines and Mineral Resources Hydrogeologic Report 6, 70 p.
Tanner, W. F., 1974, Mesozoic lake history of northern New Mexico, *in* Ghost Ranch: New Mexico Geological Society 25th Field Conference Guidebook, p. 219-223.
Teichert, C., 1965, Devonian rocks and paleogeography of central Arizona: U.S. GeologicalSurvey Professional Paper 464, 181 p.
Thyne, Geoffrey D; Tomasso, Mark; Bywater-Reyes, Sharon V; Budd, David A; Reyes, Brian M, Oct. 2010, Characterization of porosity and permeability for CO_2 sequestration models in the Mississippian Madison Group, Moxa Arch-LaBarge Platform, southwestern Wyoming:Contributions to Geology, vol. 45, no. 2, pp.133-150, Oct 2010.
Tompson, A. F. B., and L. W. Gelhar (1990), Numerical simulation of solute transport in three-dimensional, randomly heterogeneous porous media, *Water Resour. Res.*, ***26***(10), 2541-2562.
Trudgill, B. D., and Paz, M., 2009, Restoration of Mountain Front and Salt Structures in the Northern Paradox Basin, SE Utah *in* Houston, W. S., Wray, L. L., and Moreland, P. G., The Paradox Basin Revisited--New Developments in Petroleum Systems and Basin Analysis: Rocky Mountain Association of Geologists, p. 132-177.
Tweto, 0., 1975, Laramide (Late Cretaceous-Early Tertiary) orogeny in the southern Rocky Mountains, *in* Curtis, B.F., ed., Cenozoic history of the southern Rocky Mountains: Geological Society of America Memoir 144, p. 1-44.
Tweto, Ogden, 1977, Tectonic History of West-Central Colorado *in* Veal, Harry K., ed., Exploration Frontiers of the Central and Southern Rockies: Rocky Mountain Association of Geologists 1977 Symposium, p. 11-18.
Tweto, Ogden, 1979, Geologic Map of Colorado: U. S. Geological Survey.
Ulmer, D.S., and R.L. Laury, 1984, Diagenesis of the Mississippian Arroyo Peñasco Group, north-central New Mexico, *in* Rio Grande Rift: Northern New Mexico: New Mexico Geological Society Guidebook, 35th Field Conference, p. 91-100.
Ulmer-Scholle, D.S., 2005, Stromatolites in the Todilto Formation?, *in* Geology of the Chama Basin: New Mexico Geological Society, 56th Field Conference Guidebook, p. 380-388.
U.S. Department of Energy, 2010, Carbon sequestration atlas of the United States and Canada(Atlas III): U.S. Department of Energy, Office of Fossil Energy, National Energy Technology Laboratory (NETL), 3rd ed., 160 p.
U.S. Department of Energy, National Energy Technology Laboratory, NATCARB, 2012 Carbon Sequestration Atlas of the Unites States and Canada – Third Edition (Atlas III).
U.S. Department of Energy, National Energy Technology Laboratory, NATCARB, 2012 Carbon Sequestration Atlas of the Unites States and Canada – Forth Edition (Atlas IV).

[http://www.netl.doe.gov/technologies/carbon_seq/refshelf/atlasIV/index.html accessed 16 July 2013]
U.S. Environmental Protection Agency 2010 Greenhouse Gas Reporting Program: 2010 data sets [http://epa.gov/ghgreporting/ghgdata/2010data.html accessed 27 September 2013]
U.S. Environmental Protection Agency 2011 Greenhouse Gas Reporting Program: 2011 data sets [http://epa.gov/ghgreporting/ghgdata/2011data.html [accessed 27 September 2013]
Walter, L., P. J. Binning, S. Oladyshkin, B. Flemisch, and H. Class (2012), Brine migration resulting from CO_2 injection into saline aquifers - An approach to risk estimation including various levels of uncertainty, *International Journal of Greenhouse Gas Control*, *9*, 495-506.
Wengerd, S.A., 1959 Pennsylvanian oil possibilities of San Juan Basin, Four Corners Region: American Association Petroleum Geologists Bulletin, v. 42, p. 2214-2227.
Wengerd, S.A., and M.L. Matheny, 1958, Pennsylvanian System of Four Corners region: American Association Petroleum Geologists Bulletin, v. 43, p. 2048-2106.
Willis, B. J., and C. D. White (2000), Quantitative Outcrop Data for Flow Simulation, *Journal of Sedimentary Research*, *70*(4), 788-802.
Witkind, I.J., 2004, Geologic map of the Huntington 30' X 60' quadrangle, Carbon, Emery, Grand, and Uintah Counties, Utah: Utah Geological Survey Open-File Report 440 DM, scale 1:100,000.
Wood, D., L. Lake, R. Johns, and V. Nunez (2008), A screening model for CO2 flooding and storage in Gulf Coast reservoirs based on dimensionless groups, *SPE Reservoir Evaluation & Engineering*, *11*(3), 513-520.

APPENDIX B

Bonanza Dome

Analysis

Contents

Bonanza Dome Analysis only

BONANZA SITE

Reason for Selecting the Bonanza Site

The Bonanza site is located in the eastern Uinta Basin and is the best potential commercial CO_2 storage site in the Colorado Plateau in Utah. The Cretaceous Dakota Sandstone, Jurassic Entrada Sandstone, and Pennsylvanian-Permian Weber Sandstone, which are the three target storage reservoirs, are all present at the site and are at a depth greater than the required 3000-foot (1000-m) drill depth. Water quality for each formation also exceeds the TDS minimum of 10,000 ppm and the site meets the minimum storage capacity requirement of 30 million metric tonnes (MMT). The coal-fired Bonanza power plant, which is located on the site, is about 30 miles (48 km) south of Vernal Utah and access to the area is well developed (figure 1).

The Bonanza site is a down-dip extension of the Hells Hole field, which straddles the Utah-Colorado border in Rio Blanco County, Colorado and Uintah County, Utah (Moretti Jr., and others, 1992). Production of oil and gas is from stratigraphically trapped, fluvial and marine sandstones of the Dakota Sandstone. The field is located on the northwestern plunge of the West Douglas Creek Anticline and is bounded on the west by a north-south trending, high-angle reverse fault and to the south by east-west trending normal fault.

Methods

Well control within the Bonanza site is limited, with the majority of the wells located in the northwest portion of the site (figure 2). All wells penetrate the Dakota, but penetration of the deeper Entrada and Weber is limited to two wells. Using electronic wireline logs, the top of the Dakota was picked and correlated between wells. The formation tops data was then used to create structure contour maps. Because data for the Entrada and Weber is limited, structure contour maps were created for these formations by projecting from the Dakota structure contour map. A normal, roughly east-west trending fault, detected on seismic surveys by local operators, is reported to exist at depth within the Bonanza site. This fault is shown on all maps, but was not used in drawing the structure contour maps as the exact location and throw are unknown.

The structure contour data were gridded in ArcMap® and subtracted from a digital elevation model (DEM) grid to get overburden maps, or drill depth grids of the top of each reservoir. The structure, overburden, porosity, pressure, and temperature data for each reservoir were imported into the EGI storage capacity spreadsheet and the CO_2 storage capacity was calculated for 0.51%, 2.0%, and 5.4% efficiency.

Because well data is limited in the Bonanza site, isopach maps for the Weber and Entrada were generated using data from our regional study and were created in ArcMap®. Isopach maps for the Dakota were generated from correlated formation tops and wireline logs from wells in the Bonanza site area. Gross thickness of Dakota sandstone was calculated from gamma ray logs using a 60 API cutoff. Net thickness of sandstone with porosity of 6% or better was then calculated from porosity logs. We used 6% as the minimum porosity for good reservoir quality.

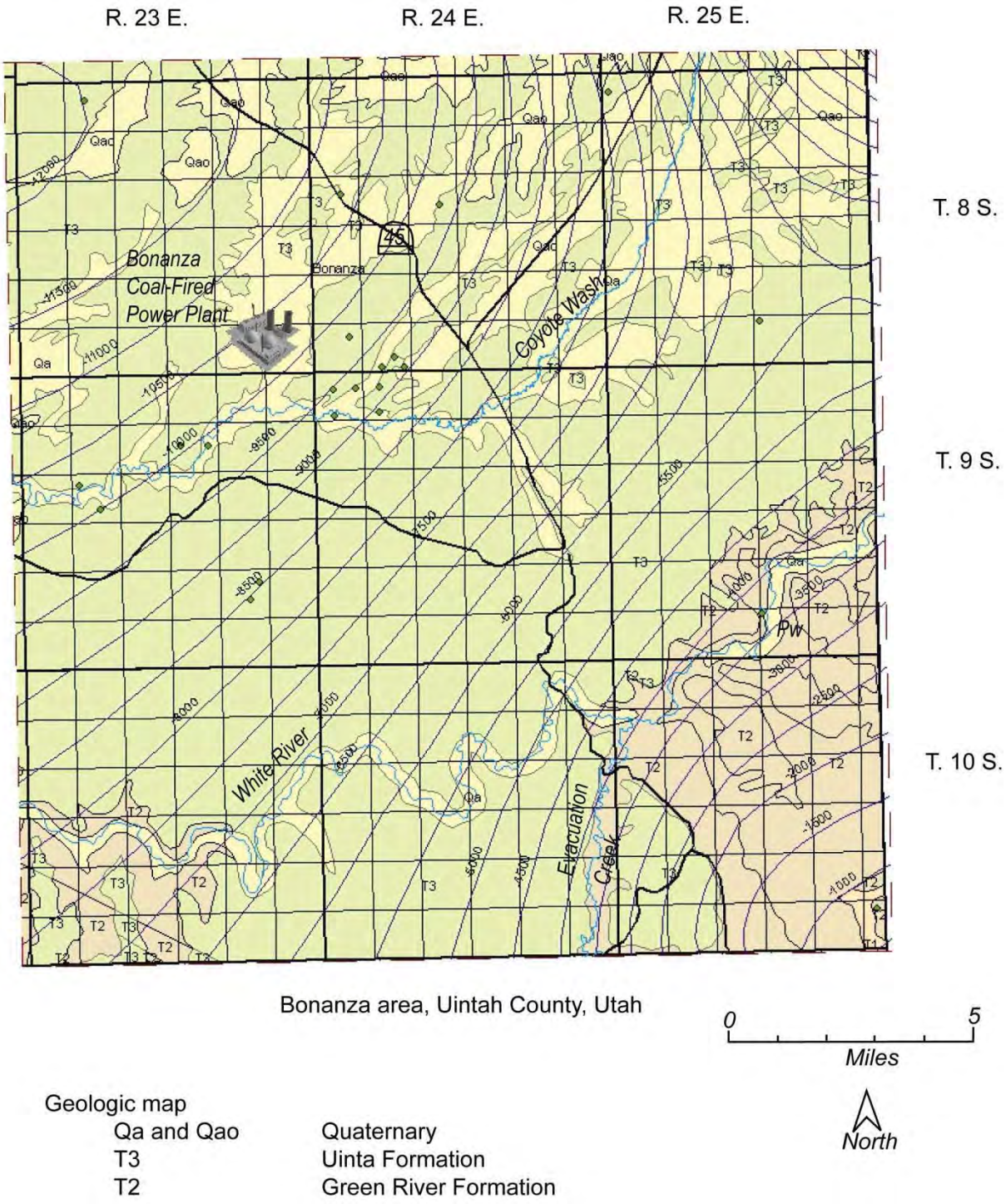


Figure 2. Geologic map of the Bonanza site from Hintze and others, 2000. Structure contours are top of Dakota Sandstone from Roberts (2003), contour interval is 500 feet (150 m), mean sea level datum. Green circles are wells that penetrated the Dakota Sandstone. Pw is the one well in the Bonanza that penetrated the Entrada and Weber Sandstones.

Pennsylvanian – Permian Weber Sandstone

The Weber Sandstone is Pennsylvanian (lower part) to Early Permian (upper part) separated by an unconformity (Hintze and Kowallis, 2009). In the eastern Uinta Basin and Bonanza site area, it is an eolian dune deposit including dune, interdune, and sand sheet facies and is a medium- to fine-grain, well sorted subarkosic to quartz arenite (Chidsey, Jr., and Sprinkel, 2005).

The isopach map shows that the Weber is thickest in the northwest portion of the area and thins significantly to the southeast (figure 3). Thickness ranges from ~250 to 300 feet (76-92 m) near the Bonanza power plant. Overburden ranges from ~9000 feet (2745 m) in the southeast to 19,000 feet (5795 m) in the northwest (figure 4).

To calculate the storage capacity for the Weber Sandstone, we used an average porosity of 7%, an average thickness of 186 feet (57 m), and an average depth of 14,604 feet (4454 m) over an area of 328 miles^2 (table 1). The storage capacity at 2.0% efficiency is 51.25 MMT (table 2).

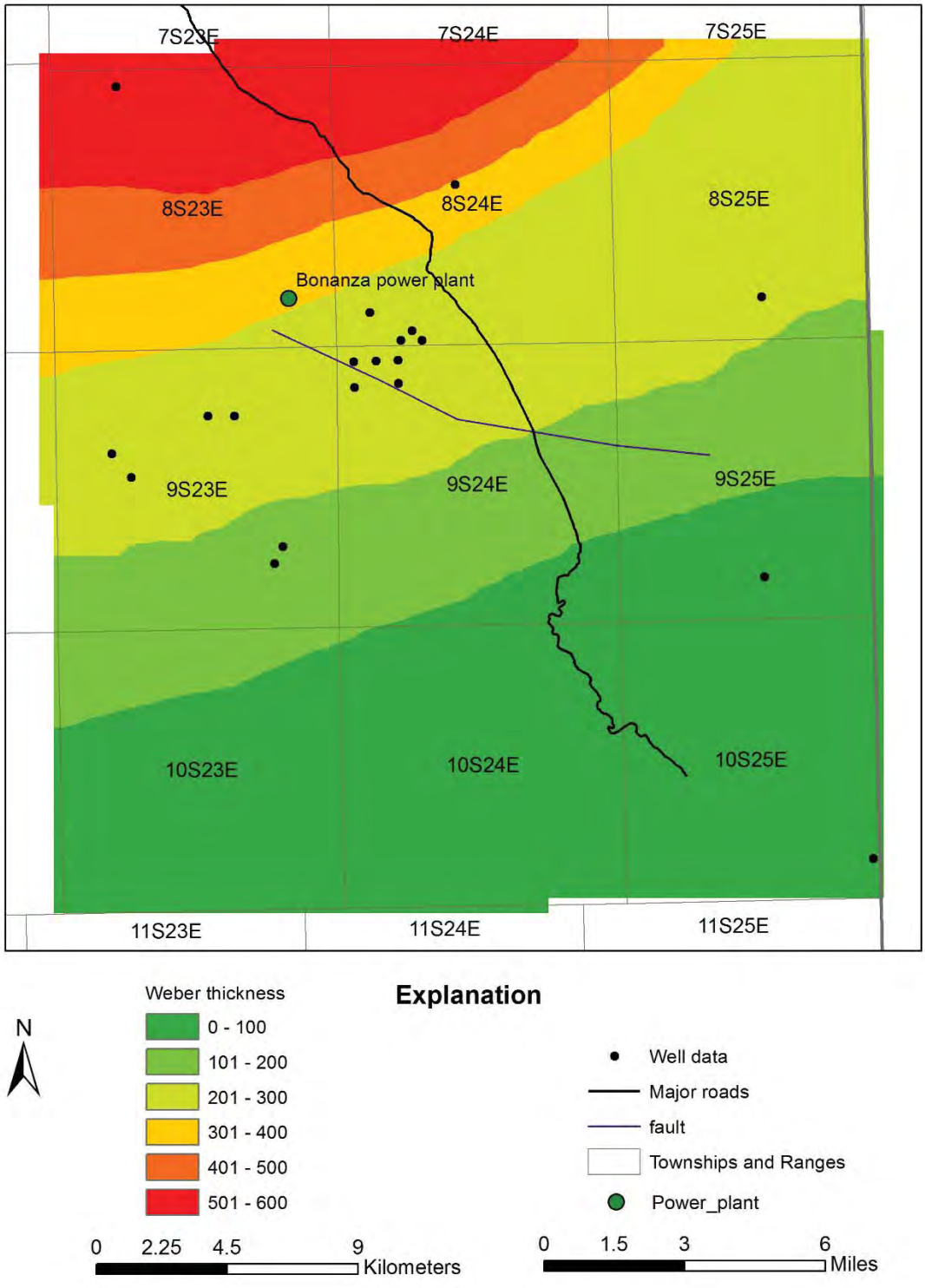


Figure 3. Isopach map of the Weber Sandstone, contour interval 100 feet (30 m).

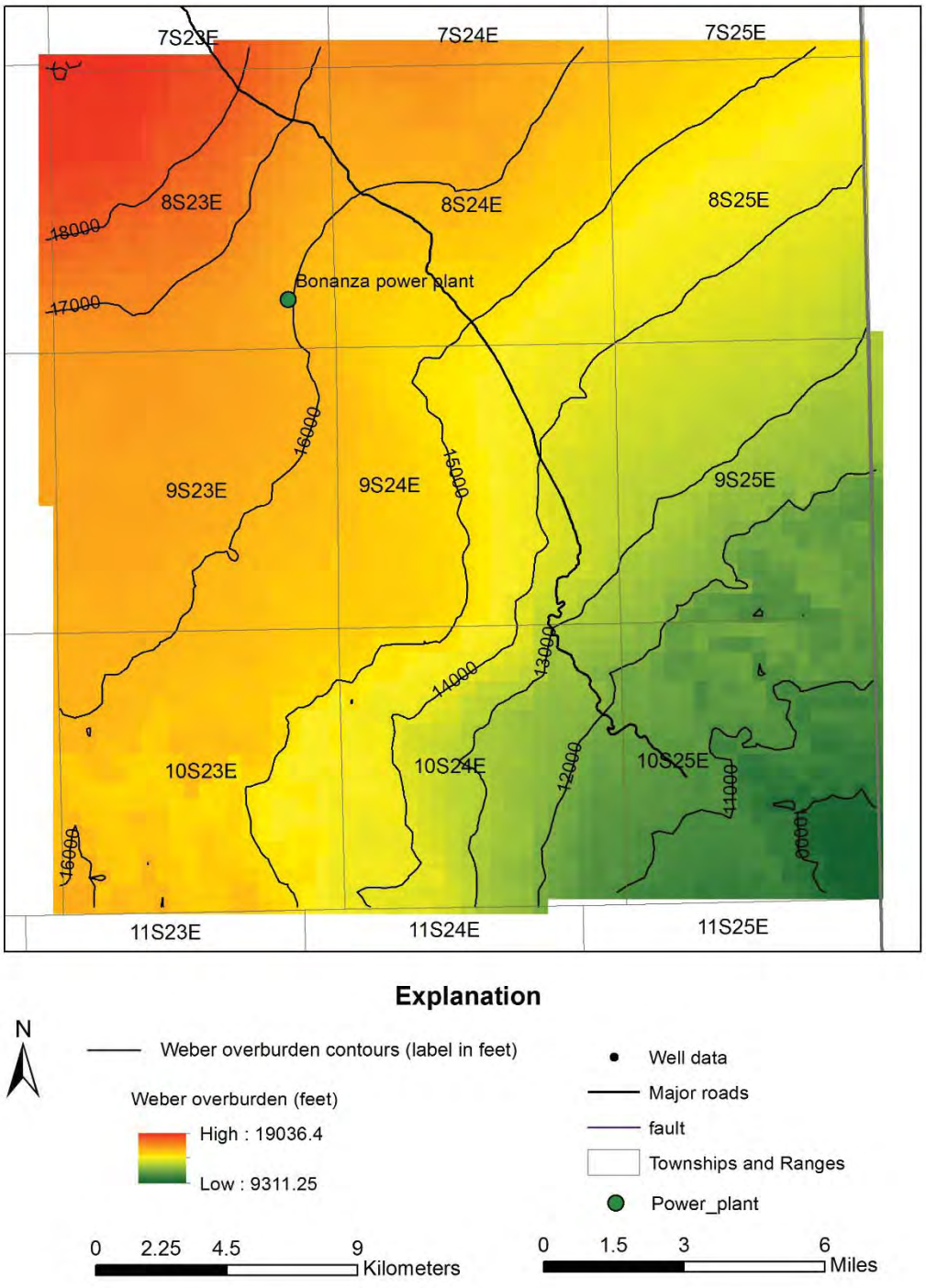


Figure 4. Thickness of the Weber Sandstone overburden, contour interval 1000 feet (300 m).

Table 1. Parameters used to calculate the CO_2 storage capacity of the Dakota, Entrada, and Weber reservoirs in the Bonanza Site. Ft = feet, m = meters, km^2 = kilometers squared, F = degrees Fahrenheit, C = degrees Celsius, D = depth, psi = pounds per square inch, and kpal = kiloPascals.

	Area	Average Depth	Average Reservoir Thickness	Average Porosity	Temperature Gradient	Pressure Gradient
Dakota	328 $miles^2$ 850 km^2	12,122 ft 3695 m	20 ft 6 m	12%	55 °F + (0.015*D) 28 °C/km	0.45 psi/ft 3.1 kPal/ft
Entrada	326 miles2 845 km2	13,016 ft 3967 m	94 ft 29 m	16%	55 °F + (0.015*D) 28 °C/km	0.45 psi/ft 3.1 kPal/ft
Weber	328 $miles^2$ 850 km^2	14,604 ft 4451 m	186 ft 57 m	7%	55 °F + (0.015*D) 28 °C/km	0.45 psi/ft 3.1 kPal/ft

Table 2. CO_2 storage capacity of the Dakota, Entrada, and Weber reservoirs in the Bonanza Site using three different efficiency factors.

CO_2 Storage Capacity in Million Metric Tonnes			
	Efficiency Factors		
	0.5%	2.0%	5.4%
Dakota	2.29	8.97	24.21
Entrada	14.22	55.78	150.59
Weber	13.07	51.25	138.38
TOTAL	***29.58***	***116.0***	***313.18***

Jurassic Entrada Sandstone

In the Bonanza site area, the Entrada is coastal dune facies and high quality reservoir. The isopach map shows that the unit thins slightly to the west and is ~60 to 90 (18-27 m) feet thick near the power plant (figure 5). The overburden map shows the unit has range of ~7700 to 17,500 feet (2349-5338 m) of overburden throughout the area and shallows to the southeast (figure 6).

Total storage capacity for the Entrada at 2.0% efficiency is 55.78 MMT (table 2). For this calculation we used an average porosity of 16%, an average reservoir thickness of 94 feet (29 m), and an average depth of 13,016 feet (3970 m) over 326 $miles^2$ (table 1).

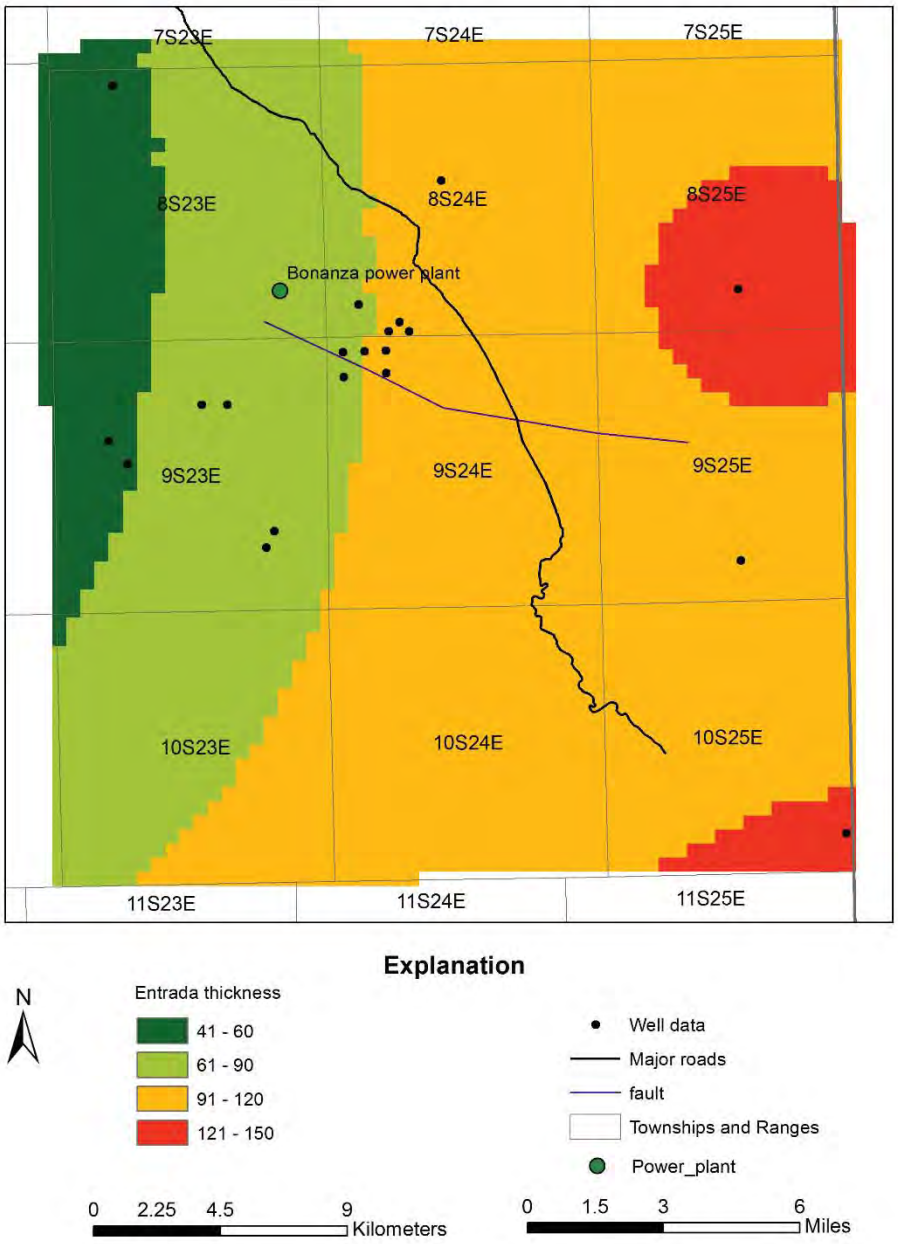


Figure 5. Isopach map of the Entrada Sandstone, contour interval 20 feet (6 m).

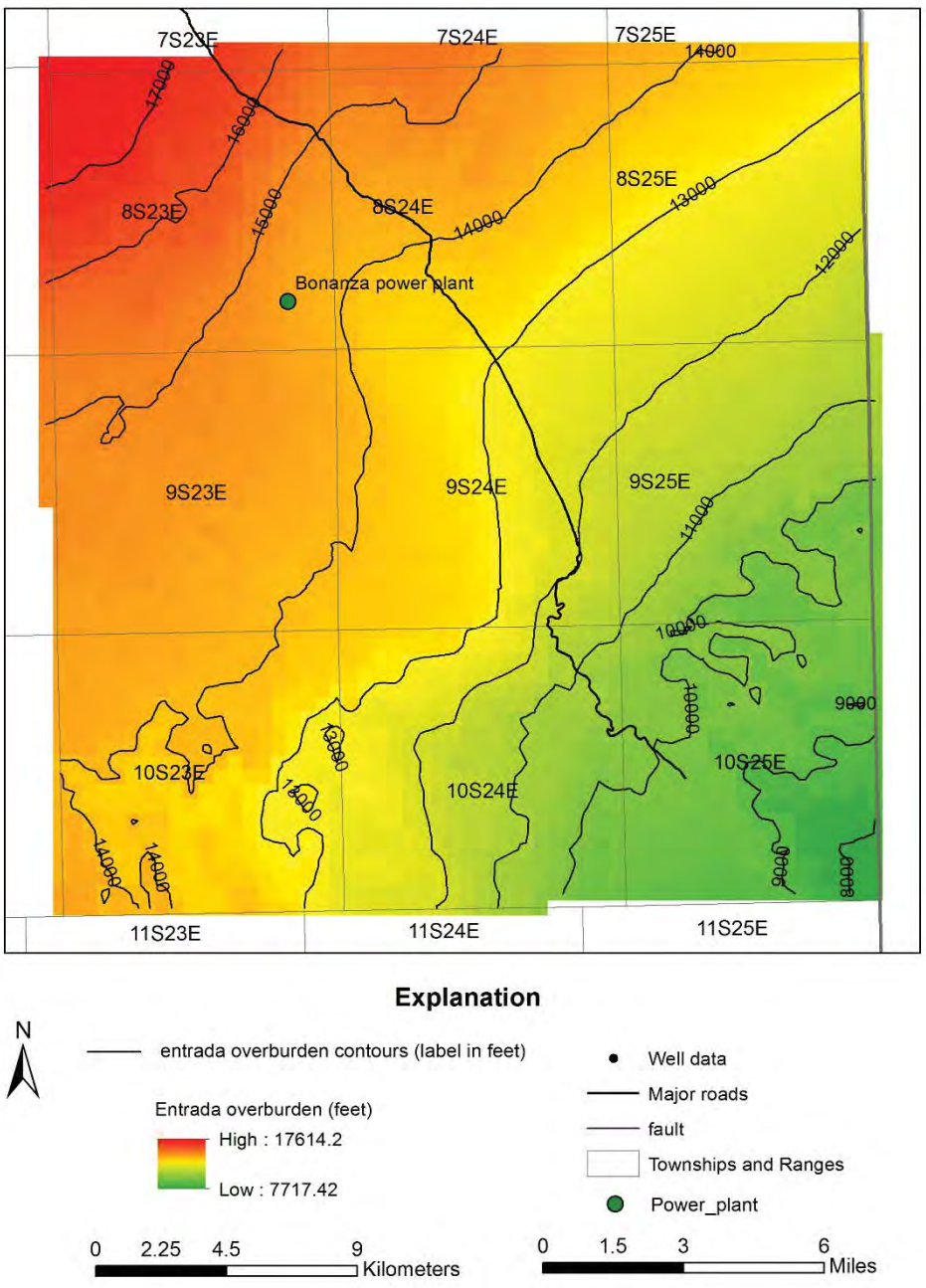


Figure 6. Thickness of the Entrada Sandstone overburden, contour interval is 1000 feet (300 m).

Cretaceous Dakota Sandstone

The Dakota Sandstone is a highly heterogeneous collection of fluvial channels, overbanks, and marginal-marine deposits. Fluvial systems often incise to varying degrees into older fluvial and over bank deposits and the subsequent valley and channel filling results in reservoirs of different thickness, width, and connectivity (Currie and others 2012). The primary reservoir facies in the Dakota are channel and near shore marine sandstone beds.

Structure contour maps show southeastward shallowing of the Dakota Sandstone, following geomorphology of the Uinta Basin (figure 7). The elevation of the Dakota near the Bonanza power plant averages ~ -8000 ft (-2440 m), while the overburden averages ~ 13,000 feet (3965 m) (figure 8). The average formation thickness of Dakota is 108 feet (33 m). The reservoir, or gross sandstone, thickness ranges between 31 to 87 feet (9.5-27 m) (figure 9), while the net reservoir sandstone with greater than 6% porosity ranges between 6 and 36 feet (2-11 m) (figure 10).

To calculate storage capacity, we used an average porosity of 12% (taken from wireline logs and published reports), an average net sandstone thickness of 20 feet (6 m), and an average depth of 12,122 feet (3697 m) over an area of 328 miles^2 (table 1). The storage capacity for the Dakota Sandstone at 2.0% efficiency is 8.97 MMT (table 2).

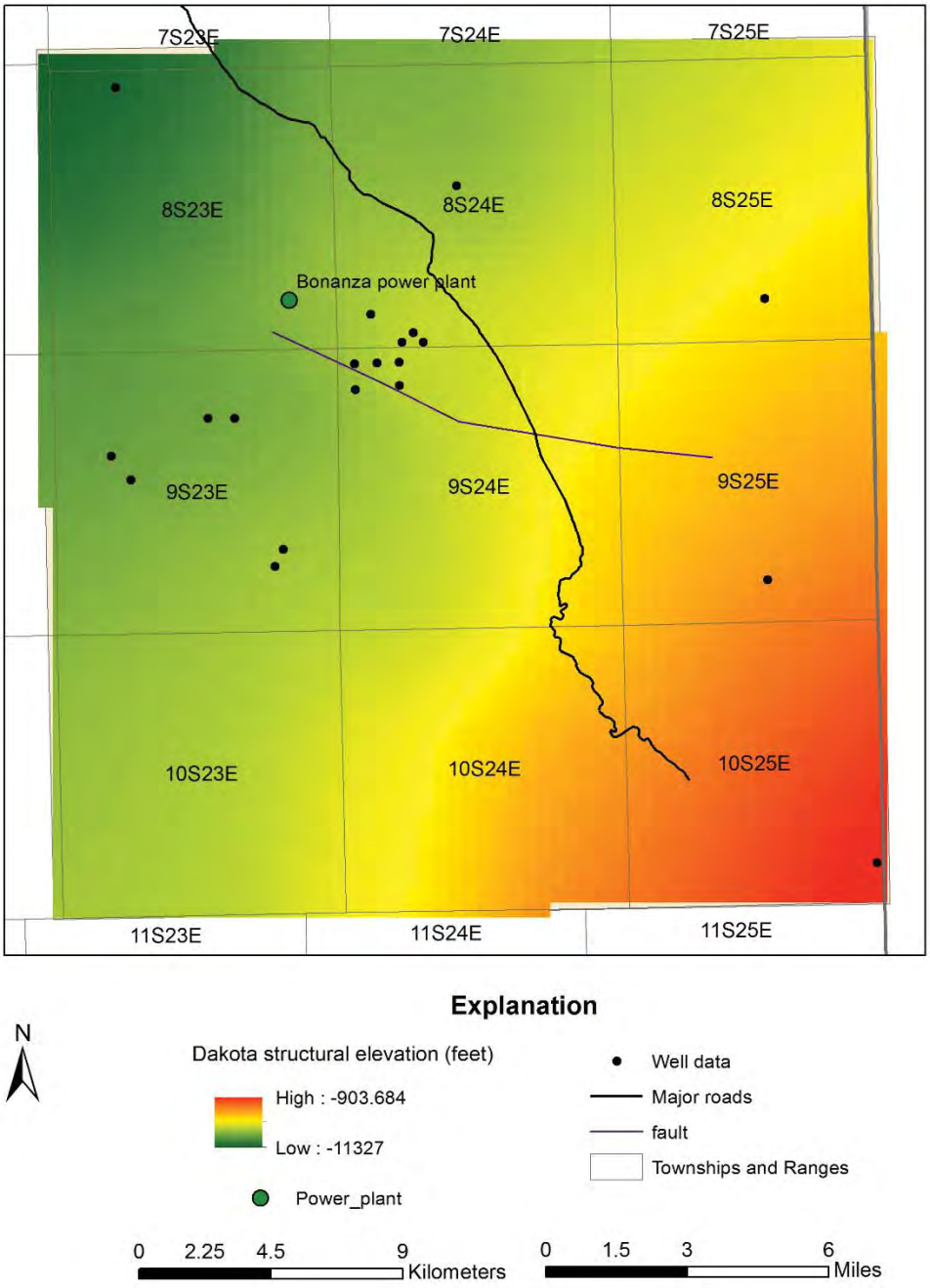


Figure 7. Structure contour map of the Dakota Sandstone in feet.

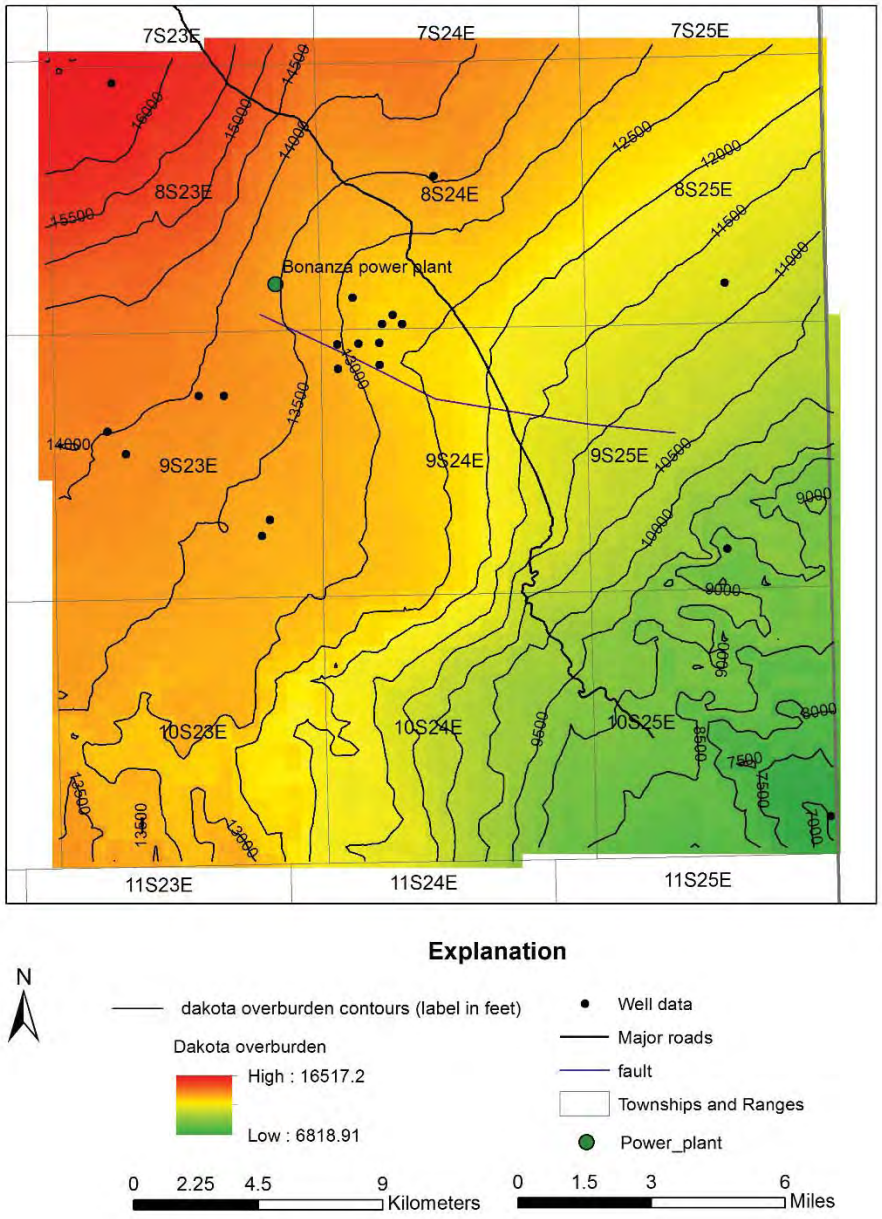


Figure 8. Thickness of the Dakota Sandstone overburden, contour interval is 500 feet (150 m).

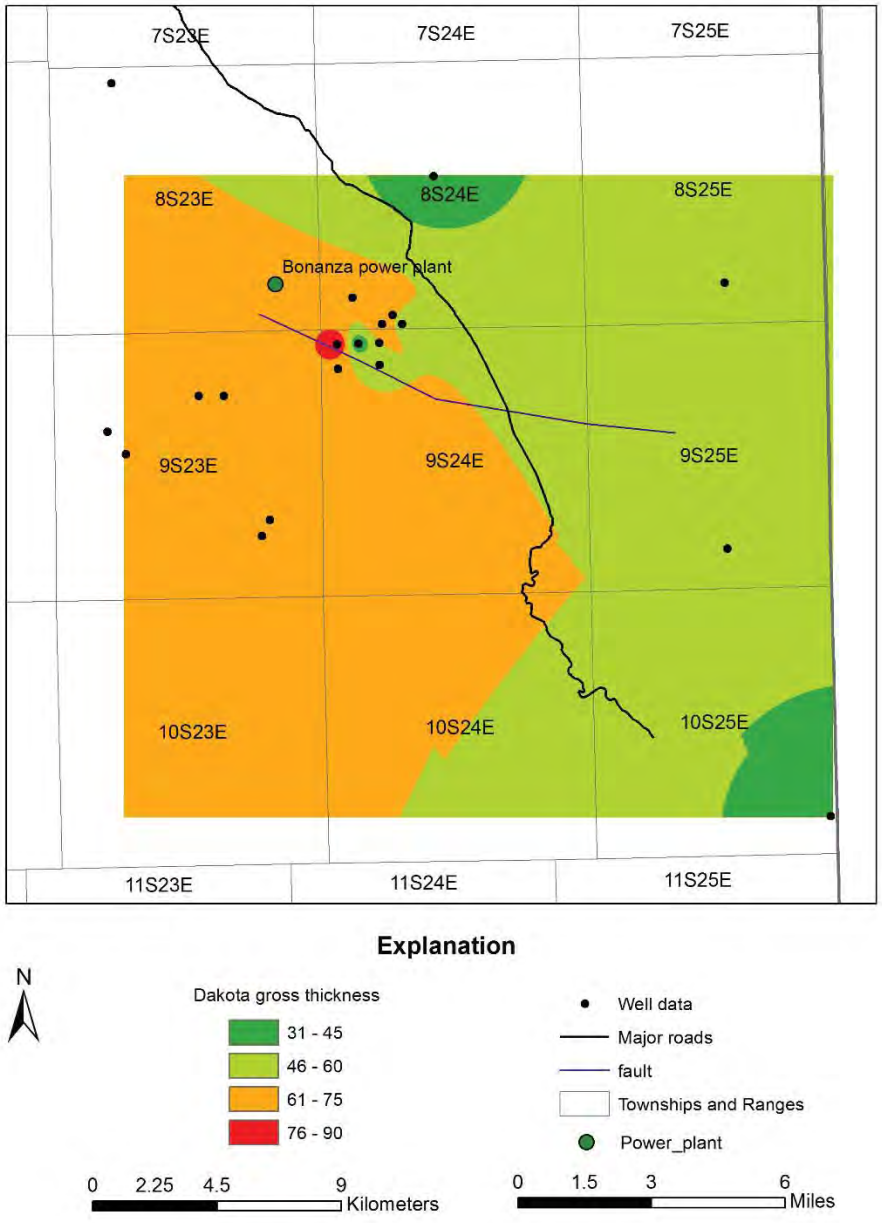


Figure 9. Thickness of sandstone within the Dakota Sandstone, contour interval is 14 feet (4 m).

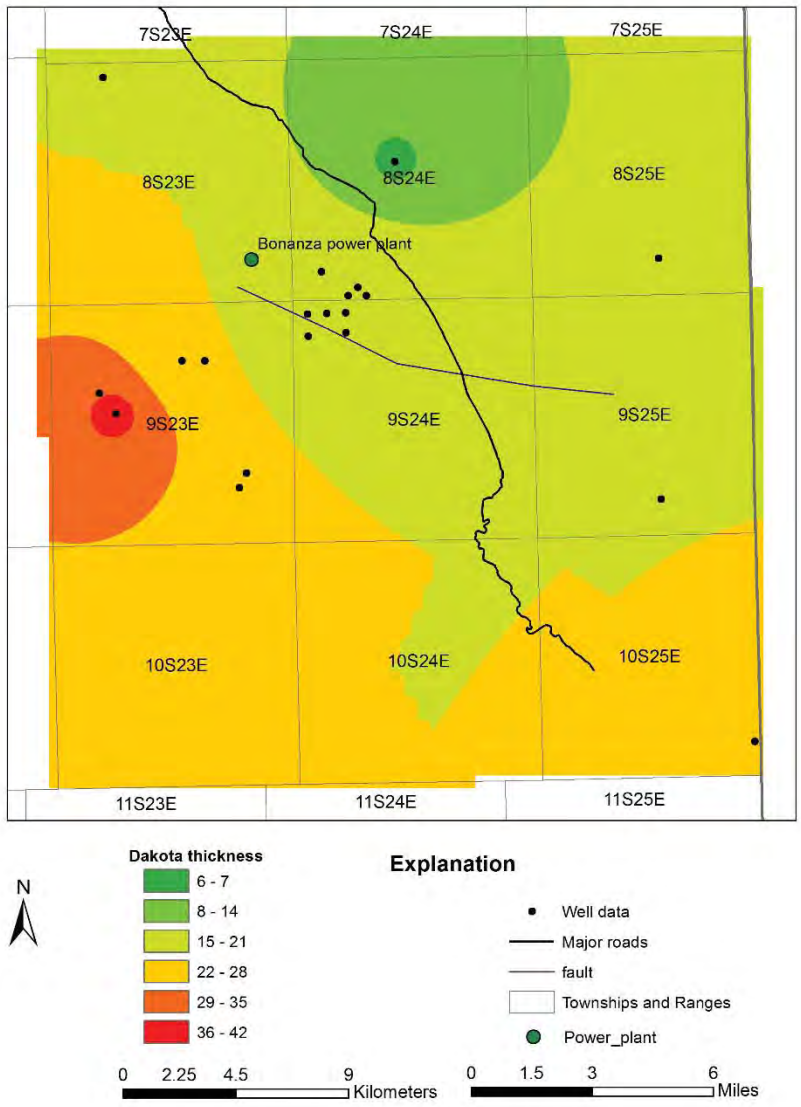


Figure 10. Thickness map showing the net reservoir sandstone within the Dakota with porosity greater than 6%. Contour interval is 6% porosity.

Summary and Recommendations

The combined storage capacity for the Weber, Entrada, and Dakota Sandstones in the Bonanza site is 116 MMT at 2.0% efficiency and 313 MMT at 5.4% efficiency. Because the sand bodies in the Dakota are thin, lenticular channel deposits with generally low average porosity (12%), it has the least storage capacity. The dune deposits of the Entrada and Weber have the greatest potential for CO_2 storage capacity in the Bonanza site. Of the two sites in Utah selected for potential commercial CO_2 storage, the Bonanza site is the best qualified with much

more storage capacity than the Woodside site. The Bonanza site also has well developed access and a power plant located on site.

References

Chidsey, Jr., T.C., and Sprinkel, D.A., 2005, Petroleum geology of Ashley Valley oil field and hydrocarbon potential of the surrounding area, Uintah County, Uutah, *in* Dehler, C.M., Pederson, J.L., Sprinkel, D.S., and Kowallis, B.J., editors, Uinta Mountain Geology: Utah Geological Association Publication 33, p. 347-368.

Currie, B.S., McPherson, M.L., Hokanson, W., Pierson, J.S., Homan, M.B., Pyden, T., Schellenbach, W., Purcell, R., and Nicklaus, D., 2012, Reservoir characterization of the Lower Cretaceous Cedar Mountain and Dakota Formations, northern Uinta Basin, Utah: UGS Open-File Report 597, CD-ROM.

Hintze, L.F., and Kowallis, B.J., 2009, Geologic history of Utah: Brigham Young University Geology Studies Special Publication 9, 225 p.

Hintze, L.F., Willis, G.C., Laes, D.Y.M., Sprinkel, D.A., and Brown, K.D., 2000, Digital geologic map of Utah: Utah Geological Survey Map 179DM, scale 1:500,000.

Moretti Jr., G., Lipinski, P., Gustafson, F., and Slaughter, A., 1992, Dakota Sandstone deposition and trap door structure of Hells Hole field, eastern Uinta Basin, Utah and Colorado in Fouch, T.D., Nuccio, V.F., and Chidsey, Jr., T.C., editors, Hydrocarbon and mineral resources of the Uinta Basin, Utah and Colorado: Utah Geological Association Guidebook 20, p. 313-323.

Roberts, L.N.R., 2003, Structure contour map of the top of the Dakota Sandstone, Uinta-Piceance Province, Utah and Colorado, *in* USGS Uinta-Piceance Assessment Team compilers, Petroleum systems and geologic assessment of oil and gas in the Uinta-Piceance Province, Utah and Colorado, USGS DDS-69B, 14 p.

APPENDIX C

Woodside Analysis

Contents

Woodside Analysis only

WOODSIDE DOME STORAGE SITE

Reason for Selecting the Woodside Site

Woodside Dome was ranked number 2 during the preliminary site evaluation. The Cretaceous Dakota Sandstone crops out along the flanks of Woodside Dome, and the Jurassic Entrada and Navajo Sandstones are also too shallow (<3000 feet [1000 m]) for consideration at this location but have regional significance. The Permian White Rim Sandstone (age equivalent to the upper Weber Sandstone) along with the deeper Mississippian Redwall Limestone combined had sufficient storage capacity to meet the minimum capacity required for consideration as a potential CO_2 storage site.

The Pennsylvanian Hermosa Group has storage potential but was not evaluated in this study. Woodside Dome has easy access, and is a double plunging anticline (figure 1) with potentially well-defined traps for the reservoirs. A few deep wells have been drilled along the crest of the anticline providing some subsurface reservoir and seal data. Woodside is near undeveloped coal beds and a potential site for a new power plant. It is close enough to the power plants in the Castle Valley area to the west that a CO_2 pipeline could be constructed.

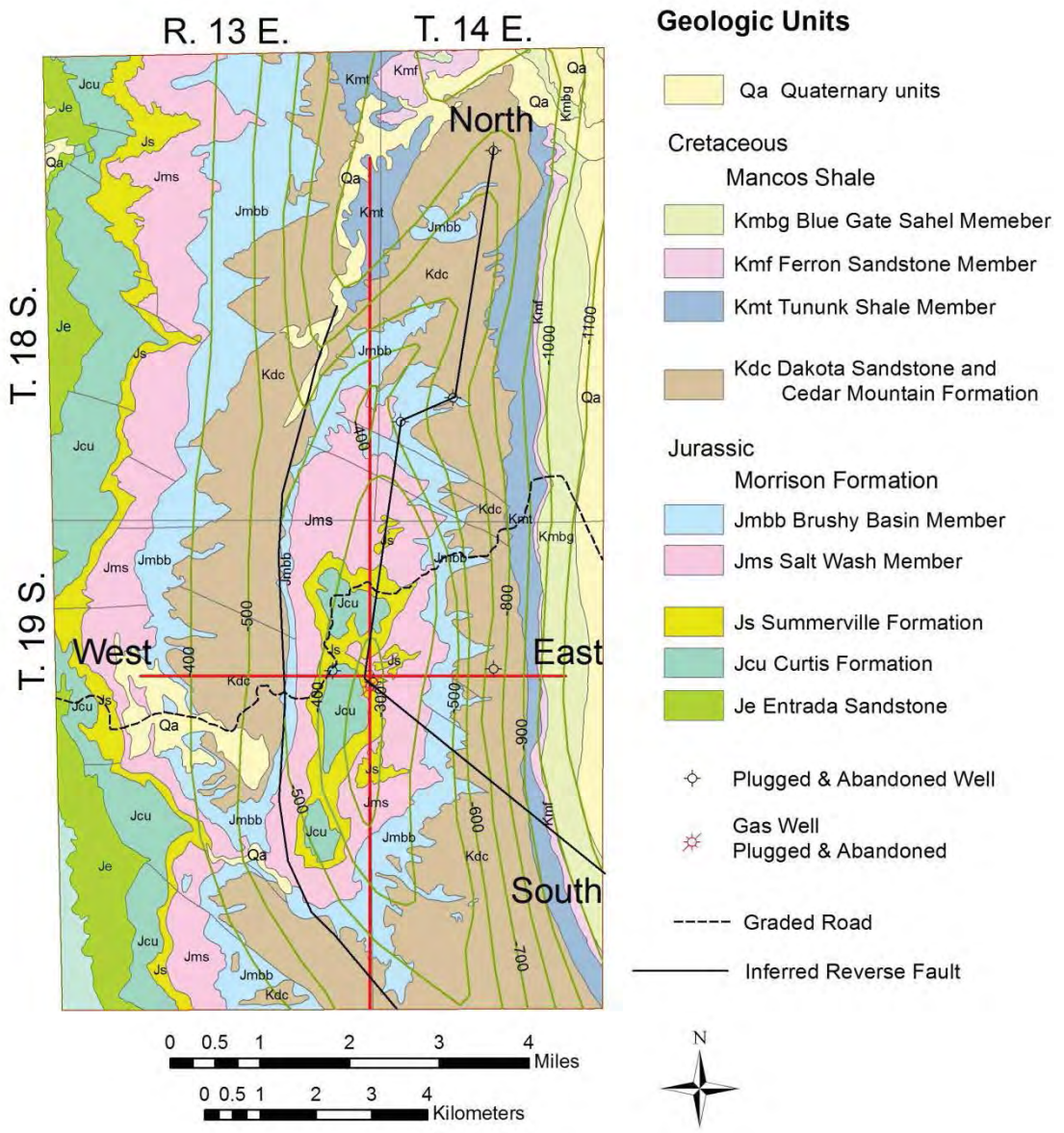


Figure 1. Structure contour map on the top of the Mississippian Redwall Limestone. Contour interval is 100 meters, mean sea-level datum. Geologic map of Woodside Dome anticline in Emery County, Utah, was clipped from Witkind (2004). Oldest formation exposed along the crest of the anticline is the Jurassic Curtis Formation (Jcu). See figure 2 for west-to-east and south-to-north structural cross sections (red lines), and figure 3 for Redwall Limestone well log cross section (black line).

Methods

South-to-north and west-to-east cross sections (figure 2) were constructed using formation contacts from the geologic map, formation strikes and dips collected from the outcrop, and well data. Well logs in the Woodside area were digitized in a LAS format so wells could be more easily correlated and reservoir porosity calculated. A well database was developed in Excel® containing well locations, name, unique API number, and drill depths of all formations penetrated. The structural elevations along the cross sections and elevations from the well database were used to construct structure contour maps of the tops of the Redwall Limestone, White Rim Sandstone, and Permian Black Box Dolomite. The structure data were gridded in ArcMap® and subtracted from a digital elevation model (DEM) grid to produce overburden maps, or drill depth grids of the top of each reservoir. The structure, overburden, porosity, pressure, and temperature data for each reservoir were imported into the EGI storage capacity spreadsheet and the CO_2 storage capacity was calculated for 0.5%, 2.0%, and 5.4% efficiency.

There are no usable outcrops of the Redwall Limestone near Woodside so only well data were available. Seven wells have been drilled at Woodside but only one penetrated a complete section of the Redwall (figure 3). Porosity logs were digitized and the data were used to determine porosity range, average porosity, and net thickness of the reservoir, defined by having 4% or more porosity.

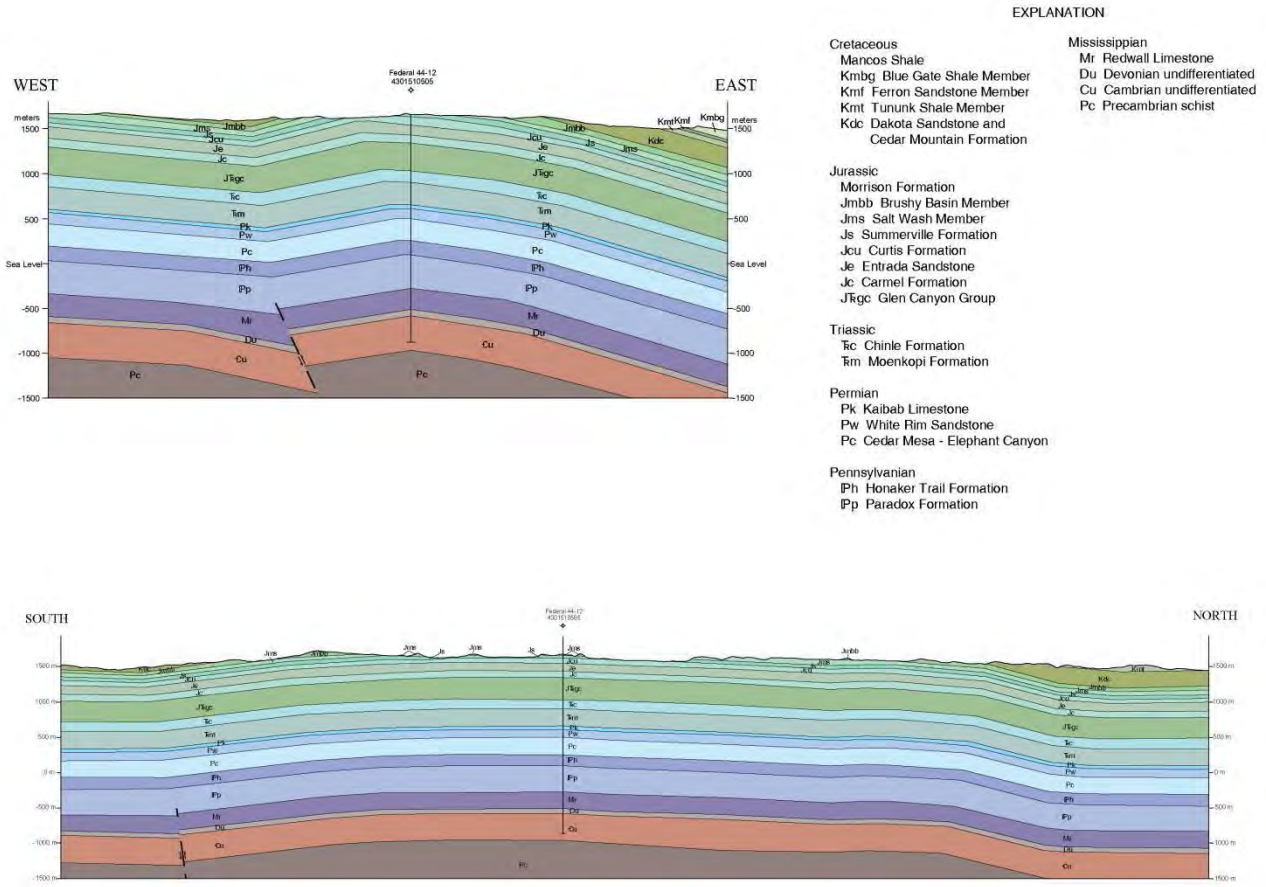


Figure 2. West-to-east and south-to-north cross sections of Woodside anticline based on surface geology and limited well control. Depth and horizontal distance are in meters, no vertical exaggeration. See figure 1 for location of cross sections. We used Kaibab Limestone (Pk) on the cross sections for the equivalent Black Box Dolomite. From Morgan and others, 2013.

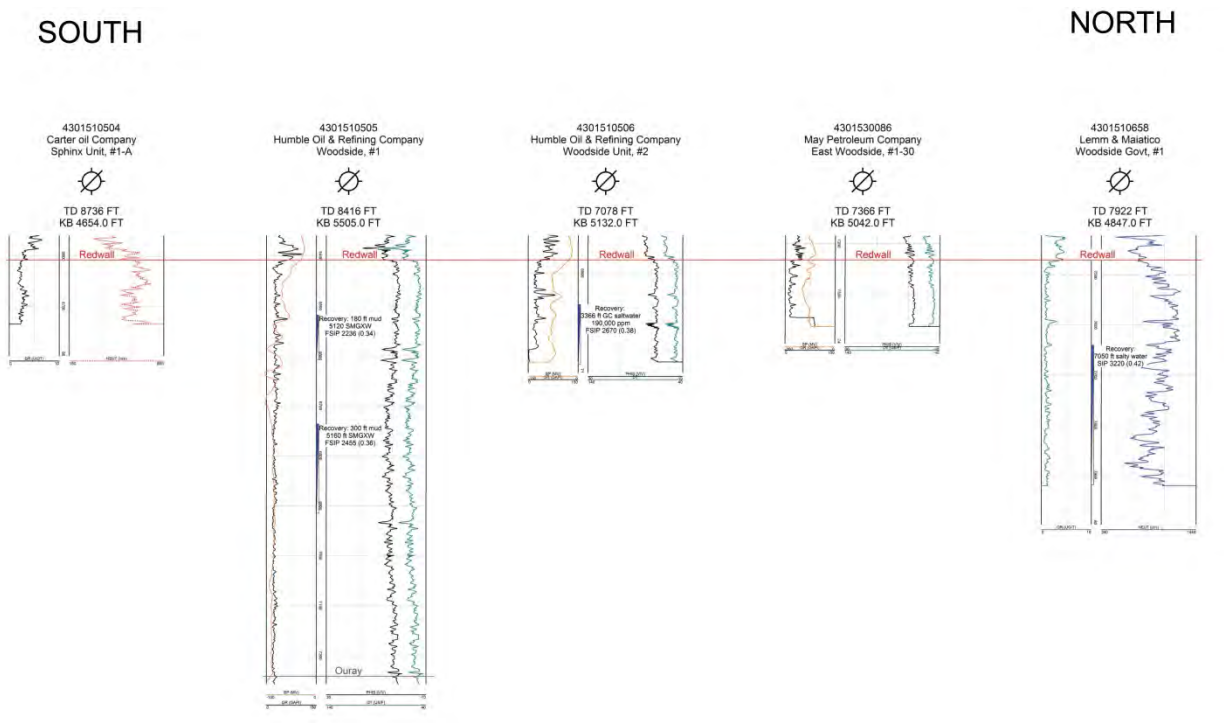


Figure 3. South-to-north well log cross section of the Mississippian Redwall Limestone at Woodside Dome. The deepest penetration is the Woodside 1 well which drilled 830 feet (253 m) of Redwall encountering 347 feet (106 m) of 4% or more porosity. See figure 1 for location of cross section.

The Black Box Dolomite (Kaibab Formation) and White Rim Sandstone are exposed in many areas of the San Rafael Swell (SRS) within miles of the Woodside Dome. The UGS contracted with Professor Thomas Morris of Brigham Young University to investigate the Black Box and White Rim reservoirs on outcrop and in the wells at Woodside Dome (Harston and Morris, 2013). Walter Harston, a graduate student under Professor Morris, measured, described, sampled, and collected gamma-ray data over several exposures of the Black Box and a nearly complete section of White Rim in Black Box Canyon of the San Rafael River (figure 3). Field work by Harston and Morris was done using metric measurements. Thin sections were used for detailed petrographic descriptions of the two formations. Plug samples (90) were used to determine porosity and permeability of various facies within the Black Box and White Rim. Gamma-ray data collected every meter (3 feet) from the outcrop were used to generate synthetic log curves that could be correlated to geophysical well logs at Woodside.

Geologic Characterization

Mississippian Redwall Limestone

Bedding strikes and dips were collected from the outcrops at Woodside and added to the geologic map of Witkind (2004). Using the geologic map and well log correlations, two cross sections were constructed: one north to south, and one west to east (figure 2).

The structural elevations along the cross sections and elevations from the well database were used to construct a structure contour map (figure 1) and overburden map on the top of the Redwall Limestone. The area of structural closure was determined from the mapping, and average reservoir thickness, porosity, pressure and temperature were determined from the well logs and tests (table 1). We used the EGI storage capacity spreadsheet to calculate the CO_2 storage capacity for 0.5%, 2.0%, and 5.4% efficiency (table 2). The calculated storage capacity is significantly less than originally estimated (table 3). We originally calculated an area of 40 square miles (100 km^2) based on the surface geologic map of the Woodside anticline but the area of closure at depth may only be 12 to 17 square miles (30-45 km^2). The area of closure is poorly constrained, so we used a very conservative estimation; the area could be much larger.

Table 1. Parameters used to calculate the CO_2 storage capacity of the Redwall Limestone, White Rim Sandstone, and Black Box Dolomite at Woodside. Ft = feet, m = meters, km^2 = kilometers squared, D = depth, F = degrees Fahrenheit, C = degrees Celsius, psi = pounds per square inch, and kPal = kiloPascals.

	Area	Average Depth	Reservoir Thickness	Average Porosity in percent (%)	Temperature Gradient	Pressure Gradient
Redwall	16.6 $miles^2$ 43 km^2	6749 ft 2058 m	345 ft 105 m	5%	55º F + (0.013*D) 0.03º C/m	0.42 psi/ft 9.5 kPal/m
White Rim	11.9 $miles^2$ 31 km^2	3445 ft 1050 m	420 ft 128 m	15%	55º F + (0.012*D) 0.04º C/m	0.42 psi/ft 9.5 kPal/m
Black Box	13.5 $miles^2$ 35 km^2	3422 ft 1043 m	75 ft 23 m	16%	55º F + (0.012*D) 0.04º C/m	0.42 psi/ft 9.5 kPal/m

Table 2. CO_2 storage capacity of the Redwall Limestone, White Rim Sandstone, and Black Box Dolomite at Woodside using three efficiency factors.

CO_2 Storage Capacity in Million Metric Tonnes			
	Efficiency Factors		
	0.5%	2.0%	5.4%
Redwall	0.8	3.2	8.8
White Rim	2.0	7.9	21.4
Black Box	0.4	1.5	4.1
Total	***3.2***	***12.6***	***34.3***

Table 3. Comparison of the preliminary and (final) parameters and resulting storage capacity calculations at an efficiency factor of 5.4%. Black Box Dolomite was not originally evaluated as a potential storage reservoir. The parameter that had the largest change in the final characterization was the area. Diff = difference between preliminary and (final) capacity calculations.

Preliminary (Final) Parameters and Storage Capacity							
	Area ($miles^2$)	Thickness (feet)	Porosity in percent (%)	Temperature Gradient	Pressure Gradient	Capacity (MMT) 5.4%	Diff %
Redwall	40 (16.6)	700 (345)	4% (5%)	60°F + (0.01*D) (55°F + [0.013*D])	0.45 psi/ft (0.42 psi/ft)	35.3 (8.8)	25%
White Rim	40 (11.9)	450 (420)	7% (15%)	60°F + (0.01*D) (55°F + [0.013*D])	0.45 psi/ft (0.42 psi/ft)	36.7 (21.4)	58%
Total						72 (30.2)	42%

Permian Black Box Dolomite and White Rim Sandstone

Outcrops of the Permian White Rim Sandstone and Black Box Dolomite in the northern SRS, Emery County, Utah were studied (figure 3) by Harston and Morris (2013). The outcrop data were then applied to interpretation of the well data at Woodside.

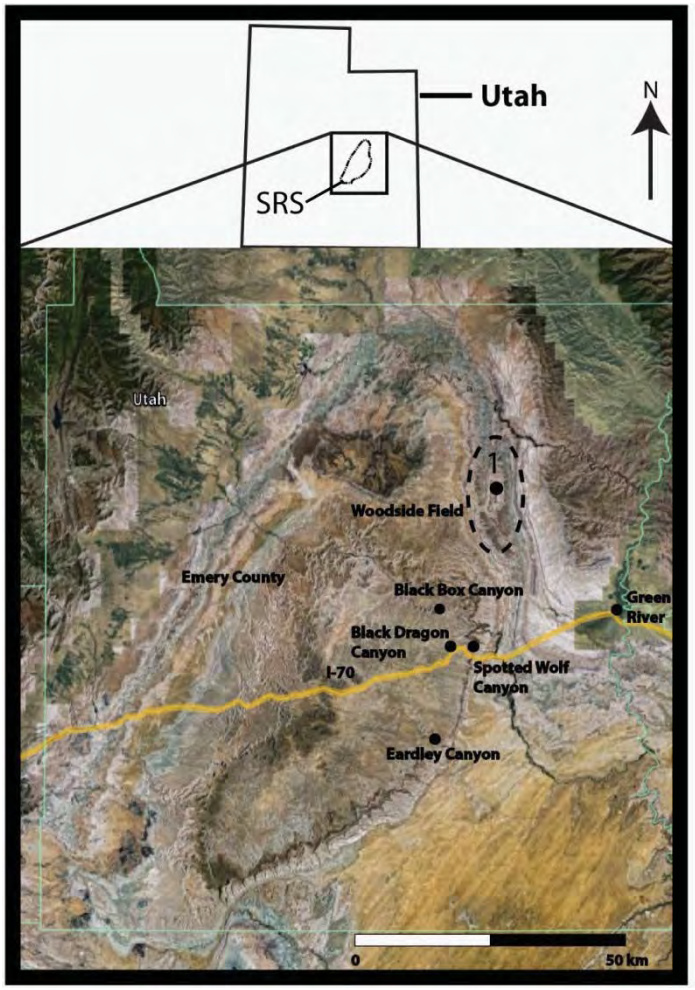


Figure 4. Location map of the SRS and Woodside Dome area in central Utah. A stratigraphic section of the White Rim, Black Box, and lower portion of the Moenkopi was measured, described, and sampled at Black Box Canyon (figure 5). Additional stratigraphic sections of the upper portion of the White Rim and Black Box were described from the Spotted Wolf Canyon and Black Dragon Canyon areas (figures 14 and 15). Location 1 in the Woodside field is the Bill Barrett Corporation Woodside 1 well. From Hartson and Morris unpublished contract report, Google Earth Pro licensed to Dr. Morris.

Black Box Canyon is the closest outcrop to the Woodside Dome study site that has a nearly complete section of White Rim Sandstone. More than 150 meters (490 feet) of White Rim were measured and described at Black Box Canyon (figure 5). Three primary facies were identified in the White Rim: a basal sand sheet facies (figure 6), an eolian dune facies (figure 7) that makes up the majority of the formation, and a reworked upper transitional facies (figure 8). Point count analyses of thin sections identified all three facies as quartz arenites from a continental block provenance (figures 9, 10, and 11). The eolian dune facies and most samples of the transitional facies exhibit good reservoir quality with porosities generally above 15% and permeabilities above 100 millidarcies (mD) (figure 12). The sand sheet facies generally has porosities from 7 to 12% with permeabilities ranging from 0.1 to 20 mD.

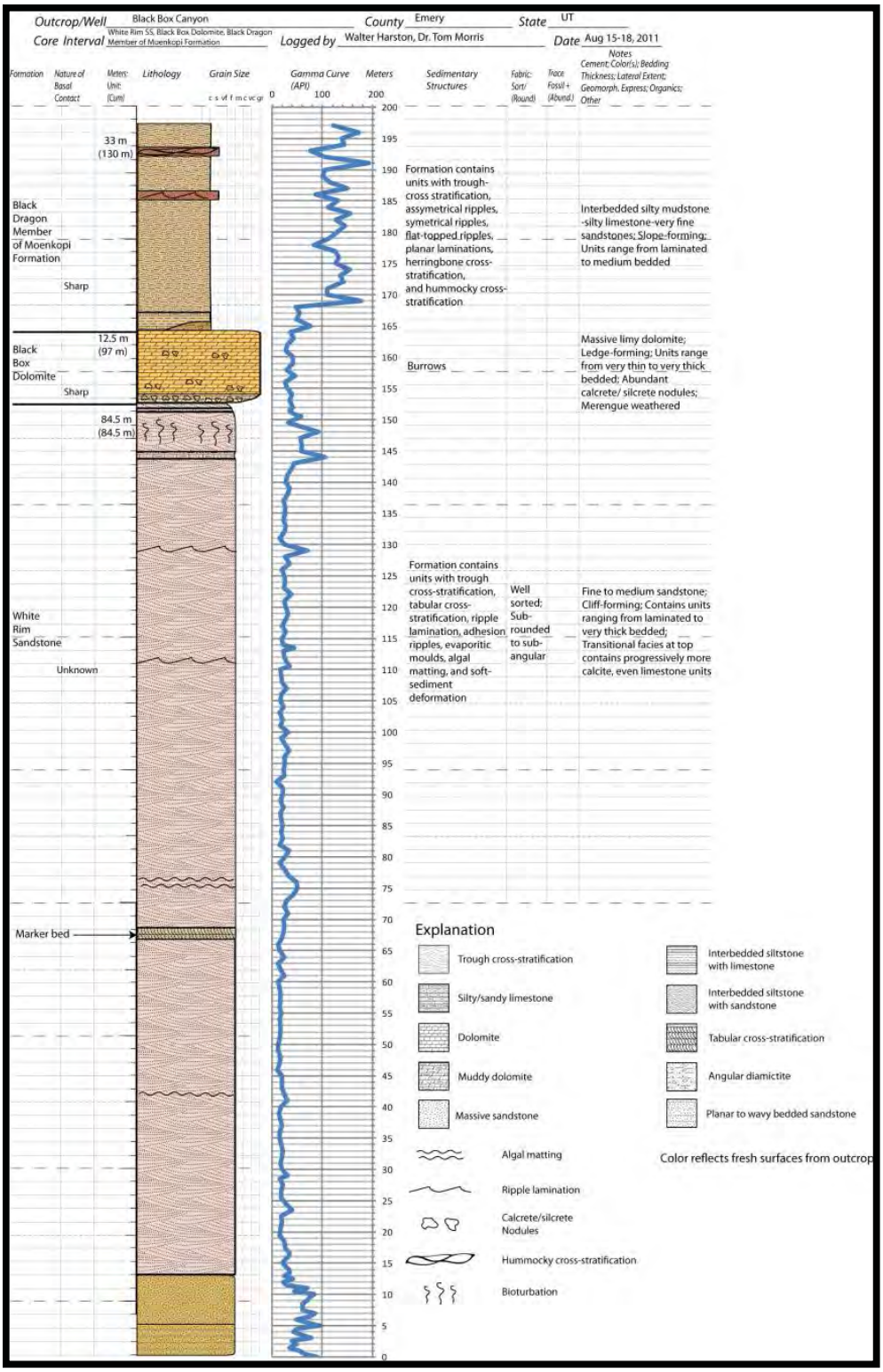
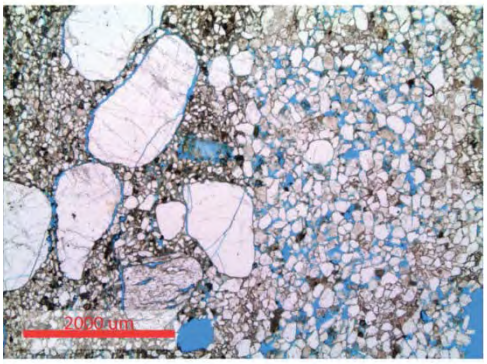


Figure 5. White Rim stratigraphic measured section from Black Box Canyon. The base of the White Rim is not exposed but the section is believed to be nearly complete.



A

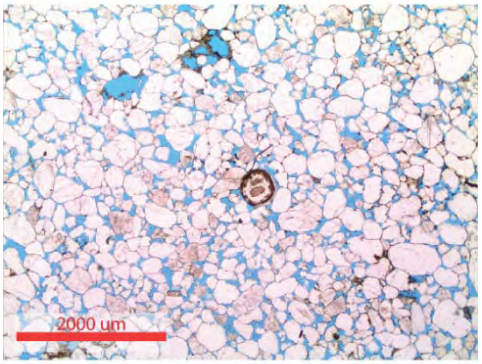


B

Figure 6. Basal sand sheet facies of the erg margin, White Rim Sandstone: A) Outcrop photograph of low-angle foresets terminating into very coarse lags observed at Black Box Canyon. B) Photomicrograph of sand sheet facies at Black Box Canyon.



A

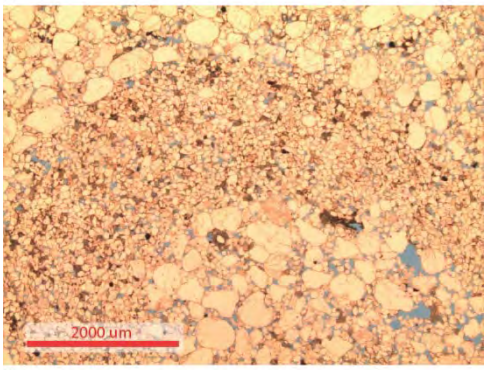


B

Figure 7. Trough cross-stratified sandstone beds of the eolian dune facies of the erg proper, White Rim Sandstone. A) Outcrop photograph of medium- to high-angle foresets at Black Box Canyon. Foreset angles are highlighted with yellow bars. B) Photomicrograph of trough cross-stratified sandstone from Black Dragon Canyon East. Note the sub-rounded to rounded grains and the chertified ooid in the center.



A



B

Figure 8. Bioturbated bed in the reworked upper transitional facies, White Rim Sandstone. A) Outcrop photograph of bioturbated bed at Black Box Canyon. Note faint vertical burrows of the Skolithos trace fossil assemblage. B) Photomicrograph of a bioturbated bed from Black Dragon Canyon West.

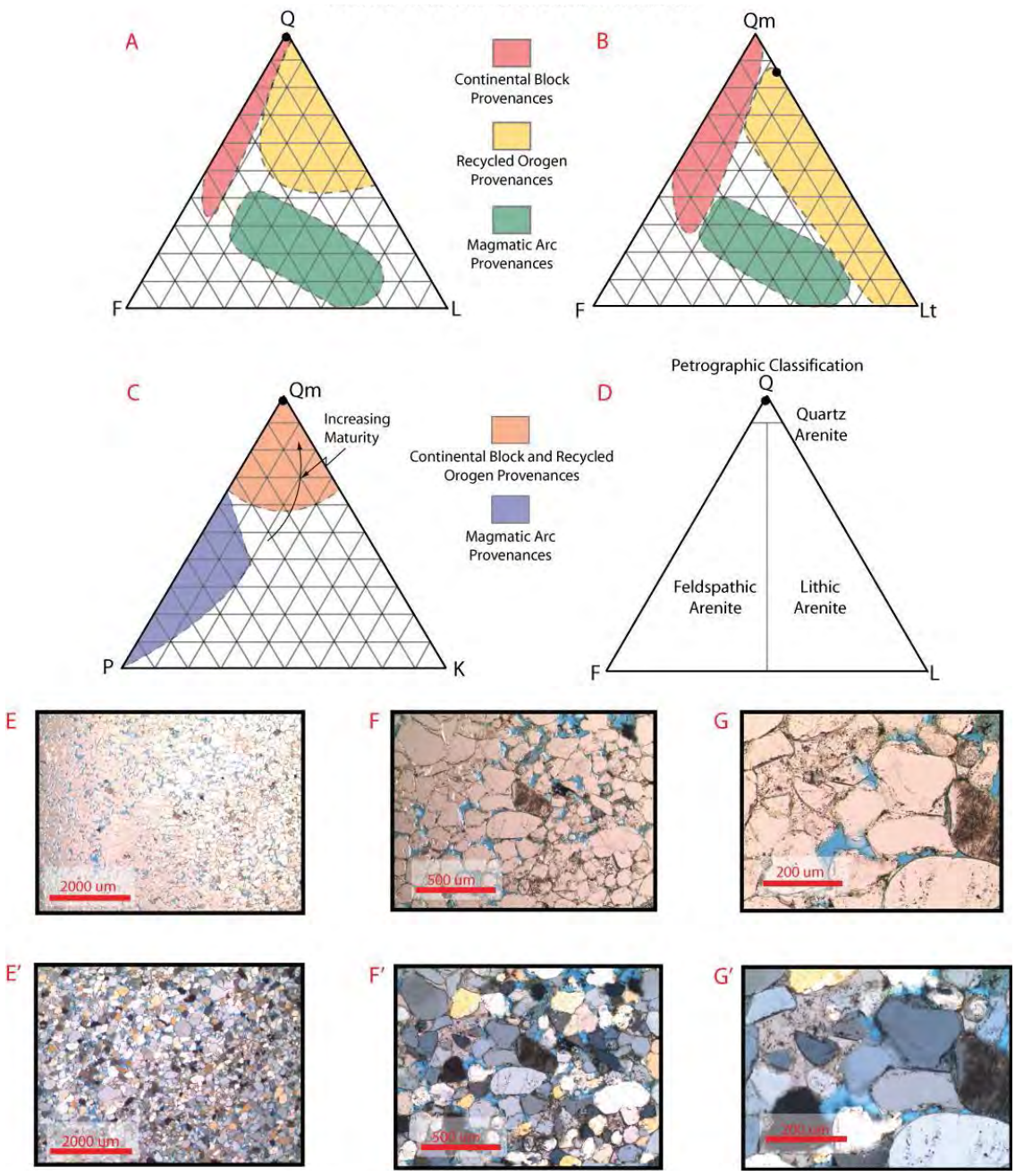


Figure 9. Photomicrographs and ternary diagrams of the sand sheet facies of the White Rim Sandstone. Photomicrographs are of one thin section at different magnification. E, F, and G are in transmitted light and E', F', and G' were taken in cross-polarized light. Q = quartz, F = feldspar, L = lithics, Qm = monocrystalline quartz, K = potassium feldspar, P = plagioclase, Lt = lithics including all forms of quartz other than monocrystalline.

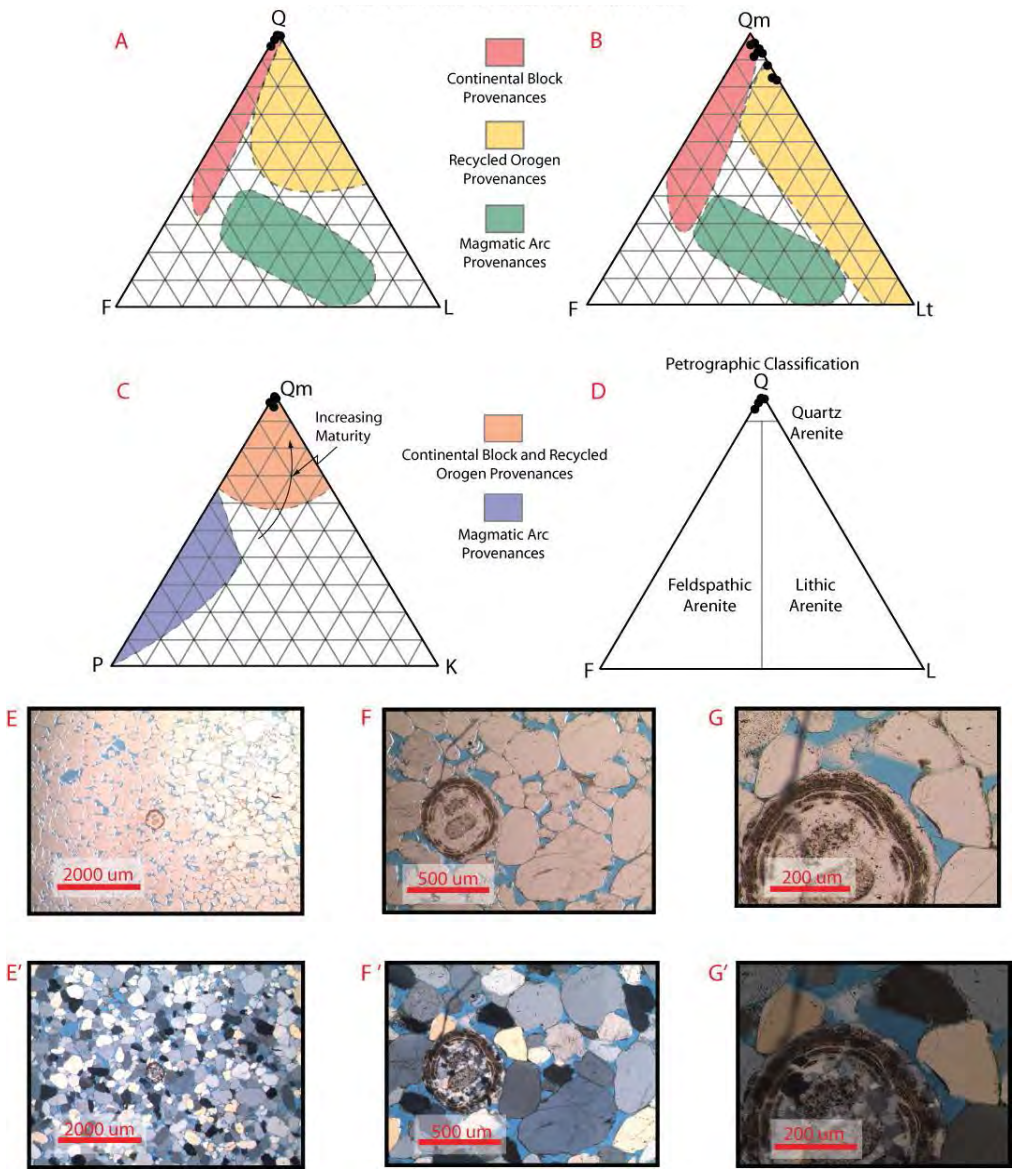


Figure 10. Photomicrographs and ternary diagrams of the eolian dune facies of the WRS. Photomicrographs are of one thin section at different magnification. E, F, and G are in transmitted light and E', F', and G' were taken in cross-polarized light. Q = quartz, F = feldspar, L = lithics, Qm = monocrystalline quartz, K = potassium feldspar, P = plagioclase, Lt = lithics including all forms of quartz other than monocrystalline. Note rounded ooid.

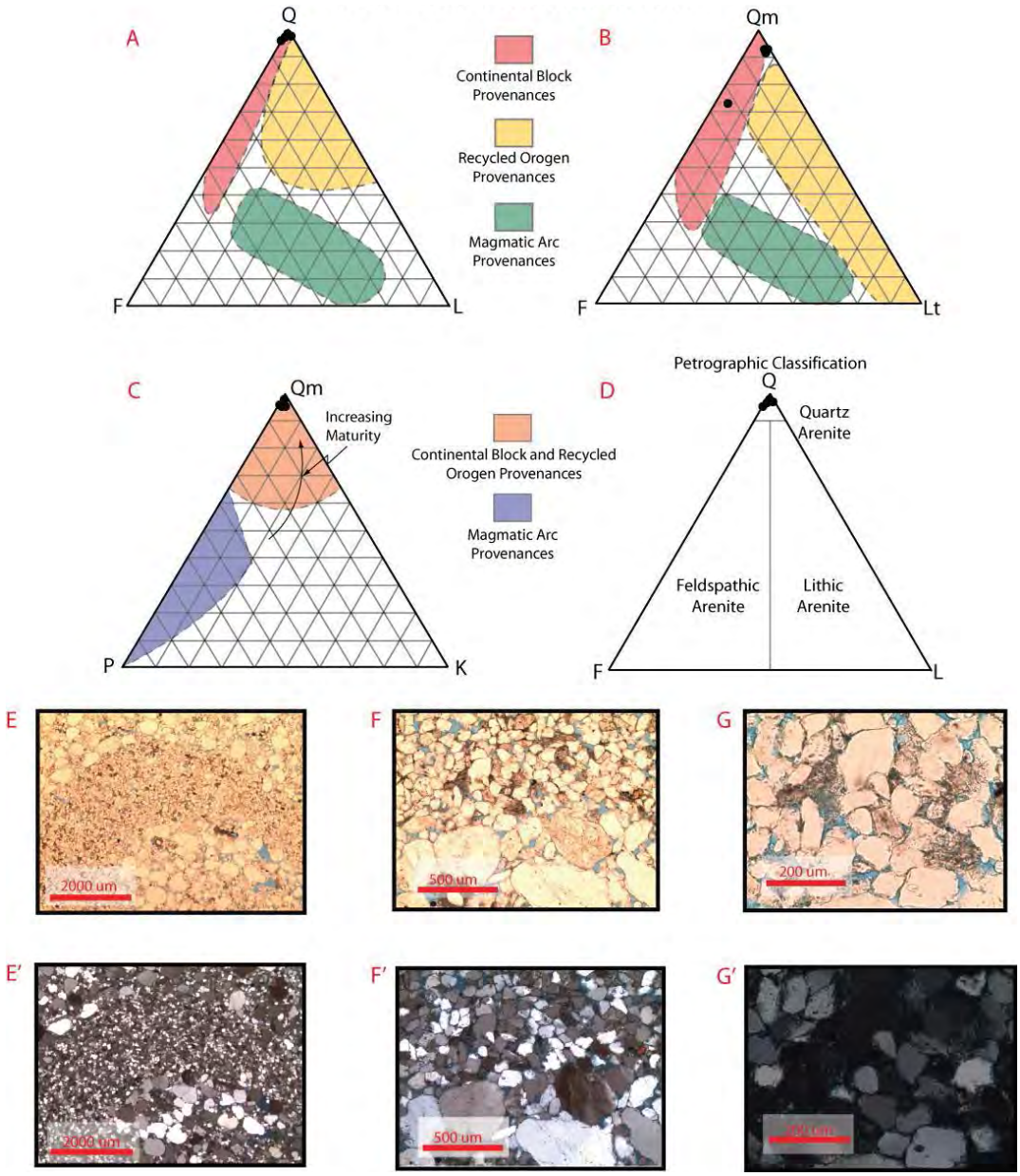


Figure 11. Photomicrographs and ternary diagrams of the transitional facies of the WRS. Photomicrographs are of one thin section at different magnification. E, F, and G are in transmitted light and E', F', and G' are taken in cross-polarized light. Q = quartz, F = feldspar, L = lithics, Qm = monocrystalline quartz, K = potassium feldspar, P = plagioclase, Lt = lithics including all forms of quartz other than monocrystalline.

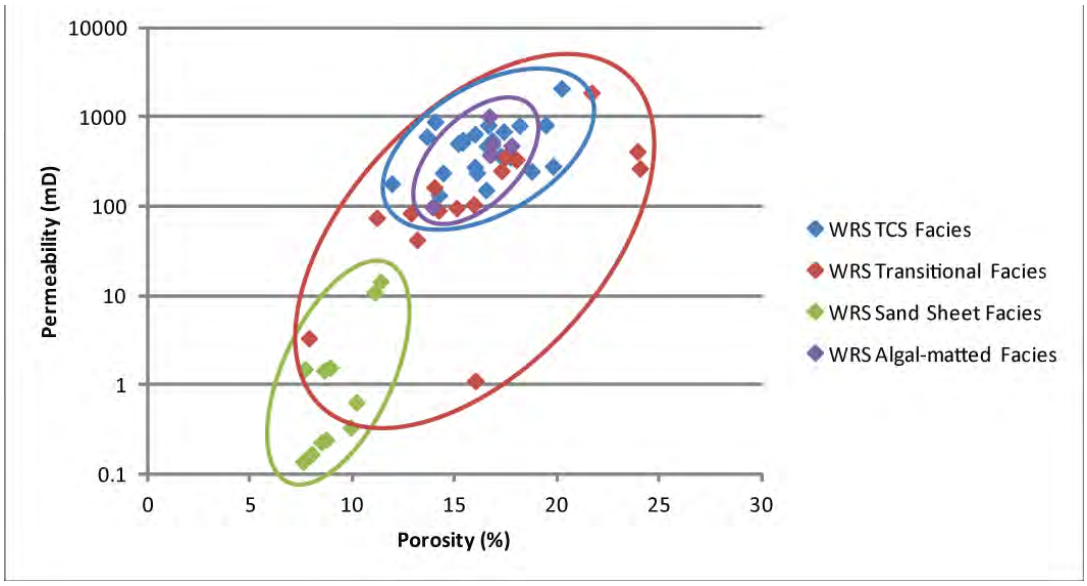


Figure 12. Porosity (%) and permeability (mD) cross plot of core plugs collected from the White Rim Sandstone outcrop. TCS is the trough cross-stratified eolian dune facies, and the algal-matted facies are interdunal deposits in the eolian dune facies. The eolian dune facies has the best reservoir properties, the transitional facies has the most heterogeneous reservoir properties, and the sand sheet facies has the lowest quality reservoir properties.

The Black Box Dolomite and overlying lower Triassic Moenkopi Formation were described at Black Box Canyon (figures 4 and 5). The basal caliche zone (figure 13) of the Black Box is a seal for the White Rim reservoir. The overlying sandy dolomite, massive dolomite, and sandstone facies have good reservoir properties; as a result, the Black Box can be considered both a seal and reservoir. Several stratigraphic sections of the Black Box were described in the Spotted Wolf Canyon and Black Dragon Canyon areas (figure 4) to understand the heterogeneity within the formation (figures 14 and 15). The thickness of the Black Box is highly variable and the unit is absent in many parts of the SRS, placing Moenkopi on White Rim. The Black Box is divided into four facies: (1) basal caliche facies, (2) massive dolomite facies comprising most of the formation, (3) sandstone facies, and (4) sandy dolomite facies. The basal caliche is the only facies that does not have good reservoir qualities (figure 16).



Figure 13. Black Box caliche facies forms the light-colored receding exposure overlain by the more resistant massive dolomite facies at Black Box Canyon.

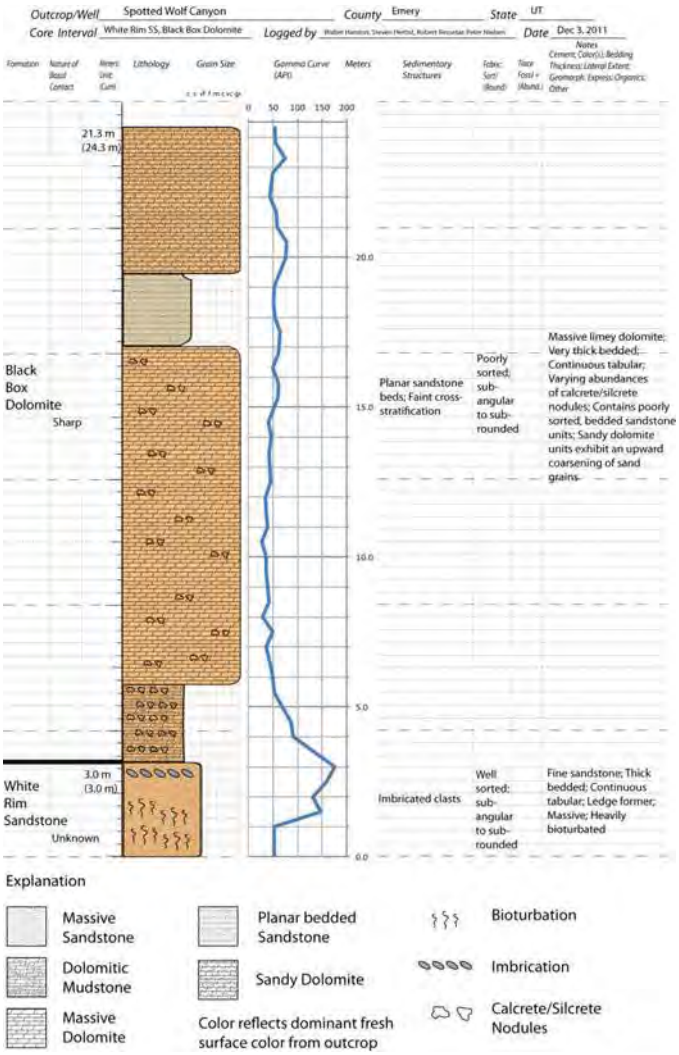


Figure 14. Stratigraphic measured section and gamma-ray curve of the Black Box and underlying transitional facies of the White Rim at Spotted Wolf Canyon.

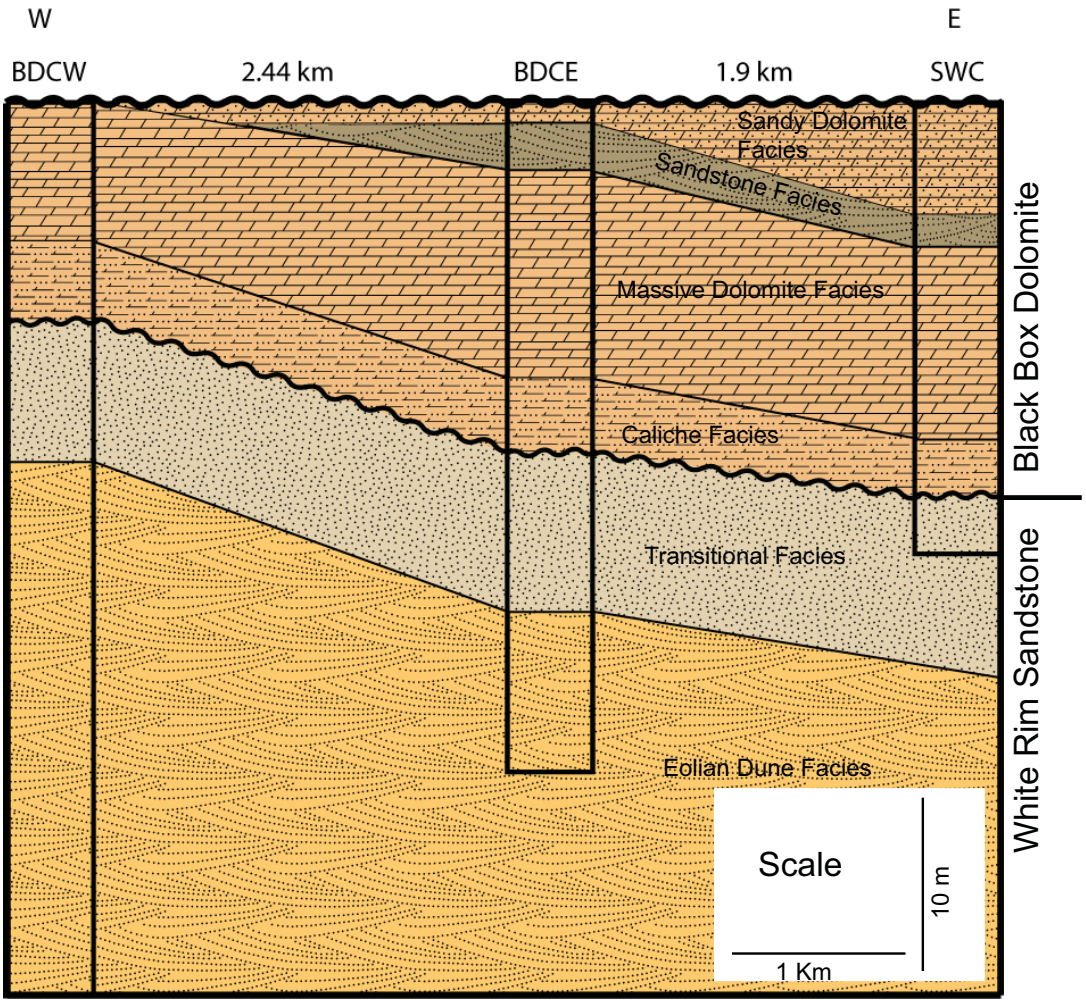


Figure 15. West-to-east cross section of the Black Box Dolomite and upper portion of the White Rim Sandstone. There is significant heterogeneity within the Black Box and thinning over the White Rim. BDCW = Black Dragon Canyon West, BDCE = Black Dragon Canyon East, and SWC = Spotted Wolf Canyon.

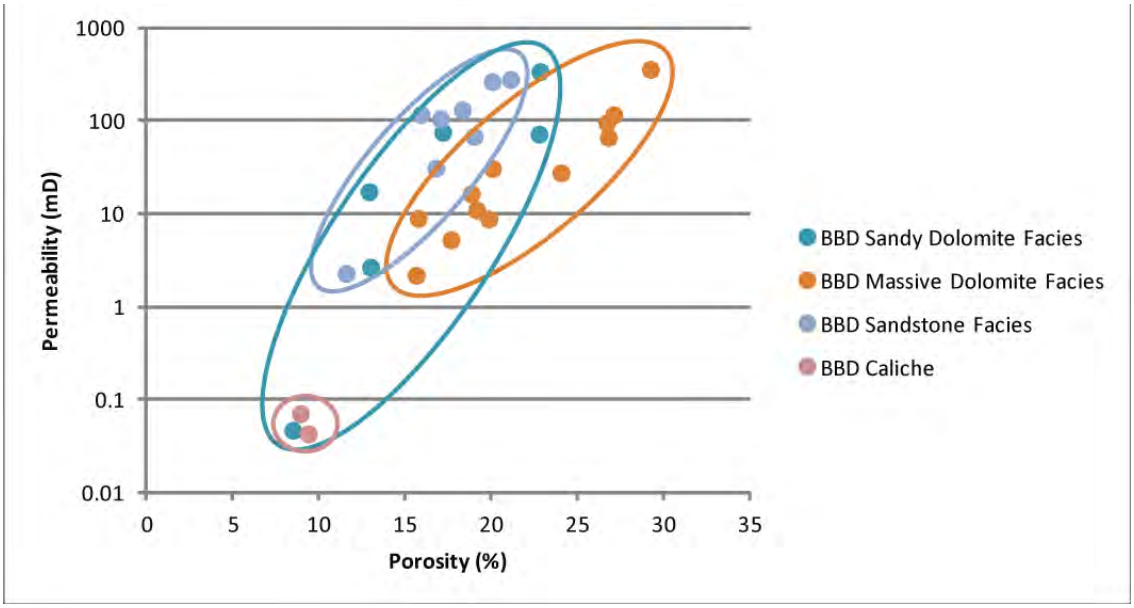


Figure 16. Porosity (%) and permeability (mD) cross plot of outcrop core plug samples of the Black Box Dolomite. The caliche is the only facies with poor reservoir properties.

There is good correlation of the gamma-ray curve from the Black Box Canyon stratigraphic section to the geophysical well log of the most recent well (Bill Barrett Corporation, Woodside 1) drilled at Woodside Dome (figures 4 and 17). The surface gamma-ray curve and detailed lithologic descriptions were very helpful in defining formation boundaries in the geophysical well logs.

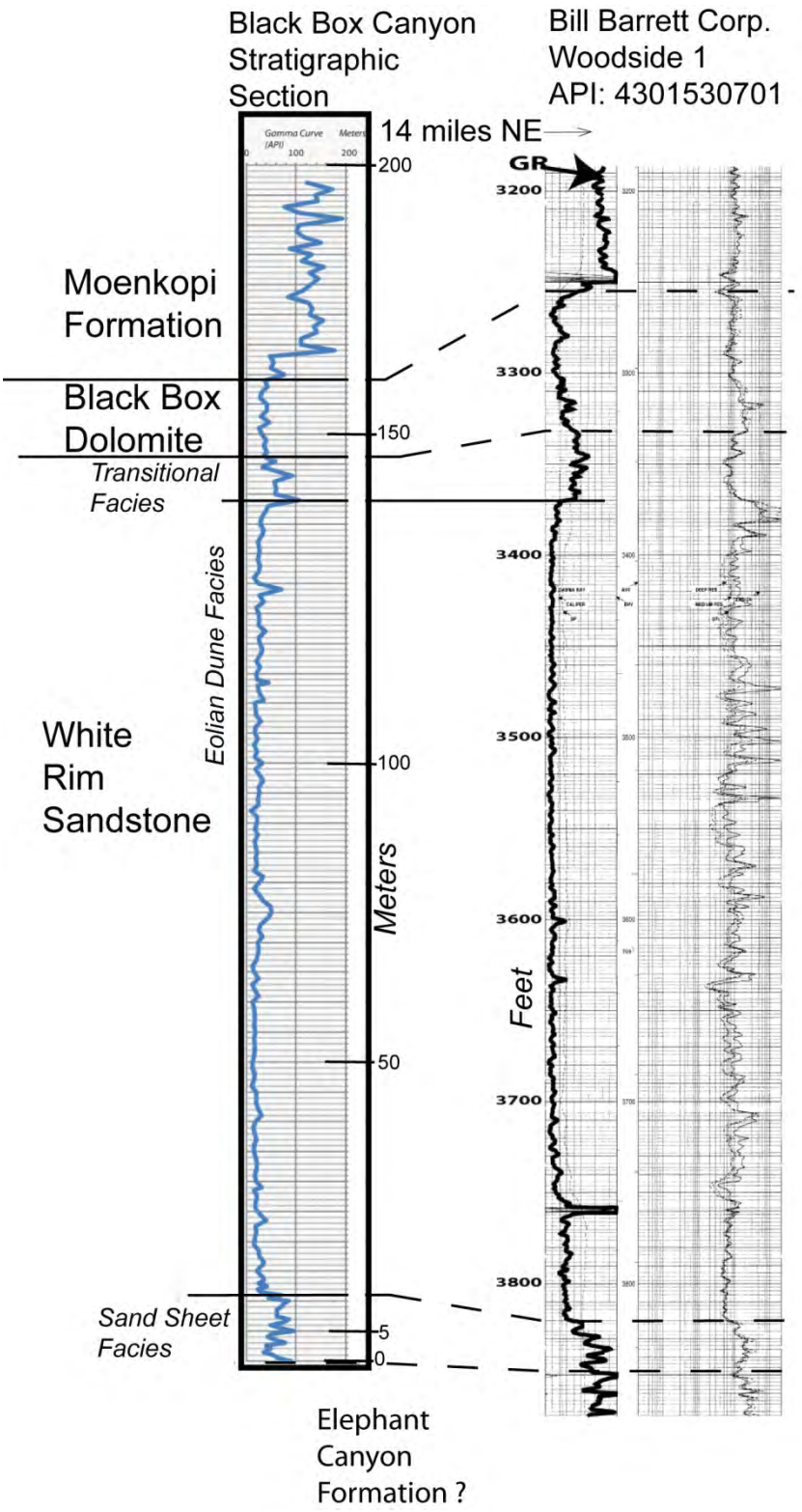


Figure 17. Preliminary correlation of gamma-ray curves from the Black Box Canyon measured section and the Woodside 1 well (figure 4) drilled by Bill Barrett Corporation on the crest of the Woodside Dome. Logs at approximate same vertical scale although units are different.

A thickness map of the White Rim Sandstone was constructed from the well data (figure 18). The structural elevations along the cross sections and elevations from the well database were used to construct structure contour maps and overburden maps on the top of the White Rim and Black Box Dolomite (figure 19). The area of structural closure was determined from the mapping; average reservoir thickness, porosity, pressure and temperature were determined from the well logs and tests (table 1). The White Rim and Black Box data were imported into the EGI storage capacity spreadsheet and the CO_2 storage capacity was calculated for 0.5%, 2.0%, and 5.4% efficiency (table 2).

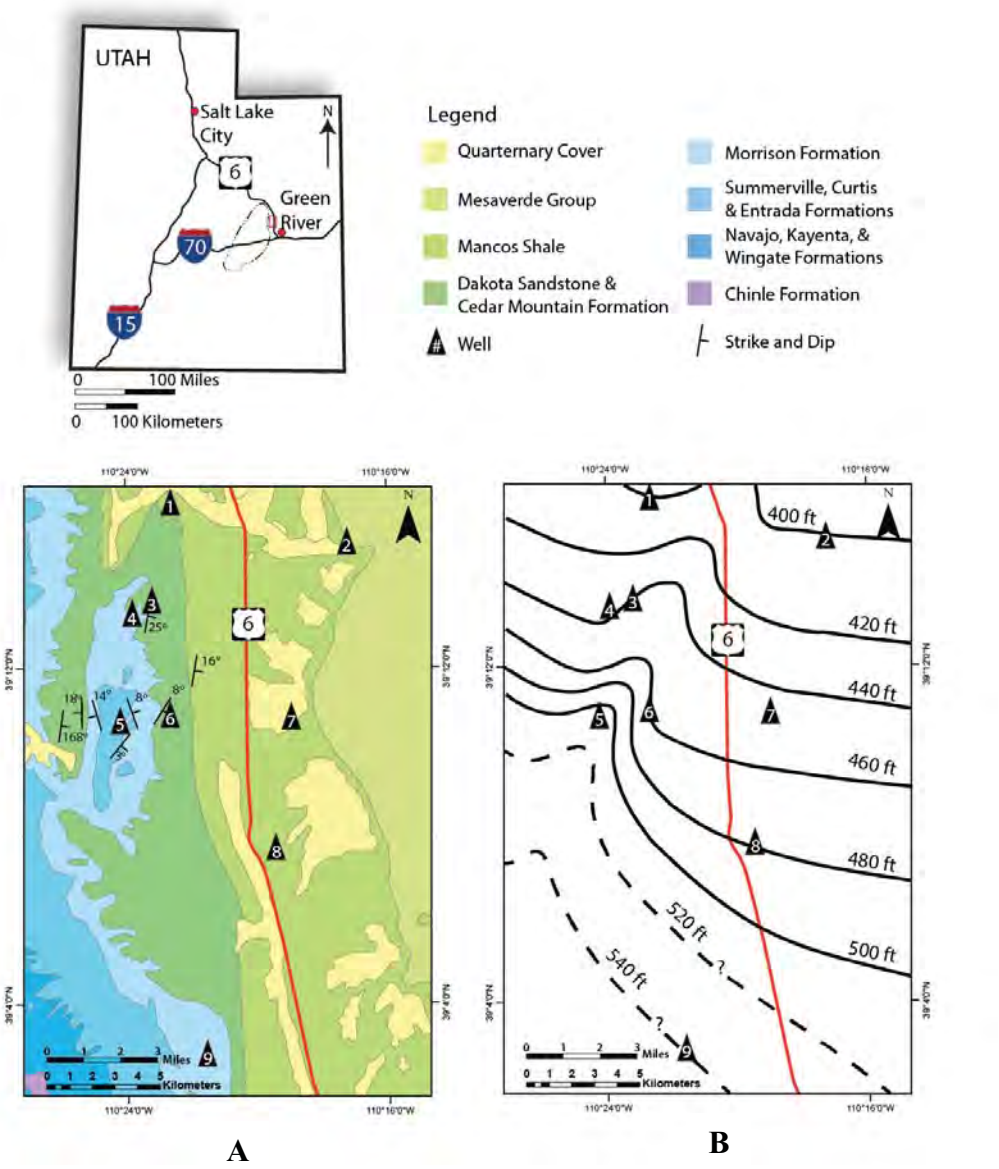


Figure 18. Surficial geologic map with strike and dip information (A) and isopach map (B) of the White Rim Sandstone at Woodside Dome (contour interval = 20 ft). Thicknesses from subsurface well data were corrected according to the dip of the strata. The exact dip of inclined strata is not known at Well #9, but the well appears to be near the crest so we assumed flat lying strata. The White Rim thins to the north and appears to have a northeast-southwest trending paleotopographic high. From Harston and Morris, 2013.

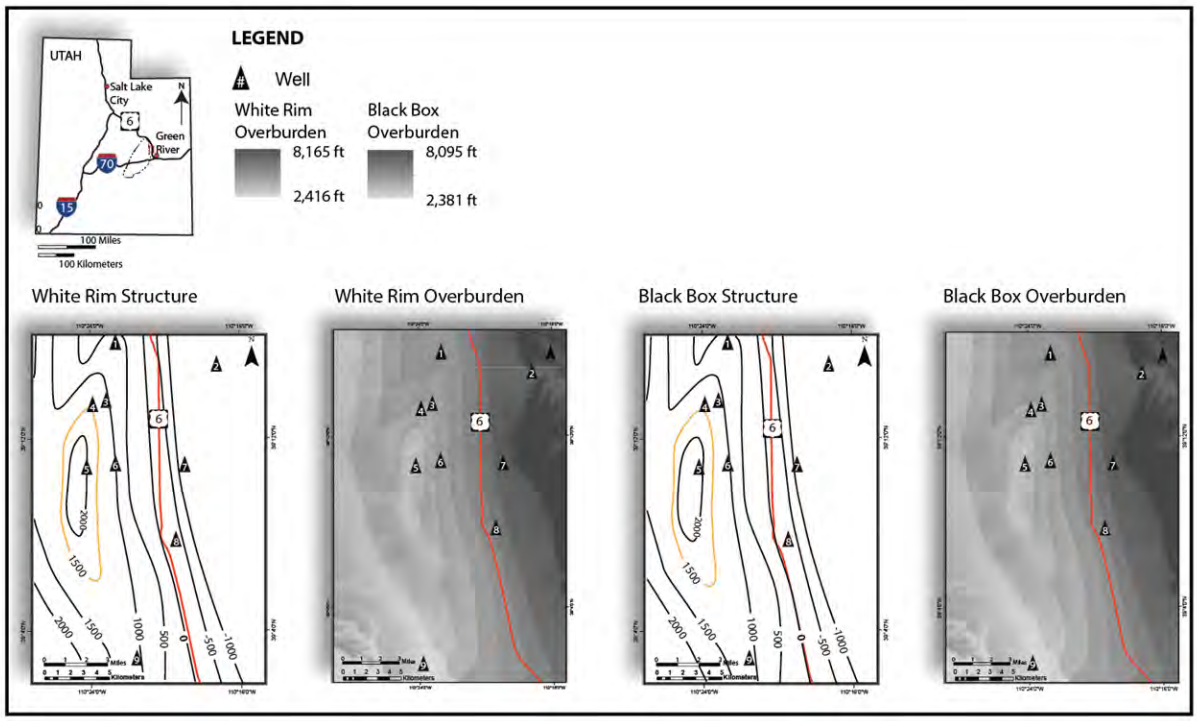


Figure 19. Structure and overburden maps for the top of the White Rim Sandstone and Black Box Dolomite. From Harston and Morris, 2013.

Summary and Recommendations

Woodside Dome is a well-defined anticline (at the surface) on public lands with good access. The Entrada and Navajo Sandstones are very shallow at Woodside but are regionally significant as potential CO_2 storage reservoirs. Potential storage reservoirs at Woodside include the Black Box Dolomite, White Rim Sandstone, Redwall Limestone, and possibly numerous beds in the Pennsylvanian Hermosa Group, which were not evaluated.

The Woodside Dome study site has the potential for 3.2 to 34.3 MMT of CO_2 storage capacity in the Redwall Limestone, White Rim Sandstone, and Black Box Dolomite. The White Rim has the most storage capacity. The Redwall has low storage capacity due to the low porosity (5%), which is based on the sonic log from one well that penetrated the entire formation. Coring the Redwall at Woodside would provide much better porosity data and much needed permeability data. If the actual porosity is more than the log indicates, the CO_2 storage capacity would greatly increase.

The calculated CO_2 storage capacity at Woodside Dome is much less than originally estimated. The parameter having the most effect is the area of closure; originally we estimated 40 square miles (100 km^2) based on the surficial extent of the anticline but we mapped a more conservative areal extent of the subsurface reservoirs (12 to 17 square miles [30-45 km^2]). Structural closure of the deeper reservoirs is controlled by a blind reverse fault. Seismic data could show the fault has greater throw and length than we mapped; this would greatly increase the CO_2 storage capacity of all the reservoirs.

The Woodside Dome site would benefit from further evaluated, including acquisition of seismic data, and coring the Entrada, Navajo, Black Box, White Rim, and Redwall reservoirs. The knowledge gained would increase our understanding of the CO_2 storage capacity of Woodside and the regional storage potential of these reservoirs.

References

Harston, W.A., and Morris, T.H., 2013, Facies analysis of the Permian White Rim Sandstone, Black Box Dolomite, and Black Dragon Member of the Triassic Moenkopi Formation for CO_2 sequestration at Woodside field, San Rafael Swell, Utah, Part I, *in* Morris, T.H., and Ressetar, R., editors, The San Rafael Swell and Henry Mountains basin—geologic centerpiece of Utah: Utah Geological Association Publication 42, p. 145-172**.**

Morgan, C.D., Carney, S., and Nielsen, P., 2013, Recent characterization of Gordon Creek, Farnham Dome, and Woodside fields, Carbon and Emery Counties, Utah, *in* Morris, T.H., and Ressetar, R., editors, The San Rafael Swell and Henry Mountains basin—geologic centerpiece of Utah: Utah Geological Association Publication 42, p. 393-414**.**

Witkind, I.J., 2004, Geologic map of the Huntington 30' X 60' quadrangle, Carbon, Emery, Grand, and Uintah Counties, Utah: Utah Geological Survey Open-File Report 440 DM, scale 1:100,000.

APPENDIX D

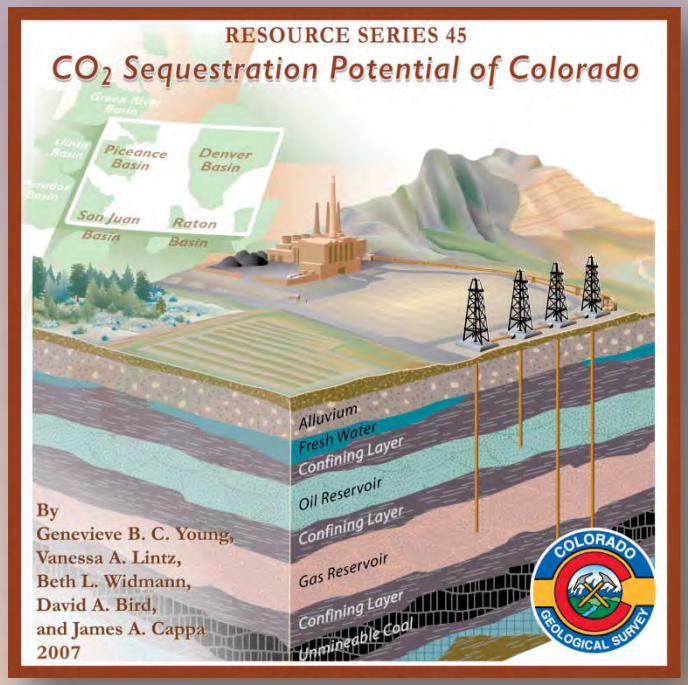
CGS Presentation Materials

Contents

Topic

CO2 Sequestration Presentation to Tri-States Generation and Transmission Board

Carbon Sequestration in Colorado and the Craig Project

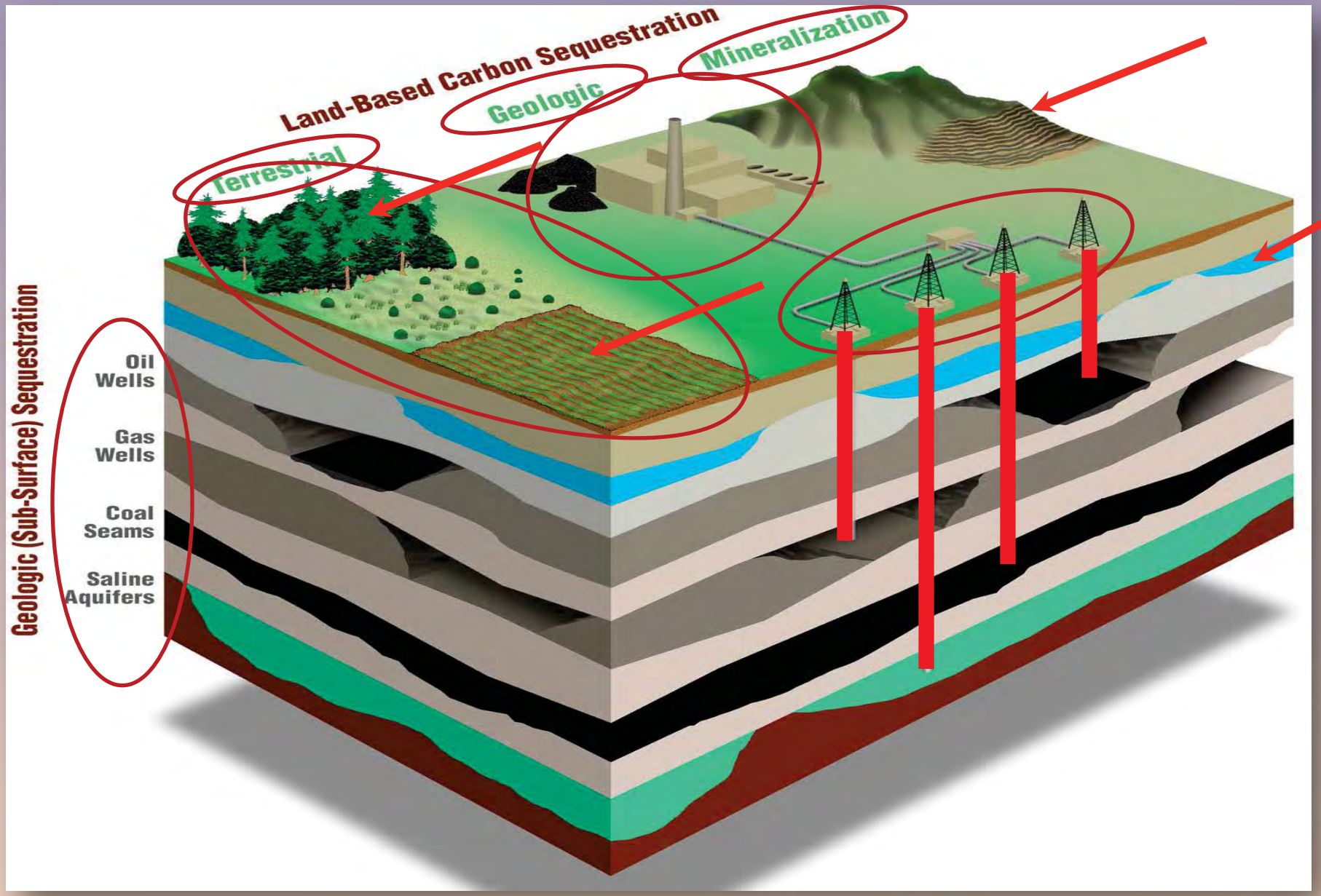


Vince Matthews, Ph.D.

State Geologist and Director

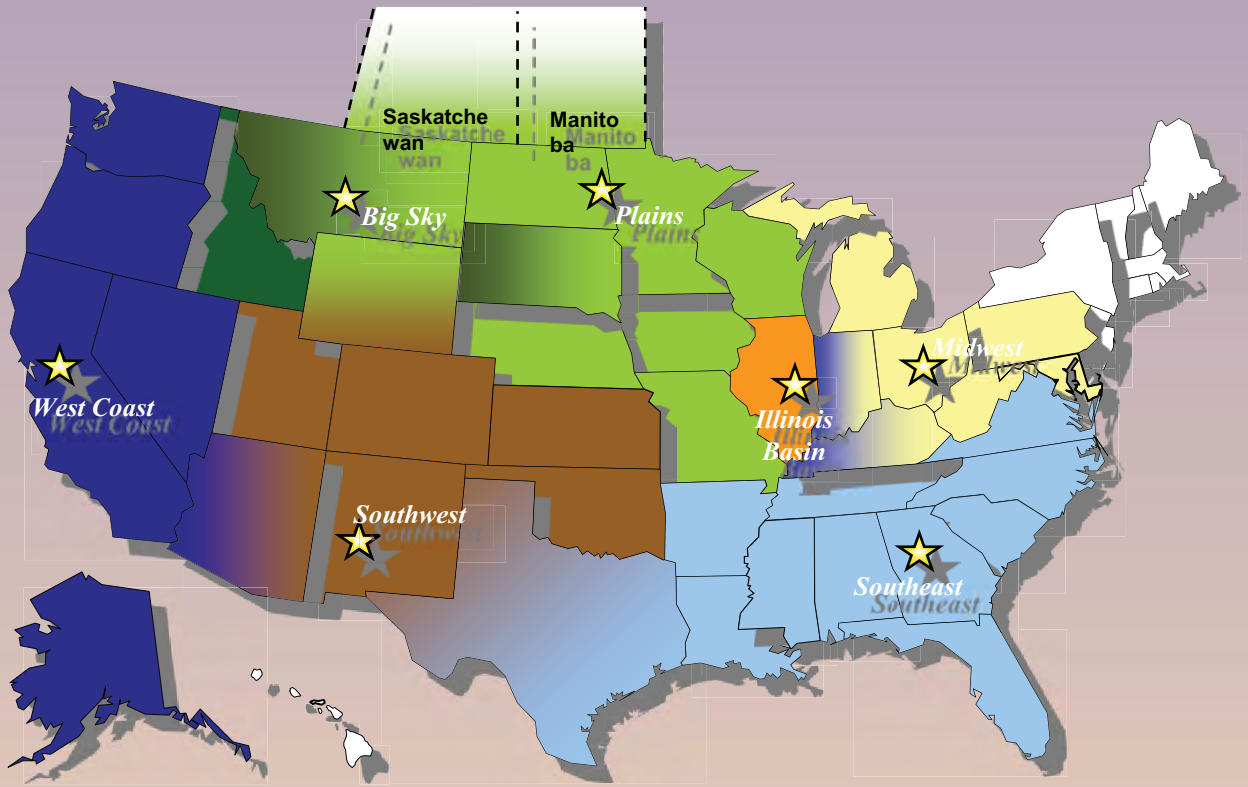
Tri-States Generation and Transmission Board Meeting

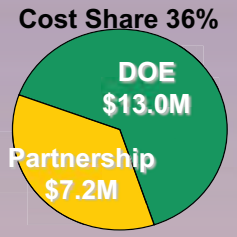
November 10, 2009


Land-Based Carbon Sequestration
Mineralization
Geologic
Terrestrial
Geologic (Sub-Surface) Sequestration
Oil Wells
Gas Wells
Coal Seams
Saline Aquifers

Regional Carbon Sequestration Partnerships

Seven Partnerships Established in Five Geographic Regions

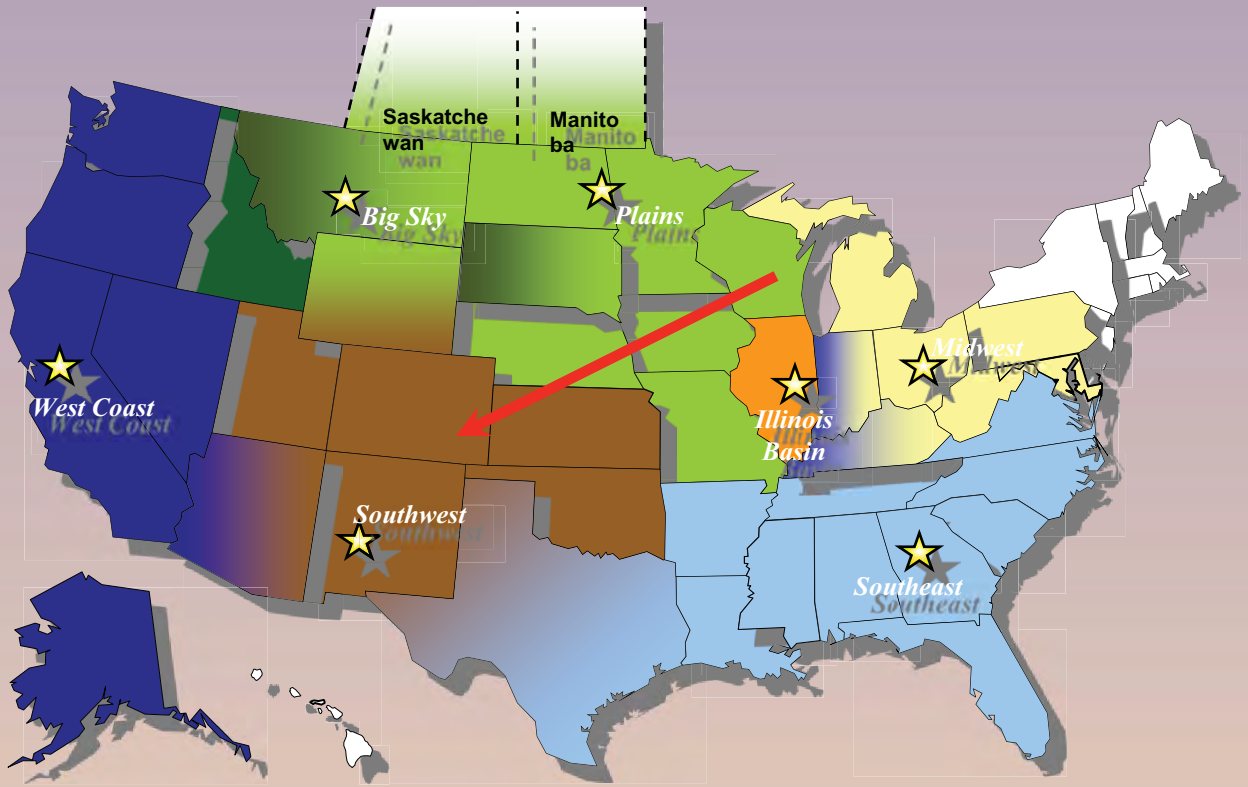




Representing:

154 Organizations
2 Canadian Provinces
3 Indian Nations
40 States

Southwest Regional Partnership on Carbon Sequestration



Three-Phased Approach

Phase I (Planning) 2003-05

-7 Projects
-$1.5 million per project
-Overall ~ 40% cost share



Phase II (Proof-of-Concepts 2005-09

- ~ $3 to $5 million per year/project
- minimum 20% cost share
- ~ 5 Regions





Phase III (Deployment) 2009-19

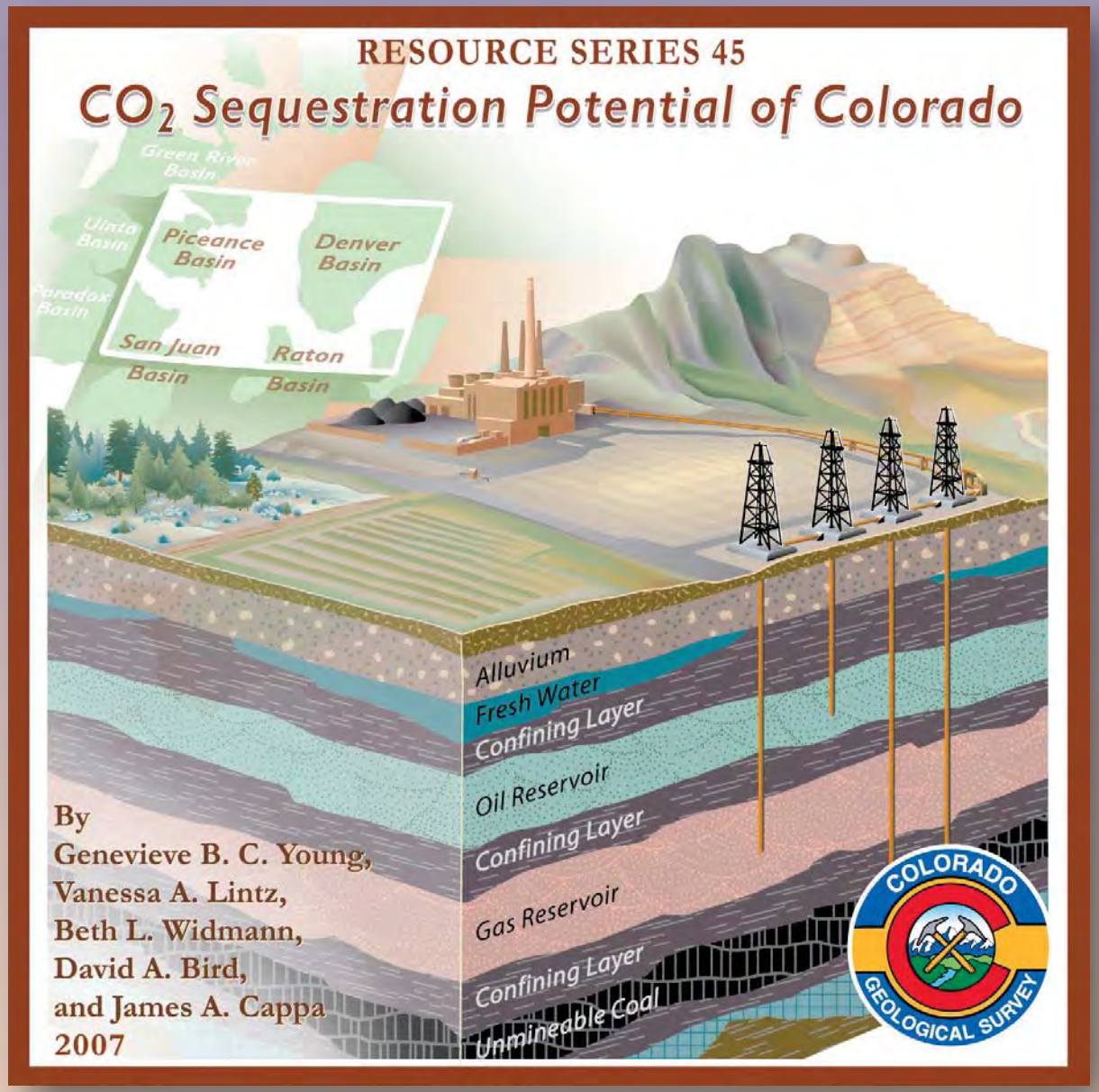
- ~ $65 million per project
- > 20% cost share
- ~ 5 Projects

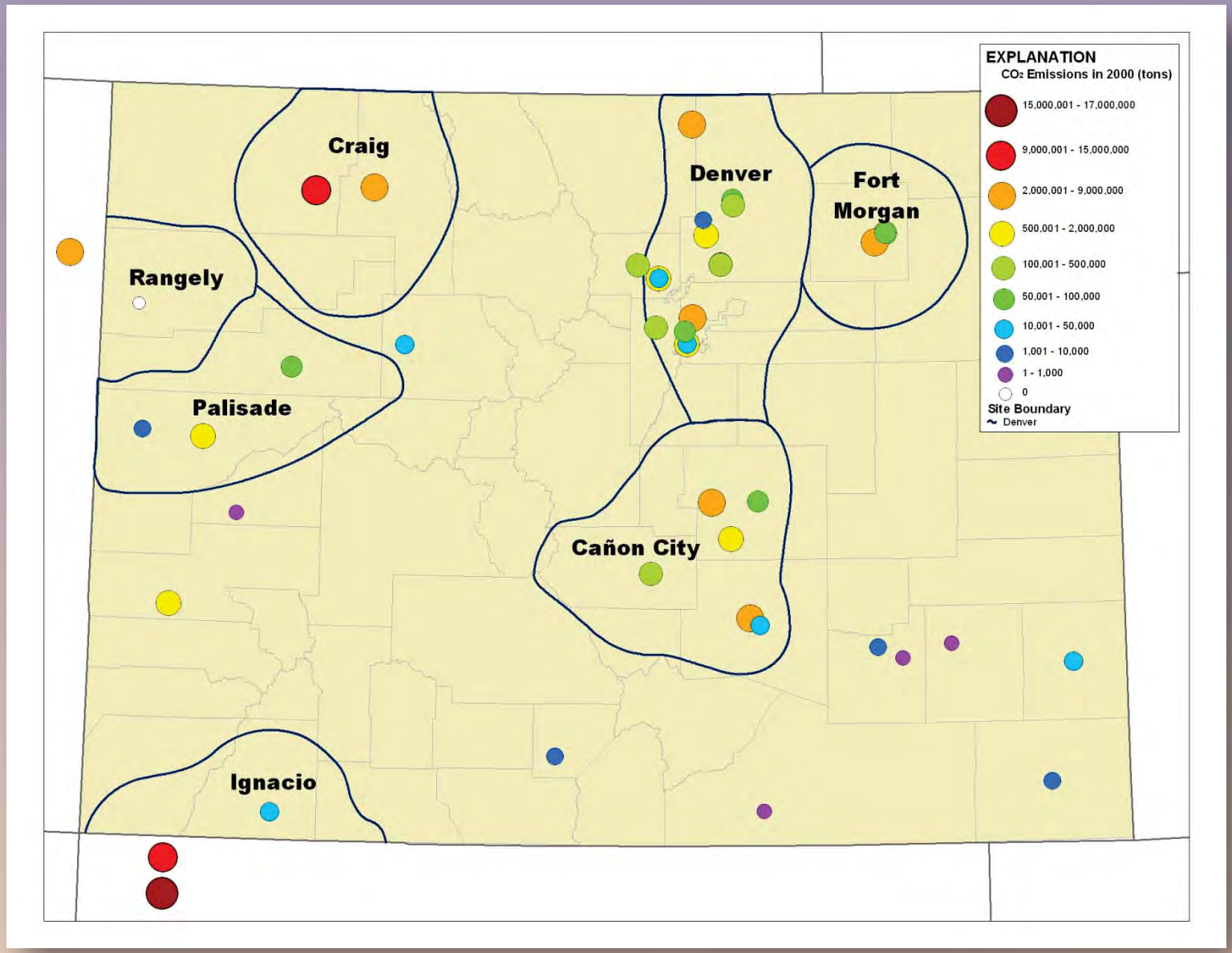
Phase I 2003-05

Characterize the Major Colorado Sources

Delineate Pilot Study Areas around major sources

Identify and characterize the various geologic sinks in potential pilot areas


RESOURCE SERIES 45
CO_2 Sequestration Potential of Colorado
Green River Basin
Uinta Basin
Piceance Basin
Denver Basin
Paradox Basin
San Juan Basin
Raton Basin
Alluvium
Fresh Water
Confining Layer
Oil Reservoir
Confining Layer
Gas Reservoir
Confining Layer
Unmineable Coal
By
Genevieve B. C. Young,
Vanessa A. Lintz,
Beth L. Widmann,
David A. Bird,
and James A. Cappa
2007
COLORADO
GEOLOGICAL SURVEY


EXPLANATION
CO2 Emissions in 2000 (tons)
15,000,001 - 17,000,000
9,000,001 - 15,000,000
2,000,001 - 9,000,000
500,001 - 2,000,000
100,001 - 500,000
50,001 - 100,000
10,001 - 50,000
1,001 - 10,000
1 - 1,000
0
Site Boundary
Denver
Craig
Rangely
Palisade
Denver
Fort Morgan
Cañon City
Ignacio

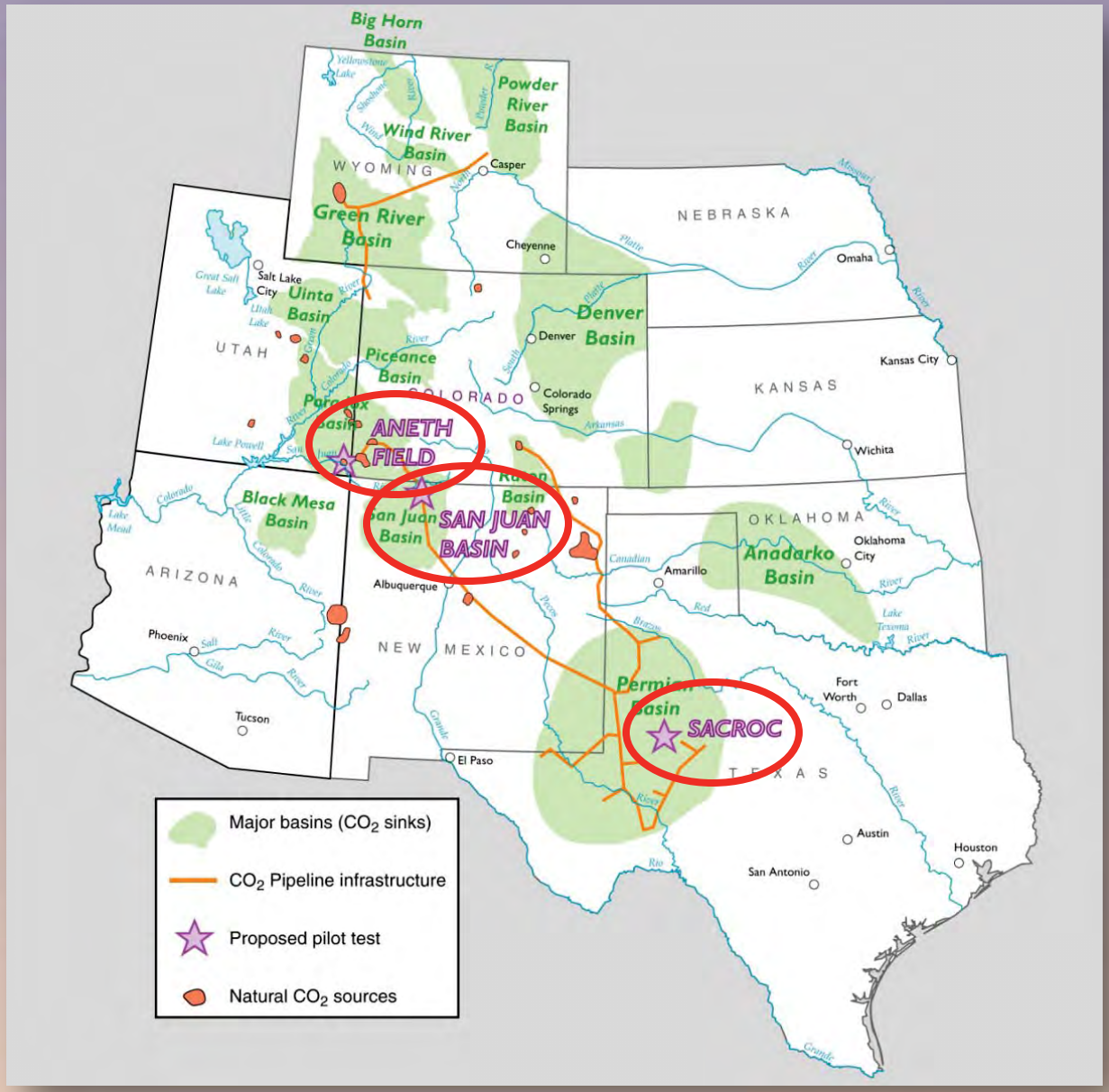
Phase II 2005-09

Detailed Geology

Modeling of the reservoir performance

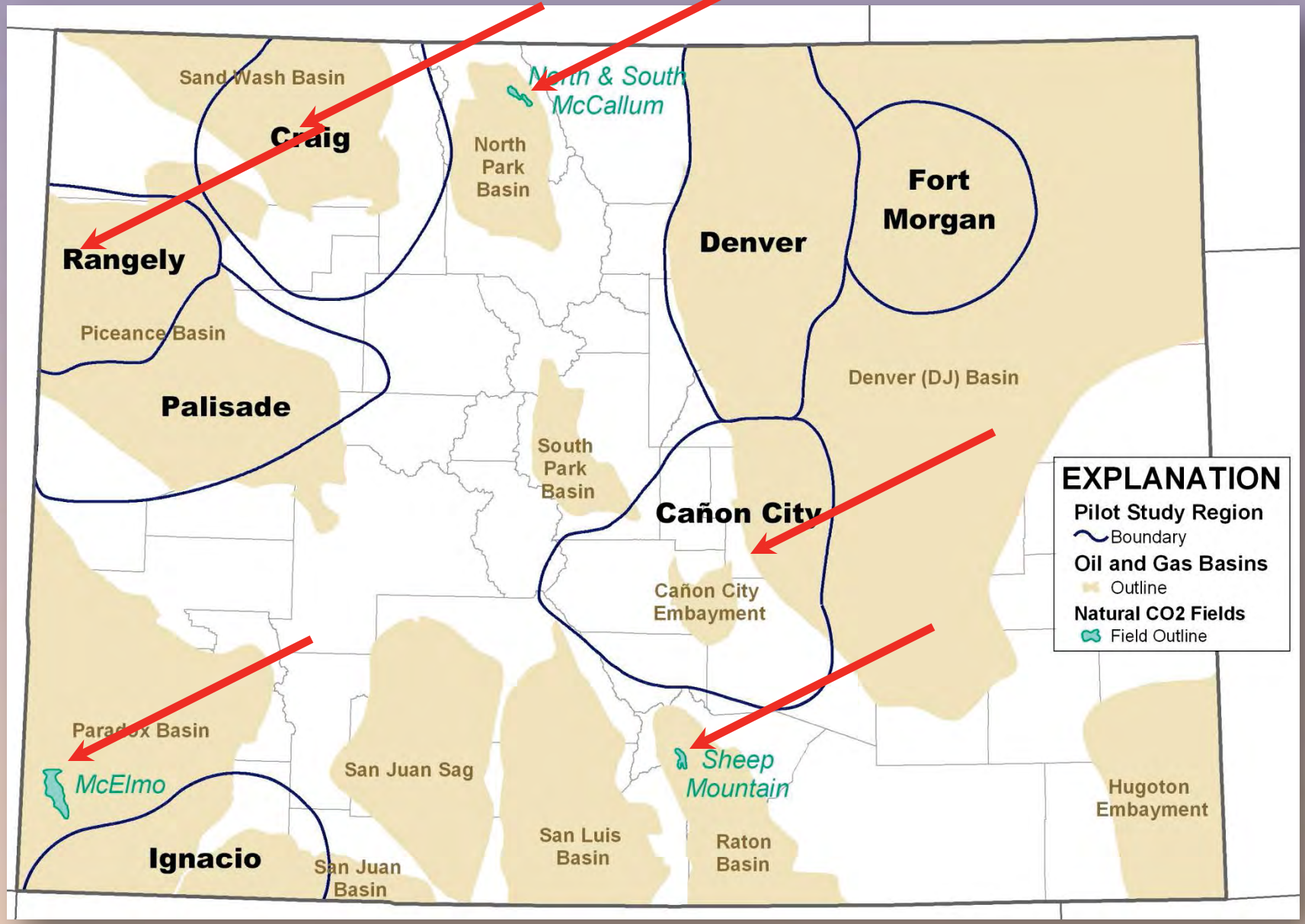
Do the project and measure results

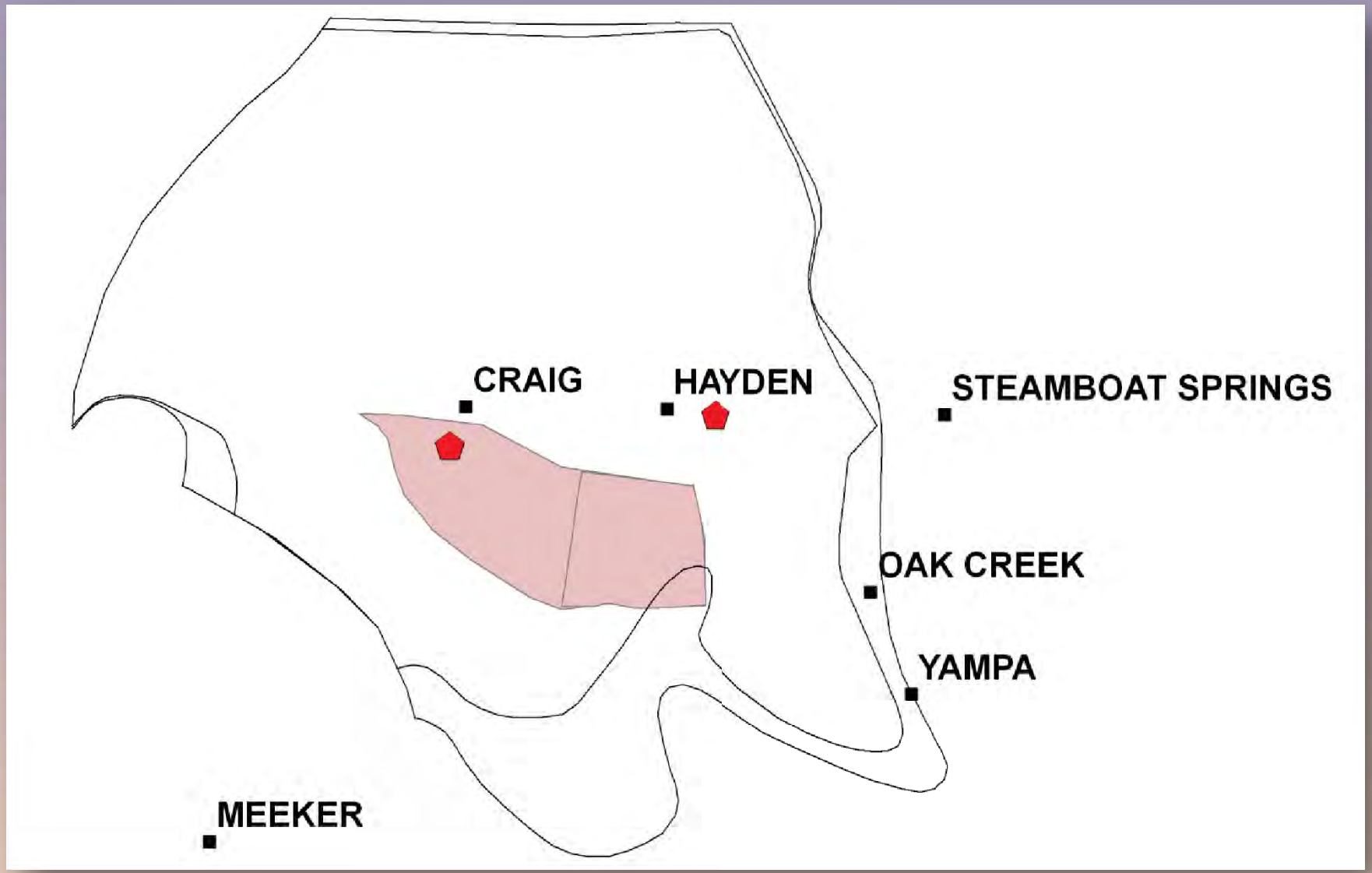
SWP Phase II Pilots



MMV Operations

- Direct methods
  - Injection rate monitoring
  - Production well LI-COR
  - Abandoned well LI-COR
  - Gas piezometers LI-COR
  - *In situ* P/T well monitoring (fiber optic sensors)
  - *Tiltmeter arrays with InSAR*
  - *Spinner surveys*
  - H2O chemistry & isotopes
  - Fluid/gas chemistry & isotope analysis
- Indirect methods
  - *2-D seismic surveys*
  - Crosswell seismic
  - Passive seismic
  - Borehole integrity by resistivity monitoring
  - *VSP*
  - ASTLI
  - Integrated seismic model
  - State-of-the-art reservoir models


Sand Wash Basin
Craig
North & South McCallum
North Park Basin
Fort Morgan
Denver
Rangely
Piceance Basin
Palisade
Denver (DJ) Basin
South Park Basin
Cañon City
Cañon City Embayment
EXPLANATION
Pilot Study Region
Boundary
Oil and Gas Basins
Outline
Natural CO2 Fields
Field Outline
Paradox Basin
McElmo
San Juan Sag
Sheep Mountain
Hugoton Embayment
San Luis Basin
Raton Basin
Ignacio
San Juan Basin


CRAIG
HAYDEN
STEAMBOAT SPRINGS
OAK CREEK
YAMPA
MEEKER

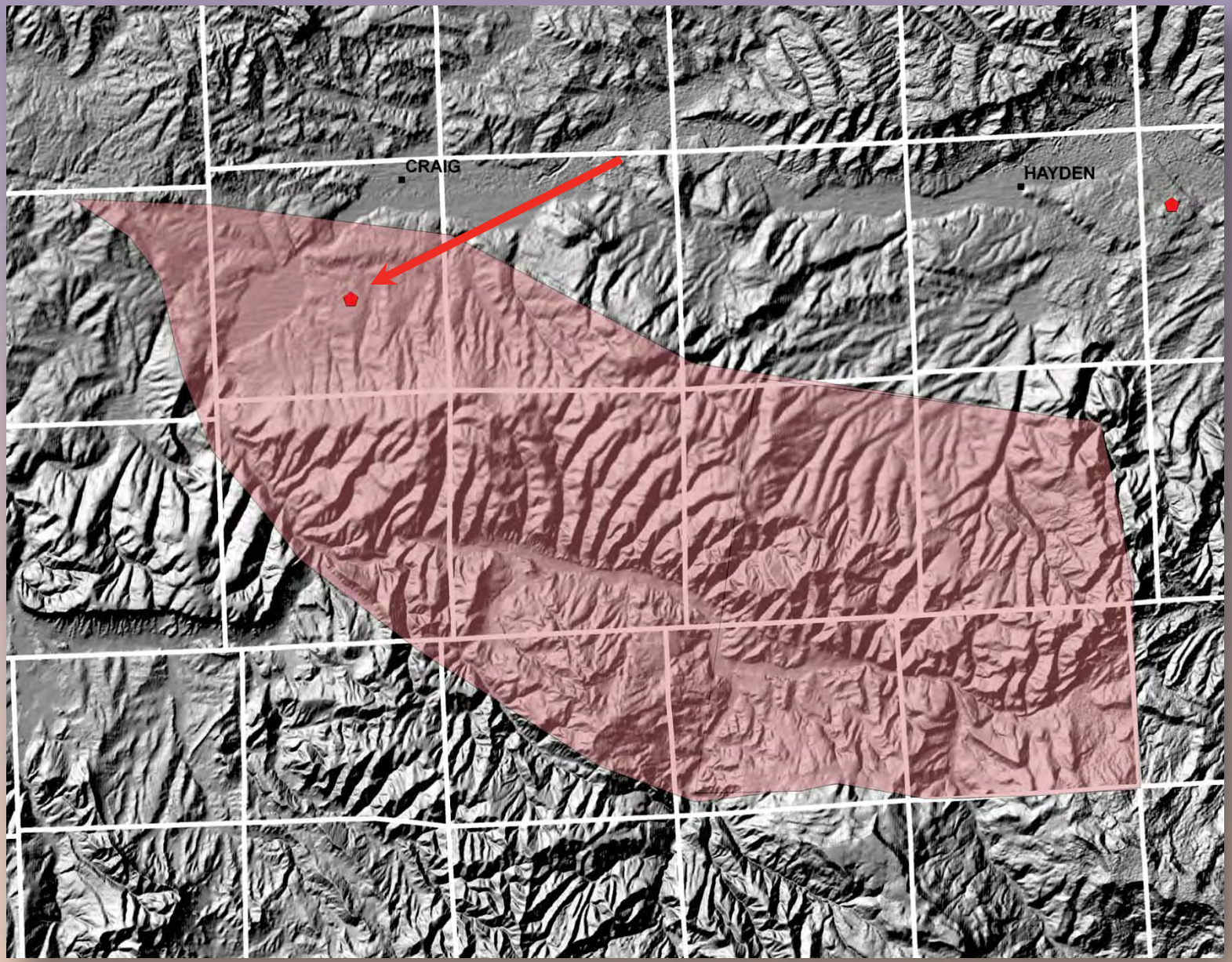
The Award

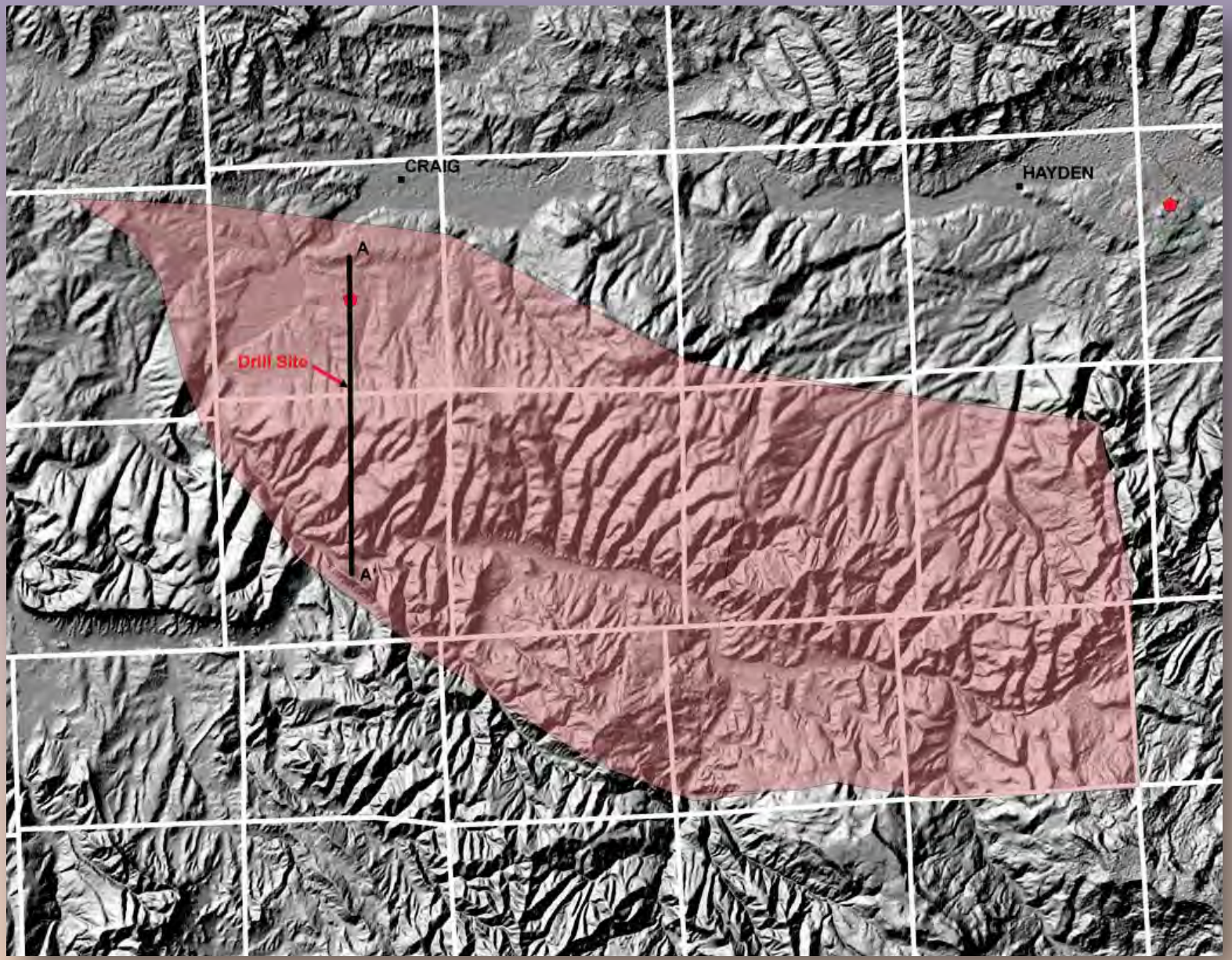
$4.8 million Project

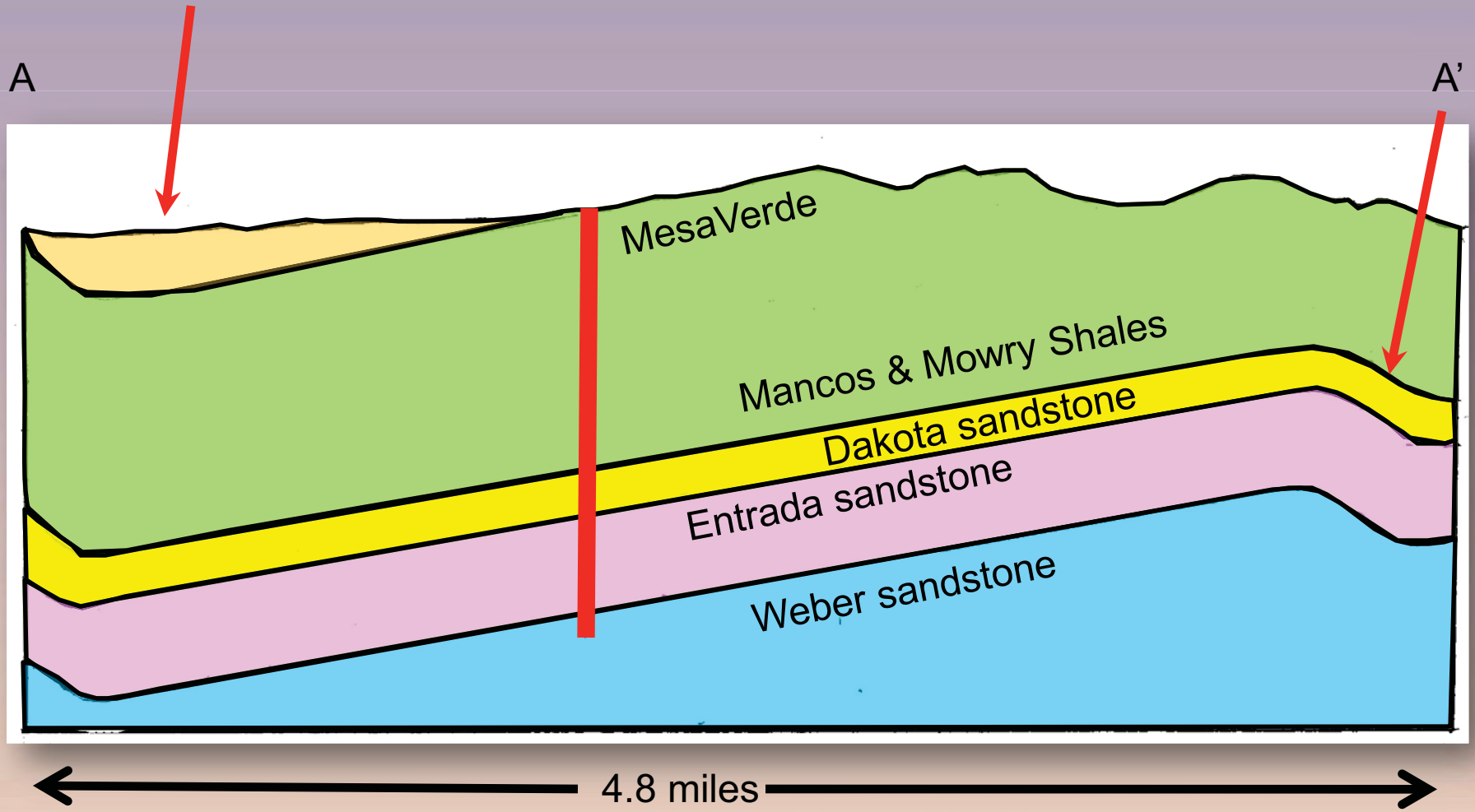
$3.8 million from Department of Energy

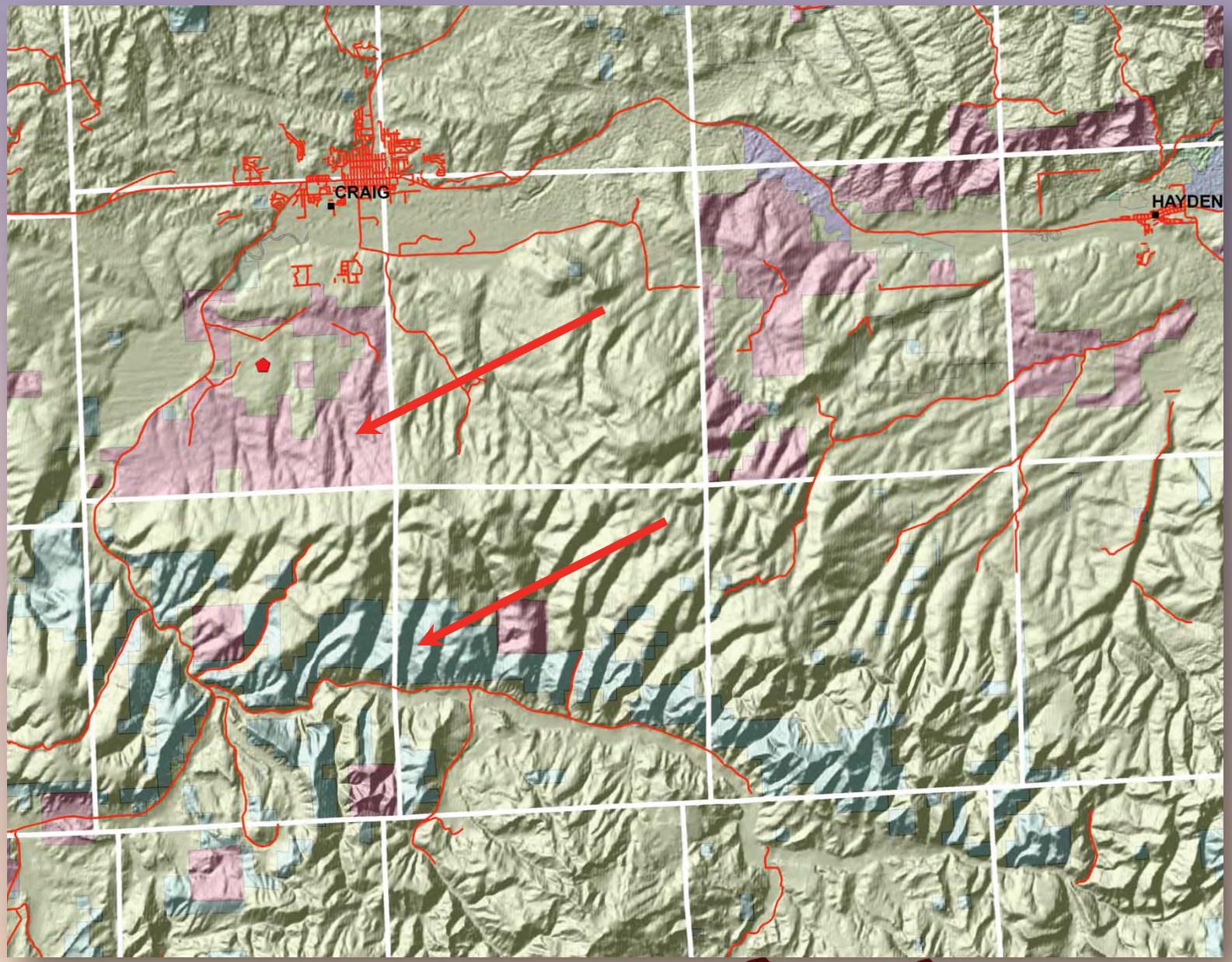
$1.0 million from Partners (20%)


Craig Power Station
Drill Site


CRAIG
HAYDEN

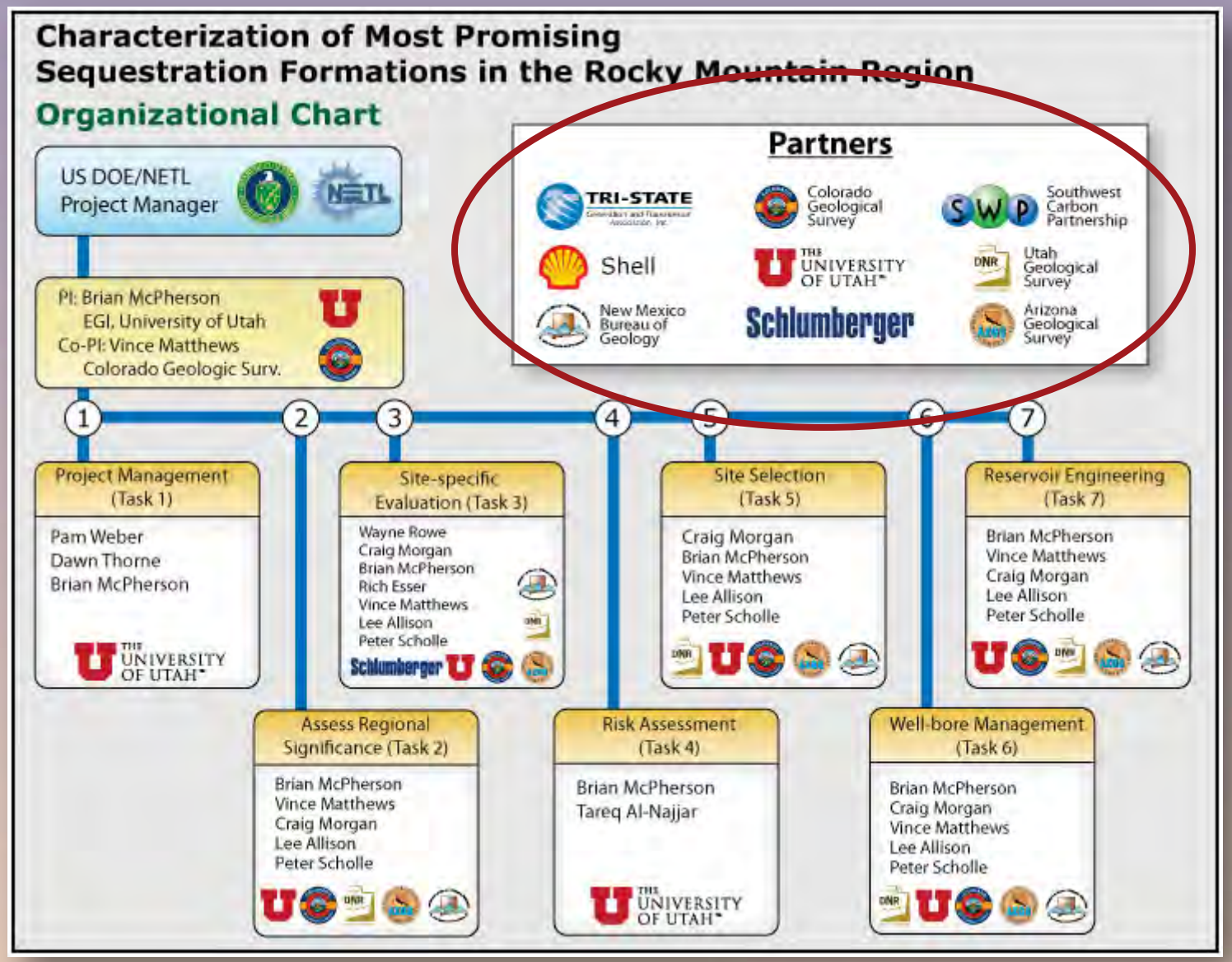

CRAIG
HAYDEN
A
A'
Drill Site


A
A'
MesaVerde
Mancos & Mowry Shales
Dakota sandstone
Entrada sandstone
Weber sandstone
4.8 miles


CRAIG
HAYDEN

Characterization of Most Promising Sequestration Formations in the Rocky Mountain Region

Organizational Chart



The Partners

Tri-State Generation and Transmission- $300K

Shell Exploration & Production- $200K

Colorado Geological Survey- $162K

Schlumberger Carbon Management- $150K

University of Utah – Energy & Geoscience Institute - $125K

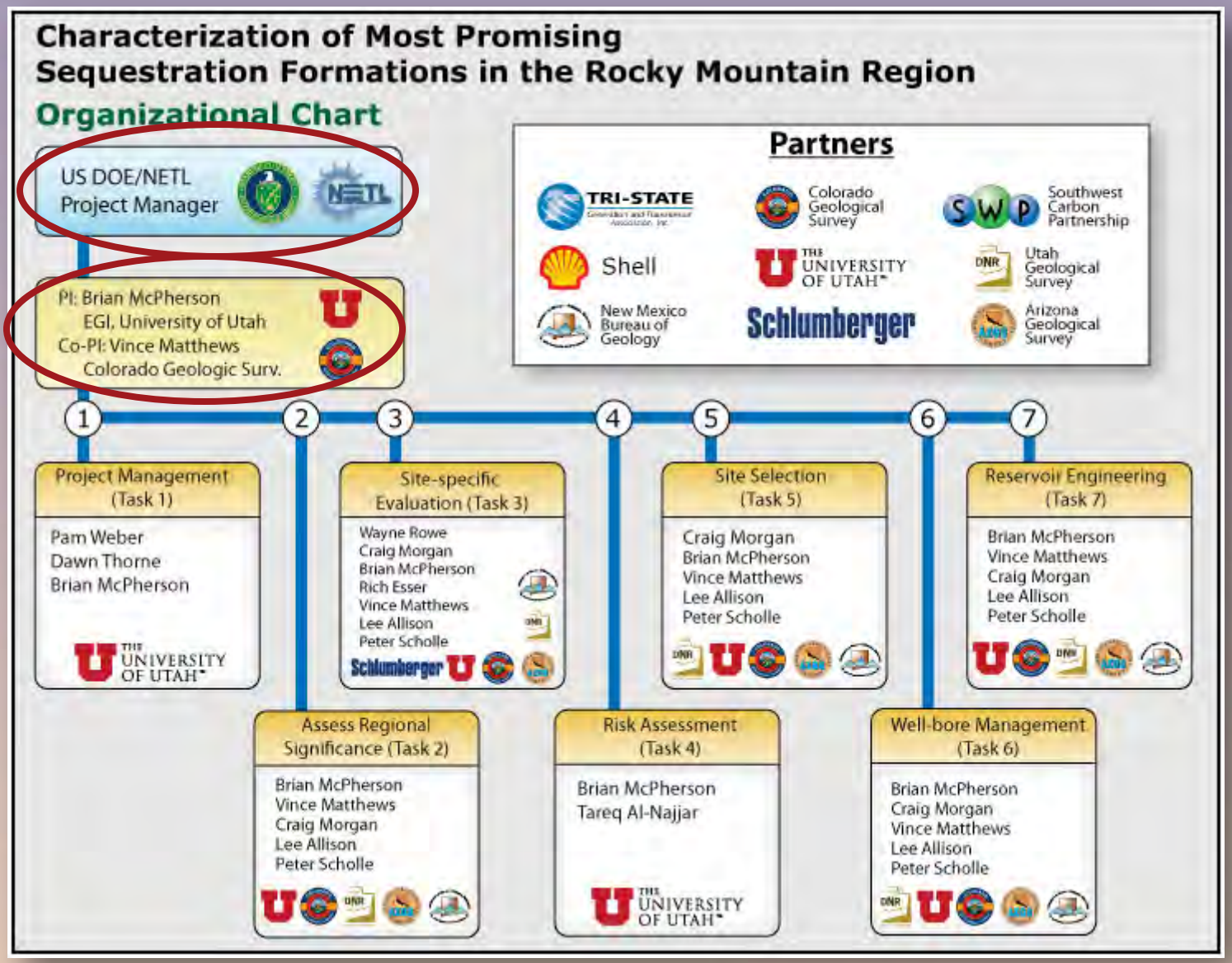
Utah Geological Survey- $22K

Arizona Geological Survey- $19K

New Mexico Geological Survey- $19K

Characterization of Most Promising Sequestration Formations in the Rocky Mountain Region

Organizational Chart



The Co- Principal Investigators



Dr. Brian McPherson – University of Utah

Associate Professor, Civil Engineering and Environmental Sciences

Director, Carbon Science & Engineering, Energy & Geoscience Institute

Director, Southwest Partnership for Carbon Sequestration

Dr. Vince Matthews – Colorado Geological Survey

Penn Virginia Resources – President

Union Pacific Resources – Vice President & Regional Manager

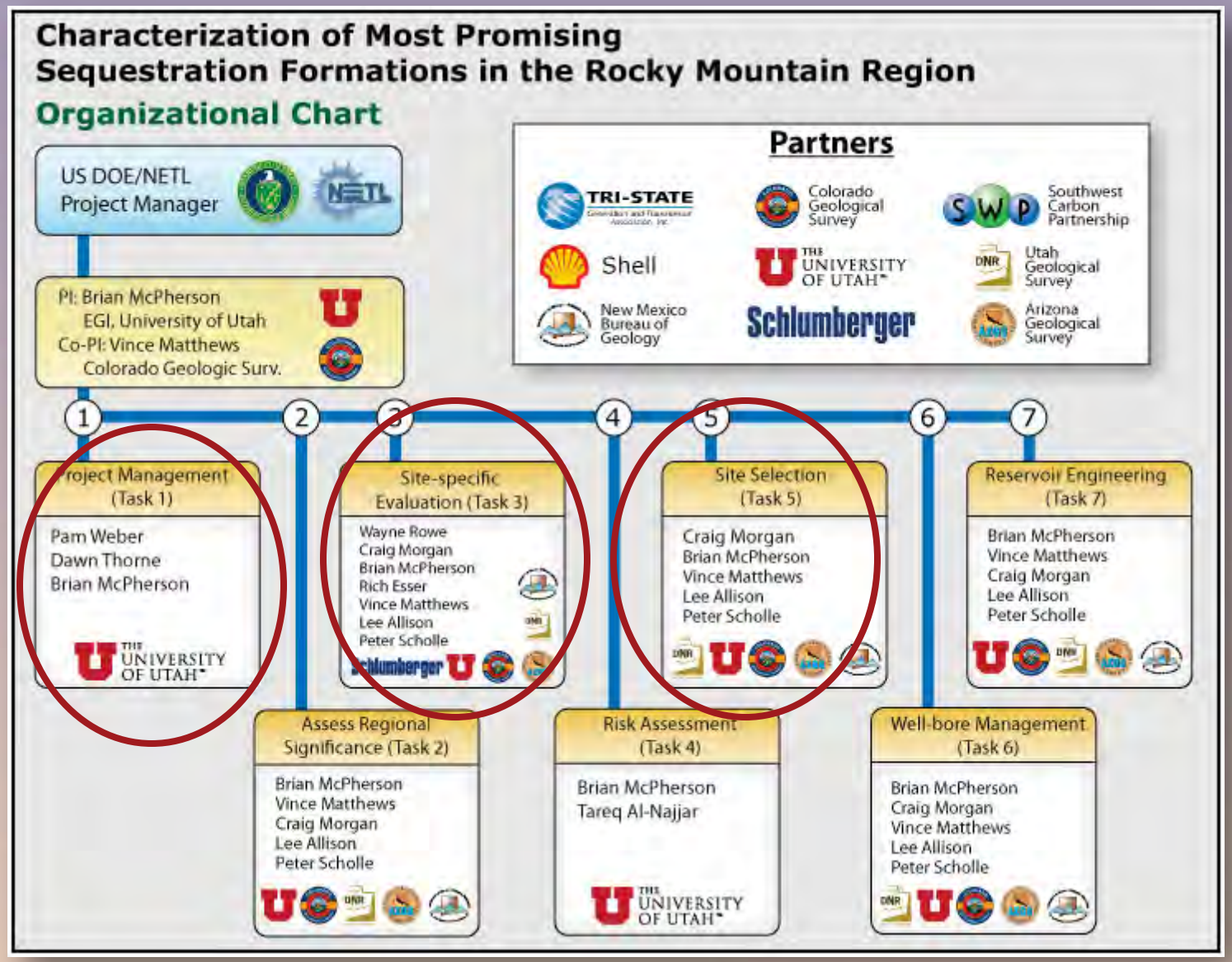
Lear– Rocky Mountain Division Manager

Amoco – Division Exploration Manager

University of California, University of Northern Colorado, University of Texas, Arizona State University

Characterization of Most Promising Sequestration Formations in the Rocky Mountain Region

Organizational Chart



The Plan – Year 1

Characterize the Structure

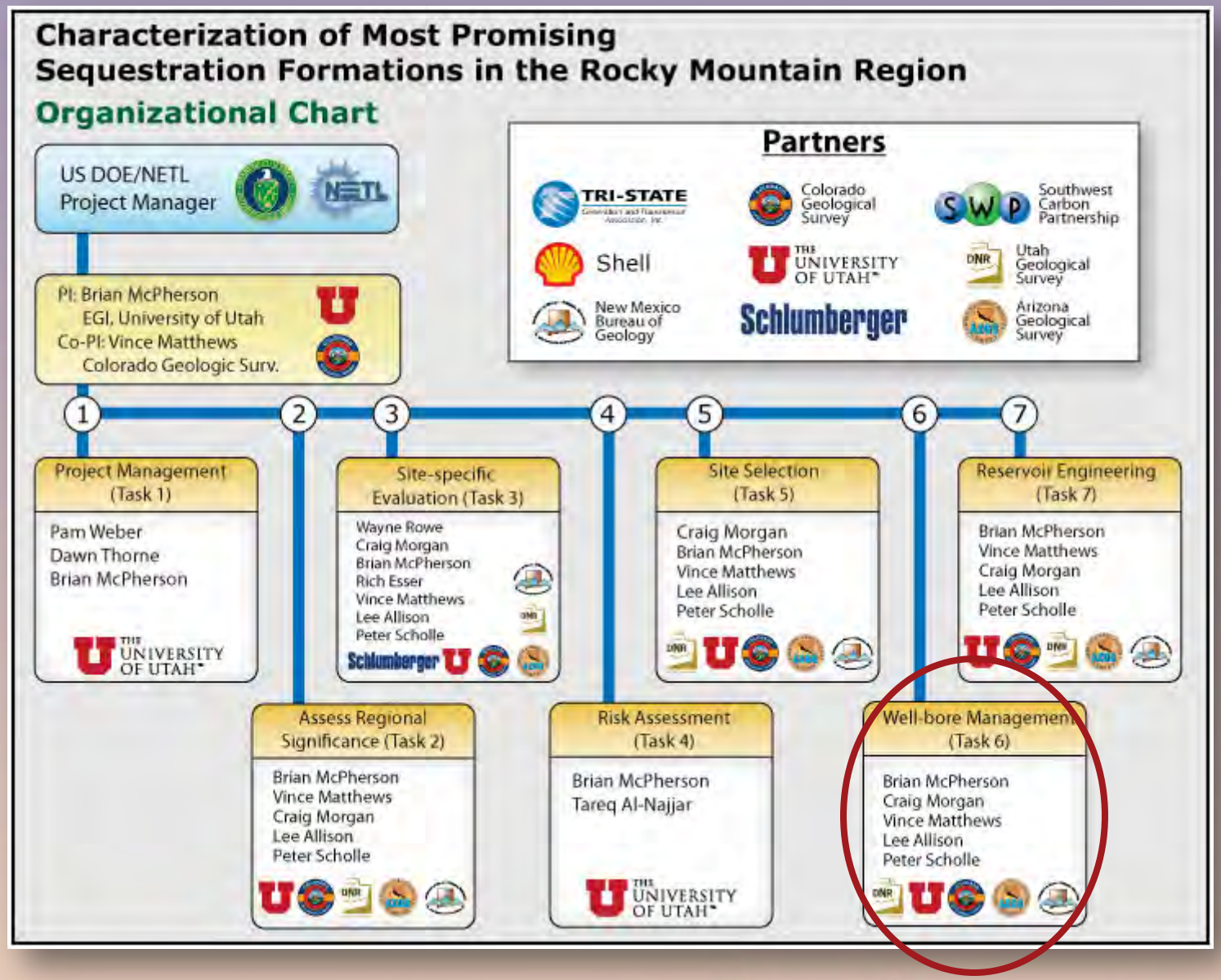
- Build database
  Purchase seismic
- Process & interpret seismic
- Map surface structure
- Shoot seismic line

Pick location for drill hole

Permit well

Characterization of Most Promising Sequestration Formations in the Rocky Mountain Region

Organizational Chart



The Plan – Year 2

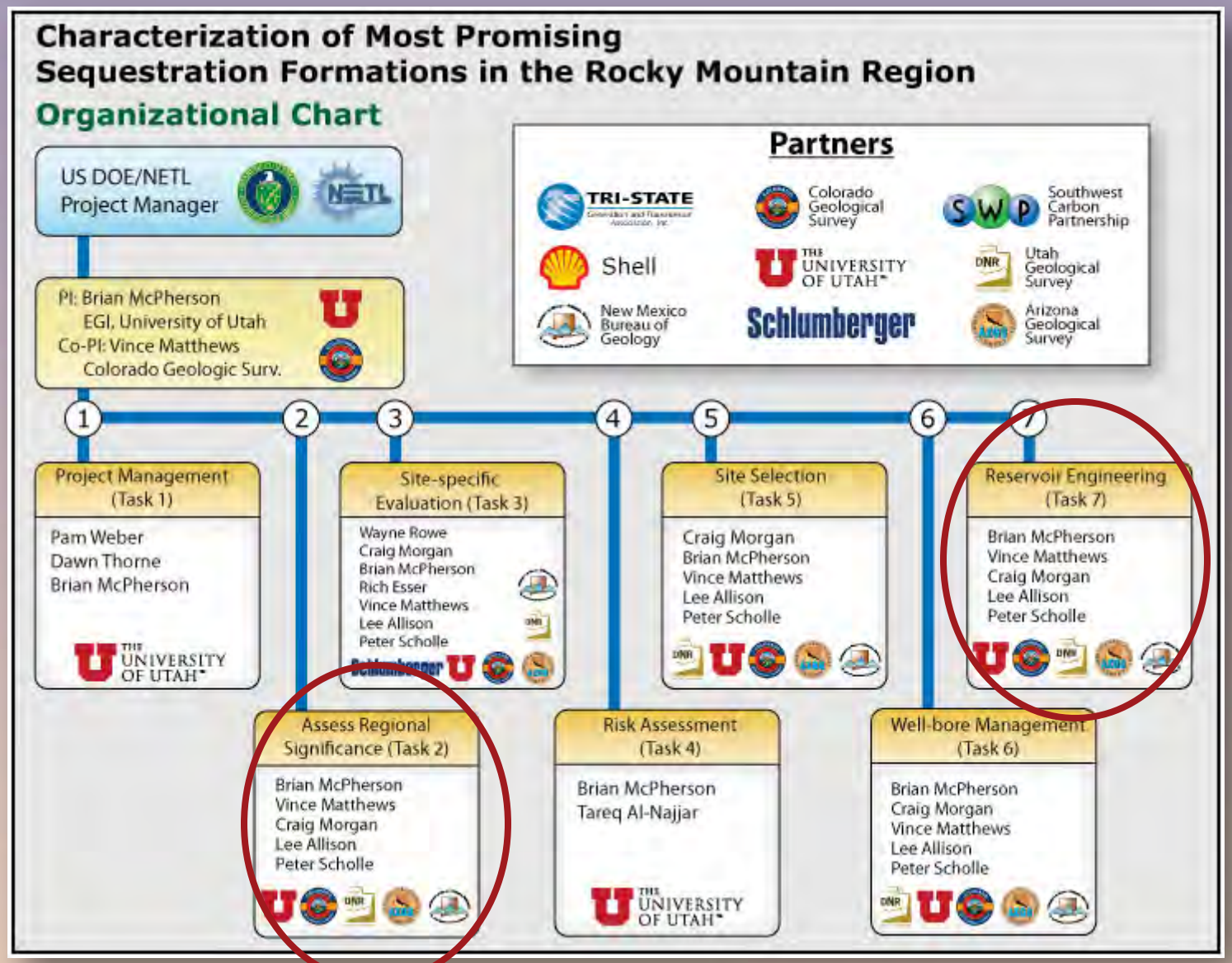
Drill Well

- Core Shale
- Core Sandstones
- Sample Waters
- Analyze Samples
- CO_2 Injectivity Experiments on cores

Begin Engineering Analysis & Reservoir Modeling

Characterization of Most Promising Sequestration Formations in the Rocky Mountain Region

Organizational Chart



The Plan – Year 3

Model Reservoir

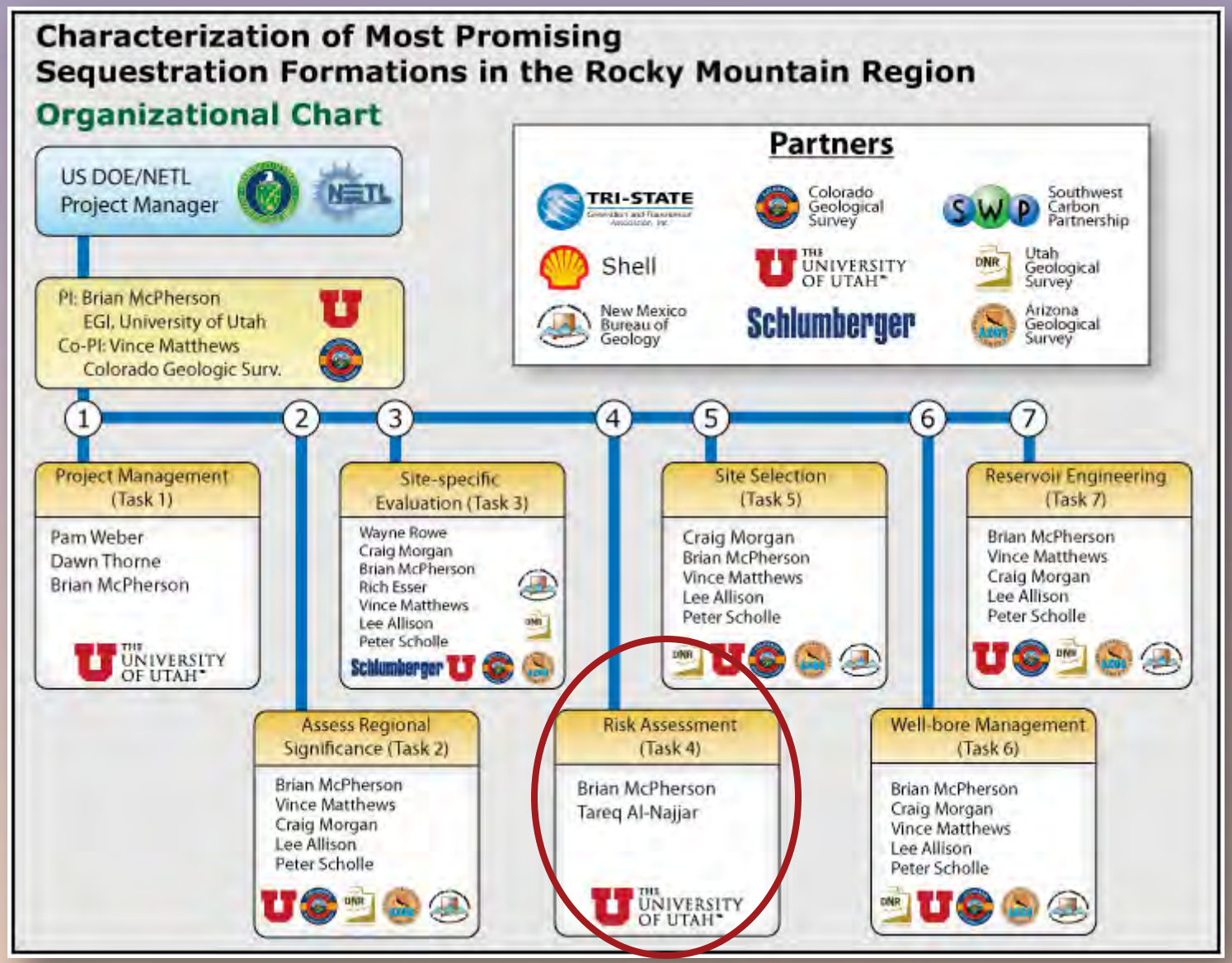
- Storage Volume
- CO2 Migration
- Potential Leakage Pathways
- Develop Optimal Injection Program
- Final Report

Extend results to Colorado Plateau

- UU-EGI Regional storage Model
- AZ, NM, UT, CO Geosurveys

Characterization of Most Promising Sequestration Formations in the Rocky Mountain Region

Organizational Chart



Risk Assesment

Programmatic risk

resource and management risks that may impede project progress or costs

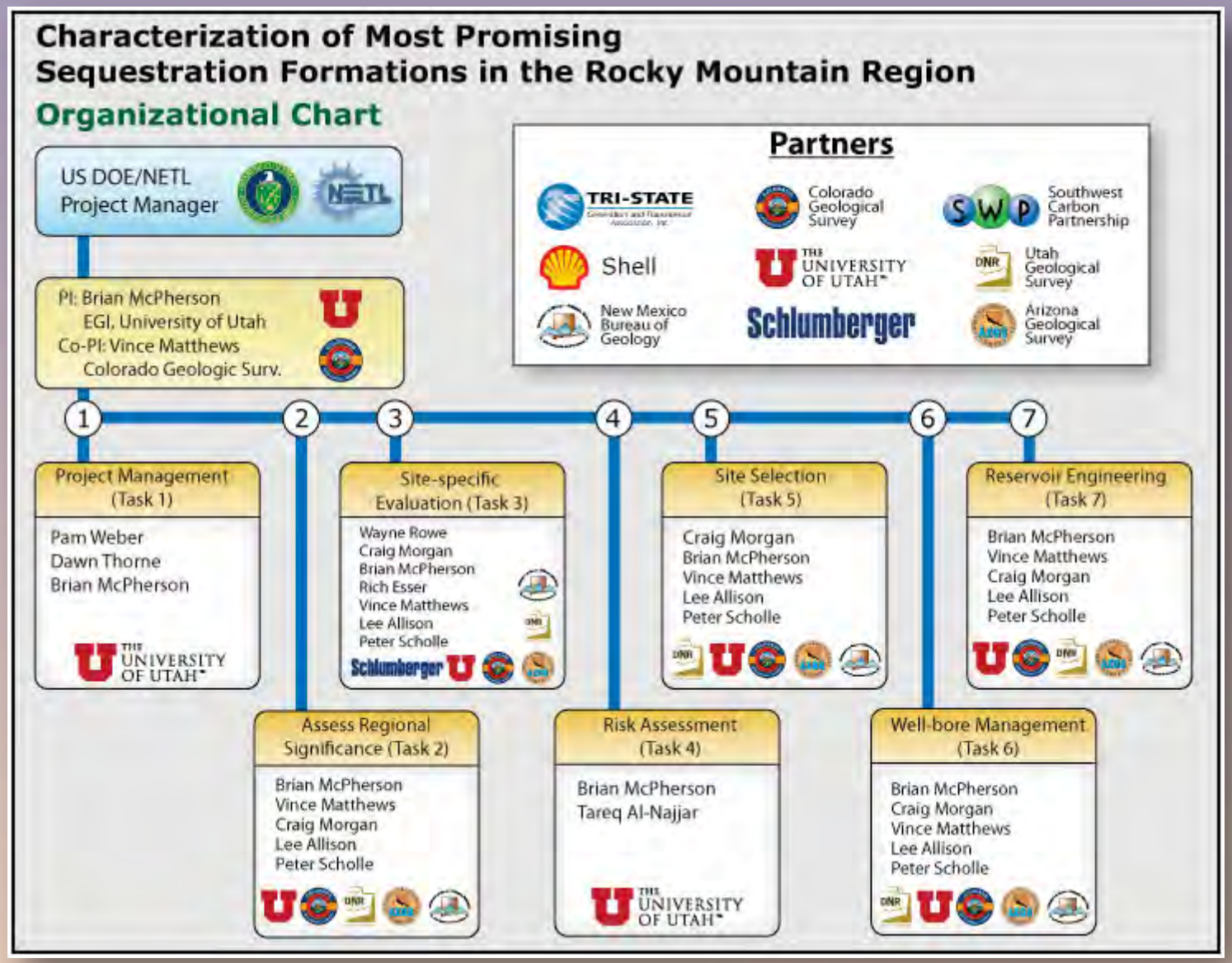
Sequestration (technical) Risks

risks inherent to the scientific and engineering objective of sequestering CO2.

Questions?

Characterization of Most Promising Sequestration Formations in the Rocky Mountain Region

Organizational Chart



APPENDIX E

Public Engagement

Contents

Topic

Carbon Capture Board

Carbon Capture Fact Sheet

Communications Plan

Craig Daily Press Ad

Project Overview Board

RMCCS Open House Postcard

RMCCS Press Release

How a Well is Drilled Fact Sheet

Seismic Survey Fact Sheet

Probabilistic Board

Stratigraphy Board

Underground Storage Safety Brochure

CARBON CAPTURE & SEQUESTRATION

Carbon Capture and Sequestration (CCS) is an integrated suite of technologies that are being developed to prevent large quantities of the greenhouse gas carbon dioxide (CO_2) from being released into the atmosphere for use on an industrial scale. As the name implies, the process seeks to efficiently capture the CO_2, typically from large industrial processes, before it is emitted into the atmosphere. The CO_2 is then compressed into a liquid, transported to a carefully selected and safe storage site and injected into a deep rock formation where it remains stored away from the atmosphere.

There are three major stages involved in this technology:

Capture: Carbon capture separates CO_2 from the other gases produced at large industrial process facilities (coal and natural gas power plants, oil and gas plants, steel mills, cement plants, etc). CCS is being pursued as a key option to reduce emissions of CO_2. The current technology for carbon capture is very expensive requiring between 25 and 35% of the energy generation associated with CO_2 emissions to capture and compress the CO_2 into a liquid for underground storage.

Transport: Once separated, the CO_2 is compressed and transported (via pipelines, trucks, ships or other methods) to a suitable site for geological storage. Large scale industrial operation such as a power plant would require a pipeline to transport the volume of CO_2 that is generated.

Storage: At the storage site, CO_2 is injected into deep underground rock formations, at depths of one kilometer or more.

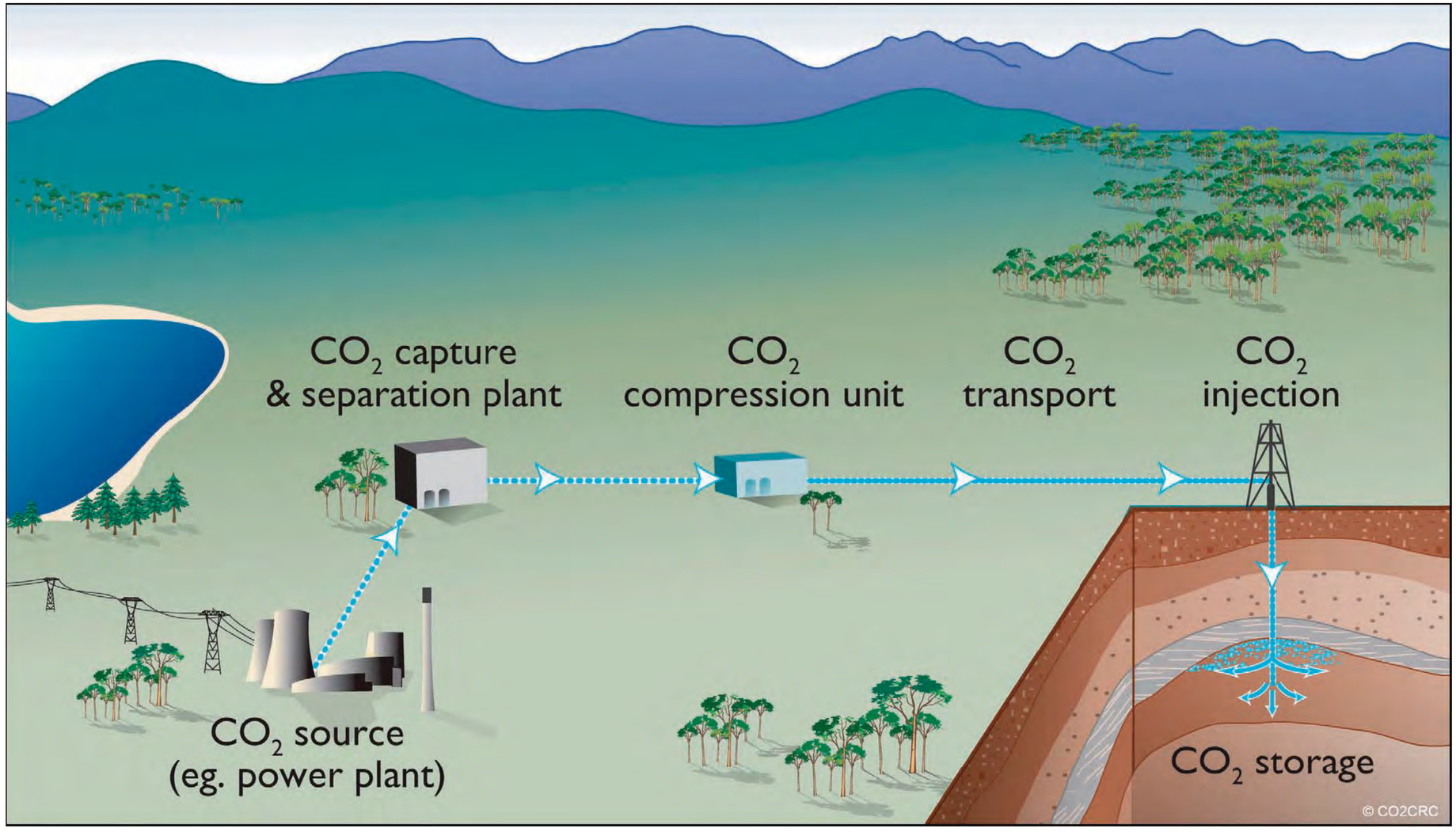


Image courtesy of CO2CRC

ROCKY MOUNTAIN CARBON CAPTURE AND SEQUESTRATION

www.rmccs.org

CARBON CAPTURE AND SEQUESTRATION

Carbon Capture and Sequestration (CCS) is an integrated suite of technologies that are being developed to prevent large quantities of the greenhouse gas carbon dioxide (CO_2) from being released into the atmosphere for use on an industrial scale. As the name implies, the process seeks to efficiently capture the CO_2, typically from large industrial processes, before it is emitted into the atmosphere. The CO_2 is then compressed into a liquid, transported to a carefully selected and safe storage site and injected into a deep rock formation where it remains stored away from the atmosphere.

There are three major stages involved in this technology:

Capture: Carbon capture separates CO_2 from the other gases produced at large industrial process facilities (coal and natural gas power plants, oil and gas plants, steel mills, cement plants, etc). CCS is being pursued as a key option to reduce emissions of CO_2. The current technology for carbon capture is very expensive requiring between 25 and 35% of the energy generation associated with CO_2 emissions to capture and compress the CO_2 into a liquid for underground storage.

Transport: Once separated, the CO_2 is compressed and transported (via pipelines, trucks, ships or other methods) to a suitable site for geological storage. Large scale industrial operation such as a power plant would require a pipeline to transport the volume of CO_2 that is generated.

Storage: At the storage site, CO_2 is injected into deep underground rock formations, at depths of one kilometer or more.

Why do we need CCS

Electricity generated from fossil fuels accounts for more than 40 percent of the world's energy-related CO_2 emissions (2011, IEA CO_2 Emissions from Fuel Combustion). Another 25 percent of CO_2 emissions comes from large-scale industrial processes such as iron and steel production, cement making, natural gas processing and petroleum refining. Demand for fossil fuels is on the rise, especially in developing countries where a significant percentage of the population currently has no access to electricity, impacting the public welfare and an ability to prosper.

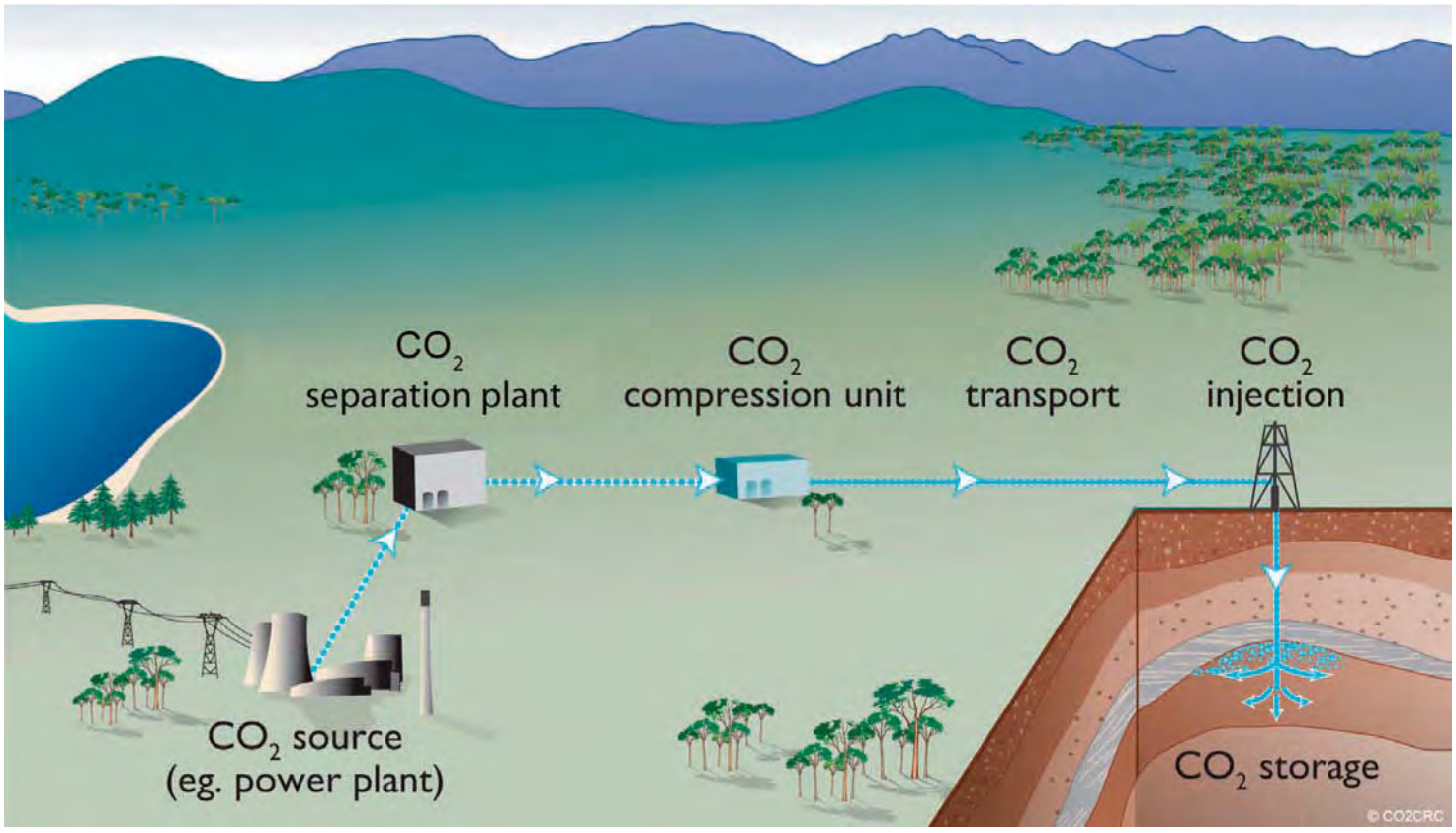


Image courtesy of CO2CRC

It is hoped that carbon capture and sequestration technologies can be developed into an economically viable option that can be implemented on a large industrial scale to reduce emissions of CO_2 from these large scale industrial sources.

How do you capture CO_2?

CO_2 can be separated from a carbon emission source either before or after it has been combusted to produce energy or other products (cement, steel, etc.). There are three ways to capture CO_2 from the combustion process:

- pre-combustion technology;
- post-combustion technology; and
- oxyfuel combustion.

Transporting the CO_2

Once separated from other elements of the flue gas (gas exiting via a chimney or 'flue'), the CO_2 is compressed to make it easier to transport and inject. While CO_2 is still a gas, when in what's called a supercritical state, it behaves like a liquid.

Today, CO_2 is already being transported by pipeline, ship and road tanker primarily for use in the food industry or to recover more oil and gas from oil and gas fields. The scale of transportation required for widespread deployment of CCS is far more significant than this small-scale transport, and will involve the transportation of dense, concentrated CO_2.

Where can you safely store CO_2?

The final major stage of the CCS process sees the CO_2 injected into deep underground rock formations, often at depths of one kilometer or more. At this depth, the temperature and pressure keep the CO_2 as a dense fluid. The CO_2 slowly moves through the porous rock, filling the tiny spaces known as 'pore space'.
Possible storage sites include depleted oil or gas fields, or rocks which contain unpotable saline waters. Acceptable storage sites have an impermeable trap (also known as a 'cap-rock') above them. The seal and other geological features prevent the CO_2 from migrating to the surface. Such sites are scientifically evaluated to ensure they are capable of securely containing fluids and gases for millions of years.

Once injected, a range of technologies are used to monitor the CO_2's movement underground. Measurement, monitoring and verification processes are important to ensure that the CO_2 is safely and stored.

The Intergovernmental Panel on Climate Change estimates the world's potential storage capacity at two trillion tonnes, although there could be a 'much larger potential'. (2005, IPCC Special Report).

What can you do with the captured CO_2?

Generally speaking, there are three possibilities:

1. As mentioned above, the CO_2 can be stored in secure deep underground geological formations.
2. CO_2 can also be used as a value-added commodity. This can result in a portion of the CO_2 being stored, such as in concrete that has been cured using CO_2, or in plastic materials derived from biomass which also use CO_2 as one of the ingredients.
3. It is also possible to convert CO_2 into biomass. This can be achieved through, for example, algae farming using CO_2 as a feedstock. The harvested algae can then be processed into bio-fuels which can take the place of non-biological carbon sources.

RMCCS
ROCKY MOUNTAIN CARBON CAPTURE AND SEQUESTRATION

Communications Plan for Rocky Mountain Carbon Capture and Sequestration Project

Objectives

- **Define and prioritize** the stakeholder groups impacted by the project.
- **Finalize** necessary messages, materials and communications channels.
- **Prepare public relations efforts** as project advances.
- **Determine** long-term campaign strategies, issues, milestones and initiatives of this strategy.

Key Audiences and Stakeholders

Project partners

- Colorado Geological Survey
- Schlumberger Carbon Services
- University of Utah
- Arizona Geological Survey
- New Mexico Bureau of Geology & Mineral Resources
- Utah Geological Survey
- Tri-State Generation & Transmission

State Government Stakeholders

- Colorado State Legislature
- Colorado Air Quality Control Commission
- Utah State Legislature
- Utah Department of Environmental Quality
- Arizona State Legislature

- Arizona Department of Environmental Quality
- Colorado State Land Board

City/County Stakeholders

- Moffatt County Commissioners
  - Tom Gray
  - Audrey Danner
  - Tom Mathers
- Craig City Government
  - Terry Carwile, Mayor
  - Don Jones, City Council
  - Gene Bilodeau**,** City Council
  - Joe Bird, City Council
  - Jennifer Riley, City Council
  - Ray Beck, City Council
  - Byron Willems, City Council
- Tri-State Coops
- Trapper Mine
- Other Coal Producers
- Landowners
- Mineral Rights Owners

External Influencers

- Media
  - Craig Daily Press, Bryan Smith
  - CBS Channel 4, Paul Day
  - AZ Media
  - UT Media, USTAR
- Community/Special Interest
  - Craig Chamber of Commerce
  - Environmental groups
- Oil & Gas Producers

Strategy and Planning

- **Ensure proper communications are made** regarding the purpose and goals of the project.

- **Identify target audiences** that have an interest in the project.

- **Create a list of opportunities** that provide avenues for RMCCS to communicate its messages including state/city/county government meetings, media and special interest groups.

- **Identify major project milestones** to ensure proper communications tactics are deployed in timely fashion.

    - September drilling characterization well
    - Coring different formations, down hole logging
    - Sending core to different work groups for analysis
    - Apply data

Materials

- **Develop fact sheets** including general project overview, seismic testing, carbon capture and sequestration, and the drilling process.

- **Develop a project press kit** to contain a project fact sheet, project partner fact sheets, FAQs, project timeline, and press releases as new milestones are reached in the project.

- **Develop legislative outreach packet** that can be used to communicate with state legislators.

- **Implement improvements and upgrades to the project Web site** as needed.
    - Project fact sheets
    - Project timeline
    - Press releases
    - Links to media coverage
    - Portal to accept public questions and comments on the project
    - Physical demonstration of sequestration
    - Core sample absorption demonstration

Media Relations

- **Create and distribute news announcements** regarding relevant project milestones, events, community initiatives and other topics as needed.

- **Build substantive relationships with local and regional press** that promote consistent and accurate media coverage and capitalize on opportunities to be proactive with news media.

- **Track media coverage** and assess for message continuity and impact.

Community/Civic Relations

- **Plan field day** at well site when rig arrives for community members. Field day will include core absorption demonstration and a general overview of the sequestration process.

- **Plan public meetings** in Craig, Denver and other locations to educate the public and stakeholders on the purpose and progress of the project.

- **Indentify primary spokespersons for media** during Moffat County Commissioner meetings and other forums.

- **Identify and determine appropriate venues** where RMCCS can deliver project updates to key audiences and stakeholders.

- **Continue to foster relationships and conduct regular meetings and briefings** with key stakeholders and external influencers to ensure project communications are as proactive as possible.

- **Develop feedback mechanisms** including an email address and phone number where key audiences can ask questions and receive appropriate feedback as it relates to the project.

- **Leverage the Tri-State blog and Twitter page** as a secondary method of communications regarding project milestones. Identify other secondary communication channels.

Programs, Tools and Tactics

- **Initiative-specific message and talking point platforms**
  Develop key messages used by individuals to educate regarding the project.

- **Reporter "beat system"**
  Build substantive relationships with journalists to promote consistent and accurate media coverage and capitalize on opportunities to be proactive with the news media.

- **Project information kit**
  Create an information kit targeted for key local and regional media. The information kit will contain documents such as fact sheets and FAQs.

- **Web site**
  Improve the project-specific Web site to communicate key messaging related to the project.

- **Op-Eds, LTEs**
  Develop news opinion-editorials and letters to the editor for use by the project team as needed.

- **Social media**
  Leverage Tri-State's social media tools when appropriate to provide secondary tools for communications. These include a blog, Twitter page and YouTube page. Identify other project partner social media opportunities.

COMMENTS DIRECTED TO:

Sarah Carlisle
303-254-3396
scarlisle@tristategt.org

YOU ARE INVITED TO ATTEND THE
ROCKY MOUNTAIN CARBON CAPTURE AND SEQUESTRATION OPEN HOUSE

January 24, 2012 from 4:00 pm to 7:00 pm at

Trapper Mining, Inc.
25910 S. Highway 13
Craig, CO 81625

A rig tour will be offered at 3:00 p.m.

Please RSVP to Sarah Carlisle at 303-254-3396 or *scarlisle@tristategt.org*.

The Rocky Mountain Carbon Capture and Sequestration Project is studying rock formations at Trapper Mining, Inc. in Craig, Colorado to evaluate potential carbon dioxide storage options. The project consists of analyzing surface and subsurface rock formations, drilling a well, creating a detailed geologic model of the underground rock formations and assessing risk for carbon sequestration and seismic testing. Visit *www.rmccs.org* for more information.



227

20827001

PROJECT OVERVIEW

Overview

Geologic formations in western Colorado are being studied for their ability to sequester carbon dioxide underground in a major research assessment conducted by a partnership called the Rocky Mountain Carbon Capture and Sequestration (RMCCS) team. The team is comprised of the Arizona Geological Survey, Colorado Geological Survey, the New Mexico Bureau of Geology and Mineral Resources, Schlumberger Carbon Services, Shell Production Company, Tri-State Generation and Transmission, the University of Utah and the Utah Geological Survey. The Project is funded by the American Reinvestment and Recovery Act.

The RMCCS team is using geologic and geophysical methods and tools to characterize rock formations in and around the town of Craig, Colorado for their potential to provide long-term storage of carbon dioxide drilling.

"This project will provide a fundamental geological baseline of the potential for major candidate rock formations in the region to safely store carbon dioxide," said co-principal investigator Dr. Brian McPherson, director of the Carbon Science and Engineering Research Center at the University of Utah's Energy & Geoscience Institute. "Such baseline is absolutely critical before commercial-scale sequestration can be deployed."

The team has identified the Cretaceous Dakota Sandstone, the Jurassic Entrada Sandstone and the Pennsylvanian Weber Sandstone as three of the most promising geologic sequestration formations for the southwestern U.S. and the Rocky Mountain region, in particular. The project consists of analyzing existing subsurface geologic data in the region, conducting new seismic surveys, drilling a well to characterize the rock formations, analyzing subsurface formation samples for their ability to store carbon dioxide, and creating a detailed geologic model of underground rock formations.

Project Goal

The goal of the three-year project is to evaluate the ability of the subsurface rock formations and the geologic structure in NW Colorado to provide a safe, long-term option to store carbon dioxide and to better understand the potential for the carbon sequestration throughout the Rocky Mountain region. The project will evaluate the sequestration potential of deep saline formation on a large, Laramide-age structure south of Craig, Colorado.

Previous studies of the Craig area indicate that at 4% efficiency, two saline formation (Weber and Entrada) have the capacity for sequestering 46.3 billion tons of CO_2. The current project area comprises about 1/10th of the area previously analyzed. Therefore, the current project has the potential of sequestering 4.6 billion tons of CO_2.

The project not only is important locally due to the location of Craig station, but also has regional implications because the Entrada and Dakota formations are widespread in the Rocky Mountains and Colorado Plateau. Given the thickness of the rock formations and the size of the subsurface geologic structure, it conceivably could serve as a regional sequestration sink for power plants, natural gas processing plants, cement plants, oil shale development and other industries that are a significant part of western Colorado's economy.

Timeline of Project

In the summer of 2009, the Rocky Mountain Carbon Capture and Sequestration group was formed and consisted of the Arizona Geological Survey, Colorado Geological Survey, the New Mexico Bureau of Geology and Mineral Resources, Schlumberger Carbon Services, Shell Production Company, Tri-State Generation and Transmission, the University of Utah and the Utah Geological Survey. The group was awarded $3.8 million from the Department of Energy's National Energy Technology Laboratory (DOE/NETL) with a $1 million match required from the partners.

In the summer of 2010, the coalition submitted a proposal to the DOE to increase the level of funding of the project from $4.8 million to $11 million, which was accepted.

The Colorado Geological Survey and Utah Geological Survey then sent a crew of geologists to the site to take measurements of the rock layers at the surface in order to better understand what might be encountered below ground. The field crew took approximately 1,700 measurements.

The Colorado Geological Survey and Schlumberger Carbon Services have reviewed the existing petroleum-industry and seismic data in the project area. The group has selected the final well site and began preparations for the permitting of the 9,600-foot-deep well and the acquisition of a new seismic survey located on State of Colorado lands.

In 2012, the well will be drilled, cored and analyzed. A detailed geologic model will be generated of the subsurface rock formations. The Energy and Geoscience Institute (EGI) at the University of Utah will analyze the materials gathered from the well, model the reservoir and assess the risk for the project. The four state geological surveys will then use the information gathered for the project to assess the carbon dioxide sequestration potential for NW Colorado, the Colorado Plateau and the Southern Rocky Mountains

www.rmccs.org

ROCKY MOUNTAIN CARBON CAPTURE AND SEQUESTRATION

Tri-State Generation and Transmission Association, Inc.
1100 W. 116th Avenue
Westminster, CO 80234

YOU ARE INVITED TO ATTEND THE
ROCKY MOUNTAIN CARBON CAPTURE AND SEQUESTRATION OPEN HOUSE

January 24, 2012, from 4:00 p.m.-7:00 p.m. at

Trapper Mining, Inc.
25910 S. Highway 13
Craig, CO 81625

A rig tour will be offered at 3:00 p.m.

Please RSVP to Sarah Carlisle at 303-254-3396 or *scarlisle@tristategt.org*.

The Rocky Mountain Carbon Capture and Sequestration Project is characterizing rock formations at Trapper Mining, Inc. in Craig, Colorado to evaluate potential carbon dioxide storage options. The project consists of analyzing surface and subsurface rock formations, drilling a well, creating a detailed geologic model of the underground rock formations and assessing risk for carbon sequestration and seismic testing. Visit *www.rmccs.org* for more information.

RMCCS
ROCKY MOUNTAIN CARBON CAPTURE AND SEQUESTRATION



A Touchstone Energy® Cooperative

FOR IMMEDIATE RELEASE

August 16, 2012

MEDIA CONTACT:
Sarah Carlisle
303-254-3396
scarlisle@tristategt.org

Coalition Discovers Potential for Carbon Storage Below the Rocky Mountains

Public and Private Sector Researchers Partner to Determine Feasibility of Sequestering Billions of Tons of Carbon Dioxide Underground

Denver, Colo. – A coalition of industry, government and academic interests has entered the home stretch of a major research initiative and has determined that there is the potential for long-term carbon storage deep below the Rocky Mountains. Earlier today in Denver, project representatives showed off rock samples from 9,745 feet below the landscape of northwest Colorado –samples that hold important clues regarding the area's potential for future carbon sequestration activities. The coalition believes that this area could store up to about 4.6 billion tons of carbon dioxide (CO2) emissions.

The research is being conducted by the Rocky Mountain Carbon Capture and Sequestration Partnership (RMCCS), a group formed in 2009 and comprised of Colorado Geological Survey, Arizona Geological Survey, New Mexico Bureau of Geology & Mineral Resources, Schlumberger Carbon Services, University of Utah, Utah Geological Survey and Tri-State Generation and Transmission Association. The work is funded largely by an $8.8 million grant from the U.S. Department of Energy as part of a national effort to identify safe and secure long-term storage capacity for CO2.

"With our partners, we have made progress in evaluating the ability to sequester carbon emissions across the Rocky Mountain region," said Ken Anderson, executive vice president and general manager of Tri-State. "Developing options to manage carbon emissions is important to help manage the risks that come with carbon regulation and ensure consumers continue to have affordable and reliable electricity."

The rock samples on display today came from a test well drilled below the Trapper Mine in Craig, Colo., which supplies coal to Tri-State's nearby 1,311-megawatt Craig Station electric generation plant. The rock samples are helping RMCCS scientists evaluate the potential of deep saline aquifers-for safely and permanently storing carbon dioxide (CO2), a byproduct produced during the combustion of fossil fuels during the energy production process. Preliminary data indicate that northwest Colorado may be capable

of safely storing several billion tons of CO2. The RMCCS team will continue to analyze the data they have collected to determine the fate of any potentially injected CO2. A full analysis will be ready in mid to late 2013.

Vince Matthews, co-principal investigator who assembled the key partners for the project, said "If the testing, modeling, and economics work out for this structure; it could serve as a regional sink for industries desiring to sequester CO2 such as oil shale, cement plants, coal plants, and natural gas processing facilities. This could lead to new job opportunities for northwest Colorado, and perhaps throughout the Colorado Plateau."

The project has regional implications because the formations at this site – the Cretaceous Dakota Sandstone, Jurassic Entrada Sandstone and Pennsylvanian Weber Sandstone – are widespread throughout the Rocky Mountains and the Colorado Plateau, which straddles Utah, Arizona, New Mexico and Colorado. The geologic structure of these formations in northwest Colorado may be capable of storing up to 4.6 billion tons of CO2 or more. Additional CO2 storage capacity may exist in other areas within the region.

"This project will provide a fundamental geological baseline of the potential for major candidate rock formations in the region to safely store carbon dioxide," said co-principal investigator Dr. Brian McPherson, director of the Carbon Science and Engineering Research Center at the University of Utah's Energy & Geoscience Institute. "Such baseline is absolutely critical before commercial-scale sequestration can be deployed."

The RMCCS project is one of several carbon sequestration studies being conducted around the United States. If perfected, sequestration processes could provide options to address energy, environmental and economic concerns.

Detailed information about the project is available at www.RMCCS.org.

Fact sheets and additional information can also be found online at www.rmccs.org/news

###

How is a well drilled?

To drill a well, a drilling rig, like a crane, is temporarily assembled on site (Figure 1). Typically about 150 feet (46 meters) tall, the rig is only there for the duration of the drilling operation, perhaps several months, before it is dismantled and moved away. The rig is used to handle long lengths of drill pipe connecting the surface to a special drill bit (Figure 2), which is chosen depending on the type of rock it has to drill through. Drilling fluid is pumped down the drill pipe and through the bit. The fluid cools the bit and transports the cuttings to the surface. It also supports the walls in the well and lubricates the drilling bit. Drilling through the rock layers causes wear to the drill bit, which may have to be changed several times (Figure 3).

Periodically, drilling is interrupted and logs are performed. Logging is the measurement of rock and fluid properties. The logging measurements are used to evaluate the suitability of the strata for secure carbon dioxide (CO_2) storage. If favorable, the construction of the well continues with the casing process.

The casing is installed in steps and it prevents the well from collapsing. It also isolates different rock layers. To stabilize the casing and to avoid leakage, the casing is cemented to the rock. Each casing string is cemented all the way back to surface. The hole is smaller after the first casing. Hence, a smaller bit has to be used for the next drilling step. The deeper the well is, the smaller the diameter of the hole becomes.

The integrity of the casing and cement is essential for fluid isolation between the rock layers. It is important to evaluate the cement and the bond where the cement and casing interface. Tools are used to provide measurements to give a qualitative indication of the percent of the casing bonded, the type of cement, and some casing properties.

To protect the casing from corrosion and wear and to transport the CO_2 from the surface to the storage formation, tubing is installed. The tubing is run inside the casing to the depth of the injection zone. To connect the well to the storage formation, holes are made in the casing. These holes are called perforations and are created by directional explosions.

CO_2 pumped into the tubing from the surface then flows into the rock formations for long-term storage (Figure 4).

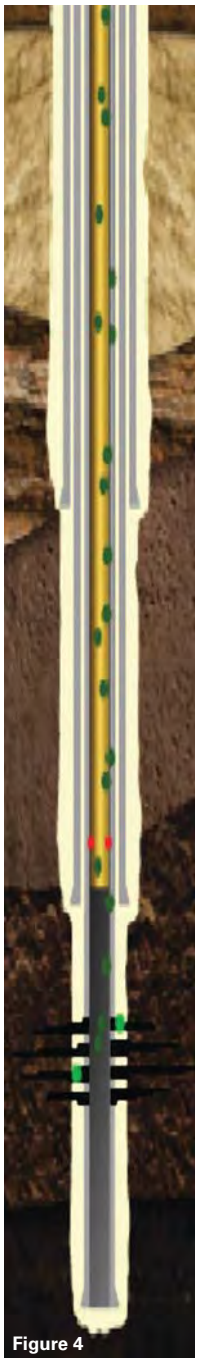
Careful planning, selection of the materials and systems used, intricate design, and execution of the jobs as planned all help to guarantee long-term integrity of the wells.


Figure 1


Figure 2



Figure 3


Figure 4

Schlumberger
Carbon Services

What is a seismic survey?

A seismic survey is needed to better understand geological formations in the subsurface before storing carbon dioxide deep underground. This enables imaging of the many layers of rock below the surface by using sound waves. Collection and processing of the data allows the creation of three-dimensional images of the subsurface and can be compared to an ultrasound test that a doctor might perform on a human body, just at a different scale and frequency.

How is a seismic survey conducted?

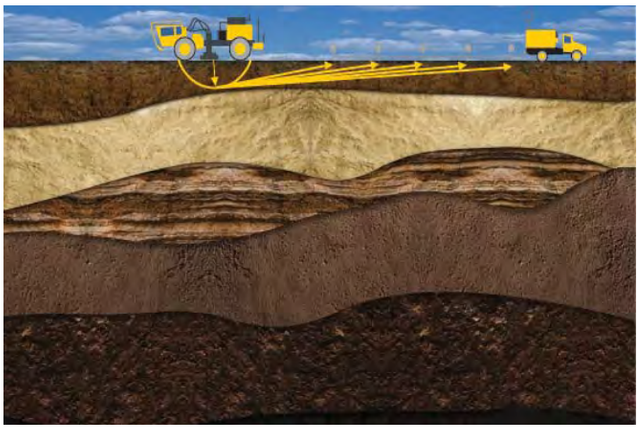
Receivers or sensors, called geophones, are installed at the surface to register echoes from geological layers. Geophones consist of a 3-inch aboveground portion, which can be seen in the image to the right, and a 3-inch belowground spike, which holds the unit securely in the ground. To create the echoes, or waves, special trucks are used. The trucks are equipped with large pads that send vibrations through the earth.

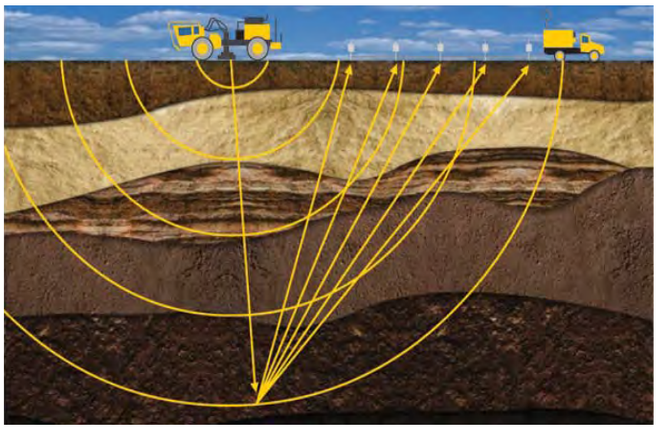
First, a survey crew will move down roads to gather surface measurements and details. These measurements will determine where to place the series of cables equipped with geophones. Once the geophones are placed, trucks will move in tandem down the road lowering a vibration pad onto the surface every few feet. The waves created travel deep underground and are reflected back as echoes from the different rock layers. The reflections are picked up by a recording truck, which captures the data for computer processing and analysis.



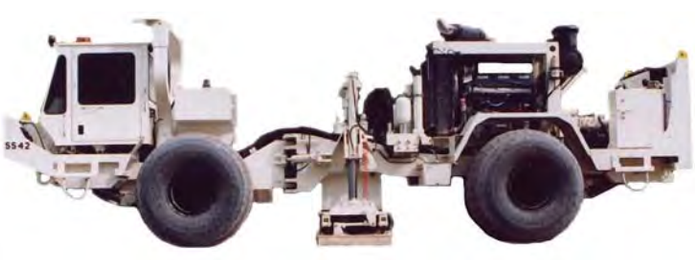
Geophone receivers are installed at the surface to register echoes from geological layers

From the timing of the reflection data, the depths of the layers can be determined, and an image of the subsurface can be formed. Any surface sign that the survey has taken place is repaired and within a few short weeks everything is back to the way it was.





The images above show how the sound waves transmitted by the vibration trucks bounce off each layer of rock and are collected by the geophones and transmitted to the data, or recorder, truck. As the sound waves travel deeper they continue to bounce off each rock layer.





Above are images of two different trucks that you might see in your area when the seismic survey is conducted. Notice the vibrator pads located in the center of the vehicle underside.

Preliminary Probabilistic AOR Prediction of CO_2 Sequestration in Craig Site, CO

Si-Yong Lee[1,2] (sylee@egi.utah.edu), and Brian McPherson[1,2]

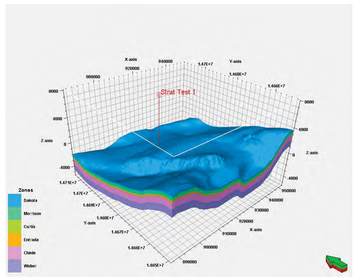
[1] Energy and Geoscience Institute, University of Utah, Salt Lake City, UT 84108

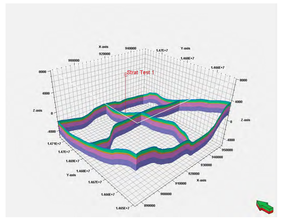
[2] Department of Civil and Environmental Engineering, University of Utah, Salt Lake City, UT 84112

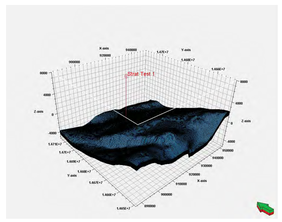
Introduction

The University of Utah performed the pre-injection phase risk assessment with the response surface method (RSM) and Monte Carlo simulation approach. We completed the preliminary evaluation of the area of review (AOR) due to the theoretical CO_2 injection (1 Mt/yr for 2 years) in the Craig site, CO. Our AOR assessment task involves the utilization of response surface method (RSM) associated with the Box-Behnken design (BBD) of experiment and corresponding numerical modeling experiments.

Static Model







Numerical Settings

Number of elements	**200 x 200 x 20 (800,000)**
Size of each element (m)	**Δx=330 ft, Δy=330 ft, Δz=varying**
Initial pressure condition	**Hydrostatic**
Initial temp. condition (°C)	**Constant**
Boundary conditions	**Constant pressure (lateral), no flow (top and bottom)**
Porosity	**Uniform porosity (0.1)**
CO2 Injection	**1,000,000 metric tons for 2 years**
Simulation period	**100 years**

Area of Review

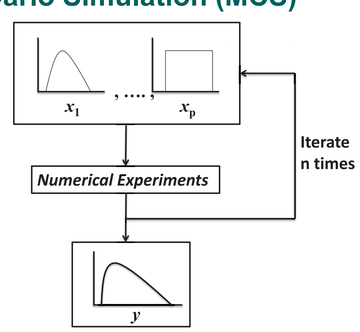
- CO_2 sequestration well is subject to EPA UIC Class VI category

-Def. : the region surrounding the geologic sequestration project where USDWs may be endangered by injection activities

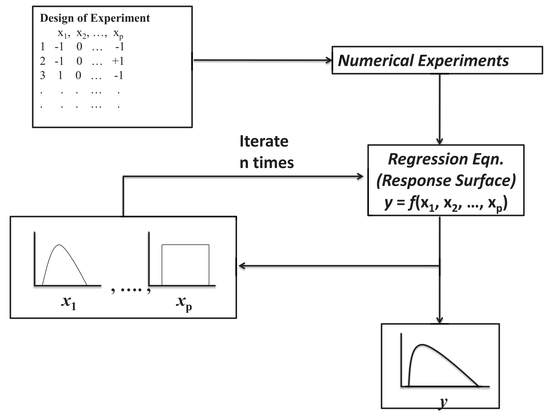
- Use of computational modeling tool

- Necessity of probabilistic assessment due to the uncertainty in the subsurface environment

Monte Carlo Simulation (MCS)



MCS through Response Surface Methodology

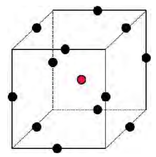


Response Surface Methodology

- Regression modeling
- Commonly referring to second-order model fit to the data/responses from the design of experiment.
- Utilized in probabilistic design to efficiently estimate a statistical linear model.

Box-Behnken Designs (BBD)

- 3-level design (-1, 0, 1)
- Each factor or independent variable is placed at one of the three equally spaced values.
- Requires 2k(k-1)+1 runs (13 runs, k=3).



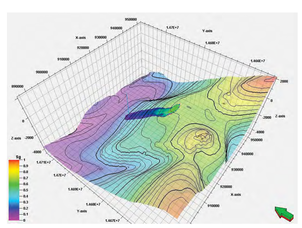
Input Parameters (independent variables)

4 factors

		Low (-1)	Mid (0)	High (+1)
X1	**Weber Thickness (ft)**	**200**	**500**	**800**
X2	**Weber Permeability (mD)**	**13.5**	**100**	**738.9**
X3	**Anisotropy Ratio**	**0.1**	**0.55**	**1**
X4	**Reservoir Temperature (F)**	**150**	**174**	**198**

Dependent Variables (responses or output)

- Area of Review
- x-dir 1st moment
- y-dir 1st moment



Model Fitting

$$y = \beta_0 + \sum_{i=1}^{k} \beta_i X_i + \sum_{\substack{i=1,j=2 \\ i<j}}^{k} \beta_{ij} X_i X_j + \sum_{i=1}^{k} \beta_{ii} X_i^2 + \varepsilon$$

Matrix form : $\boldsymbol{y = X\beta + \varepsilon}$

- A response surface model is fit using least squares regression.

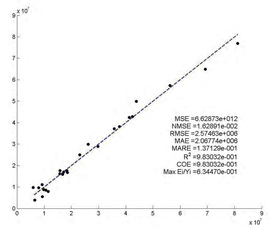
-Least squares estimator of $\boldsymbol{\beta}$ is $\hat{\boldsymbol{\beta}} = (\mathbf{X'X})^{-1}\mathbf{X'y}$

$$\hat{\boldsymbol{y}} = \boldsymbol{X}\hat{\boldsymbol{\beta}}$$

- Stepwise regression

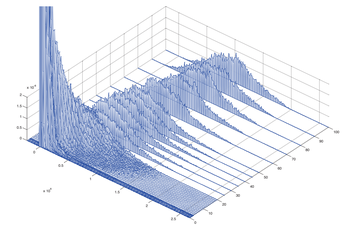
Observed vs. Predicted

At t= 7,300 days



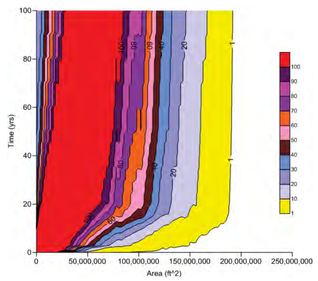
PDFs

Probability density functions for the CO2 plume extent at 45 time steps given the design of experiment.

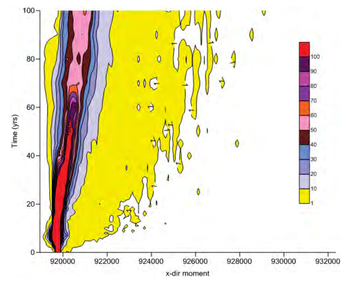


Results (contour map of frequencies)

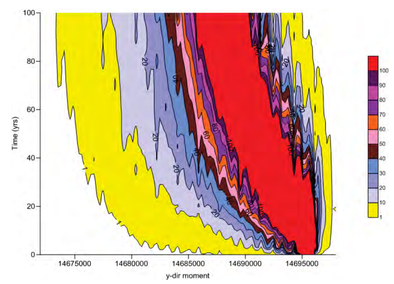
(a) CO_2 plume extent (ft^2)



(b) X-dir spatial moment of CO_2 plume



(c) Y-dir spatial moment of CO_2 plume



Summary

➢ Given the range/distributions of input variables and injection scenario, AOR in the Craig site tends to rapidly increase the range in the responses after injection ceases.

➢ It was noted that the CO_2 plume keeps growing even after 100 years. This could be related to the low irreducible gas saturation and no-hysteresis condition in the relative permeability function. Under the conservative perspective, this can provide the maximum CO_2 plume migration, but better prediction should be made from the relative permeability function that we will find from the collected core samples

➢ X- and y-dir 1st moment results well captured the center of CO_2 plume moving toward east and south, respectively

➢ We have shown that the response surface method combined with Monte Carlo simulation can be applied to the evaluation of AOR in the Craig site. Probabilistic assessment of AOR used in our work gave more realistic results accounting for the uncertainty in the subsurface environment.

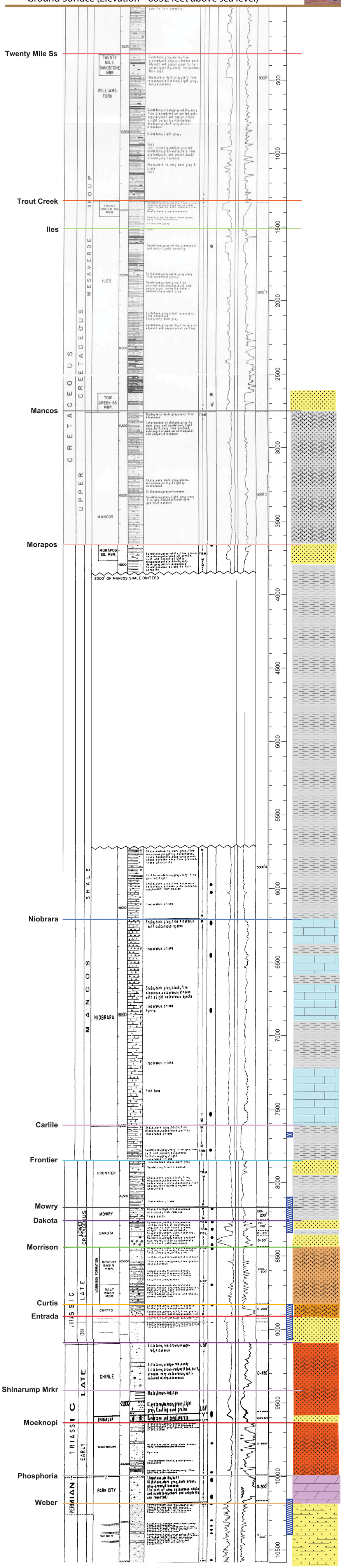
RMCCS Stratigraphic Test Well - Drilling Update
January 20, 2012, 8:00AM

Trapper Mine Site near Craig, Colorado
Drilling Start Date - January 15, 2012



CURRENT DEPTH: 1393 Feet
CURRENT FORMATION: Trout Creek Sandstone Member of the Isle

Depth (ft)	Date	# of Days Drilling	Drilled Last 24 Hours (ft)	Comments
266	01/16/2012	1	171	Drilling begins
487	01/17/2012	2	221	Drilling through Twenty Mile Sandstone Member of the Williams Fork
888	01/18/2012	3	401	Drilling through the Williams Fork.
1393	01/19/2012	4	505	Drilling through the Williams Fork and the Trout Creek Member of the Isle.
	01/20/2012	5	0	No Progress



This figure shows the rock layers (formations) that will be encountered during drilling of the RMCCS test well. Descriptions for each rock are shown, along with typical measurements that are important for engineers and geologists to "know" which rock layer they are drilling through. Color shaded patterns on the right side of figure represent different types of rocks that will be drilled including sandstones (yellow), siltstones (orange), shales and muds (grey), and calcareous rocks (blue/purple). Blue hashed boxes show the approximate depths and rock types for which rock samples (cylindrical cores) will be collected.

For, the RMCCS project, a primary goal is to collect samples from three rock formations that are good candidates for the injection and storage of carbon dioxide: the Dakota, Entrada, and Weber sandstones. All have potentially good storage in void spaces between individual sand grains.

As important as the potential storage targets, are the rocks that will 'seal' the carbon dioxide in place after injection. These are typically impermeable shales and other very fine grained rocks. Samples will also be collected from important sealing rocks.

The project website (*www.rmccs.org*) shows daily updates of the drilling activity including the current drilling depth, the amount drilled in the past 24 hours, and the current rock formation that is being penetrated. Additionally comments regarding drilling activity, such as core being collected, casing being placed, and logging tools being run, will be posted. At any time, you can visit the website and select "Click here for Recent Updates!" for up-to-date information on drilling and the project just as you see here.

ROCKY MOUNTAIN CARBON CAPTURE AND SEQUESTRATION

www.rmccs.org

Safe, long-term underground geologic storage (sequestration) of CO_2 requires that it be conducted properly. This means thorough planning and geologic analysis of the storage site, safe operating practices and careful monitoring of the underground CO_2 during injection, and continued monitoring for some time afterward.

Reliable geological surveys can prove the presence of impermeable rock barriers and the capability of deep rock formations to hold fluids. Geologic storage will use established techniques and equipment used over many years by industry, although more advanced technologies designed specifically for CO_2 injection are also being developed.



Rock samples from potential storage sites are used to analyze the rocks and the properties that affect the safety and security of storage.

Storage sites will be monitored so that any undesirable CO_2 movement can be readily detected and fixed.





Specially-designed devices can monitor any changes in air quality or underground water quality due to the presence of CO_2. Similarly, monitoring techniques such as seismic imaging can monitor the location and conditions of the CO_2 underground.

Geologic storage of CO_2 can be a vital part of the solution to the problem of global climate change. Methods and technologies are developing rapidly, as are the legal frameworks to regulate them. Geologic storage projects undertaken over the next ten years will be critical for demonstrating CO_2 storage in diverse geologic settings and will establish the basis for widespread global application.

For More Information

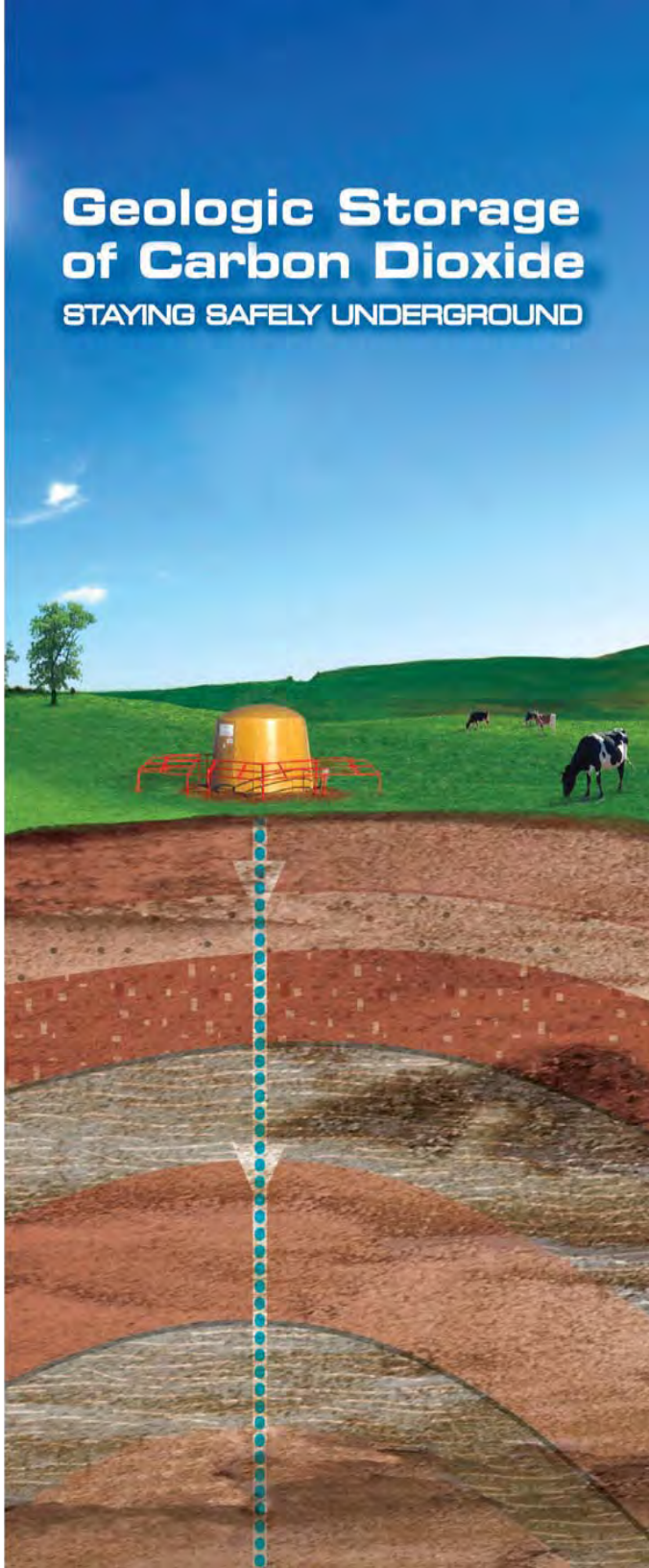
The best assurance of safe and secure geologic storage is a project that is well designed and conducted properly and carefully. More detailed explanations, including questions to ask about proposed projects to ensure that they are being conducted properly, can be found in the booklet, "Geologic Storage of Carbon Dioxide: Staying Safely Underground."

Commissioned by
International Energy Agency (IEA)
Working Party on Fossil Fuels
with funding from Chevron, CO2CRC,
the IEA GHG Weyburn-Midale CO_2 Storage
and Monitoring Project, and Rio Tinto

Developed by Bluewave Resources, LLC
Graphics courtesy of CO2CRC

Geologic Storage of Carbon Dioxide

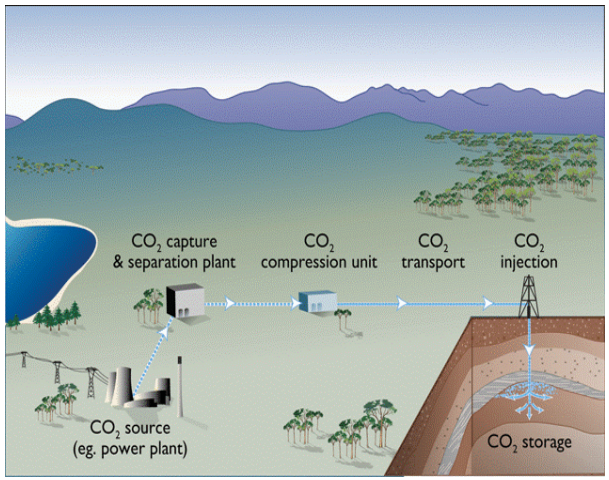
STAYING SAFELY UNDERGROUND



GEOLOGIC STORAGE OF CARBON DIOXIDE: STAYING SAFELY UNDERGROUND

CO_2 is a natural substance in the air that is vital to life. It is widely used for many purposes from carbonating drinks to filling fire extinguishers. As a greenhouse gas, its presence in the atmosphere traps heat from the sun. Normally, this keeps the climate warm enough for life to continue. However, the burning of fossil fuels is increasing CO_2 levels in the atmosphere above naturally-occurring levels, contributing to global climate change.

Geologic storage of carbon dioxide (CO_2) is the underground disposal of CO_2 from large industrial sources such as power plants. Carbon Capture and Storage (CCS), also known as Carbon Capture and Sequestration, includes geologic storage as one of its components.

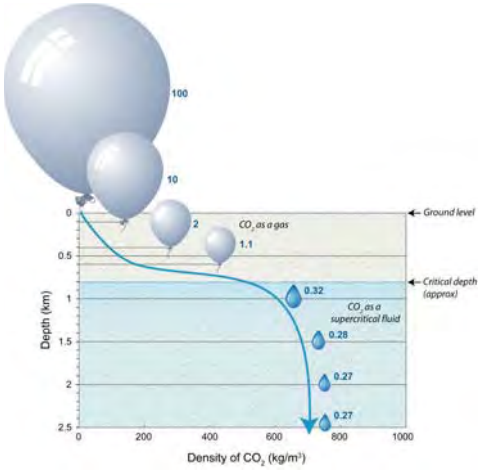


In CCS, CO_2 is captured before it can be emitted into the atmosphere. It is then compressed into a dense fluid, transported to the injection site and disposed of underground in suitable rock formations.

CCS is one tool—along with energy efficiency, fuel switching and renewable energy sources—essential to reducing CO_2 levels. Many studies show that by far the most effective and least-costly way to reduce CO_2 levels to avoid climate change is to use all CO_2 reduction tools, including CCS.

Geologic storage projects have already successfully stored millions of tons of CO_2 without detectable leakage, some for many years. For example, the Sleipner Project in Norway has injected over 10 million tons of CO_2 with no leakage. Similarly, the IEA GHG Weyburn-Midale CO_2 Storage and Monitoring Project in Canada has injected over 5 million tons of CO_2 into a depleted oil field. Extensive monitoring by an international team of scientists has detected no leakage. Many new projects are planned in the years to come.

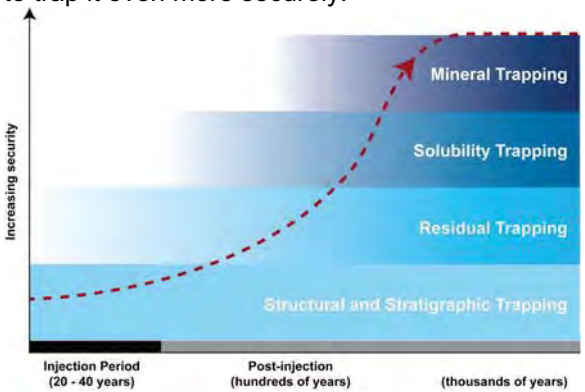
In geologic storage, CO_2 is injected under high pressure into deep, stable rocks in which there are countless, tiny pores that trap natural fluids. Some types of rock formations have securely trapped fluids, including CO_2, for long periods, even millions of years. The CO_2 will be injected into these types of formations.



CO_2 will be injected at depths below 0.8 km (2600 feet). CO_2 increases in density with depth and becomes a supercritical fluid below 0.8 km. Supercritical fluids take up less space and diffuse better than either gases or ordinary liquids through storage rocks. The blue numbers show the volume of CO_2 at each depth compared to the volume of 100 at the surface.

Several types of rock formations are suitable for CO_2 storage. These include depleted oil and gas reservoirs, deep saline formations and deep, unmineable coal seams. Deep, porous rock formations with trapped natural fluids such as oil, natural gas or highly salty and unusable water are common throughout the world. Geologists have found that these formations have the capacity to securely hold vast amounts of CO_2, potentially equivalent to hundreds of years of man-made emissions.

The same geologic forces that kept the original fluids in place will also secure the liquid CO_2. Once injected, it will be far below the surface and separated from usable groundwater by thick, impermeable barriers of dense rock. This is either structural or stratigraphic trapping depending on the geology. In residual trapping, CO_2 is trapped in tiny pores within the storage rocks. Over time, the liquid CO_2 will dissolve in water already in the rock formation and then may combine chemically with minerals in the rocks to trap it even more securely.



As time goes on, increasingly secure trapping mechanisms come into play and the overall security of storage increases.

APPENDIX F

Sand Wash Basin Data

Contents

Topic

Published Tops

Published Porosity & Permeability Studies

Regional Locator Maps

Stratigraphic Correlation Chart

Sand Wash Data Maps

Petrel Cross Sections

CO2 Migration Paths (Blockage?)

Porosity Maps

Data Sources for Published Tops

Published cross sections were used to locate as many formation tops as possible. Tops from the published cross sections were manually entered into the Petra project and their sources were noted as "PUB" and used as a framework for the regional correlations. The published cross sections included:

- Irwin (1972) chaired a committee of the Rocky Mountain Association of Geologists that published 22 cross sections in the state of Colorado. Cross Sections 7, 10, 11, 12, 13, 14, 15, 16, 17, 20, and 21 covered the Colorado Study Area. The tops shown on the cross sections extended from the Wasatch to the Precambrian.

- Hasket (1959) correlated the Niobrara in the Sand Wash Basin.

- Finn and Johnson (2005) refined the cross section of Hasket (1959) by correlating the benches of the Niobrara (Buck Peak, Tow Creek and Wolf Mountain).

- The intertonguing relationship between the Mesaverde and Mancos was illustrated by Hettinger and Kirschbaum (2002) in an east-west cross section through the Uinta and Piceance basins.

- Johnson (2002) made a detailed north-south cross section of the Mancos in the Piceance Basin starting from the base of the Mesaverde and extending to the top of the Dakota Sandstone.

- Kirschbaum (2002) made a north-south cross section along the Colorado-Utah state line correlating the basal Mancos through the Mowry, Dakota and Cedar Mountain.

- Quigley (1959) correlated the Dakota and Cedar Mountain along the Douglas Creek Arch.

- Kaiser, et al (1993) included many cross sections through the Lewis and Mesaverde in the deeper portion of the Sand Wash Basin.

In addition, the IHS database that provided well data for this project included tops that had been reported by operators. These were posted on well logs during the correlation process. They were considered, but were often inconsistent and were not used if they disagreed with the published cross sections or my correlations.

Published Porosity and Permeabilty Values from Field Studies

Field Name	Loc	Formation	Depth	Avg. Por. %	Avg. Perm. md	Water Rw	Water TDS ppm	Reference
Craig Dome	T6N R91W	Rimrock		20	50			RMAG 1961 O&G Field Vol. p.98
Douglas Creek	T2-3N R102-103W	Emery		no info				RMAG 1961 p. 114.
N. Douglas Creek	T1S R101-102W	Morapos	812	20	100	1	6,954	RMAG 1961 p. 116
Craig Dome	T6N R91W	Morapos		10	1			RMAG 1961 O&G Field Vol. p.98
Greater Douglas Ck Area	T1N-5S, R100-104W	Mancos B		9-12 (logs) 10-11(cores)	<0.1 md	0.238	23,851	RMAG 1982 O&G Fields p. 184
Moffat	T4-5N, R91W	Mancos						RMAG 1954, O&G Fields p 229
Buck Peak	T6N R90W	Niob (Buck Pk)		fractured	?			RMAG 1961 O&G Field Vol. p. 74
Curtis	T6N R86W	Niobrara		fractured				RMAG 1961 p. 102
Sage Ck & N Sage Ck	T5N R87-88W	Niobrara		fracture			no water	RMAG 1961 p. 226
Tow Creek	T6N R86W	Niobrara		fractures			24,572	RMAG 1954 p. 274
Tow Creek Anticline	T6N R86-87W	Niobrara					24,572	
Iles Dome	T4N, R92W	Mowry						RMAG 1961 O&G Field Vol. p. 158
NW CO		Dakota		10-20 %	low to 500			Special Completion Practices, RMAG 1962, p. 126
Douglas Creek	T2-3N R102-103W	Dakota	4326	12.5	50-1675md	0.095	77,820	RMAG 1961 p. 114.
Douglas Creek	T2-3S, R101-102W	Dakota/Lakota		13	50-1675 md			RMAG 1954 p. 126
Elk Spgs & Winter Valley	T4-5N, R98W	Dakota		>12%		0.08		McMillan RMAG 1986 p. 247
Elk Spgs & Winter Valley	T4-5N R98W	Dakota		16		2.96	3,200	RMAG 1961 p. 124
Maudlin Gulch	T4N R95W	Dakota	5754	17	4.8	1.7	3,991	RMAG 1982 O&G Fields p. 338
Wilson Creek	T3N R94W	Dakota						Stone, RMAG 1986, p. 234.
Moffat	T4-5N, R91W	Dakota						RMAG 1954, O&G Fields p 229
Thornberg	T3N R91W	Dakota		12.5	45			RMAG 1954 p. 270
Thornburg	T3N, R91W	Dakota		12.6	54			RMAG 1961 O&G Field Vol. p. 246
Indian Run	T4N, R89-90W	Dakota	2900	15	33		no rpt.	RMAG 1961 O&G Field Vol. p. 156
Pinnacle	T3N, R86W	Dakota/Lakota		8.5	35	<1		RMAG 1962 P. 80
NW CO		Morrison		20+	10+			Special Completion Practices, RMAG 1962, p. 126
Maudlin Gulch	T4N R95W	Morrison					5,018	RMAG 1954 p. 202
Maudlin Gulch	T4N R95W	Morrison	6061	20	35-170 md	1.5	5,018	RMAG 1961 p.176
Maudlin Gulch	T4N R95W	Morrison	6060	12-20%	8.3	1.75	3,752	RMAG 1982 O&G Fields p. 338
Danforth Hills	T5N R95W	Morrison		17-23%	35-170 md			RMAG 1961 O&G Field Vol. p. 104
Wilson Creek	T2-3N R94W	Morrison		19.4	11		2,342	RMAG 1954 p. 288
Wilson Creek	T2-3N R94W	Morrison		19.4	11		2,342	RMAG 1961 p. 258
Wilson Creek	T3N R94W	Salt Wash	6500 avg	16 (10-23)	66		2,342	Stone, RMAG 1986, p. 234.
Iles Dome	T4N R92W	Morr, Entr.		no info				RMAG 1954
Iles Dome	T4N, R92W	Morrison		20	215			RMAG 1961 O&G Field Vol. p. 158
Moffat	T4-5N, R91W	Morrison						RMAG 1954, O&G Fields p 229
NW CO		Entrada		10-20 %	low to 500			Special Completion Practices, RMAG 1962, p. 126
Maudlin Gulch	T4N R95W	Entrada						RMAG 1954 p. 202
Maudlin Gulch	T4N R95W	Entrada	6391	20	400 av	0.55	14,024	RMAG 1961 p.176
Maudlin Gulch	T4N R95W	Entrada	6391	20	32.3	0.54	13,277	RMAG 1982 O&G Fields p. 338
Danforth Hills	T5N R95W	Entrada		20	400			RMAG 1961 O&G Field Vol. p. 104
Wilson Creek	T3N R94W	Entrada	6700 avg	19.6 (14-27)	38		16,566	Stone, RMAG 1986, p. 234.
Wilson Creek	T2-3N R94W	Entrada		19.7	35		16,566	RMAG 1954 p. 288
Wilson Creek	T2-3N R94W	Entrada		19.7	35		16,566	RMAG 1961 p. 258
Iles Dome	T4N, R92W	Entrada		13	?			RMAG 1961 O&G Field Vol. p. 158
Moffat	T4-5N, R91W	Entrada		17	20		2,499	RMAG 1954, O&G Fields p 229
Thornburg	T3N, R91W	Entrada		14.8	52			RMAG 1961 O&G Field Vol. p. 246
Pagoda	T4N R89W	Shinarump	4002	11.7	72			RMAG 1961 p. 208
Pinnacle	T3N, R86W	Shinarump		7				RMAG 1962 P. 80
Oak Creek	T3N, R86W	Shinarump						RMAG 1962 p. 77
NW CO		Weber		5-15 %	low			Special Completion Practices, RMAG 1962, p. 126
N. Douglas Creek	T1S R101-102W	Weber	7517	9	5.8			RMAG 1961 p. 116
Rangely	T1-3N R102-103W	Weber		16	20		108,053	RMAG 1954, p. 252
Rangely	T1-2N R 101-103W	Weber		12.5 av	10 av	0.08	109,268	RMAG 1961 p. 224
Rangely	T2N, R102W	Weber	6500	12 av (25max)	2 av (see*)			Bowker & Jackson 1989 RMAG p. 65
Rangely	T2N, R102W			local & extensive fractures				Bowker & Jackson 1989 RMAG p. 65
Rangely	T2N, R102W	Web Ark ss & slts (perm barriers)		3.5	0.023			Bowker & Jackson 1989 RMAG p. 76
Rangely	T2N, R102W	Weber cross laminated facies		7.5	0.298			Bowker & Jackson 1989 RMAG p. 76
Rangely	T2N, R102W	Weber massive (bioturb)		7.1	0.249			Bowker & Jackson 1989 RMAG p. 76
Elk Spgs & Winter Valley	T4-5N, R98W	Weber		fractured				McMillan RMAG 1986 p. 247
Elk Spgs & Winter Valley	T4-5N R98W	Weber	6097	4.5		2	4,900	RMAG 1961 p. 124
Elk Springs	T5N R98W	Weber		4.9	0 - 1.9 md			RMAG 1954 p. 130
Maudlin Gulch	T4N R95W	Weber	8323	11	2 av	0.3	29,430	RMAG 1961 p.176
Maudlin Gulch	T4N R95W	Weber	8323	12	3.4	0.29	30,742	RMAG 1982 O&G Fields p. 338
Danforth Hills	T5N R95W	Weber		6-13%	1-5 md			RMAG 1961 O&G Field Vol. p. 104
Thornberg	T3N R91W	Weber		4.4	0.6			RMAG 1954 p. 270
Thornburg	T3N, R91W	Weber		4.45	2		1,800	RMAG 1961 O&G Field Vol. p. 246
* 2 av along laminae, 0.4 across laminae (200max)								

[1] Table 1. Published porosity and permeability values by formation for oil and gas fields within the Sand Wash Basin study area.

Back to Text

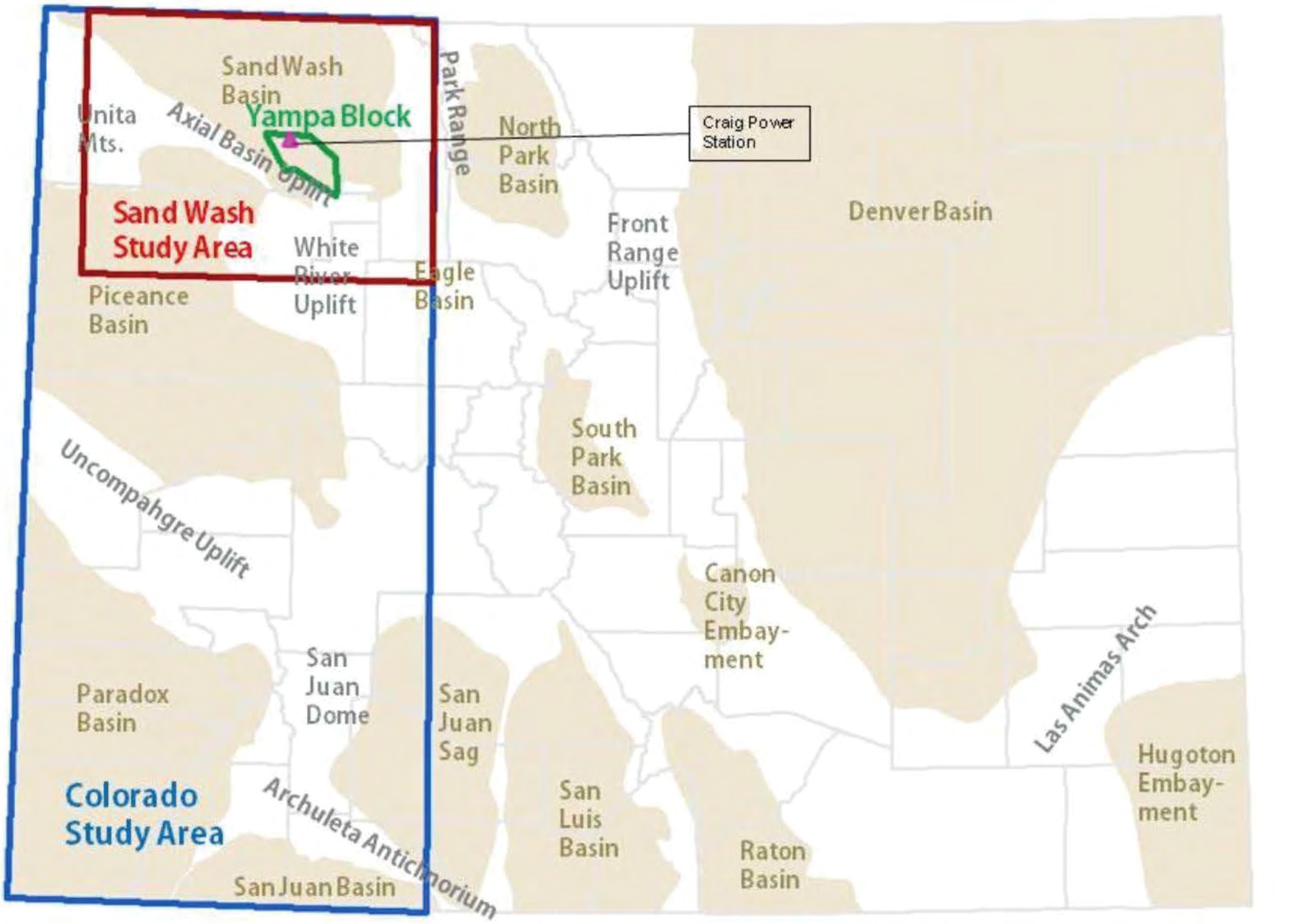


Figure 1. The extents of the three scales of study areas encompassed by this report and the basins and uplifts in Colorado.

Back to Text Pg.1

Back to Text Pg.13

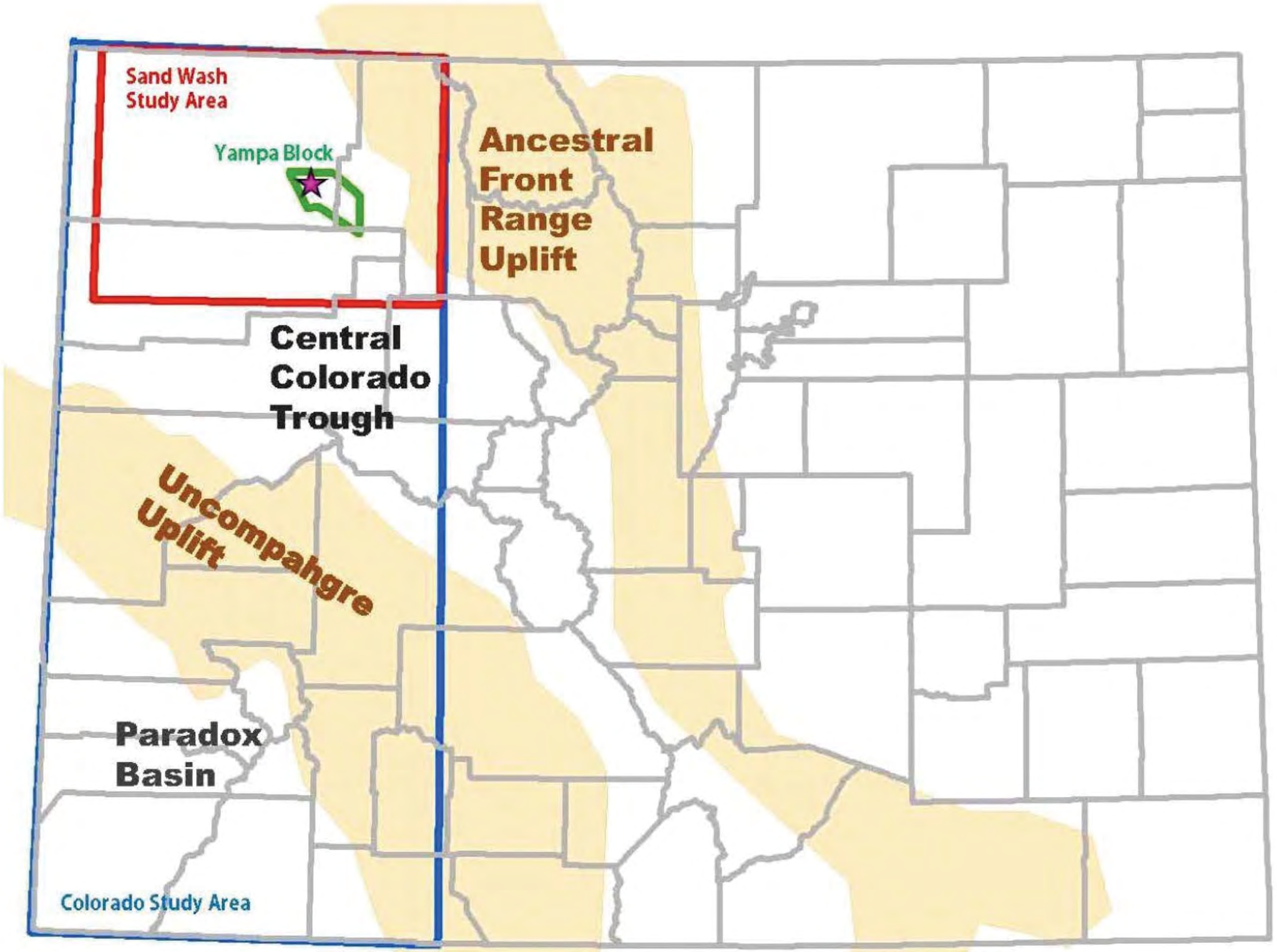


Figure 2. Locations of Ancestral Rockies uplifts and basins (Mallory, 1972, p. 132).

Back to Text

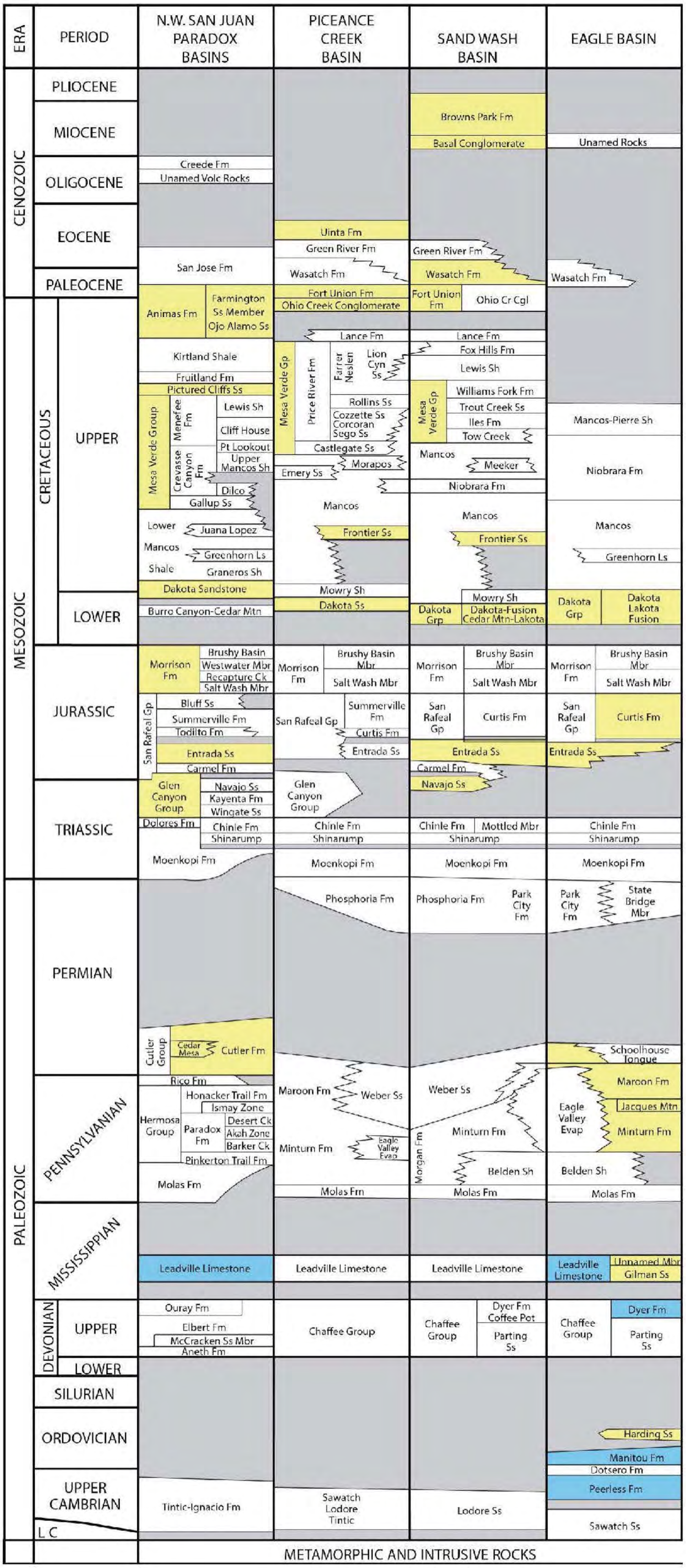


Figure 3. Stratigraphic chart for basins in the Colorado study area. (Irwin, 1977.)

Back to Text

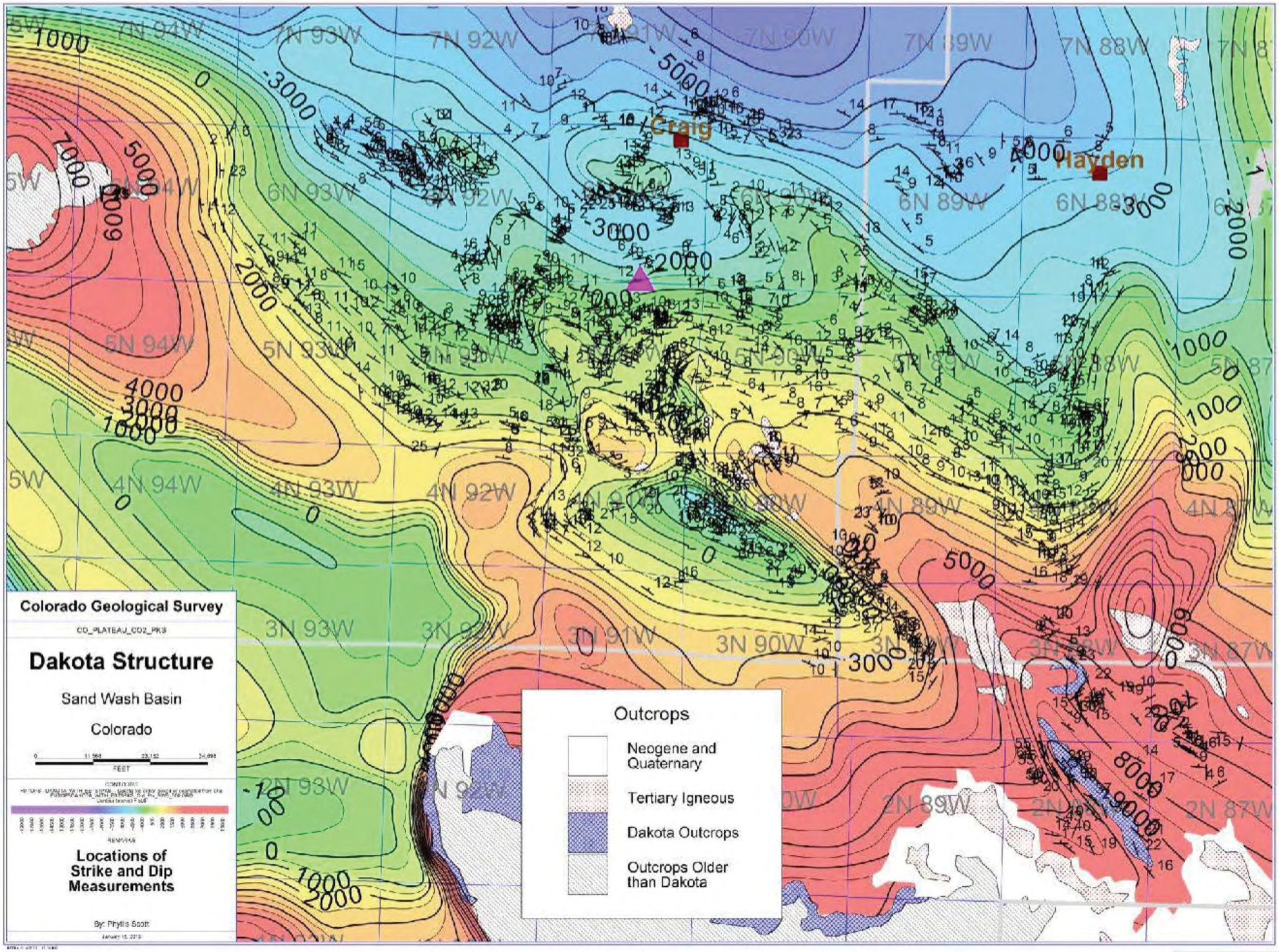


Figure 6. Locations of strike and dip measurements made by the Colorado Geological Survey superimposed on Dakota structure map.

Back to Text

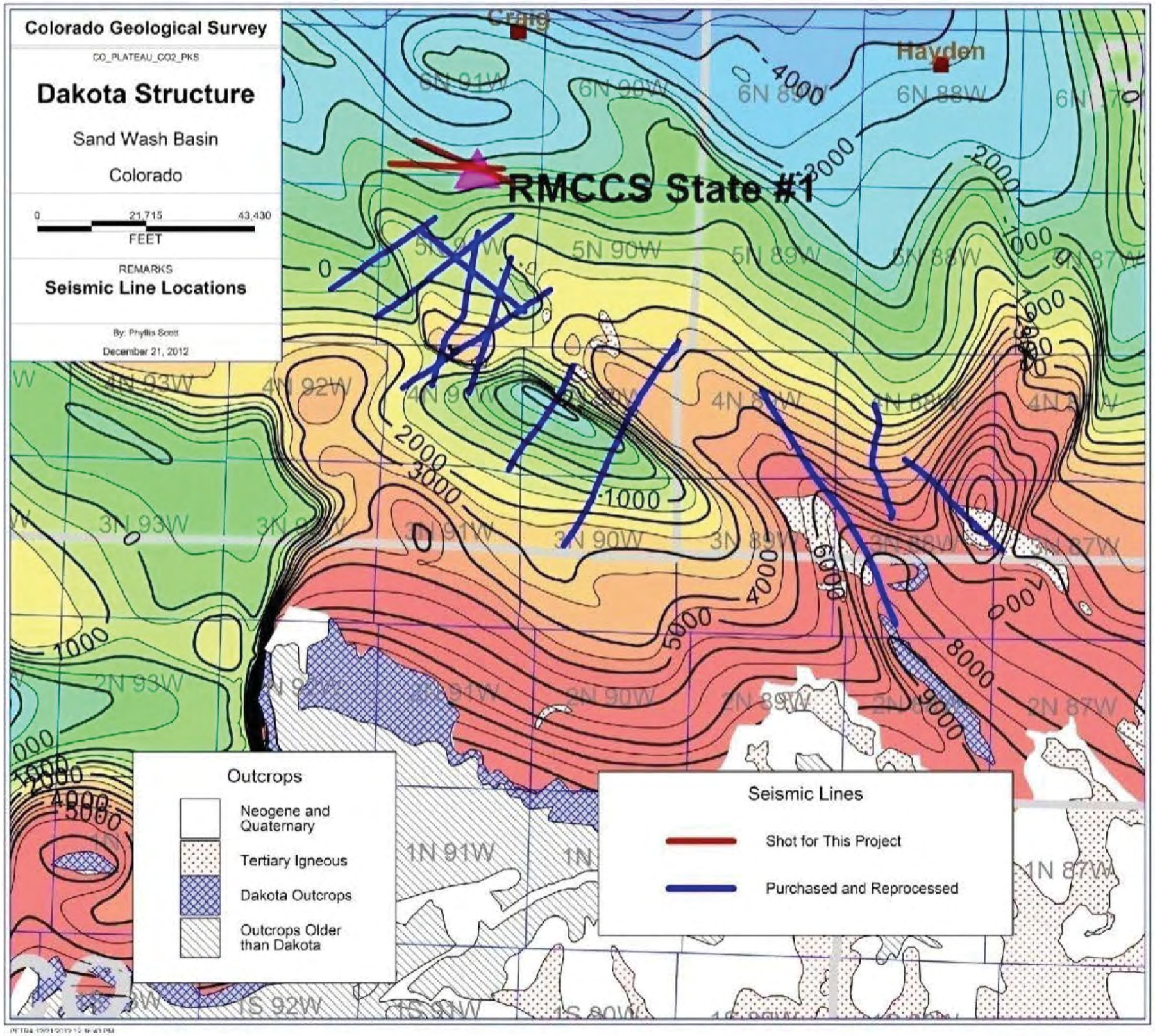


Figure 7. Locations of seismic lines that were shot or purchased for this study superimposed on Dakota structure map.

Back to Text

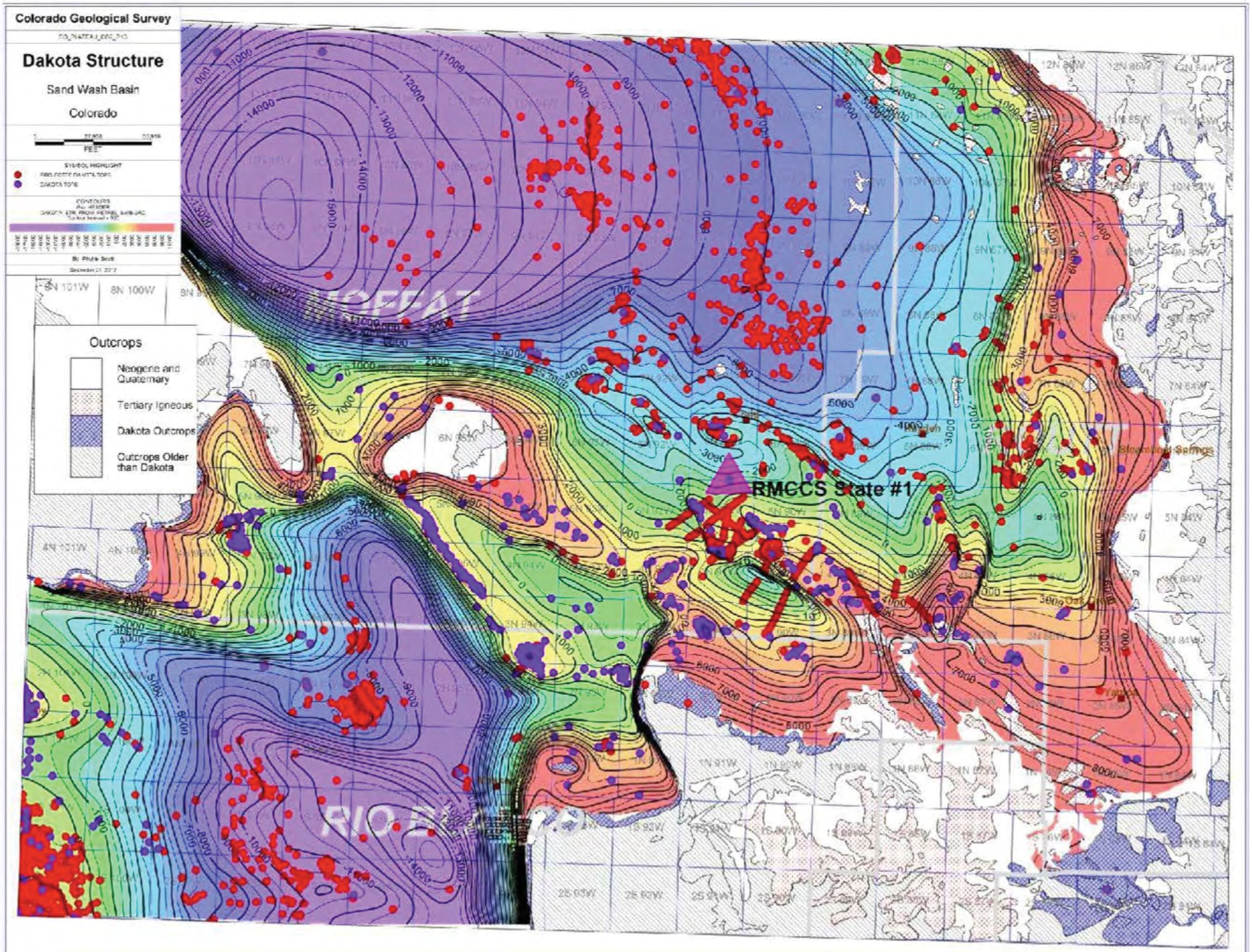


Figure 8. Structure map on top of the Dakota Sandstone saline aquifer, Sand Wash Basin study area. Locations of Dakota tops shown as purple dots; projected Dakota tops shown as red dots.

Back to Text

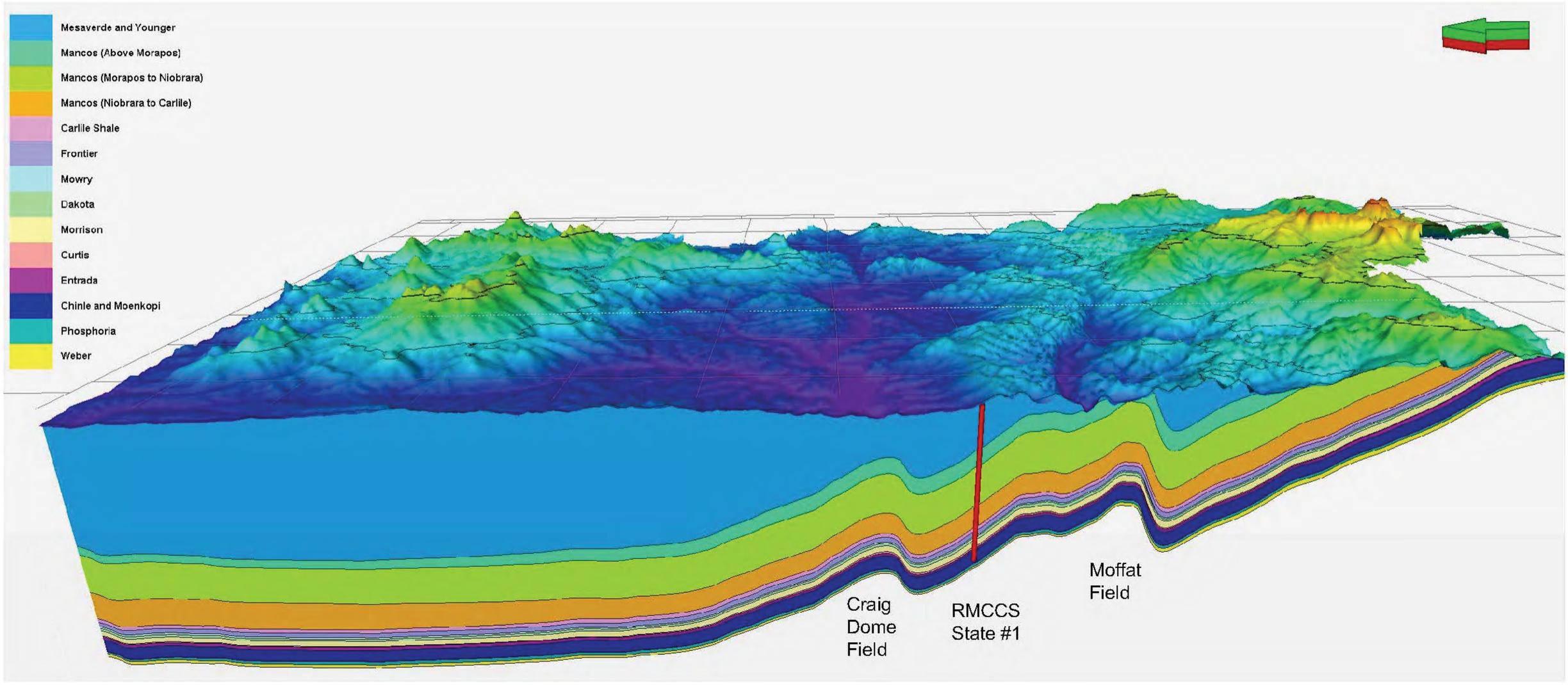


Figure 9. North-South cross section through Sand Wash Basin Petrel model. Wyoming border is at the left of the image and the White River Uplift is on the right. The RMCCS State #1 stratigraphic test well is shown in red.

Back to Text

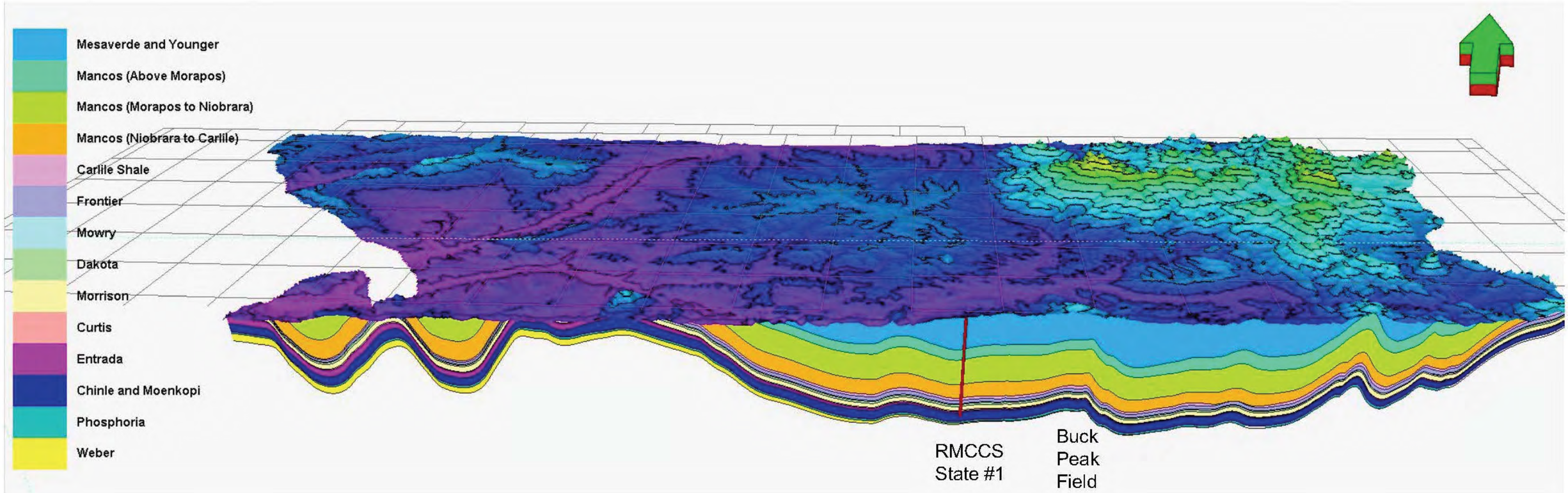


Figure10. West-East cross section through Sand Wash Basin Petrel model. The Uinta Mountains are on the left and the Park Range is on the rightt. The RMCCS State #1 stratigraphic test well is shown in red.

Back to Text

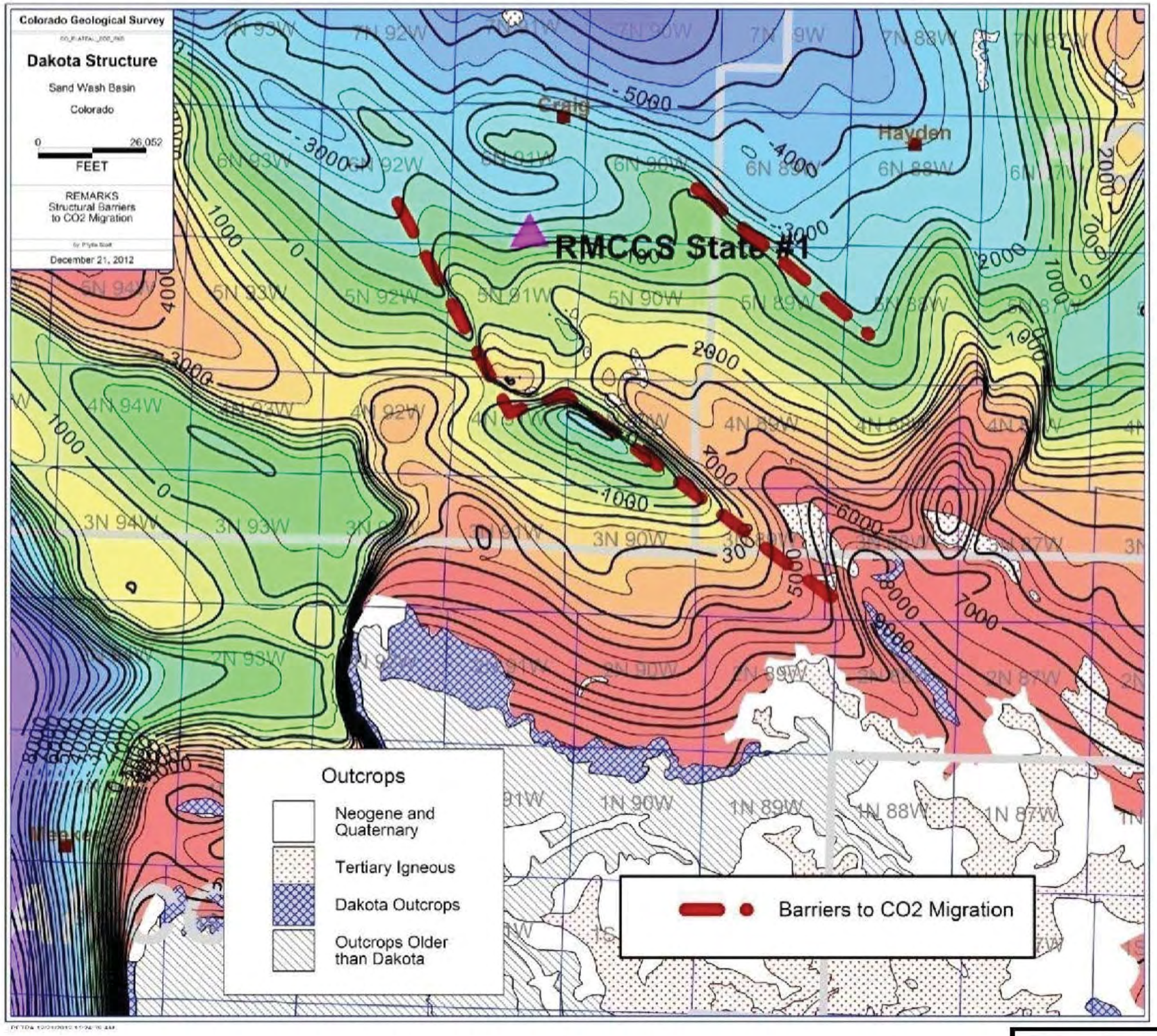


Figure 22. Barriers to CO_2 migration superimposed on Dakota structure map.

Back to Text

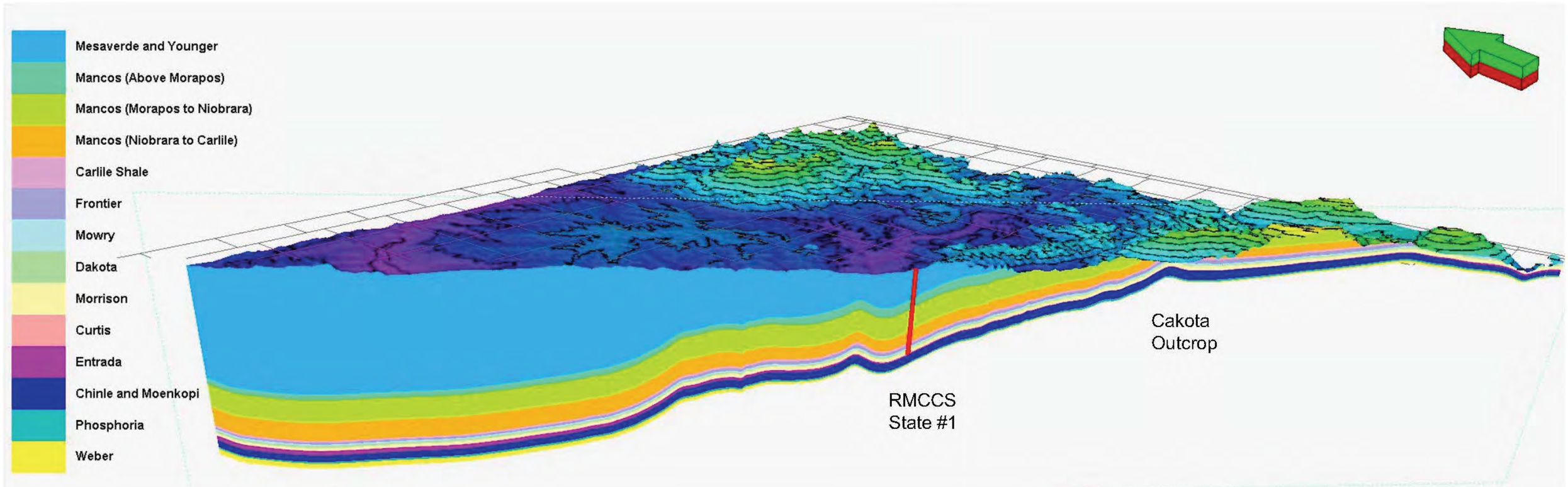


Figure 23. Northwest-Southeastast cross section through Sand Wash Basin Petrel model showing the possible pathway from the RMCCS State #1 well to the Dakota outcrop to the southeast. The model shows small undulations in the saline aquifers; it is not known if these are sufficient to trap injected CO_2. There may be fault barriers or permeability barriers that were not identified in the Petrel model.

Back to Text

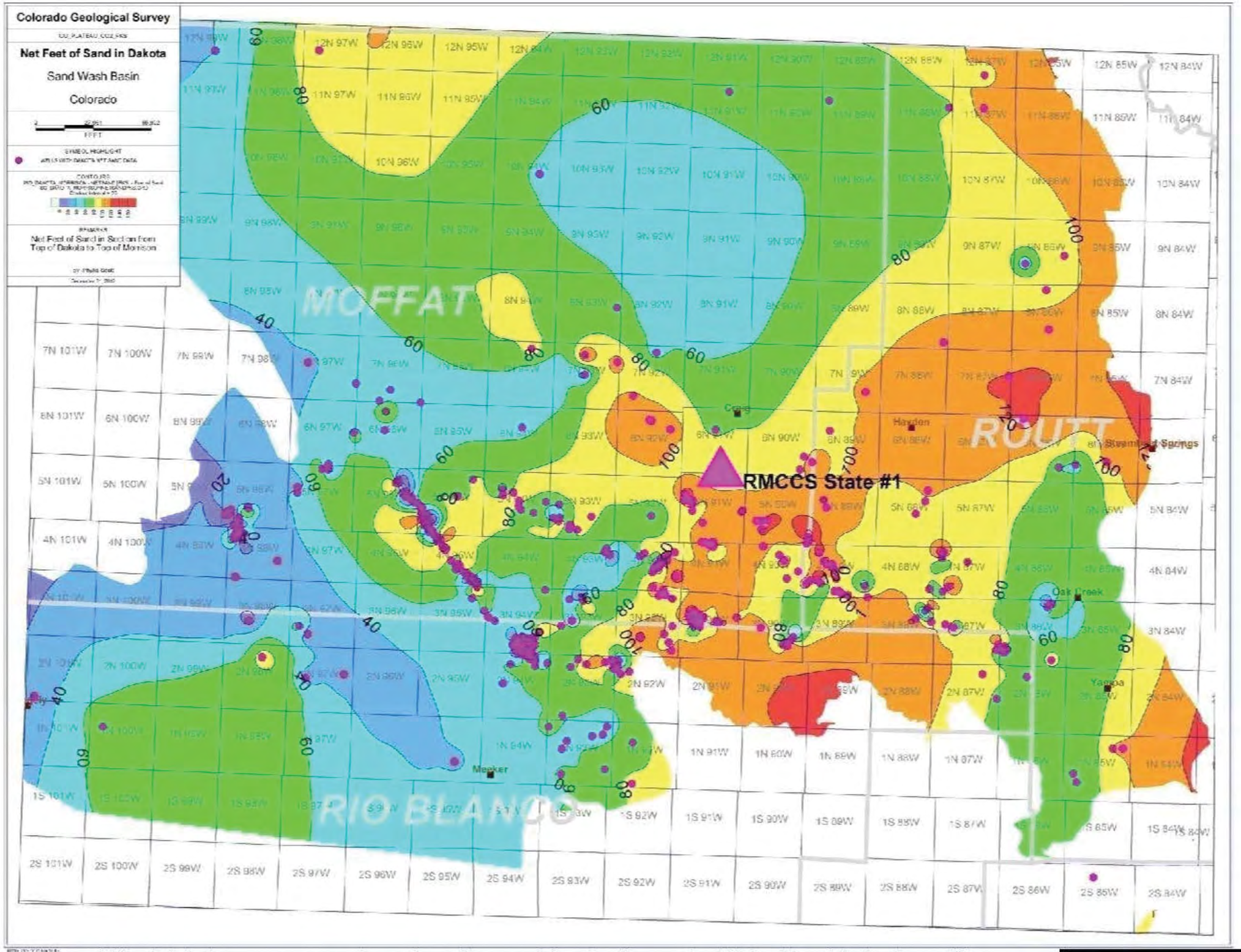


Figure 28. Thickness map showing the net feet of sand within the Dakota saline aquifer as interpreted from raster logs in the Sand Wash Basin. Contour interval is 20 feet.

Back to Text

Figure 41. Weber Average Porosity in Sands

33 Well Data Points

Purple Line = Outline of 3000 Foot Depth of Burial of Weber Formation

Back to Text

Figure 41

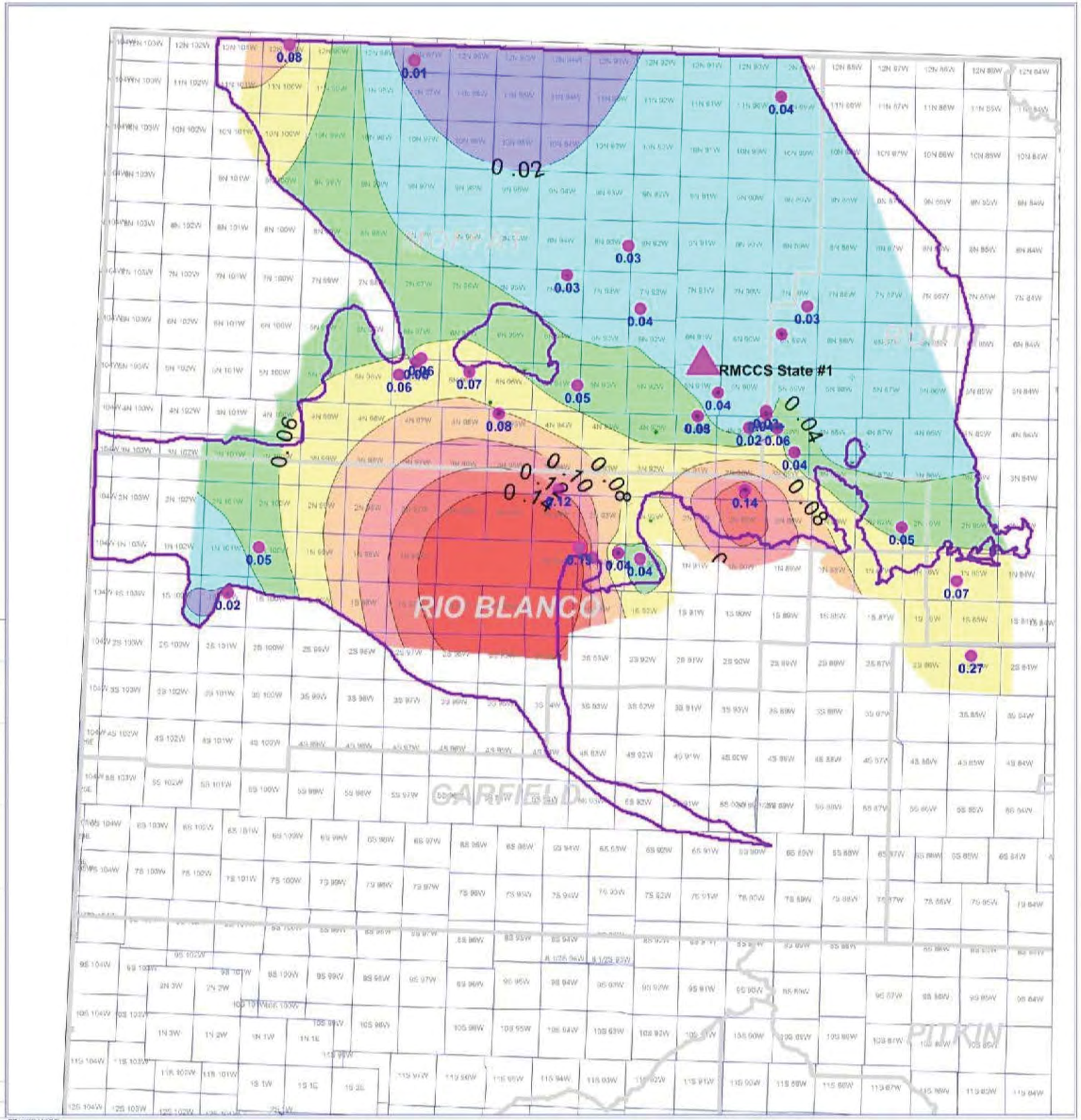


Figure 42. Weber Porosity Thickness (Average Porosity Times Net Feet of Sand)

33 Well Data Points

Purple Line = Outline of 3000 Foot Depth of Burial of Weber Formation

Back to Text

Figure 42

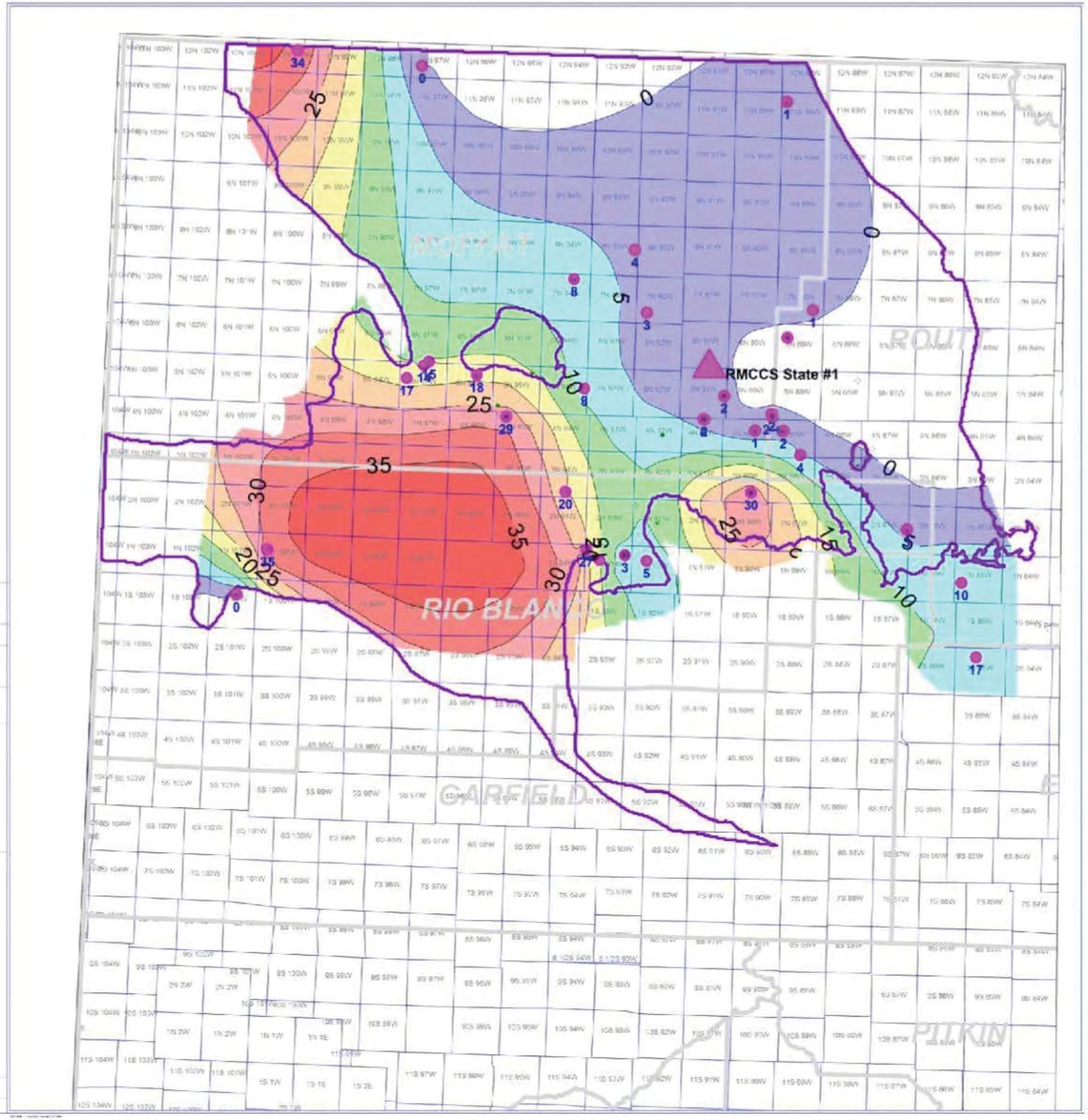


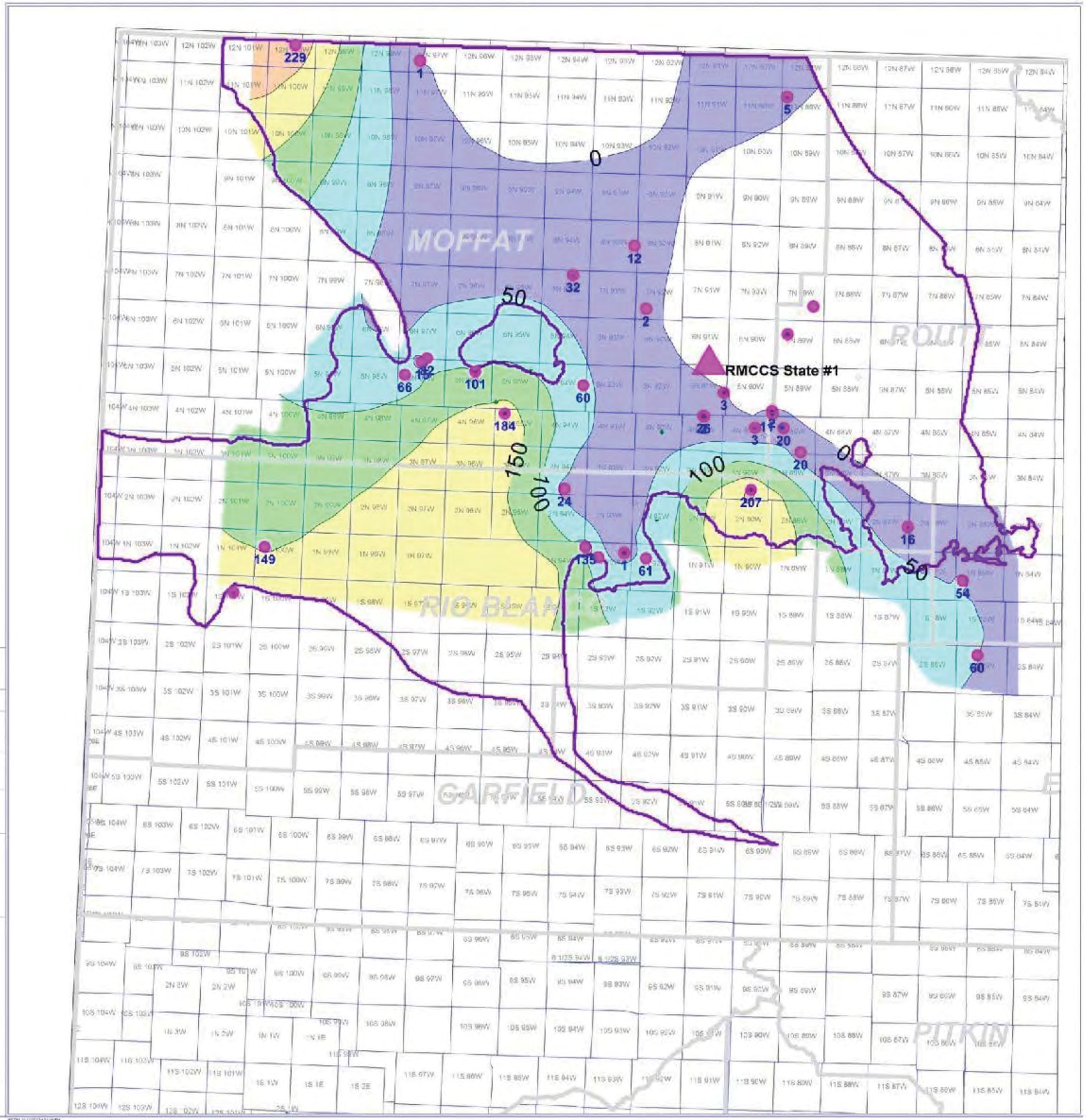
Figure 43. Weber Effective Net Sand (Net Feet of Sand with Porosity > 6%)

31 Well Data Points

Purple Line = Outline of 3000 Foot Depth of Burial of Weber Formation

Back to Text

Figure 43



Colorado Geological Survey

CO_PLATEAU_CO2_PKS

Western Colorado

FEET

WELLS WITH WEBER GR LAS

CONTOURS
WEBER_MAROON - NET_SD_6PCT [PKS] - Net
WEBER_MAROONNET_SD_6PCTPKS.GRD
Contour Interval = 50

REMARKS

Weber Formation Net Feet of Sand with Porosity > 6%

By: Phyllis Scott

November 12, 2013

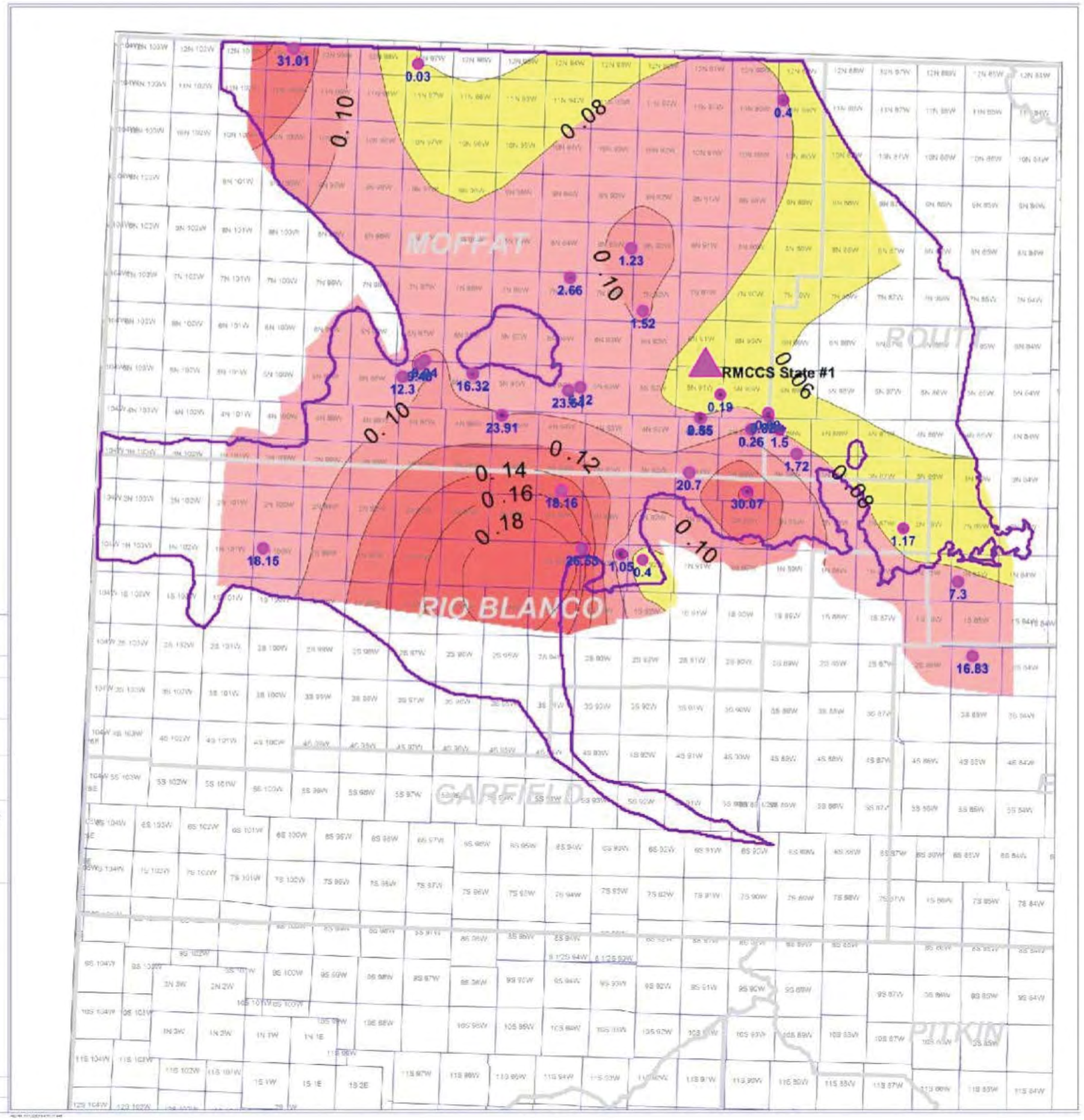
Figure 44. Weber Effective Average Porosity (in Sands with Porosity > 6%)

31 Well Data Points

Purple Line = Outline of 3000 Foot Depth of Burial of Weber Formation

Back to Text

Figure 44



Colorado Geological Survey

CO_PLATEAU_CO2_PKS

Western Colorado

FEET

WELLS WITH WEBER GR LAS

CONTOURS
WEBER_MAROON - PHIA_6PCT [PKS] - PHI A > 6% por
WEBER_MAROONPHIA_6PCTPKS.GRD
Contour Interval = 0.0199999995529652

REMARKS

Weber Formation Average Porosity (PHIA) for Net Sands

By: Phyllis Scott

November 12, 2013

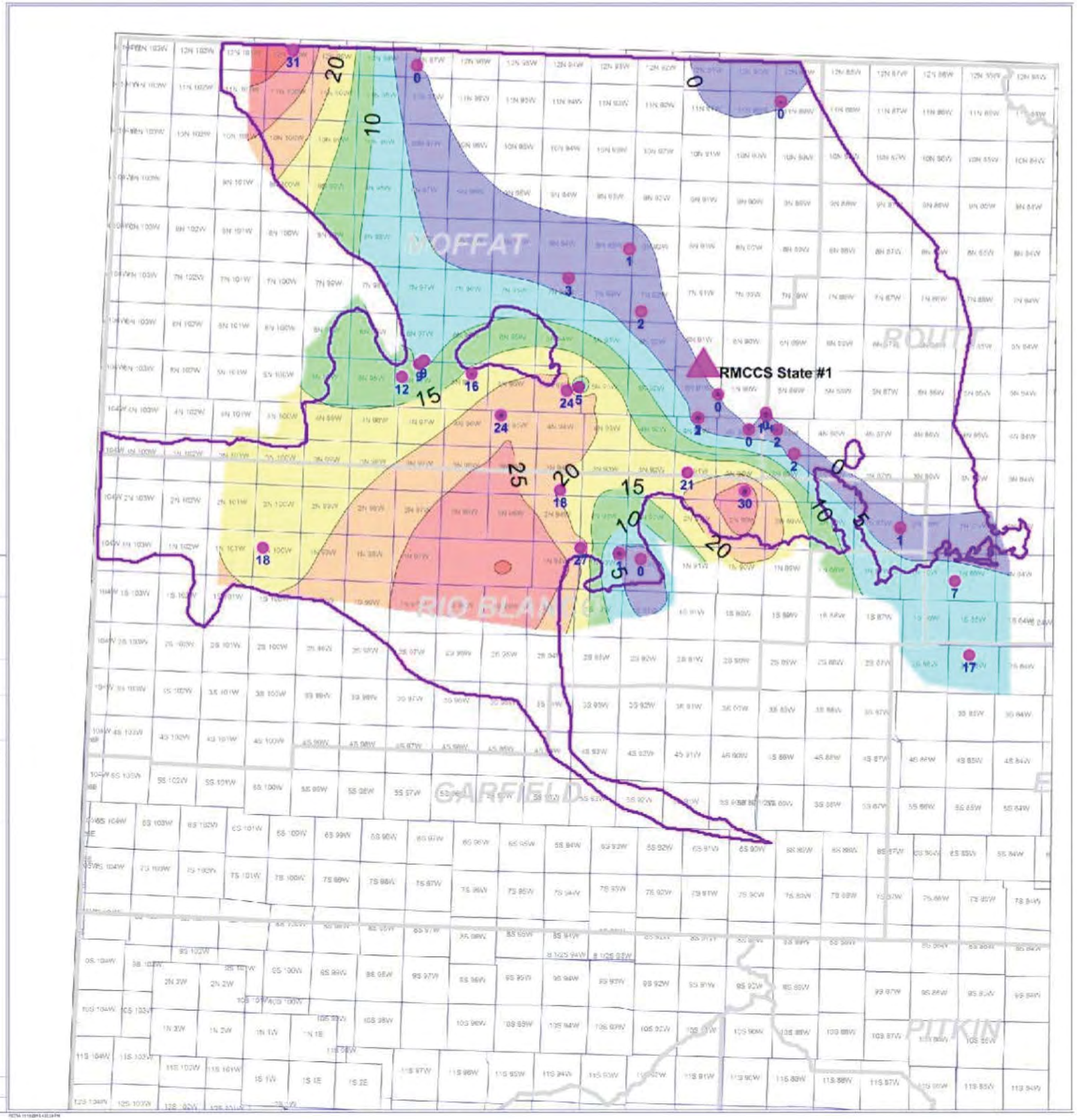
Figure 45. Weber Effective Porosity Thickness (Net Feet of Sand Times Average Porosity) in Sands with Porosity > 6%)

31 Well Data Points

Purple Line = Outline of 3000 Foot Depth of Burial of Weber Formation

Back to Text

Figure 45



APPENDIX G

Basic Summary of Drilling and Safety Plan

Project Overview

The primary goal of the project is to characterize three of the most promising carbon sequestration formations in the Rocky Mountain Region (including the Colorado Plateau) of the western U.S. In its regional capacity analyses for the Carbon Sequestration Atlas of the United States and Canada (NETL, 2009), the Southwest Partnership (SWP) identified the Cretaceous Dakota Sandstone, the Jurassic Entrada Sandstone, and the Pennsylvanian Weber Sandstone as three of the most promising geologic sequestration formations for the southwestern U.S. and the Rocky Mountain region in particular. Dakota and Entrada are ubiquitous throughout the region, and thus represent common sequestration candidates for most point sources in the region.

Work Description

Schlumberger Carbon Services will drill a characterization well to a depth of approximately 10,400' to determine if three formations are suitable for carbon sequestration. A well pad will be constructed on state section 34 of 6N-91W, Moffat County, CO. This section is within the boundaries of Trapper Mine. Patterson-UTI Rig 166 will move in and rig up on the well pad. A wellsite supervisor, rig supervisor, HSE Supervisor and wellsite geologist will have trailers on the well pad. The rig crew will have living quarters offsite and will be transported to and from site by MSHA certified drivers. Surface casing will be set at a depth of 1,500' and a string of protection pipe set at 5,500'. The well will be drilled to total depth and key zones cored. Once total depth is achieved wireline logs will be acquired and fluid samples extracted from each targeted formation. The well will then be plugged and abandoned according to Colorado Oil & Gas Conservation Commission guideline and the well pad reclaimed and returned to initial conditions. No further work is anticipated.

Site Specific Hazard Training

All members of the survey crew and all workers performing any activity on the site will receive complete and thorough site specific hazard training, including an approximately one hour class session and one hour field session. The training will be conducted by the project HSE Supervisor under the supervision of Trapper Mine safety and Environmental personnel in accordance to MSHA requirements. Each crew member will carry documentation certifying completion of the training at all times while on the mine premises. All access to the drill site will be coordinated by the site HSE supervisor. All vehicles accessing the site will be met at the gate and directly escorted to the site and will be escorted back to the gate once the work or delivery is complete. Any movement off the direct route to the drill site will only be performed by personnel with current comprehensive miner training.

An on-site safety meeting will be held at the beginning of each day to review the day's plan and coordinate activities with mine operations. Safety meeting notes will be recorded and copies provided upon request.

Operational Safety Plan Overview

1. All Workers will complete Trapper Site Specific Training and carry documentation at all times.
2. All workers will be restricted to the well location
3. Workers will be escorted from the Trapper Gate directly to the rig site by MSHA compliant transport vehicles operated by MSHA trained HSE Supervisors.
4. All project vehicles entering the mine site will be MSHA compliant.
5. Any workers performing any operation outside the well pad will have completed the New Miner Comprehensive training.
6. A MSHA certified electrician will be on call

Crew MSHA compliance

All crew and equipment will fully comply with the MSHA Code of Federal Regulations. In particular, all crew members will wear hard hats, safety vests with reflectors, safety glasses and steel-toe boots at all times on location. All vehicles will be in good shape with no leaking fluids and will be equipped with 12 ft whip flags for visibility and have fire extinguishers that are certified within the past six months. Parked vehicles will be chocked on the down-hill side with the parking brake engaged. All crew electrical equipment will be inspected by an MSHA certified electrician to assure compliance and any electrical work will be performed under the direct supervision of an MSHA certified electrician.

Timing

Rig crew will work two twelve hour shifts, changing at approximately 6 am and 6 pm. The crew will be housed offsite and transported to and from the rig by the HSE supervisor. Work will last a period of approximately 60 consecutive days. The anticipated survey dates are from December 20, 2011 to February 6, 2012. There will be supervision, emergency vehicles on standby, snow removal equipment on standby and full satellite communication 24 hrs a day.

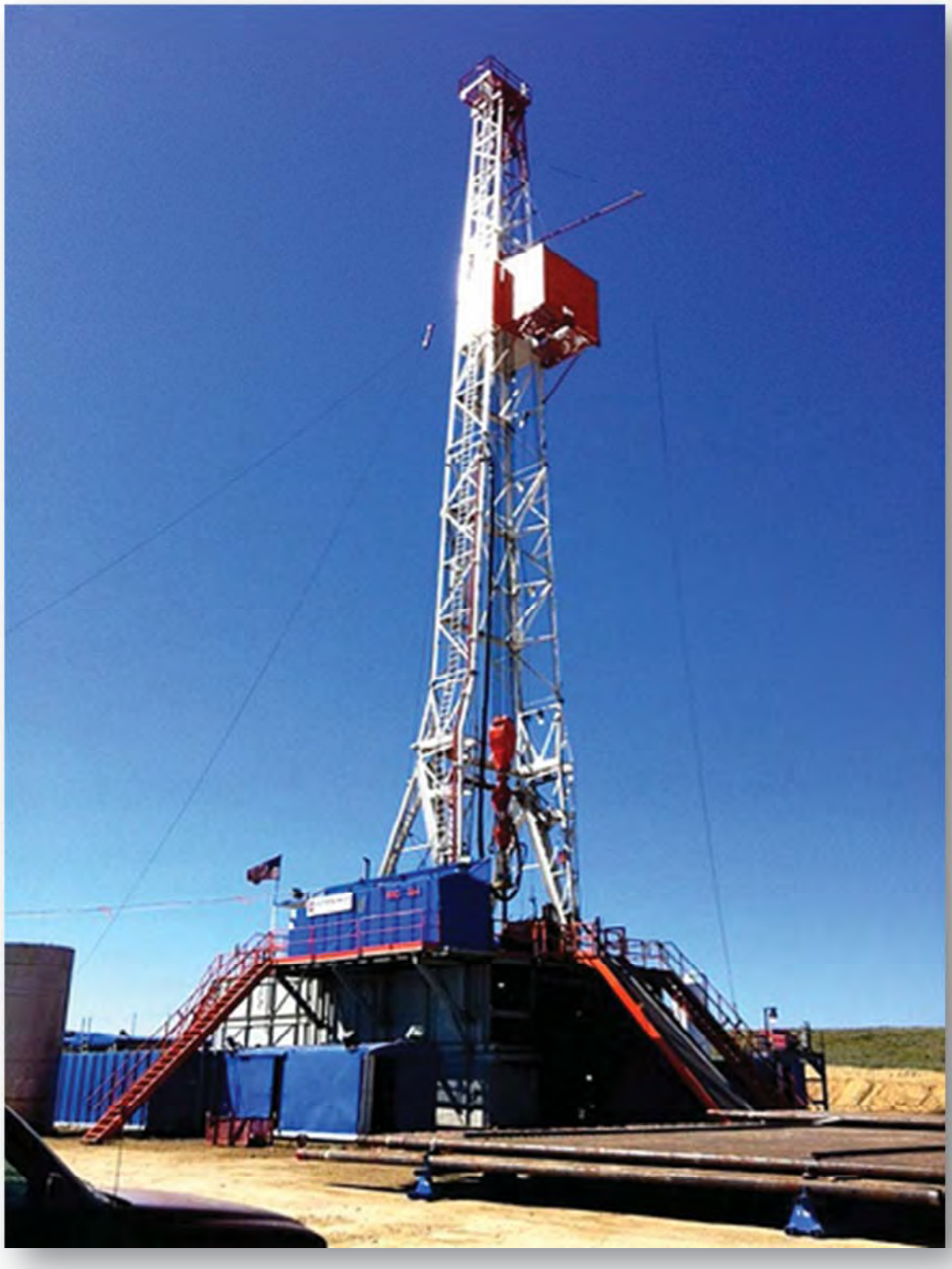
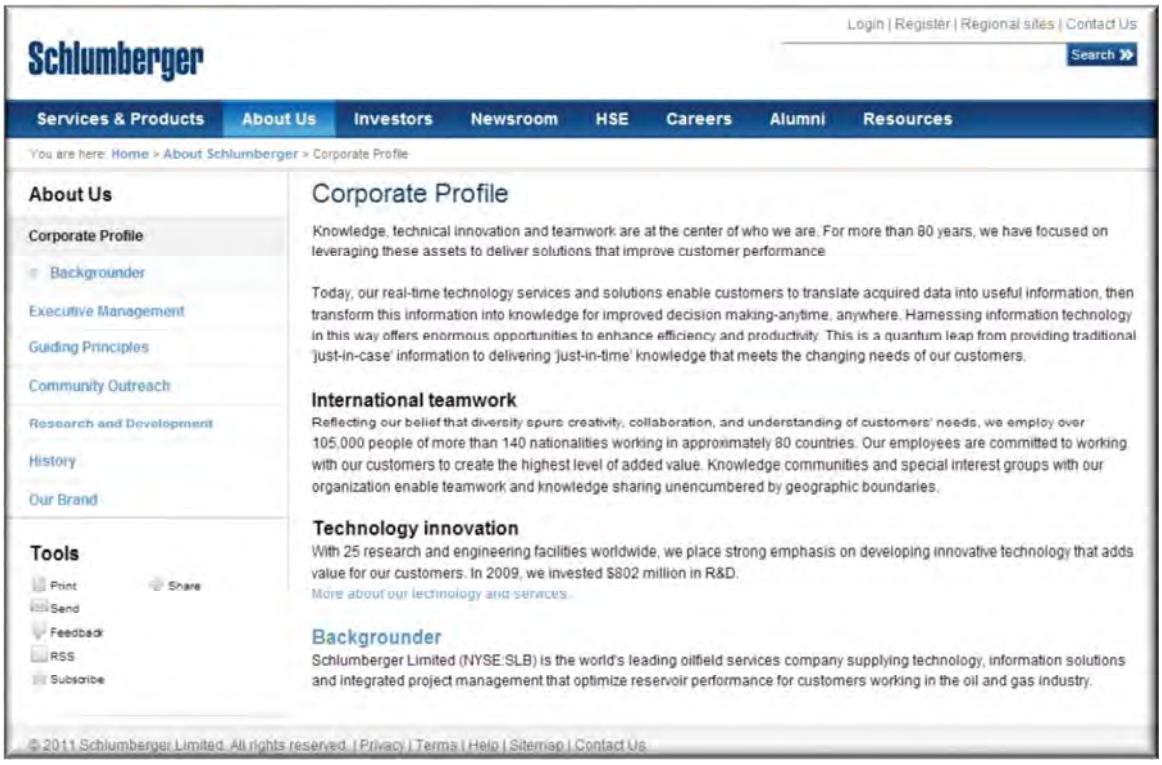


Figure 1. Patterson-UTI Rig 166



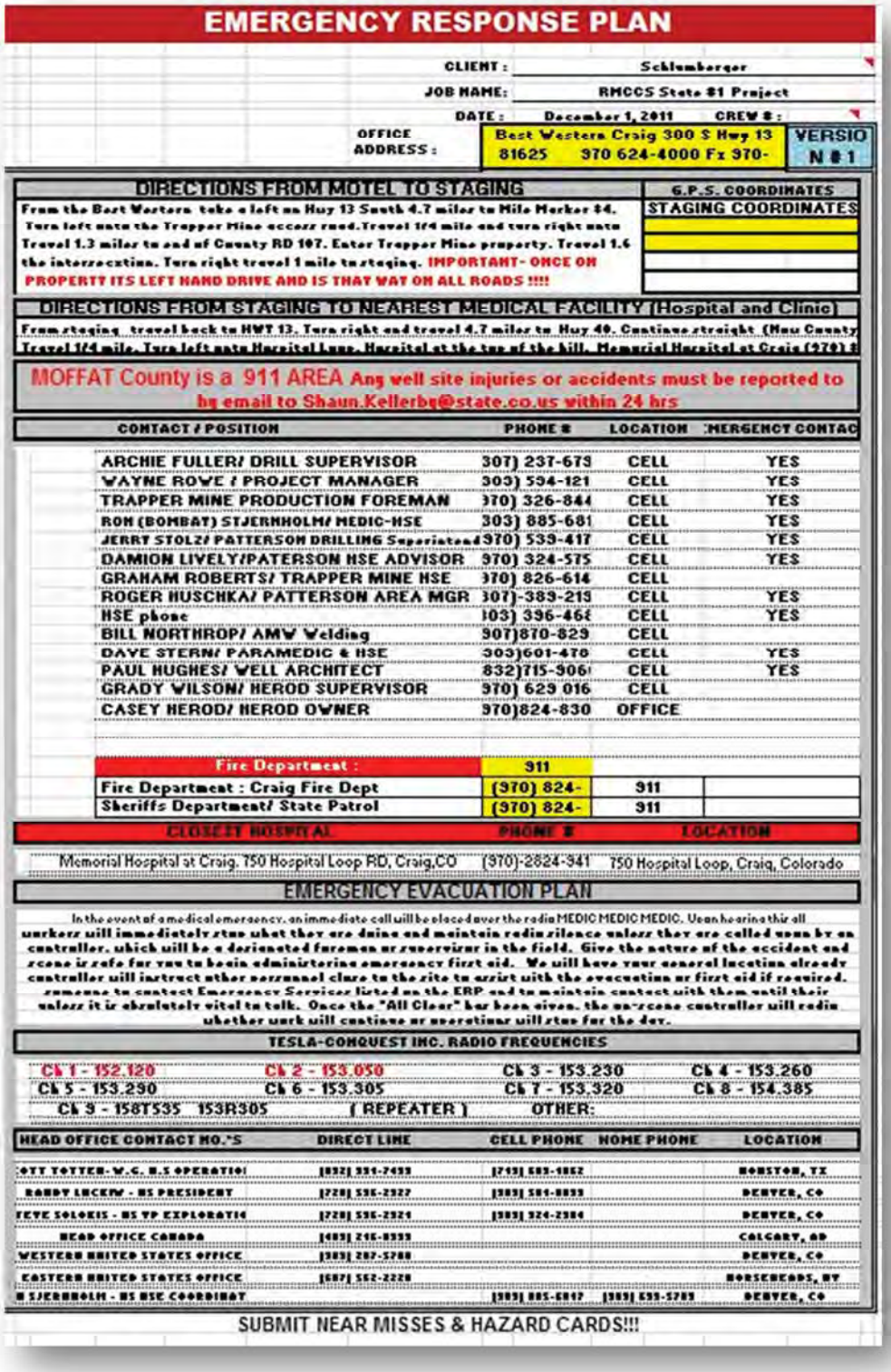
Figure 2. Site map with key operational points



http://www.slb.com/about/who.aspx



http://www.slb.com/hse.aspx



EMERGENCY RESPONSE PLAN

CLIENT : Schlumberger

JOB NAME: RMCCS State #1 Project

DATE : December 1, 2011 CREW # :

OFFICE ADDRESS : Best Western Craig 300 S Hwy 13 81625 970 624-4000 Fx 970- | VERSION # 1

DIRECTIONS FROM MOTEL TO STAGING

From the Best Western take a left on Hwy 13 South 4.7 miles to Mile Marker 84. Turn left onto the Trapper Mine access road.Travel 1/4 mile and turn right onto Travel 1.3 miles to end of County RD 107. Enter Trapper Mine property. Travel 1.6 the intersection. Turn right travel 1 mile to staging. IMPORTANT- ONCE ON PROPERTY ITS LEFT HAND DRIVE AND IS THAT WAY ON ALL ROADS !!!!

G.P.S. COORDINATES

STAGING COORDINATES

DIRECTIONS FROM STAGING TO NEAREST MEDICAL FACILITY (Hospital and Clinic)

From staging travel back to HWY 13. Turn right and travel 4.7 miles to Hwy 40. Continue straight (Now County Travel 1/4 mile. Turn left onto Hospital Loop. Hospital at the top of the hill. Memorial Hospital at Craig (970) 8

MOFFAT County is a 911 AREA Any well site injuries or accidents must be reported to by email to Shaun.Kellerby@state.co.us within 24 hrs

CONTACT / POSITION	PHONE #	LOCATION	EMERGENCY CONTAC
ARCHIE FULLER/ DRILL SUPERVISOR	307) 237-673	CELL	YES
WAYNE ROWE / PROJECT MANAGER	305) 534-121	CELL	YES
TRAPPER MINE PRODUCTION FOREMAN	970) 326-844	CELL	YES
RON (BOMBAT) STJERNHOLM/ MEDIC-HSE	303) 885-681	CELL	YES
JERRY STOLZ/ PATTERSON DRILLING Superintend	970) 539-417	CELL	YES
DAMION LIVELY/PATERSON HSE ADVISOR	970) 324-575	CELL	YES
GRAHAM ROBERTS/ TRAPPER MINE HSE	970) 826-614	CELL	
ROGER HUSCHKA/ PATTERSON AREA MGR	307)-383-215	CELL	YES
HSE phone	303) 396-468	CELL	YES
BILL NORTHROP/ AMW Welding	907)870-829	CELL	
DAVE STERN/ PARAMEDIC & HSE	303)601-478	CELL	YES
PAUL HUGHES/ WELL ARCHITECT	832)715-906	CELL	YES
GRADY WILSON/ HEROD SUPERVISOR	970) 629 016	CELL	
CASEY HEROD/ HEROD OWNER	970)824-830	OFFICE	

Fire Department :	911		
Fire Department : Craig Fire Dept	(970) 824-	911	
Sheriffs Department/ State Patrol	(970) 824-	911	

CLOSEST HOSPITAL	PHONE #	LOCATION
Memorial Hospital at Craig, 750 Hospital Loop RD, Craig,CO	(970)-2824-341	750 Hospital Loop, Craig, Colorado

EMERGENCY EVACUATION PLAN

In the event of a medical emergency, an immediate call will be placed over the radio MEDIC MEDIC MEDIC. Upon hearing this all workers will immediately stop what they are doing and maintain radio silence unless they are called upon by an controller, which will be a designated foreman or supervisor in the field. Give the nature of the accident and scene is safe for you to begin administering emergency first aid. We will have your general location already controller will instruct other personnel close to the site to assist with the evacuation or first aid if required. someone to contact Emergency Services listed on the ERP and to maintain contact with them until their unless it is absolutely vital to talk. Once the "All Clear" has been given, the on-scene controller will radio whether work will continue or operations will stop for the day.

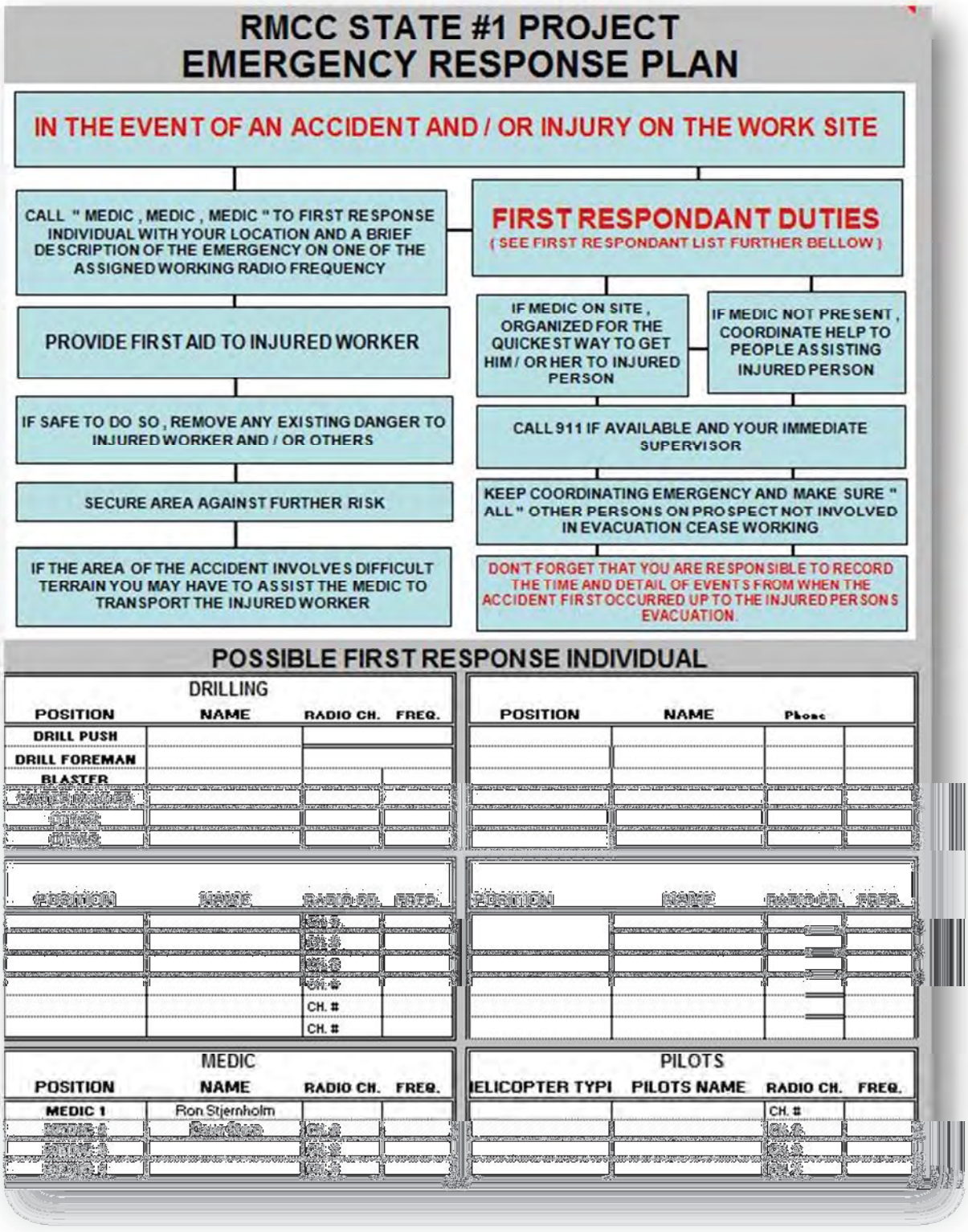
TESLA-CONQUEST INC. RADIO FREQUENCIES

Ch 1 - 152.120	Ch 2 - 153.050	Ch 3 - 153.230	Ch 4 - 153.260
Ch 5 - 153.290	Ch 6 - 153.305	Ch 7 - 153.320	Ch 8 - 154.385
Ch 9 - 158T535 153R305	(REPEATER)	OTHER:	

HEAD OFFICE CONTACT NO.'S	DIRECT LINE	CELL PHONE	HOME PHONE	LOCATION
OTT TOTTEN-W.C. U.S OPERATIO	(832) 351-7433	(713) 583-1852		HOUSTON, TX
RANDY LUCKOW - US PRESIDENT	(720) 535-2327	(303) 564-8833		DENVER, CO
STEVE SOLOKUS - US VP EXPLORATIO	(720) 535-2321	(303) 324-2384		DENVER, CO
HEAD OFFICE CANADA	(403) 215-8333			CALGARY, AB
WESTERN UNITED STATES OFFICE	(303) 297-5788			DENVER, CO
EASTERN UNITED STATES OFFICE	(607) 562-2228			HORSEHEADS, NY
B SJERNHOLM - US HSE COORDINAT		(303) 885-6817	(303) 659-5785	DENVER, CO

SUBMIT NEAR MISSES & HAZARD CARDS!!!

Emergency Response Plan (page 1)



Emergency Response Plan (page 2)

APPENDIX H

Drilling Chronology

Contents

Topic

Brief Chronology of Significant Events

APPENDIX H - Drilling Chronology

October 2011

The drilling contract terms and conditions with Patterson-UTI Rig 166 were agreed to and signed by Patterson on October 11, 2011. A copy of the drilling contract is included in Appendix O. The contract was executed once we received land access from Trapper Mine. The Colorado Oil and Gas Conservation Commission Form 2 "Application for Permit-to-Drill" for RMCCS STATE NO. 1 was issued on October 28. A waiver of the winter elk stipulations from December 1 through April 15, were granted by the Division of Wildlife. Advance notice to drill was issued to Moffat County and the Colorado Land Board. The well "Stormwater Plan" was approved by the Division for Health and Environment on October 26. The final approval necessary to begin location construction was the access agreement with Trapper Mine., home base for rig 166. Rig 166 at the time was drilling a long lateral near Worland, WY. At the time the estimation for finishing that well was November 20, 2011 so preparation activity was underway to be ready to begin drilling the RMCCS well in early December. Copies of the well permits are detailed in Appendix O.

November 2011

The agreement with Trapper Mine was executed on November 1, 2011 representing the final approval necessary to begin location construction. The pad construction and mud pit work began on November 10 and was completed by Anson Construction, out of Craig, on November 30. Trailer and wellsite accommodations were ready to be moved in the first week in December. The "Drill the Well On Paper" exercise was conducted November 10 and 11 in FT Lupton, CO, home base for rig 166. Participation was excellent with thirty participants from Patterson, Schlumberger, Colorado Geologic Survey and various third parties. At that time Rig 166 was drilling a long lateral near Worland, WY. The current estimation for finishing that well was December 14 when the rig would mobilize to Craig to begin drilling the RMCCS well. Unfortunately, the well operator had significant difficulty drilling the horizontal well ultimately delaying our spud by 45 days from the original expected date.



Figure 5.3 - Well pad construction.

December 2011

By December 1st our well pad and pits were built, all drilling permits obtained, conductor pipe set, blow-out preventer ready and everything necessary to begin drilling was in place and waiting for Patterson rig 166 to be released by the well operator. Under standard oilfield drilling contracts, once a rig begins drilling for a well operator, the rig is bound to the well operator until they are "released". When we signed the contract with Patterson in October, the RMCCS well

was the next well on the rig 166 schedule after a wildcat lateral underway near Worland, WY. The anticipated release was date November 14. Due to severe drilling difficulties the well operator did not finally complete drilling their well until December 28, fifty days later than anticipated. Patterson 166 was released for beginning work on the RMCCS well on January 2nd.

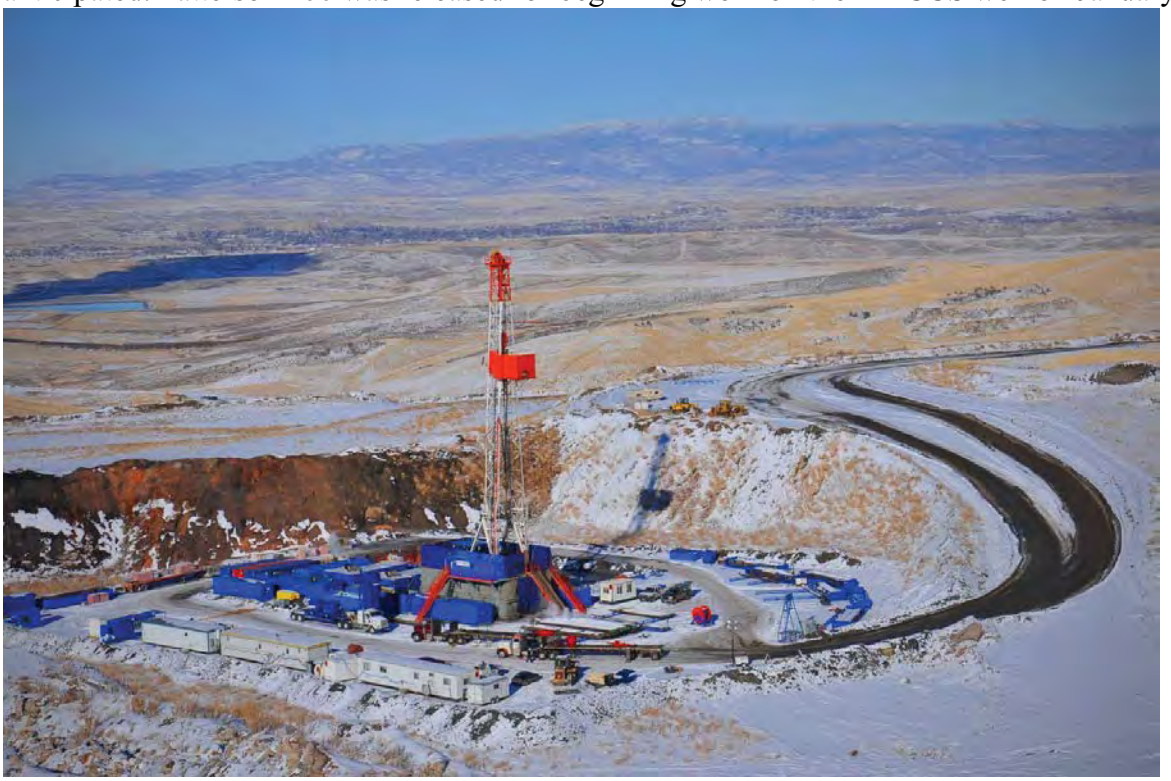


Figure 5.4 – Patterson 166 during drilling operations on Trapper mine, Craig, CO.

January 2012

On January 3rd, trucking company, Hempfill-Speedy, began loading and making the 350 mile move to Craig. By January 7 the entire rig was at the location and the mast went in the air on January 10. It would take another five days to get the rig operational and fully compliant with Mining Safety and Health Administration (MSHA) regulations. Drilling a well on land regulated by MSHA introduced significant challenges and the lessons learned in drilling this well will be invaluable for future projects. The primary impact of MSHA fall in two categories: site access and rig compliance. Every worker entering the mine site must receive "Site Specific Miner Training" and vehicles must be inspected and certified to meet regulations. The project engaged MSHA Safety specialists, Stjernholm Consulting, led by Ron Stjernholm and associate David Stern. The project used the Best Western Motel, five miles south of the site, as the base of operations. All access to the site was coordinated by the safety supervisors. Workers received their training at the hotel and vehicles were brought up to specification. They were then led through the Trapper Mine gate using a special code and taken to the drill site where they received special rig orientation and safety training. Overall, site access was extremely effective and 293 workers were trained for activity directly associated with the well. Preparing the rig to meet MSHA regulations proved to be much more difficult. The rig was pre-inspected while on location at the previous well. Although this provided some advance preparation, it required two MSHA certified welding crews and three MSHA certified electricians four extra days to bring the rig to full compliance. The rig was inspected and approved by the MSHA Craig District Lead

inspector on January 13. The inspector indicated he was very pleased with the rig, the well pad, trailers and vehicles parked at the drill site and made no citations.

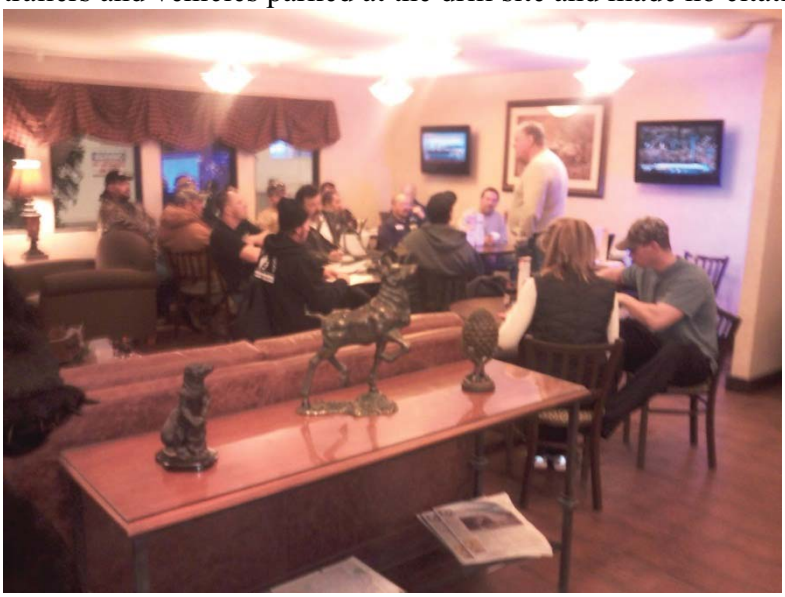


Figure 5.5 MSHA Safety training, Best Western Lobby, Craig, CO.

On January 15 at 05:00 the rig began drilling the RMCCS State No. 1. Within twelve hours of spud we began experiencing lost drilling fluid, or "lost circulation". This means the drilling fluid used to: remove the rock debris created by the drill bit, lubricate the drill bits, prevent the bore from collapsing and preventing potential blowouts, began flowing into the layers being penetrated. It was believed by the wellsite geologist that the seepage was into the many coal seams encountered in the near-surface strata. Extra water haulers were called in and special lost circulation techniques were employed to slow the flow. Lost circulation was a consistent problem throughout the entire initial stages of drilling and reduced the penetration rate significantly, increasing the cost of material used for the drilling fluid. Although lost circulation is a fairly common occurrence, the volume experienced in drilling the upper well strata was significant. Once the well reached a depth of 1,394' the 13 3/8" casing was set and cemented to surface.

Drilling continued through the next section with a 12 ¼ inch drill bit towards an intermediate casing point of 5,400'. By January 3,1 the well was at a depth of 4,818' with all deviation surveys less than 2.5 degrees.

February 2012

On February 1 the well was at a depth of 4,818', drilling towards the intermediate casing point of 5,400'. On February 2, we had well loggers on location and ran the Platform Express-Sonic Scanner to surface casing. These tools provide basic rock properties to construct the geologic model of the subsurface, including porosity, mineralogy, fluid saturation, as well as rock mechanical properties and measurements necessary to correlate the seismic data from time to depth reference.

The rig then ran 9 5/8" intermediate casing string and was cemented up to 700' above the shoe. The intermediate casing completely shut off any further losses of drilling fluid into the formation. Unfortunately, the lost circulation experienced throughout January had been continuing, even if largely under control. Various drilling fluid additives, such as lost circulation

material (LCM), were added and it was necessary to continually haul extra water loads to keep the reserves at an adequate level.

By early February it was becoming clear that the combination of higher mobilization cost due to rig scarcity, three additional days to get the rig up to MSHA safety standards, and the slower penetration rate and added mud costs due to lost circulation, were all contributing to higher drilling costs than budgeted a year earlier. It is common practice in the oil and gas industry to have a reserve fund of 10% - 25% to for foreseen events adding significantly to well cost. This is particularly true in the first penetration into an area, which is traditionally referred to as a "wildcat" well, such as the RMCCS well. Since our budget did not have a contingency reserve, several meetings were conducted with the project leadership and the NETL and a series of cost VS budget scenarios looking forward were reviewed.

By February 9, the penetration had reached the Niobrara core point. Shell, a partner in the project from its inception, provided an additional $335,000 specifically to core the Niobrara Shale. After two unsuccessful attempts to get core in the upper Niobrara, it was decided to drill ahead to the primary zone of interest and successfully retrieve 60' of full core from the Niobrara. The Niobrara formation is a potential unconventional additional target for future geologic storage not in the original plan.

During the second week of February, to compensate for the projected shortfall, an additional $650,000 was shifted from regional characterization to the drilling budget. As we continued drilling into the reservoir section the well trajectory began drifting away from vertical and deviating towards the south. If this drift continued the drilling manager for Schlumberger was concerned it would dramatically increase the risk of getting stuck during coring and well logging. If the drill string or logging tools became stuck, it could easily exhaust the remaining budget significantly compromising most of the site specific scientific objectives of the project. It was decided to add directional steering capabilities with motors to increase RPM. The main strategy was to limit deviation, keep dog-leg severity to a minimum and increase rate of penetration (ROP) to offset the additional cost. The penetration rate initially improved dramatically to up to 50 FPH, but drilling ahead was much slower and tougher than anticipated.

By February 16, the rig had reached the next core section, the Mowry seal and Dakota sandstone. The original plan had been to go in with a core barrel just above the Dakota top to sample the seal directly above the Dakota and core into the sandstone target. However, uncertainty over the Dakota top precluded us from attempting this. Instead, we cored the Mowry Shale and recovered 26' of full core and then drilled ahead to the Dakota. What appeared to be the top of the main Dakota sandstone turned out to be a thin sand layer. With little well control in the area surrounding the well, precise formation correlation was impossible leading to calling the Dakota core point a bit prematurely. Unfortunately, we ended up retrieving 44' of lower Mowry seal, rather than Dakota sandstone. The positive aspect of this was getting additional and rare core from the sealing formation above the Dakota. Due to mounting cost pressure we were not able to make a third attempt in this section and proceeded to the next target, the Entrada Sandstone. To help the geologists better correlate where the drill bit was in relation to the geologic structure, a Gamma Ray measurement was added to the bottom-hole assembly. Adding this measurement while drilling should be considered in future wells when attempting to core in areas with sparse well data. By February 19 the rig reached the next potential interval for potential geologic storage, Curtis seal and Entrada sandstone formations. Here, 22' of Curtis Shale and 26' of Entrada sandstone full core was successfully recovered.

On February 29 we were at a depth of 9,706'. Projecting drilling cost from that point forward it was determined there were insufficient funds to continue drilling to the final potential reservoir sand, the Weber formation. It would have been necessary to average 50 FPH drilling rate from the Entrada to penetrate the Weber sand. Unfortunately, we were averaging 5 FPH through the tough shale between the Entrada and Weber formations.

March 2012

A conference call was conducted on the morning of March 1 between the project technical team and the NETL and the decision to stop at that depth was made. The final depth for the RMCCS ST 1 was 9,745 attained on March 1, 2012. Logging operations began 0530 March 2. The first run in the well was the Platform Express, providing basic formation resistivity, bulk density, compensated neutron and gamma ray. The second descent included the Combinable Magnetic Resonance (CMR) providing detailed information on pore size and distribution and can be used to estimate permeability. Also in the tool string was the Elemental Capture Spectroscopy tool for detailed mineralogical makeup. The third descent into the well with the Rotary Sidewall Coring Tool with core plugs acquired at key depths to fill in gaps from the full core. We were successful in obtaining 92 out of a possible 100 cores. The final descent into the well was for the Formation Micro Imager (FMI) and Sonic Scanner. The FMI provides an electrical image of the wellbore and is used to identify sedimentary features, formation dip, and the identification of faults and fractures. The Sonic Scanner provides bi-directional rock acoustic energy and velocity that is used to correlate seismic data from the time domain to depth and can be used to estimate the mechanical properties of the rock, including fracture gradient and stress. The well logging operation was completed on March 4th.

With all data gathering complete, we conducted the final plugging of the well on March 4 by placing two open hole plugs across the Entrada and Dakota sandstone, as well as the intermediate casing shoe. Perforations were placed just below surface casing and cement circulated there, as per Colorado Oil & Gas Commission requirements. A diagram of the final well configuration is included in Appendix O and forms provided to the COGCC are detailed. The rig was released on Tuesday March 6. There were 19,416 Man/hours including all rig workers, service providers, consultants and others engaged in the drilling of this well without a single incident, first-aid or other recordable of any kind. Additionally, 293 individuals received site-specific MSHA training.

APPENDIX I

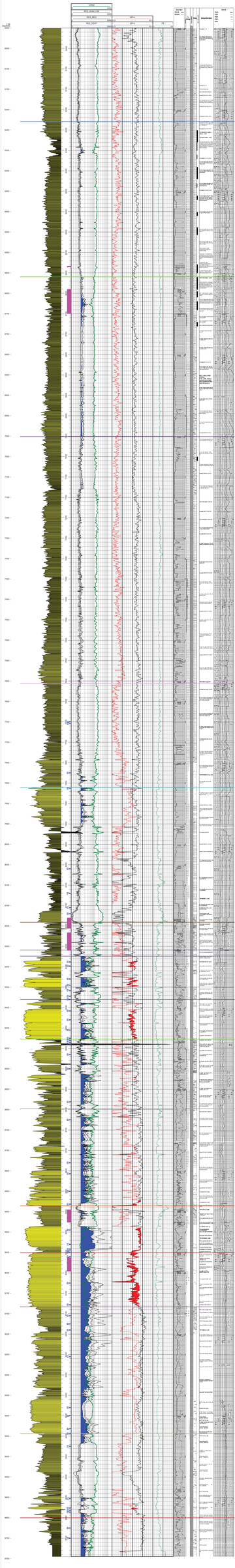
Detailed Well Logs 6000’ – 9750’

Contents

Topic

Combined Geophysical Interpretive and Sample Logs

RMCCS_State_#1
Schlumberger Carbon Services
RMCCS State
1
6,850
T6N R91W S34
SW SE



APPENDIX J

Shell Core Analysis Results for Niobrara

Contents

Topic

Niobrara Well Log

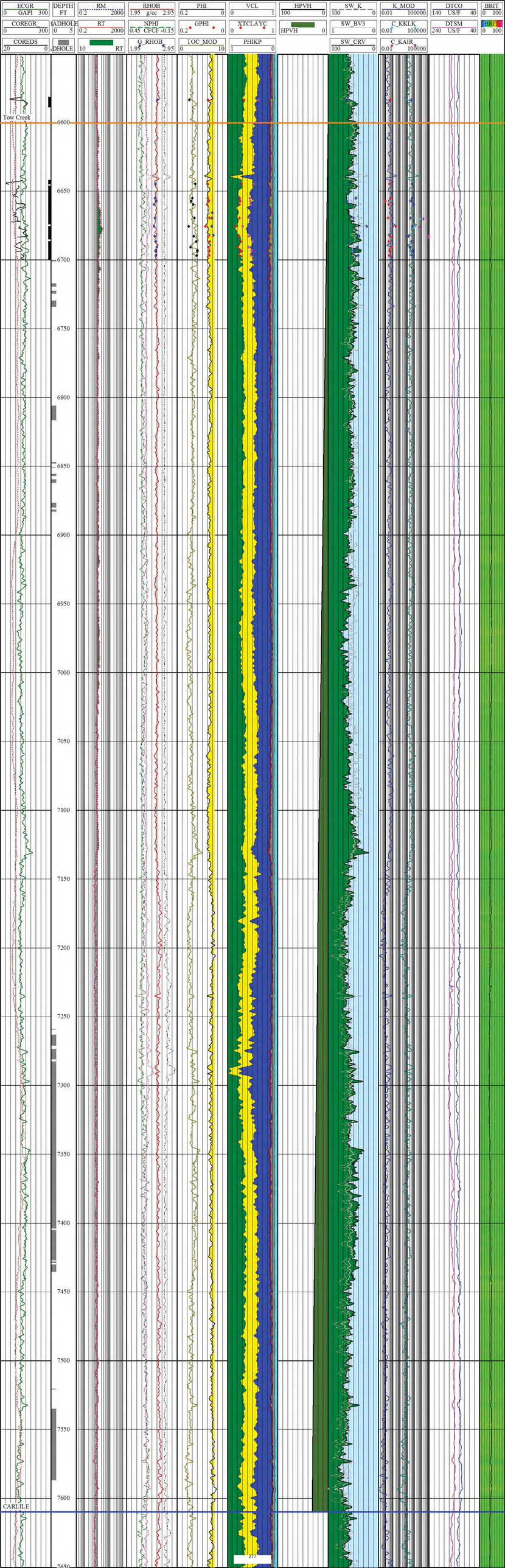
Niobrara Processed Well Log

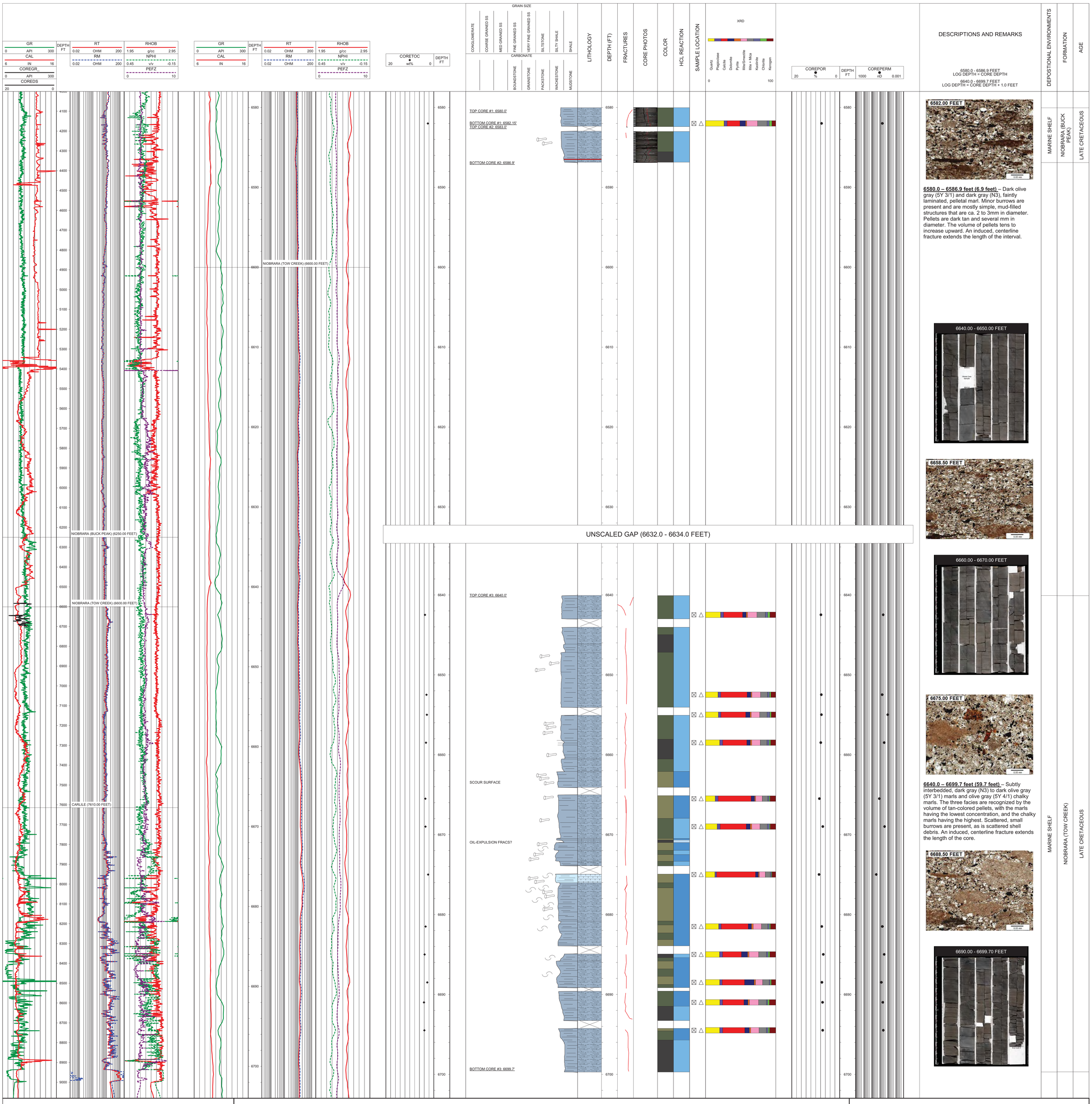
ECGR		DEPTH	RM		RHOB		DTCO	
0	GAPI 300	FT	0.2	2000	1.95	g/cc 2.95	140	US/F 40
COREGR		BADHOLE	RT		NPHI		DTSM	
0	300	0 5	0.2	2000	0.45	CFCF -0.15	240	US/F 40
COREDS		DHOLE			G_RHOB_			
20	0		10	RT	1.95	2.95		

Tow Creek

CARLILE

6600
6650
6700
6750
6800
6850
6900
6950
7000
7050
7100
7150
7200
7250
7300
7350
7400
7450
7500
7550
7600
7650


ECGR
0 GAPI 300
DEPTH
FT
RM
0.2 2000
RHOB
1.95 g/cc 2.95
PHI
0.2 0
VCL
0 1
HPVH
100 0
SW_K
100 0
K_MOD
0.01 100000
DTCO
140 US/F 40
BRIT
0 100
COREGR
0 300
ADHOLE
0 5
RT
0.2 2000
NPHI
0.45 CFCF -0.15
GPHI
0.2 0
XTCLAYC
0 1
HPVH 0
SW_BV3
1 0
C_KKLK
0.01 100000
DTSM
240 US/F 40
BRIT
0 100
COREDS
20 0
DHOLE
10 RT
G_RHOB
1.95 2.95
TOC_MOD
0 10
PHIKP
1 0
SW_CRV
100 0
C_KAIR
0.01 100000
Tow Creek
6600
6650
6700
6750
6800
6850
6900
6950
7000
7050
7100
7150
7200
7250
7300
7350
7400
7450
7500
7550
7600
CARLILE
277



DESCRIPTIONS AND REMARKS

6580.0 - 6586.9 FEET
LOG DEPTH = CORE DEPTH

6640.0 - 6699.7 FEET
LOG DEPTH = CORE DEPTH + 1.0 FEET

DEPOSITIONAL ENVIRONMENTS: MARINE SHELF

FORMATION: NIOBRARA (BUCK PEAK); NIOBRARA (TOW CREEK)

AGE: LATE CRETACEOUS

6580.0 – 6586.9 feet (6.9 feet) – Dark olive gray (5Y 3/1) and dark gray (N3), faintly laminated, pelletal marl. Minor burrows are present and are mostly simple, mud-filled structures that are ca. 2 to 3mm in diameter. Pellets are dark tan and several mm in diameter. The volume of pellets tens to increase upward. An induced, centerline fracture extends the length of the interval.

6640.0 – 6699.7 feet (59.7 feet) – Subtly interbedded, dark gray (N3) to dark olive gray (5Y 3/1) marls and olive gray (5Y 4/1) chalky marls. The three facies are recognized by the volume of tan-colored pellets, with the marls having the lowest concentration, and the chalky marls having the highest. Scattered, small burrows are present, as is scattered shell debris. An induced, centerline fracture extends the length of the core.

DEPOSITIONAL ENVIRONMENTS: MARINE SHELF

FORMATION: NIOBRARA (TOW CREEK)

AGE: LATE CRETACEOUS

Core Lab
RESERVOIR OPTIMIZATION

GEOLOGY BY: C. HALL

COMPUTER DRAFTING BY: D. DE LA FUENTE

VERTICAL SCALE 1:48

JOB NO. 120227

NFS 26

CORE LEGEND

LITHOLOGY

- Sandstone
- Muddy Sandstone
- Siltstone
- Limestone
- Argillaceous Limestone
- Chalk
- Marl
- Bentonite
- Shale
- Silty Shale
- Calcareous Shale
- Calcareous Silty Shale

SEDIMENTARY STRUCTURES

- Graded Bedding
- Bryozoa
- Burrow
- Pyrite Nodule
- Clay-Filled Vug
- Current Ripples
- Scours
- Calcareous
- Foraminifera
- Algal Cyst
- Dolomitic
- Horsetail
- Intraclast
- Nodular Bedding
- Nodule
- Crinoids
- Peloid
- Stylolite
- Fusulinids
- Plant Remains
- Sponge Spicules
- Shell Fragments
- Shell/Skeletal Fragments
- Pyrite
- Brachiopod
- Phosphate

COLOR

- N3
- 5Y 3/1

HCL REACTION

- Profuse
- Moderate
- Minor
- None

FRACTURES

- Coring-Induced Fracture
- Open/Closed Natural Fracture
- Mineralized Fracture

CONTACTS

SAMPLE LOCATION

- Thin Section
- FD Full Diameter
- SCAL
- X-Ray
- D Desorption

(MAY INCLUDE ROCK MECHANICS, PROPANT EMBEDMENT, ACOUSTIC ANISOTROPY, GEOCHEMISTRY, GRI, FRACTURE CONDUCTIVITY, AND/OR FLUID SENSITIVITY)

CORE DESCRIPTION PANEL

SHELL EXPLORATION & PRODUCTION CO.

RMCCS STATE #1

TRAPPER MINE FIELD

MOFFAT COUNTY, COLORADO

PANEL 1 OF 1

APPENDIX K

University of Utah Core Analysis Results

Contents

Topic

Plug Matrix

Slabbed-Core Images

X-Ray Diffraction Results

Spectral Gamma - CoreLab

Fracture Analysis - CoreLab

Routine Core Analysis - U of U

Routine Core Analysis - CoreLab

Routine Core Analysis - TerraTek

Mercury Injection Capillary Pressure - TerraTek

Centrifuge Capillary Pressure - CoreLab

Mercury Injection Capillary Pressure - CoreLab

Relative Permeability - TerraTek

RMCCS State #1 Sample List

Depth	Plug orientation	Plug No.	Formation	Size (inch diameter)	Max Size (inches)	Recovery Size	Notes	CQI	XRD	SEM	Petrography	Porosity	Permeability	Relative Perm	Capillary Pressure	UCS	Triax	TWC	Brazile	Bulk Comp	Pore Volume Comp	TOC	Reaction Kinetics	Plug orientation	Comments
																Destructive									
8188.17			Mowry				Thin Section (1x2) - Dana Ulmer-Scholle				NMT														
8188.92			Mowry				Thin Section (1x2) - Dana Ulmer-Scholle				NMT														
8191.6	Hor		Mowry	1.0																				Hor	
8191.65	Vert	2V	Mowry	1.0	0.2	1		D																Vert	
8191.65	Vert	2VB	Mowry	1.0	1.1	4		B				TT	TT											Vert	Service company
8191.85	45°	2°B	Mowry	1.0	1.3	4		B																45°	
8192	Hor	3H	Mowry	1.0	1.0	3		B				TT	TT											Hor	Service company
8192.1	Vert	3V	Mowry	1.0	0.9	3		A																Vert	
8192.4	45°	3°	Mowry	1.0	0.8	3		C	NMT															45°	
8193.5			Mowry				Thin Section (1x2) - Dana Ulmer-Scholle				NMT														
8194.4	Hor	3HB	Mowry	1.0	1.1	4		B																Hor	
8195.1	Hor	4H	Mowry	1.0	NR			D																Hor	
8195.1	Vert	4V	Mowry	1.0	0.3	1		D																Vert	
8195.65	45°	4°	Mowry	1.0	NR			D																45°	
8197.3	Hor	4HB	Mowry	1.0	0.2	1		C																Hor	
8197.67			Mowry				Thin Section (2x3) - Dana Ulmer-Scholle				NMT														
8198.1	Hor	5H	Mowry	1.0	NR			D	NMT															Hor	
8198.15	Vert	5V	Mowry	1.0	0.7	3		C																Vert	
8199.45	Hor	5HB	Mowry	1.0	1.6	4		B																Hor	
8199.45	Vert	5VB	Mowry	1.0	NR			D																Vert	
8200.5	Hor	7HA	Mowry	1.0	NR			C																Hor	
8200.6	Hor	7HB	Mowry	1.0	1.3	4		B																Hor	
8200.5	Vert	7VA	Mowry	1.0	0.4	2		D																Vert	
8201.1	Vert	7VB	Mowry	1.0	0.7	3		D																Vert	
8201.5	45°	7°	Mowry	1.0	0.8	3		B																45°	
8201.5	45°	7°B	Mowry	1.0	0.4	2		D																45°	
8203	Hor		Mowry	1.0	1.5	4		A																Hor	
8203.75	Hor		Mowry	1.0	1.5	4		A	NMT			TT	TT											Hor	Service company
8203.83			Mowry				Thin Section (2x3) - Dana Ulmer-Scholle				NMT														
8204	Hor	9H	Mowry	1.0	2.7	4		A			NMT					UU								Hor	
8204	Hor	9HB	Mowry	1.0	1.6	4		A																Hor	
8204.3	Vert	9V	Mowry	1.0	0.9	3		B																Vert	
8204.3	Vert	9VB	Mowry	1.0	0.9	3		B																Vert	
8205	45°	9°	Mowry	1.0	NR			D																45°	
8205	45°	10°	Mowry	1.0	1.3	4		A																45°	
8206	Hor	10H	Mowry	1.0	1.6	4		A				TT	TT											Hor	
8206	Hor	10HB	Mowry	1.0	1.3	4		A				CL	CL		CL									Hor	
8206	Vert	10V	Mowry	1.0	1.0	3		A																Vert	
8206	Vert	10VB	Mowry	1.0	1.6	4		A																Vert	
8216	Hor		Mowry	1.0																				Hor	
8216	Hor	11HB	Mowry	1.0	NR			D																Hor	
8216	Vert	11V	Mowry	1.0	NR			D																Vert	
8217			Mowry				TOC analyzed by Shell (Jerome Hall)																		
8217.3	Hor		Mowry	1.0																				Hor	
8217.3	Hor	12HB	Mowry	1.0	1.1	4		A																Hor	
8217.6	Vert	12V	Mowry	1.0	1.2	4		A																Vert	
8217.6	Vert	12VB	Mowry	1.0	NR			D																Vert	
8217.5	45°	12°	Mowry	1.0	0.3	2		D																45°	
8217.5	45°	12°B	Mowry	1.0	1.0	3		A																45°	
8218.3	Hor	13H	Mowry	1.0	0.8	3		B				TT	TT											Hor	Service company
8218.9	Vert	13V	Mowry	1.0	2.6	4		A	NMT	UU	NMT						UU			UU	UU			Vert	
8219	Hor	14H	Mowry	1.0	NR			D																Hor	
8219	45°		Mowry	1.0																				45°	
8219.35	Vert	14V	Mowry	1.0	0.5	2		C																Vert	
8221	Hor	15H	Mowry	1.0	0.3	2		C																Hor	
8221	Hor	15HB	Mowry	1.0	1.4	4		A																Hor	
8221	Vert	15V	Mowry	1.0	0.7	3		B																Vert	
8223.15	Hor	16H	Mowry	1.0	1.9	4		A																Hor	
8223.15	Hor	16HB	Mowry	1.0	1.9	4		A																Hor	
8223.45	Vert	16V	Mowry	1.0	1.3	4		A																Vert	
8223.45	Vert	16VB	Mowry	1.0	1.0	3		A																Vert	
8223.5	45°	16°	Mowry	1.0	0.2	1		C																45°	
8223.5	45°	16°B	Mowry	1.0	0.3	2		B	NMT															45°	
8224			Mowry				TOC analyzed by Shell (Jerome Hall)																		
8225.5			Mowry				Thin Section (1x2) - Dana Ulmer-Scholle				NMT														
8226.5	Hor	17H	Mowry	1.0	1.6	4		A																Hor	
8226.6	Hor	17HB	Mowry	1.0	1.8	4		A																Hor	
8226.8	Vert	17V	Mowry	1.0	0.7	3		B																Vert	
8226.8	Vert	17VB	Mowry	1.0	0.7	3		B																Vert	
8226.15	45°	17°	Mowry	1.0	0.5	2		B																45°	
8228.9	Hor	18H	Mowry	1.0	1.5	4		A				TT	TT											Hor	Service company
8228.9	Vert	18V	Mowry	1.0	1.2	4		A																Vert	
8228.55	45°	18°	Mowry	1.0	NR			D																45°	
8229			Mowry				TOC analyzed by Shell (Jerome Hall)																		
8229.5			Mowry				Thin Section (1x2) - Dana Ulmer-Scholle				NMT														
8230.5			Mowry				Thin Section (1x2) - Dana Ulmer-Scholle				NMT														
8230.9	Hor		Mowry	1.0																				Hor	
8230.9	Vert	19V	Mowry	1.0	0.3	2		C	NMT															Vert	
8232.5			Mowry				Thin Section (1x2) - Dana Ulmer-Scholle				NMT														
8233	Hor	20H	Mowry	1.0	NR			D																Hor	
8233.7	Hor	20HB	Mowry	1.0	NR			D																Hor	
8233.4	Vert	20V	Mowry	1.0	0.8	3		B																Vert	
8233.4	Vert	20VB	Mowry	1.0	0.7	3		C																Vert	
8233.75	45°	20°	Mowry	1.0	1.0	3		A																45°	
8233.75	45°	20°B	Mowry	1.0	0.7	3		B																45°	
8235	Hor	21H	Mowry	1.0	1.3	4		A		UU		TT	TT		TT									Hor	Service company
8235	Hor	21HB	Mowry	1.0	1.8	4		A				CL	CL		CL									Hor	
8235	Vert		Mowry	1.0																				Vert	
8235	Vert	21VB	Mowry	1.0	0.9	3		A																Vert	
8235	45°		Mowry	1.0																				45°	
8237			Mowry				TOC analyzed by Shell (Jerome Hall)																		
8238	Hor	22H	Mowry	1.0	0.1	1		C																Hor	
8238	Vert	22V	Mowry	1.0	1.4	4		A																Vert	
8240	Hor	23H	Mowry	1.0	1.5	4		A																Hor	
8240	Vert	23V	Mowry	1.0	NR			D																Vert	
8240.4	45°	23°	Mowry	1.0	0.9	3		C																45°	
8241	Hor	24H	Mowry	1.0	NR			D																Hor	
8241	Vert	24V	Mowry	1.0	1.8	4		B																Vert	
8241	45°	24°	Mowry	1.0	0.2	1		D																45°	
8243.15	Hor	25HA	Mowry	1.0	1.1	4		A				TT	TT											Hor	Service company
8243	Hor	25HB	Mowry	1.0	3.7	4		D			NMT					UU								Hor	
8243.58			Mowry				Thin Section (1x2) - Dana Ulmer-Scholle				NMT														
8242.85	Vert	25V	Mowry	1.0	0.3	2		C	NMT															Vert	
8242.85	Vert		Mowry	1.0																				Vert	
8242.5	45°	25°	Mowry	1.0	0.8	3		B																45°	
8244			Mowry				TOC analyzed by Shell (Jerome Hall)																		
8244.05	Hor	26H	Mowry	1.0	NR			D																Hor	
8244.55	Vert	26V	Mowry	1.0	0.3	1		D																Vert	
8244.2	45°	26°	Mowry	1.0	0.3	2		B																45°	
8245	Hor	27H	Mowry	1.0	NR			D																Hor	
8245	Vert	27V	Mowry	1.0	0.4	2		B																Vert	
8246	Hor	28H	Mowry	1.0	1.0	3		C																Hor	
8246	Vert	28V	Mowry	1.0	0.7	3		B																Vert	
8246.33			Mowry				Thin Section (2x3) - Dana Ulmer-Scholle				NMT														
8246.35	45°	28°	Mowry	1.0	0.3	2		B																45°	
8246.8	Hor	29H	Mowry	1.0	0.4	2		C																Hor	
8246.8	Vert	29V	Mowry	1.0	0.3	2		B																Vert	
8246.9	45°	29°	Mowry	1.0	0.4	2		A																45°	
8249			Mowry				TOC analyzed by Shell (Jerome Hall)																		
8249.6	Hor	30H	Mowry	1.0	0.6	3		C																Hor	
8249.6	Vert		Mowry	1.0																				Vert	
8250	Hor	31H	Mowry	1.0	1.0	3		A																Hor	Service company
8250	Vert	31V	Mowry	1.0	1.1	4		A																Vert	
8250.5	45°	31°	Mowry	1.0	NR			D																45°	
8250.9	Hor	32H	Mowry	1.0	NR			D																Hor	
8250.85	Vert	32V	Mowry	1.0	0.3	2		B	NMT															Vert	
8251.25			Mowry				Thin Section (1x2) - Dana Ulmer-Scholle				NMT														
8252.17			Mowry				Thin Section (2x3) - Dana Ulmer-Scholle				NMT														
8253.3	Hor	33H	Mowry	1.0	1.4	4		A				TT	TT											Hor	
8253.3	Vert	33V	Mowry	1.0	1.2	4		A																Vert	
8253.5	45°	33°	Mowry	1.0	NR			D																45°	
8254.3	Hor	34H	Mowry	1.0	0.8	3		A																Hor	
8254.3	Vert	34V	Mowry	1.0	0.6	3		A																Vert	
8254.55	45°	34°	Mowry	1.0	0.9	3		A																45°	
8255.65	Hor	35H	Mowry	1.0	0.2	1		C																Hor	
8255.65	Vert	35V	Mowry	1.0	0.6	3		A																Vert	
8255.35	45°	35°	Mowry	1.0	NR			D	NMT															45°	
8256.75			Mowry				Thin Section (2x3) - Dana Ulmer-Scholle				NMT														
8257			Mowry				TOC analyzed by Shell (Jerome Hall)																		
8258	Hor	36H	Mowry	1.0	1.7	4		A				TT	TT		TT									Hor	
8258	Vert	36V	Mowry	1.0	1.0	3		A																Vert	
8258.15	45°	36°	Mowry	1.0	0.7	3		A																45°	
8258.67			Mowry				Thin Section (2x3) - Dana Ulmer-Scholle				NMT														
8259.5	Hor	37H	Mowry	1.0	1.3	4		A				TT	TT		TT									Hor	Service company
8259.5	Vert	37V	Mowry	1.0	NR			D																Vert	
8259.5	45°	37°	Mowry	1.0	1.0	3		A																45°	
8260			Mowry				TOC analyzed by Shell (Jerome Hall)																		
8260.55	Hor	38H	Mowry	1.0	NR			C																Hor	
8260.5	Vert	38V	Mowry	1.0	1.1	4		A																Vert	
8260.55	45°	38°	Mowry	1.0	2.3	4		A								UU								45°	
8895.17			Curtis				Thin Section (2x3) - Dana Ulmer-Scholle				NMT														
8896.1	Hor	41HA	Curtis	1.0	1.7	4		A				TT	TT		TT									Hor	Service company
8896.1	Vert	41VA	Curtis	1.0	2.0	4		A			NMT						UU			UU	UU			Vert	
8897.2	Hor	42HA	Curtis	1.0	1.0	4		A																Hor	
8897.4	Vert		Curtis	1.0																				Vert	
8897.2	45°	42°	Curtis	1.0	0.7	3		A																45°	
8898.5	Hor	43HA	Curtis	1.0	2.1	4		A																Hor	
8898.5	Vert	43VA	Curtis	1.0	2.5	4		A	NMT								UU							Vert	
8899.92			Curtis				Thin Section (2x3) - Dana Ulmer-Scholle				NMT														
8900.5	Hor	44HA	Curtis	1.0	3.2	4		A																Hor	
8900.5	Vert	44V	Curtis	1.0	2.0	4		A																Vert	
8902	Hor	45H	Curtis	1.0	NR			C																Hor	
8902.8	Vert	45V	Curtis	1.0	0.8	3		A																Vert	
8903.5	Hor	46H	Curtis	1.0	3.2	4		A								UU								Hor	
8903.5	Vert	46V	Curtis	1.0	2.5	4		A																Vert	
8904	Hor	47H	Curtis	1.0	3.0	4		A				TT	TT											Hor	Service company
8904	45°		Curtis	1.0																				45°	
8904	Vert	47V	Curtis	1.0	2.4	4		A	NMT		NMT					UU							UU	Vert	
8904.92			Curtis				Thin Section (1x2) - Dana Ulmer-Scholle				NMT														
8905.5	Hor	48H	Curtis	1.0	2.6	4		A							TT									Hor	Too fractured for testing
8905	Vert	48V	Curtis	1.0	0.3	1		D																Vert	

																		Destructive																
Depth	Plug orientation	Plug No.	Formation	Size (inch diameter)	Max Size (inches)	Recovery Size	Notes	CQI	XRD	SEM	Petrography	Porosity	Permeability	Relative Perm	Capillary Pressure	UCS	Triax	TWC	Brazile	Bulk Comp	Pore Volume Comp	TOC	Reaction Kinetics	Plug orientation	Comments
8906.7	Hor	49H	Curtis	1.0	0.5	2		C																	Hor	
8906.7	Vert	49V	Curtis	1.0	0.5	2		B																	Vert	
8906	45°	49°	Curtis	1.0	0.3	2		D																	45°	
8907	Hor	50H	Curtis	1.0	NR			D																	Hor	
8907.8	Vert	50V	Curtis	1.0	0.4	2		C																	Vert	
8908.2	Vert	51V	Curtis	1.0	0.3	2		C																	Vert	
8909	Hor	52H	Curtis	1.0	NR			D																	Hor	
8910	Vert	53V	Curtis	1.0	1.5	4	two segments; shorter one 0.8"	A																	Vert	
8911	45°	54°	Curtis	1.0	1.3	4		A																	45°	
8911.33			Curtis				Thin Section (1x2) - Dana Ulmer-Scholle				NMT															
8911.6	Hor	54H	Curtis	1.0	1.8	4		A																	Hor	
8911.6	Vert	54V	Curtis	1.0	1.9	4		A																	Vert	
8912.58			Curtis				Thin Section (1x2) - Dana Ulmer-Scholle				NMT															
8913	Hor	55H	Curtis	1.0	1.6	4	two segments; shorter one 1.5"	A				TT	TT												Hor	
8914	Hor	56H	Curtis	1.0	NR			D																	Hor	
8915	Hor	57H	Curtis	1.0	2.5	4		A								UU									Hor	
8915	Vert	57V	Curtis	1.0	1.8	4	two segments; shorter one 0.7"	A																	Vert	
8915.5			Curtis				Thin Section (2x3) - Dana Ulmer-Scholle				NMT															
8916.35	Hor	58H	Curtis	1.0	1.1	4		A	NMT			TT	TT												Hor	Service company
8916.3	Vert	58V	Curtis	1.0	1.8	4		A																	Vert	
8917.5			Curtis				Thin Section (1x2) - Dana Ulmer-Scholle				NMT															
8918	Hor	59H	Curtis	1.0	1.0	4	two segments; shorter one NR	B															UU		Hor	
8924.8	Vert		Curtis	1.0	1.5	4		A																	Vert	
9012.1	Hor	63H	Entrada	1.5	1.5	4		A																	Hor	
9012.1	Hor	63HB	Entrada	1.5	0.3	4		A																	Hor	
9012.5	Hor	63HC	Entrada	1.5	1.1	4		A																	Hor	
9012.8	Vert	63V	Entrada	1.5	3.2	4		A				TT	TT	TT	TT										Vert	Service company
9012.8	Vert	63VB	Entrada	1.5	3.1	4		A		UU	NMT	UU	UU				UU				UU	UU			Vert	
9012.3	45°	63°	Entrada	1.5	1.7	4		A				TT	TT	TT	TT										45°	Service company
9012.3	45°	63°B	Entrada	1.5	NR	4		A																	45°	
9013.3	Hor	64H	Entrada	1.5	1.0	4		A				CL	CL		CL										Hor	
9013.6	Hor	64HB	Entrada	1.5	2.2	4		A				TT	TT	TT	TT										Hor	Service company
9013.9	Vert	64V	Entrada	1.5	0.9	4		A				TT	TT	TT	TT										Vert	
9013.9	Vert		Entrada	1.5				A																	Vert	
9013.4	45°	64°	Entrada	1.5	2.4	4		A																	45°	
9013.7	45°	64°B	Entrada	1.5	2.5	4		A				UU	UU												45°	
9013.92			Entrada				Thin Section (1x2) - Dana Ulmer-Scholle				NMT															
9015	Vert	65V	Entrada	1.5	2.2	4		A																	Vert	
9015.4	Hor		Entrada	1.5																					Hor	
9015.6	Hor	65HB	Entrada	1.5	2.1	4		A				UU	UU	UU											Hor	
9015.85	45°	65°	Entrada	1.5	3.0	4		A				UU	UU												45°	
9016.2	Vert	66V	Entrada	1.5	2.2	4		A																	Vert	
9016.5	Hor	66H	Entrada	1.5																					Hor	
9016.7	Hor	66HB	Entrada	1.5	2.7	4		A																	Hor	
9016.8	45°	66°	Entrada	1.5	1.0	3		A																	45°	
9017.1	Vert	67V	Entrada	1.5	0.8	3		A																	Vert	
9017.25	45°	67°	Entrada	1.5	1.1	4		A																	45°	
9017.3	Hor	67H	Entrada	1.5	1.1	4		A																	Hor	
9017.5	Vert		Entrada	1.5																					Vert	
9017.7	Hor	68H	Entrada	1.5	2.4	4		A																	Hor	
9017.9	45°	68°	Entrada	1.5	0.8	3		A																	45°	
9018			Entrada				Thin Section (1x2) - Dana Ulmer-Scholle				NMT															
9019.6	Vert	69V	Entrada	1.5	2.0	4		A																	Vert	
9019.8	Hor	69H	Entrada	1.5	0.5	3	two segments; other one 0.5"	A																	Hor	
9019.9	45°	69°	Entrada	1.5	1.5	4		A																	45°	
9020.2	Hor	70H	Entrada	1.5	1.4	4	two segments; shorter one 0.5"	A				UU	UU												Hor	
9020.48	45°	70°	Entrada	1.5	1.1	4		A																	45°	
9020.6	Vert	70V	Entrada	1.5	2.1	4		A																	Vert	
9020.8	Vert		Entrada	1.5																					Vert	
9021.2	Hor	71H	Entrada	1.5	2.5	4		A																	Hor	
9021.35	Hor	71HB	Entrada	1.5	2.7	4		A				UU	UU	UU											Hor	
9021.55	45°	71°	Entrada	1.5	3.0	4		A			NMT	UU	UU			UU									45°	
9021.75	45°	71°B	Entrada	1.5	0.6	3		A																	45°	
9021.9	Vert	71V	Entrada	1.5	2.4	4		A																	Vert	
9022.1	Hor	72H	Entrada	1.5	2.3	4		A																	Hor	
9022.3	Hor	72HB	Entrada	1.5	2.2	4		A																	Hor	
9022.5	45°	72°	Entrada	1.5	3.1	4		A																	45°	
9022.65	45°	72°B	Entrada	1.5	1.6	4		A																	45°	
9022.8	Vert	72V	Entrada	1.5	1.5	4		A																	Vert	
9023.35	Vert	73V	Entrada	1.5	2.6	4		A				UU	UU												Vert	
9023.55	Hor	73H	Entrada	1.5	2.7	4		A				UU	UU	UU											Hor	
9023.65	Hor	73HB	Entrada	1.5	2.7	4		A																	Hor	
9023.85	45°	73°	Entrada	1.5	2.8	4		A																	45°	
9024	45°		Entrada	1.5																					45°	
9024.15	Vert	74V	Entrada	1.5	2.7	4		A																	Vert	
9024.45	Hor	74H	Entrada	1.5	2.3	4		A																	Hor	
9024.5			Entrada				Thin Section (2x3) - Dana Ulmer-Scholle				NMT															
9024.65	Hor	74HB	Entrada	1.5	2.4	4	two segments; shorter one 0.3"	A	NMT			UU	UU												Hor	
9024.9	45°	74°	Entrada	1.5	2.3	4		A																	45°	
9025.3	Vert	75V	Entrada	1.5	1.4	4		A																	Vert	
9025.5	Hor	75H	Entrada	1.5	2.9	4		A																	Hor	
9025.75	45°	75°	Entrada	1.5	1.4	4		A																	45°	
9025.9	Vert	75VB	Entrada	1.5	1.7	4		A																	Vert	
9026.1	Vert	76V	Entrada	1.5	2.6	4		A																	Vert	
9026.35	Hor	76H	Entrada	1.5	2.2	4		A																	Hor	
9026.55	Hor		Entrada	1.5																					Hor	
9026.7	45°	76°	Entrada	1.5	3.1	4		A				UU	UU			UU									45°	
9026.9	45°	76°B	Entrada	1.5	0.7	3		A																	45°	
9027.2	Vert	77V	Entrada	1.5	2.4	4		A																	Vert	
9027.3	Hor	77H	Entrada	1.5	3.0	4		A				UU	UU			UU									Hor	
9027.45	Hor	77HB	Entrada	1.5	3.1	4		A				UU	UU	UU											Hor	
9027.8	45°	77°	Entrada	1.5	3.7	4		B				TT	TT												45°	
9028.1	Hor	78H	Entrada	1.5	2.9	4		A																	Hor	
9028.25	Hor	78HB	Entrada	1.5	2.0	4		C																	Hor	
9028.55	45°	78°	Entrada	1.5	0.3	3		B																	45°	
9028.75	45°	78°B	Entrada	1.5	1.3	4		A																	45°	
9028.9	Vert	78V	Entrada	1.5	3.5	4		C		UU	NMT						UU				UU	UU			Vert	
9029.15	Hor	79H	Entrada	1.5	2.4	4		A	NMT			TT	TT	TT	TT										Hor	Service company
9029.17			Entrada				Thin Section (2x3) - Dana Ulmer-Scholle				NMT															
9029.35	Hor	79HB	Entrada	1.5	2.6	4		B				UU	UU	UU											Hor	
9029.6	Hor	79HC	Entrada	1.5	3.3	4		A				UU	UU			UU									Hor	
9029.8	Hor	79HD	Entrada	1.5	3.2	4		A																	Hor	
9030.1	Hor	80H	Entrada	1.5	NR			F																	Hor	
9030.9	Hor	80HB	Entrada	1.5	1.3	4		A																	Hor	
9030.25	45°	80°	Entrada	1.5	1.8	4		B																	45°	
9030.55	45°	80°B	Entrada	1.5	NR			D																	45°	
9031.1	Hor	81H	Entrada	1.5	2.6	4		A																	Hor	
9031.6	Vert	81V	Entrada	1.5	2.0	4		A																	Vert	
9031.9	Vert		Entrada	1.5																					Vert	
9031.9	Vert	81VC	Entrada	1.5	2.3	4		A																	Vert	
9031.2	45°	81°	Entrada	1.5	2.5	4		A																	45°	
9031.92			Entrada				Thin Section (1x2) - Dana Ulmer-Scholle				NMT															
9032.15	Hor	82H	Entrada	1.5	3.3	4		A			NMT	UU	UU	UU		UU									Hor	
9032.5	Hor	82HB	Entrada	1.5	2.7	4		A				UU	UU	UU											Hor	
9032.9	Vert	82V	Entrada	1.5	2.4	4		A																	Vert	
9032.25	45°	82°	Entrada	1.5	1.8	4		A																	45°	
9032.6	45°	82°B	Entrada	1.5	0.2	1		D																	45°	
9033.1	Hor	83H	Entrada	1.5	3.1	4		A				UU	UU												Hor	
9033.75	Hor	83HB	Entrada	1.5	3.1	4		A																	Hor	
9033.5	Vert	83V	Entrada	1.5	0.8	3		A																	Vert	
9033.2	45°	83°	Entrada	1.5	0.8	3		A																	45°	
9033.85	45°	83°B	Entrada	1.5	1.0	4		A																	45°	
9034.1	Hor	84H	Entrada	1.5	3.1	4		A			NMT	UU	UU			UU									Hor	
9034.8	Vert	84V	Entrada	1.5	2.6	4		A																	Vert	
9034.7	45°	84°	Entrada	1.5	2.0	4		A																	45°	
9035.2	Hor		Entrada	1.5																					Hor	
9035.9	Hor	85HB	Entrada	1.5	2.1	4		A																	Hor	
9035.1	Vert	85V	Entrada	1.5	1.0	4		A																	Vert	
9035.5			Entrada				Thin Section (1x2) - Dana Ulmer-Scholle				NMT															
9035.55	Vert	85VB	Entrada	1.5	1.3	4		A																	Vert	
9035.35	45°	85°	Entrada	1.5	1.5	4		B																	45°	
9035.55	45°	85°B	Entrada	1.5	1.1	4		A																	45°	
9036.1	Hor	86H	Entrada	1.5	3.0	4		A			NMT	UU	UU			UU									Hor	
9036.5			Entrada				Thin Section (1x2) - Dana Ulmer-Scholle				NMT															
9036.6	Hor	86HB	Entrada	1.5	1.9	4		A	NMT			UU	UU												Hor	
9036.9	Vert	86V	Entrada	1.5	1.6	4		A																	Vert	
9036.25	45°	86°	Entrada	1.5	1.5	4		A																	45°	
9036.7	45°	86°B	Entrada	1.5	1.4	4		A																	45°	
9037	Hor	87H	Entrada	1.5	0.4	2		A																	Hor	
9037	Hor	87HB	Entrada	1.5	1.6	4		A																	Hor	
9037.35	Vert	87V	Entrada	1.5	2.5	4		A																	Vert	
9037.35	Vert		Entrada	1.5																					Vert	
9037.5	45°		Entrada	1.5																					45°	
9037.5	45°	87°B	Entrada	1.5	1.4	4		A																	45°	
9037.8	Hor	88H	Entrada	1.5	1.7	4		A																	Hor	
9037.8	Hor	88HB	Entrada	1.5	2.4	4		A				UU	UU	UU											Hor	
9037.9	Vert	88V	Entrada	1.5	0.2	2		A																	Vert	
9037.9	Vert	88VB	Entrada	1.5	2.1	4		A																	Vert	
9038 to 9039.75	Whole Core		Entrada	4.0	21.0			A	NMT	UU	NMT	UU	UU	UU				UU					UU	Whole Core	
9040.3	Hor	89H	Entrada	1.5	1.7	4		A																	Hor	
9040.3	Hor	89HB	Entrada	1.5	2.3	4		A																	Hor	
9040.5	Vert	89V	Entrada	1.5	0.8	3		A																	Vert	
9040.5	Vert	89VB	Entrada	1.5	0.4	2		A																	Vert	
9040.8	45°	89°	Entrada	1.5	NR																				45°	
9040.8	45°	89°B	Entrada	1.5	2.1	4		A																	45°	
9041	Hor	90H	Entrada	1.5	1.6	4		A				UU	UU												Hor	
9041	Hor	90HB	Entrada	1.5	1.8	4		B																	Hor	
9041.6	Hor	90HC	Entrada	1.5	NR																				Hor	
9041.6	Hor	90HD	Entrada	1.5	0.7	3		B																	Hor	
9041.2	Vert	90V	Entrada	1.5	1.7	4		A																	Vert	
9041.2	Vert	90VB	Entrada	1.5	1.9	4		A																	Vert	
9041.7	45°		Entrada	1.5																					45°	
9041.7	45°	90°B	Entrada	1.5	1.5	4		A																	45°	
9042.1	Hor	91H	Entrada	1.5	2.1	4		A				UU	UU	UU											Hor	
9042.1	Hor	91HB	Entrada	1.5	2.5	4		A																	Hor	
9042.1	Vert	91V	Entrada	1.5	1.0	4		A																	Vert	
9042.1	Vert	91VB	Entrada	1.5	0.8	3		A																	Vert	
9042.55	Hor	92H	Entrada	1.5	2.1	4		A																	Hor	
9042.6	Hor	92HB	Entrada	1.5	2.3	4		A																	Hor	

																	Destructive									
Depth	Plug orientation	Plug No.	Formation	Size (inch diameter)	Max Size (inches)	Recovery Size	Notes	CQI	XRD	SEM	Petrography	Porosity	Permeability	Relative Perm	Capillary Pressure	UCS	Triax	TWC	Brazile	Bulk Comp	Pore Volume Comp	TOC	Reaction Kinetics	Plug orientation	Comments
9042.9	Vert	92V	Entrada	1.5	1.7	4		A																Vert	
9043.2	Hor	93H	Entrada	1.5	NR																			Hor	
9043.2	Hor	93HB	Entrada	1.5	1.7	4		A																Hor	
9043.9	Vert	93V	Entrada	1.5	1.6	4		A																Vert	
9043.9	Vert	93VB	Entrada	1.5	1.6	4		A	NMT															Vert	
9043.58			Entrada				Thin Section (2x3) - Dana Ulmer-Scholle				NMT														
9043.7	45°	93°	Entrada	1.5	3.1	4		A			NMT	TT	TT	TT	TT		TT			TT	TT			45°	Service company
9043.7	45°	93°B	Entrada	1.5	NR																			45°	
8227.6	Hor	94H	Entrada	1.5	2.0	4		A																Hor	
8227.6	Vert	94V	Entrada	1.5	1.0	4		A																Vert	
8236	Hor	95H	Entrada	1.5	1.6	4		B																Hor	
8236	Vert	95V	Entrada	1.5	1.2	4		A																Vert	
7825.00	Sidewall	100	Carlile	0.85	1.3	4		A																Sidewall	
7863.00	Sidewall	99	Frontier	0.85	1.8	4		A																Sidewall	
7904.00	Sidewall	98	Frontier	0.85	0.3	3	4 different sections each at 0.25"	B																Sidewall	
8018.00	Sidewall	97	Frontier	0.85	NR	3	1.2" but needs smaller subcore	C																Sidewall	
8060.00	Sidewall	24	Frontier	0.85	0.5	2		A																Sidewall	
8155.00	Sidewall	96	Frontier	0.85	NR	1		D																Sidewall	
8170.00	Sidewall	95	Frontier	0.85	NR	1		F																Sidewall	
8288.00	Sidewall	42	Dakota	0.85	1.1	3		A				TT	TT		TT									Sidewall	Service company
8298.00	Sidewall	23	Dakota	0.85	0.5	2		C	NMT															Sidewall	
8326.00	Sidewall	41	Dakota	0.85	NR	1		F																Sidewall	
8330.00	Sidewall	94	Dakota	0.85	0.8	3		A																Sidewall	
8345.00	Sidewall	22	Dakota	0.85	0.7	2		A																Sidewall	
8358.00	Sidewall	40	Dakota	0.85	1.0	3		A				TT	TT	TT										Sidewall	Service company
8372.00	Sidewall	39	Dakota	0.85	NR	1		F																Sidewall	
8372.50	Sidewall	93	Dakota	0.85	0.8	4	two sections; smaller one at 0.3"	B																Sidewall	
8408.00	Sidewall	21	Dakota	0.85	0.9	3		B																Sidewall	
8430.00	Sidewall	20	Dakota	0.85	0.9	3		A																Sidewall	
8455.00	Sidewall	19	Morrison	0.85	0.7	4		C																Sidewall	
8475.00	Sidewall	18	Morrison	0.85	0.3	3		C	NMT															Sidewall	
8490.00	Sidewall	17	Morrison	0.85	1.2	3		B				TT	TT											Sidewall	Service company
8515.00	Sidewall	16	Morrison	0.85	1.5	4		A																Sidewall	
8550.00	Sidewall	38	Morrison	0.85	1.4	4		A																Sidewall	
8631.00	Sidewall	15	Morrison	0.85	1.1	4		B																Sidewall	
8675.00	Sidewall	37	Morrison	0.85	0.9	3		A																Sidewall	
8780.00	Sidewall	14	Morrison	0.85	1.3	4		A				TT	TT		TT									Sidewall	Service company
8807.00	Sidewall	36	Morrison	0.85	1.5	4		A					TT	TT										Sidewall	
8850.00	Sidewall	13	Morrison	0.85	1.3	4		A																Sidewall	
8882.00	Sidewall	35	Morrison	0.85	1.0	3		A		UU		TT	TT		TT									Sidewall	Service company
8945.00	Sidewall	12	Curtis Sand	0.85	0.7	4		C																Sidewall	
8980.00	Sidewall	11	Curtis Sand	0.85	NR	2		D	NMT															Sidewall	
8992.00	Sidewall	34	Curtis Sand	0.85	1.1	4		B				TT	TT		TT									Sidewall	Service company
8996.00	Sidewall	33	Curtis Sand	0.85	0.7	4	two sections; smaller one at 0.3"	C																Sidewall	
9010.00	Sidewall	32	Entrada	0.85	1.1	4		A																Sidewall	
9075.00	Sidewall	10	Entrada	0.85	0.2	3		D																Sidewall	
9100.00	Sidewall	31	Entrada	0.85	0.9	3		A																Sidewall	
9128.00	Sidewall	9	Entrada	0.85	1.4	4		A																Sidewall	
9155.00	Sidewall	8	Chinle	0.85	1.5	4		B																Sidewall	
9175.00	Sidewall	30	Chinle	0.85	0.5	3		C	NMT															Sidewall	
9190.00	Sidewall	29	Chinle	0.85	1.5	4		B																Sidewall	
9255.00	Sidewall	7	Chinle	0.85	1.1	4		B																Sidewall	
9380.00	Sidewall	6	Chinle	0.85	1.2	4		A				TT	TT											Sidewall	Service company
9400.00	Sidewall	5	Chinle	0.85	1.5	4		B																Sidewall	
9444.00	Sidewall	28	Chinle	0.85	1.6	4		A																Sidewall	
9475.00	Sidewall	4	Shinarump	0.85	1.2	4		A																Sidewall	
9550.00	Sidewall	3	Shinarump	0.85	NR	4		F																Sidewall	
9603.00	Sidewall	2	Shinarump	0.85	1.2	4		A				TT	TT											Sidewall	Service company
9626.00	Sidewall	27	Shinarump	0.85	0.6	4		B	NMT															Sidewall	
7699.90	Sidewall	25	Moenkopi	0.85	0.6	3		B	NMT															Sidewall	
9675.00	Sidewall	26	Moenkopi	0.85	1.4	4		A				TT	TT											Sidewall	Service company
9700.00	Sidewall	1	Moenkopi	0.85	1.5	4		A																Sidewall	

CORE QUALITY (CQI)

A	Excellent
B	Good
C	Fair
D	Poor
F	Muddy/Insufficient

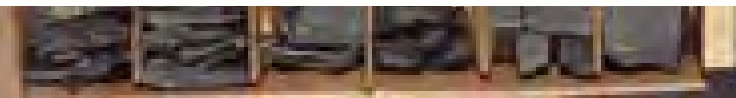
CORE RECOVERY SIZE

4	Full recovery (> 1")
3	Good recovery (>0.5" - 1")
2	Fair recovery (0.25" - .5")
1	Poor recovery (<0.25")
NR	No recovery

	Sufficient material, length, and/or diameter for specified test
	Insufficient material, length, and/or diameter for specified test
	Possibily sufficient material, length, and/or diameter for specified test



283




CORE
2





285





286





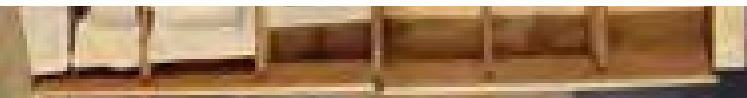
287




CORE
4



289



Sample ID	1	2	3	4	5	6	7	8	9	10
Depth (ft)	8191.6	8203	8203.75	8216	8217.3	8219	8230.9	8235V	8242.85V	8249.6V
	Bulk Mineralogy									
Quartz	39	37	37	52	73	35	24	24	25	46
K-Feldspar	0	0	0	0	0	0	0	0	0	0
Plagioclase (Albite)	5	0	2	9	7	3	3	3	6	0
Calcite	0	0	1	0	0	0	1	0	2	1
Dolomite	0	0	0	0	0	0	0	0	1	1
Halite	0	0	0	0	0	0	0	0	0	0
Siderite	0	0	0	0	0	0	0	0	0	0
Pyrite	2	1	3	2	3	5	4	2	0	1
Clay	54	62	57	37	17	57	68	71	66	51
Total	**100**	**100**	**100**	**100**	**100**	**100**	**100**	**100**	**100**	**100**

Sample ID	11	12	13	14	15	16	17	18	19	20
Depth (ft)	8897.4V	8904	8924.8V	9013.9V	9015.4	9017.5V	9020.8V	9024	9026.55	9031.9V
	Bulk Mineralogy									
Quartz	46	40	19	33	52	57	75	75	76	78
K-Feldspar	24	13	0	40	11	35	11	19	10	11
Plagioclase (Albite)	6	5	0	5	7	6	10	0	8	5
Calcite	2	17	6	0	0	0	0	0	0	0
Dolomite	8	3	2	2	2	1	0	4	3	2
Halite	0	0	0	0	0	0	0	0	0	0
Siderite	0	0	0	0	0	0	0	0	0	0
Pyrite	0	0	0	0	0	0	0	0	0	0
Clay	14	22	73	20	28	1	4	2	3	4
Total	**100**	**100**	**100**	**100**	**100**	**100**	**100**	**100**	**100**	**100**

Sample ID	21	22	23	24	25	26	27	28	29	30
Depth (ft)	9035.2	9037.35V	9041.45	8188'2"	8188'11"	8193'6"	8197'8"	8203'10"	8225'6"	8229'6"
	Bulk Mineralogy									
Quartz	53	80	58	21	20	25	22	45	44	2
K-Feldspar	37	14	34	0	0	0	0	0	0	0
Plagioclase (Albite)	8	3	6	12	0	4	0	16	6	0
Calcite	0	0	0	0	1	0	0	4	0	0
Dolomite	0	0	0	0	0	0	0	0	0	0
Halite	0	0	0	0	0	0	0	0	0	0
Siderite	0	0	0	0	0	0	0	0	0	0
Pyrite	0	0	0	2	0	1	1	2	4	21
Clay	2	3	2	65	79	70	77	33	46	77
Total	**100**	**100**	**100**	**100**	**100**	**100**	**100**	**100**	**100**	**100**

Sample ID	31	32	33	34	35	36	37	38	39	40
Depth (ft)	8230'6"	8232'6"	8243'7"	8246'4"	8251'3"	8252'2"	8256'9"	8258'8"	8895'2"	8899'11"
	Bulk Mineralogy									
Quartz	25	23	36	26	22	36	22	32	26	21
K-Feldspar	0	0	0	0	0	0	0	0	0	0
Plagioclase (Albite)	7	3	11	7	14	3	0	3	0	0
Calcite	2	0	2	0	0	1	75	0	74	79
Dolomite	0	0	1	3	0	0	0	0	0	0
Halite	0	0	0	0	0	0	0	0	0	0
Siderite	0	0	0	0	0	0	0	0	0	0
Pyrite	3	3	3	4	1	1	3	0	0	0
Clay	63	71	47	60	63	59	0	65	0	0
Total	**100**	**100**	**100**	**100**	**100**	**100**	**100**	**100**	**100**	**100**

Sample ID	41	42	43	44	45	46	47	48	49	50
Depth (ft)	8904'11"	8911'4"	8912'7"	8915'6"	8917'6"	9013'11"	9018	9024'6"	9029'2"	9031'11"
	Bulk Mineralogy									
Quartz	57	49	53	No Sample	20	45	56	42	84	85
K-Feldspar	14	0	21		11	29	17	57	7	11
Plagioclase (Albite)	0	11	0		9	11	7	0	9	0
Calcite	25	32	22		18	0	0	0	0	0
Dolomite	2	8	3		2	2	3	1	0	1
Halite	0	0	0		0	0	0	0	0	0
Siderite	0	0	0		0	0	0	0	0	0
Pyrite	0	0	1		0	0	0	0	0	0
Clay	2	0	0		40	13	17	0	0	3
Total	**100**	**100**	**100**		**100**	**100**	**100**	**100**	**100**	**100**

Sample ID	51	52	53	54	55	56	57	58	59	60
Depth (ft)	9035'6"	9036'6"	9043'7"	RM1-68DO-M01	RM1-74HB-M01	RM1-79HO-M01	RM1-86HB-M01	RM1-93VB-M01	RM1-8298-M01	RM1-8475-M01
	Bulk Mineralogy									
Quartz	81	65	46	57	91	39	20	62	94	98
K-Feldspar	8	15	29	30	0	36	18	36	0	0
Plagioclase (Albite)	8	19	6	11	8	0	45	2	6	0
Calcite	0	0	0	0	0	0	0	0	0	2
Dolomite	0	1	1	2	1	0	0	0	0	0
Halite	0	0	0	0	0	0	0	0	0	0
Siderite	0	0	0	0	0	0	0	0	0	0
Pyrite	0	0	0	0	0	0	0	0	0	0
Clay	3	0	18	0	0	25	17	0	0	0
Total	**100**	**100**	**100**	**100**	**100**	**100**	**100**	**100**	**100**	**100**

Sample ID	61	62	63	64	65	66	67	68	69	70
Depth (ft)	RM1-8980-M01	RM1-9175-M01	RM1-9626-M01	RM1-9699-M01	9012.3	RM1-03DO-M01	RM1-05HO-M01	RM1-13VO-M01	RM1-16DB-M01	RM1-19VO-M01
	Bulk Mineralogy									
Quartz	63	27	31	26	48	34	38	28	20	32
K-Feldspar	11	0	0	0	0	0	0	0	0	0
Plagioclase (A	0	0	0	0	0	0	0	0	0	0
Calcite	24	0	0	4	8	0	0	0	0	0
Dolomite	0	9	0	0	0	0	0	0	0	0
Halite	0	0	0	0	0	0	0	0	0	0
Siderite	0	0	0	0	0	0	0	0	0	0
Pyrite	0	0	0	0	1	0	1	2	2	3
Clay	2	64	69	70	43	66	61	70	78	65
Total	**100**	**100**	**100**	**100**	**100**	**100**	**100**	**100**	**100**	**100**

Sample ID	71	72	73	74	75	76	77	78	79	80	81
Depth (ft)	RM1-25VO-M01	RM1-32VO-M01	RM1-35DO-M01	RM1-11HB-M01	RM1-22HO-M01	RM1-29HO-M01	RM1-38HO-M01	RM1-43VA-M01	RM1-47VO-M01	RM1-58HO-M01	RM1-52HO-M01
	Bulk Mineralogy										
Quartz	31	35	26	37	34	32	18	17	22	9	35
K-Feldspar		0	0	0	0	0	0	0	0	0	6
Plagioclase (Albite)		0	0	0	0	0	0	0	5	0	8
Calcite	1	0	0	0	0	0	0	1	10	10	0
Dolomite	1	1	0	0	2	2	0	1	0	0	1
Halite		0	0	0	0	0	0	0	0	0	0
Siderite		0	0	0	0	0	0	0	0	0	0
Pyrite	2	1	1	2	2	8	3	0	0	0	0
Clay	65	63	73	61	62	58	79	81	63	81	50
Total	**100**	**100**	**100**	**100**	**100**	**100**	**100**	**100**	**100**	**100**	**100**

University of Utah
RMCCS State # 1
Moffat County, Colorado
2.29.2012
CL File No.: DEN-120031



Spectral Core Gamma

Core 1

Depth (feet)	Gamma (API)	Th (ppm)	U (ppm)	K (%)
8180.04	87.19	4.54	1.94	2.10
8180.25	87.45	2.89	3.10	2.07
8180.46	86.96	2.56	4.28	1.85
8180.67	86.03	1.24	5.86	1.61
8180.87	82.56	0.31	6.86	1.30
8181.08	78.84	0.27	7.90	0.88
8181.29	74.68	0.23	8.32	0.52
8181.50	71.14	0.17	8.72	0.41
8181.71	68.33	0.16	8.02	0.55
8181.92	68.82	0.14	6.93	0.85
8182.12	71.85	0.50	5.35	1.24
8182.33	77.44	3.24	3.70	1.85
8182.54	83.58	7.91	1.93	2.31
8182.75	88.64	18.79	0.70	2.52
8182.96	89.78	24.28	0.19	2.58
8183.17	86.97	26.78	0.14	2.63
8183.37	82.08	24.94	0.18	2.41
8183.58	75.84	22.62	0.17	2.30
8183.79	69.36	19.64	0.15	2.27
8184.00	64.94	10.39	0.13	2.32
8184.21	62.91	6.32	0.12	2.24
8184.42	60.13	4.57	0.13	2.23
8184.62	57.66	3.70	0.19	2.15
8184.83	56.03	3.58	0.12	2.06
8185.04	54.32	7.03	0.14	1.85
8185.25	53.97	12.08	0.11	1.76
8185.46	54.76	19.70	0.15	1.69
8185.67	57.84	21.91	0.18	1.52
8185.87	62.02	22.01	0.13	1.46
8186.08	66.04	19.41	0.39	1.42
8186.29	68.69	13.13	1.42	1.22
8186.50	72.15	10.01	2.65	0.95
8186.71	72.46	5.85	4.80	0.71
8186.92	70.75	3.67	6.86	0.42
8187.12	68.52	2.21	8.74	0.19
8187.33	66.16	1.31	10.01	0.06
8187.54	66.04	0.14	11.49	0.19
8187.75	73.40	0.28	11.49	0.13
8187.96	87.05	1.82	11.32	0.30
8188.17	108.24	5.21	10.71	0.57
8188.37	136.94	10.12	10.72	0.84
8188.58	169.82	20.61	11.00	1.07
8188.79	201.39	26.50	11.85	1.22
8189.00	230.90	30.18	12.93	1.54
8189.21	252.86	33.19	14.14	1.81
8189.42	263.83	35.77	14.19	2.15
8189.62	259.55	36.91	12.23	2.58
8189.83	242.19	35.85	9.91	2.92
8190.04	212.86	32.62	7.75	2.83
8190.25	177.90	27.42	4.99	2.65
8190.46	142.28	22.02	2.63	2.39
8190.67	114.69	13.34	1.60	2.09
8190.87	96.04	6.66	1.45	1.81
8191.08	88.52	5.42	1.06	1.71
8191.29	89.08	3.99	2.45	1.55
8191.50	95.50	3.54	4.59	1.37
8191.71	101.00	2.79	6.16	1.31
8191.92	105.43	4.39	5.86	1.37
8192.12	106.65	5.38	5.61	1.41
8192.33	106.16	8.84	4.12	1.64
8192.54	103.89	10.56	1.99	2.02
8192.75	103.11	14.42	0.69	2.04
8192.96	101.80	10.51	1.56	1.83
8193.17	100.93	6.42	2.80	1.71
8193.37	98.48	3.00	4.11	1.55
8193.58	95.55	2.43	4.93	1.21
8193.79	91.72	2.80	5.17	1.06
8194.00	89.92	4.42	4.58	1.13
8194.21	88.75	7.07	3.45	1.16
8194.42	90.09	10.33	2.48	1.17
8194.62	92.43	8.44	2.79	1.14
8194.83	96.88	5.82	3.52	1.13
8195.04	99.93	4.20	4.28	1.04
8195.25	103.40	2.29	6.16	0.80
8195.46	105.68	1.31	8.44	0.54
8195.67	106.55	2.71	9.52	0.39
8195.87	104.91	4.41	10.43	0.27
8196.08	104.52	5.85	11.61	0.15
8196.29	102.40	8.96	11.60	0.13
8196.50	99.91	14.66	10.93	0.13
8196.71	98.88	18.77	10.97	0.11
8196.92	98.72	20.47	10.66	0.07
8197.12	96.81	21.59	9.41	0.04
8197.33	95.54	21.67	8.08	0.11
8197.54	94.36	17.85	7.47	0.20
8197.75	93.08	10.02	6.28	0.48
8197.96	90.58	5.18	6.32	0.64
8198.17	89.21	2.30	7.41	0.73
8198.37	87.69	0.45	8.37	0.77
8198.58	86.56	0.11	8.15	0.93
8198.79	84.11	0.19	8.13	0.91
8199.00	82.23	0.18	6.56	1.11
8199.21	80.68	0.11	4.32	1.43
8199.42	79.66	0.11	3.27	1.60
8199.62	78.03	0.11	3.20	1.51
8199.83	77.37	0.46	2.79	1.31
8200.04	78.27	2.28	3.19	1.00
8200.25	77.97	3.84	4.48	0.58
8200.46	77.47	6.88	4.64	0.27
8200.67	77.06	11.55	3.96	0.12
8200.87	77.52	13.96	4.19	0.05
8201.08	78.06	12.68	4.66	0.01
8201.29	81.37	19.18	3.77	0.02
8201.50	88.65	20.74	3.29	0.15
8201.71	100.06	23.21	4.17	0.16
8201.92	113.08	27.17	4.41	0.24
8202.12	129.53	31.12	4.39	0.43
8202.33	146.07	31.04	5.70	0.63
8202.54	160.58	31.70	7.33	0.61
8202.75	174.13	31.08	7.76	0.95

Core 2

Depth (feet)	Gamma (API)	Th (ppm)	U (ppm)	K (%)
8216.04	177.03	34.47	12.63	0.34
8216.25	164.74	29.12	13.05	0.49
8216.46	143.98	21.44	12.32	0.85
8216.67	121.11	9.59	11.22	1.24
8216.87	101.20	3.84	11.03	1.48
8217.08	84.95	1.87	10.35	1.70
8217.29	72.94	1.78	8.75	1.77
8217.50	67.52	3.33	7.02	1.62
8217.71	69.11	5.69	5.33	1.52
8217.92	76.27	7.02	3.78	1.66
8218.12	89.79	5.60	3.97	1.75
8218.33	107.71	4.08	5.03	1.88
8218.54	127.74	4.04	7.18	2.02
8218.75	147.08	4.10	9.68	1.95
8218.96	162.49	6.53	11.40	1.72
8219.17	171.30	13.31	11.30	1.50
8219.37	173.33	21.69	10.68	1.29
8219.58	169.22	25.31	8.46	1.18
8219.79	159.41	27.43	6.18	1.17
8220.00	145.88	25.94	4.81	1.15
8220.21	130.02	23.55	4.58	0.95
8220.42	114.06	18.57	4.77	0.79
8220.62	97.91	7.84	5.97	0.67
8220.83	83.64	3.40	6.82	0.72
8221.04	72.21	1.36	6.74	0.89
8221.25	65.85	0.17	6.15	1.23
8221.46	62.63	0.13	6.07	1.48
8221.67	63.40	0.11	6.07	1.56
8221.87	67.00	0.20	6.36	1.55
8222.08	72.16	0.13	7.45	1.44
8222.29	75.04	0.12	8.02	1.40
8222.50	75.15	0.12	7.20	1.47
8222.71	72.87	0.11	5.62	1.70
8222.92	68.59	0.19	4.03	1.82
8223.12	63.11	0.18	2.13	2.00
8223.33	59.86	0.14	1.42	2.04
8223.54	58.22	0.18	2.07	1.93
8223.75	56.99	0.10	3.19	1.68
8223.96	56.98	0.16	3.22	1.68
8224.17	58.03	0.14	3.32	1.66
8224.37	56.82	0.13	2.80	1.59
8224.58	57.37	0.14	1.65	1.73
8224.79	59.79	0.13	0.58	2.04
8225.00	61.85	0.19	1.13	1.93
8225.21	62.72	0.14	1.37	1.83
8225.42	65.78	0.30	1.88	1.78
8225.62	67.75	0.36	1.95	1.75
8225.83	70.34	0.41	2.71	1.57
8226.04	72.92	0.39	3.10	1.59
8226.25	75.81	0.12	3.98	1.53
8226.46	77.79	0.17	5.19	1.40
8226.67	80.02	0.13	6.98	1.12
8226.87	77.93	0.18	7.16	0.90
8227.08	74.83	0.19	6.39	0.81
8227.29	73.59	0.15	5.22	0.75
8227.50	72.92	1.06	3.40	0.93
8227.71	71.56	2.31	1.49	1.20
8227.92	74.45	3.60	0.46	1.48
8228.12	79.77	4.42	0.16	1.71
8228.33	82.62	4.12	0.17	2.16
8228.54	83.80	2.31	0.12	2.36
8228.75	84.38	1.17	0.10	2.53
8228.96	82.23	0.35	0.13	2.68
8229.17	77.80	0.24	0.11	2.68
8229.37	75.92	1.15	0.29	2.40
8229.58	74.93	1.49	1.06	2.22
8229.79	75.56	1.46	2.27	1.91
8230.00	79.35	1.66	3.15	1.70
8230.21	85.33	1.29	4.30	1.61
8230.42	89.64	0.29	5.58	1.56
8230.62	96.11	0.10	7.10	1.32
8230.83	101.90	0.19	8.50	1.07
8231.04	103.78	0.15	10.86	0.75
8231.25	103.19	0.18	13.16	0.41
8231.46	101.87	0.14	14.63	0.12
8231.67	98.45	0.13	14.69	0.00
8231.87	95.37	0.13	13.73	0.16
8232.08	95.92	0.11	11.48	0.57
8232.29	98.77	0.18	8.39	1.01
8232.50	101.88	0.19	5.89	1.49
8232.71	102.73	0.18	3.69	2.08
8232.92	101.89	0.18	3.25	2.34
8233.12	97.20	0.12	3.56	2.19
8233.33	90.28	0.11	4.78	2.02
8233.54	84.04	0.17	5.58	1.91
8233.75	78.78	0.11	6.62	1.56
8233.96	74.75	0.14	5.95	1.51
8234.17	73.05	0.19	5.29	1.68
8234.37	71.49	0.18	4.01	1.77
8234.58	69.21	0.16	3.25	1.65
8234.79	69.96	0.11	3.68	1.48
8235.00	70.44	0.11	5.27	1.11
8235.21	71.77	0.17	6.49	0.69
8235.42	74.99	0.11	7.68	0.32
8235.62	79.81	0.19	8.79	0.07
8235.83	84.03	0.17	8.30	0.09
8236.04	89.98	0.10	6.47	0.36
8236.25	95.40	0.16	4.63	0.72
8236.46	100.91	0.60	3.21	1.11
8236.67	107.60	2.28	2.10	1.43
8236.87	114.84	4.60	1.48	1.68
8237.08	124.14	7.55	2.81	1.61
8237.29	137.34	12.26	5.48	1.37
8237.50	153.91	16.82	8.82	1.16
8237.71	172.07	19.97	11.06	1.08
8237.92	191.17	23.73	13.21	1.05
8238.12	206.42	27.09	14.18	1.23
8238.33	214.04	29.21	13.70	1.51
8238.54	211.93	31.80	12.21	1.61
8238.75	199.15	31.37	11.39	1.56

Core 3

Depth (feet)	Gamma (API)	Th (ppm)	U (ppm)	K (%)
8895.10	49.60	0.18	2.97	2.07
8895.31	55.87	0.17	2.60	2.65
8895.52	62.10	0.10	3.01	2.91
8895.72	67.75	0.17	3.49	3.11
8895.93	72.71	1.08	3.65	3.23
8896.14	75.31	3.10	2.83	3.11
8896.35	75.12	4.01	3.45	2.63
8896.56	74.28	3.87	3.83	2.34
8896.77	71.73	3.65	3.89	2.02
8896.97	68.14	2.43	3.18	1.83
8897.18	66.43	0.93	3.26	1.76
8897.39	65.90	0.53	2.58	1.94
8897.60	65.66	0.69	1.91	2.02
8897.81	66.80	1.15	1.21	2.11
8898.02	67.70	1.00	1.17	2.13
8898.22	65.15	0.66	0.72	2.14
8898.43	61.31	0.42	0.52	2.04
8898.64	57.95	0.50	0.22	2.01
8898.85	53.77	0.30	0.30	1.89
8899.06	49.67	0.66	0.35	1.80
8899.27	48.47	1.15	0.74	1.70
8899.47	48.70	1.09	1.78	1.57
8899.68	47.62	0.75	2.22	1.56
8899.89	47.60	0.57	2.56	1.73
8900.10	47.93	0.19	2.46	1.96
8900.31	46.07	0.19	2.06	2.24
8900.52	43.02	0.16	1.02	2.64
8900.72	41.01	0.15	0.58	2.83
8900.93	39.88	0.15	0.12	2.96
8901.14	39.82	0.16	0.11	3.17
8901.35	43.29	0.11	0.13	3.35
8901.56	48.87	0.38	0.19	3.31
8901.77	54.18	2.26	0.17	3.20
8901.97	56.34	4.71	0.12	3.10
8902.18	56.43	7.22	0.14	2.78
8902.39	53.28	9.78	0.18	2.38
8902.60	48.19	9.90	0.17	2.06
8902.81	42.99	6.02	0.17	1.94
8903.02	40.63	3.36	0.18	1.78
8903.22	41.27	1.81	0.12	1.71
8903.43	43.61	1.51	0.38	1.64
8903.64	47.38	2.52	0.39	1.79
8903.85	52.46	4.51	0.51	1.89
8904.06	57.23	6.87	0.54	1.99
8904.27	61.32	8.14	0.52	2.12
8904.47	64.34	6.69	0.19	2.40
8904.68	66.78	6.10	0.19	2.31
8904.89	67.89	6.47	0.11	2.09
8905.10	67.14	6.39	0.20	1.97
8905.31	62.91	6.43	0.19	1.85
8905.52	59.72	8.81	0.13	1.64
8905.72	55.88	10.57	0.17	1.73
8905.93	52.59	9.10	0.19	1.95
8906.14	51.58	9.91	0.12	2.02
8906.35	53.67	11.79	0.14	1.99
8906.56	55.33	13.60	0.14	2.05
8906.77	57.03	12.36	0.14	2.26
8906.97	59.61	15.56	0.14	2.58
8907.18	61.93	11.85	0.14	3.13
8907.39	64.57	9.32	0.19	3.85
8907.60	67.64	5.38	0.19	4.48
8907.81	70.50	3.38	0.25	4.66
8908.02	70.21	1.04	1.09	4.51
8908.22	67.56	0.31	2.34	4.06
8908.43	62.05	0.12	3.14	3.39
8908.64	53.53	0.14	3.35	2.69
8908.85	45.39	0.17	3.12	2.22
8909.06	40.45	0.16	2.28	1.89
8909.27	38.17	0.11	1.02	1.74
8909.47	38.21	0.13	0.23	1.75
8909.68	42.42	1.17	0.18	1.75
8909.89	48.16	2.86	0.41	1.62
8910.10	51.97	3.85	1.59	1.47
8910.31	53.56	3.88	2.55	1.35
8910.52	54.46	5.14	2.94	1.16
8910.72	52.65	5.43	2.94	1.06
8910.93	48.39	4.46	2.57	1.09
8911.14	45.38	3.79	1.39	1.16
8911.35	42.86	3.48	0.42	1.26
8911.56	40.84	2.19	0.11	1.34
8911.77	40.49	0.58	0.19	1.51
8911.97	42.48	0.11	1.43	1.50
8912.18	44.28	0.15	2.71	1.50
8912.39	48.37	0.13	3.79	1.36
8912.60	51.84	0.10	4.63	1.26
8912.81	54.12	0.16	5.78	0.94
8913.02	55.53	0.16	4.68	0.90
8913.22	57.20	0.18	3.41	1.06
8913.43	57.56	0.12	2.33	1.39
8913.64	58.41	0.15	1.42	1.70
8913.85	60.31	0.13	0.16	2.14
8914.06	60.95	0.19	0.18	2.36
8914.27	60.47	0.12	0.19	2.29
8914.47	59.39	0.17	0.10	2.11
8914.68	58.79	0.16	0.18	2.04
8914.89	57.55	0.19	0.13	1.99
8915.10	57.55	0.33	0.15	2.08
8915.31	57.34	0.67	0.12	2.26
8915.52	57.67	1.44	0.15	2.37
8915.72	56.91	4.01	0.11	2.38
8915.93	55.59	6.12	0.15	2.22
8916.14	53.95	5.09	0.20	2.00
8916.35	54.57	6.33	0.19	1.77
8916.56	54.55	7.13	0.12	1.63
8916.77	57.02	5.27	0.18	1.46
8916.97	61.35	6.01	0.25	1.52
8917.18	66.55	12.66	0.40	1.54
8917.39	70.47	17.13	1.00	1.58
8917.60	75.38	20.01	1.89	1.59
8917.81	77.94	22.25	2.42	1.71

Core 4

Depth (feet)	Gamma (API)	Th (ppm)	U (ppm)	K (%)
9012.00	34.96	0.15	0.94	1.86
9012.21	33.29	0.16	1.06	2.14
9012.42	33.16	0.15	0.62	2.49
9012.62	33.34	0.16	0.55	2.66
9012.83	32.64	0.20	0.57	2.68
9013.04	30.89	0.16	0.57	2.46
9013.25	29.47	0.10	0.44	2.24
9013.46	27.58	0.18	0.25	2.02
9013.67	25.30	0.33	0.10	1.77
9013.87	23.53	0.45	0.12	1.46
9014.08	23.19	0.56	0.27	1.28
9014.29	21.57	0.57	1.09	0.96
9014.50	18.02	0.52	1.17	0.65
9014.71	15.11	0.14	1.25	0.44
9014.92	12.49	0.17	1.18	0.45
9015.12	9.31	0.28	0.98	0.49
9015.33	7.44	0.49	0.16	0.78
9015.54	7.20	0.54	0.12	1.00
9015.75	6.71	0.54	0.13	1.13
9015.96	7.87	0.50	0.27	1.13
9016.17	10.06	0.12	0.96	1.05
9016.37	11.97	0.16	1.14	0.86
9016.58	15.81	0.12	1.14	0.94
9016.79	21.38	0.17	1.09	1.30
9017.00	25.62	0.17	0.96	1.60
9017.21	27.80	0.18	0.29	1.99
9017.42	29.36	0.19	0.26	2.31
9017.62	28.77	0.20	0.30	2.43
9017.83	26.33	0.13	0.30	2.35
9018.04	22.69	0.20	0.23	2.34
9018.25	19.71	0.16	0.21	2.17
9018.46	17.38	0.10	0.18	2.11
9018.67	15.25	0.19	0.17	1.94
9018.87	13.29	0.16	0.17	1.64
9019.08	11.77	0.17	0.11	1.43
9019.29	10.79	0.15	0.19	1.35
9019.50	9.03	0.16	0.15	1.15
9019.71	7.09	0.11	0.17	1.05
9019.92	5.44	0.19	0.25	1.13
9020.12	4.47	0.14	1.22	1.00
9020.33	4.00	0.14	1.96	0.88
9020.54	4.00	0.11	2.58	0.81
9020.75	4.00	0.17	2.55	0.76
9020.96	2.00	0.11	2.37	0.64
9021.17	3.00	0.12	1.40	0.73
9021.37	4.00	0.12	0.65	0.91
9021.58	4.00	0.15	0.12	1.22
9021.79	4.00	0.15	0.17	1.58
9022.00	3.00	0.14	0.18	2.02
9022.21	3.00	0.17	0.14	2.32
9022.42	4.00	0.14	0.13	2.45
9022.62	4.00	0.16	0.18	2.33
9022.83	2.00	0.11	0.16	2.08
9023.04	3.00	0.17	0.15	1.63
9023.25	4.00	0.19	0.10	1.33
9023.46	2.00	0.19	0.13	0.99
9023.67	2.00	0.14	0.15	0.75
9023.87	2.00	0.18	0.16	0.66
9024.08	2.00	0.14	0.15	0.70
9024.29	4.00	0.14	0.44	0.52
9024.50	4.00	0.14	0.88	0.43
9024.71	3.00	0.16	1.47	0.35
9024.92	3.00	0.12	1.81	0.22
9025.12	2.00	0.11	2.29	0.17
9025.33	4.72	0.18	2.35	0.27
9025.54	6.54	0.15	2.02	0.38
9025.75	9.35	0.13	2.06	0.43
9025.96	13.47	0.17	3.49	0.41
9026.17	17.81	0.11	4.20	0.36
9026.37	21.43	0.15	4.88	0.25
9026.58	25.75	0.15	6.51	0.15
9026.79	29.15	0.13	7.54	0.10
9027.00	30.09	0.10	6.01	0.17
9027.21	28.58	0.22	4.88	0.13
9027.42	25.26	0.30	3.71	0.20
9027.62	19.29	0.35	1.98	0.35
9027.83	13.08	0.43	0.32	0.52
9028.04	8.02	0.31	0.11	0.62
9028.25	5.12	0.13	0.12	0.88
9028.46	2.00	0.15	0.11	1.06
9028.67	2.00	0.18	0.14	1.08
9028.87	3.00	0.20	0.18	1.13
9029.08	2.00	0.18	0.15	1.06
9029.29	2.00	0.15	0.34	0.87
9029.50	4.39	0.13	1.45	0.65
9029.71	5.97	0.15	1.70	0.64
9029.92	7.51	0.17	1.81	0.50
9030.12	9.11	0.17	1.78	0.64
9030.33	9.74	0.11	1.48	0.80
9030.54	9.11	0.20	0.38	0.92
9030.75	7.76	0.11	0.13	0.98
9030.96	6.34	0.18	0.11	1.19
9031.17	4.73	0.14	0.12	1.25
9031.37	4.02	0.19	0.12	1.41
9031.58	2.00	0.12	0.16	1.66
9031.79	3.00	0.17	0.15	1.78
9032.00	2.00	0.15	0.19	1.76
9032.21	2.00	0.13	0.19	1.87
9032.42	3.00	0.15	0.16	1.82
9032.62	2.00	0.20	0.19	1.79
9032.83	4.00	0.13	0.12	1.89
9033.04	2.00	0.14	0.19	2.14
9033.25	3.00	0.17	0.18	2.02
9033.46	2.00	0.20	0.16	2.04
9033.67	2.00	0.17	0.14	2.00
9033.87	4.00	0.15	0.11	1.89
9034.08	5.24	0.20	0.11	1.72
9034.29	8.33	0.13	0.15	1.86
9034.50	11.12	0.19	0.11	1.79
9034.71	14.19	0.13	0.16	1.79

8202.96	188.15	30.23	8.65	1.27
8203.17	198.57	30.02	9.99	1.42
8203.37	208.18	30.92	10.94	1.58
8203.58	217.22	32.01	11.10	2.08
8203.79	222.98	34.36	11.55	2.24
8204.00	222.55	35.59	11.62	2.31
8204.21	216.89	36.42	10.54	2.37
8204.42	208.31	38.26	8.49	2.51
8204.62	193.89	38.58	7.60	2.05
8204.83	173.44	35.77	6.90	1.57
8205.04	145.49	35.98	5.76	1.11
8205.25	134.44	35.67	5.41	0.87
8205.46	118.67	33.71	6.12	0.33
8205.67	98.74	31.94	5.92	0.10
8205.90	45.23	57.03	13.01	0.14

5781.04	2.63	0.15	1.53	0.29
5781.25	7.48	0.18	2.61	0.38
5781.46	16.66	0.17	3.76	0.70
5781.67	30.54	0.19	4.84	1.52
5781.87	51.64	0.16	5.62	2.84
5782.08	77.88	0.11	6.47	4.42
5782.29	105.62	0.19	6.34	6.48
5782.5	133.03	0.14	5.68	8.77
5782.71	157.6	0.13	4.61	10.82
5782.92	174.86	0.19	4.63	12.30
5783.12	186.47	0.11	3.99	13.56

8238.96	177.37	27.75	10.60	1.34
8239.17	150.13	24.16	9.18	0.99
8239.37	122.73	21.29	7.84	0.60
8239.58	98.44	17.89	7.04	0.32
8239.79	80.93	15.14	6.23	0.13
8240.00	69.84	13.75	5.70	0.04
8240.21	65.32	12.93	5.77	0.01
8240.42	64.67	11.56	5.88	0.14
8240.62	68.38	8.88	5.86	0.07
8240.83	73.62	6.50	5.69	0.19
8241.04	81.91	7.50	4.52	0.43
8241.25	91.20	7.57	3.95	0.72
8241.46	100.34	6.54	4.00	0.98
8241.67	106.96	5.98	3.96	1.26
8241.87	114.46	5.22	4.11	1.56
8242.08	118.16	2.43	5.58	1.68
8242.29	120.46	1.69	6.37	1.68
8242.50	123.86	2.74	6.78	1.73
8242.71	127.25	5.06	6.99	1.60
8242.92	125.02	8.00	7.16	1.29
8243.12	123.02	11.90	6.95	1.00
8243.33	120.02	11.58	6.95	0.75
8243.54	115.35	10.84	6.98	0.48
8243.75	111.52	9.45	7.08	0.38
8243.96	111.19	5.87	7.57	0.50
8244.17	110.11	3.63	8.07	0.74
8244.37	109.28	2.51	9.02	0.98
8244.58	106.88	0.94	9.86	1.23
8244.79	102.33	0.13	10.88	1.40
8245.00	96.25	0.17	11.06	1.33
8245.21	91.78	0.11	10.98	1.16
8245.42	87.22	0.18	10.01	1.04
8245.62	83.92	0.16	8.94	0.98
8245.83	81.46	0.11	7.57	0.88
8246.04	81.23	0.18	6.69	0.80
8246.25	79.79	0.51	5.60	0.75
8246.46	78.27	0.84	4.90	0.77
8246.67	77.88	2.46	4.49	0.73
8246.87	79.38	4.48	4.37	0.74
8247.08	79.97	4.31	4.17	0.97
8247.29	81.27	3.44	4.56	1.20
8247.50	82.47	3.28	5.39	1.20
8247.71	82.14	1.60	6.20	1.18
8247.92	80.26	0.28	6.87	1.17
8248.12	78.58	0.18	7.54	1.02
8248.33	78.72	0.27	8.27	0.84
8248.54	82.05	0.84	8.28	0.80
8248.75	88.41	2.49	8.22	0.80
8248.96	95.61	5.00	8.46	0.69
8249.17	102.95	8.28	8.98	0.62
8249.37	108.12	11.52	8.42	0.79
8249.58	109.92	13.34	7.82	1.00
8249.79	109.61	11.42	7.38	1.14
8250.00	109.51	8.81	6.38	1.42
8250.21	110.26	7.97	4.49	1.71
8250.42	113.32	7.45	4.40	1.71
8250.62	118.88	5.92	4.98	1.63
8250.83	125.41	4.97	5.16	1.68
8251.04	131.58	3.75	5.72	1.70
8251.25	137.60	1.84	6.79	1.75
8251.46	141.60	0.55	6.64	1.99
8251.67	144.71	0.13	6.76	2.11
8251.87	147.81	0.15	7.92	2.03
8252.08	150.70	0.14	9.60	1.84
8252.29	150.41	0.11	11.26	1.50
8252.50	149.23	0.16	13.33	0.98
8252.71	145.90	0.12	14.33	0.63
8252.92	139.56	0.22	13.20	0.54
8253.12	133.91	0.26	11.28	0.63
8253.33	132.77	0.71	9.47	0.94
8253.54	133.37	1.26	6.85	1.45
8253.75	135.19	3.30	4.79	1.85
8253.96	138.45	4.79	5.06	2.01
8254.17	138.72	7.21	6.12	1.89
8254.37	133.51	8.98	7.63	1.47
8254.58	126.24	8.07	10.01	0.95
8254.79	117.74	5.08	11.96	0.50
8255.00	108.22	3.49	12.03	0.17
8255.21	101.00	1.59	11.25	0.03
8255.42	98.98	0.31	9.63	0.20
8255.62	100.18	0.86	7.03	0.58
8255.83	103.12	2.84	5.18	0.85
8256.04	109.45	4.29	5.32	0.99
8256.25	115.67	6.04	5.92	1.06
8256.46	119.30	9.91	6.34	0.96
8256.67	122.17	12.67	7.44	0.62
8256.87	126.72	11.48	8.50	0.52
8257.08	132.10	15.12	7.80	0.60
8257.29	138.32	20.76	6.48	0.72
8257.50	144.47	20.69	6.35	0.95
8257.71	146.26	20.04	6.42	1.06
8257.92	142.32	19.44	5.97	0.92
8258.12	131.81	15.29	5.87	0.70
8258.33	119.26	6.88	6.53	0.52
8258.54	107.30	3.90	6.71	0.23
8258.75	99.55	1.86	6.36	0.30
8258.96	95.51	0.66	6.02	0.69
8259.17	95.91	0.12	5.82	1.34
8259.37	97.54	0.11	4.90	2.11
8259.58	97.84	0.16	3.56	3.01
8259.79	90.96	0.17	3.52	3.50
8260.00	85.07	0.14	3.29	3.70
8260.21	80.40	0.16	2.95	3.84
8260.42	71.23	0.11	3.33	3.76
8260.65	0.20	0.12	4.95	0.74

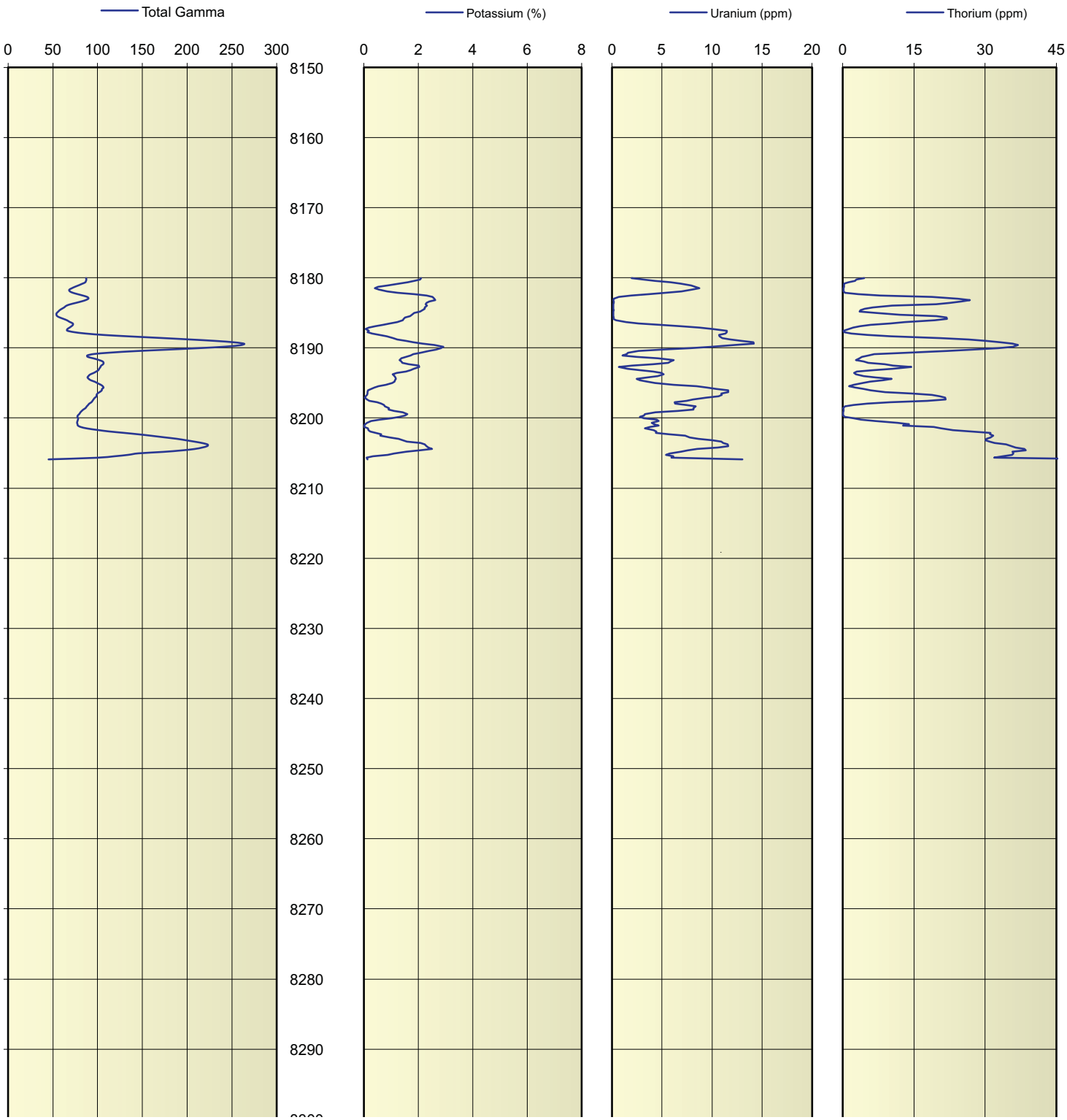
8918.02	79.75	21.75	2.94	1.78
8918.22	79.08	13.03	3.93	1.92
8918.43	77.96	7.09	4.50	2.03
8918.64	76.69	3.75	4.32	2.23
8918.85	74.62	1.25	4.47	2.31
8919.06	71.18	0.14	4.61	2.38
8919.27	71.00	0.12	3.58	2.59
8919.47	71.15	1.35	2.40	2.87
8919.68	69.89	2.48	1.68	3.07
8919.89	68.54	3.08	0.84	3.47
8920.10	69.05	4.63	0.11	3.88
8920.31	67.58	7.18	0.12	4.08
8920.52	66.34	5.26	0.18	3.97
8920.72	66.61	4.70	0.14	3.81
8920.93	69.57	5.97	0.61	3.50
8921.14	71.48	6.01	1.05	3.04
8921.35	74.54	5.31	1.29	2.67
8921.56	77.37	7.30	1.24	2.65
8921.77	80.02	9.15	1.16	2.77
8921.97	81.36	9.54	0.69	2.81
8922.18	83.35	11.18	0.25	2.88
8922.39	83.92	11.87	0.19	2.97
8922.60	83.65	8.57	0.18	3.00
8922.81	81.42	5.68	0.11	2.90
8923.02	76.61	3.53	0.14	2.92
8923.22	69.62	1.36	0.11	3.01
8923.43	64.07	0.16	0.19	3.14
8923.64	59.70	0.17	0.11	3.26
8923.85	57.86	0.69	0.15	3.55
8924.06	60.26	2.43	0.20	3.89
8924.27	66.25	5.70	0.10	4.33
8924.47	69.74	7.22	0.70	4.39
8924.68	77.06	11.76	3.18	4.41
8924.89	81.01	14.18	4.06	4.44
8925.10	84.40	15.01	5.63	4.33
8925.31	85.83	9.24	9.14	3.71
8925.55	133.24	36.35	36.68	1.99

9034.92	17.56	0.13	0.17	1.76
9035.12	19.11	0.17	0.15	1.58
9035.33	17.97	0.10	0.10	1.41
9035.54	18.53	0.10	0.16	1.43
9035.75	20.37	0.14	0.10	1.55
9035.96	20.99	0.14	0.16	1.78
9036.17	22.36	0.12	0.12	2.21
9036.37	24.28	0.17	0.18	2.56
9036.58	24.18	0.16	0.12	2.99
9036.79	21.88	0.11	0.12	3.08
9037.00	19.49	0.13	0.13	2.97
9037.21	16.36	0.15	0.15	2.69
9037.42	14.22	0.13	0.12	2.45
9037.62	11.93	0.10	0.18	2.02
9037.83	10.73	0.16	0.13	1.83
9038.04	9.81	0.16	0.13	1.75
9038.25	9.08	0.15	0.19	1.77
9038.46	7.58	0.14	0.11	1.79
9038.67	6.49	0.11	0.65	1.58
9038.87	5.09	0.17	0.89	1.31
9039.08	3.93	0.16	1.08	1.13
9039.29	2.00	0.15	1.14	0.98
9039.50	4.00	0.13	1.22	0.77
9039.71	3.00	0.16	0.58	1.09
9039.92	4.00	0.15	0.35	1.65
9040.12	4.00	0.11	0.15	2.15
9040.33	4.61	0.17	0.14	2.59
9040.54	5.50	0.14	0.11	3.22
9040.75	5.49	0.16	0.14	3.40
9040.96	5.79	0.16	0.13	3.18
9041.17	5.79	0.19	0.14	2.81
9041.37	4.89	0.11	0.10	2.38
9041.58	4.12	0.10	0.17	1.84
9041.79	5.34	0.11	0.15	1.61
9042.00	5.99	0.10	0.15	1.50
9042.21	6.84	0.13	0.18	1.50
9042.42	8.28	0.15	0.16	1.55
9042.62	9.72	0.16	0.13	1.49
9042.83	9.51	0.13	0.10	1.32
9043.04	11.91	0.14	0.17	1.43
9043.25	15.03	0.19	0.11	1.58
9043.46	19.36	0.14	0.16	1.88
9043.67	25.46	0.16	0.11	2.47
9043.87	34.89	0.16	0.11	2.92
9044.08	42.35	0.15	3.04	2.78
9044.29	47.37	0.16	3.88	2.92
9044.50	53.20	0.15	5.38	2.91
9044.71	60.52	0.12	8.73	2.29
9044.95	39.65	0.14	46.05	0.13

5783.33	193.11	0.15	3.36	14.28
5783.54	195.6	0.16	2.95	14.52
5783.75	195.59	0.15	2.81	14.62
5783.96	196.55	0.13	1.87	14.66
5784.17	197.07	0.17	1.53	14.48
5784.37	197.75	0.18	1.33	14.41
5784.58	197.34	0.18	1	14.26
5784.79	195.2	0.13	0.79	14.16
5785	189.37	0.19	0.58	14.19
5785.21	179.26	0.11	0.29	14.00
5785.42	162.98	0.18	0.13	13.19
5785.62	141.85	0.14	0.53	11.77
5785.83	116.71	0.15	1.51	9.61
5786.04	88.53	0.17	2.4	7.02
5786.25	59.83	0.14	2.56	4.51
5786.46	36.19	0.11	3.51	2.43
5786.67	18.63	0.19	4.22	1.06
5786.87	7.08	0.18	4	0.35
5787.08	1.48	0.16	4.1	0.06
5787.29	1.58	0.11	4.61	0.11
5787.5	2.6	0.11	3.72	0.08
5787.71	2.74	0.13	2.6	0.13
5787.92	2.71	0.16	1.84	0.25
5788.12	2.64	0.15	0.84	0.38
5788.33	3.14	1.42	0.14	0.45
5788.54	6.67	3.71	0.19	0.41
5788.75	14.67	6.35	0.18	0.48
5788.96	24.52	9.79	0.18	0.49
5789.17	34.88	8.72	0.1	0.62
5789.37	42.57	5.76	0.44	0.79
5789.58	45.56	3.11	0.57	1.08
5789.79	43.73	1.01	0.82	1.25
5790	41.2	0.15	1.75	1.35
5790.21	38.2	0.16	2.14	1.19
5790.42	38.78	0.19	2.3	1.07
5790.62	43.05	0.12	3.33	0.77
5790.83	48.79	0.17	4.26	0.50
5791.04	51.48	0.16	3.45	0.46
5791.25	51.39	0.16	2.95	0.64
5791.46	45.06	0.14	2.46	0.70
5791.67	33.5	0.17	1.29	0.83
5791.87	21.47	0.19	0.11	0.87
5792.08	11.44	0.87	0.19	0.72
5792.29	4.64	3.02	0.17	0.49
5792.5	4.71	6.39	0.19	0.38
5792.71	11	12.45	0.19	0.27
5792.92	18.34	18.98	0.16	0.21
5793.12	27.46	18.47	0.15	0.23
5793.33	36.53	15.82	0.17	0.19
5793.54	42.97	14.04	0.19	0.12
5793.75	46.78	13.75	0.15	0.15
5793.96	50.68	18.87	0.13	0.18
5794.17	52.51	21.33	0.16	0.16
5794.37	53.51	22.27	0.2	0.26
5794.58	53.35	20.17	0.1	0.27
5794.79	53.58	11.66	0.33	0.35
5795	54.71	5.33	1.53	0.50
5795.21	58.84	2.05	3.59	0.46
5795.42	64.17	0.28	5.48	0.37
5795.62	69.79	0.16	6.83	0.46
5795.83	74.72	0.12	8.14	0.33
5796.04	76.55	0.13	7.9	0.13
5796.25	73.87	0.2	5.94	0.29
5796.46	69.14	0.16	4.08	0.49
5796.67	65.17	0.53	2.62	0.48
5796.87	61.22	0.75	1.09	0.64
5797.08	58.58	0.7	0.14	0.88
5797.29	56.35	0.66	0.25	0.88
5797.5	55.36	0.6	1.37	0.70
5797.71	53.53	0.14	3	0.61
5797.92	50.66	0.12	4.4	0.43
5798.12	46.18	0.15	5.26	0.18
5798.33	43.35	0.16	6.04	0.04
5798.54	40.67	0.15	5.95	0.00
5798.75	39.35	0.26	5.53	0.12
5798.96	39	0.26	5.87	0.01
5799.17	41.91	0.25	7.08	0.01
5799.37	45.08	0.12	7.42	0.07
5799.58	47.99	0.12	7.52	0.13
5799.79	49.42	0.15	6.7	0.24
5800	50.88	1.7	4.96	0.26
5800.21	49.16	5.21	2.88	0.27
5800.42	43.15	10.58	1.53	0.21
5800.62	34.66	20.9	0.39	0.15
5800.83	25	24.75	0.16	0.04
5801.04	15.16	22.51	0.11	0.01
5801.25	8.62	15.97	0.15	0.16
5801.46	9.88	7.81	1.31	0.15
5801.67	15.71	2.87	2.89	0.17
5801.87	25.47	0.5	4.55	0.11
5802.08	37.29	0.11	5.39	0.05
5802.29	47.36	0.46	5.28	0.07
5802.5	52.97	1.8	4.13	0.15
5802.71	56.55	2.52	2.54	0.30
5802.92	57.64	3.01	0.89	0.47
5803.12	58.52	4.43	0.11	0.55
5803.33	60.21	3.19	0.13	0.71
5803.54	63.98	2.46	0.82	0.72
5803.75	69.42	3.65	1.77	0.62
5803.96	75.52	5.62	2.94	0.45
5804.17	78.15	5.89	4.1	0.32
5804.37	80.15	8.59	4.53	0.18
5804.58	79.7	10.42	3.85	0.32
5804.79	77.56	11.25	2.9	0.45
5805	75.15	10.84	1.74	0.84
5805.21	74.6	12.79	0.58	1.27
5805.42	73.29	15.89	0.15	1.65
5805.62	73.79	18.39	0.17	1.77
5805.83	74.68	18.2	0.11	2.04
5806.04	76.95	19.45	0.15	1.93
5806.25	80.12	19.58	0.74	1.78
5806.46	83.71	18.79	1.19	1.51
5806.67	85.63	19.04	1.61	1.27
5806.87	86.36	19.75	1.66	0.87
5807.08	85.19	18.98	1.72	0.61
5807.29	83.55	18.12	1.3	0.34
5807.5	81.57	11.36	1.46	0.21
5807.71	79.81	6.38	1.22	0.20
5807.92	78.92	3.24	1.33	0.33
5808.12	79.3	1.18	1.17	0.56
5808.33	78.18	0.11	1.07	0.85
5808.54	79.19	0.11	0.62	1.06

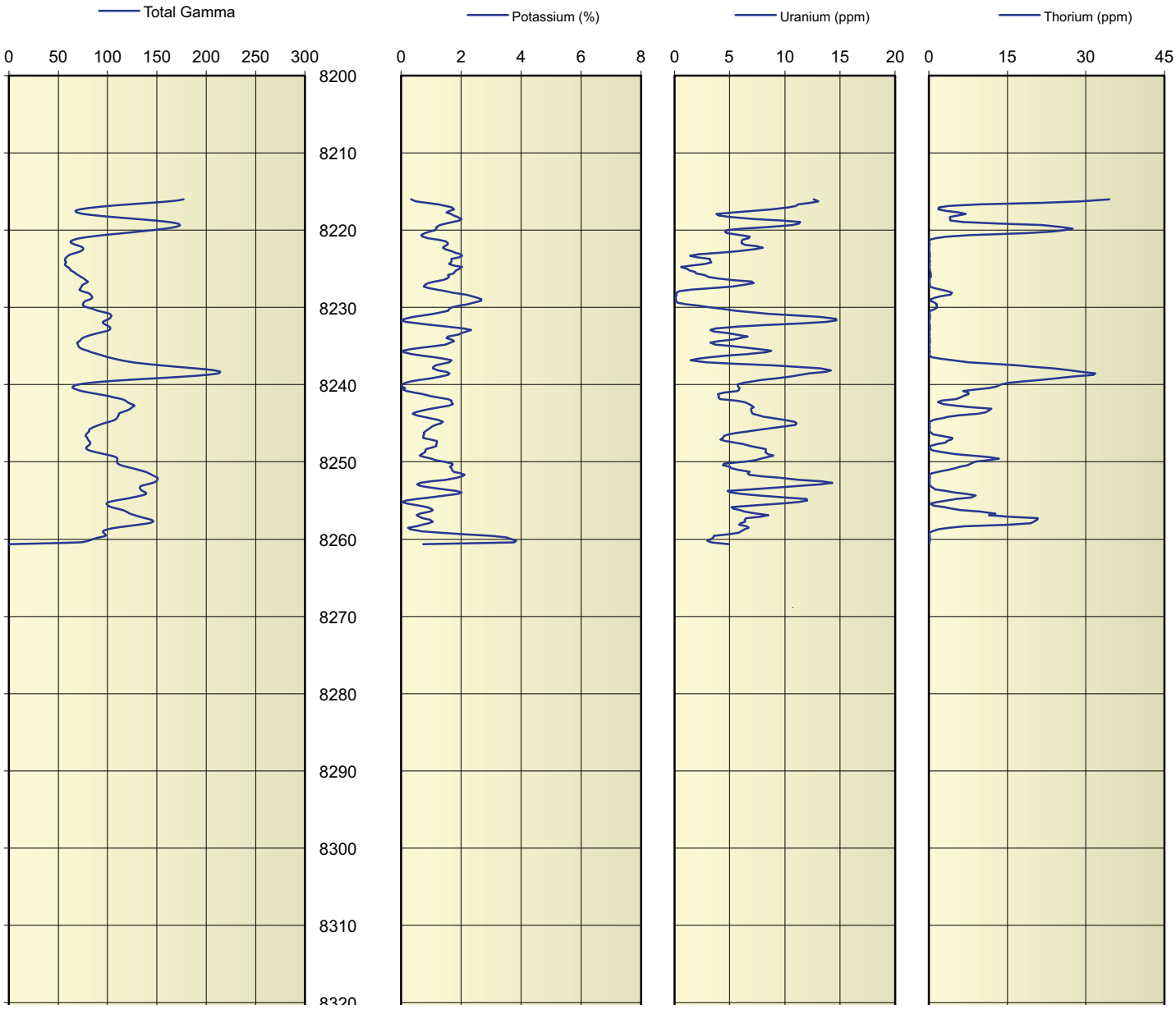
5808.75	81.25	0.19	0.89	1.25
5808.96	83.21	0.11	1.46	1.40
5809.17	83.26	0.12	1.76	1.55
5809.37	84.38	0.18	1.71	1.82
5809.58	83.25	0.14	1.55	2.21
5809.79	81.29	0.1	1.1	2.47
5810	79.72	0.13	0.37	2.54
5810.21	79.48	0.16	0.19	2.36
5810.42	80.91	0.2	1.04	1.83
5810.62	85.11	1.5	2.65	1.19
5810.83	90.54	4.29	4.62	0.64
5811.04	95.26	7.61	6.42	0.26
5811.25	98.88	13.56	8.26	0.03
5811.46	97.18	17.54	9.28	0.15
5811.67	87.33	12.72	9.43	0.15
5811.87	72.45	7.4	8.93	0.15
5812.08	54.94	4.32	8.62	0.14
5812.29	37.62	1.63	7.68	0.20
5812.5	25.69	0.31	5.85	0.02
5812.71	23.38	0.74	4.11	0.16
5812.92	28.24	0.88	2.85	0.33
5813.12	39.09	0.79	1.61	0.61
5813.33	53.13	0.81	1.15	0.91
5813.54	67.27	0.87	1.96	1.21
5813.75	78.5	0.21	3.12	1.36
5813.96	86.78	0.13	3.51	1.60
5814.17	93.27	0.43	3.67	1.73
5814.37	97.18	1.59	3.2	1.96
5814.58	98.48	2.87	2.24	2.19
5814.79	97.84	3.89	1.07	2.45
5815	95.84	5.92	0.49	2.47
5815.21	89.69	6.88	0.19	2.48
5815.42	81.27	5.13	0.11	2.13
5815.62	72.88	5.11	0.16	1.72
5815.83	65.03	4.1	0.12	1.35
5816.04	58.52	2.46	0.18	1.14
5816.25	54.35	1.22	0.12	0.87
5816.46	52.48	0.97	0.13	0.90
5816.67	50.18	0.13	0.18	0.98
5816.87	47.45	0.14	0.19	1.03
5817.08	41.31	0.18	0.53	0.99
5817.29	39.12	0.1	1.63	1.00
5817.5	35.61	0.2	2.06	0.97
5817.71	31.61	0.11	2.87	0.92
5817.95	41.05	0.15	22.31	0.19

University of Utah
RMCCS State # 1
Moffat County, Colorado
Spectral Core Gamma
Scale 5" = 100'

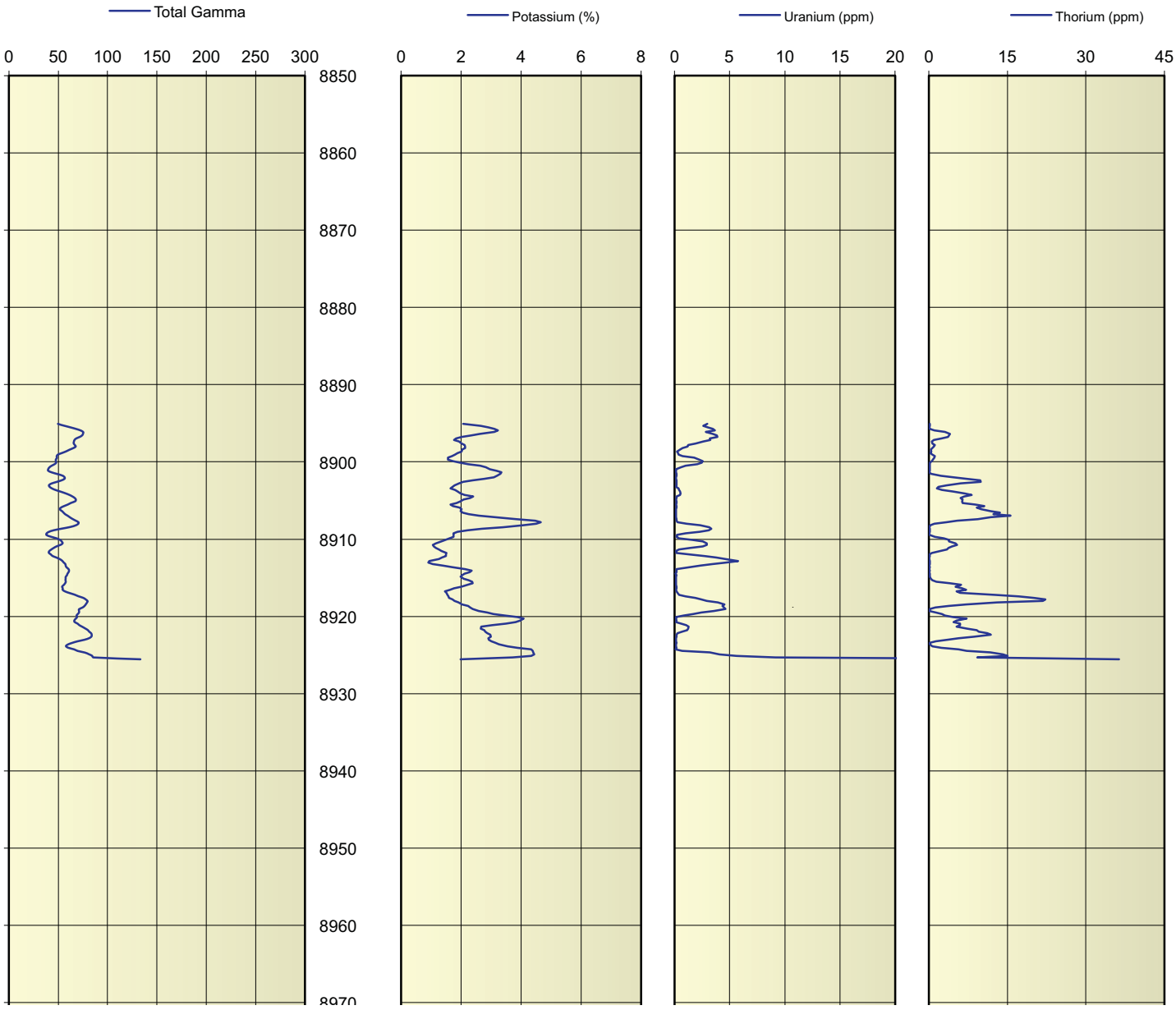


Core Lab
RESERVOIR OPTIMIZATION

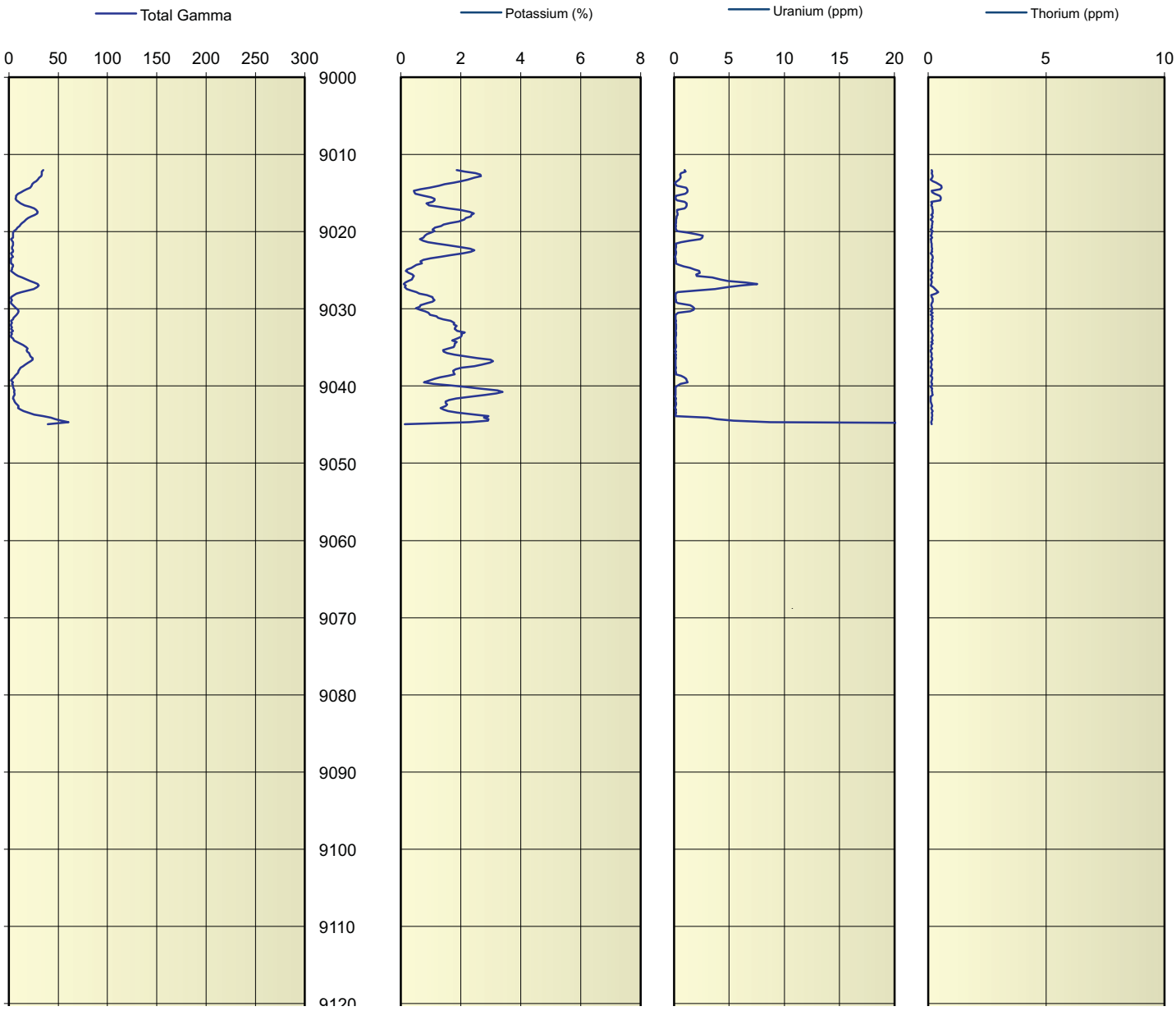
University of Utah
RMCCS State # 1
Moffat County, Colorado
Spectral Core Gamma
Scale 5" = 100'



University of Utah
RMCCS State # 1
Moffat County, Colorado
Spectral Core Gamma
Scale 5" = 100'



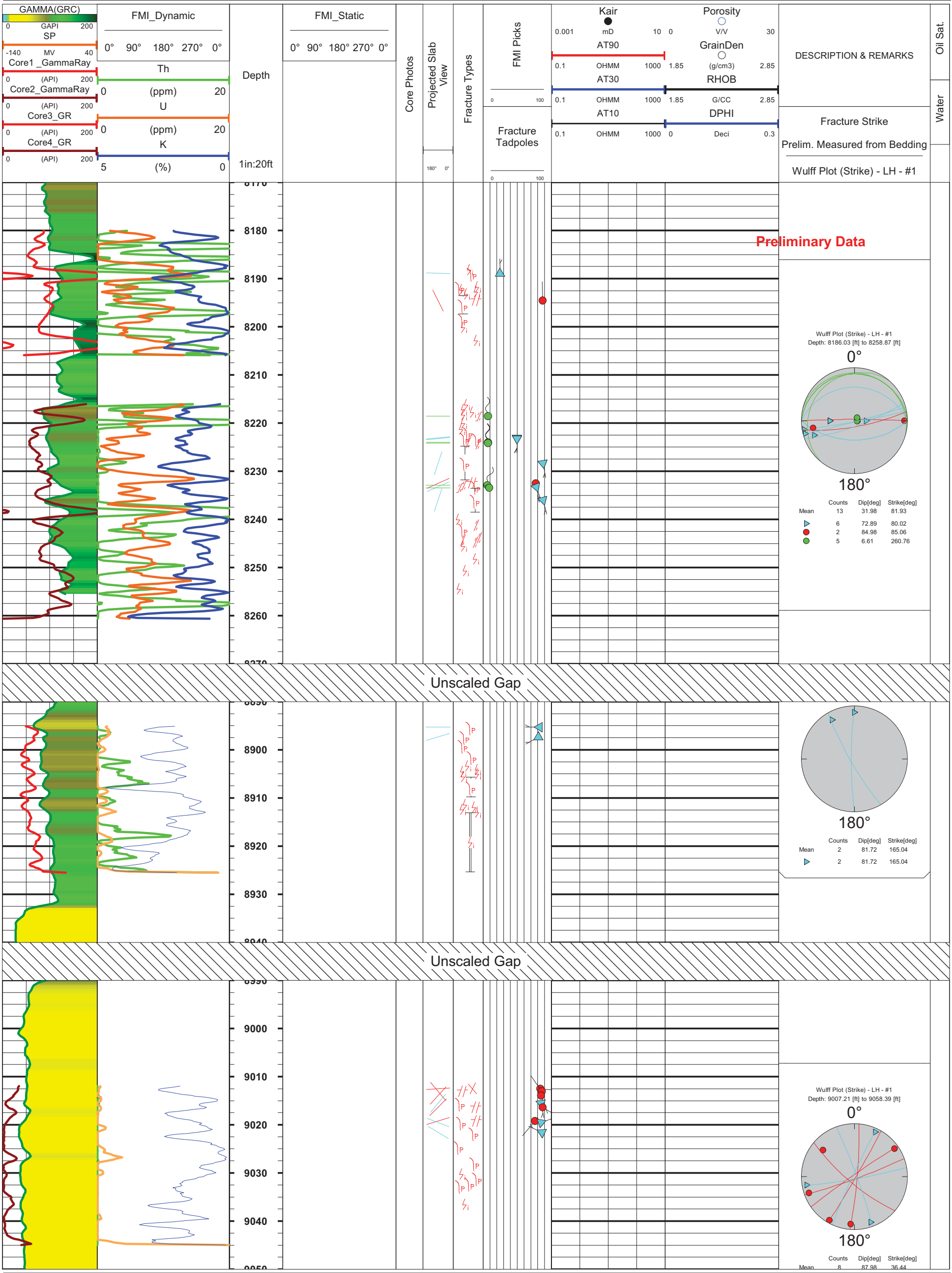
University of Utah
RMCCS State # 1
Moffat County, Colorado
Spectral Core Gamma
Scale 5" = 100'



GENERAL FRACTURE DESCRIPTION

COMPANY: Schlumberger Carbon Services / Univ. of Utah
WELL: RMCC State #1
FIELD: Trapper Mine
LOCATION: Moffat, Colorado

Interpretation by: Ron Cormier
Date: February 2012
Job#: DEN-120031G



GENERAL FRACTURE DESCRIPTION

COMPANY: Schlumberger Carbon Services / Univ. of Utah
WELL: RMCC State #1
FIELD: Trapper Mine
LOCATION: Moffat, Colorado

Interpretation by: Ron Cormier
Date: February 2012
Job#: DEN-120031G

FRACTURES:

FRACTURE TYPES:

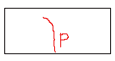

Calcite/Dolomite


Slickenside


Petal - Coring Induced



Coring Induced



Induced Petal Fracture


Conjugate set of fractures


Extension fracture

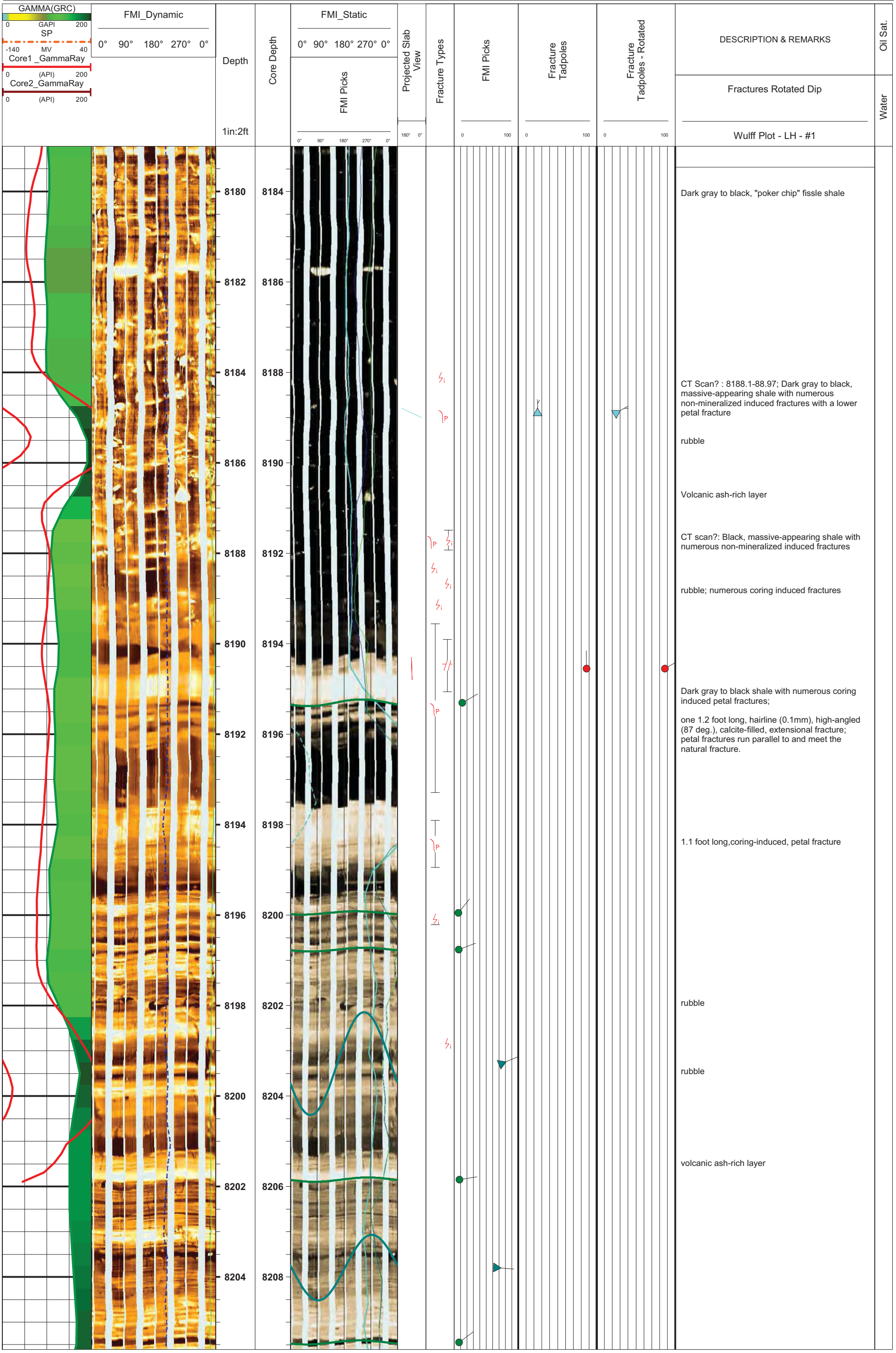

Fracture with slickensides


Shear fracture with slickensides

GENERAL FRACTURE DESCRIPTION

COMPANY: Schlumberger Carbon Services / Univ. of Utah
WELL: RMCC State #1
FIELD: Trapper Mine (Core 1-2)
LOCATION: Moffat, Colorado

Interpretation by: Ron Cormier
Date: April 2012
Job#: HOU-120305G



GAMMA(GRC)
0 GAPI 200
SP
-140 MV 40
Core1 _GammaRay
0 (API) 200
Core2_GammaRay
0 (API) 200

FMI_Dynamic
0° 90° 180° 270° 0°

Depth
1in:2ft

Core Depth

FMI_Static
0° 90° 180° 270° 0°
FMI Picks
0° 90° 180° 270° 0°

Projected Slab View
180° 0°

Fracture Types

FMI Picks
0 100

Fracture Tadpoles
0 100

Fracture Tadpoles - Rotated
0 100

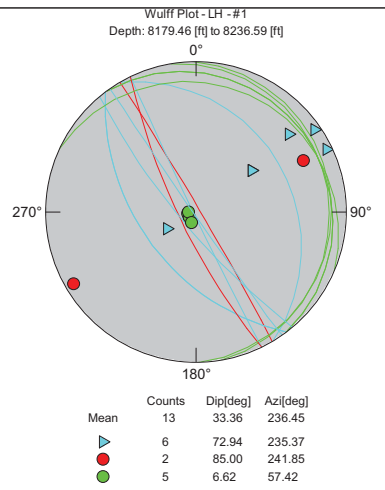
DESCRIPTION & REMARKS

Fractures Rotated Dip

Wulff Plot - LH - #1

Oil Sat.

Water



Depth	Core Depth	DESCRIPTION & REMARKS
8206	8210	
8208	8212	
8210	8214	
8212	8216	indurated, dark gray shale with a induced fracture running down the middle of the core "poker chip" fissle shale
8214	8218	indurated, parallel laminated, dark gray shale with scattered induced fractures
8216	8220	slickenside feature dipping with bedding at 7.0 degrees, striations are oriented with dip; possible shear
8218	8222	dark gray shale interbedde with (4) thin-bedded, greenish gray, volcanic-ash, claystones; small induced fracture at 8220.0'
8220	8224	0.5 ft. long, stair stepping, induced fracture very short, petal fractures that are plunging updip slickenside features dipping with bedding at 7.0 degrees, striations are oriented with dip; possible shear fractures
8222	8226	
8224	8228	very long, coring induced, petal fracture; probagation waves are formed along the fracture plane; lower termination is in a bed with numerous slickenside shear fractures
8226	8230	
8228	8232	0.7' long, hairline (0.15 mm), high angle (77 deg.), calcite-filled, extensional fracture that generally plunges updip; upper termination in bedding; CT Scan? 8232.2-32.9' a few shear fracture with slickensides dipping 15 to 50 deg. from bedding; bounded by petal fractures
8230	8234	
8232	8236	long, coring induced, petal fracture that has a lower termination in the volcanic ash-rich claystone
8234	8238	

GAMMA(GRC) 0 GAPI 200 | SP -140 MV 40 | Core1 _GammaRay 0 (API) 200 | Core2_GammaRay 0 (API) 200

FMI_Dynamic 0° 90° 180° 270° 0°

Depth 1in:2ft

Core Depth

FMI_Static 0° 90° 180° 270° 0°

FMI Picks 0° 90° 180° 270° 0°

Projected Slab View 180° 0°

Fracture Types

FMI Picks 0 100

Fracture Tadpoles 0 100

Fracture Tadpoles - Rotated 0 100

DESCRIPTION & REMARKS

Fractures Rotated Dip

Wulff Plot - LH - #1

Oil Sat.

Water

Depth	Core Depth	DESCRIPTION & REMARKS
8236	8240	volcanic ash-rich, claystone
		induced fracture
8238	8242	low angle fracture with slickenside features that is oriented with beddind; possible shear fracture
		very short petal fracture; laminated volcanic, ash-rich claystone at 8242.7'
8240	8244	several very thin-bedded to laminated, volcanic ash-rich claystone interbeds; and several low-angled, fractures with slickenside features that could be shear fractures.
8242	8246	
8244	8248	long, erratic, coring induced fractures
8246	8250	
8248	8252	short coring induced fracture; and two very thin-bedded, volcanic ash-rich claystones
8250	8254	erratic, coring induced fracture that is bound by very thin-bedded, volcanic-ash rich claystones
8252	8256	
8254	8258	dark gray, shale interbedded by several thin-bedded to laminated, volcanic ash-rich claystones (8257.5'; 58.5'; 59.0; 59.9')
8256	8260	
8258	8262	
8260	8264	

GENERAL FRACTURE DESCRIPTION

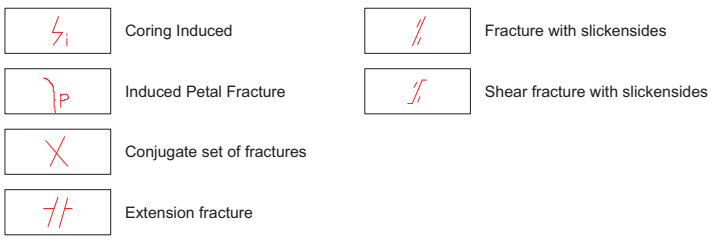
COMPANY: Schlumberger Carbon Services / Univ. of Utah
WELL: RMCC State #1
FIELD: Trapper Mine (Core 1-2)
LOCATION: Moffat, Colorado

Interpretation by: Ron Cormier
Date: April 2012
Job#: HOU-120305G

FRACTURES:



FRACTURE TYPES:

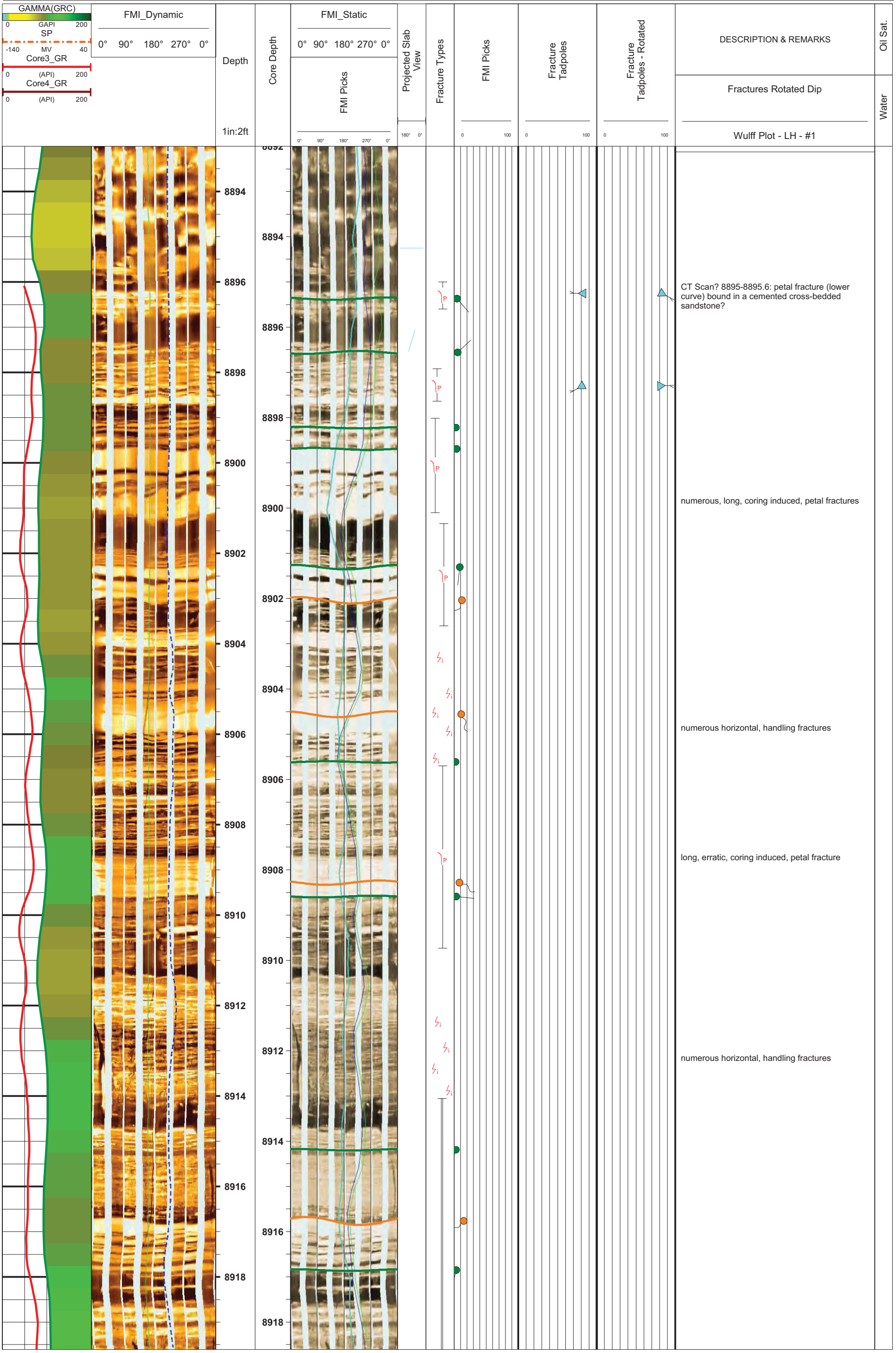


FMI FRACTURES:



COMPANY: Schlumberger Carbon Services / Univ. of Utah
WELL: RMCC State #1
FIELD: Trapper Mine
LOCATION: Moffat, Colorado

Interpretation by: Ron Cormier
Date: April 2012
Job#: HOU-120305G



GAMMA(GRC)
0 GAPI 200
SP
-140 MV 40
Core3_GR
0 (API) 200
Core4_GR
0 (API) 200

FMI_Dynamic
0° 90° 180° 270° 0°

Depth
1in:2ft

Core Depth

FMI_Static
0° 90° 180° 270° 0°
FMI Picks
0° 90° 180° 270° 0°

Projected Slab View
180° 0°

Fracture Types

FMI Picks
0 100

Fracture Tadpoles
0 100

Fracture Tadpoles - Rotated
0 100

DESCRIPTION & REMARKS

Fractures Rotated Dip

Wulff Plot - LH - #1

Oil Sat.

Water

numerous, handling fractures that break off the core in rings; core is nearly too fraible to handle

	Counts	Dip[deg]	Azi[deg]
Mean	2	81.72	101.84
▷	2	81.72	101.84

GAMMA(GRC)
0 GAPI 200
SP
-140 MV 40
Core3_GR
0 (API) 200
Core4_GR
0 (API) 200

FMI_Dynamic
0° 90° 180° 270° 0°

Depth
1in:2ft

Core Depth

FMI_Static
0° 90° 180° 270° 0°
FMI Picks
0° 90° 180° 270° 0°

Projected Slab View
180° 0°

Fracture Types

FMI Picks
0 100

Fracture Tadpoles
0 100

Fracture Tadpoles - Rotated
0 100

DESCRIPTION & REMARKS

Fractures Rotated Dip

Wulff Plot - LH - #1

Oil Sat.

Water

8950
8952
8954
8956
8958
8960
8962
8964
8966
8968
8970
8972
8974
8976

GAMMA(GRC)
0 GAPI 200
SP
-140 MV 40
Core3_GR
0 (API) 200
Core4_GR
0 (API) 200

FMI_Dynamic
0° 90° 180° 270° 0°

Depth
1in:2ft

Core Depth

FMI_Static
0° 90° 180° 270° 0°
FMI Picks
0° 90° 180° 270° 0°

Projected Slab View
180° 0°

Fracture Types

FMI Picks
0 100

Fracture Tadpoles
0 100

Fracture Tadpoles - Rotated
0 100

DESCRIPTION & REMARKS

Fractures Rotated Dip

Wulff Plot - LH - #1

Oil Sat.

Water

8978
8980
8982
8984
8986
8988
8990
8992
8994
8996
8998
9000
9002
9004
9006

Wulff Plot - LH - #1
Depth: 8992.88 [ft] to 9021.32 [ft]
0°

GAMMA(GRC) 0 GAPI 200
SP -140 MV 40
Core3_GR 0 (API) 200
Core4_GR 0 (API) 200

FMI_Dynamic 0° 90° 180° 270° 0°

Depth

1in:2ft

Core Depth

FMI_Static 0° 90° 180° 270° 0°

FMI Picks

Projected Slab View 180° 0°

Fracture Types

FMI Picks 0 100

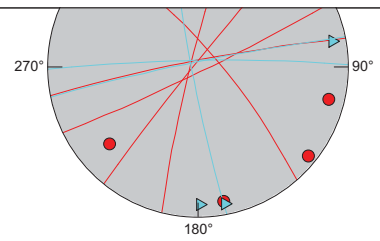
Fracture Tadpoles 0 100

Fracture Tadpoles - Rotated 0 100

DESCRIPTION & REMARKS

Fractures Rotated Dip

Wulff Plot - LH - #1



	Counts	Dip[deg]	Azi[deg]
Mean	8	85.87	333.90
●	5	87.33	320.76
▷	3	85.90	358.10

Oil Sat.

Water

9008 9010 9012 9014 9016 9018 9020 9022 9024 9026 9028 9030 9032 9034 9036

CT Scan 9012-14.6': calcite cemented sandstone with long extensional fractures; some of the fractures are partially open and may be filled with ferroan calcite; the fractures have mutiples and there is a conjugate set

petal fracture only has a slight curve

0.4' long, thin aperture (0.3 mm), calcite-filled (ferroan?), extensional fracture within a cross-bedded, calcite cemented, sandstone

classic petal fracture with mutiples; 0.9' long, hairline (0.1mm), calcite-filled, extensional fracture

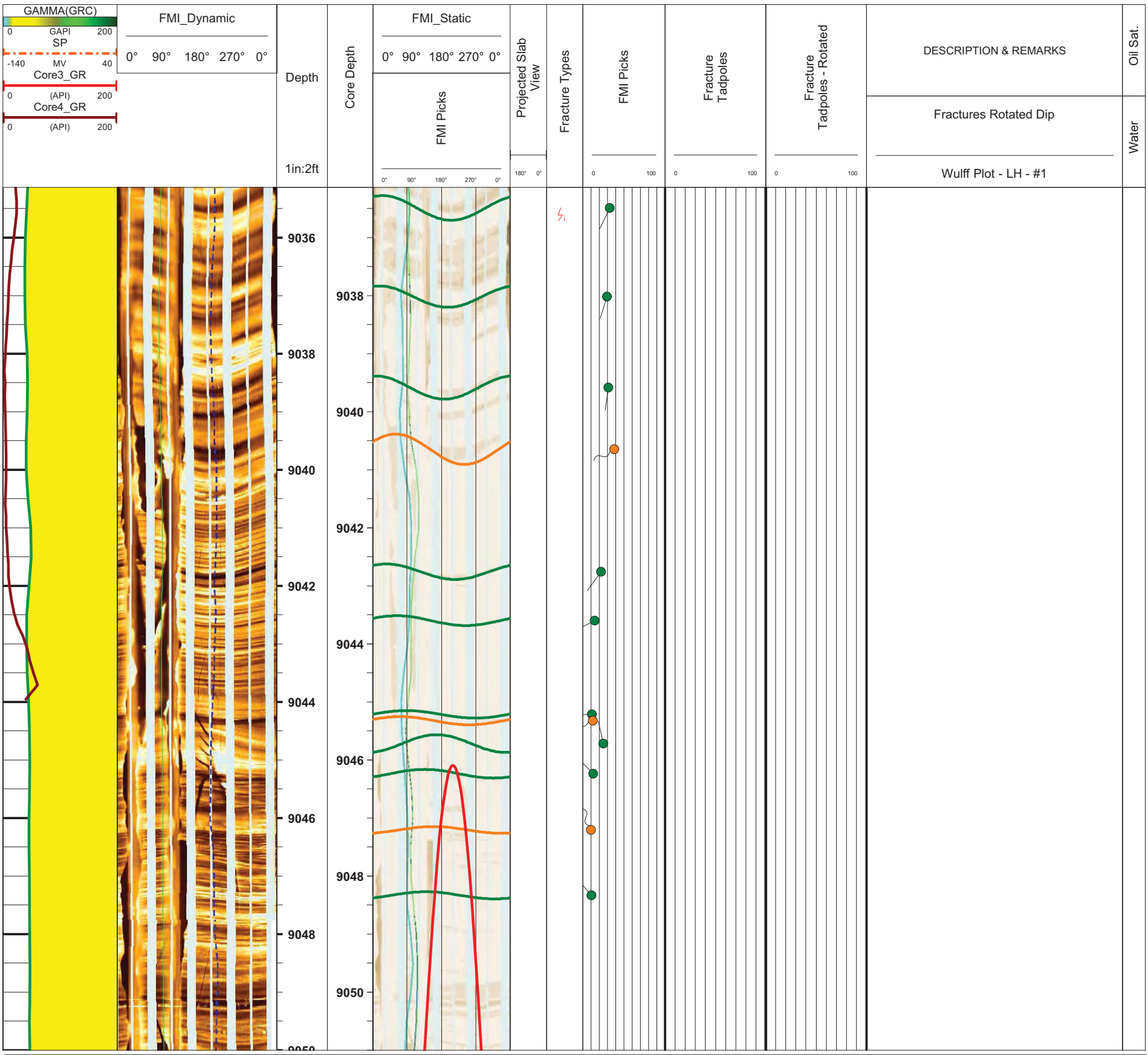
2.8' long petal fracture that is curved at the top and bottom of the fracture; major bedding change ~120 degrees within the interval; azimuth reflecs the new bedding direction

9026.5' bedding change of 80 deg.

coring induced, petal fracture; major bedding change of 130 degrees

CT Scan?: 9029.5-31.0'; showing the induced and petal fractures

numerous, coring induced petal fractures



GENERAL FRACTURE DESCRIPTION

COMPANY: Schlumberger Carbon Services / Univ. of Utah
WELL: RMCC State #1
FIELD: Trapper Mine
LOCATION: Moffat, Colorado

Interpretation by: Ron Cormier
Date: April 2012
Job#: HOU-120305G

FRACTURES:

Calcite/Dolomite
Slickenside
Petal - Coring Induced

FRACTURE TYPES:

Coring Induced
Fracture with slickensides
Induced Petal Fracture
Shear fracture with slickensides
Conjugate set of fractures
Extension fracture

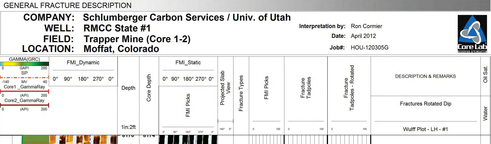
FMI FRACTURES:

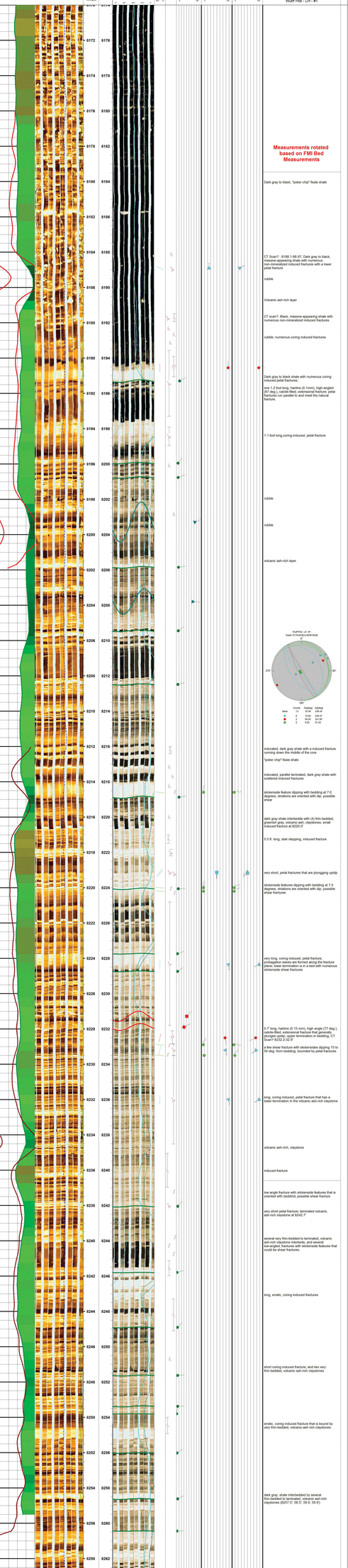
Bedding
Scour/Erosional Contact
FMI_Resistive_Fracture
FMI_Drilling_Induced
FMI_Fault

GENERAL FRACTURE DESCRIPTION

COMPANY: Schlumberger Carbon Services / Univ. of Utah
WELL: RMCC State #1
FIELD: Trapper Mine (Core 1-2)
LOCATION: Moffat, Colorado

Interpretation by: Ron Cormier
Date: April 2012
Job#: HOU-120305G





Measurements rotated based on FMI Bed Measurements

Dark gray to black, "poker chip" fissle shale

CT Scan7: 8188.1-88.97; Dark gray to black, massive-appearing shale with numerous non-mineralized induced fractures with a lower petal fracture

rubble

Volcanic ash-rich layer

CT scan7: Black, massive-appearing shale with numerous non-mineralized induced fractures

rubble; numerous coring induced fractures

Dark gray to black shale with numerous coring induced petal fractures;

one 1.2 foot long, hairline (0.1mm), high-angled (67 deg.), calcite-filled, extensional fracture; petal fractures run parallel to and meet the natural fracture

1.1 foot long,coring-induced, petal fracture

rubble

rubble

volcanic ash-rich layer

indurated, dark gray shale with a induced fracture running down the middle of the core

"poker chip" fissle shale

indurated, parallel laminated, dark gray shale with scattered induced fractures

slickenside feature dipping with bedding at 7.0 degrees, striations are oriented with dip; possible shear

dark gray shale interbedde with (4) thin-bedded, greenish gray, volcanic-ash, claystones; small induced fracture at 8225.0'

0.5 ft. long, stair stepping, induced fracture

very short, petal fractures that are plungging updip

slickenside features dipping with bedding at 7.0 degrees, striations are oriented with dip; possible shear fractures

very long, coring induced, petal fracture; prodagation waves are formed along the fracture plane; lower termination is in a bed with numerous slickenside shear fractures

0.7' long, hairline (0.15 mm), high angle (77 deg.), calcite-filled, extensional fracture that generally parallels the natural; termination in bedding; CT Scan7 8232.2'-.33'

a few shear fracture with slickensides dipping 15 to 50 deg. from bedding; bounded by petal fractures

long, coring induced, petal fracture that has a lower termination in the volcanic ash-rich claystone

volcanic ash-rich, claystone

induced fracture

low angle fracture with slickenside features that is oriented with bedding; possible shear fracture

very short petal fracture; laminated volcanic, ash-rich claystone at 8242.7'

several very thin-bedded to laminated, volcanic ash-rich claystone interbeds; and several low-angled, fractures with slickenside features that could be shear features.

long, erratic, coring induced fractures

short coring induced fracture, and two very thin-bedded, volcanic ash-rich claystones

erratic, coring induced fracture that is bound by very thin-bedded, volcanic-ash rich claystones

dark gray, shale interbedded by several thin-bedded to laminated, volcanic ash-rich claystones (8257.5'-.58.5'; 59.0'-.59.5')

GENERAL FRACTURE DESCRIPTION

COMPANY: Schlumberger Carbon Services / Univ. of Utah
WELL: RMCC State #1
FIELD: Trapper Mine (Core 1-2)
LOCATION: Moffat, Colorado

Interpretation by: Ron Cormier
Date: April 2012
Job#: HOU-120305G

FRACTURES:

- Calcite/Dolomite
- Slickenside
- Petal - Coring Induced

FRACTURE TYPES:

- Coring Induced
- Induced Petal Fracture
- Conjugate set of fractures
- Extension fracture
- Fracture with slickensides
- Shear fracture with slickensides

FMI FRACTURES:

- Bedding
- FMI_Resistive_Fracture
- FMI_Drilling_Induced
- FMI_Fault

GENERAL FRACTURE DESCRIPTION

COMPANY: Schlumberger Carbon Services / Univ. of Utah
WELL: RMCC State #1
FIELD: Trapper Mine
LOCATION: Moffat, Colorado

Interpretation by: Ron Conner
Date: April 2012
Job#: HOU-1200093

ZAVA CORP

FMI_Dynamic
FMI_Static
0° 90° 180° 270° 0°
Image Orientation
Top of Image

Depth
Core Depth
Pad Rose
Fracture Density
Fracture Count
Fracture Type
Fracture Porosity
Fracture Permeability
Fracture Aperture
Dip
Azimuth
DESCRIPTION & REMARKS
Fractures Rotated Dip
Wulff Plot - Lo's - #1

CT Scan? 6900.8900.0 axial fracture (lower fracture is a connected vug feature) 6900.8900 specification?

numerous, long, curving inducved, petal fractures

numerous horizontal, handling fractures

long, erratic, curving inducved, petal fractures

numerous horizontal, handling fractures

numerous, handling fractures that break off the core through core; it seems less stable for analysis

Wulff Plot: Lo's - #1
Upper Hemisphere Equal Area

Dip
Azimuth
Number
Color
Dip
Azimuth
Number
Color
0 - 30
0 - 90
30 - 60
90 - 180
60 - 90
180 - 270
90 - 120
270 - 360

CT Scan 8012.15.01 calcite cemented sandstone with numerous fractures. Most of the visible fractures are partially open and may be the path of the core breaks. Some fractures are healed and there is a conjugate set

petal fracture only has a slight curve

CT Fmg. Non apertural (0.5 mm), calcite filled (fenestral?), subhorizontal fracture within a cross-bedded, calcite-cemented, sandstone

Steam cal/fe fracture with crystalline, 0.5" long, opening (2-3 mm), calcite-filled, subplanar fracture

curving inducved, petal fracture, major bedding change at 7100 degrees

CT Scan? 8035.5-51.5? - showing the inducved and petal fractures

numerous, curving inducved petal fractures

GENERAL FRACTURE DESCRIPTION

COMPANY: Schlumberger Carbon Services / Univ. of Utah
WELL: RMCC State #1
FIELD: Trapper Mine
LOCATION: Moffat, Colorado

Interpretation by: Ron Conner
Date: April 2012
Job#: HOU-1200093

FRACTURES:

Natural Sinusoids
Sinusoidal
Petal - Curving Inducved

FRACTURE TYPES:

Curving Inducved
Inducved Petal Fracture
Conjugate set of fractures
Extensive Fracture
Fracture with sinusoidales
Shear fracture with sinusoidales

FMI FRACTURES:

Bedding
Broad Sinusoidal Conduct
FMI_Resistive_Fracture
FMI_Drilling_Inducved
FMI_Pad

RMCCS1
SLC UTAH
Anthony Rice

	Sample ID	Depth (ft)	Dry Weight (gm)	Grain Volume (cc)	Grain Density (gm/cc)	Bulk Density (gm/cc)	Pore Volume (cc)	Porosity (%)	HG Bulk Volume	Length (inch)	Dia (inch)	Caliper Bulk Volume	Temp (F)	Date	Time	AM/PM	Project	PV or GV			
1	79HC	9029.6	197.94	75.3986	2.625		0	0	0	3	1.4705	83.492	76	3/8/13	3:21:58	PM	RMCCS	pv			
2	79HC	9029.6	197.94	75.398	2.625		0	0	0	3	1.4705	83.492	76	3/8/13	3:24:06	PM	RMCCS	pv			
3	79HC	9029.6	197.94	75.3974	2.625		0	0	0	3	1.4705	83.492	76	3/8/13	3:25:37	PM	RMCCS	pv			
4	79HC	9029.6	197.94	75.3972	2.625		0	0	0	3	1.4705	83.492	76	3/8/13	3:27:08	PM	RMCCS	pv			
5	79HC	9029.6	197.94	75.3974	2.625		0	0	0	3	1.4705	83.492	76	3/8/13	3:28:41	PM	RMCCS	pv			
				75.3977																	
6	79HC	9029.6	197.94	75.3977	2.625		8.6652	10.308	0	3	1.4705	83.492	76	3/8/13	5:02:25	PM	RMCCS	gv	avg	75.3977	pv
7	79HC	9029.6	197.94	75.3977	2.625		8.6632	10.306	0	3	1.4705	83.492	76	3/8/13	5:04:40	PM	RMCCS	gv	avg	75.3977	pv
8	79HC	9029.6	197.94	75.3977	2.625		8.6605	10.303	0	3	1.4705	83.492	76	3/8/13	5:07:14	PM	RMCCS	gv	avg	75.3977	pv
9	79HC	9029.6	197.94	75.3977	2.625		8.6635	10.306	0	3	1.4705	83.492	76	3/8/13	5:09:48	PM	RMCCS	gv	avg	75.3977	pv
10	79HC	9029.6	197.94	75.3977	2.625		8.6574	10.3	0	3	1.4705	83.492	76	3/8/13	5:12:30	PM	RMCCS	gv	avg	75.3977	pv
11	79HC	9029.6	197.94	75.3977	2.625		8.6574	10.3	0	3	1.4705	83.492	76	3/11/13	8:08:28	AM	RMCCS	gv	avg	75.3977	pv
				75.3977		2.37077	8.6612	10.3038													

	Sample ID	Depth (ft)	Dry Weight (gm)	Grain Volume (cc)	Grain Density (gm/cc)	Bulk Density (gm/cc)	Pore Volume (cc)	Porosity (%)	HG Bulk Volume	Length (inch)	Dia (inch)	Caliper Bulk Volume	Temp (F)	Date	Time					
12	83h	9033.1	207.45	78.3806	2.647		0	0	0	3.001	1.4695	83.406	76	3/11/13	2:41:53	PM	RMCCS	gv	avg	75.3977 pv
13	83h	9033.1	207.45	78.3828	2.647		0	0	0	3.001	1.4695	83.406	76	3/11/13	2:45:39	PM	RMCCS	gv	avg	75.3977 pv
14	83h	9033.1	207.45	78.3822	2.647		0	0	0	3.001	1.4695	83.406	76	3/11/13	2:47:19	PM	RMCCS	gv	avg	75.3977 pv
15	83h	9033.1	207.45	78.3797	2.647		0	0	0	3.001	1.4695	83.406	76	3/11/13	2:48:59	PM	RMCCS	gv	avg	75.3977 pv
16	83h	9033.1	207.45	78.3782	2.647		0	0	0	3.001	1.4695	83.406	76	3/11/13	2:50:37	PM	RMCCS	gv	avg	75.3977 pv
				78.3807																
17	83h	9033.1	207.45	0	0		0	0	0	3.001	1.4695	83.406	76	3/11/13	2:57:37	PM	RMCCS	gv	avg	75.3977 pv
18	83h	9033.1	207.45	78.3726	2.647		0	0	0	3.001	1.4695	83.406	76	3/11/13	2:58:52	PM	RMCCS	gv	avg	75.3977 pv
19	83h	9033.1	207.45	78.6988	2.636		0	0	0	3.001	1.4695	83.406	76	3/11/13	3:03:57	PM	RMCCS	gv	avg	75.3977 pv
20	83h	9033.1	207.45	78.3711	2.647		0	0	0	3.001	1.4695	83.406	76	3/11/13	3:08:30	PM	RMCCS	gv	avg	75.3977 pv
21	83h	9033.1	207.45	78.6523	2.638		0	0	0	3.001	1.4695	83.406	76	3/11/13	3:12:55	PM	RMCCS	gv		
22	83h	9033.1	207.45	78.3631	2.647		0	0	0	3.001	1.4695	83.406	76	3/11/13	3:18:07	PM	RMCCS	gv		
23	83h	9033.1	207.45	78.3641	2.647		0	0	0	3.001	1.4695	83.406	76	3/11/13	3:25:49	PM	RMCCS	gv		
24	83h	9033.1	207.45	78.412	2.646		0	0	0	3.001	1.4695	83.406	76	3/11/13	3:27:24	PM	RMCCS	gv		
25	83h	9033.1	207.45	78.3759	2.647		0	0	0	3.001	1.4695	83.406	76	3/11/13	3:28:48	PM	RMCCS	gv		
26	83h	9033.1	207.45	78.3934	2.646		0	0	0	3.001	1.4695	83.406	76	3/11/13	3:30:22	PM	RMCCS	gv		
27	83h	9033.1	207.45	78.39	2.646		0	0	0	3.001	1.4695	83.406	76	3/11/13	3:31:53	PM	RMCCS	gv		
28	83h	9033.1	207.45	78.3807	2.647		4.0086	4.865	0	3.001	1.4695	83.406	76	3/15/13	4:48:17	PM	RMCCS	gv	AVE	78.3807 PV
29	83h	9033.1	207.45	78.3807	2.647		3.987	4.84	0	3.001	1.4695	83.406	76	3/15/13	5:08:56	PM	RMCCS	gv	AVE	78.3807 PV
30	83h	9033.1	207.45	78.3807	2.647		3.9854	4.839	0	3.001	1.4695	83.406	76	3/15/13	5:17:05	PM	RMCCS	gv	AVE	78.3807 PV
				78.3807		2.48723	3.99367	4.848												

	Sample ID	Depth (ft)	Dry Weight (gm)	Grain Volume (cc)	Grain Density (gm/cc)	Bulk Density (gm/cc)	Pore Volume (cc)	Porosity (%)	HG Bulk Volume	Length (inch)	Dia (inch)	Caliper Bulk Volume	Temp (F)	Date	Time					
31	77hb	9027.45	216.81	81.3734	2.664		0	0	0	2.9995	1.471	83.534	76	3/19/13	2:05:07	PM	RMCCS	gv		
32	77hb	9027.45	216.81	81.5829	2.658		0	0	0	2.9995	1.471	83.534	76	3/19/13	2:08:04	PM	RMCCS	gv		
33	77hb	9027.45	216.81	81.6197	2.656		0	0	0	2.9995	1.471	83.534	76	3/19/13	2:11:14	PM	RMCCS	gv		
34	77hb	9027.45	216.81	81.7232	2.653		0	0	0	2.9995	1.471	83.534	76	3/19/13	2:14:05	PM	RMCCS	gv		
35	77hb	9027.45	216.81	81.8041	2.65		0	0	0	2.9995	1.471	83.534	76	3/19/13	2:16:47	PM	RMCCS	gv		
36	77hb	9027.45	216.81	81.7807	2.651		0	0	0	2.9995	1.471	83.534	76	3/19/13	2:19:30	PM	RMCCS	gv		
37	77hb	9027.45	216.81	81.7013	2.654		0	0	0	2.9995	1.471	83.534	76	3/19/13	2:22:28	PM	RMCCS	gv		
38	77hb	9027.45	216.81	81.4105	2.663		0	0	0	2.9995	1.471	83.534	76	3/19/13	2:26:45	PM	RMCCS	gv	30	sec
39	77hb	9027.45	216.81	81.6581	2.655		0	0	0	2.9995	1.471	83.534	76	3/19/13	2:29:49	PM	RMCCS	gv	30	sec
40	77hb	9027.45	216.81	81.6103	2.657		0	0	0	2.9995	1.471	83.534	76	3/19/13	2:32:54	PM	RMCCS	gv	30	sec
41	77hb	9027.45	216.81	81.3929	2.664		0	0	0	2.9995	1.471	83.534	76	3/19/13	2:38:05	PM	RMCCS	gv	1	min
42	77hb	9027.45	216.81	81.5329	2.659		0	0	0	2.9995	1.471	83.534	76	3/19/13	2:41:33	PM	RMCCS	gv	1	min
43	77hb	9027.45	216.81	81.5128	2.66		0	0	0	2.9995	1.471	83.534	76	3/19/13	2:44:49	PM	RMCCS	gv	1	min
44	77hb	9027.45	216.81	81.5084	2.66		0	0	0	2.9995	1.471	83.534	76	3/19/13	2:48:12	PM	RMCCS	gv	1	min
45	77hb	9027.45	216.81	81.4629	2.661		0	0	0	2.9995	1.471	83.534	76	3/19/13	2:52:50	PM	RMCCS	gv	2	min
46	77hb	9027.45	216.81	81.4637	2.661		0	0	0	2.9995	1.471	83.534	76	3/19/13	2:57:20	PM	RMCCS	gv	2	min
47	77hb	9027.45	216.81	81.4602	2.662		0	0	0	2.9995	1.471	83.534	76	3/19/13	3:01:48	PM	RMCCS	gv	2	min
48	77hb	9027.45	216.81	81.4598	2.662		0	0	0	2.9995	1.471	83.534	76	3/19/13	3:07:15	PM	RMCCS	gv	3	min
49	77hb	9027.45	216.81	81.4587	2.662		0	0	0	2.9995	1.471	83.534	76	3/19/13	3:12:49	PM	RMCCS	gv	3	min
50	77hb	9027.45	216.81	81.4581	2.662		0	0	0	2.9995	1.471	83.534	76	3/19/13	3:18:17	PM	RMCCS	gv	3	min
51	77hb	9027.45	216.81	81.4553	2.662		0	0	0	2.9995	1.471	83.534	76	3/19/13	3:25:57	PM	RMCCS	gv	5	min
52	77hb	9027.45	216.81	81.456	2.662		0	0	0	2.9995	1.471	83.534	76	3/19/13	3:33:37	PM	RMCCS	gv	5	min
53	77hb	9027.45	216.81	81.4554	2.662		0	0	0	2.9995	1.471	83.534	76	3/19/13	3:42:21	PM	RMCCS	gv	5	min
54	77HB	9027.45	216.81	81.4583	2.662		0	0	0	2.9995	1.471	83.534	76	3/20/13	1:21:21	PM			20	min
55	77HB	9027.45	216.81	81.4419	2.662		0	0	0	2.9995	1.471	83.534	76	3/20/13	1:23:37	PM			20	min
56	77HB	9027.45	216.81	81.4462	2.662		0	0	0	2.9995	1.471	83.534	76	3/20/13	1:47:13	PM			20	min
57	77HB	9027.45	216.81	81.4465	2.662		0	0	0	2.9995	1.471	83.534	76	3/20/13	2:09:22	PM			20	min
58	77HB	9027.45	216.81	81.4465	2.662		0	0	0	2.9995	1.471	83.534	76	3/20/13	3:10:23	PM			20	min
319	77HB	9027.45	216.86	81.4479	2.663		1.8102	2.174	0	2.999	1.471	83.52	77.4	6/25/13	4:35:04	PM	grain	density	derived	before.
320	77HB	9027.45	216.86	81.4479	2.663		1.8807	2.257	0	2.999	1.471	83.52	77.4	6/25/13	4:42:39	PM	grain	density	derived	before.
321	77HB	9027.45	216.86	81.4479	2.663		1.93	2.315	0	2.999	1.471	83.52	77.4	6/25/13	4:57:58	PM	grain	density	derived	before.
322	77HB	9027.45	216.86	81.4479	2.663		2.4334	2.901	0	2.999	1.471	83.52	77.4	6/25/13	5:26:08	PM	grain	density	derived	before.
323	77HB	9027.45	216.86	81.4479	2.663		2.4311	2.898	0	2.999	1.471	83.52	77.4	6/26/13	8:31:43	AM	grain	density	derived	before.
324	77HB	9027.45	216.86	81.4479	2.663		2.4187	2.884	0	2.999	1.471	83.52	77.4	6/26/13	9:45:09	AM	grain	density	derived	before.
325	77HB	9027.45	216.86	81.4479	2.663		2.4163	2.881	0	2.999	1.471	83.52	77.4	6/26/13	10:49:38	AM	grain	density	derived	before.
326	77HB	9027.45	216.86	81.4479	2.663		1.9006	2.28	0	2.999	1.471	83.52	77.4	6/27/13	8:59:03	AM	vessel	temp	162.9	poro
327	77HB	9027.45	216.86	81.4479	2.663		1.8412	2.211	0	2.999	1.471	83.52	77.4	6/27/13	9:27:56	AM	vessel	temp	162.9	poro
328	77HB	9027.45	216.86	81.4479	2.663		1.9015	2.281	0	2.999	1.471	83.52	77.4	6/27/13	11:42:05	AM	vessel	temp	162.9	poro
				81.4479		2.59547	1.8811	2.25733												
				81.4479		2.59547	1.8811	2.25733												

	Sample ID	Depth (ft)	Dry Weight (gm)	Grain Volume (cc)	Grain Density (gm/cc)	Bulk Density (gm/cc)	Pore Volume (cc)	Porosity (%)	HG Bulk Volume	Length (inch)	Dia (inch)	Caliper Bulk Volume	Temp (F)	Date	Time					
59	76	9026.7	209.1	78.4975	2.664		0	0	0	3	1.468	83.208	76	3/21/13	4:02:19	PM	gv			
60	76	9026.7	209.1	78.4986	2.664		0	0	0	3	1.468	83.208	76	3/21/13	5:07:45	PM	gv			
61	76	9026.7	209.1	78.498	2.664		0	0	0	3	1.468	83.208	76	3/21/13	5:32:27	PM	gv			
62	76	9026.7	209.1	78.4859	2.664		0	0	0	3	1.468	83.208	76	3/22/13	3:26:00	PM	gv			
63	76	9026.7	209.1	78.4964	2.664		0	0	0	3	1.468	83.208	76	3/22/13	4:09:38	PM	gv			
64	76	9026.7	209.1	78.5066	2.663		0	0	0	3	1.468	83.208	76	3/22/13	4:16:40	PM	gv			
65	76	9026.7	209.1	78.5079	2.663		0	0	0	3	1.468	83.208	76	3/22/13	4:18:35	PM	gv			
66	76	9026.7	209.1	78.5107	2.663		0	0	0	3	1.468	83.208	76	3/22/13	4:20:20	PM	gv			
67	76	9026.7	209.1	78.5811	2.661		0	0	0	3	1.468	83.208	76	3/22/13	4:22:10	PM	gv			
68	76	9026.7	209.1	78.5217	2.663		0	0	0	3	1.468	83.208	76	3/22/13	4:23:59	PM	gv			
69	76	9026.7	209.1	78.5104	2.663		4.9307	5.909	0	3	1.468	83.208	76	3/22/13	5:16:34	PM	gv	avg	78.5104	pv
70	76	9026.7	209.1	78.5104	2.663		4.5737	5.505	0	3	1.468	83.208	76	3/22/13	5:27:05	PM	gv	avg	78.5104	pv
71	76	9026.7	209.1	78.5104	2.663		4.7041	5.653	0	3	1.468	83.208	76	3/22/13	5:30:00	PM	gv	avg	78.5104	pv
72	76	9026.7	209.1	78.5104	2.663		4.7714	5.729	0	3	1.468	83.208	76	3/22/13	5:33:03	PM	gv	avg	78.5104	pv
73	76	9026.7	209.1	78.5104	2.663		4.7601	5.716	0	3	1.468	83.208	76	3/22/13	5:36:24	PM	gv	avg	78.5104	pv
74	76	9026.7	209.1	78.5104	2.663		4.8076	5.77	0	3	1.468	83.208	76	3/22/13	5:40:00	PM	gv	avg	78.5104	pv
75	76	9026.7	209.1	78.5104	2.663		4.7656	5.723	0	3	1.468	83.208	76	3/22/13	5:44:31	PM	gv	avg	78.5104	pv
76	76	9026.7	209.1	78.5104	2.663		4.9033	5.878	0	3	1.468	83.208	76	3/22/13	6:17:53	PM	gv	avg	78.5104	pv
77	76	9026.7	209.1	78.5104	2.663		4.8892	5.862	0	3	1.468	83.208	76	3/22/13	6:33:31	PM	gv	avg	78.5104	pv
				78.5104		2.51298	4.90773	5.883												

			Dry Weight (gm)	Grain Volume (cc)	Grain Density (gm/cc)	Bulk Density (gm/cc)	Pore Volume (cc)	Porosity (%)	HG Bulk Volume	Length (inch)	Dia (inch)	Caliper Bulk Volume	Temp (F)	Date	Time			
78	77H		9027.3	209.46	78.3521	2.673	0	0	0	2.915	1.47	81.071	76	3/25/13	3:21:14 PM	gv		
79	77H		9027.3	209.46	78.3074	2.675	0	0	0	2.915	1.47	81.071	76	3/25/13	3:26:54 PM	gv		
80	77H		9027.3	209.46	78.31	2.675	0	0	0	2.915	1.47	81.071	76	3/25/13	3:30:48 PM	gv		
81	77H		9027.3	209.46	78.3123	2.675	0	0	0	2.915	1.47	81.071	76	3/25/13	3:33:31 PM	gv		
82	77H		9027.3	209.46	78.3065	2.675	0	0	0	2.915	1.47	81.071	76	3/25/13	3:50:51 PM	gv		
83	77H		9027.3	209.46	78.3065	2.675	3.1229	3.835	0	2.915	1.47	81.071	76	3/25/13	4:45:08 PM	gv	avg	78.3177 pv
84	77H		9027.3	209.46	78.3065	2.675	2.1183	2.634	0	2.915	1.47	81.071	76	3/25/13	5:02:37 PM	gv	avg	78.3177 pv
85	77H		9027.3	209.46	78.3065	2.675	3.0814	3.786	0	2.915	1.47	81.071	76	3/25/13	5:06:37 PM	gv	avg	78.3177 pv
86	77H		9027.3	209.46	78.3065	2.675	2.9086	3.581	0	2.915	1.47	81.071	76	3/25/13	5:11:19 PM	gv	avg	78.3177 pv
87	77H		9027.3	209.46	78.3065	2.675	3.1002	3.808	0	2.915	1.47	81.071	76	3/25/13	5:31:53 PM	gv	avg	78.3177 pv
88	77H		9027.3	209.46	78.3065	2.675	3.098	3.806	0	2.915	1.47	81.071	76	3/25/13	5:56:43 PM	gv	avg	78.3177 pv
					78.3087	2.58366	3.06222	3.7632										

			Dry Weight (gm)	Grain Volume (cc)	Grain Density (gm/cc)	Bulk Density (gm/cc)	Pore Volume (cc)	Porosity (%)	HG Bulk Volume	Length (inch)	Dia (inch)	Caliper Bulk Volume	Temp (F)	Date	Time			
89	82H		9032.15	197.66	75.3626	2.623	0	0	0	2.9065	1.47	80.834	76	3/26/13	11:21:36 AM	gv		
90	82H		9032.15	197.66	75.3624	2.623	0	0	0	2.9065	1.47	80.834	76	3/26/13	11:23:21 AM	gv		
91	82H		9032.15	197.66	75.3619	2.623	0	0	0	2.9065	1.47	80.834	76	3/26/13	11:26:12 AM	gv		
92	82H		9032.15	197.66	75.361	2.623	0	0	0	2.9065	1.47	80.834	76	3/26/13	11:28:09 AM	gv		
93	82H		9032.15	197.66	75.3596	2.623	0	0	0	2.9065	1.47	80.834	76	3/26/13	11:29:56 AM	gv		
94	82H		9032.15	197.66	75.3586	2.623	0	0	0	2.9065	1.47	80.834	76	3/26/13	11:45:07 AM	gv		
95	82H		9032.15	197.66	75.3586	2.623	0	0	0	2.9065	1.47	80.834	76	3/26/13	12:49:26 PM	gv		
96	82H		9032.15	197.66	75.3607	2.623	6.4606	7.896	0	2.9065	1.47	80.834	76	3/26/13	1:29:49 PM	gv	avg	75.3607 pv
97	82H		9032.15	197.66	75.3607	2.623	6.1248	7.516	0	2.9065	1.47	80.834	76	3/26/13	1:39:09 PM	gv	avg	75.3607 pv
98	82H		9032.15	197.66	75.3607	2.623	6.287	7.7	0	2.9065	1.47	80.834	76	3/26/13	1:51:14 PM	gv	avg	75.3607 pv
99	82H		9032.15	197.66	75.3607	2.623	6.4456	7.879	0	2.9065	1.47	80.834	76	3/26/13	1:55:57 PM	gv	avg	75.3607 pv
100	82H		9032.15	197.66	75.3607	2.623	6.3831	7.809	0	2.9065	1.47	80.834	76	3/26/13	1:59:23 PM	gv	avg	75.3607 pv
101	82H		9032.15	197.66	75.3607	2.623	6.4263	7.857	0	2.9065	1.47	80.834	76	3/26/13	2:14:09 PM	gv	avg	75.3607 pv
102	82H		9032.15	197.66	75.3607	2.623	6.4302	7.862	0	2.9065	1.47	80.834	76	3/26/13	2:26:42 PM	gv	avg	75.3607 pv
103	82H		9032.15	197.66	75.3607	2.623	6.4258	7.857	0	2.9065	1.47	80.834	76	3/26/13	2:40:07 PM	gv	avg	75.3607 pv
					75.3607	2.44526	6.4286	7.86										

			Dry Weight (gm)	Grain Volume (cc)	Grain Density (gm/cc)	Bulk Density (gm/cc)	Pore Volume (cc)	Porosity (%)	HG Bulk Volume	Length (inch)	Dia (inch)	Caliper Bulk Volume	Temp (F)	Date	Time			
104	71hb		9021.35	185.27	71.7882	2.581	0	0	0	2.8555	1.4695	79.362	76	3/26/13	2:59:31 PM	gv		
105	71hb		9021.35	185.27	71.7889	2.581	0	0	0	2.8555	1.4695	79.362	76	3/26/13	3:01:18 PM	gv		
106	71hb		9021.35	185.27	71.7893	2.581	0	0	0	2.8555	1.4695	79.362	76	3/26/13	3:04:20 PM	gv		
107	71hb		9021.35	185.27	71.791	2.581	0	0	0	2.8555	1.4695	79.362	76	3/26/13	3:07:22 PM	gv		
108	71hb		9021.35	185.27	71.7928	2.581	0	0	0	2.8555	1.4695	79.362	76	3/26/13	3:17:36 PM	gv		
109	71hb		9021.35	185.27	71.7939	2.581	0	0	0	2.8555	1.4695	79.362	76	3/26/13	3:27:09 PM	gv		
110	71hb		9021.35	185.27	71.7907	2.581	9.984	12.209	0	2.8555	1.4695	79.362	76	3/26/13	8:32:37 PM	gv	avg	71.7907 pv
111	71hb		9021.35	185.27	71.7907	2.581	9.0972	11.247	0	2.8555	1.4695	79.362	76	3/26/13	8:49:07 PM	gv	avg	71.7907 pv
112	71hb		9021.35	185.27	71.7907	2.581	9.8773	12.094	0	2.8555	1.4695	79.362	76	3/26/13	8:51:40 PM	gv	avg	71.7907 pv
113	71hb		9021.35	185.27	71.7907	2.581	9.8688	12.085	0	2.8555	1.4695	79.362	76	3/26/13	8:54:14 PM	gv	avg	71.7907 pv
114	71hb		9021.35	185.27	71.7907	2.581	9.8864	12.104	0	2.8555	1.4695	79.362	76	3/26/13	8:59:37 PM	gv	avg	71.7907 pv
115	71hb		9021.35	185.27	71.7907	2.581	9.9606	12.184	0	2.8555	1.4695	79.362	76	3/26/13	9:24:47 PM	gv	avg	71.7907 pv
116	71hb		9021.35	185.27	71.7907	2.581	9.948	12.17	0	2.8555	1.4695	79.362	76	3/26/13	9:46:08 PM	gv	avg	71.7907 pv
					71.7907	2.33449	9.92085	12.141										

			Dry Weight (gm)	Grain Volume (cc)	Grain Density (gm/cc)	Bulk Density (gm/cc)	Pore Volume (cc)	Porosity (%)	HG Bulk Volume	Length (inch)	Dia (inch)	Caliper Bulk Volume	Temp (F)	Date	Time			
117	73H		9023.55	194.57	75.3504	2.582	0	0	0	2.8925	1.468	80.226	76	3/27/13	8:41:31 AM	gv		
118	73H		9023.55	194.57	75.3429	2.582	0	0	0	2.8925	1.468	80.226	76	3/27/13	8:50:53 AM	gv		
119	73H		9023.55	194.57	75.3442	2.582	0	0	0	2.8925	1.468	80.226	76	3/27/13	8:52:39 AM	gv		
120	73H		9023.55	194.57	75.3448	2.582	0	0	0	2.8925	1.468	80.226	76	3/27/13	8:54:19 AM	gv		
121	73H		9023.55	194.57	75.3458	2.582	0	0	0	2.8925	1.468	80.226	76	3/27/13	9:00:59 AM	gv		
122	73H		9023.55	194.57	75.3459	2.582	0	0	0	2.8925	1.468	80.226	76	3/27/13	9:03:00 AM	gv		
123	73H		9023.55	194.57	75.3473	2.582	0	0	0	2.8925	1.468	80.226	76	3/27/13	9:18:14 AM	gv		
124	73H		9023.55	194.57	75.3459	2.582	7.1646	8.683	0	2.8925	1.468	80.226	76	3/27/13	2:47:07 PM	gv	avg	75.3459 pv
125	73H		9023.55	194.57	75.3459	2.582	7.0176	8.52	0	2.8925	1.468	80.226	76	3/27/13	2:58:23 PM	gv	avg	75.3459 pv
126	73H		9023.55	194.57	75.3459	2.582	7.0538	8.56	0	2.8925	1.468	80.226	76	3/27/13	3:01:37 PM	gv	avg	75.3459 pv
127	73H		9023.55	194.57	75.3459	2.582	7.1469	8.664	0	2.8925	1.468	80.226	76	3/27/13	3:16:43 PM	gv	avg	75.3459 pv
128	73H		9023.55	194.57	75.3459	2.582	7.1399	8.656	0	2.8925	1.468	80.226	76	3/27/13	3:31:19 PM	gv	avg	75.3459 pv
129	73H		9023.55	194.57	75.3459	2.582	7.1315	8.647	0	2.8925	1.468	80.226	76	3/27/13	3:45:13 PM	gv	avg	75.3459 pv
					75.3459	2.42527	7.14573	8.6625										

			Dry Weight (gm)	Grain Volume (cc)	Grain Density (gm/cc)	Bulk Density (gm/cc)	Pore Volume (cc)	Porosity (%)	HG Bulk Volume	Length (inch)	Dia (inch)	Caliper Bulk Volume	Temp (F)	Date	Time			
130	65		9015.85	192.35	75.8823	2.535	0	0	0	3.001	1.462	82.557	76	3/28/13	10:57:10 AM	gv		
131	65		9015.85	192.35	75.8829	2.535	0	0	0	3.001	1.462	82.557	76	3/28/13	11:03:32 AM	gv		
132	65		9015.85	192.35	75.8822	2.535	0	0	0	3.001	1.462	82.557	76	3/28/13	11:05:05 AM	gv		
133	65		9015.85	192.35	75.882	2.535	0	0	0	3.001	1.462	82.557	76	3/28/13	11:07:26 AM	gv		
134	65		9015.85	192.35	75.8828	2.535	0	0	0	3.001	1.462	82.557	76	3/28/13	11:10:23 AM	gv		
135	65		9015.85	192.35	75.8842	2.535	0	0	0	3.001	1.462	82.557	76	3/28/13	11:51:21 AM	gv		
136	65		9015.85	192.35	75.8872	2.535	0	0	0	3.001	1.462	82.557	76	3/28/13	12:12:20 PM	gv		
137	65		9015.85	192.35	75.8834	2.535	10.6326	12.29	0	3.001	1.462	82.557	76	3/28/13	2:26:18 PM	gv	ave	75.8834 pv
138	65		9015.85	192.35	75.8834	2.535	10.4736	12.128	0	3.001	1.462	82.557	76	3/28/13	2:56:59 PM	gv	ave	75.8834 pv
139	65		9015.85	192.35	75.8834	2.535	10.5056	12.161	0	3.001	1.462	82.557	76	3/28/13	2:59:05 PM	gv	ave	75.8834 pv
140	65		9015.85	192.35	75.8834	2.535	10.5174	12.173	0	3.001	1.462	82.557	76	3/28/13	3:01:18 PM	gv	ave	75.8834 pv
141	65		9015.85	192.35	75.8834	2.535	10.5308	12.186	0	3.001	1.462	82.557	76	3/28/13	3:04:18 PM	gv	ave	75.8834 pv
142	65		9015.85	192.35	75.8834	2.535	10.6139	12.271	0	3.001	1.462	82.557	76	3/28/13	3:43:21 PM	gv	ave	75.8834 pv
					75.8834	2.32991	10.6233	12.2805										

			Dry Weight (gm)	Grain Volume (cc)	Grain Density (gm/cc)	Bulk Density (gm/cc)	Pore Volume (cc)	Porosity (%)	HG Bulk Volume	Length (inch)	Dia (inch)	Caliper Bulk Volume	Temp (F)	Date	Time			
143	71		9021.55	194.34	75.4258	2.577	0	0	0	2.988	1.469	82.988	76	3/28/13	4:39:06 PM	gv		
144	71		9021.55	194.34	75.4241	2.577	0	0	0	2.988	1.469	82.988	76	3/28/13	4:40:40 PM	gv		
145	71		9021.55	194.34	75.4213	2.577	0	0	0	2.988	1.469	82.988	76	3/28/13	5:08:30 PM	gv		
146	71		9021.55	194.34	75.4225	2.577	0	0	0	2.988	1.469	82.988	76	3/28/13	5:10:04 PM	gv		
147	71		9021.55	194.34	75.4212	2.577	0	0	0	2.988	1.469	82.988	76	3/28/13	5:12:33 PM	gv		
148	71		9021.55	194.34	75.423	2.577	10.2314	11.945	0	2.988	1.469	82.988	76	3/29/13	11:32:03 AM	gv	avg	75.423 pv
149	71		9021.55	194.34	75.423	2.577	10.1106	11.821	0	2.988	1.469	82.988	76	3/29/13	11:51:56 AM	gv	avg	75.423 pv
150	71		9021.55	194.34	75.423	2.577	10.1234	11.834	0	2.988	1.469	82.988	76	3/29/13	11:54:34 AM	gv	avg	75.423 pv
151	71		9021.55	194.34	75.423	2.577	10.135	11.846	0	2.988	1.469	82.988	76	3/29/13	11:57:27 AM	gv	avg	75.423 pv
152	71		9021.55	194.34	75.423	2.577	10.1999	11.913	0	2.988	1.469	82.988	76	3/29/13	12:21:28 PM	gv	avg	75.423 pv
153	71		9021.55	194.34	75.423	2.577	10.2089	11.922	0	2.988	1.469	82.988	76	3/29/13	12:45:30 PM	gv	avg	75.423 pv
					75.423	2.34178	10.2134	11.9267										

			Dry Weight (gm)	Grain Volume (cc)	Grain Density (gm/cc)	Bulk Density (gm/cc)	Pore Volume (cc)	Porosity (%)	HG Bulk Volume	Length (inch)	Dia (inch)	Caliper Bulk Volume	Temp (F)	Date	Time			
154	63VB		9012.8	188.89	77.5157	2.437	0	0	0	3.001	1.452	81.431	76	3/29/13	1:19:31 PM	gv		
155	63VB		9012.8	188.89	77.5329	2.436	0	0	0	3.001	1.452	81.431	76	3/29/13	1:21:23 PM	gv		
156	63VB		9012.8	188.89	77.5399	2.436	0	0	0	3.001	1.452	81.431	76	3/29/13	1:23:07 PM	gv		
157	63VB		9012.8	188.89	77.5903	2.434	0	0	0	3.001	1.452	81.431	76	3/29/13	1:34:35 PM	gv		
158	63VB		9012.8	188.89	77.5908	2.434	0	0	0	3.001	1.452	81.431	76	3/29/13	1:36:41 PM	gv		
159	63VB		9012.8	188.89	77.6053	2.434	0	0	0	3.001	1.452	81.431	76	3/29/13	1:47:10 PM	gv		

160	63VB	9012.8	188.89	77.617	2.434		0	0	0	3.001	1.452	81.431	76	3/29/13	1:57:54 PM	gv							
161	63VB	9012.8	188.89	77.6308	2.433		0	0	0	3.001	1.452	81.431	76	3/29/13	2:27:58 PM	gv							
162	63VB	9012.8	188.89	77.5974	2.434		0	0	0	3.001	1.452	81.431	76	3/29/13	2:50:05 PM	gv							
163	63VB	9012.8	188.89	77.6061	2.434		0	0	0	3.001	1.452	81.431	76	3/29/13	3:03:03 PM	gv							
164	63VB	9012.8	188.89	77.6123	2.434		0	0	0	3.001	1.452	81.431	76	3/29/13	3:22:07 PM	gv							
165	63VB	9012.8	188.89	77.6063	2.434		10.5825	12	0	3.001	1.452	81.431	76	4/1/13	10:08:46 AM	gv	avg	77.6063	pv				
166	63VB	9012.8	188.89	77.6063	2.434		10.5423	11.96	0	3.001	1.452	81.431	76	4/1/13	10:43:30 AM	gv	avg	77.6063	pv				
167	63VB	9012.8	188.89	77.6063	2.434		10.5282	11.946	0	3.001	1.452	81.431	76	4/1/13	10:46:12 AM	gv	avg	77.6063	pv				
168	63VB	9012.8	188.89	77.6063	2.434		10.5212	11.939	0	3.001	1.452	81.431	76	4/1/13	10:49:03 AM	gv	avg	77.6063	pv				
169	63VB	9012.8	188.89	77.6063	2.434		10.5788	11.996	0	3.001	1.452	81.431	76	4/1/13	11:03:24 AM	gv	avg	77.6063	pv				
170	63VB	9012.8	188.89	77.6063	2.434		10.5802	11.998	0	3.001	1.452	81.431	76	4/1/13	11:16:45 AM	gv	avg	77.6063	pv				
171	63VB	9012.8	188.89	77.6063	2.434		10.5751	11.992	0	3.001	1.452	81.431	76	4/1/13	11:39:35 AM	gv	avg	77.6063	pv				
172	63VB	9012.8	188.89	77.6063	2.434		10.5841	12.001	0	3.001	1.452	81.431	76	4/1/13	11:45:51 AM	gv	avg	77.6063	pv				
				77.6063		2.31963	10.5801	11.9974															

		Dry Weight (gm)	Grain Volume (cc)	Grain Density (gm/cc)	Bulk Density (gm/cc)	Pore Volume (cc)	Porosity (%)	HG Bulk Volume	Length (inch)	Dia (inch)	Caliper Bulk Volume	Temp (F)	Date	Time								
173	73V	9023.35	171.04	69.2272	2.471		0	0	0	2.693	1.468	74.693	76	4/1/13	2:07:39 PM	gv							
174	73V	9023.35	171.04	69.2223	2.471		0	0	0	2.693	1.468	74.693	76	4/1/13	2:09:27 PM	gv							
175	73V	9023.35	171.04	69.2222	2.471		0	0	0	2.693	1.468	74.693	76	4/1/13	2:13:15 PM	gv							
176	73V	9023.35	171.04	69.2223	2.471		0	0	0	2.693	1.468	74.693	76	4/1/13	2:24:43 PM	gv							
177	73V	9023.35	171.04	69.2235	2.471		10.548	13.223	0	2.693	1.468	74.693	76	4/1/13	9:21:40 PM	gv	avg	69.2235	pv				
178	73V	9023.35	171.04	69.2235	2.471		10.514	13.186	0	2.693	1.468	74.693	76	4/1/13	9:57:22 PM	gv	avg	69.2235	pv				
179	73V	9023.35	171.04	69.2235	2.471		10.4696	13.137	0	2.693	1.468	74.693	76	4/1/13	9:59:46 PM	gv	avg	69.2235	pv				
180	73V	9023.35	171.04	69.2235	2.471		10.4812	13.15	0	2.693	1.468	74.693	76	4/1/13	10:20:19 PM	gv	avg	69.2235	pv				
181	73V	9023.35	171.04	69.2235	2.471		10.5346	13.208	0	2.693	1.468	74.693	76	4/1/13	10:23:28 PM	gv	avg	69.2235	pv				
				69.2235		2.28991	10.548	13.2057															

		Dry Weight (gm)	Grain Volume (cc)	Grain Density (gm/cc)	Bulk Density (gm/cc)	Pore Volume (cc)	Porosity (%)	HG Bulk Volume	Length (inch)	Dia (inch)	Caliper Bulk Volume	Temp (F)	Date	Time								
182	84H	9034.1	188.03	78.1704	2.405		0	0	0	2.696	1.4685	74.827	76	4/1/13	10:43:01 PM	gv							
183	84H	9034.1	188.03	78.2246	2.404		0	0	0	2.696	1.4685	74.827	76	4/1/13	10:56:58 PM	gv							
184	84H	9034.1	188.03	78.2619	2.403		0	0	0	2.696	1.4685	74.827	76	4/1/13	10:58:44 PM	gv							
185	84H	9034.1	188.03	78.2187	2.404		0	0	0	2.696	1.4685	74.827	76	4/1/13	11:19:12 PM	gv							
186	84H	9034.1	188.03	78.2174	2.404		0	0	0	2.696	1.4685	74.827	76	4/1/13	11:22:41 PM	gv							
187	84H	9034.1	188.03	78.2202	2.404		3.974	4.835	0	2.696	1.4685	74.827	76	4/2/13	10:56:13 AM	gv	ave	78.2202	pv				
188	84H	9034.1	188.03	78.2202	2.404		3.9582	4.817	0	2.696	1.4685	74.827	76	4/2/13	11:15:57 AM	gv	ave	78.2202	pv				
189	84H	9034.1	188.03	78.2202	2.404		3.9108	4.762	0	2.696	1.4685	74.827	76	4/2/13	11:20:04 AM	gv	ave	78.2202	pv				
190	84H	9034.1	188.03	78.2202	2.404		3.9752	4.836	0	2.696	1.4685	74.827	76	4/2/13	11:36:32 AM	gv	ave	78.2202	pv				
191	84H	9034.1	188.03	78.2202	2.404		3.979	4.841	0	2.696	1.4685	74.827	76	4/2/13	11:50:34 AM	gv	ave	78.2202	pv				
				78.2202		2.51286	3.9716	4.83225															

		Dry Weight (gm)	Grain Volume (cc)	Grain Density (gm/cc)	Bulk Density (gm/cc)	Pore Volume (cc)	Porosity (%)	HG Bulk Volume	Length (inch)	Dia (inch)	Caliper Bulk Volume	Temp (F)	Date	Time								
192	86H	9036.1	183.2	69.21	2.647		0	0	0	2.587	1.472	72.144	76	4/2/13	1:11:01 PM	gv							
193	86H	9036.1	183.2	69.2442	2.646		0	0	0	2.587	1.472	72.144	76	4/2/13	1:13:25 PM	gv							
194	86H	9036.1	183.2	69.2596	2.645		0	0	0	2.587	1.472	72.144	76	4/2/13	1:15:12 PM	gv							
195	86H	9036.1	183.2	69.2561	2.645		0	0	0	2.587	1.472	72.144	76	4/2/13	1:27:43 PM	gv							
196	86H	9036.1	183.2	69.2549	2.645		0	0	0	2.587	1.472	72.144	76	4/2/13	1:52:46 PM	gv							
197	86H	9036.1	183.2	69.245	2.646		2.4417	3.406	0	2.587	1.472	72.144	76	4/2/13	10:26:35 PM	gv	avg	69.245	pv				
198	86H	9036.1	183.2	69.245	2.646		2.4234	3.381	0	2.587	1.472	72.144	76	4/2/13	11:40:57 PM	gv	avg	69.245	pv				
199	86H	9036.1	183.2	69.245	2.646		2.4156	3.371	0	2.587	1.472	72.144	76	4/2/13	11:59:13 PM	gv	avg	69.245	pv				
				69.245		2.53937	2.4269	3.386															

		Dry Weight (gm)	Grain Volume (cc)	Grain Density (gm/cc)	Bulk Density (gm/cc)	Pore Volume (cc)	Porosity (%)	HG Bulk Volume	Length (inch)	Dia (inch)	Caliper Bulk Volume	Temp (F)	Date	Time								
200	64B	9013.7	160.29	66.7606	2.401		0	0	0	2.5455	1.453	69.166	76	4/3/13	12:15:43 AM	gv	bad	ground	smple				
201	64B	9013.7	160.29	66.8032	2.399		0	0	0	2.5455	1.453	69.166	76	4/3/13	9:49:49 AM	gv	bad	ground	smple				
202	64B	9013.7	160.29	66.7733	2.401		0	0	0	2.5455	1.453	69.166	76	4/3/13	9:51:44 AM	gv	bad	ground	smple				
203	64B	9013.7	160.29	66.766	2.401		0	0	0	2.5455	1.453	69.166	76	4/3/13	9:53:12 AM	gv	bad	ground	smple				
204	64B	9013.7	160.29	66.761	2.401		0	0	0	2.5455	1.453	69.166	76	4/3/13	9:55:12 AM	gv	bad	ground	smple				
205	64B	9013.7	160.29	66.7631	2.401		0	0	0	2.5455	1.453	69.166	76	4/3/13	10:09:25 AM	gv	bad	ground	smple				
206	64B	9013.7	160.29	66.7712	2.401		9.384	12.322	0	2.5455	1.453	69.166	76	4/3/13	3:28:16 PM	gv	bad	ground	smple	avg	66.7712	pv	
207	64B	9013.7	160.29	66.7712	2.401		9.343	12.275	0	2.5455	1.453	69.166	76	4/3/13	7:05:08 PM	gv	bad	ground	smple	avg	66.7712	pv	
208	64B	9013.7	160.29	66.7712	2.401		9.338	12.269	0	2.5455	1.453	69.166	76	4/3/13	7:29:15 PM	gv	bad	ground	smple	avg	66.7712	pv	
				66.7712		2.31747	9.355	12.2887															

		Dry Weight (gm)	Grain Volume (cc)	Grain Density (gm/cc)	Bulk Density (gm/cc)	Pore Volume (cc)	Porosity (%)	HG Bulk Volume	Length (inch)	Dia (inch)	Caliper Bulk Volume	Temp (F)	Date	Time								
209	82HB	9032.5	177.62	66.9323	2.654		0	0	0	3.535	1.47	98.314	76	4/3/13	11:07:19 PM	gv							
210	82HB	9032.5	177.62	66.9634	2.652		0	0	0	3.535	1.47	98.314	76	4/3/13	11:09:01 PM	gv							
212	82HB	9032.5	177.62	66.9726	2.652	Below	Zero		0	0	3.535	1.47	98.314	76	4/3/13	11:26:33 PM	gv						
213	82HB	9032.5	177.62	66.9693	2.652		0	0	0	3.535	1.47	98.314	76	4/3/13	11:28:10 PM	gv							
214	82HB	9032.5	177.62	66.9911	2.651		3.71	5.247	0	2.535	1.47	70.502	76	4/4/13	12:17:54 AM	gv	ave	66.9911					
215	82HB	9032.5	177.62	66.9911	2.651		3.5873	5.083	0	2.535	1.47	70.502	76	4/4/13	8:44:15 AM	gv	ave	66.9911	pv				
216	82HB	9032.5	177.62	66.9911	2.651		3.5756	5.067	0	2.535	1.47	70.502	76	4/4/13	8:47:13 AM	gv	ave	66.9911	pv				
217	82HB	9032.5	177.62	66.9911	2.651		3.584	5.078	0	2.535	1.47	70.502	76	4/4/13	8:50:33 AM	gv	ave	66.9911	pv				
218	82HB	9032.5	177.62	66.9911	2.651		3.5996	5.099	0	2.535	1.47	70.502	76	4/4/13	8:54:05 AM	gv	ave	66.9911	pv				
219	82HB	9032.5	177.62	66.9911	2.651		3.6545	5.173	0	2.535	1.47	70.502	76	4/4/13	9:07:55 AM	gv	ave	66.9911	pv				
220	82HB	9032.5	177.62	66.9911	2.651		3.6547	5.173	0	2.535	1.47	70.502	76	4/4/13	9:21:11 AM	gv	ave	66.9911	pv				
				66.9594		2.51936	3.67307	5.19767															

		Dry Weight (gm)	Grain Volume (cc)	Grain Density (gm/cc)	Bulk Density (gm/cc)	Pore Volume (cc)	Porosity (%)	HG Bulk Volume	Length (inch)	Dia (inch)	Caliper Bulk Volume	Temp (F)	Date	Time								
221	79HB	9029.35	159.78	66.1312	2.416		0	0	0	2.5305	1.4685	70.234	76	4/4/13	9:43:25 AM	gv							
222	79HB	9029.35	159.78	66.1322	2.416		0	0	0	2.5305	1.4685	70.234	76	4/4/13	9:45:18 AM	gv							
223	79HB	9029.35	159.78	66.1325	2.416		0	0	0	2.5305	1.4685	70.234	76	4/4/13	9:47:36 AM	gv							
224	79HB	9029.35	159.78	66.1531	2.415		0	0	0	2.5305	1.4685	70.234	76	4/4/13	10:01:02 AM	gv							
225	79HB	9029.35	159.78	66.1629	2.415		0	0	0	2.5305	1.4685	70.234	76	4/4/13	10:14:26 AM	gv							
226	79HB	9029.35	159.78	66.1615	2.415		0	0	0	2.5305	1.4685	70.234	76	4/4/13	10:25:44 AM	gv							
227	79HB	9029.35	159.78	66.1592	2.415		10.226	13.387	0	2.5305	1.4685	70.234	76	4/5/13	2:47:29 PM	gv	ave	66.1592	pv				
228	79HB	9029.35	159.78	66.1592	2.415		10.1902	13.347	0	2.5305	1.4685	70.234	76	4/5/13	2:50:30 PM	gv	ave	66.1592	pv				
229	79HB	9029.35	159.78	66.1592	2.415		10.1667	13.32	0	2.5305	1.4685	70.234	76	4/5/13	2:53:50 PM	gv	ave	66.1592	pv				
230	79HB	9029.35	159.78	66.1592	2.415		10.2152	13.375	0	2.5305	1.4685	70.234	76	4/5/13	3:06:13 PM	gv	ave	66.1592	pv				
231	79HB	9029.35	159.78	66.1592	2.415		10.214	13.374	0	2.5305	1.4685	70.234	76	4/5/13	3:19:31 PM	gv	ave	66.1592	pv				
				66.1592		2.27497	10.2114	13.3708															

		Dry Weight (gm)	Grain Volume (cc)	Grain Density (gm/cc)	Bulk Density (gm/cc)	Pore Volume (cc)	Porosity (%)	HG Bulk Volume	Length (inch)	Dia (inch)	Caliper Bulk Volume	Temp (F)	Date	Time								
232	74HB	9024.65	172.52	65.0317	2.653		0	0	0	2.5	1.469	69.434	76	4/5/13	3:31:09 PM	gv							
233	74HB	9024.65	172.52	65.0614	2.652		0	0	0	2.5	1.469	69.434	76	4/5/13	3:45:28 PM	gv							
234	74HB	9024.65	172.52	65.0602	2.652		0	0	0	2.5	1.469	69.434	76	4/5/13	3:56:41 PM	gv							
235	74HB	9024.65	172.52	65.0539	2.652		0	0	0	2.5	1.469	69.434	76	4/8/13	9:51:34 AM	gv	ave	69.1036	pv				
236	74HB	9024.65	172.52	65.0849	2.651		0	0	0	2.5	1.469	69.434	76	4/8/13	11:04:18 AM	gv	ave	69.1036	pv				
237	74HB	9024.65	172.52	65.0797	2.651		0	0	0	2.5	1.469	69.434	76	4/8/13	12:04:42 PM	gv	ave	69.1036	pv				
238	74HB	9024.65	172.52	65.077	2.651		0	0	0	2.5	1.469	69.434	76	4/8/13	12:13:13 PM	gv	ave	69.1036	pv				
239	74HB	9024.65	172.52	65.0802	2.651		0	0	0	2.5	1.469	69.434	76	4/8/13	12:14:52 PM	gv	ave	69.1036	pv				
240	74HB	9024.65	172.52	65.0824	2.651		0	0	0	2.5	1.469	69.434	76	4/8/13	1:34:46 PM	gv	ave	69.1036	pv				
241	74HB	9024.65	172.52	65.0745	2.651		0	0	0	2.5	1.469	69.434	76	4/8/13	3:42:33 PM	gv							

242	74HB	9024.65	172.52	65.0745	2.651		4.7057	6.744	0	2.5	1.469	69.434	76	4/9/13	10:29:34 AM	gv	avg	69.1036	pv		
243	74HB	9024.65	172.52	65.069	2.651		4.6712	6.698	0	2.5	1.469	69.434	76	4/9/13	11:01:41 AM	gv	avg	65.069	pv		
244	74HB	9024.65	172.52	65.069	2.651		4.6493	6.669	0	2.5	1.469	69.434	76	4/9/13	11:05:30 AM	gv	avg	65.069	pv		
245	74HB	9024.65	172.52	65.069	2.651		4.6926	6.727	0	2.5	1.469	69.434	76	4/9/13	11:28:38 AM	gv	avg	65.069	pv		
246	74HB	9024.65	172.52	65.069	2.651		4.6988	6.735	0	2.5	1.469	69.434	76	4/9/13	11:53:16 AM	gv	avg	65.069	pv		
				65.0691		2.48466	4.69903	6.73533													
		Dry Weight (gm)	Grain Volume (cc)	Grain Density (gm/cc)	Bulk Density (gm/cc)	Pore Volume (cc)	Porosity (%)	HG Bulk Volume	Length (inch)	Dia (inch)	Caliper Bulk Volume	Temp (F)	Date	Time							
247	88HB	9037.8	162.83	61.5633	2.645		0	0	0	2.302	1.469	63.935	76	4/9/13	2:49:35 PM	gv					
248	88HB	9037.8	162.83	61.5878	2.644		0	0	0	2.302	1.469	63.935	76	4/9/13	2:51:43 PM	gv					
249	88HB	9037.8	162.83	61.6032	2.643		0	0	0	2.302	1.469	63.935	76	4/9/13	2:53:43 PM	gv					
250	88HB	9037.8	162.83	61.6292	2.642		0	0	0	2.302	1.469	63.935	76	4/9/13	2:55:38 PM	gv					
251	88HB	9037.8	162.83	61.5896	2.644		0	0	0	2.302	1.469	63.935	76	4/9/13	3:06:50 PM	gv					
252	88HB	9037.8	162.83	61.5868	2.644		0	0	0	2.302	1.469	63.935	76	4/9/13	3:19:32 PM	gv					
253	88HB	9037.8	162.83	61.5881	2.644		0	0	0	2.302	1.469	63.935	76	4/9/13	3:34:00 PM	gv					
254	88HB	9037.8	162.83	61.5803	2.644		0	0	0	2.302	1.469	63.935	76	4/9/13	3:57:48 PM	gv					
255	88HB	9037.8	162.83	61.5803	2.644		2.9999	4.645	0	2.302	1.469	63.935	76	4/10/13	11:46:16 AM	gv	avg	61.5865	pv		
256	88HB	9037.8	162.83	61.5803	2.644		2.9476	4.568	0	2.302	1.469	63.935	76	4/10/13	12:53:18 PM	gv	avg	61.5865	pv		
257	88HB	9037.8	162.83	61.5803	2.644		2.9096	4.512	0	2.302	1.469	63.935	76	4/10/13	12:56:29 PM	gv	avg	61.5865	pv		
258	88HB	9037.8	162.83	61.5803	2.644		2.9895	4.63	0	2.302	1.469	63.935	76	4/10/13	1:20:12 PM	gv	avg	61.5865	pv		
259	88HB	9037.8	162.83	61.5803	2.644		2.9868	4.626	0	2.302	1.469	63.935	76	4/10/13	1:46:02 PM	gv	avg	61.5865	pv		
260	88HB	9037.8	162.83	61.5803	2.644		2.986	4.625	0	2.302	1.469	63.935	76	4/10/13	2:15:26 PM	gv	avg	61.5865	pv		
				61.5865		2.54681	2.99055	4.6315													
		Dry Weight (gm)	Grain Volume (cc)	Grain Density (gm/cc)	Bulk Density (gm/cc)	Pore Volume (cc)	Porosity (%)	HG Bulk Volume	Length (inch)	Dia (inch)	Caliper Bulk Volume	Temp (F)	Date	Time							
261	65HB	9015.6	141.07	53.6662	2.629		0	0	0	2.132	1.465	58.892	76	4/10/13	3:00:40 PM	gv					
262	65HB	9015.6	141.07	53.6728	2.628		0	0	0	2.132	1.465	58.892	76	4/10/13	3:02:18 PM	gv					
263	65HB	9015.6	141.07	53.6738	2.628		0	0	0	2.132	1.465	58.892	76	4/10/13	3:04:17 PM	gv					
264	65HB	9015.6	141.07	53.6713	2.628		0	0	0	2.132	1.465	58.892	76	4/10/13	3:17:17 PM	gv					
265	65HB	9015.6	141.07	53.6703	2.628		0	0	0	2.132	1.465	58.892	76	4/10/13	3:28:45 PM	gv					
266	65HB	9015.6	141.07	53.6688	2.629		0	0	0	2.132	1.465	58.892	76	4/10/13	3:40:55 PM	gv					
267	65HB	9015.6	141.07	53.6705	2.628		6.2775	10.472	0	2.132	1.465	58.892	76	4/11/13	5:35:48 PM	gv	avg	53.6705	pv		
268	65HB	9015.6	141.07	53.6705	2.628		6.2614	10.448	0	2.132	1.465	58.892	76	4/11/13	7:01:51 PM	gv	avg	53.6705	pv		
269	65HB	9015.6	141.07	53.6705	2.628		6.2751	10.468	0	2.132	1.465	58.892	76	4/11/13	7:06:03 PM	gv	avg	53.6705	pv		
270	65HB	9015.6	141.07	53.6705	2.628		6.261	10.447	0	2.132	1.465	58.892	76	4/11/13	7:33:02 PM	gv	avg	53.6705	pv		
271	65HB	9015.6	141.07	53.6705	2.628		6.2699	10.46	0	2.132	1.465	58.892	76	4/11/13	8:04:51 PM	gv	avg	53.6705	pv		
				53.6705		2.3954	6.26898	10.459													
		Dry Weight (gm)	Grain Volume (cc)	Grain Density (gm/cc)	Bulk Density (gm/cc)	Pore Volume (cc)	Porosity (%)	HG Bulk Volume	Length (inch)	Dia (inch)	Caliper Bulk Volume	Temp (F)	Date	Time							
272	91H	9042.1	148.34	56.3074	2.634		0	0	0	2.1045	1.4615	57.855	76	4/11/13	11:56:12 PM	gv					
273	91H	9042.1	148.34	56.306	2.635		0	0	0	2.1045	1.4615	57.855	76	4/12/13	12:03:30 AM	gv					
274	91H	9042.1	148.34	56.3073	2.634		0	0	0	2.1045	1.4615	57.855	76	4/12/13	12:09:47 AM	gv					
275	91H	9042.1	148.34	56.2407	2.638		0	0	0	2.1045	1.4615	57.855	76	4/12/13	8:32:52 AM	gv					
276	91H	9042.1	148.34	56.2801	2.636		0	0	0	2.1045	1.4615	57.855	76	4/12/13	8:53:59 AM	gv					
277	91H	9042.1	148.34	56.2867	2.635		0	0	0	2.1045	1.4615	57.855	76	4/12/13	9:15:42 AM	gv					
278	91H	9042.1	148.34	56.2975	2.635		2.5616	4.352	0	2.1045	1.4615	57.855	76	4/12/13	10:49:58 AM	gv					
279	91H	9042.1	148.34	56.2975	2.635		2.4979	4.248	0	2.1045	1.4615	57.855	76	4/12/13	8:31:05 PM	gv	avg	56.2975	pv		
280	91H	9042.1	148.34	56.2975	2.635		2.4871	4.231	0	2.1045	1.4615	57.855	76	4/12/13	9:16:05 PM	gv	avg	56.2975	pv		
281	91H	9042.1	148.34	56.2975	2.635		2.4758	4.212	0	2.1045	1.4615	57.855	76	4/12/13	9:54:07 PM	gv	avg	56.2975	pv		
282	91H	9042.1	148.34	56.2975	2.635		2.4836	4.225	0	2.1045	1.4615	57.855	76	4/12/13	10:35:12 PM	gv	avg	56.2975	pv		
				56.2975		2.564	2.4861	4.229													
		Dry Weight (gm)	Grain Volume (cc)	Grain Density (gm/cc)	Bulk Density (gm/cc)	Pore Volume (cc)	Porosity (%)	HG Bulk Volume	Length (inch)	Dia (inch)	Caliper Bulk Volume	Temp (F)	Date	Time							
283	86HB	9036.6	139.68	52.7777	2.647		0	0	0	1.924	1.4705	53.546	76	4/12/13	11:28:33 PM	gv					
284	86HB	9036.6	139.68	52.9009	2.64		0	0	0	1.924	1.4705	53.546	76	4/12/13	11:44:16 PM	gv					
285	86HB	9036.6	139.68	52.7465	2.648		0	0	0	1.924	1.4705	53.546	76	4/15/13	9:20:49 AM	gv					
286	86HB	9036.6	139.68	52.8526	2.643		0	0	0	1.924	1.4705	53.546	76	4/15/13	9:26:42 AM	gv					
287	86HB	9036.6	139.68	52.7995	2.645		0	0	0	1.924	1.4705	53.546	76	4/15/13	9:40:14 AM	gv					
288	86HB	9036.6	139.68	52.8047	2.645		0	0	0	1.924	1.4705	53.546	76	4/15/13	10:14:44 AM	gv					
289	86HB	9036.6	139.68	52.8042	2.645		0	0	0	1.924	1.4705	53.546	76	4/15/13	10:27:15 AM	gv					
290	86HB	9036.6	139.68	52.8028	2.645		2.1408	3.896	0	1.924	1.4705	53.546	76	4/15/13	11:39:31 AM	gv	avg	52.8028	pv		
291	86HB	9036.6	139.68	52.8028	2.645		2.1064	3.836	0	1.924	1.4705	53.546	76	4/15/13	12:49:58 PM	gv	avg	52.8028	pv		
292	86HB	9036.6	139.68	52.8028	2.645		2.0643	3.762	0	1.924	1.4705	53.546	76	4/15/13	12:53:34 PM	gv	avg	52.8028	pv		
293	86HB	9036.6	139.68	52.8028	2.645		2.1309	3.879	0	1.924	1.4705	53.546	76	4/15/13	1:16:44 PM	gv	avg	52.8028	pv		
294	86HB	9036.6	139.68	52.8028	2.645		2.1311	3.879	0	1.924	1.4705	53.546	76	4/15/13	1:40:14 PM	gv	avg	52.8028	pv		
295	86HB	9036.6	139.68	52.8028	2.645		2.1326	3.882	0	1.924	1.4705	53.546	76	4/15/13	2:03:35 PM	gv	avg	52.8028	pv		
				52.8028		2.6086	2.13153	3.88													
		Dry Weight (gm)	Grain Volume (cc)	Grain Density (gm/cc)	Bulk Density (gm/cc)	Pore Volume (cc)	Porosity (%)	HG Bulk Volume	Length (inch)	Dia (inch)	Caliper Bulk Volume	Temp (F)	Date	Time							
296	70H	9020.2	100.27	37.9014	2.646		0	0	0	1.475	1.467	40.855	76	4/15/13	2:33:40 PM	gv					
297	70H	9020.2	100.27	37.9293	2.644		0	0	0	1.475	1.467	40.855	76	4/15/13	2:35:37 PM	gv					
298	70H	9020.2	100.27	37.9387	2.643		0	0	0	1.475	1.467	40.855	76	4/15/13	2:37:09 PM	gv					
299	70H	9020.2	100.27	37.9355	2.643		0	0	0	1.475	1.467	40.855	76	4/15/13	2:54:43 PM	gv					
300	70H	9020.2	100.27	37.9351	2.643		0	0	0	1.475	1.467	40.855	76	4/15/13	3:06:26 PM	gv					
301	70H	9020.2	100.27	37.9331	2.643		0	0	0	1.475	1.467	40.855	76	4/15/13	3:20:14 PM	gv					
302	70H	9020.2	100.27	37.9322	2.643		0	0	0	1.475	1.467	40.855	76	4/15/13	3:35:31 PM	gv					
303	70H	9020.2	100.27	37.9321	2.643		0	0	0	1.475	1.467	40.855	76	4/15/13	3:48:26 PM	gv					
304	70H	9020.2	100.27	37.9336	2.643		3.573	8.608	0	1.475	1.467	40.855	76	4/16/13	11:27:04 AM	gv	avg	37.9336	pv00000		
305	70H	9020.2	100.27	37.9336	2.643		3.5534	8.565	0	1.475	1.467	40.855	76	4/16/13	12:50:51 PM	gv	avg	37.9336	pv		
306	70H	9020.2	100.27	37.9336	2.643		3.5159	8.482	0	1.475	1.467	40.855	76	4/16/13	12:53:41 PM	gv	avg	37.9336	pv		
307	70H	9020.2	100.27	37.9336	2.643		3.5607	8.581	0	1.475	1.467	40.855	76	4/16/13	1:16:27 PM	gv	avg	37.9336	pv		
308	70H	9020.2	100.27	37.9336	2.643		3.5636	8.588	0	1.475	1.467	40.855	76	4/16/13	1:39:36 PM	gv	avg	37.9336	pv		
309	70H	9020.2	100.27	37.9336	2.643		3.56	8.58	0	1.475	1.467	40.855	76	4/16/13	2:02:29 PM	gv	avg	37.9336	pv		
310	70H	9020.2	100.27	37.9336	2.643		3.5574	8.574	0	1.475	1.467	40.855	76	4/16/13	2:25:25 PM	gv	avg	37.9336	pv		
				37.9337		2.45429	3.56135	8.58267													
		Dry Weight (gm)	Grain Volume (cc)	Grain Density (gm/cc)	Bulk Density (gm/cc)	Pore Volume (cc)	Porosity (%)	HG Bulk Volume	Length (inch)	Dia (inch)	Caliper Bulk Volume	Temp (F)	Date	Time							
311	90h	9041	96.56	36.6988	2.631		0	0	0	1.3795	1.465	38.106	76	4/16/13	9:17:05 PM	gv					
312	90h	9041	96.56	36.6882	2.632		0	0	0	1.3795	1.465	38.106	76	4/16/13	9:26:30 PM	gv					
313	90h	9041	96.56	36.6681	2.633		0	0	0	1.3795	1.465	38.106	76	4/16/13	10:01:28 PM	gv					
314	90h	9041	96.56	36.6695	2.633		0	0	0	1.3795	1.465	38.106	76	4/16/13	10:07:16 PM	gv					
315	90h	9041	96.56	36.6656	2.634		0	0	0	1.3795	1.465	38.106	76	4/16/13	10:13:13 PM	gv					
316	90h	9041	96.56	36.6806	2.632		2.4305	6.214	0	1.3795	1.465	38.106	76	4/16/13	11:37:21 PM	gv	ave	36.6806	pv		
317	90h	9041	96.56	36.6806	2.632		2.4247	6.2	0	1.3795	1.465	38.106	76	4/17/13	12:05:56 AM	gv	ave	36.6806	pv		
318	90h	9041	96.56	36.6806	2.632		2.4266	6.205	0	1.3795	1.465	38.106	76	4/17/13	12:18:31 AM	gv	ave	36.6806	pv		
				36.6935		2.53398	2.42727	6.20633													

CMS-300 ROTARY SIDEWALL ANALYSIS

University of Utah

RMCCS State #1

Moffat County, Colorado

CL File Number: Den-130027

Date: 4/26/13

This report is based entirely upon the core samples, soils, solids, liquids, or gases, together with related observational data, provided solely by the client. The conclusions, inferences, deductions and opinions rendered herein reflect the examination, study, and testing of these items, and represent the best judgement of Core Laboratories. Any reliance on the information contained herein concerning the profitability or productivity of any well, sand, or drilling activity is at the sole risk of the client, and Core Laboratories, neither extends nor makes any warranty or representation whatsoever with respect to same. This report has been prepared for the exclusive and confidential use of the client and no other party.

University of Utah
RMCCS State #1
Moffat County, Colorado

CL File No.: Den-130027
Date: 4/26/13
Analyst(s): NS, JK

CMS-300 ROTARY SIDEWALL ANALYSIS

Sample Number	Depth (ft)	Net Confining Stress (psig)	Porosity (%)	Permeability		b(air) psi	Beta ft(-1)	Alpha (microns)	Grain Density (g/cm3)	Footnote
				Klinkenberg (md)	Kair (md)					
1	8288.00	Ambient	5.33	***	***	***	***	***	2.647	
1	8288.00	3605	4.95	0.0035	0.0132	88.41	7.64E+14	8.56E+03	2.647	
2	8358.00	Ambient	5.71	***	***	***	***	***	2.677	
2	8358.00	3636	5.66	0.0125	0.0192	15.63	1.99E+13	8.27E+02	2.677	(3)
3	8490.00	Ambient	1.01	***	***	***	***	***	2.622	
3	8490.00	3693	***	***	***	***	***	***	***	(2)
4	8780.00	Ambient	3.69	***	***	***	***	***	2.716	
4	8780.00	3819	***	***	***	***	***	***	***	(2)
5	8807.00	Ambient	6.48	***	***	***	***	***	2.675	
5	8807.00	3831	5.22	0.0012	0.0055	129.41	6.07E+15	2.29E+04	2.675	
6	8882.00	Ambient	8.76	***	***	***	***	***	2.662	
6	8882.00	3864	7.83	0.0176	0.0498	52.49	5.14E+12	2.99E+02	2.662	(3)
7	8992.00	Ambient	1.47	***	***	***	***	***	2.680	
7	8992.00	3912	***	***	***	***	***	***	***	(2)
8	9380.00	Ambient	4.11	***	***	***	***	***	2.690	
8	9380.00	4080	2.83	0.0001	0.0009	301.95	3.06E+17	1.03E+05	2.690	
9	9603.00	Ambient	0.97	***	***	***	***	***	2.626	
9	9603.00	4177	***	***	***	***	***	***	***	(2)
10	9675.00	Ambient	3.26	***	***	***	***	***	2.771	
10	9675.00	4209	***	***	***	***	***	***	***	(2)

Footnotes :

(1) : Denotes fractured or chipped sample. Permeability and/or porosity may be optimistic.

(2) : Sample permeability below the measurement range of CMS-300 equipment at indicated net confining stress (NCS). Data unavailable.

(3) : Denotes very short sample, porosity may be optimistic due to lack of conformation of boot material to plug surface.

(4) : Sample contains bitumen or other solid hydrocarbon residue.

(5) : Denotes sample unsuitable for measurement at stress. Porosity determined using Archimedes bulk volume at ambient conditions.

Permeability greater than 0.1 mD measured using helium gas. Permeability less than 0.1 mD measured using nitrogen gas. All b values converted to b (air)

APPENDIX A: EXPLANATION OF CMS-300 TERMS "b", "Beta, and "Alpha"

K_x	=	Equivalent non-reactive liquid permeability, corrected for gas slippage, mD
K_{air}	=	Permeability to Air, calculated using K_x and b, mD
b	=	Klinkenberg slip factor, psi
β (Beta)	=	Forcheimer inertial resistance factor, ft^{-1}
α (Alpha)	=	A factor equal to the product of Beta and K_x. This factor is employed in determining the pore level heterogeneity index, H_i.
H_i	=	$\log_{10}(\alpha\phi/RQI)$ α, microns = $3.238E^{-9}\ \beta K_x$
Ø	=	Porosity, fraction
RQI	=	Reservoir Quality Index, microns
RQI	=	$0.0314(K/\phi)^{0.5}$

For further information please refer to:

Jones, S.C.: "Two-Point Determination of Permeability and PV vs. Net Confining Stress" SPE Formation Evaluation (March 1988) 235-241.

Jones S.C.: "A Rapid Accurate Unsteady-State Klinkenberg Permeameter," Soc. Pet. Eng. J. (Oct. 1972) 383-397.

Jones, S.C.: "Using the Inertial Coefficient, β, To Characterize Heterogeneity in Reservoir Rock: SPE 16949 (September 1987).

Amaefule, J.O.; Kersey, D.G.; Marschall, D.M.; Powell, J.D.; Valencia, L.E.; Keelan, D.K.: "Reservoir Description: A Practical Synergistic Engineering and Geological Approach Based on Analysis of Core Data,: SPE Technical Conference (Oct. 1988) SPE 18167.

University of Utah
RMCCS State #1
Moffat County, Colorado

CL File No.: Den-130027
Date: 4/26/13
Analyst(s): NS, JK

CMS-300 ROTARY SIDEWALL ANALYSIS PROTOCOL

Sample Preparation
Samples trimmed into right cylinders with a diamond-blade trim saw. All sample trims were archived

Core Extraction
Plugs selected for routine core analysis were placed in Soxhlet extraction cycling between a chloroform /methanol (87:13) azeotrope and methanol.

Sample Drying
Samples were oven dried at 240° F to weight equilibrium (+/- 0.001 g).

Porosity
Porosity was determined using Boyle's Law technique by measuring grain volume at ambient conditions & pore volume at indicated net confining stresses (NCS)

Grain Density
Grain density values were calculated by direct measurement of grain volume and weight on dried plug samples.
Grain volume was measured by Boyle's Law technique.

Permeability
Klinkenberg permeability was measured on each sample using unsteady-state method at indicated NCS.

Fluid Saturations
Fluid saturations were determined by the Dean Stark technique using the following fluid properties:

Brine	1.032 g/cc (50000 ppm TDS)
Oil	0.845 g/cc (36° API)

Schlumberger

ROUTINE CORE ANALYSIS

Prepared for: University of Utah

Well: RMCCS-1

Formations: Various

Location: Craig, Colorado

Prepared by:

Schlumberger Reservoir Laboratories

6350 W. Sam Houston Parkway N, Suite 200

Houston, Texas 77041, USA

(713) 482-0700

Date: Apr 16 2013

Project No: 2012USHC-P113

Quality Assurance Process

Schlumberger is committed to providing unsurpassed services in reservoir sampling and analyses while maintaining high standards of safety and quality. Our objective is to deliver the most accurate and reliable sampling processes and fluid and rock property measurements available in the industry. This objective requires persistent innovation and ongoing development of state-of-the-art technologies and equipment.

A rigorous quality assurance program, continuous employee training and enforcement of strict safety standards maintain our compliance with Quality, Health, Safety and Environment (QHSE) requirements. Proactive integration of QHSE objectives and management goals at every level supports the communication and implementation of QHSE policies and standards. Schlumberger requires that qualified engineering technologists perform all laboratory measurements according to specified analytical procedures designed for obtaining accurate and reliable data.

The lab-generated data undergoes the following five levels of quality checks to establish the integrity of the reported results.

a) Establish quality of measurement during data generation.
b) Lab supervisor and manager confirm the overall quality of the generated data.
c) Project manager reviews and processes generated data and generates reports.
d) Technical advisors confirm consistency of reported data.
e) Project manager finalizes reports.

Hence the completion of each project requires that a qualified and experienced team of engineers perform a variety of independent reviews of all technical data to confirm the consistency and accuracy of the report as per pre-established quality checklists designed for each operation and based on the level of complexity. All property measurements and calculation procedures are maintained in company archives for a period of one year. This information is available for review by clients upon request.

The file and laboratory records information is listed below to provide access reference to all records related to this project. For any questions, please do not hesitate to contact the undersigned project manager.

File No.: 2012USHC-P113

Laboratory Procedures

Brent Duncan
Routine Core Analysis Supervisor

Reviewed by

X	Mark Andersen	Core Physics Domain Head
X	Joe Loman	Core Analysis Technical Advisor

Project Management

Micah Alexander
Project Manager

Table of Contents

Quality assurance i
Routine core analysis 1

List of Tables

Table 1. Routine core analysis result summary 2

List of Figures

Figure 1. Permeability vs porosity cross plot 4

Routine core analysis

Twenty (20) core samples were received from the University of Utah.

The samples were cleaned in a Soxhlet extractor with methanol to remove salt. All plugs were dried in a convection oven at 106°C until the weight stabilized. Afterwards, they were kept in a desiccator when not being tested.

Air permeability and porosity were measured using a CoreTest AP-608 based on the unsteady-state pulse decay method at a confining pressures of 800 and 3500 psi. Grain volumes were measured using helium expansion based on Boyle's Law at ambient conditions. Bulk volume was calculated by the summation of pore volume and grain volume. Porosity was determined from the calculated bulk volume.

The routine core properties are summarized in Table 1. The permeability-porosity relationship is shown in Figure 1.

Schlumberger

TABLE 1. ROUTINE CORE ANALYSIS RESULT SUMMARY

Formation	Sample ID	Depth (ft)	Net Confining Stress (psi)	Grain Density (g/cm3)	Helium Porosity (%)	Air Permeability (mD)	Klinkenberg Air Permeability (mD)	Comments
Mowry	RM1-O2VB-P01	8191.7	800	2.52	1.98	0.003	0.001	Shale, black, thin very fine grain horizontal sand laminations
Mowry	RM1-O2VB-P01	8191.7	3500	2.52	2.17	0.001	*	
Mowry	RM1-O3HO-P01	8192.0	800	2.56	1.09	0.001	*	Shale, black, thin laminations
Mowry	RM1-O3HO-P01	8192.0	3500	2.56	0.98	*	*	
Mowry	RM1-10HO-P01	8206.0	800	2.65	6.70	0.003	0.001	Sandstone, gray, very fine grain, very well cemented
Mowry	RM1-10HO-P01	8206.0	3500	2.65	5.95	0.001	*	
Mowry	RM1-13HO-P01	8218.3	800	2.55	1.84	0.521	0.403	Shale, black, very thin fractured laminations
Mowry	RM1-13HO-P01	8218.3	3500	2.55	1.39	0.103	0.065	
Mowry	RM1-18HO-P01	8228.9	800	2.52	2.11	0.001	*	Shale, black, some laminations
Mowry	RM1-18HO-P01	8228.9	3500	2.52	1.55	*	*	
Mowry	RM1-21HO-P01	8235.0	800	2.51	2.19	0.004	0.001	Shale, black, thin laminations
Mowry	RM1-21HO-P01	8235.0	3500	2.51	1.98	*	*	
Mowry	RM1-25HA-P01	8243.2	800	2.50	1.39	0.033	0.017	Shale, black, very thin vertical calcareous laminations, trace fractures
Mowry	RM1-25HA-P01	8243.2	3500	2.50	1.29	0.009	0.004	
Mowry	RM1-33HO-P01	8253.3	800	2.55	0.71	*	*	Shale, black, very thin laminations
Mowry	RM1-33HO-P01	8253.3	3500	2.55	0.60	*	*	
Mowry	RM1-36HO-P01	8258.0	800	2.57	1.03	0.004	0.002	Shale, black, very thin fractured laminations
Mowry	RM1-36HO-P01	8258.0	3500	2.57	0.630	*	*	
Mowry	RM1-37HO-P01	8259.5	800	2.58	2.26	0.006	0.003	Shale, gray
Mowry	RM1-37HO-P01	8259.5	3500	2.58	1.95	0.001	*	
Curtis	RM1-41HA-P01	8896.1	800	2.66	0.64	0.001	*	Sandstone, gray, very fine grain
Curtis	RM1-41HA-P01	8896.1	3500	2.66	0.51	*	*	

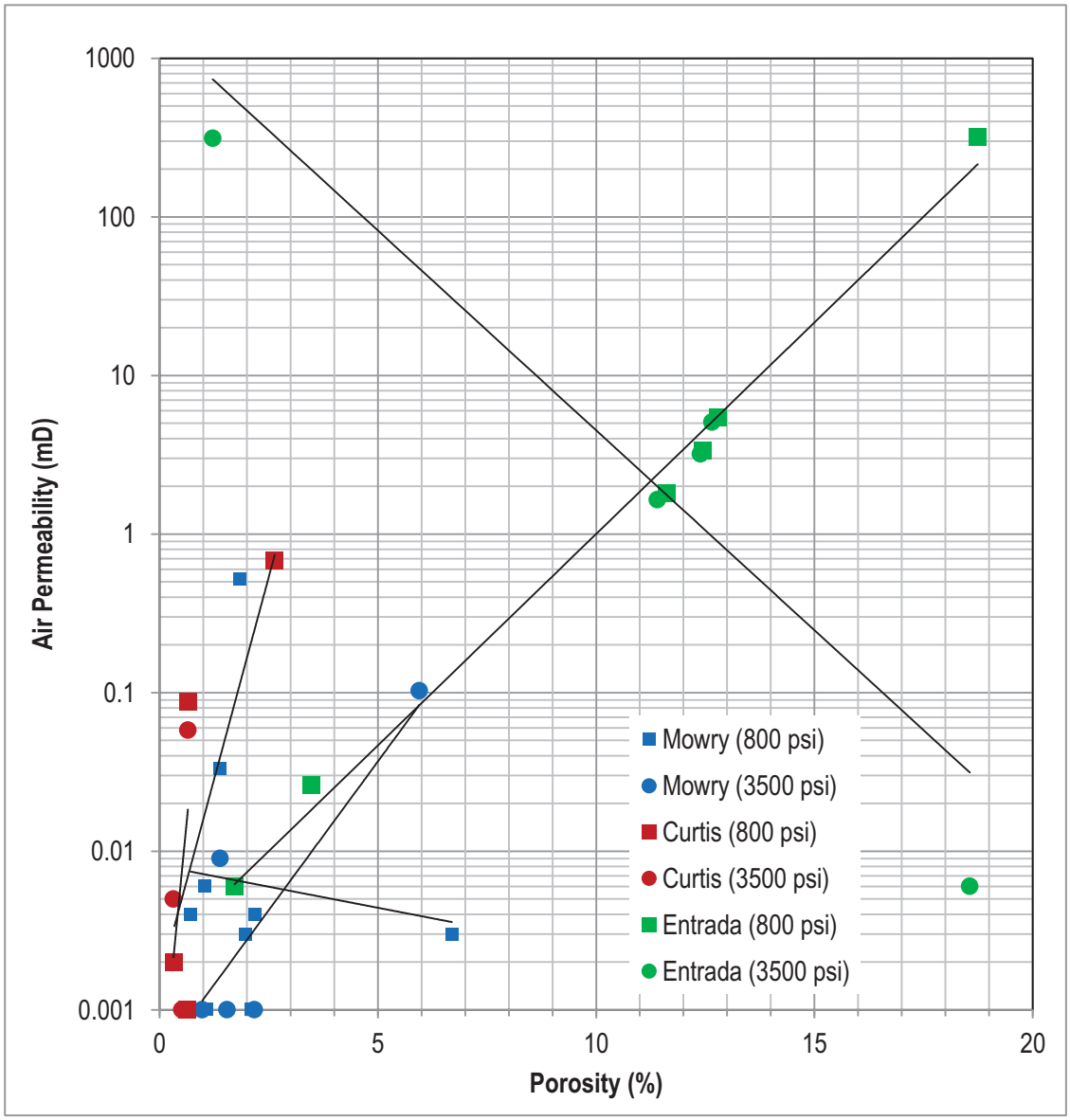
Schlumberger

TABLE 1. ROUTINE CORE ANALYSIS RESULT SUMMARY

Formation	Sample ID	Depth (ft)	Net Confining Stress (psi)	Grain Density (g/cm3)	Helium Porosity (%)	Air Permeability (mD)	Klinkenberg Air Permeability (mD)	Comments
Curtis	RM1-47HO-P01	8904.0	800	2.66	0.34	0.002	0.001	Sandstone, gray, very fine grain
Curtis	RM1-47HO-P01	8904.0	3500	2.66	0.32	0.001	*	
Curtis	RM1-55HO-P01	8913.0	800	2.66	0.65	0.087	0.054	Siltstone, shaley, very fine laminations, trace fractures
Curtis	RM1-55HO-P01	8913.0	3500	2.66	0.65	0.005	0.002	
Curtis	RM1-58HO-P01	8916.4	800	2.69	2.64	0.677	0.536	Sandstone, tan, very fine grain, shaley and calcareous laminations
Curtis	RM1-58HO-P01	8916.4	3500	2.69	2.58	0.058	0.033	
Entrada	RM1-63DO-P01	9012.3	800	2.65	11.6	1.79	1.54	Sandstone, tan, fine grain, fractured
Entrada	RM1-63DO-P01	9012.3	3500	2.65	11.4	1.65	1.40	
Entrada	RM1-63VO-P01	9013.9	800	2.65	12.4	3.38	3.00	Sandstone, tan, fine grain
Entrada	RM1-63VO-P01	9013.9	3500	2.65	12.4	3.21	2.84	
Entrada	RM1-64HB-P01	9015.6	800	2.65	12.8	5.44	4.93	Sandstone, tan, fine grain
Entrada	RM1-64HB-P01	9015.6	3500	2.65	12.7	5.08	4.59	
Entrada	RM1-77DO-P01	9027.8	800	2.65	1.72	0.006	0.002	Sandstone, tan, fine grain, laminated
Entrada	RM1-77DO-P01	9027.8	3500	2.65	1.22	*	*	
Entrada	RM1-79HO-P01	9029.2	800	2.64	18.7	319.	314.	Sandstone, tan, fine grain
Entrada	RM1-79HO-P01	9029.2	3500	2.64	18.6	312.	307.	
Entrada	RM1-93DO-P01	9043.7	800	2.65	3.64	0.026	0.013	Sandstone, tan, fine grain, laminated
Entrada	RM1-93DO-P01	9043.7	3500	2.65	3.48	0.006	0.002	

*Permeability below equipment limit.

FIGURE 1. PERMEABILITY VS POROSITY CROSS PLOT



Trendline Equations	
Mowry (800 psi)	$y = 0.0081e^{-0.122x}$
Mowry (3500 psi)	$y = 0.0005e^{0.8639x}$
Curtis (800 psi)	$y = 0.0015e^{2.346x}$
Curtis (3500 psi)	$y = 0.0003e^{6.5097x}$
Entrada (800 psi)	$y = 0.0022e^{0.6142x}$
Entrada (3500 psi)	$y = 1494e^{-0.58x}$

Schlumberger

Mercury Injection Capillary Pressure

Prepared for: University of Utah

Well: RMCCS-1

Formations: Various

Location: Craig, Colorado

Prepared by:

Schlumberger Reservoir Laboratories

6350 W. Sam Houston Parkway North, Suite 200

Houston, Texas 77041, USA

(713) 482-0700

Date: May 28 2013

Project #: 2012USHC-P113

Table of Contents

Quality Assurance iii
Executive Summary 1
Experimental Data and Analysis 2

List of Tables

Table 1. Mercury Injection Capillary Pressure Result Summary 4

List of Figures

Figure 1. Mercury/Air Capillary Pressure Result Summary 5

Appendix A - Mercury Injection Data

List of Tables

Table A.1 Mercury Injection Capillary Pressure Data For Sample RM1-21HO-P01 7
Table A.2 Mercury Injection Capillary Pressure Data For Sample RM1-36HO-P01 16
Table A.3 Mercury Injection Capillary Pressure Data For Sample RM1-37HO-P01 25
Table A.4 Mercury Injection Capillary Pressure Data For Sample RM1-41HA-P01 34
Table A.5 Mercury Injection Capillary Pressure Data For Sample RM1-48HO-P01 43
Table A.6 Mercury Injection Capillary Pressure Data For Sample RM1-63DO-P01 52
Table A.7 Mercury Injection Capillary Pressure Data For Sample RM1-63VO-P01 61
Table A.8 Mercury Injection Capillary Pressure Data For Sample RM1-64HB-P01 70
Table A.9 Mercury Injection Capillary Pressure Data For Sample RM1-79HO-P01 79
Table A.10 Mercury Injection Capillary Pressure Data For Sample RM1-93DO-P01 88

List of Figures

Figure A.1 Mercury/Air Capillary Pressure For Sample RM1-21HO-P01 13
Figure A.2 Calculated Air /Brine Capillary Pressure And Height Above Free Water For Sample RM1-21HO-P01 14
Figure A.3 Pore Throat Size Distribution For Sample RM1-21HO-P01 15
Figure A.4 Mercury/Air Capillary Pressure For Sample RM1-36HO-P01 22
Figure A.5 Calculated Air /Brine Capillary Pressure And Height Above Free Water For Sample RM1-36HO-P01 23
Figure A.6 Pore Throat Size Distribution For Sample RM1-36HO-P01 24
Figure A.7 Mercury/Air Capillary Pressure For Sample RM1-37HO-P01 31
Figure A.8 Calculated Air /Brine Capillary Pressure And Height Above Free Water For Sample RM1-37HO-P01 32
Figure A.9 Pore Throat Size Distribution For Sample RM1-37HO-P01 33
Figure A.10 Mercury/Air Capillary Pressure For Sample RM1-41HA-P01 40
Figure A.11 Calculated Air /Brine Capillary Pressure And Height Above Free Water For Sample RM1-41HA-P01 41
Figure A.12 Pore Throat Size Distribution For Sample RM1-41HA-P01 42
Figure A.13 Mercury/Air Capillary Pressure For Sample RM1-48HO-P01 49
Figure A.14 Calculated Air /Brine Capillary Pressure And Height Above Free Water For Sample RM1-48HO-P01 50
Figure A.15 Pore Throat Size Distribution For Sample RM1-48HO-P01 51

Table of Contents

List of Figures continued

Figure A.16 Mercury/Air Capillary Pressure For Sample RM1-63DO-P01 58
Figure A.17 Calculated Air /Brine Capillary Pressure And Height Above Free Water For Sample RM1-63DO-P01 59
Figure A.18 Pore Throat Size Distribution For Sample RM1-63DO-P01 60
Figure A.19 Mercury/Air Capillary Pressure For Sample RM1-63VO-P01 67
Figure A.20 Calculated Air /Brine Capillary Pressure And Height Above Free Water For Sample RM1-63VO-P01 68
Figure A.21 Pore Throat Size Distribution For Sample RM1-63VO-P01 69
Figure A.22 Mercury/Air Capillary Pressure For Sample RM1-64HB-P01 76
Figure A.23 Calculated Air /Brine Capillary Pressure And Height Above Free Water For Sample RM1-64HB-P01 77
Figure A.24 Pore Throat Size Distribution For Sample RM1-64HB-P01 78
Figure A.25 Mercury/Air Capillary Pressure For Sample RM1-79HO-P01 85
Figure A.26 Calculated Air /Brine Capillary Pressure And Height Above Free Water For Sample RM1-79HO-P01 86
Figure A.27 Pore Throat Size Distribution For Sample RM1-79HO-P01 87
Figure A.28 Mercury/Air Capillary Pressure For Sample RM1-93DO-P01 94
Figure A.29 Calculated Air /Brine Capillary Pressure And Height Above Free Water For Sample RM1-93DO-P01 95
Figure A.30 Pore Throat Size Distribution For Sample RM1-93DO-P01 96

Quality Assurance Process

Schlumberger is committed to providing unsurpassed services in reservoir sampling and analyses while maintaining high standards of safety and quality. Our objective is to deliver the most accurate and reliable sampling processes and fluid and rock property measurements available in the industry. This objective requires persistent innovation and ongoing development of state-of-the-art technologies and equipment.

A rigorous quality assurance program, continuous employee training and enforcement of strict safety standards maintain our compliance with Quality, Health, Safety and Environment (QHSE) requirements. Proactive integration of QHSE objectives and management goals at every level supports the communication and implementation of QHSE policies and standards. Schlumberger requires that qualified engineering technologists perform all laboratory measurements according to specified analytical procedures designed for obtaining accurate and reliable data.

The lab-generated data undergoes the following five levels of quality checks to establish the integrity of the reported results.

a) Establish quality of measurement during data generation.
b) Lab supervisor and manager confirm the overall quality of the generated data.
c) Project manager reviews and processes generated data and generates reports.
d) Technical advisors confirm consistency of reported data.
e) Project manager finalizes reports.

Hence the completion of each project requires that a qualified and experienced team of engineers perform a variety of independent review of all technical data to confirm the consistency and accuracy of the report as per pre-established quality checklists designed for each operation and based on the level of complexity. All property measurements and calculation procedures are maintained in company archives for a period of one year. This information is available for review by clients upon request.

The file and laboratory records information is listed below to provide access reference to all records related to this project. For any questions, please do not hesitate to contact the undersigned project manager.

File No.: 2012USHC-P113

Laboratory Procedures

George Assad
SCAL Lab Manager

Reviewed by

X	Leslie Zhang	Lead Project Manager
X	Debbie Steele	Project Manager

Project Management

Micah Alexander
Project Manager

Executive Summary

Objective

The main objective for this work is to measure the drainage-only mercury injection capillary pressure (MICP) on ten samples from Craig, Colorado. Samples were cleaned with chloroform/methanol azeotrope before testing. They were dried at 90 deg C overnight prior to MICP measurements.

Results

Ten samples were subjected to drainage-only mercury injection capillary pressure measurement. The median pore throat size ranges from 0.006 to 15.6 microns. The mercury intrusion entry pressure ranges from 6.77 to 10,031 psi. The results indicated pore throat size distribution of the samples is 0% micropores, 3.38% to 100% mesopores and 0% to 96.6% macropores.

Mercury injection capillary pressure results are summarized in Table 1 and plotted in Figure 1. Detailed mercury injection data and graphical results for each sample are presented in Appendix A.

Experimental Data and Analysis

Mercury-air capillary pressure was measured using Micromeritics AutoPore IV 9520 mercury porosimeter. The samples were broken to pieces small enough to fit within the glass penetrometers. The samples were then evacuated under vacuum. Mercury was injected at multiple pressures up to 60,000 psi. The volume of mercury injected at each pressure increment is automatically recorded until the maximum pressure is achieved.

The apparent mercury injection volume was corrected for conformance determined for each sample. The conformance is the volume of mercury pressed into surface roughness and around sample edges after the penetrometer chamber is initially filled with mercury, due to mercury being an extremely non-wetting phase. Mercury injection data are presented in tabular and graphic form in Appendix A. Swanson permeability was calculated from the mercury injection results using the method of Swanson (1981).

In general, pores can be divided into micro, meso and macro pores. As defined in *An Introduction To The Physical Characterization of Materials by Mercury Intrusion Porosimetry with Emphasis On Reduction And Presentation Of Experimental Data* by Paul A. Webb of the Micromeritics Instrument Corp., pore throat diameters smaller than .002 microns are micropores, macropores are larger than .05 microns, and mesopores between .002 and .05 microns.

Mercury porosimetry is based on the capillary law governing liquid penetration into small pores. Assuming cylindrical pores, pore throat size can be calculated from the Washburn equation:

$$r = \frac{2\sigma \cos\theta}{P_c}$$

where
- r = radius of pore throat aperture;
- Pc = capillary pressure;
- σ = surface tension of mercury;
- θ = contact angle of mercury in air.

The surface tension of mercury is 485 dyne/cm. The contact angle of the mercury in air on rock varies with rock composition, however, 140° is generally accepted by industry and will be used in the data analysis.

Application of mercury capillary data to sub-surface conditions requires the conversion of mercury capillary pressure data to sub-surface hydrocarbon-water and/or gas-water capillary pressure data. Conversions of pressure from one fluid system to the others are calculated using the example formula:

$$Pc_{(g/w)} = \frac{(\sigma \cos\theta)_{(g/w)}}{(\sigma \cos\theta)_{(m/a)}} \bullet Pc_{(m/a)}$$

where
- $Pc_{(g/w)}$ = capillary pressure for gas-brine system;
- $Pc_{(m/a)}$ = capillary pressure for mercury-air system;
- $(\sigma \cos\theta)_{(g/w)}$ = surface tension of brine•cosine of contact angle of brine in air;
- $(\sigma \cos\theta)_{(m/a)}$ = surface tension of mercury•cosine of contact angle of mercury in air;

For the derived air/water data, the contact angle of 0 degree, and surface tension of 72 dyne/cm will be used.

Height above free water is calculated using the following equation:

$$H = \frac{Pc_{(m/a)}\,(\sigma \cos\theta)_R}{(\sigma \cos\theta)_{(m/a)}\,(\rho_w - \rho_h)}$$

where $Pc_{(m/a)}$ = capillary pressure for mercury-air system;

$(\sigma \cos\theta)_{(m/a)}$ = surface tension of mercury•cosine of contact angle of mercury in air;

$(\sigma \cos\theta)_R$ = Interfacial tension •cosine of contact angle of reservoir fluid;

ρ_w = reservoir density gradient of water;

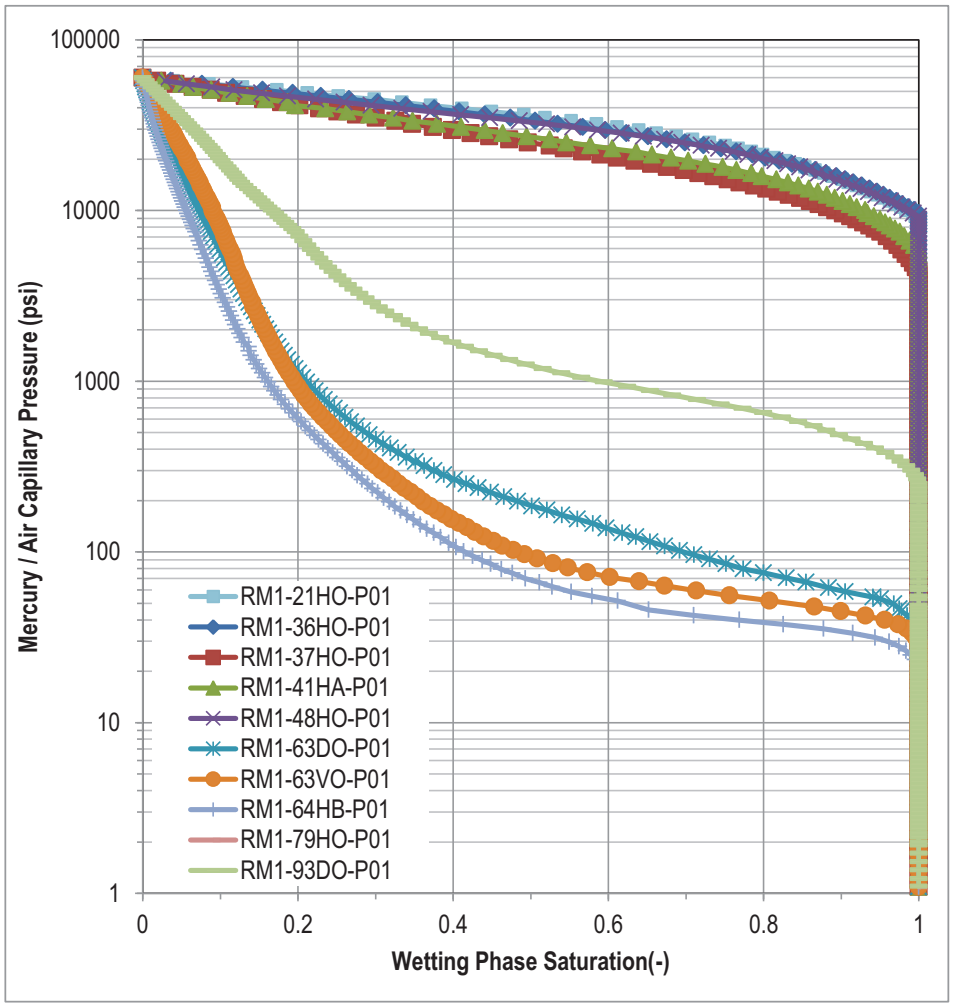
ρ_h = reservoir density gradient of hydrocarbon.

Typical density gradient of water is 0.434 psi/ft, density gradient of oil is 0.346 psi/ft, and density gradient of gas is 0.100 psi/ft. Density gradient can be calculated if the reservoir fluid density is known.

TABLE 1. MERCURY INJECTION CAPILLARY PRESSURE RESULT SUMMARY

Formation	Sample ID	Depth (ft)	Hg Inj Porosity (%)	Median Pore Throat Dia (micron)	Pore Throat Types			Mercury/Air Entry Pressure (psi)	Air/Brine Entry Pressure (psi)	Swanson Air Permeability (mD)
					Micropores Dia ≤ 0.002 µm (%PV)	Mesopores Dia .002-.05 µm (%PV)	Macropores Dia > .05 µm (%PV)			
Mowry	RM1-21HO-P01	8235.0	2.77	0.006	0.000	100	0.000	9229	1789	0.00002
Mowry	RM1-36HO-P01	8258.0	1.42	0.006	0.000	100	0.000	10031	1944	0.00001
Mowry	RM1-37HO-P01	8259.5	2.32	0.009	0.000	100	0.000	4655	902	0.00002
Curtis	RM1-41HA-P01	8896.1	1.19	0.008	0.000	100	0.000	6271	1215	0.00001
Curtis	RM1-48HO-P01	8905.5	1.55	0.007	0.000	100	0.000	9621	1864	0.00001
Entrada	RM1-63DO-P01	9012.3	9.78	1.16	0.000	11.8	88.2	35.5	6.88	1.04
Entrada	RM1-63VO-P01	9013.9	12.2	2.29	0.000	12.6	87.4	31.5	6.11	4.30
Entrada	RM1-64HB-P01	9015.6	13.0	3.15	0.000	9.09	90.9	23.3	4.52	8.18
Entrada	RM1-79HO-P01	9029.2	17.8	15.6	0.000	3.38	96.6	6.77	1.31	192
Entrada	RM1-93DO-P01	9043.7	3.79	0.175	0.000	25.1	74.9	267	51.7	0.007

FIGURE 1. MERCURY/AIR CAPILLARY PRESSURE RESULT SUMMARY



Appendix A

Mercury Injection Data

Table A.1 Mercury Injection Capillary Pressure Data For Sample RM1-21HO-P01

Sample ID: RM1-21HO-P01 Swanson Air Permeability, mD: 0.00002
Depth, ft: 8235.00 Hg Porosity, percent: 2.77

Mercury/Air Pressure (psi)	Equivalent Air/Brine Pressure (psi)	Mercury Saturation (fraction)	Incremental Mercury Saturation (fraction)	Wetting Phase Saturation (fraction)	Pore Throat Diameter (micron)	Height above Free Water (G/W) (ft)
1.09	0.211	0.000	0.0000	1.000	198	0.632
1.20	0.233	0.000	0.0000	1.000	179	0.699
1.36	0.263	0.000	0.0000	1.000	159	0.787
1.52	0.294	0.000	0.0000	1.000	142	0.881
1.69	0.328	0.000	0.0000	1.000	127	0.983
1.77	0.344	0.000	0.0000	1.000	122	1.03
1.89	0.367	0.000	0.0000	1.000	114	1.10
2.00	0.388	0.000	0.0000	1.000	108	1.16
2.12	0.411	0.000	0.0000	1.000	102	1.23
2.25	0.437	0.000	0.0000	1.000	95.6	1.31
2.38	0.462	0.000	0.0000	1.000	90.4	1.38
2.53	0.489	0.000	0.0000	1.000	85.4	1.47
2.68	0.519	0.000	0.0000	1.000	80.5	1.55
2.83	0.549	0.000	0.0000	1.000	76.1	1.64
3.00	0.582	0.000	0.0000	1.000	71.8	1.74
3.18	0.617	0.000	0.0000	1.000	67.7	1.85
3.37	0.653	0.000	0.0000	1.000	64.0	1.96
3.57	0.693	0.000	0.0000	1.000	60.3	2.07
3.78	0.733	0.000	0.0000	1.000	57.0	2.19
4.01	0.778	0.000	0.0000	1.000	53.7	2.33
4.25	0.824	0.000	0.0000	1.000	50.7	2.47
4.51	0.873	0.000	0.0000	1.000	47.8	2.61
4.78	0.925	0.000	0.0000	1.000	45.1	2.77
5.06	0.981	0.000	0.0000	1.000	42.6	2.94
5.37	1.040	0.000	0.0000	1.000	40.2	3.11
5.69	1.102	0.000	0.0000	1.000	37.9	3.30
6.03	1.169	0.000	0.0000	1.000	35.7	3.50
6.39	1.238	0.000	0.0000	1.000	33.7	3.71
6.77	1.313	0.000	0.0000	1.000	31.8	3.93
7.18	1.392	0.000	0.0000	1.000	30.0	4.17
7.61	1.475	0.000	0.0000	1.000	28.3	4.42
8.07	1.565	0.000	0.0000	1.000	26.7	4.68
8.56	1.659	0.000	0.0000	1.000	25.2	4.97
9.08	1.759	0.000	0.0000	1.000	23.8	5.27
9.62	1.865	0.000	0.0000	1.000	22.4	5.58
10.2	1.976	0.000	0.0000	1.000	21.1	5.92
10.8	2.096	0.000	0.0000	1.000	19.9	6.28

Table A.1 Mercury Injection Capillary Pressure Data For Sample RM1-21HO-P01

Sample ID: RM1-21HO-P01 Swanson Air Permeability, mD: 0.00002
Depth, ft: 8235.00 Hg Porosity, percent: 2.77

Mercury/Air Pressure (psi)	Equivalent Air/Brine Pressure (psi)	Mercury Saturation (fraction)	Incremental Mercury Saturation (fraction)	Wetting Phase Saturation (fraction)	Pore Throat Diameter (micron)	Height above Free Water (G/W) (ft)
11.5	2.222	0.000	0.0000	1.000	18.8	6.65
12.2	2.356	0.000	0.0000	1.000	17.7	7.06
12.9	2.499	0.000	0.0000	1.000	16.7	7.48
13.7	2.652	0.000	0.0000	1.000	15.7	7.94
14.5	2.814	0.000	0.0000	1.000	14.8	8.42
15.4	2.987	0.000	0.0000	1.000	14.0	8.94
16.3	3.167	0.000	0.0000	1.000	13.2	9.48
17.3	3.362	0.000	0.0000	1.000	12.4	10.1
18.4	3.569	0.000	0.0000	1.000	11.7	10.7
19.5	3.788	0.000	0.0000	1.000	11.0	11.3
20.7	4.018	0.000	0.0000	1.000	10.4	12.0
22.0	4.265	0.000	0.0000	1.000	9.79	12.8
23.4	4.526	0.000	0.0000	1.000	9.23	13.6
24.9	4.818	0.000	0.0000	1.000	8.67	14.4
26.4	5.112	0.000	0.0000	1.000	8.17	15.3
28.0	5.425	0.000	0.0000	1.000	7.70	16.2
29.7	5.755	0.000	0.0000	1.000	7.26	17.2
31.5	6.105	0.000	0.0000	1.000	6.84	18.3
33.4	6.479	0.000	0.0000	1.000	6.45	19.4
35.5	6.876	0.000	0.0000	1.000	6.08	20.6
37.6	7.294	0.000	0.0000	1.000	5.73	21.8
39.9	7.742	0.000	0.0000	1.000	5.40	23.2
42.4	8.213	0.000	0.0000	1.000	5.09	24.6
45.0	8.717	0.000	0.0000	1.000	4.79	26.1
46.4	8.986	0.000	0.0000	1.000	4.65	26.9
49.5	9.599	0.000	0.0000	1.000	4.35	28.7
53.1	10.3	0.000	0.0000	1.000	4.06	30.8
54.4	10.5	0.000	0.0000	1.000	3.96	31.6
58.6	11.4	0.000	0.0000	1.000	3.68	34.0
61.7	12.0	0.000	0.0000	1.000	3.49	35.8
66.7	12.9	0.000	0.0000	1.000	3.23	38.7
70.5	13.7	0.000	0.0000	1.000	3.06	40.9
75.6	14.6	0.000	0.0000	1.000	2.85	43.9
79.8	15.5	0.000	0.0000	1.000	2.70	46.3
85.4	16.6	0.000	0.0000	1.000	2.52	49.6
90.9	17.6	0.000	0.0000	1.000	2.37	52.8
96.5	18.7	0.000	0.0000	1.000	2.23	56.0

Table A.1 Mercury Injection Capillary Pressure Data For Sample RM1-21HO-P01

Sample ID: RM1-21HO-P01 Swanson Air Permeability, mD: 0.00002
Depth, ft: 8235.00 Hg Porosity, percent: 2.77

Mercury/Air Pressure (psi)	Equivalent Air/Brine Pressure (psi)	Mercury Saturation (fraction)	Incremental Mercury Saturation (fraction)	Wetting Phase Saturation (fraction)	Pore Throat Diameter (micron)	Height above Free Water (G/W) (ft)
102	19.8	0.000	0.0000	1.000	2.11	59.3
108	21.0	0.000	0.0000	1.000	1.99	62.9
115	22.3	0.000	0.0000	1.000	1.87	66.7
123	23.8	0.000	0.0000	1.000	1.76	71.2
130	25.1	0.000	0.0000	1.000	1.66	75.2
139	26.9	0.000	0.0000	1.000	1.56	80.4
147	28.5	0.000	0.0000	1.000	1.46	85.4
156	30.3	0.000	0.0000	1.000	1.38	90.7
165	31.9	0.000	0.0000	1.000	1.31	95.6
176	34.2	0.000	0.0000	1.000	1.22	102
186	36.1	0.000	0.0000	1.000	1.16	108
199	38.5	0.000	0.0000	1.000	1.08	115
211	40.9	0.000	0.0000	1.000	1.02	122
224	43.4	0.000	0.0000	1.000	0.962	130
238	46.1	0.000	0.0000	1.000	0.906	138
251	48.6	0.000	0.0000	1.000	0.859	146
266	51.6	0.000	0.0000	1.000	0.810	154
284	55.0	0.000	0.0000	1.000	0.760	165
300	58.1	0.000	0.0000	1.000	0.720	174
320	61.9	0.000	0.0000	1.000	0.674	185
338	65.5	0.000	0.0000	1.000	0.638	196
359	69.6	0.000	0.0000	1.000	0.600	208
382	74.0	0.000	0.0000	1.000	0.564	222
406	78.7	0.000	0.0000	1.000	0.531	236
429	83.1	0.000	0.0000	1.000	0.503	249
457	88.5	0.000	0.0000	1.000	0.472	265
485	94.1	0.000	0.0000	1.000	0.444	282
514	99.7	0.000	0.0000	1.000	0.419	298
546	106	0.000	0.0000	1.000	0.395	317
578	112	0.000	0.0000	1.000	0.373	335
615	119	0.000	0.0000	1.000	0.351	357
653	127	0.000	0.0000	1.000	0.330	379
693	134	0.000	0.0000	1.000	0.311	402
735	142	0.000	0.0000	1.000	0.293	427
780	151	0.000	0.0000	1.000	0.276	453
827	160	0.000	0.0000	1.000	0.261	480
878	170	0.000	0.0000	1.000	0.246	509

Table A.1 Mercury Injection Capillary Pressure Data For Sample RM1-21HO-P01

Sample ID: RM1-21HO-P01 Swanson Air Permeability, mD: 0.00002
Depth, ft: 8235.00 Hg Porosity, percent: 2.77

Mercury/Air Pressure (psi)	Equivalent Air/Brine Pressure (psi)	Mercury Saturation (fraction)	Incremental Mercury Saturation (fraction)	Wetting Phase Saturation (fraction)	Pore Throat Diameter (micron)	Height above Free Water (G/W) (ft)
930	180	0.000	0.0000	1.000	0.232	540
988	192	0.000	0.0000	1.000	0.218	574
1050	204	0.000	0.0000	1.000	0.205	609
1115	216	0.000	0.0000	1.000	0.193	647
1185	230	0.000	0.0000	1.000	0.182	688
1255	243	0.000	0.0000	1.000	0.172	728
1334	258	0.000	0.0000	1.000	0.162	774
1414	274	0.000	0.0000	1.000	0.152	820
1500	291	0.000	0.0000	1.000	0.144	870
1595	309	0.000	0.0000	1.000	0.135	925
1694	328	0.000	0.0000	1.000	0.127	983
1795	348	0.000	0.0000	1.000	0.120	1042
1909	370	0.000	0.0000	1.000	0.113	1108
2025	392	0.000	0.0000	1.000	0.106	1175
2147	416	0.000	0.0000	1.000	0.100	1246
2277	441	0.000	0.0000	1.000	0.095	1321
2421	469	0.000	0.0000	1.000	0.089	1405
2567	498	0.000	0.0000	1.000	0.084	1490
2726	528	0.000	0.0000	1.000	0.079	1581
2893	561	0.000	0.0000	1.000	0.075	1678
3069	595	0.000	0.0000	1.000	0.070	1781
3257	631	0.000	0.0000	1.000	0.066	1889
3457	670	0.000	0.0000	1.000	0.062	2006
3672	712	0.000	0.0000	1.000	0.059	2130
3897	755	0.000	0.0000	1.000	0.055	2261
4132	801	0.000	0.0000	1.000	0.052	2398
4387	850	0.000	0.0000	1.000	0.049	2545
4655	902	0.000	0.0000	1.000	0.046	2701
4942	958	0.000	0.0000	1.000	0.044	2867
5242	1016	0.000	0.0000	1.000	0.041	3041
5565	1079	0.000	0.0000	1.000	0.039	3229
5907	1145	0.000	0.0000	1.000	0.036	3427
6270	1215	0.000	0.0000	1.000	0.034	3638
6653	1289	0.000	0.0000	1.000	0.032	3860
7061	1368	0.000	0.0000	1.000	0.031	4097
7495	1452	0.000	0.0000	1.000	0.029	4349
7811	1514	0.000	0.0000	1.000	0.028	4532

Table A.1 Mercury Injection Capillary Pressure Data For Sample RM1-21HO-P01

Sample ID: RM1-21HO-P01 Swanson Air Permeability, mD: 0.00002
Depth, ft: 8235.00 Hg Porosity, percent: 2.77

Mercury/Air Pressure (psi)	Equivalent Air/Brine Pressure (psi)	Mercury Saturation (fraction)	Incremental Mercury Saturation (fraction)	Wetting Phase Saturation (fraction)	Pore Throat Diameter (micron)	Height above Free Water (G/W) (ft)
8144	1578	0.000	0.0000	1.000	0.026	4725
8492	1646	0.000	0.0000	1.000	0.025	4927
8851	1715	0.000	0.0000	1.000	0.024	5135
9229	1789	0.004	0.0044	0.996	0.023	5355
9622	1865	0.007	0.0031	0.993	0.022	5583
10028	1943	0.016	0.0090	0.984	0.021	5819
10456	2026	0.023	0.0064	0.977	0.021	6067
10900	2112	0.030	0.0070	0.970	0.020	6324
11363	2202	0.037	0.0075	0.963	0.019	6593
11844	2295	0.046	0.0083	0.954	0.018	6872
12349	2393	0.053	0.0076	0.947	0.017	7165
12873	2495	0.062	0.0087	0.938	0.017	7469
13419	2601	0.071	0.0087	0.929	0.016	7786
13991	2711	0.080	0.0096	0.920	0.015	8118
14585	2826	0.091	0.0103	0.909	0.015	8462
15204	2946	0.098	0.0076	0.902	0.014	8822
15849	3071	0.111	0.0128	0.889	0.014	9196
16524	3202	0.122	0.0113	0.878	0.013	9587
17225	3338	0.134	0.0115	0.866	0.013	9994
17957	3480	0.147	0.0127	0.853	0.012	10419
18719	3628	0.159	0.0125	0.841	0.012	10861
19517	3782	0.172	0.0129	0.828	0.011	11324
20343	3942	0.186	0.0144	0.814	0.011	11803
21208	4110	0.201	0.0148	0.799	0.010	12306
22110	4285	0.216	0.0146	0.784	0.010	12828
23049	4467	0.233	0.0170	0.767	0.009	13373
24020	4655	0.249	0.0165	0.751	0.009	13937
25049	4854	0.270	0.0204	0.730	0.009	14534
26113	5060	0.291	0.0217	0.709	0.008	15151
27215	5274	0.313	0.0212	0.687	0.008	15791
28379	5500	0.338	0.0256	0.662	0.008	16466
29582	5733	0.361	0.0227	0.639	0.007	17164
30838	5976	0.389	0.0279	0.611	0.007	17893
32149	6230	0.415	0.0264	0.585	0.007	18653
33516	6495	0.448	0.0327	0.552	0.006	19447
34938	6771	0.482	0.0336	0.518	0.006	20272
36422	7058	0.509	0.0272	0.491	0.006	21133

Table A.1 Mercury Injection Capillary Pressure Data For Sample RM1-21HO-P01

Sample ID: RM1-21HO-P01 Swanson Air Permeability, mD: 0.00002
Depth, ft: 8235.00 Hg Porosity, percent: 2.77

Mercury/Air Pressure (psi)	Equivalent Air/Brine Pressure (psi)	Mercury Saturation (fraction)	Incremental Mercury Saturation (fraction)	Wetting Phase Saturation (fraction)	Pore Throat Diameter (micron)	Height above Free Water (G/W) (ft)
37967	7358	0.550	0.0416	0.450	0.006	22029
39567	7668	0.589	0.0383	0.411	0.005	22958
41266	7997	0.629	0.0401	0.371	0.005	23943
42997	8332	0.666	0.0371	0.334	0.005	24947
44826	8687	0.702	0.0357	0.298	0.005	26009
46740	9058	0.748	0.0462	0.252	0.005	27119
48720	9442	0.788	0.0399	0.212	0.004	28268
50789	9843	0.827	0.0392	0.173	0.004	29469
52944	10260	0.871	0.0442	0.129	0.004	30719
55194	10696	0.914	0.0433	0.086	0.004	32024
57540	11151	0.961	0.0460	0.039	0.004	33385
59983	11624	1.000	0.0395	0.000	0.004	34803

Figure A.1 Mercury/Air Capillary Pressure For Sample RM1-21HO-P01

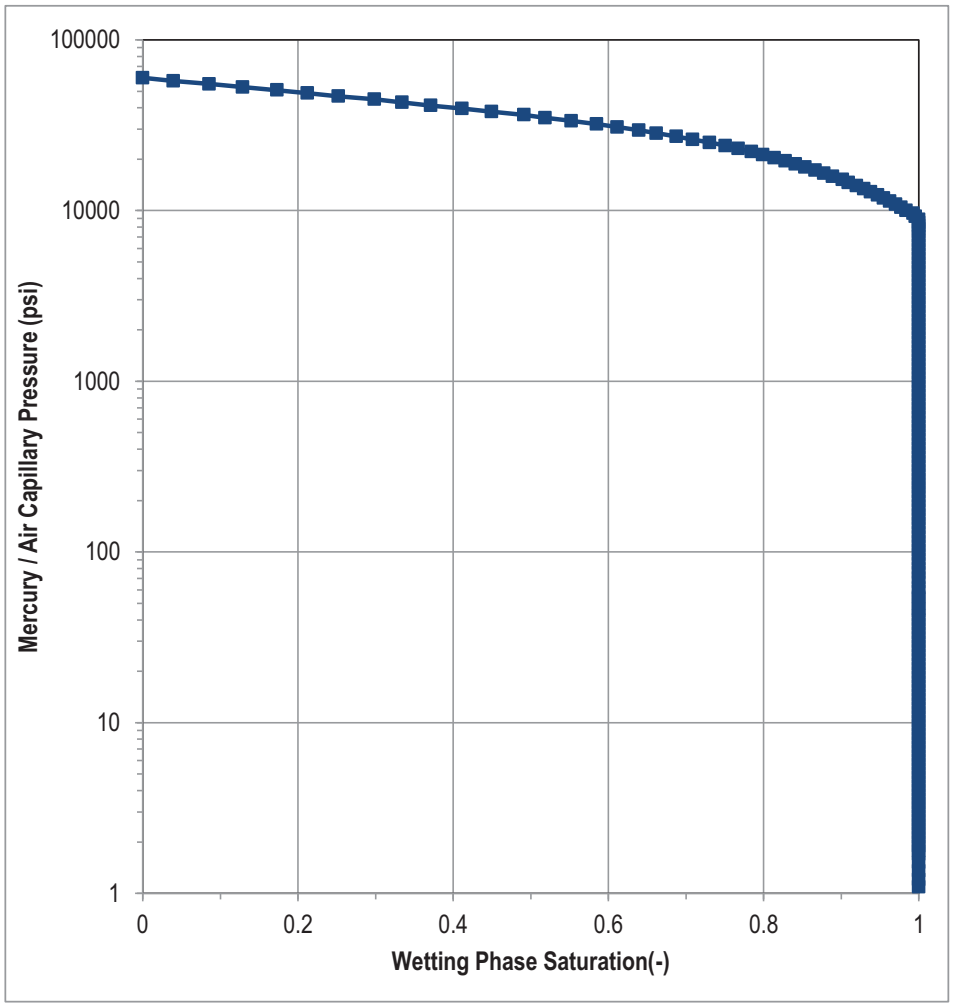


Figure A.2 Calculated Air /Brine Capillary Pressure And Height Above Free Water For Sample RM1-21HO-P01

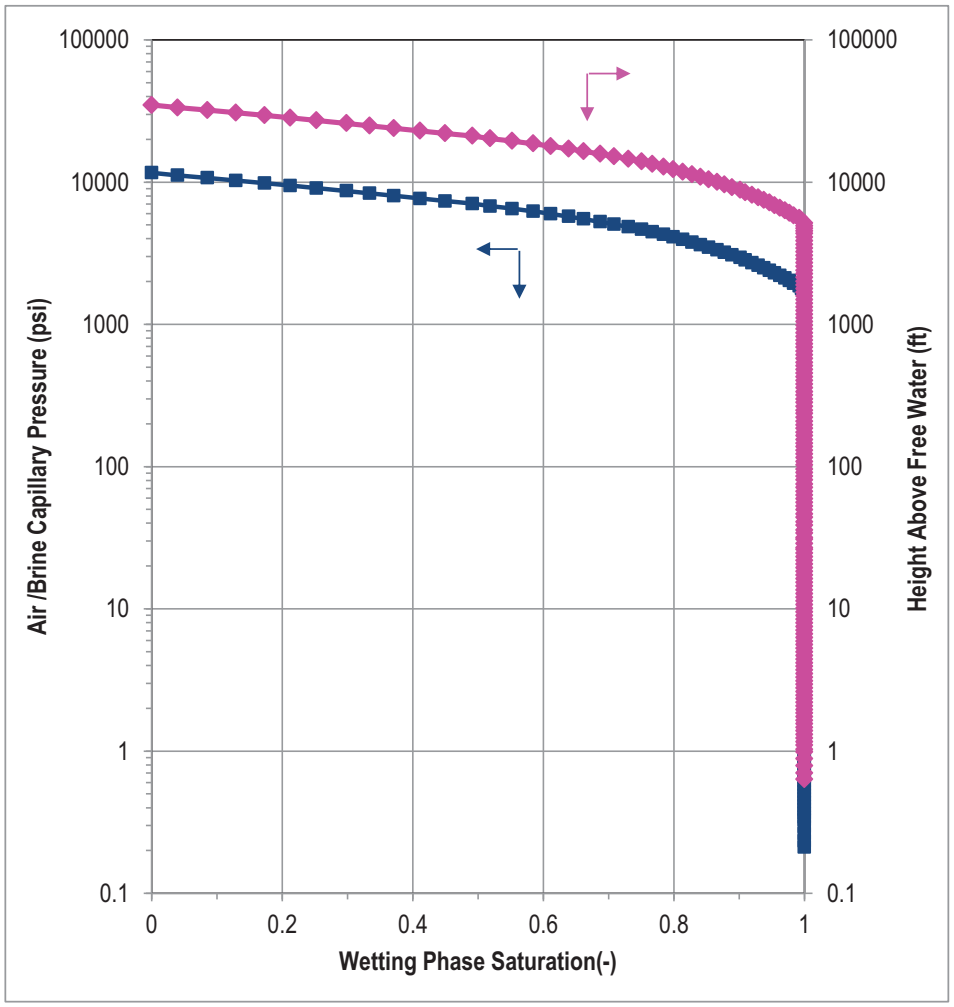


Figure A.3 Pore Throat Size Distribution For Sample RM1-21HO-P01

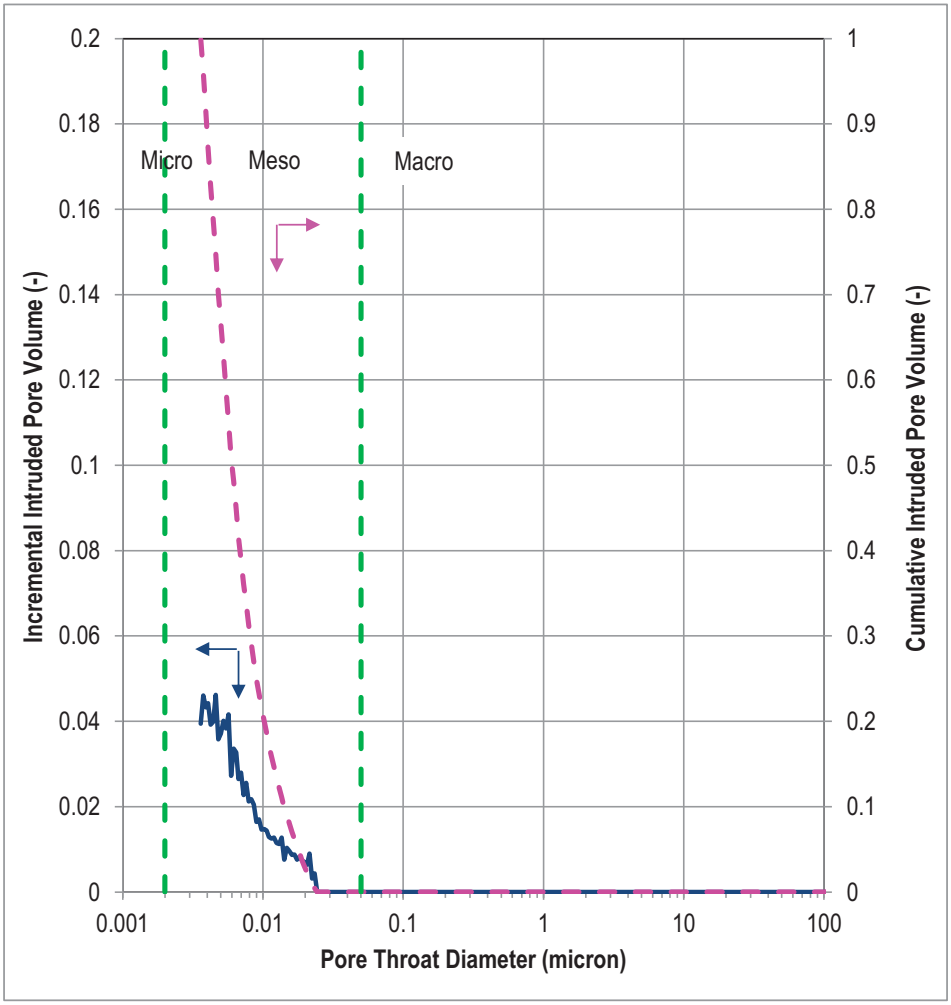


Table A.2 Mercury Injection Capillary Pressure Data For Sample RM1-36HO-P01

Sample ID: RM1-36HO-P01 Swanson Air Permeability, mD: 0.00001
Depth, ft: 8258.00 Hg Porosity, percent: 1.42

Mercury/Air Pressure (psi)	Equivalent Air/Brine Pressure (psi)	Mercury Saturation (fraction)	Incremental Mercury Saturation (fraction)	Wetting Phase Saturation (fraction)	Pore Throat Diameter (micron)	Height above Free Water (G/W) (ft)
1.09	0.212	0.000	0.0000	1.000	197	0.633
1.20	0.232	0.000	0.0000	1.000	180	0.696
1.36	0.263	0.000	0.0000	1.000	159	0.788
1.52	0.295	0.000	0.0000	1.000	142	0.883
1.70	0.330	0.000	0.0000	1.000	127	0.987
1.75	0.339	0.000	0.0000	1.000	123	1.01
1.91	0.369	0.000	0.0000	1.000	113	1.11
2.00	0.387	0.000	0.0000	1.000	108	1.16
2.13	0.412	0.000	0.0000	1.000	101	1.23
2.25	0.436	0.000	0.0000	1.000	95.8	1.31
2.38	0.462	0.000	0.0000	1.000	90.4	1.38
2.52	0.489	0.000	0.0000	1.000	85.5	1.46
2.68	0.519	0.000	0.0000	1.000	80.4	1.56
2.84	0.550	0.000	0.0000	1.000	76.0	1.65
3.01	0.583	0.000	0.0000	1.000	71.6	1.75
3.18	0.617	0.000	0.0000	1.000	67.7	1.85
3.37	0.654	0.000	0.0000	1.000	63.9	1.96
3.58	0.693	0.000	0.0000	1.000	60.2	2.08
3.79	0.734	0.000	0.0000	1.000	56.9	2.20
4.01	0.778	0.000	0.0000	1.000	53.7	2.33
4.26	0.826	0.000	0.0000	1.000	50.6	2.47
4.51	0.873	0.000	0.0000	1.000	47.8	2.61
4.78	0.926	0.000	0.0000	1.000	45.1	2.77
5.07	0.982	0.000	0.0000	1.000	42.5	2.94
5.37	1.04	0.000	0.0000	1.000	40.2	3.11
5.69	1.10	0.000	0.0000	1.000	37.9	3.30
6.03	1.17	0.000	0.0000	1.000	35.8	3.50
6.40	1.24	0.000	0.0000	1.000	33.7	3.71
6.78	1.31	0.000	0.0000	1.000	31.8	3.93
7.19	1.39	0.000	0.0000	1.000	30.0	4.17
7.62	1.48	0.000	0.0000	1.000	28.3	4.42
8.07	1.56	0.000	0.0000	1.000	26.7	4.69
8.56	1.66	0.000	0.0000	1.000	25.2	4.97
9.08	1.76	0.000	0.0000	1.000	23.7	5.27
9.62	1.87	0.000	0.0000	1.000	22.4	5.58
10.2	1.98	0.000	0.0000	1.000	21.1	5.92
10.8	2.10	0.000	0.0000	1.000	19.9	6.28

Table A.2 Mercury Injection Capillary Pressure Data For Sample RM1-36HO-P01

Sample ID: RM1-36HO-P01 Swanson Air Permeability, mD: 0.00001
Depth, ft: 8258.00 Hg Porosity, percent: 1.42

Mercury/Air Pressure (psi)	Equivalent Air/Brine Pressure (psi)	Mercury Saturation (fraction)	Incremental Mercury Saturation (fraction)	Wetting Phase Saturation (fraction)	Pore Throat Diameter (micron)	Height above Free Water (G/W) (ft)
11.5	2.22	0.000	0.0000	1.000	18.8	6.65
12.2	2.36	0.000	0.0000	1.000	17.7	7.06
12.9	2.50	0.000	0.0000	1.000	16.7	7.48
13.7	2.65	0.000	0.0000	1.000	15.8	7.93
14.5	2.81	0.000	0.0000	1.000	14.8	8.43
15.4	2.99	0.000	0.0000	1.000	14.0	8.94
16.4	3.17	0.000	0.0000	1.000	13.2	9.49
17.4	3.36	0.000	0.0000	1.000	12.4	10.1
18.4	3.57	0.000	0.0000	1.000	11.7	10.7
19.5	3.79	0.000	0.0000	1.000	11.0	11.3
20.7	4.02	0.000	0.0000	1.000	10.4	12.0
22.0	4.26	0.000	0.0000	1.000	9.79	12.8
23.3	4.52	0.000	0.0000	1.000	9.23	13.5
24.9	4.82	0.000	0.0000	1.000	8.67	14.4
26.3	5.10	0.000	0.0000	1.000	8.19	15.3
28.0	5.42	0.000	0.0000	1.000	7.70	16.2
29.7	5.75	0.000	0.0000	1.000	7.26	17.2
31.5	6.10	0.000	0.0000	1.000	6.84	18.3
33.4	6.48	0.000	0.0000	1.000	6.45	19.4
35.5	6.87	0.000	0.0000	1.000	6.08	20.6
37.6	7.29	0.000	0.0000	1.000	5.73	21.8
39.9	7.74	0.000	0.0000	1.000	5.40	23.2
42.4	8.22	0.000	0.0000	1.000	5.08	24.6
45.0	8.73	0.000	0.0000	1.000	4.79	26.1
46.2	8.95	0.000	0.0000	1.000	4.67	26.8
49.6	9.61	0.000	0.0000	1.000	4.35	28.8
51.2	9.93	0.000	0.0000	1.000	4.21	29.7
56.7	11.0	0.000	0.0000	1.000	3.80	32.9
58.5	11.3	0.000	0.0000	1.000	3.68	33.9
63.5	12.3	0.000	0.0000	1.000	3.39	36.8
66.7	12.9	0.000	0.0000	1.000	3.23	38.7
71.5	13.9	0.000	0.0000	1.000	3.01	41.5
76.0	14.7	0.000	0.0000	1.000	2.84	44.1
79.7	15.4	0.000	0.0000	1.000	2.71	46.2
85.7	16.6	0.000	0.0000	1.000	2.52	49.7
91.3	17.7	0.000	0.0000	1.000	2.36	53.0
96.3	18.7	0.000	0.0000	1.000	2.24	55.9

Table A.2 Mercury Injection Capillary Pressure Data For Sample RM1-36HO-P01

Sample ID: RM1-36HO-P01 Swanson Air Permeability, mD: 0.00001
Depth, ft: 8258.00 Hg Porosity, percent: 1.42

Mercury/Air Pressure (psi)	Equivalent Air/Brine Pressure (psi)	Mercury Saturation (fraction)	Incremental Mercury Saturation (fraction)	Wetting Phase Saturation (fraction)	Pore Throat Diameter (micron)	Height above Free Water (G/W) (ft)
102	19.7	0.000	0.0000	1.000	2.12	59.0
109	21.1	0.000	0.0000	1.000	1.98	63.3
115	22.2	0.000	0.0000	1.000	1.88	66.5
123	23.9	0.000	0.0000	1.000	1.75	71.5
131	25.3	0.000	0.0000	1.000	1.65	75.9
138	26.8	0.000	0.0000	1.000	1.56	80.2
147	28.5	0.000	0.0000	1.000	1.47	85.2
155	30.1	0.000	0.0000	1.000	1.39	90.0
165	32.0	0.000	0.0000	1.000	1.31	95.7
177	34.3	0.000	0.0000	1.000	1.22	103
187	36.3	0.000	0.0000	1.000	1.15	109
198	38.4	0.000	0.0000	1.000	1.09	115
212	41.0	0.000	0.0000	1.000	1.02	123
224	43.4	0.000	0.0000	1.000	0.962	130
238	46.2	0.000	0.0000	1.000	0.904	138
252	48.8	0.000	0.0000	1.000	0.857	146
267	51.8	0.000	0.0000	1.000	0.806	155
285	55.1	0.000	0.0000	1.000	0.757	165
301	58.3	0.000	0.0000	1.000	0.716	175
319	61.8	0.000	0.0000	1.000	0.676	185
341	66.1	0.000	0.0000	1.000	0.632	198
360	69.7	0.000	0.0000	1.000	0.599	209
381	73.9	0.000	0.0000	1.000	0.565	221
406	78.7	0.000	0.0000	1.000	0.531	236
431	83.5	0.000	0.0000	1.000	0.500	250
456	88.4	0.000	0.0000	1.000	0.472	265
486	94.3	0.000	0.0000	1.000	0.443	282
514	100	0.000	0.0000	1.000	0.419	298
547	106	0.000	0.0000	1.000	0.394	317
580	112	0.000	0.0000	1.000	0.371	337
615	119	0.000	0.0000	1.000	0.350	357
650	126	0.000	0.0000	1.000	0.331	377
693	134	0.000	0.0000	1.000	0.311	402
737	143	0.000	0.0000	1.000	0.292	428
782	152	0.000	0.0000	1.000	0.276	454
829	161	0.000	0.0000	1.000	0.260	481
881	171	0.000	0.0000	1.000	0.245	511

Table A.2 Mercury Injection Capillary Pressure Data For Sample RM1-36HO-P01

Sample ID: RM1-36HO-P01 Swanson Air Permeability, mD: 0.00001
Depth, ft: 8258.00 Hg Porosity, percent: 1.42

Mercury/Air Pressure (psi)	Equivalent Air/Brine Pressure (psi)	Mercury Saturation (fraction)	Incremental Mercury Saturation (fraction)	Wetting Phase Saturation (fraction)	Pore Throat Diameter (micron)	Height above Free Water (G/W) (ft)
937	182	0.000	0.0000	1.000	0.230	544
990	192	0.000	0.0000	1.000	0.218	574
1054	204	0.000	0.0000	1.000	0.205	611
1118	217	0.000	0.0000	1.000	0.193	648
1184	229	0.000	0.0000	1.000	0.182	687
1255	243	0.000	0.0000	1.000	0.172	728
1336	259	0.000	0.0000	1.000	0.161	775
1419	275	0.000	0.0000	1.000	0.152	823
1504	291	0.000	0.0000	1.000	0.143	873
1594	309	0.000	0.0000	1.000	0.135	925
1695	328	0.000	0.0000	1.000	0.127	983
1799	349	0.000	0.0000	1.000	0.120	1044
1910	370	0.000	0.0000	1.000	0.113	1108
2023	392	0.000	0.0000	1.000	0.107	1174
2149	416	0.000	0.0000	1.000	0.100	1247
2279	442	0.000	0.0000	1.000	0.095	1322
2418	469	0.000	0.0000	1.000	0.089	1403
2570	498	0.000	0.0000	1.000	0.084	1491
2726	528	0.000	0.0000	1.000	0.079	1581
2894	561	0.000	0.0000	1.000	0.074	1679
3070	595	0.000	0.0000	1.000	0.070	1781
3260	632	0.000	0.0000	1.000	0.066	1892
3461	671	0.000	0.0000	1.000	0.062	2008
3671	711	0.000	0.0000	1.000	0.059	2130
3896	755	0.000	0.0000	1.000	0.055	2260
4137	802	0.000	0.0000	1.000	0.052	2400
4388	850	0.000	0.0000	1.000	0.049	2546
4657	903	0.000	0.0000	1.000	0.046	2702
4941	958	0.000	0.0000	1.000	0.044	2867
5245	1016	0.000	0.0000	1.000	0.041	3043
5568	1079	0.000	0.0000	1.000	0.039	3230
5907	1145	0.000	0.0000	1.000	0.036	3427
6271	1215	0.000	0.0000	1.000	0.034	3638
6655	1290	0.000	0.0000	1.000	0.032	3862
7063	1369	0.000	0.0000	1.000	0.031	4098
7496	1453	0.000	0.0000	1.000	0.029	4349
7816	1515	0.000	0.0000	1.000	0.028	4535

Table A.2 Mercury Injection Capillary Pressure Data For Sample RM1-36HO-P01

Sample ID: RM1-36HO-P01 Swanson Air Permeability, mD: 0.00001
Depth, ft: 8258.00 Hg Porosity, percent: 1.42

Mercury/Air Pressure (psi)	Equivalent Air/Brine Pressure (psi)	Mercury Saturation (fraction)	Incremental Mercury Saturation (fraction)	Wetting Phase Saturation (fraction)	Pore Throat Diameter (micron)	Height above Free Water (G/W) (ft)
8145	1578	0.000	0.0000	1.000	0.026	4726
8492	1646	0.000	0.0000	1.000	0.025	4927
8853	1716	0.000	0.0000	1.000	0.024	5137
9229	1789	0.000	0.0000	1.000	0.023	5355
9622	1865	0.000	0.0000	1.000	0.022	5583
10031	1944	0.006	0.0057	0.994	0.021	5820
10457	2027	0.014	0.0078	0.986	0.021	6067
10900	2112	0.021	0.0075	0.979	0.020	6324
11364	2202	0.029	0.0077	0.971	0.019	6594
11847	2296	0.037	0.0085	0.963	0.018	6874
12351	2393	0.045	0.0080	0.955	0.017	7166
12875	2495	0.054	0.0084	0.946	0.017	7470
13421	2601	0.063	0.0095	0.937	0.016	7787
13990	2711	0.073	0.0103	0.927	0.015	8117
14586	2827	0.084	0.0107	0.916	0.015	8463
15206	2947	0.095	0.0108	0.905	0.014	8823
15852	3072	0.106	0.0110	0.894	0.014	9197
16525	3202	0.120	0.0137	0.880	0.013	9588
17227	3338	0.133	0.0138	0.867	0.013	9995
17959	3480	0.148	0.0147	0.852	0.012	10420
18720	3628	0.164	0.0155	0.836	0.012	10862
19517	3782	0.180	0.0160	0.820	0.011	11324
20346	3943	0.198	0.0183	0.802	0.011	11805
21209	4110	0.214	0.0165	0.786	0.010	12306
22111	4285	0.235	0.0207	0.765	0.010	12829
23050	4467	0.255	0.0199	0.745	0.009	13374
24030	4657	0.277	0.0223	0.723	0.009	13942
25050	4855	0.301	0.0240	0.699	0.009	14535
26114	5061	0.325	0.0237	0.675	0.008	15152
27224	5276	0.349	0.0238	0.651	0.008	15796
28380	5500	0.377	0.0281	0.623	0.008	16467
29575	5731	0.404	0.0271	0.596	0.007	17160
30843	5977	0.433	0.0291	0.567	0.007	17896
32152	6231	0.465	0.0324	0.535	0.007	18655
33517	6495	0.494	0.0289	0.506	0.006	19447
34939	6771	0.526	0.0319	0.474	0.006	20272
36422	7058	0.559	0.0330	0.441	0.006	21133

Table A.2 Mercury Injection Capillary Pressure Data For Sample RM1-36HO-P01

Sample ID: RM1-36HO-P01 Swanson Air Permeability, mD: 0.00001
Depth, ft: 8258.00 Hg Porosity, percent: 1.42

Mercury/Air Pressure (psi)	Equivalent Air/Brine Pressure (psi)	Mercury Saturation (fraction)	Incremental Mercury Saturation (fraction)	Wetting Phase Saturation (fraction)	Pore Throat Diameter (micron)	Height above Free Water (G/W) (ft)
37959	7356	0.592	0.0330	0.408	0.006	22024
39570	7668	0.624	0.0320	0.376	0.005	22959
41254	7995	0.661	0.0365	0.339	0.005	23936
43005	8334	0.697	0.0364	0.303	0.005	24952
44827	8687	0.734	0.0369	0.266	0.005	26009
46742	9058	0.770	0.0363	0.230	0.005	27121
48721	9442	0.807	0.0363	0.193	0.004	28268
50794	9844	0.845	0.0387	0.155	0.004	29472
52946	10260	0.884	0.0384	0.116	0.004	30720
55194	10696	0.924	0.0399	0.076	0.004	32024
57538	11150	0.964	0.0403	0.036	0.004	33384
59986	11625	1.000	0.0360	0.000	0.004	34805

Figure A.4 Mercury/Air Capillary Pressure For Sample RM1-36HO-P01

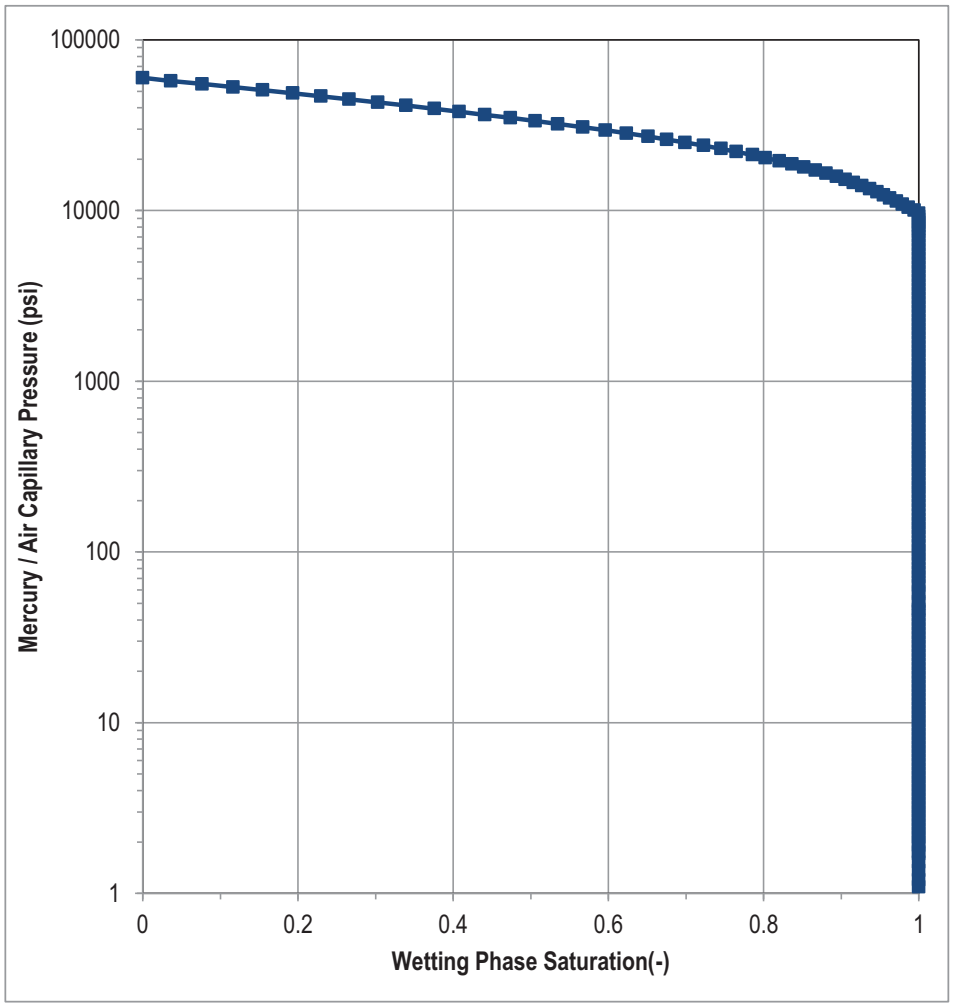


Figure A.5 Calculated Air /Brine Capillary Pressure And Height Above Free Water For Sample RM1-36HO-P01

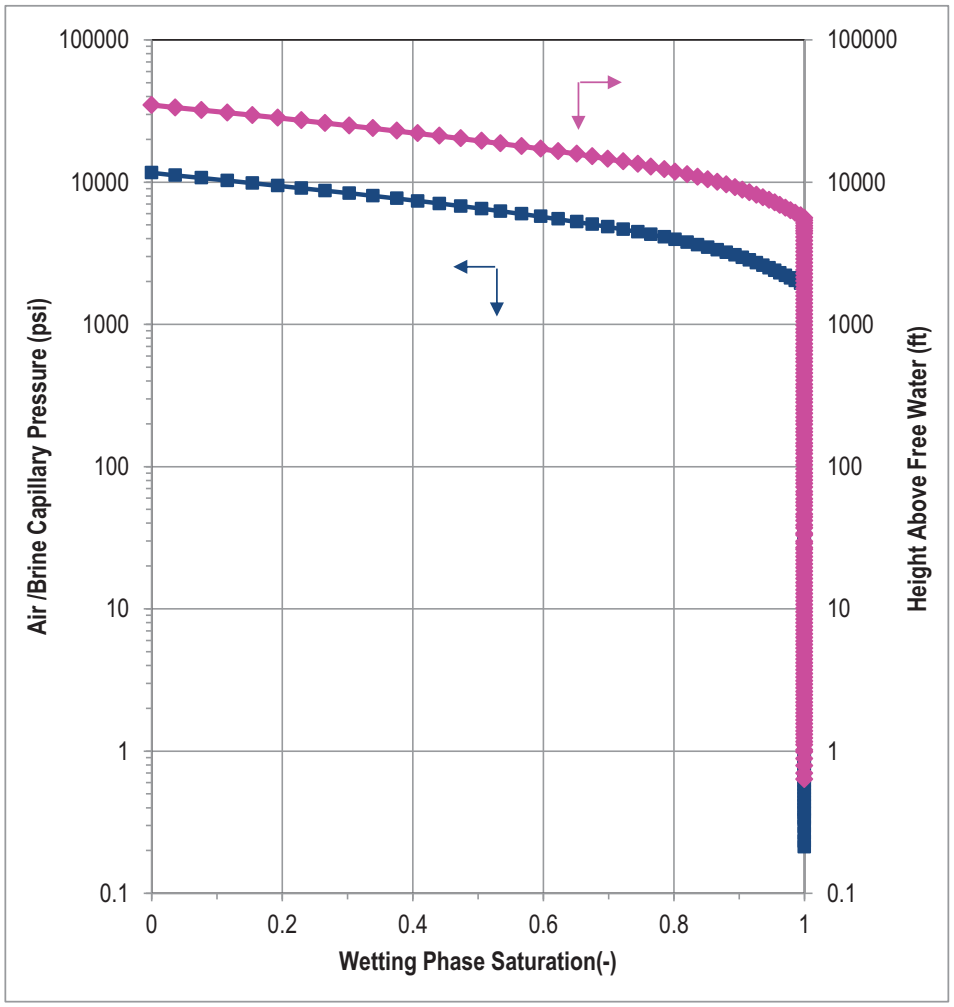


Figure A.6 Pore Throat Size Distribution For Sample RM1-36HO-P01

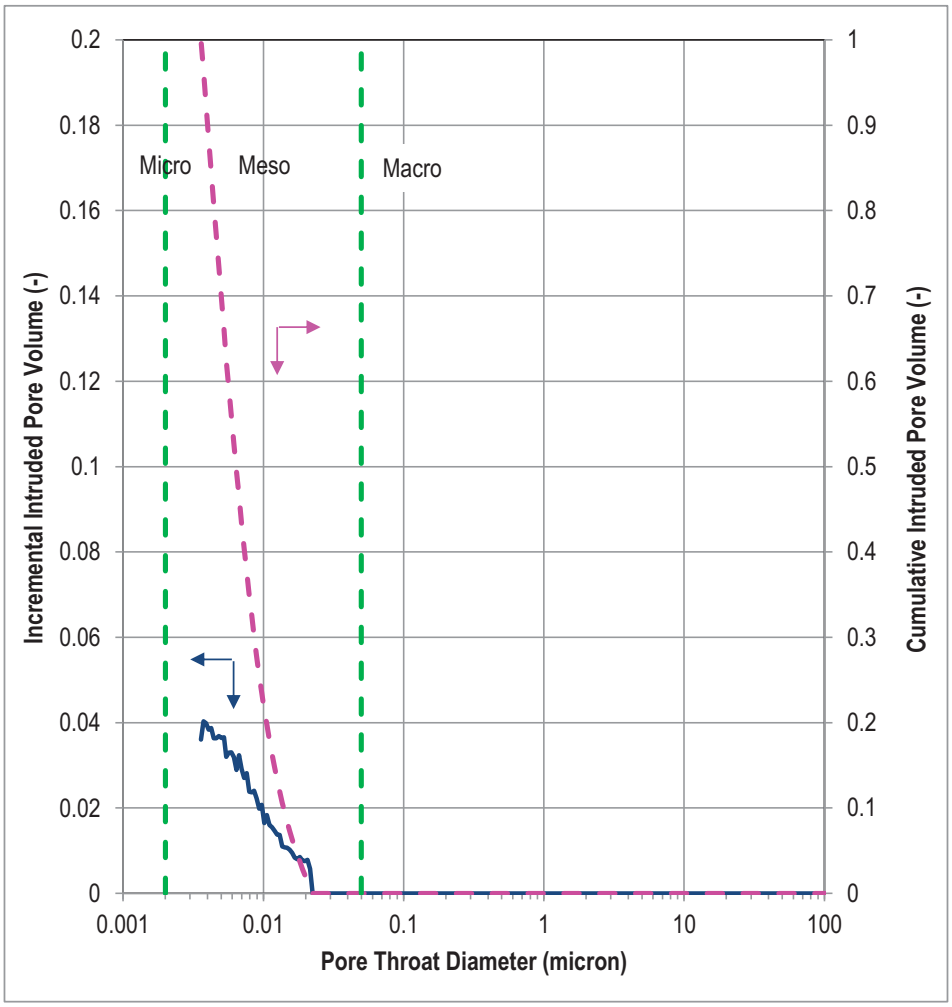


Table A.3 Mercury Injection Capillary Pressure Data For Sample RM1-37HO-P01

Sample ID: RM1-37HO-P01 Swanson Air Permeability, mD: 0.00002
Depth, ft: 8259.50 Hg Porosity, percent: 2.32

Mercury/Air Pressure (psi)	Equivalent Air/Brine Pressure (psi)	Mercury Saturation (fraction)	Incremental Mercury Saturation (fraction)	Wetting Phase Saturation (fraction)	Pore Throat Diameter (micron)	Height above Free Water (G/W) (ft)
1.09	0.212	0.000	0.0000	1.000	197	0.633
1.20	0.232	0.000	0.0000	1.000	180	0.696
1.36	0.263	0.000	0.0000	1.000	159	0.788
1.52	0.295	0.000	0.0000	1.000	142	0.883
1.70	0.330	0.000	0.0000	1.000	127	0.987
1.75	0.339	0.000	0.0000	1.000	123	1.01
1.91	0.369	0.000	0.0000	1.000	113	1.11
2.00	0.387	0.000	0.0000	1.000	108	1.16
2.13	0.412	0.000	0.0000	1.000	101	1.23
2.25	0.436	0.000	0.0000	1.000	95.8	1.31
2.38	0.462	0.000	0.0000	1.000	90.4	1.38
2.52	0.489	0.000	0.0000	1.000	85.5	1.46
2.68	0.519	0.000	0.0000	1.000	80.4	1.56
2.84	0.550	0.000	0.0000	1.000	76.0	1.65
3.01	0.583	0.000	0.0000	1.000	71.6	1.75
3.18	0.617	0.000	0.0000	1.000	67.7	1.85
3.37	0.654	0.000	0.0000	1.000	63.9	1.96
3.58	0.693	0.000	0.0000	1.000	60.2	2.08
3.79	0.734	0.000	0.0000	1.000	56.9	2.20
4.01	0.778	0.000	0.0000	1.000	53.7	2.33
4.26	0.826	0.000	0.0000	1.000	50.6	2.47
4.51	0.873	0.000	0.0000	1.000	47.8	2.61
4.78	0.926	0.000	0.0000	1.000	45.1	2.77
5.07	0.982	0.000	0.0000	1.000	42.5	2.94
5.37	1.04	0.000	0.0000	1.000	40.2	3.11
5.69	1.10	0.000	0.0000	1.000	37.9	3.30
6.03	1.17	0.000	0.0000	1.000	35.8	3.50
6.40	1.24	0.000	0.0000	1.000	33.7	3.71
6.78	1.31	0.000	0.0000	1.000	31.8	3.93
7.19	1.39	0.000	0.0000	1.000	30.0	4.17
7.62	1.48	0.000	0.0000	1.000	28.3	4.42
8.07	1.56	0.000	0.0000	1.000	26.7	4.69
8.56	1.66	0.000	0.0000	1.000	25.2	4.97
9.08	1.76	0.000	0.0000	1.000	23.7	5.27
9.62	1.87	0.000	0.0000	1.000	22.4	5.58
10.2	1.98	0.000	0.0000	1.000	21.1	5.92
10.8	2.10	0.000	0.0000	1.000	19.9	6.28

Table A.3 Mercury Injection Capillary Pressure Data For Sample RM1-37HO-P01

Sample ID: RM1-37HO-P01 Swanson Air Permeability, mD: 0.00002
Depth, ft: 8259.50 Hg Porosity, percent: 2.32

Mercury/Air Pressure (psi)	Equivalent Air/Brine Pressure (psi)	Mercury Saturation (fraction)	Incremental Mercury Saturation (fraction)	Wetting Phase Saturation (fraction)	Pore Throat Diameter (micron)	Height above Free Water (G/W) (ft)
11.5	2.22	0.000	0.0000	1.000	18.8	6.65
12.2	2.36	0.000	0.0000	1.000	17.7	7.06
12.9	2.50	0.000	0.0000	1.000	16.7	7.48
13.7	2.65	0.000	0.0000	1.000	15.8	7.93
14.5	2.81	0.000	0.0000	1.000	14.8	8.43
15.4	2.99	0.000	0.0000	1.000	14.0	8.94
16.4	3.17	0.000	0.0000	1.000	13.2	9.49
17.4	3.36	0.000	0.0000	1.000	12.4	10.1
18.4	3.57	0.000	0.0000	1.000	11.7	10.7
19.5	3.79	0.000	0.0000	1.000	11.0	11.3
20.7	4.02	0.000	0.0000	1.000	10.4	12.0
22.0	4.26	0.000	0.0000	1.000	9.79	12.8
23.3	4.52	0.000	0.0000	1.000	9.23	13.5
24.9	4.82	0.000	0.0000	1.000	8.67	14.4
26.3	5.10	0.000	0.0000	1.000	8.19	15.3
28.0	5.42	0.000	0.0000	1.000	7.70	16.2
29.7	5.75	0.000	0.0000	1.000	7.26	17.2
31.5	6.10	0.000	0.0000	1.000	6.84	18.3
33.4	6.48	0.000	0.0000	1.000	6.45	19.4
35.5	6.87	0.000	0.0000	1.000	6.08	20.6
37.6	7.29	0.000	0.0000	1.000	5.73	21.8
39.9	7.74	0.000	0.0000	1.000	5.40	23.2
42.4	8.22	0.000	0.0000	1.000	5.08	24.6
45.0	8.73	0.000	0.0000	1.000	4.79	26.1
46.4	9.00	0.000	0.0000	1.000	4.64	26.9
47.2	9.15	0.000	0.0000	1.000	4.56	27.4
52.4	10.2	0.000	0.0000	1.000	4.11	30.4
55.8	10.8	0.000	0.0000	1.000	3.86	32.4
59.0	11.4	0.000	0.0000	1.000	3.65	34.2
63.5	12.3	0.000	0.0000	1.000	3.40	36.8
67.1	13.0	0.000	0.0000	1.000	3.21	39.0
70.7	13.7	0.000	0.0000	1.000	3.05	41.0
76.1	14.7	0.000	0.0000	1.000	2.83	44.1
80.2	15.5	0.000	0.0000	1.000	2.69	46.5
85.9	16.7	0.000	0.0000	1.000	2.51	49.9
90.3	17.5	0.000	0.0000	1.000	2.39	52.4
95.7	18.5	0.000	0.0000	1.000	2.25	55.5

Table A.3 Mercury Injection Capillary Pressure Data For Sample RM1-37HO-P01

Sample ID: RM1-37HO-P01 Swanson Air Permeability, mD: 0.00002
Depth, ft: 8259.50 Hg Porosity, percent: 2.32

Mercury/Air Pressure (psi)	Equivalent Air/Brine Pressure (psi)	Mercury Saturation (fraction)	Incremental Mercury Saturation (fraction)	Wetting Phase Saturation (fraction)	Pore Throat Diameter (micron)	Height above Free Water (G/W) (ft)
102	19.7	0.000	0.0000	1.000	2.12	58.9
108	20.9	0.000	0.0000	1.000	2.00	62.5
114	22.0	0.000	0.0000	1.000	1.90	66.0
123	23.8	0.000	0.0000	1.000	1.76	71.2
130	25.2	0.000	0.0000	1.000	1.66	75.5
138	26.7	0.000	0.0000	1.000	1.57	79.8
145	28.1	0.000	0.0000	1.000	1.49	84.2
155	30.1	0.000	0.0000	1.000	1.39	90.2
165	32.0	0.000	0.0000	1.000	1.31	95.7
176	34.1	0.000	0.0000	1.000	1.23	102
185	35.9	0.000	0.0000	1.000	1.16	107
198	38.3	0.000	0.0000	1.000	1.09	115
208	40.3	0.000	0.0000	1.000	1.04	121
224	43.4	0.000	0.0000	1.000	0.963	130
236	45.8	0.000	0.0000	1.000	0.913	137
251	48.7	0.000	0.0000	1.000	0.858	146
266	51.5	0.000	0.0000	1.000	0.811	154
282	54.6	0.000	0.0000	1.000	0.765	164
301	58.4	0.000	0.0000	1.000	0.715	175
318	61.7	0.000	0.0000	1.000	0.677	185
340	65.9	0.000	0.0000	1.000	0.634	197
358	69.4	0.000	0.0000	1.000	0.602	208
383	74.2	0.000	0.0000	1.000	0.563	222
405	78.6	0.000	0.0000	1.000	0.532	235
430	83.4	0.000	0.0000	1.000	0.501	250
456	88.4	0.000	0.0000	1.000	0.472	265
482	93.5	0.000	0.0000	1.000	0.447	280
514	99.6	0.000	0.0000	1.000	0.419	298
545	106	0.000	0.0000	1.000	0.395	316
582	113	0.000	0.0000	1.000	0.371	337
613	119	0.000	0.0000	1.000	0.352	355
653	127	0.000	0.0000	1.000	0.330	379
690	134	0.000	0.0000	1.000	0.312	400
733	142	0.000	0.0000	1.000	0.294	425
781	151	0.000	0.0000	1.000	0.276	453
830	161	0.000	0.0000	1.000	0.260	482
877	170	0.000	0.0000	1.000	0.246	509

Table A.3 Mercury Injection Capillary Pressure Data For Sample RM1-37HO-P01

Sample ID: RM1-37HO-P01 Swanson Air Permeability, mD: 0.00002
Depth, ft: 8259.50 Hg Porosity, percent: 2.32

Mercury/Air Pressure (psi)	Equivalent Air/Brine Pressure (psi)	Mercury Saturation (fraction)	Incremental Mercury Saturation (fraction)	Wetting Phase Saturation (fraction)	Pore Throat Diameter (micron)	Height above Free Water (G/W) (ft)
931	180	0.000	0.0000	1.000	0.232	540
990	192	0.000	0.0000	1.000	0.218	575
1051	204	0.000	0.0000	1.000	0.205	610
1118	217	0.000	0.0000	1.000	0.193	649
1185	230	0.000	0.0000	1.000	0.182	687
1258	244	0.000	0.0000	1.000	0.171	730
1334	258	0.000	0.0000	1.000	0.162	774
1415	274	0.000	0.0000	1.000	0.152	821
1503	291	0.000	0.0000	1.000	0.143	872
1593	309	0.000	0.0000	1.000	0.135	924
1694	328	0.000	0.0000	1.000	0.127	983
1797	348	0.000	0.0000	1.000	0.120	1043
1907	370	0.000	0.0000	1.000	0.113	1106
2023	392	0.000	0.0000	1.000	0.107	1174
2146	416	0.000	0.0000	1.000	0.100	1245
2280	442	0.000	0.0000	1.000	0.095	1323
2417	468	0.000	0.0000	1.000	0.089	1403
2566	497	0.000	0.0000	1.000	0.084	1489
2723	528	0.000	0.0000	1.000	0.079	1580
2893	561	0.000	0.0000	1.000	0.075	1678
3072	595	0.000	0.0000	1.000	0.070	1782
3258	631	0.000	0.0000	1.000	0.066	1890
3461	671	0.000	0.0000	1.000	0.062	2008
3669	711	0.000	0.0000	1.000	0.059	2129
3894	755	0.000	0.0000	1.000	0.055	2260
4134	801	0.000	0.0000	1.000	0.052	2399
4387	850	0.000	0.0000	1.000	0.049	2545
4655	902	0.004	0.0037	0.996	0.046	2701
4941	957	0.007	0.0036	0.993	0.044	2867
5245	1016	0.012	0.0043	0.988	0.041	3043
5566	1079	0.017	0.0052	0.983	0.039	3229
5906	1144	0.022	0.0055	0.978	0.036	3427
6269	1215	0.027	0.0051	0.973	0.034	3638
6653	1289	0.034	0.0070	0.966	0.032	3860
7061	1368	0.041	0.0069	0.959	0.031	4097
7497	1453	0.049	0.0081	0.951	0.029	4350
7813	1514	0.057	0.0072	0.943	0.028	4533

Table A.3 Mercury Injection Capillary Pressure Data For Sample RM1-37HO-P01

Sample ID: RM1-37HO-P01 Swanson Air Permeability, mD: 0.00002
Depth, ft: 8259.50 Hg Porosity, percent: 2.32

Mercury/Air Pressure (psi)	Equivalent Air/Brine Pressure (psi)	Mercury Saturation (fraction)	Incremental Mercury Saturation (fraction)	Wetting Phase Saturation (fraction)	Pore Throat Diameter (micron)	Height above Free Water (G/W) (ft)
8144	1578	0.064	0.0072	0.936	0.026	4725
8491	1645	0.072	0.0079	0.928	0.025	4927
8852	1715	0.080	0.0088	0.920	0.024	5136
9229	1789	0.088	0.0079	0.912	0.023	5355
9619	1864	0.098	0.0094	0.902	0.022	5581
10028	1943	0.107	0.0097	0.893	0.021	5819
10456	2026	0.118	0.0104	0.882	0.021	6067
10899	2112	0.129	0.0110	0.871	0.020	6324
11362	2202	0.140	0.0112	0.860	0.019	6593
11846	2296	0.153	0.0127	0.847	0.018	6873
12350	2393	0.167	0.0145	0.833	0.017	7165
12873	2495	0.182	0.0142	0.818	0.017	7469
13419	2600	0.197	0.0150	0.803	0.016	7786
13989	2711	0.212	0.0157	0.788	0.015	8117
14585	2826	0.231	0.0186	0.769	0.015	8462
15203	2946	0.246	0.0154	0.754	0.014	8821
15850	3072	0.265	0.0184	0.735	0.014	9196
16523	3202	0.284	0.0192	0.716	0.013	9587
17225	3338	0.303	0.0188	0.697	0.013	9994
17948	3478	0.325	0.0220	0.675	0.012	10414
18717	3627	0.345	0.0201	0.655	0.012	10860
19518	3782	0.366	0.0215	0.634	0.011	11324
20344	3943	0.389	0.0224	0.611	0.011	11804
21208	4110	0.410	0.0215	0.590	0.010	12305
22109	4285	0.434	0.0236	0.566	0.010	12828
23048	4467	0.457	0.0237	0.543	0.009	13373
24027	4656	0.476	0.0182	0.524	0.009	13941
25049	4854	0.504	0.0281	0.496	0.009	14534
26114	5061	0.528	0.0240	0.472	0.008	15151
27222	5275	0.553	0.0256	0.447	0.008	15795
28378	5500	0.577	0.0241	0.423	0.008	16466
29584	5733	0.601	0.0241	0.399	0.007	17165
30840	5977	0.626	0.0245	0.374	0.007	17894
32150	6230	0.653	0.0270	0.347	0.007	18654
33515	6495	0.674	0.0212	0.326	0.006	19446
34939	6771	0.700	0.0254	0.300	0.006	20272
36421	7058	0.725	0.0254	0.275	0.006	21132

Table A.3 Mercury Injection Capillary Pressure Data For Sample RM1-37HO-P01

Sample ID: RM1-37HO-P01 Swanson Air Permeability, mD: 0.00002
Depth, ft: 8259.50 Hg Porosity, percent: 2.32

Mercury/Air Pressure (psi)	Equivalent Air/Brine Pressure (psi)	Mercury Saturation (fraction)	Incremental Mercury Saturation (fraction)	Wetting Phase Saturation (fraction)	Pore Throat Diameter (micron)	Height above Free Water (G/W) (ft)
37972	7359	0.749	0.0241	0.251	0.006	22032
39567	7668	0.772	0.0233	0.228	0.005	22957
41265	7997	0.798	0.0254	0.202	0.005	23943
43000	8333	0.821	0.0235	0.179	0.005	24949
44840	8690	0.845	0.0236	0.155	0.005	26017
46738	9057	0.868	0.0233	0.132	0.005	27118
48712	9440	0.892	0.0242	0.108	0.004	28264
50791	9843	0.912	0.0198	0.088	0.004	29470
52940	10259	0.936	0.0234	0.064	0.004	30716
55192	10696	0.958	0.0220	0.042	0.004	32023
57539	11151	0.981	0.0234	0.019	0.004	33385
59982	11624	1.000	0.0189	0.000	0.004	34802

Figure A.47 Mercury/Air Capillary Pressure For Sample RM1-37HO-P01

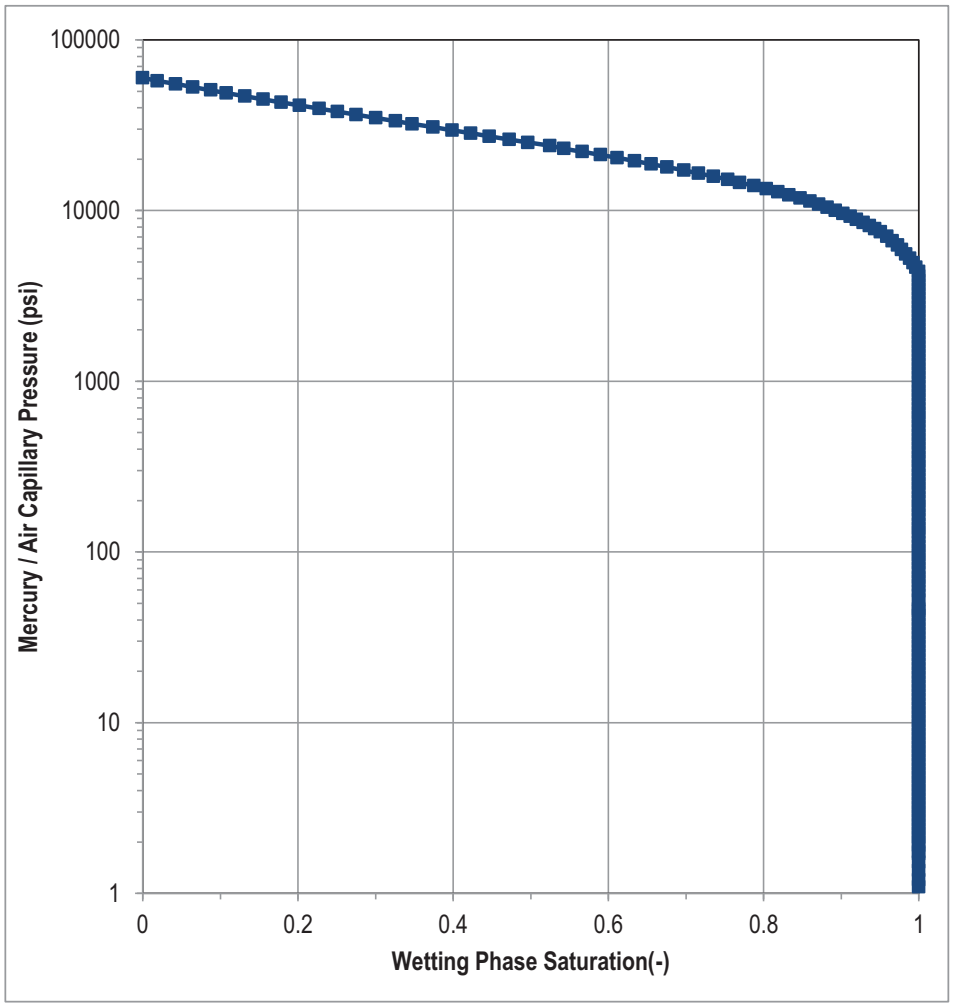


Figure A.8 Calculated Air /Brine Capillary Pressure And Height Above Free Water For Sample RM1-37HO-P01

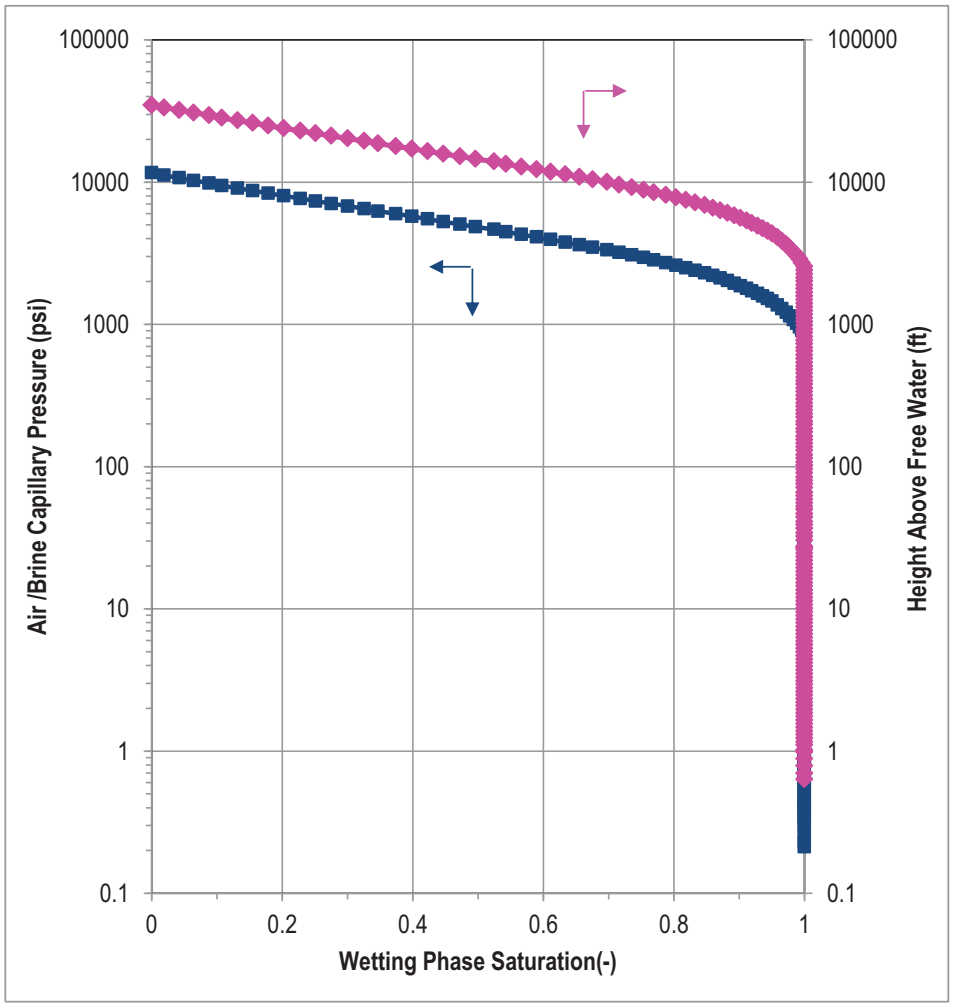


Figure A.9 Pore Throat Size Distribution For Sample RM1-37HO-P01

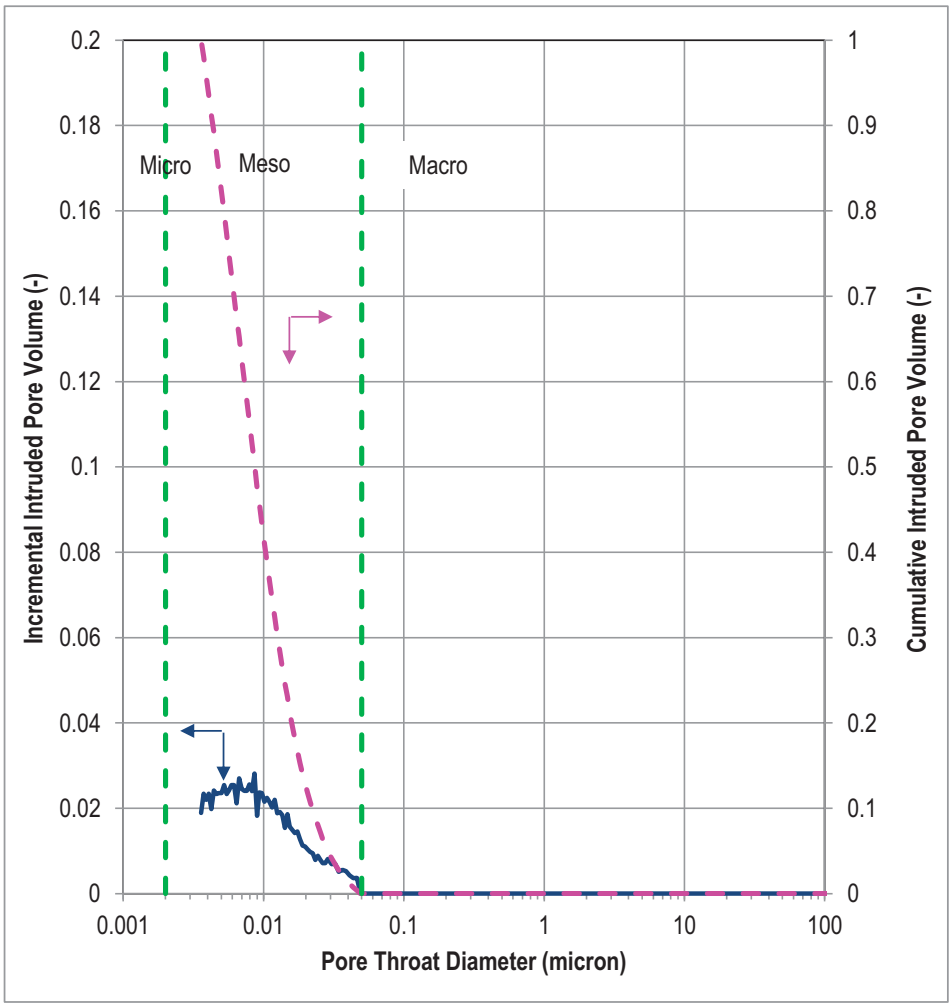


Table A.4 Mercury Injection Capillary Pressure Data For Sample RM1-41HA-P01

Sample ID: RM1-41HA-P01 Swanson Air Permeability, mD: 0.000006
Depth, ft: 8896.10 Hg Porosity, percent: 1.19

Mercury/Air Pressure (psi)	Equivalent Air/Brine Pressure (psi)	Mercury Saturation (fraction)	Incremental Mercury Saturation (fraction)	Wetting Phase Saturation (fraction)	Pore Throat Diameter (micron)	Height above Free Water (G/W) (ft)
1.09	0.211	0.000	0.0000	1.000	198	0.633
1.20	0.233	0.000	0.0000	1.000	179	0.697
1.35	0.262	0.000	0.0000	1.000	159	0.785
1.52	0.294	0.000	0.0000	1.000	142	0.879
1.51	0.294	0.000	0.0000	1.000	142	0.879
1.70	0.330	0.000	0.0000	1.000	127	0.99
1.73	0.335	0.000	0.0000	1.000	125	1.00
1.90	0.369	0.000	0.0000	1.000	113	1.10
2.00	0.387	0.000	0.0000	1.000	108	1.16
2.13	0.412	0.000	0.0000	1.000	101.4	1.23
2.25	0.436	0.000	0.0000	1.000	95.8	1.31
2.39	0.462	0.000	0.0000	1.000	90.4	1.38
2.52	0.489	0.000	0.0000	1.000	85.5	1.46
2.67	0.518	0.000	0.0000	1.000	80.6	1.55
2.84	0.550	0.000	0.0000	1.000	75.9	1.65
3.00	0.582	0.000	0.0000	1.000	71.8	1.74
3.18	0.617	0.000	0.0000	1.000	67.7	1.85
3.37	0.654	0.000	0.0000	1.000	63.9	1.96
3.57	0.692	0.000	0.0000	1.000	60.4	2.07
3.79	0.734	0.000	0.0000	1.000	56.9	2.20
4.01	0.778	0.000	0.0000	1.000	53.7	2.33
4.25	0.824	0.000	0.0000	1.000	50.7	2.47
4.51	0.874	0.000	0.0000	1.000	47.8	2.62
4.77	0.925	0.000	0.0000	1.000	45.2	2.77
5.06	0.98	0.000	0.0000	1.000	42.6	2.94
5.37	1.04	0.000	0.0000	1.000	40.2	3.11
5.69	1.10	0.000	0.0000	1.000	37.9	3.30
6.03	1.17	0.000	0.0000	1.000	35.7	3.50
6.39	1.24	0.000	0.0000	1.000	33.7	3.71
6.78	1.31	0.000	0.0000	1.000	31.8	3.93
7.18	1.39	0.000	0.0000	1.000	30.0	4.17
7.62	1.48	0.000	0.0000	1.000	28.3	4.42
8.07	1.56	0.000	0.0000	1.000	26.7	4.68
8.56	1.66	0.000	0.0000	1.000	25.2	4.97
9.08	1.76	0.000	0.0000	1.000	23.7	5.27
9.6	1.87	0.000	0.0000	1.000	22.4	5.58
10.2	1.98	0.000	0.0000	1.000	21.1	5.92

Table A.4 Mercury Injection Capillary Pressure Data For Sample RM1-41HA-P01

Sample ID: RM1-41HA-P01 Swanson Air Permeability, mD: 0.000006
Depth, ft: 8896.10 Hg Porosity, percent: 1.19

Mercury/Air Pressure (psi)	Equivalent Air/Brine Pressure (psi)	Mercury Saturation (fraction)	Incremental Mercury Saturation (fraction)	Wetting Phase Saturation (fraction)	Pore Throat Diameter (micron)	Height above Free Water (G/W) (ft)
10.8	2.10	0.000	0.0000	1.000	19.9	6.28
11.5	2.22	0.000	0.0000	1.000	18.8	6.66
12.2	2.36	0.000	0.0000	1.000	17.7	7.06
12.9	2.50	0.000	0.0000	1.000	16.7	7.48
13.7	2.65	0.000	0.0000	1.000	15.8	7.94
14.5	2.82	0.000	0.0000	1.000	14.8	8.43
15.4	2.99	0.000	0.0000	1.000	14.0	8.94
16.4	3.17	0.000	0.0000	1.000	13.2	9.49
17.3	3.36	0.000	0.0000	1.000	12.4	10.1
18.4	3.57	0.000	0.0000	1.000	11.7	10.7
19.5	3.79	0.000	0.0000	1.000	11.0	11.3
20.7	4.02	0.000	0.0000	1.000	10.4	12.0
22.0	4.27	0.000	0.0000	1.000	9.79	12.8
23.3	4.53	0.000	0.0000	1.000	9.23	13.5
24.9	4.82	0.000	0.0000	1.000	8.67	14.4
26.4	5.11	0.000	0.0000	1.000	8.17	15.3
28.0	5.42	0.000	0.0000	1.000	7.70	16.2
29.7	5.76	0.000	0.0000	1.000	7.26	17.2
31.5	6.11	0.000	0.0000	1.000	6.84	18.3
33.4	6.48	0.000	0.0000	1.000	6.45	19.4
35.5	6.88	0.000	0.0000	1.000	6.07	20.6
37.6	7.29	0.000	0.0000	1.000	5.73	21.8
39.9	7.74	0.000	0.0000	1.000	5.40	23.2
42.4	8.21	0.000	0.0000	1.000	5.09	24.6
45.0	8.71	0.000	0.0000	1.000	4.79	26.1
45.6	8.85	0.000	0.0000	1.000	4.72	26.5
48.2	9.33	0.000	0.0000	1.000	4.47	27.9
52.8	10.2	0.000	0.0000	1.000	4.08	30.7
56.3	10.9	0.000	0.0000	1.000	3.83	32.7
57.1	11.1	0.000	0.0000	1.000	3.77	33.1
62.1	12.0	0.000	0.0000	1.000	3.47	36.1
66.8	12.9	0.000	0.0000	1.000	3.23	38.7
70.5	13.7	0.000	0.0000	1.000	3.06	40.9
76.2	14.8	0.000	0.0000	1.000	2.83	44.2
80.7	15.6	0.000	0.0000	1.000	2.67	46.8
84.9	16.4	0.000	0.0000	1.000	2.54	49.2
91.3	17.7	0.000	0.0000	1.000	2.36	53.0

Table A.4 Mercury Injection Capillary Pressure Data For Sample RM1-41HA-P01

Sample ID: RM1-41HA-P01 Swanson Air Permeability, mD: 0.000006
Depth, ft: 8896.10 Hg Porosity, percent: 1.19

Mercury/Air Pressure (psi)	Equivalent Air/Brine Pressure (psi)	Mercury Saturation (fraction)	Incremental Mercury Saturation (fraction)	Wetting Phase Saturation (fraction)	Pore Throat Diameter (micron)	Height above Free Water (G/W) (ft)
96	18.6	0.000	0.0000	1.000	2.25	55.6
103	19.9	0.000	0.0000	1.000	2.10	59.7
109	21.1	0.000	0.0000	1.000	1.98	63.1
115	22.3	0.000	0.0000	1.000	1.88	66.7
123	23.8	0.000	0.0000	1.000	1.76	71.1
130	25.2	0.000	0.0000	1.000	1.66	75.5
139	26.9	0.000	0.0000	1.000	1.55	80.4
146	28.2	0.000	0.0000	1.000	1.48	84.5
156	30.3	0.000	0.0000	1.000	1.38	90.7
165	31.9	0.000	0.0000	1.000	1.31	96
176	34.0	0.000	0.0000	1.000	1.23	102
186	36.1	0.000	0.0000	1.000	1.16	108
198	38.4	0.000	0.0000	1.000	1.09	115
209	40.5	0.000	0.0000	1.000	1.03	121
222	43.0	0.000	0.0000	1.000	0.971	129
237	45.9	0.000	0.0000	1.000	0.909	138
250	48.5	0.000	0.0000	1.000	0.861	145
266	51.5	0.000	0.0000	1.000	0.811	154
284	55.1	0.000	0.0000	1.000	0.759	165
300	58.1	0.000	0.0000	1.000	0.719	174
320	62.0	0.000	0.0000	1.000	0.674	186
339	65.7	0.000	0.0000	1.000	0.635	197
360	69.8	0.000	0.0000	1.000	0.598	209
382	74.0	0.000	0.0000	1.000	0.564	222
404	78.3	0.000	0.0000	1.000	0.534	234
431	83.5	0.000	0.0000	1.000	0.500	250
456	88.5	0.000	0.0000	1.000	0.472	265
484	93.8	0.000	0.0000	1.000	0.445	281
515	100	0.000	0.0000	1.000	0.419	299
546	106	0.000	0.0000	1.000	0.394	317
579	112	0.000	0.0000	1.000	0.372	336
615	119	0.000	0.0000	1.000	0.351	357
653	127	0.000	0.0000	1.000	0.330	379
694	134	0.000	0.0000	1.000	0.311	402
733	142	0.000	0.0000	1.000	0.294	426
778	151	0.000	0.0000	1.000	0.277	451
829	161	0.000	0.0000	1.000	0.260	481

Table A.4 Mercury Injection Capillary Pressure Data For Sample RM1-41HA-P01

Sample ID: RM1-41HA-P01 Swanson Air Permeability, mD: 0.000006
Depth, ft: 8896.10 Hg Porosity, percent: 1.19

Mercury/Air Pressure (psi)	Equivalent Air/Brine Pressure (psi)	Mercury Saturation (fraction)	Incremental Mercury Saturation (fraction)	Wetting Phase Saturation (fraction)	Pore Throat Diameter (micron)	Height above Free Water (G/W) (ft)
879	170	0.000	0.0000	1.000	0.245	510
934	181	0.000	0.0000	1.000	0.231	542
990	192	0.000	0.0000	1.000	0.218	575
1053	204	0.000	0.0000	1.000	0.205	611
1116	216	0.000	0.0000	1.000	0.193	647
1184	229	0.000	0.0000	1.000	0.182	687
1256	243	0.000	0.0000	1.000	0.172	729
1332	258	0.000	0.0000	1.000	0.162	773
1415	274	0.000	0.0000	1.000	0.152	821
1505	292	0.000	0.0000	1.000	0.143	873
1596	309	0.000	0.0000	1.000	0.135	926
1692	328	0.000	0.0000	1.000	0.127	982
1795	348	0.000	0.0000	1.000	0.120	1041
1906	369	0.000	0.0000	1.000	0.113	1106
2023	392	0.000	0.0000	1.000	0.107	1174
2147	416	0.000	0.0000	1.000	0.100	1246
2280	442	0.000	0.0000	1.000	0.095	1323
2421	469	0.000	0.0000	1.000	0.089	1405
2570	498	0.000	0.0000	1.000	0.084	1491
2725	528	0.000	0.0000	1.000	0.079	1581
2894	561	0.000	0.0000	1.000	0.074	1679
3071	595	0.000	0.0000	1.000	0.070	1782
3257	631	0.000	0.0000	1.000	0.066	1890
3458	670	0.000	0.0000	1.000	0.062	2007
3669	711	0.000	0.0000	1.000	0.059	2129
3897	755	0.000	0.0000	1.000	0.055	2261
4134	801	0.000	0.0000	1.000	0.052	2398
4388	850	0.000	0.0000	1.000	0.049	2546
4657	902	0.000	0.0000	1.000	0.046	2702
4943	958	0.000	0.0000	1.000	0.044	2868
5244	1016	0.000	0.0000	1.000	0.041	3043
5566	1079	0.000	0.0000	1.000	0.039	3229
5909	1145	0.000	0.0000	1.000	0.036	3429
6271	1215	0.006	0.0058	0.994	0.034	3639
6654	1289	0.012	0.0057	0.988	0.032	3861
7063	1369	0.018	0.0069	0.982	0.031	4098
7495	1453	0.025	0.0061	0.975	0.029	4349

Table A.4 Mercury Injection Capillary Pressure Data For Sample RM1-41HA-P01

Sample ID: RM1-41HA-P01 Swanson Air Permeability, mD: 0.000006
Depth, ft: 8896.10 Hg Porosity, percent: 1.19

Mercury/Air Pressure (psi)	Equivalent Air/Brine Pressure (psi)	Mercury Saturation (fraction)	Incremental Mercury Saturation (fraction)	Wetting Phase Saturation (fraction)	Pore Throat Diameter (micron)	Height above Free Water (G/W) (ft)
7813	1514	0.030	0.0059	0.970	0.028	4533
8144	1578	0.037	0.0068	0.963	0.026	4725
8493	1646	0.043	0.0061	0.957	0.025	4928
8851	1715	0.050	0.0065	0.950	0.024	5135
9229	1789	0.058	0.0081	0.942	0.023	5355
9621	1864	0.066	0.0084	0.934	0.022	5582
10030	1944	0.069	0.0028	0.931	0.021	5820
10456	2026	0.080	0.0111	0.920	0.021	6067
10900	2112	0.089	0.0086	0.911	0.020	6325
11362	2202	0.098	0.0096	0.902	0.019	6593
11845	2296	0.108	0.0100	0.892	0.018	6873
12348	2393	0.118	0.0102	0.882	0.017	7165
12873	2495	0.130	0.0115	0.870	0.017	7469
13420	2601	0.141	0.0116	0.859	0.016	7787
13990	2711	0.155	0.0134	0.845	0.015	8117
14585	2826	0.168	0.0136	0.832	0.015	8462
15205	2947	0.183	0.0148	0.817	0.014	8822
15851	3072	0.202	0.0187	0.798	0.014	9197
16524	3202	0.215	0.0135	0.785	0.013	9587
17226	3338	0.235	0.0193	0.765	0.013	9995
17956	3480	0.253	0.0179	0.747	0.012	10418
18720	3628	0.275	0.0221	0.725	0.012	10862
19514	3782	0.297	0.0220	0.703	0.011	11322
20339	3942	0.319	0.0222	0.681	0.011	11801
21207	4110	0.344	0.0246	0.656	0.010	12304
22107	4284	0.364	0.0206	0.636	0.010	12827
23050	4467	0.395	0.0306	0.605	0.009	13374
24029	4657	0.423	0.0286	0.577	0.009	13942
25049	4854	0.454	0.0307	0.546	0.009	14534
26114	5061	0.476	0.0215	0.524	0.008	15152
27222	5275	0.505	0.0295	0.495	0.008	15795
28378	5500	0.536	0.0310	0.464	0.008	16466
29585	5733	0.559	0.0234	0.441	0.007	17165
30839	5976	0.590	0.0303	0.410	0.007	17894
32149	6230	0.620	0.0307	0.380	0.007	18653
33515	6495	0.652	0.0316	0.348	0.006	19446
34939	6771	0.677	0.0250	0.323	0.006	20272

Table A.4 Mercury Injection Capillary Pressure Data For Sample RM1-41HA-P01

Sample ID: RM1-41HA-P01 Swanson Air Permeability, mD: 0.000006
Depth, ft: 8896.10 Hg Porosity, percent: 1.19

Mercury/Air Pressure (psi)	Equivalent Air/Brine Pressure (psi)	Mercury Saturation (fraction)	Incremental Mercury Saturation (fraction)	Wetting Phase Saturation (fraction)	Pore Throat Diameter (micron)	Height above Free Water (G/W) (ft)
36424	7059	0.708	0.0310	0.292	0.006	21134
37969	7358	0.736	0.0283	0.264	0.006	22030
39583	7671	0.765	0.0285	0.235	0.005	22967
41263	7996	0.803	0.0387	0.197	0.005	23942
42996	8332	0.813	0.0098	0.187	0.005	24947
44838	8689	0.841	0.0278	0.159	0.005	26016
46743	9059	0.865	0.0240	0.135	0.005	27121
48721	9442	0.888	0.0230	0.112	0.004	28269
50792	9843	0.912	0.0235	0.088	0.004	29470
52947	10261	0.935	0.0234	0.065	0.004	30721
55194	10696	0.950	0.0149	0.050	0.004	32024
57534	11150	0.976	0.0260	0.024	0.004	33382
59983	11624	1.000	0.0241	0.000	0.004	34803

Figure A.10 Mercury/Air Capillary Pressure For Sample RM1-41HA-P01

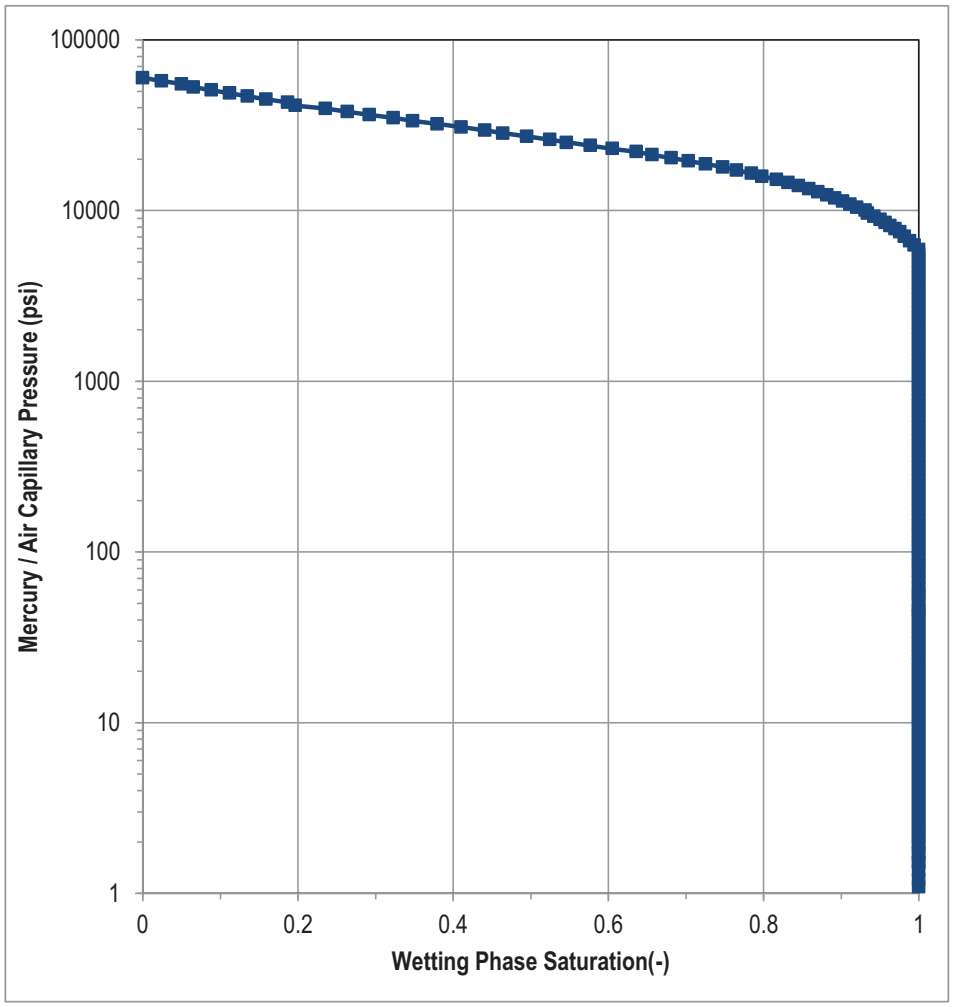


Figure A.11 Calculated Air /Brine Capillary Pressure And Height Above Free Water For Sample RM1-41HA-P01

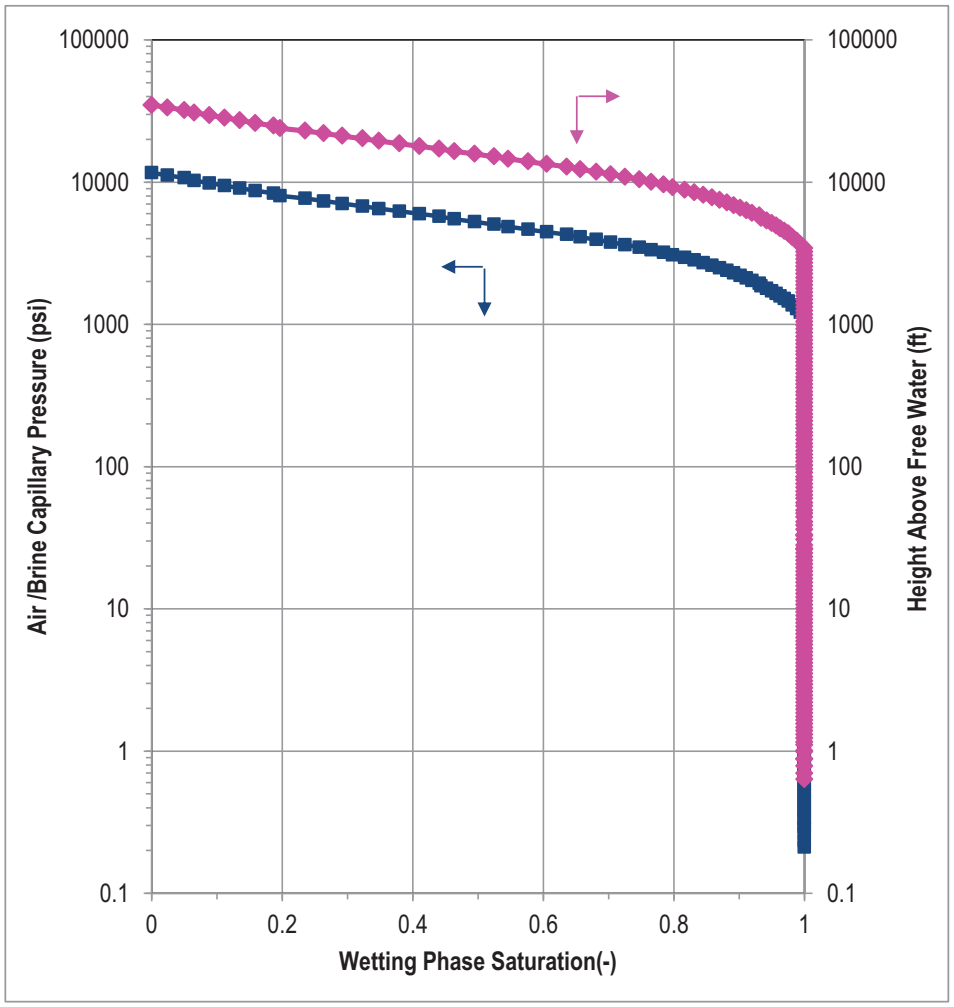


Figure A.12 Pore Throat Size Distribution For Sample RM1-41HA-P01

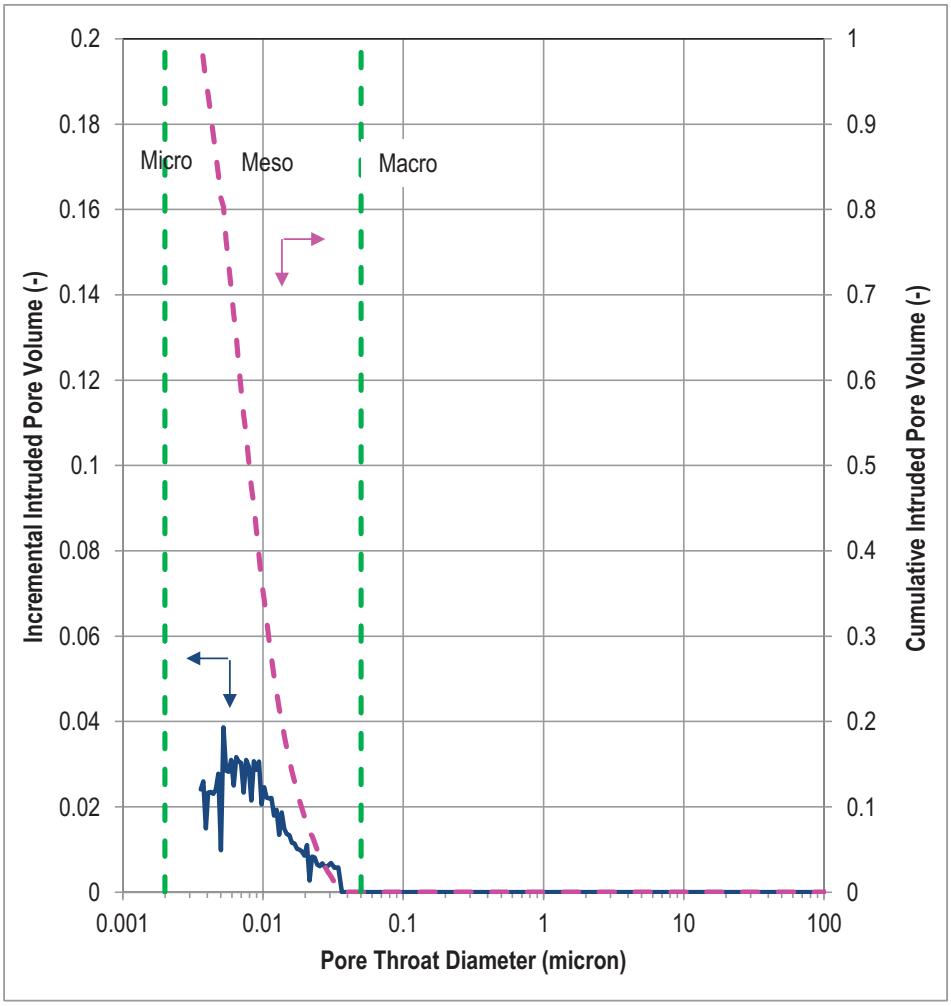


Table A.5 Mercury Injection Capillary Pressure Data For Sample RM1-48HO-P01

Sample ID: RM1-48HO-P01 Swanson Air Permeability, mD: 0.000008
Depth, ft: 8905.50 Hg Porosity, percent: 1.55

Mercury/Air Pressure (psi)	Equivalent Air/Brine Pressure (psi)	Mercury Saturation (fraction)	Incremental Mercury Saturation (fraction)	Wetting Phase Saturation (fraction)	Pore Throat Diameter (micron)	Height above Free Water (G/W) (ft)
1.09	0.211	0.000	0.0000	1.000	198	0.633
1.20	0.233	0.000	0.0000	1.000	179	0.697
1.35	0.262	0.000	0.0000	1.000	159	0.785
1.52	0.294	0.000	0.0000	1.000	142	0.879
1.51	0.294	0.000	0.0000	1.000	142	0.879
1.70	0.330	0.000	0.0000	1.000	127	0.988
1.73	0.335	0.000	0.0000	1.000	125	1.00
1.90	0.369	0.000	0.0000	1.000	113	1.10
2.00	0.387	0.000	0.0000	1.000	108	1.16
2.13	0.412	0.000	0.0000	1.000	101	1.23
2.25	0.436	0.000	0.0000	1.000	95.8	1.31
2.39	0.462	0.000	0.0000	1.000	90.4	1.38
2.52	0.489	0.000	0.0000	1.000	85.5	1.46
2.67	0.518	0.000	0.0000	1.000	80.6	1.55
2.84	0.550	0.000	0.0000	1.000	75.9	1.65
3.00	0.582	0.000	0.0000	1.000	71.8	1.74
3.18	0.617	0.000	0.0000	1.000	67.7	1.85
3.37	0.654	0.000	0.0000	1.000	63.9	1.96
3.57	0.692	0.000	0.0000	1.000	60.4	2.07
3.79	0.734	0.000	0.0000	1.000	56.9	2.20
4.01	0.778	0.000	0.0000	1.000	53.7	2.33
4.25	0.824	0.000	0.0000	1.000	50.7	2.47
4.51	0.874	0.000	0.0000	1.000	47.8	2.62
4.77	0.925	0.000	0.0000	1.000	45.2	2.77
5.06	0.980	0.000	0.0000	1.000	42.6	2.94
5.37	1.04	0.000	0.0000	1.000	40.2	3.11
5.69	1.10	0.000	0.0000	1.000	37.9	3.30
6.03	1.17	0.000	0.0000	1.000	35.7	3.50
6.39	1.24	0.000	0.0000	1.000	33.7	3.71
6.78	1.31	0.000	0.0000	1.000	31.8	3.93
7.18	1.39	0.000	0.0000	1.000	30.0	4.17
7.62	1.48	0.000	0.0000	1.000	28.3	4.42
8.07	1.56	0.000	0.0000	1.000	26.7	4.68
8.56	1.66	0.000	0.0000	1.000	25.2	4.97
9.08	1.76	0.000	0.0000	1.000	23.7	5.27
9.62	1.87	0.000	0.0000	1.000	22.4	5.58
10.2	1.98	0.000	0.0000	1.000	21.1	5.92

Table A.5 Mercury Injection Capillary Pressure Data For Sample RM1-48HO-P01

Sample ID: RM1-48HO-P01 Swanson Air Permeability, mD: 0.000008
Depth, ft: 8905.50 Hg Porosity, percent: 1.55

Mercury/Air Pressure (psi)	Equivalent Air/Brine Pressure (psi)	Mercury Saturation (fraction)	Incremental Mercury Saturation (fraction)	Wetting Phase Saturation (fraction)	Pore Throat Diameter (micron)	Height above Free Water (G/W) (ft)
10.8	2.10	0.000	0.0000	1.000	19.9	6.28
11.5	2.22	0.000	0.0000	1.000	18.8	6.66
12.2	2.36	0.000	0.0000	1.000	17.7	7.06
12.9	2.50	0.000	0.0000	1.000	16.7	7.48
13.7	2.65	0.000	0.0000	1.000	15.8	7.94
14.5	2.82	0.000	0.0000	1.000	14.8	8.43
15.4	2.99	0.000	0.0000	1.000	14.0	8.94
16.4	3.17	0.000	0.0000	1.000	13.2	9.5
17.3	3.36	0.000	0.0000	1.000	12.4	10.1
18.4	3.57	0.000	0.0000	1.000	11.7	10.7
19.5	3.79	0.000	0.0000	1.000	11.0	11.3
20.7	4.02	0.000	0.0000	1.000	10.40	12.0
22.0	4.27	0.000	0.0000	1.000	9.79	12.8
23.3	4.53	0.000	0.0000	1.000	9.23	13.5
24.9	4.82	0.000	0.0000	1.000	8.67	14.4
26.4	5.11	0.000	0.0000	1.000	8.17	15.3
28.0	5.42	0.000	0.0000	1.000	7.70	16.2
29.7	5.76	0.000	0.0000	1.000	7.26	17.2
31.5	6.11	0.000	0.0000	1.000	6.84	18.3
33.4	6.48	0.000	0.0000	1.000	6.45	19.4
35.5	6.88	0.000	0.0000	1.000	6.07	20.6
37.6	7.29	0.000	0.0000	1.000	5.73	21.8
39.9	7.74	0.000	0.0000	1.000	5.40	23.2
42.4	8.21	0.000	0.0000	1.000	5.09	24.6
45.0	8.71	0.000	0.0000	1.000	4.79	26.1
45.6	8.83	0.000	0.0000	1.000	4.73	26.4
48.1	9.32	0.000	0.0000	1.000	4.48	27.9
52.8	10.2	0.000	0.0000	1.000	4.08	30.6
56.2	10.9	0.000	0.0000	1.000	3.83	32.6
57.1	11.1	0.000	0.0000	1.000	3.78	33.1
62.1	12.0	0.000	0.0000	1.000	3.47	36.0
66.7	12.9	0.000	0.0000	1.000	3.23	38.7
70.4	13.6	0.000	0.0000	1.000	3.06	40.8
76.1	14.7	0.000	0.0000	1.000	2.83	44.1
80.6	15.6	0.000	0.0000	1.000	2.67	46.8
84.8	16.4	0.000	0.0000	1.000	2.54	49.2
91.2	17.7	0.000	0.0000	1.000	2.36	52.9

Table A.5 Mercury Injection Capillary Pressure Data For Sample RM1-48HO-P01

Sample ID: RM1-48HO-P01 Swanson Air Permeability, mD: 0.000008
Depth, ft: 8905.50 Hg Porosity, percent: 1.55

Mercury/Air Pressure (psi)	Equivalent Air/Brine Pressure (psi)	Mercury Saturation (fraction)	Incremental Mercury Saturation (fraction)	Wetting Phase Saturation (fraction)	Pore Throat Diameter (micron)	Height above Free Water (G/W) (ft)
96	18.6	0.000	0.0000	1.000	2.25	55.6
103	19.9	0.000	0.0000	1.000	2.10	59.6
109	21.1	0.000	0.0000	1.000	1.98	63.0
115	22.3	0.000	0.0000	1.000	1.88	66.6
122	23.7	0.000	0.0000	1.000	1.76	71.1
130	25.2	0.000	0.0000	1.000	1.66	75.5
139	26.8	0.000	0.0000	1.000	1.56	80.4
146	28.2	0.000	0.0000	1.000	1.48	84.5
156	30.3	0.000	0.0000	1.000	1.38	90.6
165	31.9	0.000	0.0000	1.000	1.31	95.5
176	34.0	0.000	0.0000	1.000	1.23	102
186	36.1	0.000	0.0000	1.000	1.16	108
198	38.4	0.000	0.0000	1.000	1.09	115
209	40.5	0.000	0.0000	1.000	1.03	121
222	43.0	0.000	0.0000	1.000	0.972	129
237	45.9	0.000	0.0000	1.000	0.910	137
250	48.5	0.000	0.0000	1.000	0.862	145
266	51.5	0.000	0.0000	1.000	0.811	154
284	55.1	0.000	0.0000	1.000	0.759	165
300	58.1	0.000	0.0000	1.000	0.719	174
320	62.0	0.000	0.0000	1.000	0.674	186
339	65.7	0.000	0.0000	1.000	0.635	197
360	69.8	0.000	0.0000	1.000	0.598	209
382	74.0	0.000	0.0000	1.000	0.564	222
404	78.2	0.000	0.0000	1.000	0.534	234
431	83.5	0.000	0.0000	1.000	0.500	250
456	88.4	0.000	0.0000	1.000	0.472	265
484	93.8	0.000	0.0000	1.000	0.445	281
514	100	0.000	0.0000	1.000	0.419	299
546	106	0.000	0.0000	1.000	0.395	317
579	112	0.000	0.0000	1.000	0.372	336
615	119	0.000	0.0000	1.000	0.351	357
653	127	0.000	0.0000	1.000	0.330	379
694	134	0.000	0.0000	1.000	0.311	402
733	142	0.000	0.0000	1.000	0.294	425
778	151	0.000	0.0000	1.000	0.277	451
829	161	0.000	0.0000	1.000	0.260	481

Table A.5 Mercury Injection Capillary Pressure Data For Sample RM1-48HO-P01

Sample ID: RM1-48HO-P01 Swanson Air Permeability, mD: 0.000008
Depth, ft: 8905.50 Hg Porosity, percent: 1.55

Mercury/Air Pressure (psi)	Equivalent Air/Brine Pressure (psi)	Mercury Saturation (fraction)	Incremental Mercury Saturation (fraction)	Wetting Phase Saturation (fraction)	Pore Throat Diameter (micron)	Height above Free Water (G/W) (ft)
879	170	0.000	0.0000	1.000	0.245	510
934	181	0.000	0.0000	1.000	0.231	542
990	192	0.000	0.0000	1.000	0.218	575
1053	204	0.000	0.0000	1.000	0.205	611
1115	216	0.000	0.0000	1.000	0.193	647
1184	229	0.000	0.0000	1.000	0.182	687
1256	243	0.000	0.0000	1.000	0.172	729
1332	258	0.000	0.0000	1.000	0.162	773
1415	274	0.000	0.0000	1.000	0.152	821
1505	292	0.000	0.0000	1.000	0.143	873
1595	309	0.000	0.0000	1.000	0.135	926
1692	328	0.000	0.0000	1.000	0.127	982
1795	348	0.000	0.0000	1.000	0.120	1041
1905	369	0.000	0.0000	1.000	0.113	1106
2023	392	0.000	0.0000	1.000	0.107	1174
2147	416	0.000	0.0000	1.000	0.100	1246
2280	442	0.000	0.0000	1.000	0.095	1323
2421	469	0.000	0.0000	1.000	0.089	1405
2570	498	0.000	0.0000	1.000	0.084	1491
2725	528	0.000	0.0000	1.000	0.079	1581
2894	561	0.000	0.0000	1.000	0.074	1679
3071	595	0.000	0.0000	1.000	0.070	1782
3257	631	0.000	0.0000	1.000	0.066	1890
3458	670	0.000	0.0000	1.000	0.062	2007
3669	711	0.000	0.0000	1.000	0.059	2129
3897	755	0.000	0.0000	1.000	0.055	2261
4134	801	0.000	0.0000	1.000	0.052	2398
4388	850	0.000	0.0000	1.000	0.049	2546
4656	902	0.000	0.0000	1.000	0.046	2702
4943	958	0.000	0.0000	1.000	0.044	2868
5244	1016	0.000	0.0000	1.000	0.041	3043
5566	1079	0.000	0.0000	1.000	0.039	3229
5909	1145	0.000	0.0000	1.000	0.036	3428
6271	1215	0.000	0.0000	1.000	0.034	3639
6654	1289	0.000	0.0000	1.000	0.032	3861
7063	1369	0.000	0.0000	1.000	0.031	4098
7495	1453	0.000	0.0000	1.000	0.029	4349

Table A.5 Mercury Injection Capillary Pressure Data For Sample RM1-48HO-P01

Sample ID: RM1-48HO-P01 Swanson Air Permeability, mD: 0.000008
Depth, ft: 8905.50 Hg Porosity, percent: 1.55

Mercury/Air Pressure (psi)	Equivalent Air/Brine Pressure (psi)	Mercury Saturation (fraction)	Incremental Mercury Saturation (fraction)	Wetting Phase Saturation (fraction)	Pore Throat Diameter (micron)	Height above Free Water (G/W) (ft)
7813	1514	0.000	0.0000	1.000	0.028	4533
8144	1578	0.000	0.0000	1.000	0.026	4725
8493	1646	0.000	0.0000	1.000	0.025	4928
8851	1715	0.000	0.0000	1.000	0.024	5135
9229	1788	0.000	0.0000	1.000	0.023	5355
9621	1864	0.007	0.0070	0.993	0.022	5582
10030	1944	0.014	0.0068	0.986	0.021	5820
10456	2026	0.022	0.0077	0.978	0.021	6067
10900	2112	0.030	0.0081	0.970	0.020	6324
11362	2202	0.036	0.0066	0.964	0.019	6593
11845	2295	0.047	0.0105	0.953	0.018	6873
12348	2393	0.055	0.0084	0.945	0.017	7165
12873	2495	0.065	0.0096	0.935	0.017	7469
13420	2601	0.074	0.0094	0.926	0.016	7787
13990	2711	0.084	0.0102	0.916	0.015	8117
14585	2826	0.095	0.0107	0.905	0.015	8462
15205	2947	0.105	0.0104	0.895	0.014	8822
15851	3072	0.117	0.0116	0.883	0.014	9197
16524	3202	0.129	0.0122	0.871	0.013	9587
17226	3338	0.141	0.0119	0.859	0.013	9995
17956	3480	0.153	0.0119	0.847	0.012	10418
18720	3628	0.169	0.0156	0.831	0.012	10861
19514	3782	0.185	0.0163	0.815	0.011	11322
20339	3942	0.204	0.0188	0.796	0.011	11801
21206	4110	0.220	0.0161	0.780	0.010	12304
22107	4284	0.239	0.0188	0.761	0.010	12827
23050	4467	0.258	0.0190	0.742	0.009	13374
24029	4657	0.280	0.0224	0.720	0.009	13942
25049	4854	0.305	0.0249	0.695	0.009	14534
26114	5061	0.327	0.0221	0.673	0.008	15152
27222	5275	0.354	0.0272	0.646	0.008	15795
28378	5500	0.383	0.0288	0.617	0.008	16466
29584	5733	0.414	0.0305	0.586	0.007	17165
30839	5976	0.446	0.0318	0.554	0.007	17894
32149	6230	0.479	0.0338	0.521	0.007	18653
33515	6495	0.515	0.0353	0.485	0.006	19446
34939	6771	0.553	0.0379	0.447	0.006	20272

Table A.5 Mercury Injection Capillary Pressure Data For Sample RM1-48HO-P01

Sample ID: RM1-48HO-P01 Swanson Air Permeability, mD: 0.000008
Depth, ft: 8905.50 Hg Porosity, percent: 1.55

Mercury/Air Pressure (psi)	Equivalent Air/Brine Pressure (psi)	Mercury Saturation (fraction)	Incremental Mercury Saturation (fraction)	Wetting Phase Saturation (fraction)	Pore Throat Diameter (micron)	Height above Free Water (G/W) (ft)
36424	7059	0.590	0.0373	0.410	0.006	21134
37969	7358	0.628	0.0384	0.372	0.006	22030
39583	7671	0.666	0.0378	0.334	0.005	22967
41263	7996	0.705	0.0394	0.295	0.005	23942
42996	8332	0.740	0.0350	0.260	0.005	24947
44838	8689	0.777	0.0366	0.223	0.005	26016
46743	9058	0.813	0.0362	0.187	0.005	27121
48721	9442	0.847	0.0335	0.153	0.004	28269
50791	9843	0.882	0.0353	0.118	0.004	29470
52946	10261	0.911	0.0288	0.089	0.004	30720
55194	10696	0.943	0.0325	0.057	0.004	32024
57534	11150	0.971	0.0274	0.029	0.004	33382
59983	11624	1.000	0.0292	0.000	0.004	34803

Figure A.13 Mercury/Air Capillary Pressure For Sample RM1-48HO-P01

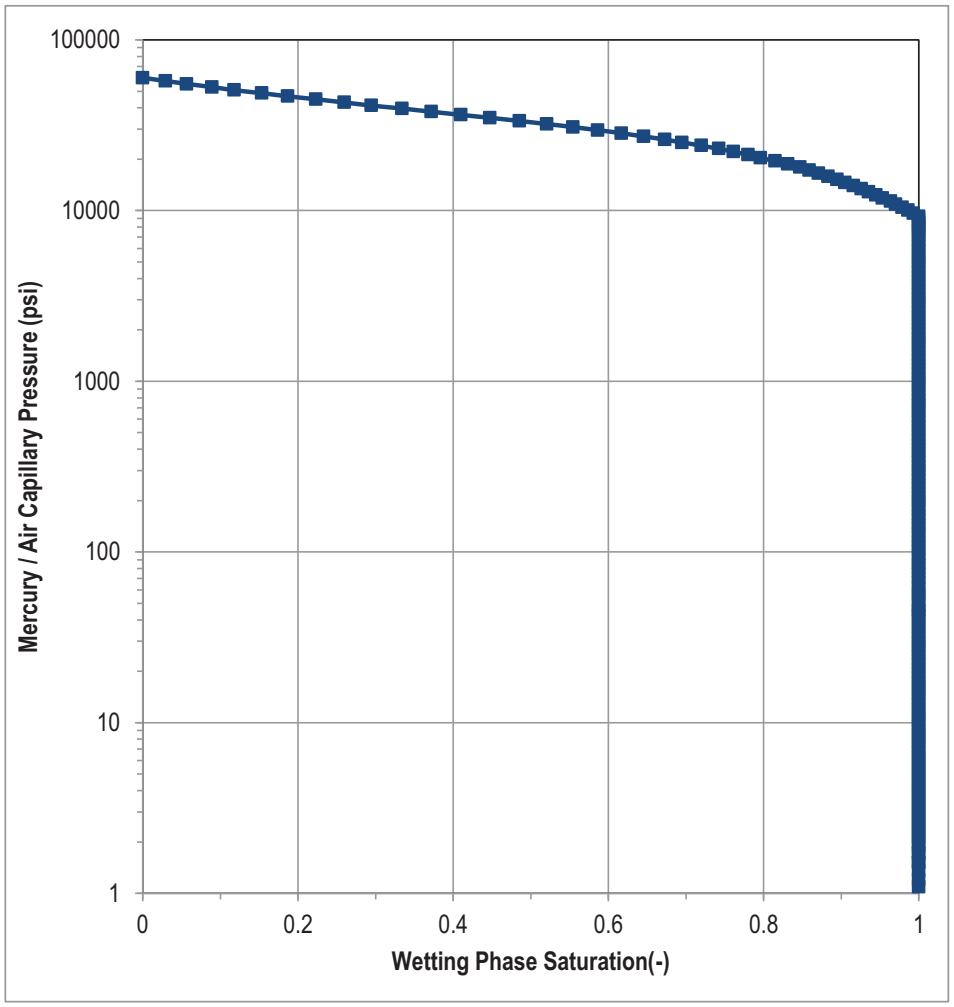


Figure A.14 Calculated Air /Brine Capillary Pressure And Height Above Free Water For Sample RM1-48HO-P01

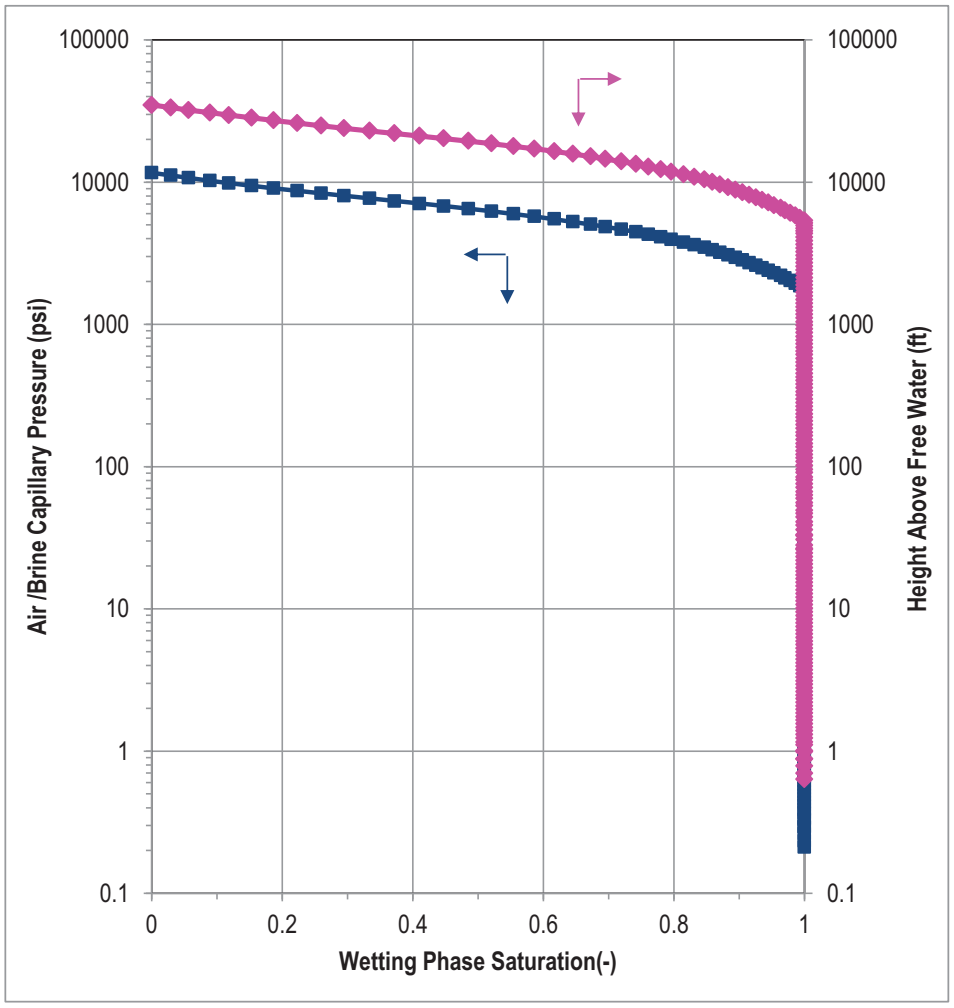


Figure A.15 Pore Throat Size Distribution For Sample RM1-48HO-P01

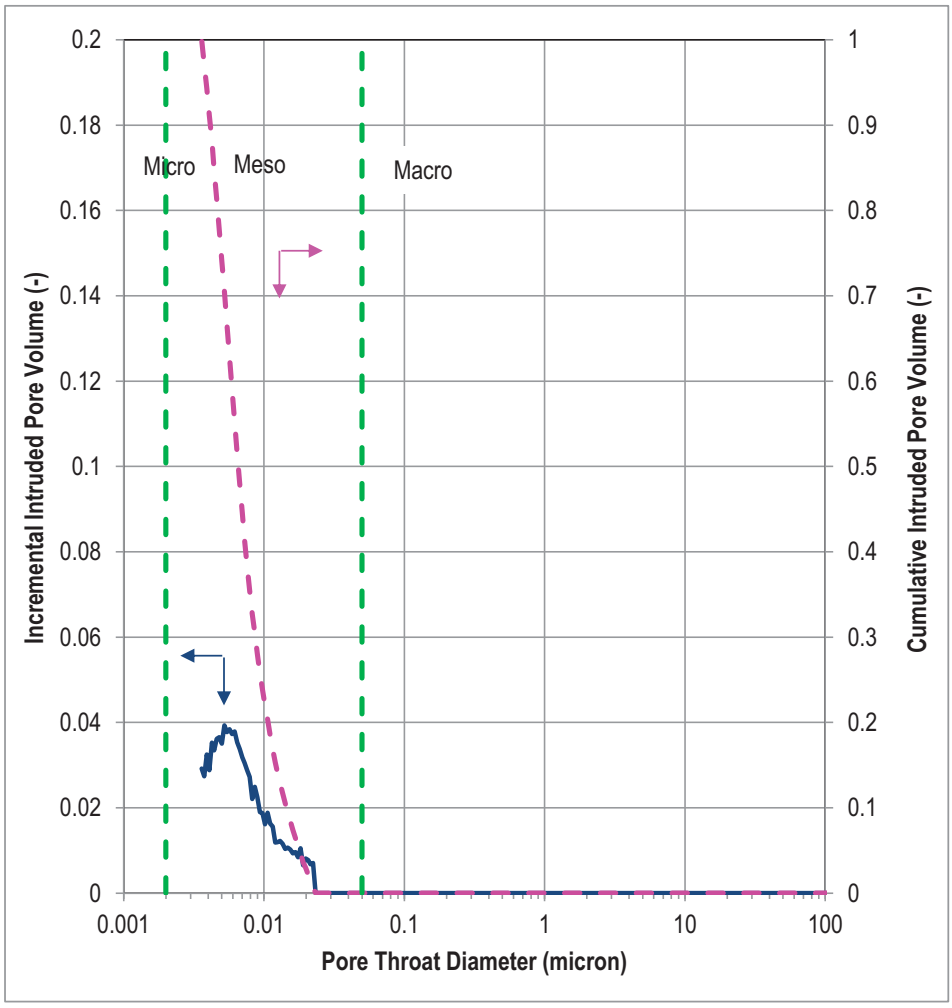


Table A.6 Mercury Injection Capillary Pressure Data For Sample RM1-63DO-P01

Sample ID: RM1-63DO-P01 Swanson Air Permeability, mD: 1.04
Depth, ft: 9012.30 Hg Porosity, percent: 9.78

Mercury/Air Pressure (psi)	Equivalent Air/Brine Pressure (psi)	Mercury Saturation (fraction)	Incremental Mercury Saturation (fraction)	Wetting Phase Saturation (fraction)	Pore Throat Diameter (micron)	Height above Free Water (G/W) (ft)
1.09	0.211	0.000	0.0000	1.000	198	0.632
1.20	0.233	0.000	0.0000	1.000	179	0.699
1.36	0.263	0.000	0.0000	1.000	159	0.787
1.52	0.294	0.000	0.0000	1.000	142	0.881
1.69	0.328	0.000	0.0000	1.000	127	0.983
1.77	0.344	0.000	0.0000	1.000	122	1.03
1.89	0.367	0.000	0.0000	1.000	114	1.10
2.00	0.388	0.000	0.0000	1.000	108	1.16
2.12	0.411	0.000	0.0000	1.000	102	1.23
2.25	0.437	0.000	0.0000	1.000	96	1.31
2.38	0.462	0.000	0.0000	1.000	90.4	1.38
2.53	0.489	0.000	0.0000	1.000	85.4	1.47
2.68	0.519	0.000	0.0000	1.000	80.5	1.55
2.83	0.549	0.000	0.0000	1.000	76.1	1.64
3.00	0.582	0.000	0.0000	1.000	71.8	1.74
3.18	0.617	0.000	0.0000	1.000	67.7	1.85
3.37	0.653	0.000	0.0000	1.000	64.0	1.96
3.57	0.693	0.000	0.0000	1.000	60.3	2.07
3.78	0.733	0.000	0.0000	1.000	57.0	2.19
4.01	0.778	0.000	0.0000	1.000	53.7	2.33
4.25	0.824	0.000	0.0000	1.000	50.7	2.47
4.51	0.873	0.000	0.0000	1.000	47.8	2.61
4.78	0.925	0.000	0.0000	1.000	45.1	2.77
5.06	0.981	0.000	0.0000	1.000	42.6	2.94
5.37	1.040	0.000	0.0000	1.000	40.2	3.11
5.69	1.10	0.000	0.0000	1.000	37.9	3.30
6.03	1.17	0.000	0.0000	1.000	35.7	3.50
6.39	1.24	0.000	0.0000	1.000	33.7	3.71
6.77	1.31	0.000	0.0000	1.000	31.8	3.93
7.18	1.39	0.000	0.0000	1.000	30.0	4.17
7.61	1.48	0.000	0.0000	1.000	28.3	4.42
8.07	1.56	0.000	0.0000	1.000	26.7	4.68
8.56	1.66	0.000	0.0000	1.000	25.2	4.97
9.08	1.76	0.000	0.0000	1.000	23.8	5.27
9.62	1.86	0.000	0.0000	1.000	22.4	5.58
10.20	1.98	0.000	0.0000	1.000	21.1	5.92
10.8	2.10	0.000	0.0000	1.000	19.9	6.28

Table A.6 Mercury Injection Capillary Pressure Data For Sample RM1-63DO-P01

Sample ID: RM1-63DO-P01 Swanson Air Permeability, mD: 1.04
Depth, ft: 9012.30 Hg Porosity, percent: 9.78

Mercury/Air Pressure (psi)	Equivalent Air/Brine Pressure (psi)	Mercury Saturation (fraction)	Incremental Mercury Saturation (fraction)	Wetting Phase Saturation (fraction)	Pore Throat Diameter (micron)	Height above Free Water (G/W) (ft)
11.5	2.22	0.000	0.0000	1.000	18.8	6.65
12.2	2.36	0.000	0.0000	1.000	17.7	7.06
12.9	2.50	0.000	0.0000	1.000	16.7	7.48
13.7	2.65	0.000	0.0000	1.000	15.7	7.94
14.5	2.81	0.000	0.0000	1.000	14.8	8.42
15.4	2.99	0.000	0.0000	1.000	14.0	8.94
16.3	3.17	0.000	0.0000	1.000	13.2	9.48
17.3	3.36	0.000	0.0000	1.000	12.4	10.1
18.4	3.57	0.000	0.0000	1.000	11.7	10.7
19.5	3.79	0.000	0.0000	1.000	11.0	11.3
20.7	4.02	0.000	0.0000	1.000	10.4	12.0
22.0	4.27	0.000	0.0000	1.000	9.79	12.8
23.4	4.53	0.000	0.0000	1.000	9.23	13.6
24.9	4.82	0.000	0.0000	1.000	8.67	14.4
26.4	5.11	0.000	0.0000	1.000	8.17	15.3
28.0	5.42	0.000	0.0000	1.000	7.70	16.2
29.7	5.75	0.000	0.0000	1.000	7.26	17.2
31.5	6.11	0.000	0.0000	1.000	6.84	18.3
33.4	6.48	0.000	0.0000	1.000	6.45	19.4
35.5	6.88	0.003	0.0026	0.997	6.08	20.6
37.6	7.29	0.005	0.0029	0.995	5.73	21.8
39.9	7.74	0.010	0.0041	0.990	5.40	23.2
42.4	8.21	0.015	0.0052	0.985	5.09	24.6
45.0	8.72	0.022	0.0075	0.978	4.79	26.1
46.4	8.99	0.025	0.0030	0.975	4.65	26.9
49.5	9.60	0.032	0.0068	0.968	4.35	28.7
53.0	10.28	0.049	0.0172	0.951	4.06	30.8
54.4	10.5	0.059	0.0097	0.941	3.96	31.6
58.5	11.3	0.095	0.0357	0.905	3.68	34.0
61.6	11.9	0.116	0.0215	0.884	3.50	35.8
66.6	12.9	0.145	0.0291	0.855	3.24	38.6
70.3	13.6	0.171	0.0256	0.829	3.07	40.8
75.4	14.6	0.200	0.0293	0.800	2.86	43.7
79.6	15.4	0.226	0.0259	0.774	2.71	46.2
85.2	16.5	0.248	0.0221	0.752	2.53	49.4
90.6	17.6	0.269	0.0211	0.731	2.38	52.6
96.2	18.6	0.290	0.0205	0.710	2.24	55.8

Table A.6 Mercury Injection Capillary Pressure Data For Sample RM1-63DO-P01

Sample ID: RM1-63DO-P01 Swanson Air Permeability, mD: 1.04
Depth, ft: 9012.30 Hg Porosity, percent: 9.78

Mercury/Air Pressure (psi)	Equivalent Air/Brine Pressure (psi)	Mercury Saturation (fraction)	Incremental Mercury Saturation (fraction)	Wetting Phase Saturation (fraction)	Pore Throat Diameter (micron)	Height above Free Water (G/W) (ft)
102	19.7	0.308	0.0183	0.692	2.12	59.1
108	20.9	0.327	0.0192	0.673	1.99	62.7
115	22.2	0.346	0.0191	0.654	1.88	66.5
122	23.7	0.365	0.0181	0.635	1.76	71.0
129	25.0	0.382	0.0178	0.618	1.67	74.9
138	26.8	0.403	0.0204	0.597	1.56	80.2
147	28.4	0.420	0.0171	0.580	1.47	85.2
156	30.2	0.440	0.0202	0.560	1.38	90.4
164	31.8	0.460	0.0199	0.540	1.31	95.3
176	34.1	0.479	0.0192	0.521	1.23	102.0
186	36.0	0.499	0.0197	0.501	1.16	108
198	38.4	0.517	0.0182	0.483	1.09	115
210	40.7	0.535	0.0176	0.465	1.03	122
223	43.3	0.552	0.0169	0.448	0.96	130
237	46.0	0.567	0.0159	0.433	0.909	138
250	48.5	0.583	0.0158	0.417	0.861	145
265	51.4	0.598	0.0149	0.402	0.812	154
283	54.8	0.612	0.0136	0.388	0.762	164
299	57.9	0.625	0.0128	0.375	0.721	173
319	61.8	0.637	0.0125	0.363	0.676	185
337	65.4	0.648	0.0113	0.352	0.639	196
358	69.4	0.660	0.0118	0.340	0.602	208
381	73.9	0.671	0.0104	0.329	0.565	221
405	78.5	0.681	0.0101	0.319	0.532	235
428	82.9	0.690	0.0095	0.310	0.504	248
456	88.3	0.699	0.0090	0.301	0.473	264
485	93.9	0.708	0.0088	0.292	0.445	281
514	99.5	0.716	0.0084	0.284	0.420	298
545	106	0.724	0.0080	0.276	0.395	316
577	112	0.732	0.0077	0.268	0.373	335
614	119	0.739	0.0073	0.261	0.351	356
653	126	0.746	0.0068	0.254	0.330	379
692	134	0.753	0.0069	0.247	0.311	402
734	142	0.759	0.0063	0.241	0.294	426
780	151	0.766	0.0062	0.234	0.276	452
826	160	0.772	0.0063	0.228	0.261	479
877	170	0.778	0.0059	0.222	0.246	509

Table A.6 Mercury Injection Capillary Pressure Data For Sample RM1-63DO-P01

Sample ID: RM1-63DO-P01 Swanson Air Permeability, mD: 1.04
Depth, ft: 9012.30 Hg Porosity, percent: 9.78

Mercury/Air Pressure (psi)	Equivalent Air/Brine Pressure (psi)	Mercury Saturation (fraction)	Incremental Mercury Saturation (fraction)	Wetting Phase Saturation (fraction)	Pore Throat Diameter (micron)	Height above Free Water (G/W) (ft)
929	180	0.783	0.0054	0.217	0.232	539
988	191	0.789	0.0054	0.211	0.218	573
1049	203	0.794	0.0052	0.206	0.205	609
1114	216	0.799	0.0049	0.201	0.193	647
1184	230	0.803	0.0047	0.197	0.182	687
1255	243	0.808	0.0049	0.192	0.172	728
1333	258	0.813	0.0046	0.187	0.162	773
1413	274	0.817	0.0043	0.183	0.153	820
1499	291	0.822	0.0043	0.178	0.144	870
1594	309	0.826	0.0040	0.174	0.135	925
1693	328	0.830	0.0041	0.170	0.127	982
1794	348	0.834	0.0041	0.166	0.120	1041
1908	370	0.838	0.0038	0.162	0.113	1107
2024	392	0.841	0.0038	0.159	0.107	1174
2146	416	0.845	0.0038	0.155	0.100	1245
2276	441	0.849	0.0037	0.151	0.095	1321
2420	469	0.852	0.0036	0.148	0.089	1404
2566	497	0.856	0.0036	0.144	0.084	1489
2725	528	0.860	0.0036	0.140	0.079	1581
2892	560	0.863	0.0033	0.137	0.075	1678
3068	595	0.866	0.0028	0.134	0.070	1780
3256	631	0.870	0.0040	0.130	0.066	1889
3456	670	0.873	0.0033	0.127	0.062	2005
3671	711	0.876	0.0032	0.124	0.059	2130
3896	755	0.879	0.0031	0.121	0.055	2260
4131	801	0.882	0.0029	0.118	0.052	2397
4386	850	0.886	0.0032	0.114	0.049	2545
4654	902	0.889	0.0031	0.111	0.046	2701
4941	958	0.892	0.0030	0.108	0.044	2867
5241	1016	0.895	0.0028	0.105	0.041	3041
5565	1078	0.897	0.0029	0.103	0.039	3229
5906	1145	0.900	0.0028	0.100	0.036	3427
6269	1215	0.903	0.0029	0.097	0.034	3637
6652	1289	0.906	0.0028	0.094	0.032	3860
7060	1368	0.909	0.0028	0.091	0.031	4097
7494	1452	0.911	0.0028	0.089	0.029	4348
7810	1514	0.914	0.0020	0.086	0.028	4532

Table A.6 Mercury Injection Capillary Pressure Data For Sample RM1-63DO-P01

Sample ID: RM1-63DO-P01 Swanson Air Permeability, mD: 1.04
Depth, ft: 9012.30 Hg Porosity, percent: 9.78

Mercury/Air Pressure (psi)	Equivalent Air/Brine Pressure (psi)	Mercury Saturation (fraction)	Incremental Mercury Saturation (fraction)	Wetting Phase Saturation (fraction)	Pore Throat Diameter (micron)	Height above Free Water (G/W) (ft)
8143	1578	0.916	0.0022	0.084	0.026	4725
8491	1645	0.918	0.0021	0.082	0.025	4926
8850	1715	0.920	0.0019	0.080	0.024	5135
9228	1788	0.922	0.0021	0.078	0.023	5354
9621	1865	0.924	0.0020	0.076	0.022	5583
10027	1943	0.926	0.0021	0.074	0.021	5818
10455	2026	0.928	0.0020	0.072	0.021	6066
10899	2112	0.930	0.0020	0.070	0.020	6324
11362	2202	0.932	0.0021	0.068	0.019	6592
11843	2295	0.934	0.0020	0.066	0.018	6872
12348	2393	0.936	0.0019	0.064	0.017	7164
12872	2495	0.939	0.0028	0.061	0.017	7469
13418	2600	0.940	0.0011	0.060	0.016	7786
13990	2711	0.942	0.0022	0.058	0.015	8117
14584	2826	0.944	0.0020	0.056	0.015	8462
15203	2946	0.946	0.0021	0.054	0.014	8821
15848	3071	0.948	0.0020	0.052	0.014	9196
16523	3202	0.950	0.0020	0.050	0.013	9587
17224	3338	0.952	0.0019	0.048	0.013	9994
17956	3480	0.954	0.0021	0.046	0.012	10418
18718	3627	0.956	0.0024	0.044	0.012	10861
19516	3782	0.958	0.0018	0.042	0.011	11323
20342	3942	0.960	0.0012	0.040	0.011	11803
21208	4110	0.961	0.0015	0.039	0.010	12305
22109	4284	0.963	0.0019	0.037	0.010	12828
23048	4466	0.965	0.0020	0.035	0.009	13373
24019	4655	0.967	0.0021	0.033	0.009	13936
25048	4854	0.968	0.0014	0.032	0.009	14533
26112	5060	0.970	0.0017	0.030	0.008	15151
27214	5274	0.972	0.0020	0.028	0.008	15790
28379	5500	0.974	0.0018	0.026	0.008	16466
29581	5733	0.975	0.0010	0.025	0.007	17163
30837	5976	0.977	0.0016	0.023	0.007	17892
32148	6230	0.978	0.0018	0.022	0.007	18653
33516	6495	0.980	0.0016	0.020	0.006	19446
34938	6771	0.982	0.0018	0.018	0.006	20271
36421	7058	0.983	0.0014	0.017	0.006	21132

Table A.6 Mercury Injection Capillary Pressure Data For Sample RM1-63DO-P01

Sample ID: RM1-63DO-P01 Swanson Air Permeability, mD: 1.04
Depth, ft: 9012.30 Hg Porosity, percent: 9.78

Mercury/Air Pressure (psi)	Equivalent Air/Brine Pressure (psi)	Mercury Saturation (fraction)	Incremental Mercury Saturation (fraction)	Wetting Phase Saturation (fraction)	Pore Throat Diameter (micron)	Height above Free Water (G/W) (ft)
37967	7358	0.985	0.0018	0.015	0.006	22029
39567	7668	0.987	0.0017	0.013	0.005	22957
41265	7997	0.989	0.0018	0.011	0.005	23943
42996	8332	0.990	0.0014	0.010	0.005	24947
44825	8687	0.990	0.0000	0.010	0.005	26008
46739	9058	0.991	0.0011	0.009	0.005	27119
48720	9442	0.993	0.0019	0.007	0.004	28268
50789	9843	0.995	0.0015	0.005	0.004	29469
52943	10260	0.996	0.0015	0.004	0.004	30718
55193	10696	0.997	0.0010	0.003	0.004	32024
57539	11151	0.999	0.0016	0.001	0.004	33385
59983	11624	1.000	0.0013	0.000	0.004	34803

Figure A.16 Mercury/Air Capillary Pressure For Sample RM1-63DO-P01

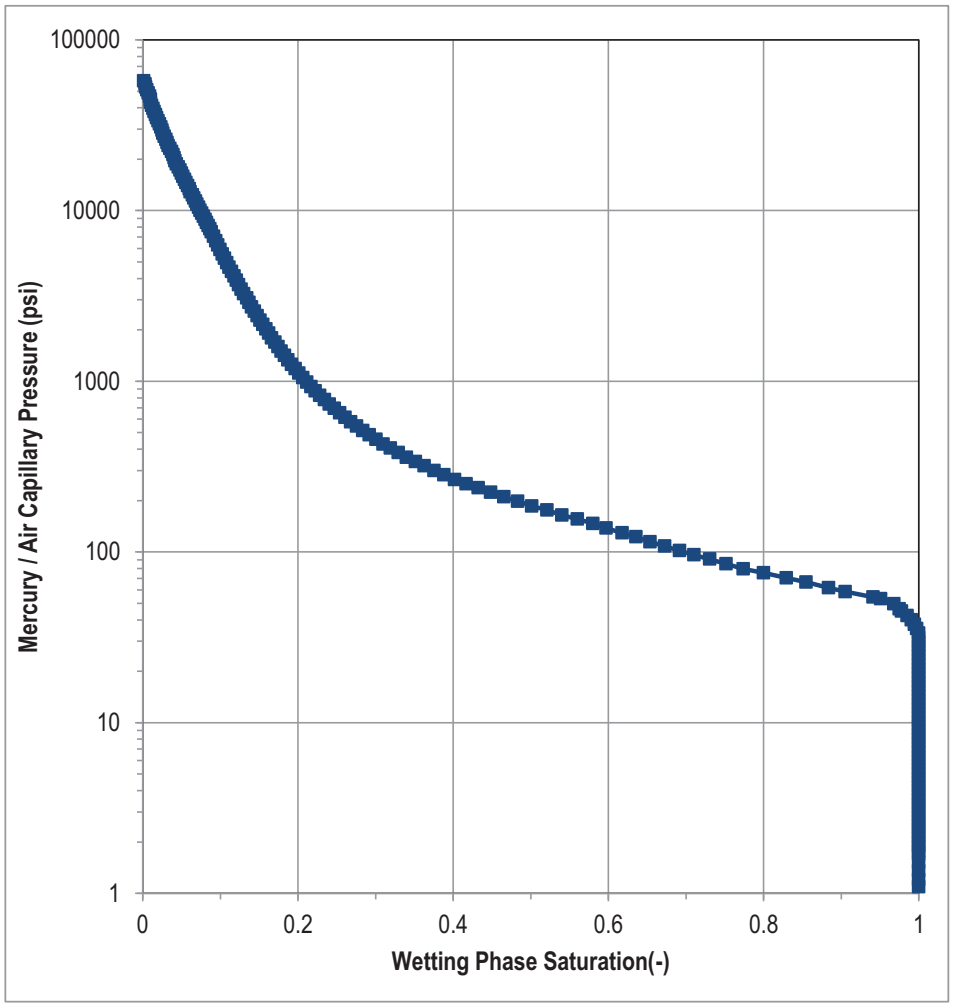


Figure A.17 Calculated Air /Brine Capillary Pressure And Height Above Free Water For Sample RM1-63DO-P01

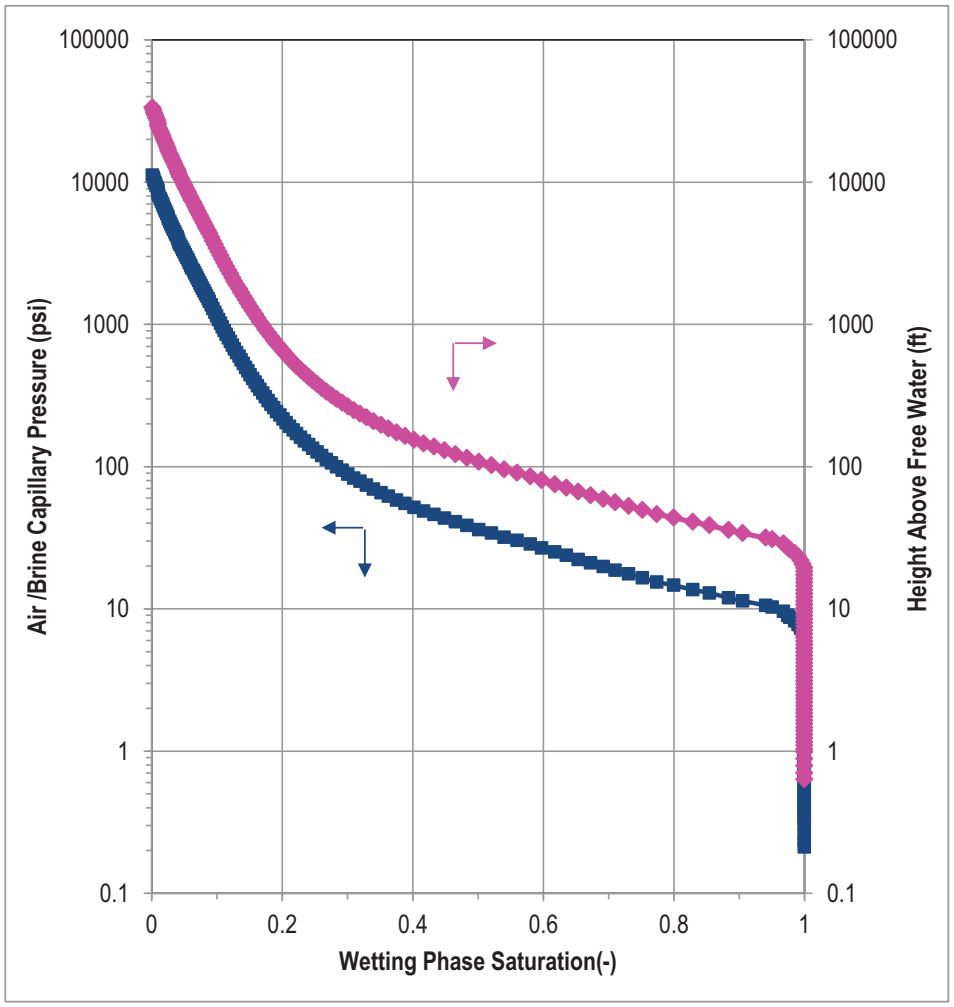


Figure A.18 Pore Throat Size Distribution For Sample RM1-63DO-P01

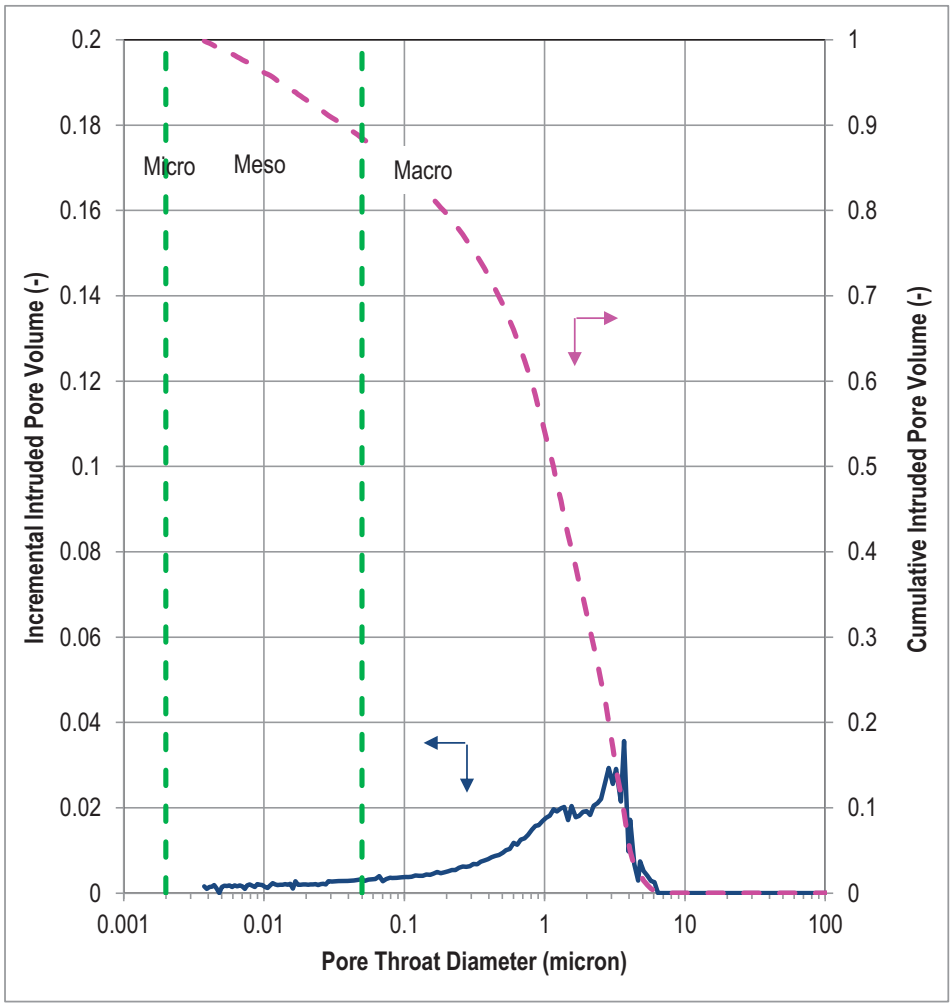


Table A.7 Mercury Injection Capillary Pressure Data For Sample RM1-63VO-P01

Sample ID: RM1-63VO-P01 Swanson Air Permeability, mD: 4.30
Depth, ft: 9013.90 Hg Porosity, percent: 12.2

Mercury/Air Pressure (psi)	Equivalent Air/Brine Pressure (psi)	Mercury Saturation (fraction)	Incremental Mercury Saturation (fraction)	Wetting Phase Saturation (fraction)	Pore Throat Diameter (micron)	Height above Free Water (G/W) (ft)
1.09	0.211	0.000	0.0000	1.000	198	0.632
1.20	0.233	0.000	0.0000	1.000	179	0.699
1.36	0.263	0.000	0.0000	1.000	159	0.787
1.52	0.294	0.000	0.0000	1.000	142	0.881
1.69	0.328	0.000	0.0000	1.000	127	0.983
1.77	0.344	0.000	0.0000	1.000	122	1.03
1.89	0.367	0.000	0.0000	1.000	114	1.10
2.00	0.388	0.000	0.0000	1.000	108	1.16
2.12	0.411	0.000	0.0000	1.000	102	1.23
2.25	0.437	0.000	0.0000	1.000	96	1.31
2.38	0.462	0.000	0.0000	1.000	90.4	1.38
2.53	0.489	0.000	0.0000	1.000	85.4	1.47
2.68	0.519	0.000	0.0000	1.000	80.5	1.55
2.83	0.549	0.000	0.0000	1.000	76.1	1.64
3.00	0.582	0.000	0.0000	1.000	71.8	1.74
3.18	0.617	0.000	0.0000	1.000	67.7	1.85
3.37	0.653	0.000	0.0000	1.000	64.0	1.96
3.57	0.693	0.000	0.0000	1.000	60.3	2.07
3.78	0.733	0.000	0.0000	1.000	57.0	2.19
4.01	0.778	0.000	0.0000	1.000	53.7	2.33
4.25	0.824	0.000	0.0000	1.000	50.7	2.47
4.51	0.873	0.000	0.0000	1.000	47.8	2.61
4.78	0.925	0.000	0.0000	1.000	45.1	2.77
5.06	0.981	0.000	0.0000	1.000	42.6	2.94
5.37	1.04	0.000	0.0000	1.000	40.2	3.11
5.69	1.10	0.000	0.0000	1.000	37.9	3.30
6.03	1.17	0.000	0.0000	1.000	35.7	3.50
6.39	1.24	0.000	0.0000	1.000	33.7	3.71
6.77	1.31	0.000	0.0000	1.000	31.8	3.93
7.18	1.39	0.000	0.0000	1.000	30.0	4.17
7.61	1.48	0.000	0.0000	1.000	28.3	4.42
8.07	1.56	0.000	0.0000	1.000	26.7	4.68
8.56	1.66	0.000	0.0000	1.000	25.2	4.97
9.08	1.76	0.000	0.0000	1.000	23.8	5.27
9.62	1.86	0.000	0.0000	1.000	22.4	5.58
10.2	1.98	0.000	0.0000	1.000	21.1	5.92
10.8	2.10	0.000	0.0000	1.000	19.9	6.28

Table A.7 Mercury Injection Capillary Pressure Data For Sample RM1-63VO-P01

Sample ID: RM1-63VO-P01 Swanson Air Permeability, mD: 4.30
Depth, ft: 9013.90 Hg Porosity, percent: 12.2

Mercury/Air Pressure (psi)	Equivalent Air/Brine Pressure (psi)	Mercury Saturation (fraction)	Incremental Mercury Saturation (fraction)	Wetting Phase Saturation (fraction)	Pore Throat Diameter (micron)	Height above Free Water (G/W) (ft)
11.5	2.22	0.000	0.0000	1.000	18.8	6.65
12.2	2.36	0.000	0.0000	1.000	17.7	7.06
12.9	2.50	0.000	0.0000	1.000	16.7	7.48
13.7	2.65	0.000	0.0000	1.000	15.7	7.94
14.5	2.81	0.000	0.0000	1.000	14.8	8.42
15.4	2.99	0.000	0.0000	1.000	14.0	8.94
16.3	3.17	0.000	0.0000	1.000	13.2	9.48
17.3	3.36	0.000	0.0000	1.000	12.4	10.1
18.4	3.57	0.000	0.0000	1.000	11.7	10.7
19.5	3.79	0.000	0.0000	1.000	11.0	11.3
20.7	4.02	0.000	0.0000	1.000	10.4	12.0
22.0	4.27	0.000	0.0000	1.000	9.79	12.8
23.4	4.53	0.000	0.0000	1.000	9.23	13.6
24.9	4.82	0.000	0.0000	1.000	8.67	14.4
26.4	5.11	0.000	0.0000	1.000	8.17	15.3
28.0	5.42	0.000	0.0000	1.000	7.70	16.2
29.7	5.75	0.000	0.0000	1.000	7.26	17.2
31.5	6.11	0.004	0.0038	0.996	6.84	18.3
33.4	6.48	0.008	0.0047	0.992	6.45	19.4
35.5	6.88	0.016	0.0071	0.984	6.08	20.6
37.6	7.29	0.026	0.0109	0.974	5.73	21.8
39.9	7.74	0.044	0.0175	0.956	5.40	23.2
42.4	8.21	0.069	0.0248	0.931	5.09	24.6
45.0	8.72	0.101	0.0318	0.899	4.79	26.1
47.7	9.25	0.135	0.0339	0.865	4.52	27.7
51.8	10.04	0.192	0.0578	0.808	4.16	30.0
55.6	10.78	0.244	0.0518	0.756	3.88	32.3
59.3	11.5	0.287	0.0428	0.713	3.64	34.4
63.4	12.3	0.328	0.0409	0.672	3.40	36.8
67.3	13.0	0.361	0.0327	0.639	3.20	39.1
71.2	13.8	0.398	0.0376	0.602	3.03	41.3
76.1	14.7	0.427	0.0291	0.573	2.83	44.1
80.9	15.7	0.452	0.0251	0.548	2.66	47.0
85.8	16.6	0.471	0.0190	0.529	2.51	49.8
91.3	17.7	0.492	0.0206	0.508	2.36	53.0
96.9	18.8	0.508	0.0161	0.492	2.23	56.2
103	19.9	0.523	0.0147	0.477	2.10	59.5

Table A.7 Mercury Injection Capillary Pressure Data For Sample RM1-63VO-P01

Sample ID: RM1-63VO-P01 Swanson Air Permeability, mD: 4.30
Depth, ft: 9013.90 Hg Porosity, percent: 12.2

Mercury/Air Pressure (psi)	Equivalent Air/Brine Pressure (psi)	Mercury Saturation (fraction)	Incremental Mercury Saturation (fraction)	Wetting Phase Saturation (fraction)	Pore Throat Diameter (micron)	Height above Free Water (G/W) (ft)
108	21.0	0.537	0.0140	0.463	1.99	62.9
116	22.4	0.548	0.0115	0.452	1.86	67.1
123	23.8	0.561	0.0127	0.439	1.76	71.2
131	25.3	0.572	0.0111	0.428	1.65	75.8
139	27.0	0.582	0.0101	0.418	1.55	80.8
148	28.6	0.593	0.0107	0.407	1.46	85.6
156	30.1	0.602	0.0095	0.398	1.39	90.2
165	32.1	0.612	0.0094	0.388	1.30	96.0
174	33.8	0.620	0.0088	0.380	1.24	101
185	35.9	0.630	0.0091	0.370	1.16	108
197	38.2	0.639	0.0092	0.361	1.09	114
210	40.7	0.646	0.0076	0.354	1.03	122
224	43.4	0.655	0.0083	0.345	0.96	130
237	45.9	0.663	0.0080	0.337	0.91	137
251	48.6	0.670	0.0075	0.330	0.859	146
268	51.9	0.677	0.0073	0.323	0.805	155
283	54.9	0.685	0.0076	0.315	0.761	164
300	58.1	0.692	0.0072	0.308	0.719	174
319	61.9	0.699	0.0071	0.301	0.675	185
339	65.6	0.706	0.0069	0.294	0.637	196
359	69.6	0.713	0.0068	0.287	0.600	208
381	73.8	0.720	0.0067	0.280	0.566	221
405	78.5	0.727	0.0068	0.273	0.532	235
431	83.5	0.733	0.0067	0.267	0.500	250
456	88.4	0.739	0.0059	0.261	0.472	265
485	94.1	0.745	0.0062	0.255	0.444	282
513	99.4	0.751	0.0054	0.249	0.420	298
545	106	0.757	0.0056	0.243	0.396	316
580	112	0.762	0.0057	0.238	0.372	337
614	119	0.768	0.0055	0.232	0.351	356
651	126	0.773	0.0052	0.227	0.331	378
693	134	0.778	0.0053	0.222	0.311	402
734	142	0.783	0.0050	0.217	0.294	426
780	151	0.788	0.0043	0.212	0.276	453
827	160	0.792	0.0045	0.208	0.261	480
880	170	0.796	0.0044	0.204	0.245	510
933	181	0.800	0.0037	0.200	0.231	541

Table A.7 Mercury Injection Capillary Pressure Data For Sample RM1-63VO-P01

Sample ID: RM1-63VO-P01 Swanson Air Permeability, mD: 4.30
Depth, ft: 9013.90 Hg Porosity, percent: 12.2

Mercury/Air Pressure (psi)	Equivalent Air/Brine Pressure (psi)	Mercury Saturation (fraction)	Incremental Mercury Saturation (fraction)	Wetting Phase Saturation (fraction)	Pore Throat Diameter (micron)	Height above Free Water (G/W) (ft)
989	192	0.804	0.0043	0.196	0.218	574
1051	204	0.808	0.0035	0.192	0.205	610
1118	217	0.812	0.0039	0.188	0.193	649
1187	230	0.815	0.0035	0.185	0.182	689
1258	244	0.819	0.0034	0.181	0.171	730
1337	259	0.822	0.0033	0.178	0.161	776
1418	275	0.825	0.0033	0.175	0.152	823
1501	291	0.828	0.0031	0.172	0.144	871
1597	309	0.831	0.0031	0.169	0.135	926
1692	328	0.834	0.0030	0.166	0.127	982
1795	348	0.837	0.0029	0.163	0.120	1041
1905	369	0.840	0.0029	0.160	0.113	1105
2025	392	0.843	0.0028	0.157	0.106	1175
2145	416	0.846	0.0028	0.154	0.100	1245
2279	442	0.849	0.0028	0.151	0.095	1322
2421	469	0.851	0.0029	0.149	0.089	1405
2568	498	0.854	0.0025	0.146	0.084	1490
2724	528	0.857	0.0034	0.143	0.079	1581
2893	561	0.859	0.0014	0.141	0.074	1679
3072	595	0.862	0.0031	0.138	0.070	1782
3257	631	0.864	0.0022	0.136	0.066	1890
3458	670	0.866	0.0024	0.134	0.062	2006
3671	711	0.869	0.0026	0.131	0.059	2130
3895	755	0.871	0.0022	0.129	0.055	2260
4136	802	0.874	0.0027	0.126	0.052	2400
4384	850	0.877	0.0029	0.123	0.049	2544
4655	902	0.879	0.0023	0.121	0.046	2701
4941	957	0.881	0.0017	0.119	0.044	2867
5244	1016	0.882	0.0015	0.118	0.041	3043
5564	1078	0.884	0.0018	0.116	0.039	3228
5907	1145	0.887	0.0031	0.113	0.036	3427
6270	1215	0.890	0.0028	0.110	0.034	3638
6655	1290	0.892	0.0021	0.108	0.032	3861
7062	1368	0.895	0.0026	0.105	0.031	4097
7495	1453	0.897	0.0017	0.103	0.029	4349
7813	1514	0.899	0.0020	0.101	0.028	4533
8146	1579	0.900	0.0019	0.100	0.026	4726

Table A.7 Mercury Injection Capillary Pressure Data For Sample RM1-63VO-P01

Sample ID: RM1-63VO-P01 Swanson Air Permeability, mD: 4.30
Depth, ft: 9013.90 Hg Porosity, percent: 12.2

Mercury/Air Pressure (psi)	Equivalent Air/Brine Pressure (psi)	Mercury Saturation (fraction)	Incremental Mercury Saturation (fraction)	Wetting Phase Saturation (fraction)	Pore Throat Diameter (micron)	Height above Free Water (G/W) (ft)
8493	1646	0.902	0.0019	0.098	0.025	4928
8853	1716	0.904	0.0017	0.096	0.024	5137
9228	1788	0.906	0.0022	0.094	0.023	5354
9621	1864	0.909	0.0024	0.091	0.022	5582
10029	1943	0.910	0.0015	0.090	0.021	5819
10455	2026	0.911	0.0004	0.089	0.021	6066
10900	2112	0.913	0.0023	0.087	0.020	6324
11363	2202	0.915	0.0021	0.085	0.019	6593
11844	2295	0.917	0.0018	0.083	0.018	6872
12349	2393	0.919	0.0023	0.081	0.017	7165
12873	2495	0.921	0.0019	0.079	0.017	7469
13419	2601	0.923	0.0019	0.077	0.016	7786
13990	2711	0.925	0.0026	0.075	0.015	8117
14586	2827	0.927	0.0010	0.073	0.015	8463
15204	2946	0.929	0.0023	0.071	0.014	8821
15850	3072	0.931	0.0021	0.069	0.014	9197
16522	3202	0.933	0.0020	0.067	0.013	9586
17225	3338	0.935	0.0022	0.065	0.013	9994
17957	3480	0.937	0.0019	0.063	0.012	10419
18720	3628	0.939	0.0023	0.061	0.012	10862
19515	3782	0.942	0.0028	0.058	0.011	11323
20343	3942	0.943	0.0004	0.057	0.011	11804
21207	4110	0.945	0.0024	0.055	0.010	12304
22109	4285	0.947	0.0023	0.053	0.010	12828
23049	4467	0.950	0.0027	0.050	0.009	13373
24028	4656	0.952	0.0019	0.048	0.009	13942
25049	4854	0.954	0.0025	0.046	0.009	14534
26113	5061	0.956	0.0018	0.044	0.008	15151
27223	5276	0.958	0.0024	0.042	0.008	15795
28378	5499	0.960	0.0020	0.040	0.008	16466
29584	5733	0.963	0.0024	0.037	0.007	17165
30842	5977	0.965	0.0022	0.035	0.007	17895
32150	6230	0.967	0.0019	0.033	0.007	18654
33513	6495	0.970	0.0027	0.030	0.006	19445
34938	6771	0.972	0.0020	0.028	0.006	20272
36410	7056	0.974	0.0023	0.026	0.006	21126
37955	7355	0.976	0.0024	0.024	0.006	22022

Table A.7 Mercury Injection Capillary Pressure Data For Sample RM1-63VO-P01

Sample ID: RM1-63VO-P01 Swanson Air Permeability, mD: 4.30
Depth, ft: 9013.90 Hg Porosity, percent: 12.2

Mercury/Air Pressure (psi)	Equivalent Air/Brine Pressure (psi)	Mercury Saturation (fraction)	Incremental Mercury Saturation (fraction)	Wetting Phase Saturation (fraction)	Pore Throat Diameter (micron)	Height above Free Water (G/W) (ft)
39572	7669	0.980	0.0036	0.020	0.005	22960
41266	7997	0.980	0.0000	0.020	0.005	23943
42998	8333	0.980	0.0001	0.020	0.005	24948
44828	8687	0.983	0.0028	0.017	0.005	26010
46735	9057	0.985	0.0024	0.015	0.005	27117
48723	9442	0.988	0.0026	0.012	0.004	28270
50790	9843	0.990	0.0025	0.010	0.004	29469
52942	10260	0.993	0.0022	0.007	0.004	30718
55192	10696	0.995	0.0023	0.005	0.004	32023
57539	11151	0.997	0.0023	0.003	0.004	33385
59982	11624	1.000	0.0028	0.000	0.004	34803

Figure A.19 Mercury/Air Capillary Pressure For Sample RM1-63VO-P01

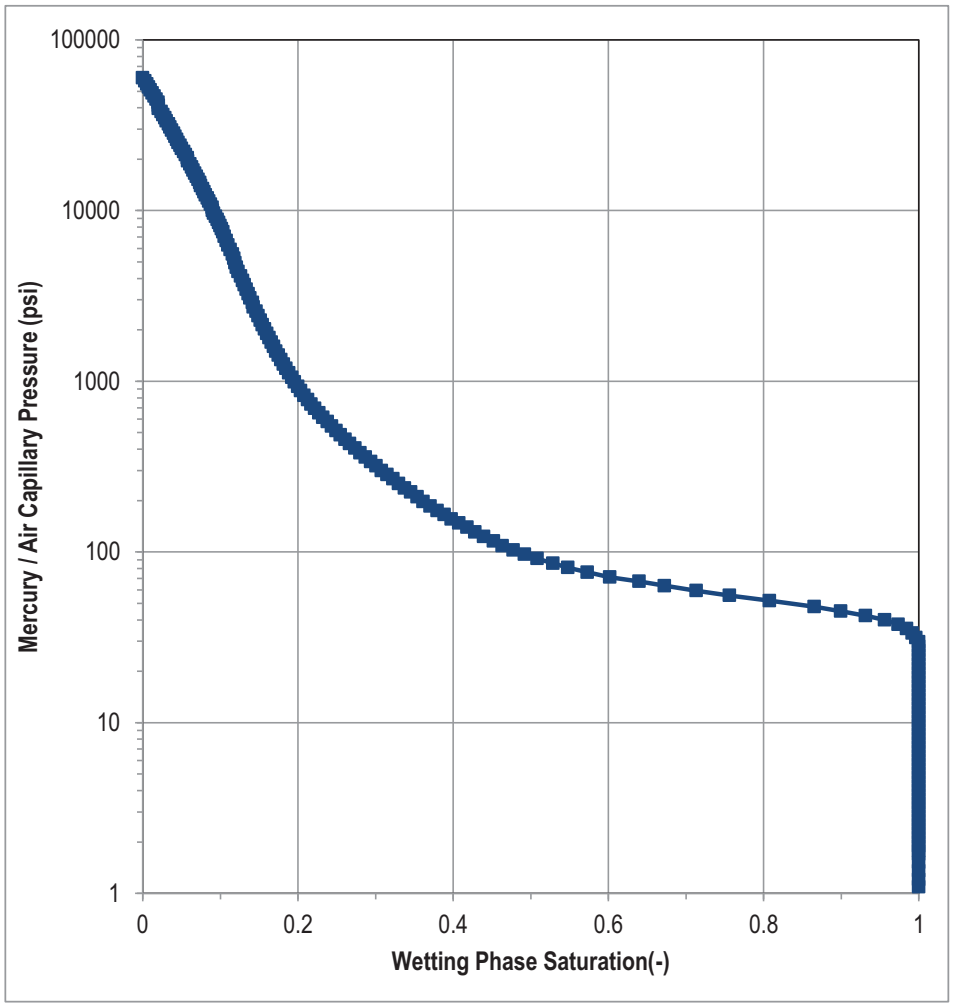


Figure A.20 Calculated Air /Brine Capillary Pressure And Height Above Free Water For Sample RM1-63VO-P01

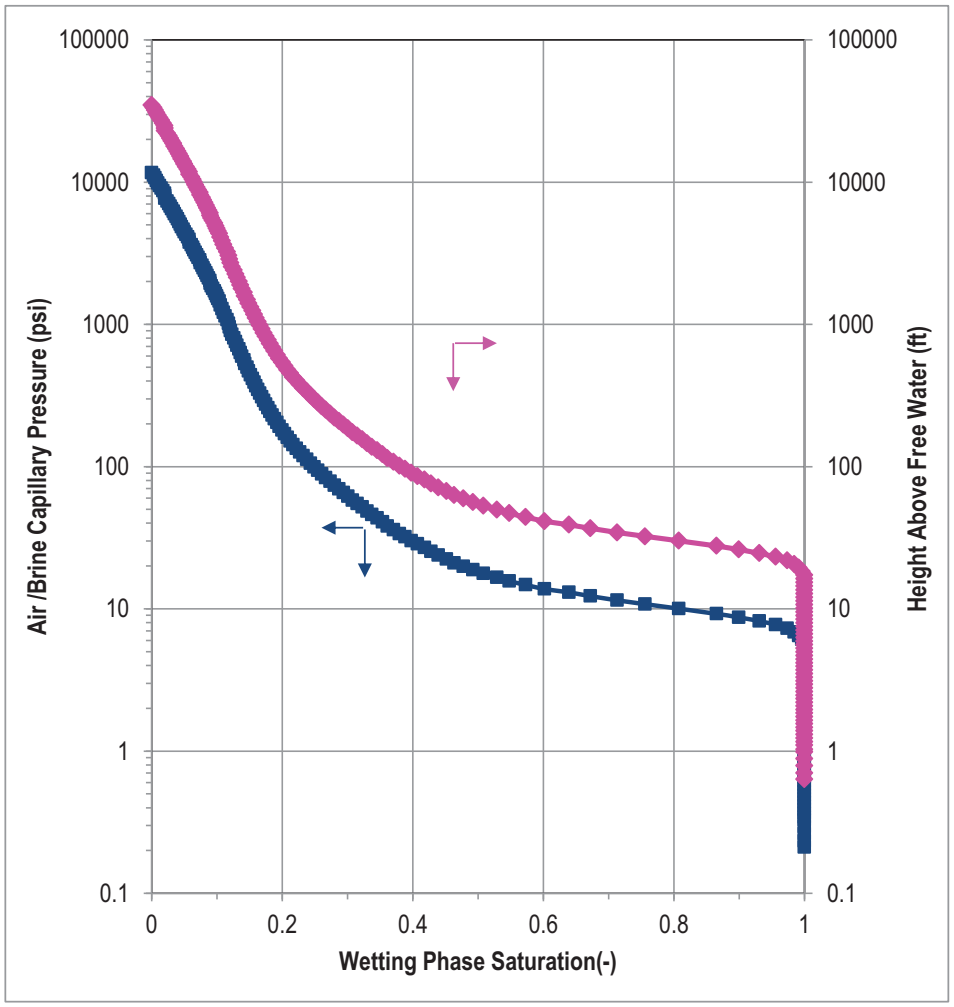


Figure A.21 Pore Throat Size Distribution For Sample RM1-63VO-P01

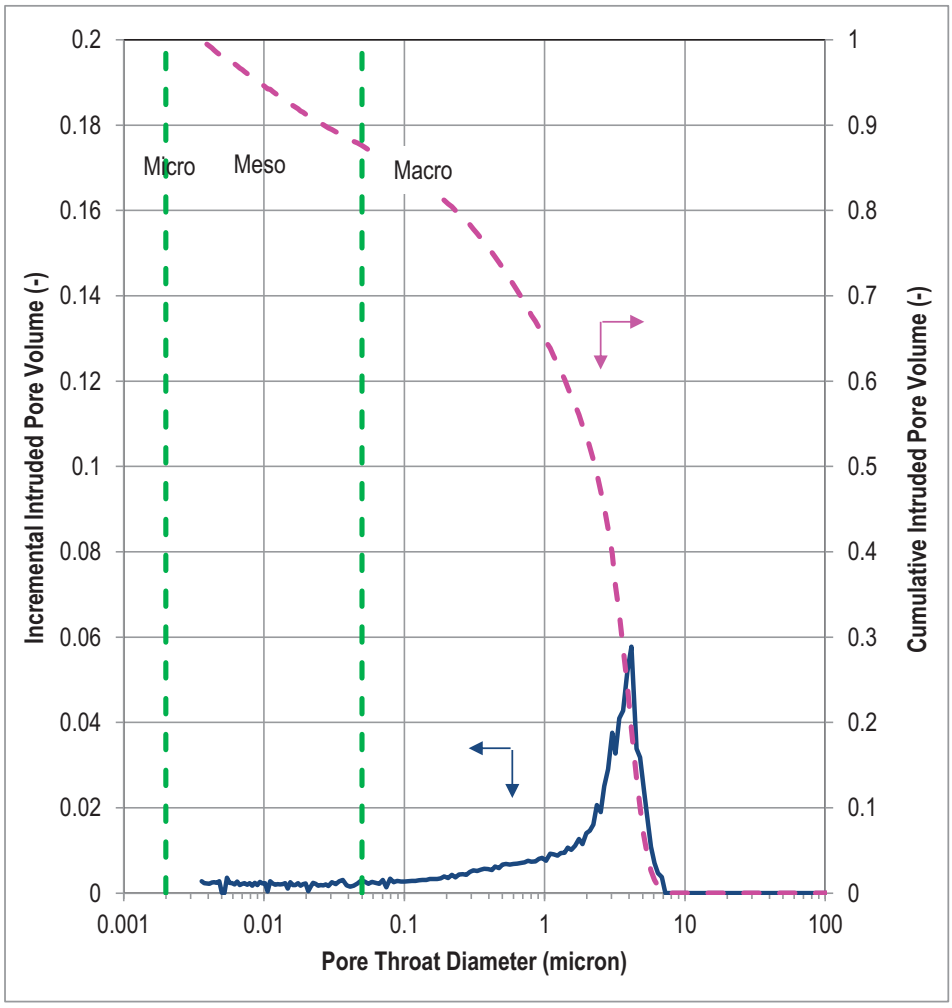


Table A.8 Mercury Injection Capillary Pressure Data For Sample RM1-64HB-P01

Sample ID: RM1-64HB-P01 Swanson Air Permeability, mD: 8.18
Depth, ft: 9015.60 Hg Porosity, percent: 13.0

Mercury/Air Pressure (psi)	Equivalent Air/Brine Pressure (psi)	Mercury Saturation (fraction)	Incremental Mercury Saturation (fraction)	Wetting Phase Saturation (fraction)	Pore Throat Diameter (micron)	Height above Free Water (G/W) (ft)
1.09	0.212	0.000	0.0000	1.000	197	0.633
1.20	0.232	0.000	0.0000	1.000	180	0.696
1.36	0.263	0.000	0.0000	1.000	159	0.788
1.52	0.295	0.000	0.0000	1.000	142	0.883
1.70	0.330	0.000	0.0000	1.000	127	0.987
1.75	0.339	0.000	0.0000	1.000	123	1.01
1.91	0.369	0.000	0.0000	1.000	113	1.11
2.00	0.387	0.000	0.0000	1.000	108	1.16
2.13	0.412	0.000	0.0000	1.000	101	1.23
2.25	0.436	0.000	0.0000	1.000	95.8	1.31
2.38	0.462	0.000	0.0000	1.000	90.4	1.38
2.52	0.489	0.000	0.0000	1.000	85.5	1.46
2.68	0.519	0.000	0.0000	1.000	80.4	1.56
2.84	0.550	0.000	0.0000	1.000	76.0	1.65
3.01	0.583	0.000	0.0000	1.000	71.6	1.75
3.18	0.617	0.000	0.0000	1.000	67.7	1.85
3.37	0.654	0.000	0.0000	1.000	63.9	1.96
3.58	0.693	0.000	0.0000	1.000	60.2	2.08
3.79	0.734	0.000	0.0000	1.000	56.9	2.20
4.01	0.778	0.000	0.0000	1.000	53.7	2.33
4.26	0.826	0.000	0.0000	1.000	50.6	2.47
4.51	0.873	0.000	0.0000	1.000	47.8	2.61
4.78	0.926	0.000	0.0000	1.000	45.1	2.77
5.07	0.982	0.000	0.0000	1.000	42.5	2.94
5.37	1.04	0.000	0.0000	1.000	40.2	3.11
5.69	1.10	0.000	0.0000	1.000	37.9	3.30
6.03	1.17	0.000	0.0000	1.000	35.8	3.50
6.40	1.24	0.000	0.0000	1.000	33.7	3.71
6.78	1.31	0.000	0.0000	1.000	31.8	3.93
7.19	1.39	0.000	0.0000	1.000	30.0	4.17
7.62	1.48	0.000	0.0000	1.000	28.3	4.42
8.07	1.56	0.000	0.0000	1.000	26.7	4.69
8.56	1.66	0.000	0.0000	1.000	25.2	4.97
9.08	1.76	0.000	0.0000	1.000	23.7	5.27
9.62	1.87	0.000	0.0000	1.000	22.4	5.58
10.2	1.98	0.000	0.0000	1.000	21.1	5.92
10.8	2.10	0.000	0.0000	1.000	19.9	6.28

Table A.8 Mercury Injection Capillary Pressure Data For Sample RM1-64HB-P01

Sample ID: RM1-64HB-P01 Swanson Air Permeability, mD: 8.18
Depth, ft: 9015.60 Hg Porosity, percent: 13.0

Mercury/Air Pressure (psi)	Equivalent Air/Brine Pressure (psi)	Mercury Saturation (fraction)	Incremental Mercury Saturation (fraction)	Wetting Phase Saturation (fraction)	Pore Throat Diameter (micron)	Height above Free Water (G/W) (ft)
11.5	2.22	0.000	0.0000	1.000	18.8	6.65
12.2	2.36	0.000	0.0000	1.000	17.7	7.06
12.9	2.50	0.000	0.0000	1.000	16.7	7.48
13.7	2.65	0.000	0.0000	1.000	15.8	7.93
14.5	2.81	0.000	0.0000	1.000	14.8	8.43
15.4	2.99	0.000	0.0000	1.000	14.0	8.94
16.4	3.17	0.000	0.0000	1.000	13.2	9.49
17.4	3.36	0.000	0.0000	1.000	12.4	10.1
18.4	3.57	0.000	0.0000	1.000	11.7	10.7
19.5	3.79	0.000	0.0000	1.000	11.0	11.3
20.7	4.02	0.000	0.0000	1.000	10.4	12.0
22.0	4.26	0.000	0.0000	1.000	9.79	12.8
23.3	4.52	0.005	0.0048	0.995	9.23	13.5
24.9	4.82	0.010	0.0055	0.990	8.67	14.4
26.3	5.10	0.016	0.0061	0.984	8.19	15.3
28.0	5.42	0.026	0.0092	0.974	7.70	16.2
29.7	5.75	0.038	0.0126	0.962	7.26	17.2
31.5	6.10	0.056	0.0183	0.944	6.84	18.3
33.4	6.48	0.085	0.0284	0.915	6.45	19.4
35.5	6.87	0.123	0.0379	0.877	6.08	20.6
37.6	7.29	0.175	0.0519	0.825	5.73	21.8
39.9	7.74	0.231	0.0566	0.769	5.40	23.2
42.4	8.22	0.290	0.0590	0.710	5.08	24.6
45.8	8.88	0.348	0.0579	0.652	4.70	26.6
51.7	10.02	0.388	0.0398	0.612	4.17	30.0
55.1	10.7	0.421	0.0332	0.579	3.91	32.0
58.2	11.3	0.448	0.0267	0.552	3.70	33.8
62.7	12.1	0.472	0.0246	0.528	3.44	36.4
66.3	12.9	0.489	0.0166	0.511	3.25	38.5
69.8	13.5	0.507	0.0181	0.493	3.09	40.5
75.2	14.6	0.524	0.0167	0.476	2.87	43.6
79.3	15.4	0.538	0.0141	0.462	2.72	46.0
85.0	16.5	0.552	0.0137	0.448	2.54	49.3
89.4	17.3	0.563	0.0111	0.437	2.41	51.9
95	18.4	0.575	0.0124	0.425	2.27	55.0

Table A.8 Mercury Injection Capillary Pressure Data For Sample RM1-64HB-P01

Sample ID: RM1-64HB-P01 Swanson Air Permeability, mD: 8.18
Depth, ft: 9015.60 Hg Porosity, percent: 13.0

Mercury/Air Pressure (psi)	Equivalent Air/Brine Pressure (psi)	Mercury Saturation (fraction)	Incremental Mercury Saturation (fraction)	Wetting Phase Saturation (fraction)	Pore Throat Diameter (micron)	Height above Free Water (G/W) (ft)
101	19.5	0.587	0.0115	0.413	2.14	58.4
107	20.7	0.596	0.0098	0.404	2.02	61.9
113	21.8	0.606	0.0095	0.394	1.91	65.4
122	23.6	0.616	0.0103	0.384	1.77	70.6
129	25.0	0.625	0.0088	0.375	1.67	74.9
137	26.5	0.634	0.0090	0.366	1.58	79.2
144	27.9	0.642	0.0083	0.358	1.50	83.6
154	29.9	0.651	0.0090	0.349	1.40	89.5
164	31.8	0.660	0.0083	0.340	1.31	95.1
175	33.8	0.668	0.0081	0.332	1.23	101
184	35.7	0.675	0.0072	0.325	1.17	107
196	38.1	0.682	0.0073	0.318	1.10	114
207	40.1	0.689	0.0072	0.311	1.04	120
223	43.2	0.697	0.0078	0.303	0.97	129
235	45.6	0.704	0.0070	0.296	0.917	136
250	48.5	0.710	0.0062	0.290	0.862	145
265	51.3	0.717	0.0070	0.283	0.815	154
281	54.4	0.724	0.0064	0.276	0.768	163
300	58.2	0.730	0.0065	0.270	0.718	174
317	61.5	0.737	0.0065	0.263	0.680	184
339	65.7	0.743	0.0063	0.257	0.636	197
357	69.2	0.749	0.0061	0.251	0.604	207
382	74.0	0.755	0.0061	0.245	0.565	221
404	78.3	0.761	0.0061	0.239	0.533	235
429	83.2	0.768	0.0062	0.232	0.502	249
455	88.2	0.773	0.0060	0.227	0.474	264
481	93.2	0.779	0.0055	0.221	0.448	279
513	99.4	0.785	0.0058	0.215	0.420	298
544	105	0.790	0.0055	0.210	0.396	316
580	112	0.796	0.0055	0.204	0.371	337
611	118	0.801	0.0053	0.199	0.353	355
652	126	0.807	0.0056	0.193	0.331	378
689	133	0.812	0.0048	0.188	0.313	400
731	142	0.817	0.0049	0.183	0.295	424
780	151	0.822	0.0053	0.178	0.276	452
829	161	0.826	0.0042	0.174	0.260	481
875	170	0.830	0.0044	0.170	0.246	508

Table A.8 Mercury Injection Capillary Pressure Data For Sample RM1-64HB-P01

Sample ID: RM1-64HB-P01 Swanson Air Permeability, mD: 8.18
Depth, ft: 9015.60 Hg Porosity, percent: 13.0

Mercury/Air Pressure (psi)	Equivalent Air/Brine Pressure (psi)	Mercury Saturation (fraction)	Incremental Mercury Saturation (fraction)	Wetting Phase Saturation (fraction)	Pore Throat Diameter (micron)	Height above Free Water (G/W) (ft)
929	180	0.834	0.0040	0.166	0.232	539
989	192	0.838	0.0040	0.162	0.218	574
1050	203	0.842	0.0038	0.158	0.205	609
1117	216	0.846	0.0039	0.154	0.193	648
1183	229	0.850	0.0038	0.150	0.182	687
1257	244	0.853	0.0036	0.147	0.171	729
1332	258	0.857	0.0035	0.143	0.162	773
1413	274	0.861	0.0039	0.139	0.153	820
1501	291	0.863	0.0025	0.137	0.144	871
1592	308	0.863	0.0000	0.137	0.135	924
1692	328	0.869	0.0060	0.131	0.127	982
1796	348	0.872	0.0029	0.128	0.120	1042
1906	369	0.875	0.0029	0.125	0.113	1106
2021	392	0.878	0.0027	0.122	0.107	1173
2145	416	0.881	0.0027	0.119	0.100	1245
2279	442	0.883	0.0027	0.117	0.095	1322
2416	468	0.886	0.0028	0.114	0.089	1402
2565	497	0.889	0.0026	0.111	0.084	1488
2722	527	0.891	0.0026	0.109	0.079	1579
2891	560	0.894	0.0026	0.106	0.075	1678
3071	595	0.897	0.0026	0.103	0.070	1782
3257	631	0.899	0.0026	0.101	0.066	1890
3459	670	0.902	0.0025	0.098	0.062	2007
3668	711	0.904	0.0025	0.096	0.059	2128
3893	754	0.907	0.0024	0.093	0.055	2259
4133	801	0.909	0.0025	0.091	0.052	2398
4386	850	0.911	0.0024	0.089	0.049	2545
4654	902	0.914	0.0024	0.086	0.046	2700
4939	957	0.916	0.0023	0.084	0.044	2866
5244	1016	0.918	0.0023	0.082	0.041	3043
5564	1078	0.921	0.0024	0.079	0.039	3228
5904	1144	0.923	0.0023	0.077	0.037	3426
6268	1215	0.925	0.0023	0.075	0.034	3637
6651	1289	0.928	0.0022	0.072	0.032	3859
7060	1368	0.930	0.0022	0.070	0.031	4096
7495	1453	0.932	0.0023	0.068	0.029	4349
7812	1514	0.934	0.0019	0.066	0.028	4532

Table A.8 Mercury Injection Capillary Pressure Data For Sample RM1-64HB-P01

Sample ID: RM1-64HB-P01 Swanson Air Permeability, mD: 8.18
Depth, ft: 9015.60 Hg Porosity, percent: 13.0

Mercury/Air Pressure (psi)	Equivalent Air/Brine Pressure (psi)	Mercury Saturation (fraction)	Incremental Mercury Saturation (fraction)	Wetting Phase Saturation (fraction)	Pore Throat Diameter (micron)	Height above Free Water (G/W) (ft)
8143	1578	0.936	0.0017	0.064	0.026	4725
8490	1645	0.937	0.0017	0.063	0.025	4926
8851	1715	0.939	0.0017	0.061	0.024	5135
9228	1788	0.941	0.0017	0.059	0.023	5354
9617	1864	0.942	0.0016	0.058	0.022	5580
10027	1943	0.944	0.0017	0.056	0.021	5818
10455	2026	0.946	0.0016	0.054	0.021	6066
10898	2112	0.947	0.0016	0.053	0.020	6323
11361	2202	0.949	0.0016	0.051	0.019	6592
11845	2295	0.950	0.0016	0.050	0.018	6873
12348	2393	0.952	0.0017	0.048	0.017	7165
12872	2494	0.954	0.0016	0.046	0.017	7468
13417	2600	0.956	0.0017	0.044	0.016	7785
13988	2711	0.957	0.0014	0.043	0.015	8116
14584	2826	0.959	0.0016	0.041	0.015	8462
15202	2946	0.960	0.0015	0.040	0.014	8821
15848	3071	0.962	0.0016	0.038	0.014	9196
16522	3202	0.963	0.0015	0.037	0.013	9586
17224	3338	0.965	0.0016	0.035	0.013	9994
17947	3478	0.966	0.0016	0.034	0.012	10413
18716	3627	0.968	0.0017	0.032	0.012	10859
19517	3782	0.970	0.0016	0.030	0.011	11324
20343	3942	0.971	0.0014	0.029	0.011	11804
21207	4110	0.972	0.0014	0.028	0.010	12305
22108	4284	0.974	0.0015	0.026	0.010	12828
23048	4466	0.975	0.0014	0.025	0.009	13373
24026	4656	0.977	0.0013	0.023	0.009	13940
25049	4854	0.978	0.0015	0.022	0.009	14534
26113	5060	0.979	0.0012	0.021	0.008	15151
27221	5275	0.981	0.0013	0.019	0.008	15794
28378	5499	0.982	0.0014	0.018	0.008	16465
29584	5733	0.983	0.0012	0.017	0.007	17165
30840	5977	0.985	0.0013	0.015	0.007	17894
32149	6230	0.986	0.0012	0.014	0.007	18654
33514	6495	0.987	0.0012	0.013	0.006	19446
34939	6771	0.988	0.0012	0.012	0.006	20272
36421	7058	0.989	0.0012	0.011	0.006	21132

Table A.8 Mercury Injection Capillary Pressure Data For Sample RM1-64HB-P01

Sample ID: RM1-64HB-P01 Swanson Air Permeability, mD: 8.18
Depth, ft: 9015.60 Hg Porosity, percent: 13.0

Mercury/Air Pressure (psi)	Equivalent Air/Brine Pressure (psi)	Mercury Saturation (fraction)	Incremental Mercury Saturation (fraction)	Wetting Phase Saturation (fraction)	Pore Throat Diameter (micron)	Height above Free Water (G/W) (ft)
37972	7359	0.990	0.0010	0.010	0.006	22032
39567	7668	0.991	0.0010	0.009	0.005	22957
41265	7997	0.992	0.0010	0.008	0.005	23943
43000	8333	0.993	0.0010	0.007	0.005	24949
44840	8690	0.994	0.0009	0.006	0.005	26017
46738	9057	0.995	0.0010	0.005	0.005	27118
48712	9440	0.996	0.0008	0.004	0.004	28264
50791	9843	0.997	0.0007	0.003	0.004	29470
52939	10259	0.998	0.0010	0.002	0.004	30716
55192	10696	0.999	0.0008	0.001	0.004	32023
57539	11151	0.999	0.0008	0.001	0.004	33385
59982	11624	1.000	0.0007	0.000	0.004	34802

Figure A.22 Mercury/Air Capillary Pressure For Sample RM1-64HB-P01

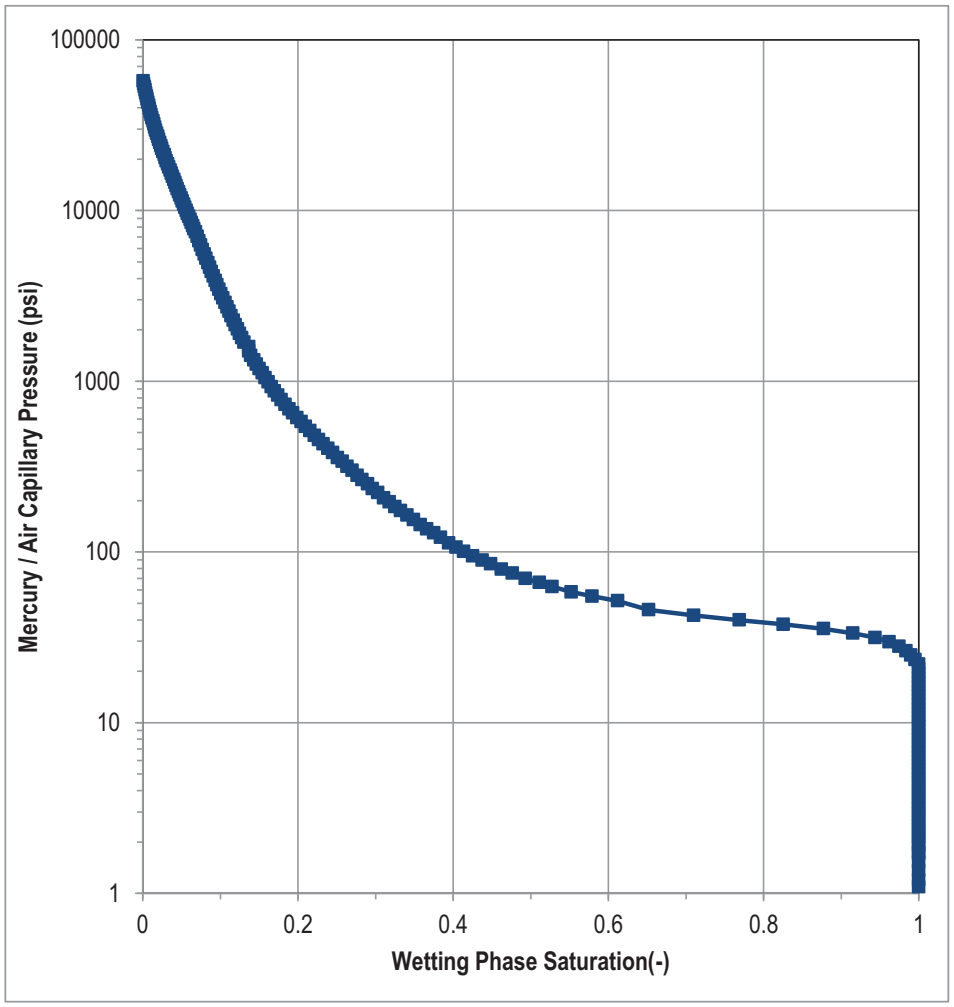


Figure A.23 Calculated Air /Brine Capillary Pressure And Height Above Free Water For Sample RM1-64HB-P01

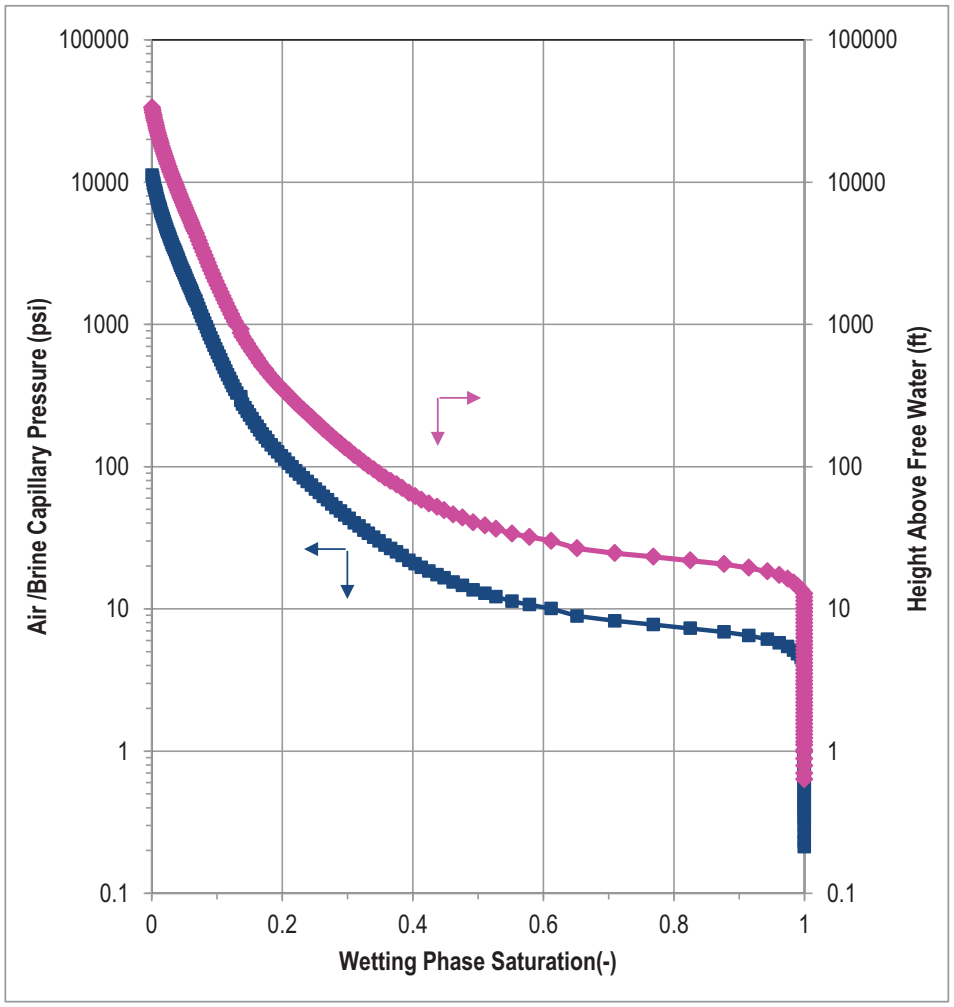


Figure A.24 Pore Throat Size Distribution For Sample RM1-64HB-P01

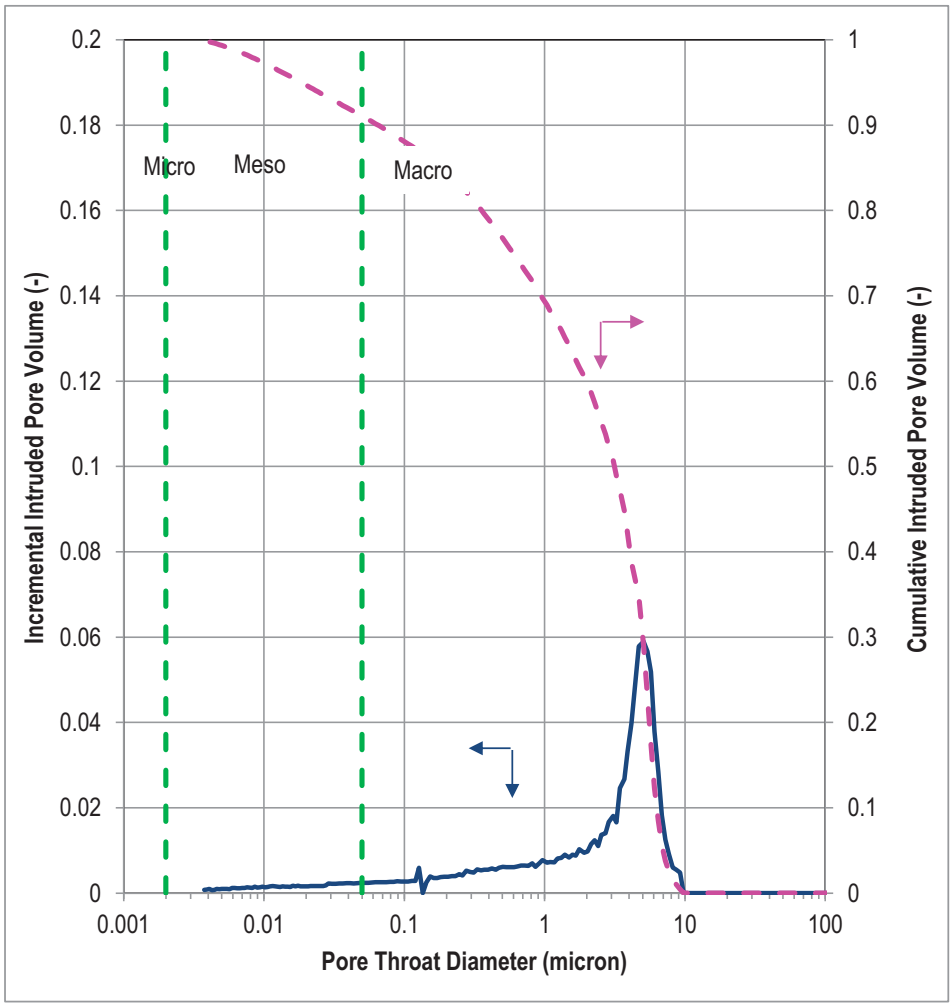


Table A.9 Mercury Injection Capillary Pressure Data For Sample RM1-79HO-P01

Sample ID: RM1-79HO-P01 Swanson Air Permeability, mD: 192
Depth, ft: 9029.20 Hg Porosity, percent: 17.8

Mercury/Air Pressure (psi)	Equivalent Air/Brine Pressure (psi)	Mercury Saturation (fraction)	Incremental Mercury Saturation (fraction)	Wetting Phase Saturation (fraction)	Pore Throat Diameter (micron)	Height above Free Water (G/W) (ft)
1.09	0.211	0.000	0.0000	1.000	198	0.632
1.20	0.233	0.000	0.0000	1.000	179	0.699
1.36	0.263	0.000	0.0000	1.000	159	0.787
1.52	0.294	0.000	0.0000	1.000	142	0.881
1.69	0.328	0.000	0.0000	1.000	127	0.983
1.77	0.344	0.000	0.0000	1.000	122	1.03
1.89	0.367	0.000	0.0000	1.000	114	1.10
2.00	0.388	0.000	0.0000	1.000	108	1.16
2.12	0.411	0.000	0.0000	1.000	102	1.23
2.25	0.437	0.000	0.0000	1.000	95.6	1.31
2.38	0.462	0.000	0.0000	1.000	90.4	1.38
2.53	0.489	0.000	0.0000	1.000	85.4	1.47
2.68	0.519	0.000	0.0000	1.000	80.5	1.55
2.83	0.549	0.000	0.0000	1.000	76.1	1.64
3.00	0.582	0.000	0.0000	1.000	71.8	1.74
3.18	0.617	0.000	0.0000	1.000	67.7	1.85
3.37	0.653	0.000	0.0000	1.000	64.0	1.96
3.57	0.693	0.000	0.0000	1.000	60.3	2.07
3.78	0.733	0.000	0.0000	1.000	57.0	2.19
4.01	0.778	0.000	0.0000	1.000	53.7	2.33
4.25	0.824	0.000	0.0000	1.000	50.7	2.47
4.51	0.873	0.000	0.0000	1.000	47.8	2.61
4.78	0.925	0.000	0.0000	1.000	45.1	2.77
5.06	0.981	0.000	0.0000	1.000	42.6	2.94
5.37	1.04	0.000	0.0000	1.000	40.2	3.11
5.69	1.10	0.000	0.0000	1.000	37.9	3.30
6.03	1.17	0.000	0.0000	1.000	35.7	3.50
6.39	1.24	0.000	0.0000	1.000	33.7	3.71
6.77	1.31	0.004	0.0043	0.996	31.8	3.93
7.18	1.39	0.009	0.0051	0.991	30.0	4.17
7.61	1.48	0.015	0.0060	0.985	28.3	4.42
8.07	1.56	0.024	0.0088	0.976	26.7	4.68
8.56	1.66	0.037	0.0127	0.963	25.2	4.97
9.08	1.76	0.059	0.0220	0.941	23.8	5.27
9.62	1.86	0.098	0.0396	0.902	22.4	5.58
10.2	1.98	0.168	0.0692	0.832	21.1	5.92
10.8	2.10	0.254	0.0868	0.746	19.9	6.28

Table A.9 Mercury Injection Capillary Pressure Data For Sample RM1-79HO-P01

Sample ID: RM1-79HO-P01 Swanson Air Permeability, mD: 192
Depth, ft: 9029.20 Hg Porosity, percent: 17.8

Mercury/Air Pressure (psi)	Equivalent Air/Brine Pressure (psi)	Mercury Saturation (fraction)	Incremental Mercury Saturation (fraction)	Wetting Phase Saturation (fraction)	Pore Throat Diameter (micron)	Height above Free Water (G/W) (ft)
11.5	2.22	0.336	0.0820	0.664	18.8	6.65
12.2	2.36	0.401	0.0650	0.599	17.7	7.06
12.9	2.50	0.453	0.0512	0.547	16.7	7.48
13.7	2.65	0.495	0.0426	0.505	15.7	7.94
14.5	2.81	0.529	0.0338	0.471	14.8	8.42
15.4	2.99	0.557	0.0280	0.443	14.0	8.94
16.3	3.17	0.580	0.0236	0.420	13.2	9.48
17.3	3.36	0.602	0.0212	0.398	12.4	10.1
18.4	3.57	0.622	0.0198	0.378	11.7	10.7
19.5	3.79	0.641	0.0193	0.359	11.0	11.3
20.7	4.02	0.658	0.0167	0.342	10.4	12.0
22.0	4.27	0.673	0.0150	0.327	9.79	12.8
23.4	4.53	0.685	0.0129	0.315	9.23	13.6
24.9	4.82	0.698	0.0122	0.302	8.67	14.4
26.4	5.11	0.708	0.0106	0.292	8.17	15.3
28.0	5.42	0.718	0.0095	0.282	7.70	16.2
29.7	5.75	0.726	0.0087	0.274	7.26	17.2
31.5	6.11	0.734	0.0077	0.266	6.84	18.3
33.4	6.48	0.741	0.0068	0.259	6.45	19.4
35.5	6.88	0.748	0.0068	0.252	6.08	20.6
37.6	7.29	0.754	0.0061	0.246	5.73	21.8
39.9	7.74	0.759	0.0056	0.241	5.40	23.2
42.4	8.21	0.765	0.0052	0.235	5.09	24.6
45.0	8.72	0.770	0.0049	0.230	4.79	26.1
46.4	8.99	0.771	0.0019	0.229	4.65	26.9
50.5	9.79	0.777	0.0051	0.223	4.27	29.3
54.4	10.54	0.782	0.0054	0.218	3.96	31.6
58.1	11.3	0.787	0.0049	0.213	3.71	33.7
62.3	12.1	0.792	0.0047	0.208	3.46	36.1
66.2	12.8	0.795	0.0037	0.205	3.26	38.4
70.1	13.6	0.801	0.0060	0.199	3.07	40.7
75.0	14.5	0.806	0.0050	0.194	2.87	43.5
79.9	15.5	0.811	0.0048	0.189	2.70	46.4
84.8	16.4	0.815	0.0045	0.185	2.54	49.2
90.4	17.5	0.821	0.0053	0.179	2.39	52.4
95.9	18.6	0.826	0.0049	0.174	2.25	55.6
102	19.7	0.830	0.0047	0.170	2.12	58.9

Table A.9 Mercury Injection Capillary Pressure Data For Sample RM1-79HO-P01

Sample ID: RM1-79HO-P01 Swanson Air Permeability, mD: 192
Depth, ft: 9029.20 Hg Porosity, percent: 17.8

Mercury/Air Pressure (psi)	Equivalent Air/Brine Pressure (psi)	Mercury Saturation (fraction)	Incremental Mercury Saturation (fraction)	Wetting Phase Saturation (fraction)	Pore Throat Diameter (micron)	Height above Free Water (G/W) (ft)
107	20.8	0.836	0.0051	0.164	2.01	62.4
115	22.2	0.840	0.0044	0.160	1.88	66.6
122	23.6	0.845	0.0049	0.155	1.77	70.7
130	25.1	0.849	0.0045	0.151	1.66	75.3
138	26.8	0.854	0.0044	0.146	1.56	80.3
147	28.4	0.858	0.0047	0.142	1.47	85.1
155	30.0	0.863	0.0043	0.137	1.39	89.7
165	31.9	0.867	0.0041	0.133	1.31	95.5
173	33.6	0.871	0.0041	0.129	1.24	101
185	35.8	0.875	0.0041	0.125	1.17	107
196	38.0	0.879	0.0043	0.121	1.10	114
209	40.6	0.883	0.0033	0.117	1.03	121
223	43.3	0.886	0.0037	0.114	0.97	130
236	45.7	0.890	0.0034	0.110	0.91	137
250	48.5	0.893	0.0032	0.107	0.862	145
267	51.7	0.896	0.0031	0.104	0.808	155
282	54.7	0.899	0.0031	0.101	0.763	164
299	57.9	0.902	0.0030	0.098	0.722	173
319	61.7	0.905	0.0029	0.095	0.677	185
338	65.4	0.908	0.0027	0.092	0.638	196
358	69.4	0.910	0.0026	0.090	0.602	208
380	73.6	0.913	0.0025	0.087	0.567	220
404	78.4	0.915	0.0026	0.085	0.533	235
430	83.3	0.918	0.0026	0.082	0.501	250
456	88.3	0.920	0.0021	0.080	0.473	264
484	93.9	0.922	0.0022	0.078	0.445	281
512	99.3	0.924	0.0019	0.076	0.421	297
544	105.4	0.926	0.0020	0.074	0.396	316
579	112	0.928	0.0020	0.072	0.372	336
613	119	0.930	0.0020	0.070	0.352	356
650	126	0.932	0.0018	0.068	0.331	377
693	134	0.934	0.0019	0.066	0.311	402
733	142	0.935	0.0016	0.065	0.294	425
779	151	0.937	0.0016	0.063	0.277	452
826	160	0.938	0.0014	0.062	0.261	479
879	170	0.940	0.0015	0.060	0.245	510
932	181	0.941	0.0014	0.059	0.231	541

Table A.9 Mercury Injection Capillary Pressure Data For Sample RM1-79HO-P01

Sample ID: RM1-79HO-P01 Swanson Air Permeability, mD: 192
Depth, ft: 9029.20 Hg Porosity, percent: 17.8

Mercury/Air Pressure (psi)	Equivalent Air/Brine Pressure (psi)	Mercury Saturation (fraction)	Incremental Mercury Saturation (fraction)	Wetting Phase Saturation (fraction)	Pore Throat Diameter (micron)	Height above Free Water (G/W) (ft)
988	191	0.943	0.0013	0.057	0.218	573
1050	203	0.944	0.0012	0.056	0.205	609
1117	217	0.945	0.0013	0.055	0.193	648
1186	230	0.946	0.0011	0.054	0.182	688
1257	244	0.947	0.0011	0.053	0.171	729
1336	259	0.948	0.0012	0.052	0.161	775
1417	275	0.950	0.0011	0.050	0.152	822
1500	291	0.951	0.0010	0.049	0.144	870
1596	309	0.952	0.0010	0.048	0.135	926
1691	328	0.953	0.0011	0.047	0.127	981
1794	348	0.954	0.0010	0.046	0.120	1041
1904	369	0.955	0.0011	0.045	0.113	1105
2024	392	0.956	0.0008	0.044	0.106	1174
2144	416	0.956	0.0009	0.044	0.101	1244
2278	441	0.957	0.0009	0.043	0.095	1322
2420	469	0.959	0.0012	0.041	0.089	1404
2567	497	0.960	0.0009	0.040	0.084	1489
2724	528	0.961	0.0010	0.039	0.079	1580
2893	561	0.961	0.0009	0.039	0.075	1678
3071	595	0.963	0.0010	0.037	0.070	1782
3257	631	0.963	0.0007	0.037	0.066	1890
3457	670	0.964	0.0010	0.036	0.062	2006
3670	711	0.965	0.0009	0.035	0.059	2130
3894	755	0.966	0.0008	0.034	0.055	2259
4136	801	0.966	0.0003	0.034	0.052	2400
4383	849	0.967	0.0011	0.033	0.049	2543
4655	902	0.969	0.0013	0.031	0.046	2701
4940	957	0.970	0.0010	0.030	0.044	2866
5244	1016	0.970	0.0008	0.030	0.041	3042
5563	1078	0.971	0.0006	0.029	0.039	3228
5906	1145	0.972	0.0007	0.028	0.036	3427
6269	1215	0.972	0.0008	0.028	0.034	3637
6654	1290	0.973	0.0007	0.027	0.032	3861
7061	1368	0.974	0.0007	0.026	0.031	4097
7494	1452	0.975	0.0006	0.025	0.029	4348
7813	1514	0.975	0.0006	0.025	0.028	4533
8145	1578	0.976	0.0006	0.024	0.026	4726

Table A.9 Mercury Injection Capillary Pressure Data For Sample RM1-79HO-P01

Sample ID: RM1-79HO-P01 Swanson Air Permeability, mD: 192
Depth, ft: 9029.20 Hg Porosity, percent: 17.8

Mercury/Air Pressure (psi)	Equivalent Air/Brine Pressure (psi)	Mercury Saturation (fraction)	Incremental Mercury Saturation (fraction)	Wetting Phase Saturation (fraction)	Pore Throat Diameter (micron)	Height above Free Water (G/W) (ft)
8492	1646	0.976	0.0005	0.024	0.025	4927
8852	1715	0.977	0.0006	0.023	0.024	5136
9227	1788	0.977	0.0005	0.023	0.023	5354
9620	1864	0.978	0.0005	0.022	0.022	5582
10028	1943	0.978	0.0004	0.022	0.021	5818
10454	2026	0.979	0.0006	0.021	0.021	6066
10899	2112	0.979	0.0005	0.021	0.020	6324
11362	2202	0.980	0.0005	0.020	0.019	6593
11844	2295	0.980	0.0004	0.020	0.018	6872
12348	2393	0.981	0.0005	0.019	0.017	7165
12872	2495	0.981	0.0005	0.019	0.017	7469
13419	2600	0.982	0.0004	0.018	0.016	7786
13989	2711	0.982	0.0005	0.018	0.015	8117
14585	2826	0.983	0.0005	0.017	0.015	8462
15203	2946	0.983	0.0005	0.017	0.014	8821
15849	3071	0.984	0.0005	0.016	0.014	9196
16522	3202	0.984	0.0004	0.016	0.013	9586
17224	3338	0.985	0.0006	0.015	0.013	9994
17957	3480	0.985	0.0006	0.015	0.012	10419
18720	3628	0.986	0.0005	0.014	0.012	10862
19515	3782	0.986	0.0000	0.014	0.011	11323
20343	3942	0.987	0.0007	0.013	0.011	11803
21206	4110	0.987	0.0006	0.013	0.010	12304
22108	4284	0.988	0.0004	0.012	0.010	12828
23048	4467	0.988	0.0007	0.012	0.009	13373
24028	4656	0.989	0.0004	0.011	0.009	13941
25049	4854	0.989	0.0005	0.011	0.009	14534
26113	5060	0.990	0.0005	0.010	0.008	15151
27222	5275	0.990	0.0005	0.010	0.008	15795
28378	5499	0.991	0.0005	0.009	0.008	16465
29583	5733	0.991	0.0005	0.009	0.007	17164
30841	5977	0.992	0.0005	0.008	0.007	17894
32149	6230	0.992	0.0006	0.008	0.007	18654
33512	6494	0.993	0.0005	0.007	0.006	19444
34937	6771	0.993	0.0006	0.007	0.006	20271
36409	7056	0.994	0.0005	0.006	0.006	21125
37955	7355	0.994	0.0005	0.006	0.006	22022

Table A.9 Mercury Injection Capillary Pressure Data For Sample RM1-79HO-P01

Sample ID: RM1-79HO-P01 Swanson Air Permeability, mD: 192
Depth, ft: 9029.20 Hg Porosity, percent: 17.8

Mercury/Air Pressure (psi)	Equivalent Air/Brine Pressure (psi)	Mercury Saturation (fraction)	Incremental Mercury Saturation (fraction)	Wetting Phase Saturation (fraction)	Pore Throat Diameter (micron)	Height above Free Water (G/W) (ft)
39571	7669	0.995	0.0004	0.005	0.005	22960
41265	7997	0.995	0.0005	0.005	0.005	23943
42997	8333	0.996	0.0004	0.004	0.005	24948
44828	8687	0.996	0.0006	0.004	0.005	26010
46735	9057	0.997	0.0005	0.003	0.005	27116
48722	9442	0.997	0.0005	0.003	0.004	28269
50789	9843	0.998	0.0004	0.002	0.004	29469
52941	10260	0.998	0.0005	0.002	0.004	30717
55191	10696	0.999	0.0006	0.001	0.004	32023
57538	11150	0.999	0.0005	0.001	0.004	33385
59981	11624	1.000	0.0006	0.000	0.004	34802

Figure A.25 Mercury/Air Capillary Pressure For Sample RM1-79HO-P01

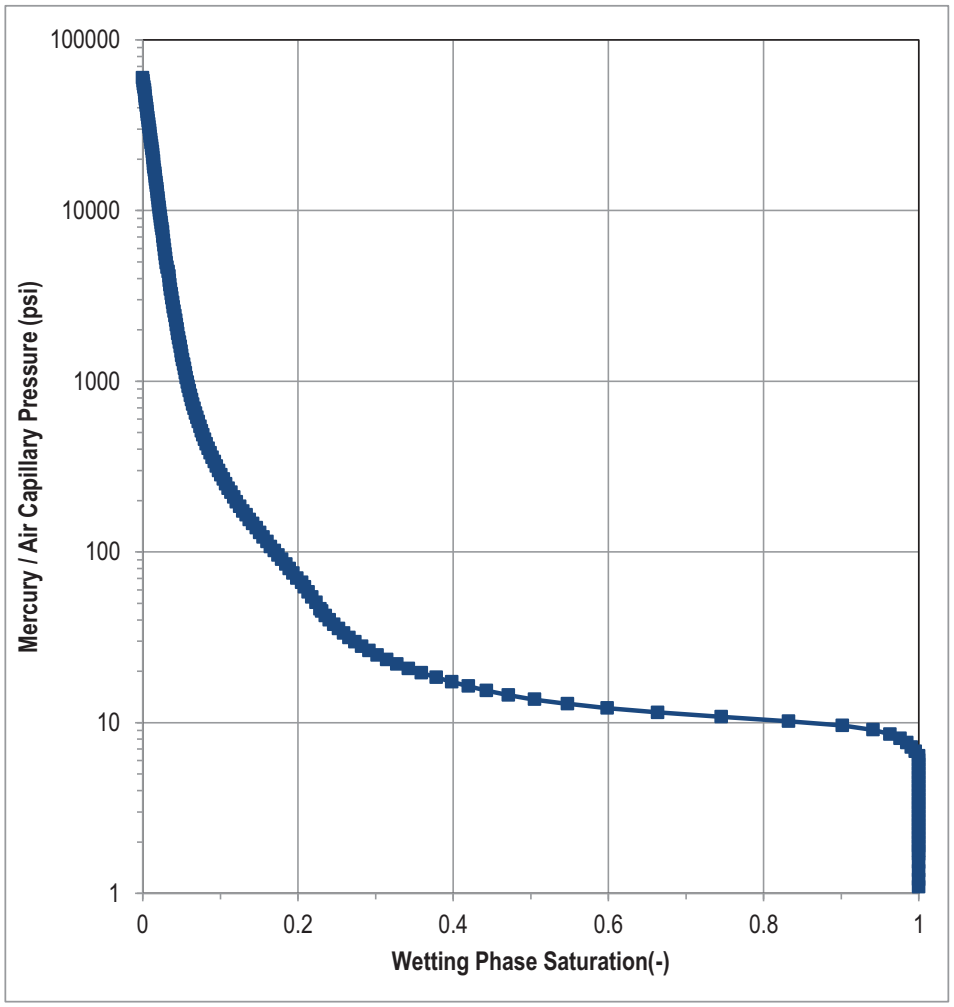


Figure A.26 Calculated Air /Brine Capillary Pressure And Height Above Free Water For Sample RM1-79HO-P01

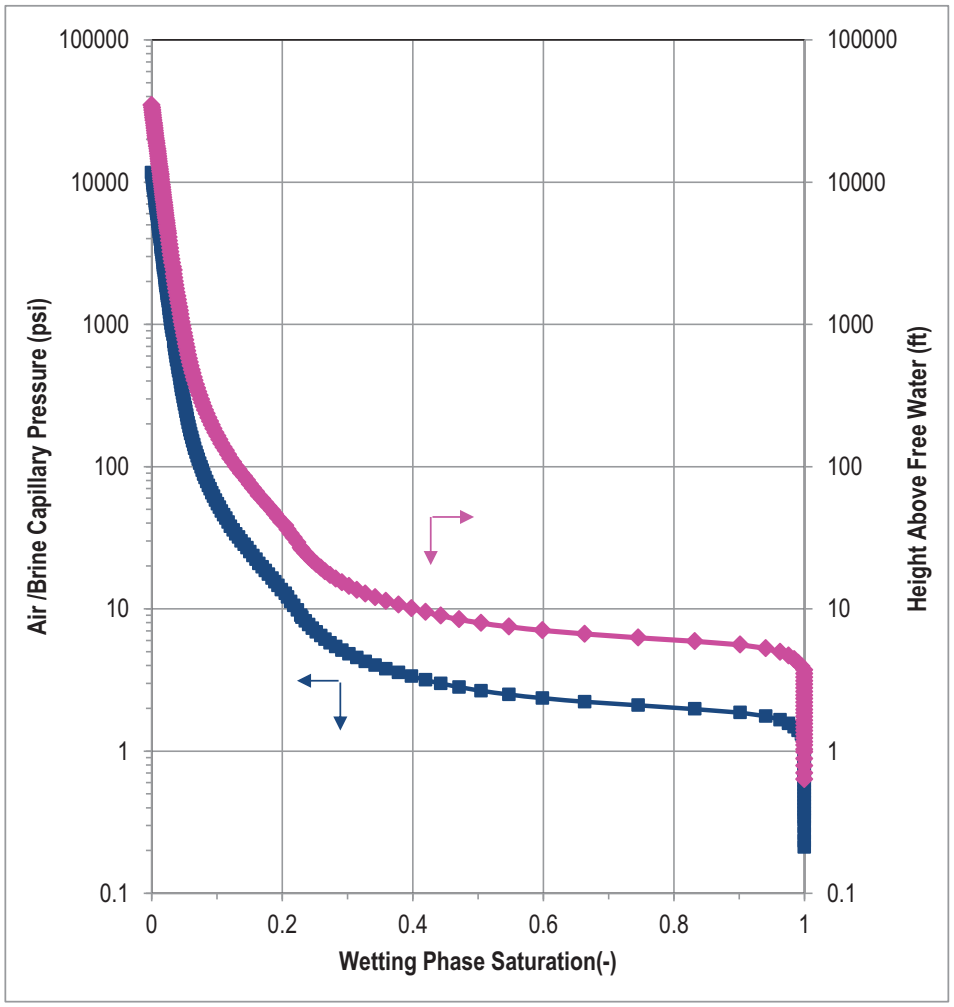


Figure A.27 Pore Throat Size Distribution For Sample RM1-79HO-P01

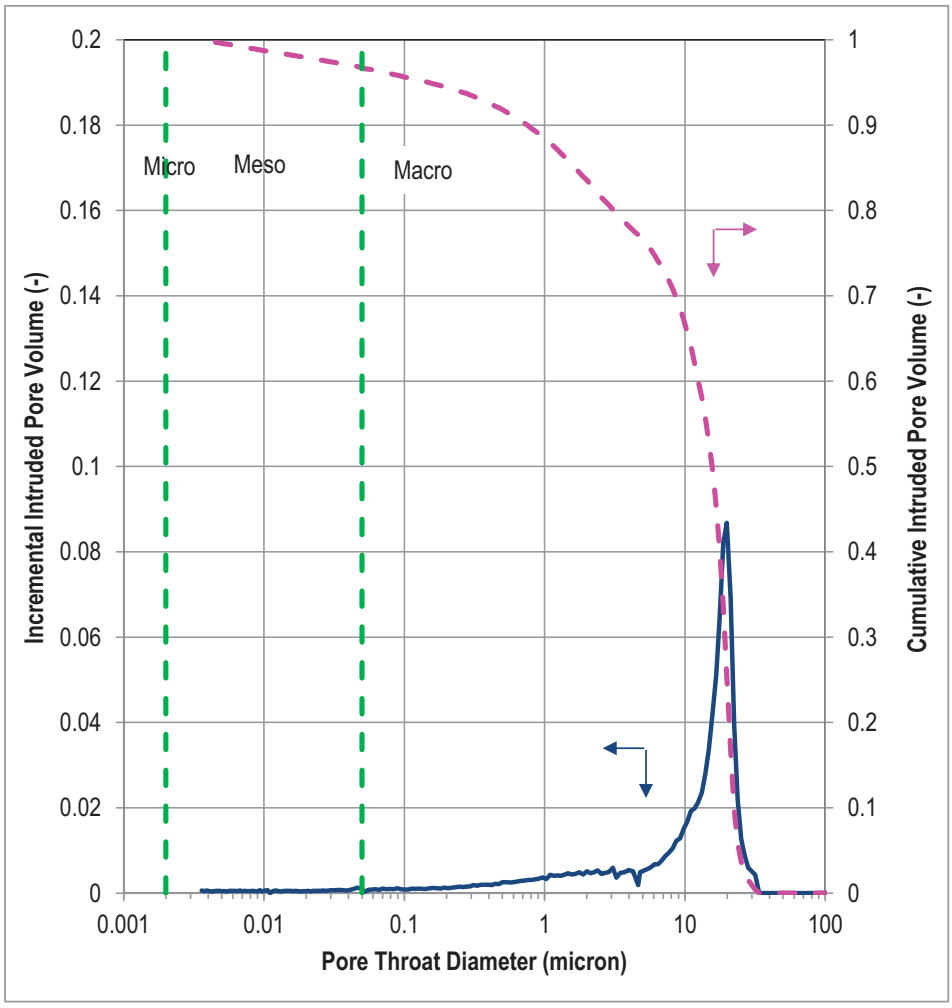


Table A.10 Mercury Injection Capillary Pressure Data For Sample RM1-93DO-P01

Sample ID: RM1-93DO-P01 Swanson Air Permeability, mD: 0.007
Depth, ft: 9043.70 Hg Porosity, percent: 3.79

Mercury/Air Pressure (psi)	Equivalent Air/Brine Pressure (psi)	Mercury Saturation (fraction)	Incremental Mercury Saturation (fraction)	Wetting Phase Saturation (fraction)	Pore Throat Diameter (micron)	Height above Free Water (G/W) (ft)
1.10	0.213	0.000	0.0000	1.000	196	0.637
1.22	0.236	0.000	0.0000	1.000	177	0.705
1.37	0.266	0.000	0.0000	1.000	157	0.795
1.53	0.296	0.000	0.0000	1.000	141	0.887
1.71	0.332	0.000	0.0000	1.000	126	0.994
1.91	0.370	0.000	0.0000	1.000	113	1.11
2.00	0.387	0.000	0.0000	1.000	108	1.16
2.14	0.414	0.000	0.0000	1.000	101	1.24
2.26	0.437	0.000	0.0000	1.000	95.5	1.31
2.39	0.463	0.000	0.0000	1.000	90.2	1.39
2.53	0.491	0.000	0.0000	1.000	85.1	1.47
2.68	0.520	0.000	0.0000	1.000	80.3	1.56
2.84	0.551	0.000	0.0000	1.000	75.8	1.65
3.01	0.584	0.000	0.0000	1.000	71.5	1.75
3.19	0.618	0.000	0.0000	1.000	67.6	1.85
3.38	0.655	0.000	0.0000	1.000	63.7	1.96
3.58	0.694	0.000	0.0000	1.000	60.2	2.08
3.80	0.735	0.000	0.0000	1.000	56.8	2.20
4.02	0.779	0.000	0.0000	1.000	53.6	2.33
4.26	0.825	0.000	0.0000	1.000	50.6	2.47
4.52	0.875	0.000	0.0000	1.000	47.7	2.62
4.79	0.927	0.000	0.0000	1.000	45.0	2.78
5.07	0.983	0.000	0.0000	1.000	42.5	2.94
5.38	1.04	0.000	0.0000	1.000	40.1	3.12
5.70	1.10	0.000	0.0000	1.000	37.8	3.31
6.04	1.17	0.000	0.0000	1.000	35.7	3.50
6.40	1.24	0.000	0.0000	1.000	33.7	3.71
6.78	1.31	0.000	0.0000	1.000	31.8	3.94
7.19	1.39	0.000	0.0000	1.000	30.0	4.17
7.62	1.48	0.000	0.0000	1.000	28.3	4.42
8.08	1.57	0.000	0.0000	1.000	26.7	4.69
8.57	1.66	0.000	0.0000	1.000	25.2	4.97
9.09	1.76	0.000	0.0000	1.000	23.7	5.27
9.63	1.87	0.000	0.0000	1.000	22.4	5.59
10.21	1.98	0.000	0.0000	1.000	21.1	5.93
10.8	2.10	0.000	0.0000	1.000	19.9	6.28
11.5	2.22	0.000	0.0000	1.000	18.8	6.66

Table A.10 Mercury Injection Capillary Pressure Data For Sample RM1-93DO-P01

Sample ID: RM1-93DO-P01 Swanson Air Permeability, mD: 0.007
Depth, ft: 9043.70 Hg Porosity, percent: 3.79

Mercury/Air Pressure (psi)	Equivalent Air/Brine Pressure (psi)	Mercury Saturation (fraction)	Incremental Mercury Saturation (fraction)	Wetting Phase Saturation (fraction)	Pore Throat Diameter (micron)	Height above Free Water (G/W) (ft)
12.2	2.36	0.000	0.0000	1.000	17.7	7.06
12.9	2.50	0.000	0.0000	1.000	16.7	7.49
13.7	2.65	0.000	0.0000	1.000	15.8	7.94
14.5	2.81	0.000	0.0000	1.000	14.8	8.43
15.4	2.99	0.000	0.0000	1.000	14.0	8.94
16.4	3.17	0.000	0.0000	1.000	13.2	9.49
17.4	3.36	0.000	0.0000	1.000	12.4	10.1
18.4	3.57	0.000	0.0000	1.000	11.7	10.7
19.6	3.79	0.000	0.0000	1.000	11.0	11.3
20.7	4.02	0.000	0.0000	1.000	10.4	12.0
22.0	4.26	0.000	0.0000	1.000	9.80	12.8
23.4	4.53	0.000	0.0000	1.000	9.23	13.6
24.8	4.80	0.000	0.0000	1.000	8.69	14.4
26.3	5.10	0.000	0.0000	1.000	8.19	15.3
27.9	5.41	0.000	0.0000	1.000	7.72	16.2
29.7	5.75	0.000	0.0000	1.000	7.26	17.2
31.5	6.11	0.000	0.0000	1.000	6.84	18.3
33.4	6.48	0.000	0.0000	1.000	6.45	19.4
35.5	6.87	0.000	0.0000	1.000	6.08	20.6
37.6	7.29	0.000	0.0000	1.000	5.73	21.8
40.0	7.75	0.000	0.0000	1.000	5.39	23.2
42.4	8.22	0.000	0.0000	1.000	5.08	24.6
45.0	8.72	0.000	0.0000	1.000	4.79	26.1
46.9	9.09	0.000	0.0000	1.000	4.59	27.2
48.6	9.42	0.000	0.0000	1.000	4.43	28.2
52.9	10.24	0.000	0.0000	1.000	4.08	30.7
55.1	10.67	0.000	0.0000	1.000	3.91	32.0
59.9	11.6	0.000	0.0000	1.000	3.60	34.8
62.4	12.1	0.000	0.0000	1.000	3.46	36.2
66.8	12.9	0.000	0.0000	1.000	3.23	38.8
71.8	13.9	0.000	0.0000	1.000	3.00	41.6
75.4	14.6	0.000	0.0000	1.000	2.86	43.8
80.5	15.6	0.000	0.0000	1.000	2.68	46.7
85.3	16.5	0.000	0.0000	1.000	2.53	49.5
90.9	17.6	0.000	0.0000	1.000	2.37	52.8
96.5	18.7	0.000	0.0000	1.000	2.23	56.0
102	19.7	0.000	0.0000	1.000	2.12	59.1

Table A.10 Mercury Injection Capillary Pressure Data For Sample RM1-93DO-P01

Sample ID: RM1-93DO-P01 Swanson Air Permeability, mD: 0.007
Depth, ft: 9043.70 Hg Porosity, percent: 3.79

Mercury/Air Pressure (psi)	Equivalent Air/Brine Pressure (psi)	Mercury Saturation (fraction)	Incremental Mercury Saturation (fraction)	Wetting Phase Saturation (fraction)	Pore Throat Diameter (micron)	Height above Free Water (G/W) (ft)
108	21.0	0.000	0.0000	1.000	1.99	62.9
116	22.4	0.000	0.0000	1.000	1.87	67.0
122	23.7	0.000	0.0000	1.000	1.76	70.9
130	25.1	0.000	0.0000	1.000	1.66	75.3
139	26.8	0.000	0.0000	1.000	1.56	80.4
146	28.3	0.000	0.0000	1.000	1.48	84.7
156	30.2	0.000	0.0000	1.000	1.38	90.4
165	32.0	0.000	0.0000	1.000	1.31	95.7
175	33.9	0.000	0.0000	1.000	1.23	101
186	36.0	0.000	0.0000	1.000	1.16	108
198	38.3	0.000	0.0000	1.000	1.09	115
210	40.8	0.000	0.0000	1.000	1.02	122
223	43.2	0.000	0.0000	1.000	0.97	129
237	46.0	0.000	0.0000	1.000	0.91	138
251	48.7	0.000	0.0000	1.000	0.858	146
267	51.7	0.002	0.0018	0.998	0.809	155
283	54.8	0.005	0.0030	0.995	0.763	164
301	58.3	0.009	0.0046	0.991	0.717	174
319	61.9	0.016	0.0066	0.984	0.675	185
340	65.8	0.023	0.0072	0.977	0.634	197
359	69.6	0.031	0.0082	0.969	0.600	208
382	74.0	0.043	0.0116	0.957	0.565	222
406	78.6	0.056	0.0136	0.944	0.531	235
430	83.4	0.070	0.0139	0.930	0.501	250
457	88.6	0.087	0.0162	0.913	0.471	265
485	93.9	0.103	0.0163	0.897	0.445	281
515	99.7	0.119	0.0163	0.881	0.419	299
547	106	0.136	0.0163	0.864	0.394	317
579	112	0.155	0.0198	0.845	0.372	336
616	119	0.176	0.0206	0.824	0.350	357
654	127	0.200	0.0243	0.800	0.330	379
693	134	0.227	0.0265	0.773	0.311	402
734	142	0.255	0.0284	0.745	0.294	426
778	151	0.286	0.0306	0.714	0.277	452
829	161	0.318	0.0319	0.682	0.260	481
879	170	0.346	0.0288	0.654	0.245	510
934	181	0.376	0.0294	0.624	0.231	542

Table A.10 Mercury Injection Capillary Pressure Data For Sample RM1-93DO-P01

Sample ID: RM1-93DO-P01 Swanson Air Permeability, mD: 0.007
Depth, ft: 9043.70 Hg Porosity, percent: 3.79

Mercury/Air Pressure (psi)	Equivalent Air/Brine Pressure (psi)	Mercury Saturation (fraction)	Incremental Mercury Saturation (fraction)	Wetting Phase Saturation (fraction)	Pore Throat Diameter (micron)	Height above Free Water (G/W) (ft)
989	192	0.406	0.0298	0.594	0.218	574
1051	204	0.435	0.0291	0.565	0.205	610
1117	216	0.461	0.0258	0.539	0.193	648
1184	229	0.484	0.0239	0.516	0.182	687
1257	244	0.506	0.0219	0.494	0.171	729
1335	259	0.528	0.0215	0.472	0.161	775
1417	275	0.548	0.0197	0.452	0.152	822
1502	291	0.567	0.0190	0.433	0.143	872
1598	310	0.585	0.0182	0.415	0.135	927
1692	328	0.601	0.0164	0.399	0.127	982
1795	348	0.617	0.0155	0.383	0.120	1042
1905	369	0.631	0.0143	0.369	0.113	1105
2023	392	0.644	0.0130	0.356	0.107	1174
2147	416	0.656	0.0120	0.344	0.100	1246
2281	442	0.666	0.0099	0.334	0.094	1324
2422	469	0.676	0.0104	0.324	0.089	1405
2567	497	0.687	0.0109	0.313	0.084	1489
2725	528	0.696	0.0086	0.304	0.079	1581
2891	560	0.705	0.0087	0.295	0.075	1677
3068	595	0.713	0.0080	0.287	0.070	1780
3258	631	0.721	0.0082	0.279	0.066	1890
3458	670	0.728	0.0076	0.272	0.062	2006
3670	711	0.736	0.0072	0.264	0.059	2130
3896	755	0.742	0.0068	0.258	0.055	2260
4134	801	0.749	0.0065	0.251	0.052	2399
4386	850	0.755	0.0064	0.245	0.049	2545
4656	902	0.761	0.0059	0.239	0.046	2701
4942	958	0.767	0.0058	0.233	0.044	2867
5244	1016	0.772	0.0053	0.228	0.041	3042
5566	1079	0.778	0.0055	0.222	0.039	3230
5909	1145	0.783	0.0052	0.217	0.036	3429
6269	1215	0.788	0.0050	0.212	0.034	3638
6654	1289	0.793	0.0052	0.207	0.032	3861
7063	1369	0.798	0.0048	0.202	0.031	4098
7495	1452	0.803	0.0047	0.197	0.029	4348
7814	1514	0.807	0.0044	0.193	0.028	4534
8145	1578	0.812	0.0051	0.188	0.026	4726

Table A.10 Mercury Injection Capillary Pressure Data For Sample RM1-93DO-P01

Sample ID: RM1-93DO-P01 Swanson Air Permeability, mD: 0.007
Depth, ft: 9043.70 Hg Porosity, percent: 3.79

Mercury/Air Pressure (psi)	Equivalent Air/Brine Pressure (psi)	Mercury Saturation (fraction)	Incremental Mercury Saturation (fraction)	Wetting Phase Saturation (fraction)	Pore Throat Diameter (micron)	Height above Free Water (G/W) (ft)
8492	1646	0.816	0.0041	0.184	0.025	4927
8853	1716	0.820	0.0043	0.180	0.024	5136
9229	1788	0.825	0.0043	0.175	0.023	5355
9620	1864	0.829	0.0044	0.171	0.022	5582
10030	1944	0.834	0.0044	0.166	0.021	5820
10455	2026	0.838	0.0043	0.162	0.021	6066
10900	2112	0.842	0.0046	0.158	0.020	6324
11362	2202	0.847	0.0043	0.153	0.019	6593
11845	2296	0.851	0.0045	0.149	0.018	6873
12349	2393	0.855	0.0043	0.145	0.017	7165
12875	2495	0.859	0.0038	0.141	0.017	7470
13420	2601	0.864	0.0048	0.136	0.016	7786
13990	2711	0.869	0.0046	0.131	0.015	8117
14584	2826	0.873	0.0045	0.127	0.015	8462
15204	2946	0.877	0.0037	0.123	0.014	8822
15850	3072	0.880	0.0033	0.120	0.014	9196
16524	3202	0.884	0.0034	0.116	0.013	9587
17225	3338	0.887	0.0036	0.113	0.013	9994
17957	3480	0.891	0.0034	0.109	0.012	10419
18720	3628	0.894	0.0038	0.106	0.012	10862
19516	3782	0.898	0.0036	0.102	0.011	11323
20343	3942	0.902	0.0035	0.098	0.011	11803
21207	4110	0.904	0.0029	0.096	0.010	12305
22109	4284	0.908	0.0037	0.092	0.010	12828
23049	4467	0.911	0.0031	0.089	0.009	13373
24027	4656	0.915	0.0036	0.085	0.009	13941
25049	4854	0.919	0.0037	0.081	0.009	14534
26113	5061	0.922	0.0036	0.078	0.008	15151
27223	5276	0.926	0.0038	0.074	0.008	15795
28378	5499	0.930	0.0039	0.070	0.008	16465
29584	5733	0.933	0.0036	0.067	0.007	17165
30840	5977	0.937	0.0039	0.063	0.007	17894
32151	6231	0.941	0.0042	0.059	0.007	18655
33516	6495	0.945	0.0037	0.055	0.006	19446
34940	6771	0.949	0.0042	0.051	0.006	20273
36423	7058	0.953	0.0036	0.047	0.006	21133
37957	7356	0.957	0.0040	0.043	0.006	22023

Table A.10 Mercury Injection Capillary Pressure Data For Sample RM1-93DO-P01

Sample ID: RM1-93DO-P01 Swanson Air Permeability, mD: 0.007
Depth, ft: 9043.70 Hg Porosity, percent: 3.79

Mercury/Air Pressure (psi)	Equivalent Air/Brine Pressure (psi)	Mercury Saturation (fraction)	Incremental Mercury Saturation (fraction)	Wetting Phase Saturation (fraction)	Pore Throat Diameter (micron)	Height above Free Water (G/W) (ft)
39572	7669	0.961	0.0040	0.039	0.005	22960
41261	7996	0.965	0.0041	0.035	0.005	23940
42999	8333	0.969	0.0039	0.031	0.005	24949
44839	8690	0.973	0.0038	0.027	0.005	26017
46726	9055	0.977	0.0038	0.023	0.005	27111
48722	9442	0.981	0.0040	0.019	0.004	28270
50794	9843	0.984	0.0034	0.016	0.004	29471
52942	10260	0.988	0.0042	0.012	0.004	30718
55192	10696	0.992	0.0040	0.008	0.004	32023
57538	11151	0.996	0.0039	0.004	0.004	33385
59982	11624	1.000	0.0038	0.000	0.004	34802

Figure A.28 Mercury/Air Capillary Pressure For Sample RM1-93DO-P01

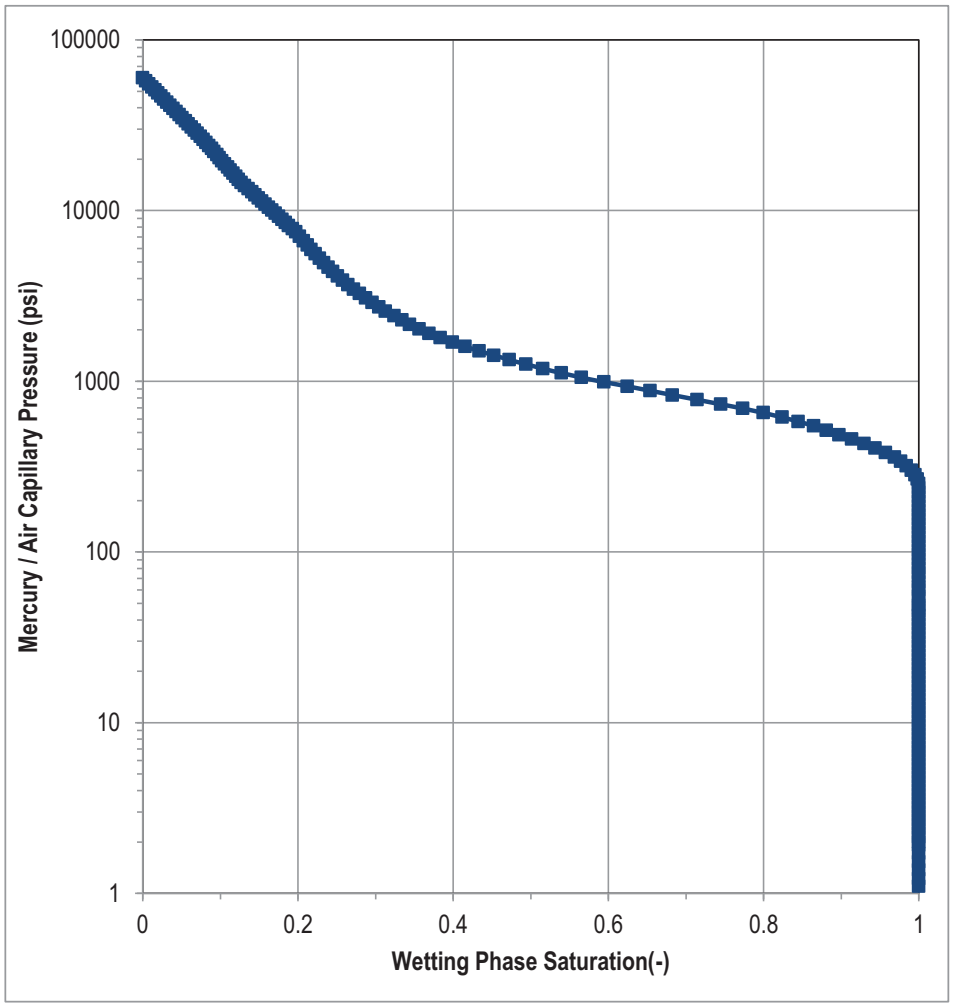


Figure A.29 Calculated Air /Brine Capillary Pressure And Height Above Free Water For Sample RM1-93DO-P01

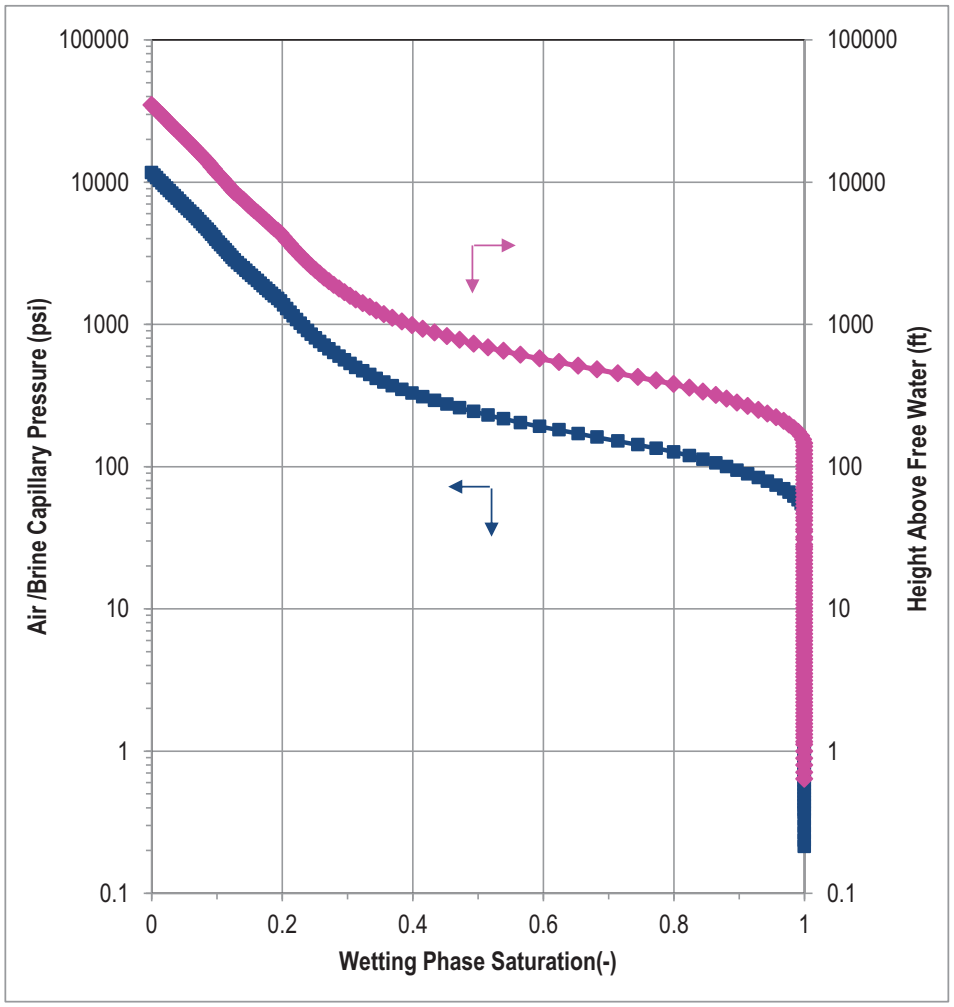
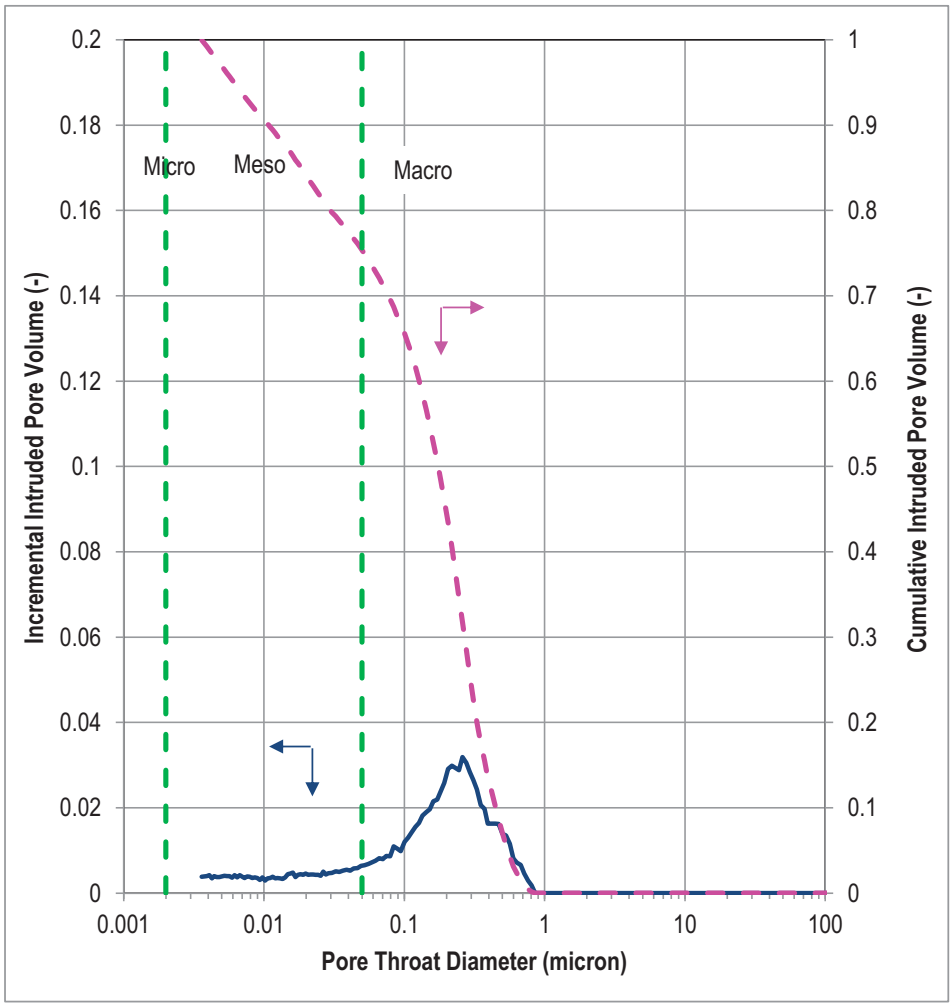


Figure A.30 Pore Throat Size Distribution For Sample RM1-93DO-P01



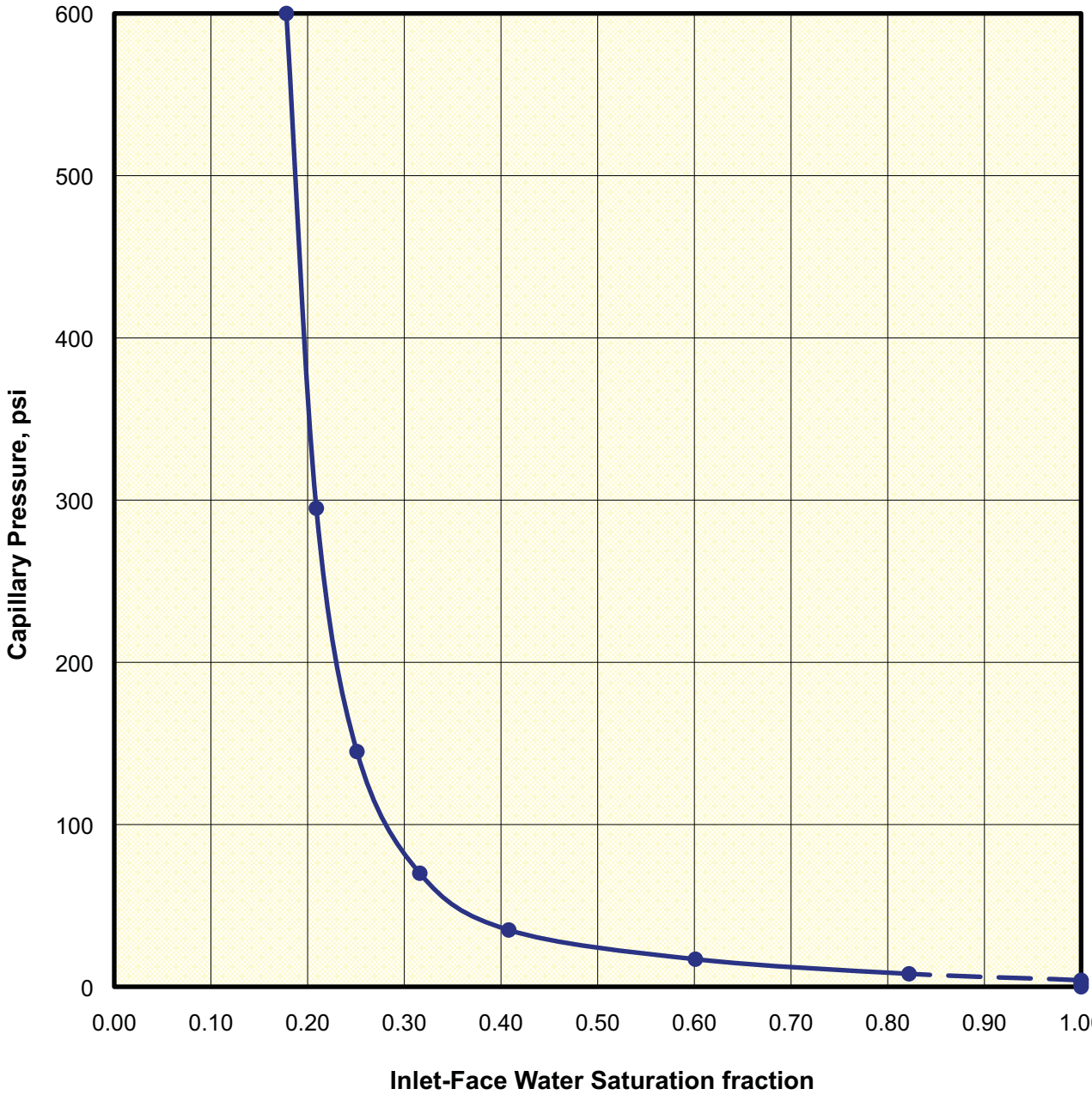
GAS-WATER CAPILLARY PRESSURE

High Speed Centrifuge Method

Ambient Conditions

University of Utah
RMCCS State #1 Well
Entrada Formation
File: HOU-130069

Sample Number:	RM1-64HO-P01
Depth, feet:	9013.0
Klinkenberg Permeability, md:	2.48
Porosity, fraction:	0.137
Initial Saturation, fraction:	1.000
Saturant:	Synthetic Formation Brine



Core Laboratories

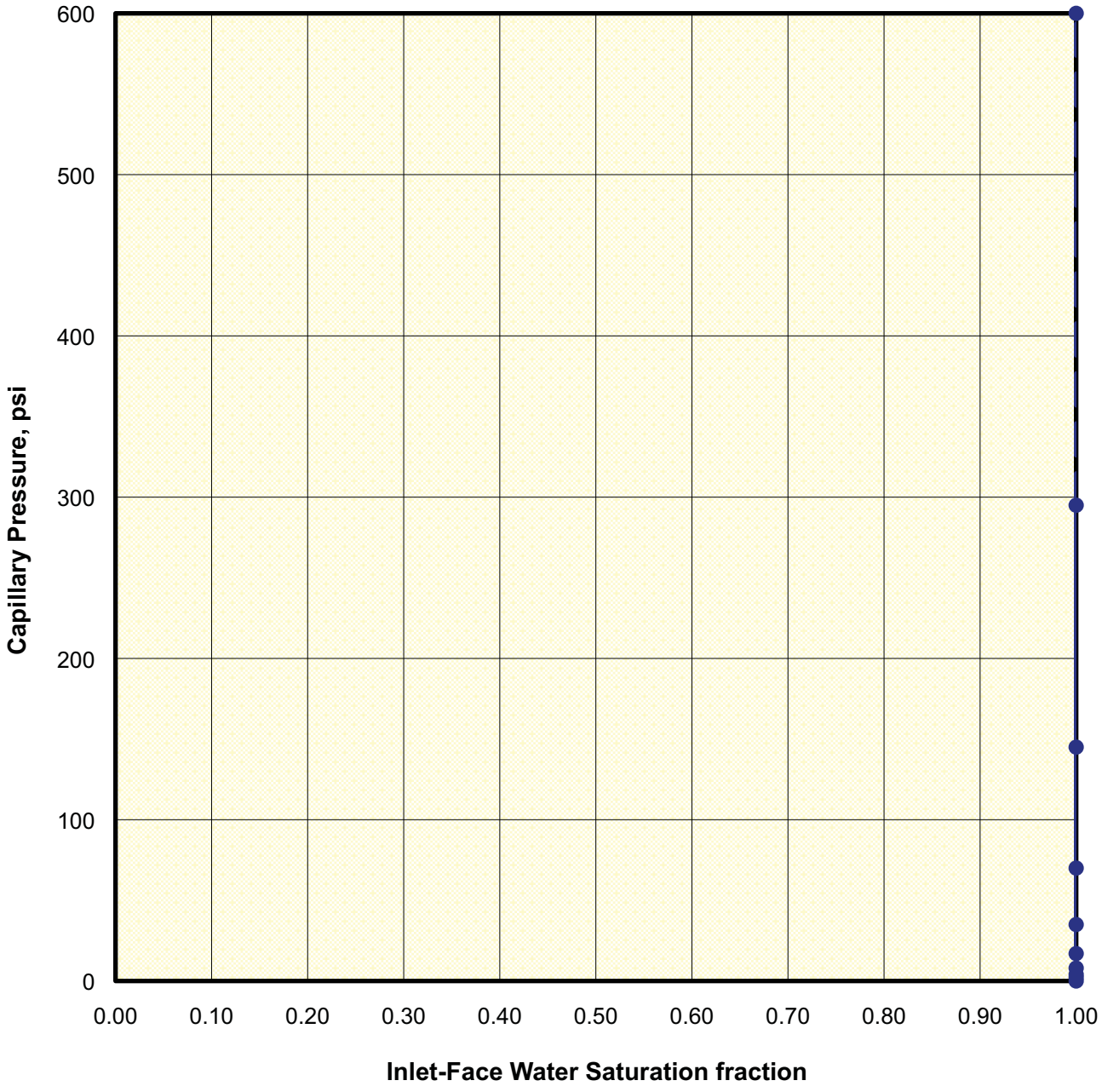
GAS-WATER CAPILLARY PRESSURE

High Speed Centrifuge Method

Ambient Conditions

University of Utah
RMCCS State #1 Well
Mowry Formation
File: HOU-130069

Sample Number:	RM1-21HB-P01
Depth, feet:	8235.0
Klinkenberg Permeability, md:	7.02
Porosity, fraction:	0.039
Initial Saturation, fraction:	1.000
Saturant:	Synthetic Formation Brine



Core Laboratories

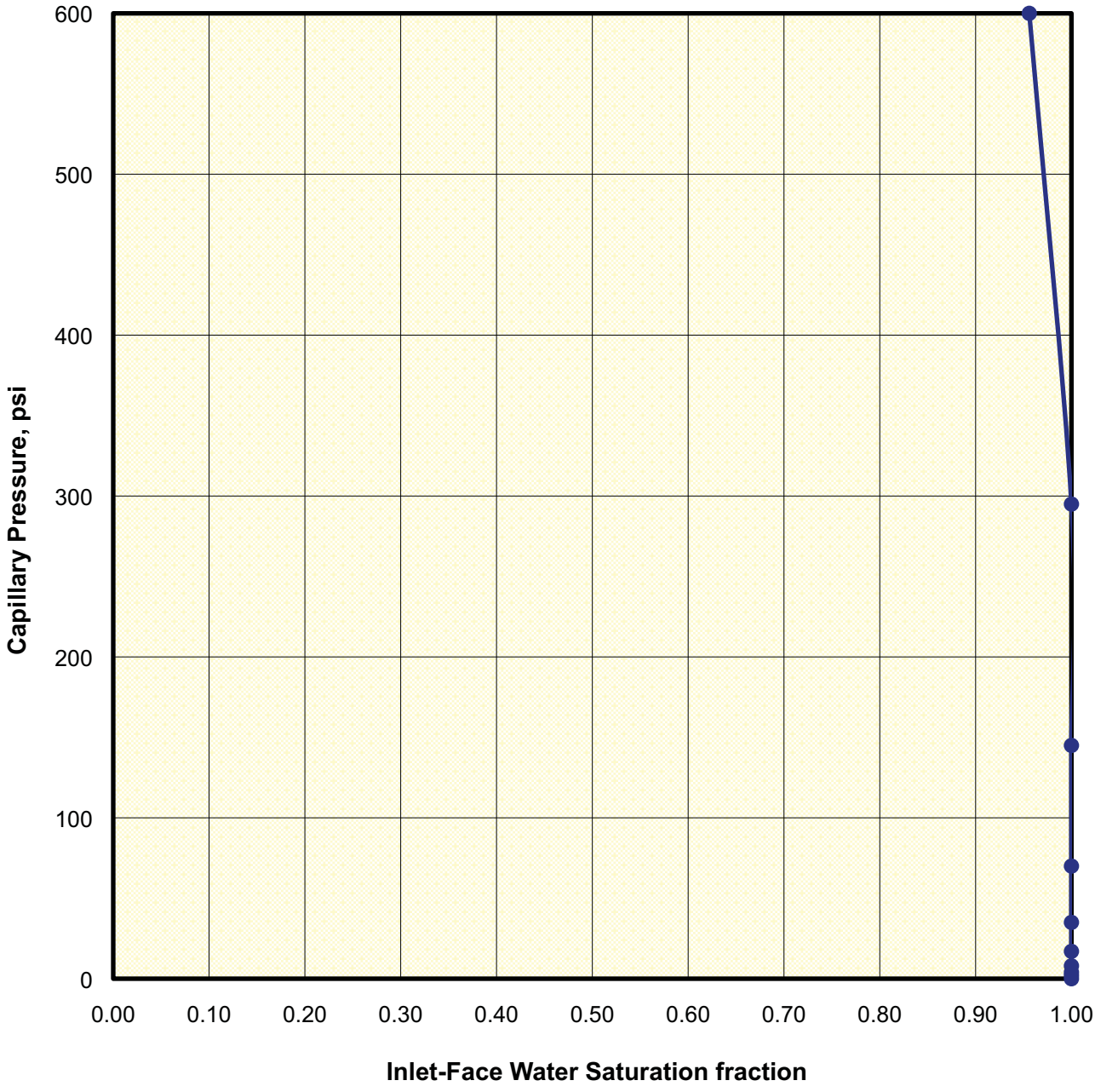
GAS-WATER CAPILLARY PRESSURE

High Speed Centrifuge Method

Ambient Conditions

University of Utah
RMCCS State #1 Well
Mowry Formation
File: HOU-130069

Sample Number:	RM1-10HB-P01
Depth, feet:	8206.0
Klinkenberg Permeability, md:	0.911
Porosity, fraction:	0.061
Initial Saturation, fraction:	1.000
Saturant:	Synthetic Formation Brine



Core Laboratories

Core Lab
RESERVOIR OPTIMIZATION

CAPILLARY PRESSURE

High Speed Centrifuge Method
Gas-Water System

Company: University of Utah
Well: RMCCS State #1
File: HOU-130069

Displaced Phase: Water
Displacing Phase: Gas (air)
Confining Stress, psi: Ambient
Temperature, ° F: 72
Saturant: Synthetic Formation Brine

Capillary Pressure, psi:	0	2	4	8	17	35	70	145	295	600

Sample Number	Depth, feet	Klinkenberg Permeability millidarcies	* Porosity, fraction	Initial Saturation fraction	Inlet-Face Water Saturation, fraction pore volume								
Mowry Formation													
RM1-10HB-P01	8206.0	0.911	0.061	1.000	1.000	1.000	1.000	1.000	1.000	1.000	1.000	1.000	0.956
RM1-21HB-P01	8235.0	7.02	0.039	1.000	1.000	1.000	1.000	1.000	1.000	1.000	1.000	1.000	1.000
Entrada Formation													
RM1-64HO-P01	9013.0	2.48	0.137	1.000	1.000	1.000	0.822	0.601	0.408	0.316	0.251	0.209	0.178

Permeabilities are optimistic due to fracture(s) in samples.
* Porosities calculated from saturated pore volumes.

MERCURY INJECTION DATA SUMMARY

Company: University of Utah
Well: RMCCS State #1
Formation: Mowry
File: HOU-130069

Sample:	RM1-10HB-901m	un-stressed	Host Plug 800psi	Host Plug 3580psi
Depth, feet:	8206.00			
Klinkenberg Permeability, md:		N/A	0.911*	0.0941*
Permeability to Air, md:		N/A	1.01*	0.115*
Swanson Permeability, md:		5.71E-04	-	-
Porosity, fraction:		0.064	0.061	0.054
maximum Sb/Pc, fraction:		3.50E-04		
R35, microns:		0.0130		
R50 (median pore throat radius):		0.0110		

*Permeability may be optimistic due to fracutre(s) in sample.

Injection Pressure, psia	Mercury Saturation, fraction	Pseudo-Wetting Saturation, fraction	Pore Throat Radius, microns	J Values	Conversion to other Laboratory Fluid Systems, psia G-W	G-O	O-W	Estimated Height Above Free Water, feet G-W	O-W
0.83	0.000	1.000	130	0.000046	0.161	0.0536	0.0929	0.335	0.667
1.10	0.000	1.000	97.9	0.000060	0.213	0.0711	0.123	0.445	0.884
1.41	0.000	1.000	76.4	0.000078	0.273	0.0911	0.158	0.570	1.13
1.75	0.000	1.000	61.6	0.000096	0.339	0.113	0.196	0.707	1.41
2.13	0.000	1.000	50.6	0.000117	0.413	0.138	0.238	0.861	1.71
2.57	0.000	1.000	41.9	0.000141	0.498	0.166	0.288	1.04	2.07
3.06	0.000	1.000	35.2	0.000168	0.593	0.198	0.342	1.24	2.46
3.62	0.000	1.000	29.8	0.000199	0.702	0.234	0.405	1.46	2.91
4.20	0.000	1.000	25.7	0.000231	0.814	0.271	0.470	1.70	3.38
4.85	0.000	1.000	22.2	0.000267	0.940	0.313	0.543	1.96	3.90
5.53	0.000	1.000	19.5	0.000304	1.07	0.357	0.619	2.23	4.44
6.27	0.000	1.000	17.2	0.000345	1.22	0.405	0.702	2.53	5.04
7.05	0.000	1.000	15.3	0.000388	1.37	0.455	0.789	2.85	5.67
7.90	0.000	1.000	13.6	0.000434	1.53	0.510	0.884	3.19	6.35
8.80	0.000	1.000	12.2	0.000484	1.71	0.568	0.985	3.56	7.07
9.73	0.000	1.000	11.1	0.000535	1.89	0.629	1.09	3.93	7.82
10.8	0.000	1.000	9.99	0.000593	2.09	0.697	1.21	4.36	8.68
11.9	0.000	1.000	9.07	0.000653	2.30	0.767	1.33	4.81	9.56
13.4	0.000	1.000	8.05	0.000736	2.59	0.865	1.50	5.42	10.8
15.3	0.000	1.000	7.06	0.000840	2.96	0.986	1.71	6.18	12.3
17.6	0.000	1.000	6.13	0.000966	3.40	1.13	1.97	7.11	14.1
20.4	0.000	1.000	5.27	0.00112	3.96	1.32	2.29	8.24	16.4
23.6	0.000	1.000	4.56	0.00130	4.58	1.53	2.64	9.54	19.0
26.9	0.000	1.000	4.01	0.00148	5.21	1.74	3.01	10.9	21.6
31.3	0.000	1.000	3.44	0.00172	6.07	2.02	3.50	12.6	25.2
36.5	0.000	1.000	2.95	0.00201	7.07	2.36	4.08	14.8	29.3
42.1	0.000	1.000	2.56	0.00231	8.16	2.72	4.71	17.0	33.8
48.3	0.000	1.000	2.23	0.00266	9.37	3.12	5.41	19.5	38.8
55.2	0.000	1.000	1.95	0.00304	10.7	3.57	6.18	22.3	44.4
62.0	0.000	1.000	1.74	0.00341	12.0	4.01	6.94	25.1	49.8
70.6	0.000	1.000	1.53	0.00388	13.7	4.56	7.90	28.5	56.7
80.0	0.000	1.000	1.35	0.00440	15.5	5.17	8.95	32.3	64.3
90.6	0.000	1.000	1.19	0.00498	17.6	5.85	10.1	36.6	72.8
103	0.000	1.000	1.05	0.00566	19.9	6.64	11.5	41.6	82.8
115	0.000	1.000	0.939	0.00631	22.2	7.41	12.8	46.5	92.4
131	0.000	1.000	0.822	0.00721	25.4	8.47	14.7	52.9	105
147	0.000	1.000	0.731	0.00810	28.6	9.52	16.5	59.4	118
168	0.000	1.000	0.642	0.00924	32.5	10.8	18.8	67.9	135
190	0.000	1.000	0.568	0.0104	36.8	12.3	21.2	76.8	153
213	0.000	1.000	0.506	0.0117	41.3	13.8	23.8	86.1	171
241	0.000	1.000	0.448	0.0132	46.6	15.5	26.9	97.4	194
276	0.000	1.000	0.391	0.0152	53.4	17.8	30.8	112	222
313	0.000	1.000	0.345	0.0172	60.6	20.2	35.0	126	252
352	0.000	1.000	0.306	0.0194	68.2	22.7	39.4	142	283
398	0.000	1.000	0.270	0.0219	77.2	25.7	44.6	161	320
449	0.000	1.000	0.240	0.0247	86.9	29.0	50.2	181	361
509	0.000	1.000	0.212	0.0280	98.7	32.9	57.0	206	409
578	0.000	1.000	0.186	0.0318	112	37.4	64.7	234	465
653	0.000	1.000	0.165	0.0359	127	42.2	73.0	264	525
734	0.000	1.000	0.147	0.0403	142	47.4	82.1	297	590
829	0.000	1.000	0.130	0.0456	161	53.5	92.7	335	666
944	0.000	1.000	0.114	0.0519	183	61.0	106	382	759
1080	0.000	1.000	0.0999	0.0593	209	69.6	121	436	868
1220	0.000	1.000	0.0884	0.0670	236	78.7	136	493	981

Sample: RM1-10HB-901m

Median Pore Throat, µm	pore radius, µm	System	Approximate Threshold Data, Entry Pressure, psia Lab	Resv	Height, ft
0.0110	0.0321	A-Hg	3356.5	-	n/a
		G-W	650.5	451.7	1356
		O-W	375.5	234.7	2698
		A-Hg	23143	(kPa)	

Pressure, psia	Increm. Hg sat'n fraction	Cumulative Kf
0.550	0.0000	0.00E+00
0.83	0.0000	0.00E+00
1.10	0.0000	0.00E+00
1.41	0.0000	0.00E+00
1.75	0.0000	0.00E+00
2.13	0.0000	0.00E+00
2.57	0.0000	0.00E+00
3.06	0.0000	0.00E+00
3.62	0.0000	0.00E+00
4.20	0.0000	0.00E+00
4.85	0.0000	0.00E+00
5.53	0.0000	0.00E+00
6.27	0.0000	0.00E+00
7.05	0.0000	0.00E+00
7.90	0.0000	0.00E+00
8.80	0.0000	0.00E+00
9.73	0.0000	0.00E+00
10.8	0.0000	0.00E+00
11.9	0.0000	0.00E+00
13.4	0.0000	0.00E+00
15.3	0.0000	0.00E+00
17.6	0.0000	0.00E+00
20.4	0.0000	0.00E+00
23.6	0.0000	0.00E+00
26.9	0.0000	0.00E+00
31.3	0.0000	0.00E+00
36.5	0.0000	0.00E+00
42.1	0.0000	0.00E+00
48.3	0.0000	0.00E+00
55.2	0.0000	0.00E+00
62.0	0.0000	0.00E+00
70.6	0.0000	0.00E+00
80.0	0.0000	0.00E+00
90.6	0.0000	0.00E+00
103	0.0000	0.00E+00
115	0.0000	0.00E+00
131	0.0000	0.00E+00
147	0.0000	0.00E+00
168	0.0000	0.00E+00
190	0.0000	0.00E+00
213	0.0000	0.00E+00
241	0.0000	0.00E+00
276	0.0000	0.00E+00
313	0.0000	0.00E+00
352	0.0000	0.00E+00
398	0.0000	0.00E+00
449	0.0000	0.00E+00
509	0.0000	0.00E+00
578	0.0000	0.00E+00
653	0.0000	0.00E+00
734	0.0000	0.00E+00
829	0.0000	0.00E+00
944	0.0000	0.00E+00
1080	0.0000	0.00E+00
1220	0.0000	0.00E+00

Pore Throat Radius, µm	Hg Sat'n, fraction cumulative	frequency
<0.0025	0.017	0.017
0.0050	0.122	0.105
0.0075	0.253	0.130
0.010	0.418	0.166
0.025	0.989	0.571
0.050	1.000	0.011
0.075	1.000	0.000
0.10	1.000	0.000
0.25	1.000	0.000
0.50	1.000	0.000
0.75	1.000	0.000
1.0	1.000	0.000
2.5	1.000	0.000
5.0	1.000	0.000
7.5	1.000	0.000
10	1.000	0.000
25	1.000	0.000
50	1.000	0.000
75	1.000	0.000
100	1.000	0.000
>100	1.000	0.000

Conversion Parameters	air/water	air/oil	oil/water
Laboratory Theta -->	0.0	0.0	30.0
Laboratory IFT -->	72.0	24.0	48.0
Reservoir Theta -->	0.0	0.0	30.0
Reservoir IFT	50.0	0.0	30.0
Laboratory TcosTheta -->	72.0	24.0	41.6
Reservoir TcosTheta -->	50.0	0.0	26.0
A-Hg Contact Angle:	140		
A-Hg IFT:	485		
A-Hg TcosTheta:	371.5		
Density Gradients, psi/foot		(typical)	
Water:	**0.433**	0.433	
Oil:	**0.346**	0.346	
Gas:	**0.100**	0.100	

Sample Parameters	
Weight, g	21.788
PVol, cc	0.552
GVol, cc	8.044
BVol, cc	8.597
GDens, gm/cc	2.709
Bdens, gm/cc	2.534

R35 Line	
0.001	0.35
100	0.35
Micro boundary	
0.5	0
0.5	1
Macro boundary	
2.5	0
2.5	1

Gas-Water Pc Test Pc	I-F Sw
0	
25	
50	
100	
200	
300	
450	
650	
900	
1200	

Total Surface Area
m^2/g

Qv value is from:

estimated	CoCw	NMR	CEC	BJ adsb H2O

Qv Correction

1	Salinity, g/L
0.00	Qv, e/L
1.000	A = phi(eff)/phi(tot)
-	Qv, e/L for ~good match
-	Qv from companion

Thomeer and Swanson Parameters

PS1 (large pore system) G Factor	Pd	BV(inf)	PS2 (fine pore system) G Factor	Pd	BV(inf)	PS3 (fine pore system) G Factor	Pd	BV(inf)		BV TOTAL
										0.00
Thomeer K, md:		#DIV/0!	Swanson K md:		0.00					
Swanson Point is at mas Bv corr/Pc =		0.0003	Pc =	12496	Bv=	4.372				

MERCURY INJECTION DATA SUMMARY

Company: University of Utah
Well: RMCCS State #1
Formation: Mowry
File: HOU-130069

Sample:	**RM1-10HB-901m**	un-	Host Plug	
Depth, feet:	8206.00	stressed	800psi	3580psi
Klinkenberg Permeability, md:		N/A	0.911*	0.0941*
Permeability to Air, md:		N/A	1.01*	0.115*
Swanson Permeability, md:		5.71E-04	-	-
Porosity, fraction:		0.064	0.061	0.054
maximum Sb/Pc, fraction:		3.50E-04		
R35, microns:		0.0130		
R50 (median pore throat radius):		0.0110		

*Permeability may be optimistic due to fracutre(s) in sample.

Injection Pressure, psia	Mercury Saturation, fraction	Pseudo-Wetting Saturation, fraction	Pore Throat Radius, microns	J Values	Conversion to other Laboratory Fluid Systems, psia G-W	G-O	O-W	Estimated Height Above Free Water, feet G-W	O-W
1370	0.000	1.000	0.0788	0.0752	265	88.4	153	554	1100
1540	0.000	1.000	0.0701	0.0846	298	99.3	172	622	1240
1750	0.000	1.000	0.0616	0.0962	339	113	196	707	1410
1980	0.000	1.000	0.0545	0.109	383	128	221	800	1590
2220	0.000	1.000	0.0486	0.122	430	143	248	897	1780
2510	0.000	1.000	0.0430	0.138	486	162	281	1010	2020
2830	0.000	1.000	0.0381	0.156	548	183	316	1140	2270
3220	0.000	1.000	0.0335	0.177	624	208	360	1300	2590
3660	0.003	0.997	0.0295	0.201	709	236	409	1480	2940
4150	0.009	0.991	0.0260	0.228	804	268	464	1680	3340
4700	0.017	0.983	0.0229	0.258	910	303	525	1900	3780
5300	0.035	0.965	0.0203	0.291	1030	342	593	2140	4260
5970	0.079	0.921	0.0181	0.328	1160	385	668	2410	4800
6750	0.158	0.842	0.0160	0.371	1310	436	755	2730	5430
7650	0.263	0.737	0.0141	0.421	1480	494	855	3090	6150
8650	0.381	0.619	0.0125	0.476	1680	559	967	3500	6950
9790	0.499	0.501	0.0110	0.538	1900	632	1100	3960	7870
11000	0.601	0.399	0.00976	0.607	2140	713	1230	4450	8840
12500	0.681	0.319	0.00862	0.687	2420	807	1400	5050	10000
14100	0.740	0.260	0.00763	0.777	2740	912	1580	5700	11300
16000	0.789	0.211	0.00674	0.879	3100	1030	1790	6470	12900
18100	0.830	0.170	0.00596	0.994	3500	1170	2020	7310	14500
20400	0.865	0.135	0.00527	1.12	3960	1320	2290	8240	16400
23100	0.893	0.107	0.00466	1.27	4480	1490	2590	9340	18600
26200	0.918	0.082	0.00412	1.44	5070	1690	2930	10600	21100
29600	0.940	0.060	0.00364	1.63	5730	1910	3310	12000	23800
33500	0.959	0.041	0.00322	1.84	6490	2160	3750	13500	26900
37800	0.972	0.028	0.00285	2.08	7330	2440	4230	15300	30400
43000	0.983	0.017	0.00250	2.37	8340	2780	4810	17400	34600
48400	0.988	0.012	0.00223	2.66	9380	3130	5420	19600	38900
55000	0.993	0.007	0.00196	3.02	10700	3550	6150	22200	44200

Sample: RM1-10HB-901m

Median Pore Throat, µm	pore radius, µm	System	Approximate Threshold Data, Entry Pressure, psia Lab	Resv	Height, ft
0.0110	0.0321	**A-Hg**	3356.5	-	n/a
		G-W	650.5	451.7	1356
		O-W	375.5	234.7	2698
		A-Hg	23143	(kPa)	

Pore Throat Radius, µm	Hg Sat'n, fraction cumulative	frequency
<0.0025	0.017	0.017
0.0050	0.122	0.105
0.0075	0.253	0.130
0.010	0.418	0.166
0.025	0.989	0.571

Pressure, psia	Increm. Hg sat'n fraction	Cumulative Kf
0.550	0.0000	0.00E+00
1370	0.0000	0.00E+00
1540	0.0000	0.00E+00
1750	0.0000	0.00E+00
1980	0.0000	0.00E+00
2220	0.0000	0.00E+00
2510	0.0000	0.00E+00
2830	0.0000	0.00E+00
3220	0.0000	0.00E+00
3660	0.0034	2.26E-02
4150	0.0051	4.88E-02
4700	0.0081	8.14E-02
5300	0.0186	1.40E-01
5970	0.0439	2.48E-01
6750	0.0784	4.00E-01
7650	0.1055	5.59E-01
8650	0.1180	6.98E-01
9790	0.1182	8.07E-01
11000	0.1021	8.80E-01
12500	0.0799	9.25E-01
14100	0.0593	9.52E-01
16000	0.0481	9.68E-01
18100	0.0413	9.79E-01
20400	0.0352	9.87E-01
23100	0.0282	9.91E-01
26200	0.0248	9.95E-01
29600	0.0220	9.97E-01
33500	0.0186	9.98E-01
37800	0.0136	9.99E-01
43000	0.0102	1.00E+00
48400	0.0059	1.00E+00
55000	0.0051	1.00E+00

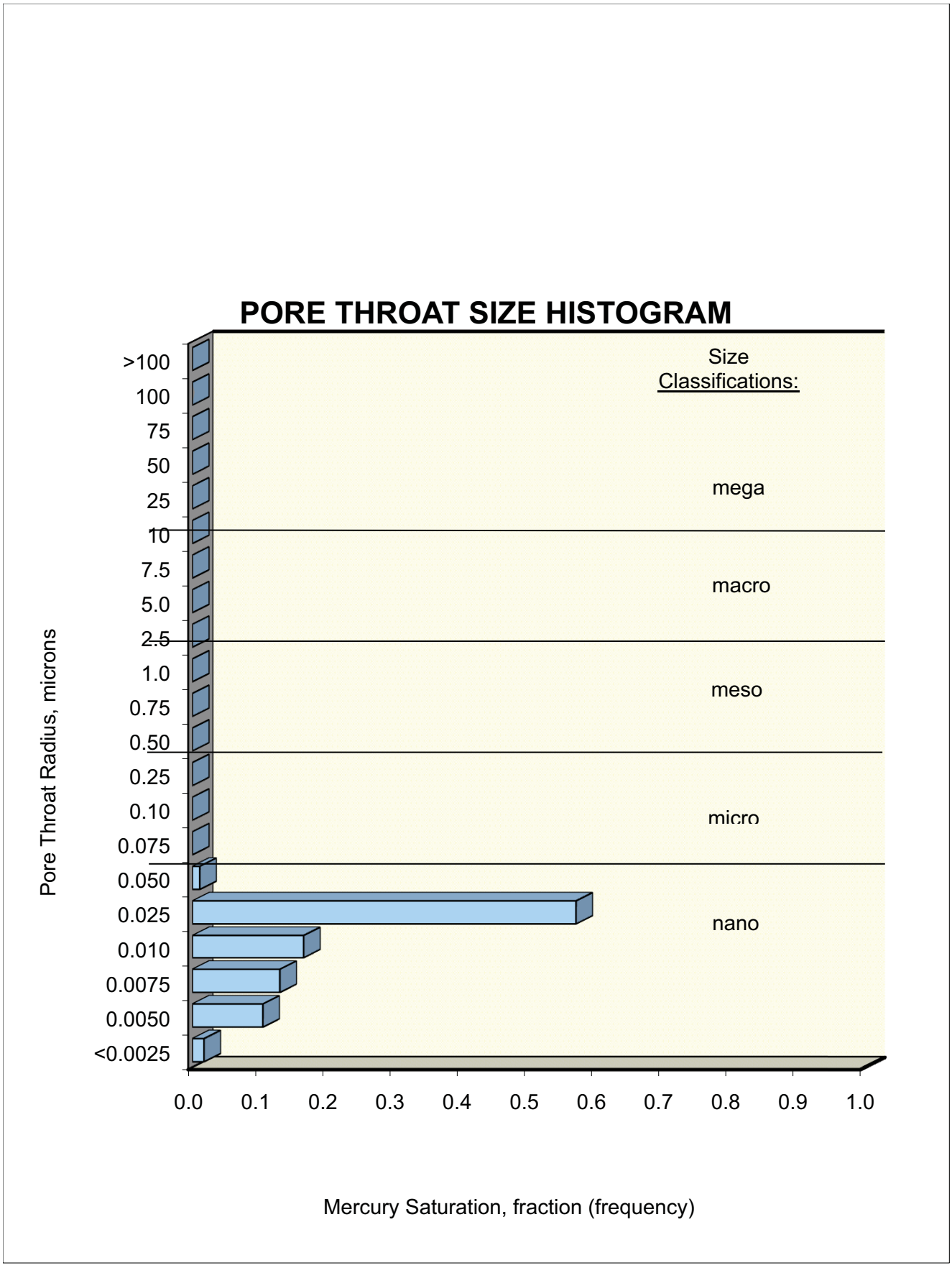
Conversion Parameters

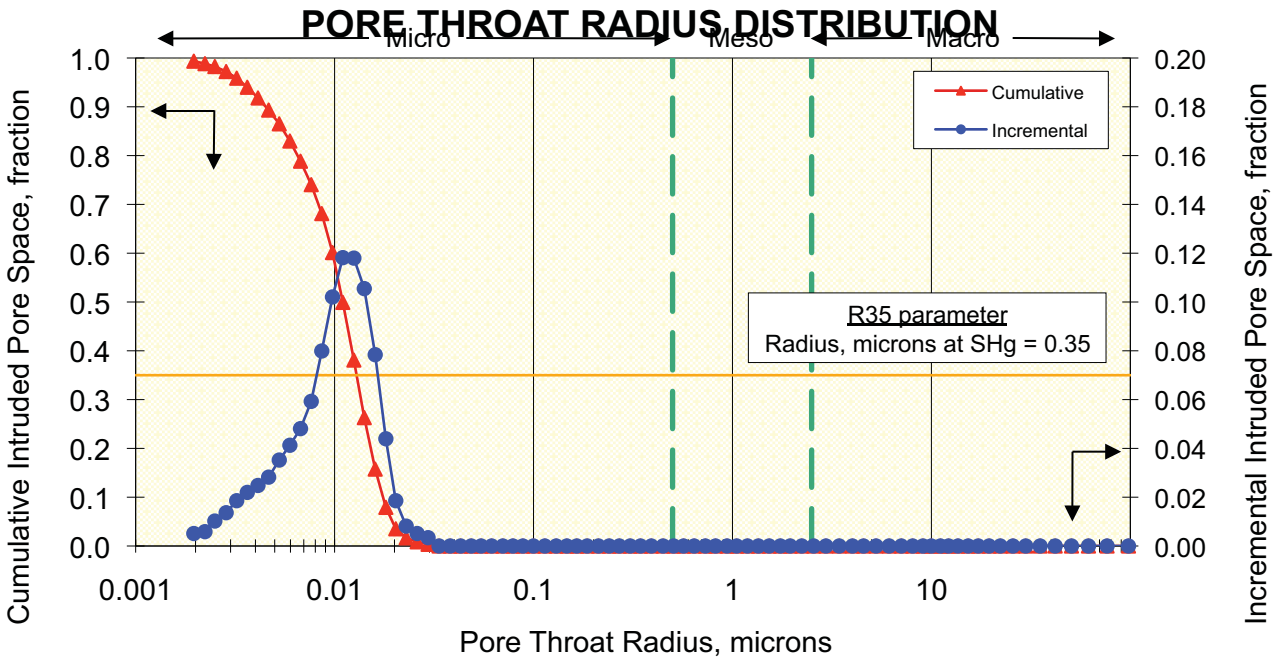
	air/water	air/oil	oil/water
Laboratory Theta -->	0.0	0.0	30.0
Laboratory IFT -->	72.0	24.0	48.0
Reservoir Theta -->	0.0	0.0	30.0
Reservoir IFT	50.0	0.0	30.0
Laboratory TcosTheta -->	72.0	24.0	41.6
Reservoir TcosTheta -->	50.0	0.0	26.0
A-Hg Contact Angle:	140		
A-Hg IFT:	485		
A-Hg TcosTheta:	371.5		

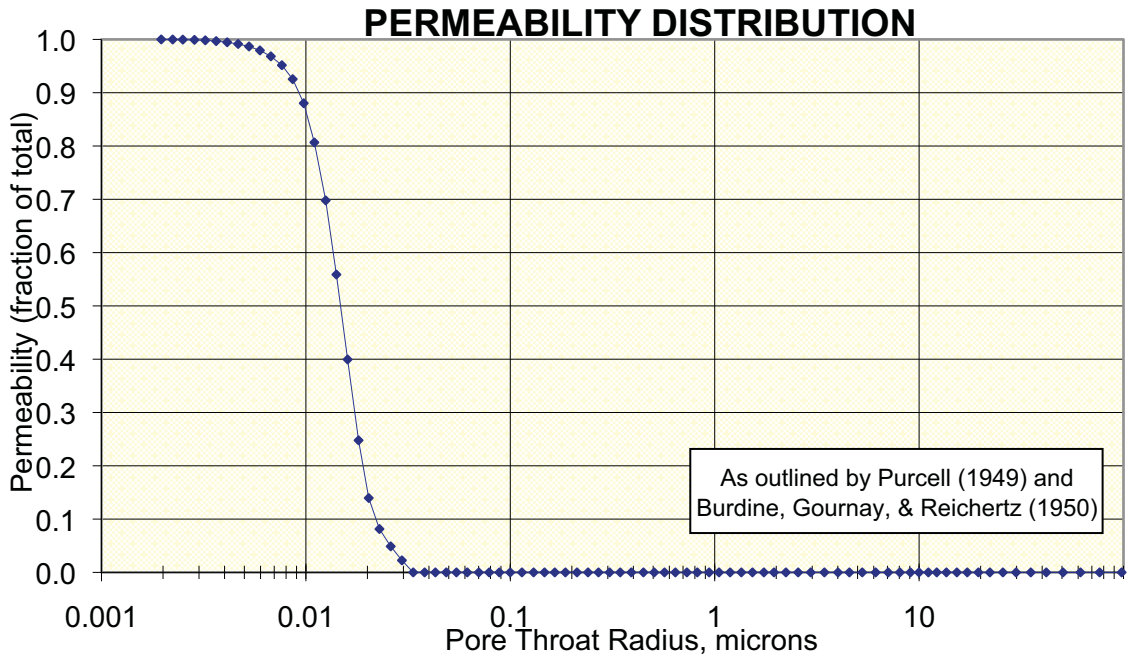
Density Gradients, psi/foot		(typical)
Water:	**0.433**	0.433
Oil:	**0.346**	0.346
Gas:	**0.100**	0.100

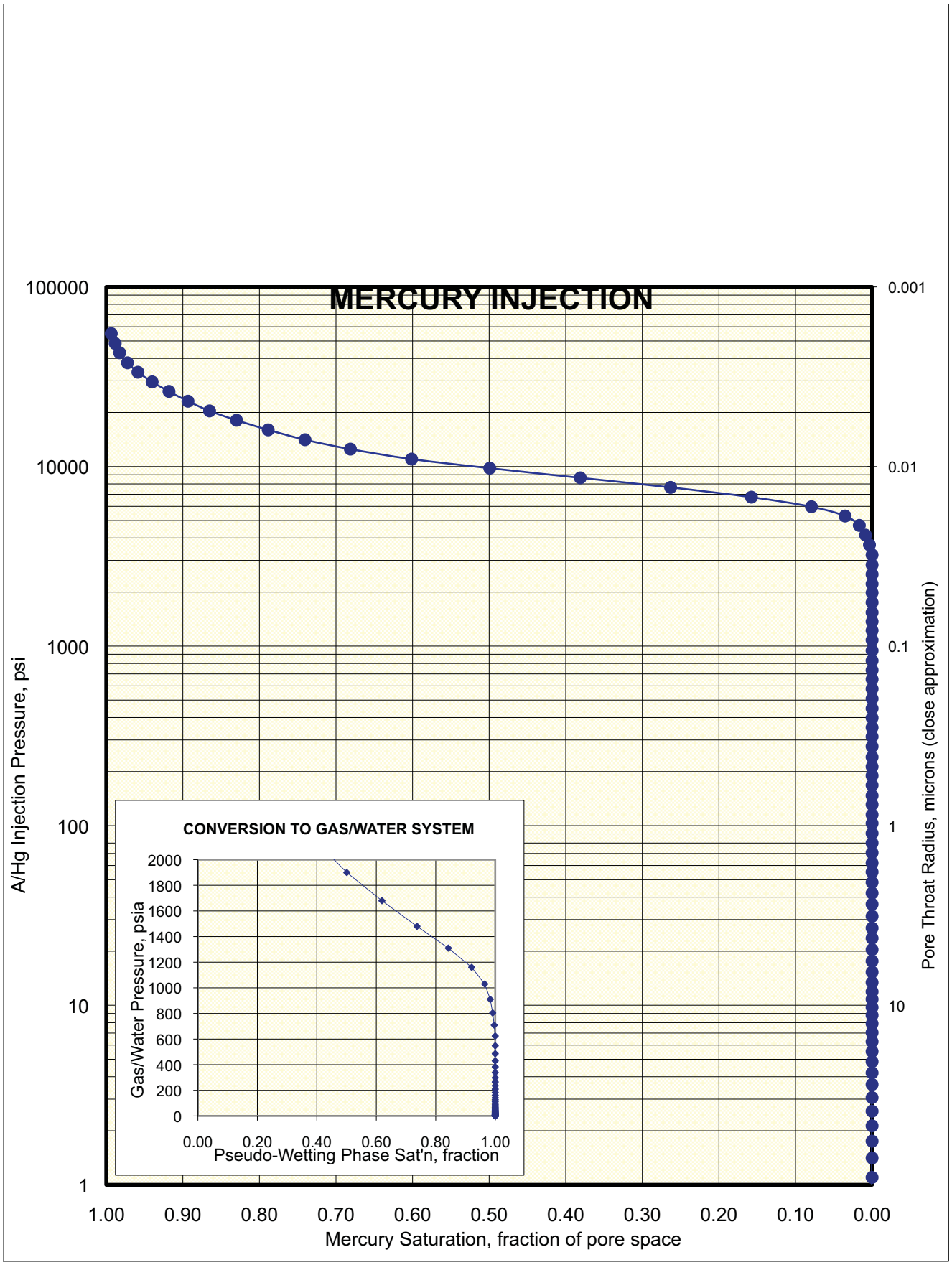
Sample Parameters

Gas-Water Pc Test	
Pc	I-F Sw
0	
25	
50	
100	
200	
300	
450	


PORE THROAT SIZE HISTOGRAM
Size
Classifications:
mega
macro
meso
micro
nano
>100
100
75
50
25
10
7.5
5.0
2.5
1.0
0.75
0.50
0.25
0.10
0.075
0.050
0.025
0.010
0.0075
0.0050
<0.0025
Pore Throat Radius, microns
0.0
0.1
0.2
0.3
0.4
0.5
0.6
0.7
0.8
0.9
1.0
Mercury Saturation, fraction (frequency)


PORE THROAT RADIUS DISTRIBUTION
Micro
Meso
Macro
Cumulative
Incremental
R35 parameter
Radius, microns at SHg = 0.35
Cumulative Intruded Pore Space, fraction
Incremental Intruded Pore Space, fraction
Pore Throat Radius, microns
1.0
0.9
0.8
0.7
0.6
0.5
0.4
0.3
0.2
0.1
0.0
0.20
0.18
0.16
0.14
0.12
0.10
0.08
0.06
0.04
0.02
0.00
0.001
0.01
0.1
1
10


PERMEABILITY DISTRIBUTION
As outlined by Purcell (1949) and
Burdine, Gournay, & Reichertz (1950)
Permeability (fraction of total)
Pore Throat Radius, microns
1.0
0.9
0.8
0.7
0.6
0.5
0.4
0.3
0.2
0.1
0.0
0.001
0.01
0.1
1
10


MERCURY INJECTION
A/Hg Injection Pressure, psi
100000
10000
1000
100
10
1
Pore Throat Radius, microns (close approximation)
0.001
0.01
0.1
1
10
1.00
0.90
0.80
0.70
0.60
0.50
0.40
0.30
0.20
0.10
0.00
Mercury Saturation, fraction of pore space
CONVERSION TO GAS/WATER SYSTEM
Gas/Water Pressure, psia
2000
1800
1600
1400
1200
1000
800
600
400
200
0
0.00
0.20
0.40
0.60
0.80
1.00
Pseudo-Wetting Phase Sat'n, fraction

MERCURY INJECTION DATA SUMMARY

Company: University of Utah
Well: RMCCS State #1
Formation: Mowry
File: HOU-130069

Sample: RM1-21HB-P01m	un-stressed	Host Plug 800psi	Host Plug 3580psi
Depth, feet: 8235.00			
Klinkenberg Permeability, md:	N/A	7.02*	0.580*
Permeability to Air, md:	N/A	7.45*	0.727*
Swanson Permeability, md:	2.62E-05	-	-
Porosity, fraction:	0.035	0.029	0.016
maximum Sb/Pc, fraction:	5.67E-05		
R35, microns:	0.00315		
R50 (median pore throat radius):	0.00272		

*Permeability may be optimistic due to fracutre(s) in sample.

Injection Pressure, psia	Mercury Saturation, fraction	Pseudo-Wetting Saturation, fraction	Pore Throat Radius, microns	J Values	Conversion to other Laboratory Fluid Systems, psia G-W	G-O	O-W	Estimated Height Above Free Water, feet G-W	O-W
5.99	0.000	1.000	18.0	0.000096	1.16	0.387	0.670	2.42	4.81
6.73	0.000	1.000	16.0	0.000108	1.30	0.435	0.753	2.72	5.41
7.44	0.000	1.000	14.5	0.000119	1.44	0.481	0.832	3.01	5.98
8.31	0.000	1.000	13.0	0.000133	1.61	0.537	0.930	3.36	6.68
9.25	0.000	1.000	11.6	0.000148	1.79	0.598	1.03	3.74	7.43
10.3	0.000	1.000	10.4	0.000165	2.00	0.667	1.15	4.16	8.28
11.5	0.000	1.000	9.38	0.000184	2.23	0.742	1.29	4.65	9.24
12.8	0.000	1.000	8.41	0.000205	2.48	0.827	1.43	5.17	10.3
14.3	0.000	1.000	7.56	0.000228	2.76	0.921	1.60	5.78	11.5
15.9	0.000	1.000	6.78	0.000254	3.08	1.03	1.78	6.43	12.8
17.7	0.000	1.000	6.08	0.000283	3.43	1.14	1.98	7.15	14.2
19.9	0.000	1.000	5.42	0.000318	3.85	1.28	2.23	8.04	16.0
22.1	0.000	1.000	4.87	0.000354	4.29	1.43	2.48	8.93	17.8
24.7	0.000	1.000	4.37	0.000395	4.78	1.59	2.76	9.98	19.9
26.9	0.000	1.000	4.01	0.000430	5.21	1.74	3.01	10.9	21.6
29.7	0.000	1.000	3.63	0.000475	5.75	1.92	3.32	12.0	23.9
32.0	0.000	1.000	3.37	0.000511	6.20	2.07	3.58	12.9	25.7
36.4	0.000	1.000	2.96	0.000582	7.06	2.35	4.07	14.7	29.3
40.9	0.000	1.000	2.63	0.000654	7.93	2.64	4.58	16.5	32.9
45.5	0.000	1.000	2.37	0.000728	8.82	2.94	5.09	18.4	36.6
51.4	0.000	1.000	2.10	0.000822	9.95	3.32	5.75	20.8	41.3
56.7	0.000	1.000	1.90	0.000907	11.0	3.66	6.34	22.9	45.6
65.4	0.000	1.000	1.65	0.00105	12.7	4.23	7.32	26.4	52.6
71.8	0.000	1.000	1.50	0.00115	13.9	4.63	8.03	29.0	57.7
79.6	0.000	1.000	1.35	0.00127	15.4	5.14	8.91	32.2	64.0
89.1	0.000	1.000	1.21	0.00143	17.3	5.76	9.97	36.0	71.6
98.0	0.000	1.000	1.10	0.00157	19.0	6.33	11.0	39.6	78.8
111	0.000	1.000	0.970	0.00178	21.5	7.17	12.4	44.9	89.2
124	0.000	1.000	0.869	0.00198	24.0	8.01	13.9	50.1	99.7
138	0.000	1.000	0.782	0.00220	26.7	8.90	15.4	55.8	111
154	0.000	1.000	0.698	0.00247	29.9	9.98	17.3	62.2	124
172	0.000	1.000	0.626	0.00275	33.4	11.1	19.3	69.5	138
192	0.000	1.000	0.562	0.00307	37.2	12.4	21.5	77.6	154
215	0.000	1.000	0.501	0.00344	41.7	13.9	24.1	86.9	173
238	0.000	1.000	0.453	0.00380	46.1	15.4	26.6	96.2	191
266	0.000	1.000	0.404	0.00426	51.6	17.2	29.8	108	214
298	0.000	1.000	0.362	0.00476	57.7	19.2	33.3	120	240
332	0.000	1.000	0.324	0.00532	64.4	21.5	37.2	134	267
370	0.000	1.000	0.291	0.00592	71.8	23.9	41.4	150	297
413	0.000	1.000	0.261	0.00660	80.0	26.7	46.2	167	332
458	0.000	1.000	0.235	0.00733	88.8	29.6	51.3	185	368
513	0.000	1.000	0.210	0.00820	99.3	33.1	57.3	207	412
572	0.000	1.000	0.188	0.00916	111	37.0	64.0	231	460
639	0.000	1.000	0.169	0.0102	124	41.3	71.5	258	514
713	0.000	1.000	0.151	0.0114	138	46.0	79.7	288	573
793	0.000	1.000	0.136	0.0127	154	51.2	88.7	320	637
884	0.000	1.000	0.122	0.0141	171	57.1	98.9	357	711
985	0.000	1.000	0.109	0.0158	191	63.6	110	398	792
1100	0.000	1.000	0.0980	0.0176	213	71.0	123	445	884
1230	0.000	1.000	0.0879	0.0196	238	79.2	137	497	989
1370	0.000	1.000	0.0787	0.0219	265	88.4	153	554	1100
1520	0.000	1.000	0.0707	0.0244	295	98.4	170	614	1220
1700	0.000	1.000	0.0634	0.0272	329	110	190	687	1370
1890	0.000	1.000	0.0569	0.0303	367	122	212	764	1520

Sample: RM1-21HB-P01m

Median Pore Throat, µm	Approximate Threshold Data, pore radius, µm	System	Entry Pressure, psia Lab	Resv	Height, ft
0.00272	0.0168	A-Hg	6430.2	-	n/a
		G-W	1246.1	865.4	2599
		O-W	719.4	449.7	5168
		A-Hg	44336	(kPa)	

Pressure, psia	Increm. Hg sat'n fraction	Cumulative Kf
5.010	0.0000	0.00E+00
5.99	0.0000	0.00E+00
6.73	0.0000	0.00E+00
7.44	0.0000	0.00E+00
8.31	0.0000	0.00E+00
9.25	0.0000	0.00E+00
10.3	0.0000	0.00E+00
11.5	0.0000	0.00E+00
12.8	0.0000	0.00E+00
14.3	0.0000	0.00E+00
15.9	0.0000	0.00E+00
17.7	0.0000	0.00E+00
19.9	0.0000	0.00E+00
22.1	0.0000	0.00E+00
24.7	0.0000	0.00E+00
26.9	0.0000	0.00E+00
29.7	0.0000	0.00E+00
32.0	0.0000	0.00E+00
36.4	0.0000	0.00E+00
40.9	0.0000	0.00E+00
45.5	0.0000	0.00E+00
51.4	0.0000	0.00E+00
56.7	0.0000	0.00E+00
65.4	0.0000	0.00E+00
71.8	0.0000	0.00E+00
79.6	0.0000	0.00E+00
89.1	0.0000	0.00E+00
98.0	0.0000	0.00E+00
111	0.0000	0.00E+00
124	0.0000	0.00E+00
138	0.0000	0.00E+00
154	0.0000	0.00E+00
172	0.0000	0.00E+00
192	0.0000	0.00E+00
215	0.0000	0.00E+00
238	0.0000	0.00E+00
266	0.0000	0.00E+00
298	0.0000	0.00E+00
332	0.0000	0.00E+00
370	0.0000	0.00E+00
413	0.0000	0.00E+00
458	0.0000	0.00E+00
513	0.0000	0.00E+00
572	0.0000	0.00E+00
639	0.0000	0.00E+00
713	0.0000	0.00E+00
793	0.0000	0.00E+00
884	0.0000	0.00E+00
985	0.0000	0.00E+00
1100	0.0000	0.00E+00
1230	0.0000	0.00E+00
1370	0.0000	0.00E+00
1520	0.0000	0.00E+00
1700	0.0000	0.00E+00
1890	0.0000	0.00E+00

Pore Throat Radius, µm	Hg Sat'n, fraction cumulative	frequency
<0.0025	0.390	0.390
0.0050	0.874	0.485
0.0075	0.935	0.060
0.010	0.959	0.025
0.025	1.000	0.041
0.050	1.000	0.000
0.075	1.000	0.000
0.10	1.000	0.000
0.25	1.000	0.000
0.50	1.000	0.000
0.75	1.000	0.000
1.0	1.000	0.000
2.5	1.000	0.000
5.0	1.000	0.000
7.5	1.000	0.000
10	1.000	0.000
25	1.000	0.000
50	1.000	0.000
75	1.000	0.000
100	1.000	0.000
>100	1.000	0.000

Conversion Parameters	air/water	air/oil	oil/water
Laboratory Theta -->	0.0	0.0	30.0
Laboratory IFT -->	72.0	24.0	48.0
Reservoir Theta -->	0.0	0.0	30.0
Reservoir IFT	50.0	0.0	30.0
Laboratory TcosTheta -->	72.0	24.0	41.6
Reservoir TcosTheta -->	50.0	0.0	26.0
A-Hg Contact Angle:	140		
A-Hg IFT:	485		
A-Hg TcosTheta:	371.5		
Density Gradients, psi/foot		(typical)	
Water:	**0.433**	0.433	
Oil:	**0.346**	0.346	
Gas:	**0.100**	0.100	

Sample Parameters	
Weight, g	15.575
PVol, cc	0.219
GVol, cc	6.062
BVol, cc	6.288
GDens, gm/cc	2.569
Bdens, gm/cc	2.477

R35 Line	
0.001	0.35
100	0.35
Micro boundary	
0.5	0
0.5	1
Macro boundary	
2.5	0
2.5	1

Gas-Water Pc Test	
Pc	I-F Sw
0	
25	
50	
100	
200	
300	
450	
650	
900	
1200	

Total Surface Area
m^2/g

Qv value is from:

estimated	CoCw	NMR	CEC	BJ adsb H2O

Qv Correction

1	Salinity, g/L
0.00	Qv, e/L
1.000	A = phi(eff)/phi(tot)
-	Qv, e/L for ~good match
-	Qv from companion

Thomeer and Swanson Parameters

PS1 (large pore system) G Factor	Pd	BV(inf)	PS2 (fine pore system) G Factor	Pd	BV(inf)	PS3 (fine pore system) G Factor	Pd	BV(inf)		BV TOTAL
										0.00
Thomeer K, md:		#DIV/0!	Swanson K md:		0.00					
Swanson Point is at mas Bv corr/Pc =		0.0001	Pc =		54962	Bv=		3.117		

MERCURY INJECTION DATA SUMMARY

Company: University of Utah
Well: RMCCS State #1
Formation: Mowry
File: HOU-130069

*Permeability may be optimistic due to fracutre(s) in sample.

Sample: RM1-21HB-P01m	un-stressed	Host Plug 800psi	Host Plug 3580psi
Depth, feet: 8235.00			
Klinkenberg Permeability, md:	N/A	7.02*	0.580*
Permeability to Air, md:	N/A	7.45*	0.727*
Swanson Permeability, md:	2.62E-05	-	-
Porosity, fraction:	0.035	0.029	0.016
maximum Sb/Pc, fraction:	5.67E-05		
R35, microns:	0.00315		
R50 (median pore throat radius):	0.00272		

Injection Pressure, psia	Mercury Saturation, fraction	Pseudo-Wetting Saturation, fraction	Pore Throat Radius, microns	J Values	Conversion to other Laboratory Fluid Systems, psia G-W	G-O	O-W	Estimated Height Above Free Water, feet G-W	O-W
2110	0.000	1.000	0.0510	0.0338	409	136	236	853	1700
2360	0.000	1.000	0.0457	0.0377	456	152	264	954	1900
2620	0.000	1.000	0.0411	0.0420	509	170	294	1060	2110
2930	0.000	1.000	0.0368	0.0468	567	189	327	1180	2360
3260	0.000	1.000	0.0330	0.0522	632	211	365	1320	2620
3640	0.000	1.000	0.0296	0.0582	705	235	407	1470	2930
4050	0.000	1.000	0.0266	0.0649	786	262	454	1640	3260
4520	0.000	1.000	0.0238	0.0723	876	292	506	1830	3630
5040	0.000	1.000	0.0214	0.0805	976	325	563	2040	4050
5610	0.000	1.000	0.0192	0.0898	1090	363	628	2270	4510
6260	0.000	1.000	0.0172	0.100	1210	404	700	2530	5030
6980	0.007	0.993	0.0154	0.112	1350	451	781	2820	5610
7780	0.014	0.986	0.0139	0.124	1510	502	870	3140	6250
8670	0.022	0.978	0.0124	0.139	1680	560	970	3500	6970
9670	0.031	0.969	0.0111	0.155	1870	624	1080	3910	7770
10800	0.041	0.959	0.0100	0.172	2090	696	1210	4360	8680
12000	0.049	0.951	0.00897	0.192	2330	776	1340	4850	9650
13400	0.060	0.940	0.00804	0.214	2600	865	1500	5420	10800
14900	0.068	0.932	0.00722	0.239	2890	965	1670	6020	12000
16600	0.086	0.914	0.00647	0.266	3230	1080	1860	6710	13300
18600	0.099	0.901	0.00581	0.297	3600	1200	2080	7520	15000
20700	0.117	0.883	0.00521	0.331	4010	1340	2310	8370	16600
23100	0.139	0.861	0.00467	0.369	4470	1490	2580	9340	18600
25700	0.169	0.831	0.00419	0.411	4980	1660	2880	10400	20700
28700	0.221	0.779	0.00376	0.458	5550	1850	3210	11600	23100
31900	0.288	0.712	0.00337	0.511	6190	2060	3570	12900	25600
35600	0.385	0.615	0.00303	0.570	6900	2300	3980	14400	28600
39700	0.506	0.494	0.00271	0.635	7690	2560	4440	16000	31900
44200	0.641	0.359	0.00244	0.708	8570	2860	4950	17900	35500
49300	0.781	0.219	0.00219	0.789	9550	3180	5520	19900	39600
55000	0.894	0.106	0.00196	0.879	10700	3550	6150	22200	44200

Sample: RM1-21HB-P01m

Median Pore Throat, µm	pore radius, µm	System	Approximate Threshold Data, Entry Pressure, psia Lab	Resv	Height, ft
0.00272	0.0168	**A-Hg**	6430.2	-	n/a
		G-W	1246.1	865.4	2599
		O-W	719.4	449.7	5168
		A-Hg	44336	(kPa)	

Pore Throat Radius, µm	Hg Sat'n, fraction cumulative	frequency
<0.0025	0.390	0.390
0.0050	0.874	0.485
0.0075	0.935	0.060
0.010	0.959	0.025
0.025	1.000	0.041

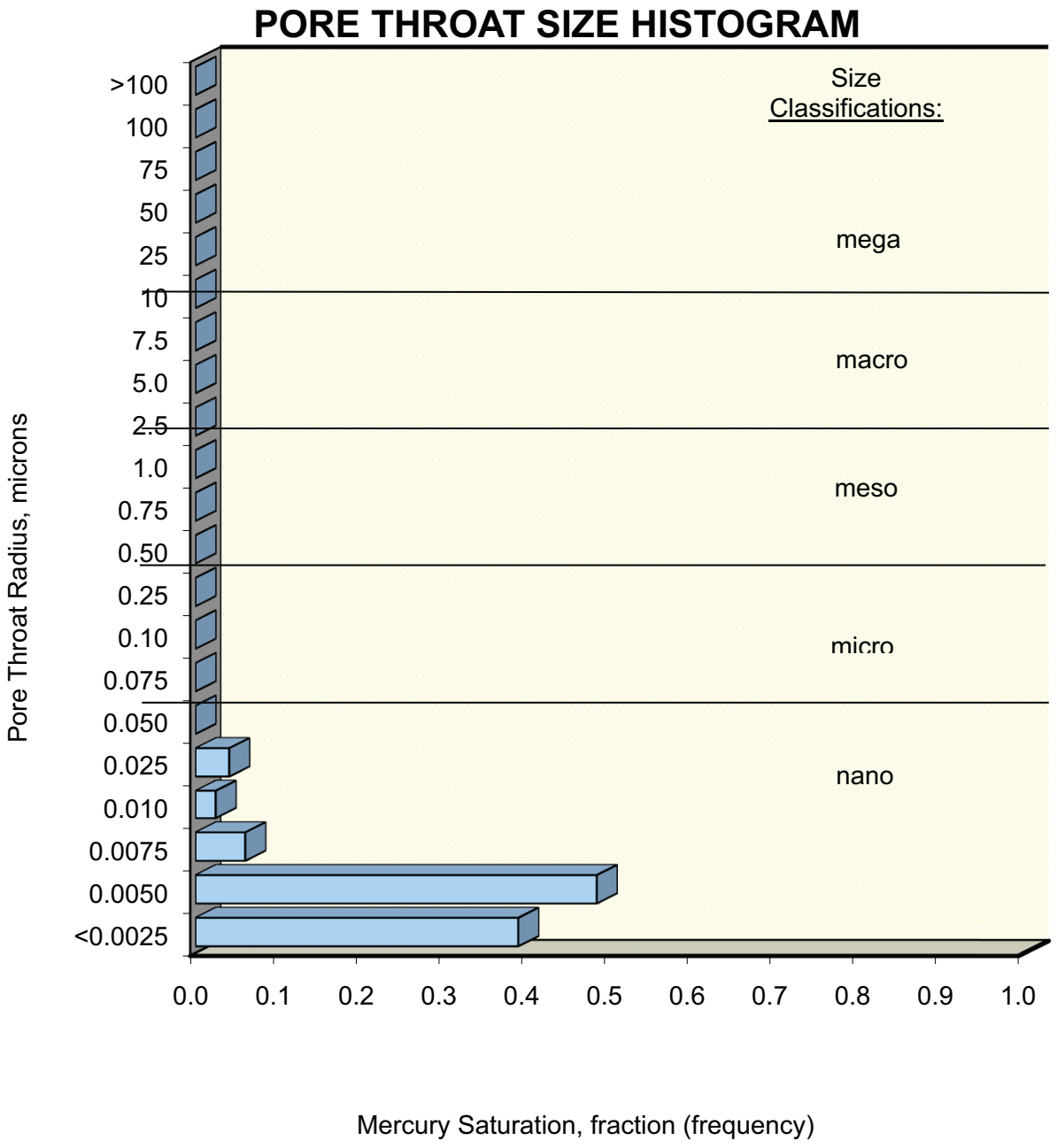
Pressure, psia	Increm. Hg sat'n fraction	Cumulative Kf
5.010	0.0000	0.00E+00
2110	0.0000	0.00E+00
2360	0.0000	0.00E+00
2620	0.0000	0.00E+00
2930	0.0000	0.00E+00
3260	0.0000	0.00E+00
3640	0.0000	0.00E+00
4050	0.0000	0.00E+00
4520	0.0000	0.00E+00
5040	0.0000	0.00E+00
5610	0.0000	0.00E+00
6260	0.0000	0.00E+00
6980	0.0066	9.88E-02
7780	0.0077	1.91E-01
8670	0.0072	2.61E-01
9670	0.0099	3.38E-01
10800	0.0094	3.97E-01
12000	0.0077	4.36E-01
13400	0.0110	4.80E-01
14900	0.0088	5.09E-01
16600	0.0171	5.54E-01
18600	0.0138	5.83E-01
20700	0.0177	6.13E-01
23100	0.0221	6.43E-01
25700	0.0298	6.76E-01
28700	0.0519	7.22E-01
31900	0.0673	7.70E-01
35600	0.0966	8.25E-01
39700	0.1214	8.81E-01
44200	0.1352	9.31E-01
49300	0.1397	9.73E-01
55000	0.1132	1.00E+00

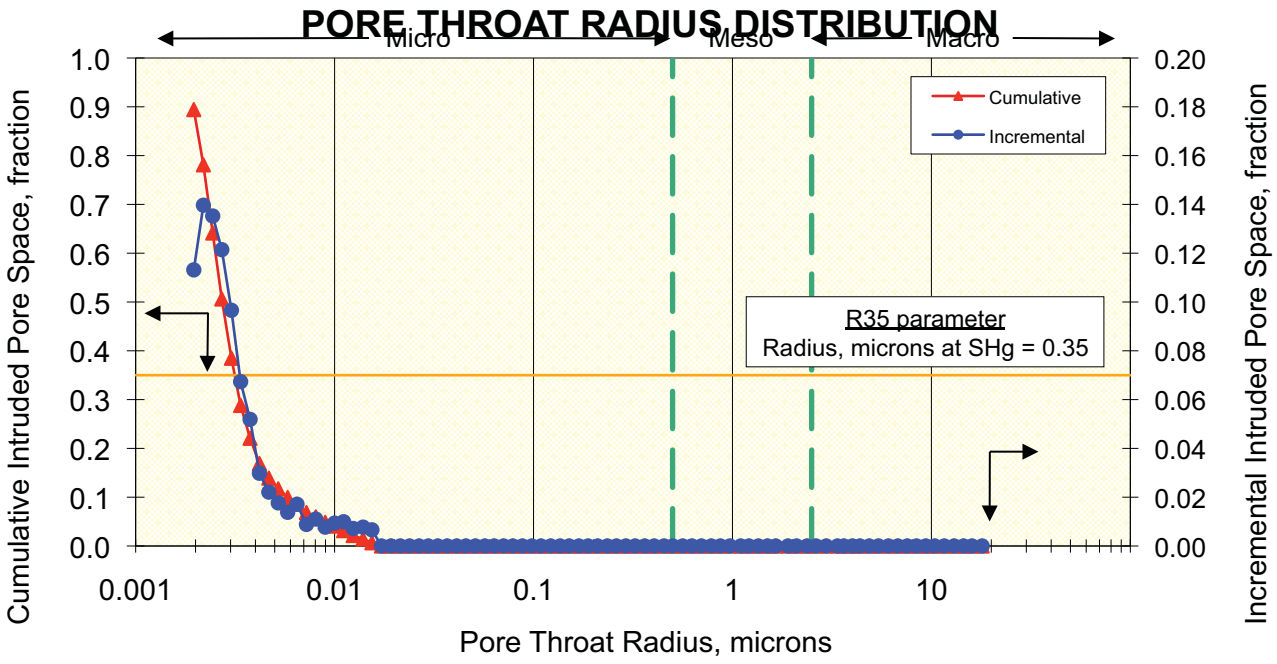
Conversion Parameters

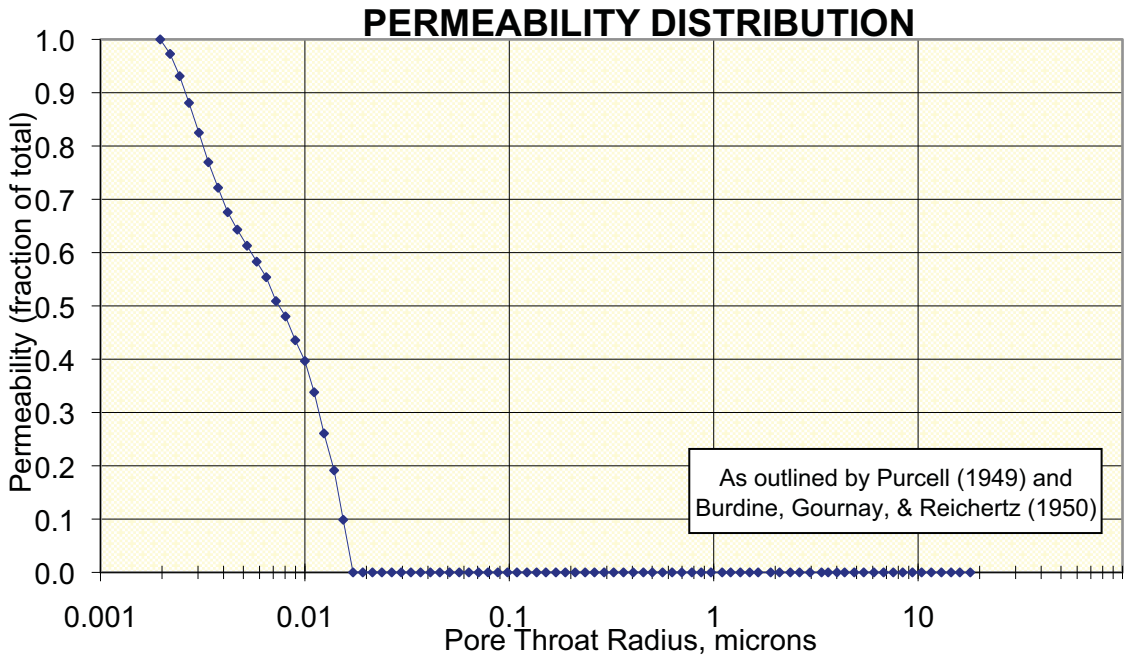
	air/water	air/oil	oil/water
Laboratory Theta -->	0.0	0.0	30.0
Laboratory IFT -->	72.0	24.0	48.0
Reservoir Theta -->	0.0	0.0	30.0
Reservoir IFT	50.0	0.0	30.0
Laboratory TcosTheta -->	72.0	24.0	41.6
Reservoir TcosTheta -->	50.0	0.0	26.0
A-Hg Contact Angle:	140		
A-Hg IFT:	485		
A-Hg TcosTheta:	371.5		
Density Gradients, psi/foot		(typical)	
Water:	**0.433**	0.433	
Oil:	**0.346**	0.346	
Gas:	**0.100**	0.100	

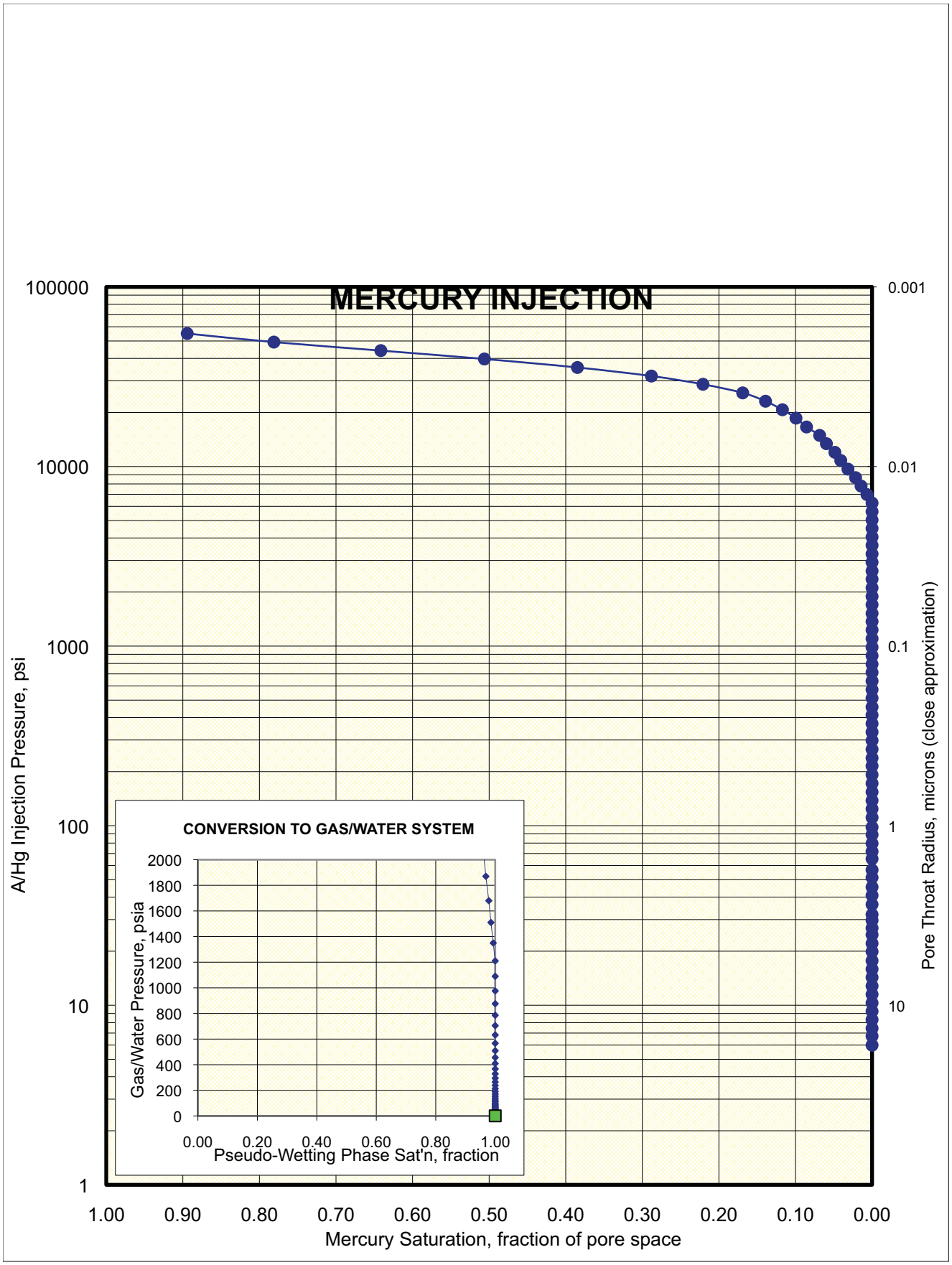
Sample Parameters

Gas-Water Pc Test Pc	I-F Sw
0	
25	
50	
100	
200	
300	
450	


PORE THROAT SIZE HISTOGRAM
Size
Classifications:
mega
macro
meso
micro
nano
>100
100
75
50
25
10
7.5
5.0
2.5
1.0
0.75
0.50
0.25
0.10
0.075
0.050
0.025
0.010
0.0075
0.0050
<0.0025
Pore Throat Radius, microns
0.0
0.1
0.2
0.3
0.4
0.5
0.6
0.7
0.8
0.9
1.0
Mercury Saturation, fraction (frequency)


PORE THROAT RADIUS DISTRIBUTION
Micro
Meso
Macro
Cumulative
Incremental
R35 parameter
Radius, microns at SHg = 0.35
Cumulative Intruded Pore Space, fraction
Incremental Intruded Pore Space, fraction
Pore Throat Radius, microns
1.0
0.9
0.8
0.7
0.6
0.5
0.4
0.3
0.2
0.1
0.0
0.20
0.18
0.16
0.14
0.12
0.10
0.08
0.06
0.04
0.02
0.00
0.001
0.01
0.1
1
10


PERMEABILITY DISTRIBUTION
As outlined by Purcell (1949) and
Burdine, Gournay, & Reichertz (1950)
Permeability (fraction of total)
Pore Throat Radius, microns
1.0
0.9
0.8
0.7
0.6
0.5
0.4
0.3
0.2
0.1
0.0
0.001
0.01
0.1
1
10



Core Laboratories

MERCURY INJECTION DATA SUMMARY

Company: University of Utah
Well: RMCCS State #1
Formation: Entrada
File: HOU-130069

Sample: RM1-64HO-P01m	un-stressed	Host Plug 800psi	Host Plug 3930psi
Depth, feet: 9013.00			
Klinkenberg Permeability, md:	N/A	2.48	2.11
Permeability to Air, md:	N/A	3.20	2.70
Swanson Permeability, md:	7.79	-	-
Porosity, fraction:	0.131	0.144	0.134
maximum Sb/Pc, fraction:	0.098		
R35, microns:	2.06		
R50 (median pore throat radius):	1.59		

Injection Pressure, psia	Mercury Saturation, fraction	Pseudo-Wetting Saturation, fraction	Pore Throat Radius, microns	J Values	Conversion to other Laboratory Fluid Systems, psia G-W	G-O	O-W	Estimated Height Above Free Water, feet G-W	O-W
0.83	0.000	1.000	130	0.00374	0.161	0.0536	0.0929	0.335	0.667
1.10	0.000	1.000	97.9	0.00495	0.213	0.0711	0.123	0.445	0.884
1.41	0.000	1.000	76.4	0.00635	0.273	0.0911	0.158	0.570	1.13
1.75	0.000	1.000	61.6	0.00788	0.339	0.113	0.196	0.707	1.41
2.13	0.000	1.000	50.6	0.00959	0.413	0.138	0.238	0.861	1.71
2.57	0.000	1.000	41.9	0.0116	0.498	0.166	0.288	1.04	2.07
3.06	0.000	1.000	35.2	0.0138	0.593	0.198	0.342	1.24	2.46
3.62	0.000	1.000	29.8	0.0163	0.702	0.234	0.405	1.46	2.91
4.20	0.000	1.000	25.7	0.0189	0.814	0.271	0.470	1.70	3.38
4.85	0.000	1.000	22.2	0.0218	0.940	0.313	0.543	1.96	3.90
5.53	0.000	1.000	19.5	0.0249	1.07	0.357	0.619	2.23	4.44
6.27	0.000	1.000	17.2	0.0282	1.22	0.405	0.702	2.53	5.04
7.05	0.000	1.000	15.3	0.0317	1.37	0.455	0.789	2.85	5.67
7.90	0.000	1.000	13.6	0.0356	1.53	0.510	0.884	3.19	6.35
8.80	0.000	1.000	12.2	0.0396	1.71	0.568	0.985	3.56	7.07
9.73	0.000	1.000	11.1	0.0438	1.89	0.629	1.09	3.93	7.82
10.8	0.000	1.000	9.99	0.0486	2.09	0.697	1.21	4.36	8.68
11.9	0.000	1.000	9.07	0.0535	2.30	0.767	1.33	4.81	9.56
13.4	0.000	1.000	8.05	0.0603	2.59	0.865	1.50	5.42	10.8
15.3	0.000	1.000	7.06	0.0687	2.96	0.986	1.71	6.18	12.3
17.6	0.000	1.000	6.13	0.0791	3.40	1.13	1.97	7.11	14.1
20.4	0.002	0.998	5.27	0.0920	3.96	1.32	2.29	8.24	16.4
23.6	0.005	0.995	4.56	0.106	4.58	1.53	2.64	9.54	19.0
27.3	0.012	0.988	3.95	0.123	5.29	1.76	3.05	11.0	21.9
31.4	0.026	0.974	3.43	0.141	6.09	2.03	3.52	12.7	25.2
36.6	0.056	0.944	2.95	0.165	7.09	2.36	4.09	14.8	29.4
42.0	0.149	0.851	2.57	0.189	8.14	2.71	4.70	17.0	33.8
48.0	0.283	0.717	2.25	0.216	9.30	3.10	5.37	19.4	38.6
54.7	0.384	0.616	1.97	0.246	10.6	3.53	6.12	22.1	44.0
61.3	0.458	0.542	1.76	0.276	11.9	3.96	6.86	24.8	49.3
69.8	0.511	0.489	1.54	0.314	13.5	4.51	7.81	28.2	56.1
79.2	0.549	0.451	1.36	0.356	15.3	5.11	8.86	32.0	63.7
89.7	0.580	0.420	1.20	0.404	17.4	5.79	10.0	36.3	72.1
102	0.609	0.391	1.06	0.459	19.7	6.58	11.4	41.2	82.0
114	0.633	0.367	0.947	0.512	22.0	7.35	12.7	46.1	91.6
130	0.657	0.343	0.828	0.585	25.2	8.40	14.6	52.5	104
146	0.675	0.325	0.737	0.658	28.3	9.45	16.4	59.0	117
167	0.695	0.305	0.646	0.751	32.3	10.8	18.7	67.5	134
188	0.712	0.288	0.572	0.849	36.5	12.2	21.1	76.0	151
212	0.727	0.273	0.509	0.954	41.0	13.7	23.7	85.7	170
239	0.741	0.259	0.450	1.08	46.4	15.5	26.8	96.6	192
274	0.756	0.244	0.393	1.24	53.2	17.7	30.7	111	220
311	0.770	0.230	0.346	1.40	60.3	20.1	34.8	126	250
351	0.781	0.219	0.307	1.58	68.0	22.7	39.3	142	282
397	0.794	0.206	0.271	1.79	77.0	25.7	44.4	160	319
447	0.806	0.194	0.241	2.01	86.7	28.9	50.0	181	359
508	0.819	0.181	0.212	2.29	98.4	32.8	56.8	205	408
577	0.830	0.170	0.187	2.60	112	37.3	64.5	233	464
651	0.840	0.160	0.165	2.93	126	42.1	72.9	263	523
732	0.850	0.150	0.147	3.30	142	47.3	81.9	296	588
827	0.859	0.141	0.130	3.72	160	53.4	92.6	334	665
943	0.868	0.132	0.114	4.24	183	60.9	105	381	758
1080	0.876	0.124	0.100	4.85	209	69.6	120	436	868
1220	0.884	0.116	0.0885	5.48	236	78.6	136	493	981

Sample: RM1-64HO-P01m

Median Pore Throat, µm	Approximate Threshold Data, pore radius, µm	System	Entry Pressure, psia Lab	Resv	Height, ft
1.59	5.89	A-Hg	18.3	-	n/a
		G-W	3.5	2.5	7
		O-W	2.0	1.3	15
		A-Hg	126	(kPa)	

Pore Throat Radius, µm	Hg Sat'n, fraction cumulative	frequency
<0.0025	0.001	0.001
0.0050	0.012	0.010
0.0075	0.020	0.008
0.010	0.029	0.009
0.025	0.059	0.030
0.050	0.088	0.029
0.075	0.107	0.020
0.10	0.124	0.016
0.25	0.197	0.074
0.50	0.271	0.074
0.75	0.327	0.056
1.0	0.378	0.051
2.5	0.823	0.445
5.0	0.997	0.174
7.5	1.000	0.003
10	1.000	0.000
25	1.000	0.000
50	1.000	0.000
75	1.000	0.000
100	1.000	0.000
>100	1.000	0.000

Pressure, psia	Increm. Hg sat'n fraction	Cumulative Kf
0.550	0.0000	0.00E+00
0.83	0.0000	0.00E+00
1.10	0.0000	0.00E+00
1.41	0.0000	0.00E+00
1.75	0.0000	0.00E+00
2.13	0.0000	0.00E+00
2.57	0.0000	0.00E+00
3.06	0.0000	0.00E+00
3.62	0.0000	0.00E+00
4.20	0.0000	0.00E+00
4.85	0.0000	0.00E+00
5.53	0.0000	0.00E+00
6.27	0.0000	0.00E+00
7.05	0.0000	0.00E+00
7.90	0.0000	0.00E+00
8.80	0.0000	0.00E+00
9.73	0.0000	0.00E+00
10.8	0.0000	0.00E+00
11.9	0.0000	0.00E+00
13.4	0.0000	0.00E+00
15.3	0.0000	0.00E+00
17.6	0.0000	0.00E+00
20.4	0.0020	2.00E-02
23.6	0.0027	3.92E-02
27.3	0.0068	7.60E-02
31.4	0.0142	1.34E-01
36.6	0.0305	2.27E-01
42.0	0.0929	4.38E-01
48.0	0.1343	6.70E-01
54.7	0.1009	8.04E-01
61.3	0.0736	8.80E-01
69.8	0.0535	9.24E-01
79.2	0.0375	9.47E-01
89.7	0.0312	9.63E-01
102	0.0295	9.74E-01
114	0.0238	9.81E-01
130	0.0234	9.87E-01
146	0.0189	9.90E-01
167	0.0197	9.93E-01
188	0.0170	9.95E-01
212	0.0146	9.96E-01
239	0.0139	9.97E-01
274	0.0150	9.98E-01
311	0.0143	9.98E-01
351	0.0111	9.99E-01
397	0.0133	9.99E-01
447	0.0119	9.99E-01
508	0.0129	1.00E+00
577	0.0107	1.00E+00
651	0.0105	1.00E+00
732	0.0098	1.00E+00
827	0.0084	1.00E+00
943	0.0094	1.00E+00
1080	0.0084	1.00E+00
1220	0.0072	1.00E+00

Conversion Parameters

	air/water	air/oil	oil/water
Laboratory Theta -->	0.0	0.0	30.0
Laboratory IFT -->	72.0	24.0	48.0
Reservoir Theta -->	0.0	0.0	30.0
Reservoir IFT	50.0	0.0	30.0
Laboratory TcosTheta -->	72.0	24.0	41.6
Reservoir TcosTheta -->	50.0	0.0	26.0
A-Hg Contact Angle:	140		
A-Hg IFT:	485		
A-Hg TcosTheta:	371.5		
Density Gradients, psi/foot		(typical)	
Water:	**0.433**	0.433	
Oil:	**0.346**	0.346	
Gas:	**0.100**	0.100	

Sample Parameters	
Weight, g	9.238
PVol, cc	0.520
GVol, cc	3.464
BVol, cc	3.982
GDens, gm/cc	2.667
Bdens, gm/cc	2.320

R35 Line	
0.001	0.35
100	0.35
Micro boundary	
0.5	0
0.5	1
Macro boundary	
2.5	0
2.5	1

Gas-Water Pc Test	
Pc	I-F Sw
0	
25	
50	
100	
200	
300	
450	
650	
900	
1200	

Total Surface Area
m^2/g

Qv value is from:

estimated	CoCw	NMR	CEC	BJ adsb H2O

Qv Correction

1	Salinity, g/L
0.00	Qv, e/L
1.000	A = phi(eff)/phi(tot)
-	Qv, e/L for ~good match
-	Qv from companion

Thomeer and Swanson Parameters

PS1 (large pore system) G Factor	Pd	BV(inf)	PS2 (fine pore system) G Factor	Pd	BV(inf)	PS3 (fine pore system) G Factor	Pd	BV(inf)	BV TOTAL
									0.00
Thomeer K, md:	#DIV/0!		Swanson K md:	7.79					
Swanson Point is at mas Bv corr/Pc =	0.0975		Pc =	61		Bv=	5.981		

MERCURY INJECTION DATA SUMMARY

Company: University of Utah
Well: RMCCS State #1
Formation: Entrada
File: HOU-130069

Sample: RM1-64HO-P01m	un-stressed	Host Plug 800psi	Host Plug 3930psi
Depth, feet: 9013.00			
Klinkenberg Permeability, md:	N/A	2.48	2.11
Permeability to Air, md:	N/A	3.20	2.70
Swanson Permeability, md:	7.79	-	-
Porosity, fraction:	0.131	0.144	0.134
maximum Sb/Pc, fraction:	0.098		
R35, microns:	2.06		
R50 (median pore throat radius):	1.59		

Injection Pressure, psia	Mercury Saturation, fraction	Pseudo-Wetting Saturation, fraction	Pore Throat Radius, microns	J Values	Conversion to other Laboratory Fluid Systems, psia G-W	G-O	O-W	Estimated Height Above Free Water, feet G-W	O-W
1370	0.890	0.110	0.0789	6.15	265	88.3	153	554	1100
1540	0.896	0.104	0.0701	6.92	298	99.3	172	622	1240
1750	0.903	0.097	0.0617	7.87	339	113	196	707	1410
1980	0.909	0.091	0.0545	8.90	383	128	221	800	1590
2220	0.914	0.086	0.0486	9.98	430	143	248	897	1780
2510	0.919	0.081	0.0430	11.3	486	162	280	1010	2020
2830	0.924	0.076	0.0381	12.7	548	183	316	1140	2270
3220	0.929	0.071	0.0335	14.5	623	208	360	1300	2590
3660	0.935	0.065	0.0295	16.5	709	236	409	1480	2940
4150	0.940	0.060	0.0260	18.7	804	268	464	1680	3340
4690	0.944	0.056	0.0230	21.1	910	303	525	1900	3770
5300	0.948	0.052	0.0203	23.8	1030	342	592	2140	4260
5970	0.952	0.048	0.0181	26.9	1160	385	667	2410	4800
6750	0.957	0.043	0.0160	30.4	1310	436	755	2730	5430
7650	0.961	0.039	0.0141	34.4	1480	494	855	3090	6150
8650	0.965	0.035	0.0125	38.9	1680	558	967	3500	6950
9790	0.968	0.032	0.0110	44.1	1900	632	1090	3960	7870
11000	0.972	0.028	0.00976	49.7	2140	713	1230	4450	8840
12500	0.976	0.024	0.00862	56.3	2420	807	1400	5050	10000
14100	0.980	0.020	0.00763	63.6	2740	912	1580	5700	11300
16000	0.983	0.017	0.00674	71.9	3100	1030	1790	6470	12900
18100	0.985	0.015	0.00596	81.4	3500	1170	2020	7310	14500
20400	0.987	0.013	0.00527	92.0	3960	1320	2290	8240	16400
23100	0.990	0.010	0.00466	104	4480	1490	2590	9340	18600
26200	0.992	0.008	0.00412	118	5070	1690	2930	10600	21100
29600	0.994	0.006	0.00364	133	5730	1910	3310	12000	23800
33500	0.996	0.004	0.00322	151	6490	2160	3750	13500	26900
37800	0.997	0.003	0.00285	170	7330	2440	4230	15300	30400
43000	0.999	0.001	0.00250	194	8340	2780	4810	17400	34600
48400	1.000	0.000	0.00223	218	9380	3130	5420	19600	38900
55000	1.000	0.000	0.00196	248	10700	3550	6150	22200	44200

Sample: RM1-64HO-P01m

Median Pore Throat, µm	pore radius, µm	System	Approximate Threshold Data, Entry Pressure, psia Lab	Resv	Height, ft
1.59	5.89	**A-Hg**	18.3	-	n/a
		G-W	3.5	2.5	7
		O-W	2.0	1.3	15
		A-Hg	126	(kPa)	

Pressure, psia	Increm. Hg sat'n fraction	Cumulative Kf
0.550	0.0000	0.00E+00
1370	0.0066	1.00E+00
1540	0.0061	1.00E+00
1750	0.0066	1.00E+00
1980	0.0057	1.00E+00
2220	0.0051	1.00E+00
2510	0.0055	1.00E+00
2830	0.0051	1.00E+00
3220	0.0051	1.00E+00
3660	0.0055	1.00E+00
4150	0.0049	1.00E+00
4690	0.0037	1.00E+00
5300	0.0045	1.00E+00
5970	0.0043	1.00E+00
6750	0.0043	1.00E+00
7650	0.0041	1.00E+00
8650	0.0039	1.00E+00
9790	0.0037	1.00E+00
11000	0.0037	1.00E+00
12500	0.0039	1.00E+00
14100	0.0039	1.00E+00
16000	0.0029	1.00E+00
18100	0.0027	1.00E+00
20400	0.0020	1.00E+00
23100	0.0023	1.00E+00
26200	0.0020	1.00E+00
29600	0.0020	1.00E+00
33500	0.0018	1.00E+00
37800	0.0016	1.00E+00
43000	0.0014	1.00E+00
48400	0.0012	1.00E+00
55000	0.0000	1.00E+00

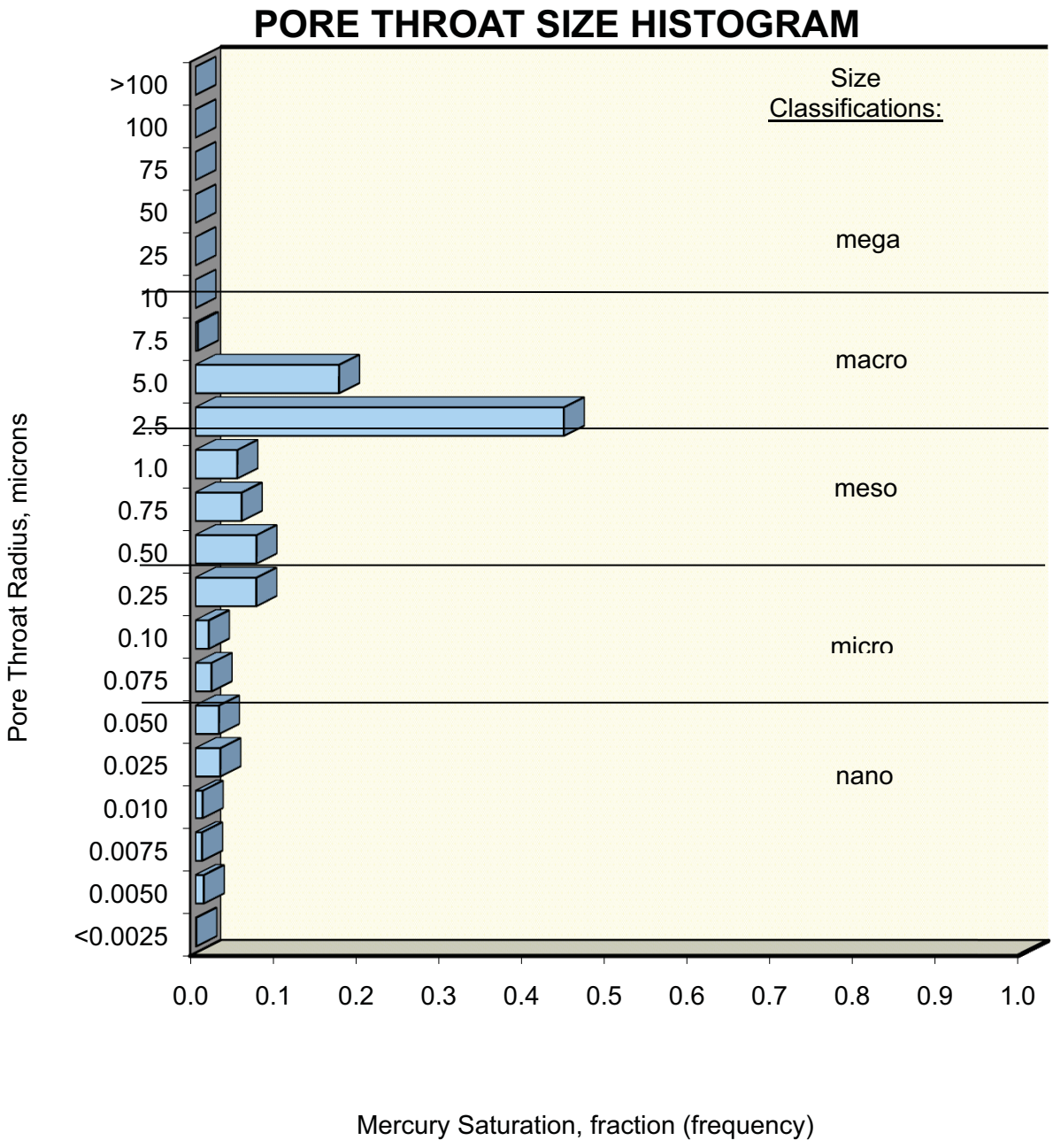
Pore Throat Radius, µm	Hg Sat'n, fraction cumulative	frequency
<0.0025	0.001	0.001
0.0050	0.012	0.010
0.0075	0.020	0.008
0.010	0.029	0.009
0.025	0.059	0.030

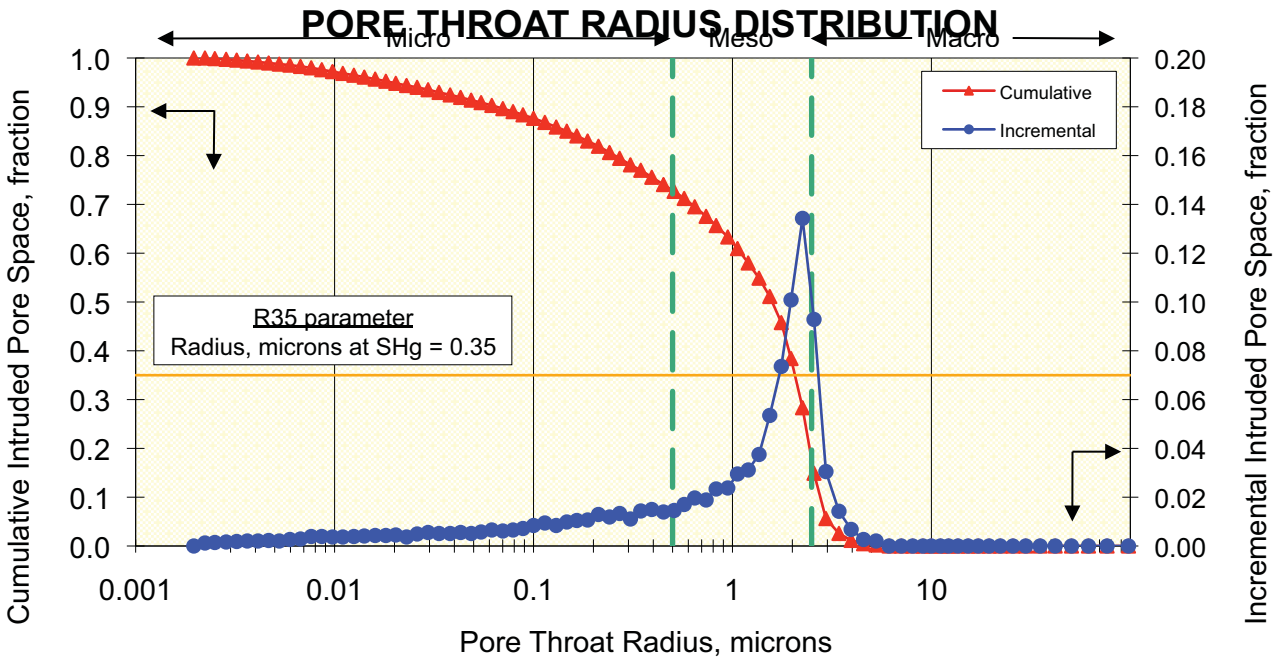
Conversion Parameters

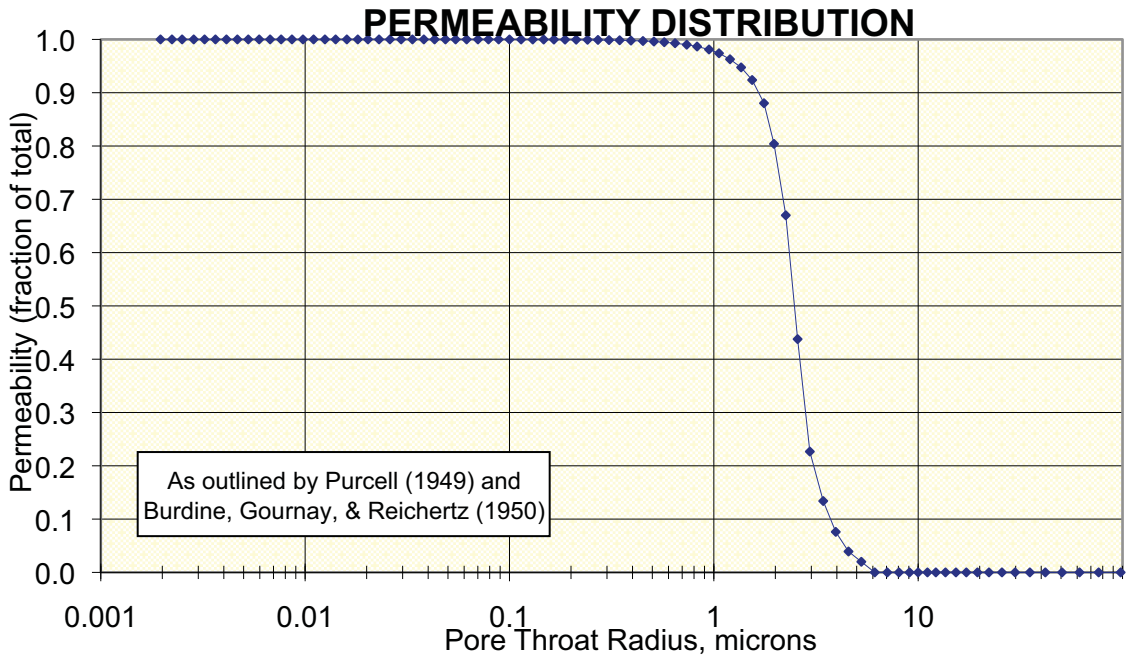
	air/water	air/oil	oil/water
Laboratory Theta -->	0.0	0.0	30.0
Laboratory IFT -->	72.0	24.0	48.0
Reservoir Theta -->	0.0	0.0	30.0
Reservoir IFT	50.0	0.0	30.0
Laboratory TcosTheta -->	72.0	24.0	41.6
Reservoir TcosTheta -->	50.0	0.0	26.0
A-Hg Contact Angle:	140		
A-Hg IFT:	485		
A-Hg TcosTheta:	371.5		
Density Gradients, psi/foot		(typical)	
Water:	**0.433**	0.433	
Oil:	**0.346**	0.346	
Gas:	**0.100**	0.100	

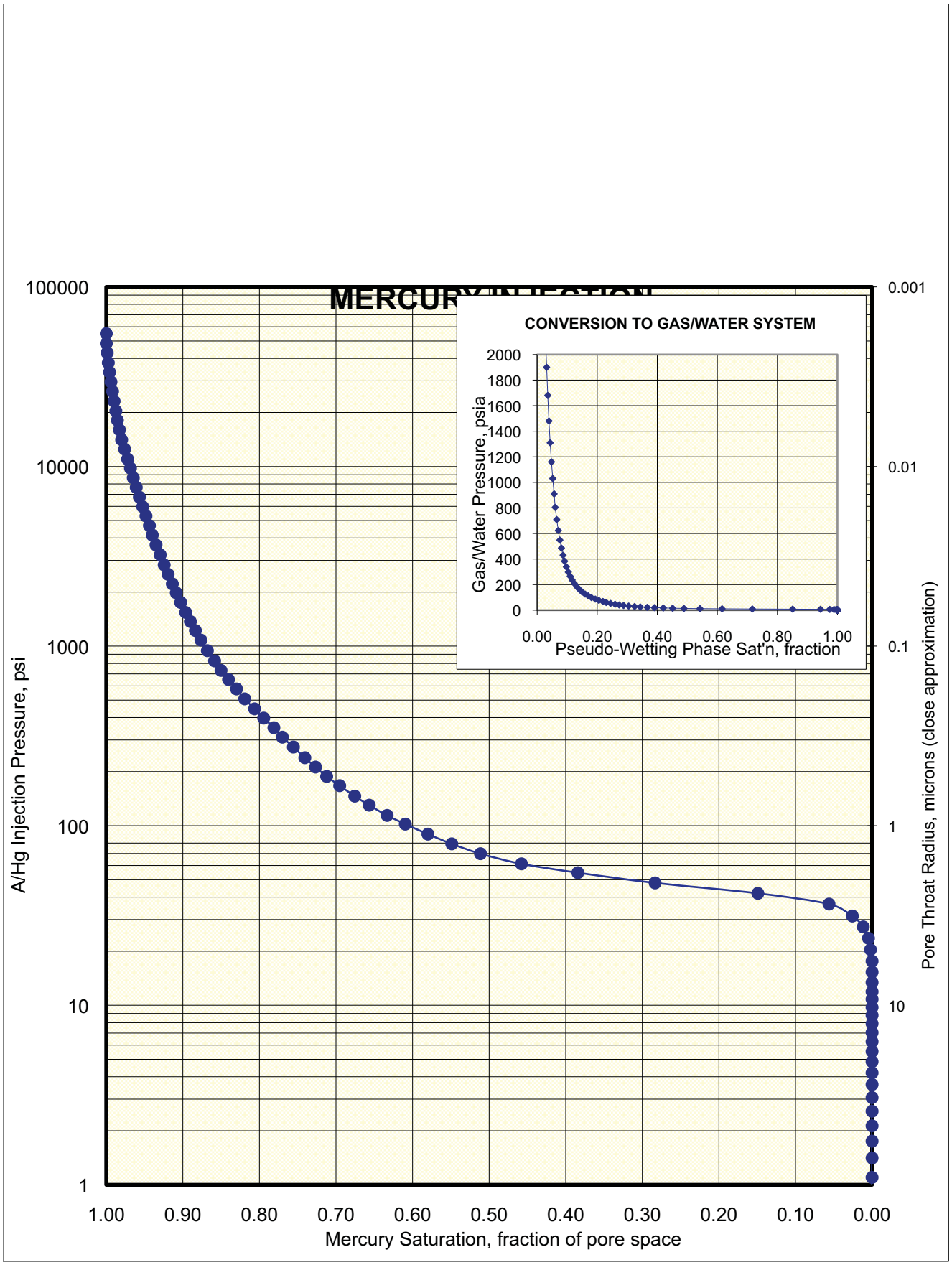
Sample Parameters

Gas-Water Pc Test Pc	I-F Sw
0	
25	
50	
100	
200	
300	
450	


PORE THROAT SIZE HISTOGRAM
Size
Classifications:
mega
macro
meso
micro
nano
>100
100
75
50
25
10
7.5
5.0
2.5
1.0
0.75
0.50
0.25
0.10
0.075
0.050
0.025
0.010
0.0075
0.0050
<0.0025
Pore Throat Radius, microns
0.0
0.1
0.2
0.3
0.4
0.5
0.6
0.7
0.8
0.9
1.0
Mercury Saturation, fraction (frequency)


PORE THROAT RADIUS DISTRIBUTION
Micro
Meso
Macro
Cumulative
Incremental
R35 parameter
Radius, microns at SHg = 0.35
Cumulative Intruded Pore Space, fraction
Incremental Intruded Pore Space, fraction
Pore Throat Radius, microns
1.0
0.9
0.8
0.7
0.6
0.5
0.4
0.3
0.2
0.1
0.0
0.20
0.18
0.16
0.14
0.12
0.10
0.08
0.06
0.04
0.02
0.00
0.001
0.01
0.1
1
10


PERMEABILITY DISTRIBUTION
As outlined by Purcell (1949) and
Burdine, Gournay, & Reichertz (1950)
Permeability (fraction of total)
Pore Throat Radius, microns
1.0
0.9
0.8
0.7
0.6
0.5
0.4
0.3
0.2
0.1
0.0
0.001
0.01
0.1
1
10


MERCURY INJECTION
CONVERSION TO GAS/WATER SYSTEM
Gas/Water Pressure, psia
2000
1800
1600
1400
1200
1000
800
600
400
200
0
0.00
0.20
0.40
0.60
0.80
1.00
Pseudo-Wetting Phase Sat'n, fraction
A/Hg Injection Pressure, psi
100000
10000
1000
100
10
1
Pore Throat Radius, microns (close approximation)
0.001
0.01
0.1
1
10
1.00
0.90
0.80
0.70
0.60
0.50
0.40
0.30
0.20
0.10
0.00
Mercury Saturation, fraction of pore space

Schlumberger

Unsteady-State Relative Permeabilty Report

Prepared for: University of Utah

Well: RMCCS-1

Formation: Entrada

Location: Craig, Colorado

Prepared by:

Schlumberger Reservoir Laboratories

6350 W. Sam Houston Parkway N, Suite 200

Houston, Texas 77041, USA

(713) 482-0709

Date: Aug 13 2013

Project No: 2012USHC-P113

Quality Assurance Process

Schlumberger is committed to providing unsurpassed services in reservoir sampling and analyses while maintaining high standards of safety and quality. Our objective is to deliver the most accurate and reliable sampling processes and fluid and rock property measurements available in the industry. This objective requires persistent innovation and ongoing development of state-of-the-art technologies and equipment.

A rigorous quality assurance program, continuous employee training and enforcement of strict safety standards maintain our compliance with quality, health, safety and environment (QHSE) requirements. Proactive integration of QHSE objectives and management goals at every level supports the communication and implementation of QHSE policies and standards. Schlumberger requires that qualified engineering technologists perform all laboratory measurements according to specified analytical procedures designed for obtaining accurate and reliable data.

The lab-generated data undergoes the following five levels of quality checks to establish the integrity of the reported results.

a) Establish quality of measurement during data generation.
b) Lab supervisor and manager confirm the overall quality of the generated data.
c) Project manager reviews and processes generated data and generates reports.
d) Technical advisors confirm consistency of reported data.
e) Project manager finalizes reports.

Hence the completion of each project requires that a qualified and experienced team of engineers perform a variety of independent reviews of all technical data to confirm the consistency and accuracy of the report as per pre-established quality checklists designed for each operation and based on the level of complexity. All property measurements and calculation procedures are maintained in company archives for a period of one year. This information is available for review by clients upon request.

The file and laboratory records information is listed below to provide access reference to all records related to this project. For any questions, please do not hesitate to contact the undersigned project manager.

File No: 2012USHC-P113

Laboratory Procedures

George Assad
Special Core Analysis Manager

Project Management

Micah Alexander
Project Manager

Reviewed by

X	Leslie Zhang	Lead Project Manager
X	Debbie Steele	Senior Project Manager

Table of Contents

Quality Assurance i
Relative Permeability by Unsteady-State Method 1

List of Tables

Table 1. Formation Brine Composition 2
Table 2. Fluid Viscosity 3
Table 3. Unsteady-State Supercritical CO2 Flood Result Summary 4
Table 4. Relative Permeability Data - Sample RM1-63DO-P01 5
Table 5. Relative Permeability Data - Sample RM1-63VO-P01 7
Table 6. Relative Permeability Data - Sample RM1-64HB-P01 9
Table 7. Relative Permeability Data - Sample RM1-79HO-P01 11

List of Figures

Figure 1. Relative Permeability - Sample RM1-63DO-P01 6
Figure 2. Relative Permeability - Sample RM1-63VO-P01 8
Figure 3. Relative Permeability - Sample RM1-64HB-P01 10
Figure 4. Relative Permeability - Sample RM1-79HO-P01 12

Unsteady-State Relative Permeability Discussion

Four (4) plugs from the RMCCS-1 well were selected for the unsteady-state supercritical carbon dioxide (CO2)-water relative permeability study. Formation brine and supercritical CO2 were used in the tests.

The formation brine recipe was provided by the client. The brine composition was calculated and is presented in table 1. Formation brine was made with de-ionized water and filtered through a 0.45 micron filter. Viscosity of the formation brine was measured by Anton Paar viscometer at a temperature of about 75°C. Viscosity data are shown in table 2.

Samples were Soxhlet cleaned and convection dried until the weights were stable. The plugs were vacuum and then pressure saturated with formation brine. A plug was then loaded into a core holder. A pore pressure of 1500 psi and a net confining pressure of 3500 psi were used in the test. Tests were conducted at 75°C.

The absolute brine permeability (Kw) was measured first using the formation brine at three flow rates. After measuring the brine permeability, the flow system's dead volumes were flushed with supercritical CO2 until no brine could be seen in the effluent. Supercritical CO2 displaced the brine at a constant rate until pressure differential and brine production were stable. The relative permeability data are shown in tables 4 through 7. Presented relative permeability data were determined using the Welge/Corey method. The absolute Kw was used as the base permeability in the relative permeability calculations. Results can be found in figures 1 through 4.

The endpoint supercritical CO2 permeability was measured at residual water saturation (Swr). The plugs were then unloaded, and the Dean-Stark extraction was conducted to confirm the final water saturation.

Table 1. Formation Brine Composition

Chemical Name	Formula	Mass for 1 liter solution (grams)
Potassium Chloride	KCl	0.18
Sodium Chloride	NaCl	5.78
Sodium Bicarbonate	$NaHCO_3$	0.05
Magnesium Chloride	$MgCl_2*6H_2O$	2.62
Calcium Chloride	$CaCl_2*2H_2O$	0.37
Sodium Sulfate	Na_2SO_4	0.97
Sodium Bromine	NaBr	0.02
Strontium Chloride	$SrCl_2*6H_2O$	0.01

Table 2. Fluid Viscosities

Fluid Name	Temperature (°C)	Viscosity (cP)
Formation brine	73.0	0.470
Supercritical CO2 @ 1515 psi	73.0	0.023

Table 3. Unsteady-State Supercritical CO2 Flood Result Summary

Sample ID	Depth (ft)	Porosity (%)	Air Permeability (mD)	Absolute Brine Permeability (mD)	Effective Supercritical CO2 Permeability (mD)	Residual Brine Saturation (%)
RM1-63DO-P01	9012.3	11.4	1.65	0.238	0.091	79.0
RM1-63VO-P01	9013.9	12.4	3.21	0.536	0.179	61.4
RM1-64HB-P01	9015.6	12.7	5.08	1.33	0.370	55.6
RM1-79HO-P01	9029.2	18.6	312	184	11.54	51.6

Table 4. Unsteady-State Relative Permeability Data - Sample RM1-63DO-P01

Water Saturation (fraction)	KrCO2 (fraction)	Krw (fraction)	KrCO2/Krw
1.000	0.000	1.000	0.000
0.990	0.001	0.903	0.001
0.979	0.004	0.810	0.005
0.969	0.009	0.723	0.012
0.958	0.015	0.640	0.024
0.948	0.024	0.563	0.042
0.937	0.034	0.490	0.070
0.927	0.047	0.423	0.111
0.916	0.061	0.360	0.170
0.906	0.077	0.303	0.256
0.895	0.096	0.250	0.382
0.885	0.116	0.203	0.571
0.874	0.138	0.160	0.860
0.864	0.161	0.123	1.318
0.853	0.187	0.090	2.080
0.843	0.215	0.063	3.438
0.832	0.244	0.040	6.112
0.822	0.276	0.023	12.267
0.811	0.309	0.010	30.942
0.801	0.345	0.003	137.904
0.790	0.382	0.000	-

Figure 1. Unsteady-State Relative Permeability - Sample RM1-63DO-P01

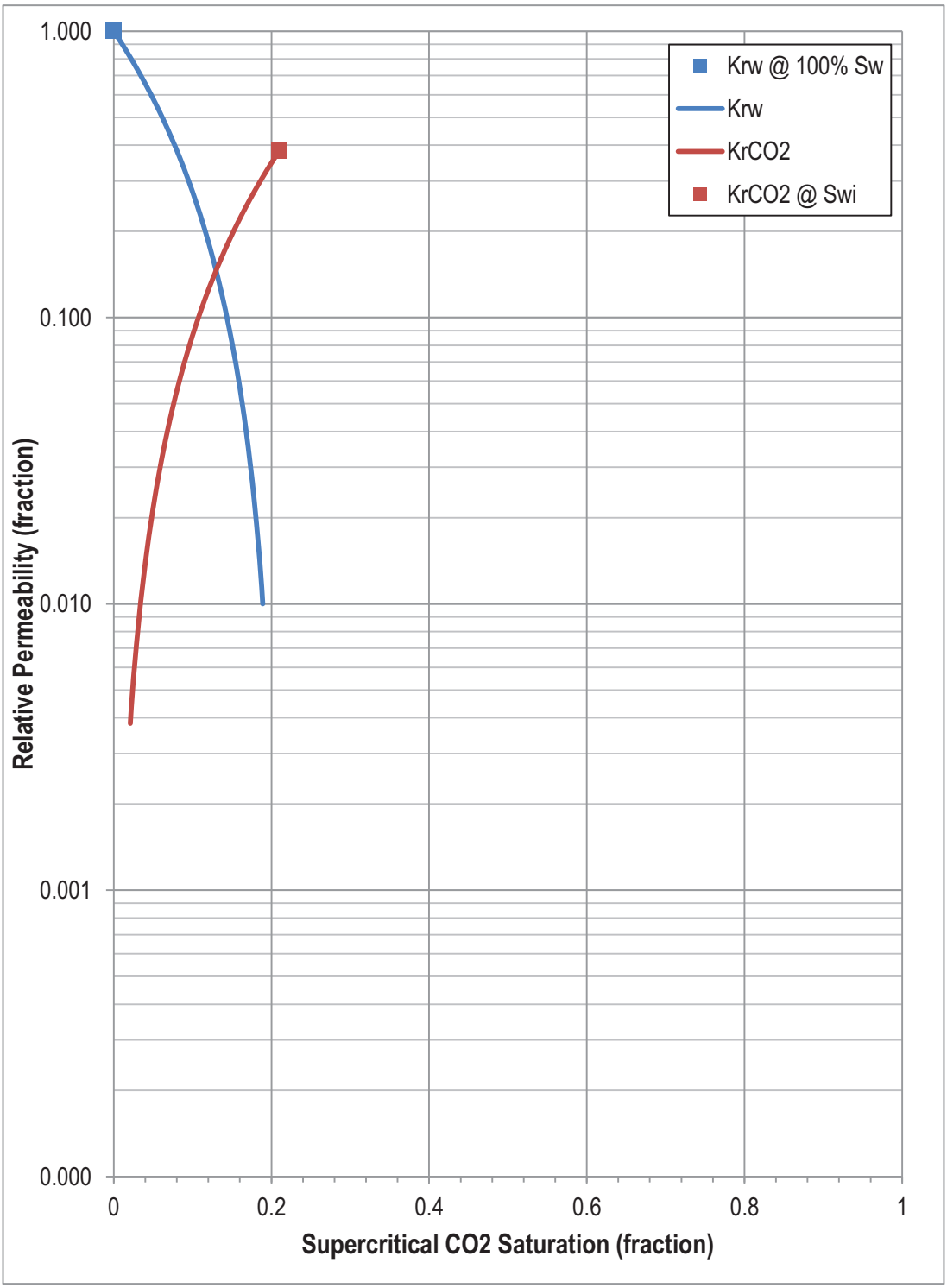


Table 5. Unsteady-State Relative Permeability Data - Sample RM1-63VO-P01

Water Saturation (fraction)	KrCO2 (fraction)	Krw (fraction)	KrCO2/Krw
1.000	0.000	1.000	0.000
0.981	0.001	0.903	0.001
0.961	0.003	0.810	0.004
0.942	0.007	0.723	0.010
0.923	0.013	0.640	0.021
0.904	0.021	0.563	0.037
0.884	0.030	0.490	0.060
0.865	0.040	0.423	0.095
0.846	0.053	0.360	0.146
0.826	0.067	0.303	0.220
0.807	0.082	0.250	0.329
0.788	0.100	0.203	0.492
0.769	0.119	0.160	0.741
0.749	0.139	0.123	1.136
0.730	0.161	0.090	1.793
0.711	0.185	0.063	2.964
0.691	0.211	0.040	5.269
0.672	0.238	0.023	10.574
0.653	0.267	0.010	26.673
0.634	0.297	0.003	118.876
0.614	0.329	0.000	-

Figure 2. Unsteady-State Relative Permeability - Sample RM1-63VO-P01

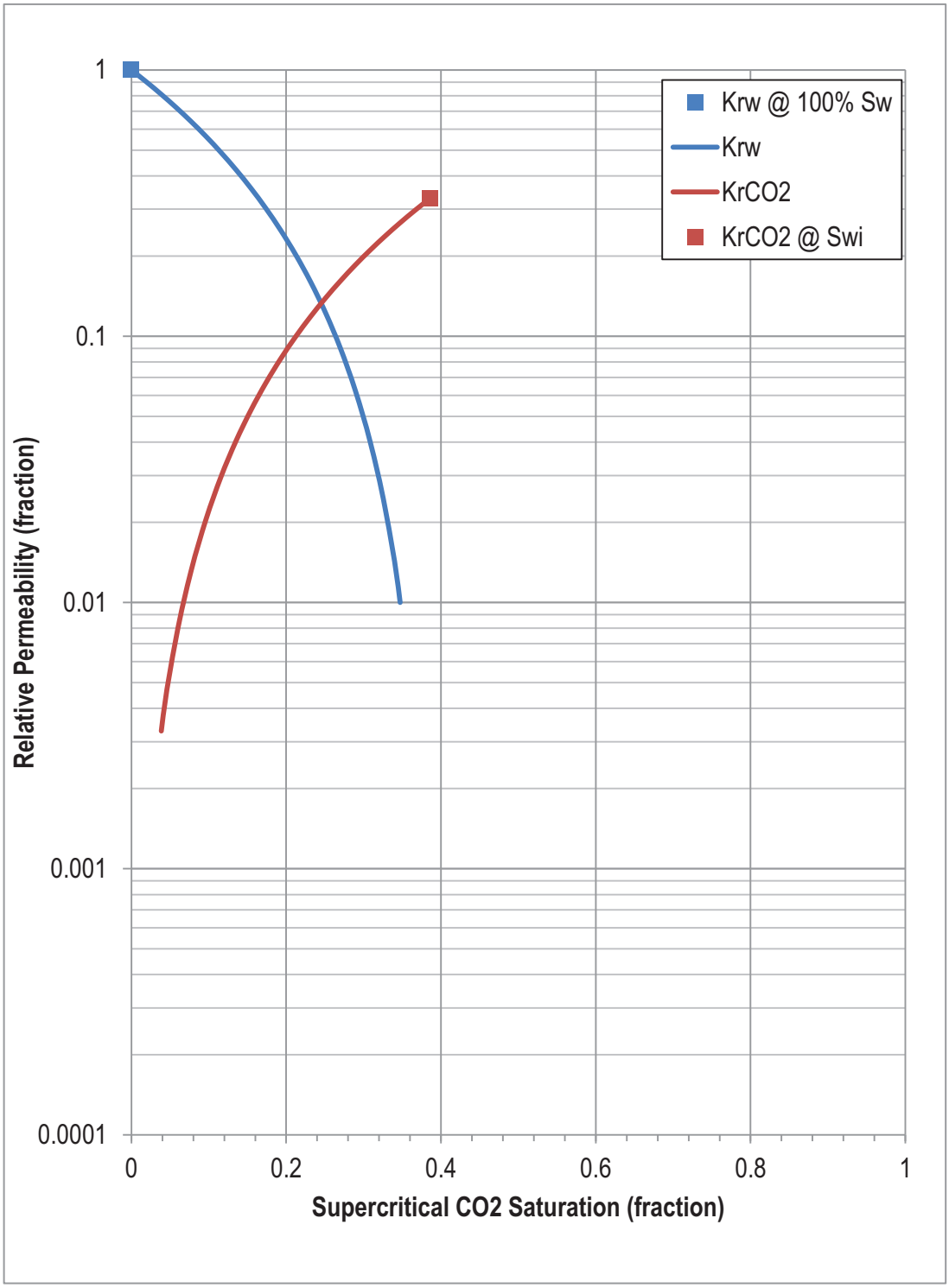


Table 6. Unsteady-State Relative Permeability Data - Sample RM1-64HB-P01

Water Saturation (fraction)	KrCO2 (fraction)	Krw (fraction)	KrCO2/Krw
1.000	0.000	1.000	0.000
0.978	0.001	0.903	0.001
0.956	0.003	0.810	0.003
0.933	0.006	0.723	0.009
0.911	0.011	0.640	0.017
0.889	0.017	0.563	0.031
0.867	0.025	0.490	0.051
0.845	0.034	0.423	0.080
0.822	0.044	0.360	0.123
0.800	0.056	0.303	0.186
0.778	0.069	0.250	0.277
0.756	0.084	0.203	0.414
0.734	0.100	0.160	0.624
0.711	0.117	0.123	0.957
0.689	0.136	0.090	1.510
0.667	0.156	0.063	2.497
0.645	0.178	0.040	4.439
0.623	0.200	0.023	8.908
0.600	0.225	0.010	22.469
0.578	0.250	0.003	100.140
0.556	0.277	0.000	-

Figure 3. Unsteady-State Relative Permeability - Sample RM1-64HB-P01

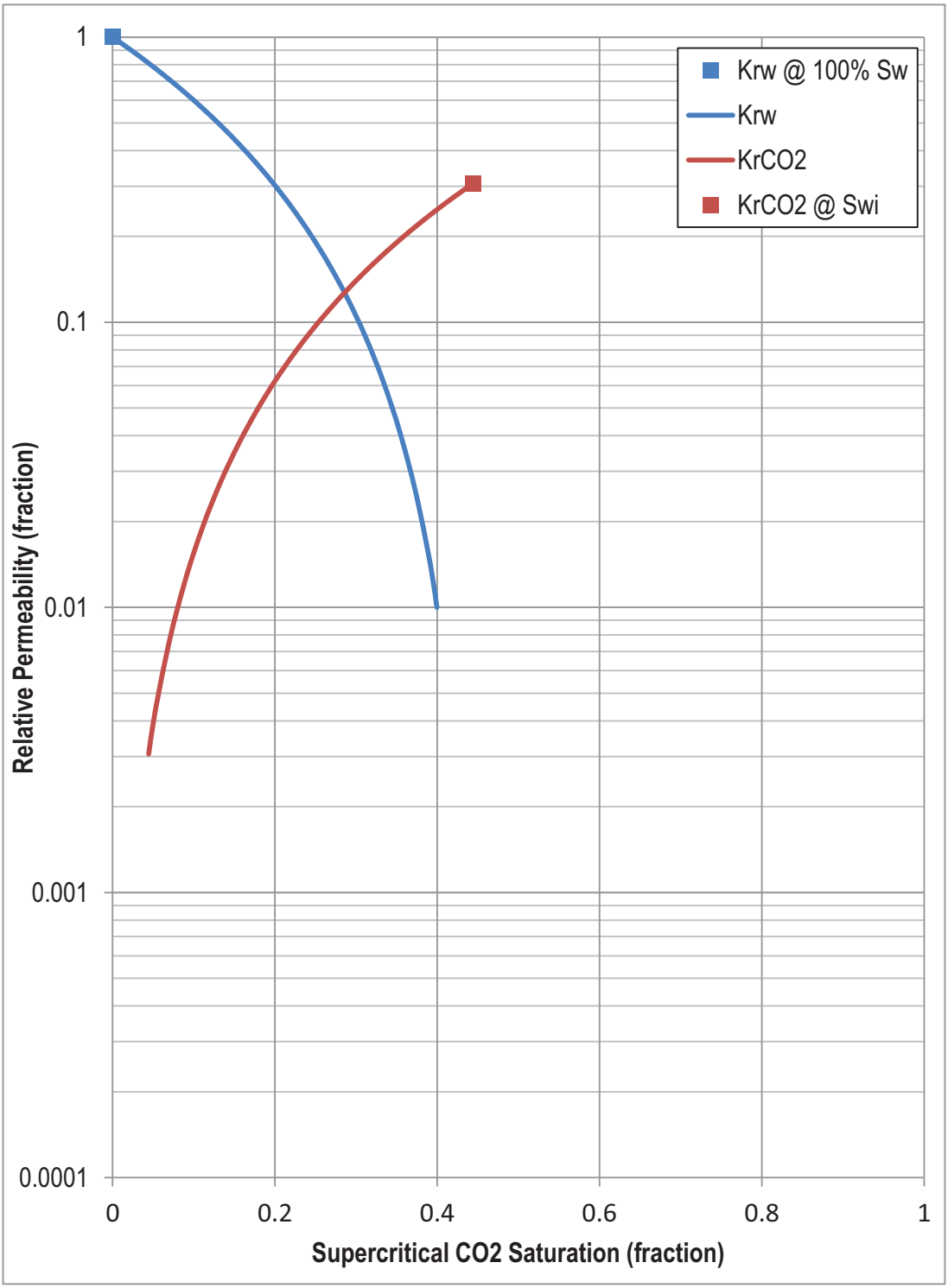
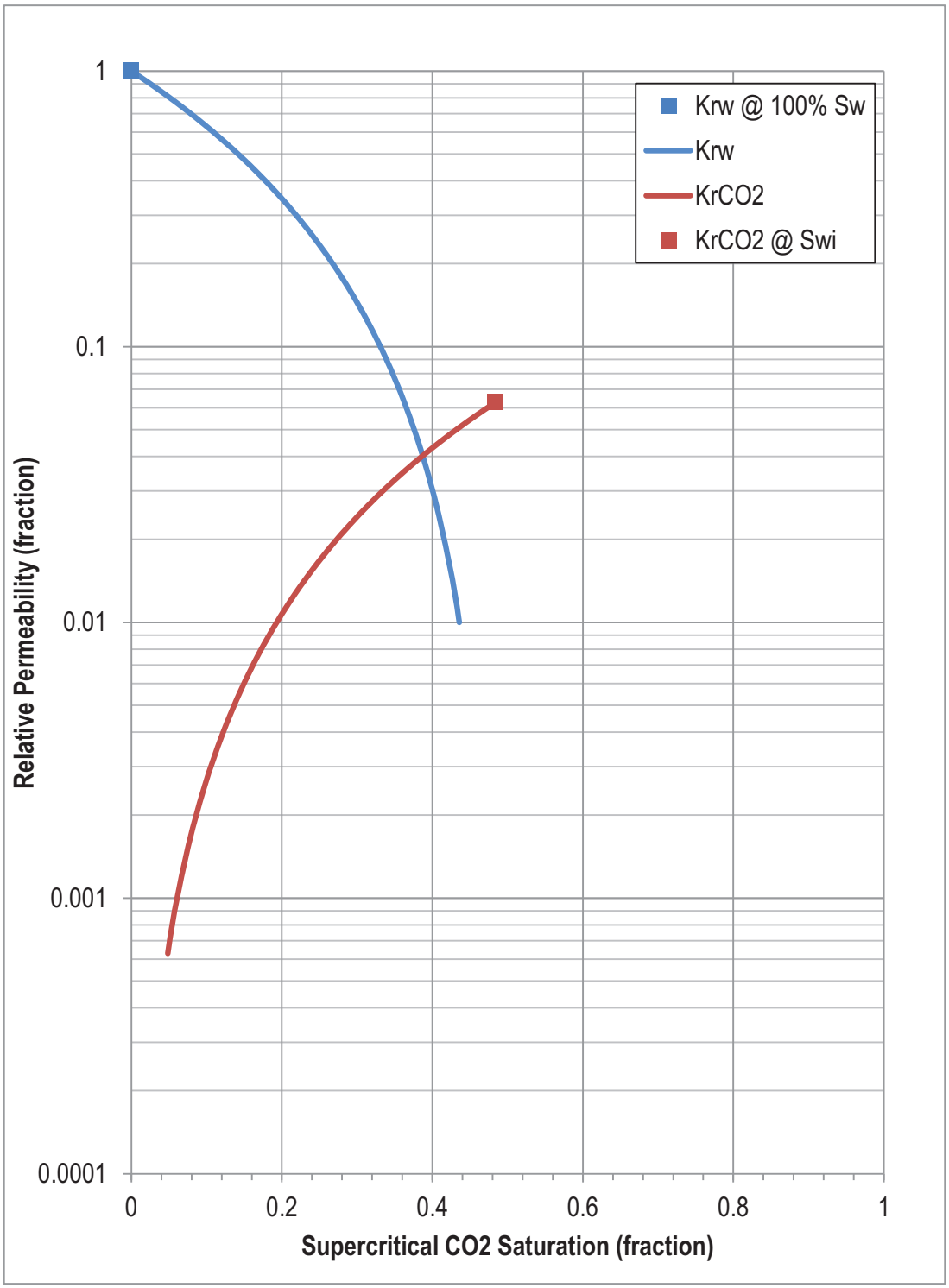


Table 7. Unsteady-State Relative Permeability Data - Sample RM1-79HO-P01

Water Saturation (fraction)	KrCO2 (fraction)	Krw (fraction)	KrCO2/Krw
1.000	0.000	1.000	0.000
0.976	0.000	0.903	0.000
0.952	0.001	0.810	0.001
0.927	0.001	0.723	0.002
0.903	0.003	0.640	0.004
0.879	0.004	0.563	0.007
0.855	0.006	0.490	0.012
0.831	0.008	0.423	0.018
0.806	0.010	0.360	0.028
0.782	0.013	0.303	0.042
0.758	0.016	0.250	0.063
0.734	0.019	0.203	0.094
0.710	0.023	0.160	0.142
0.685	0.027	0.123	0.217
0.661	0.031	0.090	0.342
0.637	0.035	0.063	0.566
0.613	0.040	0.040	1.007
0.588	0.045	0.023	2.020
0.564	0.051	0.010	5.095
0.540	0.057	0.003	22.708
0.516	0.063	0.000	-

Figure 4. Unsteady-State Relative Permeability - Sample RM1-79HO-P01



APPENDIX L

Selected Petrographic Descriptions

& Images

Table of Contents

Dakota Sandstone Only

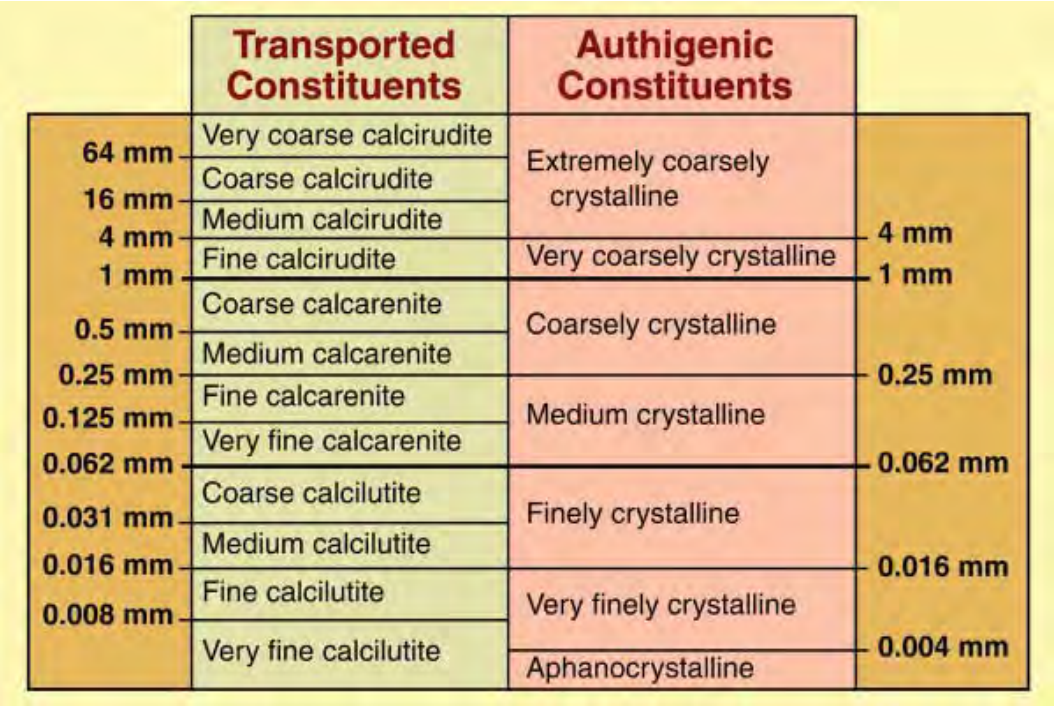
Petrographic Observations for Rocky Mountain CSS State #1 Well

General Information

Photo caption format and key: Well and depth Photo description; Polarization (PPL = plane polarized light; XPL = cross-polarized light; RL = reflected light); scale bar length; digital image file name.

Most of the photos were taken on an Olympus BX 53 with a Canon Digital Rebel 2Ti (18 MP). The Olympus BX 53 is equipped a CooLED epifluorescence with 365 and 470 wavelengths. With epifluorescence, both hydrocarbons/organics and pink fluorescent epoxy fluoresce. Hydrocarbons/organics usually range from green to yellow (at 470 wavelength) and white to blue (at 365 wavelength). The dyed epoxy used for some of the thin sections fluoresces orange at the 470 wavelength. A few were taken Nikon Polarizing microscope with the same camera.

Crystal and grain size terminology used for carbonate rocks (AAPG Memoir 77)



Grain size terminology used for clastic terrigenous rocks (from Wentworth 1922)

Millimeters (mm)	Micrometers (μm)	Phi (ϕ)	Wentworth size class		Rock type
4096		-12.0	Boulder		
256		-8.0	Cobble	Gravel	Conglomerate/ Breccia
64		-6.0	Pebble		
4		-2.0	Granule		
2.00		-1.0	Very coarse sand		
1.00		0.0	Coarse sand		
1/2 0.50	500	1.0	Medium sand	Sand	Sandstone
1/4 0.25	250	2.0	Fine sand		
1/8 0.125	125	3.0	Very fine sand		
1/16 0.0625	63	4.0	Coarse silt		
1/32 0.031	31	5.0	Medium silt		
1/64 0.0156	15.6	6.0	Fine silt	Silt	Siltstone
1/128 0.0078	7.8	7.0	Very fine silt		
1/256 0.0039	3.9	8.0			
0.00006	0.06	14.0	Clay	Mud	Claystone

Abbreviations:

VRFs- Volcanic rock fragments
IRFs- Plutonic igneous rock fragments
SRFs- Sedimentary rock fragments

About the thin section descriptions:

Within the descriptions, the percentages given in the grains, matrix, cements and porosity all add up to 100%. The XRD data and observed percentages do not match exactly since porosity is not included in the XRD data. Other sources of error between the observed and XRD data, is the fact that the sample for the XRD is not from exactly the same area as the thin section, and that visual estimates can have significant error associated with them.

Dakota Formation

Depositional Environment:

This unit has been called Dakota Group, but it is probably better to assign it to the lowermost member of Naturita Formation (Young, 1960, 1965).

Early Cretaceous (~Cedar Mesa) Paleogeographic Map
(from Ron Blakey, Northern Arizona University)



Based on one thin section, it is difficult to say definitively what was the depositional environment for the section; however, based on the conglomeratic nature of the sediments and the composition (quartz, quartzite, feldspars and chert/chalcedony), these deposits were formed most likely in a fluvial or alluvial channel deposit feeding from highlands to the west of the Craig well site. The distance is moderately far because of the dominance of quartz grains and the scarcity of feldspars and other grains.

Diagenesis:

Only one thin section was made from Dakota Formation section. The diagenetic sequence for that thin section was:

- Early feldspar (both K-spar and plagioclase) overgrowths

- Quartz overgrowths
- Leaching of K-spar and chert/chalcedony grains
- Kaolinite and illite cements
- Pyrite replacement (very minor)

Because of the early quartz cementation, the sands were well cemented prior to significant burial, and few compactional fabrics were found.

Porosity makes up about 12% of the thin section with most of the porosity being secondary intraparticle, vuggy and intercrystalline (10%) and primary interparticle (2%).

Bibliography

Young, R.G., 1960, Dakota Group of Colorado Plateau: American Association of Petroleum Geologists, Bulletin, V. 44, p. 156-194.

Young, R.G., 1965, Type Section of Naturita Formation: American Association of Petroleum Geologists, Bulletin, V. 49, p. 1512-1531.

http://jan.ucc.nau.edu/~rcb7/ColoPlatCret_CedarMtn.jpg (Blakey Map)

RMCSS State #1 8298.0 ft (RM1-8298-M02)

Total Clays	Calcite	Dolomite	Quartz	K-spar	Plag.	Pyrite	Anhyd.	Por.	Perm. (air)
%	%	%	%	%	%	%	%	%	mD
			94		6				

Rock name: Quartz Arenite.

Basic rock description:

Grains – Quartz sand/conglomerate (64%), quartz silt (1%), plagioclase (1%), K-spar (5%) and lithics (chert and chalcedony, 5%).

Matrix – No matrix except in the pore that contains residual debris in it.

Avg. Grain Size: 0.28 mm (medium sand)
Max. Grain Size: 0.65 mm (coarse sand)
Sorting: Moderate
Angularity: Well rounded to sub-angular

Fabric – No visible bedding.

Depositional interpretation:

Possible fluvial or alluvial channel deposits.

Diagenesis:

Cementation – Cementation occurred in multiple episodes. K-spar and plagioclase cements (1%) occurred prior to quartz cements (8%). Kaolinite (3%) and minor illite (<1%) followed.

Replacement – Minor pyrite replacement (<1%).

Leaching – K-spar grains and chert/chalcedony grains have been leached. Leaching appears to be early, prior to significant cementation.

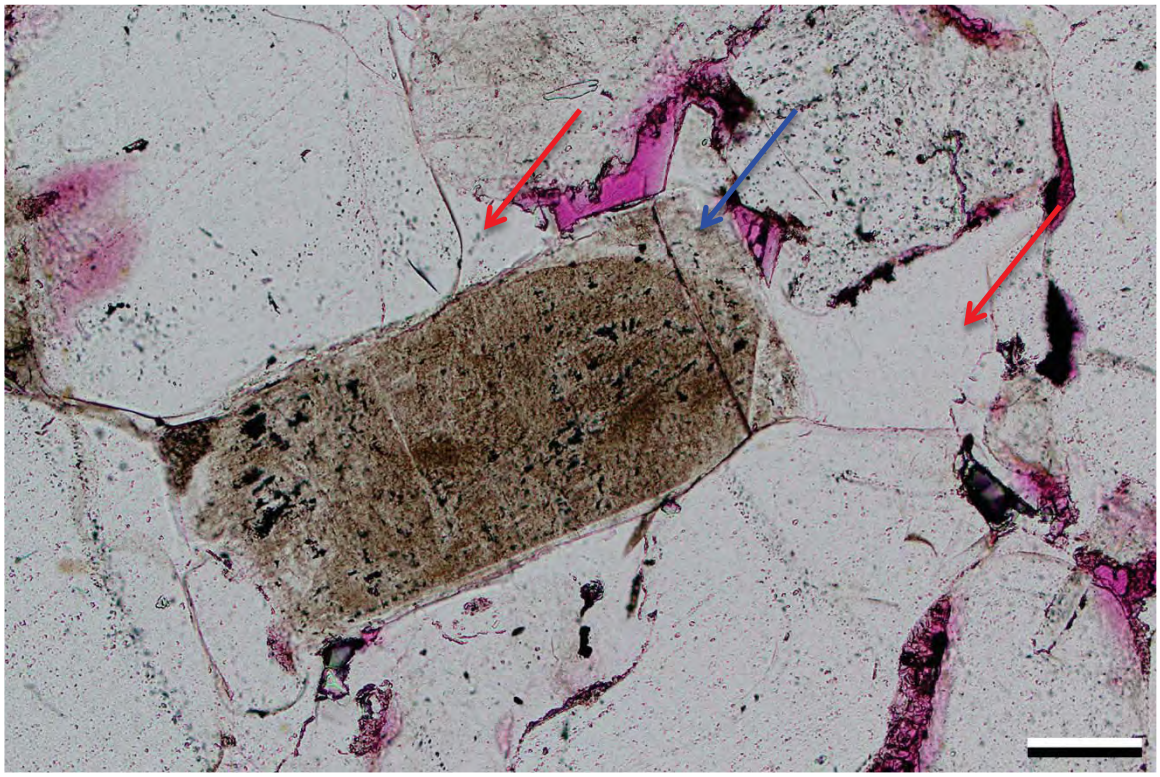
Other – Little to no compaction due to quartz cementation.

Porosity analysis: Visible porosity is approximately 12%.

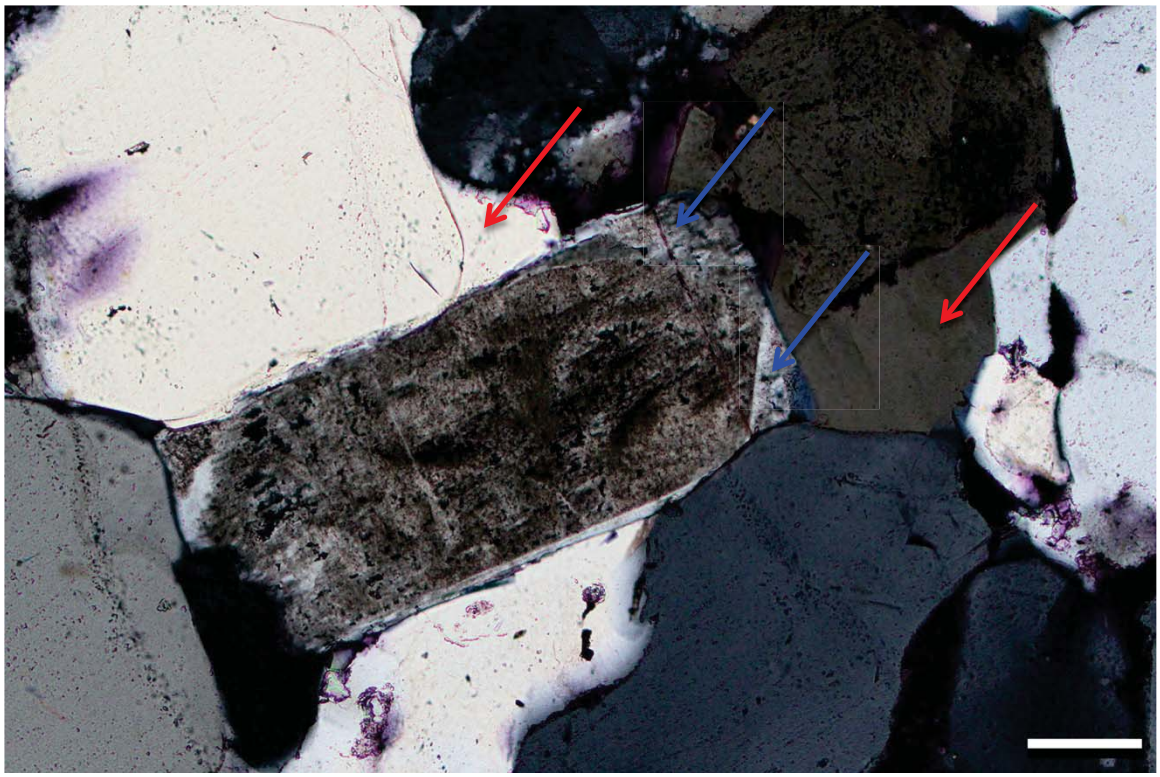
Porosity Types – Primary interparticle porosity (2%) and secondary porosity (10%). Secondary porosity types include intraparticle (leached K-spar and chert/chalcedony), vuggy, intercrystalline (kaolinite).

Porosity Controls – Compaction; quartz, feldspar and kaolinite cementation.

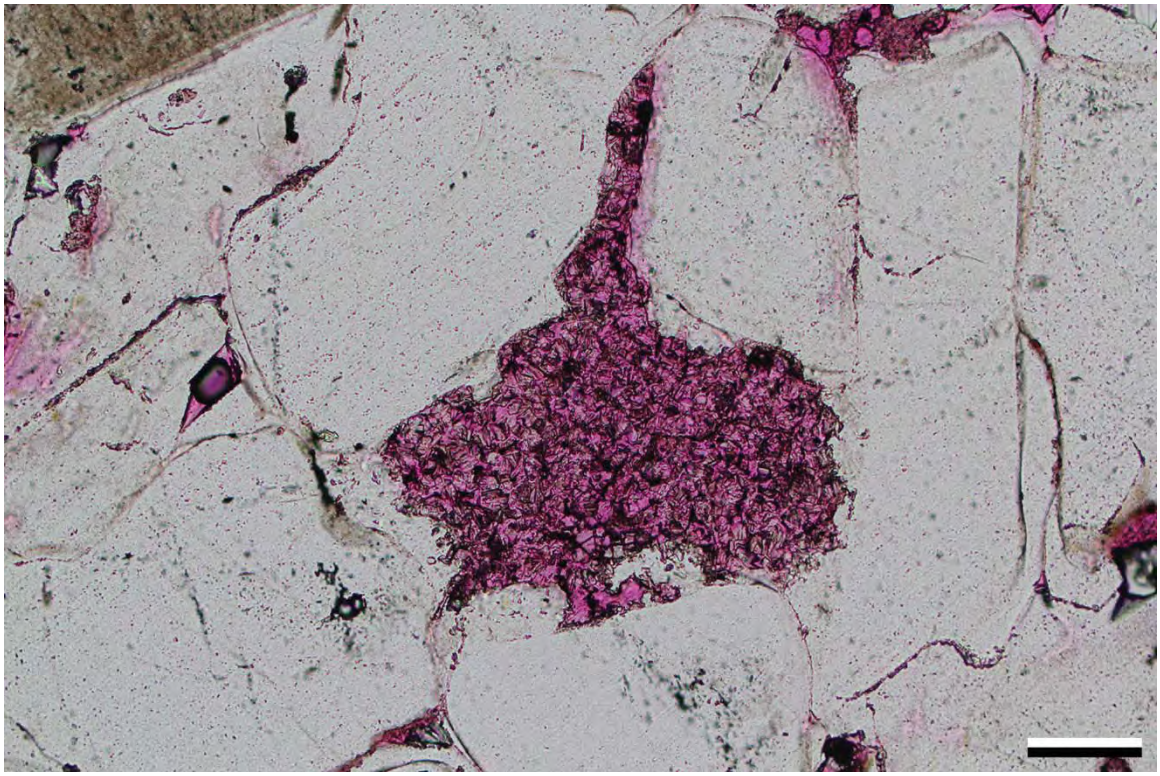
Photomicrographs for RMCSS State #1 8298.0 ft



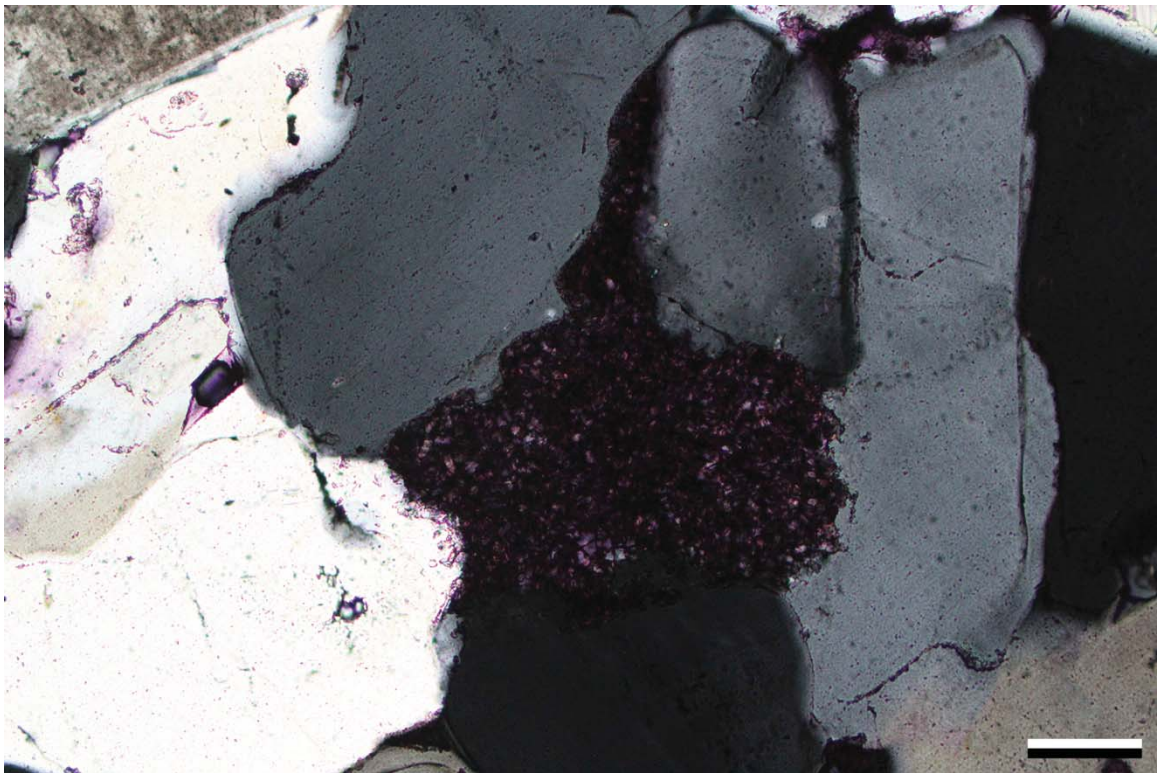
RMCSS State #1 8298'. K-spar (blue arrow) and quartz (red) overgrowths. It is difficult to determine the timing, but it appears that the feldspar overgrowths may have occurred first. PPL; Scale bar = 0.1 mm; IMG_7436; Cretaceous Dakota Fm., Craig, CO.



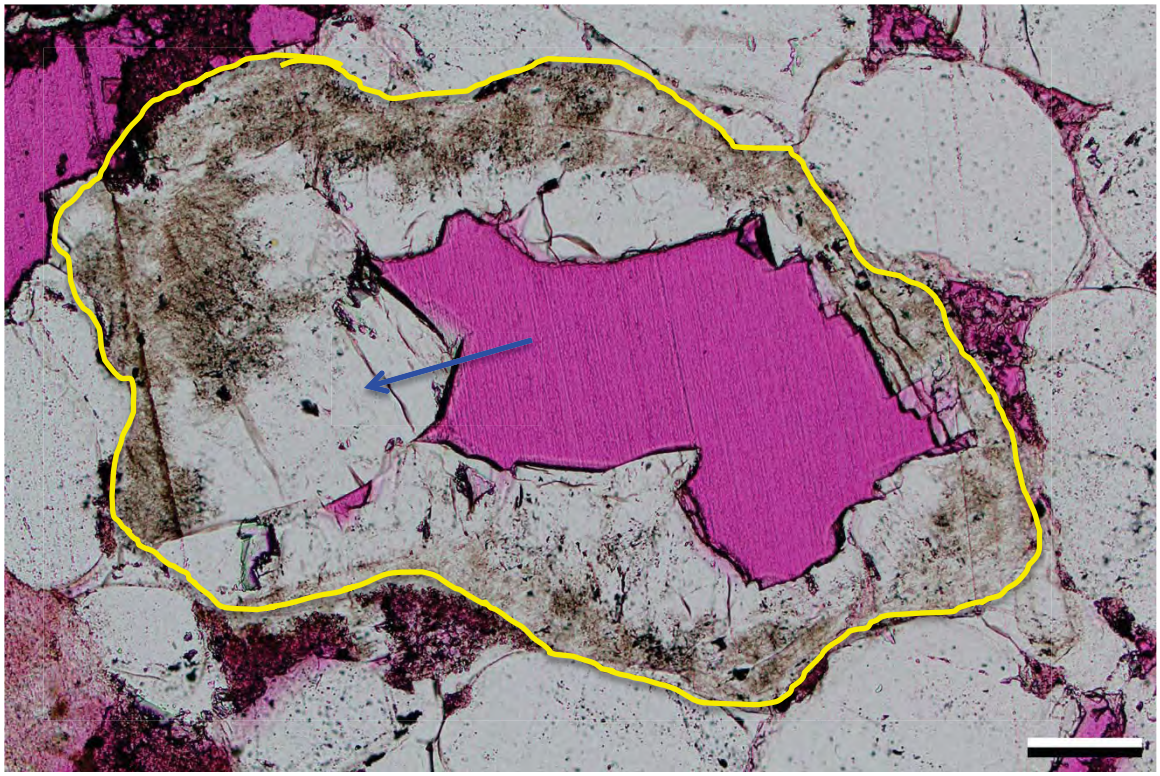
RMCSS State #1 8298'. Same view as previous photomicrograph. XPL; Scale bar = 0.1 mm; IMG_7437; Cretaceous Dakota Fm., Craig, CO.



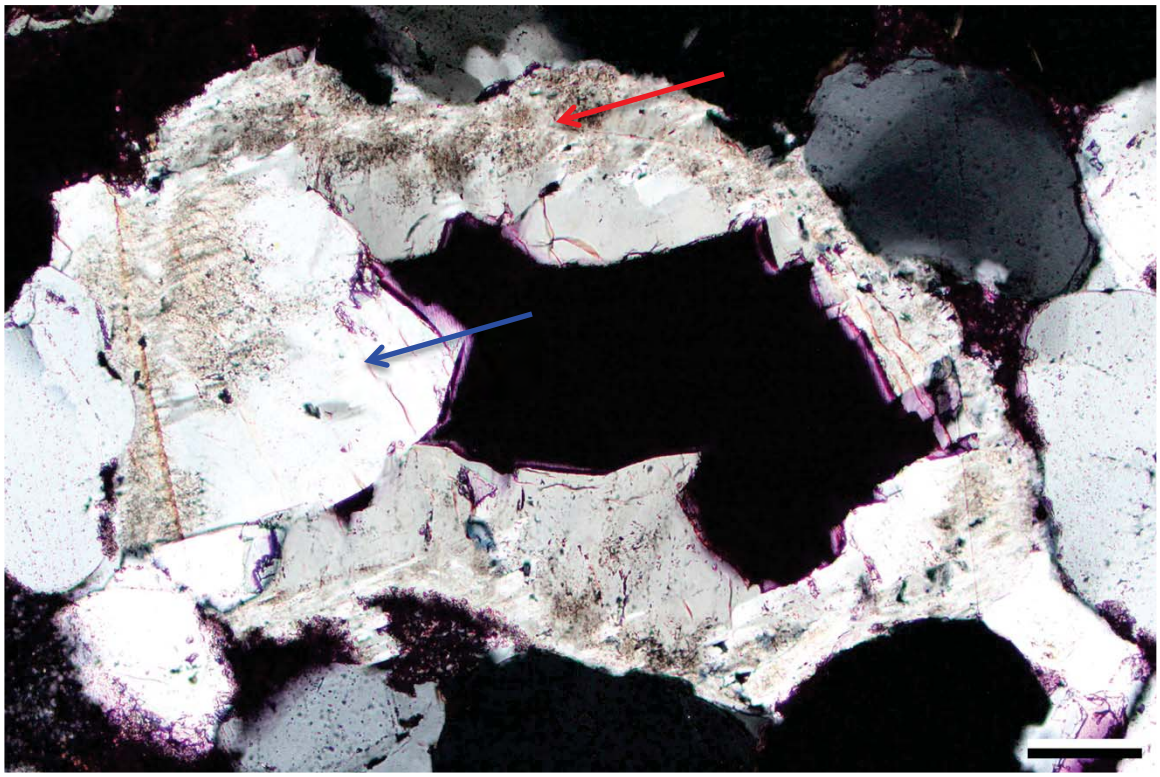
RMCSS State #1 8298'. Kaolinite books filling primary porosity (with intercrystalline porosity in pink) closely follow feldspar and quartz overgrowths. PPL; Scale bar = 0.1 mm; IMG_7438; Cretaceous Dakota Fm., Craig, CO.



RMCSS State #1 8298'. Same view as previous photomicrograph. XPL; Scale bar = 0.1 mm; IMG_7439; Cretaceous Dakota Fm., Craig, CO.



RMCSS State #1 8298'. Secondary porosity after partial dissolution of a K-spar grain (yellow outline) that was later infilled with K-spar cements (blue arrow). PPL; Scale bar = 0.1 mm; IMG_7440; Cretaceous Dakota Fm., Craig, CO.



RMCSS State #1 8298'. Same view as previous photomicrograph. XPL; Scale bar = 0.1 mm; IMG_7441; Cretaceous Dakota Fm., Craig, CO.

APPENDIX M

University of Utah Report for Capacity Assessment

Contents

Topic

Capacity Assessment Methodologies

Regional Capacity and Significance

List of Abbreviations....2
Background/Introduction....3
General CO_2-capacity-calculation methodology....4
Previous Southwest Region Atlas methods:....4
NATCARB saline formation CO_2 storage resource estimates methodology....5
Methodology workflow update....6
Regional data preparation:....6
CO_2 Storage-capacity calculations....9
Creation of GIS CO_2 storage capacity point database.....10
Edge matching formation data across state boundaries:....12
Integration of the regional, 1-km-spaced Rocky Mountain-CO_2-capacity GIS database....16
Aggregating (upscaling) the data into 10-km^2 NATCARB predefined polygons 18
Rocky Mountain Carbon Capture and Sequestration Project CO_2 capacity data....20
Comparison of 2013 project most promising CO_2 capacity data to previous data for the 3 main saline formations on the Colorado Plateau:....26
Significance of Regional Capacity Results....28
Significance of Regional Capacity Estimates in Context of Previous Estimates....28
Significance of Regional Capacity Estimates in Context of Years of Emissions....28
Significance of Regional Capacity Estimates as Compared to Eastern USA....30
Conclusions....31
References....

List of Abbreviations

AGS	Arizona Geological Survey
ARRA	American Recovery and Reconstruction Act
AZ	Arizona
CCS	Carbon Capture and Storage
CGS	Colorado Geological Survey
CO	Colorado
CO2	Carbon dioxide
CSV	Comma Separated Values (text file)
DEM	Digital Elevation Model
DOE	Department of Energy
EGI	Energy and Geosciences Institute
ESRI	Environmental Systems Research Institute
gdb	Geodatabase
GHG	Green House Gas
GIS	Geographic Information System
GT	Gigatonnes (= 1 billion Tonnes)
mpk	Map package
NATCARB	National Carbon Sequestration Database and Geographic Information system
NETL	National Energy Technology Laboratory
NM	New Mexico
NMBGMR	New Mexico Bureau of Geology and Mineral Resources
RCSP	Regional Carbon Sequestration Partnerships
RMCCS	Rocky Mountain Carbon Capture and Storage
shp	Shape file (GIS file)
TDS	Total Dissolved Solids
U.S.	United States
UGS	Utah Geological Survey
USDW	Underground source of Drinking Water
UT	Utah
xls	Excel spreadsheet file

Background/Introduction

This report describes the workflow created to process data for 'Characterization of most promising sequestration formation in the Rocky Mountain Region' project. One of the project tasks was to assess the regional significance of these ubiquitous regional formations. The project also required refining existing carbon capacity estimates based on existing data to determine if formations can store 30 million tons of CO_2. The national NATCARB Carbon Sequestration database was updated with the generated regional data. It was therefor necessary to integrate the regional deep saline geology information into a coherent and consistent single dataset across state and sedimentary basin boundaries. These data also have to comply with NETL's NATCARB data structure from which data can be queried to estimate CO_2 storage capacities on a national scale. The Colorado Geological Survey (CGS), the Arizona Geological Survey (AGS), New Mexico Bureau of Geology & Mineral Resources (NMBGMR) and the Utah Geological Survey (UGS) together with the University of Utah contributed to this task in particular.

The University of Utah developed a workflow that could be used or adapted by each of the four State geological surveys. The workflow allowed AGS, CGS, NMBGMR and UGS to transform their regionally compiled data into a format from which data could be integrated across state boundaries. Eventually, the data for all the formations were merged into a single database. The database provides the original data and their derived attributes. The resulting capacity data can be queried at a 1-km^2 scale or can be aggregated into 10 km^2 polygons conforming to NETL's NATCARB saline formation Atlas format. Geologists from the State surveys created the regional data for the saline formations and the University of Utah spearheaded the coordination, the development of a workflow that can be used for future regional data compilations, the data integration across the state boundaries and the aggregation of the data at the 10 km scale. University of Utah then formatted the regional data in accordance with the NATCARB saline-atlas template.

Several steps were required to convert the regional data provided by the geological surveys before calculating the regional CO_2 capacity values. After the surveys compiled the regional data for their state, the University of Utah's role was initially focused on creating a common workflow system that served as a framework. The states were asked to create their original input data in a GIS format from which the required parameters could be extracted at a 1-km^2 spatial resolution. While the states were working on this task, the University developed an excel spreadsheet based on the CO_2 capacity spreadsheet used previously for capacity calculations in the southwestern US. Besides the CO_2-density macro, a new worksheet was generated to prepare the data points for integration into the GIS database. The manipulated GIS data became the input for the NATCARB Carbon Atlas format. The purpose of the spreadsheet is to replace a visual basic script used for previous NATCARB Atlas capacity calculations. It used to run within ArcGIS™ version 9, but did not run properly anymore under version 10. Since ESRI™ is phasing out Visual Basic scripts in their GIS software and the expertise to modify the script was not available in the project team, it was decided to look for an alternative solution. Mimicking the functionality of the script in an Excel spreadsheet had the advantage that the method is more transparent to the GIS analyst. A drawback of the spreadsheet calculations is a greater potential for operator mistakes.

This study determined that the potential CO_2-storage capacity for the three main regional saline formations ranges between 9.8 and 103.9 billion metric tons depending on the efficiency factor. When compared to the 2012 Atlas IV data the total CO_2 storage capacity of these three formations decreased by approximately 8%. Including the stratigraphic equivalents increased the total CO_2-storage-capacity-estimate to a range between 13.6 and 143.7 billion tonnes depending on the efficiency factor. Since not all the equivalent formations were included in the Atlas IV data, a comparison cannot be made. The relatively simple, volumetrically based, regional-resource estimates did not take geologic complexity, presence or absence of seals, or different trapping mechanisms into account. The numbers also do not take economical or technical constraints into account.

In summary, this report describes the general GIS workflow process applied to transform the data delivered by the four involved State Geological Surveys into the NATCARB Atlas structure. Additionaly, this reports touches on the specific issues stemming from different groups processing their data more or less independently. And, it outlines remaining problems and presents suggestions for how to improve the data and the workflow process.

General CO_2-capacity-calculation methodology

Previous Southwest Region Atlas methods**:**

The first CO_2 capacity data for the South West Region were created by drawing generalized cross sections through the sedimentary basin to derive average data for thickness and depth of the formations. Average, local geothermal gradients were used to calculate reservoir temperatures. The hydrostatic pressure at the top of the formation was derived by applying the hydrostatic pressure gradient of 1MPa/km (0.433 psi/ft) to the depth of the top of the formation. These values allow calculating the CO_2 density at depth. Average porosity values for the formation were applied to derive the pore volume. Combining the total pore volume with the average CO_2 mass – derived from the CO_2 density – provided the initial CO_2 capacity values. In a later version of the methodology low, medium and high efficiency factors were applied to the total CO_2-storage capacity. These efficiency factors, corresponding to P10, P50 and P90 probability distributions derived from Monte Carlo simulations reflect the fraction of the pore space that will be occupied by the injected CO_2 (U.S. DOE 2012). For the NATCARB Atlas III data, the methodology was modified to include information extracted from well data in the public domain and commercial well databases. Existing well depth and thickness values were interpolated between the wells and extrapolated to the extent of the basin. Where only one data point was readily available, that data point's values were assigned to the entire basin, which creates a lot of uncertainty. For the NATCARB Atlas III southwest region data, the CO_2 density was calculated using an iterative method based on the Modified Redlich-Kwong equation of state and standard thermodynamic equations (Han and McPherson 2008). Previous versions of southwest regional Atlas data used a 3000' (914.4m) depth of the top of formation cut-off to estimate the CO_2 capacities. This is a slight deviation from the NATCARB Atlas protocol, which suggests an 800m minimum depth (U.S. DOE 2010). To maintain consistency within the southwest regional data, to which this project's data eventually will be merged, that cut-off of 3000' was maintained. No thickness or maximum depth data cut-off values were imposed on the CO_2 capacity

estimates. For Atlas IV the range of the efficiency factors was tightened from a 0.4 - 5.5 to 0.51 – 5.4. The data from the current ARRA project will be merged with the Atlas V data, the anticipated 2014 version of the NATCARB CO_2 Atlas. At the moment of this writing, no updated NATCARB calculation methodology or database structure has been communicated to the project. The methodology described in the rest of this report reflects an update of how the improved regional saline data prepared by the state surveys was processed in preparation for eventually being merged with the RCSP Atlas V data.

NATCARB saline formation CO_2 storage resource estimates methodology

Carbon dioxide (CO_2) capacity calculations require several input data parameters. This project used the volumetric calculation method described in the NATCARB Atlas (U.S. DOE 2010) given by the following equation:

$$G_{CO2} = A_t h_g \square_{tot} \square E_{saline}$$

This formula generates the **CO_2 storage resource mass estimates** (G_{CO2}) based on combining data for the total area (A_t), gross formation thickness (h_g), total porosity ($\square_{tot}$), CO2 density ($\square$) and the storage efficiency factor (E_{saline}). The first two input parameters account for the total bulk volume; the CO_2 density converts the reservoir volume of CO_2 to mass while the storage-efficiency factor reflects the fraction of the total pore volume that will be occupied by the injected CO_2.

The **total area** represents the extent of the formation 3000' below the topographic surface. To be able to take the variations in the other contributing variables across the extent of the formation into account, the total area was discretized into a centroid-centered grid with 1-km^2 cells using GIS techniques, which will be explained later. An equal area projection was used to assure that the area of the each cell was not distorted and kept equal throughout the project region. The CO_2 storage capacity was calculated for each of the 1-km^2 cells of the formation that is present below 3000'. The formation totals were obtained by summing the data of the contributing cells.

The **gross formation thickness** for each cell was extracted from the 1 km^2 discretized regional isopach maps provided by the four geological surveys of the states participating in the project. The volume of the formation at the center of cell was obtained by multiplying the thickness with its area (1 km^2).

Multiplying the bulk volume by the **porosity**, a parameter provided by the surveys, generated the available pore volume. Generally, an average constant porosity value was applied for the entire formation across the basin except for the Uinta Basin Weber formation, for which location dependent values derived by spatially interpolating existing well porosity data.

The **CO_2 density** at the top of the formation was calculated based on the modified Redlich-Kwong equation of state using an Excel Visual Basic macro. The algorithm in this macro requires temperature and pressure as variable input parameters depending on the depth. Neither of those 2 variables is readily available from well data but they can be approximated from the depth of the top of the formation. The top of the formation and not the middle of the formation depth was selected as reference point because the super critical CO_2 fluid will rise to the top from the buoyancy effect. The temperature was approximated using the geothermal gradient, whereas the hydrostatic gradient was used for pressure. The geothermal gradient can either be calculated from measured bottom

hole temperatures or set to one corresponding to heat flow within the sedimentary basin. The density parameter combined with the pore volume allows for the conversion to CO_2 mass

The **efficiency factors** applied to the CO_2 mass reflect the fraction of the pore space that will be occupied by the injected CO_2. Three different factor magnitudes are used reflecting a low, medium and high estimate: 0.51%, 2% and 5.4%

Methodology workflow update

The general workflow for converting the regional geologic information provided by the four state geological surveys, to CO_2 capacity numbers compliant with the NATCARB saline Atlas data format consisted of 6 major steps listed in Table 1. ESRI's™ ArcGIS software package was used for the GIS platform and Microsoft Excel™ was used for the spreadsheet calculations.

Table 1: Major methodology workflow steps:

Workflow step	Processing environment	Data Scale	Responsibility
1. Regional Data Preparation	GIS	Regional	AZ, CO, NM & UT Geological Surveys
2. CO2 storage capacity calculations	Spreadsheet	1 km^2	State Surveys and University of Utah
3. Creation of GIS CO2 storage capacity point database	GIS	1 km^2	University of Utah
4. Edge matching formation data across state boundaries	GIS & spreadsheet	1 km^2	University of Utah & State Surveys
5. Integration of the regional 1-km-spaced Rocky Mountain CO_2 capacity GIS database	GIS	1 km^2	University of Utah
6. Aggregating (upscaling) the data into 10 km^2 NATCARB predefined polygons	GIS	10 km^2	University of Utah

<u>Regional data preparation:</u>

a. State Geological Survey Regional Data

The partnering State Geological Surveys generated the input parameters required for the CO_2 storage capacity equation applying different methods. The surveys will report on the details of their regional data compilations in separate reports while this report will provide an overview of the parameters and touch upon their workflow where needed. The states assessments generally resulted in two contoured surfaces for each deep saline formation of interest within a basin (Figure 1). The first was a contoured isopach and the other a 'top of formation' structure surface. The contours were derived from available

well information, expert knowledge of the basins and ancillary data where available. By only applying computer interpolation to the well data NM was the exception to this method. The manual contouring process allowed the geologist to include structural basin knowledge that cannot easily be incorporated using mathematical interpolation of well data attributes only. These contour lines were converted to records with a 1km spacing covering the entire area where the formation occurs at depth within the sedimentary basin. Later in the workflow the 1 km^2 point data were aggregated into predefined 10 km^2 NATCARB Atlas cells. Besides the contour lines, the surveys also provided porosity data and geothermal gradients. The four required capacity estimate input values were included in the delivered spreadsheet or in the geodatabase, containing formation records at the 1-km^2 scale.

There were several reasons why the data were prepared at 1-km^2. First of all it allowed for a better approximation of the regional geological interpretation into discretized cells. It also facilitated matching discrepancies between formation data along State boundaries. Southwest regional data submitted to previous NATCARB Atlas versions were generated as a 1 km^2 points before reformatting them to the predefined 10 km^2 polygon cells. Keeping the 1 km^2 scale assured continuity in the data generation methodology. A final reason was that the Colorado plateau area was small enough to allow us to work at such a relative fine scale. The intermediary data file sizes were not that too large to become an obstacle to manage the data workflow.

To facilitate equidistant 1 km sample spacing across state boundaries, the NATCARB 10 km^2 saline polygon template was subset to the polygons belonging to the four participating states only. From these polygons a 1 km^2 base raster was created, preserving the NATCARB Lambert Azimuthal Equal Area projection (Appendix 1). All of the other grids created during the capacity-calculation process were snapped to this base ensuring that the centroids of the grid cells representing different attributes were all exactly geo-located. This procedure allows an exact match by location during the spatial joining of point-data attributes extracted from the grids. Using a uniform grid based on a single projection also ensured that each record of the merged state formation databases represent exactly 1 km^2. It also prevented mismatches of the grids at the state lines. Taking care of the projection at the end of the workflow would have introduced errors in the variables for which the area was a contributing parameter, i.e. all volumes. Establishing a common projection at the onset of the project and having a base dataset to snap all project-derived grids greatly facilitated the data processing workflow.

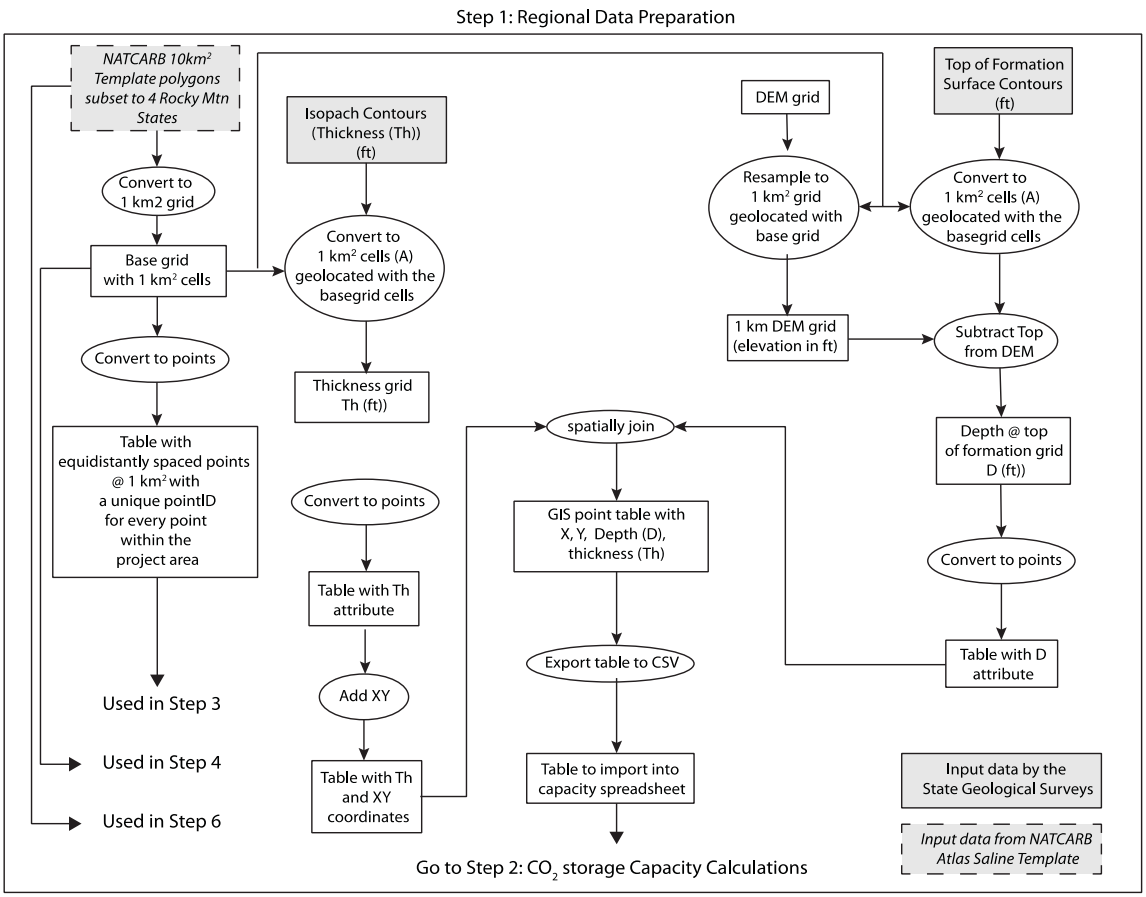


Figure 1: Workflow step 1: Regional data preparation

The base raster also facilitated solving edge matching formation data across state boundaries. Edge matching is a GIS procedure used to align features along the boundaries of two separate data sets. Associating the unique ID number of each 1 km^2 cell with the 1 km^2 GIS capacity data records allowed for summarizing the CO_2 storage capacity numbers over all the saline formations or over a selected subset after merging all the 1 km spaced capacity records of the individual formations into a single feature class.

Before the overburden data could be derived from the top of formation data, a 1 km DEM grid - also geo-located with the base raster – was required as well. The University of Utah did the preparation of the base raster while the DEMS were prepared by the state surveys.

b. Generating discretized thickness and overburden (depth) data

Spatially discretized thickness-of-formation and depth-of-the-formation attributes were obtained by converting the isopach and the top of formation contour data to 1 km grids geo-located to the base, raster layer using standard GIS techniques (figure 1). Several techniques were used by the different surveys. Subtracting the top of formation raster from the DEM, generated a grid with depth of formation values. The accuracy of this depth grid depends on the accuracy of the interpolation of input well data and the generalization of the DEM grid, which was resampled from higher spatial resolution cells to 1 km^2 cells. This procedure was performed for each of the formations of interest,

mainly by the state surveys and occasionally with cooperation of the University of Utah. NM was the exception to this procedure. They used the data attributes available in their state well records database and interpolated the thickness and top of formation straight to a terrain model, skipping the contouring process.

The thickness of the Weber Formation is the most uncertain of the three main, deep-saline formations. It is stratigraphically the oldest formation and occurs at great depth. Not many wells penetrated the entire Weber Formation. The deepest top-of-formation-depth was interpolated in the Unita Basin at over 35,000 feet. At the Craig project site, the Weber was deeper than predicted from adjacent logs and geophysical data. Because of overall drilling-cost overruns, the drilling was stopped before reaching the Weber Formation.

c. Converting the thickness and depth data to database records:

Both the depth and thickness, grid-cell values were converted to a point feature dataset. This created fairly large database files. These two attributes were combined into a single table using a join-by location operation. Only records for which both attributes were present were kept. After X and Y coordinates were explicitly added as fields to the database containing the joined depth and thickness values, the database was exported from GIS to a comma-delimited text file, file format which allows for easy interchange of the data with other software packages.

CO_2 Storage-capacity calculations

a. CO_2 density calculations:

The text file generated at the end of step 3.3.1.c was copied into the EGI capacity Excel spreadsheet (EGI capacity calculation spreadsheet), which contained the CO_2 density-calculation macro (Han and McPherson, 2008). The main inputs for the macro are temperature and pressure (Figure 2). These attributes are derived from the depth values in the text file using a certain geothermal and pressure gradient. The geothermal gradient was generally the same by basin, except for UT who applied different gradients for different formations. In the Uinta Basin one gradient was used for the Dakota and the Entrada and another for the Weber formation. Colorado spatially interpolated the gradient derived from bottom hole temperature data. Once temperature and the pressure values at the top of the formation were calculated using the spreadsheet formulas, the CO_2 density values were generated by running the Visual Basic macro.

b. CO_2 capacity calculations:

A separate worksheet was developed in which all of the derived attributes (X coordinate, Y coordinate, temperature, pressure, depth, thickness and CO_2 density) for all the records were copied into. Before calculating the CO_2 volumes a few formula-based fields for additional attributes were generated (volume, pore volume and CO_2 mass). The CO_2-density, macro output was converted to metric units so the CO_2 volume could be generated in metric tonnes, the NATCARB Atlas reporting unit. The volume of each cell was generated by multiplying the area (1-km^2 for each data point, defined by the raster cell from which the attributes were extracted) by the thickness of the formation at that cell. Multiplying the cell volume by the porosity, generated the pore volume. The CO_2 mass was obtained by multiplying the pore volume by the CO_2 density. The CO_2 storage

capacity volumes at the 1 km scale were calculated by applying the low (0.51%), medium (2%) and high (5.4%) efficiency factors to the CO_2 mass. This worksheet contains all the data from which a new point feature class can be generated in GIS.

Although the spreadsheet with the formulas was provided to the surveys, not all of them followed the template, or some made changes to them to suit their data. Before the data could be imported into GIS, it was necessary to generate a common set of field names that were exactly the same for all the formation data files within a state, as well as in files from the different states. This was necessary in order to merge the formation data from the different states into a single formation point database. Having a different set of fieldnames for the different formations would prevent merging the across-state-integrated-formation data into a single GIS feature class. Utah's data, which were provided in geodatabase feature classes by formation, still needed to be modified to adjust the field names. Because adjusting the fieldnames outside the GIS environment is a faster process compared to applying GIS database techniques, the records were exported to a CSV file, modified in a spreadsheet and then reloaded into GIS.

c. Formation contour at 3000' depth:

Finally, to be able to format the CO_2 capacity numbers into the pre-defined NATCARB Atlas format, a polygon representing the outline of the formation at 3000' depth was required. Some State Geological Surveys provided these contour lines, other only provided the 1 km spaced points and the limiting extent was screen digitized by University of Utah.

<u>Creation of GIS CO_2 storage capacity point database.</u>

a. Importing the 1-km^2-CO_2-capacity data into GIS

- Point data by formation:

An additional field was added to the database to indicate whether the record represented an original data point generated by the State Geological Surveys, or if it was added to fill in missing data points. The binary field values were marked as 'N'' for an original data record, or 'Y' for the records representing points created to enforce spatial data continuity. Another field was added by spatially joining the GIS point data to points converted to the 1-km-spaced base, Rocky Mountain raster grid. Doing this made it possible to associate a unique point-ID to each formation record (Figure 3). This point-ID was consistent for all formations for which records at the same locations are available, i.e. for cells for which there are data in multiple stratigraphic formations. The unique point-ID was added by spatially joining the 1-km-spaced-CO_2-capacity data to the points that were converted, base-raster cells.

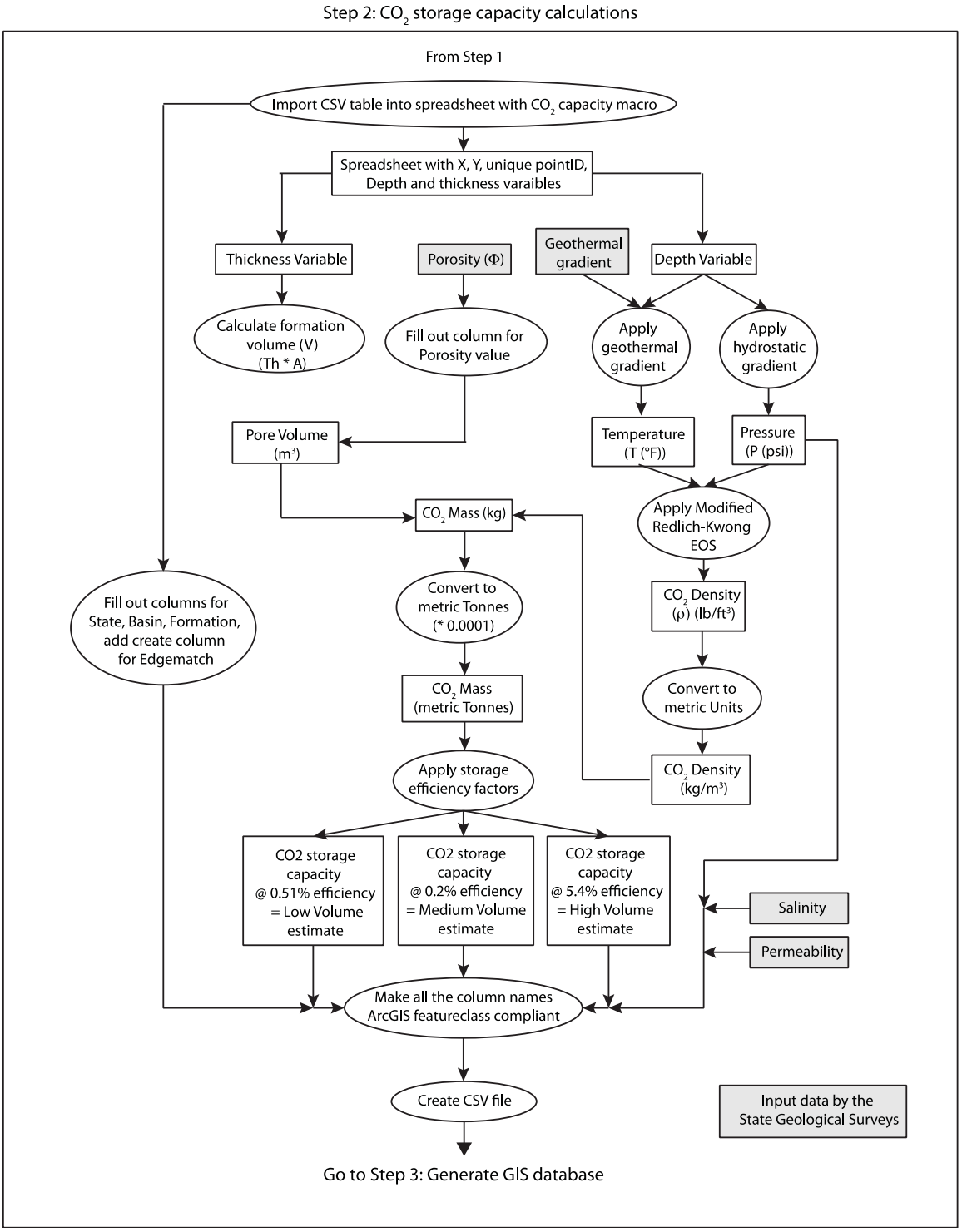


Figure 2: Workflow step 2 – CO_2 Capacity calculations

The final step consisted of quality checking the data. Different test are required for numeric defined fields and text defined ones. The numeric tests relied on simple methods such as making sure the magnitude and the data ranges were within expected values. We also gridded the different numeric parameters to check for discontinuities in the data that didn't have a reasonable geological explanation, or was caused by differences in data-generation methodology was also applied. Magnitude inconsistencies often indicated parameter unit problems requiring unit conversions of the values. Negative thickness values resulting from interpolating geological conditions were eliminated. The interpolation algorithm generated negative thickness values between the lines representing contours of zero thickness. Data records with a depth at the top of formation less than 3000' were eliminated too. The text-defined, database fields were checked for spelling consistency across all records.

- Formation polygon outlines at 3000' depth:

Besides a database with 1-km-spaced points for each deep saline formation, a polygon outline of these formations at the 3000' cut-off depth needed to be prepared for use during the edge matching process, Further, this was necessary to calculate the 'resource_area' field for the NATCARB saline-atlas field at the 10 km^2scale. These formation outlines were created by combining polygons provided by either the State Geological Surveys or the outlines that were screen digitized around the point locations. For formations with multiple, spatially-separated polygons, the single part features were combined into a multipart feature so that each formation is represented by a single record in the formation-outline, merged database.

Edge matching formation data across state boundaries:

Spatial edge matching problems occur at borders between data sets. This problem most commonly takes place when line or polygon features have to be joined. In this project superimposing administrative state boundaries on geologically continuous data created these artificial edges. Because the 1-km points in the formation data sets for this project actually represent a discretization of a data parameter in the area (polygon) of the formation below 3000' depth; issues related to spatial continuity need to be addressed.

Four different situations needed to be dealt with. The easiest one to correct was the one where duplicate points existed. There were a few instances where a narrow strip of cross-boundary data points were included in the records of both adjacent states. Rectifying this problem required deleting the one point of duplicated spatial records: the points within the state of the survey that created the data were maintained; those that crossed into the neighboring state were removed.

A second crossover problem happened where points were located in a neighboring state whereas the state that should have generated the point did not have a data point at that location. In this case, the depth and pressure parameters were kept but the porosity and geothermal gradient was adjusted to correspond to the rules and values set by the state in which the point is located. This required recalculations of the CO_2 capacity.

Dealing with missing records was more difficult to handle. A first cause for missing data points along state lines can be attributed to each state using their own state outline to define their data. Small spatial discrepancies along the state boundaries caused

some of the 1 km points not to be included in the 1 km^2 data set of either state. Although the missing points represent a 1 km gap, this does not necessarily imply that the state boundaries are offset by the same amount. Having what should have been a common state boundary line instead pass just on either side of the 1 km grid centroid, will cause the exclusion of the point in the data sets of both states resulting in the gap when the

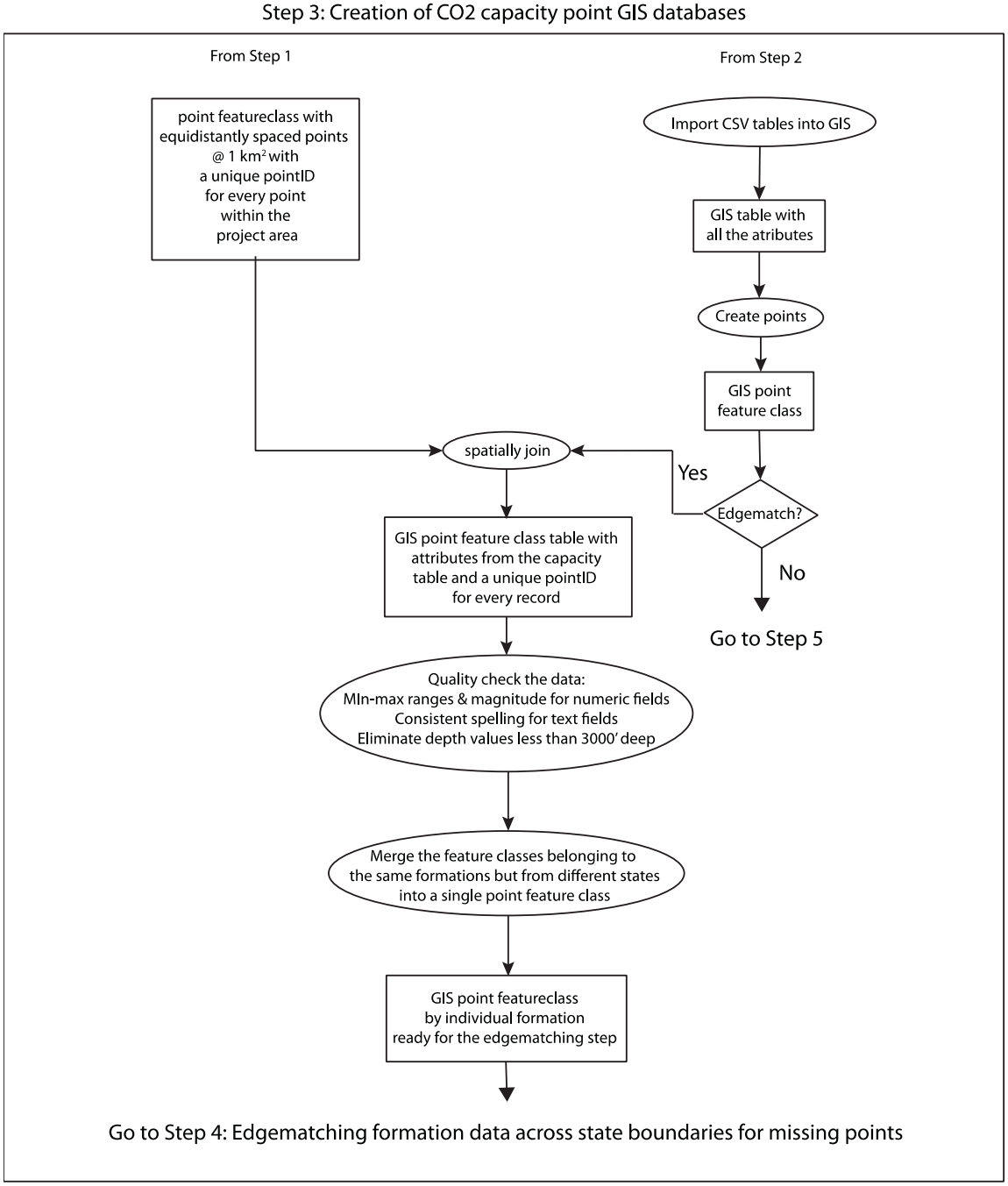


Figure 3: Workflow step 3 - Creation of quality-checked, GIS-CO_2-capacity database with a set of database fieldnames consistent across the saline formations for the 4 Rocky Mountain States.

points are merged. This problem could have been prevented by providing a topologically correct, state boundary file containing the outlines of the four states involved at the onset of the project.

Finally, a few problems occurred where there was an offset of the 3000' depth contour at state borders (Figure 4). This problem was most likely caused by the surveys only using their state's data as the source for their interpretations, while excluding data points that were across state boundaries. By using only single-state-source data, extrapolation to the state boundary was based on best-knowledge, ancillary information, rather than actual data just across state boundaries. Including data from wells across state lines could have resulted in a tighter interpretation at the boundary while also reducing uncertainty. The range of the offset of the 3000' contour line was in the order of a few kilometers where ancillary basin data were used to generate the depth and thickness maps. The offsets were much larger where 1-km-spaced data were created by computer based interpolation between wells with known records only, and not manually extrapolated to the 3000' depth boundary using best knowledge practices. In this situation matching up the 3000' depth contour line involved discussions between the partners of each involved state.

After agreeing on how to spatially match the data across the state boundary, the polygon boundary of the area was edited to reflect the modification. This polygon was used to extract all the equidistant 1 km-spaced points from the Rocky Mountain base grid that was created at the onset of the workflow. This new database contained location records for the points generated by the State geological surveys as well as for the missing points. The missing points at this step have no data values for any of the parameters besides the XY coordinate locations and the unique point-ID number. A new binary field, representing either an existing data point or a new data point was added to this newly created table. Joining the formation points subset of the basin (where the edge matching is required) to the newly created table using the common field (the base layer point-ID) allows for updating the just-created, binary-valued field in the ArcGIS field calculator. The points that were already processed will have a 'N'-value while the 'null'-value for the points for which capacities were replaced with a 'Y'-value. A new raster was created from the binary values to later be used as a mask to extract the unknown thickness and depth data. Temperature can be derived from the depth values when a constant geothermal gradient was used but where the geothermal gradient changed spatially, the temperature data for the missing points were interpolated as well. Just as with all other grids generated during the workflow thus far, this binary mask was snapped to the base grid created at the onset of the workflow. Attributing the unknown points with the state in which they plot was the last preparatory step required before generating parameters for the unknown data points. One state used spatially varying porosity values, but the edge matching procedure of the formation did not require generating additional points.

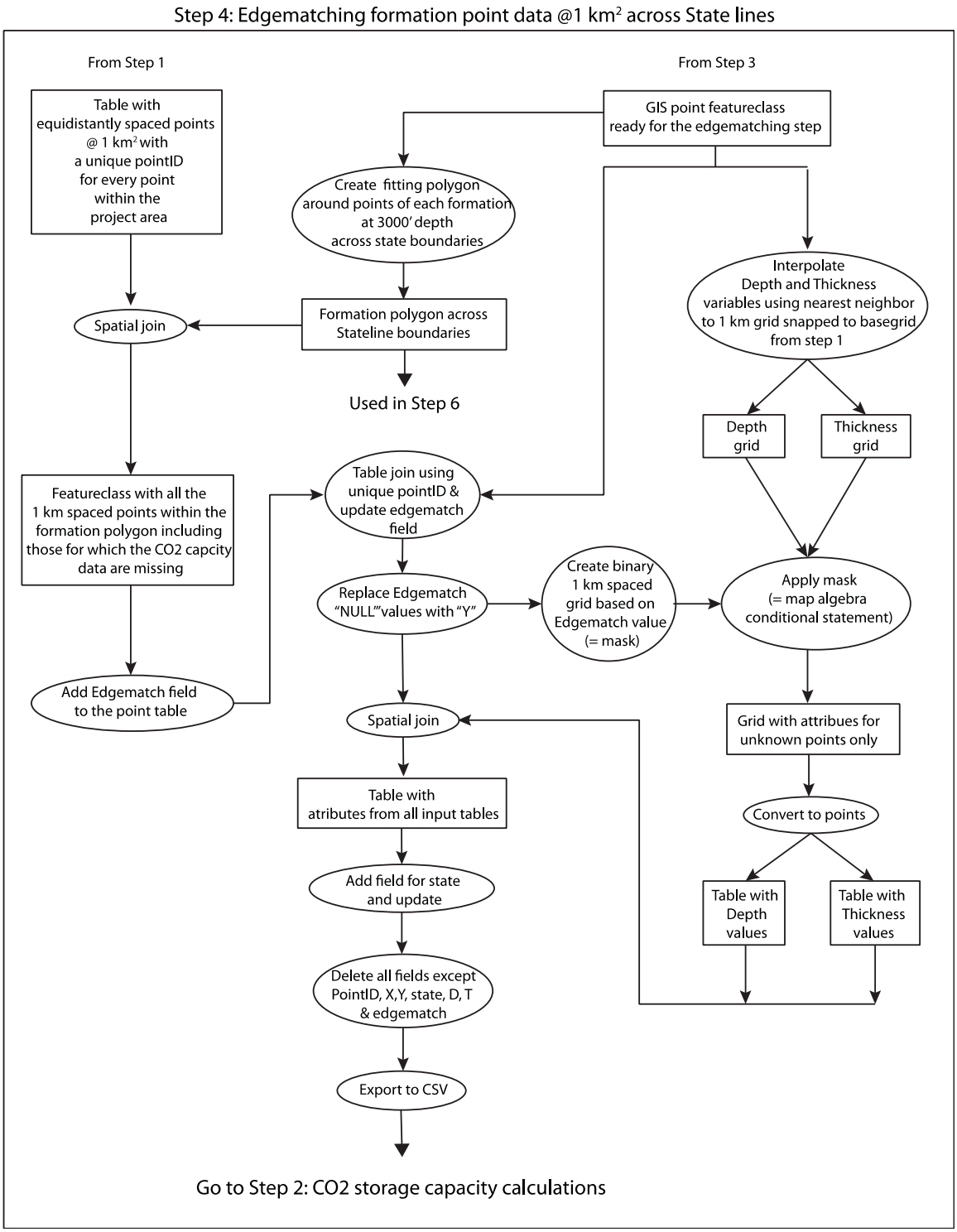


Figure 4: Workflow Step 4 – edgematching formation data across state boundaries

Depth and thickness values were derived at the missing locations by interpolating the values, using a natural neighbor algorithm, from the existing data provided by the state geological surveys. Both output grids were geolocated with the base grid and the values of the new points were extracted using a raster-calculator, conditional statement

invoking the binary mask. The retained points, extracted from the interpolated parameter grids, were spatially joined with one another as well as with the table containing the unique point-ID variable, the associated state code and the XY coordinates. This table combining all the parameters was exported to a CSV file and manipulated in the capacity spreadsheet in a similar manner as described under step 2 of the workflow. The porosity and geothermal gradient were assigned following the numbers of the state in which the point was located. Once the worksheet was structured the same, having all the parameters calculated and fieldnames assigned, (as the spreadsheets processed with the points provided by the state geological surveys), it was loaded into ArcGIS and merged with the existing point data for that formation.

Besides problems with the spatial data continuity, the state-by-state approach resulted in data-value discontinuities across state boundaries as well. Their details will be reported in the section describing the actual data. Generally the data-discontinuity problems can be attributed to states using different, single-valued parameters for porosity and the geothermal gradient. Or, some states set a constant value for all their records in a certain formation for the area covering their state while others used a spatially varying one (ex. porosity and geothermal gradient). Changes in thickness and depth across state boundaries occurred because the bounding basal and top, strata were not precisely defined ahead of time (e.g., Entrada). In one instance, a different constant geothermal gradient was used within a state for different formations within the same sedimentary basin. Not all states provided data for the parameters that were not required to calculate the CO_2 storage capacity (permeability and salinity).

The Utah Geological Survey created a web-based, ArcGIS online site to which the other surveys were invited to upload their preliminary contour data with the anticipation this could be used by the participating states to compare their deliverables to those in adjacent states and make adjustments if needed. The UGS did adjust their Entrada maps after noticing CO had used different layers to constrain the formation. AZ uploaded their data as well. NM did not generate contour maps, only terrain maps, and did not make use of this tool. As a result, the data continuity along New Mexico's stateliness was more difficult to match than along the other borders.

Integration of the regional, 1-km-spaced Rocky Mountain-CO_2-capacity GIS database

After the same database structure was created for each formation table, the quality control was completed. The points for each formation were edge matched across the state boundaries, and all the properties of corresponding fields in the different formation databases were defined exactly the same, i.e. enforcing data integrity on the database. Then, the tables for all the formations were merged into a single, point-feature class containing all the data records for all the formations (Figure 5). The CO_2 capacity numbers - as well as others such as thickness and pore volume - can then be summarized in tables by state, formation and/or sedimentary basin. The total capacity numbers can also be summed for each 1-km point using the unique ID number that was extracted from the base grid and associated with each data point. The 1-km data can be summarized either by a subset of the formations or by all of them. The 1-km^2 cell summaries allow for generating maps illustrating the spatial variability of the parameter.

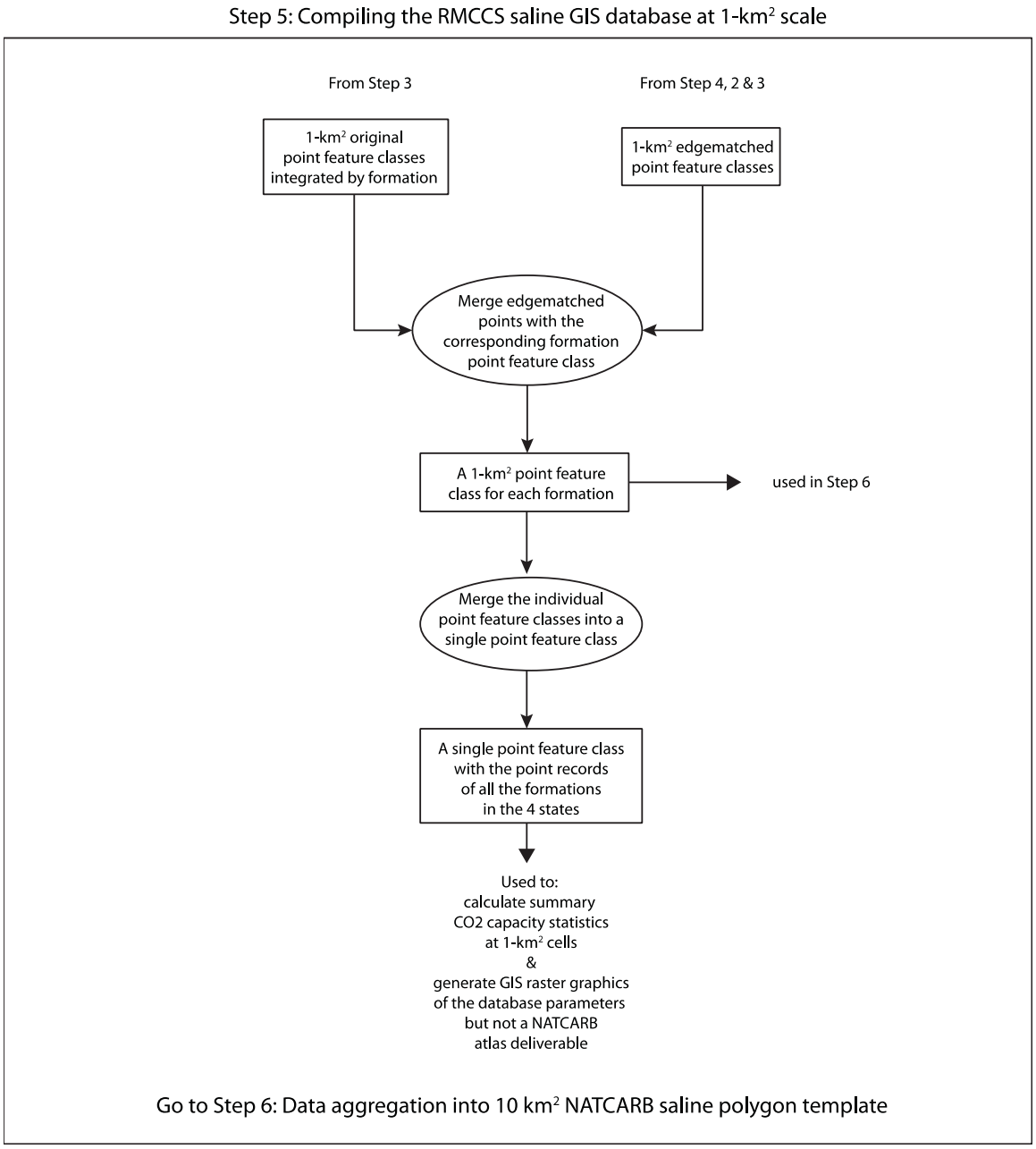


Figure 5: Workflow step 5 – Compiling the integrated, saline-formation CO_2-capacity database at 1 km² scale.

Besides several problems inherent to having the states generate their data (mostly independently from one another), additional data issues exist. Some are related to extreme simplification of the geology (caused by lack of better data) such as using a single porosity value for an entire formation. This disregards geological 3D spatial heterogeneity and anisotropy. The same argument can be made for the thermal gradient. Utah tackled the single porosity problem by interpolating known porosity values from well data across the Weber and De Chelly Formations within the sedimentary basin. Colorado used a similar spatial approach for the geothermal gradient. However, the data end-user has no indication about the reliability of the generated data. The project team

had planned to address this by generating a well-density parameter for each 1-km^2 cell as well as a distance to nearest cell containing source well data. Since this study is using spatially continuously varying data, concepts of spatial autocorrelation indicate that data generated in a cell closer to a cell with existing data is most likely more reliable that data in cells further away from reported data. Due to a combination of the surveys delivering their data later than anticipated, integrating the data taking longer than planned and NETL requesting that the project data deliverables be available by the end of original project deadline, there was not sufficient time to incorporate these uncertainty indicators.

Another uncertainty issue that should be addressed to gauge the data reliability is a quantifier of the quality of the original input data, especially where wells are clustered. Not only were generalizations made under those circumstances but the end-user does not know which criteria were used. Since the data for this project were derived from databases compiled over time and for which the input data were generated by many geologists each using their own standards, it is not known how well the source data were screened for inconsistent values.

Although NETL requests saline data in the CO_2 capacity Atlas be included, most of the states did not provide salinity data. This information is often not readily available, or included in the databases they used as their source. This could be remedied by including a layer indicating USDW data in the Atlas. Just as with the uncertainty indicator(s) there was not enough time to pursue this within the timeframe of the project.

Permeability data are requested by NETL as well. This parameter generally is more heterogeneous and anisotropic than the porosity parameter. Since the permeability value is also not required to calculate storage capacity but comes into play to model injectivity, most surveys did not provide permeability data because they did not want to over-generalize. And, reliable permeability data is difficult to obtain from the public domain. Even industry does not have good datasets for permeability variations.

Aggregating (upscaling) the data into 10-km^2 NATCARB predefined polygons

Aggregation of the 1-km-scaled, formation point data into predefined 10 km^2 cells is required to make the capacity data compliant with the NATCARB carbon sequestration Atlas for saline-formations-data dictionary (appendix 2). The 1-km^2 data for each formation were processed by themselves before merging all the results into the NATCARB template. The first step consisted of spatial joining each 1-km^2-formation-point-feature class with the NATCARB saline-10K template subset to the four-state region (Figure 6). This procedure aggregated all the 1-km points located within a 10-km^2 polygon into a single value for the different parameters. During this step, the fields and the field contents belonging to the 10K template are not modified. Most of the 10-km^2 attribute fields contain 'Null'-values. The COL_ROW number is populated with a unique 10K polygon ID, comparable to the unique pointID used for the 1-km^2 points. The attributes of the 1-km^2-formation-point, feature class were summarized according to a set of merging rules. The numeric parameters were averaged (Depth, Thickness, Temperature, Pressure, Porosity, Salinity, Permeability and CO_2-density) except for the volume- (volume, pore volume) and CO_2-mass related parameters (CO_2-mass, CO_2-mass at 0.51%, at 2% and at 5.4%), which were summed. The first occurrence was extracted for the fields defined as text (basin and formation). Fields not serving any purpose at the 10 km^2 level scale were dropped during the aggregation (1 km pointID, state, edgematch

indicator, X and Y coordinates). The basin parameter is not included in the NATCARB database dictionary, but was kept for internal use.

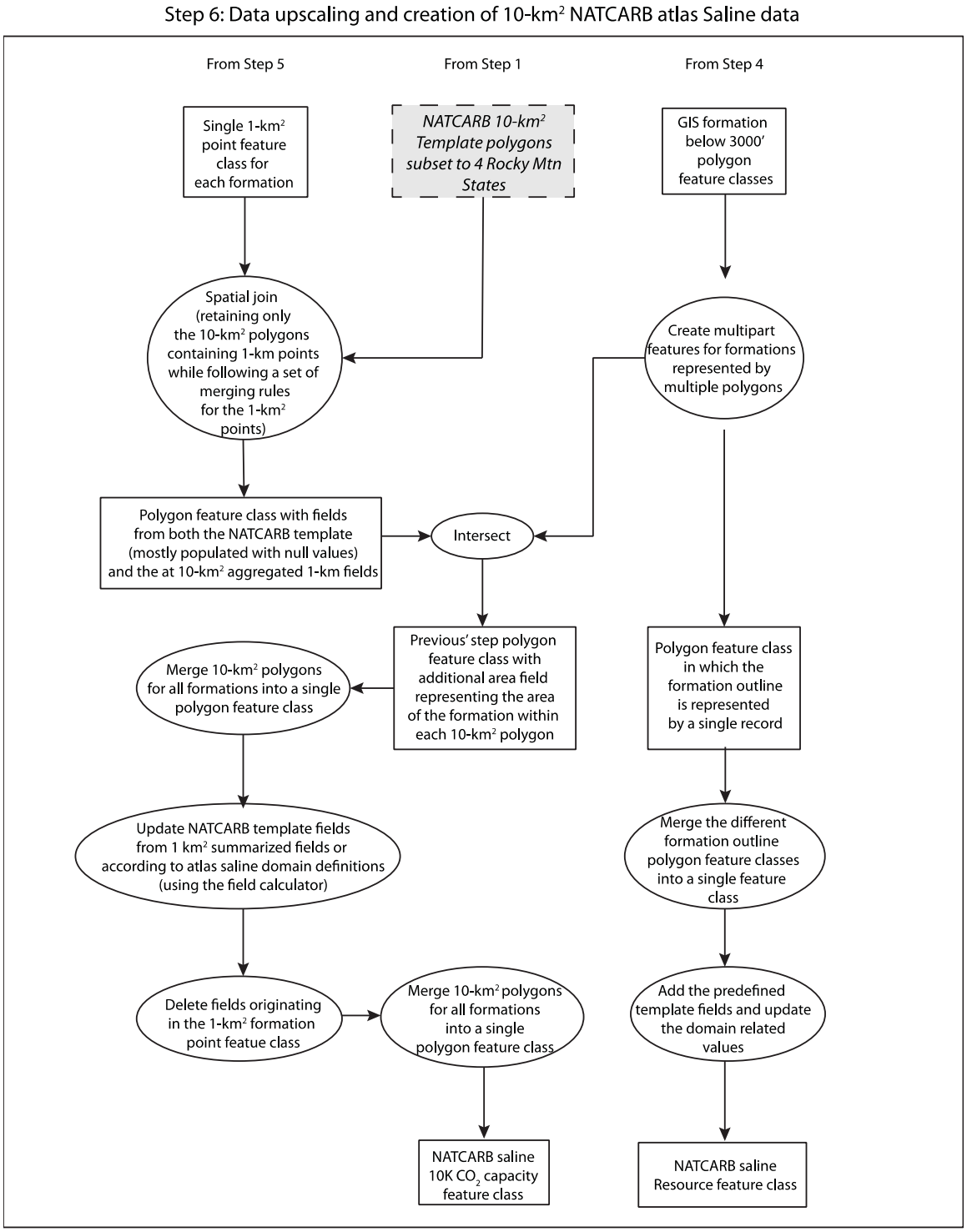


Figure 6: Workflow step 6 - Upscaling the data to 10-km² and NATCARB compliant saline data creation

For each formation, the output of the spatial-join procedure was intersected with the corresponding formation polygon 3000' depth outline. This intersection process calculated the area of the formation within each 10-km^2 polygon and stored it in a newly added area field. For most polygons this number will be 100,000,000 m^2 corresponding to the 10 by 10 km area. Near the outer edge of the formation or where there is an interior gap in the formation data, this number will be less.

Since all the 10 km^2 formation tables with the summarized 1 km^2 data and the updated area numbers had the same database structure, they could be merged into a single, new-feature-polygon class that now contained data for all the formations at the upscaled 10 km^2 level. All the NATCARB template fields are still populated with null values however. Using the field calculator, those template field values were updated by extracting the values from the corresponding statistically summarized data fields. After the NATCARB-template, null values were replaced with the information from the statistically summarized fields, the latter set of fields was removed. Finally, the up-scaling to 10-km^2 data was completed by populating the fields that have a single value for all the records, for example the RSCP field, ARRA_PROJECT field and the geodatabase-domain-related fields.

Data preparation done during the compilation procedure of the 1-km^2 data resulted in 7 structurally completely consistent data sets. This would have allowed the python script to easily handle the upscaling steps. However, writing this script would have taken longer than repeating the process for each formation using ArcGIS's GUI interface. Ninety percent of the University of Utah's Atlas data task time was spent in the following tasks:

1. Guiding, assisting and coordinating the surveys near the end phase of their data preparation time,
2. Integrating all of their 1-km^2data, including data-problem tracking and solving,
3. Developing the workflow to format the data into a common database structure, including edge matching the data across state boundaries.

Aggregating the data to make the NATCARB Atlas compliant and reporting took the remaining 10%.

Rocky Mountain Carbon Capture and Sequestration Project CO_2 capacity data

Geological surveys of the four partnering states delivered data for the three deep saline formations (Cretaceous Dakota, Jurassic Entrada and Permian Weber) occurring mostly in the northern half of the Colorado plateau, as well as four Paleozoic stratigraphic equivalent formations further to the south (Cedar Mesa, De Chelly, Hermosa and Leadville formations). These seven formations are occurring in 5 different basins: the Uinta basin and the Piceance/SandWash basins in the north; and the San Juan, Black Mesa and Paradox basins in the south. A total of 14 input data sets containing various stages of CO_2-capacity calculations were sent to the University of Utah in 4 different data formats: spreadsheets, ArcGIS file geodatabases, ArcGIS map package with raster data and shapefile depth and thickness contour lines (Table 2).

Formation	Basin	AZ	UT	CO	NM
Dakota	Piceance/SandWash			xls	
	Uinta		gdb		
	San Juan				xls
Entrada	Piceance/SandWash			xls	
	Uinta		gdb		
	San Juan				xls
Weber	Piceance/SandWash			xls	
	Uinta		mpk, xls		
Hermosa	San Juan				xls
De Chelly	Black Mesa	shp			
	Paradox		gdb, xls	xls	
Cedar Mesa	Black Mesa	xls			
Leadville	San Juan				xls

Table 2: format of submitted data to the University of Utah: gdb = ArcGIS geodatabase, mpk = ArcGIS map package, shp = ESRI shape file, xls = MS Excel.

These different files, all containing slightly different information, were reformatted into a common database structure. Data not delivered in spreadsheets were the most difficult to use in determining methodology problems because the calculations were not, or were poorly, documented. A few cases related to unspecified, variable units had to be dealt with. And, in two other situations the projection of the data was not the requested, Lambert azimuthal equal area. This required a fair number of recalculations to make the data fit the 1-km-equidistant grid laid out for the entire region, and across the state boundaries. After reformatting the point data into a common ArcGIS database, the state-boundary-crossing-formation datasets required edge-matching-problem corrections. Only then, could they be prepared to conform to NETL's smaller-scale, Carbon-sequestration-Atlas data structure.

Most files had records for depth and thickness either in the spreadsheet or in the feature class database. The only exception was the Arizona De Chelly data, which were not originally part of the to-be-submitted data. Because of a small miscommunication problem, the data were not shared until very late in the workflow process. The AGS sent two shapefiles, one with thickness contours and one with depth contours. These files were re-projected to the Atlas Lambert azimuthal equal area projection before being converted to grids from which the depth and thickness values were extracted at the 1-km^2 scale. These parameters combined with the porosity values that were provided and a geothermal gradient, allowed for the data to be processed in the capacity spreadsheet and structured according to the other data.

The porosity values together with the formation thickness data provided the bulk storage volume. Most data were processed with a single porosity value set by basin in each state. Most data sets also provided a minimum and maximum porosity value, listed in Table 3, but only the medium values were incorporated in the storage capacity calculations. The only exception to this method was the Weber calculation in the Uinta basin, where the porosity value was interpolated and depended on the location. The results of the porosity test of core from the single site characterization well, RMCCS

State #1, were not yet available when regional CO_2 capacity estimates were generated and are thus not included in the analysis.

Table 3: Rocky Mountain Carbon Sequestration Project deep saline porosity values:

		Porosity (%)		
		Min	Average	Max
Dakota	CO	-	10.0	-
	UT	2.0	12.0	22.0
	NM	2.5	6.3	13.2
Entrada	CO	-	15.0	-
	UT	8.0	16.0	24.0
	NM	7.4	9.6	22.5
Weber	UT	Varies spatially between 1.12 and 22.45 with an average of 6.22		
	CO	-	8.0	-
Hermosa	NM	3.0	9.9	14.2
De Chelly	AZ	-	14.3	-
	UT	-	20.0	-
	CO	-	10.0	-
Cedar Mesa	AZ	2.0	4.6	8.04
Leadville	NM	1.0	4.0	7.0

Applied geothermal temperature gradients generally varied by state and by formation, although in most cases the different gradient was used in the same basin for different formations (Table 4). Colorado made their geothermal gradient spatially dependent by deriving the gradient from temperatures measured in well data located across the state. The interpolated gradient data were extracted from the grid, which was geo-located to the base grid and added as an additional column to the spreadsheet.

Table 4: Rocky Mountain Carbon Sequestration Project geothermal gradients used to derive temperatures at top of formation depth for deep saline CO_2 storage formations

State	**Basin**	**Formation(s)**	**Gradient***	**Temp @ depth Formula = Surface temp (F) + gradient**
AZ	Black Mesa	Cedar Mesa De Chelly	13.5°C/km	75 + (0.0074 * D**)
CO	Piceance/ SandWash	Dakota Entrada Weber	Spatial dependent	55 + (gradient in the 1km^2 cell * D)
	Paradox	De Chelly		
	San Juan	Dakota		
UT	Uinta	Dakota Entrada	25°C/km	55 + (0.0138 * D)
		Weber	20°C/km	55 + (0.0115 * D)

	Paradox	De Chelly	20°C/km	55 + (0.0115 * D)
NM	San Juan	Dakota Entrada Hermosa Leadville	47°C/km	61 + (0.026 * D)

* Geothermal conversion factor from °C/100m to °F/100ft: 0.549 (Klett 2005)
D** = depth in feet

The New Mexico Bureau of Geology and Mineral Resources provided salinity and permeability values for the San Juan basin formations (Table 5). Other states did not contribute this info. Just as with the porosity data, the permeability test results of the single well RMCCS State #1, drilled during this project, were not available during the processing of the CO_2 capacity data.

Table 5: Salinity and Permeability data fro the NM deep saline formations

State	Formation	Salinity (TDS)	Permeability (mD)
NM	Dakota	25000	0.83
	Entrada	35000	0.09
	Hermosa	85000	0.2
	Leadville	35000	-

CO_2 capacity numbers grouped by formation but separated by state and sedimentary basin are listed in Table 6. Figure 7 shows the spatial distribution of he total capacity numbers summed over all of the formations at the 1-km^2 data-distribution scale. The total, calculated-CO_2-storage-capacity for all seven formations (using the average porosity for most data) varies between 13.6 and 143.7 billion metric tonnes depending on the efficiency factor. For the three major, deep-saline formations the values vary between 9.8 and 104.0 billion metric tonnes. The CO_2-capacity volumes summarized at the 10-km^2, Atlas scale are the same as the larger scales. However, at the larger scale, they cannot be broken out by state or sedimentary basin, only by the resource formation. The CO_2-storage-capacity volumes summarized by formation are listed in Table 7.

Table 6: Rocky Mountain Carbon Sequestration Project deep-saline, CO_2-capacity numbers derived from the 1 km^2 scaled points:

				CO2 Storage Volume (metric Tonnes)		
State	Basin	Formation	Area (km^2)	Low Efficiency (0.51%)	Medium Efficiency (2%)	High Efficiency (5.4 %)
CO	Piceance_ Sandwash	Dakota	28,522	482,624,867	1,892,646,535	5,110,145,645
CO	San Juan		3,214	68,252,705	267,657,665	722,675,695
NM	San Juan		19,599	172,502,878	676,481,873	1,826,501,060
UT	Uinta		28,834	507,104,513	1,988,645,149	5,369,341,904
CO	Piceance_ Sandwash	Entrada	30,052	1,393,361,516	5,464,162,810	14,753,239,586
CO	San Juan		4,595	127,397,634	499,598,566	1,348,916,127
NM	San Juan		16,511	300,019,280	1,176,546,181	3,176,674,688
UT	Uinta	Entrada-Navajo	29,989	4,857,039,869	19,047,215,174	51,427,480,970
CO	Piceance_ Sandwash	Weber	15,577	549,361,376	2,154,358,336	5,816,767,507
UT	Uinta		27,789	1,361,192,180	5,338,008,549	14,412,623,083
NM	San Juan	Hermosa	9,444	1,672,530,703	6,558,943,933	17,709,148,619
AZ	Black Mesa	De Chelly	10,053	1,820,718,060	7,140,070,822	19,278,191,219
CO	Paradox		1,934	13,715,122	53,784,794	145,218,943
UT	Paradox		1,579	35,650,148	139,804,502	377,472,155
AZ	Black Mesa	Cedar Mesa	17,139	168,097,713	659,206,719	1,779,858,142
NM	San Juan	Leadville	12,247	42,728,636	167,563,275	452,420,844
			Totals:	**13,572,297,199**	**53,224,694,882**	**143,706,676,188**

Table 7: CO_2 storage capacity volumes summarized by formation

	CO_2 Storage Volume (metric Giga Tonnes)		
Formation	Low Effciency (0.51%)	Medium Effciency (2%)	High Effciency (5.4%)
Dakota	1.23	4.83	13.03
Entrada	6.68	26.19	70.71
Weber	1.91	7.49	20.23
Partial Total:	**9.82**	**38.51**	**103.96**
Hermosa	1.67	6.56	17.71
Cedar Mesa	0.17	0.66	1.78
De Chelly	1.87	7.33	19.80
Leadville	0.04	0.17	0.45
Total:	**13.57**	**53.22**	**143.71**

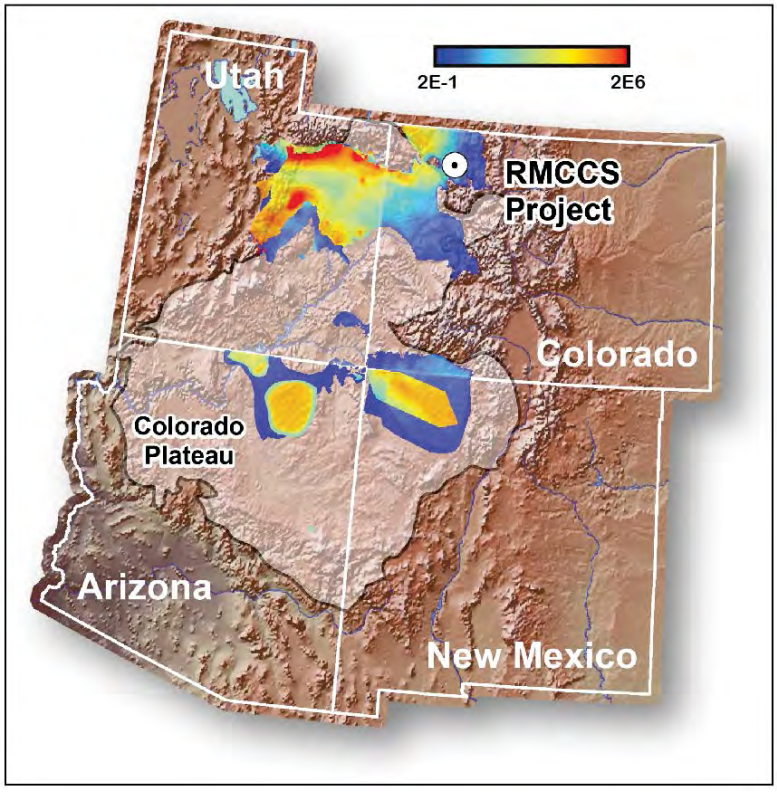


Figure 7: Spatial distribution of the CO_2 storage capacity summed over all 7 formations using a 1-km^2 cell size. The color-bar represents the medium efficiency CO_2 capacity data in metric tonnes.

Comparison of 2013 project most promising CO_2 capacity data to previous data for the 3 main saline formations on the Colorado Plateau:

Comparing this project's CO_2 storage capacity volumes to the 2012 data (NATCARB Atlas IV), subset to the Colorado Basin area, indicate the total estimated CO_2 volumes are different (Table 8 and Figure 8). The Entrada Formation CO_2 volumes increased compared to the previous data while the storage capacity in the Dakota and the Weber Formations decreased. A main contributing factor to the increased Entrada capacity is an increase of the area of the Entrada Formation, a direct contributor to the bulk volume. The decrease in the Dakota storage capacity by nearly 50% can be explained by using a porosity value that is up to less than half of the Atlas IV porosity value of 14%. The current project calculations also applied a higher geothermal gradient for the San Juan basin compared to the 2012 data, where a single geothermal gradient was used for all the data in the region the Southwest Partnership was responsible for. A combination of several factors explains the reduction of the storage capacity in the Weber Formation with nearly two thirds. The largest contributing factor is the lower average porosity. This study, used an average of 6.9%, which is less than half of the average porosity of 14.9% used in Atlas IV for the same region. The total area and the total available thickness for the Weber Formation in this study are both less than the values calculated for the previous Atlas as well.

The results of this study indicate a potential CO_2-storage capacity for the three main, regional saline formations ranging between 12.9 and 136.8 billion metric tons depending on the efficiency factor (Table 8). When compared to the 2012 Atlas IV data the total CO_2-storage capacity of these three formations decreased by approximately 8%. Including the stratigraphic equivalents, increased the total CO_2 storage capacity between 13.6 and 143.7 billion tonnes. Since not all the equivalent formations were included in the Atlas IV data, a CO_2 storage capacity comparison cannot be made.

Table 8: Difference in CO2 capacity numbers between 2012 Atlas IV and this project's three main deep saline formations on the Colorado Plateau:

			CO_2 Storage Volume (metric Giga Tonnes)		
	Formation	# of 10 km^2 cells*	Low Efficiency (0.51%)	Medium Efficinecy (2%)	High Efficiency (5.4%)
Atlas IV	Dakota	955	2.132	8.360	22.572
	Entrada	595	3.531	13.847	37.387
	Weber	626	4.964	19.468	52.563
	Total:		**10.627**	**41.675**	**112.521**
Atlas V	Dakota	943	1.230	4.825	13.029
	Entrada	964	6.678	26.188	70.706
	Weber	564	1.911	7.492	20.229
	Total:		**9.819**	**38.505**	**103.964**
IV to V Difference (V - IV)	Dakota	-12	-0.901	-3.534	-9.543
	Entrada	369	3.147	12.341	33.319
	Weber	-62	-3.054	-11.975	-32.334
	V - IV Difference:		**-0.808**	**-3.169**	**-8.557**

* Not all cells contain 100% formation at depth; those along the edge of the formation are only partially filled

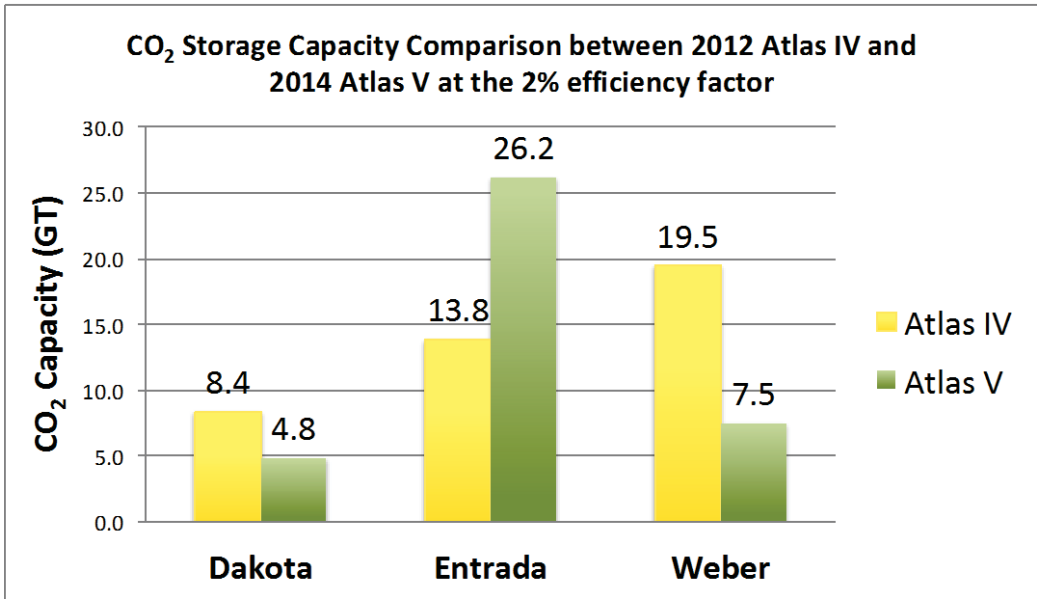


Figure 8: CO2-storage capacity comparison between Atlas IV and Atlas V data for the three main saline formations on the Colorado Plateau

The spatial differences are shown in Figure 9. The actual numbers in the figures represent the medium capacity volume for each formation. The color ramping is based on the range of the data within each formation and not on a uniform range ramp. Since the low, medium and high volumes are proportional, the color ramp would look the same for the three different efficiency classes within each formation. The differences in the numbers can be mostly explained by the different areas covered by the two different data

sets. The Atlas IV data were derived from interpolated well data that was extracted from the IHS and other public data sources. This project's data are mainly based on expert geological interpretation of the data within the basin. The current New Mexico data are an exception to the expert knowledge interpretation. One of the noticeable differences for the Dakota and the Entrada Formation is the inclusion of the CO Sand Wash Basin (part of the greater Green River Basin) into the updated data. The Entrada is also more extensively mapped in the NM San Juan basin.

The CO_2-storage-capacity numbers determined in this study for the Dakota, Entrada and Weber Formations in the Colorado Plateau for the State of Colorado compare less favorably to the numbers listed by Young et al. (2007). The previous study listed a number of 90 billion metric tonnes at the 2% efficiency while the current numbers tallied up to 10.3 billion metric tonnes.

Significance of Regional Capacity Results

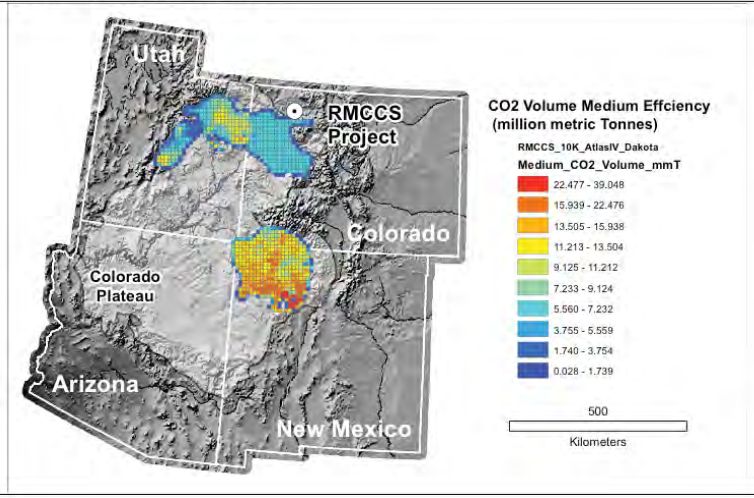
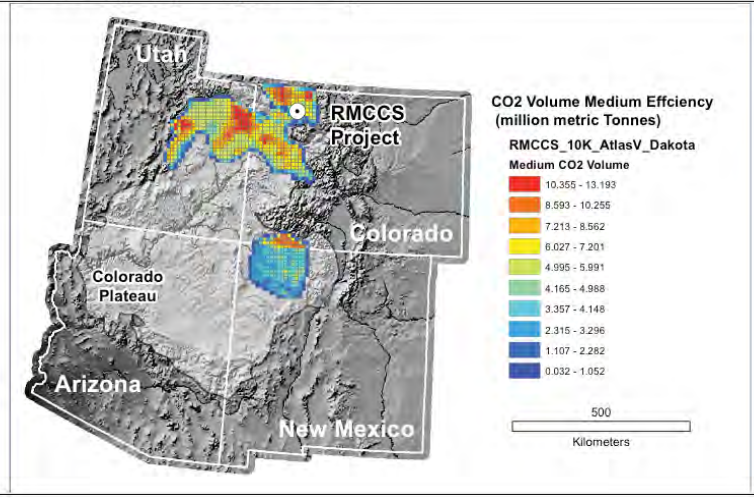
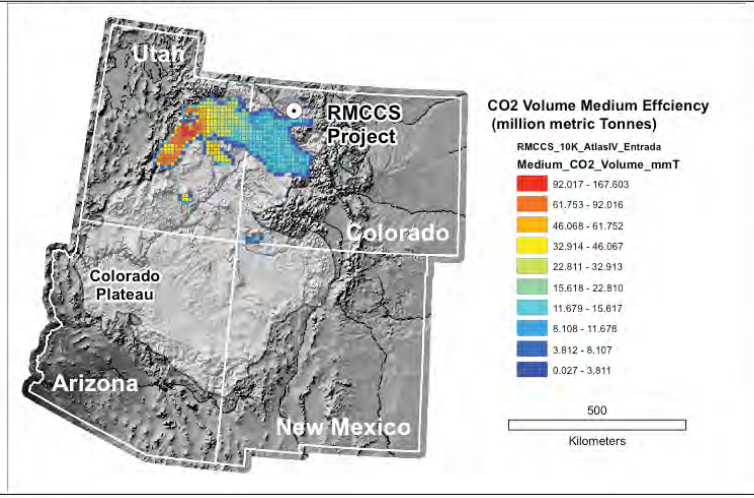
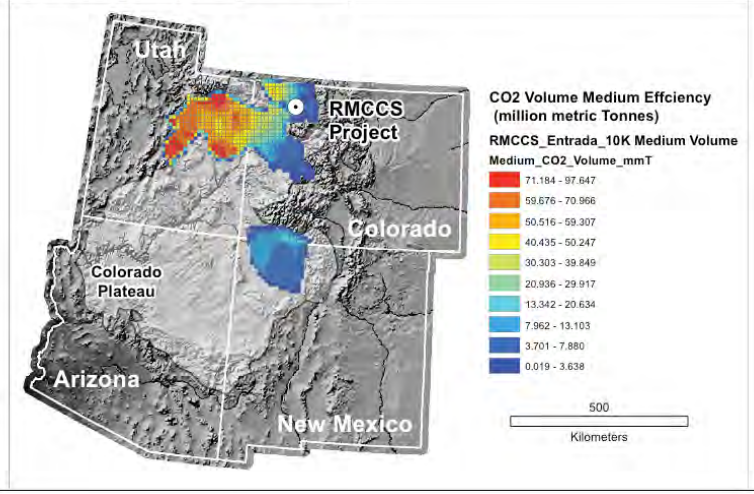
The storage capacity results of this analysis are of reasonable, robust quality, and even a qualitative analysis suggests that the estimated capacities are very significant if the results are compared to past estimates (Section 5 of this report), and if compared to other regions of the USA. Perhaps most significant about the estimated regional capacities is not the values in tons, but rather as expressed as number of years of emissions.

Significance of Regional Capacity Estimates in Context of Previous Estimates

As discussed in Section 5 of this report, the newest capacity data reported here are markedly different (Table 8). As outlined in Section 5, the primary explanation for the contrast in results include more data, better quality data, and more-robust geological analysis of those data. Because the data and interpretations are better, the regional capacity estimates may be considered to be more significant in the context of reliability and usefulness. The upshot is that regional capacity estimates will be better and more significant as more resources are invested in the analysis.

Significance of Regional Capacity Estimates in Context of Years of Emissions

Given very recent (late 2013) announcements regarding how existing coal-fired power plants and gas-fired power plants will be regulated, it will be useful to cast the capacity estimates as number of years of emissions, in addition to gross tons. Specifically, according to September, 2013 announcements by the U.S. Environmental Protection Agency, the intent of the federal government is to not require existing plants to implement CCS, but rather only new coal-fired power plants will be required to implement CCS to meet emission reduction goals. Thus, if these rules are approved, the currently operating power plants will continue emissions at their current levels, and most new power plants will likely be gas-fired. Because existing plants will not be subject to retrofit, CO_2 emissions from these point sources will not see a rapid and marked decrease any time in the coming decades. As such, what is the regional capacity of the regional Dakota, Entrada and Weber formations in number of years of current emission rates?

	NATCARB Atlas IV	RMCCS project (Atlas V)
Dakota		
	NATCARB Atlas IV	RMCCS project (Atlas V)
Entrada		

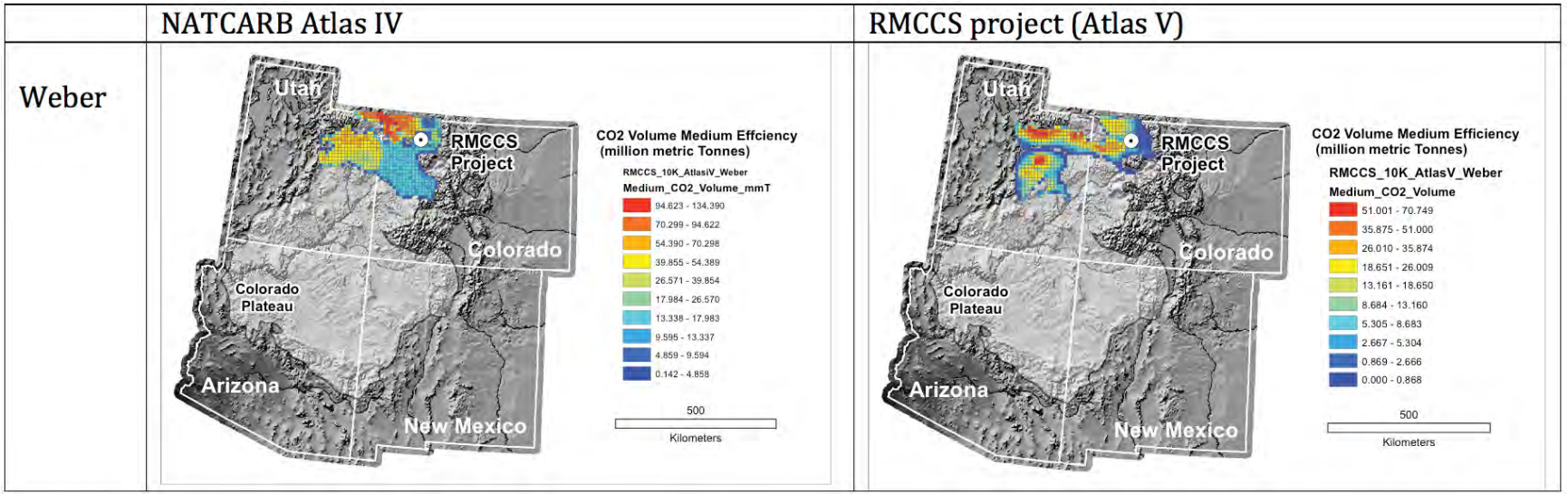


Figure 9: Spatial comparison of the CO_2-medium-efficiency-capacity volume between NATCARB Atlas IV (2012) and this project's three major, regional saline aquifer data (in preparation of Atlas V 2014) at the 10 km^2 scale.

The current total CO_2 emission rate for the combined set of coal-fired and gas-fired power plants in the region is roughly 320 million tons per year, according to a selected subset of rocky mountain emissions data (per NATCARB and its online database accessible at http://www.natcarbviewer.com/). The total storage capacity for the combined Dakota, Entrada and Weber formations is 38,505 million tons (Table 8, medium efficiency factor), translating to approximately 120 years of storage capacity. Over 120 years, it is very likely that emissions rates will not increase (per discussion immediately above), but rather should decline somewhat. Thus, it is not inappropriate to suggest that the regional capacity of these three formations will likely exceed 150 years or more.

Significance of Regional Capacity Estimates as Compared to Eastern USA

With respect to electricity generation, the Rocky Mountain region is dominated by coal. As such, we suggest that the most appropriate comparison of capacity estimates might be to another coal-dominated region of the USA. According to Atlas IV (NETL, 2012), the dominant CO2 emissions sources in Pennsylvania and surrounding states are electricity generation plants, and these plants are predominantly coal-fired.

For comparison of the Rocky Mountain regional capacity estimates to another coal-dominated region, we selected the region studied by the Midwest Regional Carbon Sequestration Partnership, or MRCSP (http://addap.tk). Data provided by Atlas IV (NETL, 2012) indicates that the total storage capacity of the MRCSP region is approximately 130, 447 million tonnes (143,793 tons), almost four times that of the Rocky Mountain regional capacity of the Dakota, Entrada and Weber formations. And, annual CO2 emissions for the entire region are approximately 670 million tonnes (739 million tons), over twice that of the Rocky Mountain region. However the storage capacity expressed in years for the MRCSP region is not too much more than that of the Rocky Mountain region: approximately 195 years. While this is 75 more years than the Rocky Mountain region, the MRCSP capacity assessment corresponds to no fewer than 13 formations (Waste Gate Fm., Sylvania Fm., Bass Islands Fm., Dundee Fm., Oriskany Fm., Lockport Fm., Medina/Tuscarora Fm., St. Peter Fm., Rose Run Fm., Potsdam Fm., Conasauga Fm., Rome Trough Fm. , and the Mt. Simon Fm.), compared to the Rocky Mountain Region analysis of just the three most promising formations, the Dakota Fm., the Entrada Fm., and the Weber Fm.

Conclusions

The derived, CO_2-capacity-storage numbers that were based on solid, geological-based, decision making; combined with available well data; were different from the numbers based on computer generated interpolations from well data only. Having input from geologists that incorporated the structure, basin, and geological discontinuities; resulted in a more realistic interpretation of the data. A computer-interpolation algorithm is not capable of such interpretation. Although it is likely that the current interpretation of the data is better than the method used in Atlas IV (data interpolation only); it is difficult to conclude this objectively without being able to test the results.

The CO_2 storage capacity numbers for the three regional, saline formations reflect a decrease of nearly 8% compared to earlier reported numbers. There are additional refinements that can be made to the input data (porosity and geothermal gradient) for the current methodology, including better structural information such as structural dip or incorporating a better representation of the sedimentary basin structure especially for the San Juan Basin. Improving this general type of information will still not be a substitute for detailed basin models based on calibrated data such as wells, seismic lines and petrophysical logs as were used for this project's model Sand Wash Basin detailed local analysis. Having an indication about data uncertainty would be beneficial to the current methodology as well.

The methodology to calculate the CO_2 storage capacities could be simplified by automating the procedure currently applied within the spreadsheet. This would involve converting the method to an arc python script. Although it would simplify and automate the workflow, it also creates a black box push button method. It became clear during the data compilation and integration process that several of the project partners did not fully understood the method until they worked through it step by step. A major disadvantage of using an automated script for the CO_2 capacity calculations is its inflexibility in handling modifications to variable input parameters such as the geothermal gradient.

Appendix 1: NATCARB CO_2 sequestration atlas projection parameters:

Projection: Lambert_Azimuthal_Equal_Area
False_Easting: 0.000000
False_Northing: 0.000000
Central_Meridian: -100.000000
Latitude_Of_Origin: 45.000000
Linear Unit: Meter (1.000000)

Geographic Coordinate System: GCS_WGS_1984
Angular Unit: Degree (0.01745329251994329)
Prime Meridian: Greenwich
(0.000000000000000000)
Datum: D_WGS_1984
Spheroid: WGS_1984
Semimajor Axis: 6378137.000000000000000000
Semiminor Axis: 6356752.314245179300000000
Inverse Flattening: 298.257223563000030000

Appendix 2: NATCARB Carbon Sequestration Atlas Saline formations database template data dictionary:

SALINE

FIELD	ALIAS	DATA_TYPE	WIDTH	UNITS	DOMAIN?	DESCRIPTION
PARTNERSHI	PARTNERSHI	Text	15		Yes	Abbreviated partnership name
RESOURE_NA	RESOURE_NA	Text	50			Name of storage resource
ASSESSED	ASSESSED	Short Integer			Yes	1 = Yes, storage resource has been assessed.; 0 = No, storage assessed.

SALINE10K

FIELD	ALIAS	DATA_TYPE	WIDTH	UNITS	DOMAIN?	DESCRIPTION
COL_ROW	COL_ROW	String	20			10K unique ID
PARTNERSHI	PARTNERSHI	Text	15		Yes	Abbreviated partnership name
RESOURE_NA	RESOURE_NA	Text	50			Name of storage resource
RSC_AREA_C	RSC_AREA_C	Double		sq. m.		Area of the storage resource within the cell in square meters
VOL_LOW*	VOL_LOW	Double		tonnes		Low (P10) storage resource estimate in metric tonnes per cell Assessed = 0
VOL_MED*	VOL_MED	Double		tonnes		Medium (P50) storage resource estimate in metric tonnes per Assessed = 0
VOL_HIGH*	VOL_HIGH	Double		tonnes		High (P90) storage resource estimate in metric tonnes per cel Assessed = 0
DEPTH_FT**	DEPTH	Long Integer		feet		Mean depth to top (from surface) of storage resource per cell
THICKNESS_F	THICKNESS	Long Integer		feet		Mean thickness of storage resource per cell to the nearest 5'
SALINITY_TD	SALINITY	Long Integer		ppm		Mean salinity (TDS) of storage resource per cell in ppm to the
PRESSURE_P	PRESSURE	Short Integer		PSI		Mean pressure at top of storage resource per cell in PSI to the
TEMPERATU	TEMPERATU	Short Integer		degrees F		Mean temperature at top of storage resource per cell in degr number
POROSITY_P	POROSITY	Float		percent		Mean porosity of storage resource per cell in percent to the r
PERMEABILI	PERMEABILI	Float		mD		Mean permeability of storage resource per cell in millidarcies
ASSESSED	ASSESSED	Short Integer			Yes	1 = Yes, storage resource has been assessed. Storage estimate storage resource has not been assessed. Storage estimates m
ARRA_PROJECT		Text	20			

* Field is defined as a DOUBLE in order to accept large numbers, but values should be rounded to nearest

** Value applies to the "storage zone" portion of the storage resource

APPENDIX N

Arizona Geological Survey Regional Studies for Capacity

Contents

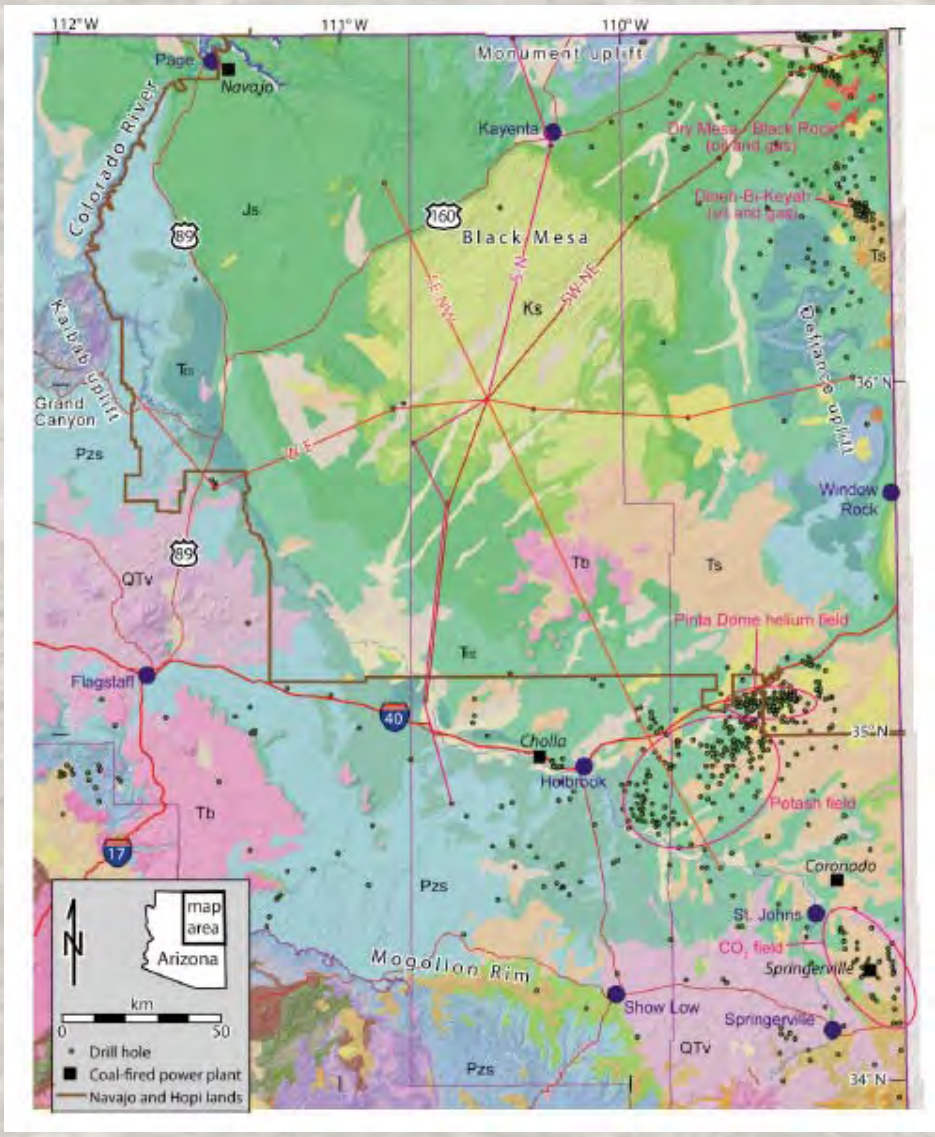
Topic

Evaluation of Paleozoic Strata

Evaluation of Cedar Mesa Formations

An Evaluation of Carbon Dioxide Sequestration Potential of Paleozoic Sandstone Units, Northeastern Arizona

Steven L. Rauzi and Jon E. Spencer
Arizona Geological Survey



OPEN-FILE REPORT OFR-12-10 V1.0

October 2012

Arizona Geological Survey

www.azgs.az.gov | repository.azgs.az.gov

Arizona Geological Survey

M. Lee Allison, State Geologist and Director

Manuscript approved for publication in October 2012
Printed by the Arizona Geological Survey
All rights reserved

For an electronic copy of this publication: www.repository.azgs.az.gov
Printed copies are on sale at the Arizona Experience Store
416 W. Congress, Tucson, AZ 85701 (520.770.3500)

For information on the mission, objectives or geologic products of the
Arizona Geological Survey visit www.azgs.az.gov.

This publication was prepared by an agency of the State of Arizona. The State of Arizona, or any agency thereof, or any of their employees, makes no warranty, expressed or implied, or assumes any legal liability or responsibility for the accuracy, completeness, or usefulness of any information, apparatus, product, or process disclosed in this report. Any use of trade, product, or firm names in this publication is for descriptive purposes only and does not imply endorsement by the State of Arizona.

Recommended Citation: Rauzi, S.L. and Spencer, J.E., An Evaluation of Carbon Dioxide Sequestration Potential of Paleozoic Sandstone Units, Northeastern Arizona. Arizona Geological Survey Open File Report, OFR-12-10, v 1.0, 24 p.

An Evaluation of Carbon Dioxide Sequestration Potential of Paleozoic Sandstone Units, Northeastern Arizona

By

Steve L. Rauzi and Jon E. Spencer
Arizona Geological Survey

Arizona Geological Survey Open File Report 12-10

October 2012

www.azgs.az.gov | www.repository.azgs.az.gov

An evaluation of CO_2 sequestration potential of Paleozoic sandstone units, northeastern Arizona

Steven L. Rauzi, Oil and Gas Administrator
Arizona Geological Survey
416 W. Congress St., #100
Tucson, AZ 85701
Steve.Rauzi@azgs.az.gov

Jon E. Spencer, Senior Geologist
Arizona Geological Survey
416 W. Congress St., #100
Tucson, AZ 85701
Jon.Spencer@azgs.az.gov

Abstract

Northeastern Arizona is underlain by the southwestern part of the Colorado Plateau, an area of gently dipping to slightly folded Paleozoic and Mesozoic strata that include porous and permeable sandstone units. Three Paleozoic sandstone units, the Cambrian Tapeats Sandstone, Devonian McCracken Sandstone, and Permian De Chelly Sandstone, were identified for study as potential targets for CO_2 sequestration in order to reduce anthropogenic emissions to the atmosphere. Well logs for 755 drill holes were used to evaluate the extent, depth, and thickness of these sandstone units. Esri® ArcMap™ software was then used to calculate the volume of each sandstone unit where the top of each unit is below 800 m depth, which is the minimum necessary for CO_2 sequestration so that the CO_2 remains in a dense, near-liquid state. Well logs were used to evaluate porosity, which was then used to calculate effective porosity that is theoretically available for CO_2 storage. We calculate that there are 9.7 km^3 of effective pore space in the De Chelly Sandstone in Black Mesa basin, with 0.43 km^3 and 0.72 km^3 effective pore space in the Tapeats and McCracken sandstone units, respectively, in the same area. The total mass of CO_2 that, potentially, could be stored in Colorado Plateau sandstone units is calculated at 8.28 billion metric tons. Qualitative information available from well logs suggests that the Tapeats and McCracken sandstones contain saline formation waters, but the character of formation waters in the De Chelly Sandstone remains poorly known.

Introduction

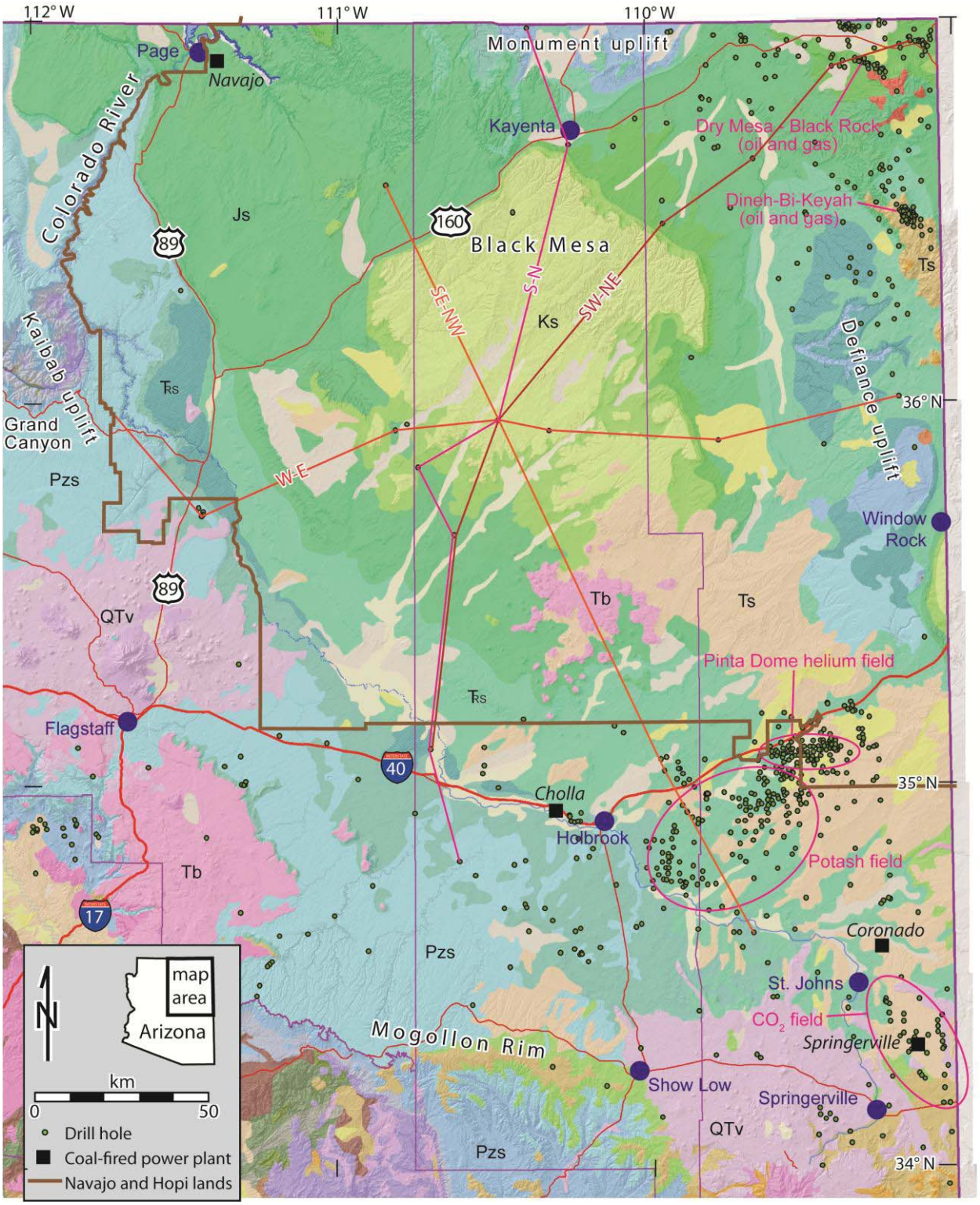
The U.S. Department of Energy (DOE), through its National Engineering Technology Laboratory (NETL), established a national program to evaluate the feasibility of separating carbon dioxide (CO_2) from industrial sources and pumping it underground for long-term storage or disposal. This program was established in response to concerns that CO_2 emissions from

fossil-fuel combustion, and from other industrial processes such as cement production from limestone, are increasing atmospheric CO_2 concentration and solar-energy absorption, thereby causing global warming. Carbon dioxide removal from industrial sources and storage in geologic reservoirs is known as "geologic sequestration." A major aspect of the DOE program is to evaluate subsurface geology to determine the potential of underground rock formations for long-term CO_2 sequestration (U.S. Department of Energy, 2010).

WESTCARB (West Coast Regional Carbon Sequestration Partnership) is a consortium of seven western U.S. States and one Canadian Province that is one of seven regional North American partnerships established to evaluate technical aspects of high-volume CO_2 capture and sequestration. The WESTCARB research program has members and collaborators, including more than 90 public agencies, private companies, and non-profit organizations. The Arizona Geological Survey began work in 2010 on *WESTCARB Phase III – Arizona Geological Characterization*. This report represents a WESTCARB assessment of CO_2 storage potential in Arizona's Paleozoic strata of the Colorado Plateau, and is part of Tasks 2 and 3 of Arizona WESTCARB Phase III (California Energy Commission Agreement Number 500-10-024).

The study area is northeastern Arizona, which consists largely of land owned by the Navajo and Hopi Indians (Fig. 1). The focus of this study is determining (1) the volume of porous and permeable Paleozoic sandstone units where the interface with overlying impermeable capping formations is below 800 m depth, (2) the effective (accessible) pore-space volume, and (3) the presence or absence of saline water in the pore space. The ultimate purpose of this study is to identify specific units and areas for further carbon-sequestration evaluation. Basin volume below 800 m depth is important because CO_2 will remain in a dense, near-liquid state at hydrostatic pressures corresponding to such depths (provided temperatures are not abnormally high). Successful sequestration requires both adequate permeability and porosity for large-volume CO_2 injection, and an impermeable cap rock that will prevent movement of CO_2 to shallower depth and escape to the atmosphere. Data on the porosity of Paleozoic strata and the salinity of included groundwater are reviewed in this report, and discussed in the context of suitability for CO_2 sequestration.

Figure 1 (next page). Map of the study area, which covers the northeastern one-fourth of Arizona. Colors represent rock units exposed at the surface and were derived from the geologic map of Arizona (Richard et al., 2000). Location of cross sections is also shown (see Appendix A for cross sections). Large blue dots represent towns. The "CO_2 field" around Springerville is under consideration for CO_2 production for use in secondary oil recovery in west Texas. Map units include Pzs – Paleozoic sedimentary rocks; Trs – Triassic sedimentary rocks; Js – Jurassic sedimentary rocks; Ks – Cretaceous sedimentary rocks, Ts – Tertiary sedimentary rocks; Tb – Tertiary basalt; QTv – Quaternary and Tertiary volcanic rocks, undivided.


112° W
111° W
110° W
Monument uplift
Page
Navajo
Colorado River
Kayenta
Dry Mesa – Black Rock (oil and gas)
Dineh-Bi-Keyah (oil and gas)
Js
160
89
Black Mesa
Ts
SE-NW
S-N
SW-NE
Ks
Kaibab uplift
Trs
Defiance uplift
36° N
Grand Canyon
Pzs
W-E
Window Rock
89
Tb
Ts
QTv
Pinta Dome helium field
Trs
Flagstaff
40
35° N
Cholla
Holbrook
Potash field
Tb
17
Coronado
Pzs
St. Johns
CO2 field
Springerville
Mogollon Rim
Show Low
Springerville
QTv
Pzs
34° N
map area
Arizona
km
0
50
Drill hole
Coal-fired power plant
Navajo and Hopi lands

Paleozoic sandstone units on the Colorado Plateau in Arizona

The Colorado Plateau in Arizona, Utah, New Mexico, and Colorado is characterized by flat-lying to gently dipping, locally gently folded Paleozoic and Mesozoic strata. These strata are most spectacularly revealed where dissected by the Colorado River in the Grand Canyon. Areas surrounding the Colorado Plateau contain a similar sequence of Paleozoic strata but are more severely affected by Mesozoic and Cenozoic magmatism, folding, faulting, and erosion.

Paleozoic strata of the Colorado Plateau were deposited on the North American craton, an area of much older igneous and metamorphic rocks that had been beveled to a fairly flat surface during hundreds of millions of years of Proterozoic weathering without mountain building. Because of minimal Paleozoic igneous and tectonic activity, Paleozoic sandstones are generally quartzose, with rounded quartz grains, and lack much of the fine clay and silt that would clog pore spaces in less mature sandstones. As a result, Paleozoic Plateau sands are generally porous and permeable, and an obvious target for studies of CO_2 sequestration potential.

The study area is centered on Black Mesa Basin in northeastern Arizona. The Paleozoic sandstone units that are the focus of this study (Fig. 2) are not thicker in Black Mesa basin. Rather, they are deformed over a large area into an approximate bowl shape, with the most deeply buried strata beneath Black Mesa on the Navajo and Hopi Nations (Fig. 1; Appendix A). The greater burial depth of Paleozoic strata in Black Mesa basin results from the greater preserved stratigraphic thickness of Mesozoic strata that make up Black Mesa and immediately surrounding areas. The bowl-shaped basin is bounded to the north by the Monument uplift, to the west by the Kaibab uplift, to the east by the Defiance uplift, and to the south by the slightly upturned south rim of the Colorado Plateau that is known as the Mogollon Rim (Fig. 1). These uplifts are the result of faulting and folding during the latest Cretaceous and Paleogene Laramide orogeny.

The three Plateau sandstone units targeted for CO_2 sequestration study are the Cambrian Tapeats Sandstone, Devonian McCracken Sandstone, and Permian De Chelly Sandstone (pronounced "dee-sháy" - derived from a Navajo word). The De Chelly Sandstone here includes the overlying Coconino Sandstone and the upper sandstone of the underlying Supai Group where these units are lithologically similar in well logs, which is characteristic of the Black Mesa Basin area. These units are interbedded with much less porous carbonates, siltstones, and evaporites. The study area covers ~90,000 km^2 (35,000 mi^2) of Apache, Navajo, and Coconino Counties in northeastern Arizona. The northern and eastern extent of the area is the Arizona state border. The southern extent is generally coincident with the Mogollon Rim, which is the approximate topographic margin of the Colorado Plateau. Grand Canyon and Flagstaff are the approximate western margin. (The area encompasses Townships 7 through 42 North and Ranges 8 through 31 East of the Gila and Salt River Baseline and Meridian and Townships 1 through 7 North and Ranges 6 through 10 West of the Navajo Baseline and Meridian).

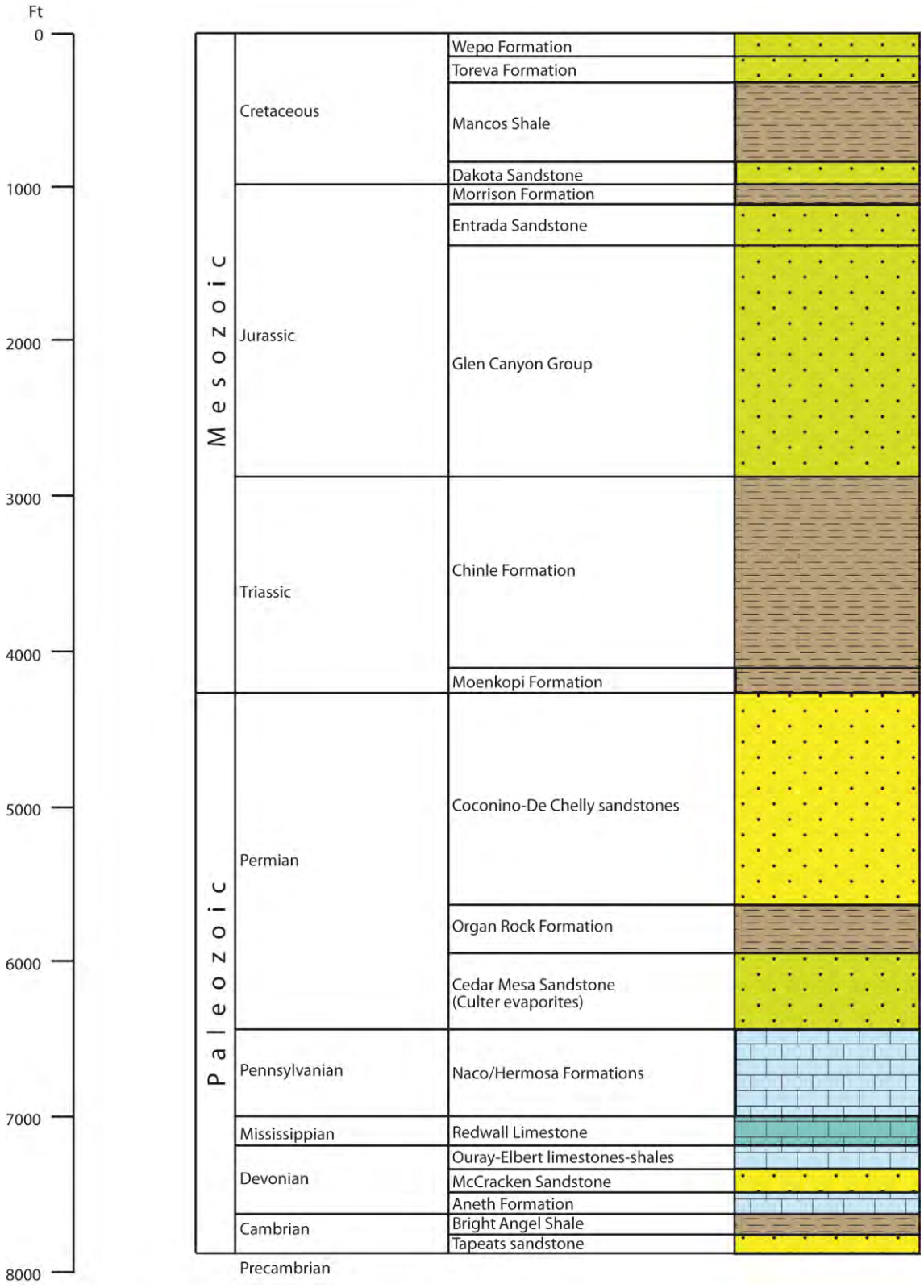


Figure 2. Stratigraphic column representing the Black Mesa and Four Corners areas. Yellow represents sandstone units under study for CO_2 sequestration potential.

Subsurface control is from 755 wells maintained on behalf of the State of Arizona Oil and Gas Conservation Commission at the Arizona Geological Survey. Depth, thickness, and porosity data are primarily from lithologic logs prepared by the American Stratigraphic Company (AmStrat). Approximate porosity indicated on the AmStrat logs represent visual examination of cuttings and core. AmStrat logs are available for most wells drilled in the 1970s and earlier. Some depth and thickness data are from formation tops reported on completion reports submitted by well operators. In some cases, depth correlations and estimates were picked by the authors in wells for which operator-identified tops or an AmStrat log were not available or where the authors disagreed with the operator or AmStrat picks. Well data used in the report are available online at the USGIN AASG website at catalog.usgin.org/geoportal/catalog/search/search.page .

All three sandstone units are present in the study area at depths greater than 800 m below the land surface. Contours are based on depth below the land surface at the location of the wells and are not based on depth relative to sea level or some other horizontal datum. For example, the three potential storage units are deeper in the Black Mesa Basin because of the higher surface elevation of Black Mesa relative to the surrounding terrain in northeastern Arizona. Some of the locally isolated deep spots depicted on the depth maps represent wells that were drilled on topographically high buttes and mesas, which are common in northeastern Arizona.

Sealing units. Impermeable sealing units overlie all three of the potential geologic storage units studied (Fig. 2; Appendix A). Shale and mudstone are the dominant rock types in the Triassic Moenkopi and Chinle Formations that overlie the Permian De Chelly - Coconino Sandstone. The Triassic Moenkopi and Chinle Formations are predominately thick shale, mudstone, and claystone intercalated with lenticular siltstone and sandstone across northeastern Arizona. The Moenkopi and Chinle Formations range in thickness from about 1700 feet near Winslow on the south to about 1000 feet near Lees Ferry on the north. Thick bentonitic mudstones and claystones are the most common rock type of the Chinle as expressed in outcrop in Petrified Forest National Park. Dense limestone and shale of the Devonian Elbert Formation, and shale, limestone, and marl of the Ouray limestone overlie the McCracken Sandstone. Dense limestone and shale of the Ouray and upper Elbert Formations form an ~175-foot-thick seal to oil produced from the McCracken Sandstone at the Walker Creek field in northeast Arizona. The Ouray and upper Elbert formations are about 295 feet thick in the Skelly well in the Black Mesa Basin. (The Skelly well is the central well where all cross sections intersect in Appendix A). Thin-bedded limestone and shale of the Cambrian Muav Limestone and Bright Angel Shale overlies the Tapeats Sandstone in the western part of the area. Devonian carbonate and shale and to a lesser extent Cambrian carbonate and shale overlie the Tapeats Sandstone in the northeastern part of the area. About 155 feet of dense dolomite with scattered anhydrite inclusions and green shale of the Devonian Aneth and Cambrian Bright Angel Shale provide a seal to the Cambrian Tapeats in the Skelly well in the Black Mesa Basin. About 110 feet of Bright Angel Shale and about 130 feet of dolomite in the Devonian Aneth Formation provides a seal to isolated accumulations of the Tapeats Sandstone in the Four Corners area.

Formation fluid salinity. Salinity data are derived primarily from drill-stem tests or production data. Drill-stem tests are usually performed while the well is being drilled. Production data are obtained after a well is completed as a producing well. Salinity data from drill-stem tests are usually described qualitatively as "salt water", "mud-cut salt water", or in some instances "fresh water". Actual salinity data measured from produced water in producing fields indicate that the formation-water salinity in the McCracken and Tapeats Sandstones is much greater than 10,000 total dissolved solids in the far northeastern corner of Arizona. Water salinity (Na^+ and Cl^-) from a production test of the McCracken Sandstone at the Walker Creek Field (Township 41 North, Range 25 East) is 41,000 ppm. Several tests of formation fluids in the De Chelly-Coconino sandstone in the Holbrook area indicate that total dissolved solids may be greater than 10,000 ppm in the deeper parts of the Black Mesa Basin. Fresh water is reported in some drill-stem tests in the Coconino Sandstone.

Depth and thickness of potential storage units

Tapeats Sandstone. The Tapeats Sandstone of Cambrian age is at least 3000 ft below ground surface in most of northeastern Arizona and is more than 7000 feet deep below Black Mesa (Figs. 3a, b). The Tapeats Sandstone is absent over much of the southern part of the study area, which is labeled the "Defiance paleotopographic high" on Figures 3a, b, and c. This area is inferred to have been elevated in Cambrian time so that it was a source of sand rather than an area of sand deposition. The Tapeats is mostly absent in the Four Corners area except for a few isolated accumulations or remnant deposits (Fig. 3c). There is some uncertainty as to whether basal sandstone in the Four Corners area is correlative with Tapeats or the Devonian McCracken Sandstone, especially where the Devonian Aneth Formation, which usually underlies the McCracken, is absent. The Tapeats Sandstone increases in thickness from zero in the Four Corners area and along the western margin of the Defiance uplift to over 300 ft where it crops out in the eastern Grand Canyon (Fig. 3c). The Tapeats Sandstone attains a thickness of 150 ft in a relatively isolated occurrence in the central part of the area south of the Defiance Uplift and just north of the Mogollon Rim (Fig. 3c).

McCracken Sandstone. The McCracken Sandstone is present at depths of >3000 feet below ground surface throughout much of the study area (Figs. 4a, b). The McCracken Sandstone as originally described by Knight and Cooper (1955) is restricted to the Four Corners region and Black Mesa Basin in the northeastern part of the study area. The isolated accumulations or remnants of sandstone in the Holbrook area in the southern part of the area are mapped with the McCracken Sandstone but actually represent local sandstone accumulations in the lower part of the Devonian Martin Formation rather than the McCracken Sandstone (Fig. 4c). Teichert (1965) used the term Beckers Butte member for the basal sandstone in the Devonian Martin Formation south of the Mogollon Rim in central Arizona. The sandstone exposed along the Verde River just north of Payson has been referred to by various investigators as either Cambrian Tapeats or "sandstone of Devonian age" for many years (Lausen and Wilson, 1925; Teichert, 1965, p. 14; Hereford, 1977). This sandstone is included with the Tapeats Sandstone in this study. The

McCracken Sandstone is thin to absent in the southern part of the study area but thickens northward across Black Mesa Basin to reach thicknesses of over 250 ft in the Four Corners region (Fig. 4c). The McCracken Sandstone is absent in the southeastern part of the area. Locally isolated accumulations of sandstone in the lower part of the Martin Formation range from 10 to 30 ft thick across most of the Holbrook area. The sandstone in the lower part of the Martin Formation attains a thickness of about 100 ft. between St. Johns and Show Low.

De Chelly - Coconino Sandstone. The De Chelly Sandstone in eastern Arizona and the Coconino Sandstone in Grand Canyon, both of Permian age, are treated here as one unit, commonly referred to simply as De Chelly Sandstone. Sandstone in the upper Supai Group (approximately the Esplanade Member) that directly underlies the De Chelly Sandstone in the Black Mesa Basin is also included here with the De Chelly Sandstone. The De Chelly Sandstone is present in northeastern Arizona at depths ranging from 2000 ft below ground surface in the Four Corners area to 4900 ft below ground surface in the Black Mesa Basin (Figs. 5a, b). The De Chelly Sandstone is present at depths generally < 1000 ft below ground surface in the southern part of the study area. The De Chelly is present at a depth of 2000 ft below ground surface in a relatively small area east of Holbrook. The De Chelly Sandstone crops out in Monument Valley to the northeast, Marble and Grand Canyons to the west, along the Mogollon Rim to the south, and in the Canyon De Chelly area to the east. The De Chelly Sandstone increases in thickness from about 300 ft in the Four Corners, Grand Canyon, and Mogollon Rims to as much as 1700 ft in the southern part of the Black Mesa Basin (Fig. 5c).

Sandstone-volume calculations - procedure

The volume of sandstone in each of the three sandstone units under study here was calculated for areas where the depth to the base of the overlying capping unit is >800 m (2625 feet) (this is the minimum depth for a capping unit according to NETL recommended methodology [Litynski et al., 2010]). This was done using Esri® ArcMap™ version 10 software, as follows:

(1) Well logs from a database of 755 oil and gas exploration drill holes were used to identify the depth to the stratigraphic top and base of the three sandstone units. Contour maps were drafted (in feet), by hand, for formation tops and formation thicknesses. Each of these six contour maps was then digitized to create six shape files, with depth and thickness as numeric attributes (in both feet and meters) of the contours.

(2) In a raster representation of a contour map, a surface is constructed that interpolates between contours. The depth and thickness contour maps were used to build raster representations of sandstone unit-top depths and unit thicknesses using the “Topo to Raster” tool in the “Raster Interpolation” tool set in the “3D Analyst Tools” in “ArcToolbox”. To do this, each contour dataset was dragged (using the computer mouse) from the table of contents in the ArcMap project to the top line in the “Topo to Raster” tool. The “field” to represent was set to “Thick_m” or “Depth _m”. “Drainage enforcement” was set to “NO_ENFORCE” because the

contour map does not represent a landscape. Raster creation was done six times, once for each depth and thickness contour set. For the Tapeats depth raster construction, the line representing the margin of the unit (zero thickness) was deleted from the depth contour map because it does not represent depth. This was done by creating a copy of the contour shape file using ArcCatalog, deleting the zero-thickness contours from the copy in ArcMap, and then using the remaining contour lines to create the raster representation of thickness. The areas of depth interpolation where Tapeats is absent in the subsurface are irrelevant to later volume calculations because these calculations were done only for areas of finite thickness.

(3) The raster representations of unit depth were then used to create a contour map with an 800m contour. This was done using the "Contour" tool in the "Raster Surface" tool set in the "3D Analysts Tools" in ArcToolbox, with a contour interval of 1312 feet (400m). These depth contour maps were copied and placed in the ArcMap Project. All contours other than the 800m contour were then deleted.

(4) The 800m lines were extended along the zero-thickness contour and along the state border, until each line formed a closed loop. Each loop was then converted to a polygon using the "Feature to Polygon" tool in the "Features" tool set in the "Data Management Tools" in ArcToolbox. The areas represented by the polygons have formation tops greater than 800m depth, thickness greater than zero, and are within Arizona. Each polygon file, representing one sandstone formation, was copied using ArcCatalog so that there were as many copies as polygons. All polygons except one were deleted from each shape file so that each shape file contained only one polygon. Each shape file (and each polygon) was then used to extract subsets of the thickness rasters for the purpose of calculating volume, as described in the next step.

(5) The parts of each thickness raster corresponding to formation-top depths below 800m, >0m thickness, and that are within Arizona, were separated into smaller rasters using the "Extract by mask" tool of the "Extraction" tool set within the "Spatial Analyst" toolbox. This produced three rasters, shown in shades of green, for the Tapeats Sandstone (Fig. 3b), one for the McCracken Sandstone (Fig. 4b), and three for the De Chelly Sandstone (Fig. 5b). The green color is darker for greater sand thickness (Figs. 3c, 4c, 5c).

(6) Each deep-basin raster area was then used to calculate basin volume below 800m depth using the "Surface volume" tool from the "Functional surface" tool set in the "3D Analyst" toolbox. "Plane Height" was set to zero so that, if all thicknesses in the raster are greater than zero by a finite amount (i.e., the minimum thickness is greater than zero), a reduced volume is not erroneously produced. Resulting table output data was compiled in an Excel spreadsheet, with three deep basins each for the De Chelly and Tapeats Sandstones, and one for the McCracken Sandstone (Table 1).

CO_2 Storage Capacity

The estimated mass of CO_2 (G_{CO2}) that could be stored in a sandstone unit is calculated with the following equation (from Litynski et al., 2010):

$$G_{CO2} = A_t \, h_g \, \phi_{total} \, \rho \, E_{saline} \quad (1)$$

where A_t is the total area in which the top of the saline formation is below 800m depth, h_g is the gross formation thickness, ϕ_{total} is the total porosity, ρ is the average density of CO_2 at the depths and temperatures that characterize the formation, and E_{saline} is the storage efficiency factor that represents the fraction of the total pore space that potentially will be occupied by stored CO_2. The ArcMap calculations presented in Table 1 represent formation volume with greater accuracy than formation volume calculated by simply multiplying total area A_t by gross thickness h_g because the ArcMap calculations account for lateral changes in thickness.

Formation porosities were estimated by well loggers based on examination of drill cuttings. This was done for 184 drill holes in the De Chelly Sandstone, 112 drill holes in the McCracken Sandstone, and 55 drill holes in the Tapeats Sandstone. The total porosity (ϕ_{total}) and standard deviation were determined for each formation (Table 2). Low and high porosities are given at the one standard deviation level for the De Chelly Sandstone, but for the other two formations, one standard deviation below the mean is approximately zero or negative. As a result, approximately similar representations of uncertainty are estimated at one-half standard deviation below the mean for the McCracken Sandstone, and one-third standard deviation for the Tapeats Sandstone (Table 2). These values were assigned to the respective formations over the entire study area, without determining different porosities for each subbasin in the De Chelly and Tapeats Sandstone units. Low, middle and high values for total pore volume were then calculated for each of the seven basins (Table 2, last three columns).

The capacity of sandstone to store CO_2 is not equivalent to its pore volume because not all pore space is accessible to an injected fluid. The storage efficiency of a saline formation (E_{saline}), which is the fraction of pore space that is actually accessible to injected CO_2, is calculated from the following equation (Litynski et al., 2010):

$$E_{saline} = E_{An/At} \, E_{hn/hg} \, E_{\phi e/\phi tot} \, E_v \, E_d \quad (2)$$

$E_{An/At}$ and $E_{hn/hg}$ are the fractions of areal extent and thickness, respectively, that have suitable physical properties for CO_2 sequestration. $E_{\phi e/\phi tot}$ is the fraction of total pore space that is interconnected and so is amenable to CO_2 sequestration. E_v represents barriers to displacement of CO_2 into formation volume, and includes such barriers as fault zones. E_d represents microscopic barriers to CO_2 movement into all pore space and includes molecular adhesion (wetting) of saline solutions to sand grains in which the saline fluids are not displaced by CO_2 influx. Storage efficiencies derived from studies of CO_2 injection into oil and gas reservoirs, and estimated by numerical simulation, are 0.51% to 5.4% for clastic rocks, with a mean value of 2.0% (Table 7 *in*

Litynski et al., 2010). The low and high values are calculated to represent the 10% and 90% probability values.

Estimates of the mass of CO_2 that can be stored in a given pore-space volume require an estimate of the density of stored CO_2, which depends on temperature and pressure. Subsurface temperatures beneath the Colorado Plateau as measured in 430 drill holes were used to calculate average surface temperature and geothermal gradient (Fig. 6). This yielded a surface temperature of 23.57°C and a gradient of 0.0134*h* where *h* is depth in meters and gradient is given in degrees C per meter depth. Using this data set in this manner is somewhat problematic because data generally were collected during drilling operations and not after an extended period (5-15 days) of inactivity. Circulating drilling fluids carry cold fluids down and bring heat back up, which decreases bottom-hole temperature. Because of variability in the time between cessation of drill-fluid circulation and down-hole temperature measurement, some measured temperatures were possibly artificially depressed and others were not. As a result, geothermal gradient is probably slightly underestimated, and scatter in measured temperatures is increased. The significance of this bias toward low temperatures is not well known, but inasmuch as it is reflected in increased scatter in temperature measurements, it does not appear to be large. Especially telling in this regard is the fact that temperatures measured at greater depth do not show greater scatter, as would be expected for greater heat loss to drill fluids for deeper wells with greater down-hole temperatures (Fig. 6).

The calculated temperature gradient was used to estimate subsurface temperatures beneath the Colorado Plateau. Hydrostatic pressure (the weight of a column of water extending upward to the surface) is assumed for conditions of CO_2 storage (Bachu, 2003). Using a hydrostatic pressure gradient and a temperature gradient as described above, CO_2 density was calculated by plotting P-T conditions for a range of depths as shown on Figure 7. Each blue dot represents hydrostatic pressure at depths represented by the numbers (in km) associated with each dot. The horizontal position of each dot is determined by the calculated temperature at each depth. Because calculated temperature at Earth's surface on the Colorado Plateau is rather high (23.6°C), CO_2 density at 800m depth is rather low (~350 kg/m^3). Because of greater subsurface buoyancy of CO_2 at lower densities, and potential for upward flow of CO_2, the 800m minimum depth for CO_2 storage may not be sufficient for long-term storage. Most of the volume under consideration for CO_2 storage is deeper, however, reaching depths of over 2km for the Tapeats Sandstone. CO_2 density at depths of ~1-2 km is ~700 – 800 kg/m^3. A value of 750 km/m^3 was used to calculate CO_2 storage capacity for Colorado Plateau sandstone units (Table 3). Our median estimate of the mass of CO_2 that can be stored in sandstone units of the Colorado Plateau is 8.28 billion tonnes, with low and high estimates of 1.34 and 32.5 billion tonnes, respectively. We calculate that 88% of this storage capacity is present in the De Chelly Sandstone sub-basin beneath Black Mesa.

Conclusion

Of the three sandstone units on the Colorado Plateau in Arizona, the De Chelly Sandstone has ~90% of the total capacity for CO_2 sequestration (7.40 billion tonnes calculated storage capacity). This is because the De Chelly Sandstone is thicker and has higher porosity than the deeper Paleozoic units. However, it is not known if formation waters present in the De Chelly Sandstone are saline. The sub-basin of the Tapeats sandstone beneath Black Mesa has a calculated CO_2 storage capacity of 540 million tonnes, while the CO_2 storage capacity of the McCracken Sandstone is calculated at 319 million tonnes. Both of these units are more likely, based on measured formation-water salinities, to contain saline pore water. If these three formations in the Black Mesa area are considered potential targets of future investigations, it is perhaps fortunate that all three can be penetrated with a single drill hole.

References cited

Bachu, S., 2003, Screening and ranking of sedimentary basins for sequestration of CO_2 in geological media in response to climate change: Environmental Geology, v. 44, p. 277-289.

Hereford, R., 1977, Deposition of the Tapeats Sandstone (Cambrian) in central Arizona: Geological Society of America Bulletin, v. 88, no. 2, p. 199-211.

Knight, R.L., and Cooper, J.R., 1955, Suggested changes in Devonian terminology in the Four Corners area, in Cooper, J.C., ed., Geology of parts of Paradox, Black Mesa, and San Juan Basins, Four Corners Field Conference: Four Corners Geological Society Guidebook, p. 56-58.

Lausen, C., and Wilson, E.D., 1925, Gold and copper deposits near Payson, Arizona: Arizona Bureau of Mines Bulletin no. 120, 44 p.

Litynski, J., Deel, D., Rodosta, T., Guthrie, G., Goodman, A, Hakala, A., Bromhal, G., and Frailey, S., 2010, Carbon sequestration atlas of the United States and Canada (Atlas III): U.S. Department of Energy, Office of Fossil Energy, National Energy Technology Laboratory (NETL), 3rd ed., Appendix B, p. 136-152.

Richard, S.M., Reynolds, S.J., Spencer, J.E., and Pearthree, P.A., 2000, Geologic map of Arizona: Arizona Geological Survey Map 35, scale 1:1,000,000.

Teichert, C., 1965, Devonian rocks and paleogeography of central Arizona: U.S. Geological Survey Professional Paper 464, 181 p.

U.S. Department of Energy, 2010, Carbon sequestration atlas of the United States and Canada (Atlas III): U.S. Department of Energy, Office of Fossil Energy, National Energy Technology Laboratory (NETL), 3rd ed., 160 p.

Figures 3, 4, 5. Depth and thickness of Paleozoic sandstone units, well locations, cross-section locations, and areas where the top of the sandstone units are below 800m depth.

Figures 3a, 4a, 5a. Contours shown here (black numbered lines) represent the depth to the top of each Paleozoic sandstone unit and were derived from analysis of well logs. The color background maps are raster representations of the contoured surface created using ArcToolbox™ tools (see text) (color interval for raster colors is arbitrary). Magenta lines bounds areas where the top of each sandstone unit is greater than 800m deep or where the sandstone pinches out to zero thickness.

Figures 3b, 4b, 5b. As in figures 3a, 4a, and 5a, but areas where the top of the relevant sandstone unit is below 800m depth are colored green, with lighter green corresponding to areas where the sandstone is thinner.

Figures 3c, 4c, 5c. As in figures 3b, 4b, and 5b, but contours and color raster background maps represent sandstone unit thickness rather than depth. The color raster background maps represent the thickness of each sandstone unit as derived from the contour map using ArcToolbox™ tools (see text) (color interval for raster colors is arbitrary). Areas where the top of the relevant sandstone unit is below 800m depth are colored green, with lighter green corresponding to areas where the sandstone is thinner. Each contiguous green area represents a raster representation of thickness. Sandstone volume was calculated for each of these rasters using ArcToolbox™ tools (see text and tables).

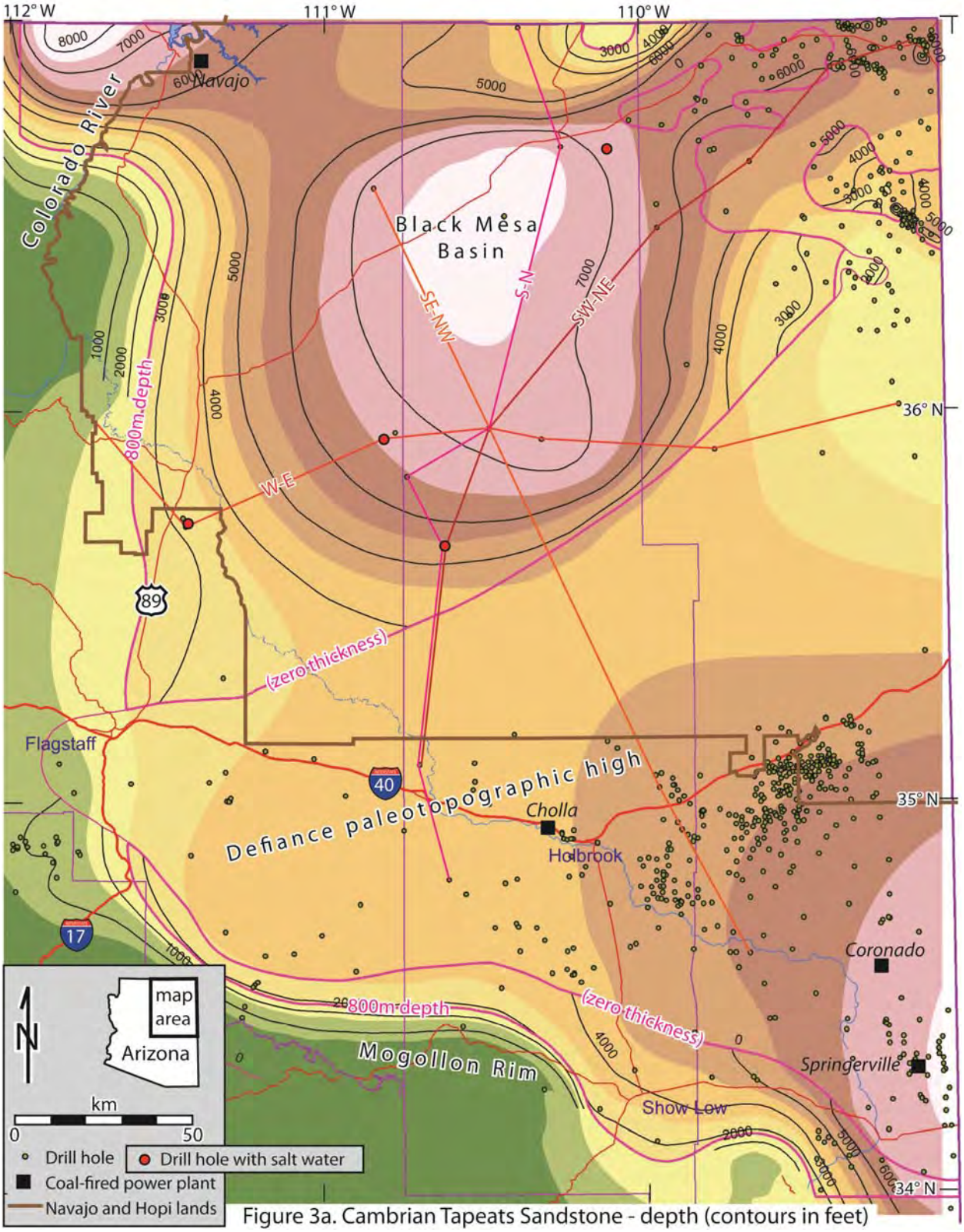


Figure 3a. Cambrian Tapeats Sandstone - depth (contours in feet)

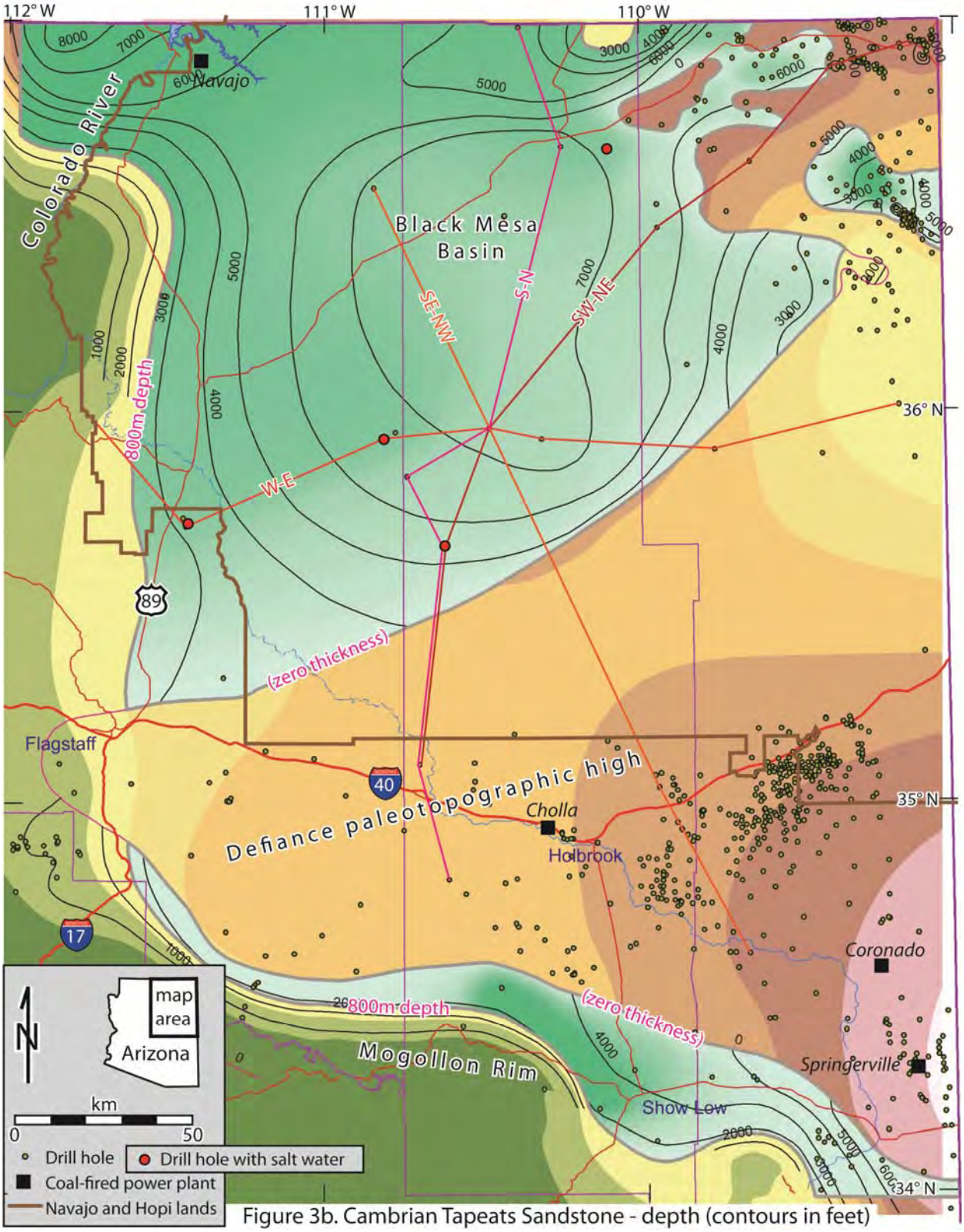


Figure 3b. Cambrian Tapeats Sandstone - depth (contours in feet)

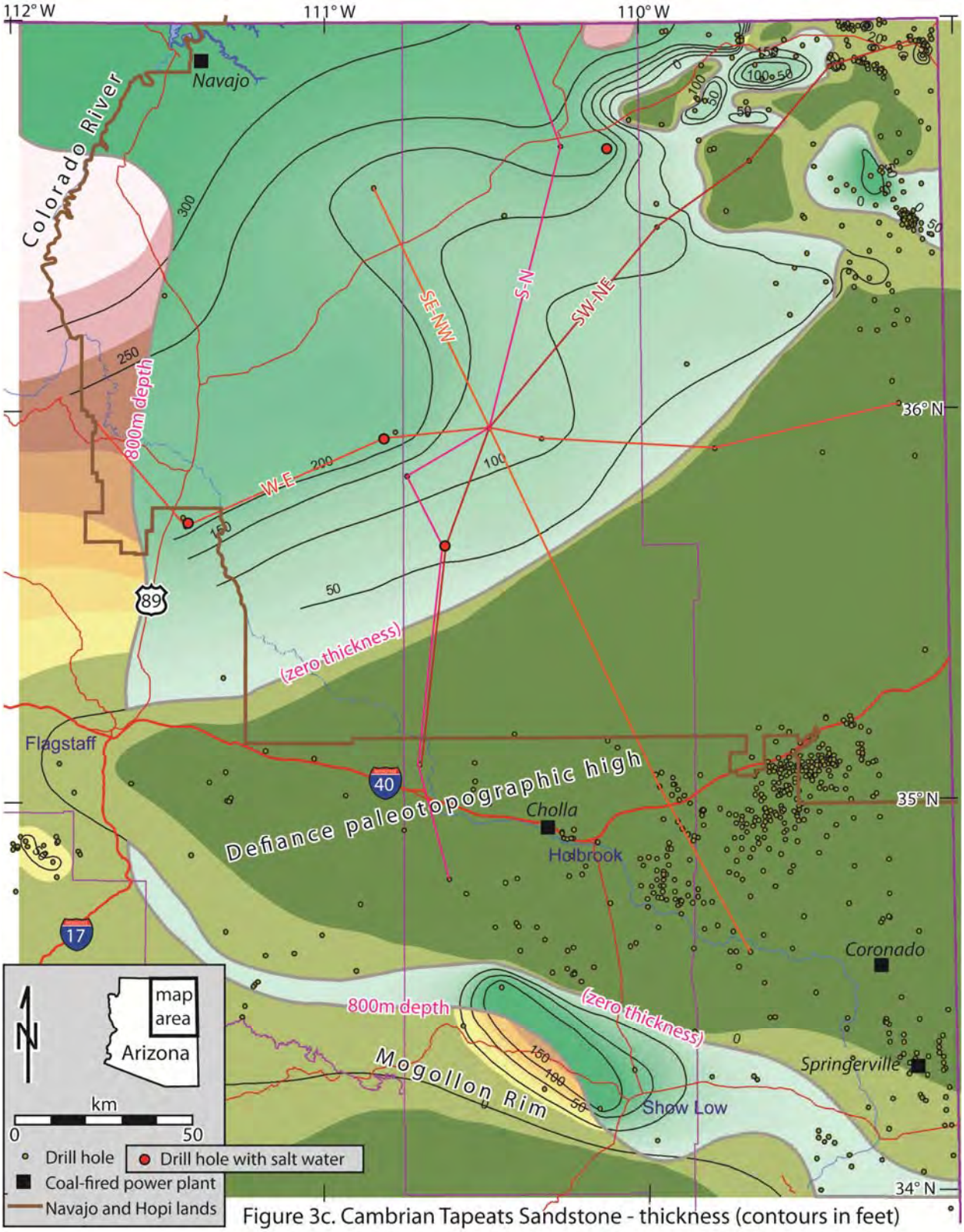


Figure 3c. Cambrian Tapeats Sandstone - thickness (contours in feet)

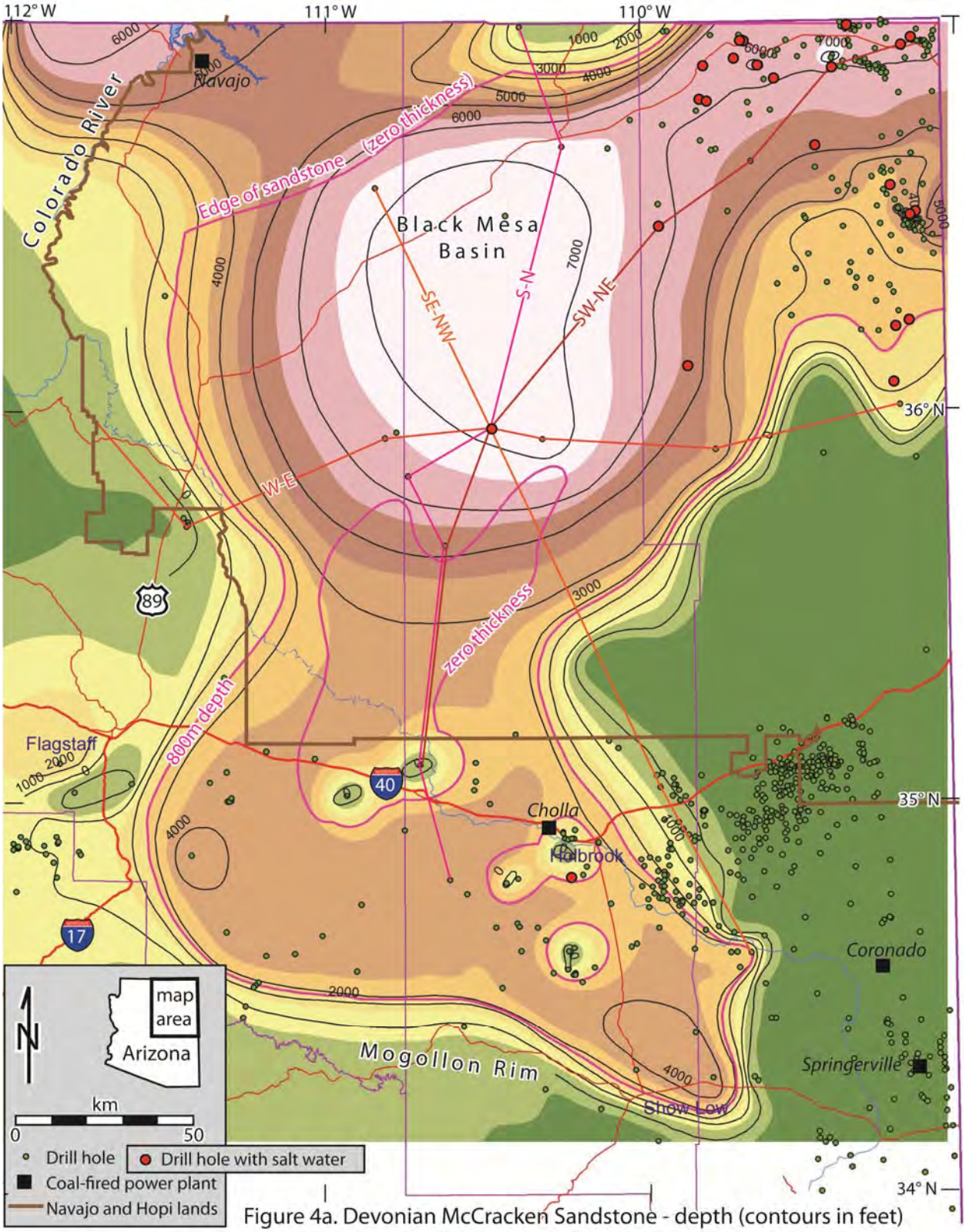


Figure 4a. Devonian McCracken Sandstone - depth (contours in feet)

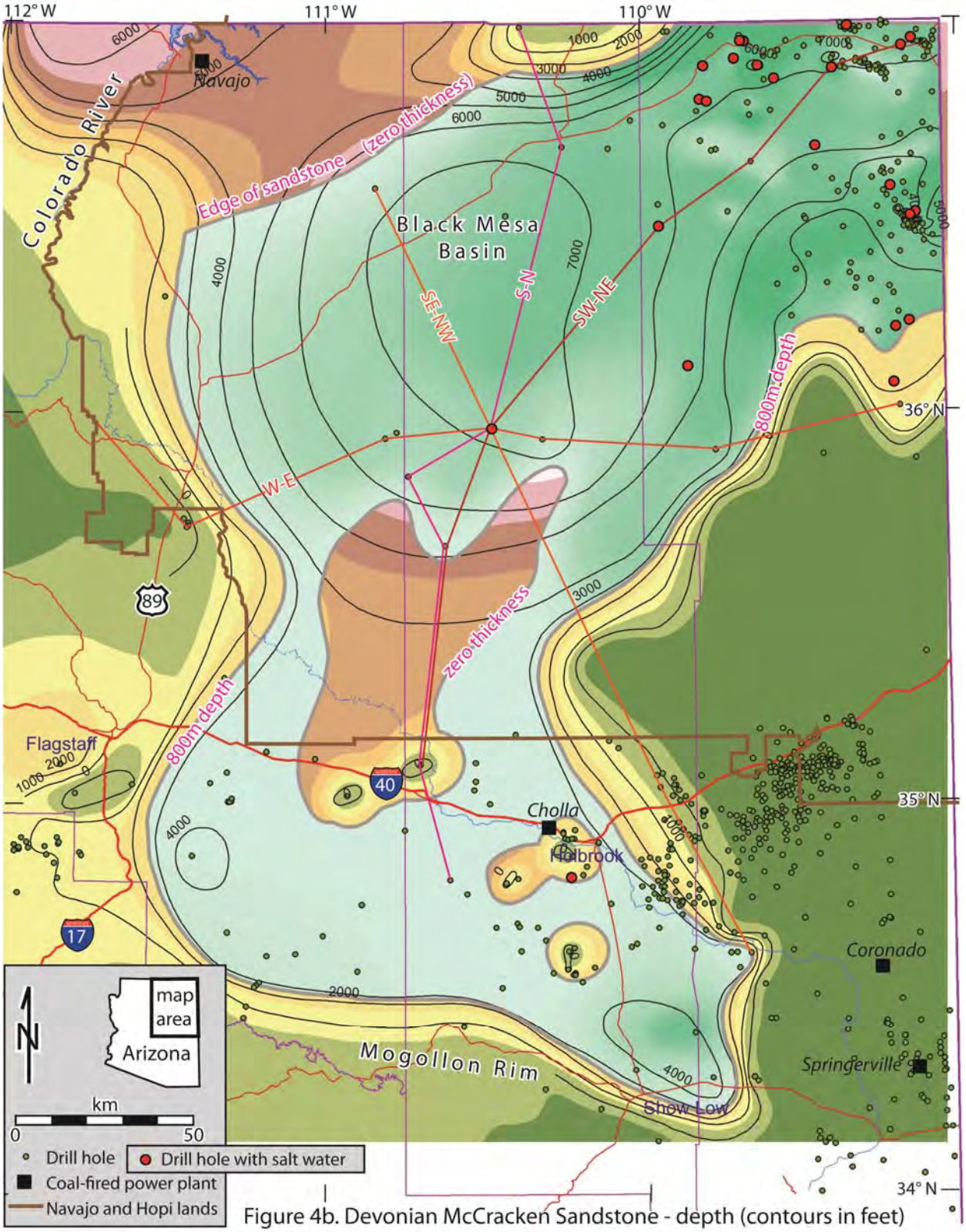


Figure 4b. Devonian McCracken Sandstone - depth (contours in feet)

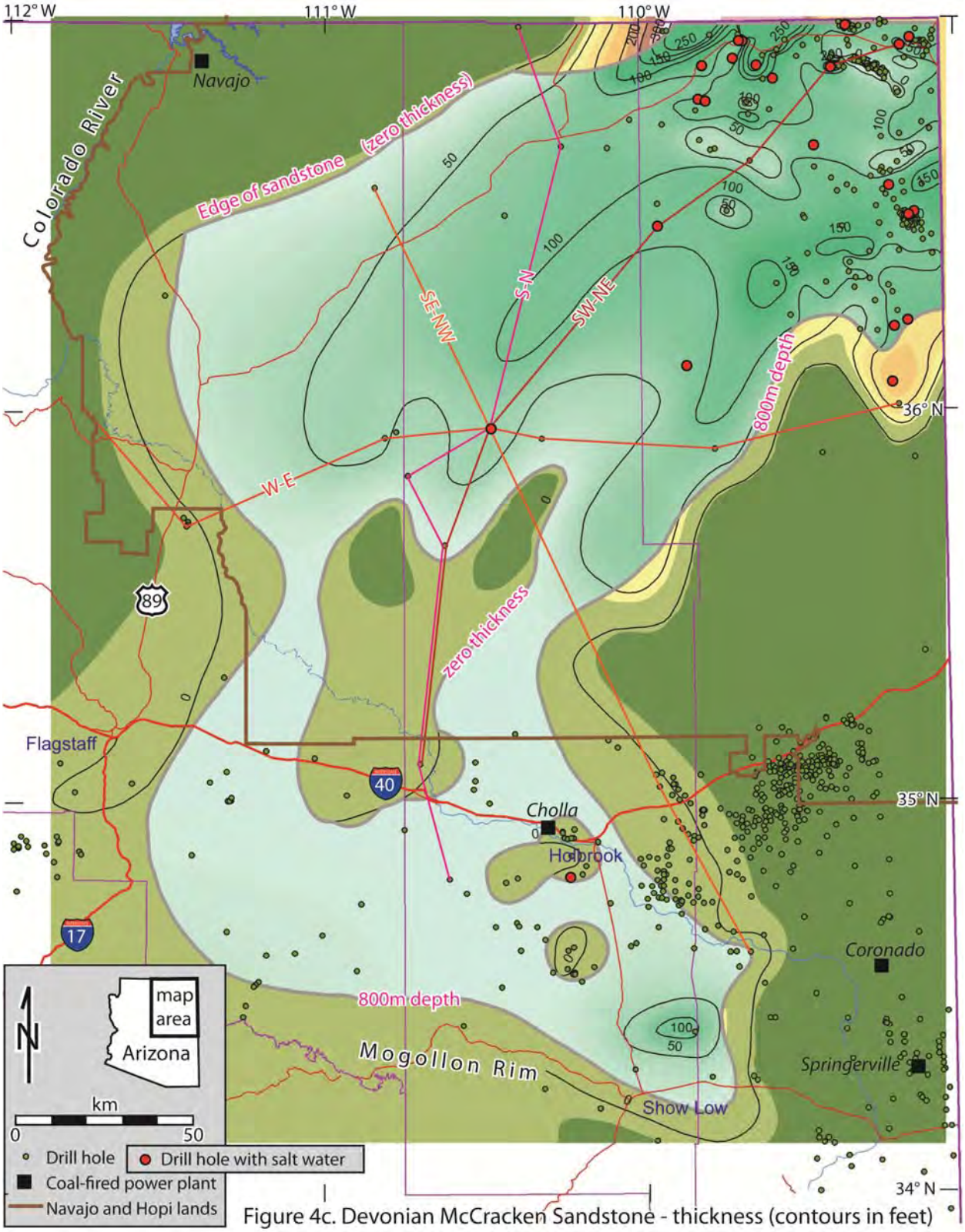


Figure 4c. Devonian McCracken Sandstone - thickness (contours in feet)

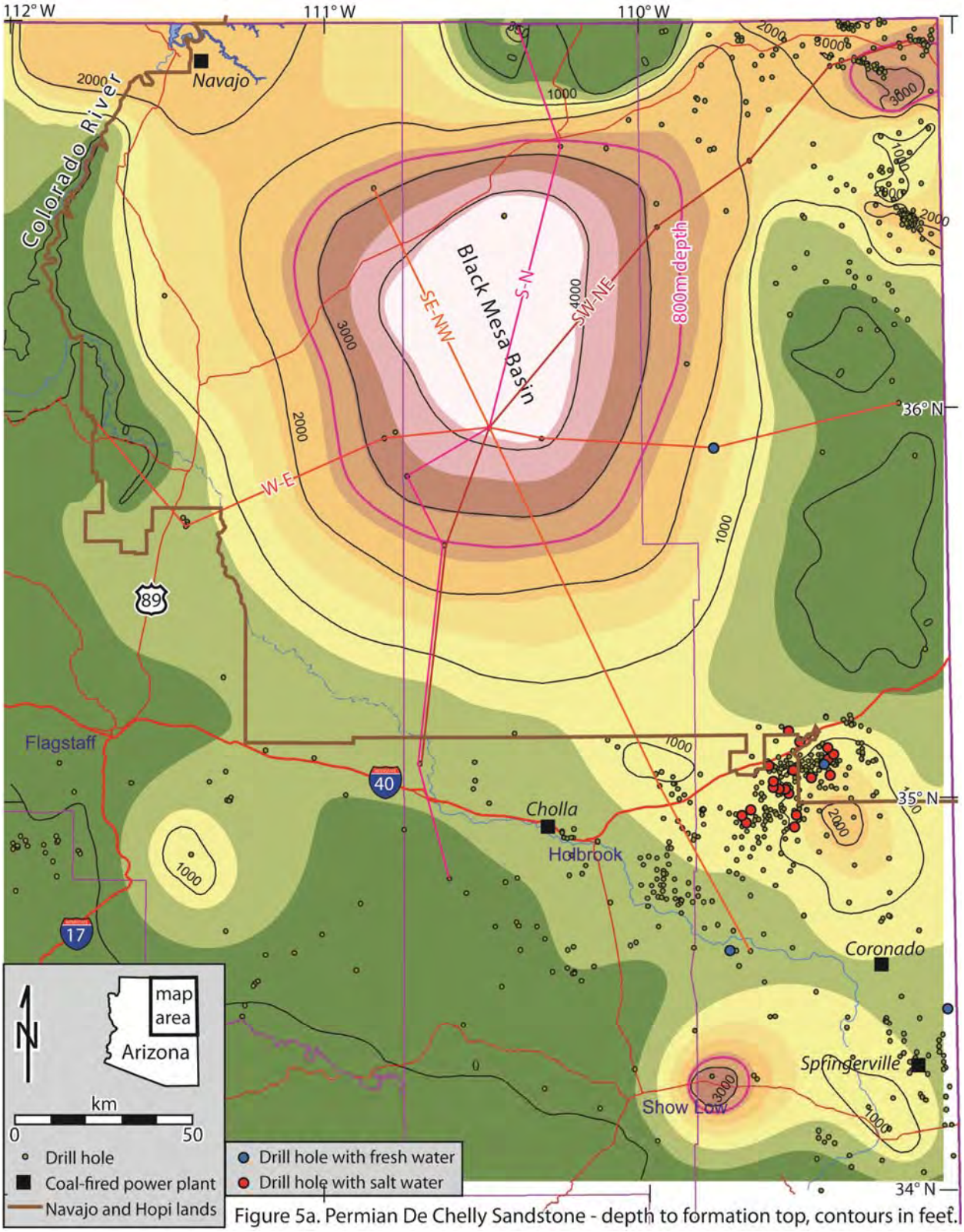


Figure 5a. Permian De Chelly Sandstone - depth to formation top, contours in feet.

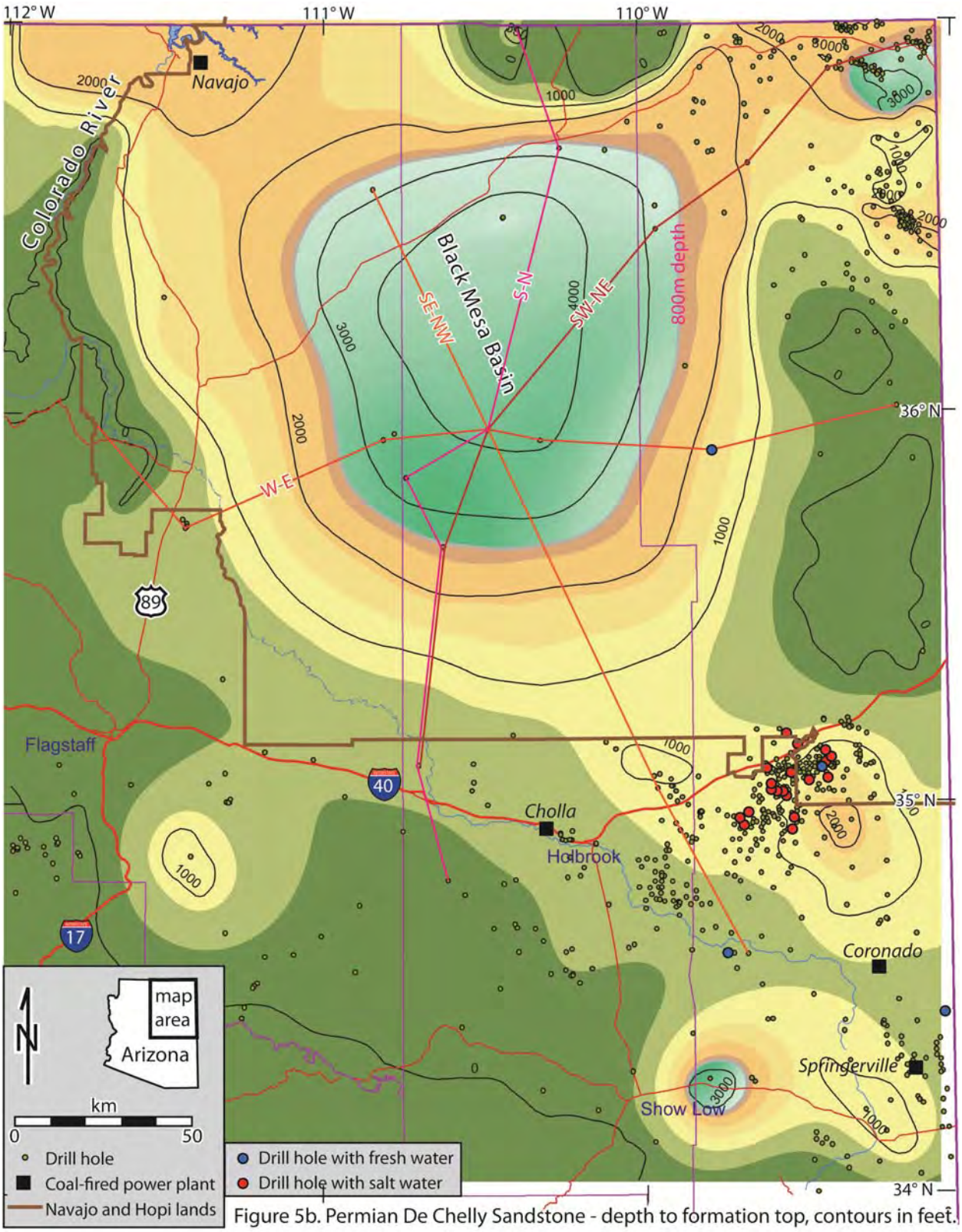


Figure 5b. Permian De Chelly Sandstone - depth to formation top, contours in feet.

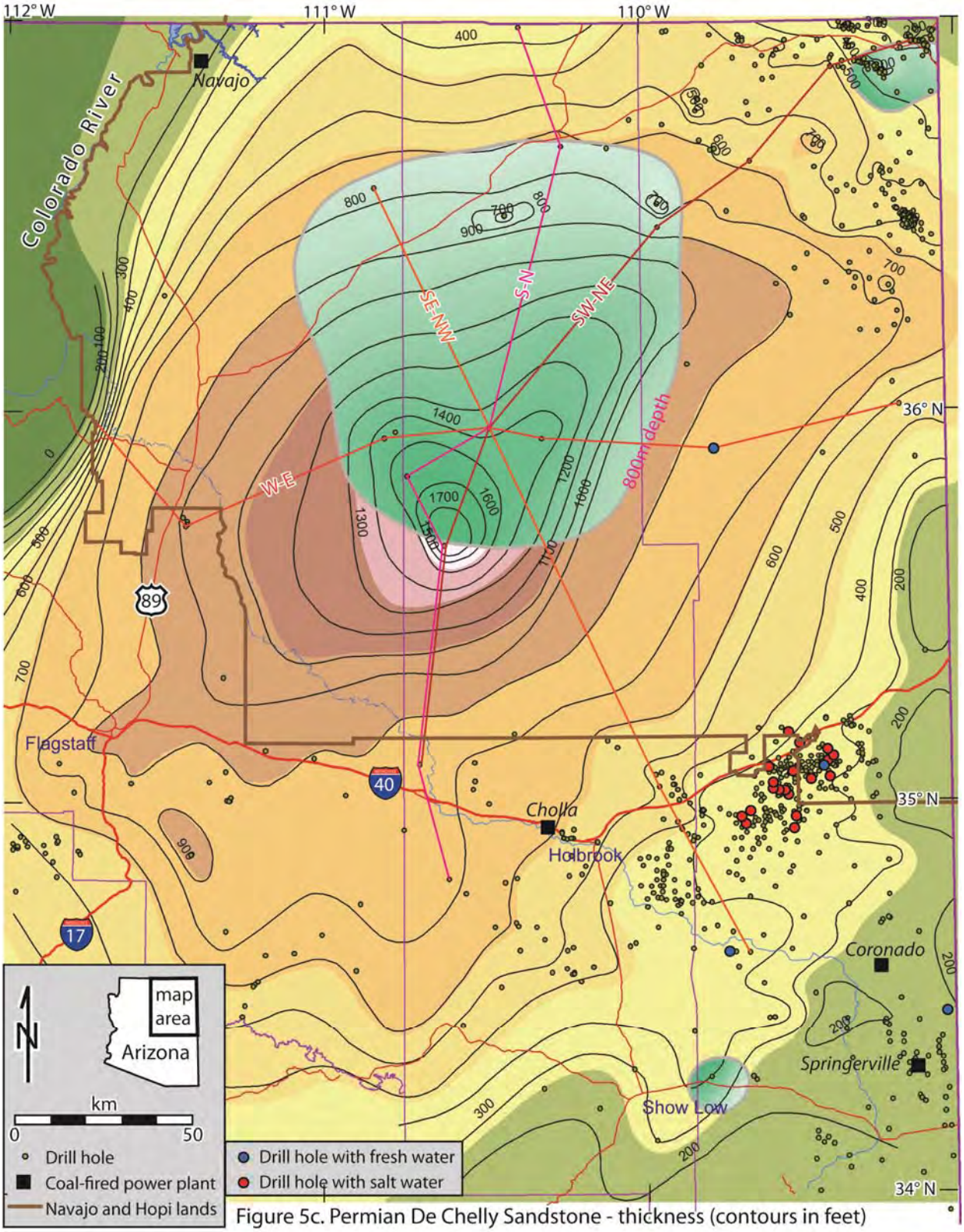


Figure 5c. Permian De Chelly Sandstone - thickness (contours in feet)

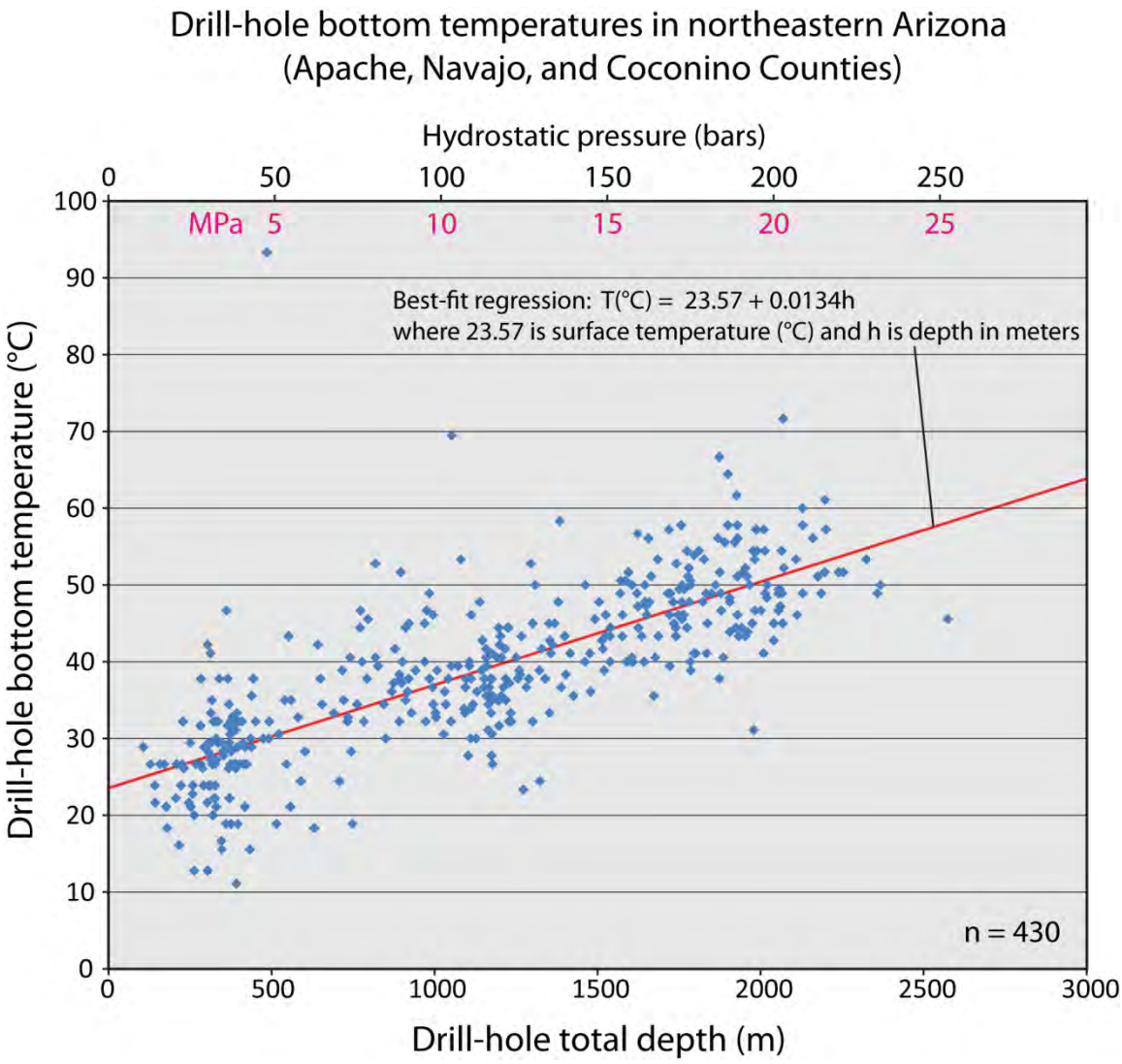


Figure 6. Drill-hole bottom temperatures from 430 bore holes in northeastern Arizona.

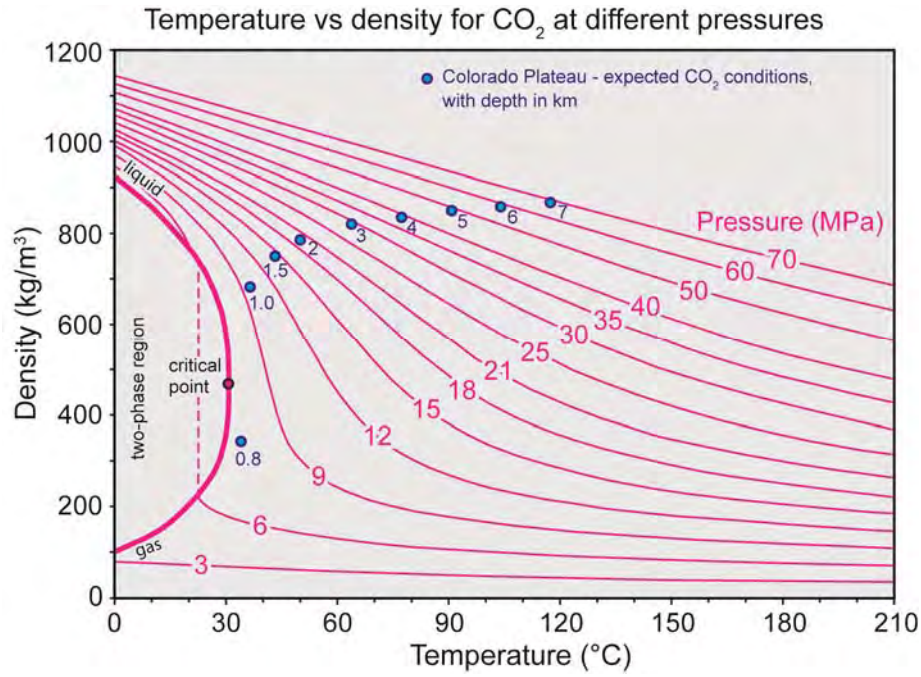


Figure 7. Temperature and density of CO_2 are plotted for a range of pressures represented by the magenta isopressure lines. For appropriate pressure, and temperature below that of the critical point, CO_2 coexists as both a gas and a liquid. To identify density conditions of CO_2 stored in sandstone units beneath the Colorado Plateau, a range of pressure and temperature conditions were evaluated, as follows. For each storage depth, a temperature was calculated from the regression line in Figure 6, and a value for hydrostatic pressure was calculated. Each blue dot, representing a depth given by the number next to each dot, was located on this diagram by its temperature (horizontal position) and by the calculated hydrostatic pressure for each depth which was used to place the dot among the magenta isopressure lines (from Bachu, 2003). At pressure corresponding to depth less than 1 km, precise density is uncertain (for example, compare results plotted here [derived from Bachu, 2003] with those from an online CO_2 density calculator at http://www.peacesoftware.de/einigewerte/co2_e.html).

Table 1. ArcMap-calculated volume and area of Paleozoic sandstone units below 800m depth on the Colorado Plateau									
Basin and unit	**Dataset**	**Plane Height**	**Reference**	**Z Factor**	**2D Area (m^2)**	**3D Area (m^2)**	**Volume (m^3)**	**2D area (km^2)**	**Volume (km^3)**
De Chelly main	..ateau2012_2\Rasters\dech_main2	0	ABOVE	1	10133348856	10133429005	3.39325E+12	10133	3393
De Chelly NE	..Plateau2012_2\Rasters\dech_ne2	0	ABOVE	1	344775438	344777719	36952468117	345	37
De Chelly SE	..Plateau2012_2\Rasters\dech_se2	0	ABOVE	1	172387719	172389150	18197437824	172	18
McCracken	..eau2012_2\Rasters\mccrac_main4	0	ABOVE	1	33578357384	33578387847	5.31312E+11	33578	531
Tapeats main	..au2012_2\Rasters\tapeats_main5	0	ABOVE	1	28661186925	28661225407	1.50136E+12	28661	1501
Tapeats south	..\Plateau2012_2\Rasters\tpts_s2	0	ABOVE	1	3644635937	3644645273	50082646390	3645	50
Tapeats NE	..\Plateau2012_2\Rasters\tpts_NE	0	ABOVE	1	603350972	603351717	3044647738	603	3

Table 2. Porosity and pore volume for Paleozoic sandstone units below 800m depth on the Colorado Plateau								
Basin and unit	**Area (km^2)**	**Volume (km^3)**	**Porosity low (%)***	**Porosity mean (%)**	**Porosity high (%)***	**Pore volume low (km^3)**	**Pore volume mean (km^3)**	**Pore volume high (km^3)**
De Chelly main	10133	3393	9.3	14.3	19.3	315.57	485.23	654.90
De Chelly NE	345	37	9.3	14.3	19.3	3.44	5.28	7.13
De Chelly SE	172	18	9.3	14.3	19.3	1.69	2.60	3.51
McCracken	33578	531	2	4	8	10.63	21.25	42.50
Tapeats main	28661	1501	1.2	2.4	6	18.02	36.03	90.08
Tapeats south	3645	50	1.2	2.4	6	0.60	1.20	3.00
Tapeats NE	603	3	1.2	2.4	6	0.04	0.07	0.18
*De Chelly Sandstone (n=184): Porosity range is +/- one standard deviation								
*McCracken Sandstone (n=112): Porosity range is plus one standard deviation, minus one half of one standard deviation								
*Tapeats Sandstone (n=55): Porosity range is plus one standard deviation, minus one third of one standard deviation								

Table 3. CO_2 storage capacity for Paleozoic sandstone units below 800m depth on the Colorado Plateau

Sandstone unit and basin	Pore volume low (km^3)	Pore volume mean (km^3)	Pore volume high (km^3)	Storage efficiency, low*	Storage efficiency, median*	Storage efficiency, high*	Effective pore volume, low (km^3)	Effective pore volume, median (km^3)	Effective pore volume, high (km^3)	CO_2 density (kg/m^3)	Potential mass of stored CO_2 (tonnes), low**	Potential mass of stored CO_2 (tonnes), median**	Potential mass of stored CO_2 (tonnes), high**
De Chelly main	315.57	485.23	654.90	0.0051	0.02	0.054	1.6	9.7	35.4	750	1.21.E+09	7.28.E+09	2.65.E+10
De Chelly NE	3.44	5.28	7.13	0.0051	0.02	0.054	0.018	0.11	0.39	750	1.31.E+07	7.93.E+07	2.89.E+08
De Chelly SE	1.69	2.60	3.51	0.0051	0.02	0.054	0.009	0.05	0.19	750	6.47.E+06	3.90.E+07	1.42.E+08
McCracken	10.63	21.25	42.51	0.0051	0.02	0.054	0.054	0.43	2.30	750	4.06.E+07	3.19.E+08	1.72.E+09
Tapeats main	18.02	36.03	90.08	0.0051	0.02	0.054	0.092	0.72	4.86	750	6.89.E+07	5.40.E+08	3.65.E+09
Tapeats south	0.60	1.20	3.00	0.0051	0.02	0.054	0.0031	0.024	0.16	750	2.30.E+06	1.80.E+07	1.22.E+08
Tapeats NE	0.04	0.07	0.18	0.0051	0.02	0.054	0.00019	0.0015	0.0099	750	1.40.E+05	1.10.E+06	7.40.E+06
										Total	1.34.E+09	8.28.E+09	3.25.E+10

*Values are approximations from various lithologies in the United States, as given by Litynski et al. (2010)

**E+09 indicates $x10^9$

Appendix A: Cross sections. Cross sections were constructed from drill logs. Locations of cross sections are shown in Figure A1 and Figures 1, 3, 4, and 5. Locations of drill holes are shown on Figures 1, 3, 4, and 5.

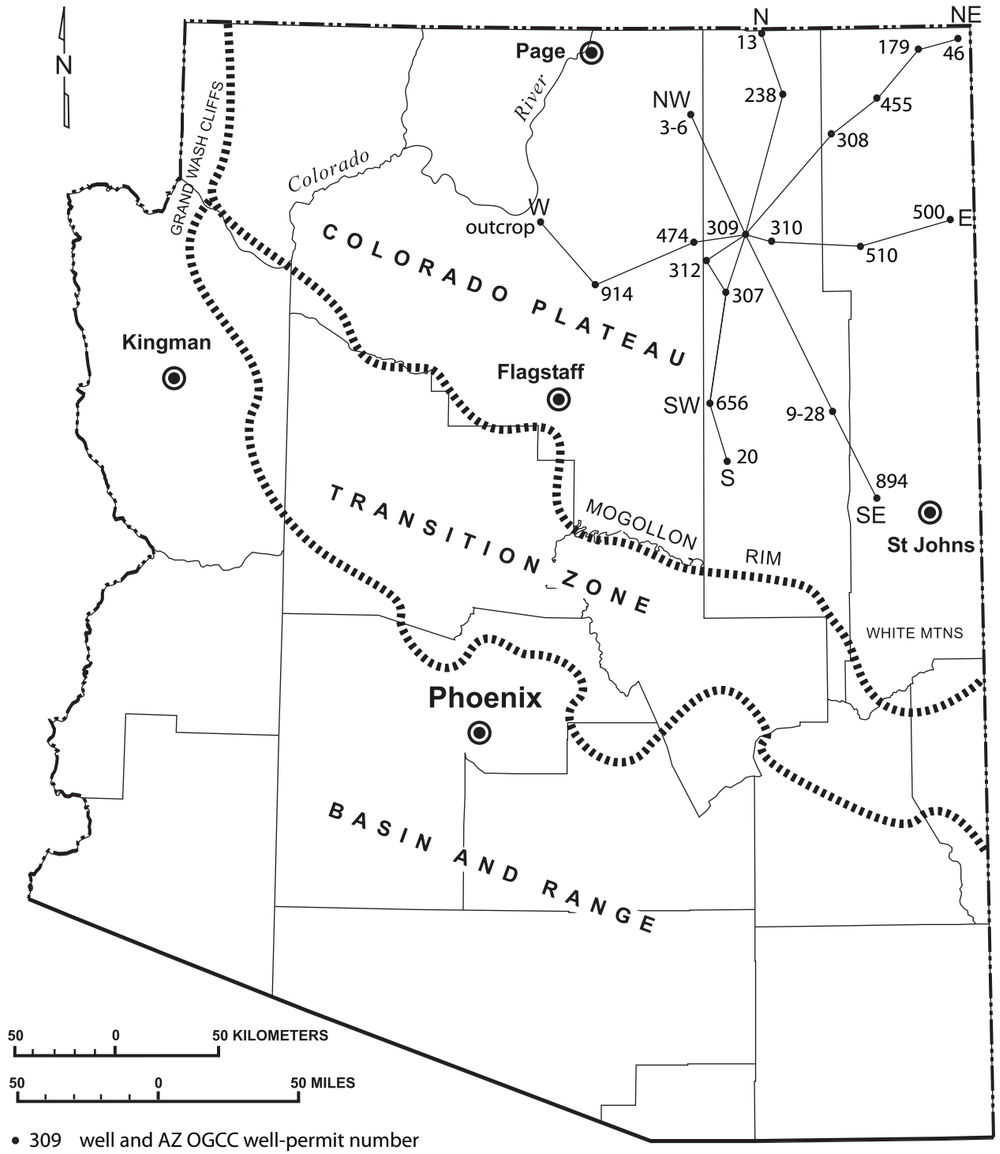


Figure A1: Location of Colorado Plateau in Arizona and section lines for cross sections.

SW

656
25-20n-15e
4856′ gl

307
15-26n-16e
5535′ gl

309
35-30n-17e
6106′ gl

308
02-35n-22e
6097′ gl

455
04-37n-25e
5191′ gl

179
06-40n-28e
6582′ gl

46
16-41n-30e
5112′ gl

NE

surface simplified

Black Mesa

Cretaceous

Toh Atin Mesa

Chinle Wash

Dahstini Wash

997 Jurassic

Jurassic Glen Canyon Group

1360 Triassic

250 Triassic

272 Coconino

1225 Triassic

2458

1115

1680 DeChelly

1410 Triassic

2860 Triassic

Triassic Chinle - Moenkopi

3297

2860 DeChelly

2638

2308

3723

2363

3000 f t depth line

Permian Coconino-DeChelly-Upper Supai sandstones

2695

3750

4230

3323

3347

2500/200,640 ft =0.7 degrees

4360

3767

3795 TD

Devonian Martin

Precambrian

700/110,000 ft =0.4 degrees

=0.4 degrees 1800/237,600 ft

5610

Lower Supai and older units

5818

4860

5412

Sea Level

5620

5780

5855

5915 TD

Tapeats

Mississippian

McCracken

Lower Devonian

Upper Cambrian

Tapeats

6984

6348

6560

6653

6754 TD

Devonian

5183

5268 TD

Precambrian

6999

7455

7700

7760

7780 TD

7318

7359 TD

5960

McCracken

6445

6640

6787 TD

SW-NE Depth Section Northeastern Arizona
Depth from surface in feet
Steven L. Rauzi
01-25-2011

Thickness of thin units exaggerated
Wells identified by permit number

Well information is on file, under
AZ OGCC permit number, at the
Arizona Geological Survey

1000′

VE = 53

10 miles

S

N

20
01-11n-16e
5535' gl

656
25-20n-15e
4856' gl

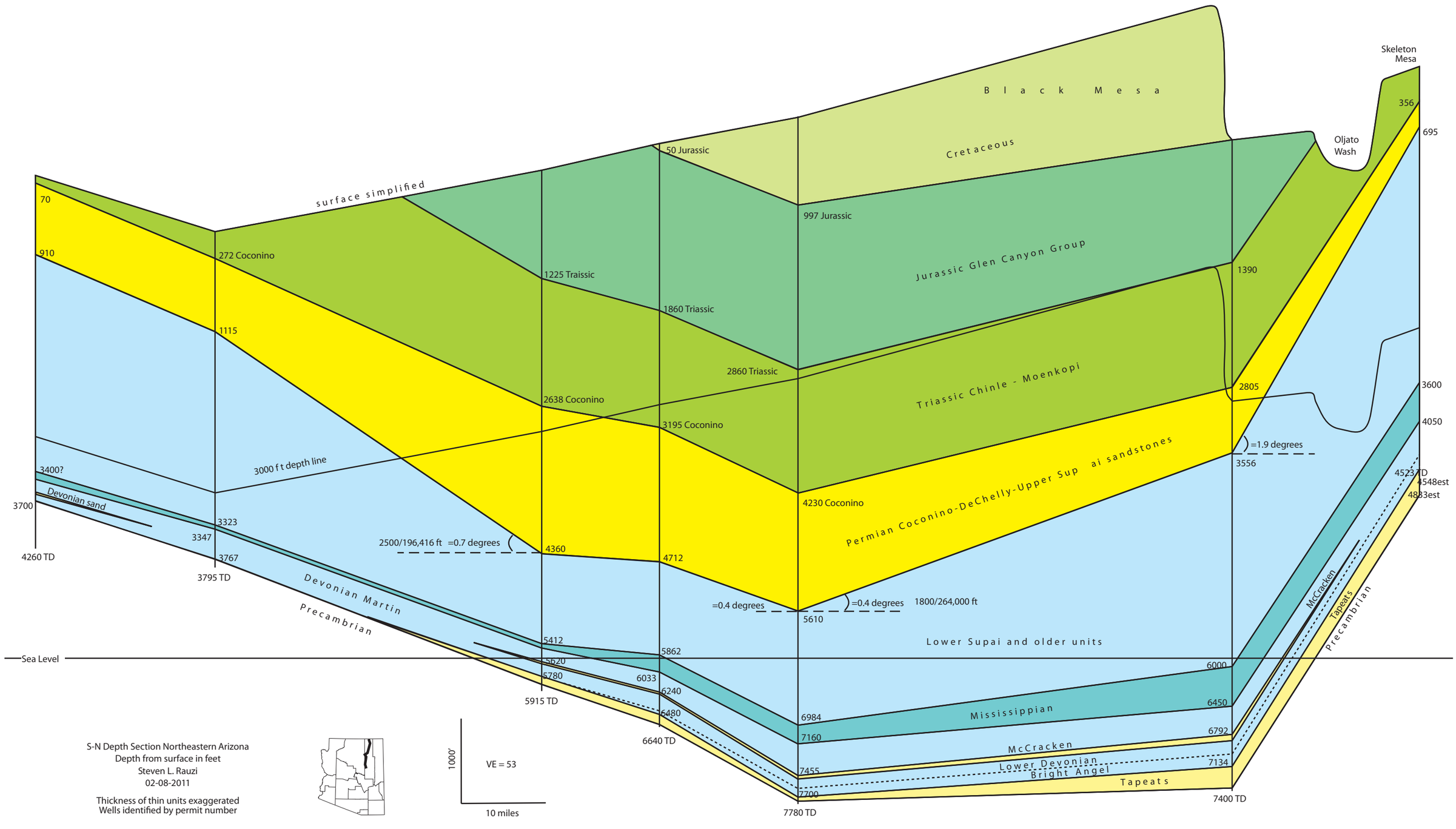
307
15-26n-16e
5915' gl

312
09-28n-15e
5808' gl

309
35-30n-17e
6106' gl

283
24-38n-19e
5857' gl

13
34-41n-18e
6694' gl



S-N Depth Section Northeastern Arizona
Depth from surface in feet
Steven L. Rauzi
02-08-2011

Thickness of thin units exaggerated
Wells identified by permit number

SE

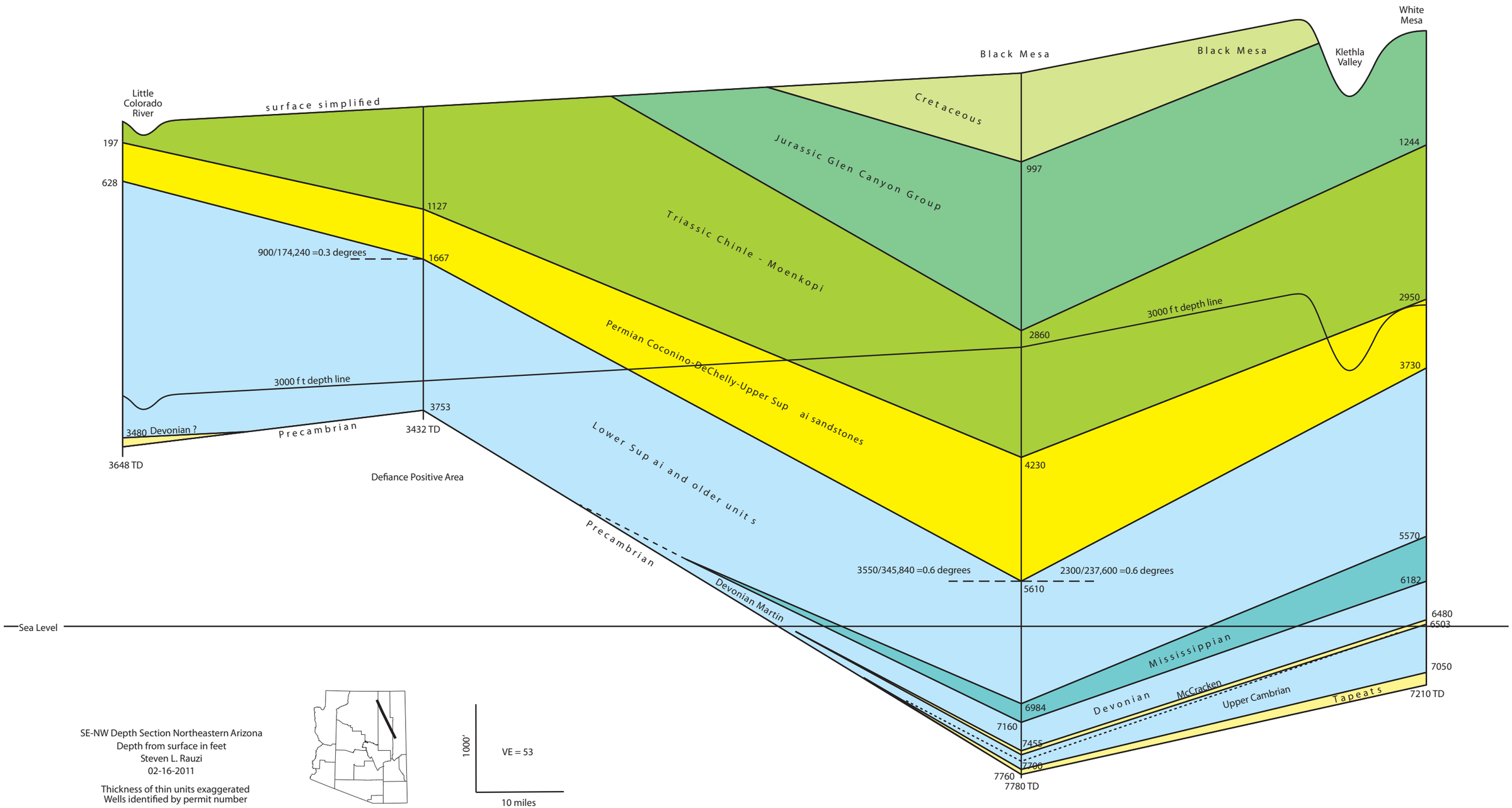
894
15-14n-25e
5552′ gl

9-28
06-19n-23e
5710′ gl

309
35-30n-17e
6106′ gl

3-6
28-37n-14e
6607′ gl

NW



SE-NW Depth Section Northeastern Arizona
Depth from surface in feet
Steven L. Rauzi
02-16-2011

Thickness of thin units exaggerated
Wells identified by permit number

W

Outcrop
24-31n-05e
6900′ gl

914
15-27n-09e
5068′ gl

474
11-29n-14e
5638′ gl

321
06-29n-15e
5634′ gl

309
35-30n-17e
6106′ gl

310
08-29n-19e
6171′ gl

510
21-29n-24e
6163′ gl

500
36-04n-07w
7558′ gl

E

Canyon DeChelly
250
839
1670
1999
2032 TD

Coconino Plateau
Kaibab-T oroweap
540
1140
2930
3270
4300
Mississippian Redwall
Upper Cambrian
Tapeats
Precambrian Super Group
Precambrian granite
Devonian
Little Colorado River
256
1264
2738
3391
3616
4266
4350 TD
Permian
surface simplified
50
997
1622
1775
3249
3395
4710
4817
5610
Cretaceous
Black Mesa
910
Jurassic Glen Canyon Group
652
Chinle Wash
Triassic Chinle - Moenkopi
1880
2760
2700
2860
3000 f t depth line
Permian Coconino-DeChelly-Upper Sup ai sandstones
4060
4230
4322
4370
4496
4552 TD
Lower Sup ai and older units
2900/196,944 =0.8 degrees
5540 =1 degree 2750/158,400 ft
Precambrian
3000 f t depth line
Sea Level
5040
6085
6345
6500
6615
6723
6750
6940 TD
6998 TD
Mississippian
Devonian
Tapeats
McCracken
6984
7038
7330
7455
7540
7700
7570
7694
7750 TD
7780 TD
Lower Devonian

W-E Depth Section Northeastern Arizona
Depth from surface in feet
Steven L. Rauzi
02-14-2011

Thickness of thin units exaggerated
Wells identified by permit number

1000′
VE = 53
10 miles

An evaluation of carbon dioxide sequestration potential of the Permian Cedar Mesa Sandstone, northeastern Arizona

Abstract

Northeastern Arizona encompasses the southwestern part of the Colorado Plateau, an area of gently dipping to slightly tilted Paleozoic and Mesozoic strata that include porous and permeable sandstone units. The Lower Permian Cedar Mesa Sandstone was identified for study as a potential target for CO_2 sequestration in order to reduce anthropogenic CO_2 emissions to the atmosphere. The Cedar Mesa Sandstone is overlain by the impermeable Organ Rock Formation, which is necessary to prevent escape of sequestered CO_2. The salinity of groundwater in the Cedar Mesa Sandstone is unknown, but must be determined before CO_2 can be sequestered because CO_2 sequestration is not permitted in potable groundwater under current regulatory conditions. Well logs for 755 drill holes were used to evaluate the extent, depth, and thickness of subsurface formations. ESRI® ArcMap™ software was then used to calculate the volume of the Cedar Mesa Sandstone where the top of the unit is below 3000 feet (915 meters) depth, which is the minimum depth necessary for CO_2 sequestration where the CO_2 is under sufficient pressure to remain in a dense, near-liquid state. Well logs were used to evaluate porosity, which was then used to calculate the amount of pore space that is theoretically available for CO_2 storage (the effective porosity). We calculate that there are between 30 km^3 and 80 km^3 of pore space in the Cedar Mesa Sandstone. The fraction of pore-space volume that is accessible to CO_2 injection is estimated to be approximately 0.5% to 5%. Applying this storage efficiency to the Cedar Mesa Sandstone indicates that 0.15 km^3 to 4.3 km^3 of pore space is accessible to injected CO_2, and that 0.114 to 3.24 billion tonnes of CO_2 could be sequestered in this pore space at a density of approximately 750 kg/m^3.

Introduction

This report represents a RMCCS assessment of CO_2 storage potential in the Lower Permian Cedar Mesa Sandstone (equivalent to the Weber Sandstone farther north), the Jurassic Entrada Sandstone, and the Cretaceous Dakota Formation in Arizona. Neither the Entrada Sandstone nor the Dakota Formation are buried at sufficient depth to be considered for CO_2 sequestration, and are not considered further in this report.

The study area is located in northeastern Arizona, in an area that is largely owned by the Navajo and Hopi Indians (Fig. 1; Appendix A). The focus of this study is determining (1) the volume of porous and permeable Permian Cedar Mesa Sandstone where the interface with overlying impermeable capping formations is below 3000 feet (915 meters) depth, (2) the effective (accessible) pore-space volume, and (3) the presence or absence of saline water in the pore space. Basin volume below 3000 feet (915 meters) depth is important because CO_2 will remain in a dense, near-liquid state at hydrostatic pressures corresponding to such depths (provided temperatures are not abnormally high). Data on the porosity of the Cedar Mesa Sandstone and the salinity of included groundwater are reviewed in this report, and discussed in the context of suitability for CO_2 sequestration. Data on the porosity of the Permian De Chelly

Sandstone (lateral equivalent of the White Rim Sandstone in southern Utah) and the salinity of included groundwater are reviewed in the previous section) and are not duplicated here. However, the De Chelly data were submitted to the RMCCS group at the University of Utah Energy Geoscience Institute (EGI) for capacity calculation in the EGI Storage Capacity Spreadsheet.

The AZGS purchased Neuralog software in 2011 to digitize Arizona well logs into computer usable LAS (log ASCII Standard) format to aid analysis for CO_2 sequestration potential. The digitizing effort focused on deep wells across northeastern Arizona including wells that penetrated Precambrian basement and wells in the oil and gas fields with the highest cumulative production (Appendix B). The AZGS developed a user-friendly web application to make the digitized well data available online to facilitate the widest possible access and use of the data. The online search and download map, the Arizona Oil and Gas Well Viewer, is hosted under the Online Data tab on the State of Arizona Oil and Gas Conservation Commission (AZOGCC) website. A total of 275 logs from 120 wells for a total of about 962 curves were digitized through September 30, 2013.

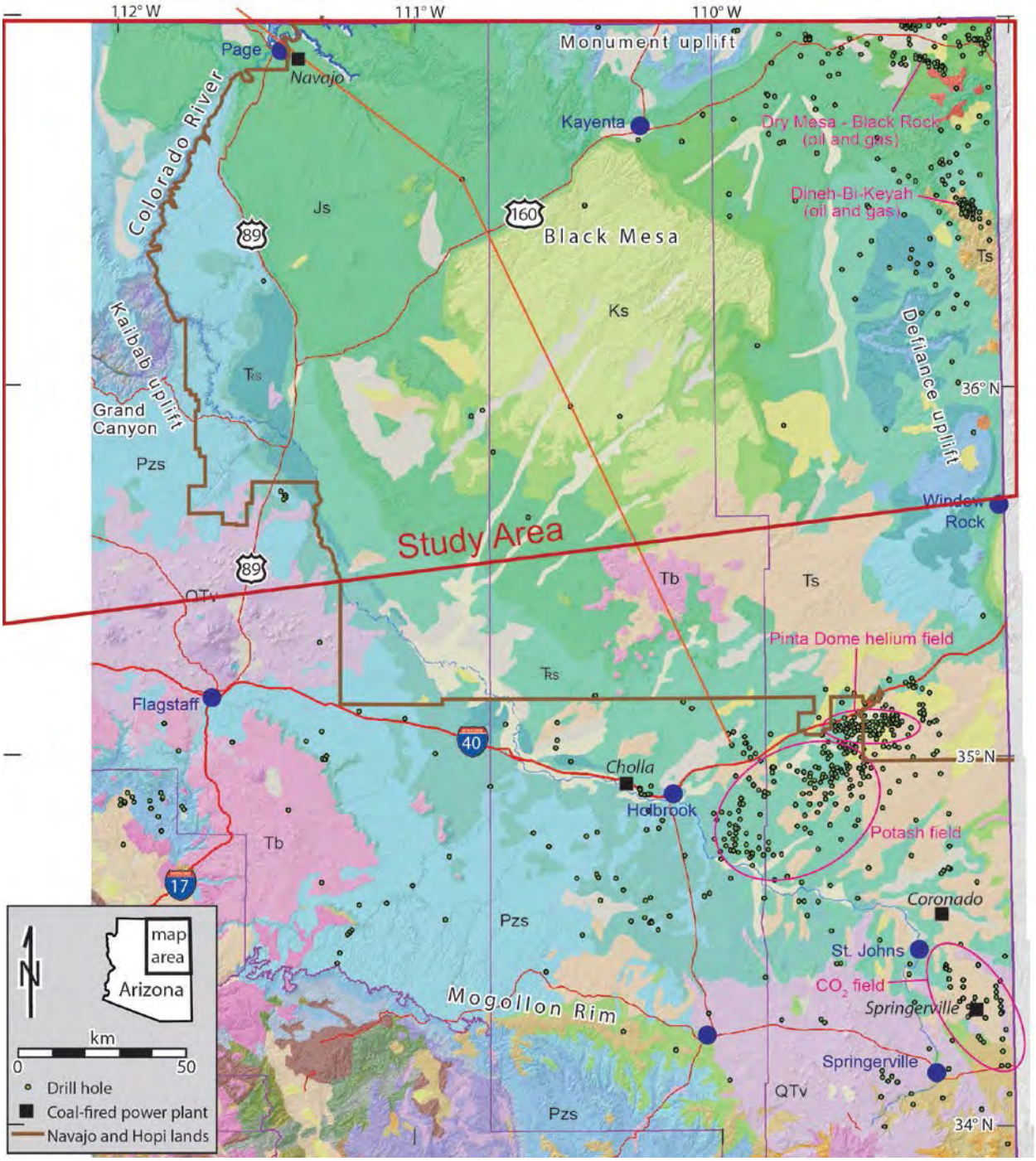


Figure 1. *Map of the study area in northeastern Arizona. Colors represent rock units exposed at the surface and were derived from the geologic map of Arizona (Richard et al., 2000). Location of cross section is also shown (see Appendix A for cross section). Large blue dots represent towns. The "CO_2 field" around Springerville is under consideration for CO_2 production for use in secondary oil recovery in west Texas. Map units include Pzs – Paleozoic sedimentary rocks; Trs – Triassic sedimentary rocks; Js – Jurassic sedimentary rocks; Ks – Cretaceous sedimentary rocks, Ts – Tertiary sedimentary rocks; Tb – Tertiary basalt; QTv – Quaternary and Tertiary volcanic rocks, undivided.*

Paleozoic Cedar Mesa Sandstone on the Colorado Plateau in Arizona

The Colorado Plateau in Arizona, Utah, New Mexico, and Colorado is characterized by flat-lying to gently dipping, locally gently folded Paleozoic and Mesozoic strata. These strata are most spectacularly revealed where dissected by the Colorado River in Grand Canyon or exposed in Monument Valley in northeastern Arizona. Areas surrounding the Colorado Plateau contain a similar sequence of Paleozoic strata but are more severely affected by Mesozoic and Cenozoic magmatism, folding, faulting, and erosion.

Paleozoic strata of the Colorado Plateau were deposited on the North American craton, an area of much older igneous and metamorphic rocks that had been beveled to a fairly flat surface during hundreds of millions of years of Proterozoic weathering without mountain building. Because of minimal Paleozoic igneous and tectonic activity in the American Southwest, Paleozoic sandstones are generally quartzose, with rounded quartz grains, and lack much of the fine clay and silt that would clog pore spaces in less mature sandstones (e.g., Sloss, 1988; Blakey and Knepp, 1989). As a result, Paleozoic Plateau sands are generally porous and permeable, and an obvious target for studies of CO_2 sequestration potential.

The study area is centered on Black Mesa Basin and the area to the northwest around the town of Page (Fig. 1). The Permian Cedar Mesa Sandstone that is the focus of this study (Fig. 2) is not thicker in Black Mesa basin. Rather, the unit is deformed over a large area into an approximate bowl shape, with the most deeply buried strata beneath Black Mesa on the Navajo and Hopi Nations (Fig. 1). The greater burial depth of Paleozoic strata in Black Mesa basin results from the greater preserved stratigraphic thickness of Mesozoic strata that make up Black Mesa and immediately surrounding areas. The bowl-shaped basin is bounded to the north by the Monument uplift, to the west by the Kaibab uplift, to the east by the Defiance uplift, and to the south by the slightly upturned south rim of the Colorado Plateau that is known as the Mogollon Rim (Fig. 1). These uplifts are the result of faulting and folding during the latest Cretaceous and Paleogene Laramide orogeny. The greater depth of the Cedar Mesa Sandstone to the northwest of Black Mesa Basin is the result, in part, of thick preserved Jurassic and Triassic strata that extend into Utah north of Page.

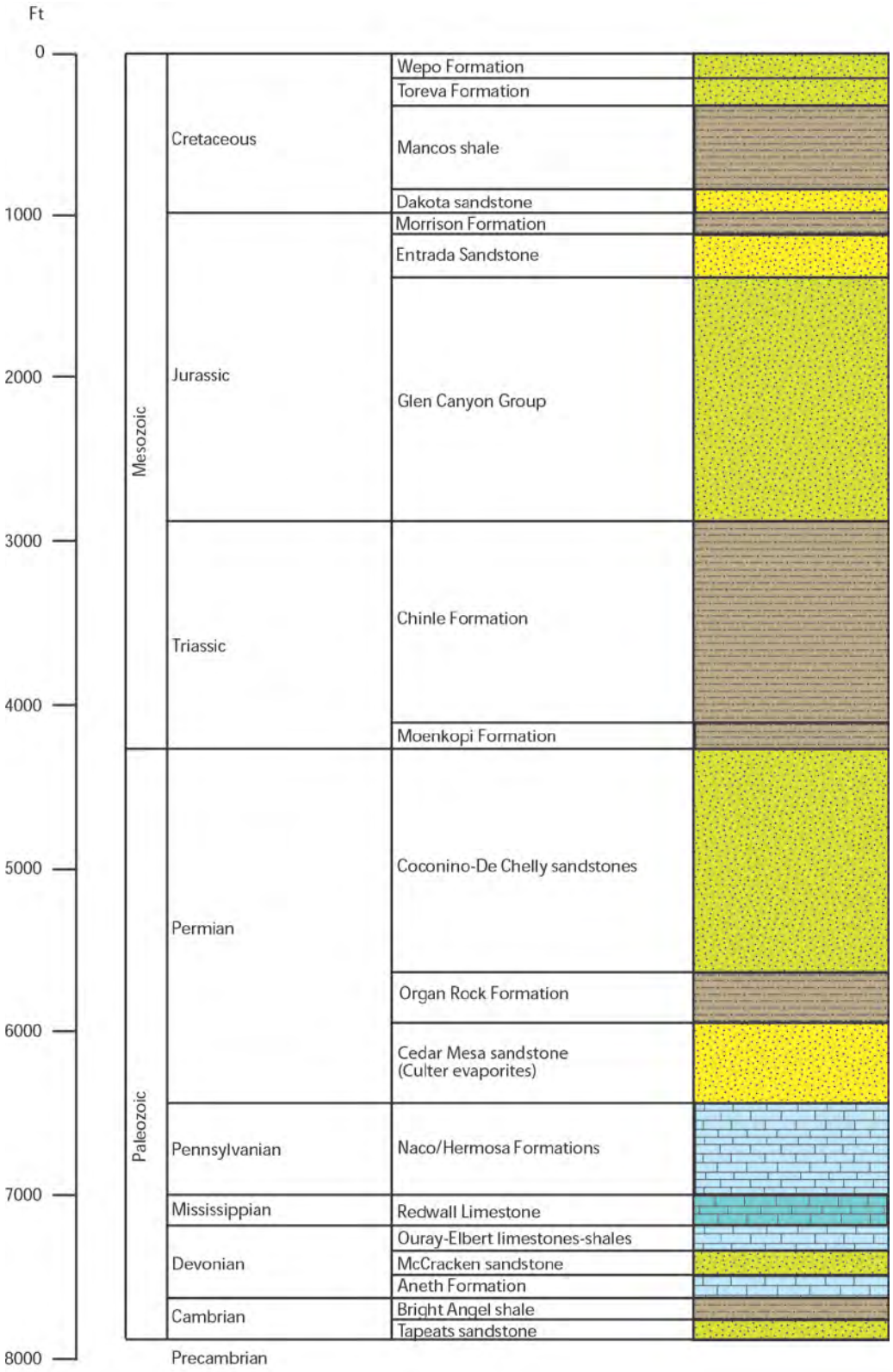


Figure 2. Stratigraphic column representing the Black Mesa and Four Corners areas. Yellow represents sandstone units under study for CO_2 sequestration potential.

Subsurface control is from 755 wells maintained on behalf of the AZOGCC at the AZGS. Depth, thickness, and porosity data are primarily from lithologic logs prepared by the American Stratigraphic Company (AmStrat). Approximate porosity indicated on the AmStrat logs represent visual examination of cuttings and core. AmStrat logs are available for most wells drilled in the 1970s and earlier. Some depth and thickness data are from formation tops reported on completion reports submitted by well operators. In some cases, depth correlations and estimates were picked by the authors in wells for which operator-identified tops or an AmStrat log were not available or where the authors disagreed with the operator or AmStrat picks. Well data used in the report are available online at the AZOGCC website at http://welldata.azogcc.az.gov/OilGasViewer.html.

Of the three units under study by RMCCS, only the Cedar Mesa Sandstone is present in the study area at depths greater than 3000 feet (915 meters). Depth and thickness contours are based on depth below the land surface at the location of the wells and are not based on depth relative to sea level or some other horizontal datum. For example, the Cedar Mesa Sandstone is deeper in the Black Mesa Basin because of the higher surface elevation of Black Mesa relative to the surrounding terrain in northeastern Arizona. Some of the locally isolated deep spots depicted on the depth maps represent wells that were drilled on topographically high buttes and mesas, which are common in northeastern Arizona.

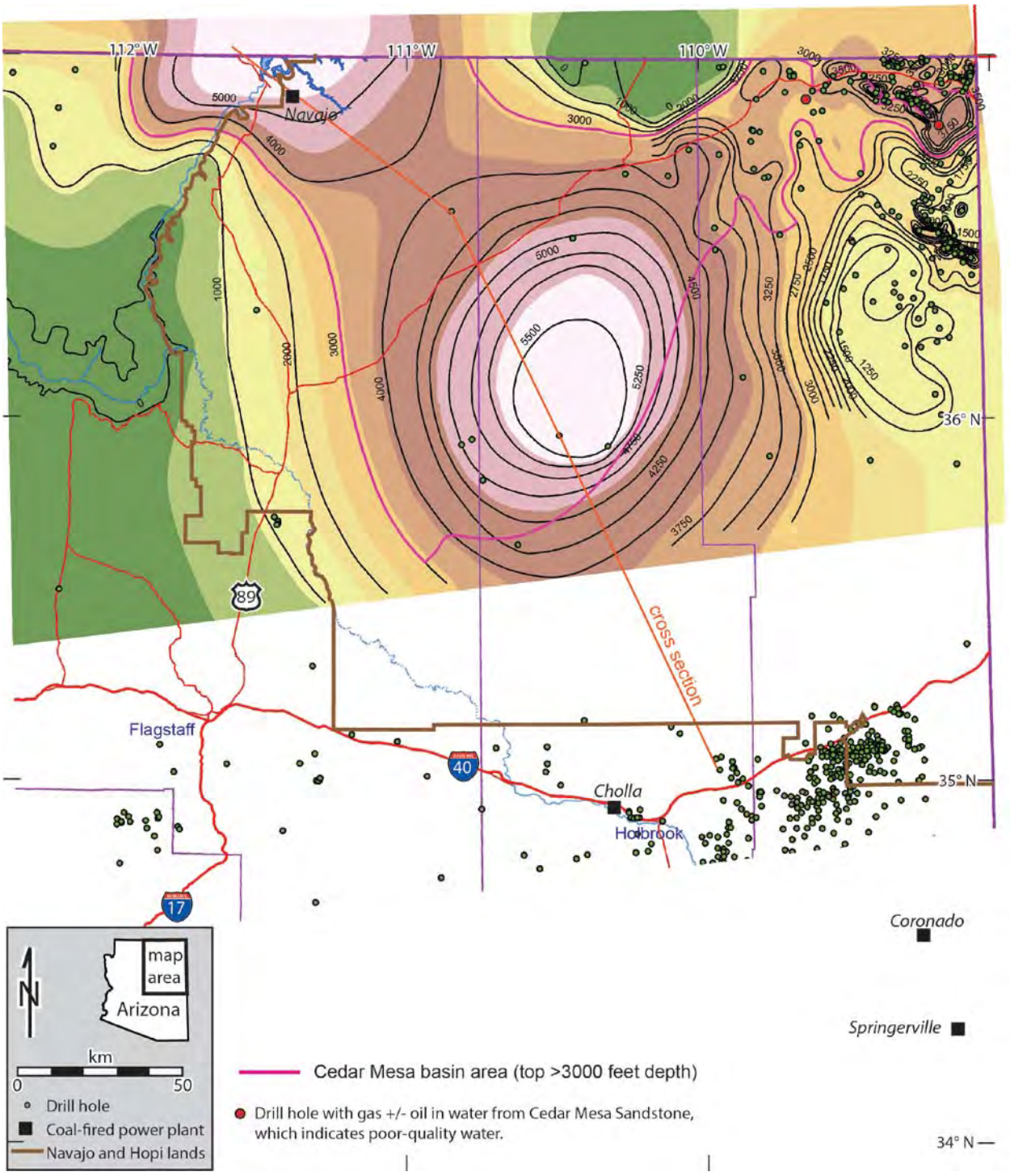
Sealing unit. The impermeable Permian Organ Rock Formation overlies the Cedar Mesa Sandstone (Fig. 2). The Organ Rock forms a distinctive redbed sequence that was deposited across all of northern Arizona (Blakey and Knepp, 1989). The Organ Rock Formation in the Sinclair Oil #1 Navajo well in Sec 28, T. 37 N., R. 14 E. is predominantly a tight, orange to brown very argillaceous, very fine grained sandy siltstone interbedded with thin shale. The shale is micaceous with limestone nodules. The Organ Rock Formation forms an effective seal directly above the Cedar Mesa Sandstone.

Formation fluid salinity. Salinity data are derived primarily from drill-stem tests or production data. Drill-stem tests are usually performed while the well is being drilled. Production data are obtained after a well is completed as a producing well. Salinity data from drill-stem tests are usually described qualitatively as “salt water”, “mud-cut salt water”, or in some instances “fresh water”. The Cedar Mesa Sandstone has not generally been the target of drilling for oil and gas exploration. As a result, only two wells in the far northeastern corner of Arizona have any data relevant to the composition of groundwater in the Cedar Mesa Sandstone. They indicate “gas-cut mud” and “slightly oil and gas cut mud.” The slight showings of hydrocarbons suggest that the formation waters in the Cedar Mesa Sandstone are not fresh because they yield minor showings of oil and gas.

Depth and thickness of the Cedar Mesa Sandstone. The Permian Cedar Mesa Sandstone pinches out to zero thickness southeastward under Black Mesa, but thickens northwestward toward the Paria Plateau west of Page where thickness is up to 700 feet (213 meters) at depths greater than 3000 feet (915 meters). The Cedar Mesa Sandstone is equivalent to the Weber Sandstone in northern Utah. To the west in the Grand Canyon region, the Cedar Mesa Sandstone is roughly equivalent to the Esplanade Member of the Supai Group. The Cedar Mesa Sandstone grades into an evaporite facies of the Cutler Group in northeastern Arizona across a line that extends generally from Flagstaff to the Four Corners. This line represents the zero thickness line on the isopach map (Fig. 5). Isolated sandbars embedded within the evaporite facies are present in northeastern Arizona north of the Defiance Uplift. These isolated sandbars provide an insignificant amount to the overall potential CO_2 sequestration capacity of the Cedar

Mesa Sandstone in Arizona. The Cedar Mesa has potential for CO_2 sequestration throughout a broad area below a depth of 3000 feet (915 meters) that extends northward from the Black Mesa Basin in Arizona to the Kaiparowits Basin in Utah and between Kaibab Uplift to the west and Monument Valley and Defiance Uplift to the east. The Cedar Mesa Sandstone is absent over much of the southern part of the study area. The Cedar Mesa Sandstone increases in thickness from zero in the Four Corners area and along the western margin of the Defiance Uplift to about 500 feet (152 meters) beneath the Navajo Generating Station near Page, Arizona. The unit is between 300 and 400 feet (91 and 122 meters) thick where it crops out as the Esplanade Sandstone in eastern Grand Canyon. The Cedar Mesa Sandstone attains localized thickness of up to 500 feet (152 meters) in isolated occurrences in the Four Corners area. Maps of the distribution, depth, and thickness of the Cedar Mesa Sandstone are shown in figures 3, 4, and 5, which also show drill holes. The cross section, represented by the orange line in the map figures, is shown in Appendix A.

Navajo Generating Station. The Navajo Generating Station (NGS) near Page is the recommended site in Arizona. The NGS is the largest coal-fired power plant and emitter of CO_2 (16 million metric tons in 2011) in Arizona. The Cedar Mesa Sandstone attains its maximum storage capacity of 138,409 metric tons per km^2 at 2% efficiency factor beneath the NGS as calculated in the EGI Storage Capacity Spreadsheet (Fig. 6). There are no deep exploratory wells in the immediate vicinity of the NGS. The depth and thickness estimates of the Cedar Mesa Sandstone beneath the NGS are based on regional hand contouring and projections from the Sinclair Oil 1 Navajo well in Arizona (Sec. 28, T. 37 N., R. 14 E.) and the Rangeland (Union Oil Company) 1 Judd Hollow well in Utah (Sec. 19, T. 43 S., R. 2 E.). The Sinclair and Rangeland wells lie approximately 38 miles southeast and 22 miles northwest of the NGS, respectively. A stratigraphic well is needed at the NGS site to determine the site-specific reservoir properties of the Cedar Mesa Sandstone and seal properties of the overlying Organ Rock Formation.



Figures 3. Depth contours (black numbered lines, in feet) represent the depth to the top of the Cedar Mesa Sandstone, and were derived from analysis of well logs. The color background maps are raster representations of the contoured surface created using ArcToolbox™ tools (see text) (color interval for raster colors is arbitrary). Magenta lines bounds areas where the top of the Cedar Mesa Sandstone is greater than 3000 feet (915 meters) deep or where the sandstone pinches out to zero thickness.

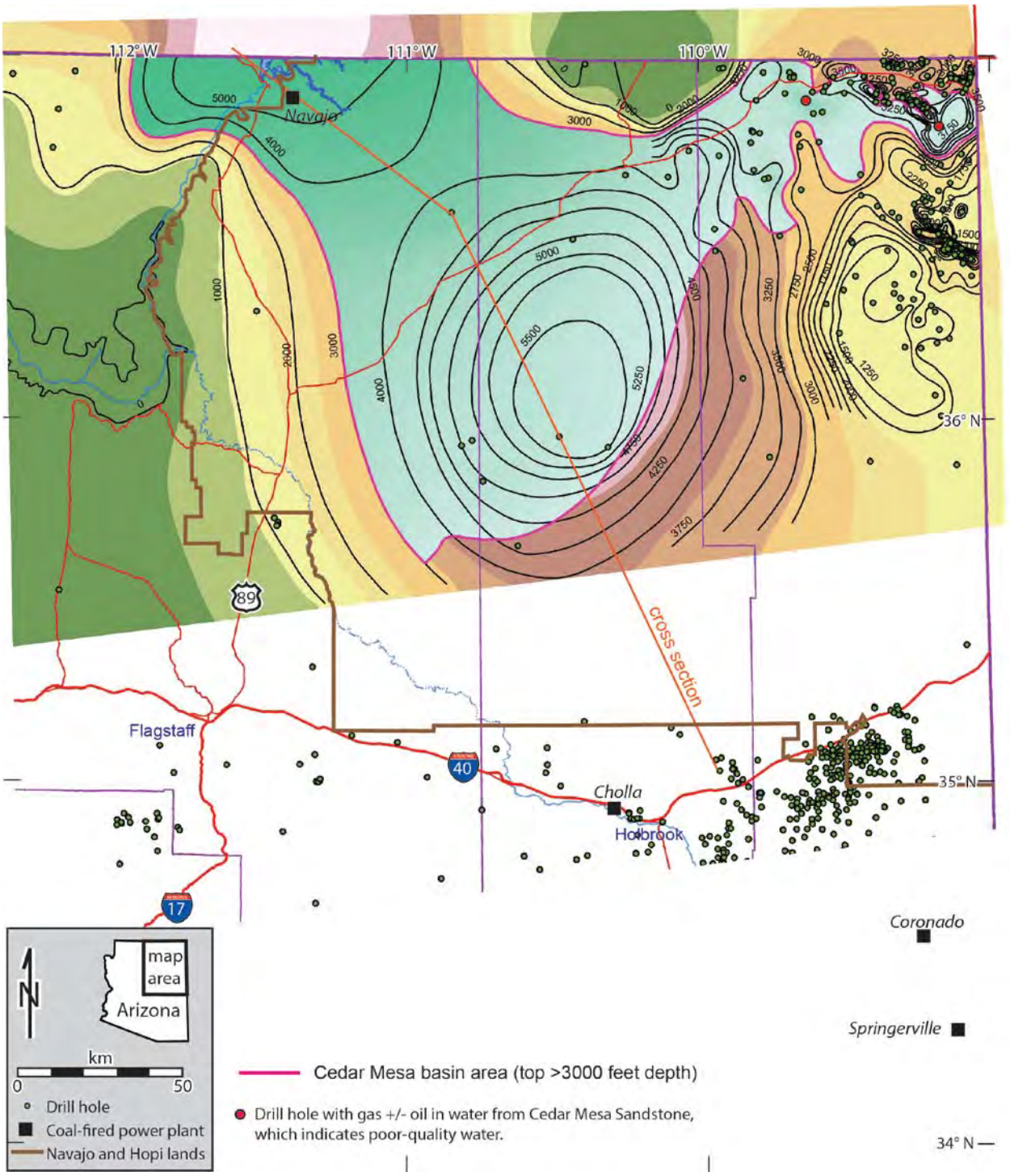


Figure 4. As in figure 3, but areas where the top of the Cedar Mesa Sandstone is below 3000 feet (915 meters) depth are colored green, with lighter green corresponding to areas where the sandstone is thinner. Depth contours are in feet.

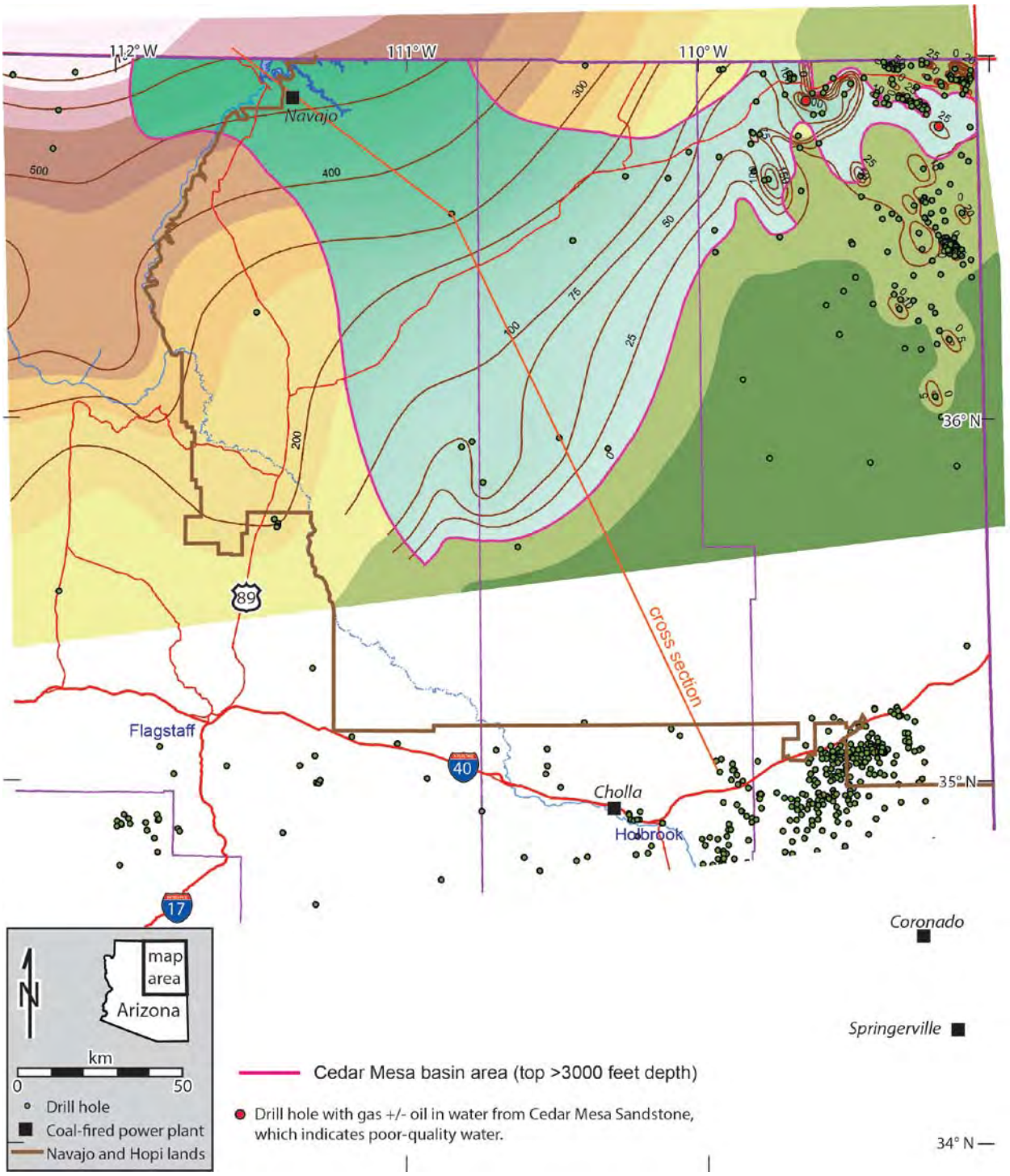


Figure 5. As in figures 3 and 4, but contours and color raster background maps represent sandstone unit thickness rather than depth (in feet). The color raster background maps represent the thickness of the Cedar Mesa Sandstone as derived from the contour map using ArcToolbox™ tools (see text) (color interval for raster colors is arbitrary). Areas where the top of the Cedar Mesa Sandstone is below 3000 feet (915 meters) depth are colored green, with lighter green corresponding to areas where the sandstone is thinner. Sandstone volume was calculated for this raster using ArcToolbox™ tools (see text and tables).

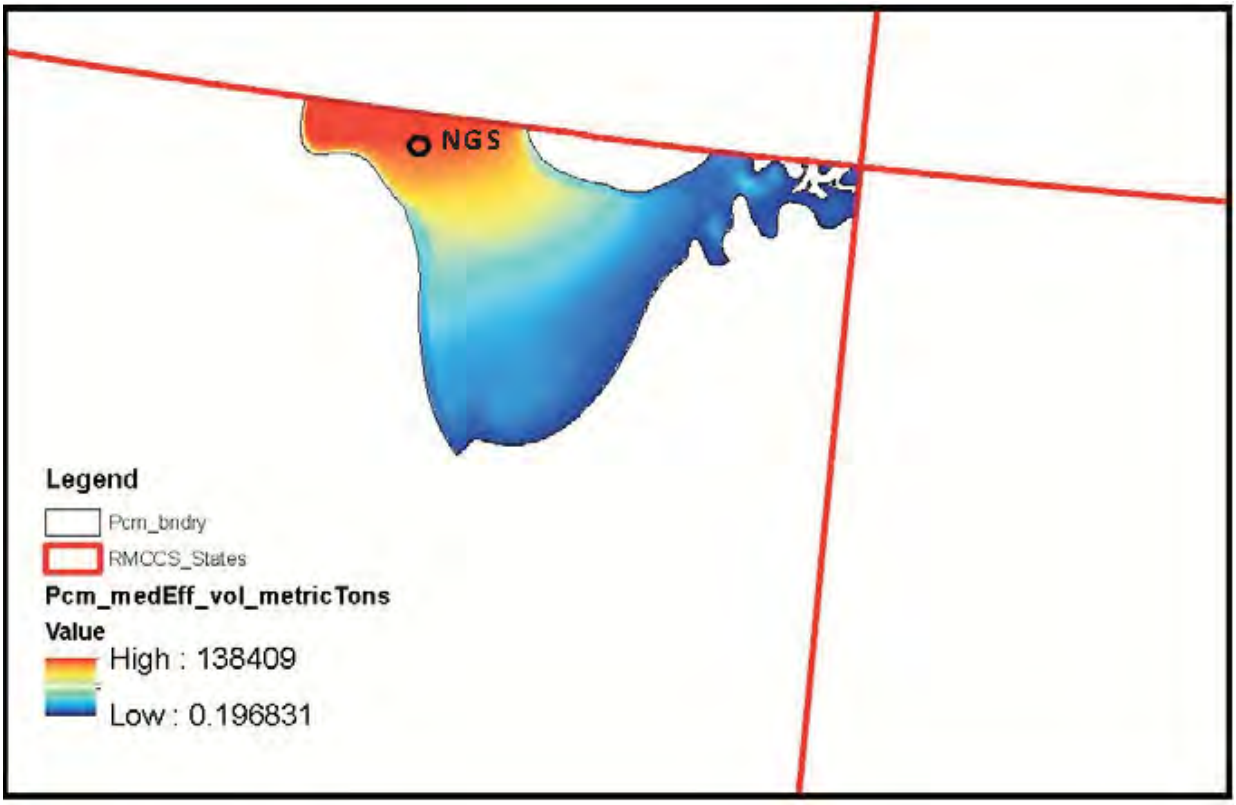


Figure 6. Map showing a CO_2 storage capacity visualization of the Cedar Mesa Sandstone in Arizona as calculated in the EGI Storage Capacity Spreadsheet. Units are in metric tons per km^2 raster cell using an average porosity of 4.62% and medium efficiency volume of 2%. The values range from a high of 138,409 metric tons per km^2 to a low of 0.2 metric tons per km^2. Note that the highest storage capacity occurs beneath the Navajo Generating Station (NGS). Pcm_bndy shows where the top of the Cedar Mesa Sandstone is below a depth of 3000 feet. Input parameters for the capacity visualization included depth (ft), thickness (ft), reservoir temperature (F), porosity (%), pore volume (m^3), and CO_2 density (kg/m^3).

Sandstone-volume calculations - procedure

The volume Cedar Mesa Sandstone in areas where the top of the formation is >3000 feet (>915 meters) deep was determined using ESRI® ArcMap™ version 10 software. Some of this procedure followed specifications required by the RMCCS program coordinators.

(1) Contours. Well logs from a database of 755 Arizona oil and gas exploration drill holes were used to identify the depth to the stratigraphic top and base of Colorado Plateau sandstone units. Contour maps were drafted by hand (by Steve Rauzi) for formation tops and thicknesses (in feet), and then each was digitized to create a shape file with depth and thickness in feet (as text values) and in meters (as numeric values calculated from values in feet). These digitized contour maps were created in the geographic coordinate system (GCS) "North American 1983" using projection NAD83, zone 12. The Cedar Mesa Sandstone contours were used for this study. Other formations were evaluated earlier using similar methodology (Rauzi and Spencer, 2012). Digital manipulations and calculations listed below were done by J. Spencer.

(2) Coordinate system transformation. Contour maps were transformed to the geographic coordinate system (GCS) WGS_1984 with a Lambert Azimuthal Equal Area projection, as required for the NATCARB Atlas geodatabase, with the following procedure.

The "Project" tool in the "Feature" toolset in the "Projections and Transformations" toolbox in the "Data Management Tools" in ArcMap v. 10.0 was opened. The "Input Dataset or Feature Class" is the original (NAD 83) shape file. A folder was created for the transformed shape files (in ArcCatalog) and used for the "Output Dataset of Feature Class" (ArcMap defaulted to the RMCCS_saline data.gdb for the output feature class, but then would fail to create the file if this default option was not changed). For "Output Coordinate System" select "Import", then navigate to one of the feature classes in the RMCCS_saline geodatabase and select it. That should fill in "Details" window with the following information:

Projection: Lambert_Azimuthal_Equal_Area
False_Easting: 0.000000
False_Northing: 0.000000
Central_Meridian: -100.000000
Latitude_Of_Origin: 45.000000
Linear Unit: Meter (1.000000)
Geographic Coordinate System: GCS_WGS_1984
Angular Unit: Degree (0.0174532925199433299)
Prime Meridian: Greenwich (0.000000000000000000)
Datum: D_WGS_1984
Spheroid: WGS_1984
Semimajor Axis: 6378137.000000000000000000
Semiminor Axis: 6356752.314245179300000000
Inverse Flattening: 298.257223563000030000

It was necessary to add a "Geographic Transformation" which is supposed to be optional. However, reprojection was not possible without selecting one of the Transformations. According to the help menu for "Project (Data Management)", the "Geographic Transformation" corresponds to a "transform_method", with the following information:

This method can be used for converting data between two geographic coordinate systems or datums. This initially optional parameter may be required if the input and output coordinate systems have different data.

The ArcGIS help topic "Choosing an appropriate transformation" states the following:

Converting between NAD 1983 and WGS 1984

Originally, NAD 1983 and WGS 1984 were considered coincident. To minimize coordinate changes, NAD 1983 is tied to the North American and Pacific (for Hawaii, and so on) plates. WGS 1984 is tied to the International Terrestrial Reference System (ITRF), which is independent of the tectonic plates. Over time, the two coordinate systems have become increasingly different.

NAD_1983_To_WGS_1984_1: Published accuracy from EPSG is 2 meters. This transformation applies to the entire North American continent. This transformation uses the geocentric translation method, with the transformation's parameters (dx, dy, and dz) all equal to zeroes. This transformation treats the NAD 1983 and WGS 1984 datums as though they are equivalent.

"NAD_1983_To_WGS_1984_1" was used to transform Arizona data.

(3) Contour-to-raster conversion. In a raster representation of a contour map, a surface is constructed that interpolates between contours. The surface is represented by a grid of regularly spaced points, each of which has an assigned value based on the interpolation between contours. The depth and thickness contour maps were used to build raster representations of Cedar Mesa unit-top depth and unit thickness using the "Topo to Raster" tool in the "Raster Interpolation" tool set in the "3D Analyst Tools" in ArcToolbox. To do this, each contour dataset was dragged (using the computer mouse) from the table of contents in the ArcMap project to the top line in the "Topo to Raster" tool. The "field" to represent was set to "ThicknessM" or "DepthMeter" (this must be a numeric field that indicates contour depth or thickness, here in meters). Output surface raster file name and path were specified, and output cell size was set to 1000 meters. "Output extent (optional)" was specified as using the same extent as the input contour shape file for thickness, and to the thickness contour shape file for depth so that the extent would be the same for both resultant raster files. "Drainage enforcement" was set to "NO_ENFORCE" because the contour map does not represent a landscape. The "Environments" button at the bottom of the "Topo to Raster" tool window was then used to open the "Environment Settings" window. To create a raster with raster points that are spatially coincident with the "RMCCS_1K" 1-km grid raster, the "Processing Extent" option was opened and the "Snap Raster" was identified as "RMCCS_1K" by navigating to that feature and selecting it. Also, under "Processing Extent", the input contour file was selected (this might be redundant with the "Output extent (optional)" setting as specified in the "Topo to Raster" tool).

For the Cedar Mesa thickness-raster construction, the zero-depth line was deleted from the thickness contour map where that line is due to modern erosional removal rather than subsurface thickness changes. The areas of thickness interpolation (especially across Grand Canyon) where Cedar Mesa Sandstone is absent are ultimately irrelevant to later volume calculations because these calculations were done only for areas where the sandstone is present at significant depth. (Also, it was not necessary to calculate depth by subtracting the elevation of the formation top from surface elevation because, from the start, depth represented depth below the surface and not elevation as would be the case for a structure-contour map.)

(4) Basin area below 3000 feet (915 meters) depth and thickness-raster subset. The basin area for calculation of basin sequestration volume is the area where the top of the Cedar Mesa Sandstone is below 3000 feet (915 meters) depth, the unit has greater-than-zero thickness, and the unit is within Arizona. A single closed loop, as a feature in a shape file, was created from a copy of the 3000 foot depth contour, which was cut where it crossed the Arizona state border or the zero thickness contour, and then extended along the zero thickness contour and state border until a single closed loop was created that outlined the Cedar Mesa calculation area. The loop was then converted to a polygon using the "Feature to Polygon" tool in the "Features" tool set in the "Data Management Tools" in ArcToolbox.

The polygon was then used to extract a subset of the thickness raster for the purpose of calculating volume. This was done using the "Extract by mask" tool of the "Extraction" tool set within the "Spatial Analyst" toolbox (output file named "thick3000"). For the RMCCS multistate CO_2 sequestration atlas, this same procedure was then done for the depth raster (output file named "depth3000") so that two rasters would exist, one for thickness and one for depth, of identical areas with identical coordinates for the raster cells. (For calculations presented in the rest of this paper that were not done only for the RMCCS atlas, a very slightly corrected raster area was used, with outputs named "thick3000B" and "depth3000B".)

(5) Joined table with xy coordinates (done only for the RMCCS multistate CO_2 sequestration atlas). Depth and thickness raster data (in two .shp files but referred to as "raster datasets" or "raster layers") were merged into a single feature class (also with a .shp file extension but referred to as a "point feature class" in the ArcMap Help menu under "raster to point") with xy coordinates. This was done in three steps: (1) The raster point data were converted using the "Raster to Point" tool in the "From Raster" toolset in the "Conversion Tools" in ArcToolbox. (2) The two resulting point-data datasets were then merged into a single point feature class using the "Spatial Join" tool in the "Overlay" toolset in the "Analysis Tools" in ArcToolbox. (3) To add coordinate data to the table of points, we used the "Add XY Coordinates" tool in the "Features" toolset in the "Data Management Tools" in ArcToolbox. This tool was used on the joined table created in the previous step to create two new fields populated with coordinate data.

(6) Export to Excel (done only for the RMCCS multistate CO_2 sequestration atlas). The joined table with xy data was opened in ArcMap. The pull-down menu associated with the upper left button ("Table Options") at the top of the table includes "Export". Selecting this option allows export of the joined table with xy data to be exported as a .txt file to any specified folder. The table was then opened in Excel, saved as an Excel file, and sent to the RMCCS group at the University of Utah for further calculations in the EGI Storage Capacity Spreadsheet.

(7) Calculation of Cedar Mesa volume below 3000 feet (915 meters) depth (done for AZGS, not for atlas). The Cedar Mesa thickness raster produced in step 4 above was then used to calculate basin volume below 3000 feet (915 meters) depth using the "Surface volume" tool from the "Functional surface" tool set in the "3D Analyst" toolbox. "Plane Height" was set to zero so that, if all thicknesses in the raster are greater than zero by a finite amount (i.e., every raster cell has thickness greater than zero), a reduced volume is not erroneously produced. The resulting table output data was entered in an Excel spreadsheet (Table 1), with similar data for the De Chelly Sandstone that was evaluated earlier for minimum depth of 800 meters (2624 feet) (Rauzi and Spencer, 2012).

CO_2 Storage Capacity

The estimated mass of CO_2 (G_{CO2}) that could be stored in a sandstone unit is calculated with the following equation (from Litynski et al., 2010):

$$G_{CO2} = A_t \, h_g \, \phi_{total} \, \rho \, E_{saline} \qquad (1)$$

where A_t is the total area in which the top of the saline formation is below 915m depth, h_g is the gross formation thickness, ϕ_{total} is the total porosity, ρ is the average density of CO_2 at the depths and temperatures that characterize the formation, and E_{saline} is the storage efficiency factor that represents the fraction of the total pore space that potentially will be occupied by stored CO_2. The ArcMap calculations presented in Table 1 represent formation volume with greater accuracy than formation volume calculated by simply multiplying total area A_t by gross thickness h_g because the ArcMap calculations account for lateral changes in thickness.

Formation porosities were estimated by well loggers based on examination of drill cuttings from 79 drill holes that penetrated at least part of the Cedar Mesa Sandstone. The total porosity (ϕ_{total}) and standard deviation were determined for the sandstone (Table 2). High porosity is given at the one standard deviation level above the mean, but this was unreasonably low for the deviation below the mean due to the skewed distribution of porosity determination. Instead, we considered a porosity of 3% as the low estimate because 66 of 79 measurements indicated porosity of 3% or higher. Low, middle, and high values for total pore volume were

then calculated for the Cedar Mesa Sandstone and compared to other Paleozoic sandstone unit volumes calculated previously (Table 2, last three columns).

The capacity of sandstone to store CO_2 is not equivalent to its pore volume because not all pore space is accessible to an injected fluid. The storage efficiency of a saline formation (E_{saline}), which is the fraction of pore space that is actually accessible to injected CO_2, is calculated from the following equation (Litynski et al., 2010):

$$E_{saline} = E_{An/At}\, E_{hn/hg}\, E_{\phi e/\phi tot}\, E_v\, E_d \quad (2)$$

$E_{An/At}$ and $E_{hn/hg}$ are the fractions of areal extent and thickness, respectively, that have suitable physical properties for CO_2 sequestration. $E_{\phi e/\phi tot}$ is the fraction of total pore space that is interconnected and so is amenable to CO_2 sequestration. E_v represents barriers to displacement of CO_2 into formation volume, and includes such barriers as fault zones. E_d represents microscopic barriers to CO_2 movement into all pore space and includes molecular adhesion (wetting) of saline solutions to sand grains in which the saline fluids are not displaced by CO_2 influx. Storage efficiencies derived from studies of CO_2 injection into oil and gas reservoirs, and estimated by numerical simulation, are 0.51% to 5.4% for clastic rocks, with a mean value of 2.0% (Table 7 *in* Litynski et al., 2010). The low and high values are calculated to represent the 10% and 90% probability values.

Estimates of the mass of CO_2 that can be stored in a given pore-space volume require an estimate of the density of stored CO_2, which depends on temperature and pressure. Subsurface temperatures beneath the Colorado Plateau as measured in 430 drill holes were used to calculate average surface temperature and geothermal gradient (Fig. 7). This yielded a surface temperature of 23.57°C and a gradient of $0.0134h$ where h is depth in meters and gradient is given in degrees C per meter depth. Using this data set in this manner is somewhat problematic because data generally were collected during drilling operations and not after an extended period (5-15 days) of inactivity. Circulating drilling fluids carry cold fluids down and bring heat back up, which decreases bottom-hole temperature. Because of variability in the time between cessation of drill-fluid circulation and down-hole temperature measurement, some measured temperatures were possibly artificially depressed and others were not. As a result, geothermal gradient is probably slightly underestimated, and scatter in measured temperatures is increased. The significance of this bias toward low temperatures is not well known, but inasmuch as it is reflected in increased scatter in temperature measurements, it does not appear to be large. Especially telling in this regard is the fact that temperatures measured at greater depth do not show greater scatter, as would be expected for greater heat loss to drill fluids for deeper wells with greater down-hole temperatures (Fig. 7).

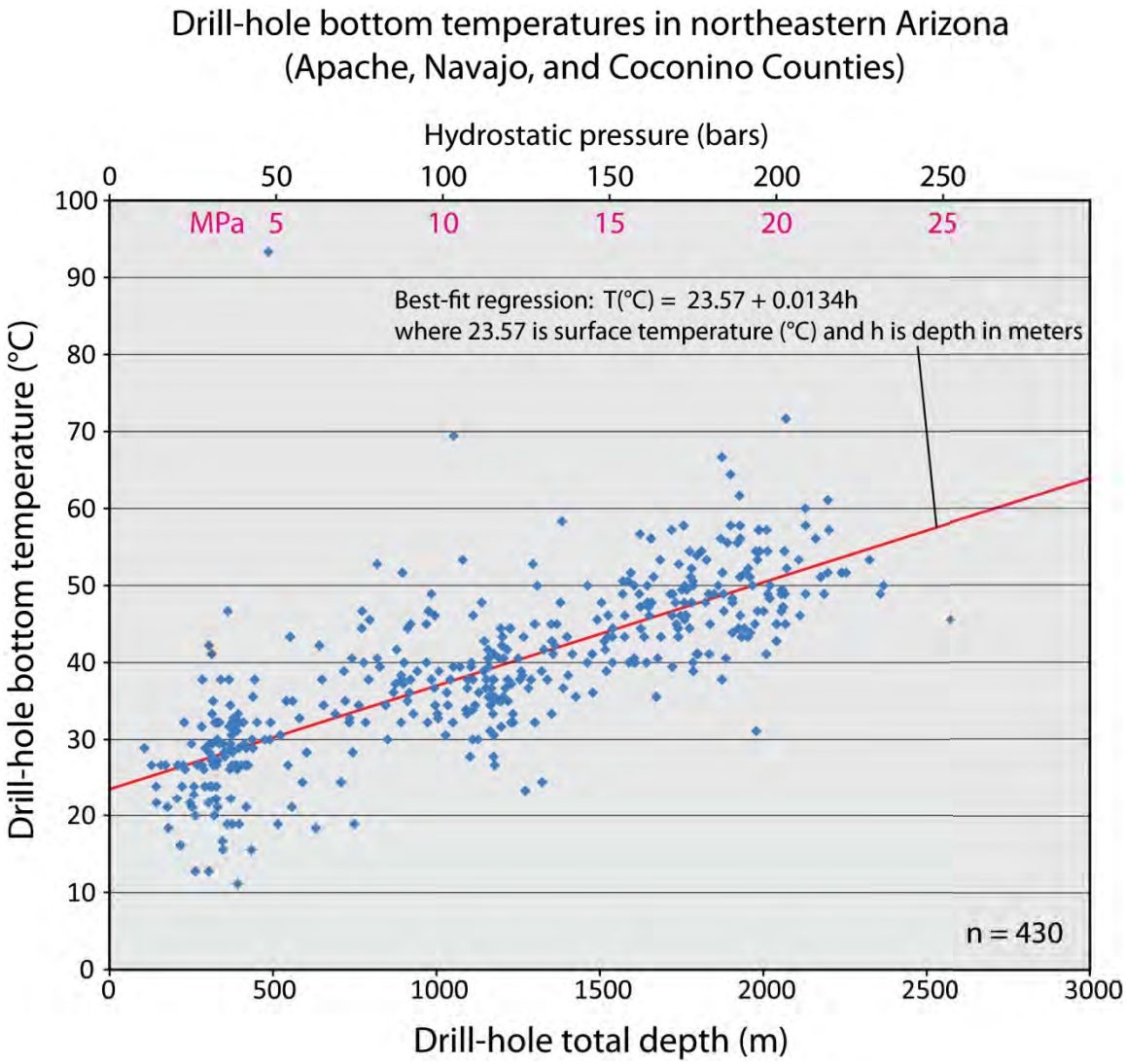


Figure 7. Drill-hole bottom temperatures from 430 bore holes in northeastern Arizona.

The calculated temperature gradient was used to estimate subsurface temperatures beneath the Colorado Plateau. Hydrostatic pressure (the weight of a column of water extending upward to the surface) is assumed for conditions of CO_2 storage (Bachu, 2003). Using a hydrostatic pressure gradient and a temperature gradient as described above, CO_2 density was calculated by plotting P-T conditions for a range of depths as shown on Figure 8. Each blue dot represents hydrostatic pressure at depths represented by the numbers (in km) associated with each dot. The horizontal position of each dot is determined by the calculated temperature at each depth. CO_2 density at 3000 feet (915 meters) depth is estimated from the graph at 750 kg/m^3. This value was used to calculate CO_2 storage capacity for Colorado Plateau sandstone units (Table 3). Most of the volume under consideration for CO_2 storage is deeper, however, reaching depths of over 5000 feet (1524 meters) in a large area near the Navajo Generating Station near Page (Figs. 3, 4) where thickness is several hundred feet (Fig. 5). Our median estimate using ArcMap tools of the mass of CO_2 that can be stored in the Cedar Mesa Sandstone in the Arizona part of the Colorado Plateau is 0.69 billion tonnes, with low and high estimates of 0.114 and 3.24

billion tonnes, respectively (a "tonne" is a metric ton, equivalent to 1000 kg). Median estimate from the EGI Storage Capacity Spreadsheet of the mass of CO_2 that can be stored in the Cedar Mesa Sandstone in the Arizona part of the Colorado Plateau is 0.66 billion tonnes, with low and high estimates of 0.168 and 1.78 billion tonnes, respectively (Table 3). The difference in median capacity values may be due, at least in part, to the use of a CO_2 density calculation procedure that accounts for variation in depth to formation top, and hence ambient pressure, in the EGI Storage Capacity Spreadsheet. The difference in low and high capacity estimates, with a greater range of values determined by the AZGS estimate, is apparently due to the fact that AZGS estimates included low and high estimates of porosity (Table 2). The median estimate from the EGI Storage Capacity Spreadsheet of the mass of CO_2 that can be stored in the De Chelly Sandstone in the Arizona part of the Colorado Plateau is 7.1 billion tonnes (Table 3).

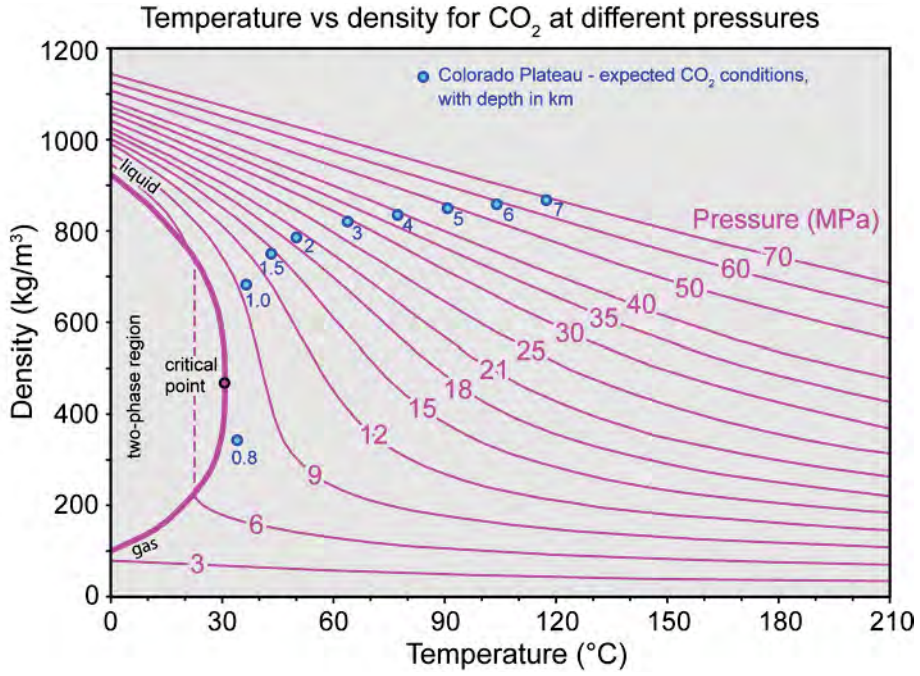


Figure 8. Temperature and density of CO_2 are plotted for a range of pressures represented by the magenta isopressure lines. For appropriate pressure, and temperature below that of the critical point, CO_2 coexists as both a gas and a liquid. To identify density conditions of CO_2 stored in sandstone units beneath the Colorado Plateau, a range of pressure and temperature conditions were evaluated, as follows. For each storage depth, a temperature was calculated from the regression line in Figure 7, and a value for hydrostatic pressure was calculated. Each blue dot, representing a depth given by the number next to each dot, was located on this diagram by its temperature (horizontal position) and by the calculated hydrostatic pressure for each depth which was used to place the dot among the magenta isopressure lines (from Bachu, 2003). At pressure corresponding to depth less than 1 km, precise density is uncertain (for example, compare results plotted here [derived from Bachu, 2003] with those from an online CO_2 density calculator at http://www.peacesoftware.de/einigewerte/co2_e.html).

Conclusion

We calculate that the Cedar Mesa Sandstone has the capacity to store approximately 0.69 billion tonnes of CO_2, which is more than for any of the other Paleozoic sandstone units on the Colorado Plateau except the De Chelly sandstone beneath Black Mesa Basin (median estimate of 7.3 billion tonnes, or ten times more; Rauzi and Spencer, 2012). However, it is not known if pore waters present in the Cedar Mesa Sandstone are saline. It seems likely that groundwater in the Cedar Mesa Sandstone is saltier than that in the De Chelly Sandstone simply because the Cedar Mesa Sandstone is more deeply buried, but this will not be known until drilling and testing are done.

References cited

Bachu, S., 2003, Screening and ranking of sedimentary basins for sequestration of CO_2 in geological media in response to climate change: Environmental Geology, v. 44, p. 277-289.

Blakey, R.C., and Knepp, R., 1989, Pennsylvanian and Permian geology of Arizona, *in* Jenny, J.P., and Reynolds, S.J., eds., Geologic evolution of Arizona: Arizona Geological Society Digest 17, p. 313-348.

Blakey, R.C., 1989, Triassic and Jurassic geology of the southern Colorado Plateau, *in* Jenny, J.P., and Reynolds, S.J., eds., Geologic evolution of Arizona: Arizona Geological Society Digest 17, p. 369-396.

Hereford, R., 1977, Deposition of the Tapeats Sandstone (Cambrian) in central Arizona: Geological Society of America Bulletin, v. 88, no. 2, p. 199-211.

Knight, R.L., and Cooper, J.R., 1955, Suggested changes in Devonian terminology in the Four Corners area, in Cooper, J.C., ed., Geology of parts of Paradox, Black Mesa, and San Juan Basins, Four Corners Field Conference: Four Corners Geological Society Guidebook, p. 56-58.

Lausen, C., and Wilson, E.D., 1925, Gold and copper deposits near Payson, Arizona: Arizona Bureau of Mines Bulletin no. 120, 44 p.

Litynski, J., Deel, D., Rodosta, T., Guthrie, G., Goodman, A, Hakala, A., Bromhal, G., and Frailey, S., 2010, Carbon sequestration atlas of the United States and Canada (Atlas III): U.S. Department of Energy, Office of Fossil Energy, National Energy Technology Laboratory (NETL), 3rd ed., Appendix B, p. 136-152.

Rauzi, S.L., and Spencer, J.E., 2012, An Evaluation of CO2 Sequestration Potential of Paleozoic Sandstone Units, Northeastern Arizona: Arizona Geological Survey Open File Report 12-10, 29 p., with appendix.

Richard, S.M., Reynolds, S.J., Spencer, J.E., and Pearthree, P.A., 2000, Geologic map of Arizona: Arizona Geological Survey Map 35, scale 1:1,000,000.

Sloss, L.L., 1988, Tectonic evolution of the craton in Phanerozoic time, *in* Sloss, L.L., ed., Sedimentary Cover - North American craton: Geological Society of America DNAG v. D-2, p. 25-51.

Teichert, C., 1965, Devonian rocks and paleogeography of central Arizona: U.S. Geological Survey Professional Paper 464, 181 p.

U.S. Department of Energy, 2010, Carbon sequestration atlas of the United States and Canada (Atlas III): U.S. Department of Energy, Office of Fossil Energy, National Energy Technology Laboratory (NETL), 3rd ed., 160 p.

Table 1. ArcMap-calculated volume and area of two Paleozoic sandstone units on the Colorado Plateau in Arizona*

Basin and unit	Dataset	Plane Height	Reference	Z Factor	2D Area (m^2)	3D Area (m^2)	Volume (m^3)	2D area (km^2)	Volume (km^3)	Minimum depth
De Chelly main	..ateau2012_2\Rasters\dech_main2	0	ABOVE	1	10133348856	10133429005	3.39325E+12	10133	3393	800 m
Cedar Mesa	..GS_Atlas\ShapeFiles\thick3000B	0	ABOVE	1	16640926196	16640951452	9.93947E+11	16641	994	914 m (3000 ft)

*For depth below threshold indicated in last column

Table 2. Porosity and pore volume for two Paleozoic sandstone units on the Colorado Plateau in Arizona

Basin and unit	Area (km^2)	Volume (km^3)	Porosity low (%)*	Porosity mean (%)	Porosity high (%)*	Pore volume low (km^3)	Pore volume mean (km^3)	Pore volume high (km^3)
De Chelly main	10133	3393	9.3	14.3	19.3	315.57	485.23	654.90
Cedar Mesa	16818	994	3	4.62	8.04	29.82	45.92	79.91

*De Chelly Sandstone (n=184): Porosity range is +/- one standard deviation

Table 3. CO_2 storage capacity for two Paleozoic sandstone units on the Colorado Plateau in Arizona

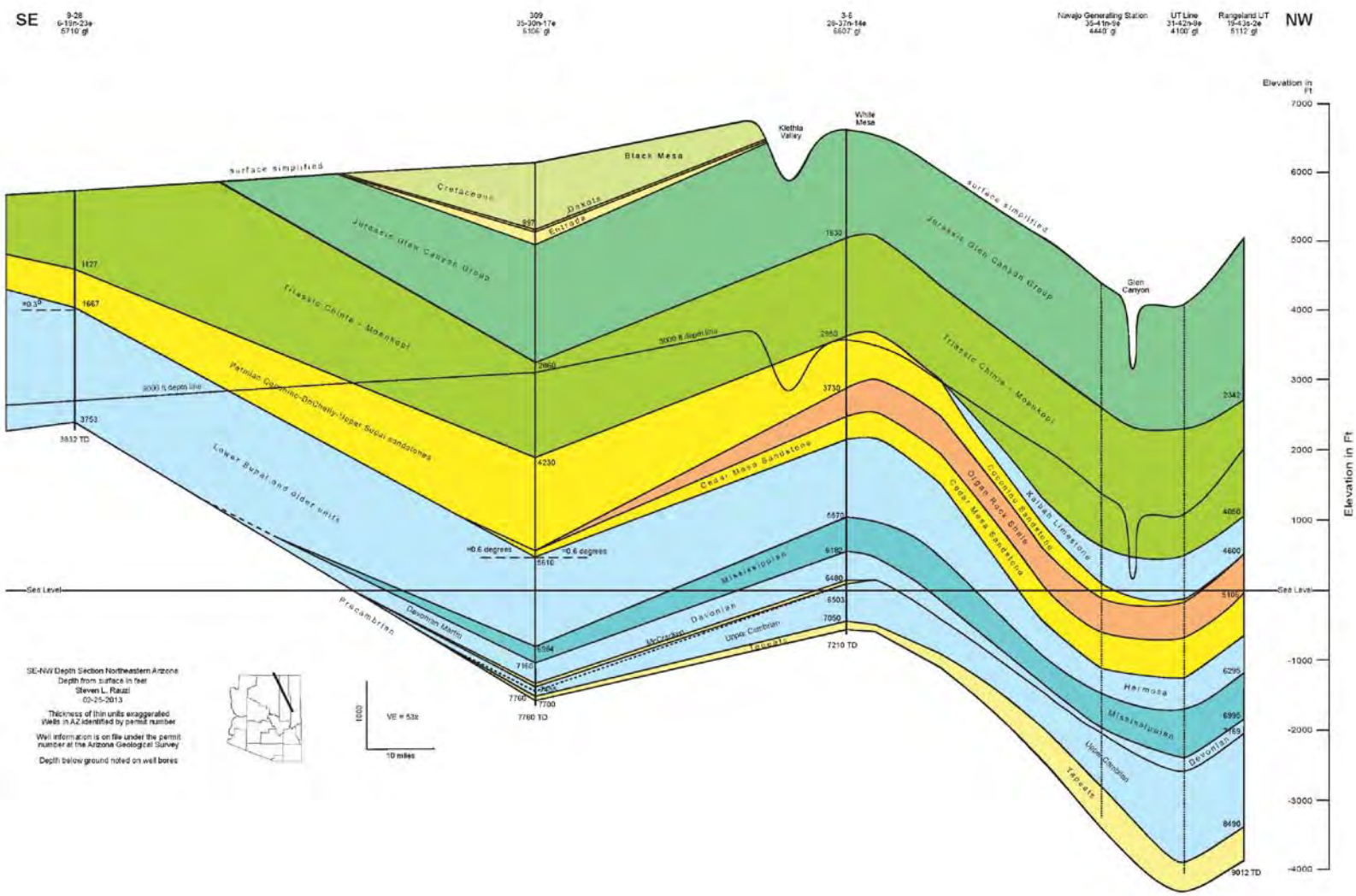
Sandstone unit and basin	Pore volume low (km^3)	Pore volume mean (km^3)	Pore volume high (km^3)	Storage efficiency, low*	Storage efficiency, median*	Storage efficiency, high*	Effective pore volume, low (km^3)	Effective pore volume, median (km^3)	Effective pore volume, high (km^3)	CO_2 density (kg/m^3)	AZGS ArcMap Potential mass of stored CO_2 (tonnes), low**	EGI Storage Capacity Spreadsheet Potential mass of stored CO_2 (tonnes), low**	AZGS ArcMap Potential mass of stored CO_2 (tonnes), median**	EGI Storage Capacity Spreadsheet Potential mass of stored CO_2 (tonnes), median**	AZGS ArcMap Potential mass of stored CO_2 (tonnes), high**	EGI Storage Capacity Spreadsheet Potential mass of stored CO_2 (tonnes), high**
De Chelly main	315.57	485.23	654.90	0.0051	0.02	0.054	1.6	9.7	35.4	750	1.2071.E+09	1.8207.E+09	7.2785.E+09	7.1401.E+09	2.6523.E+10	1.9278.E+10
Cedar Mesa***	29.82	45.92	79.91	0.0051	0.02	0.054	0.152	0.92	4.32	750	1.1406.E+08	1.6810.E+08	6.8881.E+08	6.5921.E+08	3.2365.E+09	1.7799.E+09
										Total	1.32.E+09	1.99.E+09	7.97.E+09	7.80.E+09	2.98.E+10	2.11.E+10

*Values are approximations from various lithologies in the United States, as given by Litynski et al. (2010, p. 147, Table 7)

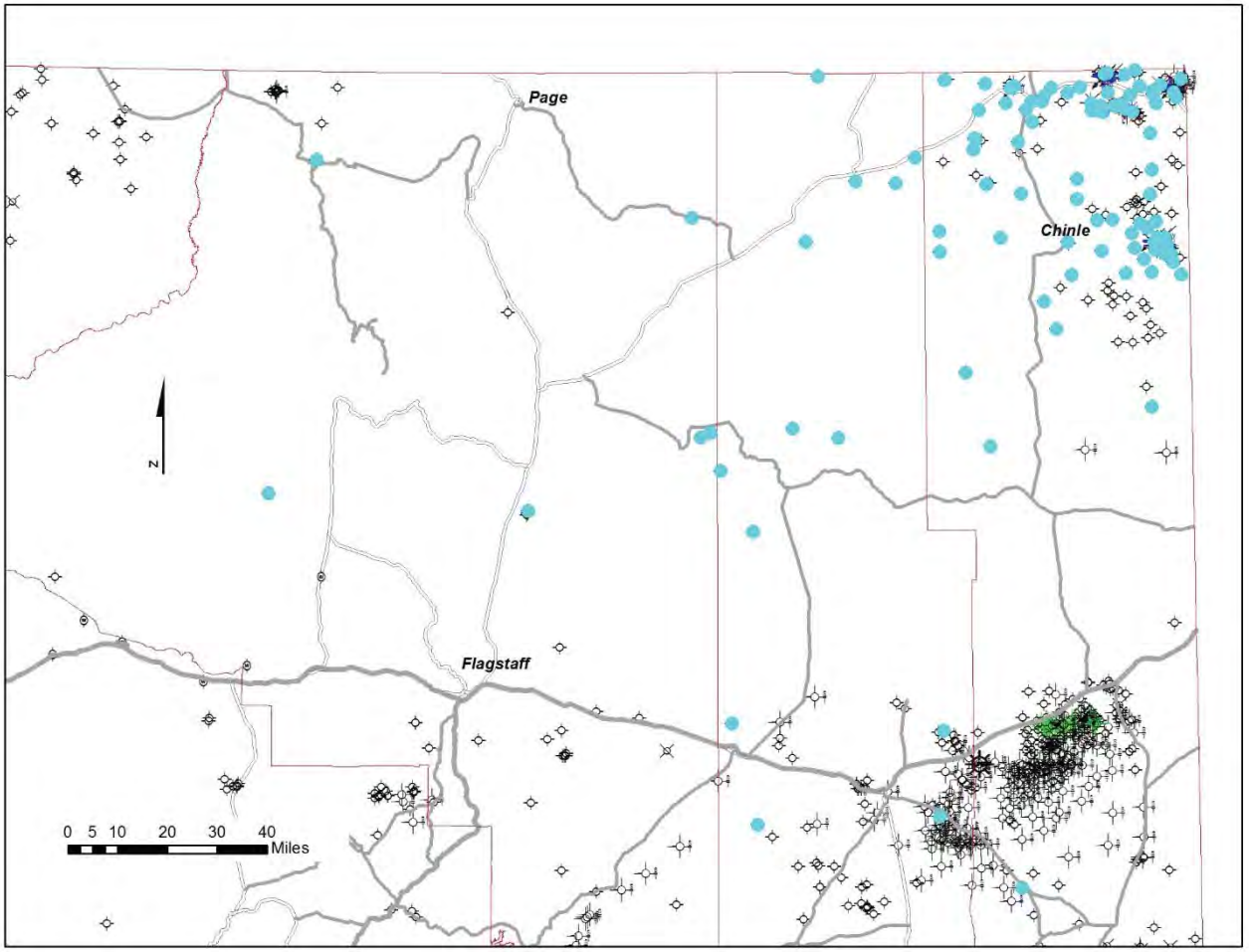
**E+09 indicates $x10^9$

***Values are for depth below 800m except for Cedar Mesa Sandstone for which value are for depth below 914m (3000 feet)

Appendix A. SE-NW Cross Section. Cross section was constructed from drill logs. Location of cross section is shown in Figures 1, 3, 4, and 5. Locations of drill holes are shown on Figures 1, 3, 4, and 5.



Appendix B. Blue dots represent wells digitized from raster tiff images to LAS (Log ASCII Standard) format using Neuralog. Approximately 268 logs from 118 wells for a total of about 938 curves were digitized. The AZGS developed a web application to make the LAS data available on the internet through an interactive search and download map hosted on the AZOGCC website



APPENDIX O

NM Bureau of Geology & Mineral Resources Regional Studies for Capacity

Contents

Topic

San Juan Basin Report

Introduction

The search for reservoirs with accompanying tight seals that occur between 3,000 and 13,000 feet, have total dissolved solids of greater that 10,000 μg/l and a capacity in excess of 500K BOEs is particularly attractive in New Mexico because of its long history of oil and gas production in the San Juan Basins. The size of many of the fields in this basin makes them prospective sequestration targets. In addition, there is the potential for deep saline aquifers to provide additional sequestration opportunities. In addition, there are several large power plants that could take advantage of identified sequestration reservoirs.

Within the San Juan Basin, several horizons were selected as possible sequestration targets: Dakota Group, Entrada Formation, Hermosa Group (equivalent to the Weber) and the Leadville Limestone. They are locally thick, porous and deep enough to be possible CO_2 sequestration targets. Associated seals for each of the units exist, but ultimately, the thick sequence of shales and siltstones of the Mancos Shale is an excellent upper seal for all the units in the basin.

CO_2 Sources for injection within the San Juan Basin

Within the San Juan Basin area, possible sources of CO_2 emissions were identified. They were the San Juan Generating Plant, Four Corners Generating Plant, Escalante Generating Plant, San Juan Gas Plant, Lybrook Gas Plant and the Giant Refinery. Of these sites, the San Juan and Four Corners Generating Plants were considered the most likely candidates for CO_2 sequestration project because the units of interest were deep enough and thick enough to meet all of the criteria for injection.

The main issues that ruled out a New Mexico site early in the selection process were:

- The lack of a partner (a source of CO_2) willing to work with the group. Both Tri-State Energy in New Mexico and PNM Resources, the operators of the two selected power plants, were contacted and declined involvement.
- The San Juan Basin is an area with complex land ownership issues. The area is a patchwork of private, state and federal lands that included both public and Indian lands. The nature of the permits and ownership issues would have made a site selection a long and uncertain affair.

These issues are not insurmountable for possible future projects, but it means that far more time will be required upfront for site selection and permitting in the San Juan Basin than the selected Craig Well site. The agreements would probably require Federal, Tribal, State and private landholders involvement in the site selection process.

Geology

Stratigraphy:

The northwestern corner of New Mexico is dominated by the broad, asymmetric San Juan Basin. It covers roughly 26,000 mi^2 (Brister and Hoffman, 2002) and is a structural and a depositional basin. The San Juan Basin is located north of Zuni Mountains, Lucero Uplift and Ignacio

monocline, west of the Nacimiento Mountains and Gallina-Archuleta Arch, south of the San Juan and La Plata Mountains and Sleeping Ute Mountain in Colorado, and east of Defiance uplift and Chuska and Carrizo Mountains and (Craigg, 2001; Figs. 1). The San Juan Basin center is filled by nearly 15,000 ft of Precambrian to Eocene rocks. Along the flanks of the basin, older sediments are turned up and exposed providing an opportunity to study the older, deeper horizons (Figs. 2 - 4). The basin is deepest on the northern and southeastern sides of this asymmetric basin.

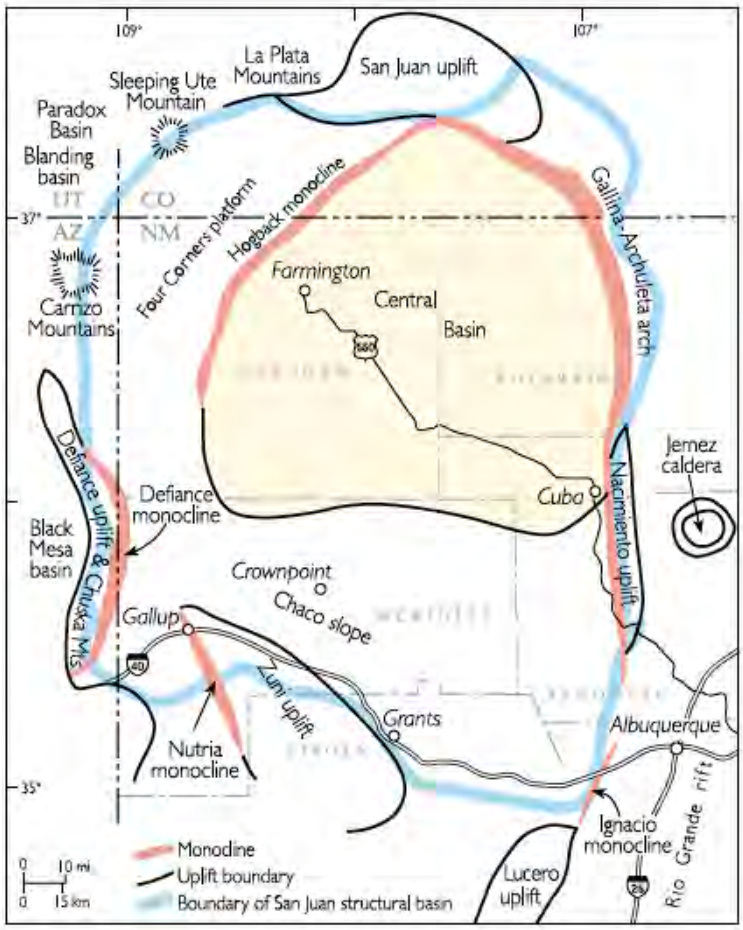


Figure 1. San Juan Basin (modified from Craigg, 2001).

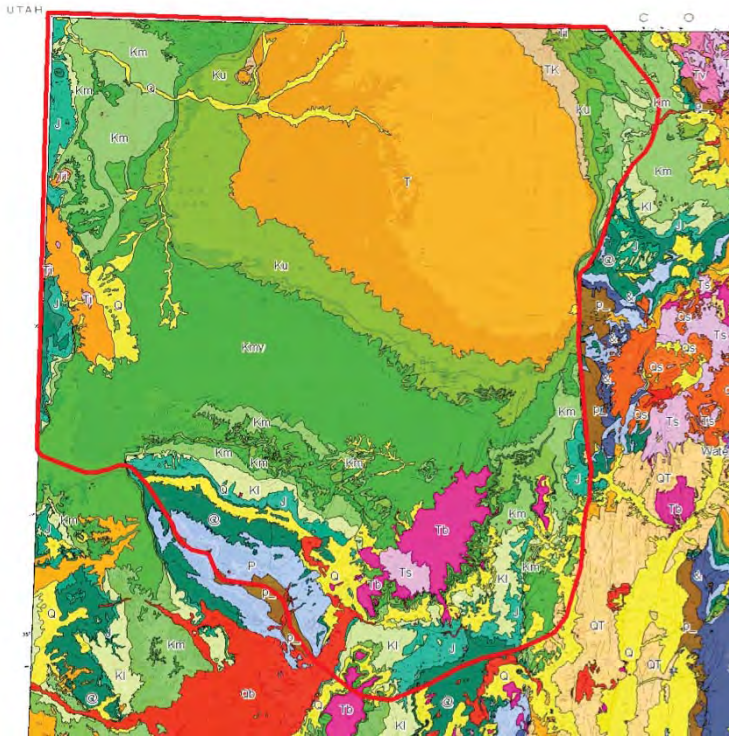


Figure 2. Generalized geologic map of the San Juan Basin and the basin outline (from NMBGMR).

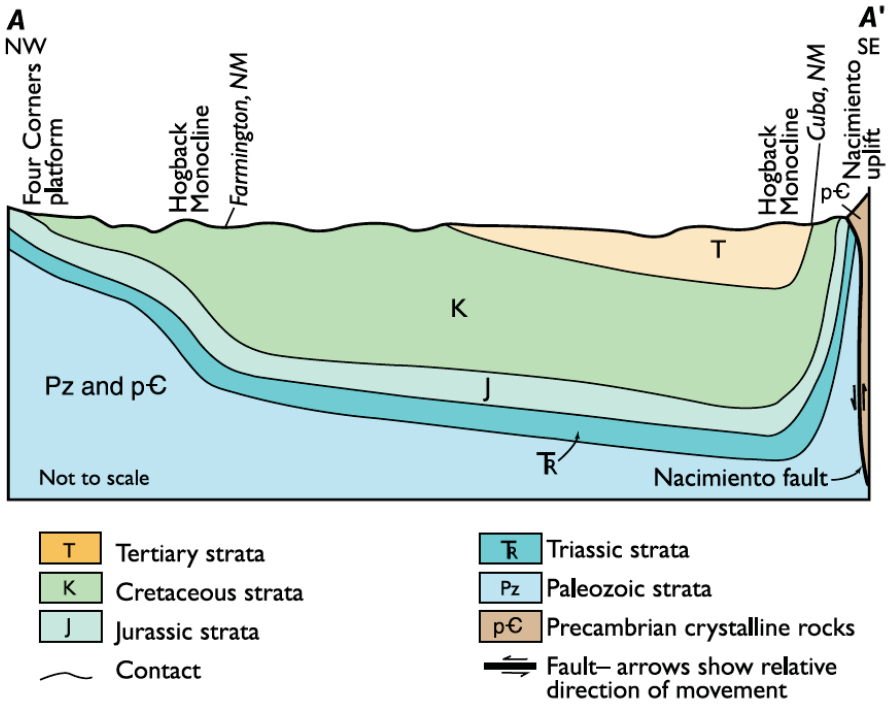


Figure 3. A northwest-southeast cross section across the San Juan Basin (from Craigg, 2001).

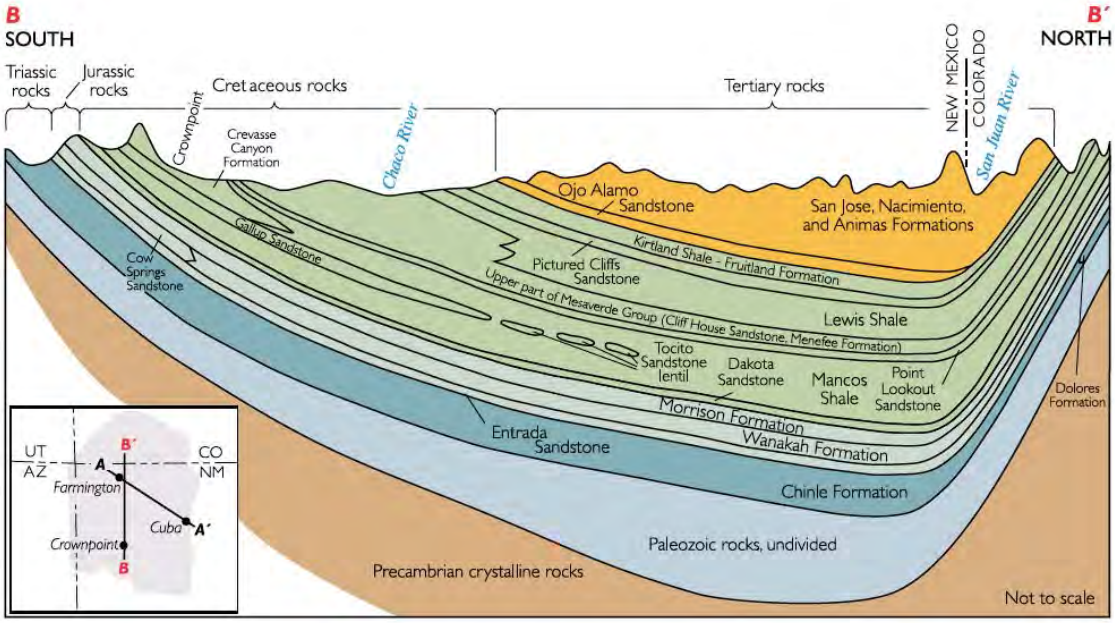


Figure 4. A north-south cross section through the San Juan Basin (from Craigg, 2001).

The stratigraphy of the basin starts with Precambrian units (Fig. 5). Precambrian rocks in the area are granites and quartzites (meta-sandstones). An unconformity exists between the Precambrian and Cambrian Ignacio Formation. The Ignacio Formation is a marine transgressive sandstone that is quartz-rich, well cemented and contains shale lenses (McLemore et al., 1986a, 1986b). The maximum thickness is approximately 100 feet, and it occurs in block-faulted erosional remnants (McLemore et al., 1986a, 1986b).

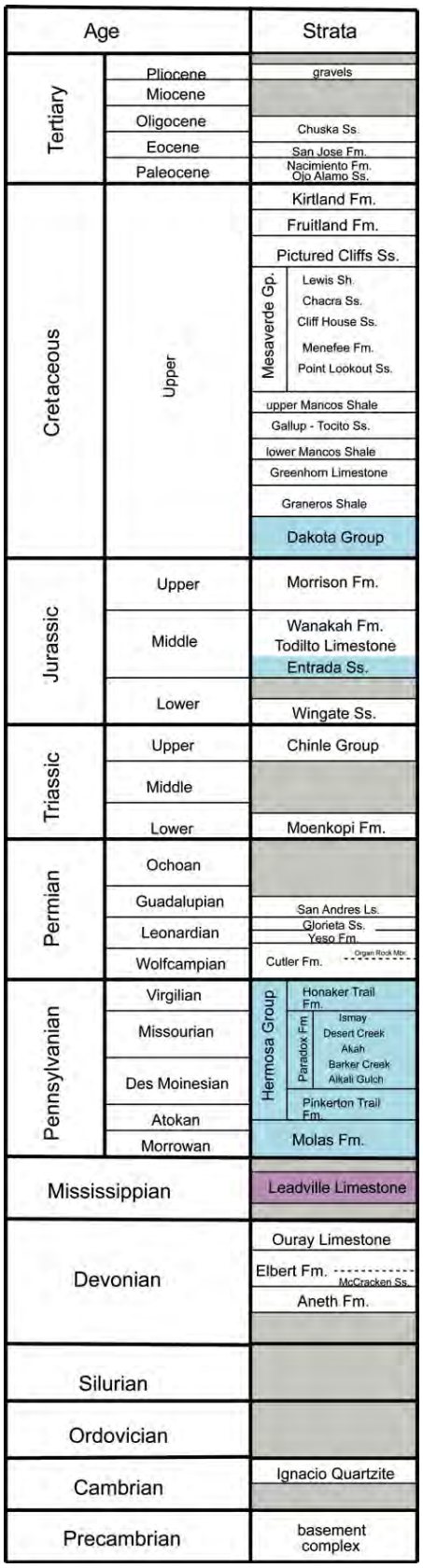


Figure 5. Idealized stratigraphic section for the San Juan Basin including the specific resources found in units.

An unconformity on top of the Ignacio Formation lasted until mid-Devonian time. The first Devonian deposit is the Aneth Formation. In places, the Aneth Formation lies directly on Precambrian surface where the Ignacio sediments were removed by erosion (McLemore et al., 1986a, 1986b). The Aneth Formation consists of dark, organic-rich, argillaceous limestones, dolomites, shales and siltstones. These units were deposited in euxinic basin (Stevenson and Baars, 1977) and are approximately 75 feet thick within the basin. The Elbert Formation is conformable with the underlying Aneth Formation. The Elbert Formation is subdivided into the McCracken Sandstone Member and an upper carbonate member.

The McCracken Sandstone Member is approximately 175 feet thick (Stevenson and Baars, 1977) and consists of fine to medium-grained, glauconitic, marine sandstones. The upper unit has a maximum thickness of 200 feet and thins across the basin to east (McLemore et al., 1986a, 1986b). It contains shallow marine limestones, shales and glauconitic sandstones.

The Ouray Formation conformably overlies the Elbert Formation and contains organic-rich, shallow marine limestones and dolomites. It varies across the San Juan Basin from over 90 feet thick to not being present due to erosion (McLemore et al., 1986a, 1986b).

The Mississippian Leadville Limestone unconformably overlies the Ouray Formation and ranges in thickness from 0 to 200 feet thick (McLemore et al., 1986a, 1986b) due to erosion or non- deposition prior to Pennsylvanian sedimentation. The shallow marine carbonates of the Leadville have been brecciated during the exposure event that followed deposition.

Mississippian strata are unconformably overlain by sediments of Pennsylvanian Molas Formation and Hermosa Group. The Molas Formation is up to 150 feet thick and is made up of red-bed terra rossa soil deposits and calcareous sandstones, siltstones and shale with minor limestones (Wengard and Matheny, 1959). Conformably overlying the Molas Formation, the Hermosa Group is a series of mostly marine deposits. They are shallow marine calcarenites and biohermal limestones and dolomites, sandstones, siltstones and shales. The upper part of Hermosa Group is a regressive sequence that grades into the overlying Permian Cutler Formation.

The Permian Cutler Formation (also referred to as the Abo Formation in early literature) is up to 1,600 feet thick, but it thins southward around the Zuni and Defiance uplifts (McLemore et al., 1986a). It is a non-marine red-bed sequence that consists fluvial and lacustrine conglomerates, sandstones and shales.

The conformable Yeso Formation ranges from fine-grained cross-bedded aeolian sandstones to marginal marine shales, limestones and evaporites (McLemore et al., 1986a, 1986b). The Glorieta Sandstone is well-sorted, quartz-rich shallow-marine sandstone. Due to its almost pure quartz content of this unit, it is a key marker horizon here in the San Juan Basin and elsewhere in New Mexico.

The San Andres Formation interfingers with the underlying Glorieta Sandstone. It is thins from 100 feet in the southern areas to being absent in the northern areas of the San Juan Basin (McLemore et al., 1986a, 1986b). It ranges from shallow marine limestones and dolomites to non-marine red beds. An unconformity overlies the Permian strata, and in areas with carbonates, karst topography formed.

Triassic time in the San Juan Basin was a time of non-marine deposition. From a thick section in Arizona, the Moenkopi Formation wedges out in the far western parts of the San Juan Basin (Akers et al., 1958). In New Mexico, the continental deposits consist of shales to sandstones (Repenning et al., 1969).

The Chinle Formation unconformably overlies the Moenkopi Formation (and Permian). The Chinle floodplain and fluvial deposits are up to 1,700 feet thick in the Colorado Plateau (Repenning et al., 1969). The Jurassic Wingate Sandstone is conformable with the Chinle Formation and formed as part of aeolian dune fields in the southwestern part of the San Juan Basin and get up to 600 feet thick.

The Jurassic Entrada Sandstone unconformably overlies the Wingate Sandstone. The Entrada Sandstones were deposited as part of large aeolian dune fields interspersed with playa lake deposits (Tanner, 1976). The Todilto Limestone conformably overlies the Entrada Sandstones.

The Todilto Limestone Member and the Summerville Member are currently assigned to the Wanakah Formation. The Todilto Limestone is composed of bedded gypsum and organic-rich, algally-laminated limestones and dolomites that were deposited in either a marginal marine or lacustrine environment. Currently, a lacustrine environment is the favored interpretation (see discussion in Ulmer-Scholle, 2005). In places, Todilto deposits fill the relief on the Entrada depositional surface.

The Todilto Limestone Member is overlain by the Summerville Member. The Summerville deposits consist of sandstones, siltstones, mudstones, minor conglomerates and gypsiferous sandstones and siltstones. In the San Juan Basin, it varies in thickness from 90 to 150 feet, and it may represent deposition on a arid coastal plain to sabkha (Anderson and Lucas, 1006)

Jurassic Morrison Formation (Salt Wash, Recapture, Westwater Canyon and Brushy Basin members) was deposited in fluvial, aeolian, sabkha to lacustrine environments and consists of sandstones, siltstones and shales.

The incursion of Cretaceous Seaway into the San Juan Basin during Upper Cretaceous time resulted in the deposition of over 6,500 ft of marine, coastal to non-marine sediments. Between Morrison and Upper Cretaceous sediments, there is an unconformity. During Upper Cretaceous sedimentation, at least 5 episodes of transgression/regression within the seaway occurred (Molenaar, 1983) resulting in deep marine, deltaic, coastal swamps, beach, alluvial and fluvial deposits.

The Dakota Sandstones represents the first transgressive cycle and is composed of sandstones, shales and coals. These sediments were deposited in fluvial environments in the northwestern part of the basin and coastal swamps to marine environments in the southeastern part of the San Juan Basin (Grant and Owen, 1974). It can exceed 200 feet in thickness.

Conformably overlying the Dakota Sandstone is the Mancos Shale. It is a complex sequence of siltstones and shales and minor sandstones representing deep marine environments to shallower marine environments. It exceeds 2,000 feet in thickness.

The Mesaverde Group is subdivided into the Point Lookout Sandstone, Menefee Formation, Cliff House Sandstone and Lewis Shale. The Point Lookout Sandstones (~200 feet) consist of

regressive coastal barrier system sandstones. The Menefee Formation (~400 feet) was deposited in coastal swamps to alluvial plains and is composed of sandstones, shales and coals. The Cliff House Sandstone consists of marine, cross-bedded sandstones with shales that are up to 800 feet thick. The contact with the overlying Lewis Shale is gradational. The Lewis Shale, a marine shale, is over 500 feet and contains numerous bentonite beds (McLemore et al., 1986a, 1986b).

Pictured Cliffs Sandstone is a quartz arenite that were deposited as part of a regressive coastal barrier island/bar system (McLemore et al., 1986b)

The Fruitland Formation sediments are non-marine coastal plain deposits formed after the last regression of the Cretaceous Seaway from the San Juan Basin area. The sandstones, shale and coals are over 300 feet thick. The Kirtland Shale is a non-marine coastal plain to alluvial sediments and thins to the southeast. At its maximum, it is over 2, 00 feet thick (Molenaar, 1977)

The Paleocene Ojo Alamo Sandstone lies unconformably on Cretaceous sediments. It is composed of sandstones with minor conglomerates and shales, followed by the Nacimiento Formation, shales with minor sandstone lenses. Nacimiento deposits were followed by sediments of the Eocene San Jose Formation. The San Jose Formation consists of conglomerates, sandstones and shales. The Pliocene Chuska Sandstone unconformably overlies the San Jose Formation, and the rocks are aeolian and fluvial deposits.

Structural History:

From Cambrian to early Pennsylvanian time, the area covered by the present-day San Juan Basin was a broad shelf adjacent to the Cordilleran passive margin (Wengard, 1959). Local uplifts during Pennsylvanian sedimentation resulted in a supply coarse-grained siliciclastics to the area. The area remained relatively flat, and slowly subsiding. Minor tilting (westward during the Permian, northeastward during the Cretaceous) was extent of the tectonic activity in the basin until the Laramide (Wengard, 1959).

The formation of the present-day San Juan Basin began during the Laramide (late Cretaceous/Early Tertiary to Eocene) with downwarping of the area (Stone et al., 1983, Tweto, 1975).

Igneous activity started approximately the same time as the Laramide Orogeny, around 70 Ma and continued until 63 Ma. During Oligocene time (35 to 26 Ma), the San Juan volcanic field produced 60,000 km^3 of volcanic material (Lipman et al., 1978). The San Juan Mountains saw renewed volcanism during Miocene to Pliocene time (Lipman et al., 1978). Most of the volcanics have been removed by subsequent erosion, but intrusives feeding the activity are still preserved.

Geothermal History:

Within the San Juan Basin, heat flow increases toward the San Juan Volcanic Field. In the area of the basin near the San Juan Volcanic field, heat flow averages 127mWm^{-2} (Clarkson and Reiter, 1988). Elsewhere in the basin, the heat flow is considered to too high to be caused only by the volcanic activities in the San Juan Mountains (Reiter and Clarkson, 1983). The thickness of sediments in the basin do not account for the anomalously high temperatures or the heating event associated with Oligocene San Juan Batholith emplacement. It is thought a large plume-like anomaly at 100 to 35 km depth (Clarkson and Reiter, 1988) is the likely source of the extra heat.

Project Deliverables

Database

The initial goals of the project was to:

- Collect and review public data from the region including well logs and previous studies, and
- Create a relational geodatabase that could be integrated GIS software to produce derivative products.

The New Bureau of Geology and Mineral Resources (NMBGMR) team created a relational geodatabase in Microsoft Access to collect all the pertinent information for the 50,000 plus wells in the San Juan Basin as well as the 100 to 200 thousand of wells elsewhere in New Mexico. The database was created for this project, but the NMBGMR designed the database in such a way that it can be expanded and upgraded as needed for future projects (Fig. 6). To date, in addition to this project, the database has been utilized for a USGS Carbon Capture and Sequestration study and two geothermal projects.

Where available, the data collected geodatabase includes:

- All formation tops available,
- Location and elevation information,
- Core and plug data —
    - Porosity and permeability data,
    - Oil/Gas/Water ratios.
    - Lithologic information,
    - Water chemistry,
- Well site tests —
    - Bottom hole temperatures,
    - Geothermal gradient data,
    - Produced water salinity and
    - Flow rates.

Figure 6. The Microsoft Access relational database scheme developed by the New Mexico Bureau of Geology and Mineral Resources. The data collected during this study populated the database as well as from other work. Queries designed in Access

Update NATCARB Database with Regional Data

NMBGMR contributed relevant data and derivative structural and isopachous maps to the RMCCS team to develop a three-dimensional, fully coupled process model of the region, including multiphase flow with thermal, mechanical and chemical processes (THMC), using all available existing data. This required the creation of several generations of maps (structure and isopachous) to refine the New Mexico dataset as well as the input of over 70,000 porosity and permeability values derived from core analyses.

Units of Interest for CO_2 Sequestration

The San Juan Basin has the second largest gas accumulations in North America, and it has a long history of production (since 1911) with more than 50,000 well penetrations in the basin (Fig. 7). The majority of oil and gas production is shallow units from the Dakota Group and younger strata (Gallup Sandstone, Mesaverde Group and Pictured Cliffs Sandstones) along anticlinal folds within the basin, but there is production from deeper horizons. Most of this deeper production is from the Pennsylvanian Hermosa Formation, but Jurassic Entrada Sandstone, the Leadville Limestone and Devonian units also have had productive fields.

Hydrocarbon maturation patterns mimic heat flow trends within the San Juan Basin and increased to the north; gas is common in the northern and central areas of the basin. The thickness of the sediment package in the deepest parts of the basin also increases the formation temperatures to the north. The San Juan Volcanic Field was also a possible heat source to produce the anomalously high temperatures found in the region. Oil is common in the western, southern and southeastern areas of the basin (Clarkson and Reiter, 1988).

This history of production (Table 1) makes the San Juan Basin both an excellent basin for CO_2 sequestration as well as utilization for enhanced oil recovery techniques. Most of the main producing reservoirs within the basin are too shallow to be possible CO2 sequestration sites, but Dakota Group and older reservoirs are deep enough. If the CO2 is being used for gas flooding and other enhanced oil recovery technologies, then the shallower horizons may have potential.

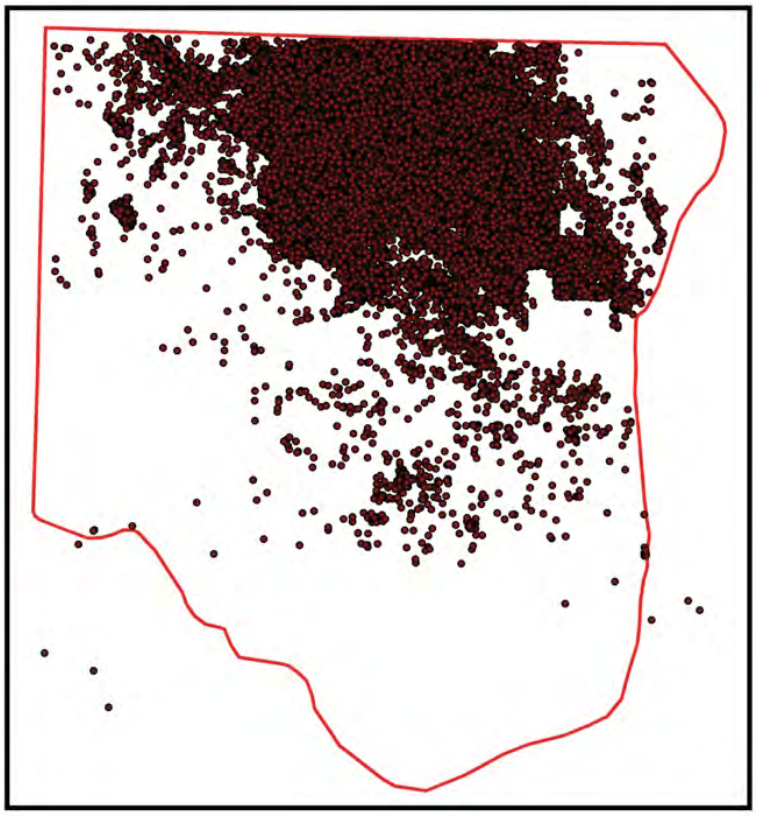


Figure 7. Distribution of wells drilled within the San Juan Basin.

Table 1: Summary of oil and gas production within the San Juan Basin. The blue areas are from Engler et al. (2001), the orange areas are from Fassett (1993) and the rest of the values are from Fassett (2010).

Formation/Period	Play		Cumulative Production	
	Oil	Gas	Oil (10^3 bbls)	Gas (Tcf)
Tertiary				
San Jose		λ	0	0.0019
Nacimiento		λ	0.7	0.0006
Ojo Alamo		λ	0	0.0003
Cretaceous				
Farmington		λ	–	–
Fruitland Sand		λ	34.6	0.0570
Fruitland Coal		λ	367.1	15.7
Fruitland/Pictured Cliffs		λ	–	–
Pictured Cliffs		λ	1,200	4.5
Lewis Shale		λ	–	–
Chacra		λ	47.6	0.3
Mesaverde		λ	47,300	12.9
Gallup	λ		59,663.2	0.552
Tocito	λ		150,000	–
Sanastee	λ		–	–
Mancos Shale	λ		41,000	–
Greenhorn	λ		–	–
Graneros	λ		–	–
Gallup-Dakota	λ		–	–
Mancos-Dakota	λ		–	–
Dakota	λ	λ	49,600	7.0
Jurassic				
Entrada	λ		6,000	–
Pennsylvanian	λ	λ	14,000	35,481
Mississippian	λ	λ	90.1	3,723
Devonian	λ		18.8	0.0141

To better understand the geology, the distribution and provide information for the CO_2 capacity spreadsheets for the selected units within the San Juan Basin, a series of maps were created in ARC-GIS. Structure maps on top of each of the units of interest and the underlying formation were constructed. The underlying formations were also mapped since they were needed later for the isopachous maps.

To create the structure maps, a surface topographic map was created (Figs. 8-9) to make certain that the elevations were consistent with the regional topography. The surface elevations, used for the digital elevation model (DEM), were the datums provided by the drillers. This is the point that the loggers would measure to the each of formation tops. These elevations range from the actual land surface to the Kelly bushing (KB) or drilling floor (DF). If values were not in the expected range, then the values were checked on Goggle Earth. Many of the drilling pads are still visible on aerial photographs.

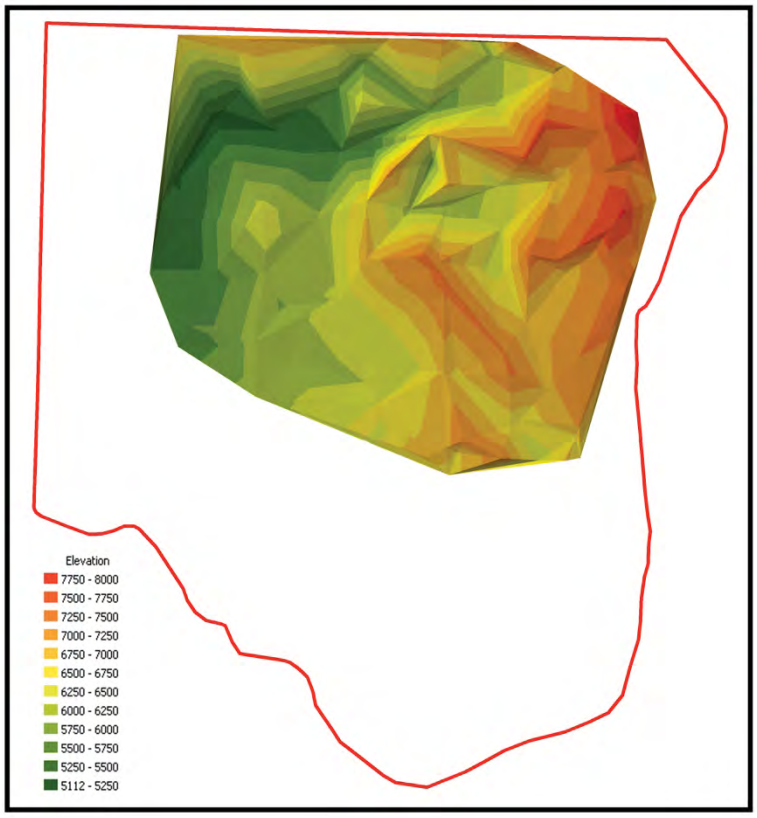


Figure 8. Structure contour map of the surface topography (ft). It lacks the fine details of the rasterized version generated from this map (Fig. 9).

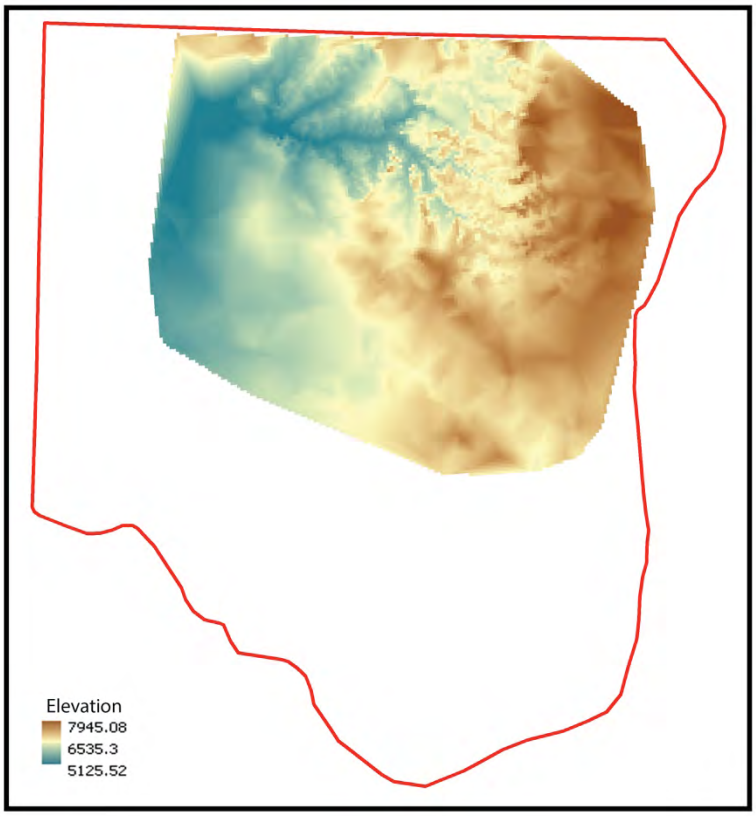


Figure 9. The rasterized version of topographic map has more detail.

After the surface topography was checked, a query was created in Microsoft Access to subtract each of the formation tops from the surface elevation to get the formation top with respect to sea level. The formation tops include the Mancos Shale, Dakota Group, Morrison Formation, Entrada Formation, Chinle Group, Hermosa Group, Molas Formation, Leadville Limestone and Ouray Limestone. Structure maps were created for each of the formations. Tops were checked, and wells that were not consistent with surrounding data, the well logs were checked or, if the logs were not available, they were omitted from the map. This was an iterative process until the maps were realistic.

To create the isopachous maps for each of the target units, for example the Mancos Shale, the structural contour map for the top of the Mancos Shale was subtracted Dakota Group to come up with a isopachous (thickness) map of the Mancos Shale. To create overburden isopachous maps for each of the target formations, the surface DEM map was subtracted from the formation's structural map.

Mancos Shale —

Geologic Characterization:

The Mancos Shale is thick sequence occurring throughout the San Juan Basin that conformably overlies the Dakota Group and grades into the overlying Pictured Cliffs Sandstone. While there are productive sandstones near the top of the Mancos, the majority of unit is composed of well-compacted, deep marine shales and siltstones that have extremely low porosities and permeabilities. This makes it a potential regional seal for CO_2 sequestration projects. Currently, companies operating in the San Juan Basin are predicting that with horizontal drilling technologies and hydraulic fracturing of the shales, the Mancos shale may be the next Bakken or Barnett play (Fig. 10). If this does happen, the sealing capabilities of the unit may be diminished. The bottom-hole temperatures (Fig. 11) support the prospective areas of gas deposits surrounded by shallower oil reservoirs.

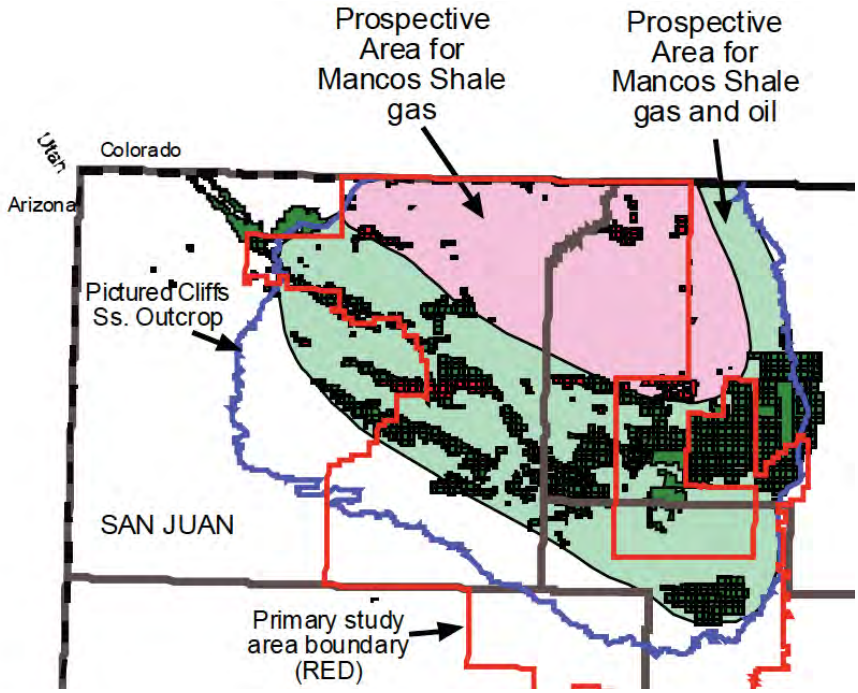


Figure 10. Areas that may see exploration growth in the Mancos Shale (from a BLM Report by Engler et al., 2001).

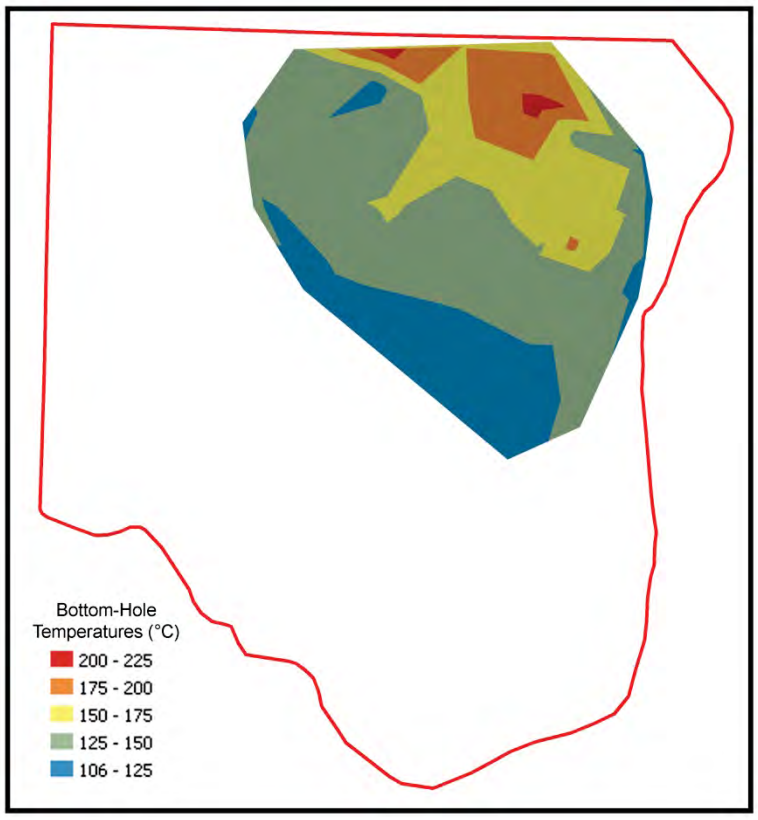


Figure 11. Bottom-hole temperatures within the Mancos Shale. The highest temperatures are in the deepest part of the basin and closer to the San Juan Volcanic field.

The stratigraphy of the Mancos Shale is complex due to the conflicting terminologies used by industry and geological surveys. The Mancos Shale (Fig. 12) can be subdivided into upper Mancos, Carlile, Lower Mancos, Greenhorn Limestone and Graneros Shale (Nummedal and Molenaar, 1995; Engler et al., 2001). In addition, the Juana Lopez, Gallup Sandstone, Tocito, El Vado, Crevasse Canyon Shale and the Niobrara Shale, all have been used by previous workers to describe members of the Mancos Shale (Engler et al., 2001; McLemore et al., 1986a, 1986b). Many times, this terminology is used incorrectly. For example, the Gallup Sandstone is part of the Carlile member, and in numerous reports, papers and production data, the Gallup Sandstone stands alone and the Tocito Sandstone is a member of the Gallup; however, the Tocito appears to be equivalent to upper Mancos, not the Gallup or Carlile (Nummedal and Molenaar, 1995).

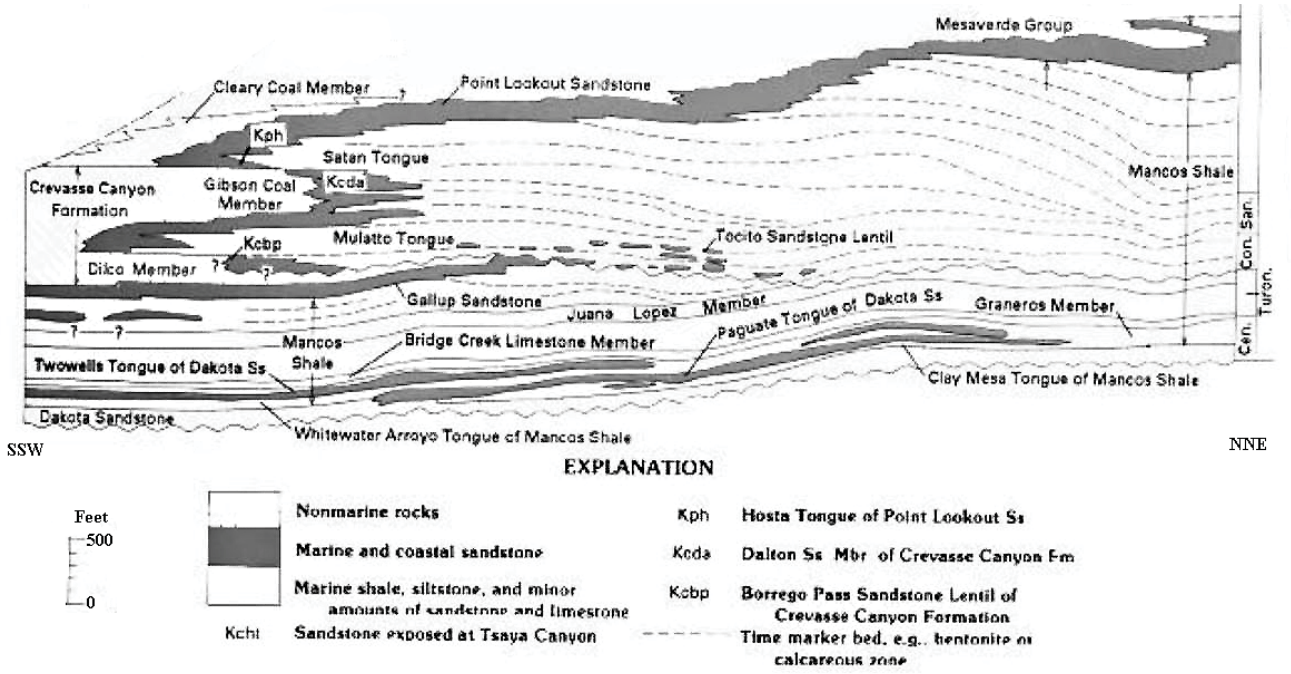


Figure 12. An idealized diagram of Mancos stratigraphy from south/southwest to north/northeast (modified from Nummedal and Molenaar, 1995).

Due to asymmetrical nature of the basin, the deepest sections of the Mancos Shale are in the northeastern part of the basin (Figs. 13 and 14). This area has been more extensively drilled than the edges, because the sediments have been buried deep enough to reach the oil and gas window. The lower Mancos is approximately 850 feet thick; and the upper Mancos Shale is approximately 1,000 to 1,400 feet thick (McLemore et al., 1986a) (Fig. 15).

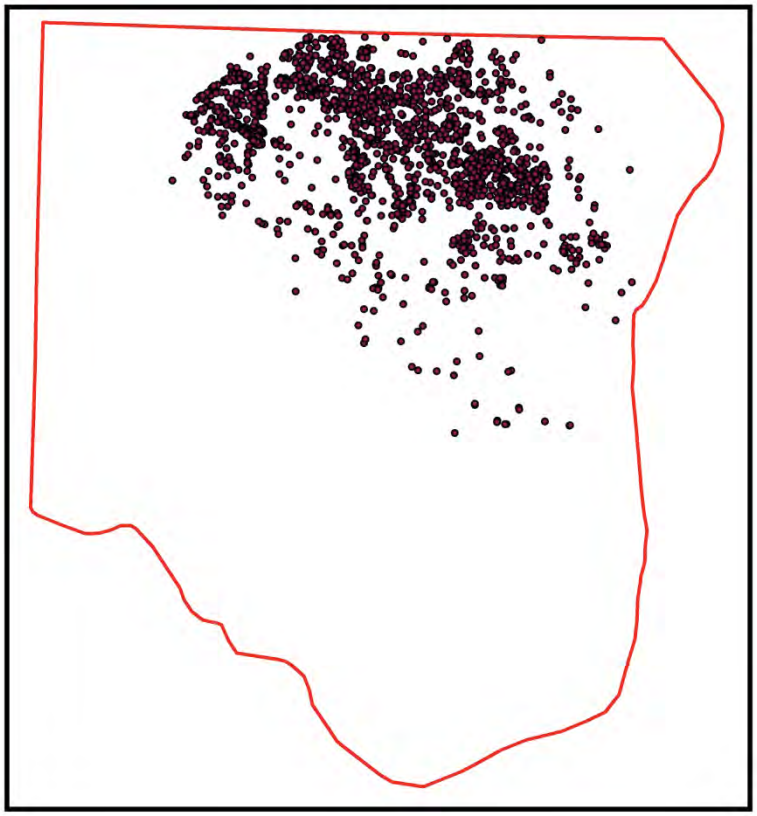


Figure 13. Distribution of wells used for mapping that penetrates the Mancos Shale.

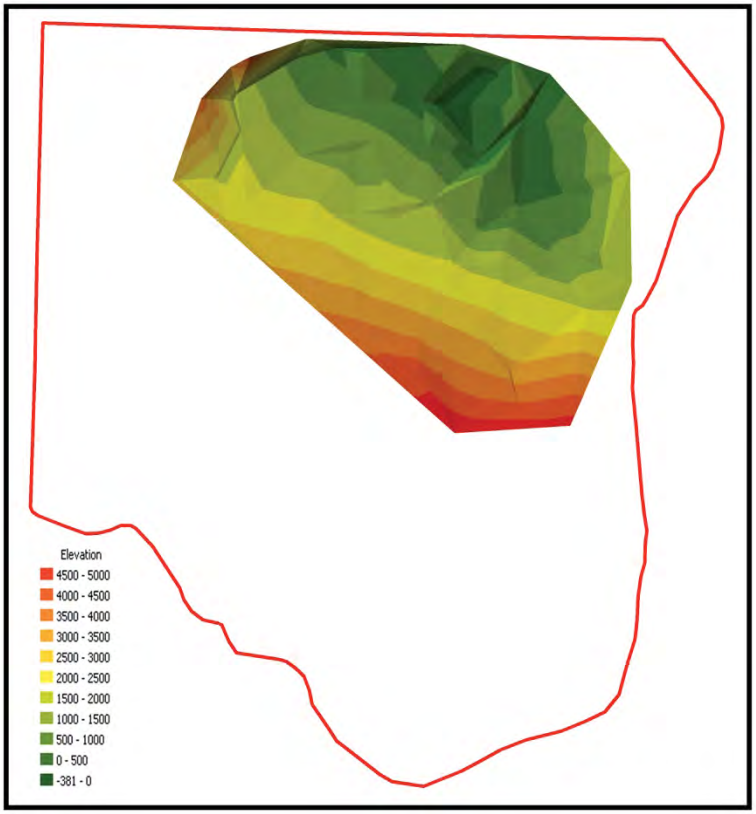


Figure 14. Structural map on top of the Mancos Shale (elevation = feet).

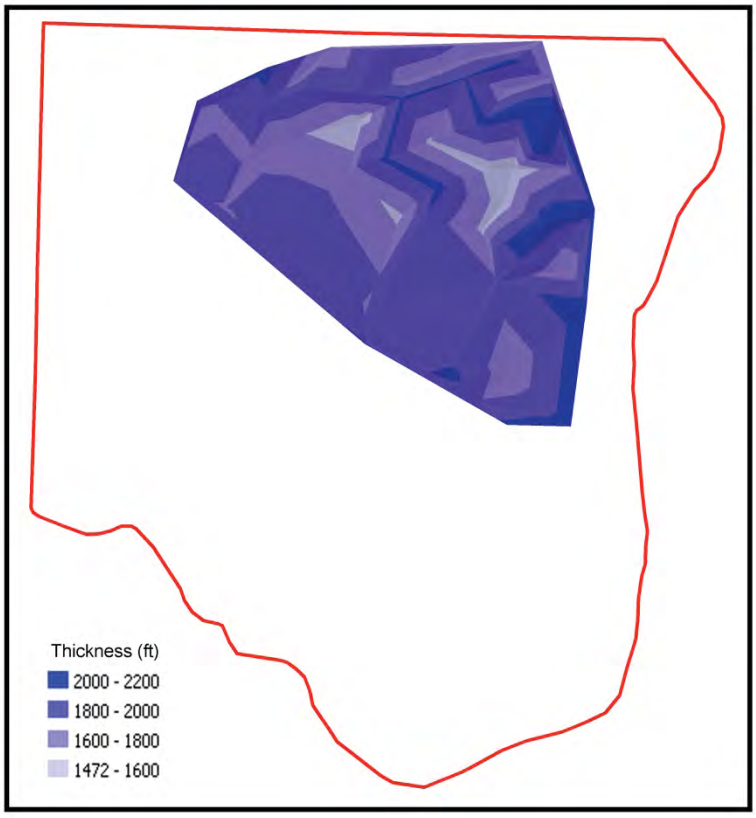


Figure 15. Isopachous map of the Mancos Shale (thickness = ft).

Based on foraminiferal zonation data, during Mancos deposition, the water depths within the Cretaceous Seaway may have been up to 300-400 feet deep, but this varied due to several transgressive/regressive events that occurred that period of the Cretaceous Period. The Graneros Shale Member is approximately 60 feet thick and is a transgressive shale unit. The Greenhorn Limestone Member sits on top of the Graneros Shale and is 40 to 70 feet thick. The Greenhorn Limestone Member represents the maximum transgression of the seawater into the Cretaceous Seaway of New Mexico (Molenaar, 1977). The Juana Lopez member represents the start of regressive event and consists of shallow marine fossiliferous calcarenites, sandstones and shales. The sediments that were deposited at the height of the regression and during next transgressive sequence are not well developed in the basin (McLemore et al., 1986a).

The Gallup Sandstones were deposited during the second regression and are shallow marine sediments. They are very fine to very coarse-grained sandstones with minor shales and coal that ranges from 25 to 135 feet in thickness (O'Sullivan et al., 1972). The next transgressive/ regressive/transgressive cycles resulted in deposition of Crevasse Canyon Shales. This unit contains shale, calcareous concretions and sandy zones.

The Mancos Shale ranges from being exposed on the edges of the basin to being buried by almost 8,000 ft of sediment in the "center" of the basin (Fig. 16).

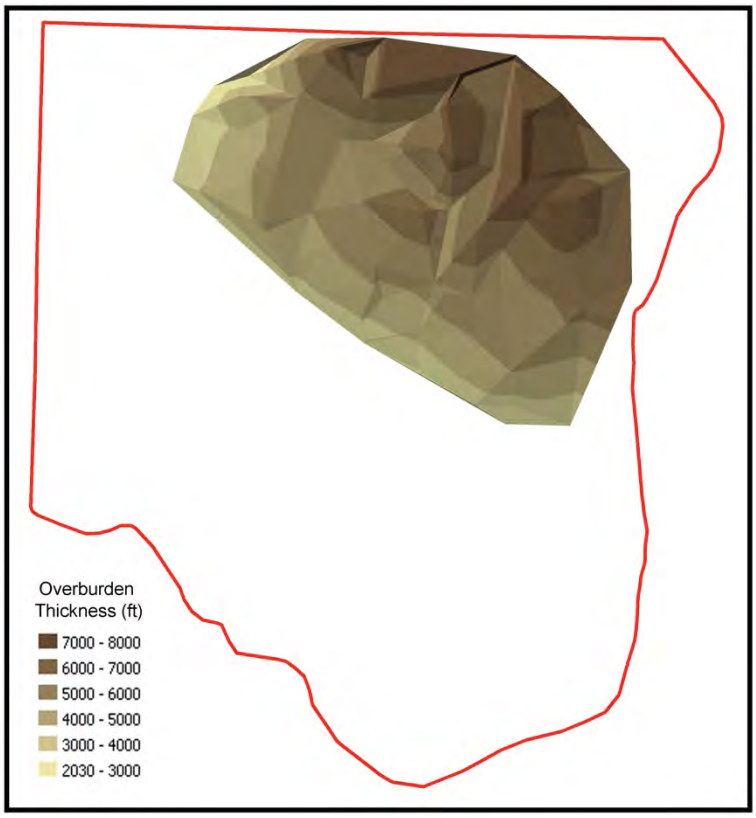


Figure 16. A map of the overburden (ft) on top of the Mancos Shale.

The Mancos Shale (excluding the Gallup Sandstone) has seen limited oil and gas production. Regionally, it has been considered the source rock for many of the younger Cretaceous plays. It is productive only where it is highly fractured, but in most areas, it is a seal.

The Gallup and basal Niobrara reservoirs (upper Mancos) have both oil and gas production and are stratigraphic traps with a minor structural control (McLemore et al., 1986a). The difficulty in determining production in the Mancos Shale is due to Gallup and Tocito Sandstones being misidentified by drillers, but it is likely that most of the production is from the Tocito Sandstone. The Tocito Sandstone is a super clean quartz sandstone deposited in an offshore marine bar facies. Reservoirs have net pays up to 125 feet, porosities up to 20% and permeabilities of 250 mD or less (McLemore et al., 1986a).

Summary and Recommendations:

The Mancos Shale is a potential regional seal, but it will depend on future exploration within the Mancos Shale. Areas that are currently highly fractured will most likely be a leaky seal; therefore, other seals will have to be evaluated.

Dakota Group —

Geologic Characterization:

The first incursion of the Cretaceous Seaway into the San Juan Basin area resulted in the deposition of the Dakota Group in the San Juan Basin. The Dakota was deposited on an unconformity surface over Morrison or Burro Canyon Formations and conformably grades into the overlying Mancos Shale.

Environments range from fluvial, coastal wetlands to deltaic deposits in northwestern part of the basin to marine sandstones and shales in the southeastern part of the basin (Grant and Owen, 1974; Fassett, 1983). Deposits range from carbonaceous sandstones and siltstones, shales, coal and conglomerates. The source of the sediment appears to be from the north and consists of reworked sediments from underlying units (Burton, 1955). The Dakota Group is up to 500 ft in thickness (Figs. 17 and 18), and it varies through the basin, but there appears to be a low that trends northwest to southeast.

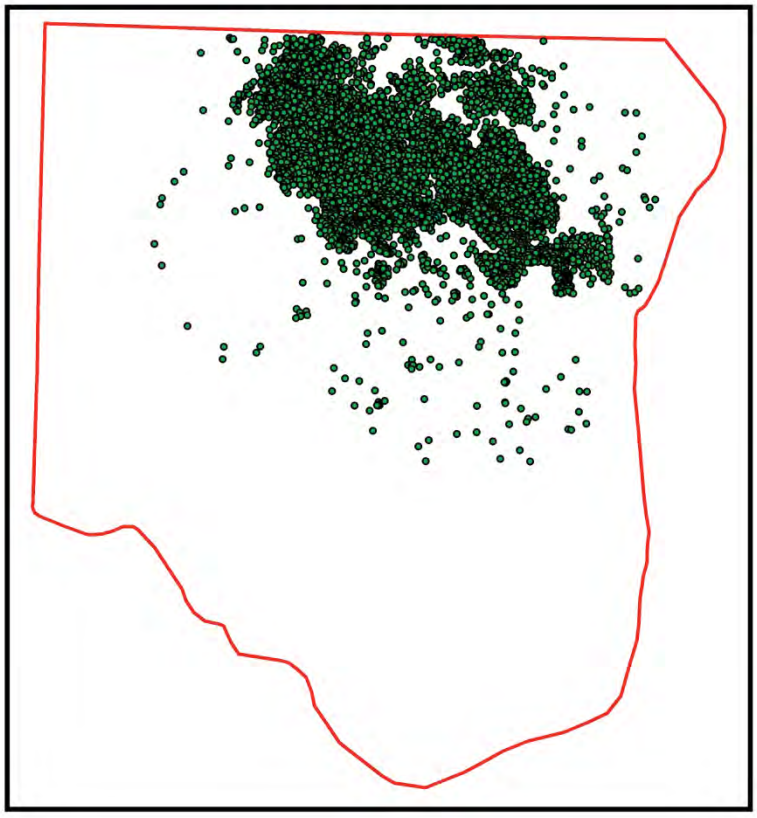


Figure 17. A well density map of Dakota Group wells.

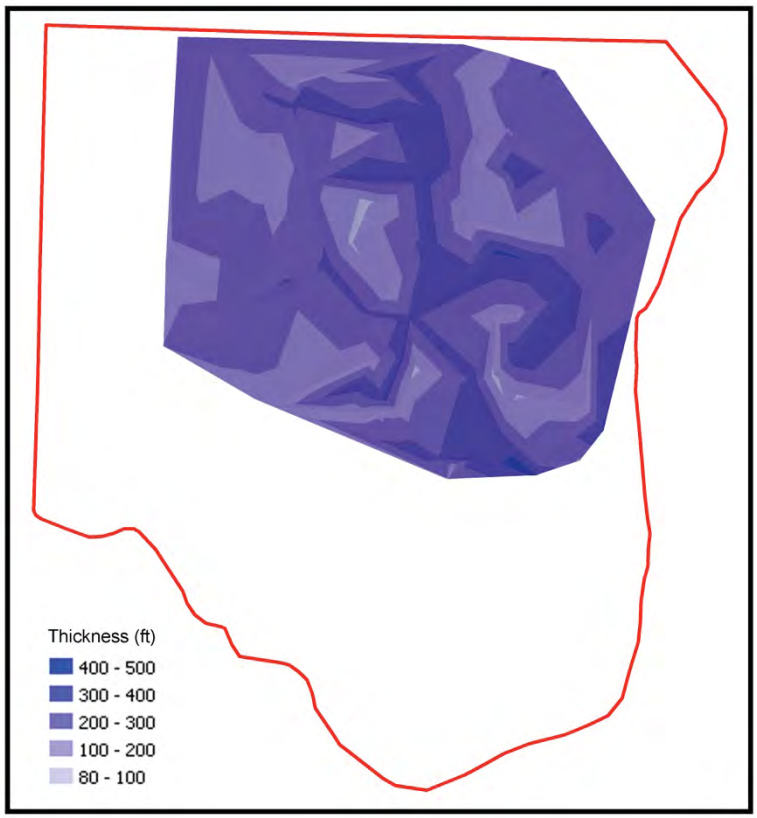


Figure 18. An isopachous map of the Dakota Group sediments (thickness = ft).

Gas production is not as well understood within the Dakota Group, but it probably has stratigraphic and hydrodynamic controls (McLemore et al., 1986a). The Dakota gas play has become a model for basin-centered gas (Figs. 19, 20). Oil reservoirs are a combination of structurally-controlled production along anticlines in shallower areas of the basin and fracture enhanced porosity and permeability. There may be minor stratigraphic controls on that production as well, including depositional environment and diagenetic controls. Most of the oil production in the Dakota Sandstone in the San Juan Basin occurs along the edge of the basin (Fassett, 1983). Fields trend northwest on the southwest structural axis, and most of the production is due fracturing (Fassett, 2006).

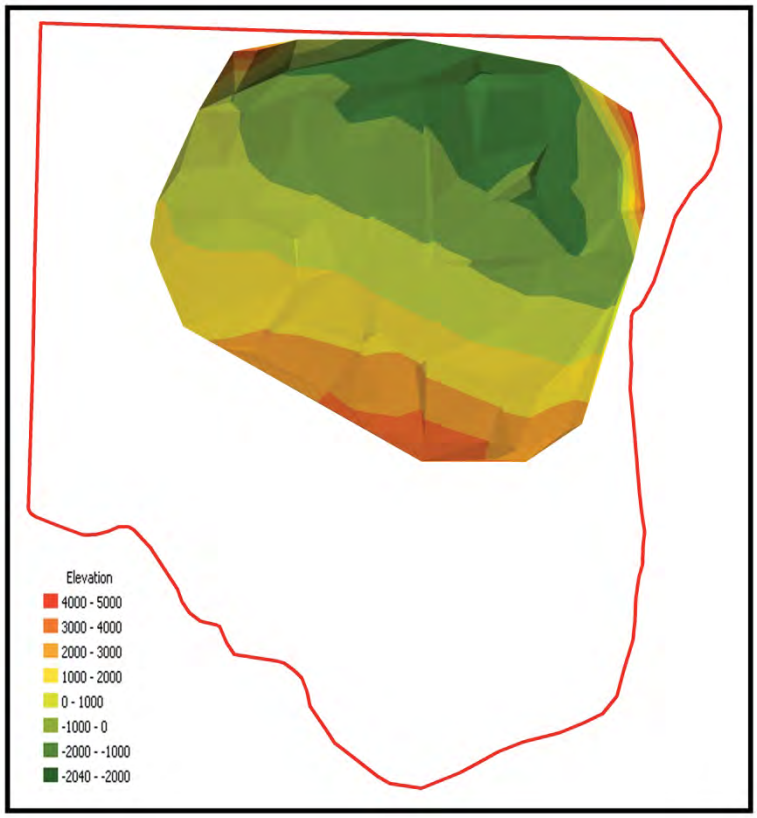


Figure 19. Structural map on top of the Dakota Group (elevation = feet).

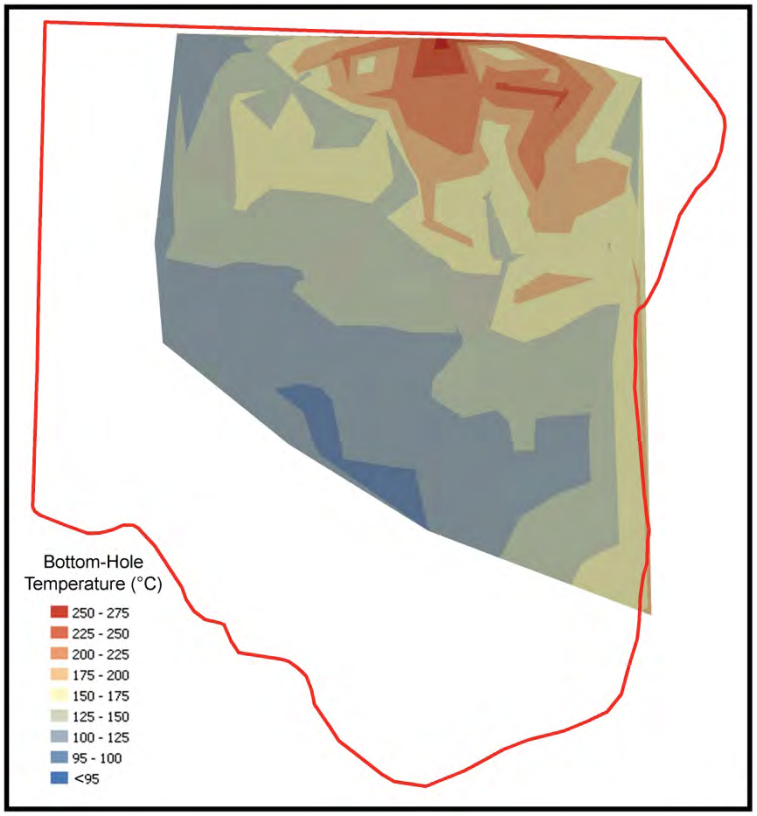


Figure 20. Bottom-hole temperatures for the Dakota Group. The highest temperatures are in the basin "center."

The Dakota is one of the prolific oil and gas reservoirs in the San Juan Basin (Table 1, Fig. 21). Dakota Sandstone reservoirs are within the transgressive/regressive marine littoral deposits on the western margin of the Cretaceous Seaway (Fassett, 1983). They are sourced from the Mancos Shale. Porosity within the Dakota Group is intergranular (Burton, 1955) and fracture. The "tight" sandstones have an average porosity of 7% and permeability of 0.15mD (Deischl, 1973), but they can go up to 15-20% porosity, 1,500 mD and 300 feet of pay (McLemore et al., 1986a). The core plug data within the database for the Dakota cores, this includes pay and tight zones, averages 6.7% porosity and 1.3 mD permeability. The maximum value for the porosity was 25.1%, and the maximum permeability was 715 mD.

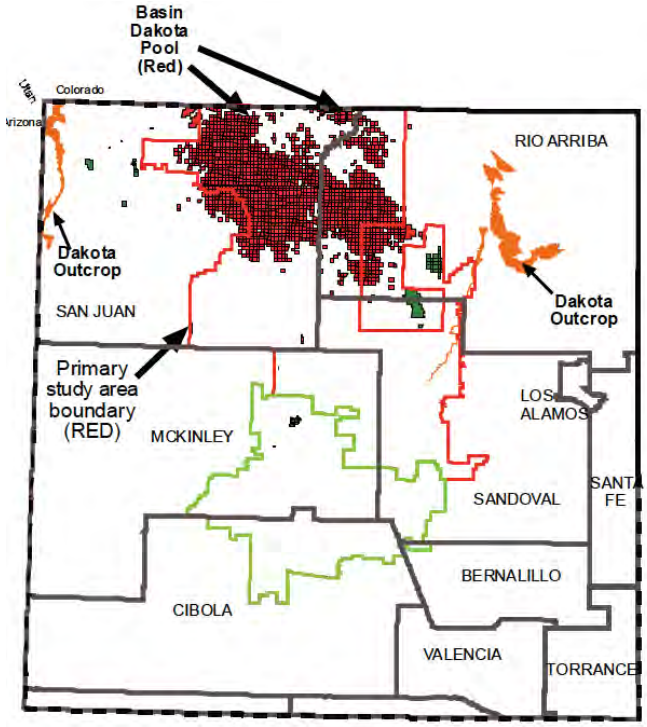


Figure 21. Dakota Group production in the San Juan Basin. The red areas are gas, and the green areas are oil production (from Engler et al., 2001).

CO2 storage Capacity:

The parameters used to calculate the CO_2 storage capacity for the Dakota Group are located in Table 2. The basin area was determined from the overburden map (Fig. 22). The area is based on the 3,000 ft contour. Since the San Juan Basin has numerous completions in the Mancos Shale, the overburden map is an accurate estimate to the CO_2 reservoir size.

The thickness varies across the basin, and the data from the Dakota isopachous map was used to determine the thickness. Porosity varies greatly throughout the section from almost zero to close to 20%. Ultimately, the capacity estimates will also vary greatly from the minimum to maximum value. Possibly, a more accurate way to calculate the net capacity is to base the thickness on the net pay.

The porosity and permeability data comes from over 5,550 values from core reports within the basin. The temperature data is from well header information as well as geothermal and heatflow surveys.

The CO2 storage capacities are presented in Table 3.

Table 2. Parameters used to calculate CO_2 storage efficiency for the Dakota Group in San Juan Basin, New Mexico.

Area (km^3)	Thickness (ft)	Porosity % (min, avg, max)	Salinity (TDS)	Permeability (mD)	Temperature (°C)	Geothermal Gradient
19,599	See Figure 18	2.5, 6.3, 13.2	25000	0.83	See Figure 20	47°C/km



Figure 22. A map of the overburden (ft) on top of the Dakota Group.

Table 3. CO_2 Storage Capacity (metric tonnes) *for the Dakota Group in San Juan Basin, New Mexico.*

Storage Efficiency		
0.51%	2%	5.4%
172,502, 878	676,481,873	1,826,501,601

Summary and Recommendations:

Based on the CO_2 storage capacity values, these Dakota marine to terrestrial sandstones have more limited capacity than comparable Dakota Colorado and Utah basins. These gas fields are close to potential CO_2 sources (power plants), and the CO_2 can be utilized to for enhanced oil recovery.

Entrada Sandstone —

Geologic Characterization:

The Entrada Sandstone of the San Juan is part of a large aeolian dune field that covered most of the Colorado Plateau. The Entrada Sandstone unconformably overlies the Wingate Sandstone, and it is conformable with the overlying Todilto Limestone Member of the Wanakah Formation.

The Entrada Sandstones consists of fine to medium, well- to poorly-sorted, moderately well-rounded, quartz arenites of large trough, cross-bedded units. In the San Juan Basin, the Entrada Sandstone ranges from 150 to 800 feet thick (Fig. 23). It thickens to the northwest and thins to southeast. The upper sandstones are sometimes bleached; whereas, the lower sections are iron stained (Anderson and Lucas, 1996). The bleached zones have a different diagenetic history, and it is this zone that is usually the reservoirs. In places, they are calcite cemented which decreases the porosity and permeability of the unit. Interbedded with these sandstones are finer-grained, planar-bedded units. These have been identified as lacustrine deposits (Anderson and Lucas, 1996), but more likely these deposits represent playa lakes that were interspersed with the dune fields.

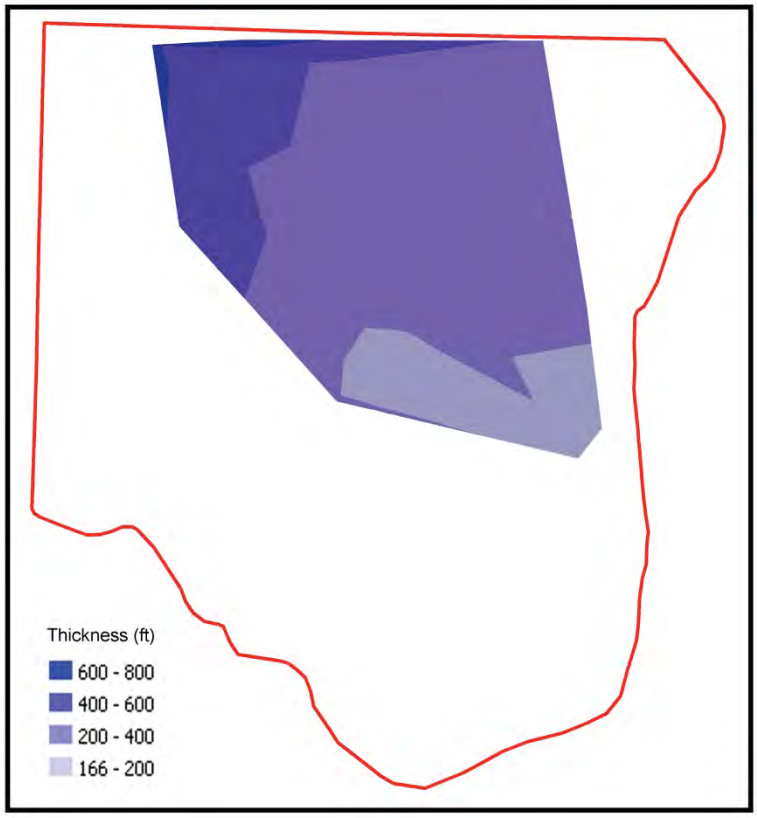


Figure 23. An isopachous map of the Entrada Sandstone (thickness = ft). Note that the unit thins from a thick in the northwest to a thin in the southeastern section of the San Juan Basin.

The Todilto Limestone conformably overlies the Entrada Sandstones. It consists of bedded gypsum and organic-rich, algally-laminated limestones and dolomites that were deposited in either a marginal marine or lacustrine environment (Kirkland et al., 1995; Anderson and Lucas, 1996; Lucas and Anderson, 1997; Lucas et al., 1985; Lucas et al., 2003; Ulmer-Scholle, 2005). Currently, a lacustrine environment is the favored interpretation. On outcrop, Todilto deposits can be seen filling the relief on the Entrada depositional surface.

The aeolian Entrada Sandstone's oil was probably sourced from the overlying organic-rich Todilto Limestone (Fassett, 1983). Most of the Entrada production comes from northwest Sandoval and southeast McKinley Counties, and almost all the reservoirs are stratigraphic traps. There is no gas production from the Entrada units at this time. Based on the work by Engler et al. (2001), the Entrada has future potential for both oil and gas (Fig. 24). Like the Dakota Group sediments, gas reservoirs should occur in areas where it is buried the deepest and has the highest temperatures (Figs. 25 to 27); and oil reservoirs will occur closer to the flanks.

Average porosity for productive Entrada units is 23% and 300 mD (Fassett, 1983), but it can be higher than 25%, have permeabilities greater than 600 mD and pay thickness of greater than 200 feet. Based on the database's measured porosity and permeability data produced for this project, the average porosity is 9.6%, and average permeability is 0.1 mD. The maximum thickness of this unit is 800 feet (Fig. 27). This is based on a Chinle Formation top, not the Wingate Formation. The Wingate is difficult to tell apart from the Entrada Sandstone and it is not present in large sections of the basin.

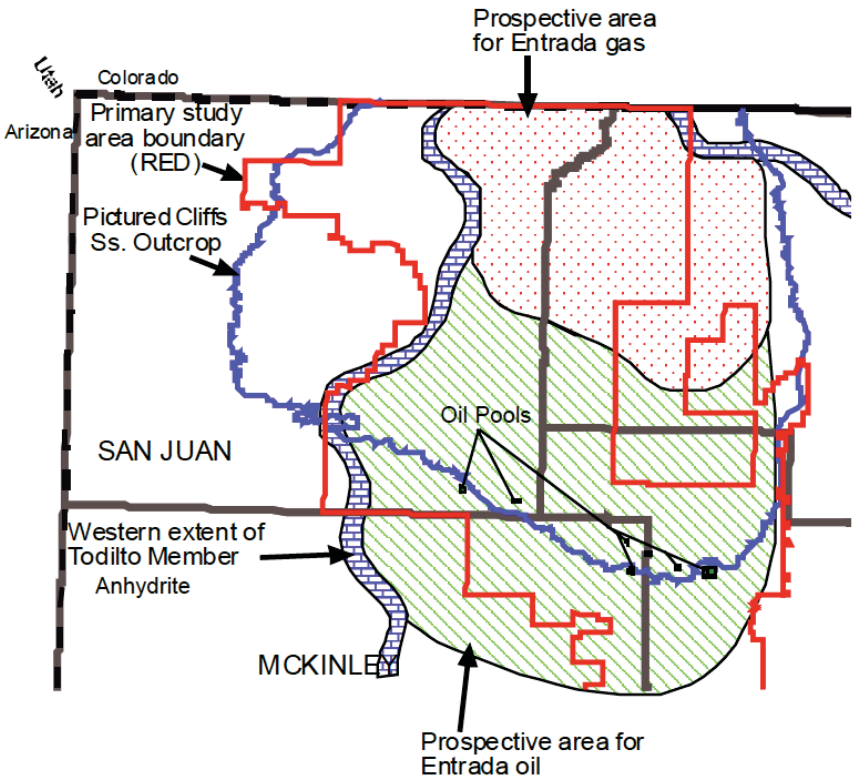


Figure 24. A map of prospective play areas for the Entrada Sandstone. Current production is oil and forms a linear trend on the map (from Engler et al., 2001).

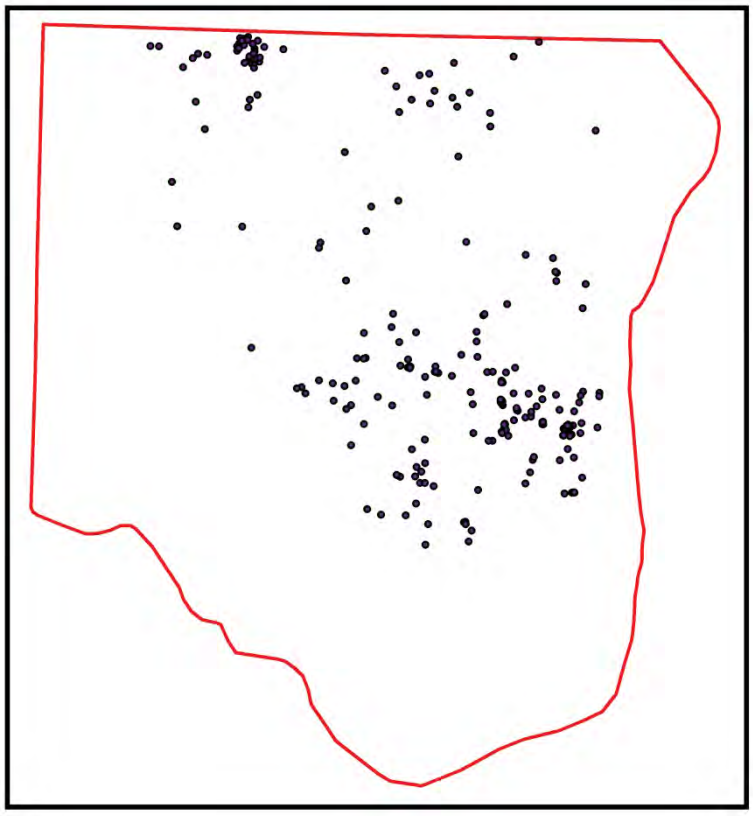


Figure 25. A map of the well density for the Entrada Sandstone.

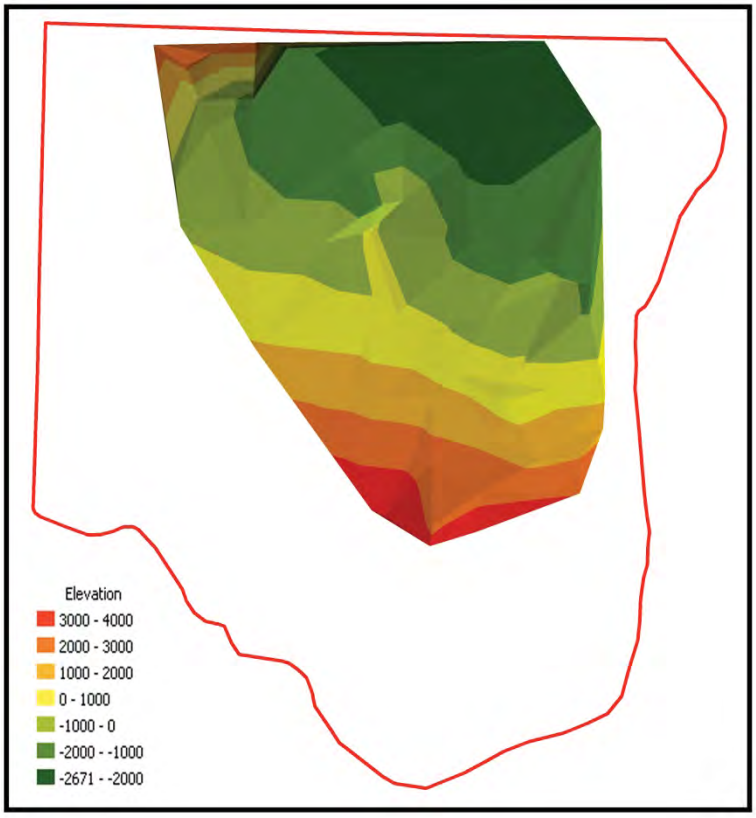


Figure 26. A structural map on the top of the Entrada Sandstone (elevation = feet).

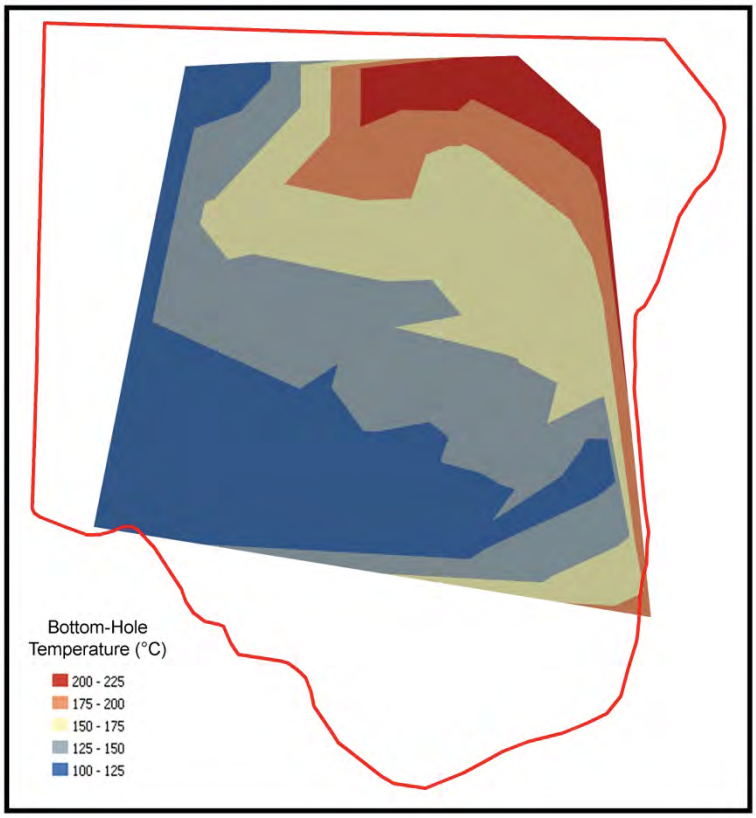


Figure 27. A map of the bottom-hole temperatures within the Entrada Sandstone.

CO2 storage Capacity:

The parameters used to calculate the CO_2 storage capacity for the Entrada Sandstone are located in Table 4. The basin area was determined from the overburden map (Fig. 28). The 3,000 ft contour is the minimum depth for injection of CO_2. Due to the fact the Entrada sandstones have been drilled less extensively than the shallower horizons, the overburden map is incomplete. The extent of the Entrada sands in the San Juan Basin is probably much greater than the 16,511 km^3 calculated.

Table 4. Parameters used to calculate CO_2 storage efficiency for the Entrada Sandstone in San Juan Basin, New Mexico.

Area (km^3)	Thickness (ft)	Porosity % (min, avg, max)	Salinity (TDS)	Permeability (mD)	Temperature (°C)	Geothermal Gradient
16,511	See Figure 23	7.4, 9.6, 22.5	35000	0.09	See Figure 27	47°C/km

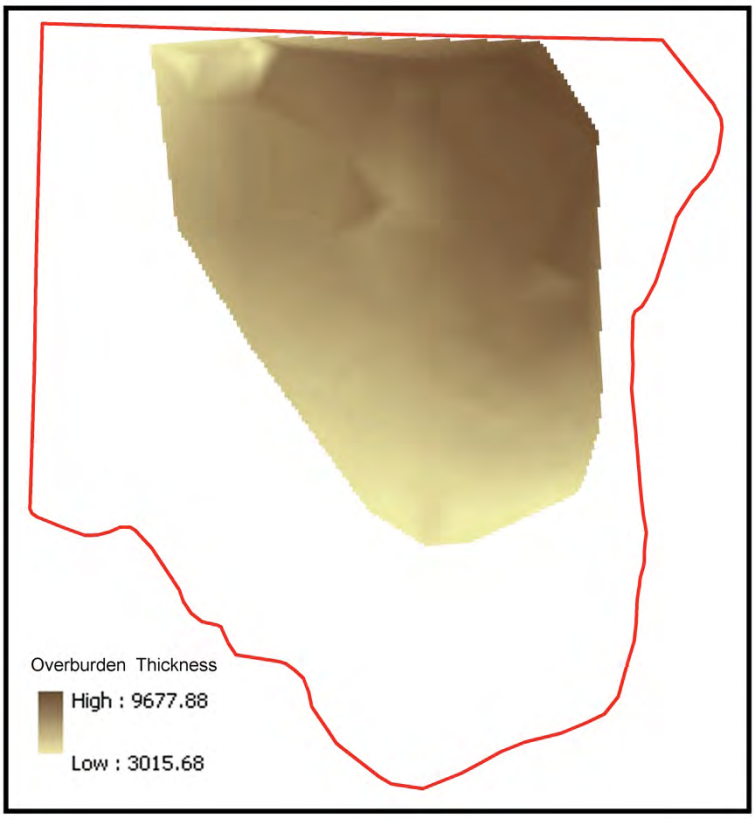


Figure 28. A map of the overburden (ft) over the Entrada Sandstone.

The thickness of the Entrada sands varies uniformly across the basin (Fig. 23), and the data from the Entrada isopachous map was used to determine the thickness. Porosity varies greatly throughout the section from almost zero to close to 25%, so the capacity estimates can also vary greatly from the minimum to maximum value.

The porosity and permeability data comes from fewer than 10 values from core reports within the basin. The temperature data is from well header information as well as geothermal and heatflow surveys.

Table 5 is the CO_2 storage capacity based on the data within Table 4.

Table 5. CO_2 Storage Capacity (metric tonnes) *for the Entrada Sandstone in San Juan Basin, New Mexico.*

Storage Efficiency		
0.51%	2%	5.4%
300,019,280	1,176,546,181	3,176,674,688

Summary and Recommendations:

Based on the CO_2 storage capacity values, the Entrada Sandstone doesn't appear to have great potential. The storage capacity calculation is in part dependent on the area of the unit, and it is derived from the overburden map. For the Entrada Sandstone, the limited well coverage impacts this value since the true boundaries of the 3,000 ft contour could not be determined. With additional drilling, the area will increase causing the storage capacity to increase. This will make the Entrada and the overlying Todilto Limestone a much more attractive reservoir and seal.

Hermosa Group —

Geologic Characterization:

The Hermosa Group (Pinkerton Trail, Paradox, Honaker Trail and Rico Formations) is conformable with the underlying Pennsylvanian Molas and overlying Permian Cutler Formations. The Hermosa Group was deposited on a broad shelf that was part of Paradox geosyncline and has thickness of over two thousand feet (Figs. 29 to 30).

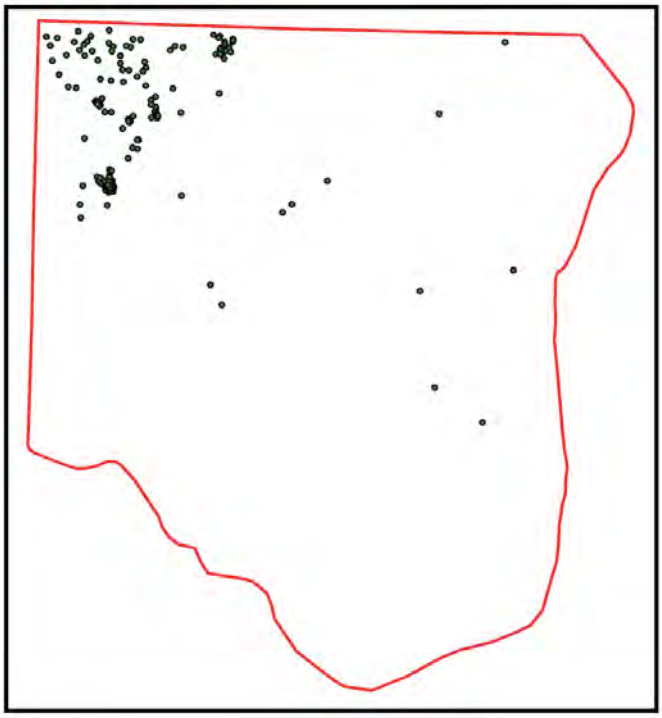


Figure 29. A well density map for the Hermosa Group. Most drilling has been in the northwestern corner of the state (and the basin). There are a few scattered wells elsewhere in the basin, but additional wells need to be drilled to develop future plays.

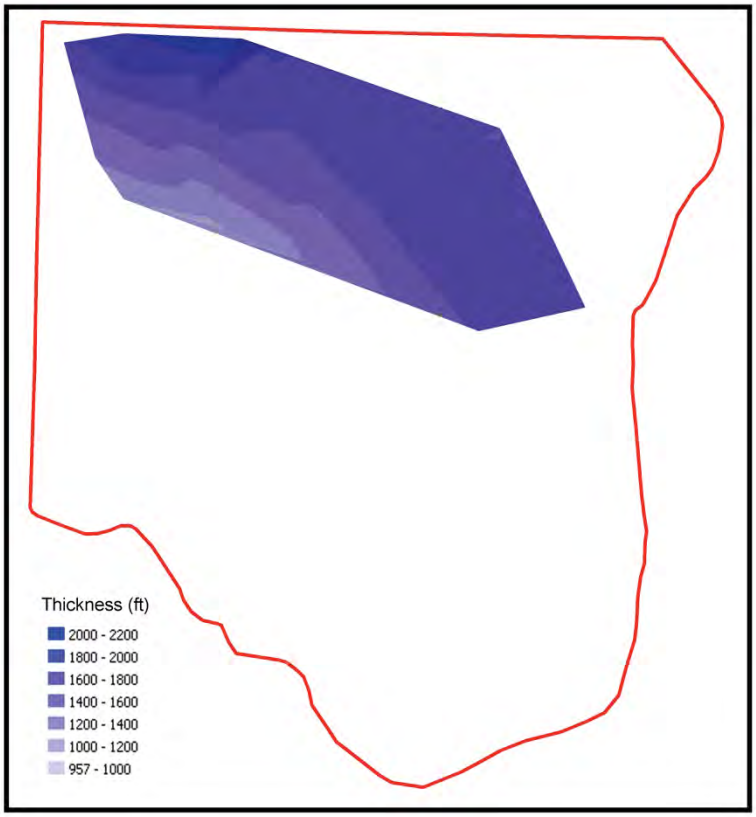


Figure 30. An isopachous map of the Hermosa Group. It is much more extensive in the basin, but there are too few wells to isopachous the rest of the San Juan Basin.

The Pinkerton Trail Formation is up to 200 feet thick and consists of marine, fossiliferous limestones and shales that formed during a marine transgressive event over the non-marine Molas Formation. The Paradox Formation contains algal bioherms surrounded by conglomeritic and cherty limestones, sandstones and siltstones and can reach a thickness of over 1,500 ft in the San Juan Basin (Wengard, 1959). The Honaker Trail Formation is also a marine carbonate unite with cherty, fossiliferous limestones and dolomites, sandstones, siltstones and shales. It can reach up to 1,000 feet in thickness. The Rico Formation varies from fully marine carbonates at its basin to non-marine red beds at the top. This unit represents a regressive sequence and grades into the overlying Permian Cutler Formation.

Most of the Pennsylvanian oil production is from the northwestern part of the basin from the Paradox Formation. These Paradox reservoirs are stratigraphic traps formed by phylloid algae bioherms located on paleo-structural highs. Net pay in these biohermal units can be up to 120 feet thick, 15% porosity and greater than 100 mD (McLemore et al., 1986a).

A few wells have been drilled in other parts of the basin and they show the Hermosa Group occurs throughout the San Juan Basin and that the thickness increases eastward (Fig. 30). The Laramide orogeny may have dissected the platform (Engler et al., 2001), but it certainly resulted in the downwarping of the present-day San Juan Basin (Fig. 31). The Hermosa Group sediments are now almost 5,000 feet below sea level.

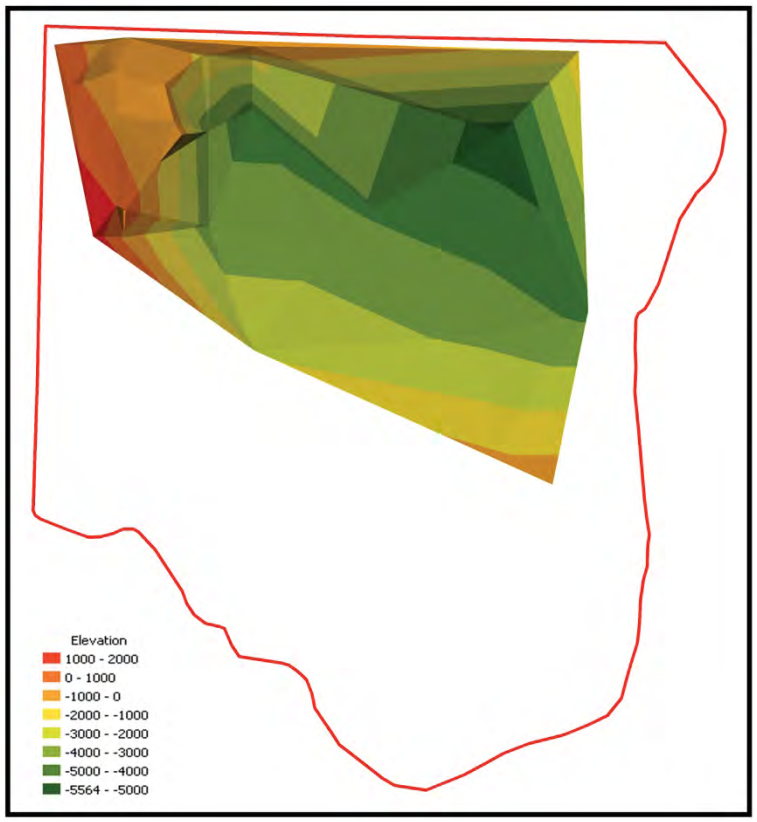


Figure 31. A structural map on the top of the Pennsylvanian Hermosa Group (elevation = ft).

The database produced for this project contains measured porosity and permeability from 40 plugs. The average porosity for Pennsylvanian cores is 5.1%, and the highest porosity measured is 21.4%. The average permeability is 42.6 mD, and the highest measured permeability was 1000 mD. There is little temperature data available for Pennsylvanian sediments (Fig. 32), but based on the underlying temperatures in the Leadville Limestone, most of the potential production in the rest of the basin is probably gas. The depth of the wells will make them expensive to drill, so any future plays will have to wait until the market drives exploration.

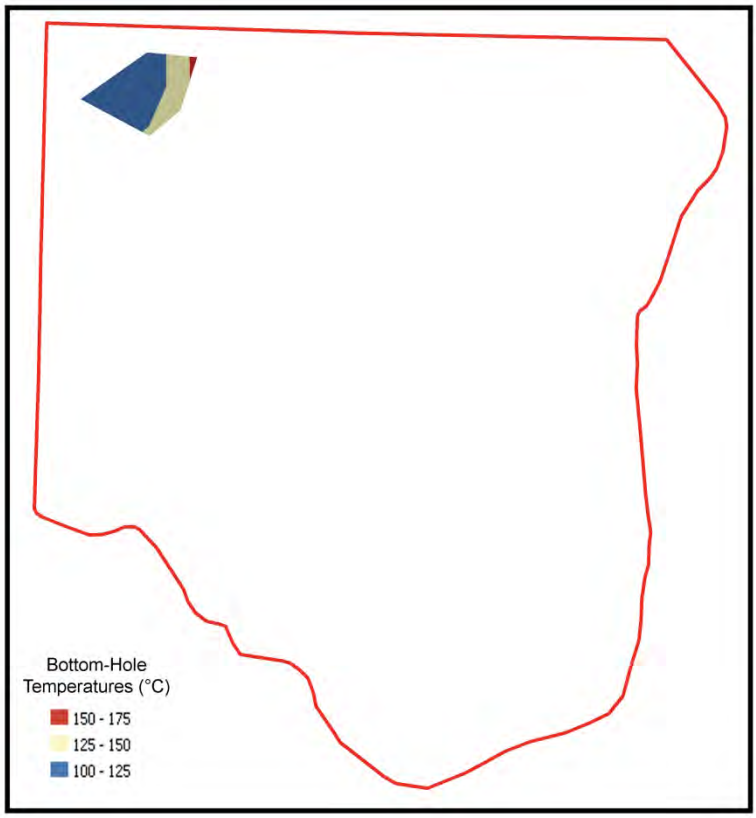


Figure 32. The very limited bottom-hole temperature data available for the Hermosa Group in the San Juan Basin.

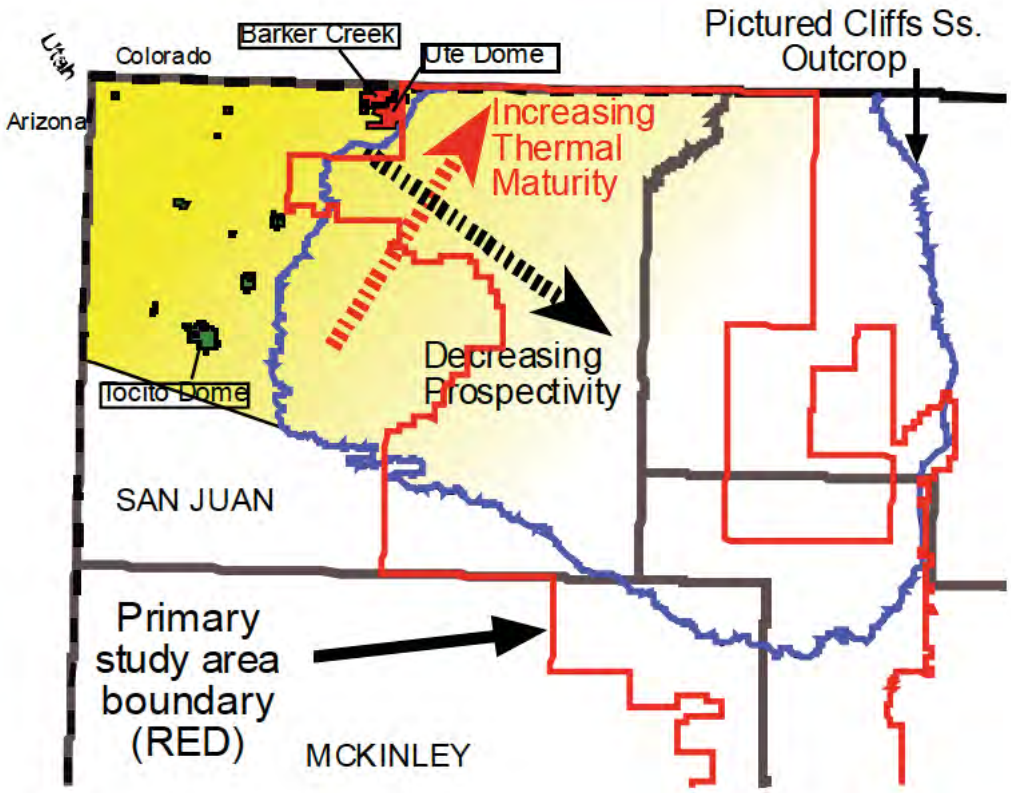


Figure 33. Possible future plays in the Hermosa Group. The diagram also shows where there was previous production; all the Pennsylvanian fields are now shut in (from Engler et al., 2001).

CO2 storage Capacity:

The parameters used to calculate the CO_2 storage capacity for the Hermosa Group are located in Table 6. The basin area was determined from the overburden map (Fig. 34) by using the 3,000 ft contour as the minimum depth for injection of CO_2. The area is a minimum value since there are not enough wells to define the extent of the Hermosa sediments.

Table 6. Parameters used to calculate CO_2 storage efficiency for the Hermosa Group in San Juan Basin, New Mexico.

Area (km^3)	Thickness (ft)	Porosity % (min, avg, max)	Salinity (TDS)	Permeability (mD)	Temperature (°C)	Geothermal Gradient
9,444	See Figure 30	3.0, 9.9, 14.2	85000	0.2	See Figure 32	47°C/km



Figure 34. A map of overburden on the Hermosa Group.

The thickness varies uniformly across the basin, and the data from the Hermosa Group isopachous map was used to determine the thickness. Porosity varies greatly throughout the section from almost zero to close to 25%, so the capacity estimates can also vary greatly from the minimum to maximum value.

The porosity and permeability data comes from less than 10 values from core reports within the basin. Since most of the Hermosa Group wells were drilled more than 50 years ago, there are only a few bottom-hole temperatures available

Table 7 is the CO_2 storage capacity based on the data within Table 6.

Table 7. CO_2 Storage Capacity (metric tonnes) *for the Hermosa Group in San Juan Basin, New Mexico.*

Storage Efficiency		
0.51%	2%	5.4%
1,672,530,703	6,558,943,933	17,709,148,619

Summary and Recommendations:

Based on the CO_2 storage capacity values, the Hermosa Group has the best potential for carbon storage. Like the Entrada Sandstone, the lack of well control in areas of the basin

means that the aerial extent is underestimated. The storage capacity value can only increase making the Hermosa Group a very attractive CO_2 reservoir.

Leadville Limestone —

Geologic Characterization:

Most of the wells that have been drilled into the Leadville Limestone are in the northwestern part of the state and the San Juan Basin (Fig. 35). In this area, the Leadville Limestone is relatively shallow (Fig. 36). Both oil and gas production within these Mississippian carbonates in the San Juan Basin occurred from a few fields (Table 1), but they have all been shut-in for the last 20 to 30 years. They were structural plays located on anticlines (Fassett, 1983). The reservoirs were porous limestones and dolomites, fossiliferous and oolitic limestones and solution-collapse breccias. Mississippian exploration has been limited over the years due to the expense of drilling into these deep strata.

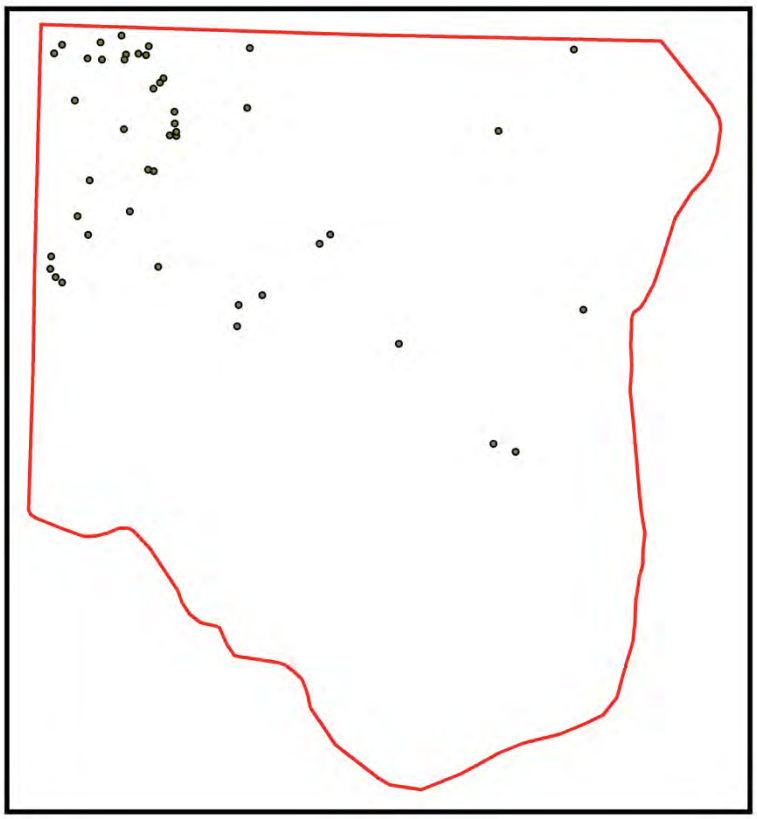


Figure 35. A well density map showing the scarcity of wells.

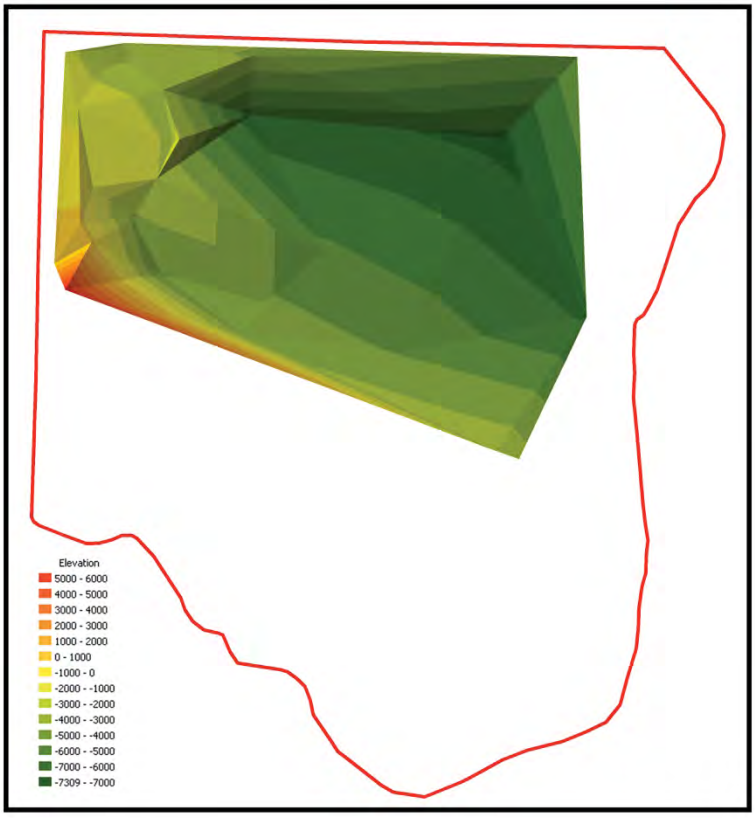


Figure 36. A structural map on top of the Leadville Limestone/ Arroyo Peñasco Group (elevation = ft).

The Mississippian Leadville Limestone unconformably overlies the Devonian Ouray Formation and ranges in thickness from 0 to over 300 feet thick in the San Juan Basin (Figs. 37 to 38). In the southern areas of the San Juan Basin, the Leadville is equivalent to the Arroyo Peñasco Group. In places, the Leadville Limestone/Arroyo Peñasco Group lies directly on the weathered Precambrian surface due to erosion of the underlying Cambrian and Devonian units (McLemore et al., 1986a). The Leadville Limestone consists of shallow marine, crinoid-rich limestones and dolomites (Fig. 39). Further to the south and east, the Arroyo Peñasco Group grades from shallow marine to supratidal carbonate and evaporite deposits. After Mississippian deposition, a major regression event resulted in an exposure that produced dissolution and brecciation within the Leadville Limestone resulting in a karst topography. Within the karstified sediments, there are porous breccia horizons that have potential as reservoirs (Armstrong and Mamet, 1977; Ulmer and Laury, 1984). The Leadville Limestone is unconformably overlain by nonmarine sediments of the Pennsylvanian Molas Formation.

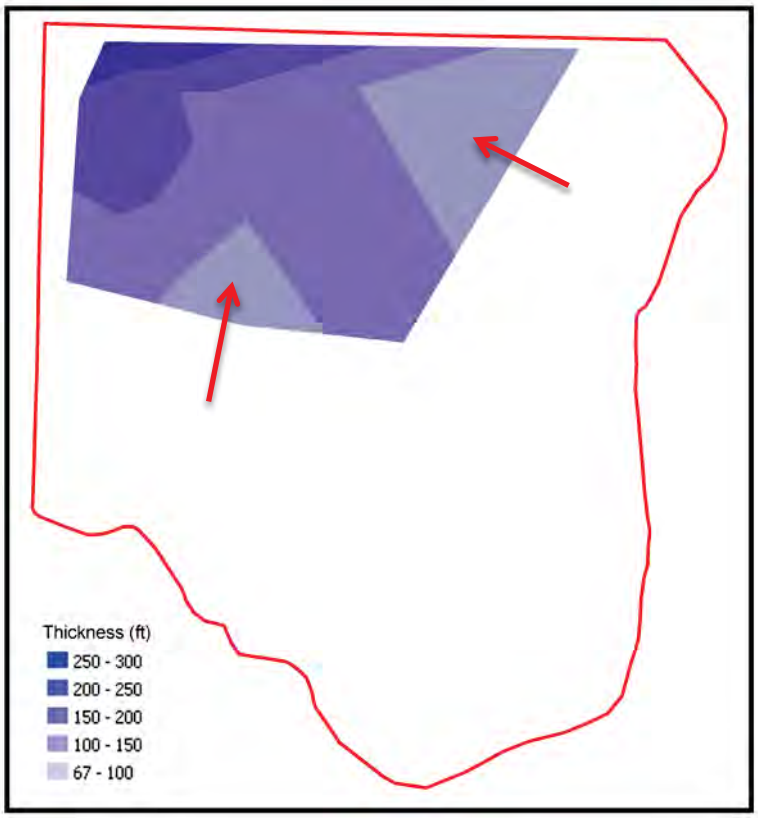


Figure 37. An isopachous map based on the wells within the database. The two arrows point to thin areas that are adjacent to the Peñasco Uplift and the Chaco Slope in Figure 37.

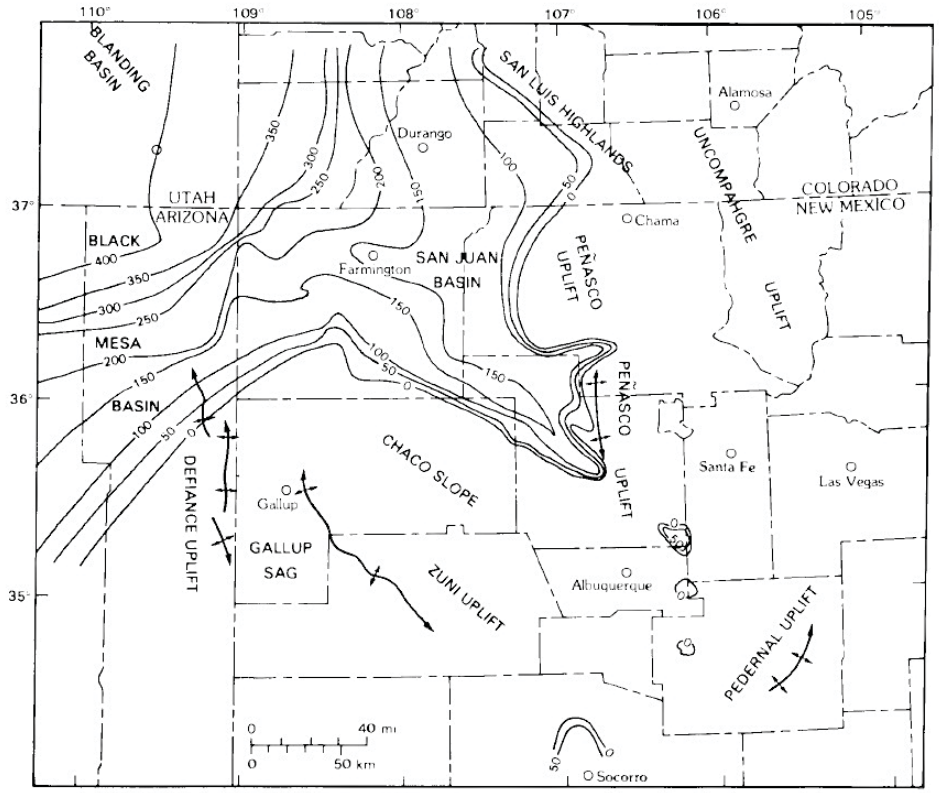


Figure 38. An isopachous map from Armstrong and Holcomb (1989) showing their interpretation of the distribution of Mississippian sediments in the San Juan Basin and adjacent areas based on well and outcrop data.

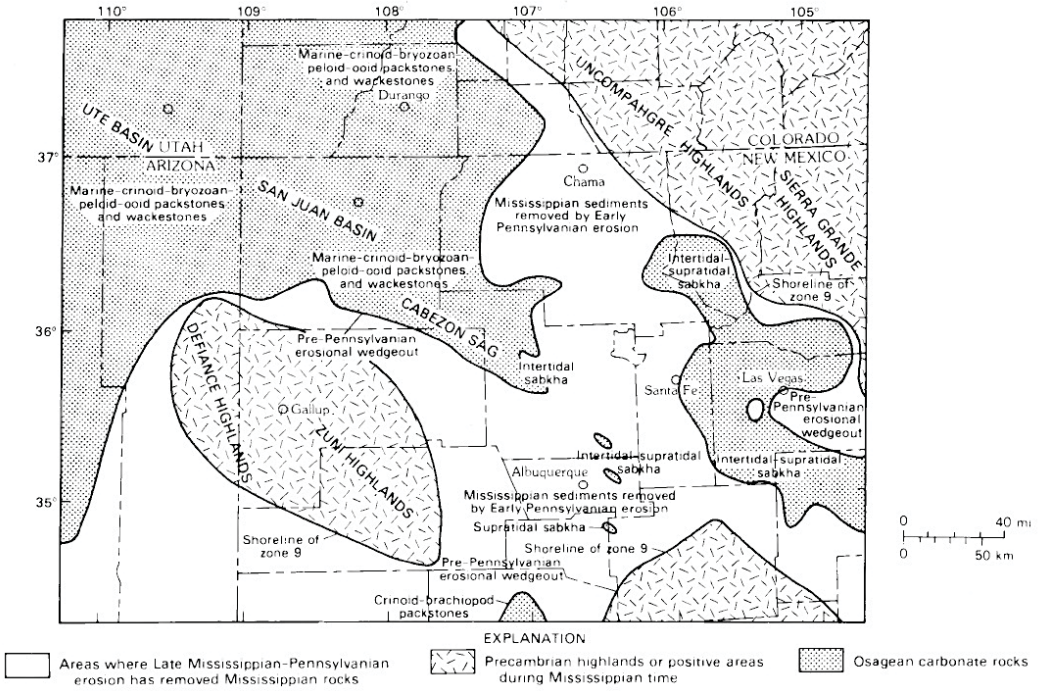


Figure 39. Deposition environments of the Leadville Limestone (from Armstrong and Holcomb, 1989).

CO2 storage Capacity:

The parameters used to calculate the CO_2 storage capacity for the Leadville Limestone are located in Table 8. The basin area was determined from the overburden map (Fig. 40) by using the 3,000 ft contour as the minimum depth for injection of CO_2. The area is a minimum value since there are not enough wells to define the extent of the Leadville Limestone. On Figure 40, all the well data is from deeper than 3,600 feet. The actual area on the map is a small part of a possible Mississippian CO_2 reservoir.

Table 8. Parameters used to calculate CO_2 storage efficiency for the Leadville Limestone in San Juan Basin, New Mexico.

Area (km^3)	Thickness (ft)	Porosity % (min, avg, max)	Salinity (TDS)	Permeability (mD)	Temperature (°C)	Geothermal Gradient
12,247	See Figure 37	1.0, 4.0, 7.0	35000	_	See Figure 41	47°C/km

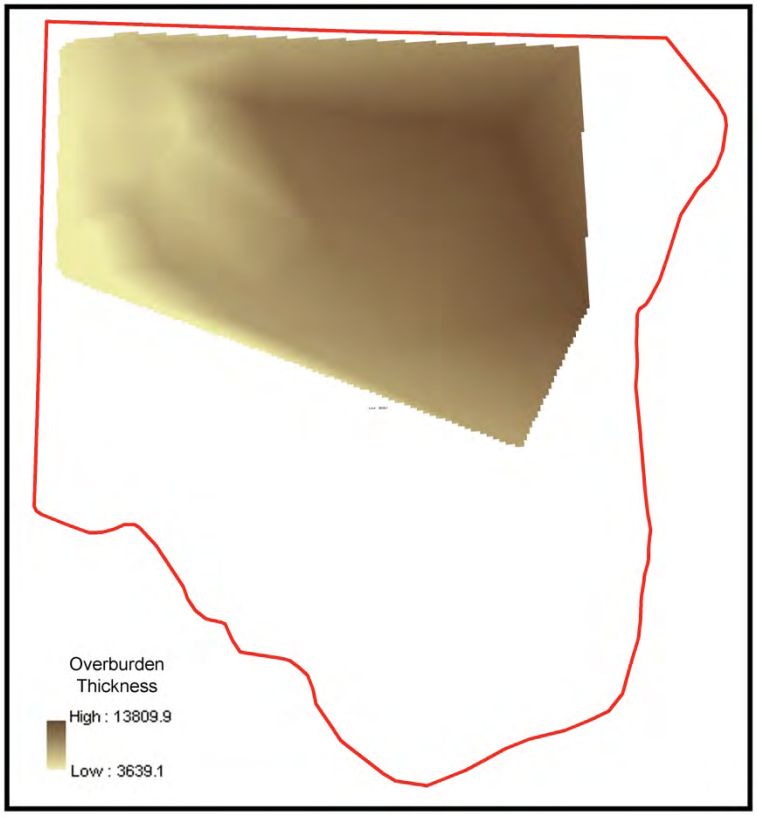


Figure 40. A map of the overburden on top of the Leadville Limestone.

The thickness varies across the basin, and it is dependent on the location of positive features on top of the Precambrian surface (Fig. 37). This data was used to determine the thickness used for the capacity equations. Porosity varies greatly throughout the section from 1% to close to 7%, so the capacity estimates can also vary from the minimum to maximum value.

The porosity and permeability data comes from less than 10 values from core reports within the basin. Since most of the Leadville wells were drilled more than 50 years ago, there is little data porosity permeability available. Unlike the Hermosa Group wells, there was enough temperature data to construct a map (Fig. 41).

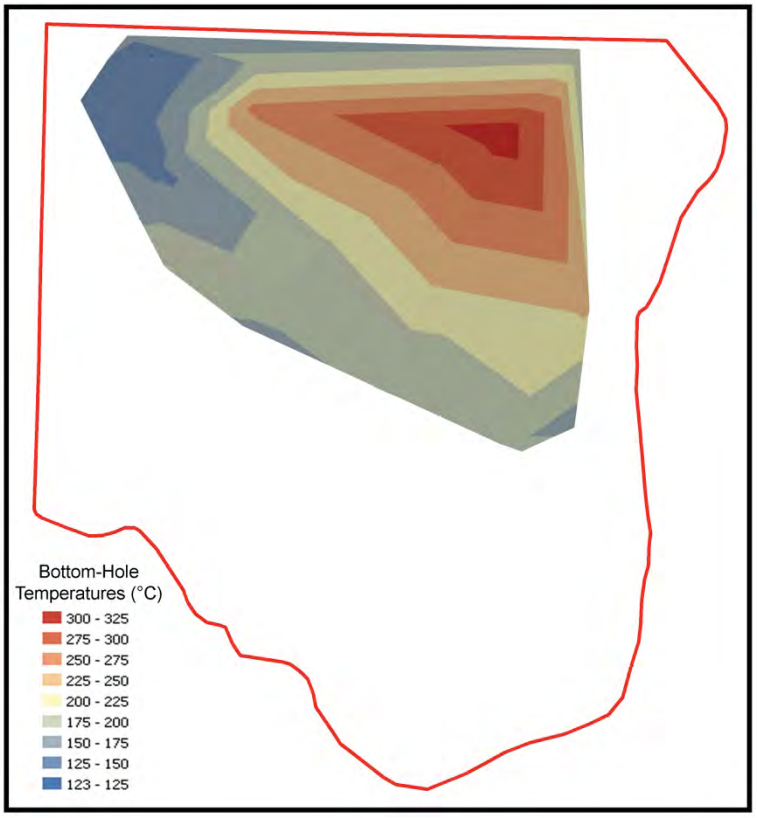


Figure 41. A map of the bottom-hole temperatures within the Leadville Limestone.

Table 9 is the CO_2 storage capacity based on the data within Table 8.

Table 9. CO_2 Storage Capacity (metric tonnes) *for the Leadville Limestone in San Juan Basin, New Mexico.*

Storage Efficiency		
0.51%	2%	5.4%
42,728,636	167,563,275	452,420,844

Summary and Recommendations:

Based on the CO_2 storage capacity values, the Leadville Limestone, like the Entrada Sandstone, doesn't appear to have great potential for CO_2 storage. The overburden map underestimates the aerial extent of the unit because of the lack well coverage; therefore, the

storage capacity calculation will increase. With additional drilling, the area will cause the storage capacity to increase as the area and thickness of the unit is better delineated. This will make the Leadville and Arroyo Peñasco Group a much more attractive reservoir.

APPENDIX P

Utah Geological Survey Regional Studies for Capacity

Contents

Topic

Introductory Text & Maps

Dakota Text & Maps

Entrada/Navajo Text & Maps

DeChelly Text & Maps

Weber/White Rim Text & Maps

CAPACITY ASSESSMENT - UGS

Executive Summary

The UGS evaluated the Pennsylvanian – Permian Weber/White Rim, Jurassic - Triassic Entrada/Navajo, and Cretaceous Dakota reservoirs in the Uinta Basin and the De Chelly reservoir in Utah's portion of the Paradox Basin. The Entrada reservoir has the best potential of the reservoirs studied; the Weber/White Rim is too deep for near-term consideration.

The Weber/White Rim reservoir has 5338 MMT (2% E) of storage capacity but the majority of the capacity is in the deepest portion of the basin. No wells have penetrated the Weber/White Rim reservoir in the deep basin and the porosity may be much lower than what has been used for the storage calculations. The Entrada/Navajo reservoir has 19,048 MMT (2% E) of storage capacity in the Uinta Basin. The dune facies of the reservoir has good quality reservoir properties and is laterally extensive. The Dakota reservoir has 1988 MMT (2% E) of storage capacity but is generally thin and laterally discontinuous. The De Chelly Sandstone in the Paradox Basin has 139 MMT (2% E) of storage capacity. The reservoir has good reservoir properties but is less than 3000 feet (1000 m) depth throughout much of the basin resulting in a very limited area of potential storage.

Geologic Setting

The majority of Utah's oil and gas production comes from the eastern half of the state which lies within the Colorado Plateau. The major basins within Utah's Colorado Plateau are the: (1) Uinta, (2) Paradox, (3) Henry Mountains, and (4) Kaiparowits. The major uplifts are the: (1) Uncompaghgre, (2) San Rafael Swell (SRS), (3) Circle Cliffs, (4) Monument, (5) Wasatch Plateau, and (6) High Plateaus (figure 1).

The Uinta Basin is an asymmetric basin with an east-west axis (figure 2). The southern portion of the basin dips gently northward and the northern portion deeps steeply to the south. Tertiary and Cretaceous strata crop out in the south and define the southern boundary of the basin. The Uinta Basin has a very thick stratigraphic section with numerous potential CO_2 storage reservoirs that have large areal extent (figure 3).

The Paradox Basin has Cretaceous and Jurassic strata exposed throughout much of the basin (figure 4), which eliminates the Cretaceous Dakota and Jurassic Entrada Sandstones as potential CO_2 storage reservoirs. The Permian White Rim Sandstone is limited to the northern Paradox Basin where it is exposed in outcrop. The Permian De Chelly and Cedar Mesa Sandstones of the Cutler Group and the Mississippian Redwall (Leadville) Limestone have the most potential for CO_2 storage in the Paradox Basin (figure 5). The De Chelly lies at a depth of 3000 feet (1000 m) or more and has sufficient areal extent to be considered as a potential CO_2 storage reservoir. The Cedar Mesa and Redwall were not evaluated.

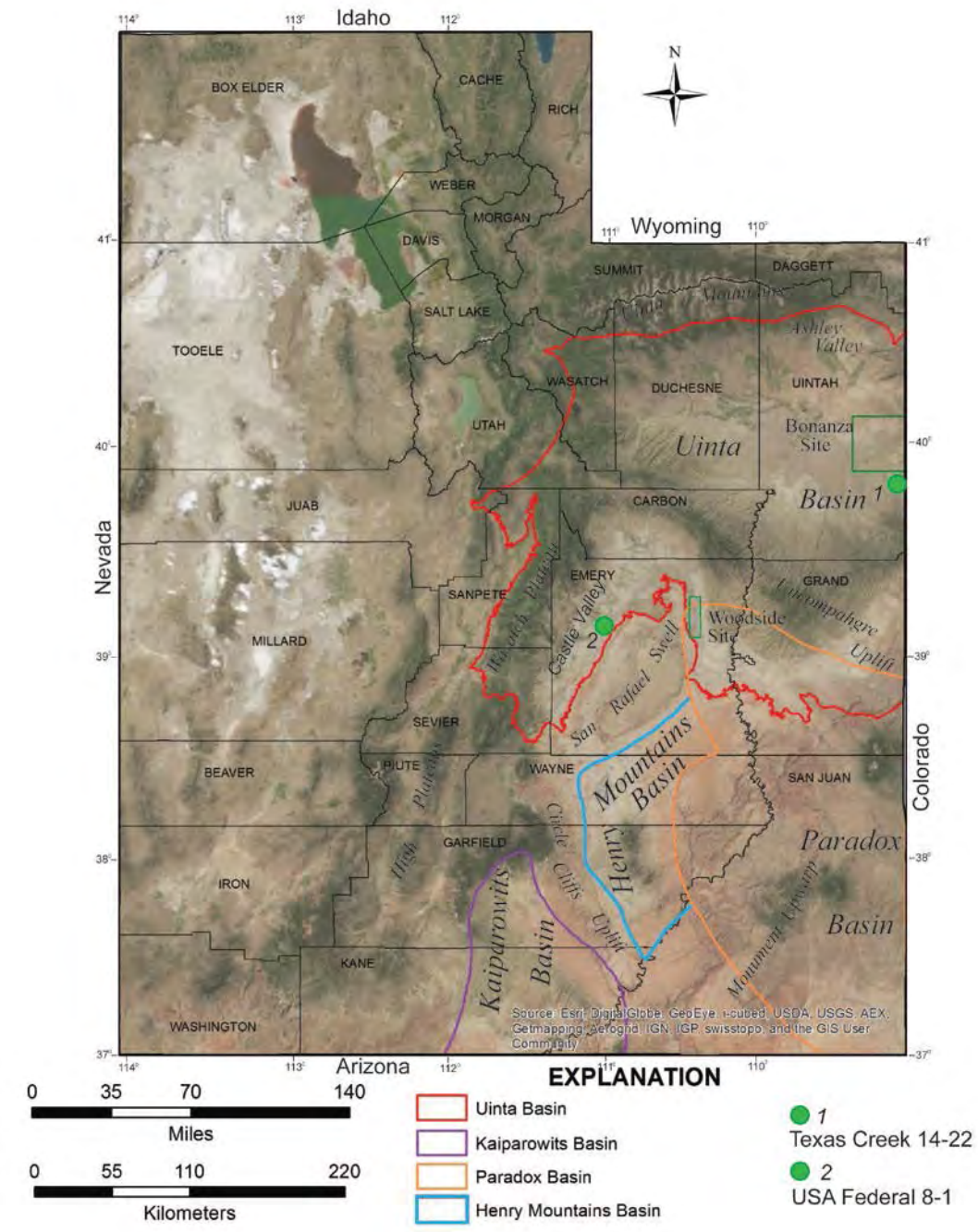


Figure 1. Map of Utah showing basins and uplifts of the Colorado Plateau. The sites Bonanza and Woodside (rectangular outlines), were evaluated as potential storage sites. Well 1 has a Weber Sandstone (?) core and 2 has a White Rim core.

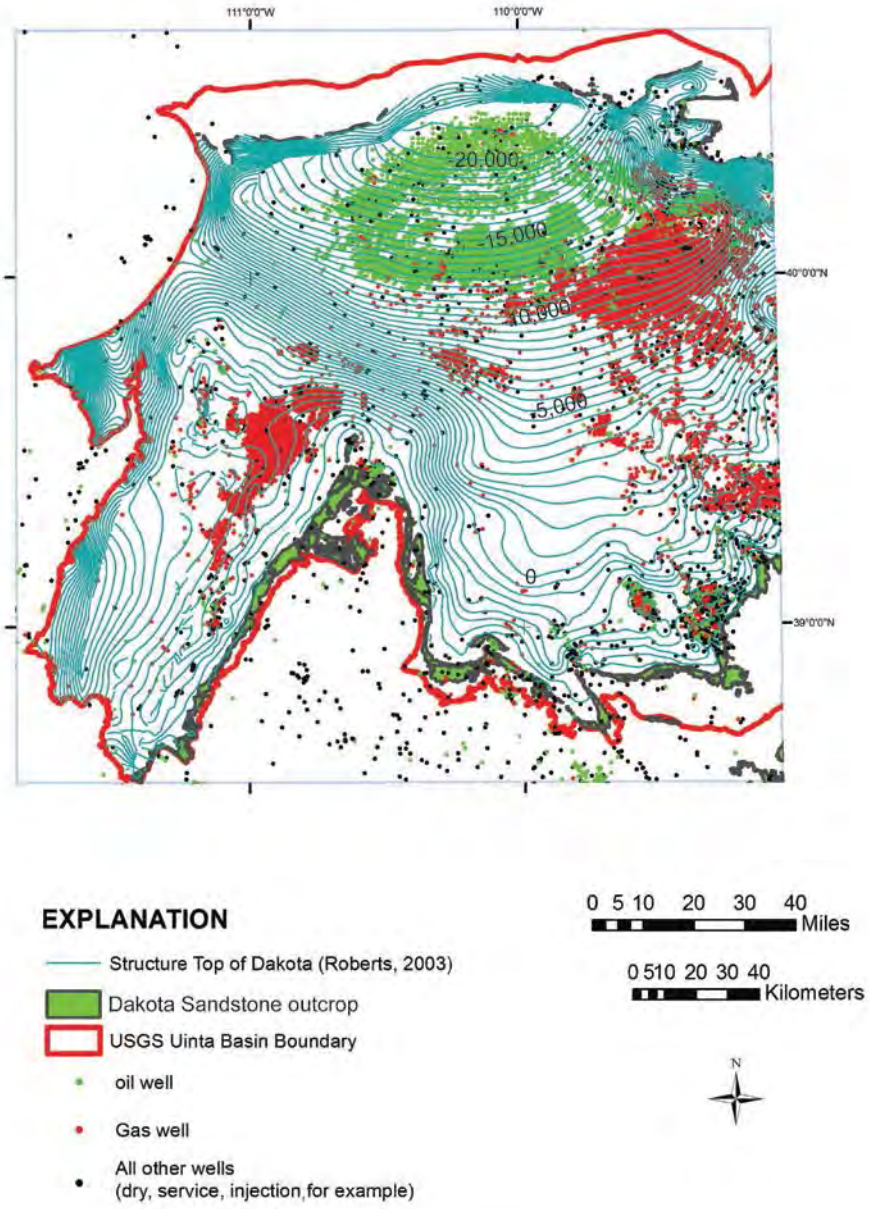


Figure 2. Structure top of the Dakota Sandstone. Contour lines digitized from Roberts (2003). The structure of most of the northern deeper basin was determined by projecting shallower wells to the Dakota. Contour interval 500 feet (150 m), mean sea level datum.

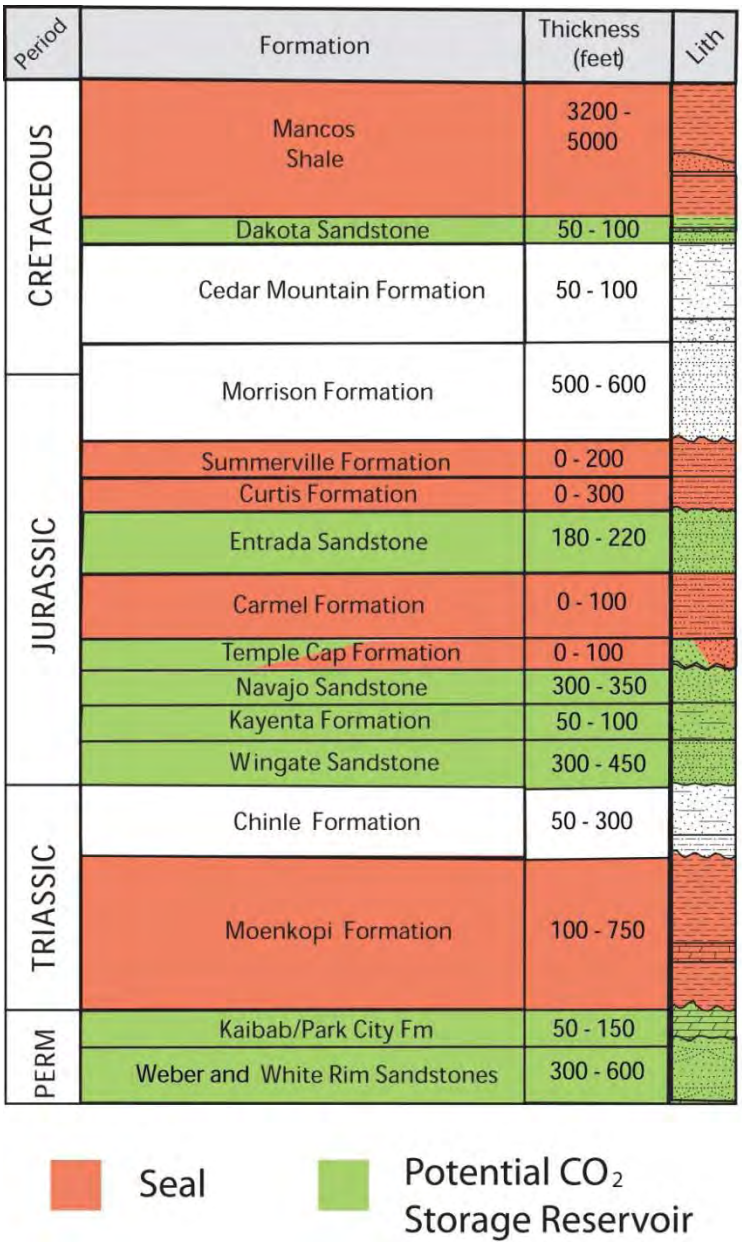


Figure 3. Stratigraphic column for the Uinta Basin showing saline reservoirs with the potential to store CO_2 and associated seals. Due to facies change, such as within the Temple Cap Formation, some formations can be a potential storage reservoir in one location and a seal in another. Thicknesses are generalized and based on Hintze and Kowallis, 2009.

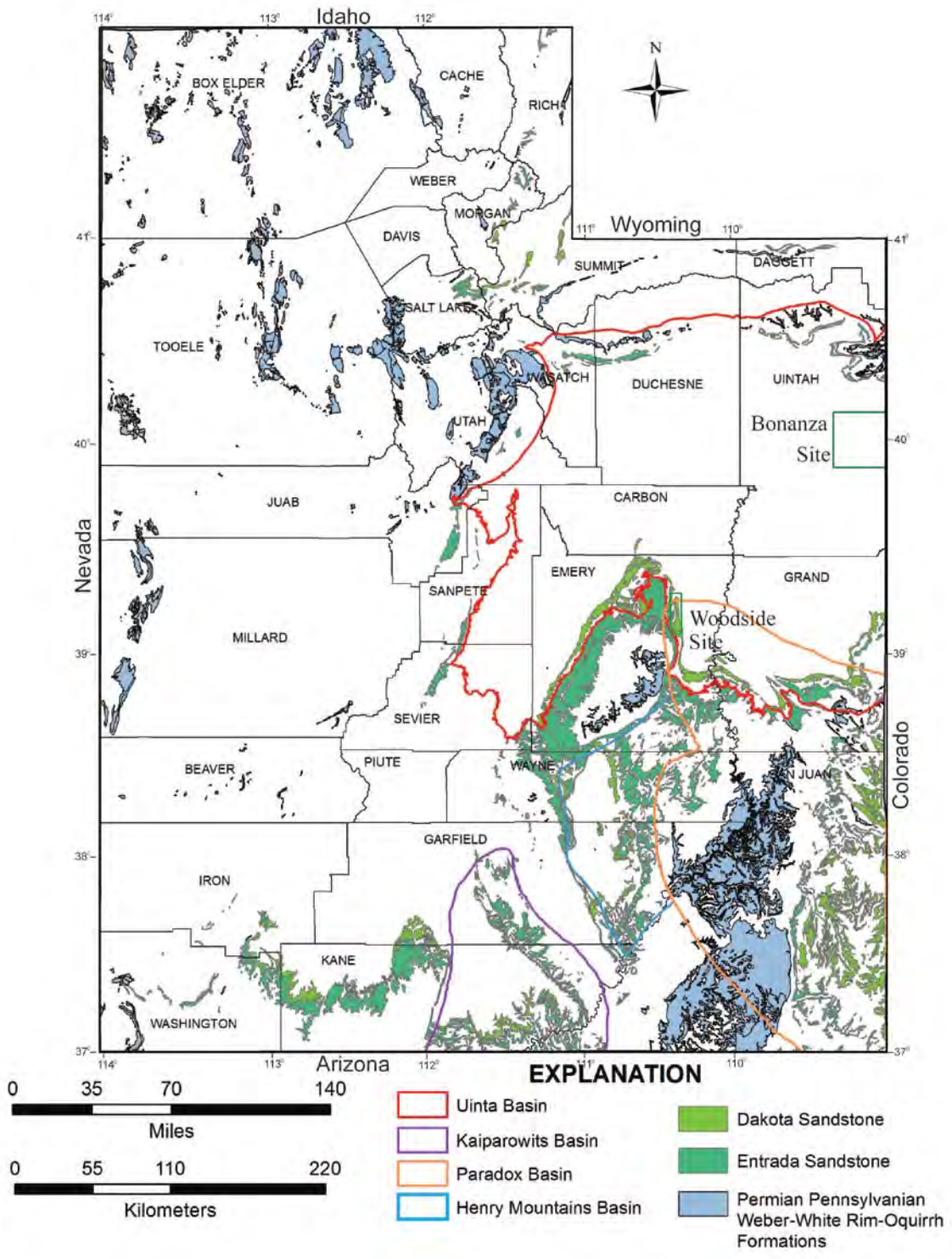


Figure 4. Map of Utah showing the basin outlines and outcrops of the Dakota, Entrada, and Weber Sandstones and equivalent formations.

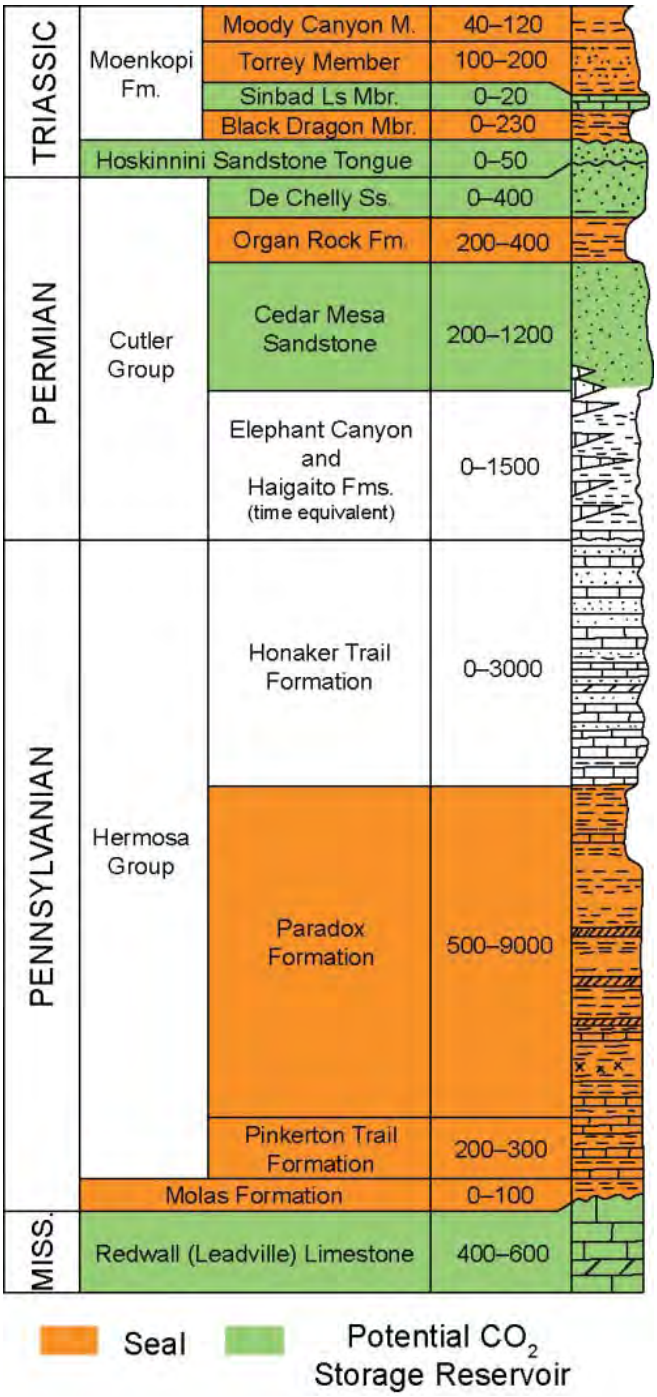


Figure 5. Stratigraphic column for the Paradox Basin showing saline reservoirs with the potential to store CO_2 and associated seals. Modified from Hintze and Kowallis, 2009.

The Henry Mountains, Kapararowits Basins, Monumnet Upwarp, Circle Cliffs, and High Plateaus were not studied for this project. These areas probably do not have significant CO_2 storage capacity in the primary reservoirs studied (Dakota, Entrada, and Weber) due to poor reservoir quality and/or shallow exposure. Much of the Wasatch Plateau and Uncompahgre Uplift lie within the Uinta Basin study area.

Methods

A database was developed in Excel® for each of the reservoirs: (1) Weber/White Rim, (2) De Chelly, (3) Entrada, and (4) Dakota. The drill depth and thickness of each reservoir were gathered from numerous well databases such as Division of Oil, Gas, and Mining and internal UGS databases. Many of the well logs were digitized into LAS format for easier correlation; others were viewed in tif image format downloaded from the Utah Division of Oil, Gas, and Mining website (http://oilgas.ogm.utah.gov). Formation boundaries in the databases were quality checked by correlating logs and then making corrections as needed. Additional formation tops were also added to the database from these well log correlations.

Regional studies rarely have sufficient data, and the data is never adequately spaced throughout the basin. Structure contour mapping using only well data misrepresents major portions of the basin. Figure 6 is a structure contour map on the top of the Dakota Sandstone using only well data. The basin axis (false axis) is shifted south (compare to figure 2) and the deepest part of the basin is shown as much shallower than it really is. This structural error results in errors in the overburden map, temperature and pressure calculations, all of which contribute to errors in the calculation of the CO_2 density and ultimately the storage

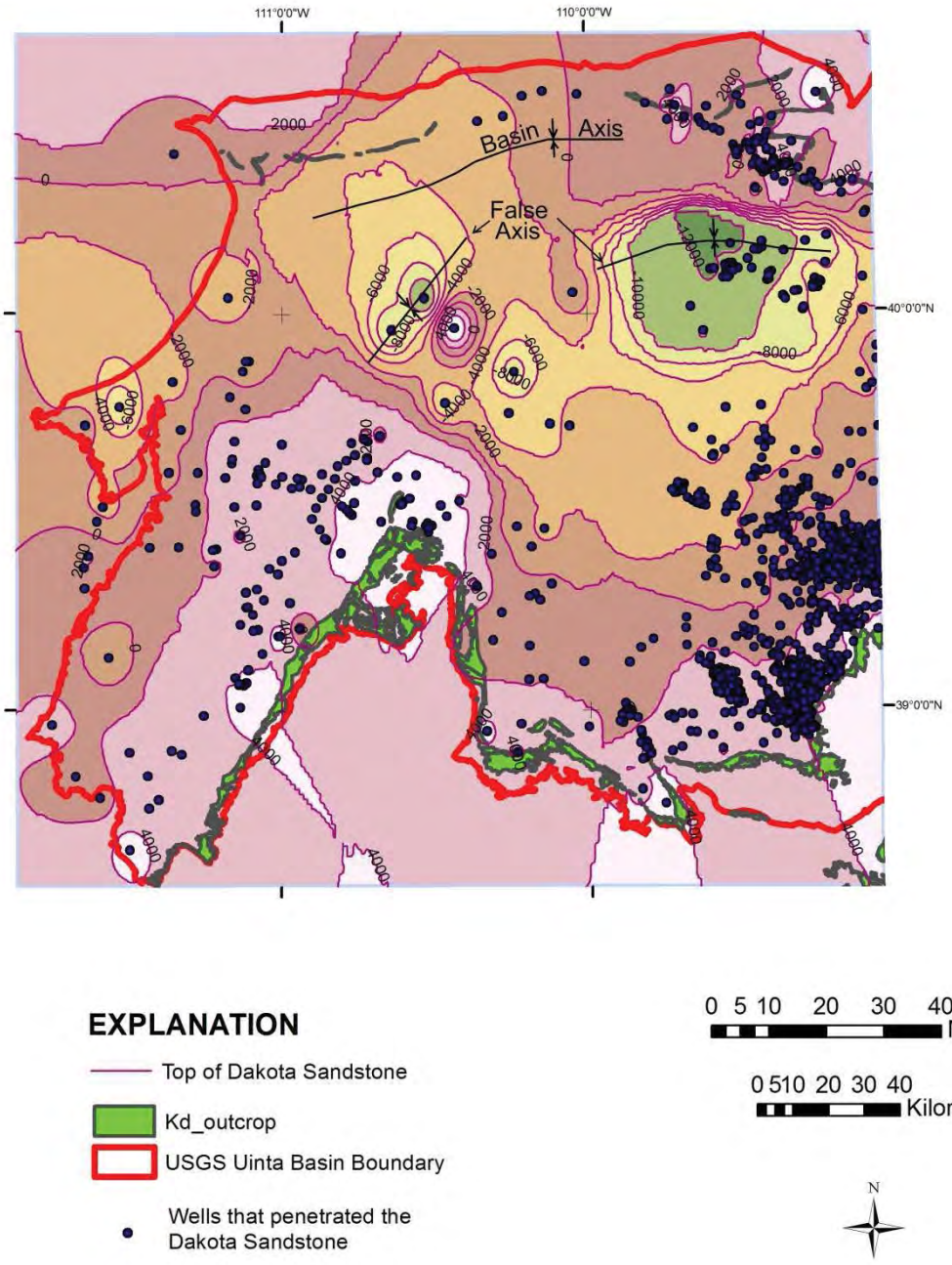


Figure 6. Structure on top of the Dakota Sandstone using only data from wells that penetrated the Dakota. The deepest portion of the basin has no Dakota data so an incorrect basin axis (labeled false axis) is mapped south of the actual axis. Contour interval 2000 feet (600 m), mean sea level datum.

capacity calculation. The Dakota structure by Roberts (2003) (figure 3) was constructed by using Dakota well tops and projecting to the Dakota the hundreds of shallower wells in the deeper part of the basin. This resulted in a very accurate structure contour map for the Uinta Basin.

The UGS took the digital structural contour data from Roberts (2003) and converted the lines to points every 2000 m (6505 ft) (figure 7). This point data was added to the UGS Dakota well database and used to grid the Dakota structure in the Uinta Basin. The structural elevations from the Entrada and Weber/White Rim well top databases were plotted on base maps. Structure contour maps of the top of Entrada and top of Weber/White Rim were hand contoured using the well data and following similar strike and dip of the Dakota structure map. The hand contoured maps were digitized and the contours were converted to point data which were added to the respective well databases. The expanded well databases were used to grid the structure of the top of the Entrada and Weber/White Rim. A structure contour map of the top of the De Chelly Sandstone was generated using well data.

A single average porosity value was assigned to each reservoir evaluated (except Weber/White Rim) based on a review of logs and published reports for the respective reservoir. Basin-wide average gradients for each reservoir were used to calculate the temperature and pressure in each grid cell. An average porosity value was determined for each Weber/White Rim well penetration based on the porosity log; temperature was taken from the log headers. These data were used to create porosity and temperature grids for the Weber/White Rim.

The well databases were used to generate structure and thickness maps of each of the reservoirs in ArcMap®. The datasets were gridded using 1 km^2 grid cells. A digital elevation model (DEM) was gridded using the same grid pattern for each reservoir. The structural elevation grids from each reservoir were subtracted from the DEM grids to produce overburden, or drill depth, grids. The grid data (structure, overburden, and thickness) with 3000 feet (1000 m) or larger overburden thickness were exported from ArcMap® and brought into an Excel® spreadsheet developed by EGI for calculating CO_2 storage capacity. We discovered the dataset exceeded the capacity of Excel® if we didn't limit the export from ArcMap® to only the grids with overburden of 3000 feet (1000 m) or more. In the spreadsheet each grid (row of data) was assigned a temperature and pressure value based on a basin-wide temperature and pressure gradient for each reservoir. A macro in the spreadsheet calculated the density of CO_2 for each grid using the pressure and temperature data. The data was then used in equations in the EGI spreadsheet to calculate CO_2 storage capacity for each grid at 0.5%, 2.0%, and 5.4% efficiency. The completed spreadsheets were brought back into ArcMap® and used to create geodatabases which were then sent to EGI for inclusion into the NATCARB database.

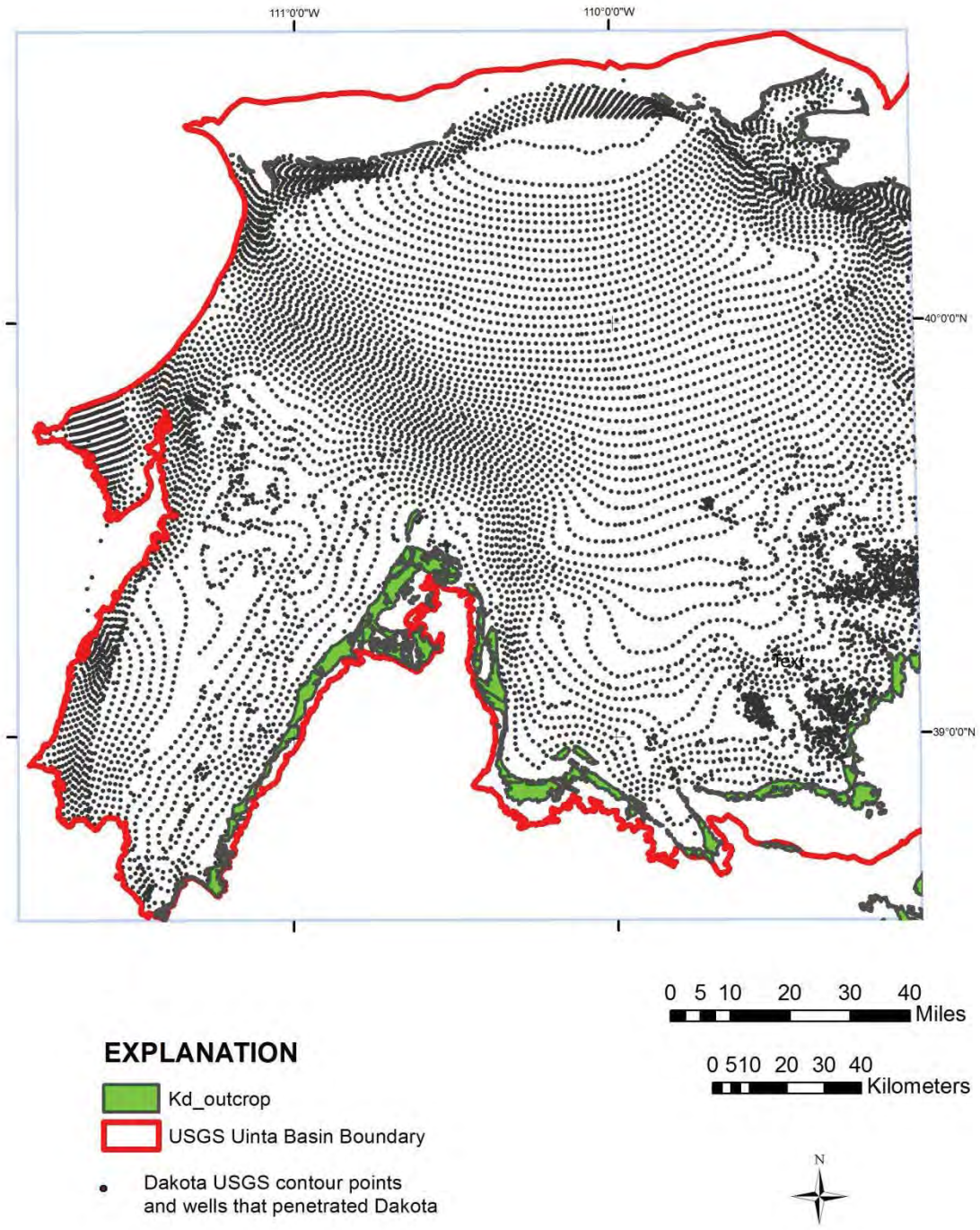


Figure 7. Points generated from Roberts (2003) structure contour map of the top of the Dakota Sandstone and wells that penetrated the Dakota. The contour point data set was added to the Dakota well database.

CO_2 Storage Capacity

The UGS mapped the Pennsylvanian-Permian Weber and Permian White Rim Sandstones, Jurassic Entrada and Jurassic-Triassic Navajo Sandstones, and Cretaceous Dakota Sandstone, in the Uinta Basin. The Permian De Chelly Sandstone of the Cutler Group was mapped in the Paradox Basin. A detailed characterization of each reservoir is in the Appendix. The CO_2 storage capacity was calculated for each reservoir based on the mapped data and regional reservoir data using EGI storage capacity spreadsheet. The parameters used for each reservoir are shown in table 1 and the calculated CO_2 storage capacities are shown in table 2. The Uinta Basin has 26,374 MMT (at 2% E) of storage capacity mostly in the Entrada/Navajo reservoir which has 19,048 MMT of storage capacity (72% of the basin total).

Table 1. Parameters used to calculate the CO_2 storage capacity of the Dakota, Entrada/Navajo, Weber/White Rim reservoirs in the Uinta Basin and the De Chelly reservoir in the Paradox Basin. Ft = feet, m = meters, km^2 = kilometers squared, F = degrees Fahrenheit, C = degrees Celsius, D = depth, psi = pounds per square inch, and kpal = kiloPascals.

	Area	Average Reservoir Thickness	Average Porosity	Temperature Gradient	Pressure Gradient
Dakota	11,100 $miles^2$ 29,000 km^2	131 ft 40 m	12%	55 °F + (0.0138*D) 25 °C/km	0.45 psi/ft 3.1 kPal/ft
Entrada/Navajo	11,600 $miles^2$ 30,000 km2	1195 ft 360 m	16%	55 °F + (0.0138*D) 25 °C/km	0.45 psi/ft 3.10 kPal/ft
Weber/White Rim	10730 $miles^2$ 27,792 km^2	430 ft 130 m	7%	Variable	1.14 psi/ft 7.9 kPal/ft
De Chelly	600 $miles^2$ 1600 km^2	150 ft 50 m	20%	55 °F + (0.0115*D) 20 °C/km	1.1 psi/ft 7.3 kPal/ft

Table 2. CO_2 storage capacity of the Dakota, Entrada/Navajo, Weber/White Rim reservoirs in the Uinta Basin (UB) and the De Chelly reservoir in the Paradox Basin using three different efficiency factors.

CO_2 Storage Capacity in Million Metric Tonnes			
	Efficiency Factors		
	0.5%	2.0%	5.4%
Dakota	508	1988	5369
Entrada/Navajo	4857	19,048	51,427
Weber/White Rim	1361	5338	14,413
UB TOTAL	***6726***	***26,374***	***71,209***
De Chelly	36	139	377
GRAND TOTAL	***6,762***	***26,513***	***71,586***

The Dakota Sandstone is dominantly a fluvial deposit with interbedded channel sandstones and flood plain mudstones resulting in a complex, highly heterogeneous reservoir. We calculated 1988 MMT (at 2% E) of CO_2 storage capacity for the Dakota in the Uinta Basin. Due to the heterogeneity of the reservoir, a more detailed study of subsurface data will identify areas of thick reservoir versus areas with little to no reservoir. The channel sandstones have the potential for numerous stratigraphic traps within the basin.

The Entrada and Navajo Sandstones are separated by the Carmel Formation, but were treated as a single reservoir to be consistent with mapping in Colorado where the Carmel is missing and the Entrada lies directly on the Nugget Sandstone (Navajo equivalent). The Entrada/Navajo reservoir has the most CO_2 storage capacity (19,048 MMT at 2% E) of the formations studied. The dune facies of the Entrada and Navajo provide thick, laterally continuous deposits throughout most of the eastern Uinta Basin and have excellent porosity and permeability.

The Weber and White Rim Sandstones were evaluated as a single reservoir (Weber/White Rim) and have the second largest CO_2 storage capacity (5338 MMT at 2% E). The Weber/White Rim reservoir is dominantly eolian coastal dune deposits with good reservoir properties. The Weber changes rapidly from north to south in the eastern Uinta Basin from a good quality quartz arenite sandstone reservoir to poorer quality arkosic alluvial fan deposits of the Maroon Formation. From east to west, the Weber becomes more quarzitic with interbedded limestone and dolomite. This facies change limits the extent and, therefore, the total storage capacity of the Weber. The White Rim is shallow and outcrops in many areas greatly limiting the extent of the reservoir available for storage.

The De Chelly Sandstone is a good quality reservoir in the Paradox Basin and we calculated 139 MMT of CO_2 storage capacity (2% E). The De Chelly crops out in many locations in the basin, and the extent of the De Chelly that is 3000 feet (1000 m) or deeper is limited, greatly reducing the storage capacity.

References

Hintze, L.F., and Kowallis, B.J., 2009, Geologic history of Utah: Brigham Young University Geology Studies Special Publication 9, 225 p.

Roberts, L.N.R., 2003, Structure contour map of the top of the Dakota Sandstone, Uinta-Piceance Province, Utah and Colorado, *in* USGS Uinta-Piceance Assessment Team compilers, Petroleum systems and geologic assessment of oil and gas in the Uinta-Piceance Province, Utah and Colorado, USGS DDS-69B, 14 p.

CRETACEOUS DAKOTA SANDSTONE

Data Resources

The Dakota Sandstone produces natural gas and is a primary exploration target throughout much of the Uinta Basin. However, wells penetrating the Dakota are located mostly in the southern, shallower part of the Uinta Basin and are sparse in the northern, deeper part. We correlated a Dakota top in 1426 wells and a gross sandstone thickness in 1330 wells. There are numerous publications on the Dakota in the Uinta Basin, some of the more recent publications with well data that we incorporated into our database are Currie and McPherson (2006, 2008), and Currie and others (2008, 2012). Structure on top of the Dakota was mapped using well data and mapping by Roberts (2003). Sandstone thickness mapping used well data and mapped thickness data by Doubs and others (2004).

Geologic Characterization

The Dakota Sandstone is overlain by the Tununk Shale Member of the Cretaceous Mancos Shale and underlain by the Cretaceous Cedar Mountain Formation. The boundary between the Dakota and Cedar Mountain can be difficult to identify and in many well records the Cedar Mountain is included with the Dakota. The Dakota Sandstone is a highly heterogeneous collection of fluvial channels, overbanks, and marginal-marine deposits. Fluvial systems often incise to varying degrees into older fluvial and over bank deposits and the subsequent valley and channel filling results in reservoirs of different thickness, width, and connectivity (Currie and others 2012). The primary reservoir facies in the Dakota are channel and near shore marine sandstone beds.

We mapped the structure on top of the Dakota Sandstone (figure 1) then generated an overburden map (figure 2) by subtracting the structure grid from a DEM grid. The net reservoir thickness (figure 3) is the gross thickness of the sandstone within the Dakota. The average reservoir thickness is 131 feet (40 m) but large variability can exist due to the lenticular nature of channel deposits. Predicting reservoir thickness in areas with very little well control is high risk but the heterogeneity of the reservoir provides good potential for development of stratigraphic traps.

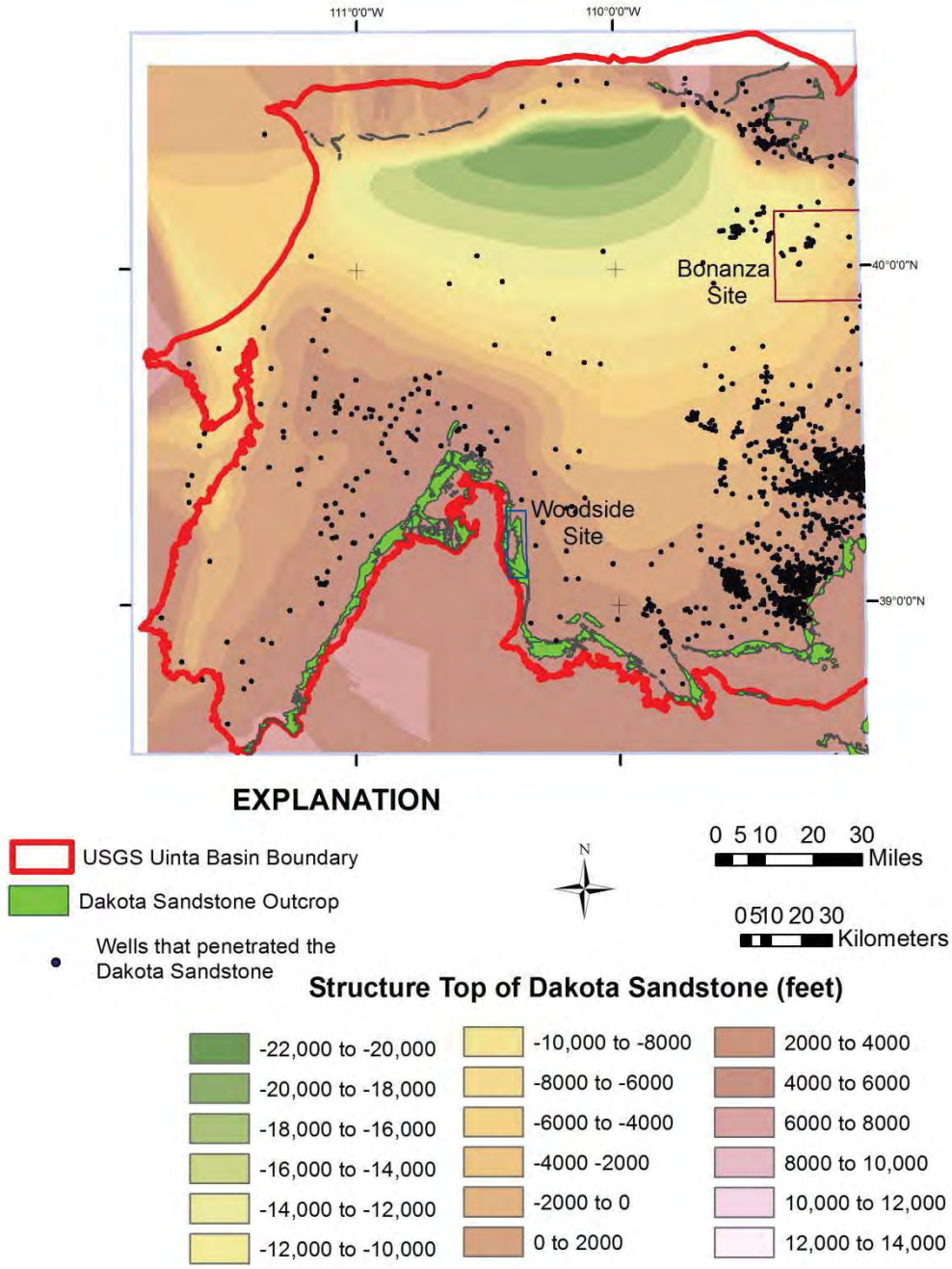


Figure 1. Structure on top of Dakota Sandstone. Contour interval 2000 feet (600 m), datum is mean sea level.

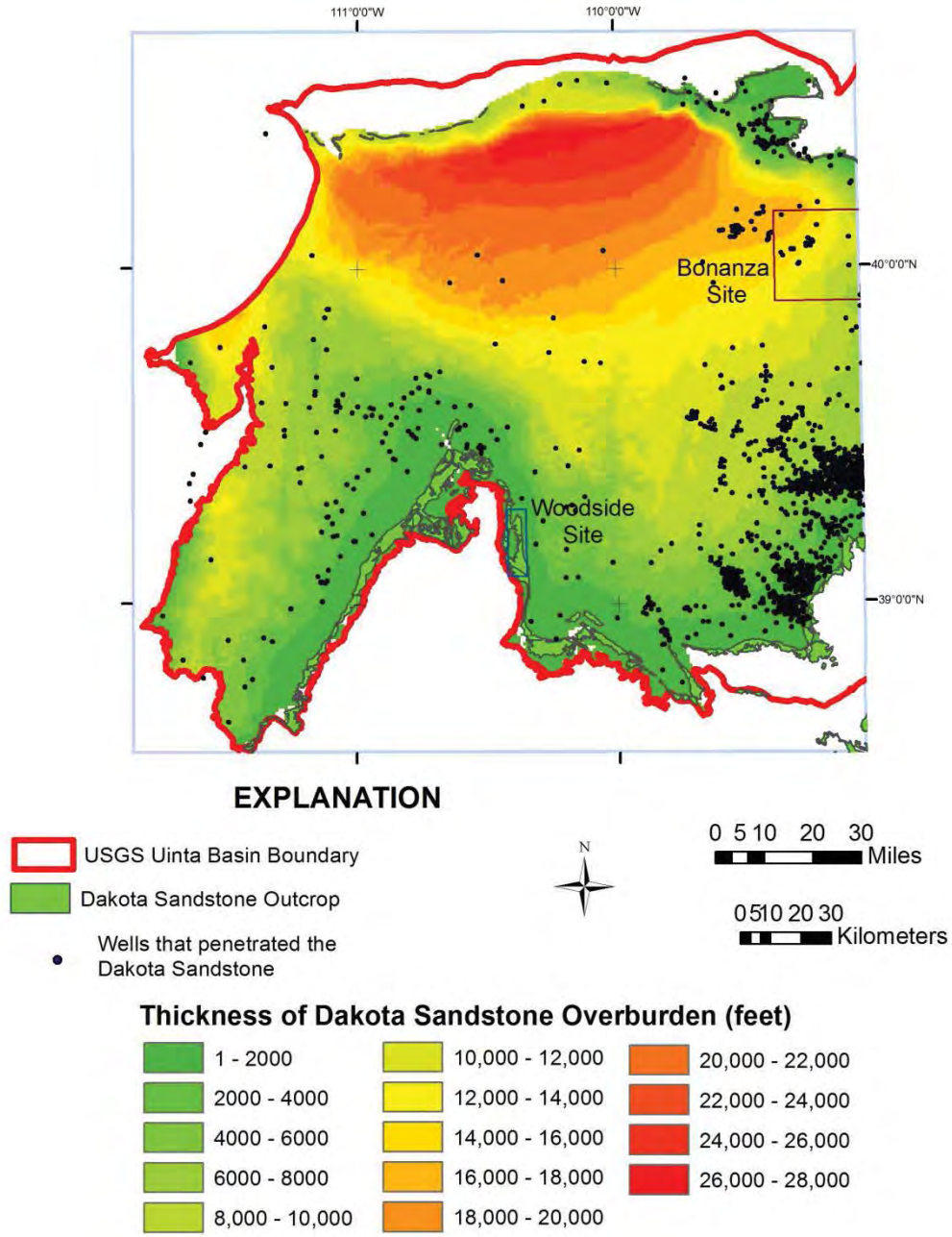


Figure 2. Thickness of the Dakota Sandstone overburden in feet. Contour interval is 2000 feet (600 m).

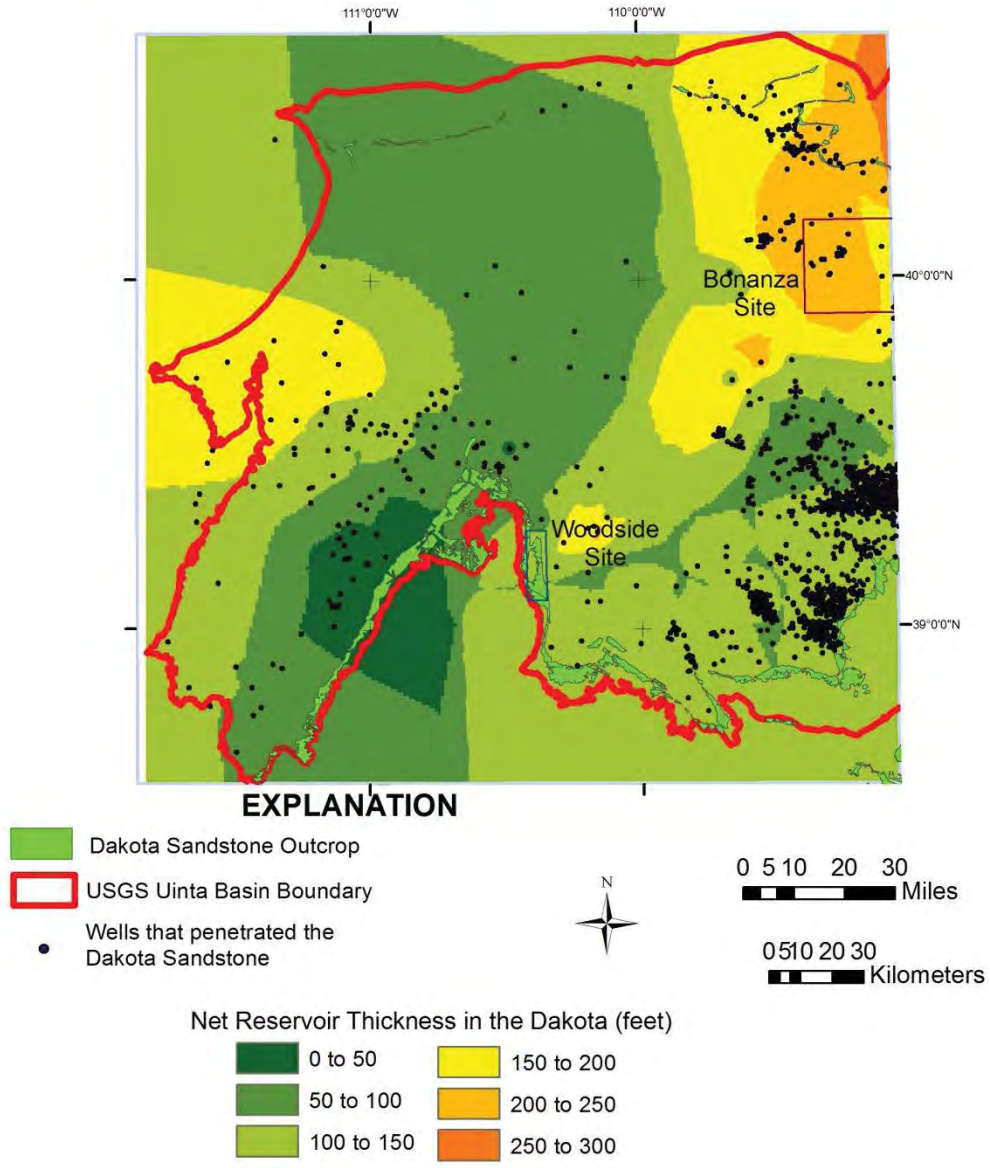


Figure 3. Net reservoir thickness (total sandstone) of the Dakota Sandstone. Reservoir is defined as the total volume of sandstone in the formation. Contour interval is 50 feet (15 m).

CO_2 Storage Capacity

We mapped the storage capacity of the Dakota reservoir using a 1 km^2 grid (figure 4). The storage capacity potential closely follows the net reservoir thickness (figure 3) indicating reservoir thickness is the dominant parameter. The Dakota has the thinnest average reservoir thickness and the lowest average porosity (table 1) of the three formations studied. As a result, in the Uinta Basin the Dakota Sandstone has the least amount of potential CO_2 storage capacity (table 2).

Table 1. Parameters used to calculate the CO_2 storage capacity of the Dakota Sandstone reservoir in the Uinta Basin. Ft = feet, m = meters, km^2 = kilometers squared, F = degrees Fahrenheit, C = degrees Celsius, D = depth, psi = pounds per square inch, and kpal = kiloPascals.

	Area	Average Reservoir Thickness	Average Porosity	Temperature Gradient	Pressure Gradient
Dakota	11,100 $miles^2$ 29,000 km^2	131 ft 40 m	12%	55 °F + (0.0138*D) 25 °C/km	0.45 psi/ft 3.1 kPal/ft

Table 2. CO_2 storage capacity of the Dakota Sandstone reservoir in the Uinta Basin using three different efficiency factors.

CO_2 Storage Capacity in Million Metric Tonnes			
	Efficiency Factors		
	0.5%	2.0%	5.4%
Dakota	508	1988	5369

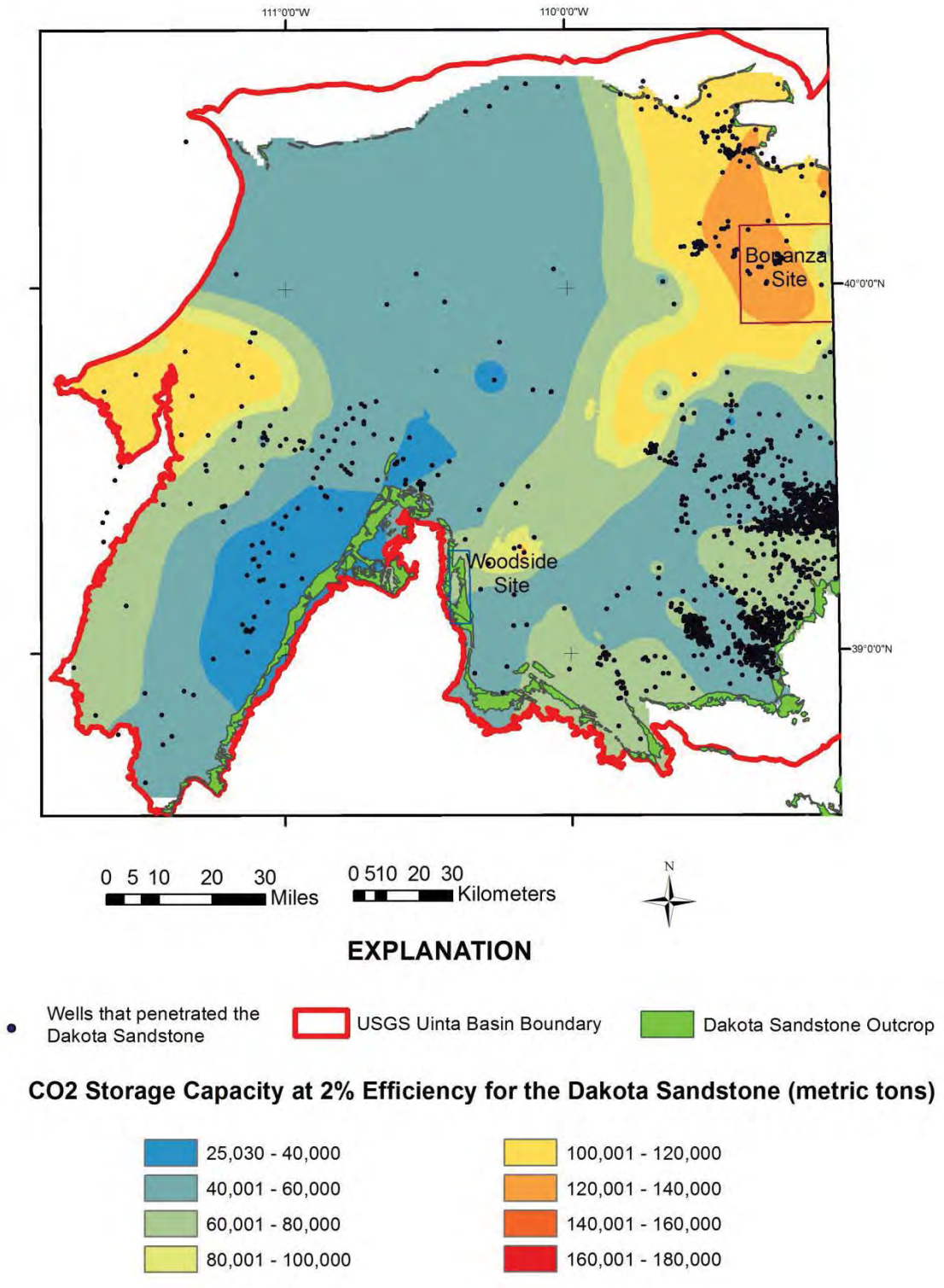


Figure 4. CO_2 storage capacity of the Dakota reservoir in metric tonnes per million square meter grid (1 km^2). The storage capacity of the Dakota closely follows the net reservoir thickness (figure 3). Calculation based on a 2% efficiency factor.

Summary and Recommendations

The Dakota Sandstone is a heterogeneous reservoir with lenticular channels and nearshore marine deposits. The depositional environment of the Dakota provides abundant opportunities for development of stratigraphic traps but creates highly variable reservoir thickness resulting in a low regional storage capacity potential relative to the Weber/Whit Rim and Entrada/Navajo reservoirs. We used a single value for porosity basin wide; the accuracy of the storage calculation can be greatly improved by more detailed porosity mapping.

References

Currie, B.S., and McPherson, M.L., 2006, Reservoir characterization of the Cretaceous Cedar Mountain and Dakota Formations, southern Uinta Basin – year-one report: UGS Open-File Report 492, CD-ROM.

Currie, B.S., and McPherson, M.L., 2008, Reservoir characterization of the Cretaceous Cedar Mountain and Dakota Formations, southern Uinta Basin – year-two report: UGS Open-File Report 516, CD-ROM.

Currie, B.S., Dark, J.P., McPherson, M.L., and Pierson, J.S., 2008, Fluvial channel architecture of the Albian-Cenomanian Dakota Formation, southern Uinta Basin , *in* Longman, M.W., and Morgan, C.D., editors, Hydrocarbon systems and production in the Uinta Basin, Utah: Utah Geological Association Publication 37, CD-ROM, 468 p. 65-80.

Currie, B.S., McPherson, M.L., Hokanson, W., Pierson, J.S., Homan, M.B., Pyden, T., Schellenbach, W., Purcell, R., and Nicklaus, D., 2012, Reservoir characterization of the Lower Cretaceous Cedar Mountain and Dakota Formations, northern Uinta Basin, Utah: UGS Open-File Report 597, CD-ROM.

Douds, A., Pancake, J., and Pratt, S., 2004, Assessing the technology needs of sub-economic natural gas resources Phase II – Anadarko and Uinta Basins: U.S. Department of Energy National Energy Technology Lab preliminary version unpublished report.

Roberts, L.N.R., 2003, Structure contour map of the top of the Dakota Sandstone, Uinta-Piceance Province, Utah and Colorado, *in* USGS Uinta-Piceance Assessment Team compilers, Petroleum systems and geologic assessment of oil and gas in the Uinta-Piceance Province, Utah and Colorado, USGS DDS-69B, 14 p.

APPENDIX - UGS

JURASSIC ENTRADA AND NAVAJO SANDSTONES

Data Resources

Natural gas is produced from the Entrada and Navajo Sandstones in the southern Uinta Basin. Oil and gas field studies by Suck and Glanville (1993) and Dyer and Donoho (2008) provide data on the Entrada reservoir. Recent data on the Navajo reservoir is discussed by Chidsey, Jr., and others (2007), Dalrymple and Morris (2007), and Morgan (2007). There are numerous well penetrations of the Entrada and Navajo (Nugget Sandstone) but much of the data is limited to the shallower southern portion of the data and there is little data showing what happens to the reservoir properties with depth. We correlated an Entrada top in 716 wells and 319 with gross thickness. We correlated a Navajo top in 457 wells and 371 wells with a gross thickness. We correlated 239 wells that had a combined thickness of Entrada and Navajo.

Geologic Characterization

The Entrada and Navajo Sandstones were evaluated as a single reservoir Entrada/Navajo, in an attempt to better match the Colorado data. The main body of the Entrada the Slick Rock Member and Navajo, are separated by the Carmel Formation or the Dewey Bridge Member of the Entrada (figure 1). In most of Colorado the Entrada rests directly on the Navajo (Nugget or Glen Canyon Group) and is difficult to determine the boundary from well logs so the Colorado geologists evaluated the Entrada and Navajo as one reservoir. The interval from the base of the Entrada to the top of the Navajo thins rapidly from west to east in the Uinta Basin and is less than 100 feet thick at the Utah Colorado border (figure 2)

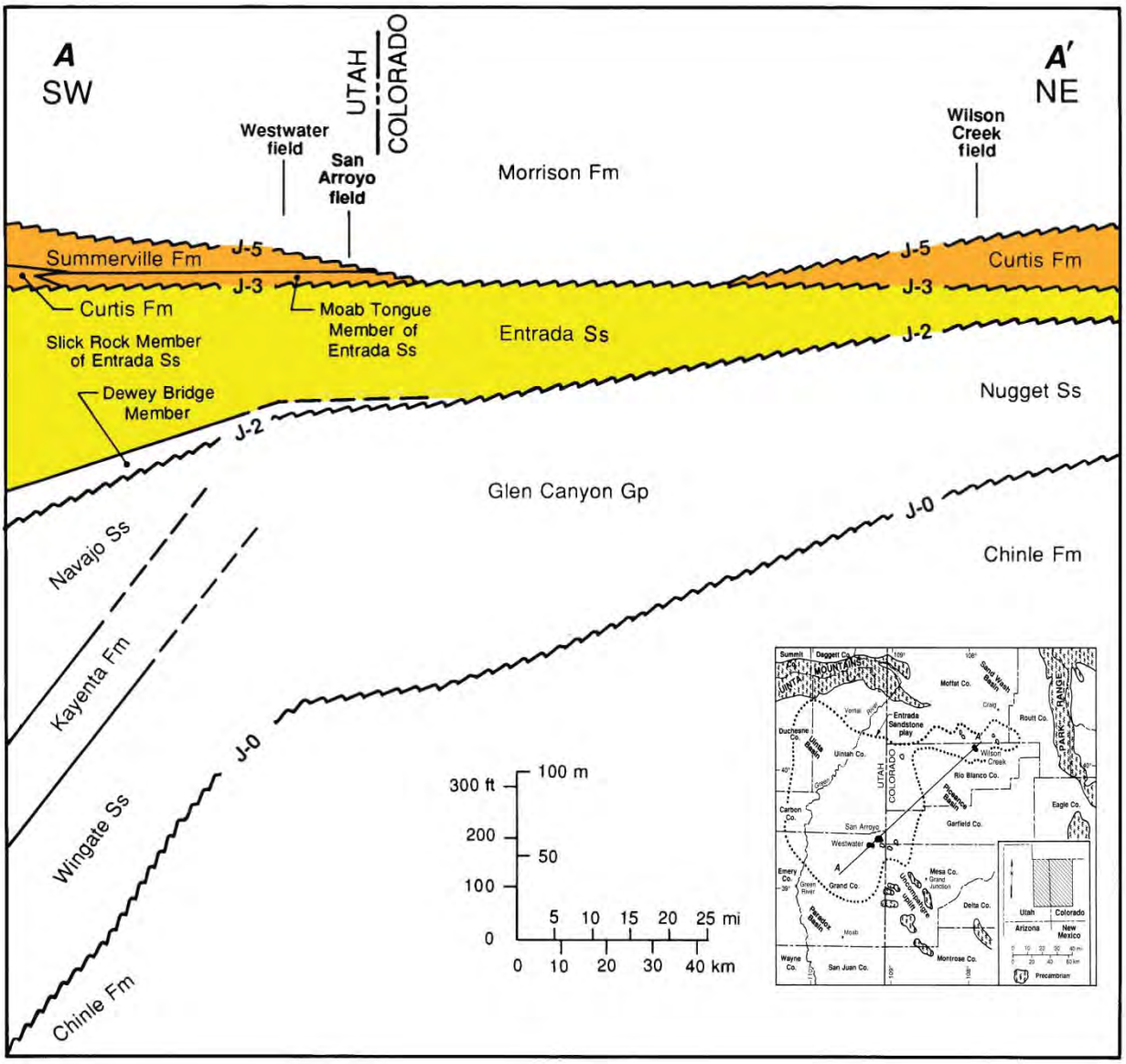


Figure 1. Southwest-to-northeast cross section showing the pinchout of the Dewey Bridge Member of the Entrada Sandstone. In most of the Uinta Basin the Carmel Formation separates the Entrada from the Navajo Sandstone. In most of Colorado the Entrada rests directly on the Navajo equivalent Glen Canyon Group or Nugget Sandstone making it difficult to distinguish between the Entrada and Navajo. Modified from Pipiringos and O'Sullivan (1978).

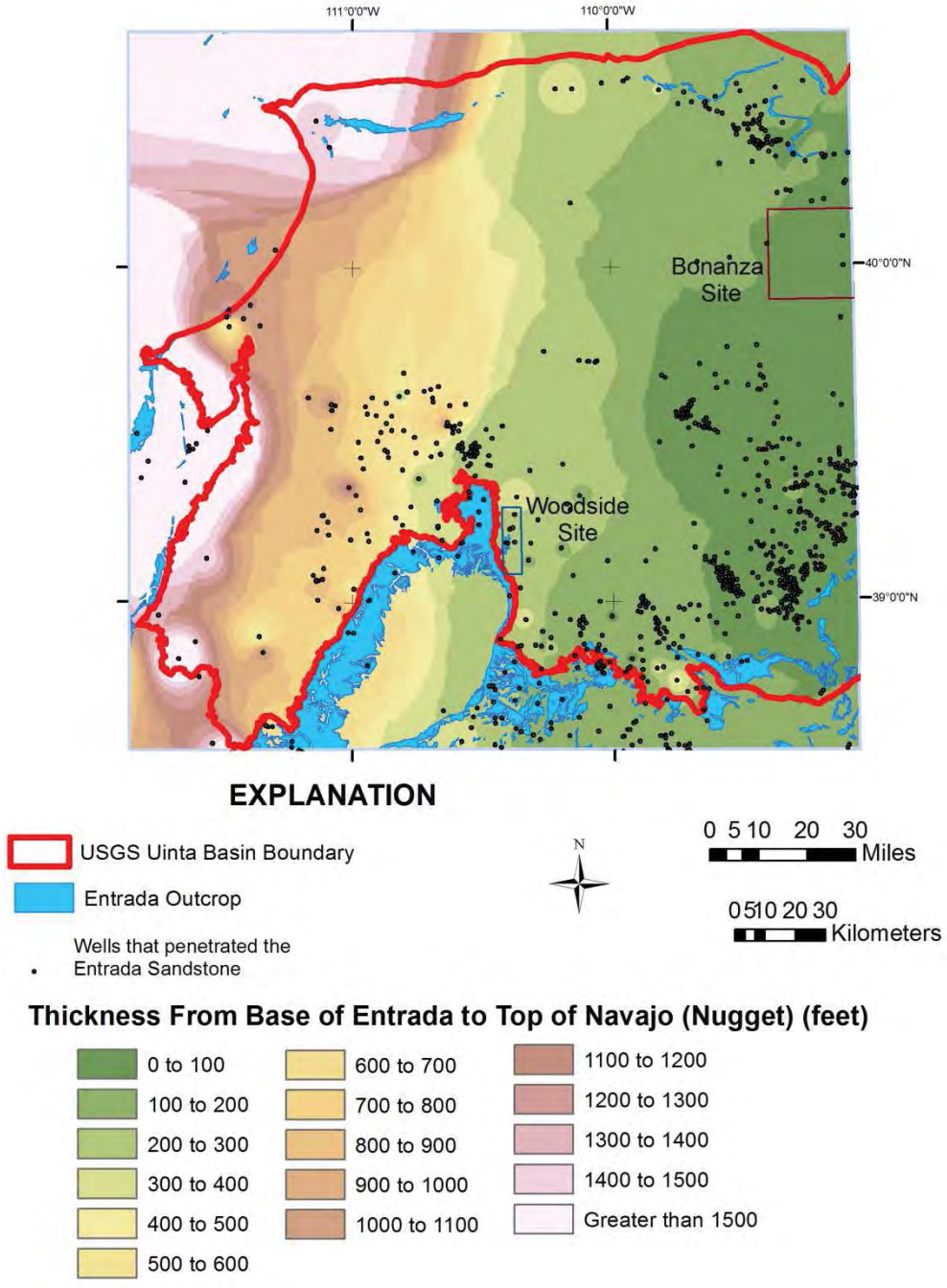


Figure 2. Thickness from the base of the Entrada Sandstone to the top of the Navajo Sandstone or equivalent Nugget Sandstone. The interval thins rapidly west to east and is less than 100 feet (30 m) thick at the Utah – Colorado border (eastern edge of map).

In the Uinta Basin the Entrada Sandstone changes from east to west from high quality reservoir coastal dune facies to tidal flat shale and siltstone with thin reservoir quality beds. Although the gross thickness of the Entrada thickens from east to west the thickness of reservoir thins dramatically due to the facies change (figure 3). This facies change is mapped (Morris, 2005) based on outcrop exposures in an area of very limited well control. The structure on top of the Entrada (figure 4) was mapped using well data and hand contouring following similar strike and dip of the Dakota Sandstone structure map. A DEM grid was subtracted from the structure grid to produce an overburden map of the Entrada (figure 5).

The gross thickness of the Navajo Sandstone was mapped using well data (figure 6). The Navajo thickness grid was added to the Entrada reservoir thickness grid to produce a combined Entrada/Navajo reservoir thickness (figure 7).

CO_2 Storage Capacity

We mapped the storage capacity of the Entrada/Navajo reservoir using a 1 km2 grid (figure 8). The storage capacity closely follows the reservoir thickness (figure 7). The Entrada/Navajo reservoir has the most storage capacity of the reservoirs studied in the Uinta Basin. The large storage capacity is due to the total thickness of the combined Entrada and Navajo Sandstones and the good quality reservoir properties of the eolian dune facies that makes up the majority of both formations. The parameters used to calculate the CO_2 storage capacity of the Entrada/Navajo reservoir are shown in table 1. The temperature and pressure gradients are calculated on the top of the Entrada Sandstone. Temperatures and pressures in the Navajo Sandstone will be greater than what was used in the EGI storage capacity spreadsheet.

Storage capacity of the Entrada/Navajo reservoir is shown in table 2.

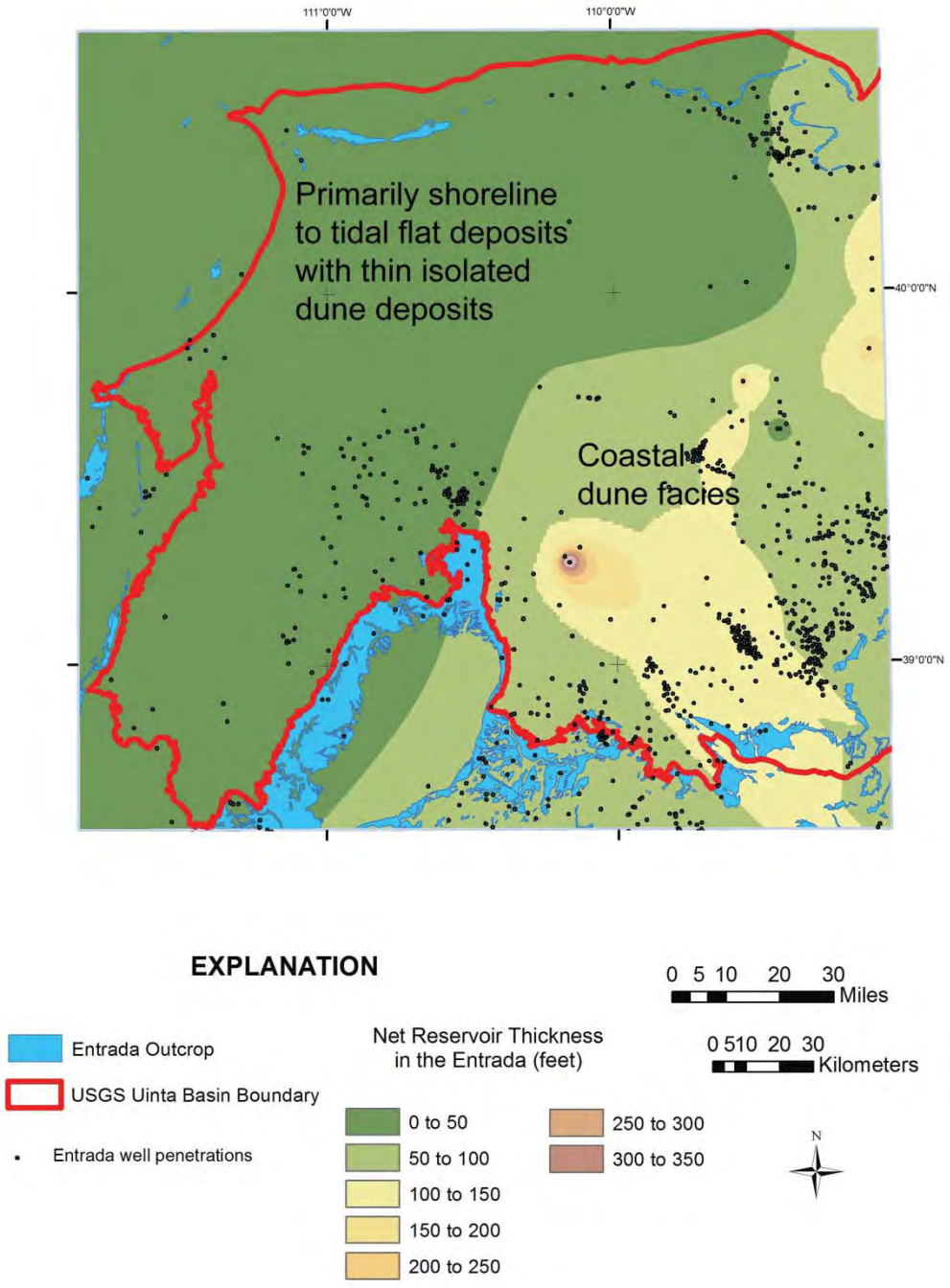


Figure 3. Thickness of the Entrada net reservoir. Contour interval is 50 feet (15 m). Reservoir strata is typically a porous eolian dune facies.

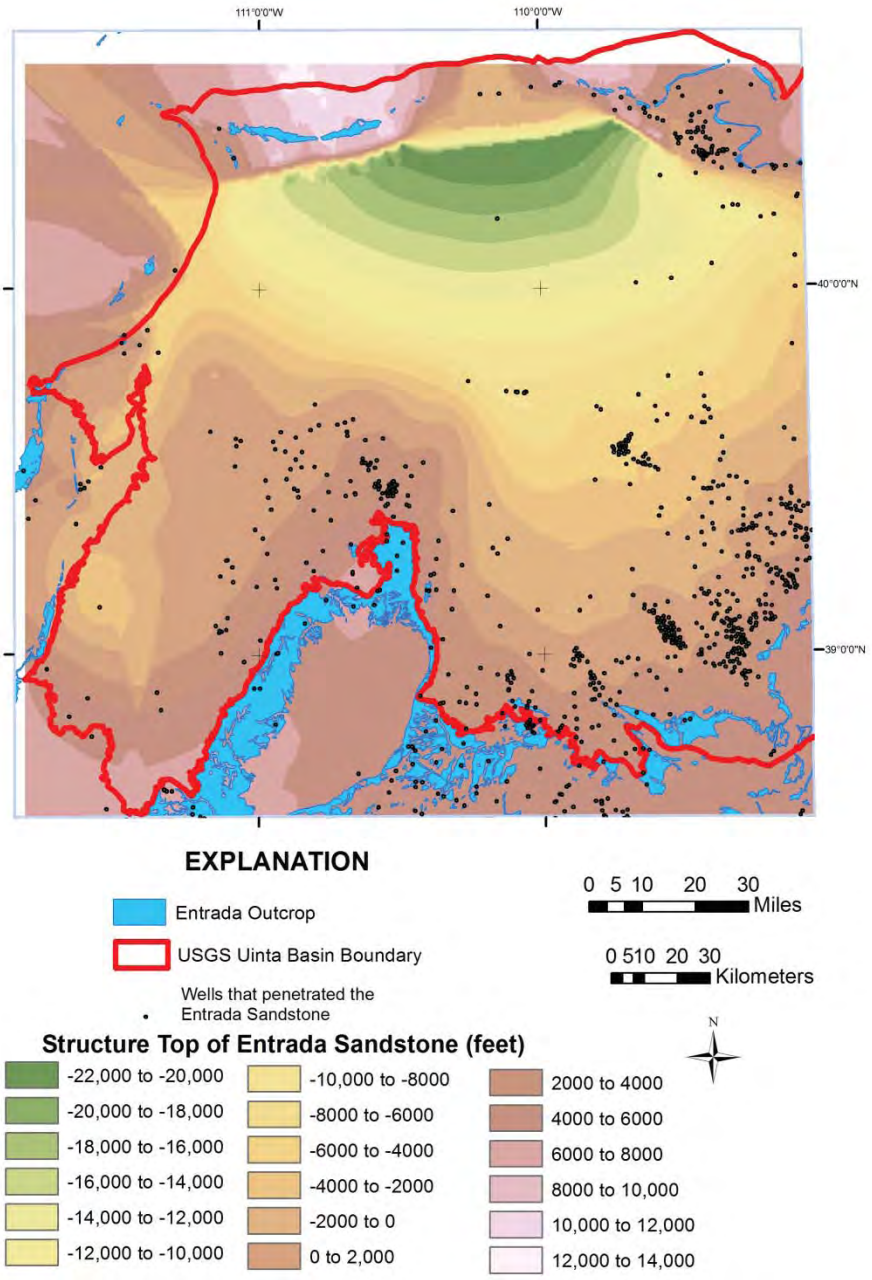


Figure 4. Structure on top of the Entrada Sandstone. Contour interval is 2000 feet (600 m) with mean sea level datum.

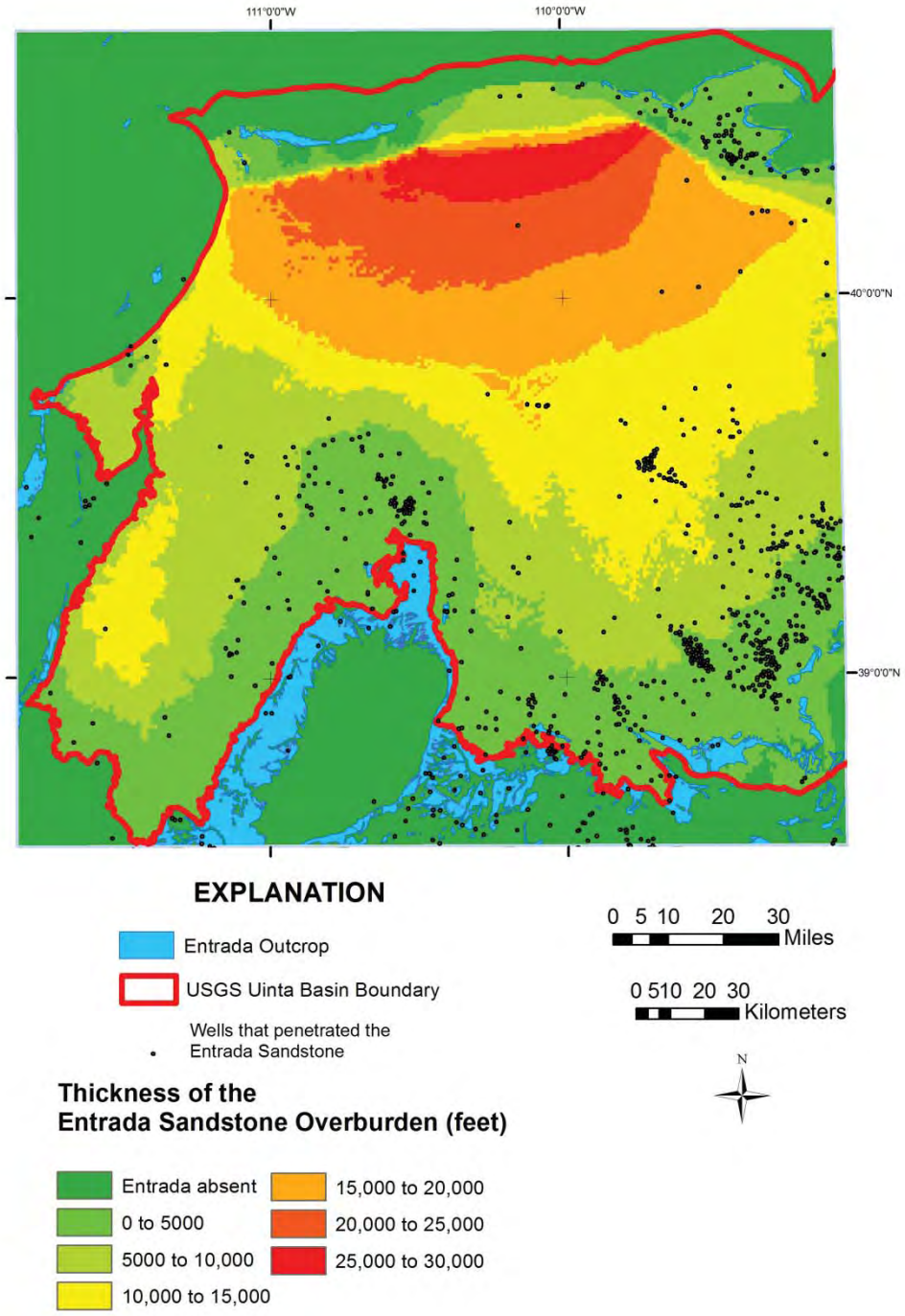


Figure 5. Thickness of the overburden above the Entrada Sandstone. Contour interval is 5000 feet (1500 m).

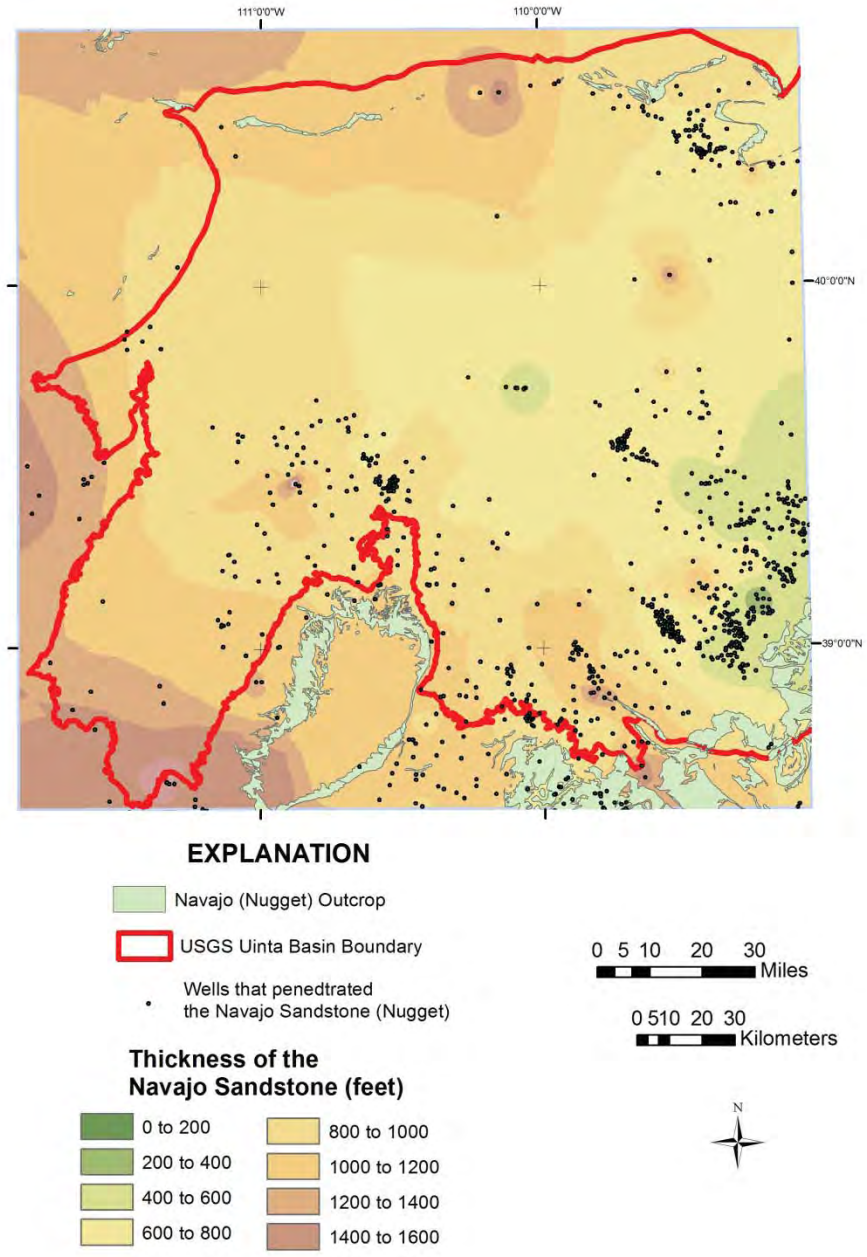


Figure 6. Thickness of the Navajo Sandstone and equivalent Nugget Sandstone. Contour interval is 200 feet (60 m).

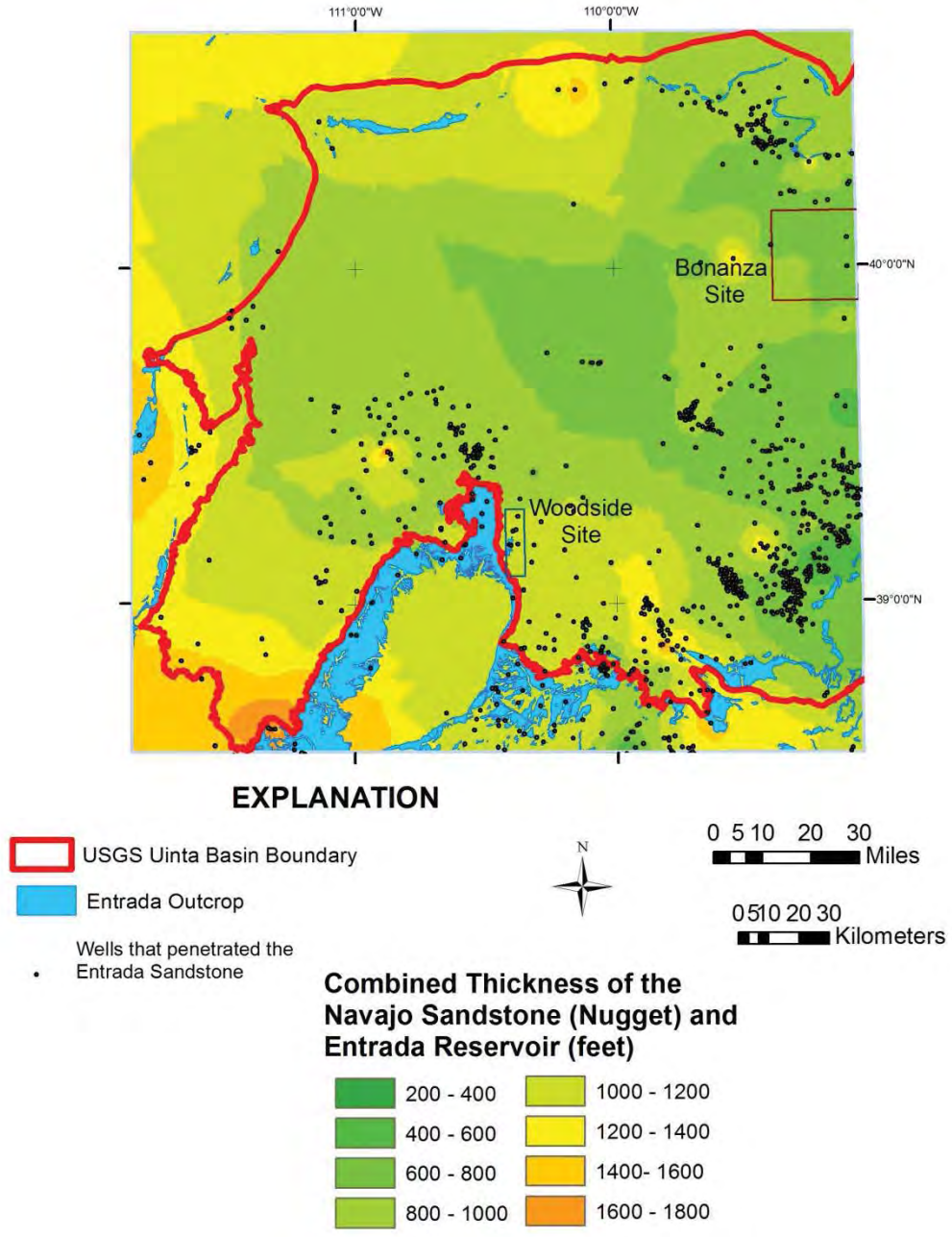


Figure 7. Combined thickness of the Entrada net reservoir and Navajo Sandstone (Nugget). Contour interval 200 feet (60 m).

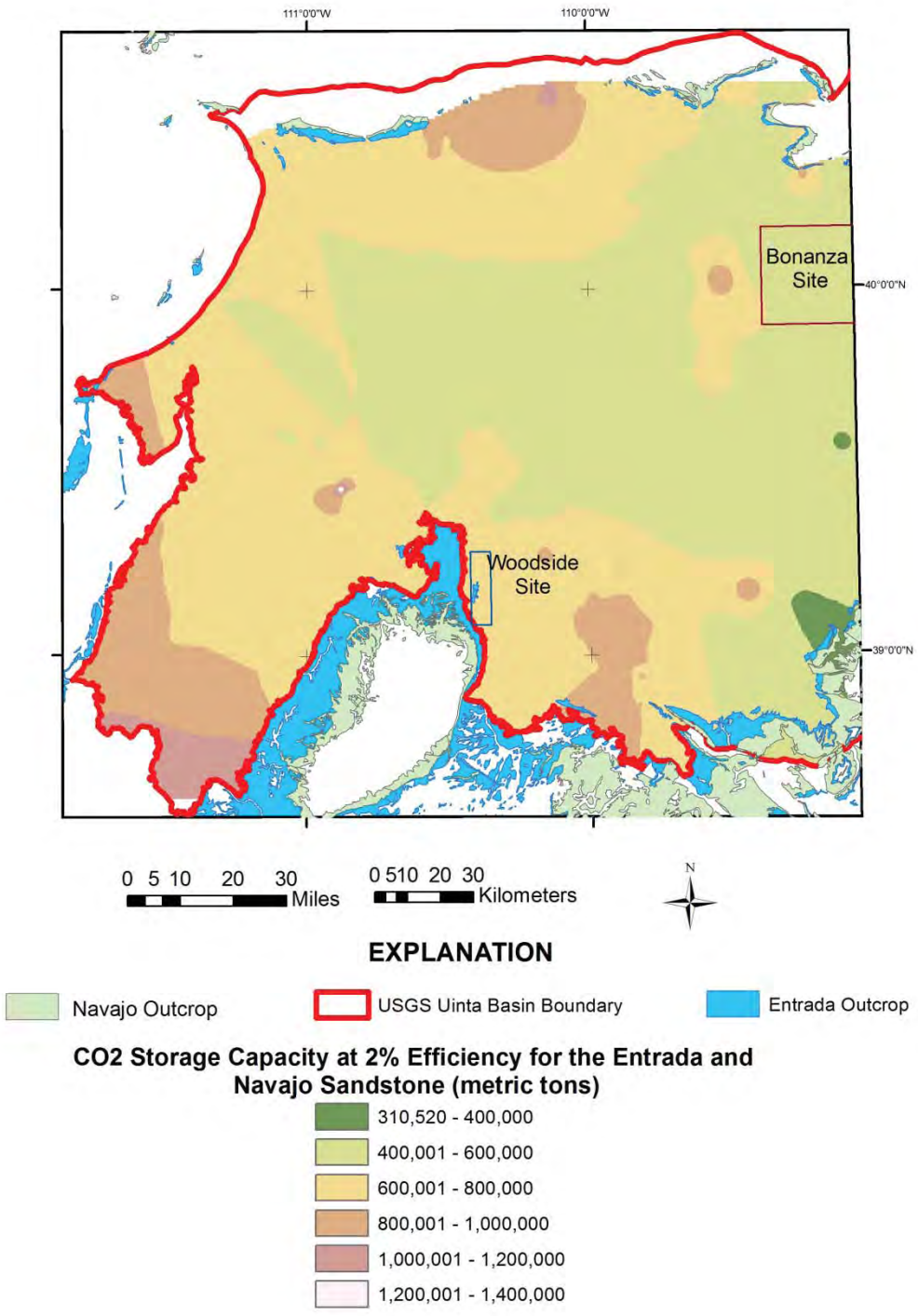


Figure 8. CO_2 storage capacity of the Entrada/Navajo reservoir in metric tonnes per million square meter grid (1 km^2).

Table 1. Parameters used to calculate the CO_2 storage capacity of the Entrada/Navajo reservoir in the Uinta Basin. Ft = feet, m = meters, km^2 = kilometers squared, F = degrees Fahrenheit, C = degrees Celsius, D = depth, psi = pounds per square inch, and kpal = kiloPascals.

	Area	Average Reservoir Thickness	Average Porosity	Temperature Gradient	Pressure Gradient
Entrada/Navajo	11,600 $miles^2$ 30,000 km^2	1195 ft 360 m	16 %	55 °F + (0.0138*D) 25 °C/km	0.45 psi/ft 3.10 kPal/ft

Table 2. CO_2 storage capacity of the Entrada/Navajo reservoir in the Uinta Basin using three different efficiency factors.

CO_2 Storage Capacity in Million Metric Tonnes			
	Efficiency Factors		
	0.5%	2.0%	5.4%
Entrada/Navajo	4857	19,048	51,427

Summary and Recommendations

The Entrada/Navajo reservoir has the most storage capacity of the formations that were studied in the Uinta Basin. The Entrada and Navajo Sandstones were combined to try to better match with the Colorado data. A zero thickness for the Entrada should be mapped in western Colorado so the two sandstones can be evaluated as separate reservoirs. Most locations in the Uinta Basin will have both sandstones and wells could injection into both, but evaluating them separately will result in more accurate data since pressures and temperatures in the Navajo will be different than what was used for the top of the Entrada.

References

Chidsey, Jr., T.C., DeHamer, J.S., Hartwick, E.E., Johnson, K.R., Schelling, D.D., Sprinkel, D.A., Strickland, D.K., Vrona, J.P., and Wavrek, D.A., 2007, Petroleum geology of the Covenant oil field, central Utah thrust belt *in* Willis, G.C., Hylland, M.D., Clark, D.L., and Chidsey, Jr., T.C., editors Central Utah – diverse geology of a dynamic landscape: Utah Geological Association Publication 36, p. 273-298.

Dalrymple, A., and Morris, T.H., 2007, Facies analysis and reservoir characterization of outcrop analogs to the Navajo Sandstone in the central Utah thrust belt exploration play *in* Willis, G.C., Hylland, M.D., Clark, D.L., and Chidsey, Jr., T.C., editors Central Utah – diverse geology of a dynamic landscape: Utah Geological Association Publication 36, p. 311-322.

Dyer, J., and Donoho, D., 2008, Gas-filled Jurassic Entrada Sandstones at Flat Rock field, Uintah County, Utah, *in* Longman, M.W., and Morgan, C.D., editors, Hydrocarbon systems and

production in the Uinta Basin, Utah: Utah Geological Association Publication 37, DVD, p. 155-178.

Morgan, C.D., 2007, Structure, reservoir characterization, and carbon dioxide resources of Farnham Dome field, Carbon County, Utah, *in* Willis, G.C., Hylland, M.D., Clark, D.L., and Chidsey, Jr., T.C., editors Central Utah – diverse geology of a dynamic landscape: Utah Geological Association Publication 36, p. 297-310.

Morris, T.H., and McBride, J.H., 2005, A multidisciplinary approach to reservoir characterization of the Entrada erg-margin gas play, Utah: UGS Open-File Report 459.

Suck, D.H., and Glanville, R.E., 1993, San Arroyo *in* Hill, B.G., and Bereskin, S.R., editors, Oil and gas fields of Utah: Utah Geological Association publication 22, unpagenated.

DE CHELLY SANDSTONE OF THE PERMIAN CUTLER GROUP

Data Resources

Hydrocarbons are not produced from the De Chelly Sandstone of the Cutler Group in Utah's Paradox Basin. As a result formation tests and cores from the De Chelly were not available. The De Chelly is generally at a shallow depth in the Paradox Basin with numerous well penetrations and good outcrop control. Twenty-one well logs have been digitized and the formation tops identified in 88 wells. The formation has been described and mapped in detail by Condon (1997). Outcrops were examined and correlated to well logs. The well data points were gridded in ArcMap and used to calculate the CO_2 storage capacity of the De Chelly.

Geologic Characterization

The De Chelly Sandstone has been identified in several geophysical logs from wells drilling to underlying oil reservoirs in the basin. It was found during review of the well logs that the Shinarump Conglomerate Member of the Triassic Chinle Formation has been misidentified as the De Chelly in many of the well reports, resulting in an overly thick De Chelly. The top of the Organ Rock Formation (base of the De Chelly) was identified and used to calculate the total thickness of the De Chelly. Three outcrops of De Chelly were sampled in the Combs Wash area near State Highway 163, southwest of Bluff, Utah. The sequence of Moenkopi Formation, De Chelly, and Organ Rock was identified at the outcrops. The thickness of the De Chelly was measured, and the formation was described and sampled. The hand samples were oriented and thin-section blanks were cut and prepared.

The outcrops of De Chelly Sandstone show eolian depositional structures with more than seven dune activation surfaces. Large dune surfaces can be seen in the outcrop and show a sharp contrast between the fluvial sandstone and shale beds in the underlying Organ Rock and the fluvial sandstone and siltstone beds in the overlying Moenkopi. An upper and lower De Chelly were observed in each outcrop separated by an erosional surface. Thin sections show predominately bimodal, poorly to well sorted, subrounded to subangular quartz crystals with hematite stain. Lineations on the grains are consistent with a windblown depositional system. The thin sections from all the outcrops show a very high intergranular porosity of approximately 20% to 25%. Connected pores within the sandstone suggest potentially high permeability.

The De Chelly Sandstone well database was brought into ArcMap® and structure (figure 1), overburden (figure 2) and, gross thickness which was used as reservoir thickness (figure 3) were gridded and mapped. Storage capacity is calculated for the reservoir at 3000 feet (1000 m) depth or deeper which greatly reduces the area of potential storage (figure 4). The grid data was exported to the EGI spreadsheet where the CO_2 storage capacity was calculated and then brought back into ArcMap® and a De Chelly geodatabase was developed.

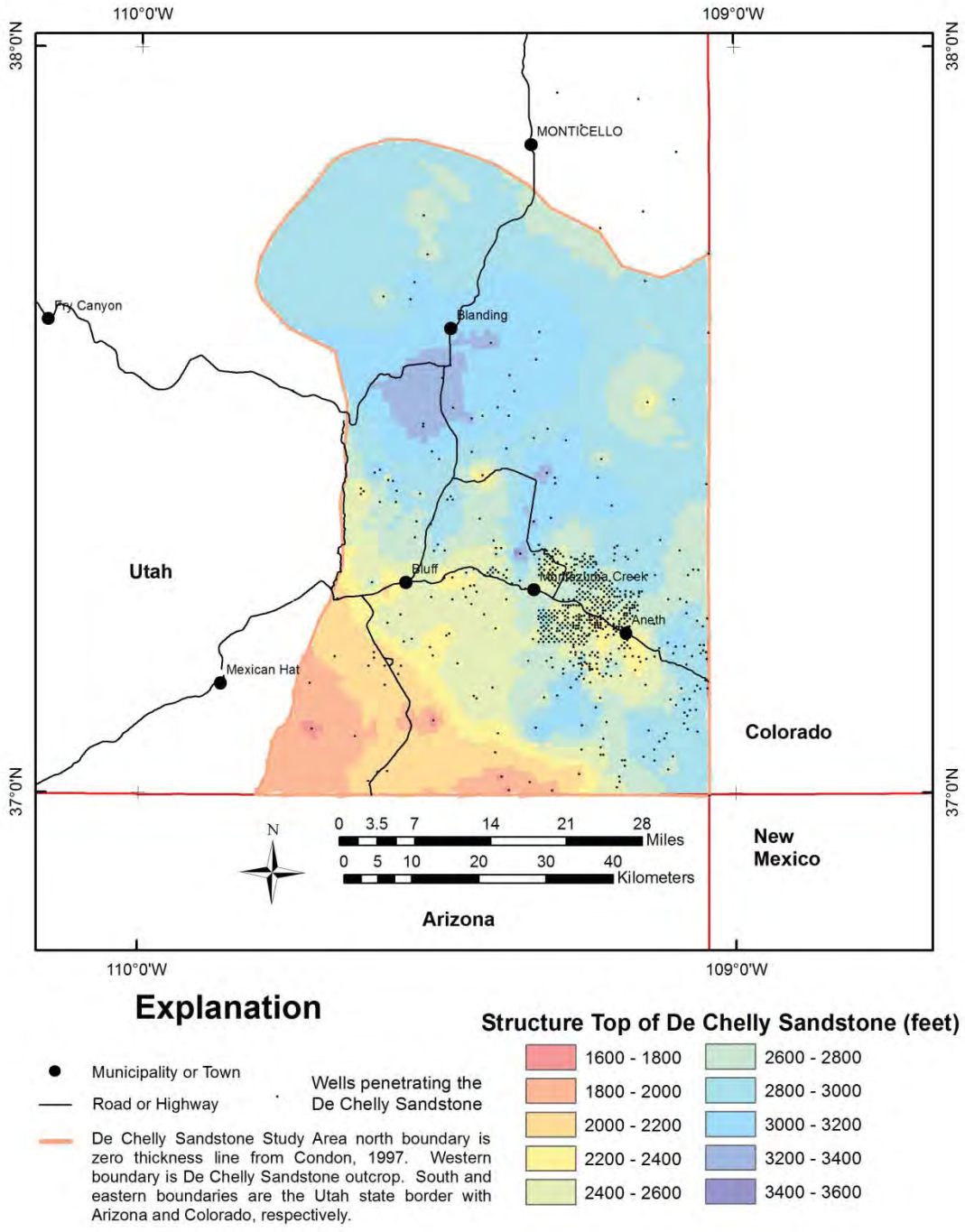


Figure 1. Structure on top of the De Chelly Sandstone. Contour interval is 200 feet (60 m), with a mean sea level datum.

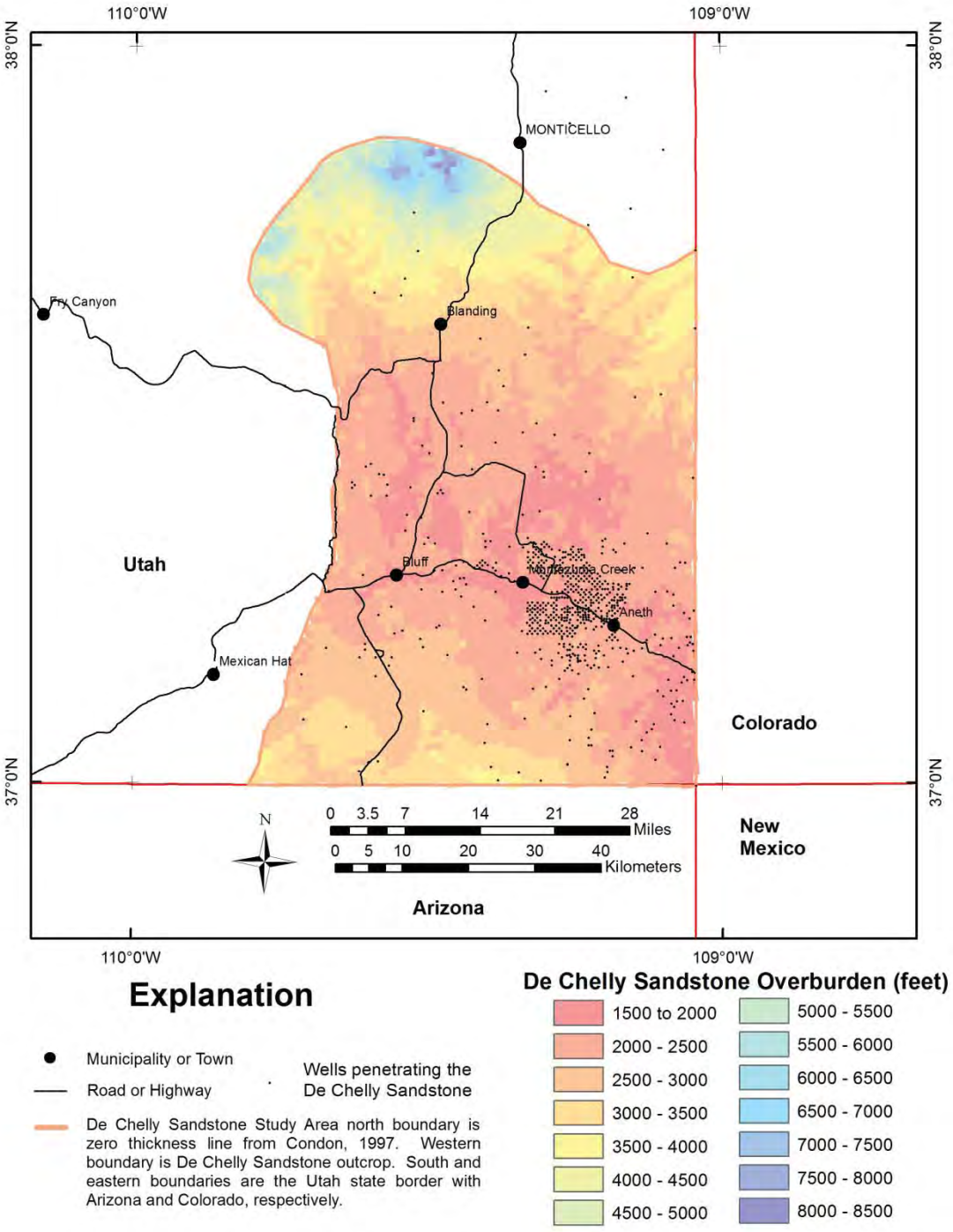


Figure 12. De Chelly Sandstone overburden thickness in feet. Contour interval is 500 feet (150 m).

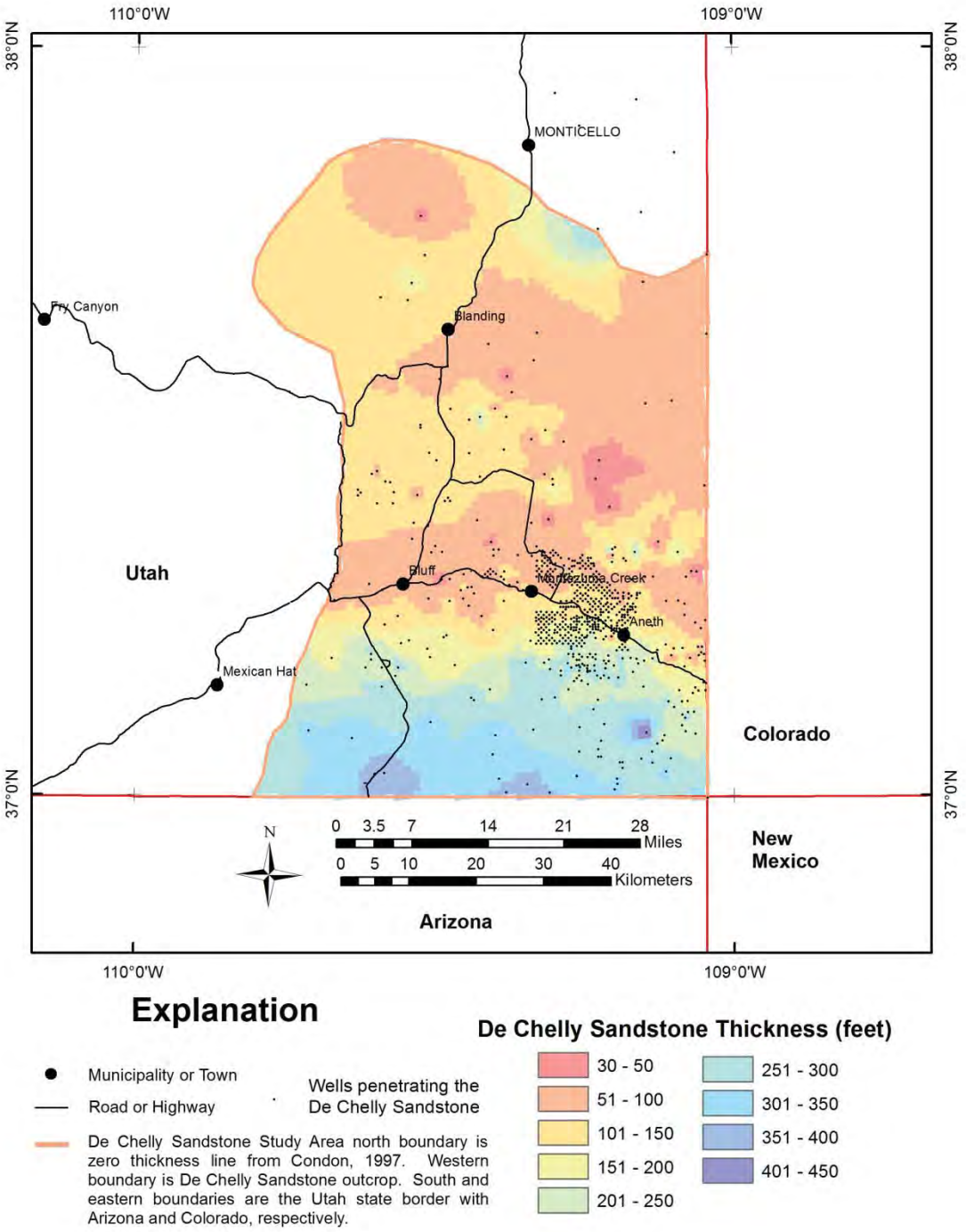


Figure 3. Gross thickness of the De Chelly Sandstone which was used as the reservoir thickness. Contour interval is 50 feet (15 m).

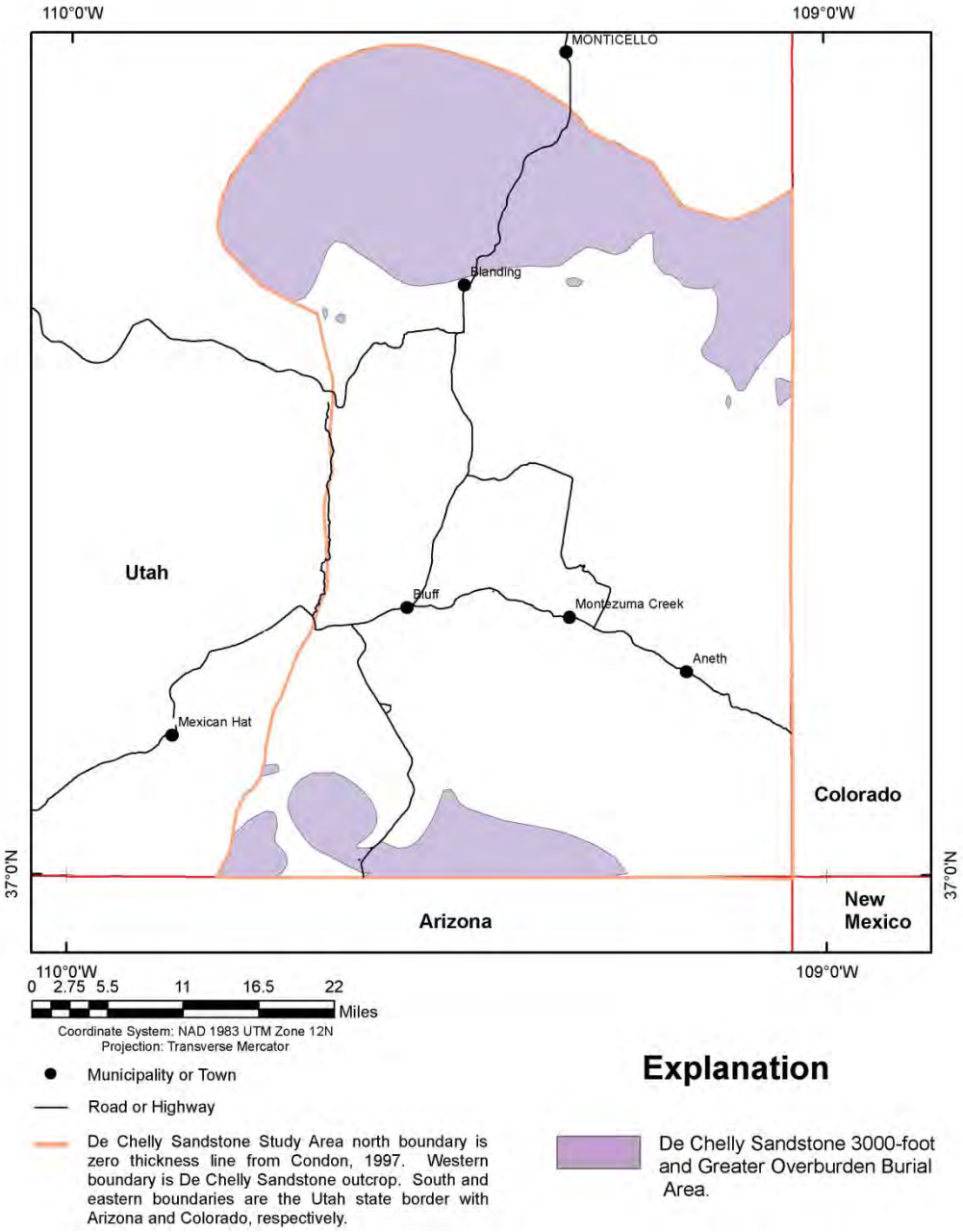


Figure 18. Map showing areas where the De Chelly Sandstone has 3000 feet (1000 m) or more overburden. The 3000-foot (1000-m) depth is the minimum depth used for calculation of potential CO_2 storage capacity.

CO_2 Storage Capacity

The parameters used to calculate the CO_2 storage capacity of the De Chelly Sandstone reservoir are shown in table 1. The pressure gradient used is too high but the error went unnoticed until after the data had been submitted to NATCARB. Recalculation of the storage capacity using a gradient of 0.44 psi/ft results in less than 1% change due to the shallow depth of the reservoir. The CO_2 storage capacity of the De Chelly reservoir provided to NATCARB is shown in table 2 and would be the same with the lower pressure gradient.

Table 1. Parameters used to calculate the CO_2 storage capacity of the De Chelly reservoir in the Paradox Basin. Ft = feet, m = meters, km^2 = kilometers squared, F = degrees Fahrenheit, C = degrees Celsius, D = depth, psi = pounds per square inch, and kpal = kiloPascals.

	Area	Average Reservoir Thickness	Average Porosity	Temperature Gradient	Pressure Gradient
De Chelly	600 $miles^2$ 1600 km^2	150 ft 50 m	20 %	55 °F + (0.0115*D) 20 °C/km	1.1 psi/ft 7.3 kPal/ft

Table 2. CO_2 storage capacity of the De Chelly reservoir in the Paradox Basin using three efficiency factors.

CO_2 Storage Capacity in Million Metric Tonnes			
	Efficiency Factors		
	0.5%	2.0%	5.4%
De Chelly	36	139	377

Summary and Recommendations

The storage capacity of the De Chelly Sandstone is reduced by the many areas in Utah's Paradox Basin where the formation outcrops or is less than 3000 feet (1000 m) deep. Although there have been numerous penetrations of the De Chelly there are very few tests and even fewer cores that can provide the petrophysical properties needed for an accurate storage calculation. Outcrop studies of the De Chelly indicate good reservoir properties. But more extensive core-hole data unaffected by surface weathering would be more reliable. One or more core holes should be drilled to determine reservoir properties, water quality, reservoir pressure and injectivity of the De Chelly Sandstone.

Reference

Condon, S.M., 1997, Geology of the Pennsylvanian and Permian Cutler Group and Permian Kaibab Limestone in the Paradox Basin, southeastern Utah and southwestern Colorado: U.S. Geological Survey Bulletin 2000-P, 46 p., 9 plates.

PENNSYLVANIAN-PERMIAN WEBER AND PERMIAN WHITE RIM SANDSTONES

Data Resources

Hydrocarbons are not produced from the Weber or White Rim Sandstone or deeper reservoirs in the Uinta Basin except at the Ashley Valley field (Chidsey, Jr., and Sprinkel, 2005; Larson, 1993) (figure 1). The Weber is more than 3000 feet (1000 m) deep in most of Ashley Valley but the formation water is less than 10,000 total dissolved solids (TDS) so the area was not evaluated for potential storage capacity. There are very few well penetrations of the Weber in the Uinta Basin. Many of the wells are old with very poor quality geophysical logs. We correlated a Weber top in 16 wells and a formation thickness in 15 wells; most of the wells were in the Ashley Valley area. There was only one core from the Weber Sandstone available for the study the Texas Creek 14-22 core in section 22, T. 11 S., R. 25 E., Uintah County (API 4304732693) (figure 1).

Reservoirs below the White Rim Sandstone (Paradox and Doughnut Formations, for example) are productive in and near, the southwest Uinta Basin and SRS area so there are numerous well penetrations through the White Rim. We correlated a White Rim top in 121 wells and a formation thickness in 119 wells. There was only one core from the White Rim Sandstone available for the study the USA Federal 8-1 White Rim core in section 8, T. 19 S., R. 9 E., Emery County (API 4301530039) (figure 1).

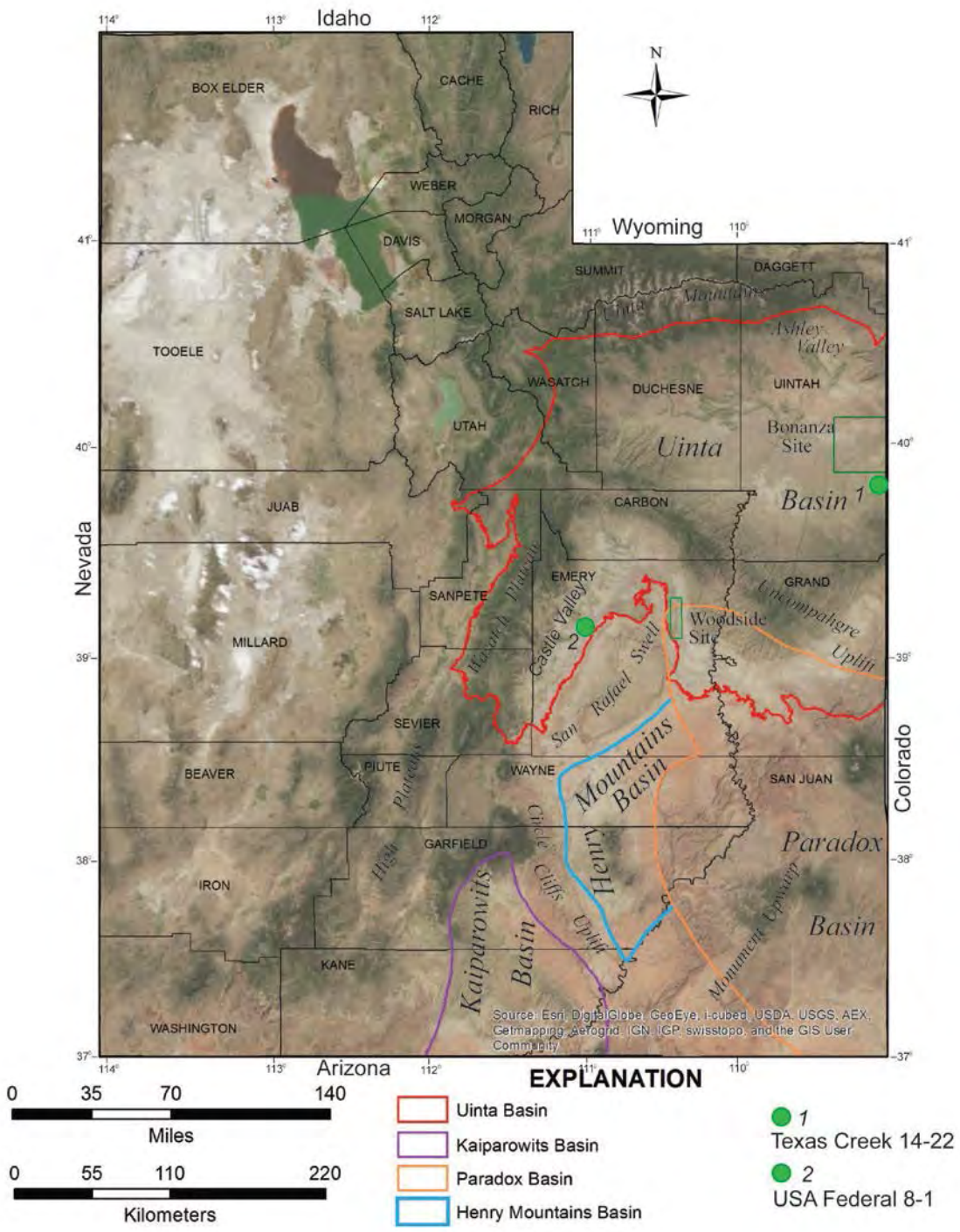


Figure 1. Map of Utah showing basins and uplifts of the Colorado Plateau. Well 1 has a Weber Sandstone (?) core and 2 has a White Rim core. Bonanza and Woodsite (green rectangles) are the UGS detailed study sites.

We choose to evaluate the Weber and White Rim Sandstones as one reservoir (Weber/White Rim). The two sandstones have similar reservoir facies and are partly time equivalent. The Weber Sandstone is Pennsylvanian (lower part) to Early Permian (upper part) separated by an unconformity (Hintze and Kowallis, 2009). Hintze and Kowallis (2009) and Franczyk (1991) show the White Rim overlying the Weber. Franczyk (1991) shows the White Rim grading northward from the SRS into mixed carbonates and clastic rocks of the lower Park City Formation along the southwest flank of the Uinta Mountains. Franczyk (1991) states her correlation of the White Rim with the Park City is "speculative."

The primary reservoir facies in the Weber/White Rim is eolian coastal dune deposits. The dune facies typically has well sorted cross-bedded sandstones with moderate to good porosity and permeability.

The Weber Sandstone overlies the Morgan Formation and is overlain by the Park City Formation. The Weber Sandstone in eastern Uinta Basin is an eolian dune deposit including dune, interdune, and sand sheet facies (Chidsey, Jr., and Sprinkel, 2005). The Weber dune field extended from Wyoming to northern Utah. The Weber dune facies in northeastern Uinta Basin interfingers with alluvial fan deposits of the Maroon Formation (figure 2). The Weber is a medium- to fine-grain, well sorted subarkosic to quartz arenite and has been described in detail by Fryberger (1990) and more recently by Chidsey, Jr., and Sprinkel (2005). In western Uinta Basin the Weber becomes more quartzitic with interbedded limestone and dolomite (Bryant, 2003; and Constenius and others, 2011).

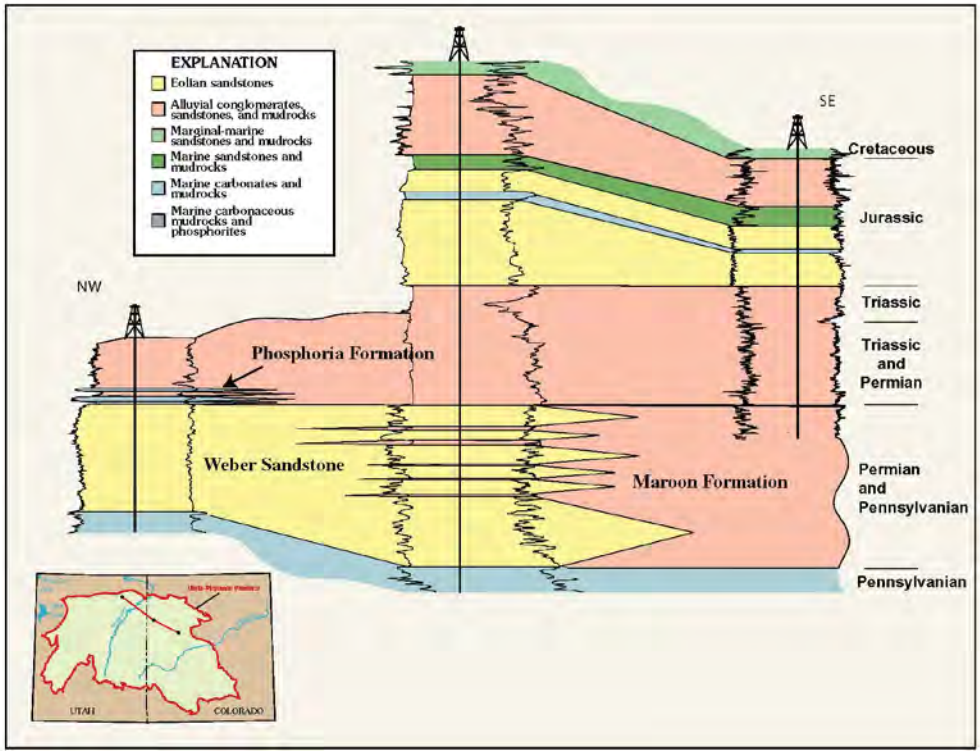


Figure 2. Northwest to southeast cross section showing the interfingering of the Weber Sandstone and Maroon Formation, from Johnson, 2003.

The Texas Creek 14-22 core is reported as a Weber core but is mostly arkosic redbeds more typical of the Maroon Formation. Core plug analysis shows average porosity of 4.1% and average permeability 0.09 milliDarcys (mD). An open-hole drill-stem test of the cored interval recovered 240 feet (75 m) of very slightly gas cut drilling mud. The Texas Creek 14-22 core does not provide representative regional reservoir properties but does help identify the southern limit of the Weber reservoir.

The White Rim Sandstone overlies the Organ Rock and Elephant Canyon Formations, and is overlain by the Permian Kaibab Formation (Black Box Dolomite of Welsh and others, 1979) or Triassic Moenkopi Formation. The White Rim is fine- to medium-grained sandstone deposited in a coastal dune environment (Huntoon, 1985; Huntoon and Chan, 1987; Chan, 1989; Harston and Morris, 2013). Harston and Morris (2013) described three primary facies in the White Rim: (1) a lower erg-margin sabkha environment of small, widely spaced dunes and interdune lag deposits, (2) a middle interval of high-angle trough cross-stratified eolian dune sets making up the majority of the formation, and (3) an upper facies lacking bedding, heavily bioturbated with some silty limestone. See the discussion on the Woodside site in this report for more detail about the White Rim. The White Rim is generally 600 to 800 feet (180–240 m) thick in the northern SRS area. Outcrop examination of the White Rim indicates a porous and permeable reservoir, but most well logs show porosity ranging from 2% to 6%, although high gas rates were tested at Gordon Creek and Woodside fields.

The USA Federal 8-1 White Rim core (figure 3) is only 31 feet (9 m) of the upper portion of the formation. Most of the core is very tight with an average porosity of 3.7%, maximum porosity 5.2%, and average permeability of 0.1 mD. An open-hole drill-stem test of the cored interval recovered 15 feet (5 m) of drilling mud. The core is described as dolomitic sandstone which may indicate a greater marine influence than is seen in outcrop along the crest of the SRS. Based on geophysical logs of wells in the region this well is not a good representation of the formation reservoir properties.

The UGS completed structure (figure 4), formation thickness (figure 5), grain density, porosity (figure 6), and temperature (figure 7) maps of the Weber/White Rim reservoir in the Uinta Basin and SRS. The structural elevation data was subtracted from a digital elevation model (DEM) to develop a drill-depth or overburden map for Weber/White Rim (figure 8). The porosity and temperature maps, with the overburden map, were used to construct a geodatabase model for the Weber/White Rim from which CO_2 storage capacity was calculated (figures 9).

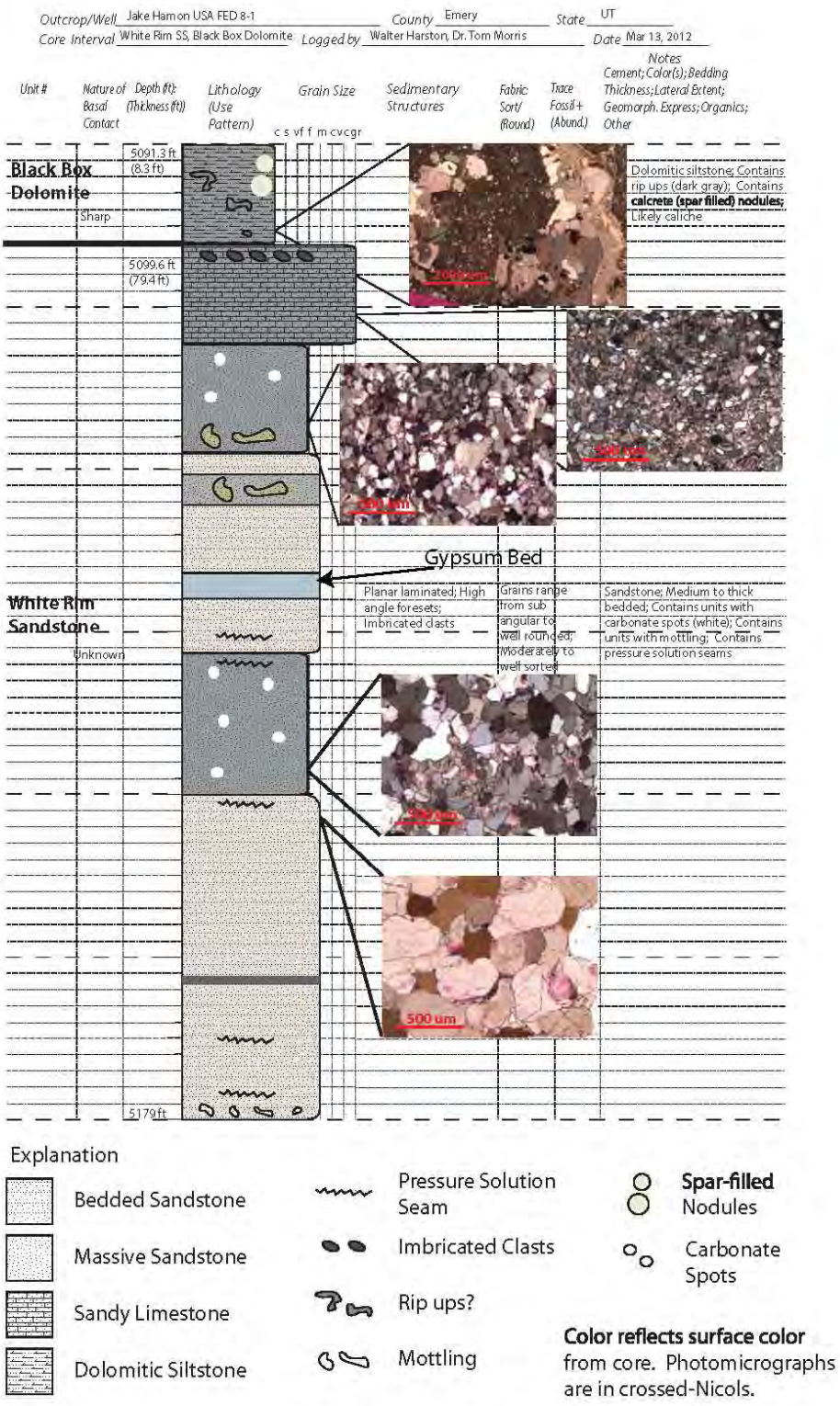


Figure 3. Generalized description of the USA Federal 8-1 core, see figure 1 for the location of the well. Core described by Harston, 2012, unpublished contact deliverable to the UGS.

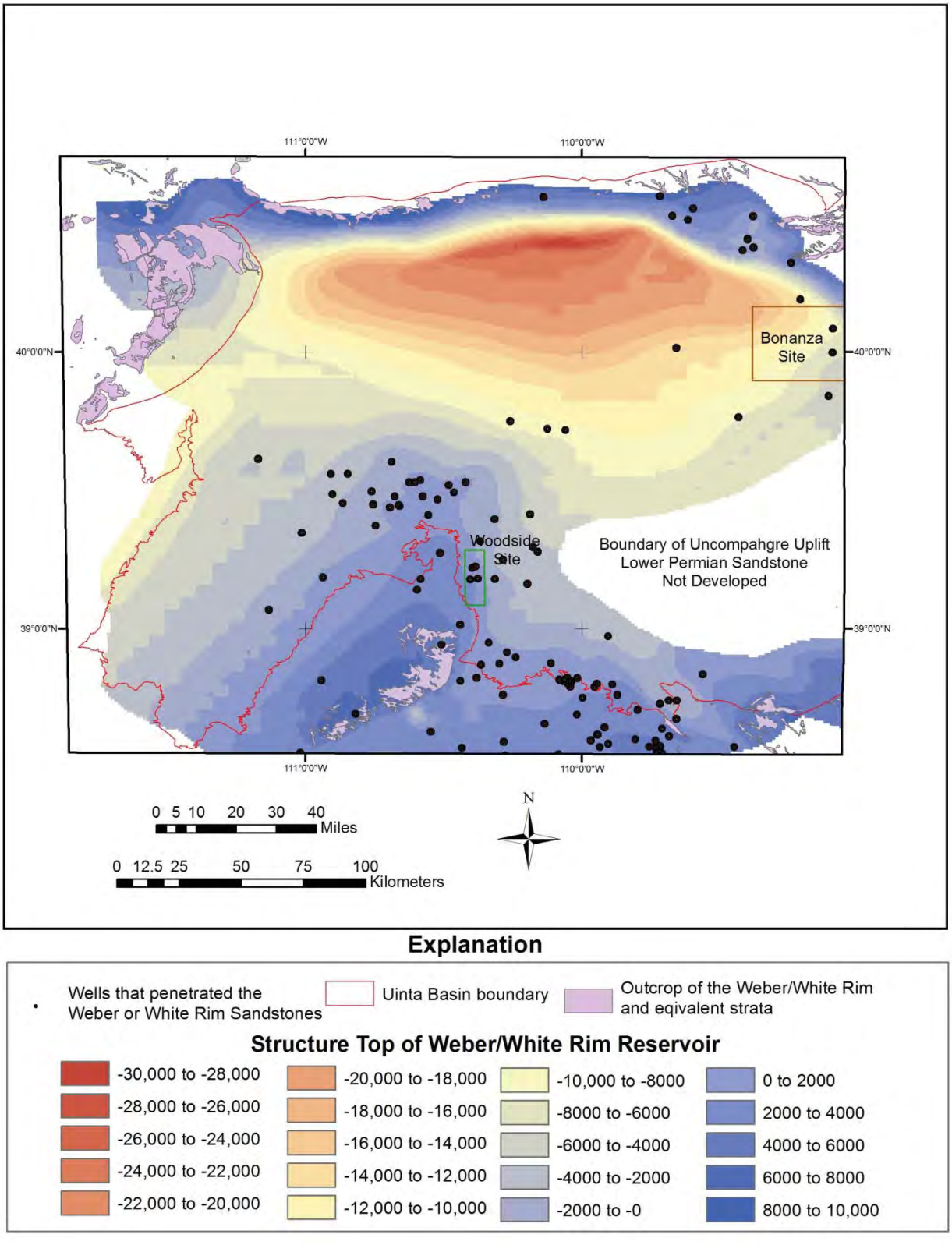


Figure 4. Structural contour map of the top of the Weber and White Rim Sandstones. Contour interval 2000 feet (600 m), mean sea level datum.

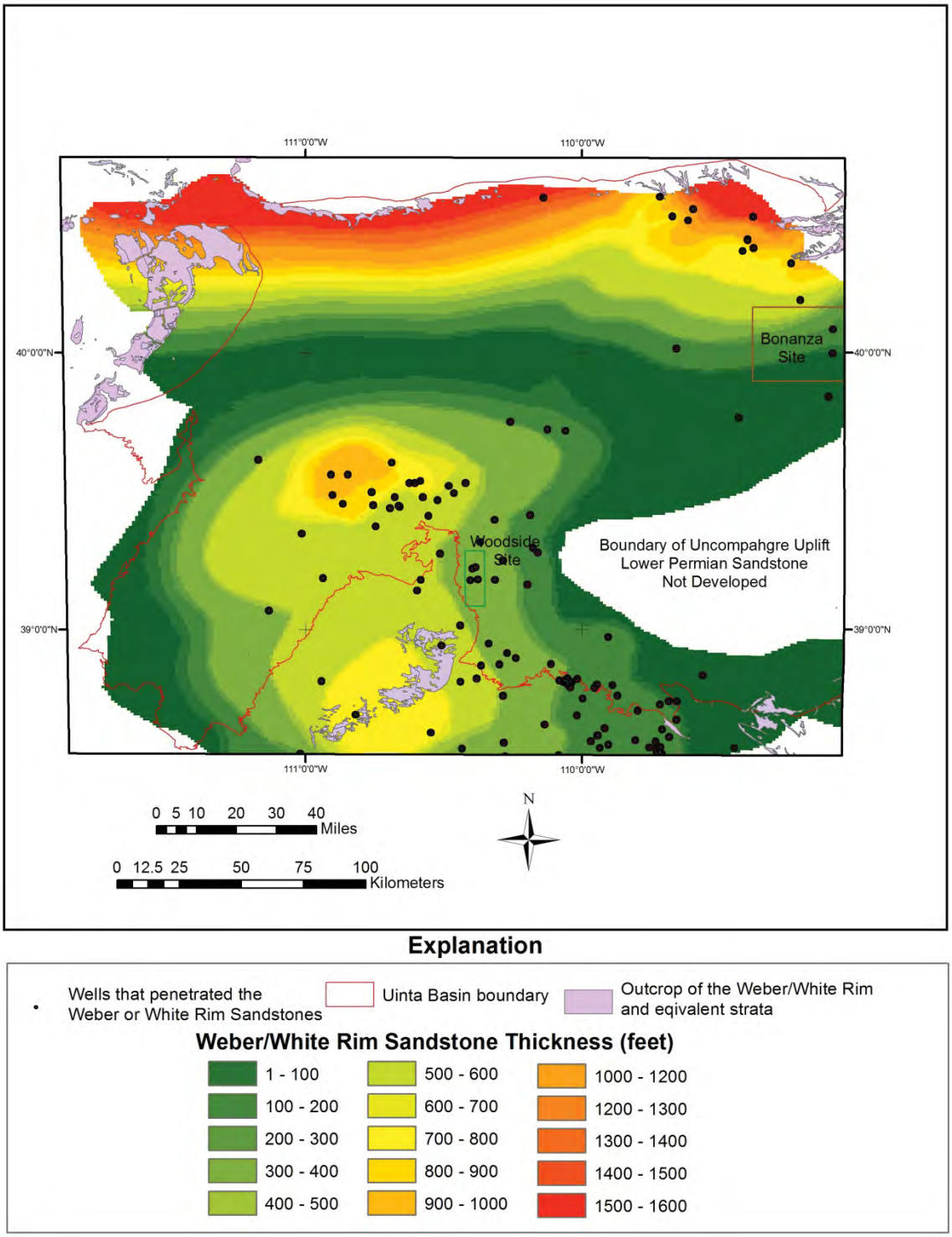


Figure 5. Generalized thickness map of the Weber/White Rim reservoir. Contour interval is 200 feet (60 m).

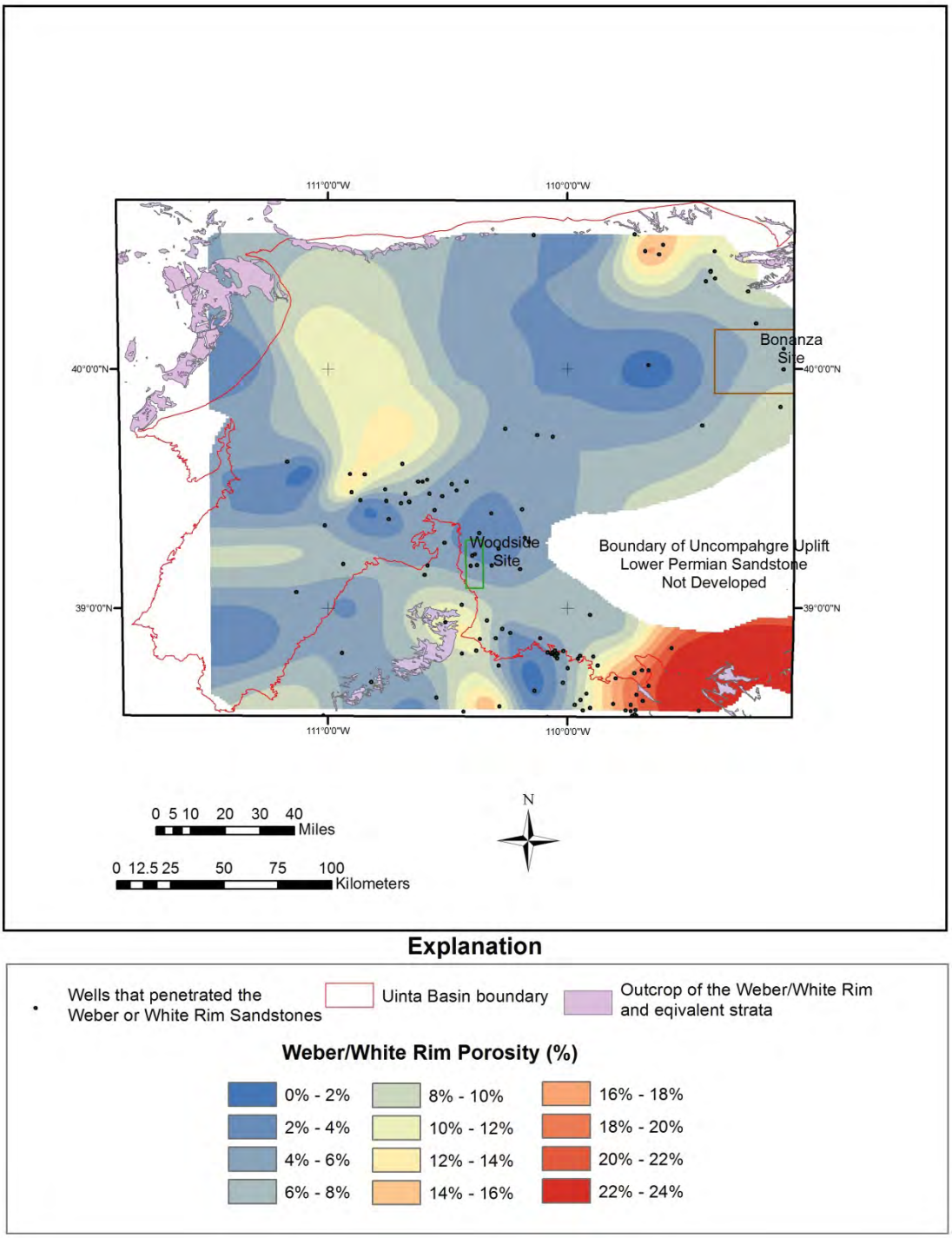


Figure 6. Average porosity in percent, of the Weber/White Rim reservoir derived from the bulk density grid using a grain density of 2.65 and cross plotted with neutron and sonic porosity if available.

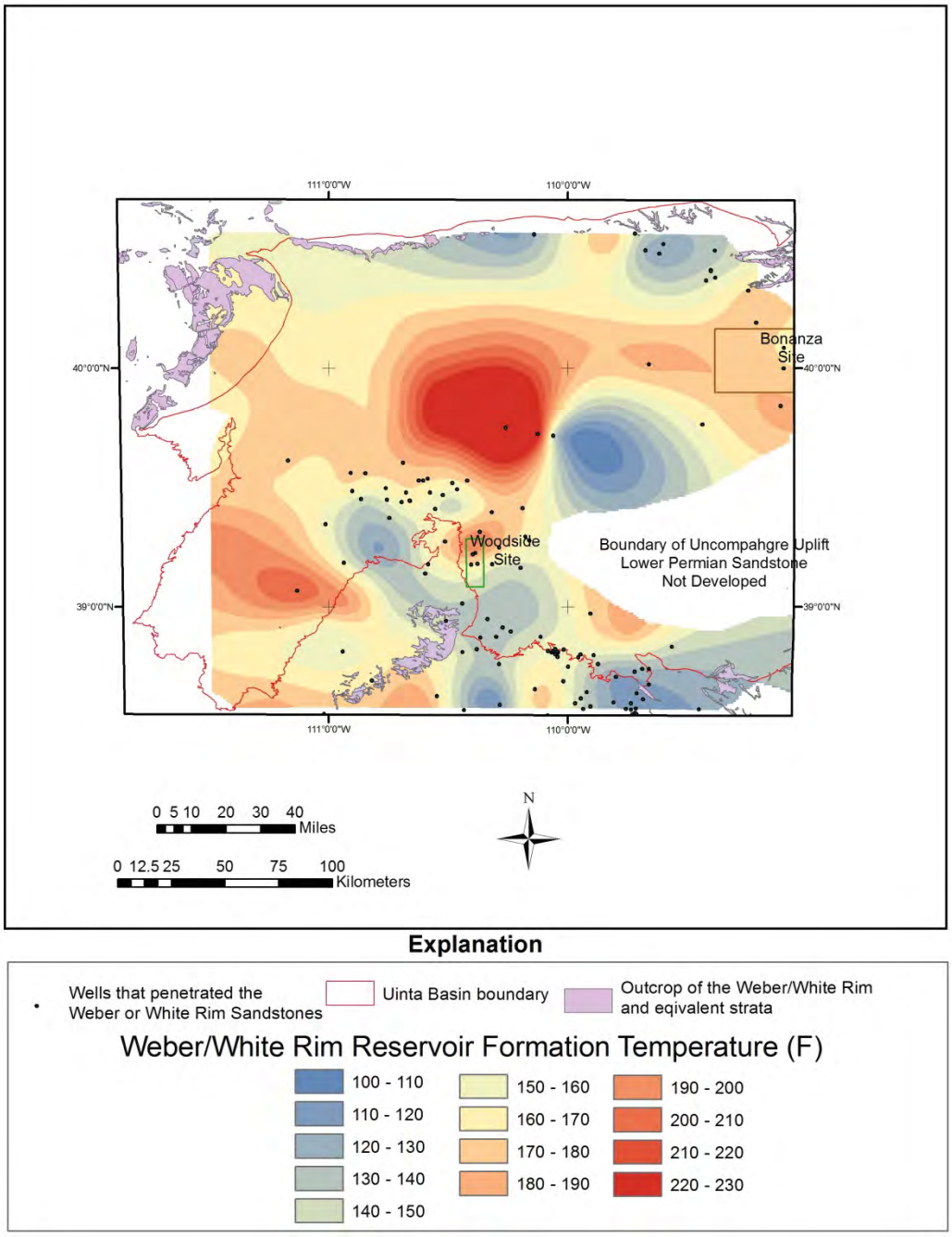


Figure 7. Temperature distribution in the Weber/White Rim reservoir in degrees Fahrenheit (F) based on bottom-hole temperatures recorded on the geophysical well logs corrected to the depth of the sandstones.

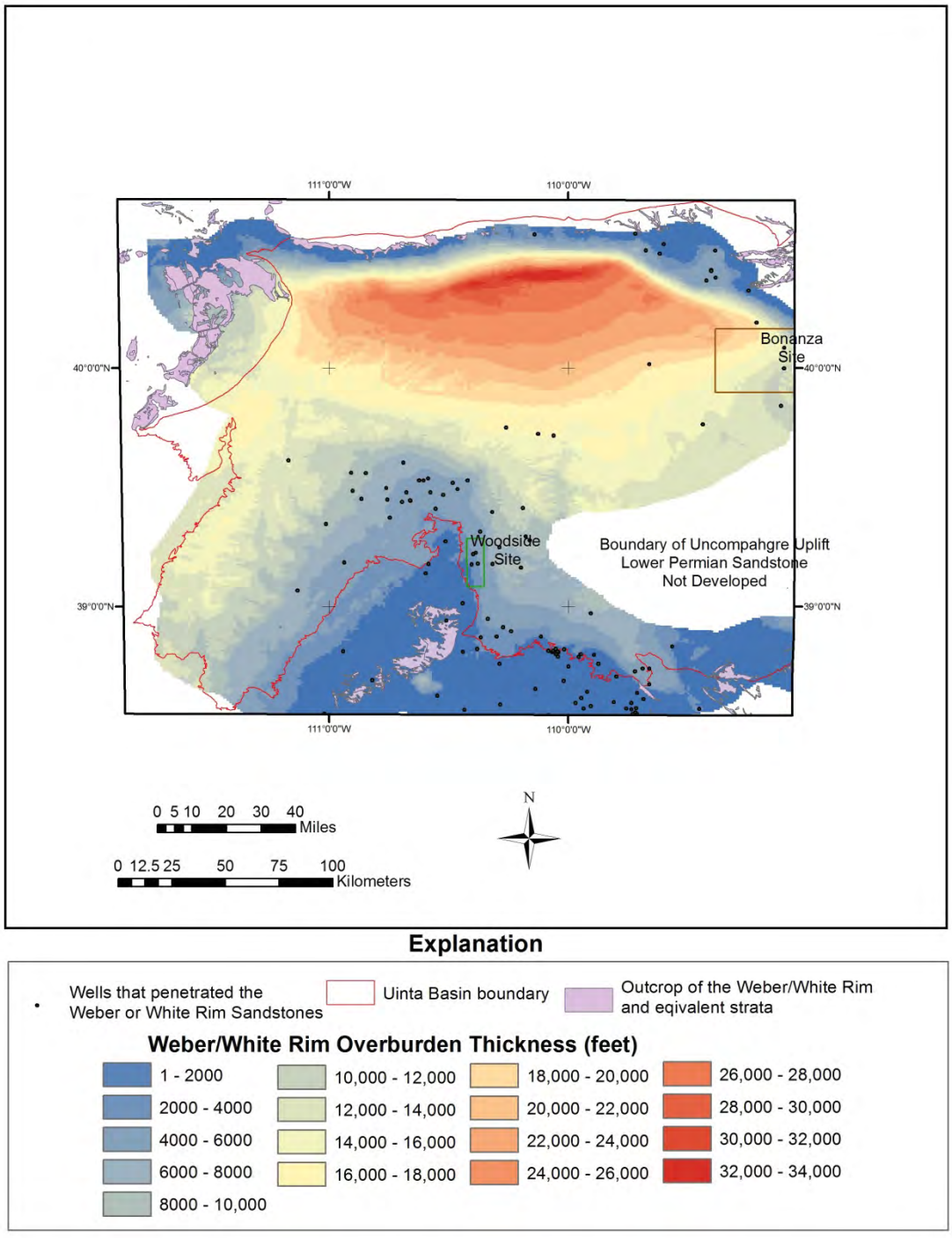


Figure 8. Overburden thickness map of the Weber/White Rim reservoir. Contour interval is 2000 feet (600 m). The overburden was calculated by subtracting the structural grid from a DEM grid.

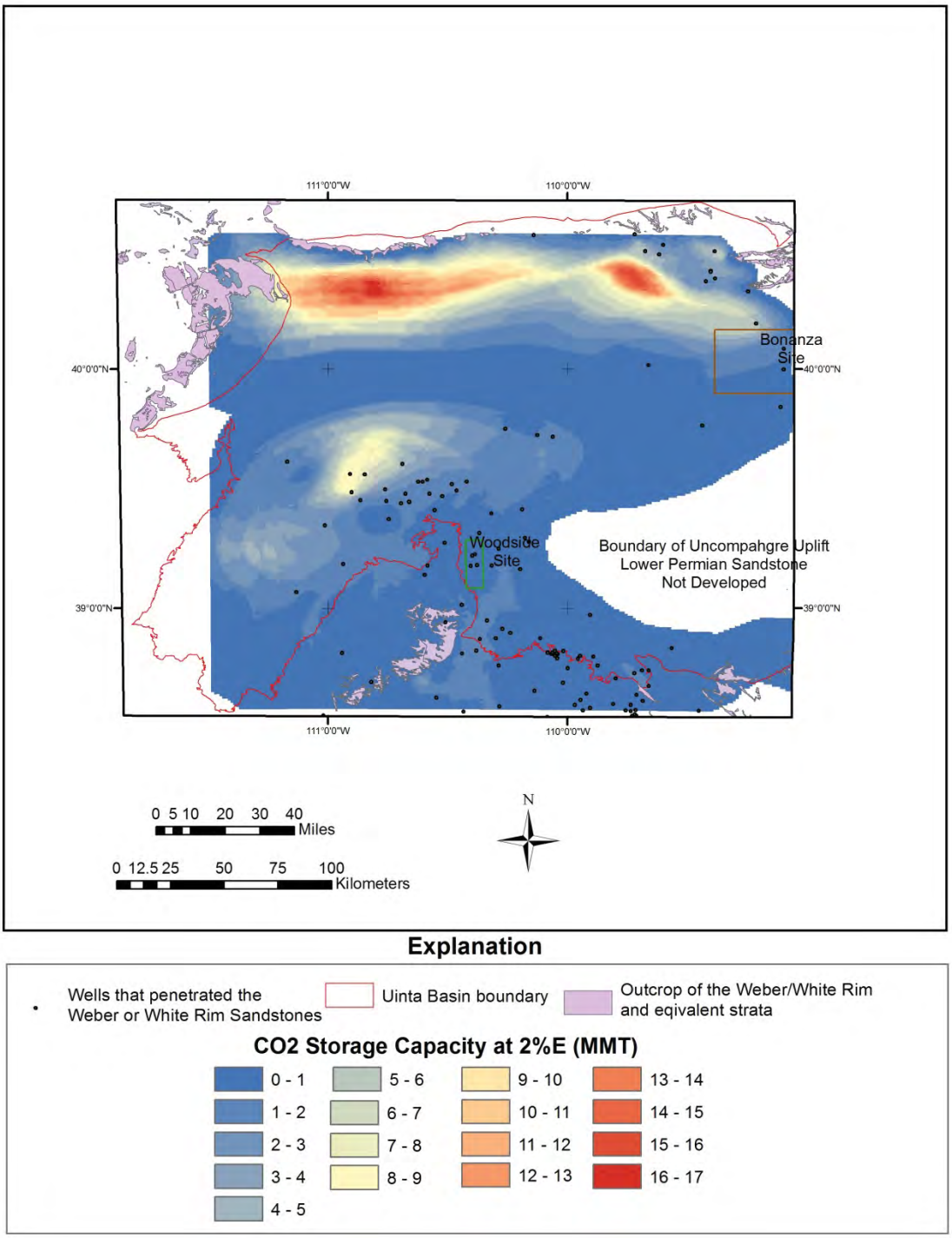


Figure 9. CO_2 storage capacity of the Weber/White Rim reservoir in million metric tonnes (MMT) per million square meter grid. Most of the storage capacity of the Weber is in the deepest part of the Uinta Basin. Calculation based on a 2.0% efficiency factor (E).

CO_2 Storage Capacity

The parameters used to calculate the CO_2 storage capacity of the Weber/White Rim reservoir are shown in table 1. The porosity, reservoir thickness, and reservoir temperature are spatially variable and are based on mapping of well data. The temperature data is from well log headings and can have a wide range of quality because the temperature of the well usually has not equilibrated before the data is collected. There are no penetrations of the Weber in the deepest part of the Uinta Basin; as a result the porosity is projected from shallower wells into the deepest part of the basin. The deepest part of the basin may have much lower porosity due to the depth of burial, than is mapped. Storage capacity of the Weber/White Rim reservoir is shown in table 2.

Table 1. Parameters used to calculate the CO_2 storage capacity of the Weber/White Rim reservoir in the Uinta Basin. Ft = feet, m = meters, km^2 = kilometers squared, F = degrees Fahrenheit, C = degrees Celsius, D = depth, psi = pounds per square inch, and kpal = kiloPascals.

	Area	Average Reservoir Thickness	Average Porosity	Temperature	Pressure Gradient
Weber/White Rim	10,730 $miles^2$ 27,792 km^2	430 ft 130 m	7%	Variable See figure 7	1.14 psi/ft 7.9 kPal/ft

Table 2. CO_2 storage capacity of the Weber/White Rim reservoir in the Uinta Basin using three efficiency factors.

CO_2 Storage Capacity in Million Metric Tonnes			
	Efficiency Factors		
	0.5%	2.0%	5.4%
Weber/White Rim	1361	5338	14,413

Summary and Recommendations

The Weber and White Rim Sandstones were evaluated as one potential reservoir unit. Both formations have good quality coastal dune reservoir facies; the Weber is Pennsylvanian and Permian in age and the White Rim is Permian. The White Rim is believed to be younger and overlies the Weber but there are no outcrops or well penetrations in the western Uinta Basin to confirm this relationship. But an adequate northern limit of the White Rim reservoir and a southern limit of Weber reservoir can be projected and the two formations should be separated for future storage calculations.

The storage capacity of the Weber Sandstone in the eastern Uinta Basin is limited by the rapid north to south change from good quality reservoir of the Weber coastal dune deposits to the arkosic redbeds of the Maroon Formation. The change from Weber to Maroon reduces the areal extend of the reservoir but provides a good updip trap in most of the basin. The Weber would probably not be a major storage reservoir in the Uinta Basin due to the depth and limited extent of the formation.

The storage capacity of the White Rim Sandstone is reduced by the many areas on the SRS where the formation outcrops or is less than 3000 feet (1000 m) deep. Many localized areas on the flanks of the SRS such as the Woodside Dome can be excellent traps for the White Rim

reservoir. Although there have been numerous penetrations of the White Rim there are very few tests and even fewer cores that can provide the petrophysical properties needed for accurate storage calculation. Outcrop studies of the White Rim and overlying Black Box Dolomite (Harston and Morris, 2013) indicate good reservoir properties. But more extensive core-hole data unaffected by surface weathering would be more reliable. There are several locations on the north plunging SRS where a core hole could be drilled at a shallow depth to sample the White Rim and deeper potential reservoirs. The Woodside Dome on the eastern flank of the SRS would be an excellent location to drill a stratigraphic test and recover core from the Entrada, Navajo, and White Rim Sandstones as well as associated reservoir seals.

References

Bryant, B., 2003, Geologic map of the Salt Lake City 30' X 60' quadrangle, north-central Utah, and Uintah County, Wyoming: Utah Geological Survey Map 190DM scale 1:100,000.

Chan, M.A., 1989, Erg margin of the Permian White Rim Sandstone, SE Utah: Sedimentary Geology, v. 36, p. 235-251.

Chidsey, Jr., T.C., and Sprinkel, D.A., 2005, Petroleum geology of Ashley Valley oil field and hydrocarbon potential of the surrounding area, Uintah County, Uutah, *in* Dehler, C.M., Pederson, J.L., Sprinkel, D.S., and Kowallis, B.J., editors, Uinta Mountain Geology: Utah Geological Association Publication 33, p. 347-368.

Contenius, K.N., Clark, D.L., King, J.K., and Ehler, J.B., 2011, Interm geologic map of the Provo 30' X 60' quadrangle, Utah, Wasatch, and Salt Lake Counties, Utah: Utah Geological Survey Open-File Report 586DM, 42 p., scale 1:62,500.

Franczyk, K.J., 1991, Stratigraphic and time-stratigraphic cross sections of Phanerozoic rocks along line C-C', Uinta and Piceance Basin area, southern Uinta Mountains to northern Henry Mountains, Utah: U. S. Geological Survey Miscellaneous Investigations Map I-2184-C, 2 sheets, scale 1:500,000.

Fryberger, S.G. 1990, Ancient eolian deposits of the Navajo and Weber Sandstones, northeast Utah and Colorado, in Fryberger, S.G., Krystinik, L.F., and Schenk, C.J., editors, Modern and ancient eolian deposits – petroleum exploration and production: Society for Sedimentary Geology (SEPM), Rocky Mountain Section Publication, Chapter 19, 12 p.

Harston, W.A., and Morris, T.H., 2013, Facies analysis of the Permian White Rim Sandstone, Black Box Dolomite, and Black Dragon Member of the Triassic Moenkopi Formation for CO_2 sequestration at Woodside field, San Rafael Swell, Utah, Part I, *in* Morris, T.H., and Ressetar, R., editors, The San Rafael Swell and Henry Mountains basin—geologic centerpiece of Utah: Utah Geological Association Publication 42, in press**.**

Hintze, L.F., and Kowallis, B.J., 2009, Geologic history of Utah: Brigham Young University Geology Studies Special Publication 9, 225 p.

Huntoon, J.E., 1985, Depositional environments and paleotopographic relief of White Rim Sandstone (Permian) in the Elaterite Basin, Canyonlands National Park and Glen Canyon National Recreation Area: Salt Lake City, University of Utah, M.S. thesis, 143 p.

Huntoon, J.E., and Chan, M.A., 1987, Marine origin of paleotopographic relief on eolian White Rim Sandstone (Permian), Elaterite Basin, Utah: American Association of Petroleum Geologists Bulletin, v. 71, p. 1035-1045.

Johnson, E.A., 2003, Geologic assessment of the Phosphoria total petroleum system, Uinta-Piceance Province, Utah and Colorado, *in* USGS Uinta-Piceance Assessment Team compilers, Petroleum systems and geologic assessment of oil and gas in the Uinta-Piceance Province, Utah and Colorado, USGS DDS-69B, 42 p.

Welsh, J.E., Stokes, W.L., and Wardlaw, B.R., 1979, Regional stratigraphic relationships of the Permian Kaibab or Black Box Dolomite of the Emery high, central Utah, *in* Baars, D.L., editor, Permianland: Four Corners Geological Society, 9th Field Conference Guidebook, p. 143-149.

APPENDIX Q

Colorado Geological Survey Regional Studies for Capacity

Contents

Topic

Descriptive Text

Maps

Colorado Study Area (CSA)

Petra

The Sand Wash study area was expanded in Petra to include the entire Colorado portion of the Colorado Plateau, called the Colorado Study Area (CSA). Areal coverage is approximately 35,000 square miles and includes the Sand Wash, Piceance, Paradox and San Juan Basins and the intervening Uncompahgre and Axial Basin Uplifts. The same procedure was followed as for the basin scale analysis: formation tops were correlated and the Dakota surface was mapped in detail using Petra. That grid was then transferred to Petrel.

This final project contains a total of 30,678 wells (this number includes the wells within the Sand Wash Basin), of which 18,796 have one or more geophysical logs. Eighty-three formations were identified and correlated and 48,700 individual tops were picked. Altogether 11,146 Dakota tops were used in the construction of the regional Dakota structure map; 2,816 were picked directly off logs and the rest were projected from shallower (or occasionally deeper) tops.

Petrel

The Dakota surface that was created in Petra was transferred to Petrel and used to create ten additional subparallel surfaces which form the the tops and bases of five saline aquifers and the Mancos seal over the CSA. These include:

Structural Surfaces Mapped in the Colorado Study Area Petrel Model

Formation Top and Base	Average Interval Thickness	Description
Mancos to Dakota	3854	The name of the group that comprises all of the formations deposited within the Cretaceous Seaway (including all formations down to the Dakota saline aquifer). The Mancos Group is the ultimate seal overlying the saline aquifers.
Dakota to Morrison	210	The Dakota is a saline aquifer comprised of fluvial and marine sands, silts and shales. Its base is the top of the Morrison.
Bluff to Summerville	163	The Bluff Sandstone consists of eolian dunes in the basal portion of the Morrison Formation. It is only present in the southern portion of the Colorado Plateau study area.
Entrada to Chinle	309	This interval includes the eolian sands of the Entrada, Navajo and Wingate where they are present. The top of the Chinle forms the base of the saline aquifer.
Weber to Maroon	403	The Weber saline aquifer is comprised of eolian sandstone. It is present only in the northern portion of the Colorado Plateau. The top of the Maroon forms its base.
DeChelly to Organ Rock	89	The DeChelly is comprised of eolian sandstone that is equivalent to the Weber saline aquifer. It is only present in the extreme southwestern portion of the Colorado Plateau study area.

Figures 11 through **18**are a series of structure and isopach maps on the top of each of

the saline aquifers and the thickness of each saline aquifer over the Colorado Plateau study area. **Figure 19** is a structure map of the top of the Mancos Shale, the ultimate seal over the saline aquifers. **Figure 20** is an isopach map of the Mancos Shale.

The digital elevation model was used to create maps showing the depths to the top of each of the targeted saline aquifers. These depth maps were used to outline the area of each aquifer present at depths of more than 3000 feet below the surface (**Figure 21**).

Colorado Geology

Structural Geology of the Colorado Study Area (CSA)

The Colorado study area (CSA) contains portions of four major structural basins: the Sand Wash in the north (including the Eagle Basin, its southeastern extension), the Piceance Basin in the west central portion of the state, and the Paradox and San Juan Basins in the south. These basins are separated by uplifted areas that are cored by Precambrian rocks. The locations of these basins and uplifts are shown in **Figure 1**.

These structural elements are the result of four major periods of deformation in the Phanerozoic: (1) the Pennsylvanian Ouachita-Marathon Orogeny that resulted in the formation of the Ancestral Rocky Mountains (Kluth, 1986); (2) the Jurassic-Cretaceous Sevier Orogeny that formed the Western Interior Cretaceous Seaway; (3) the Cenozoic Laramide Orogeny that resulted in the Rocky Mountain Uplift and the interevening present-day basins; and (4) late Cenozoic extensional faulting. These structural elements were key in controlling sedimentation. Basins provided accommodation space allowing for deposition, while uplifts furnished eroded sediments to fill the basins. Subsequent faulting, both compressional and extensional, created barriers to fluid flow within porous strata.

Pennsylvanian Structures

During the Pennsylvanian Period the collision of the continents of Laurentia (North America) and Gondwana (South America and Africa) created the supercontinent of Pangaea. As a result of this continent-to-continent collision, much of North America was subjected to extreme tectonism. In Colorado the Ancestral Rocky Mountains were formed as broad, block-faulted uplifts rather than intensely folded mountains, with the primary movement focused along Precambrian lineaments (Kluth, 1986). The Uncompahgre and Ancestral Front Range uplifts are components of the Ancestral Rockies. They trend roughly northwest and are within or adjacent to the Colorado study area. These uplifts contributed clastic sediments to the adjacent downfaulted basins. Two major basins were created in the Colorado study area between the uplifts: the Central Colorado Trough and the Paradox Basin (**Figure 2**).

The Central Colorado Trough is a northwest-trending basin between the Uncompahgre Uplift and the Ancestral Front Range Uplift. It includes the present-day Sand Wash, Piceance and Eagle Basins within the CSA, and extends to the South Park and Raton Basins in Colorado outside the study area.

In the Craig area, faults along the southern edge of the present-day Axial Basin Uplift were active during the Pennsylvanian. Stone (1986) maps them as predominantly northwest trending thrust faults whose planes dip to the northeast under the upthrust blocks; Pennsylvanian displacements of 1,000 to 3,500 feet were mapped by Stone (1986) in fault segments south of Craig. The Pennsylvanian section thickens considerably to the south and southeast.

The Paradox Basin is located in southwestern Colorado and southeastern Utah to the

southwest of the Uncompahgre Uplift. It is an asymmetric, northwest-trending basin with its maximum thickness along its northeastern edge adjacent to the Uncompahgre Uplift. That edge is interpreted to be a stack of thrust sheets that moved southwestward (Kluth and DuChene, 2009).

The structural configuration of the Paradox Basin was further complicated by salt tectonics. Stevenson and Baars (1988) state that salt attained net depositional thicknesses in excess of 3,000 feet; Peterson and Hite (1969) postulate as much as 5,000 to 6,000 feet of salt was deposited in the basin. It was thickest in the deepest part of the basin along the northeastern basin margin near the Uncompahgre mountain front. The salt began moving due to differential loading in Missouri time, shortly after it was deposited. The salt formed walls that were localized over basement faults; the walls either bent the overlying sediments into anticlines or extended to the surface as diapirs, influencing the deposition of younger sediments. The oldest salt walls are in the northeastern part of the basin closest to the Uncompahgre Uplift. As the salt was evacuated from the subsurface adjacent to the salt wall, the overlying sediments were bent downward creating a mini-basin in which a thicker clastic section accumulated. When there was no salt left beneath the mini-basin, it filled with sediments and salt movement shifted farther to the southwest creating a new salt wall (Kluth and DuChene, 2009). Salt movement affected sedimentation patterns through the Jurassic; thicker clastic sections exist between the salt walls and the clastic sections are thin or absent over the salt anticlines and diapirs.

Mesosoic-Cenozoic Structures

The Sevier Orogeny began with Late Jurassic and Early Cretaceous uplift and thrust faulting along the entire western margin of the North American continent as the Farallon Plate subducted under the North American Plate. The thrust belt runs from Canada through western Utah and eastern Nevada to Mexico with thrust fault movement from west to east, becoming progressively younger to the east. As a result of the crustal thickening from the stacked thrust sheets, a foreland basin formed to the east. This crustal downwarping, combined with high eustatic sea levels, allowed marine flooding into the basin creating the Western Interior Cretaceous Seaway. The seaway covered the entire state of Colorado as well as much of the western North American continent from Canada to Mexico, connecting the Arctic Ocean with the Gulf of Mexico at its maximum extent. It was deepest along its western margin adjacent to the Sevier mountain front. Thousands of feet of sediments, mostly shales, were deposited in the seaway; these form a seal over the underlying saline aquifers.

The Laramide Orogeny began in Late Cretaceous time and extended through the Eocene. The orogeny is thought to be caused by a flattening of the angle at which the Farallon Plate was subducted under the North American Plate. The normal 45 degrees or more subduction angle was changed to a much shallower angle, which caused the Rocky Mountain Uplift to occur almost a thousand miles from the plate boundary (Blakey and Ranney, 2008).

The result of the Laramide Orogeny was the final draining of the Western Interior Seaway and the fragmentation of the foreland into uplifts and intermontane structural basins. The boundaries between the basins and the uplifts are often dramatic and may be marked by monoclines or large scale faults. As an example, the Grand Hogback, a nearly one hundred-mile-long rim of nearly vertical beds, bounds the eastern Piceance Basin.

In the Oligocene, large scale volcanism in southern Colorado created the San Juan Mountains. In the Miocene, extensional forces caused thinning and uplift of the crust resulting in basin and range faulting and the formation of the Rio Grande Rift in central Colorado

(Chronic, 2002). The Rio Grande Rift and its accompanying uplift created the present-day, high topography in the Central part of the state.

Stratigraphy of the Colorado Study Area (CSA)

Sedimentary rocks within the Colorado study area (CSA) range in age from Cambrian through Neogene; only the Silurian System is not represented in the rock record. **Figure 3** is a chart showing stratigraphic relationships of the rock formations for each of the basins within the Colorado study area.

Cambrian through Mississippian Systems

Basal Phanerozoic rocks in the Rocky Mountain region are generally transgressive deposits that overlie the eroded Precambrian surface (Kent, 1972). Cambrian through Mississippian sands and carbonates were deposited on a broad, stable, shallow marine shelf. The uppermost Mississippian formation in the CSA is the Leadville Limestone (which is equivalent to the Madison and Redwall in adjacent states). Uplift and erosion resulted in the formation of a karst surface on the limestone throughout the region, which is called the Molas Formation. (DeVoto, 1980).

The Leadville and its equivalents produce oil and gas throughout the western United States. The Madison is a major CO_2 sequestration target in Wyoming (Thyne, et al, 2010). Therefore, the Leadville Limestone may be considered as a sequestration target in the Colorado Plateau area in the future.

Pennnsylvanian and Permian Systems

The Pennsylvanian and Permian Systems are dominated by extensive tectonism and by cyclic sedimentation. During the Pennsylvanian Period a continent-to-continent collision resulted in wide- scale tectonism over much of North America. In the CSA, the Ancestral Rocky Mountains were formed as broad, block-fault uplifts with downfaulted basins between. The uplifts contributed voluminous clastic sediments to the adjacent basins. Because of the high relief of the Pennsylvanian paleogeography and the changing tectonism, the nature and thickness of the Pennsylvanian sedimentation is highly variable over short distances.

At the same time, glaciation in the southern hemisphere caused rhythmic changes in eustatic sea level, which resulted in cyclic patterns of sedimentation that differed greatly between sea level highstands and lowstands.

The uplift of the Ancestral Rockies had a profound effect on the sedimentation in the CSA. The two deep basins that formed on downfaulted blocks in the study area, the Paradox Basin in southwest Colorado (including the San Juan Basin) and the Central Colorado Trough in northwest Colorado (including the present-day Piceance, Sand Wash and Eagle basins), were filled with cyclic deposits formed as sea level changed in response to Gondwana glaciation. During glacial periods, sea level was at a lowstand, the basins were isolated from the open ocean and evaporites in the form of halite, potash and anhydrite were deposited in the basin centers. As sea level rose in response to glacial melting with the onset of an interglacial period, shales were deposited throughout the basin. During marine highstands in interglacial periods the basins were connected with the open ocean and limestones were deposited along the basin margins (Grammer, et. al., 1996). Thick clastic wedges were deposited adjacent to

the uplifts. These deposits comprise the Pennsylvanian Paradox Formation of the Hermosa Group in the Paradox Basin and the Eagle Valley Evaporites and Minturn Formation in the Central Colorado Trough.

Permian-Pennsylvanian Saline Aquifers in the Paradox Basin

As tectonic activity decreased, the basins continued filling in Late Pennsylvanian time and into the Permian. In the Paradox Basin, evaporite deposition ceased and the carbonates, sands and shales of the Honaker Trail were deposited in a marine environment that graded into alluvial fan deposits along the basin margins. The Honaker Trail exhibits lateral thickness changes, especially around the salt diapirs, which indicates that salt movement began during Honaker Trail deposition (Trudgill and Paz, 2010). As the basin filled, the environment became more nonmarine. Clastic wedges of the Cutler Group prograded farther into the basin, forming thick fans of arkosic sandstones, conglomerates, stilstones and mudstones around the basin margins and prograding into the basin.

The DeChelly Sandstone Member of the Cutler Group consists of lithified dune fields and is present in the extreme southwestern corner of Colorado. It extends into New Mexico and Arizona, and is the equivalent of the Weber Sandstone, one of the three sequestration targets.

Permian-Pennsylvanian Saline Aquifers in the Central Colorado Trough

In the Central Colorado Trough the cyclic nature of the deposition continued, but the sedimentation was nearly all clastic and formed the interfingering Weber and Maroon formations. The Weber Sandstone is described by Johnson, Chan and Konopka (1992) as massive or cross bedded sands deposited in eolian environments during lowstands or in shallow marine or fluvial environments during highstands. It isdescribed by Masoner and Wackowski (1995) as "a series of interbedded eolian sandstones and fluvial siltstones and shales" in Rangely Field, the largest oil field in the Rocky Mountains.

The Weber Sandstone reaches a maximum of 1,000 feet thick at Dinosaur National Monument (Fryberger and Koelmel, 1986) and is the principal oil producing reservoir in Rangely Field. Therefore, it has been targeted as a regional CO_2 sequestration target. However, the thickness and composition of the Weber vary considerably, thinning to the east and south in the present-day Sand Wash and Piceance basins. Therefore, it is only a sequestration target in limited areas, particularly in the southwestern Sand Wash Basin and the northwestern Piceance Basin. An eastern extension of the Weber in the Sand Wash Basin is the Permian Schoolhouse Tongue Sandstone. This unit is 100 to 150 feet thick and extends throughout the southeastern portion of the Sand Wash Basin (Fryberger and Koelmel, 1986). It is indistinguishable from the Weber and the two have been lumped together and called "Weber" in this study.

The Weber interfingers to the south and east with fluvial and eolian sand-sheet deposits of the Maroon Formation (Johnson, Chan and Konopka, 1992) which are described by Whitaker (1975) as arkosic conglomerates and sandstones with red and maroon siltstones and shales associated with alluvial fan deposition. The Maroon Formation is not a sequestration

target because of the discontinuous nature of the sandstones and poor reservoir quality. Fryberger and Koelmel (1986) describe the interfingering between the Weber and Maroon in the Rangely Field area as an abrupt transition, with the percentage of Maroon alluvial sedimentation increasing rapidly to the south. They state: "Reservoir quality decreases proportionately with an increase in the percentage of Maroon alluvial sediments."

A marine incursion into northwestern Colorado in the Permian resulted in the deposition of the Phosphoria Formation and its correlative Park City Formation (in this report it is called "Phosphoria") which is comprised of limestone, sandstone, shale and greenish-gray cherty or phosphatic shale (Geldon, 1986). These rocks, along with the overlying Triassic siltstones and mudstones of the Moenkopi and Chinle formations, form a seal over the Weber saline aquifer.

Triassic System

The Triassic rocks in the CSA were deposited along the broad, arid coastal plain of the supercontinent of Pangea. They were deposited in the floodplains of rivers that had their headwaters in the southern Appalachian Mountains far to the east and southeast (Blakey and Ranney, 2008).

The Triassic Moenkopi consists of red and pale reddish brown claystone, siltstone, and sandy siltstone as well as minor very fine-grained, cross-stratified sandstone (Oriel and Craig, 1960). It, and its equivalent State Bridge Formation in central Colorado, is present throughout much of the northern part of the CSA. It is absent in much of the southern portion as mapped by Stewart, Poole and Wilson (1972), although it is identified by operators in many oil and gas wells within the Colorado portion of the Paradox Basin. It is unknown if the well tops are truly Moenkopi or a facies of the overlying Chinle Formation. If it is Moenkopi, it is thin within the Paradox Basin, on the order of 50 to 200 feet. The Chinle Formation unconformably overlies the Moenkopi and was also deposited by large river systems that originated in the Appalachians. It consists of "predominantly dark-reddish-brown to moderate-reddish-orange fine-grained sandstone, siltstone, and mudstone and lesser amounts of dark- gray to reddish-purple conglomeratic sandstone, limestone-pebble conglomerate, sandstone and gray limestone" (Dubiel, 1992). It reaches a maximum of 1400 feet thick in the southwestern corner of Colorado.

The lowermost member of the Chinle is the Shinarump Conglomerate that consists of coarse-grained sandstone and pebble conglomerate that was deposited in valleys eroded into the Moenkopi. Because it is valley fill, the Shinarump is not present where the Moenkopi formed highlands between valleys (Blakey and Ranney, 2008). The Shinarump produces oil and gas and could be considered a sequestration target. Its maximum net sand thickness in the Sand Wash Basin is 194 feet based on geophysical log measurements from this study.

The Moenkopi and Chinle thin over the salt anticlines in the Paradox Basin and are thicker in the downfolded strata between the anticlines. (Stewart, Poole, and Wilson, 1972).

Juarassic System

Wingate, Navajo and Entrada Eolian Sandstones

Three great Jurassic sand ergs are represented by the Wingate, Navajo and Entrada Sandstones. The oldest is the Wingate Sandstone, which may be partly Triassic in age. It is a

red, cliff-forming unit of cross-bedded sandstone deposited in eolian dunes. It is present in the southwestern part of the study area at least as far north as Grand Junction. The fluvial Kayenta Formation overlies the Wingate and caps its cliffs. Overlying the Kayenta is the Navajo Formation, which may represent the largest eolian sand deposit on Earth (Blakey and Ranney, 2008). It is composed of mostly buff to pale orange, well- rounded, well-sorted, fine-grained sandstone that was deposited in a coastal dune environment (Molenaar, 1981). Together these three formations, the Wingate, Kayenta, and Navajo, comprise the Glen Canyon Group. In the CSA area they thicken to the west and pinch out to the east.

Unconformably overlying the Glen Canyon Group is the Carmel Formation, a marine formation composed of sandstone, mudstone, gypsum and limestone (Blakey and Ranney, 2008). Conformably overlying the Carmel is the Entrada, the youngest of the three Jurassic eolian sandstones and the only one that is present over almost the entire CSA, although it has been removed by erosion over many of the present-day uplifts. The Curtis Formation, a marine deposit of sandstone and mudstone, caps and seals the Entrada in the northern part of the CSA. In southwestern Colorado, the Entrada is capped by the Summerville, which is comprised of very fine grained sandstone, mudstone and shale that was deposited in a tidal flat or marginal marine environment (Molenaar, 1981).

These predominantly eolian deposits, from the Entrada through the Wingate, thicken dramatically to the west. In the eastern Sand Wash Basin only the Entrada is present and in places it may not be present all. The intervening Kayenta and Carmel formations are not present everywhere and are difficult to discern on geophysical logs. For the purpose of this study, the entire section of the Entrada through the Wingate has been mapped as one unit that is defined by structure maps on the top of the Entrada and top of the Chinle. (The top of the Chinle correlates to the base of the Wingate or Navajo or Entrada, depending on where the lower formations are truncated by erosion or missing because of non- deposition.) The total thickness of these units ranges from zero to over 1400 feet in the valleys between the salt diapirs in the Paradox Basin. The sands are porous, permeable and regionally continuous and constitute the largest potential sequestration target on the Colorado Plateau.

Morrison Formation

Beginning in the latest Middle Jurassic time stream drainage patterns changed. They had been flowing toward the northwest, but the Nevadan Orogeny to the west shifted drainage to the northeast. (Blakey and Ranney, 2008). The shales and sands of the Morrison Formation were deposited in this fluvial system.

Four members of the Morrison have been identified: The Salt Wash Member is the lowest and was deposited in fluvial and floodplain environments by braided streams (Berman, Poleschook, and Dimelow, 1980). It is the sandiest of the members in the CSA. In the southwestern corner of the state, eolian dunes of the Bluff and Junction Creek sandstones (called Bluff in this study) were deposited in the lower portion of the Salt Wash Member; these are potential sequestration targets. The Recapture and Westwater Canyon Members overlie the Salt Wash in southwestern Colorado. These were not differentiated in this study. The uppermost member is the Brushy Basin which is comprised of colorful green, red, purple and gray bentonitic mudstones with interbedded sandstone and limestone beds, (Berman, Poleschook, and Dimelow, 1980) which comprise a seal for deeper saline aquifers.

The Morrison is present over the entire Colorado study area except where it has been removed by erosion on the uplifts. A regional unconformity is present at its top. The top of the Morrison is often difficult to distinguish on geophysical logs, especially if there are

channel sands in the upper part of the Morrison. Morrison tops reported by operators were often relied upon in this study because the colorful shales should be more easily identified from samples.

Cretaceous System

The Cretaceous System is dominated by the sediments deposited in and along the Western Interior Seaway. The seaway formed as a foreland basin in response to compressional forces to the west of the present-day Colorado Plateau that created the Sevier Orogeny.

Dakota and Lakota/Cedar Mountain/Burro Canyon Saline Aquifers

As lands to the west were uplifted, Early Cretaceous sediments were deposited by rivers as channel sands, gravels, and mudstones onto the Morrison erosional surface. These sediments are known as the Cedar Mountain in the Piceance Basin, the Lakota in the Sand Wash Basin, and the Burro Canyon in the Paradox Basin. Porosity and permeability of these units can be very good at the localized scale.

As the Sevier Orogeny continued, the continental crust to the west of the Colorado Plateau was thickened by stacked thrust sheets. This depressed the crust to the east (including present-day Colorado), creating a foreland basin which filled with a shallow ocean. As the ocean transgressed over the subsiding land, advancing from north to south, marine and fluvial sands, shales and some coals were deposited along the advancing shoreline and coastal plain. These lithologies comprise the Dakota Formation which is present over much of the western United States from the Dakotas to New Mexico.

In this study, the fluvial-deltaic sandstones of the Dakota could not be distinguished from the fluvial sandstones of the Lakota/Cedar Mountain/Burro Canyon because of their discontinuous nature. For this report the Dakota includes the interval from the top of the Dakota to the top of the Morrison.

Mancos Group

As the sea continued to advance, the Dakota shoreline moved farther to the south and east and water depths increased. Conformably overlying the Dakota is a thin bed of Mowry Shale (100 feet or less) overlain by the shales and sands of the Mancos Group that were deposited within the Cretaceous Seaway. The Mancos varies in thickness throughout the CSA. In general, it thins to the south, with thicknesses ranging from 2000 feet in the south to almost 6000 feet in the north. The axis of the basin moved east through time along with the thrust faulting of the Sevier Orogeny. The western shoreline of the seaway also moved eastward in conjunction with the advancing mountain front.

The Mancos Group consists of a succession of shales, calcareous shales, and sandstones representing a number of formations. The Mancos Group as a whole represents a definitive seal for the underlying saline aquifers targeted in this study. The Niobrara Formation, a component of the Mancos section, is 1500 feet thick in the Craig area; it contains three calcareous shale benches that are being actively explored for oil and gas, and may be a future target for sequestration in fractured media.

Toward the top of the Mancos Group, as the western shoreline of the Cretaceous Seaway was advancing eastward, the Mancos section becomes sandier. Tongues of shoreface sandstones were deposited during stillstands; these prograde for many miles into the basin and become thinner and shalier as they extend into the basin until they eventually pinch out. Each of these sandstone tongues was buried by a subsequent pulse of tectonic activity that caused subsidence of the basin and a corresponding transgression of the seaway, thereby creating

conditions for another shoreface sandstone tongue to be created. These prograding sandstone layers extend progressively farther to the southeast as they get younger, recording the advance of the western shoreline of the Cretaceous Seaway to the east. Two very extensive prograding shoreface sands in the Piceance and Sand Wash Basins are the Castlegate (which appears to be correlative with the Morapos in the Sand Wash Basin) and the Rollins (which is correlative with the Trout Creek in the Sand Wash Basin); both of these units are potentially good sequestration targets.

Mesaverde Group

With time, the western shoreline finally advanced into the area of study and sedimentation changed from predominantly marine to continental. Marine and fluvial sands, shales and coals were deposited on coastal plains and comprise the Cretaceous Mesaverde Group. The Mesaverde is thicker in the west and thins in the eastern Sand Wash and San Juan basins where the sediments appear to be more marine. A major marine transgression near the middle of the Mesaverde section was recorded in the rock record as an extensive marine shale that can be seen in the eastern part of the Sand Wash Basin. Overlying it is the prograding Trout Creek sand, which is correlative with the Rollins sand in the Piceance Basin.

For this study the top of the Mesaverde was not identified in the Piceance Basin because it was indistiguishable on geophysical logs from the overlying continental deposits of the Ohio Creek, Fort Union and Wasatch formations.

Lewis Shale

In the Sand Wash and San Juan basins a final transgression of the Cretaceous Seaway resulted in the deposition of the Lewis Shale, although the shales are of different ages in the two basins.

In the Sand Wash Basin the Lewis consists of marine shale and sandstones; the sands are fine-grained turbidity deposits (Cain, 1986). The Lewis Shale thins from east to west; it is not present in the Piceance and Paradox basins. Above the Lewis in the Sand Wash Basin is the Cretaceous Fox Hills Formation consisting of shoreline sandstones representing the final regression of the Cretaceous Western Interior Seaway.

Paleogene and Neogene Systems

At the end of the Cretaceous Period, compressive forces from the west initiated the Laramide Orogeny, which continued through the Eocene. This mountain building episode fragmented the western United States, uplifting the Rocky Mountains and creating basins in the intervening areas. Erosion reduced the mountains and filled the basins with fluvial and lacustrine deposits, forming rocks of the Fort Union, Wasatch, Green River and Uintah Formations in Colorado.

Intense igneous activity occurred in the southwestern part of the state during the Cenozoic. In the Oligocene, laccoliths were intruded in the area of the Elk Mountains and andesitic and ash flows were extruded in the San Juan volcanic field. The eruptions in the San Juan volcanic field became basaltic in the Miocene (Tweto, 1977) as the regional compressional forces of the Laramide Orogeny changed to regional extensional forces that created the Basin and Range (Stern and Constenius, 1997). The Rocky Mountains underwent another period of uplift in the Miocene and Pliocene, which lifted them to their present height. Igneous sills, dikes, and flows continued in the area through the Pliocene (Tweto, 1979) in

response to the extensional forces.

Net Sand and Porosity Distribution Mapped from Geophysical Logs

In the early stages of this study, when mapping was limited to the Sand Wash Basin Study Area, raster logs were examined in an attempt to map reservoir properties. Net sand maps were constructed by highlighting sandy intervals on raster logs and summing those intervals for each saline aquifer. This process was time consuming and imprecise.

In the final months of this study, digital well logs in LAS format became available. Digital logs were downloaded for 818 wells within the CSA that penetrated all or a portion of the saline aquifers. These logs were used to construct maps depicting the distribution of net sands, porosity, and pore volumes for each of the saline aquifers. These parameters are measured by one or more types of geophysical logs. Sands are measured by gamma ray logs and porosity is measured by density, neutron and/or sonic log.

Net Sand

Gamma ray curves were used to identify sands and construct net sand maps of the Dakota, Entrada and Weber formations. A total of 578 wells had digital gamma ray curves over all or parts of the saline aquifers. These curves were normalized using Petra™ software to adjust the curves to a common scale because of insensitivities of gamma ray tools. Net feet of sand were summed in each well for each saline aquifer and contoured to illustrate the distributions of those properties. **Figure 27** shows the net sand map for the Dakota Formation in the CSA that was constructed from the digital gamma ray curve data.

This net sand map can be compared with a net sand map that had been constructed for the Sand Wash Basin from raster logs, which is shown in **Figure 28**. Overall, the maps from the digital and raster data agree favorably. The maps created from the raster logs show more variability, probably because there are more clustered data points and the gamma ray curve was not normalized.

Average Porosity

Density, neutron, and sonic logs were used to measure the porosity within the sands of the saline aquifers. When multiple porosity logs were available, a hierarchy was established to determine which log to use. If modern density/neutron logs were available, a digital curve averaging the two values was constructed and this was used as the porosity curve for the well. If both of those curves were not available, the density curve was used, after which the sonic and finally the neutron curve was used. Petra software was used to compute the average porosity for the sandstone intervals within the Dakota, Entrada and Weber saline aquifers, and maps were constructed to show its distribution. **Figure 29** shows the average porosity within the Dakota sands.

The porosity maps, like the net sand maps, have irregularly spaced data points; where data are clustered, porosity values can be highly variable. This shows that individual data points are not representative of large areas. Areas contoured from very few data points should be viewed with caution; they are probably much more variable than the maps depict. Other inaccuracies in the average porosity maps stem from the fact that porosity values were obtained from different kinds of logs: density, neutron and sonic. These all measure different parameters and are affected to different degrees by the presence of hydrocarbons or water in the pore spaces, by the presence of fractures, and by hole rugosity. Therefore, the maps constructed from

these logs can give an estimate of general trends and ranges of values, but cannot be relied upon for specific values. Also, these maps were computer contoured and the final configuration is highly dependent on the gridding algorithm and grid spacing that were used.

Pore Volume

Porosity thickness maps were generated as the product of average porosity and net sand. Pore volume can be derived by considering mapped area. Porosity thickness maps were generated for each of the saline aquifers in each well that had both a porosity log and a gamma ray log. **Figure 30** depicts the porosity thickness for the Dakota sand intervals.

Storage Capacity

The porosity thickness grid was used in an Excel spreadsheet to calculate the storage capacity for CO_2 within the saline aquifers. This is discussed in a separate section of this study.

Effective Porosity

Sands with low porosities often have very low permeabilities and may not be available to provide storage capacity for CO_2. As an attempt to estimate how low porosity sands may not contribute to storage capacity, a porosity cutoff of six percent was used. Sands with less than six percent porosity were deemed incapable of storing CO_2. Sands with six percent or greater porosity were considered capable of storing CO_2 and their porosity was deemed "effective" porosity. A series of maps was constructed for each saline aquifer to depict effective net sand, effective average porosity and effective pore thickness. These maps are shown for the Dakota saline aquifer in **Figures 31** through **33**.

A six percent porosity cutoff is not a definitive value, but rather is an estimation to compare total porosity with some lesser effective porosity. Additional studies would be required to better determine a representative value. However, these maps illustrate another way that storage capacity estimates could be refined.

Discussion

Dakota Saline Aquifer

The map series for the Dakota saline aquifer (**Figures 27** through **33**) show high variability in net sand thickness and porosity values, which is reasonable because the formation consists of fluvial-deltaic sequences which can be highly variable over short distances. The actual variability within the formation is probably more than is shown on the maps.

There are two trends of thick sands: (1) in the southeastern Sand Wash Basin to the south of the RMCCS State #1 well, and (2) across the southern portion of the Piceance Basin. These two areas have multiple data points with thick net sands and high porosities and may represent deltas along the paleoshoreline or a stillstand in the paleoshoreline where more sands were deposited. There are other areas of seemingly thick sand intervals, but they are defined by only one or two data points, and thus, their size and extent cannot be verified with the data available.

Entrada Saline Aquifer

Figures 34 through **39** are the series of maps that were constructed for the Entrada saline aquifer (net sand, average porosity, pore thickness, effective net sand, effective average porosity, and effective pore thickness). This aquifer consists mostly of sandstone; therefore, the

net sand map closely resembles the isopach map for the formation. The net sand map (**Figure 34**) shows the steady thinning of the interval to the east as the the Navajo and Wingate sandstones are removed from the interval by erosion or non- deposition. Because most of this interval is eolian sand, the porosities and pore volumes are less variable. However, the data points still show variation and the maps are less accurate where there are few data points.

Weber Saline Aquifer

Figures 40 through **45** are the series of net sand and porosity maps that were constructed for the Weber saline aquifer. These maps are based on very few data points and are highly interpretive. The Weber eolian sands decrease to the east and interfinger with the alluvial Maroon sands. Unfortunately, many wells that were drilled into the Weber only penetrated the top portion of it, so these wells could not be used to characterize the entire Weber interval. Also, the Weber and Maroon cannot be distinguished from each other on geophysical logs, so the base of the Weber was picked using tops reported by operators. Some operators identified the Maroon top; some identified only deeper formations such as the Morgan or Minturn Formations. Each well that had raster logs and also a deeper top reported by an operator was examined to see how it compared to other nearby wells. The picture that emerged showed thickest net sands in the west. There appears to be a second area of thicker sand with greater porosities about 15 miles south of the RMCCS State #1 stratigraphic test well. The RMCCS State #1 was not able to drill deep enough to penetrate the Weber, but it is expected that the Weber would have thin sands and very little porosity at that location.

The maps of the tops and bases of the saline aquifers in the Sand Wash Basin and their equivalents were extended over the Colorado portion of the Colorado Plateau, called the Colorado Study Area (CSA). Ten maps were created at that scale, five depicting the structural tops of the saline aquifers and also the Mancos seal, and five depicting thicknesses of the saline aquifers and also the Mancos seal. These will be combined with similar maps of the Utah, Arizona and New Mexico portions of the Colorado Plateau.

Maps depicting the net feet of sand, average porosity in sand, and pore thickness were created for the Dakota, Entrada and Weber saline aquifers in the Colorado study area. These were made by identifying sands from digital gamma ray logs and porous zones from digital density, neutron or sonic logs. Maps depicting effective net feet of sand, effective average porosity, and effective pore thickness were made by summing net sand and porosity for those sands with porosities greater than or equal to six percent. The Dakota shows a great deal of variability in the distribution of sand and porous sand because of the fluvial nature of much of the sand. The Entrada maps show that both the net sand and net porous sand thickness increases to the west as the Navajo and Wingate sandstones (which are considered a part of the Entrada saline aquifer in this report) increase in thickness. The Weber saline aquifer was the most difficult to map because many wells only penetrated the topmost portion of the formation and also because the base of the Weber is hard to distinguish from the underlying Maroon Formation. For these maps, the base of the Weber was estimated from the tops of deeper formations reported by operators. The thickest Weber sands and greatest porous volumes are located to the west and south and decrease to the east. It is expected that the Weber would have thin sands and very little porosity at the location of the RMCCS State #1 well

List of Figures

1. Extents of the three scales of the study areas encompassed by this report and the basins and uplifts in Colorado.
2. Locations of Ancestral Rockies uplifts and basins.
3. Stratigraphic chart for basins in the Colorado study area.
4. Locations of all wells in the Colorado study area.
5. Locations of all wells with raster and/or digital geophysical logs in the Colorado study area.
6. Structure map on top of the Dakota saline aquifer in the Colorado study area. Contour interval is 500 feet.
7. Thickness of the Dakota saline aquifer in the Colorado study area from the top of the Dakota Formation to the top of the Morrison Formation.
8. Structure map on top of the Entrada saline aquifer in the Colorado study area.
9. Thickness of the Entrada saline aquifer in the Colorado study area from the top of the Entrada Formation to the top of the Chinle Formation.
10. Structure map on top of the Weber saline aquifer in the northern part of the Colorado study area. The structure on top of its equivalent, the DeChelly Sand, is shown in the southern part of the map.
11. Thickness of the Weber saline aquifer in the northern part of the Colorado study area from the top of the Weber Formation to the top of the Maroon Formation. In the southern part of the map the thickness shown is of the DeChelly Sandstone, which is equivalent to the Weber.
12. Structure map on top of the Bluff Sandstone in the Colorado study area.
13. Thickness of the Bluff Sandstone in the Colorado study area.
14. Structure map on top of the Mancos seal in the Colorado study area.
15. Thickness of the Mancos seal in the Colorado study area from the top of the Mancos Formation to the top of the Dakota Formation.
16. Outlines of the extents of each of the saline aquifers where they are buried more than 3000 feet below the ground surface..
17. Dakota net sand from normalized gamma ray curve.
18. Dakota Average Porosity in Net Sands
19. Dakota porosity thickness (average porosity times net feet of sand).
20. Dakota net feet of sand with porosity >6%.
21. Dakota average effective porosity for sands with porosity > 6%.
22. Dakota effective porosity thickness (average porosity times net feet of sand) for sands with porosity > 6%.
23. Entrada net sand from normalized gamma ray curves.
24. Entrada average porosity in net sand.
25. Entrada porosity thickness (average porosity times net feet of sand).
26. Entrada effective net sand (net feet of sand with porosity > 6%).
27. Entrada effective average porosity (porosity in sands > 6%).
28. Entrada effective poprosity thickness (average porosity times net feet of sand) for sands with porosity > 6%.
29. Weber net sand from normalized gamma ray curves.
30. Weber average porosity in net sands.
31. Weber porosity thickness (average porosity times net feet of sand).
32. Weber effective net sand (net feet of sand with porosity > 6%).
33. Weber effective average porosity (in sands with porosity > 6%).
34. Weber effective porosity thickness (net feet of sand times average porosity) in sands with porosity > 6%.

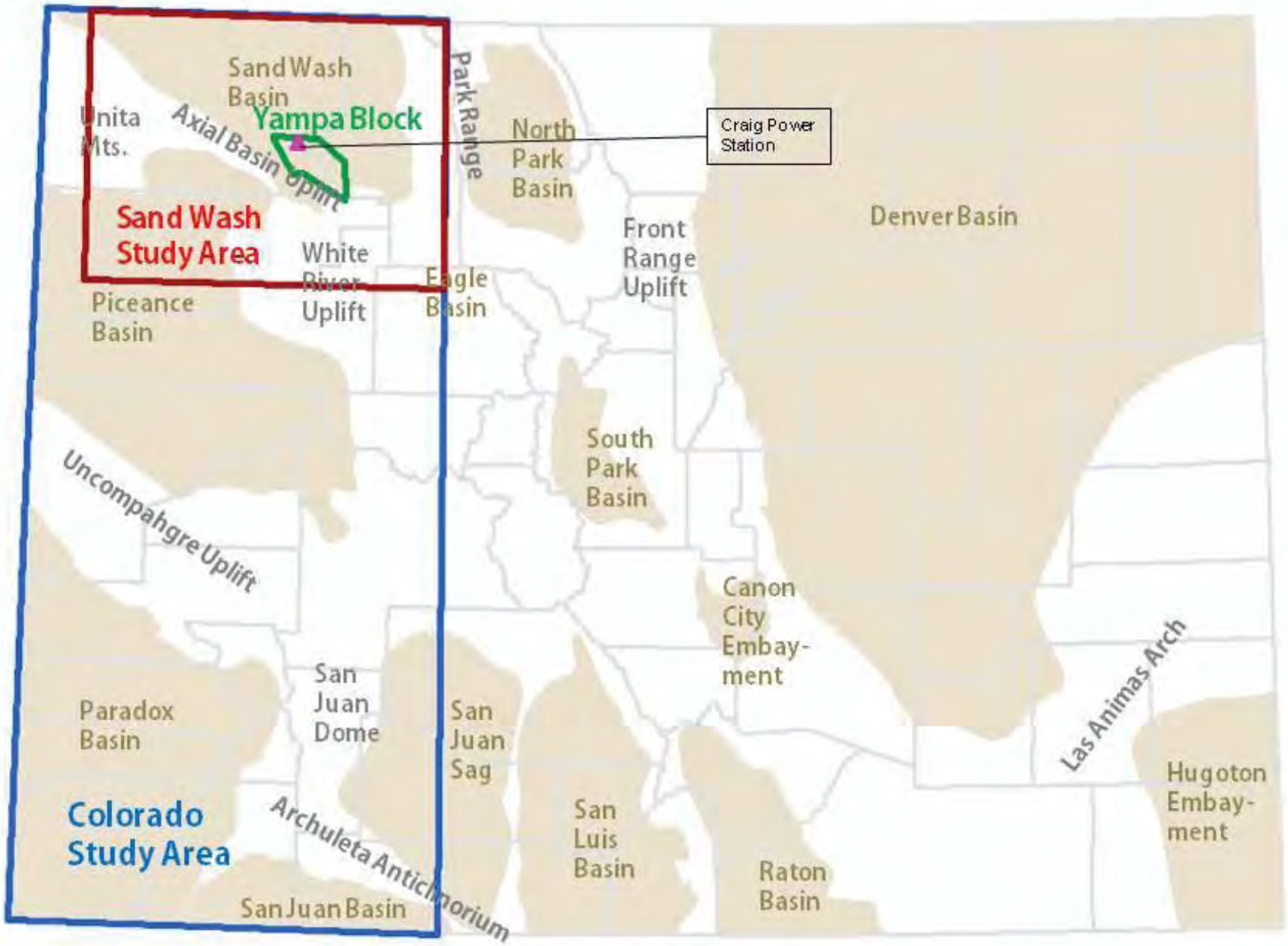


Figure 1. The extents of the three scales of study areas encompassed by this report and the basins and uplifts in Colorado.

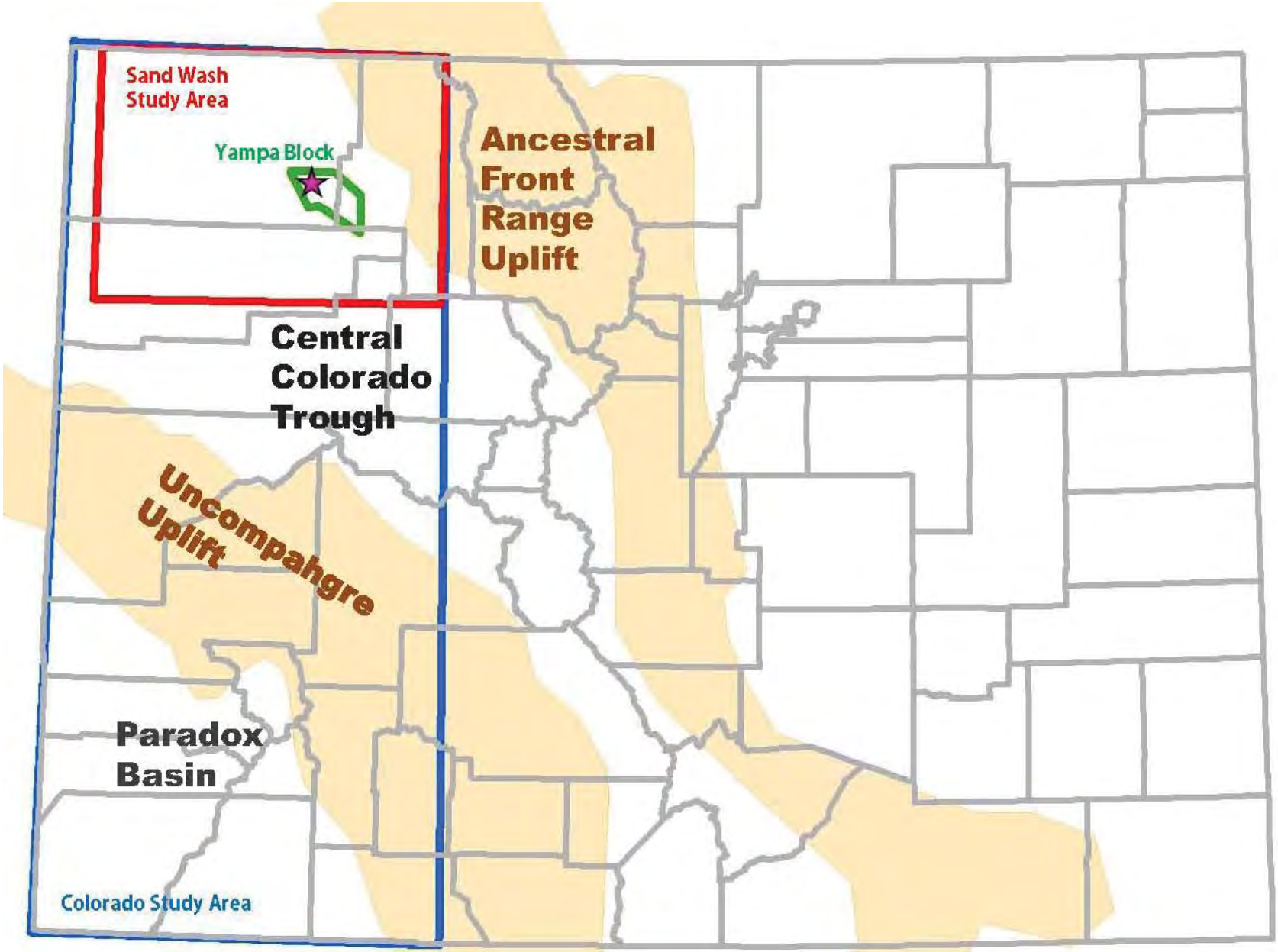


Figure 2. Locations of Ancestral Rockies uplifts and basins (Mallory, 1972, p. 132).

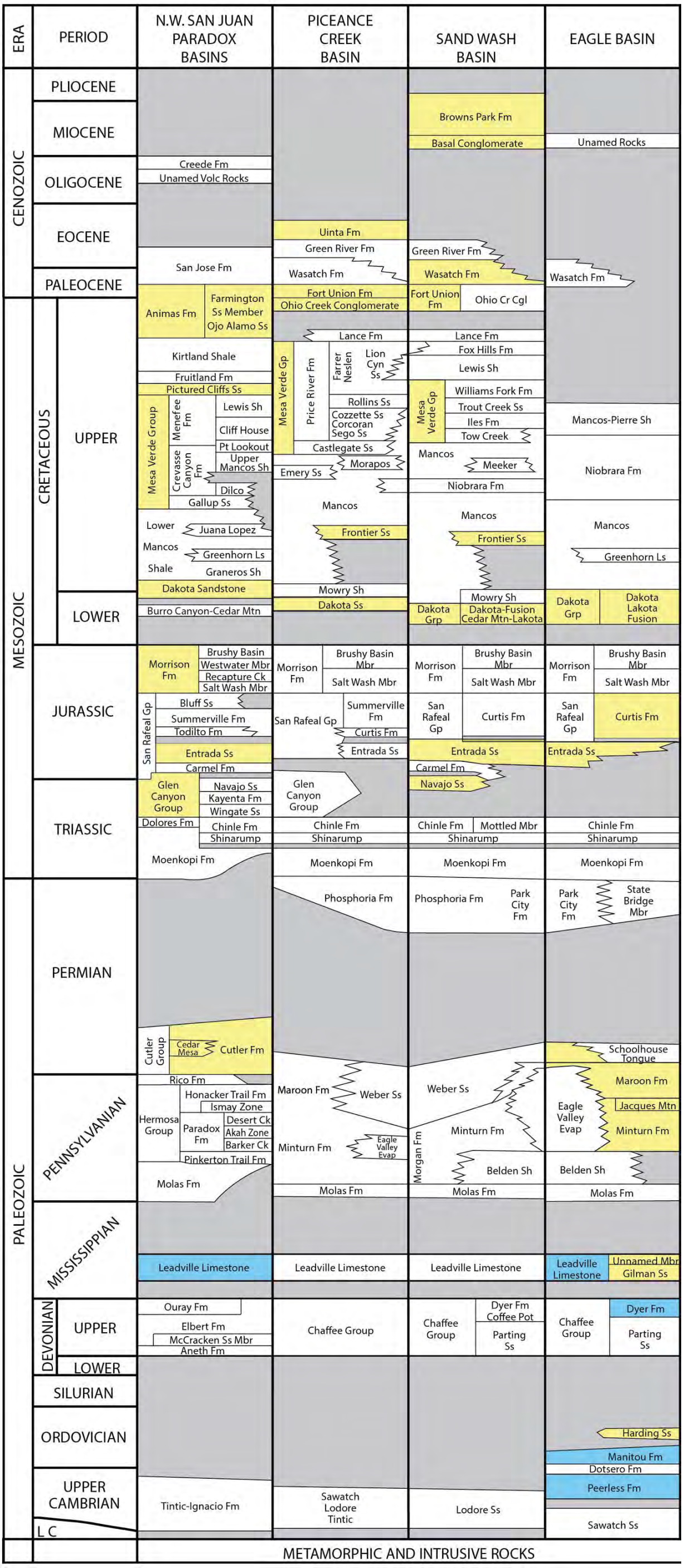


Figure 3. Stratigraphic chart for basins in the Colorado study area. (Irwin, 1977.)

Figure 4. Locations of all wells in the Colorado study area. Basins are shaded brown.

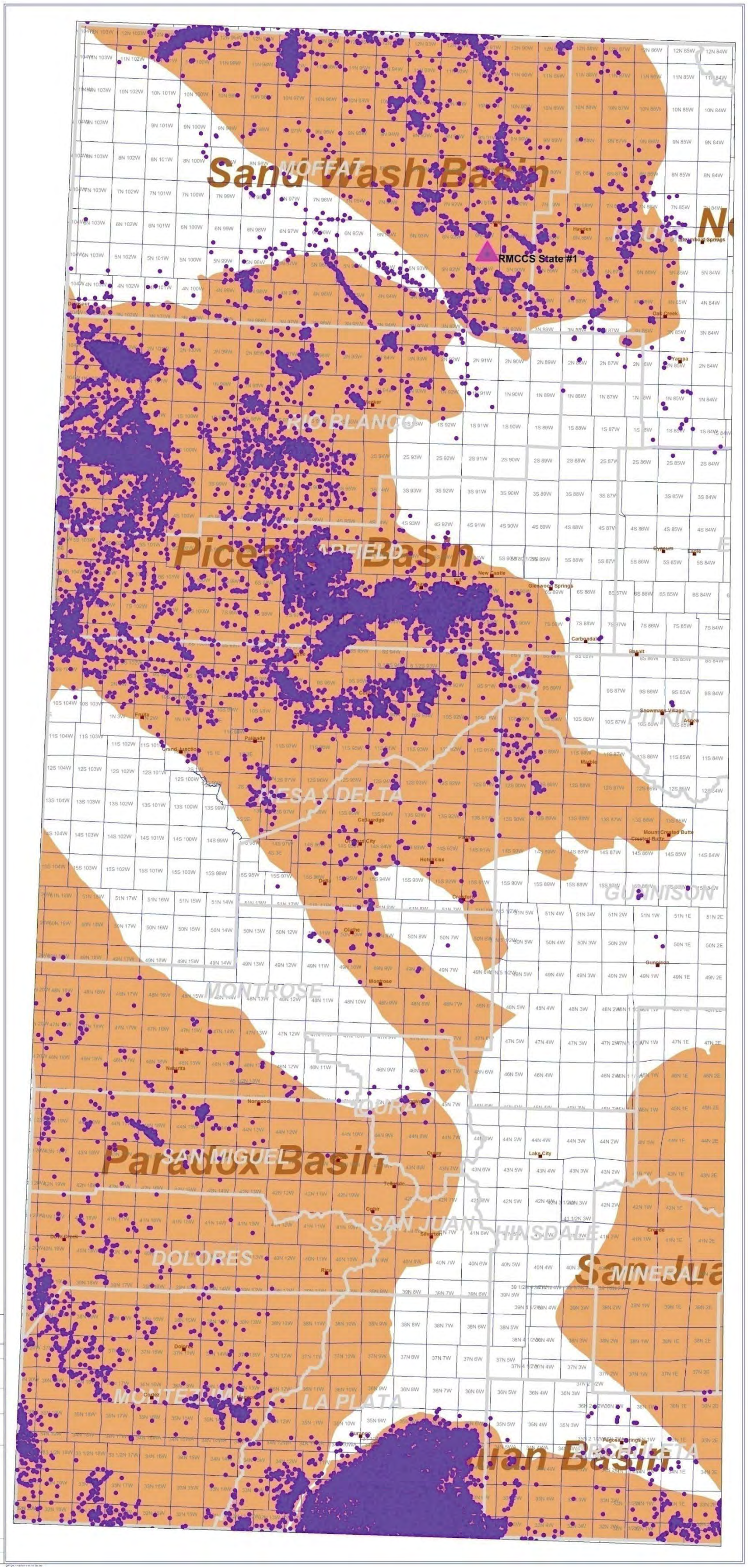


Figure 5. Locations of wells with raster and/or digital geophysical logs in the Colorado study area. Basins are Outlined in Brown.

Green Dots = Raster Logs

Turquoise Dots = Digital Logs

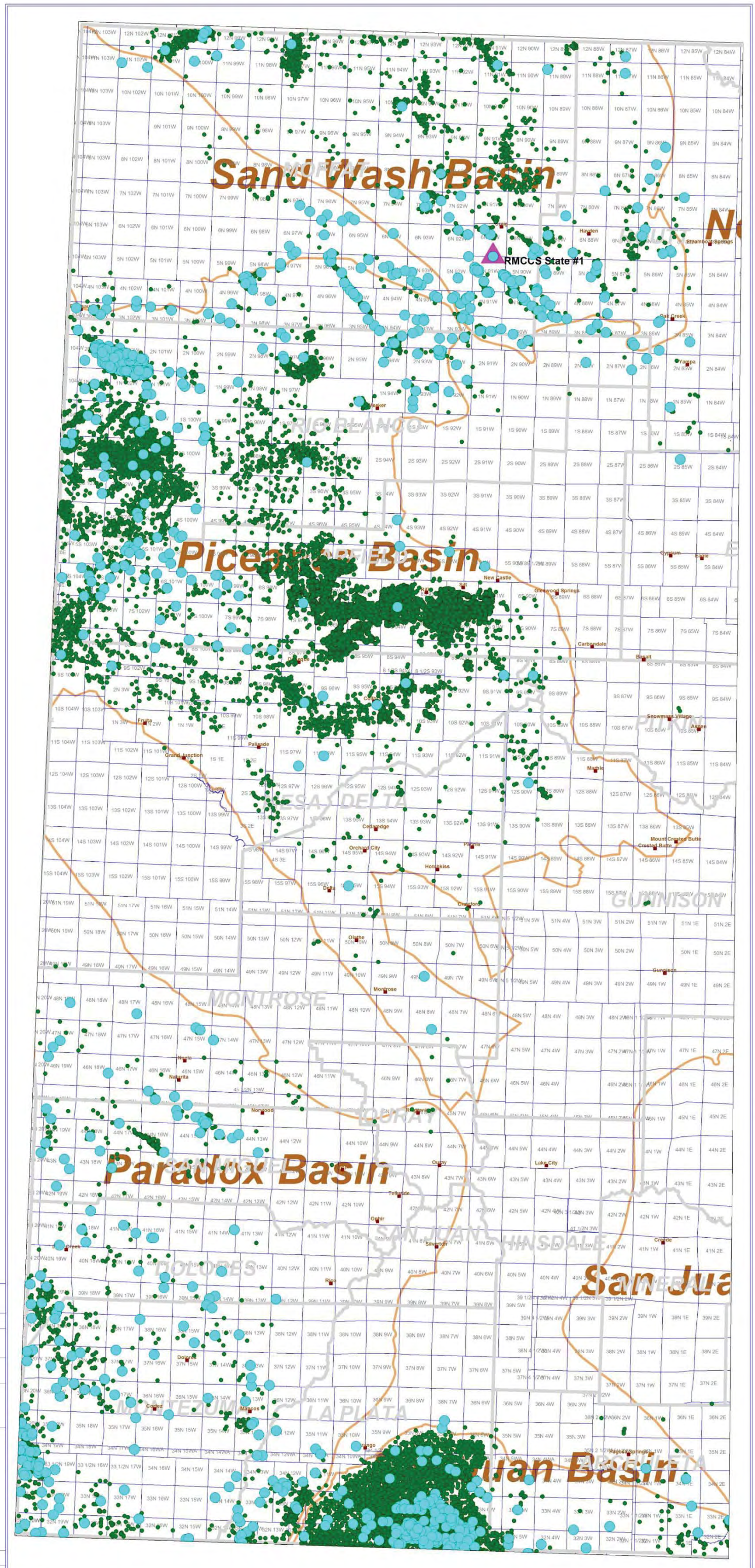


Figure 5

Figure 6. Structure map on top of the Dakota saline aquifer in the Colorado study area. Contour interval is 500 feet.

Purple Dots: Dakota top

Red Dots: Projected Dakota Top

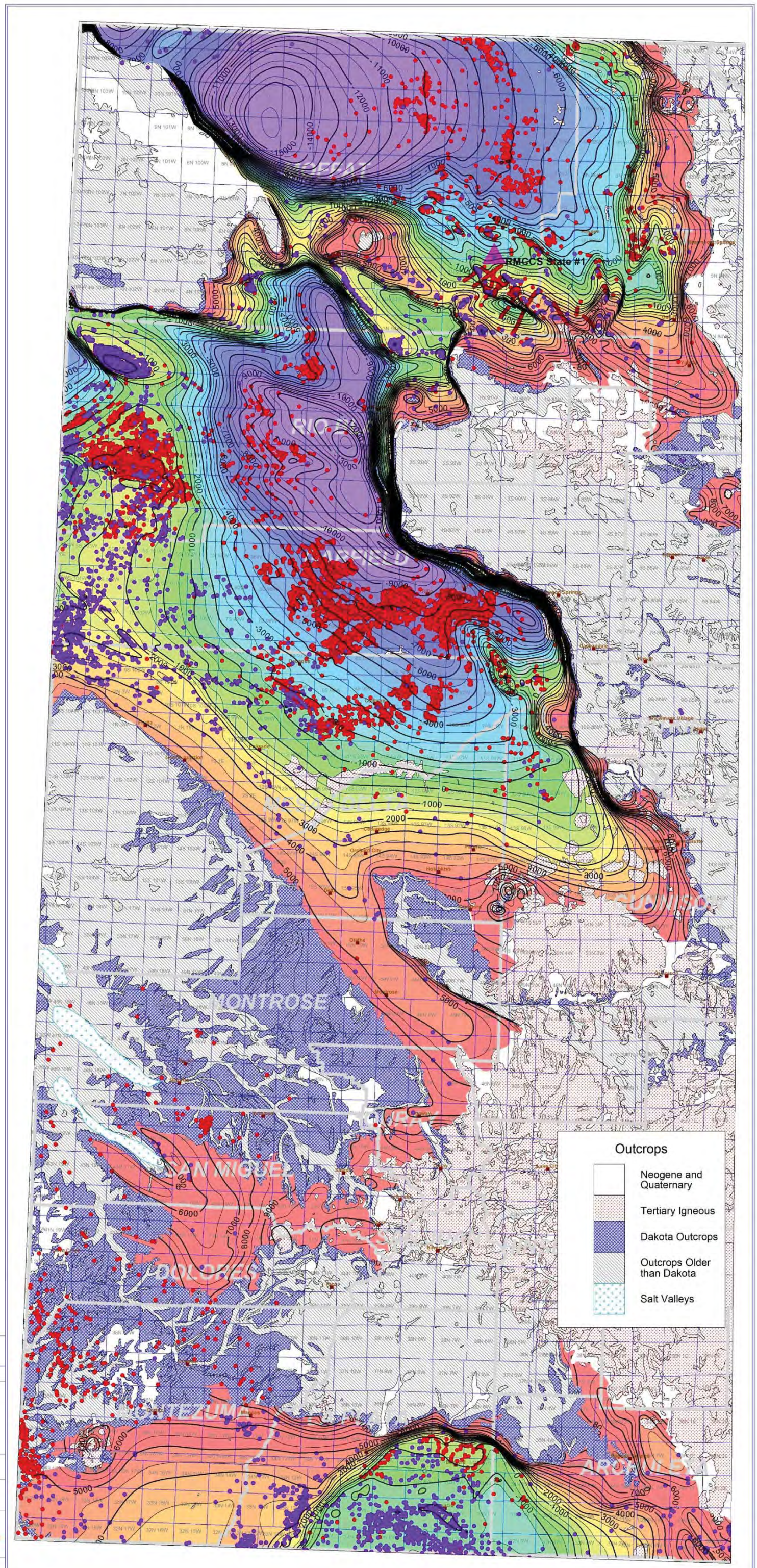


Figure 6

Figure 7. Thickness of the Dakota saline aquifer in the Colorado study area from the top of the Dakota Formation to the top of the Morrison Formation. Contour interval is 50 feet.

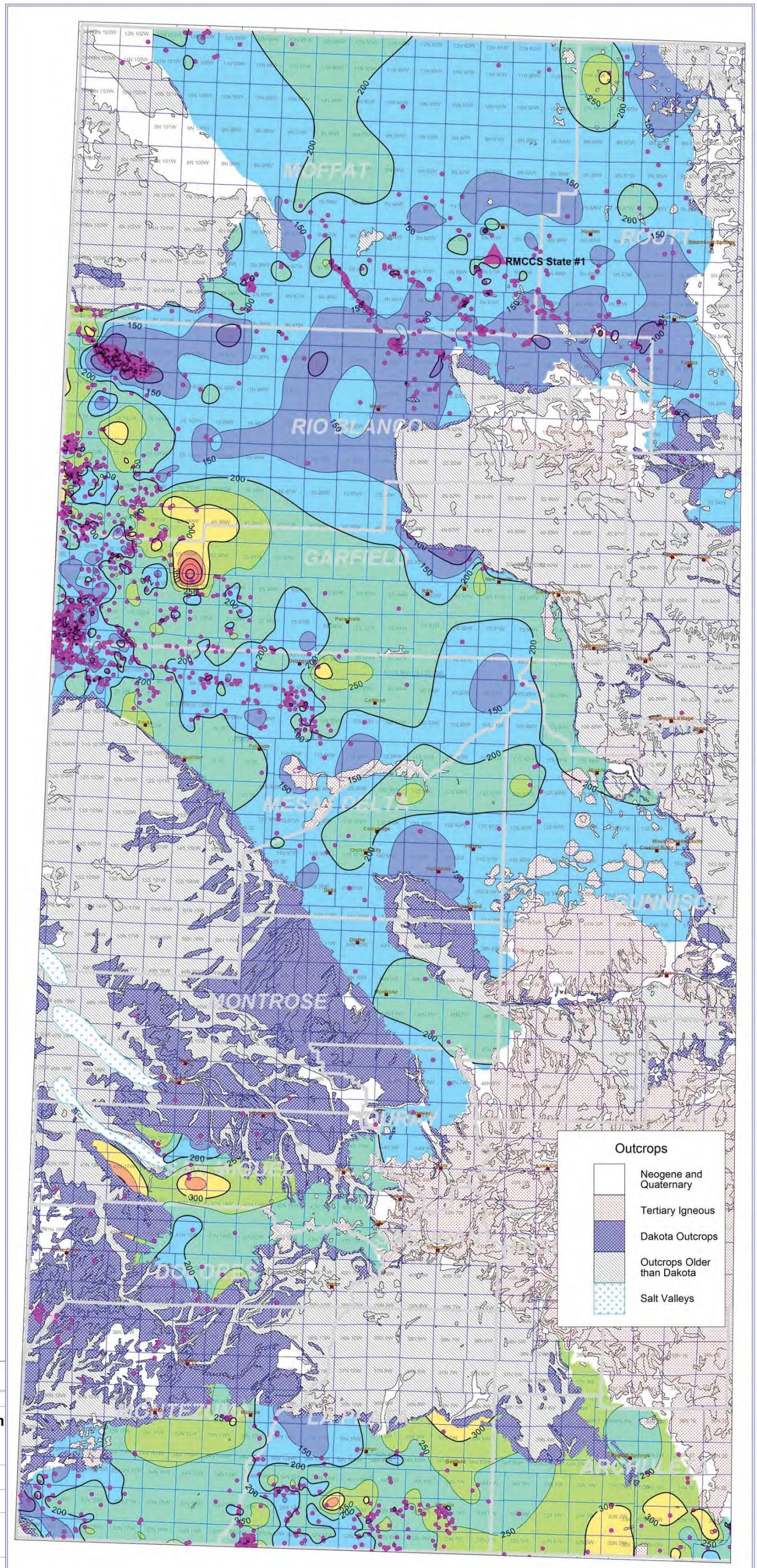


Figure 7

Figure 8. Structure map on top of the Entrada saline aquifer in the Colorado study area. Contour interval is 500 feet.

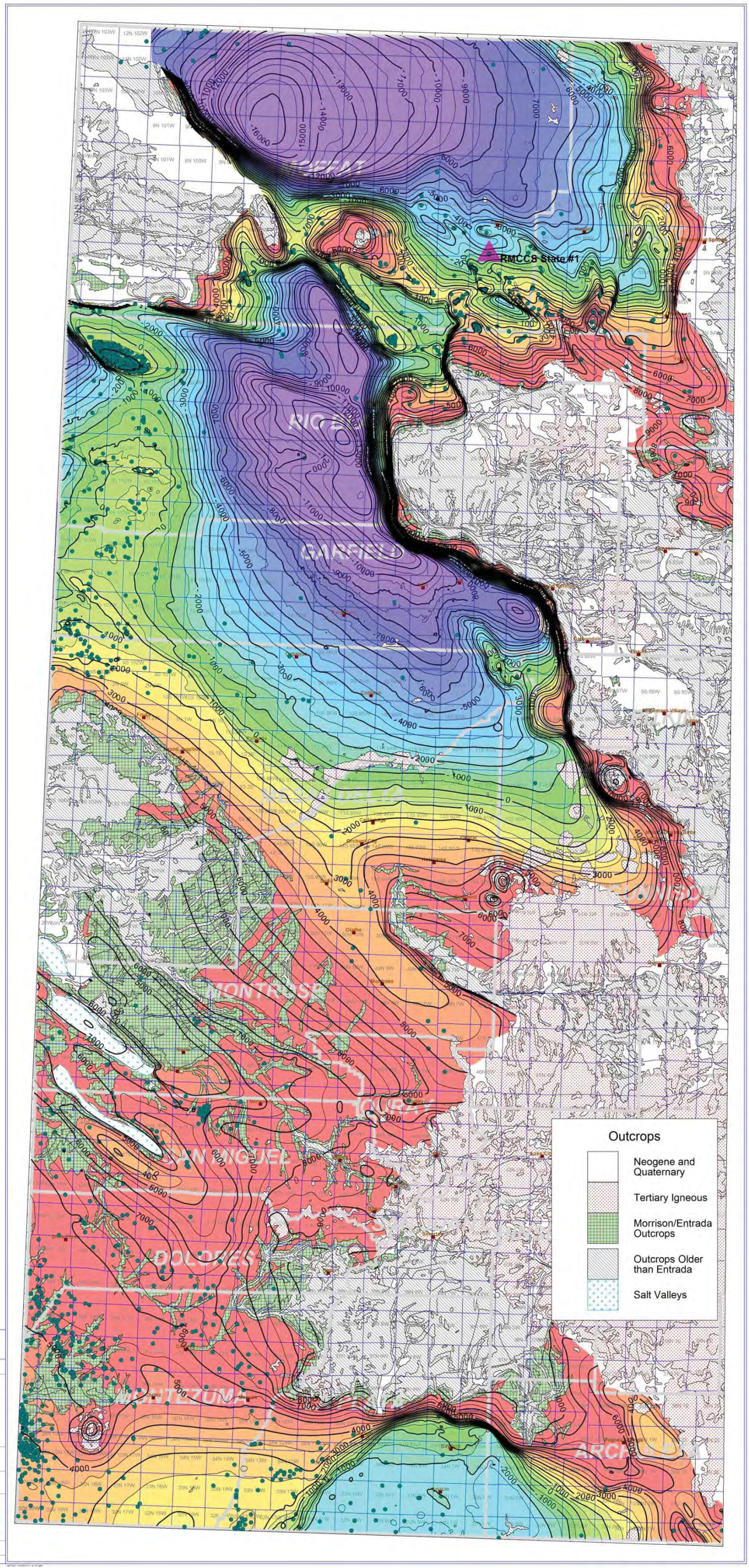


Figure 8

Figure 9. Thickness of the Entrada saline aquifer in the Colorado study area from the top of the Entrada Formation to the top of the Chinle Formation. Contour interval is 100 feet.

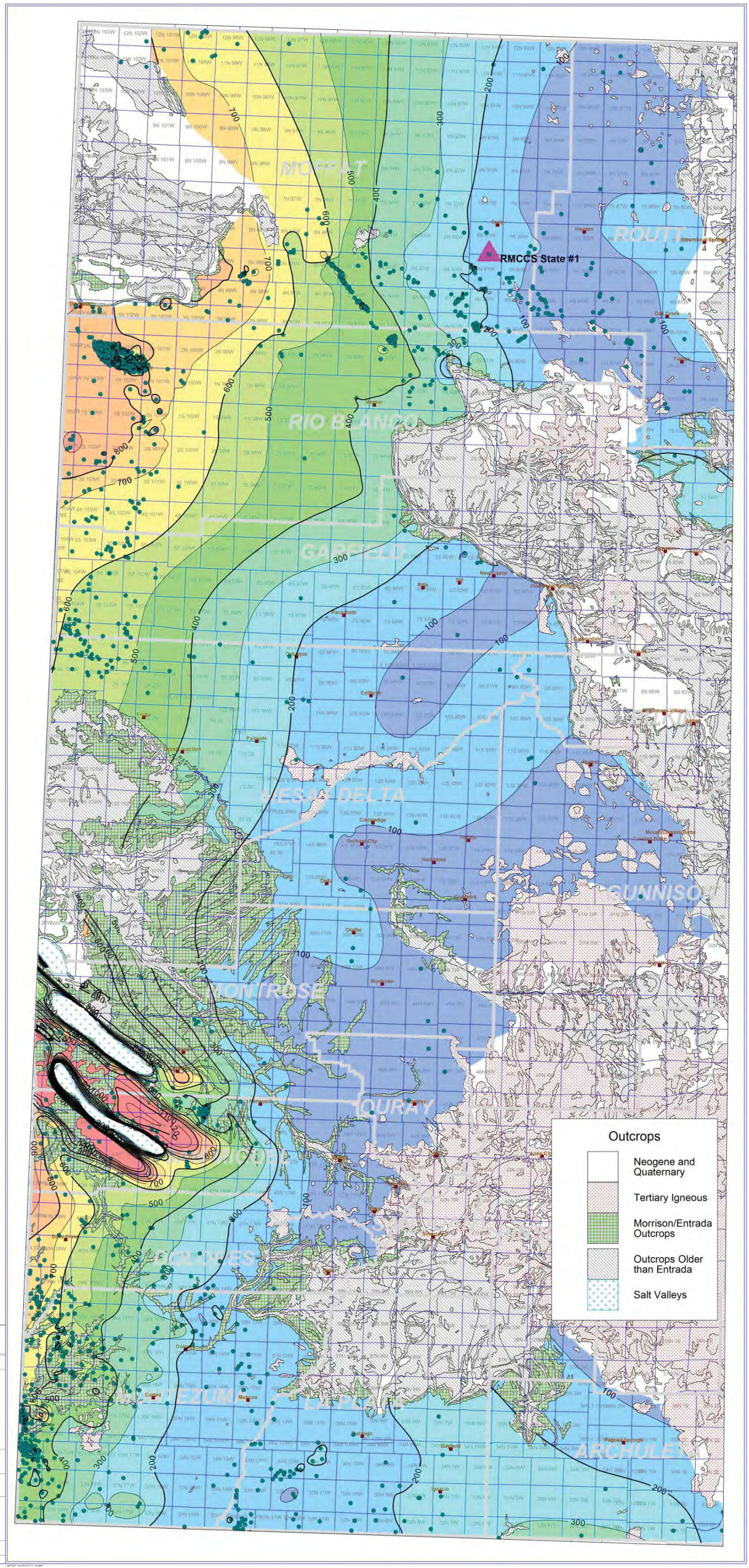


Figure 9

Colorado Geological Survey

CO_PLATEAU_CO2_PKS

Thickness: Entrada to Chinle

Includes Entrada, Navajo and Wingate

Western Colorado

0 38,563 77,126 115,689
FEET

SYMBOL HIGHLIGHT

ENTRADA TOPS

CONTOURS
Grid HEADER
THICKNESS_BETWEEN_ENTRADA_AND_CHINLE.GRD
Contour Interval = 100

0 100 200 300 400 500 600 700 800 900 1000 1100 1200 1300

By: Phyllis Scott

January 16, 2013

Figure 10. Structure map on top of the Weber saline aquifer in the northern part of the Colorado study area. The structure on top of its equivalent, the DeChelly Sand, is shown in the southern part of the map.

Contour interval is 500 feet.

Figure 10

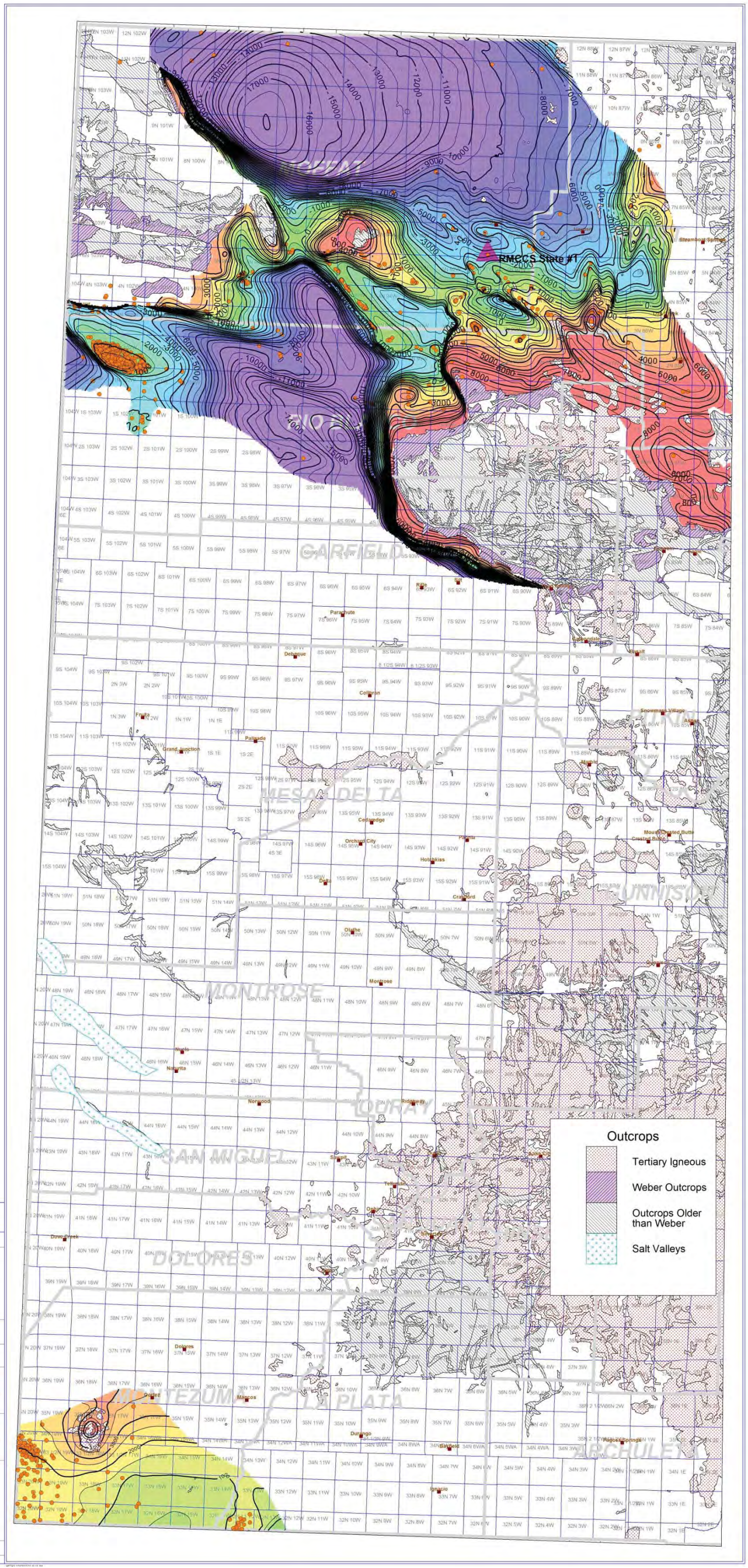


Figure 11. Thickness of the Weber saline aquifer in the northern part of the Colorado study area from the top of the Weber Formation to the top of the Maroon Formation. In the southern part of the map the thickness shown is of the DeChelly Sandstone, which is equivalent to the Weber. Contour interval is 100 feet.

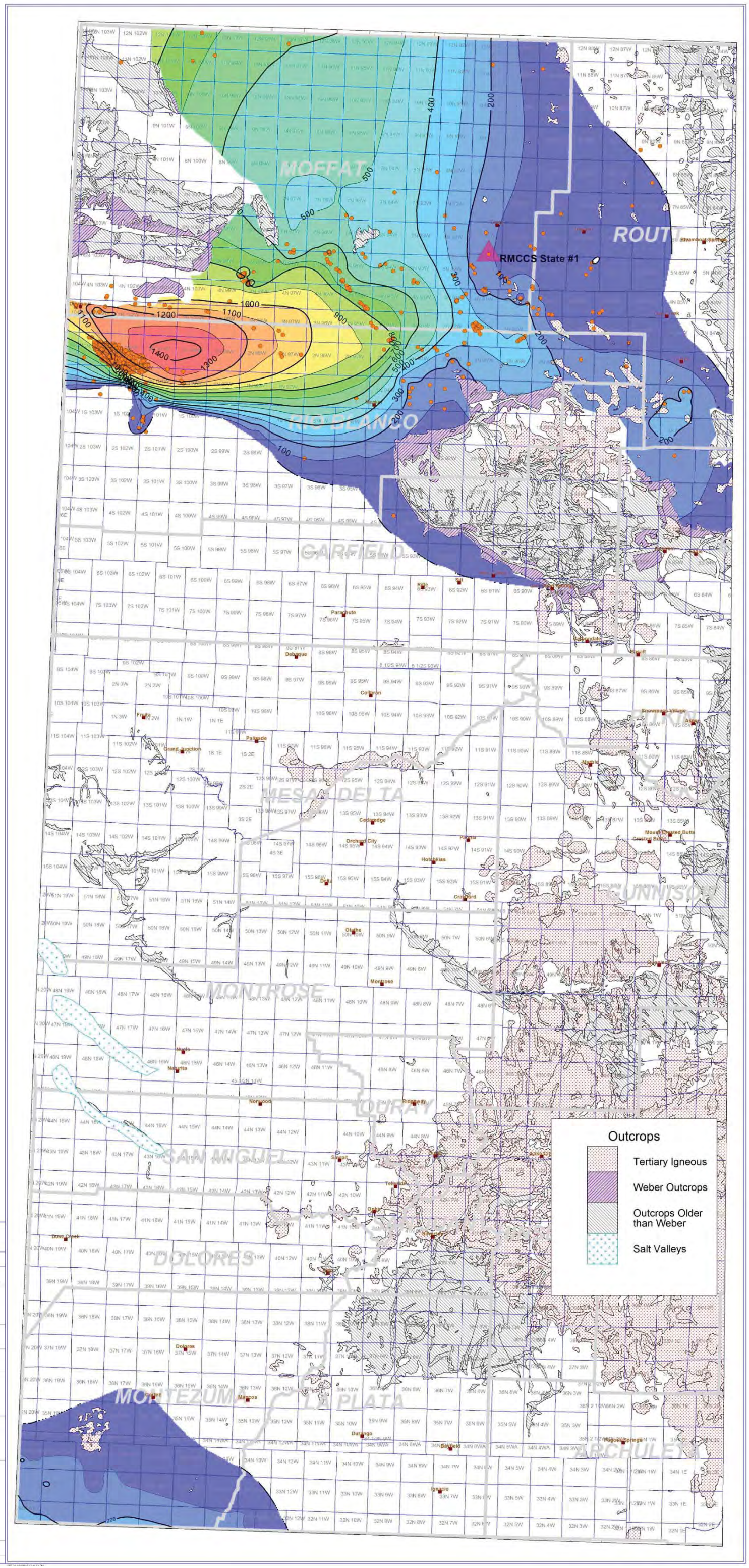


Figure 11

Figure 12. Structure map on top of the Bluff Sandstone in the Colorado study area. Contour interval is 500 feet.

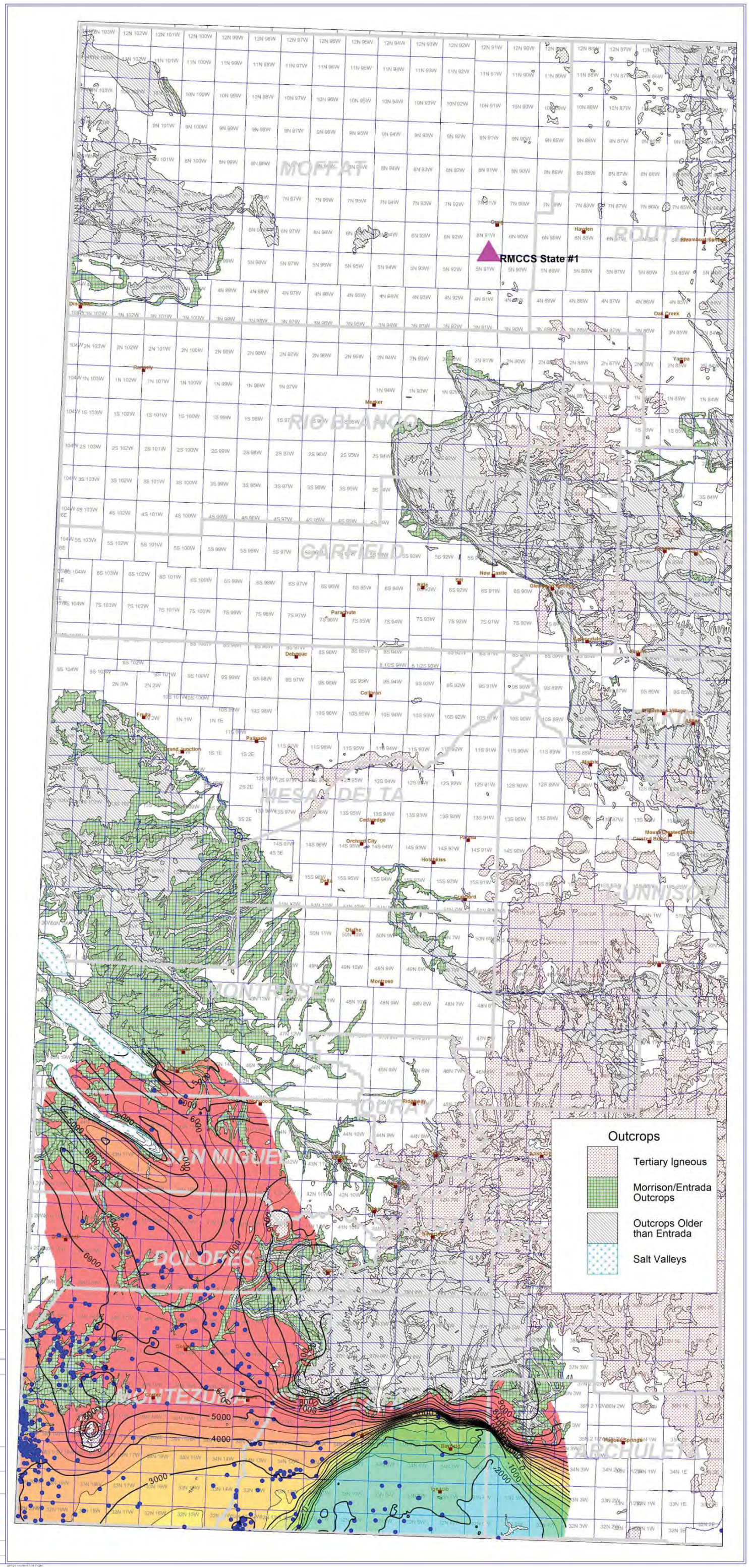


Figure 12

Figure 13. Thickness of the Bluff Sandstone in the Colorado study area. Contour interval is 100 feet.

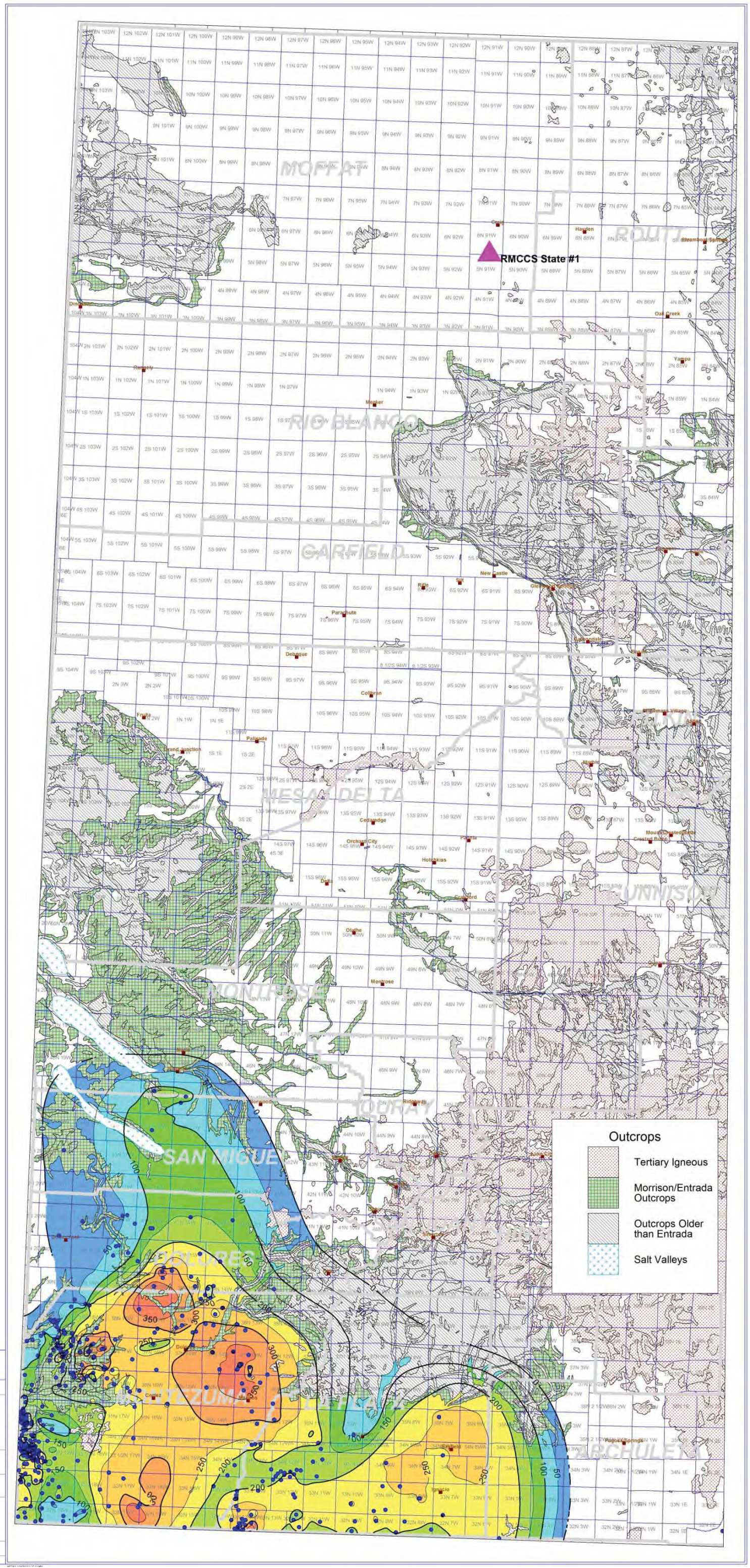


Figure 13

Figure 14. Structure map on top of the Mancos seal in the Colorado study area. Contour interval is 500 feet.

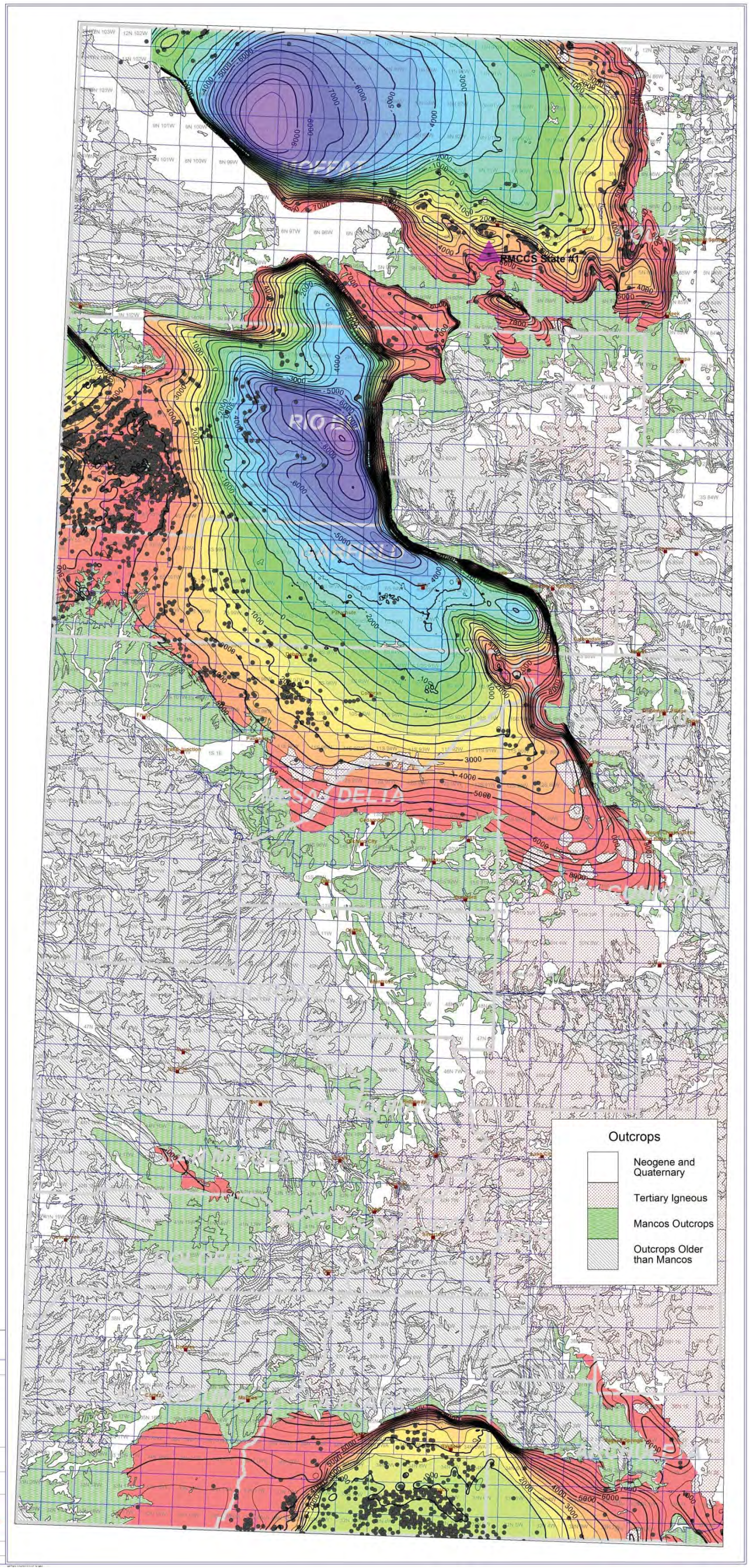


Figure 14

Figure 15. Thickness of the Mancos seal in the Colorado study area from the top of the Mancos Formation to the top of the Dakota Formation. Contour interval is 200 feet.

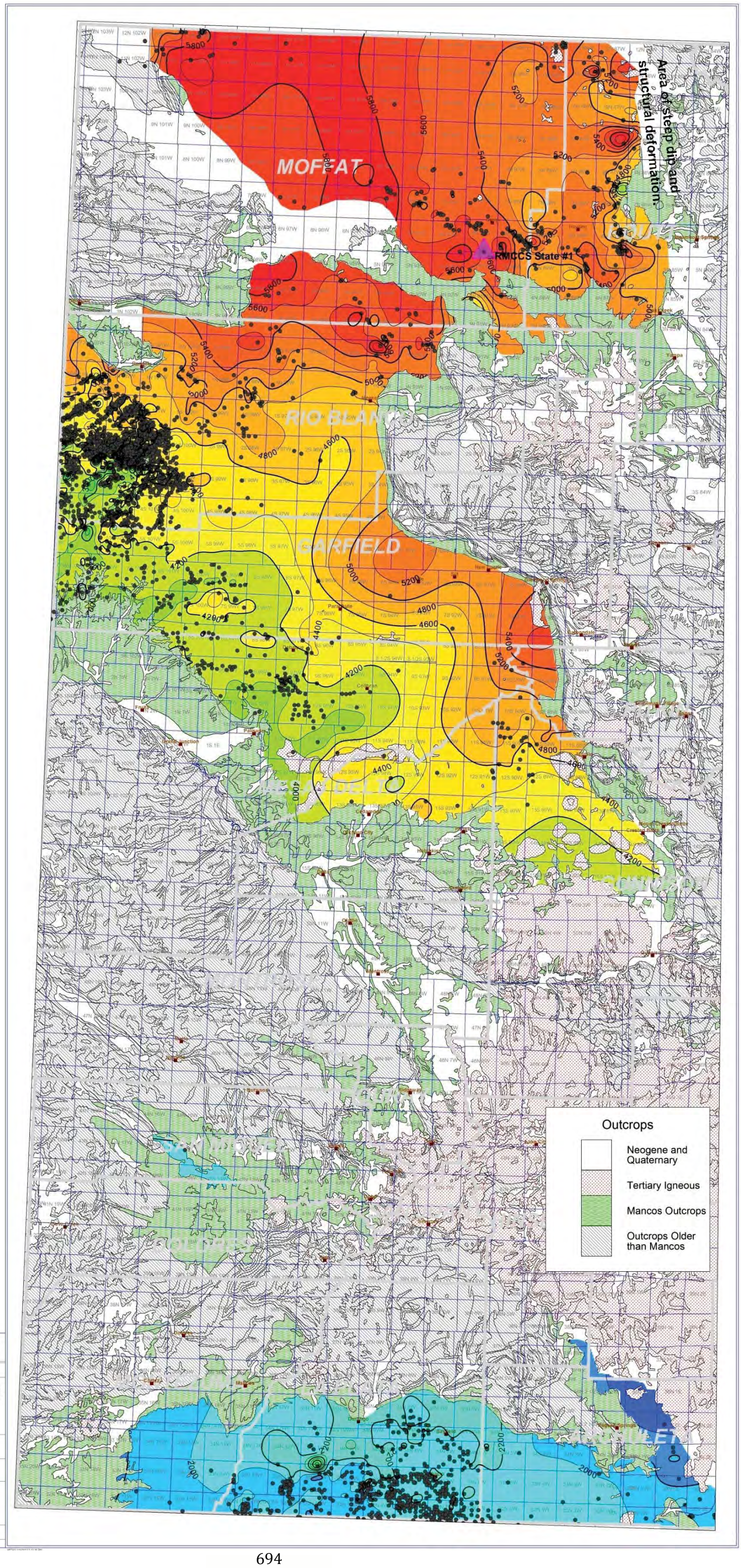


Figure 15

Figure 16. Outlines of the extents of each of the saline aquifers that are buried more than 3000 feet below the ground surface.

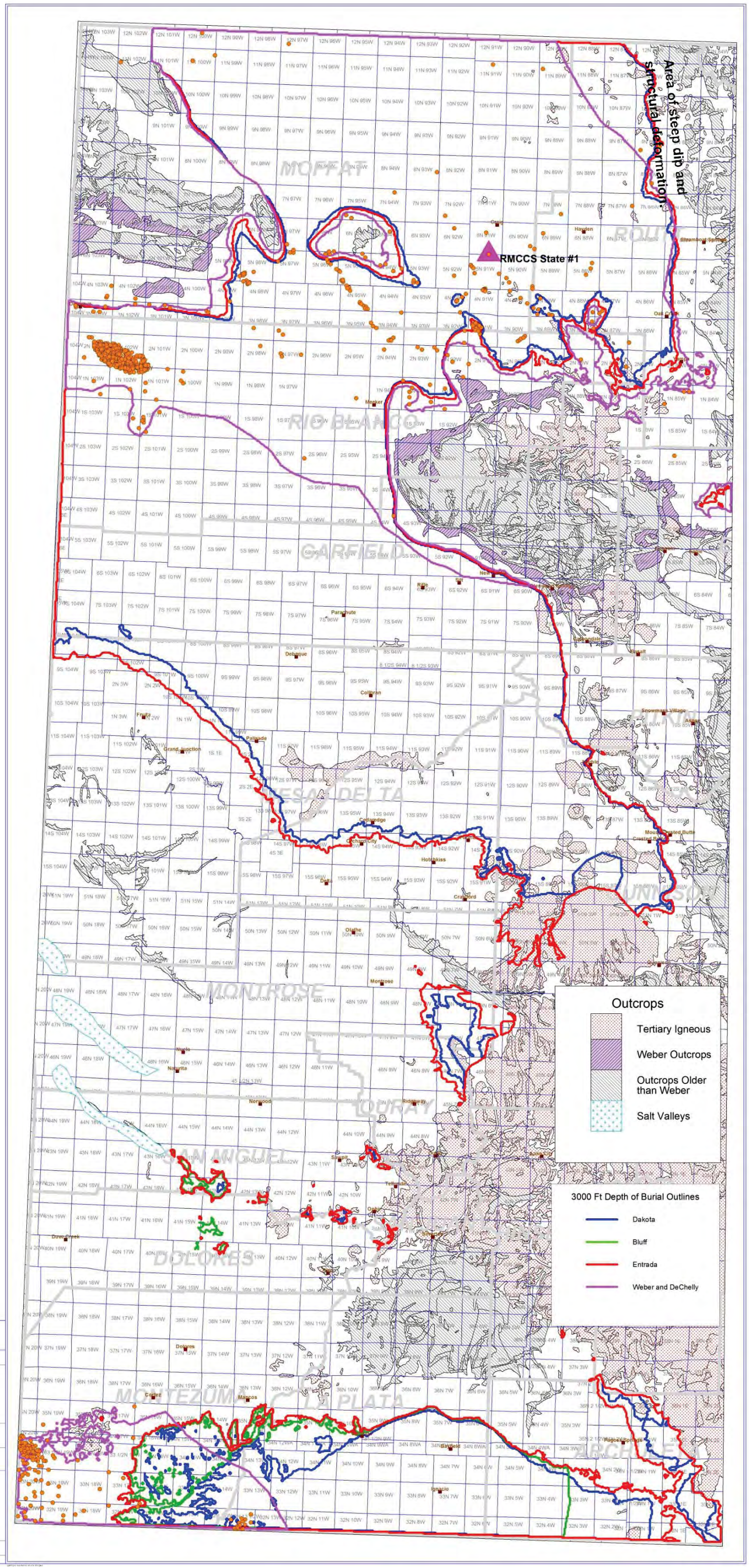


Figure 16

Colorado Geological Survey

CO_PLATEAU_CO2_PKS

3000 Ft Depth of Burial

Western Colorado

0 38,563 77,126 115,689
FEET

SYMBOL HIGHLIGHT
WEBER OR DECHELLY TOPS

REMARKS
Outlines Showing Depth of Burial of Saline Aquifers Greater than 3000 Feet

By: Phyllis Scott

February 4, 2013

Figure 17. Dakota Net Sand from Normalized Gamma Ray Curves

Sand Cutoff =
50 API Units

312 Wells

Blue Line= Outline of 3000 Foot Depth of Burial of Dakota Formation

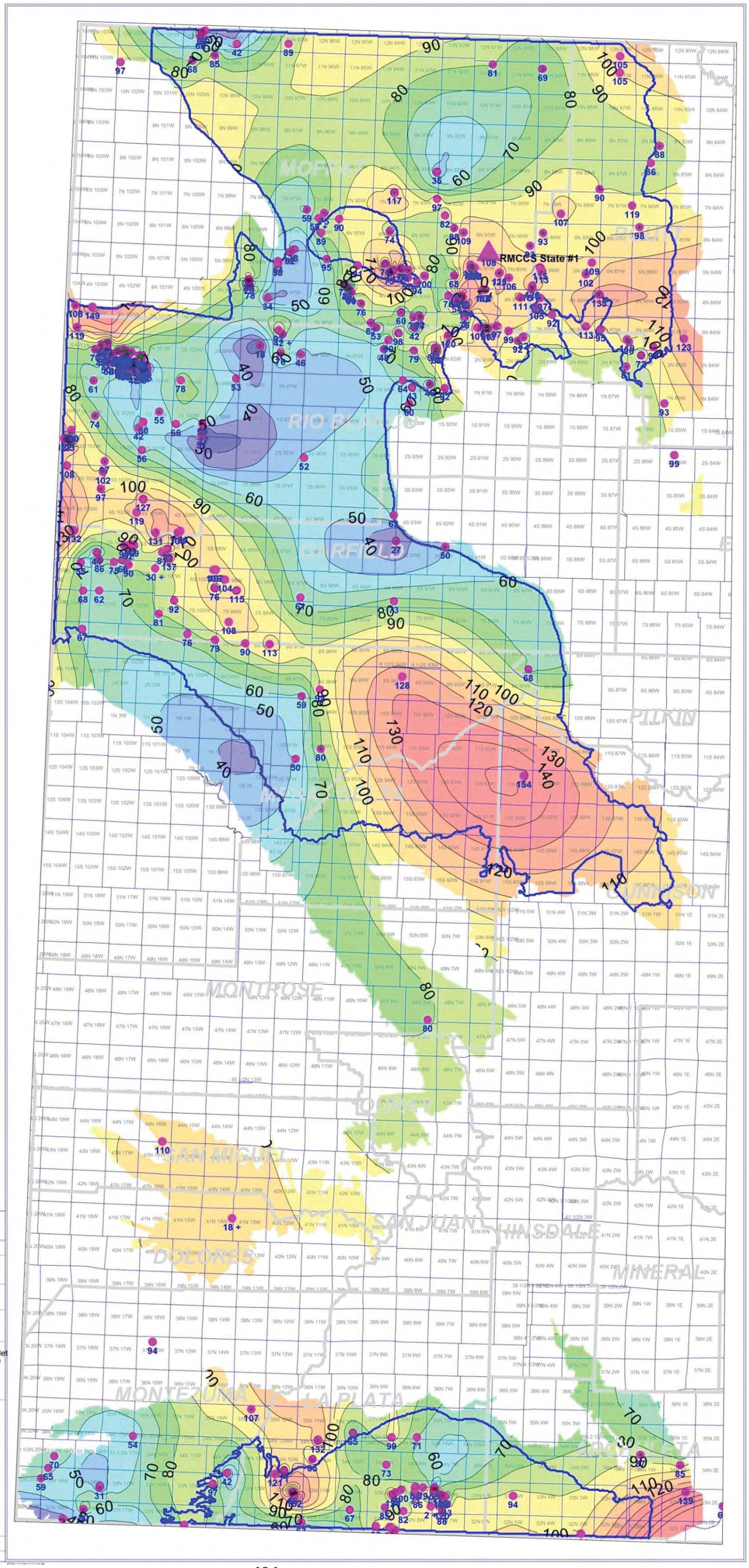


Figure 17

Figure 18. Dakota Average Porosity In Net Sands

260 Wells

Blue Line = Outline of 3000 Foot Depth of Burial of Dakota Formation

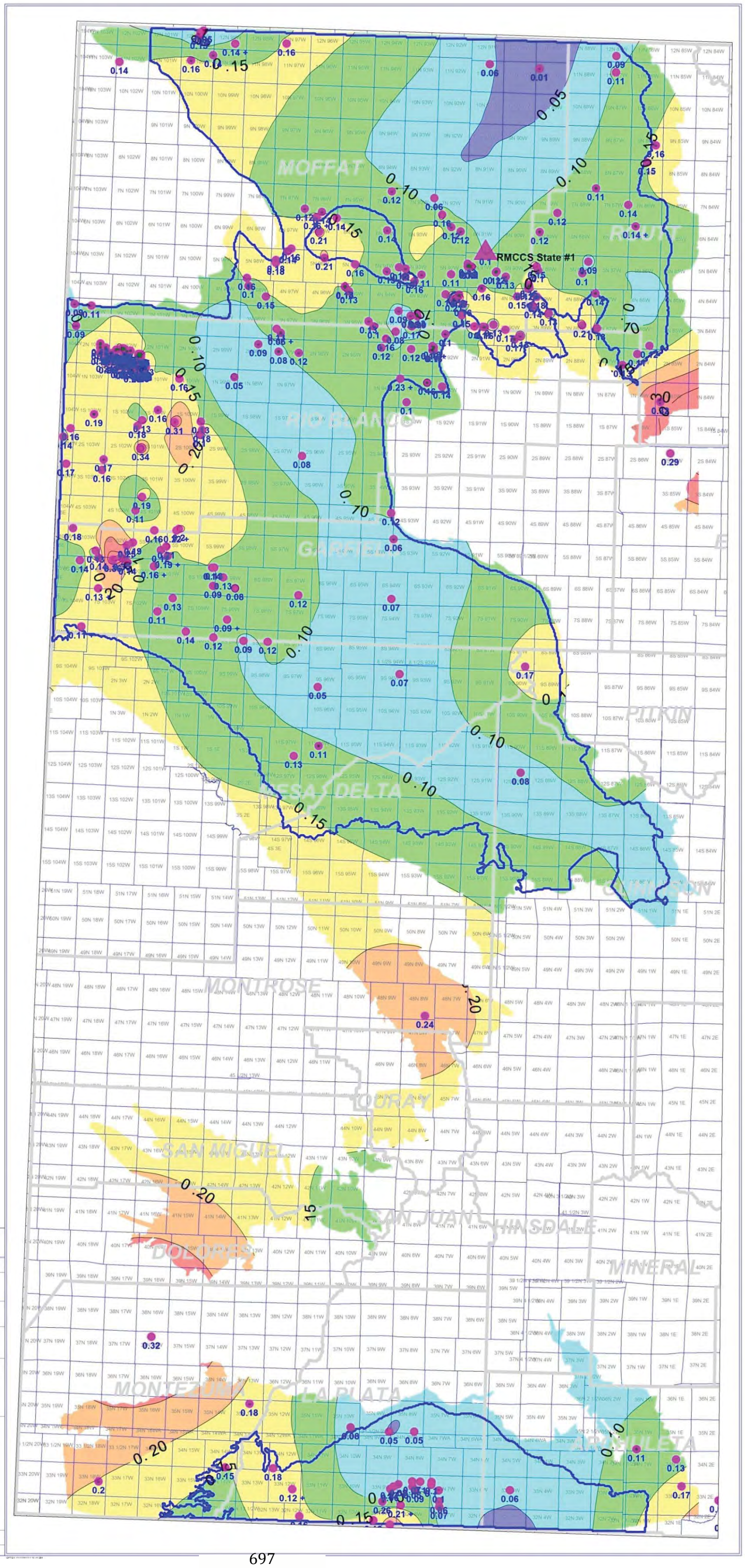


Figure 18

Figure 19. Dakota Porosity Thickness

(Average Porosity Times Net Feet of Sand)

260 Wells

Blue Line = Outline of 3000 foot Depth of Burial of Dakota Formation

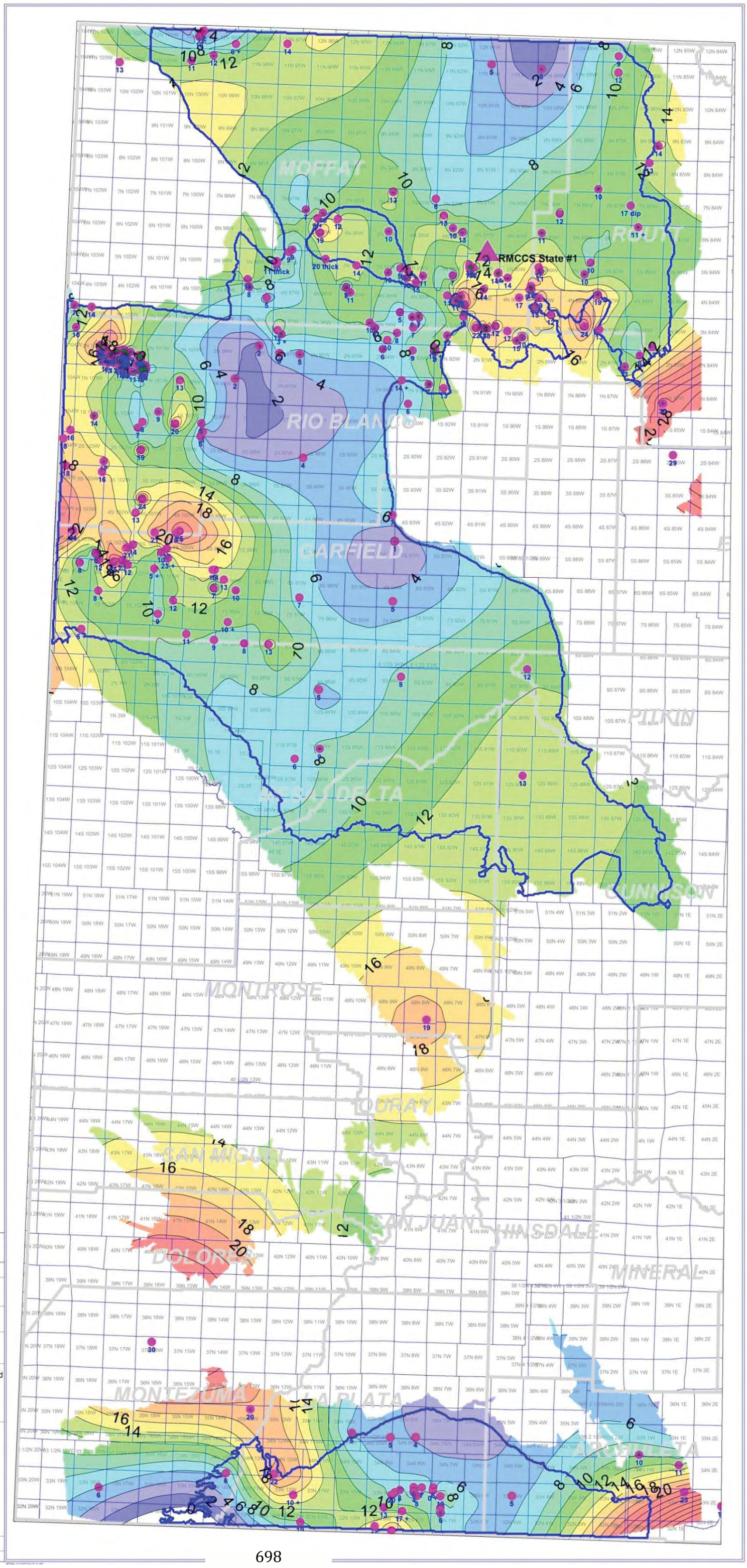


Figure 19

Figure 20. Dakota Net Feet of Sand With Porosity > 6%

259 Wells

Blue Line = Outline of 3000 Foot Depth of Burial of Dakota Formation

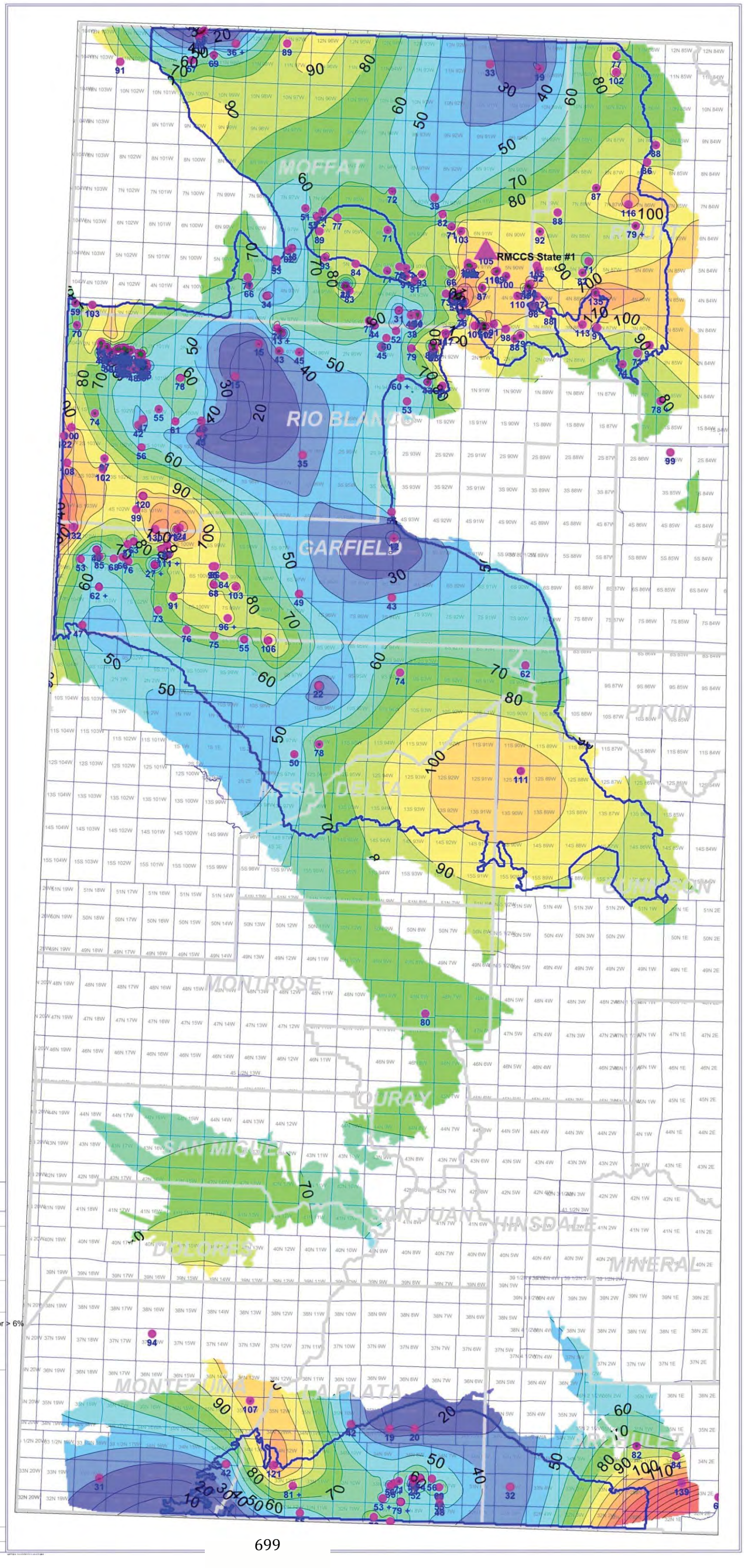


Figure 20

Figure 21. Dakota Average Effective Porosity for Sands with Porosity > 6%

259 Wells

Blue Line = Outline of 3000 Foot Depth of Burial of Dakota Formation



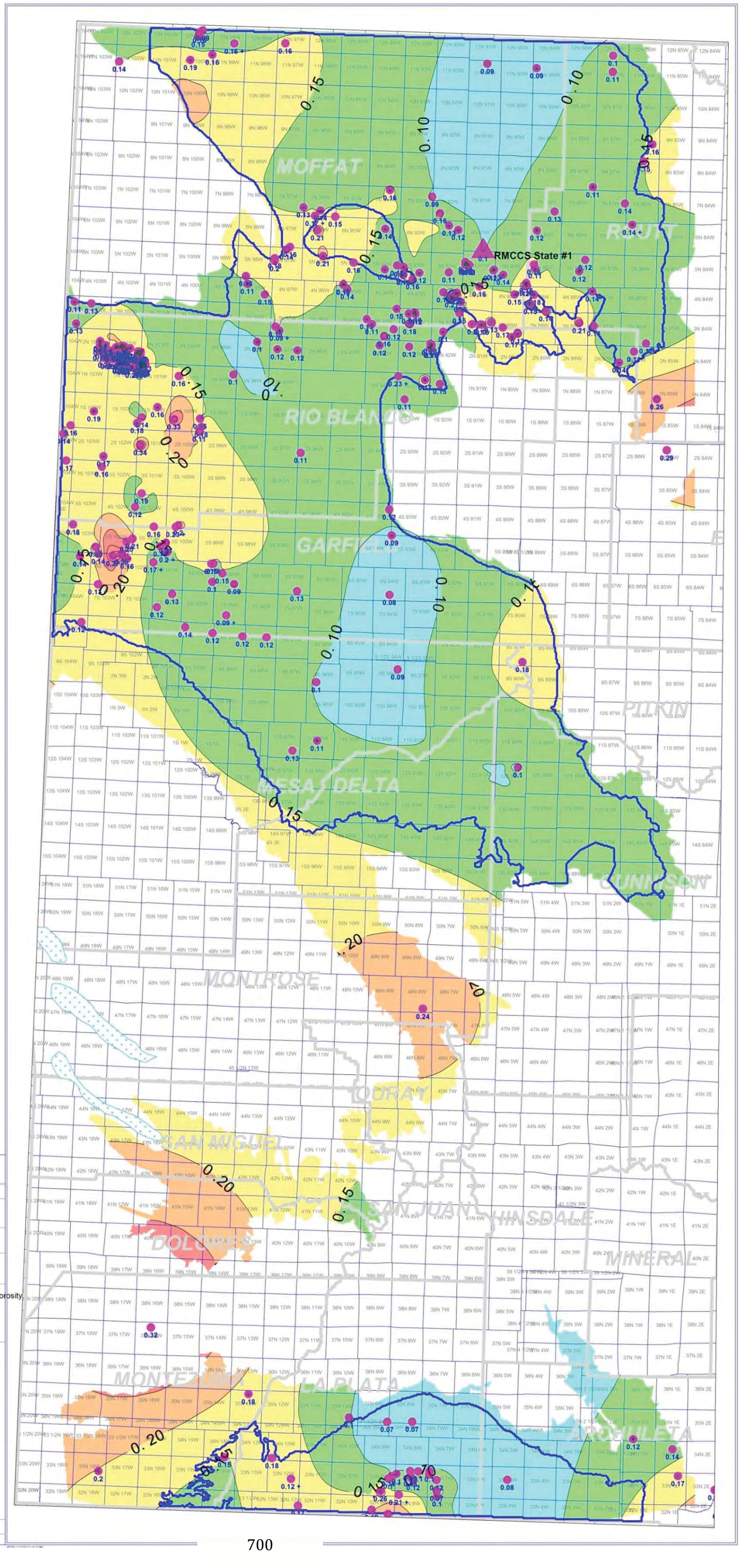


Figure 21

Colorado Geological Survey

CO_PLATEAU_CO2_PKS

Western Colorado

0 38,563 77,126 115,689
FEET

WELLS WITH DAKOTA PHIA AND PHIH

CONTOURS
O_DAKOTA_MORRISON - PHIA_6PCT - PHIA for sds > 6% porosity
ISO_DAKOTA_MORRISONPHIA_6PCT.GRD
Contour Interval = 0.0500000007450581

0.05 0.1 0.15 0.2 0.25 0.3

REMARKS

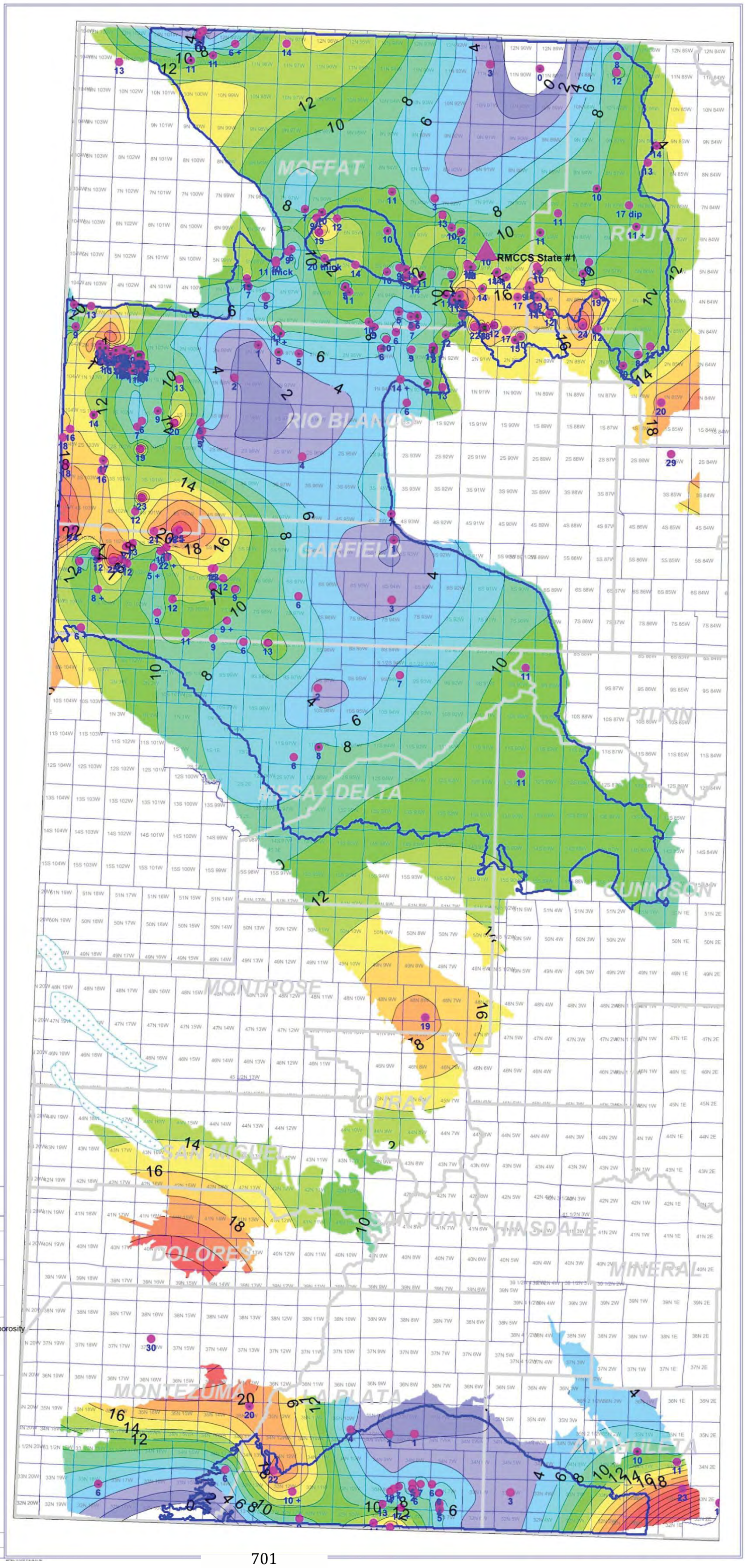
Dakota Formation Effective Average Porosity (PHIA) for Sands with Porosity > 6%

By: Phyllis Scott

November 12, 2013

Figure 22. Dakota Effective Porosity Thickness (Average Porosity Times Net Feet of Sand) for Sands with Porosity > 6%

259 Wells



Colorado Geological Survey

CO_PLATEAU_CO2_PKS

Western Colorado

0 38,563 77,126 115,689
FEET

WELLS WITH DAKOTA PHIA AND PHIH

CONTOURS
_DAKOTA_MORRISON - PHIH_6PCT - PHIH for sds > 6 pct porosity
ISO_DAKOTA_MORRISONPHIH_6PCT.GRD
Contour Interval = 2

REMARKS

Dakota Formation Effective Porosity Thickness (PhiH) for Sands with Porosity > 6%

By: Phyllis Scott

November 14, 2013

Figure 22

Figure 23. Entrada Net Sand From Gamma Ray Curves

299 Wells

Red Line = Outline of 3000 Foot Depth of Burial of Entrada Formation

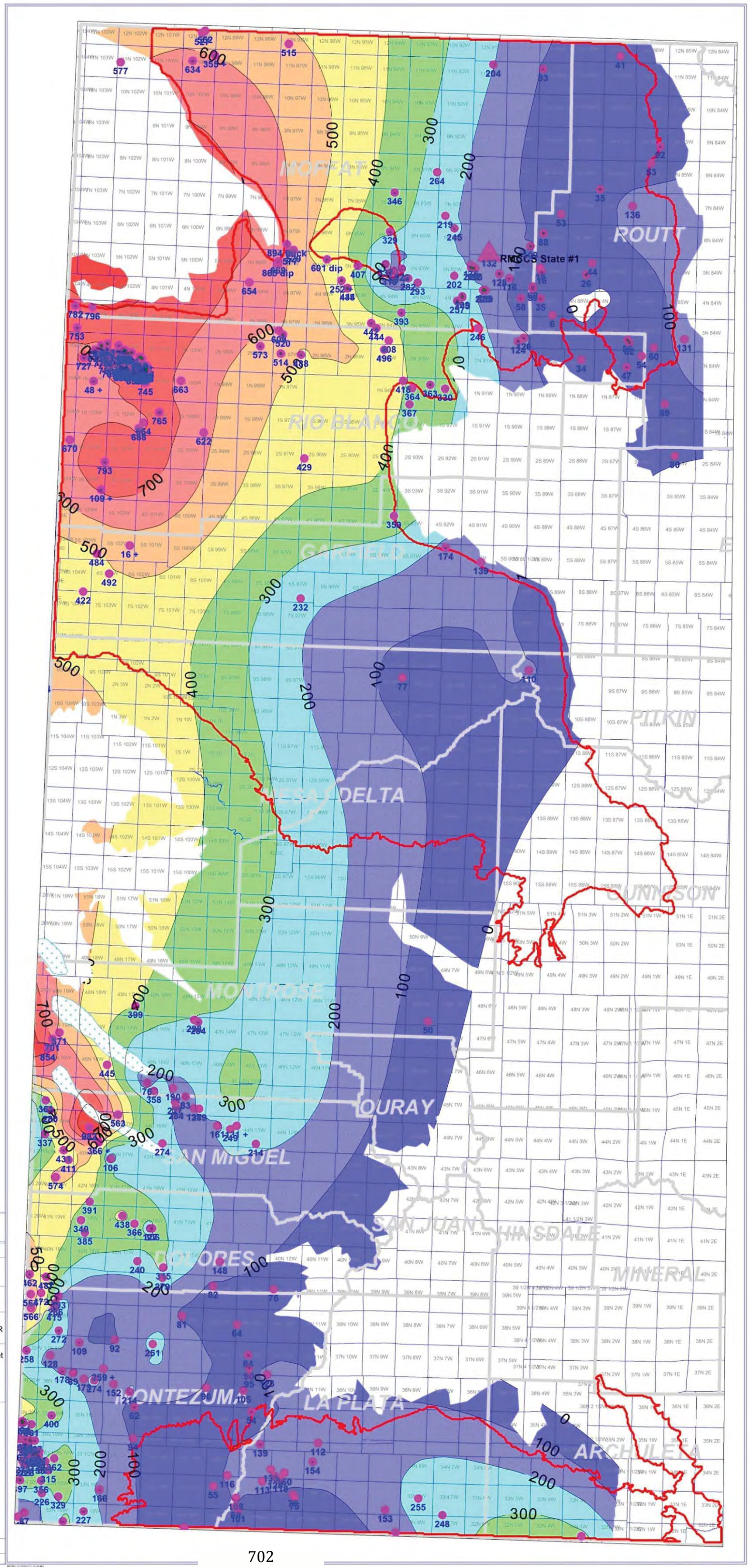


Figure 23

Colorado Geological Survey

CO_PLATEAU_CO2_PKS

Western Colorado

0 38,563 77,126 115,689
FEET

WELLS WITH ENTRADA NET SAND FROM GR

CONTOURS
ISO_ENTRADA_CHINLE - NET_SD_GR_60API [PKS] - Net
ISO_ENTRADA_CHINLENET_SD_GR_60APIPKS.GRD
Contour Interval = 100

REMARKS

Entrada Formation Net Sand (feet) from Normalized Gramma Ray Curve

By: Phyllis Scott

November 12, 2013

Figure 24. Entrada Average Porosity in Net Sands

188 Wells

Red Line = Outline of 3000 Foot Depth of Burial of Entrada Formation



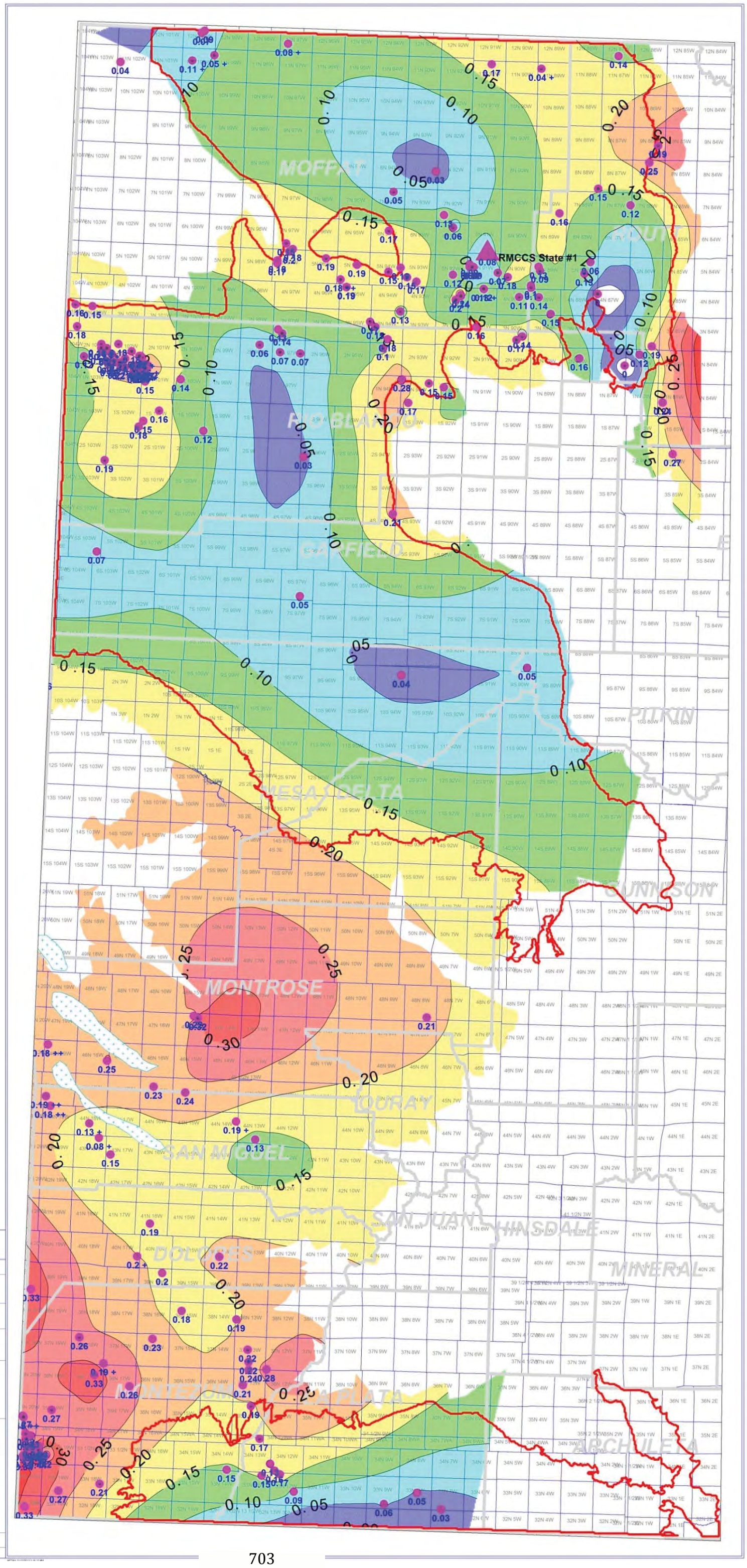


Figure 24

Colorado Geological Survey

CO_PLATEAU_CO2_PKS

Western Colorado

0 38,583 77,126 115,689
FEET

WELLS WITH ENTRADA PHIA AND PHIH

CONTOURS
ISO_ENTRADA_CHINLE - PHIA [PKS] - Phi Average
ISO_ENTRADA_CHINLEPHIAPKS.GRD
Contour Interval = 0.05

0.05 0.1 0.15 0.2 0.25 0.3 0.35

REMARKS

Entrada Formation Average Porosity in Net Sand

By: Phyllis Scott

November 12, 2013

Figure 25. Entrada Porosity Thickness (Average Porosity times Net Feet of Sand)

188 Wells

Red Line = Outline of 3000 Foot Depth of Burial of Entrada Formation

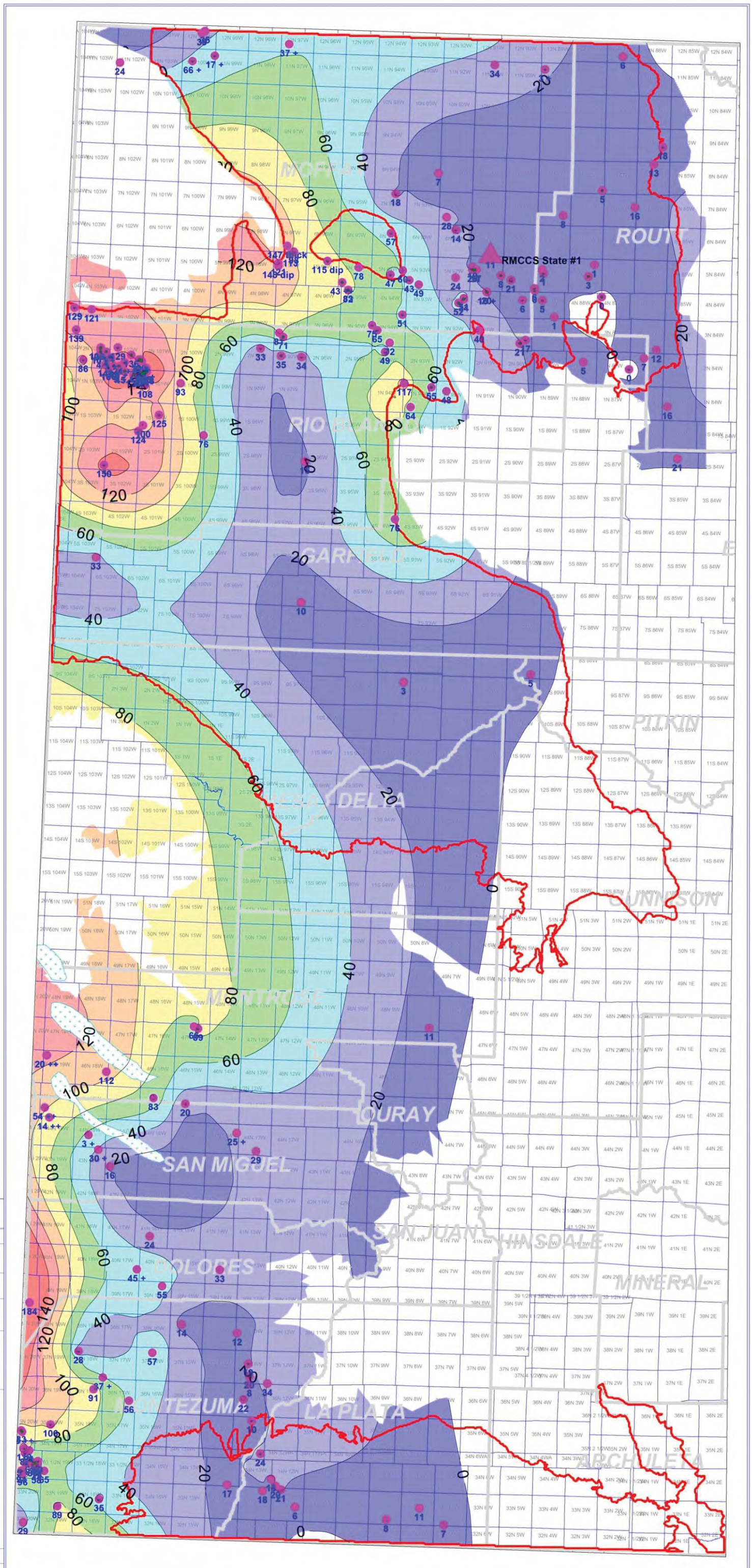


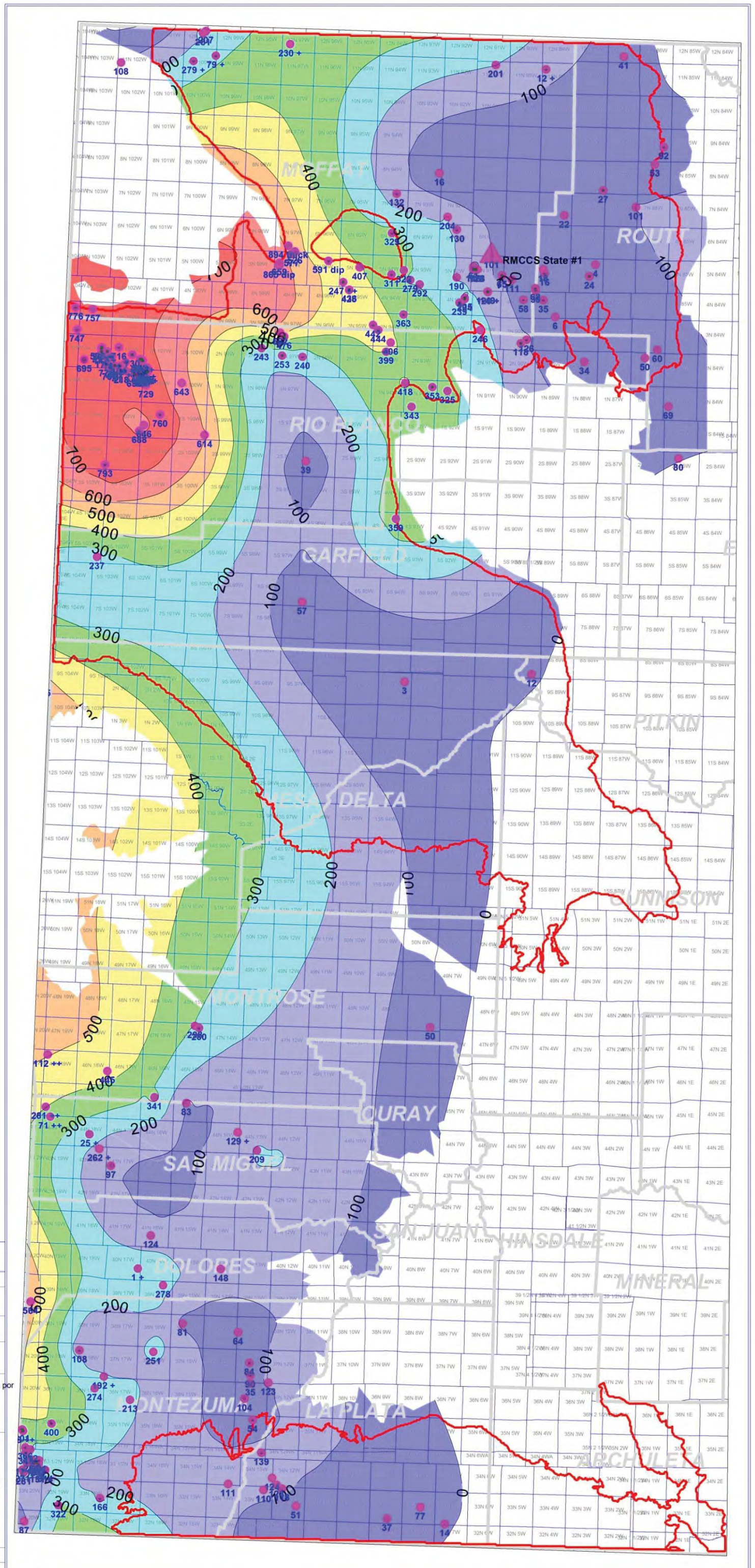
Figure 25

Figure 26. Entrada Effective Net Sand (Net Feet of Sand with Porosity > 6%)

186 Wells

Red Line = Outline of 3000 Foot Depth of Burial of Entrada Formation





Colorado Geological Survey

CO_PLATEAU_CO2_PKS

Western Colorado

0 38,563 77,126 115,689
FEET

ENTRADA NET SAND WITH POROSITY > 6%

CONTOURS
ISO_ENTRADA_CHINLE - NET_SD_GR_6PCT - Net Sd > 6% por
ISO_ENTRADA_CHINLENET_SD_GR_6PCT.GRD
Contour Interval = 100

REMARKS

Entrada Formation
Net Feet of Sand with
Porosity > 6%

By: Phyllis Scott

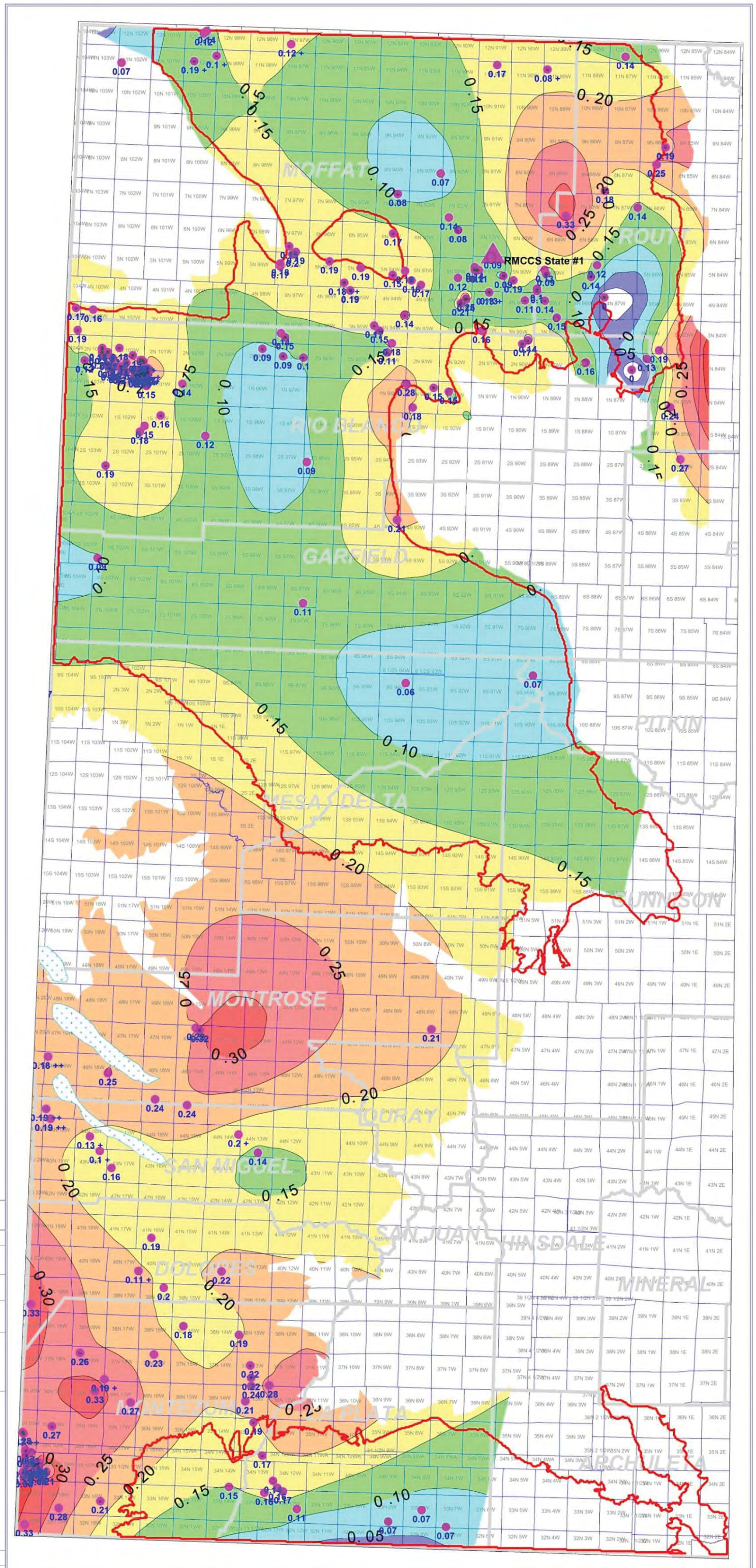
November 12, 2013

Figure 26

Figure 27. Entrada Effective Average Porosity (Porosity in Sands ☐6%)

188 Wells

Red Line = Outline of 3000 Foot Depth of Burial of Entrada Formation



Colorado Geological Survey

CO_PLATEAU_CO2_PKS

Western Colorado

0 38,563 77,126 115,689
FEET

WELLS WITH ENTRADA PHIA AND PHIH

CONTOURS
ISO_ENTRADA_CHINLE - PHIA_6PCT - Avg. Por > 6%
ISO_ENTRADA_CHINLEPHIA_6PCT.GRD
Contour Interval = 0.05

REMARKS

Entrada Formation Average Porosity (PHIA) for Sands with Porosity > 6%

By: Phyllis Scott

November 12, 2013

Figure 27

Figure 28. Entrada Effective Porosity Thickness (Average Porosity Times Net Feet of Sand) For Sands with Porosity > 6%

188 Wells

Red Line = Outline of 3000 Foot Depth of Burial of Entrada Formation

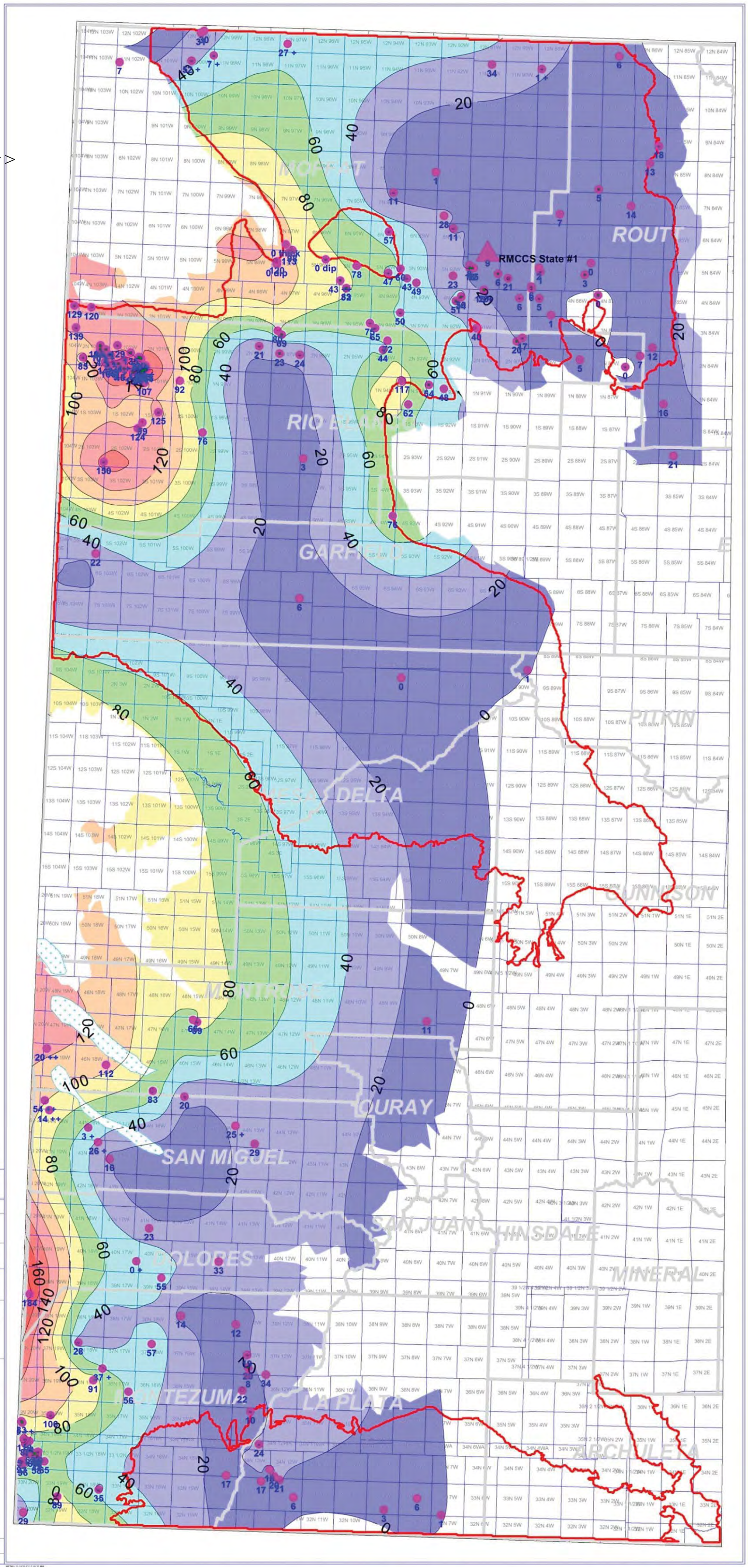


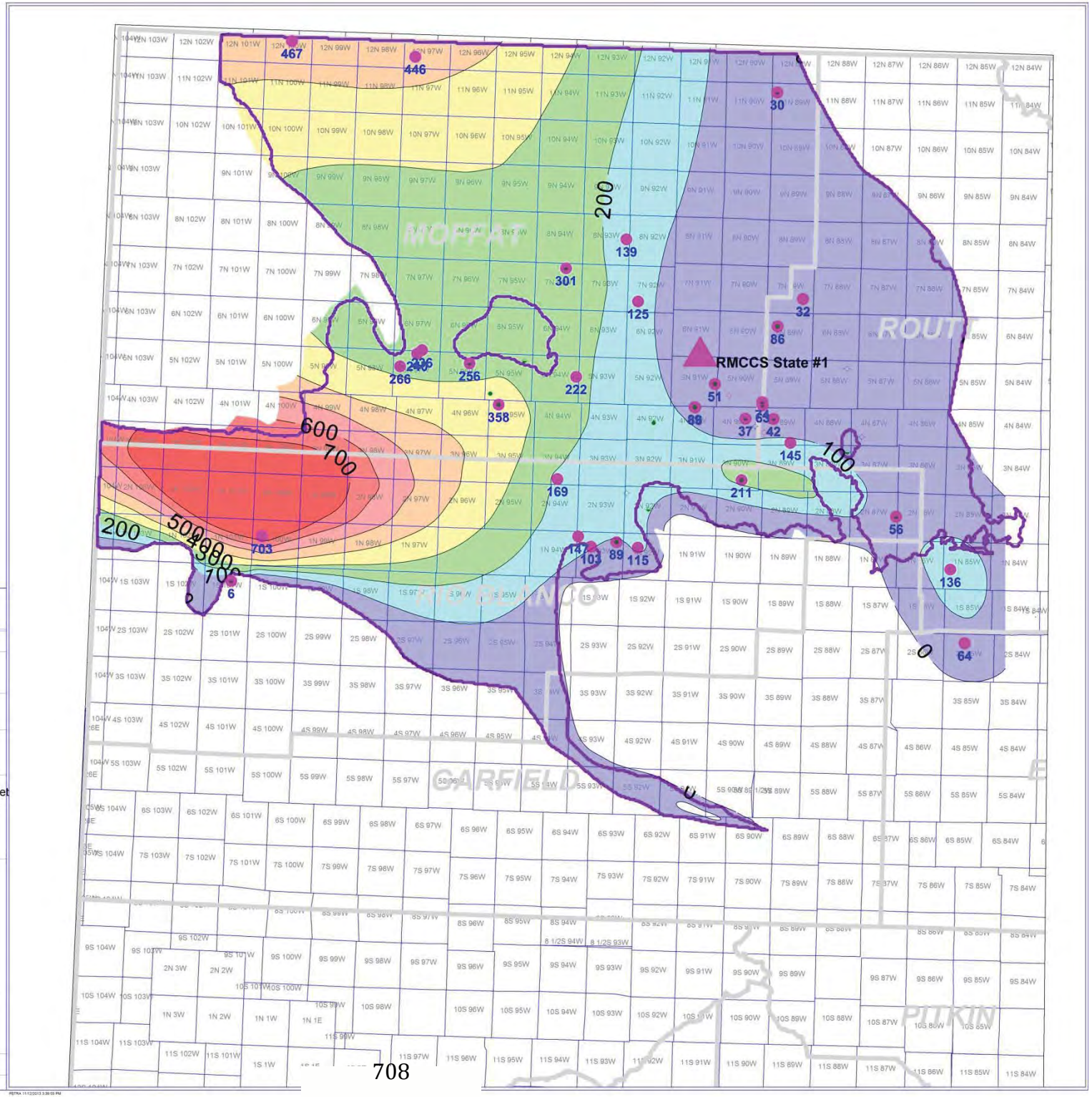
Figure 28

Figure 29. Weber Net Sand From Normalized Gamma Ray Curves

36 Wells

Purple Line = Outline of 3000 Foot Depth of Burial of Weber Formation





Colorado Geological Survey

CO_PLATEAU_CO2_PKS

Western Colorado

0 38,731 77,462 116,193
FEET

WELLS WITH WEBER GR LAS

CONTOURS
WEBER_MAROON - NET_SAND_GR_NRM_W60 [PKS] - Net
WEBER_MAROONNET_SAND_GR_NRM_W60PKS.GRD
Contour Interval = 100

REMARKS

Weber Formation Net Feet of Sand from Normalized Gamma Ray Curves

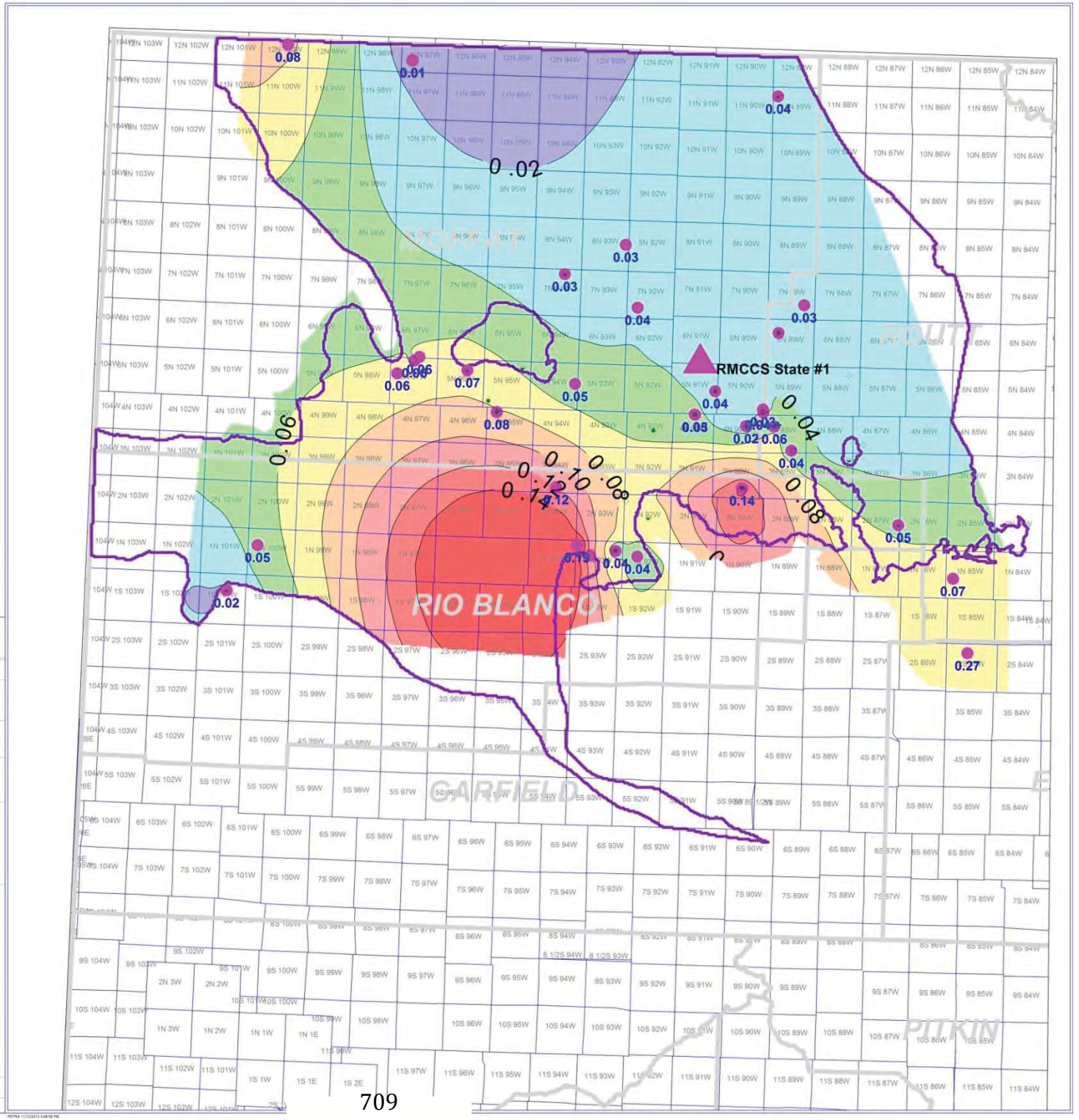
By: Phyllis Scott

November 12, 2013

Figure 30. Weber Average Porosity in Sands

33 Well Data Points

Purple Line = Outline of 3000 Foot Depth of Burial of Weber Formation



Colorado Geological Survey

CO_PLATEAU_CO2_PKS

Western Colorado

0 37,848 75,696 113,544
FEET

WELLS WITH WEBER GR LAS

CONTOURS
WEBER_MAROON - PHIA - Phi Avg aliased
WEBER_MAROONPHIA.GRD
Contour Interval = 0.02

REMARKS

Weber Formation Average Porosity (PHIA) for Net Sands

By: Phyllis Scott

November 12, 2013

Figure 31. Weber Porosity Thickness (Average Porosity Times Net Feet of Sand)

33 Well Data Points

Purple Line = Outline of 3000 Foot Depth of Burial of Weber Formation

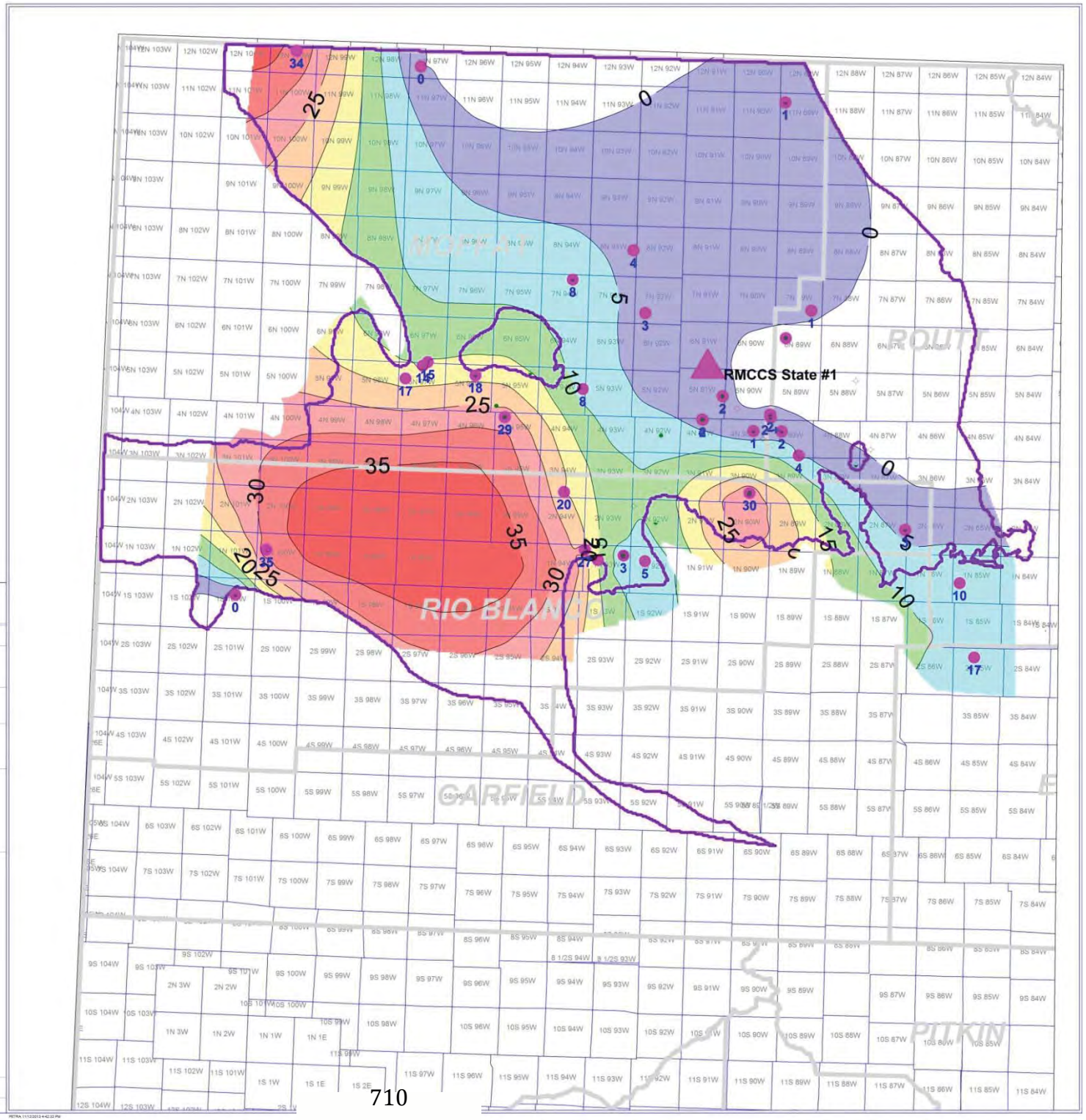
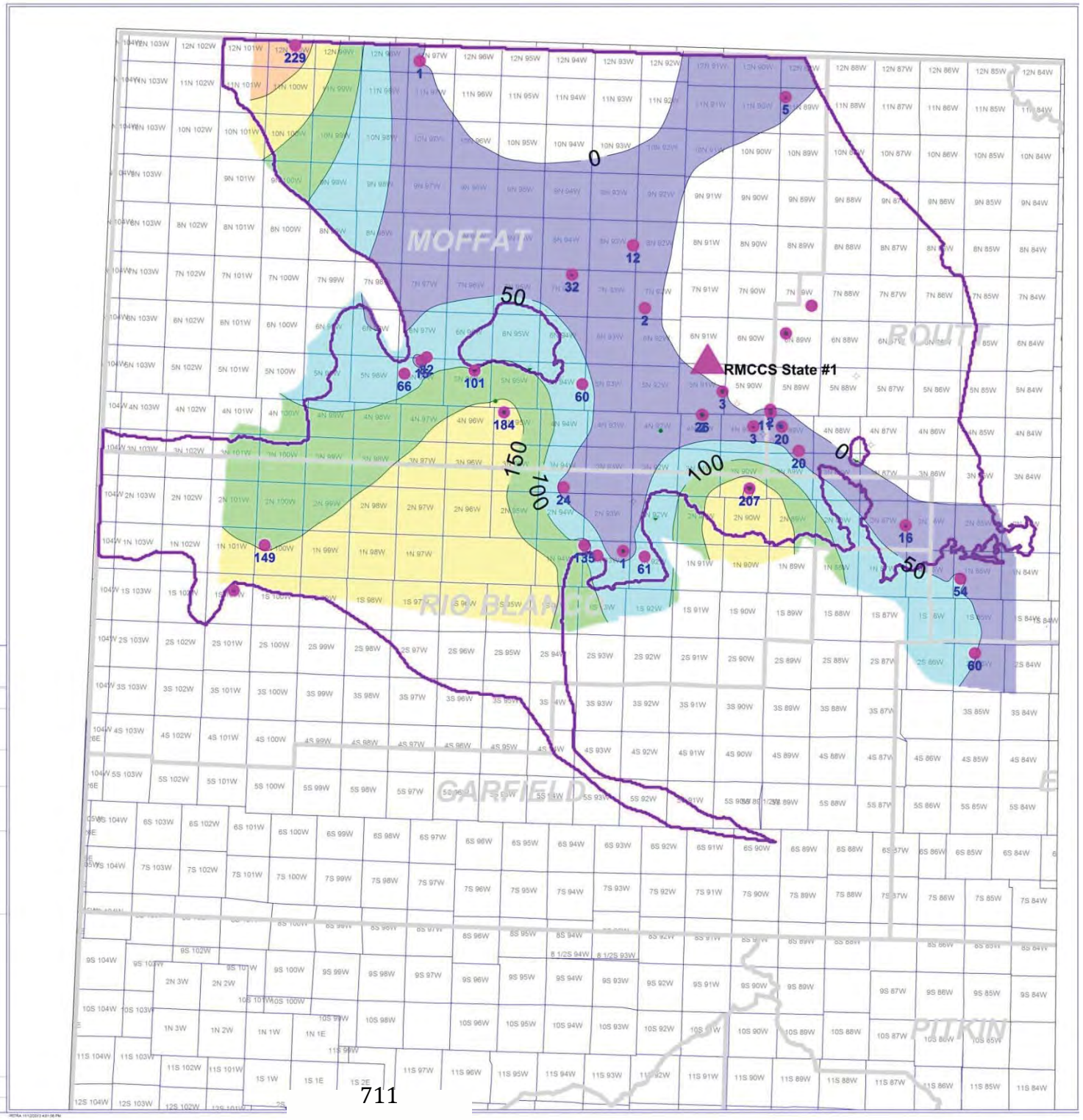


Figure 32. Weber Effective Net Sand (Net Feet of Sand with Porosity > 6%)

31 Well Data Points

Purple Line = Outline of 3000 Foot Depth of Burial of Weber Formation



Colorado Geological Survey

CO_PLATEAU_CO2_PKS

Western Colorado

0 38,045 76,090 114,135
FEET

WELLS WITH WEBER GR LAS

CONTOURS
WEBER_MAROON - NET_SD_6PCT [PKS] - Net
WEBER_MAROONNET_SD_6PCTPKS.GRD
Contour Interval = 50

REMARKS

Weber Formation Net Feet of Sand with Porosity > 6%

By: Phyllis Scott

November 12, 2013

Figure 33. Weber Effective Average Porosity (in Sands with Porosity > 6%)

31 Well Data Points

Purple Line = Outline of 3000 Foot Depth of Burial of Weber Formation

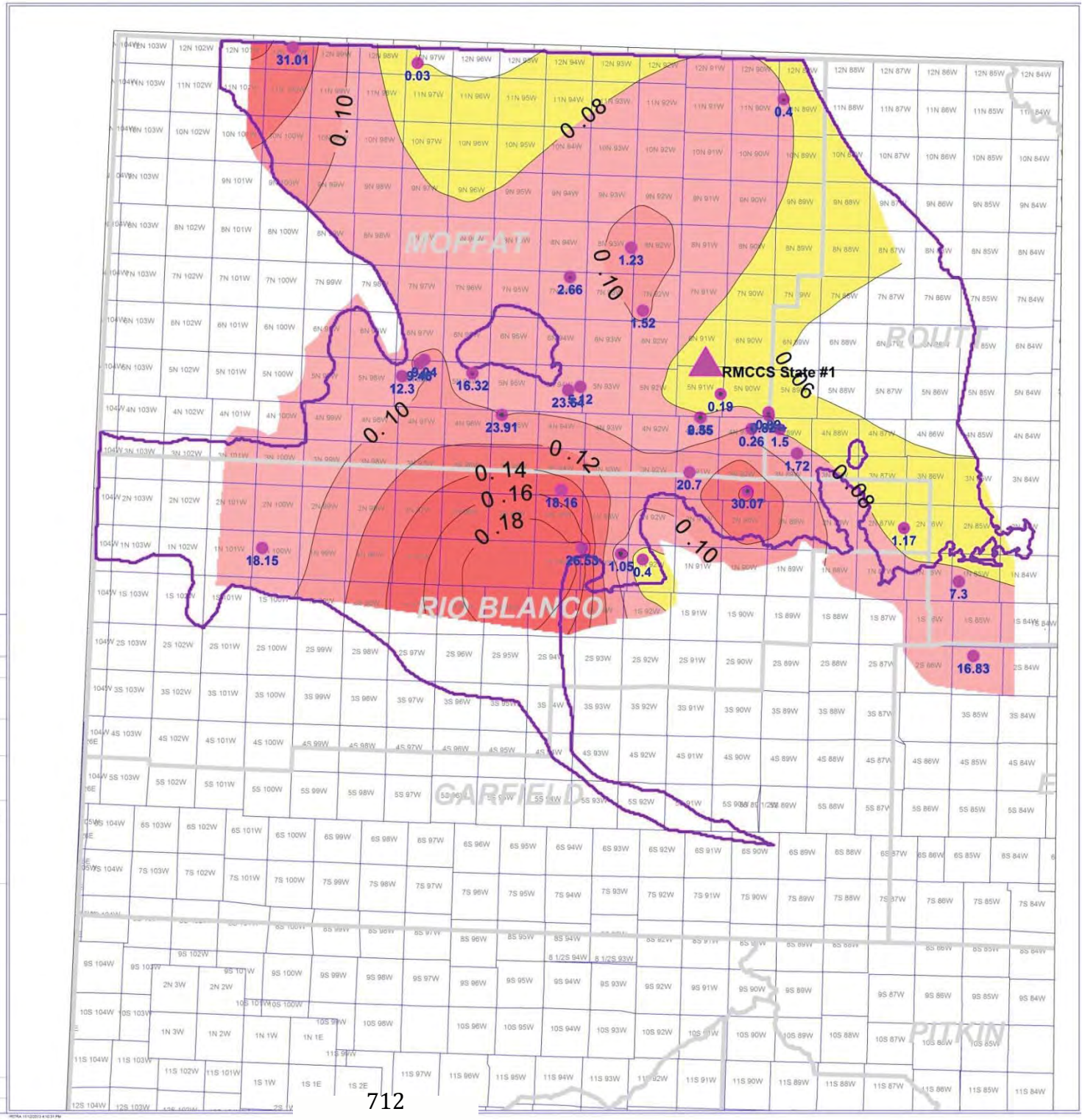


Figure 34. Weber Effective Porosity Thickness (Net Feet of Sand Times Average Porosity) in Sands with Porosity > 6%)

31 Well Data Points

Purple Line = Outline of 3000 Foot Depth of Burial of Weber Formation

